

ORGANOMETALLICS

Volume 28, Number 1, January 12, 2009

© Copyright 2009
American Chemical Society

Editor's Page

Introduction to the Editor's Historical Review in This Issue of *Organometallics*

In this issue there appears, after a long delay, Part 2 of my essay—review on the alkyls and aryls of the alkali metals lithium, sodium, and potassium. The molecules on the cover of this issue are two that are featured in this essay: on the top left is Wilhelm Schlenk's product of the addition of sodium to tetraphenylethylene, $(\text{C}_6\text{H}_5)_2\text{C}(\text{Na})\text{C}(\text{Na})(\text{C}_6\text{H}_5)_2$, shown here as Schlenk had drawn it, as a covalent molecule with C–Na single bonds, rather than as the disodium salt of the tetraphenylethylene dianion, as we know it today. The second molecule, on the bottom right, is Karl Ziegler's α -phenylisopropylpotassium, $\text{C}_6\text{H}_5(\text{CH}_3)_2\text{CK}$, the compound that he found added to the olefinic double bond and, as a consequence, could initiate the polymerization of 1,3-dienes and styrene, thus launching him on the path to his 1963 Nobel Prize in Chemistry.

Part 2 completes the account of the major routes used in the preparation of organoalkali-metal compounds, with discussions of the metal displacement and transmetalation reactions and of organolithium-derived superbases. During the course of my preparatory reading I became greatly interested in the life and work of Wilhelm Schlenk, the great pioneer of organoalkali metal chemistry—not just his work on the alkyls and aryls of sodium and lithium but on all of his other varied research in the organoalkali-metal area spanning the 20 years 1911–1931. Having immersed myself in Schlenk's papers and related contemporaneous papers of Karl Ziegler, I decided that an account of this extraordinary experimental work on such extremely reactive compounds would be of interest to our readers. Thus, discussions of Schlenk's work on the diaryl ketone alkali-metal ketyls, the colored triarylmethyl–alkali-metal compounds, and the products of alkali-metal addition to compounds that contain reactive C=C, C=N, and N=N bonds were added. As a result, Part 2 ended up being rather long.

Part 2 hopefully will be followed by a short Part 3, which will bring an account of the early work on the structure and bonding of organoalkali-metal compounds.

My thanks, as always, to Professor Arnold L. Rheingold for the cover figures.

Dietmar Seyferth

Editor

OM801048Y

Cover Essay

Alkyl and Aryl Derivatives of the Alkali Metals: Strong Bases and Reactive Nucleophiles. 2. Wilhelm Schlenk's Organoalkali-Metal Chemistry. The Metal Displacement and the Transmetalation Reactions. Metalation of Weakly Acidic Hydrocarbons. Superbases

Dietmar Seyferth

Department of Chemistry, Massachusetts Institute of Technology, Cambridge, Massachusetts 02139

Received October 30, 2008

I. Introduction

In Part 1 of this essay,¹ the preparation of organoalkali-metal compounds by reaction of organic halides with alkali metals and with organoalkali-metal compounds was discussed. In Part 2, the preparation of organoalkali-metal compounds by the metal displacement reaction (eq A) and by transmetalation (eq B) is considered.

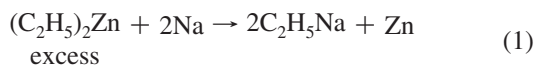


M = alkali metal; M' = another metal, usually a heavy metal (e.g. Hg, Sn, Pb)

This account includes a discussion of the seminal work in this area of Wilhelm Schlenk. In view of the importance of his pioneering contributions, I felt that a reasonably thorough discussion of all of his research in the broad area of organoalkali-metal chemistry was warranted. Toward the end of Schlenk's research activities, Karl Ziegler came on the scene and a not overly friendly interaction developed between the two when Ziegler entered the organoalkali-metal field. This required a discussion of Ziegler's work, and so the essay grew longer than I had expected when I started my writing. Add to that the last section on organolithium-derived superbases, the exciting more recent development in organoalkali-metal chemistry, and Part 2 ended up quite long, with no room left for a discussion of structures and bonding, which I had originally intended to include.

II. The Preparation of Organoalkali-Metal Compounds by the Metal Displacement Reaction. George Bowdler Buckton, 1859

In Section I of Part 1 of this essay,¹ the attempts by J. A. Wanklyn to prepare sodium alkyls were described. These involved the use of the metal displacement reaction for the first time (eq 1), but the sodium alkyl, a strong, highly polar



nucleophile and base, reacted with the excess of diethylzinc, a Lewis acid, to give an adduct, the zincate complex $NaZn(C_2H_5)_3$. This compound was much more reactive than diethylzinc, about as reactive as one might have expected ethylsodium to be, but

its two components could not be separated. The new field of organometallic chemistry was a very active one in the 1850s, after Frankland had reported the preparation of dimethylzinc in 1849. Among the chemists of the time who had begun research in organometallic chemistry was George Bowdler Buckton in England.² Buckton had reported his preparations of ethyl derivatives of mercury, tin, and lead by the action of diethylzinc on halides of these metals in 1859.³ Having prepared diethylmercury, which he wrote as HgC_4H_5 (using Berzelius' flawed atomic weight scale in which C = 6 and O = 8), Buckton was led to wonder:^{3b,d}

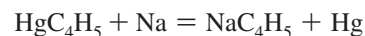
"The electro-negative character of the group $C_{n2}H_{n2+1}$ in the class of organo-metals to which zincethyl belongs, may now perhaps be considered as established. Some interest, nevertheless, attaches to the question whether sodium is capable of displacing ethyl from mercuric ethyl. An answer to this question would give us some means of judging the position of ethyl, as regards its electro-negative function towards the true metals."

Therefore, he carried out the experiment and described its outcome (but without experimental details).^{3b,d}

"At ordinary temperatures, sodium has only a slow action on mercuric ethyl, but after the lapse of a few hours a voluminous grey sponge is formed, whilst the liquid entirely disappears. This sponge-like body has the property of spontaneous combustibility in a marked degree, and is liable to explosion from apparently very slight causes. By the application of a gentle heat, a strong rush of gaseous matter is evolved which eudiometric experiments proved to be a mixture of ethylene and hydride of ethyl, obviously proceeding from the disintegration of a double molecule of ethyl."

Buckton correctly interpreted his observations:

"...probably, perhaps, sodiummethyl is first formed in the reaction, and then decomposed by heat



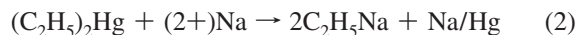
The mercury is supposed here to be inert, and in no way to determine the decomposition."

(2) For a picture and biographical sketch of Buckton, see an earlier historical essay: ; Seyferth, D. *Organometallics* 2003, 22, 2346.

(3) (a) Buckton, G. B. *Proc. R. Soc. London* 1859, 9, 309. (b) Buckton, G. B. *Proc. R. Soc. London* 1859, 9, 685. (c) Buckton, G. B. *Ann.* 1859, 109, 122, 222. (d) Buckton, G. B. *Ann.* 1859, 112, 220.

(1) Seyferth, D. *Organometallics* 2006, 25, 2.

This was the first preparation of an organosodium compound. Diethylmercury is a much weaker Lewis acid than diethylzinc; thus, no “ate” complex of mercury was formed. The report by Buckton does not indicate the amounts of reactants used, but if he had used an excess of sodium, formation of sodium amalgam would have facilitated the reaction (eq 2).

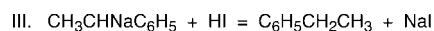
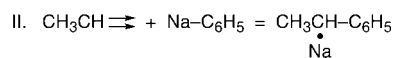
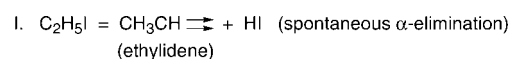


Buckton did not pursue this chemistry; no doubt he was put off by the nasty “voluminous grey sponge”. The R_2Hg/Na reaction, not surprisingly, did not attract any other organometallic chemists of the time, so organosodium chemistry remained at the starting gate.

John Ulric Nef, at the University of Chicago, at the beginning of the last century had S. F. Acree, one of his students, investigate the preparation of phenylsodium by the reaction of sodium with diphenylmercury because he wanted to seek confirmation that phenylsodium was an intermediate in the Wurtz–Fittig reaction of bromobenzene with sodium. Fittig and other workers had found that when the C_6H_5Br/Na reaction was carried out in the presence of various electrophiles such as alkyl halides, ketones, and CO_2 , phenylation of the electrophile was observed.⁴ It was assumed that phenylsodium was an intermediate in these reactions but proof, either direct or indirect, was not sought and was lacking. Nef felt that if phenylsodium could be prepared by an independent method and, if it reacted with these electrophiles in the same way as did the C_6H_5Br/Na system, this would be strong evidence in favor of the intermediacy of phenylsodium in the C_6H_5Br/Na reaction. In his preparation of phenylsodium, Acree used benzene as reaction medium, in contrast to Buckton, who did not mention using a solvent for the reaction of sodium with diethylmercury. This made all the difference. The reaction of diphenylmercury with a considerable excess of sodium wire in benzene proceeded vigorously. Sodium amalgam fell to the bottom of the flask, and a light brown powder remained suspended in the benzene.⁵ The greater the excess of sodium used, the greater was the extent of conversion to phenylsodium. A pure (as possible) sample of phenylsodium was prepared by using an excess of sodium wire in the preparation and subsequently transferring a sample of the phenylsodium as a suspension in benzene under an atmosphere of dry hydrogen to a tared flask using a pipet. The benzene then was evaporated in a stream of hydrogen, leaving behind the phenylsodium as a dry powder which was weighed in the tared bottle. Slow, careful addition of water hydrolyzed the sample to give $NaOH$ and C_6H_6 . Titration of the $NaOH$ with H_2SO_4 then followed. The percent Na found was 22.68 and 22.36 in two titrations vs a calculated value for C_6H_5Na of 23.04. A very small amount of water-insoluble diphenylmercury remained. Phenylsodium on exposure to air on a filter paper burst into flame. It was highly reactive toward water; therefore, moisture was excluded from the apparatus with a calcium chloride tube when its reactions were studied. Phenylsodium prepared in this manner reacted as expected with alkyl bromides and iodides, benzyl chloride, bromobenzene, benzophenone, benzoyl chloride, benzil, and carbon dioxide. Nef’s curious ideas (see Part I) were applied to the reaction of phenylsodium with ethyl iodide, the reaction sequence in Scheme 1 being proposed and written as shown.

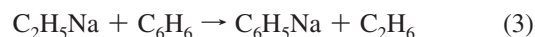
The $CH_3CH \rightleftharpoons$ species is ethylidene, which was expected to transform in part to ethylene. It was written as shown to indicate,

Scheme 1

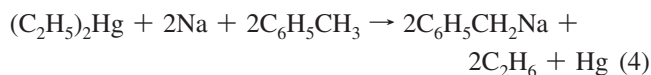


by means of the arrows, “free valences”, the electron being unknown at the time. In the case of benzyl chloride, the C_6H_5CH intermediate was expected to result in the formation of some stilbene. It was stated that “These expectations were in every way realized.” That these byproduct might have been formed by a route other than spontaneous dehydrohalogenation of the organic halide apparently was not considered.

Nearly 50 years after Buckton’s report, Paul Schorigin of the Imperial Technische Hochschule of Moscow recognized the potential value of the $(C_2H_5)_2Hg/Na$ reaction in organic synthesis. In view of the high reactivity of ethylsodium toward air and moisture and its limited thermal stability, he did not attempt to isolate it or even to preform it but carried out the $(C_2H_5)_2Hg/Na$ reaction in diethyl ether in the presence of the respective electrophile.⁶ By such means the following conversions were effected: $(C_6H_5)_2CO \rightarrow (C_6H_5)_2(C_2H_5)COH$ (40%); $C_6H_5CO_2CH_3 \rightarrow C_6H_5(C_2H_5)_2COH$ (24%); $C_6H_5CHO \rightarrow C_6H_5(C_2H_5)CHOH$ (15%). The reactions were quite exothermic. A protective atmosphere of dry nitrogen or hydrogen was used. When in separate experiments dry CO_2 had been passed into the gently heated diethyl ether solutions of $(CH_3)_2Hg$, $(C_2H_5)_2Hg$, and $(Me_2CHCH_2)_2Hg$, respectively, that contained stoichiometric amounts of sodium, hydrolytic workup gave the respective carboxylic acids in low yield. Without doubt, destructive reaction of the sodium alkyl with the diethyl ether solvent competed with its reaction with carbon dioxide and reduced the yield of carboxylic acid. However, when such in situ $(C_2H_5)_2Hg/Na/CO_2$ reactions were carried out in benzene rather than in diethyl ether solution, the major product was benzoic acid. Clearly, metalation of the benzene, i.e., metal–hydrogen exchange, had occurred (eq 3).⁷



(A similar observation had been made by Schorigin when the in situ $C_6H_5Br/Na/CO_2$ reaction was carried out in benzene (see Part I): Schorigin likened the $(C_2H_5)_2Hg/Na/C_6H_6$ reaction to the mercuration of benzene by $Hg(II)$ salts, discovered by Dimroth 10 years earlier, and was puzzled when the analogy failed to hold up when the $(C_2H_5)_2Hg/Na/CO_2$ reaction was carried out in toluene. The product was phenylacetic acid, not a toluic acid. Side chain, not nuclear, metalation obviously had occurred (eq 4). In contrast, reaction of toluene with $Hg(II)$ salts results in nuclear mercuration.



Schorigin’s explanation for benzene metalation was on the mark:

“The reaction is a result of the great lability and reactivity of sodium alkyls. The negative character of the phenyl group plays a very important role. One could view this reaction as a migration of the strongly positive sodium

(4) This chemistry has been discussed in Part I of this essay.¹

(5) Acree, S. F. *Am. Chem. J.* **1903**, 29, 588.

(6) Schorigin, P. *Ber. Dtsch. Chem. Ges.* **1908**, 41, 2717.

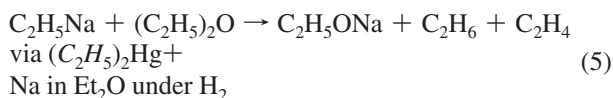
(7) Schorigin, P. *Ber. Dtsch. Chem. Ges.* **1908**, 41, 2723.

atom from a weakly negative alkyl group to a strongly negative atom complex (phenyl group)."

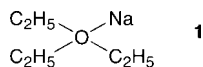
However, the side chain metalation of toluene bothered him: "But the entrance of the carboxyl group into the side chain is not in good agreement with this view." In the case of ethylbenzene, the carboxylic acid produced was $C_6H_5-CH(CH_3)CO_2H$. This regioselectivity, Schorigin said, might be due to the presence of the negative phenyl group adjacent to the methylene group.

What confused the problem of nuclear vs side-chain metalation even more was Schorigin's observation that in contrast to the results obtained with the $(C_2H_5)_2Hg/Na/toluene/CO_2$ system, when $(C_2H_5)_2Zn$ was used in place of diethylmercury, some nuclear metalation occurred in addition to side-chain metalation. However, here a different organometallic base, Wanklyn's $NaZn(C_2H_5)_3$, is involved.

In later work, Schorigin extended the side-chain metalation reaction (in the presence of CO_2) to the preparation of *m*-tolylacetic acid from *m*-xylene, of *o*-tolylacetic acid from *o*-xylene, of *p*-tolylacetic acid from *p*-methyltoluene, of 3,5-dimethylphenylacetic acid from mesitylene, and of diphenylacetic acid from diphenylmethane.⁸ Thiophene was found to be much more reactive toward $(C_2H_5)_2Hg/Na$ than benzene. It is too bad that Schorigin did not extend his metalation studies a bit further to other aromatic compounds and, especially, that he did not use electrophilic substrates other than carbon dioxide. If he had, the metalation of weak organic acids by alkali-metal alkyls would have been recognized as a general reaction earlier and probably would have been named the "Schorigin reaction" (as it should be, in any case). Schorigin confirmed that ethylsodium attacked diethyl ether, giving as gaseous products ethane and ethylene in a 1:1 molar ratio⁹ (eq 5).



The voluminous, gray-white, at times pyrophoric solid that was formed in this reaction was shown to be sodium ethoxide. Its pyrophoric nature suggests that it also contained some entrained ethylsodium. Schorigin suggested that the $C_2H_5Na/(C_2H_5)_2O$ reaction might proceed by way of an intermediate 1:1 adduct, which he wrote as **1** in analogy to the then believed constitution of the 1:1 $RMgX/Et_2O$ complex. When the $(C_2H_5)_2Hg/Na$ reaction was carried out in hexane, pyrophoric, black crusts formed on the surface of the sodium wire and the liquid phase remained clear.



Since Schorigin did some of the early, important alkylsodium chemistry and was the first to report and study the metalation of weakly acidic hydrocarbons by alkali metal-alkyls, it is of interest to learn something about him. Pavel Polievktovich Shorygin (Figure 1) (Russian transliteration vs the German one in the cited references) (1881–1939) was born in the Vladimir Province of Russia. He graduated from the Moscow Higher-Engineering School (given as the Kaiserliche Technische Hochschule zu Moskau in his papers in *Berichte*) in 1906. There, all of his organosodium research was carried out until he moved on in 1910. After employment for eight years in a Moscow

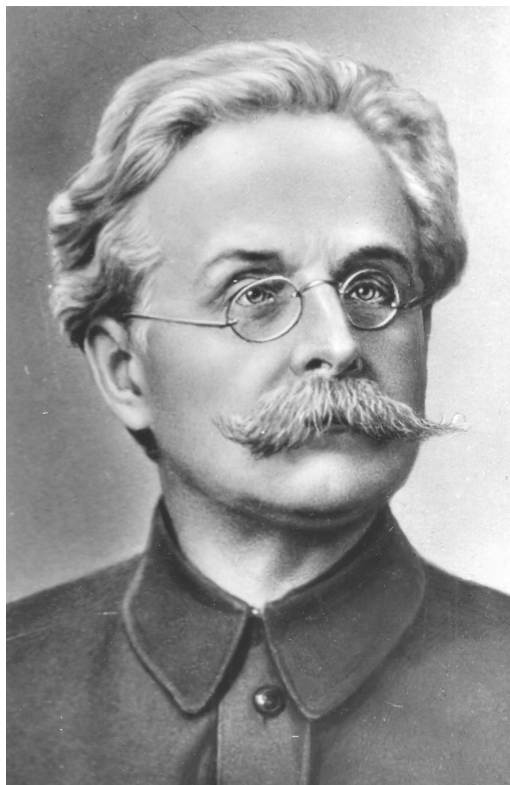


Figure 1. Pavel Polievktovich Schorigin (1881–1939), courtesy of Professor Mikhail Egorov, Director of Zelinsky Institute of Organic Chemistry, Russian Academy of Sciences; reproduced by permission.

textile mill (1910–1918), he was appointed Professor at the Moscow Veterinary and Forestry Universities of Technology in 1919. From 1925–1939 he was a member of the faculty of the Moscow Mendeleev Technological University. During this time (1931–1939) he also was a scientific leader at the Moscow Scientific Research Institute of Synthetic Fibers and (1936–1939) head of the Laboratory of High Molecular Weight Compounds at the Zelinsky Institute of Organic Chemistry of the USSR Academy of Sciences. Schorigin became Director of the Institute in 1939. In addition to his early academic research on organoalkali-metal chemistry, Schorigin's later work was devoted to the development of synthetic fibers, the synthesis of cellulose ethers, paper and pulp manufacture, and the synthesis of fragrances. His contributions were recognized by election as a Corresponding Member of the Academy of Sciences of the USSR in 1932 and to full membership in 1939.

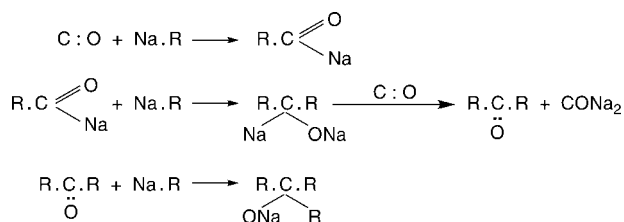
The reaction of the $C_2H_5Na/(C_2H_5)_2Zn$ adduct with carbon monoxide, reported by Wanklyn in 1866 (see ref 1), was examined in some detail by Schlubach at the Chemical Laboratory of the Bavarian Academy of Sciences in Munich using C_2H_5Na prepared from diethylmercury.¹⁰ When the $(C_2H_5)_2Hg/Na$ reaction was carried out in petroleum ether (since the reaction with CO was too vigorous in Et_2O) under an atmosphere of carbon monoxide, a rapid absorption of CO was observed. The reaction was allowed to proceed, with shaking, for 8 days. The reaction mixture was diluted with ether and allowed to stand for 24 h (otherwise, the subsequent hydrolysis step was explosive). Hydrolytic workup gave $(C_2H_5)_2CO$ and $(C_2H_5)_3COH$ as major products, a minor quantity of $C_2H_5CO_2H$, and a "not insignificant" amount of higher boiling products. A

(8) Schorigin, P. *Ber. Dtsch. Chem. Ges.* **1910**, *43*, 1938.

(9) Schorigin, P. *Ber. Dtsch. Chem. Ges.* **1910**, *43*, 1931.

(10) Schlubach, H. H. *Ber. Dtsch. Chem. Ges.* **1919**, *52*, 1910.

Scheme 2



smoother reaction occurred in the case of the $(\text{C}_2\text{H}_5)_2\text{Hg}/\text{Na}/\text{CO}$ in situ reaction in benzene. The products in this case were those resulting from carbonylation of phenylsodium, formed more rapidly by benzene metalation than the reaction of CO with ethylsodium: $(\text{C}_6\text{H}_5)_2\text{CO}$ (30%), $(\text{C}_6\text{H}_5)_3\text{COH}$ (25%), $\text{C}_2\text{H}_5\text{CO}_2\text{H}$ (16%), higher boilers (15%). Schlubach suggested the reaction course as written in Scheme 2. The first step, the formation of an acylsodium intermediate, is a reasonable one.¹¹ Schlubach used his discovery of the RNa/CO reaction to show that organosodium compounds are intermediates in the Wurtz–Fittig reaction (which had been already shown by other workers some years earlier¹). Thus, the reaction of 2 g atom of sodium shavings with 0.5 mol of bromobenzene in benzene solution under an atmosphere of CO, after hydrolytic workup, gave biphenyl, benzophenone, triphenylcarbinol, and benzoic acid, the last three being the same products as obtained in the $(\text{C}_6\text{H}_5)_2\text{Hg}/\text{Na}/\text{CO}$ reaction.¹² In a similar fashion, the $\text{C}_2\text{H}_5\text{Br}/\text{Na}/\text{CO}$ reaction in diethyl ether produced analogous products: diethyl ketone and triethylcarbinol. When a 1:1 mixture of ethyl bromide and bromobenzene was used, only CO-derived products from the latter were isolated in addition to some ethylbenzene from the reaction of $\text{C}_2\text{H}_5\text{Br}$ with phenylsodium. Obviously, the formation of phenylsodium is much more facile than that of ethylsodium in $\text{RBr} + \text{Na}$ reactions.

Subsequent to the work of Schorigin and Schlubach, the $\text{R}_2\text{Hg}/\text{Na}$ reaction has been used to prepare organosodium compounds for studies of their reactivity. Once it was known through the work of W. Schlenk (vide infra) that the organosodium compounds prepared by this procedure are fairly stable as suspensions in hydrocarbon medium, such reactions usually were carried out in a two-stage manner: (1) preparation of the organosodium compound and (2) reaction of the organosodium compound, without isolation, with the substrate. Some selected references serve as examples of the application of the $\text{R}_n\text{M}/$ alkali-metal displacement reaction to the preparation of organoalkali-metal compounds. Some merit separate mention; others are noted only by reference.¹³

Lane and Ulrich prepared *sec*-butylsodium by reaction of sodium slices with di-*sec*-butylmercury in dodecane solution

(11) In the case of the RLi/CO reaction, products derived from the initially formed acyllithium, RC(O)Li , can be isolated, usually in high yield, when the reactions are carried out at very low (-110 to -140 °C) temperature in the presence of the electrophile. Reviews: (a) Seyferth, D. *Isr. J. Chem.* **1984**, *24*, 167. (b) Seyferth, D. *Nova Acta Leopold.*, *New Series*, No. 264, **1985**, 335, and references therein.

(12) Schlubach, H. H. *Ber. Dtsch. Chem. Ges.* **1922**, *55*, 2889.

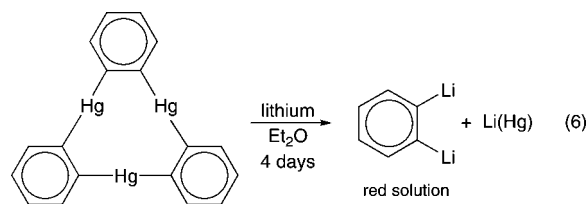
(13) (a) Carothers, W. H.; Coffman, D. D. *J. Am. Chem. Soc.* **1929**, *51*, 588. (b) Morton, A. A.; Heckenbleikner, I. *J. Am. Chem. Soc.* **1936**, *58*, 1024. (c) Whitmore, F. C.; Zook, H. D. *J. Am. Chem. Soc.* **1942**, *64*, 1783. (d) Brink, N. G.; Lane, J. F.; Wallis, E. S. *J. Am. Chem. Soc.* **1943**, *65*, 943. (e) Ulrich, S. E.; Gentes, F. H.; Lane, J. F.; Wallis, E. S. *J. Am. Chem. Soc.* **1950**, *72*, 5127. (f) Benkeser, R. A.; Trevillyan, A. E.; Hooz, J. *J. Am. Chem. Soc.* **1962**, *84*, 4971. (g) Bryce-Smith, D. *J. Chem. Soc.* **1963**, 5983. (h) Wittig, G.; Benz, E. *Chem. Ber.* **1958**, *91*, 879. (i) Hart, A. J.; O'Brien, D. H.; Russell, C. R. *J. Organomet. Chem.* **1974**, *72*, C19. (j) Waack, H.; McKeever, L. D.; Doran, M. *Chem. Commun.* **1969**, 117. (k) Waack, H.; Doran, M. A.; Baker, E. B.; Olah, G. A. *J. Am. Chem. Soc.* **1966**, *88*, 1272. (l) Asami, M.; Levy, M.; Szwarc, M. *J. Chem. Soc.* **1962**, 361.

under nitrogen at 20–25 °C. The resulting brown reaction mixture was carbonated by bubbling in dry CO_2 , and workup was effected by acid hydrolysis. The expected $\text{CH}_3\text{CH}_2\text{CH}(\text{CH}_3)\text{CO}_2\text{H}$ was obtained in less than 5% yield together with a minor amount of the malonic acid, $\text{CH}_3\text{CH}_2(\text{CH}_3)\text{C}(\text{CO}_2\text{H})_2$.^{14a} The latter was formed, as explained in Part I, by α -metalation and subsequent carbonation of the initially formed $\text{CH}_3\text{CH}_2\text{CH}(\text{CH}_3)\text{CO}_2\text{Na}$. These results suggested that *sec*-alkylsodium compounds are only marginally stable around room temperature, a fact noted by Morton and his co-workers^{14b,c} in their studies of the reactions of secondary alkyl chlorides with sodium.

The $\text{R}_2\text{Hg}/\text{M}$ reaction also was used to prepare CH_3K ,^{15a} $\text{C}_2\text{H}_5\text{Li}$ and $\text{C}_2\text{H}_5\text{K}$,^{15b} and *n*- $\text{C}_4\text{H}_9\text{K}$, *n*- $\text{C}_4\text{H}_9\text{Rb}$, and *n*- $\text{C}_4\text{H}_9\text{Cs}$.^{15c} The last of these reactions was carried out in benzene medium; thus, benzene metalation by the butylalkali-metal compounds as they were formed resulted in formation and precipitation of $\text{C}_6\text{H}_5\text{K}$, $\text{C}_6\text{H}_5\text{Rb}$, and $\text{C}_6\text{H}_5\text{Cs}$, respectively.

The metal displacement reaction also has been used in the preparation of unsaturated organoalkali-metal compounds. Canadian workers reported the preparation of the allyl compounds of sodium, potassium, rubidium, and cesium by reaction of films of the respective metal with diallylmercury in THF at -20 °C.^{16a} NMR spectroscopic studies showed these compounds to be ionic in solution in the form of contact ion pairs or clusters. Vinyl lithium also has been prepared by the metal displacement reaction. Divinylmercury^{16b} and tetravinyltin and tetravinyllead^{16c} served as vinyl group sources. The $(\text{CH}_2=\text{CH})_4\text{Pb}/\text{Li}$ reaction was carried out in diethyl ether in a creased (Morton) flask with high-speed stirring using benzophenone as a catalyst. The reaction was exothermic, causing the ether to reflux and metallic lead to precipitate as a black powder. All four vinyl groups reacted, giving vinyl lithium in 90% yield. It was isolated (filtration, removal of ether by distillation, and washing with petroleum ether) as a white solid in analytical purity (Anal. Calcd: C, 70.60; H, 8.90. Found: C, 70.77, 70.85; H, 8.93, 8.90). Solid vinyl lithium is violently pyrophoric., giving a brilliant red flash on exposure to air.

Of special interest is the synthesis of 1,2-dilithiobenzene by Wittig and Bickelhaupt (eq 6).¹⁷



The $(\text{CH}_3)_2\text{Hg}/\text{M}$ reaction also can be carried out in the gas phase.¹⁸ In the cell of the reaction chamber of a direct absorption spectrometer $(\text{CH}_3)_2\text{Hg}$ at ~ 5 m Torr was allowed to react with lithium and sodium vapors (≤ 1 mTorr in argon carrier gas) to

(14) (a) Lane, J. F.; Ulrich, S. E. *J. Am. Chem. Soc.* **1951**, *73*, 5470. (b) Morton, A. A.; Heckenbleikner, I. *J. Am. Chem. Soc.* **1936**, *58*, 1697. (c) Morton, A. A.; Davidson, J. B.; Newey, H. A. *J. Am. Chem. Soc.* **1942**, *64*, 2240.

(15) (a) Carothers, W. H.; Coffman, D. D. *J. Am. Chem. Soc.* **1930**, *52*, 1254. (b) Gilman, H.; Young, R. V. *J. Org. Chem.* **1936**, *1*, 315. (c) Gilman, H.; Jacoby, A. L.; Ludeman, H. *J. Am. Chem. Soc.* **1938**, *60*, 2336.

(16) (a) Brownstein, S.; Bywater, S.; Worsfold, D. J. *J. Organomet. Chem.* **1980**, *199*, 1. (b) Nesmeyanov, A. N.; Borisov, A. E.; Savel'eva, I. S.; Golubeva, E. I. *Izv. Akad. Nauk SSSR, Otdel. Khim. Nauk* **1958**, 1490. (c) Juenge, E. C.; Seyferth, D. *J. Org. Chem.* **1961**, *26*, 563.

(17) Wittig, G.; Bickelhaupt, F. *Chem. Ber.* **1958**, *91*, 883.

(18) Grotjahn, D. B.; Pesch, T. C.; Xia, J.; Ziurys, L. M. *J. Am. Chem. Soc.* **1997**, *119*, 12369.

produce monomeric, gaseous CH_3Li and CH_3Na molecules, respectively. It was determined that the gaseous CH_3M species are symmetric top molecules of C_{3v} symmetry with C–Li and C–Na distances of 1.959 and 2.299 Å, respectively.

III. Wilhelm Schlenk's Pioneering Work in Organoalkali-Metal Chemistry, 1911–1931

Until 1917, with one exception, alkali-metal alkyls and aryls had not been isolated as pure compounds. They had either been prepared and used in situ or they had been prepared and used without isolation in a two-step process.

As described in the previous section, S. F. Acree had reported the preparation of phenylsodium by the $(\text{C}_6\text{H}_5)_2\text{Hg}/\text{Na}$ reaction in benzene and its subsequent isolation as a light brown powder.⁵ Hydrolysis of the latter and acidimetric titration of the base thus formed indicated a purity of >90%. The phenylsodium was contaminated with a minor amount of diphenylmercury. Hilpert and Grüttner reported that they were unable to reproduce Acree's results.¹⁹ In their hands the reactions of diphenylmercury with sodium, as well as with lithium and potassium, proceeded vigorously in benzene to give insoluble and infusible dark solids. The formation of metallic mercury or of a mercury/alkali-metal amalgam was not observed; these were formed, they reported, only upon hydrolysis of the reaction mixture. Thus, in 1913, the isolation of a simple organoalkali-metal compound appeared to be in doubt.

These negative results did not deter Wilhelm Schlenk, who with his student Johanna Holtz embarked on a broad and successful investigation of the reactions of sodium and lithium with various dialkylmercury compounds as well as with diphenyl- and dibenzylmercury.²⁰

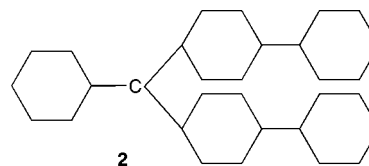
Schlenk is well-known to organometallic and other chemists whose research involves air- and moisture-sensitive compounds as the developer of glassware which is very useful in the handling of such compounds (Schlenk tubes, Schlenk flasks, Schlenk lines, etc.)

Wilhelm Johann Schlenk (1879–1943)²¹ (Figure 2) was born in Munich, Germany. As his older brother, Johann Oskar Schlenk (1874–1951) had done, Wilhelm Schlenk studied chemistry in the Chemistry Department of the Bavarian Academy of Sciences in Munich. His Ph.D. dissertation, carried out under the direction of Oskar Piloty, one of Adolf von Baeyer's lieutenants, was entitled "Über Metall-Isobutyryl-Adine." After his graduation in 1905 he worked briefly in industry but was back at the Academy in 1906 as a teaching assistant working on his Habilitation, which would gain him entry into the academic world. On its completion in 1909, he became Privatdozent (equivalent to Assistant Professor) in 1910. Schlenk's first independent research was devoted to a study of Gomberg's triphenylmethyl radical, discovered in 1900, and other triarylmethyl radicals.²² An important finding was that, in contrast to the triphenylmethyl radical, which is in large part associated in solution, the tris(4-biphenyl)methyl radical,



Figure 2. Wilhelm Johann Schlenk (ca. 1935) from the Archive of the Eberhard-Karls-Universität, Tübingen, courtesy of Dr. Michael Wischnath, Archive Director; reproduced with permission.

$(\text{C}_6\text{H}_5\text{---C}_6\text{H}_4)_3\text{C}\cdot$, is monomeric in benzene solution. Of course, Schlenk did not call this a radical—this was in 1910 and the first paper on the electronic theory of valency was published in 1916. Thus, the description of the triarylmethyl radicals in terms of unpaired electron species did not come to mind. Schlenk simply wrote the phenylbis(4-biphenyl)methyl radical as **2**. (In the journals of the day, benzene rings were written as simple hexagons, as in **2**, not as the Kekulé structure with three alternating double bonds). He talked about it as a trivalent carbon compound. The radical **2** could be isolated in good purity as greenish black crystals, which were monomeric by cryoscopy in benzene.



This new approach opened the door to studies of trivalent carbon. The triarylmethyl radicals are extremely sensitive to oxygen; the color of their solutions is instantaneously discharged by air. To deal with this problem, Schlenk used a glass apparatus (Figure 3) developed by Schmidlin in his studies of the triphenylmethyl radical²³ as well as glassware of his own devising (Figure 4).

Schlenk's interest in trivalent carbon also led him to the strange products formed by the action of alkali metals on diaryl ketones in diethyl ether solution, species well-known and much used by today's organometallic chemists. Beckmann and Paul had reported in 1891²⁴ the reaction of a 5–7-fold excess of sodium wire with benzophenone in diethyl ether under an atmosphere of hydrogen. With time a deep blue solution was

(19) Hilpert, S.; Grüttner, G. *Ber. Dtsch. Chem. Ges.* **1913**, *46*, 1675.

(20) Schlenk, W.; Holtz, J. *Ber. Dtsch. Chem. Ges.* **1917**, *50*, 262.

(21) There is a surprising lack of biographical material about Schlenk. The best source is an excellent, well-researched article by Tidwell: Tidwell, T. T. *Angew. Chem., Int. Ed.* **2001**, *40*, 331. The University of Tübingen Archives kindly provided copies of talks given at Schlenk's graveside on May 1, 1943 by Schlenk's friend and colleague, Professor Alfred Kliegl, and the Dean, Professor Ernst Back.

(22) (a) Schlenk, W.; Weickel, T. *Justus Liebig's Ann. Chem.* **1909**, *368*, 295. (b) Schlenk, W.; Weickel, T.; Herzenstein, A. *Justus Liebig's Ann. Chem.* **1910**, *372*, 1. (c) Schlenk, W.; Brauns, M. *Ber. Dtsch. Chem. Ges.* **1915**, *48*, 661.

(23) Schmidlin, J. *Ber. Dtsch. Chem. Ges.* **1908**, *41*, 423.

(24) Beckmann, E.; Paul, T. *Justus Liebig's Ann. Chem.* **1891**, *266*, 1.

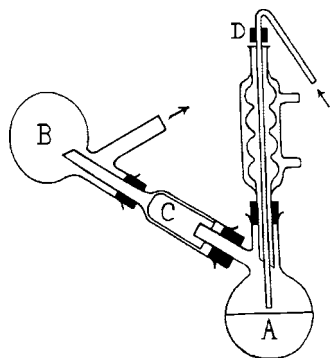


Figure 3. Glassware developed by J. Schmidlin for study of the extremely air-sensitive triphenylmethyl radical (Ber. Dtsch. Chem. Ges. 1908, 41, 423; copyright Wiley-VCH Verlag GmbH & Co. KGaA, reproduced with permission).

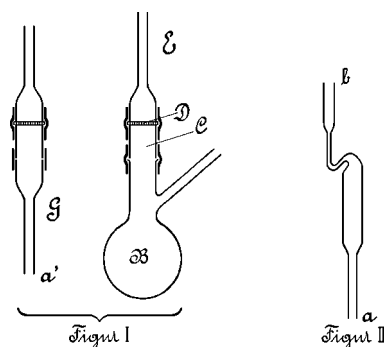


Figure 4. Glassware developed by W. Schlenk for his studies of very air-sensitive triarylmethyl radicals, later used in his organoalkali-metal chemistry work (Justus Liebigs Ann. Chem. 1910, 372, 17; copyright Wiley-VCH Verlag GmbH & Co. KGaA, reproduced with permission).

formed. After several days beautiful, deep blue crystals formed which on drying became lighter in color. This product, in solution or as the solid, was extremely air- and moisture-sensitive, which made its isolation as a pure material difficult. The blue solutions were decolorized almost instantaneously on exposure to air, and bulk samples of the blue solid oxidized so rapidly in air that the whole solid mass began to glow. Careful drying of the hydrogen and diethyl ether was imperative, and the apparatus shown in Figure 5 served in the preparation of the alkali-metal/diaryl ketone products. The reaction was carried out in the sealed separatory funnel. Upon its completion, the unreacted sodium remained behind while the ether suspension of the product which had formed was drawn off through the wide-bore stopcock into the cylindrical vessel F, in which an atmosphere of dry hydrogen was maintained. The product was retained on filter paper on the porcelain filter plate C and dried under a stream of hydrogen. Flask G contained ether, which was forced under hydrogen pressure into vessel F to wash the product collected on the filter. According to a sodium analysis, the product contained 1 g atom of sodium and 1 formula weight of benzophenone. The hydrolysis of an ether solution of the blue product gave, depending on reaction conditions, either a mixture of benzopinacol, $(\text{C}_6\text{H}_5)_2(\text{HO})\text{C}-\text{C}(\text{OH})(\text{C}_6\text{H}_5)_2$, benzophenone, and benzhydrol, $(\text{C}_6\text{H}_5)_2\text{CHOH}$, or a mixture of only benzophenone and benzhydrol. Beckmann concluded that the blue product was **3**, writing its formation as shown in eq 7 on

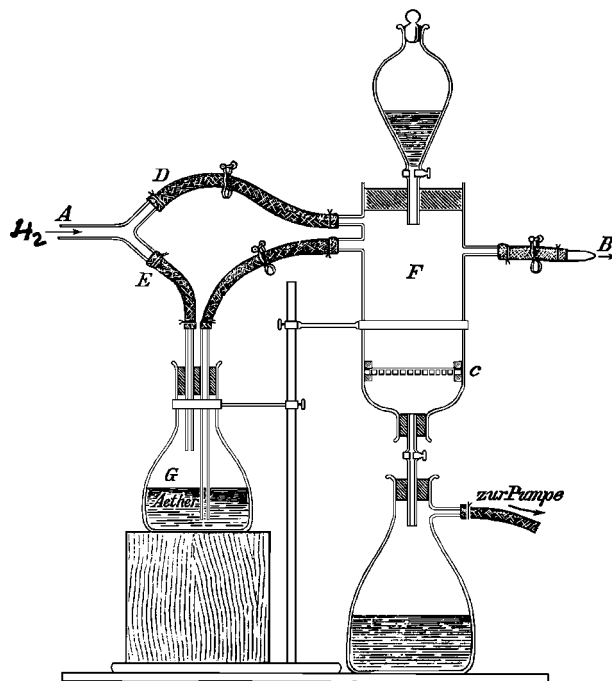
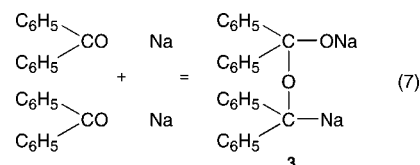
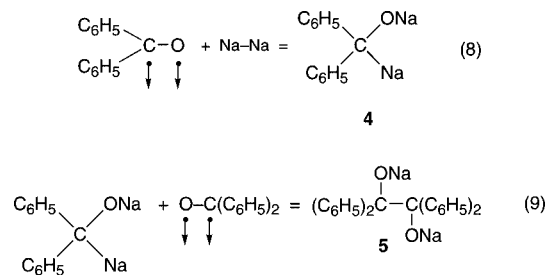


Figure 5. Apparatus developed by Beckmann and Paul for the preparation of the very air-sensitive alkali-metal/diaryl ketone products (Justus Liebigs Ann. Chem. 1891, 266, 4; copyright Wiley-VCH Verlag GmbH & Co. KGaA, reproduced with permission).

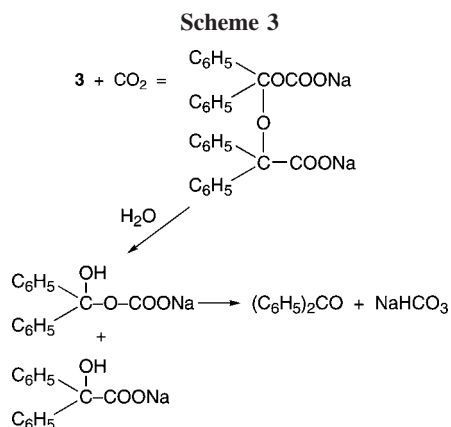
the basis of the products that the blue $(\text{C}_6\text{H}_5)_2\text{CO}/\text{Na}$ product gave on reaction with CO_2 (Scheme 3).



Acree investigated the benzophenone/sodium reaction a few years later.⁵ Following the views of Nef on reactions of sodium with organic carbonyl compounds,²⁵ he described the initial product as the disodium species **4** and said it reacted with a second molecule of benzophenone to give sodium-benzopinacol (**5**). This, he said, is marginally stable at room temperature, regenerating **4** and benzophenone, writing eqs 8 and 9 (in the Nef style²⁵). In his experiment, Acree obtained the blue ether solution and blue solid but did not isolate and analyze the latter. Instead he poured it into water. Beckmann and Paul's formulation of the $(\text{C}_6\text{H}_5)_2\text{CO}/\text{Na}$ product as **3** Acree considered "very improbable".

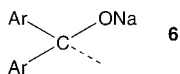


Schlenk had become interested in Beckmann and Paul's paper, which reported such extraordinary results, because it led



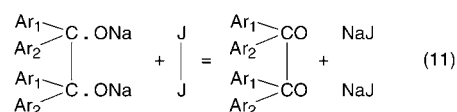
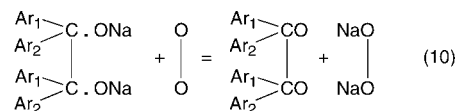
him to suspect that a new class of compounds of trivalent carbon was involved. His first publication on his work in this area was a preliminary communication without experimental details,²⁶ written, as he said, "in order to ensure us a leisurely continued investigation of this subject." To make this possible, in his last sentence he requested his chemical colleagues for the time being to leave this research area to him. As was customary in those days, nobody intruded. Times have changed!

Substituting 4-biphenyl groups for phenyl had served Schlenk well in his study of the triarylmethyl radicals, and he used the same approach in his investigation of alkali-metal–diaryl ketone products, carrying out his experiments with bis(4-biphenyl) ketone, $(\text{C}_6\text{H}_5\text{---}\text{C}_6\text{H}_4)_2\text{C}=\text{O}$, and 4-biphenyl phenyl ketone, $(\text{C}_6\text{H}_5\text{---}\text{C}_6\text{H}_4)(\text{C}_6\text{H}_5)\text{C}=\text{O}$. This turned out to bring important experimental advantages. The products obtained in the reactions of the sodium–benzophenone product with water and carbon dioxide were difficult to crystallize and separate. Substituting one or both of the phenyl groups of benzophenone by biphenyl groups alleviated these difficulties. In addition to sodium, potassium also was used in the study. A reaction of potassium with $(\text{C}_6\text{H}_5\text{---}\text{C}_6\text{H}_4)(\text{C}_6\text{H}_5)\text{C}=\text{O}$ gave a green product with a 1:1 ketone/potassium ratio (Anal. Found: K, 13.14, 13.49. Calcd: K, 13.13). A molecular weight determination of the blue sodium-derived product was of crucial importance in order to distinguish between a trivalent, monomeric species, **6**, that Schlenk had envisioned and a dimeric



species of type **3**. However, the deep blue solutions of the alkali-metal–diaryl ketone products were not true solutions but contained the blue solids in colloidal or in polymeric ("hochkomplex," Schlenk said) forms. Thus, cryoscopic molecular weight determinations were not possible. For this reason, Schlenk in this early work resorted to chemical studies. A notable similarity between the triarylmethyl radicals and the alkali-metal–diaryl ketone products was their extremely ready susceptibility to oxidation. The facility with which an ether solution of the blue sodium–benzophenone product was decolorized when exposed to air had been noted by Beckmann and Paul, but the reaction was not examined further. Schlenk and Weickel found that air oxidation of the green sodium bis(biphenyl)ketone product in ether resulted in immediate decolorization and precipitation of a voluminous white solid which was found to be a mixture of $(\text{C}_6\text{H}_5\text{---}\text{C}_6\text{H}_4)_2\text{C}=\text{O}$ and sodium peroxide. The latter could be washed out with water.

On reaction of the blue product with iodine, the ketone and sodium iodide were the products. Hydrolysis of the sodium bis(biphenyl) ketone product gave a mixture of the ketone and $(\text{C}_6\text{H}_5\text{---}\text{C}_6\text{H}_4)_2\text{CHOH}$ but no pinacol product. Of special interest was the reaction of benzopinacol with freshly prepared 1.5% sodium amalgam (but not with sodium alone) in anhydrous ether at room temperature in the absence of air, which proceeded with rapid evolution of H_2 to give a deep blue solution of what proved to be the sodium–benzophenone product of Beckmann and Paul. At first sight, Schlenk said, this result might imply that the blue solid is, as Acree had claimed, the disodium derivative of benzopinacol **5**. The reactions of the blue product with oxygen and iodine then could be written as shown in eqs 10 and 11. However, the intense colors of the alkali-metal–diaryl ketone compounds, their extremely facile oxidation and their



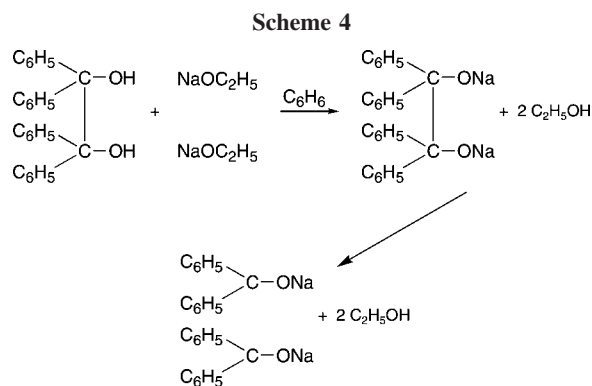
hydrolysis, which usually proceeded with C–C bond rupture, spoke against such a "normal" formulation. Schlenk also considered the formulation of Beckmann and Paul improbable in view of the benzopinacol/sodium–benzophenone product. He concluded that all the observed chemistry was best explained in terms of a trivalent carbon derivative, one with reactivity similar to that of the triarylmethyl radicals, and he favored formula **6** for the alkali-metal–diaryl ketone products.

In the full paper which followed in 1913,²⁷ the important question concerning the molecular weight of the alkali-metal–diaryl ketone products was answered. A normal ebullioscopic molecular weight determination was not possible because of the poor solubility of such products, but the solubility of the potassium–biphenyl phenyl ketone product in diethyl ether immediately following its preparation was sufficient to allow the following indirect procedure. A solution of the ketone in well-dried diethyl ether in a boiling point elevation apparatus under a purified nitrogen atmosphere was heated to the boiling point. When this had remained constant, some freshly cut (under ether) shiny small pieces of potassium were added. The green potassium–ketone product formed in solution, without precipitation. During this process the boiling point remained constant, which showed that the number of molecules in the solution had not changed. It follows that each molecule of ketone had formed one molecule of the potassium–ketone product and the latter was monomeric. Thus, Schlenk's original formulation, $(\text{C}_6\text{H}_5\text{---}\text{C}_6\text{H}_4)(\text{C}_6\text{H}_5)\text{COK}$ in this case, was correct. In a control experiment, the boiling point of a sample of diethyl ether that contained some clean pieces of potassium was determined. Subsequently a weighed quantity of the ketone was added. In spite of the rather rapid formation of the potassium–ketone product, the molecular weight of the ketone could be determined from the boiling point elevation.

Also telling was the formation of the sodium–benzophenone product by the reaction of a concentrated alcoholic solution of sodium ethoxide with a suspension of benzopinacol in benzene, a reaction that involved C–C cleavage to give the radical species (Scheme 4).

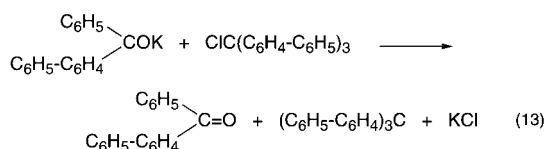
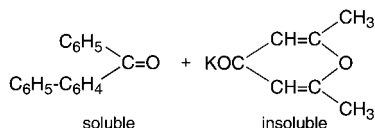
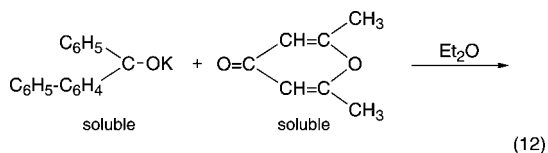
(26) Schlenk, W.; Weickel, T. *Ber. Dtsch. Chem. Ges.* **1911**, *44*, 1182.

(27) Schlenk, W.; Thal, A. *Ber. Dtsch. Chem. Ges.* **1913**, *46*, 2840.



With the constitution of the alkali-metal-diaryl ketone products settled as being monomeric, trivalent type **6** species, Schlenk proposed naming them ketyls, a name that we still use today. Further work established the scope of alkali-metal-ketone interactions. When there were C–H bonds α to the carbonyl groups, enolate formation with evolution of hydrogen occurred. In the absence of α -C–H bonds there were two possibilities: (1) formation of alkali-metal derivatives of pinacols, $\text{R}^1\text{R}^2\text{C}(\text{ONa})-\text{C}(\text{ONa})\text{R}^1\text{R}^2$, i.e., ketyl dimers, and (2) formation of alkyl metal ketyls. Which alkali metal was used did not seem to make a difference; lithium, sodium, and potassium worked equally well. In all cases metal ketyls were formed. Even magnesium, activated with iodine or as the amalgam, formed a metal ketyl. The metal used had no effect on the color of the ketyl or its reactivity, but it did affect the solubility of the ketyl.²⁸

Preparation of alkali-metal ketyls which were poorly soluble or insoluble was difficult, because the ketyl tended to coat the as yet unreacted metal. A solution to this problem was found in an alternate preparation by “transketylation”, as illustrated in eq 12 for the preparation of the bright red potassium–dimethyl- γ -pyrone by reaction of the pyrone with potassium–biphenyl phenyl ketone in diethyl ether. The two reactants and the biphenyl phenyl ketone produced were soluble, and the dimethyl- γ -pyrone potassium ketyl precipitated and was isolated in good yield. A related reaction found by Schlenk and Thal is that of $(\text{C}_6\text{H}_5-\text{C}_6\text{H}_4)_2\text{COK}$ with tris(4-biphenyl)methyl chloride (eq 13).



The Schlenk/Thal paper also is of interest for its detailed description of reaction procedures and of the Schlenkware that was used. Figure 6 shows the reaction vessel (150 cm³) used; Figures 7 and 8 illustrate the arrangements for filtration of the product, and Figure 9 depicts the apparatus used to dry and

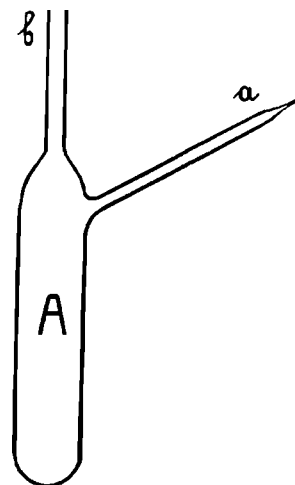


Figure 6. Schlenk's reaction vessel for use in alkali-metal-diaryl ketone reactions (Ber. Dtsch. Chem. Ges. 1913, 46, 2843; copyright Wiley-VCH Verlag GmbH & Co. KGaA, reproduced with permission).

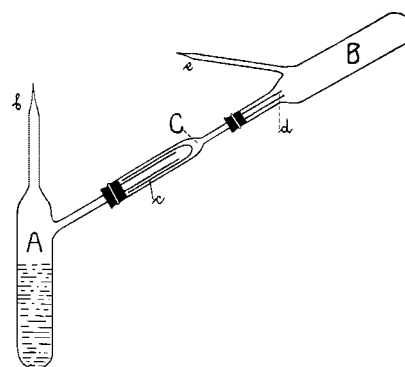


Figure 7. Schlenk's filtration apparatus for use in alkali-metal-diaryl ketone reactions (Ber. Dtsch. Chem. Ges. 1913, 46, 2844; copyright Wiley-VCH Verlag GmbH & Co. KGaA, reproduced with permission).

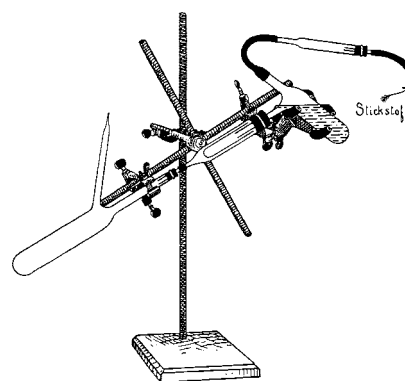


Figure 8. Schlenk's filtration apparatus for use in alkali-metal-diaryl ketone reactions (Ber. Dtsch. Chem. Ges. 1913, 46, 2845; copyright Wiley-VCH Verlag GmbH & Co. KGaA, reproduced with permission).

isolate the product. With apparatus of this kind, by thorough purification of the nitrogen protective gas (now available in cylinders) by passing over sodium oxide, then through a heated quartz tube containing reduced copper, and finally over sulfuric acid and phosphorus pentoxide and by appropriate drying of all the solvents, glassware, and rubber hoses used, so that reactants and products were protected from the air, moisture,

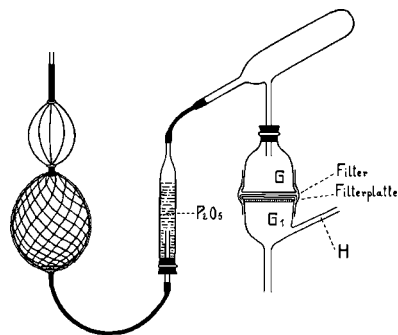
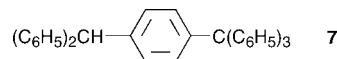


Figure 9. Schlenk's apparatus used for the drying and isolation of alkali-metal–diaryl ketone products (*Ber. Dtsch. Chem. Ges.* 1913, 46, 2845; copyright Wiley-VCH Verlag GmbH & Co. KGaA, reproduced with permission).

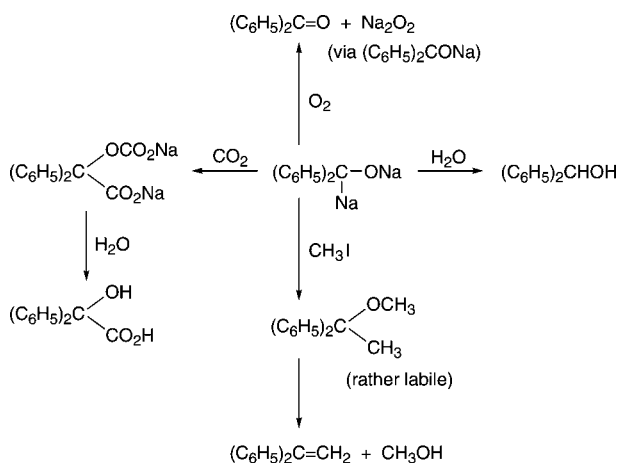


$(\text{C}_6\text{H}_5)_3\text{CNa}$ could be readily prepared by the reaction of freshly prepared sodium amalgam with triphenylchloromethane in ether. During the 12 h reaction time a dark orange-red solution of $(\text{C}_6\text{H}_5)_3\text{CNa}$ was formed in quantitative yield.³⁰ Triphenylmethylsodium could be isolated as an extremely air-sensitive tile red solid. Once it had been isolated as such, it was nearly insoluble in ether. Careful, slow air oxidation gave first the triphenylmethyl radical and then, by oxidation of the latter, the peroxide, $(\text{C}_6\text{H}_5)_3\text{COOC}(\text{C}_6\text{H}_5)_3$. Reaction of $(\text{C}_6\text{H}_5)_3\text{CNa}$ with water occurred instantaneously to give triphenylmethane. Reaction with CO_2 followed by hydrolytic workup gave triphenylacetic acid. With methyl iodide, $(\text{C}_6\text{H}_5)_3\text{CCH}_3$ was produced. Phenylbiphenyl- α -naphthylmethylsodium was prepared from the respective chloride by treatment with copper bronze and sodium in diethyl ether, a reaction which proceeded by way of the respective radical, as shown by color changes, first to brown-red (the radical) and then to the intense bluish violet of the sodium derivative. The similar formation of bis(biphenyl)- α -naphthylmethylsodium proceeded via the red radical to the black-violet sodium compound.

The nature of the triarylmethylsodium compounds was of particular interest to Schlenk in view of the electrical conductivity (for $(\text{C}_6\text{H}_5)_3\text{CNa}$ 4.8×10^{-2} at a dilution of 26.62 L per mol) of their solutions in diethyl ether. A simple dissociation to $(\text{C}_6\text{H}_5)_3\text{C}^-$ and Na^+ was considered unlikely, in view of the fact that the conductivity showed anomalously great increases with increasing concentration. Instead, Schlenk suggested that labile “ate” complexes of the type $\{[(\text{C}_6\text{H}_5)_3\text{C}]_m\text{Na}_{m-n}\}\text{Na}_n$ were present.³⁰ In 1925 Charles A. Kraus and Raphael Rosen at Brown University, who had measured the conductivities of triphenylmethylsodium and -potassium in liquid ammonia, noted that the behavior found by Schlenk and Marcus for $(\text{C}_6\text{H}_5)_3\text{CNa}$ in ether is common for all salts dissolved in solvents of low dielectric constant.³¹ Thus, the more complicated “ate” complex formulation for the solute is not appropriate.

Speaking for the $(\text{C}_6\text{H}_5)_3\text{C}^-\text{Na}^+$ formulation was the reaction reported by Schlenk and Johanna Holtz in 1916, of an ether solution of $(\text{C}_6\text{H}_5)_3\text{CNa}$ (under nitrogen) with finely powdered and well-dried tetramethylammonium chloride in a sealed tube with vigorous shaking.³² The insoluble, white ammonium salt became covered with a bright red coating within a few minutes, and the red-brown $(\text{C}_6\text{H}_5)_3\text{CNa}$ solution became light yellow. The red product could be separated from the NaCl which had been formed and the excess $[(\text{CH}_3)_4\text{N}]\text{Cl}$ by extraction with pyridine. On addition of ether to the resulting intensely blood red pyridine solution the novel compound $[(\text{CH}_3)_4\text{N}][(\text{C}_6\text{H}_5)_3\text{C}]$ was obtained as red crystals with a blue metallic sheen. These were extremely sensitive toward air, moisture, and carbon dioxide. Since the pyridine solution of $[(\text{CH}_3)_4\text{N}][(\text{C}_6\text{H}_5)_3\text{C}]$ conducted an electric current, Schlenk concluded that the compound was ionized in solution, just like ammonium halides. Nonetheless, Schlenk appeared to regard $[(\text{CH}_3)_4\text{N}][(\text{C}_6\text{H}_5)_3\text{C}]$ as a compound of pentavalent nitrogen. He wrote its formula with a bond between nitrogen and the methyl carbon atom, $(\text{C}_6\text{H}_5)_3\text{C}-\text{N}(\text{CH}_3)_4$, and titled his paper “Concerning a Compound of Nitrogen with Five Hydrocarbon Groups”. Of course, $[(\text{CH}_3)_4\text{N}][(\text{C}_6\text{H}_5)_3\text{C}]$ is a salt. Schlenk and Holtz in 1917 reported the preparation of another such ammonium compound in a reaction of benzylsodium with tetramethylammonium chloride, which Schlenk wrote as $\text{C}_6\text{H}_5\text{CH}_2\text{N}(\text{CH}_3)_4$.³³ This

Scheme 5



and carbon dioxide, Schlenk and his students were able to work with these extremely reactive compounds.

Sodium–benzophenone ketyl as well as the biphenyl-substituted ketone sodium ketyls were found to react with sodium, which was not a surprise since they are free radicals. Thus, when a $(\text{C}_6\text{H}_5)_2\text{CONa}$ solution was shaken in diethyl ether for several hours under nitrogen with an excess of sodium powder, the deep blue color of the ketyl was replaced by the dark red-violet color of the $(\text{C}_6\text{H}_5)_2\text{C}(\text{Na})\text{ONa}$ which had been formed. (This is compound **4**, which Acree thought was in equilibrium with $(\text{C}_6\text{H}_5)_2\text{C}(\text{ONa})-\text{C}(\text{ONa})\text{C}_6\text{H}_5$ in the blue $(\text{C}_6\text{H}_5)_2\text{C}=\text{O}/\text{Na}$ product solution.) The blue-green $(\text{C}_6\text{H}_5-\text{C}_6\text{H}_4)_2\text{CONa}$ solutions reacted with sodium in the same way to give the isolable disodium compound, whose ether solutions are deep blue.²⁹ The reactivity of $(\text{C}_6\text{H}_5)_2\text{C}(\text{Na})\text{ONa}$ toward some simple reagents is summarized in Scheme 5.

As might be expected, the triarylmethyl radicals reacted with sodium to give triarylmethylsodium reagents, and Schlenk undertook a study of the chemistry of Ar_3CNa compounds. In initial studies it was found that the reaction of the triphenylmethyl radical presented difficulties. Sodium powder catalyzed the known dimerization of $(\text{C}_6\text{H}_5)_3\text{C}$ to give **7**. However,

(28) In more recent times sodium–benzophenone ketyl and other alkali-metal–diaryl ketone ketyls usually are prepared in THF or in the dimethyl ethers of ethylene glycol (DME) or of higher polyethylene glycols (e.g., diglyme). It was the discovery by Scott, Walker, and Hansley of DuPont that DME is an excellent solvent for the preparation of sodium naphthalenide and the sodium-generated radical anions and dianions of other polycyclic aromatic hydrocarbons as well as of sodium–benzophenone ketyl that was the important breakthrough that made radical anion chemistry practical and useful: Scott, N. D.; Walker, J. F.; Hansley, V. L. *J. Am. Chem. Soc.* **1936**, 58, 2442.

(29) Schlenk, W.; Thal, A. *Ber. Dtsch. Chem. Ges.* **1914**, 47, 486.

(30) (a) Schlenk, W.; Marcus, E. *Ber. Dtsch. Chem. Ges.* **1914**, 47, 1664.

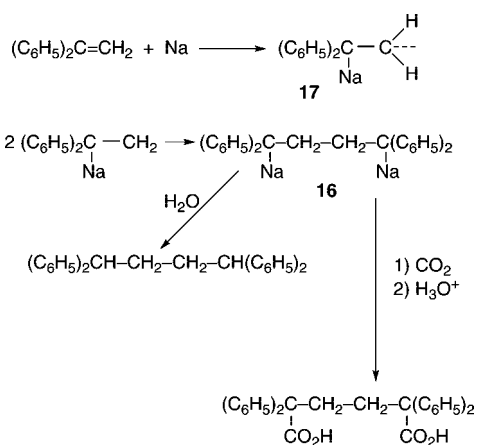
(b) Schlenk, W. *Ber. Dtsch. Chem. Ges.* **1916**, 49, 608.

(31) Kraus, C. A.; Rosen, R. *J. Am. Chem. Soc.* **1925**, 47, 2739.

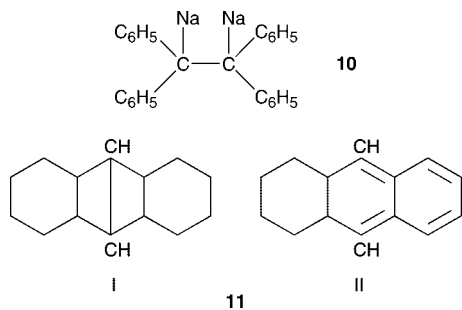
(32) Schlenk, W.; Holtz, J. *Ber. Dtsch. Chem. Ges.* **1916**, 49, 603.

(33) Schlenk, W.; Holtz, J. *Ber. Dtsch. Chem. Ges.* **1917**, 50, 274.

Scheme 7



Anthracene was a particularly interesting substrate. At the time that Schlenk wrote this paper, the structure of anthracene (**11**) was uncertain; two forms, I and II, as Schlenk drew them,

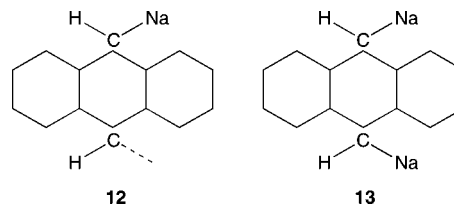


were under discussion. Form I had what was called a meso bond; Form II had an *o*-quinoid structure. Schlenk thought that he could provide crucial evidence to distinguish between the two:

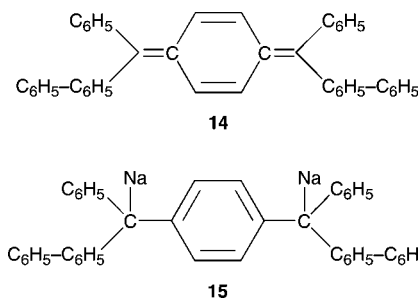
“An examination of the possible ability of sodium to add to anthracene seemed to us a suitable criterion for the correctness of one or the other of these formulas. If double bonds of the types shown in II. are present, they are connected to an aryl group and one would expect that sodium would add. If the central ring of anthracene, on the other hand, is valence-saturated, as formula I. shows, then there certainly should be no metal addition under the mild conditions that we use in our experiments.”

It was found that anthracene was especially reactive toward sodium, forming a strongly colored ether solution. This, Schlenk said, proved that anthracene had structure II. The anthracene/sodium reaction was of interest for another reason. In the preparation of the disodium adduct in diethyl ether an instantaneous reaction generated a deep blue color. This soon changed to violet (by transmitted light). This was not a concentration effect, as spectroscopic measurements showed. Schlenk’s explanation was the correct one: the blue intermediate was the monosodium adduct (a trivalent carbon species as he wrote it), **12**; the violet end product was the disodium adduct, **13**.⁴⁰ The final product, the disodium derivative, precipitated from the violet solution toward the end of the reaction as an air-sensitive, deep blue, analytically pure powder whose hydrolysis gave dihydroanthracene.

(40) Formulas **12** and **13** are reproduced as they appear in ref 39. Here also the benzene rings were not written as Kekulé structures with double bonds.



A quinomethane compound, **14**, also was examined. This compound reacted with sodium powder in diethyl ether to form a blue solution. The product was isolated as a beautiful fuchsia (bluish red) solid, the hydrolysis product of which indicated that it was **15**.



A different behavior was encountered with 1,1-diphenylethylene and styrene. The former reacted immediately with sodium powder in ether to form initially a red solution. In a reaction of 3 g of $(\text{C}_6\text{H}_5)_2\text{C}=\text{CH}_2$ with 10 g of sodium in 250 cm³ of ether the product precipitated as a brick red powder. Its hydrolysis and carbonation products, $(\text{C}_6\text{H}_5)_2\text{CHCH}_2\text{CH}_2\text{CH}(\text{C}_6\text{H}_5)_2$ and $(\text{C}_6\text{H}_5)_2\text{C}(\text{CO}_2\text{H})\text{CH}_2\text{CH}_2\text{C}(\text{CO}_2\text{H})(\text{C}_6\text{H}_5)_2$, respectively, indicated that the red product was the “dimer,” $(\text{C}_6\text{H}_5)_2\text{C}(\text{Na})\text{CH}_2\text{CH}_2\text{C}(\text{Na})(\text{C}_6\text{H}_5)_2$ (**16**). Schlenk rationalized this result in terms of the initial formation of **17**, which contained a trivalent CH_2 terminus and whose homogeneous reaction with another molecule of **17** was faster than its heterogeneous reaction with sodium (Scheme 7). On reaction of styrene with sodium powder in ether a reddish yellow color became apparent, which, however, did not increase in intensity during 1 week on the shaking machine. Examination of the reaction mixture showed that the styrene had been polymerized to a glassy solid, presumably by the catalytic action of the sodium.⁴¹

Schlenk was intrigued by the intense colors of the products of these reactions with sodium and concluded that they were due to the “labile binding of the alkali metal to the phenyl group-substituted carbon atom”, an explanation that he considered “completely sufficient”. Schlenk’s understanding of his chemistry was quite good, considering it was 1914.

Schlenk’s alkali-metal additions to unsaturated hydrocarbons over the years have provided grist for the mills of many synthetic, physical organic, and theoretical chemists. High reactivity and intense colors are always interesting. Within the same year of the Schlenk, et al. publication, Schlubach submitted a manuscript on December 17, 1914, in which he reported that the reactions of sodium with unsaturated hydrocarbons proceeded much more rapidly in anhydrous liquid ammonia.⁴² When the unsaturated hydrocarbon, in diethyl ether solution, was added to sodium in liquid ammonia, color formation was immediate and the reactions were fast and went to completion in most cases.

Two C=N bond containing compounds were examined during the course of Schlenk’s preliminary study. Benzophe-

(41) This may have been the first synthesis of polystyrene by anionic polymerization.

(42) Schlubach, H. *Ber. Dtsch. Chem. Ges.* **1915**, *48*, 12.

Table 1

Reactions of $(\text{C}_6\text{H}_5)_2\text{C}-\text{C}(\text{C}_6\text{H}_5)_2$ Na Na	
Reagent	Products
1 H ₂ O	$(\text{C}_6\text{H}_5)_2\text{CHCH}(\text{C}_6\text{H}_5)_2$
2 CO ₂	$(\text{C}_6\text{H}_5)_2\text{C} \begin{array}{c} \text{---} \\ \\ \text{CO}_2\text{Na} \end{array} \text{---} \text{C}(\text{C}_6\text{H}_5)_2$ CO ₂ Na
3 SO ₂	$(\text{C}_6\text{H}_5)_2\text{C} \begin{array}{c} \text{---} \\ \\ \text{SO}_2\text{Na} \end{array} \text{---} \text{C}(\text{C}_6\text{H}_5)_2$ SO ₂ Na
4 CH ₃ I	$(\text{C}_6\text{H}_5)_2\text{C}=\text{C}(\text{C}_6\text{H}_5)_2$ (TPE) + NaI + CH ₃ -CH ₃
5 C ₆ H ₅ Br	TPE + C ₆ H ₅ -C ₆ H ₅ + NaBr
6 C ₆ H ₅ CO ₂ CH ₃	TPE + CH ₃ -CH ₃ + C ₆ H ₅ CO ₂ Na
7 C ₆ H ₅ COCl	TPE + C ₆ H ₅ C(=O)CC ₆ H ₅ + NaCl
8 C ₂ H ₅ NCS	TPE + C ₂ H ₅ N(=S)C(=S)NC ₂ H ₅
9 Hg	TPE + Na/Hg
10 NO	TPE + Na ₂ N ₂ O ₂

Table 2

Reactions of $(\text{C}_6\text{H}_5)_2\text{C}-\text{CH}_2\text{CH}_2-\text{C}(\text{C}_6\text{H}_5)_2$ Na Na	
Reagent	Products
1 H ₂ O	$(\text{C}_6\text{H}_5)_2\text{CHCH}_2\text{CH}_2\text{CH}(\text{C}_6\text{H}_5)_2$
2 CO ₂	$(\text{C}_6\text{H}_5)_2\text{C} \begin{array}{c} \text{---} \\ \\ \text{CO}_2\text{Na} \end{array} \text{---} \text{CH}_2\text{CH}_2-\text{C}(\text{C}_6\text{H}_5)_2$ CO ₂ Na
3 CH ₃ I	$(\text{C}_6\text{H}_5)_2\text{C} \begin{array}{c} \text{---} \\ \\ \text{CH}_3 \end{array} \text{---} \text{CH}_2\text{CH}_2-\text{C}(\text{C}_6\text{H}_5)_2$ CH ₃
4 C ₆ H ₅ CH=O	$(\text{C}_6\text{H}_5)_2\text{C} \begin{array}{c} \text{---} \\ \\ \text{C}_6\text{H}_5\text{CHONa} \end{array} \text{---} \text{CH}_2\text{CH}_2-\text{C}(\text{C}_6\text{H}_5)_2$ C ₆ H ₅ CHONa
5 C ₆ H ₅ CO ₂ C ₆ H ₅	$(\text{C}_6\text{H}_5)_2\text{C} \begin{array}{c} \text{---} \\ \\ \text{C}_6\text{H}_5\text{C}=\text{O} \end{array} \text{---} \text{CH}_2\text{CH}_2-\text{C}(\text{C}_6\text{H}_5)_2$ C ₆ H ₅ C=O
6 C ₆ H ₅ CO ₂ CH ₃	$(\text{C}_6\text{H}_5)_2\text{C} \begin{array}{c} \text{---} \\ \\ \text{C} \end{array} \begin{array}{c} \text{---} \\ \\ \text{O} \end{array} \text{---} \text{C}(\text{C}_6\text{H}_5)_2$ CH ₂ -CH ₂
7 C ₂ H ₅ NCS	$(\text{C}_6\text{H}_5)_2\text{C} \begin{array}{c} \text{---} \\ \\ \text{S}=\text{C}-\text{NC}_2\text{H}_5 \end{array} \text{---} \text{CH}_2\text{CH}_2-\text{C}(\text{C}_6\text{H}_5)_2$ Na S=C-NC ₂ H ₅ Na
8 Hg	2(C ₆ H ₅) ₂ C=CH ₂ + Na/Hg

^a This system is more complicated than Schlenk ever would have imagined; cf.: (a) Jagur, J.; Levy, M.; Feld, M.; Szwarc, M. *Trans Faraday Soc.* 1962, 58, 2168 and (b) Gill, D.; Jagur-Grodzinski, D.; Szwarc, M. *Trans. Faraday Soc.* 1964, 60, 1424. ^b For a 1975 report of further reactions, see: Smith, J. G.; Talvite, J. R.; Eix, A. R. E. *J. Chem. Soc., Perkin Trans.* 1 1975, 1474.

work merited some discussion. It is the work of his student, Johanna Holtz, carried out at the University of Jena, which is directly relevant.²⁰ As Schlenk noted, "our knowledge concerning the simplest organometallic-alkali compounds is still full of gaps", and he pointed out that, since Wanklyn's work (cf. Part I), because of their great reactivity toward oxygen and their instability, nobody (except Acree) who had worked with them had tried to isolate alkali-metal alkyls and aryls. Acree had

claimed the isolation of phenylsodium, but this had been disputed by Hilpert and Grüttner (*vide supra*).

Schlenk and Holtz reported the successful preparation, isolation as nearly pure compounds, and characterization of methyl-, ethyl-, *n*-propyl-, *n*-octyl-, benzyl-, and phenylsodium, as well as methyl-, ethyl-, *n*-propyl-, and phenyllithium. All of the organosodium compounds were found to be colorless, amorphous powders that were insoluble or very poorly soluble in all inert solvents. The RNa powders, when heated, decomposed without melting. They were extremely oxygen-sensitive, inflaming in air. The RLi compounds also were white solids. Methylsodium was insoluble in hydrocarbon solvents, but ethyl- and *n*-propyllithium were readily soluble in alkanes and benzene.

In their search for a procedure for the preparation of alkylsodium compounds Schlenk and Holtz examined Wanklyn's diethylzinc/sodium reactions and confirmed his finding that an ethylsodium/diethylzinc complex was produced. All variations of the procedure were unsuccessful, in that all products contained zinc as well as sodium. Attempts to prepare alkylsodium compounds by the action of sodium on tetraalkyllead compounds only gave impure products. However, a variation of Buckton's procedure, the reaction of sodium with a dialkylmercury compound (eq 2), was successful in the preparation of the sodium alkyls mentioned above. Buckton, like most early organometallic chemists, had not used a solvent and, on reaction of sodium with neat diethylmercury, had obtained a "voluminous grey sponge" with which he could do nothing. As time went on, the advantages of using solvents in reactions of metals with organic compounds had become apparent. Schlenk and Holtz carried out their RNa preparations in petroleum ether ("Gasolin") or high-boiling ligroin. In their procedure small pieces of clean sodium were added to a dialkylmercurial in a well-dried solvent (under dry, purified nitrogen with strict exclusion of air using Schlenkware shown in Figures 5–8). Within hours or days, the sodium became covered with the insoluble sodium alkyl. The formation of a layer of sodium amalgam between the sodium surface and the thin crust of light-colored sodium alkyl initially caused problems. In some spots little drops of the liquid amalgam emerged, which made the isolation of the sodium alkyl in any kind of purity impossible when the RNa layer was shaken loose from the sodium surface. After many unsuccessful experiments it was found that this problem could be circumvented by strongly cooling (ice-salt mixture) the reaction vessel prior to the shaking step. This caused the amalgam to freeze and adhere strongly to the sodium surface. The sodium alkyl particles then could be shaken away and decanted with the liquid phase away from the heavier Na/sodium amalgam phase. The sodium alkyl suspension usually settled out from the solvent. If it did not, the mixture was centrifuged.

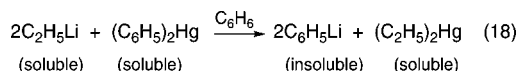
The reaction of sodium with dimethylmercury in ligroin of bp ~80° proceeded fairly slowly at room temperature, but the reaction was much more rapid when carried out at 65 °C. Methylsodium was isolated as an off-white powder flecked with small yellow-brown particles of some impurity, possibly mercury. It inflamed almost explosively in air. Because of its high reactivity, for analysis a toluene suspension of a weighed sample of the powder (under nitrogen) was decomposed by very slow addition of ethyl alcohol. Dilution with water and titration of the base which had been formed with standardized acid followed. All things considered, the results were quite good: Anal. Calcd: Na, 60.5. Found: Na, 59.2.

The reaction of sodium with diethylmercury was more rapid than that with dimethylmercury, and heating was not needed.

the reaction of metallic lithium with methyl chloride in diethyl ether, as had been described by Ziegler et al.⁴⁸

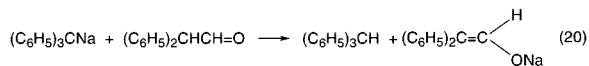
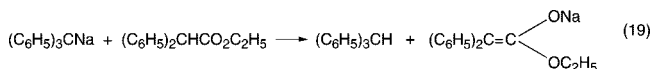
As noted above, ethyllithium was soluble in warm hydrocarbon solvents and was generally more tractable than methyllithium. Its preparation thus was easier. Finely cut pieces of metallic lithium (in excess) were added, under nitrogen, to a solution of diethylmercury in benzene, and the resulting mixture was heated at 65 °C with periodic shaking, for 3 days. The excess lithium, coated with lithium amalgam, sank to the bottom of the flask. Filtration of the mixture at 70 °C (Figure 7) gave a filtrate from which, as it cooled, large colorless crystals of ethyllithium crystallized. The crystallization was completed by cooling to 0 °C. A wash with a small amount of cold petroleum ether gave pure C₂H₅Li (Anal. Calcd: Li, 19.44. Found: Li, 19.10) which melted at 95 °C under nitrogen. It could be distilled at high temperatures, in part without decomposition. Like ethylsodium, it reacted with diethyl ether and was decomposed in the process. In air ethyllithium inflamed, burning with a bright red flame.

Phenyllithium was prepared using the same procedure. During the 5–6 day reaction time at 65 °C a microcrystalline powder was formed. Decantation from the lithium/lithium amalgam mixture followed by centrifugation of the phenyllithium suspension and washing of the isolated solid with benzene and petroleum ether gave a pure product (Anal. Calcd: Li, 8.33. Found: Li, 8.61). Even simpler was the preparation of phenyllithium in high purity by the transmetalation reaction (eq 18). Phenyllithium was isolated as a microcrystalline white powder that inflamed in air, burning with a yellow flame.



Although Schlenk described his preparations of the organoalkali-metal alkyls and phenyls adequately in ref 20 when he wrote the organoalkali-metal chapter in the Houben-Weyl series,⁴⁹ he was requested by the editor to do so in even greater detail. This he did, with detailed instructions even for nitrogen purification, including a final step of passing it through an ether solution of triphenylmethylsodium (whose color served as an indicator for the absence of oxygen).

Schlenk's activity in the area of organoalkali-metal chemistry continued into the late 1920s and early 1930s, dealing mostly with those classes of compounds discussed above. In 1931 he reported on yet another class, the alkali-metal enolates, prepared as shown in eqs 19 and 20 and isolated as the pure solids.⁵⁰



During the early years, as he had requested, Schlenk did not have competitors in his research, but this changed, with the no

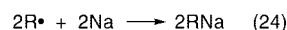
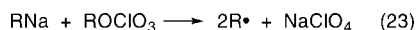
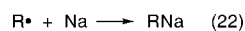
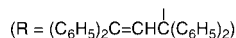
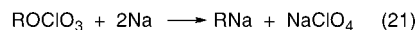
(48) Ziegler, K.; Nagel, K.; Patheiger, M. *Z. Anorg. Allg. Chem.* **1955**, 289, 345.

(49) Schlenk, W. In *Houben-Weyl, "Die Methoden der Organischen Chemie"*, 2nd ed.; Thieme: Stuttgart, Germany, 1924; Vol. IV, pp 945–978.

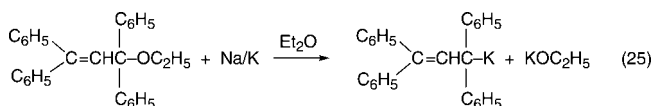
(50) (a) Schlenk, W.; Schmidt, R. *Ber. Dtsch. Chem. Ges.* **1925**, 58, 1189. (b) Schlenk, W.; Hillemann, H.; Rodloff, I. *Justus Liebig's Ann. Chem.* **1931**, 487, 135.

doubt unwelcome entrance of Karl Ziegler⁵¹ into both of his major areas of interest, trivalent carbon compounds (i.e., persistent organic free radicals) and organoalkali metal chemistry, when Ziegler began a vigorous pursuit of independent research in the early 1920s. Since Ziegler's work impacted on Schlenk's research and led to an active, not very friendly controversy between them, an account of Ziegler's research in the area of organoalkali-metal chemistry must be included in this essay.

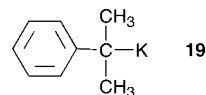
In his first full paper on organic radicals Ziegler reported an interesting alkali-metal reaction (eq 21).⁵² The reaction was believed to be one of the tetraphenylallyl radical, generated by some trace radical species, so that the postulated sequence was that shown in eqs 22–24. This led Ziegler to a new synthesis of organic radicals by interrupting the sequence of reactions at eq 23, in which a solution of the deeply colored organosodium compound was added to a suspension of the organic perchlorate in ether. The RNa solution became lighter in color and the perchlorate went into solution. However, the organic perchlorates were of limited applicability. The tetraphenylallyl perchlorate, for instance, was not very stable.



An important contribution by Ziegler in this early work was the discovery that the colored organoalkali-metal compounds can be prepared by the cleavage of appropriately substituted ethers by the alkali metals: e.g., eq 25.⁵³ Further investigation



of the ether cleavage reaction⁵⁴ led to the preparation of 2-phenylisopropylpotassium (**19**), a compound that was to be a



very useful reagent in Ziegler's subsequent organoalkali-metal research. The cleavage of 2-phenylisopropyl methyl ether with liquid sodium–potassium alloy proceeded rapidly in diethyl ether. The resulting product, **22**, a deep red ether-soluble compound, was obtained in excellent yield.

In 1928 a preliminary communication by Ziegler and Bähr⁵⁵ reported a reaction of 2-phenylisopropylpotassium that turned

(51) For a biographical sketch and picture of Ziegler see Part 1 of this essay.¹ Ziegler obtained his Ph.D. in 1920 and completed his Habilitation in 1923; therefore, his earliest independent research was carried out in 1921/1922.

(52) Ziegler, K. *Justus Liebig's Ann. Chem.* **1923**, 434, 34.

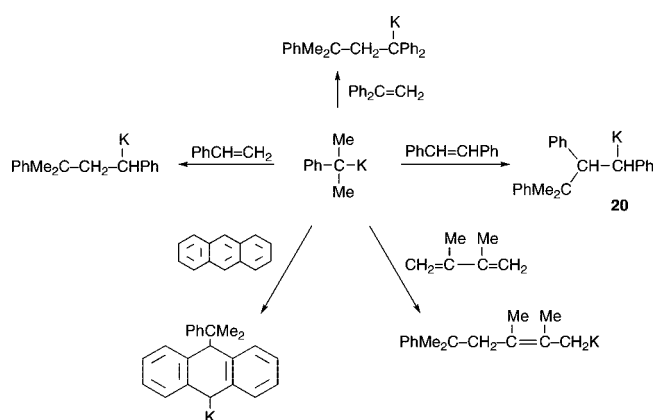
(53) Ziegler, K.; Thielmann, F. *Ber. Dtsch. Chem. Ges.* **1923**, 56, 1740.

(54) Ziegler, K.; Schnell, B. *Justus Liebig's Ann. Chem.* **1924**, 437, 227.

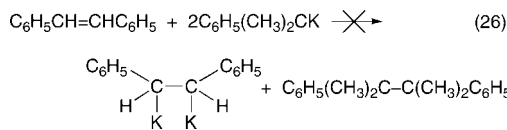
(55) (a) Ziegler, K.; Bähr, K. *Ber. Dtsch. Chem. Ges.* **1928**, 61, 253.

(b) Full paper (covering alkyllithium as well as C₆H₅(CH₃)₂CK): Ziegler, K.; Crössmann, F.; Kleiner, H.; Schäfer, O. *Justus Liebig's Ann. Chem.* **1929**, 473, 1–35. (c) Ziegler, K.; Grimm, H.; Willer, R. *Justus Liebig's Ann. Chem.* **1939**, 542, 90. (d) In 1957, when the starting ether, C₆H₅(CH₃)₂COCH₃, had become more readily available, Ziegler conducted further studies of the reactions of C₆H₅(CH₃)₂CK: Ziegler, K.; Dislich, H. *Chem. Ber.* **1957**, 90, 1107.

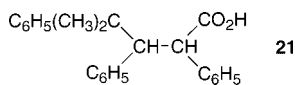
Scheme 10



out to be crucial in the further development of Ziegler's scientific career: its addition to the C=C bond of appropriately activated olefins. This was the first carbometalation reaction (Scheme 10). As Ziegler related, this was an accidental discovery. The reaction that had been sought was the preparation of a dipotassium derivative of stilbene as shown in eq 26, the potassium analogue



of the violet-brown disodium stilbene that Schlenk had reported earlier. Instead of the expected violet-brown, ether-insoluble solid, a soluble orange-yellow potassium compound resulted. Treatment of this solution with carbon dioxide followed by aqueous acid workup gave a carboxylic acid that was identified as **21**. This established that the potassium compound had been



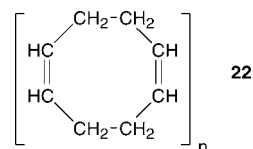
20 in Scheme 10, a result much more interesting and gratifying to Ziegler than the one he had sought. Further work showed this to be a general reaction when the C=C bond was conjugated with an aryl group or another C=C bond, as in 2,3-dimethylbuta-1,3-diene.

Interesting though it was, Ziegler put the stoichiometric reaction of $\text{C}_6\text{H}_5(\text{CH}_3)_2\text{CK}$ with activated olefins, which gave 1:1 addition products, on the back burner, for he believed that this new chemistry might provide the answer to an important problem: the question of the mechanism of the polymerization of 1,3-dienes and styrene induced by alkali metals and organoalkali-metal compounds. The process had been reported first by Carl Dietrich Harries of the University of Kiel in Germany in 1911.⁵⁶ Harries had been investigating the thermal polymerization of 1,3-dienes, trying to establish the degree of unsaturation of the resulting polymers by means of ozonolysis, a process in which he had become an expert. Around the end

(56) (a) Harries, C. *Justus Liebigs Ann. Chem.* **1911**, *383*, 157–227. A long paper that covered both the synthesis and polymerization of 1,3-butadiene, isoprene, and 2,3-dimethyl-1,3-butadiene. A good read—we don't write papers in such a casual style today. (b) C. D. Harries (1866–1923). Chemistry studies, Universities of Jena and Berlin, Ph.D. with Ferdinand Thiemann, 1889. Assistant in Univ. of Berlin, Habilitation, 1904. Professor, Univ. of Kiel. Studies on organic chemistry of ozone and natural and synthetic rubber, 1916. Director of Scientific Activities at Siemens in Berlin. Adjunct Professor, Charlottenburger Technische Hochschule in Berlin, 1919.

of 1910 he began his investigation of the interaction of sodium with 1,3-dienes. In one experiment reported by Harries 9 g of pure 1,3-butadiene and 0.5 g of sodium wire were sealed in a glass tube and warmed at 35–40 °C on a water bath for 3 h. During this time the liquid thickened around the sodium wire into a brown, gelatinous mass. No buildup of pressure was noted when the tube was opened. Addition of the contents of the tube to dilute aqueous alcohol to destroy and remove unreacted sodium converted the brown mass into a bright yellow, rubbery material in nearly quantitative yield. Freshly prepared, the product was soluble in ether, chloroform, and benzene. With time, however, the solubility decreased and the material swelled enormously when treated with solvent. The material could be vulcanized, and the vulcanized product was superior to the products derived from butadiene polymers obtained in other ways in terms of tear strength and elasticity. The C,H analysis of the product from the sodium process agreed reasonably well with that calculated for $(\text{C}_4\text{H}_6)_n$: Anal. Calcd: C, 88.89; H, 11.11. Found: C, 87.92; H, 11.10. Its ozonolysis in chloroform proceeded very slowly, giving a white, solid ozonide which, when dry, readily exploded.

As Harries noted, there were two remarkable features about the sodium-induced polymerization of dienes. First, the sodium, for the most part, was unconsumed; thus, it appeared to be a catalyst. Second, although the product resembled rubber (Kautschuk in German), it was different from natural rubber and thermally produced synthetic rubber in terms of its behavior on ozonolysis. Harries called these reactions “a surprising discovery” and called the products “Natrium-Kautschuk”. In 1911 the structures of natural and synthetic rubber were not known. Harries discussed them in terms of polymers of cyclic dimers, **22**. Isoprene, in contrast to 1,3-butadiene, was not as readily polymerized by sodium, requiring a reaction time of 50–100 h at 60 °C.



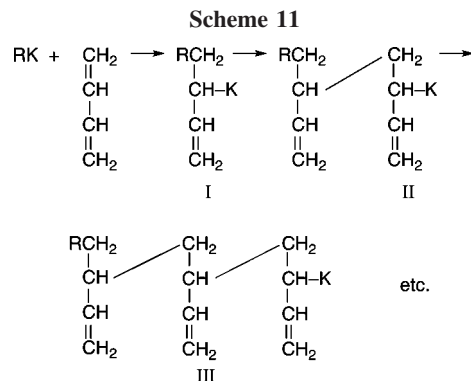
There also was industrial activity on the preparation of synthetic rubber by sodium-induced polymerization of 1,3-dienes at around the same time, as indicated by several German patents.⁵⁷ The Bayer patent^{57c} shows that such polymerizations can take place when the diene vapor comes in contact with sodium wire.

Such sodium-induced polymerizations are not restricted to 1,3-dienes. It should be recalled that Schlenk, Appenrodt, and Michael had reported the sodium-induced polymerization of styrene.³⁹

As Ziegler noted, a 1912 BASF patent⁵⁸ had shown that organoalkali-metal compounds, including $\text{NaZn}(\text{C}_2\text{H}_5)_2$ used in one example, could induce the polymerization of 1,3-dienes. He suggested that the alkali-metal-induced polymerizations proceeded via initially formed adducts of type $\text{KCH}_2\text{CH}=\text{CHCH}_2\text{K}$ and pictured the polymerization process as shown in Scheme 11, opting for 1,2-addition of RK since

(57) (a) Matthews, F. E.; Strange, E. H. Patentschrift Nr. 249868, Kaiserliches Patentamt, 1911. (b) Badische Anilin & Soda-Fabrik. Patentschrift Nr. 255787, Kaiserliches Patentamt, 1912. (c) Farbenfabriken vorm. Friedr. Bayer & Co. Patentschrift Nr. 280959, Kaiserliches Patentamt, 1912.

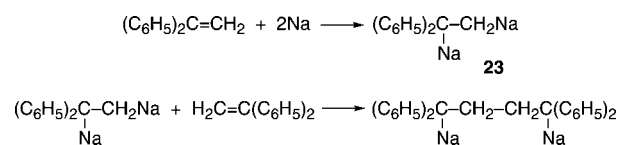
(58) Badische Anilin- & Soda-Fabrik. Patentschrift Nr. 255786, Kaiserliches Patentamt, 1912.



“Natrium-Kautschuk” was different from natural rubber and thermally produced synthetic rubbers which were formed by a 1,4-addition process. Ziegler and Bähr’s initial results were in agreement with his views: products of higher molecular weight of the $\text{C}_6\text{H}_5(\text{CH}_3)_2\text{CK}$ /styrene and 2,3-dimethyl-1,3-butadiene reactions were obtained when an excess of the olefin was used. In subsequent work Ziegler and his students studied the mechanisms of 1,3-diene and styrene polymerization catalyzed by alkali metals and organoalkali-metal compounds in much greater depth.^{59–62} The study of the catalysis of 1,3-diene polymerization by alkylsodium and alkyllithium compounds was taken up in the United States in later years, as has been discussed in Part 1.

A full paper with more details concerning the scope of the addition of organoalkali metal alkyls to activated olefins was published by Ziegler in 1929.⁶³ It was confirmed that conjugation of the $\text{C}=\text{C}$ bond with an aryl group or another $\text{C}=\text{C}$ bond was required. However, steric factors intruded and the presence of fairly acidic $\text{C}-\text{H}$ bonds that could be metalated by the alkyl alkali-metal reagent interfered. 2-Phenylisopropylpotassium was Ziegler’s reagent of choice: it was easy to prepare and soluble and it reacted rapidly. Also, investigated were the addition reactions in benzene solution of organolithium reagents (prepared by the $\text{R}_2\text{Hg}/\text{Li}$ procedure). Since these were not colored, the progress of their addition to activated olefins could be followed by the increasing intensity of the color of the adducts formed in these reactions.

Ziegler also turned his attention to Schlenk’s reports concerning the addition of alkali metals to other unsaturated hydrocarbons: ³⁹ in particular, to Schlenk’s proposed mechanism for the formation of the “dimer” $(\text{C}_6\text{H}_5)_2\text{C}(\text{Na})\text{CH}_2\text{CH}_2\text{C}(\text{Na})(\text{C}_6\text{H}_5)_2$ in the addition of sodium to 1,1-diphenylethylene. Schlenk had suggested that it proceeded by the initial formation of a monosodium adduct, the radical $(\text{C}_6\text{H}_5)_2\text{C}(\text{Na})\text{CH}_2^\cdot$, which in a subsequent step dimerized (Scheme 7). Ziegler, in contrast, suggested that a different two-step reaction course was involved: first, addition of two sodium atoms to give **23**, followed by addition of **23** to the $\text{C}=\text{C}$ bond of another molecule of 1,1-diphenylethylene (Scheme 12).⁶⁴ This, he thought, was in line with his recently discovered addition of alkyl alkali-metal compounds to activated $\text{C}=\text{C}$ bonds. Ziegler presented some arguments in favor of his mechanism. Schlenk did not take

Scheme 12

kindly to Ziegler’s paper; he rejected all of his criticisms and stuck with his original mechanism.⁶⁵ He sent preprint copies of these papers to Ziegler, and this prompted Ziegler to add what amounted to a second paper as a rebuttal to Schlenk to a paper in which he discussed more broadly the reactions of alkali metals with unsaturated compounds.⁶⁶ This controversy between Ziegler and Schlenk was not resolved.⁶⁷ It is possible that both mechanisms are right, rather than one being wrong and the other right. We now know, as noted earlier in this essay, that the addition of alkali metals to an unsaturated hydrocarbon (which involves addition of a metal s electron to the LUMO of the hydrocarbon with formation of an alkali-metal cation) can proceed in two steps: addition of one electron to form the radical anion and then addition of the second electron to form the dianion.⁶⁸ Thus, depending on reaction conditions, the initially formed radical anion, $[(\text{C}_6\text{H}_5)_2\text{CCH}_2]^\cdot\text{Na}^+$, in principle could either dimerize to give $[(\text{C}_6\text{H}_5)_2\text{CCH}_2\text{CH}_2\text{C}(\text{C}_6\text{H}_5)_2]^{2-}, 2\text{Na}^+$ directly, or add a second electron to produce the dianion, $[(\text{C}_6\text{H}_5)_2\text{CCH}_2]^{2-}, 2\text{Na}^+$, which subsequently would add to $(\text{C}_6\text{H}_5)_2\text{C}=\text{CH}_2$, as Ziegler suggested, to give the 1,1,4,4-tetraphenylbutane dianion.

With this not especially cordial exchange Schlenk stopped publishing papers on organoalkali-metal chemistry, although Bergmann continued to do so. Ziegler continued research in this area. Most notable was the preparation of alkyllithium reagents and phenyllithium by the reaction of organic halides with metallic lithium,⁶⁹ which was discussed in Part 1. In an attempt to use their new organolithiums as reagents in the preparation of the heavier alkali-metal alkyls, Ziegler and Colonius shook an alkyllithium solution with 40% liquid sodium amalgam. It was expected that the hydrocarbon-insoluble sodium alkyl would precipitate. What occurred instead was that the alkyllithium was consumed, but a solid alkylsodium compound was not formed. The same observation was made, i.e., that the RLi was consumed, when metallic mercury, rather than the amalgam, was used and it was found that the mercury now contained lithium. The alkyl groups of the alkyllithium reagent were present in the solution as the dialkylmercury compound. This reaction was the reverse of the Schlenk/Holtz alkyllithium synthesis: i.e., eq 27.

(65) (a) Schlenk, W.; Bergmann, E. *Justus Liebigs Ann. Chem.* **1930**, 479, (a) 42; (b) 58; (c) 78.

(66) Ziegler, K.; Schäfer, O. *Justus Liebigs Ann. Chem.* **1930**, 479, 150.

(67) (a) For a discussion of the Schlenk/Ziegler controversy from a contemporaneous point of view see: Wooster, C. B. *Chem. Rev.* **1932**, 11, 1. (b) A good account of the work of Schlenk and Ziegler in the organoalkali-metal area is given (in German) in: Krause, E.; von Grosse, A. *Die Chemie der metall-organischen Verbindungen*; Verlag von Gebrüder Bornträger: Berlin, 1937; Chapter 2, pp 69–109. This book also contains a useful chapter on the procedures and various apparatus for the handling of air-sensitive compounds, pp 802–811.

(68) For a brief, modern discussion of the addition of alkali metals to unsaturated hydrocarbons see: Coates, G. E.; Green, M. L. H.; Wade, K. *Organometallic Compounds*; Methuen: London, 1967; Vol. 1, The Main Group Elements, pp 54–70. Note that the “dimerizing addition” of sodium to 1,1-diphenylethylene is discussed in terms of Schlenk’s mechanism. Note also that in my discussion of the work of Schlenk and Ziegler I have written compound formulas as they wrote them, i.e., with $\text{C}-\text{Li}$, $\text{C}-\text{Na}$, and $\text{C}-\text{K}$ bonds in the case of the addition compounds.

(69) Ziegler, K.; Colonius, H. *Justus Liebigs Ann. Chem.* **1930**, 479, 135.

(59) Ziegler, K.; Kleiner, H. *Justus Liebigs Ann. Chem.* **1929**, 473, 57.

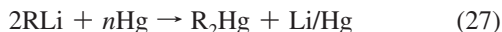
(60) Ziegler, K.; Dersch, F.; Wolltham, H. *Justus Liebigs Ann. Chem.* **1934**, 511, 13.

(61) Ziegler, K.; Jakob, L. *Justus Liebigs Ann. Chem.* **1934**, 511, 45.

(62) Ziegler, K.; Jakob, L.; Wolltham, H.; Wenz, A. *Justus Liebigs Ann. Chem.* **1934**, 511, 64.

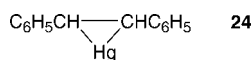
(63) Ziegler, K.; Crösmann, F.; Kleiner, H.; Schäfer, O. *Justus Liebigs Ann. Chem.* **1929**, 473, 1.

(64) Ziegler, K.; Colonius, H.; Schäfer, O. *Justus Liebigs Ann. Chem.* **1929**, 473, 36.



One experiment was reported by Ziegler and Colonius in support of this chemistry: an *n*-butyllithium solution (100 cm³ of 0.45 N reagent in cyclohexane) was shaken with 500 g of mercury at room temperature for 2 days. Subsequent treatment of an aliquot of the solution with water developed no alkalinity. The solution had the characteristic odor of di-*n*-butylmercury. Isolation of the latter was not attempted. Instead, the cyclohexane solution was heated (under nitrogen) "for some time" with small chips of lithium metal. The resulting solution was found to be 0.25 N in alkalinity. In addition, the residual mercury from this experiment evolved hydrogen on treatment with water and dilute HCl. The aqueous solution was shown spectroscopically to contain lithium.

The discovery of this new chemistry led Ziegler to propose how the remarkable reactions (which had been reported by Schlenk and Bergmann⁴³), the regeneration of the original olefin when a solution of its sodium addition product was shaken with metallic mercury (Scheme 9), occurred. Ziegler felt sure that organomercury intermediates, which he wrote as the mercurio-cyclopropane **24** in the case of stilbene, must be involved. These



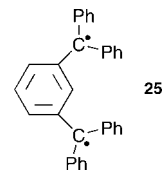
then, he said, would decompose to regenerate mercury and give the olefin. Schlenk and Bergmann had suggested that the driving force of the reaction in Scheme 9 was the high heat of formation of the sodium amalgam, but Ziegler, as noted, favored a reaction course involving unstable organomercury intermediates. These, he said, were likely to be in equilibrium with the disodium adduct, and as they decomposed, the equilibrium would keep being driven to the right. Those monosodium compounds, i.e., the substitution products RNa, which did not appear to react with mercury, according to Ziegler really did react, but the equilibrium lay far to the left and could not be driven to the right since the mercury product, present in only minute amounts, was stable. This was disputed by Bergmann, who reported that (C₆H₅)₂CHNa did react with metallic mercury, giving (C₆H₅)₂CH-CH(C₆H₅)₂ and another, unidentified isomeric product.⁷⁰ This fact, he said, spoke against Ziegler's ideas and left an explanation in thermodynamic terms the only viable one. Ziegler, in rebuttal, claimed that Bergmann's arguments were without merit.⁷¹ The formation of (C₆H₅)₂CHCH(C₆H₅)₂ in the (C₆H₅)₂CHNa/Hg reaction, he said, indicated that [(C₆H₅)₂CH]₂Hg was unstable, decomposing to tetraphenylethane and mercury. He supported this by noting his finding that the reaction of (C₆H₅)₂CHNa with mercuric chloride gave not [(C₆H₅)₂CH]₂Hg but rather (C₆H₅)₂CHCH(C₆H₅)₂ and metallic mercury. Clearly, this fit into Ziegler's supposition that the (C₆H₅)₂CHNa/Hg reaction proceeded by way of the organomercury intermediate, which was unstable at room temperature. Ziegler also cited dibenzylmercury, which was stable at room temperature and could be prepared by the reaction of benzyl lithium with metallic mercury but which decomposed to dibenzyl and mercury at 170 °C. Thus, the reaction of all organoalkali-metal compounds, whether they were addition or substitution products, with metallic mercury proceeded in the same manner. The products obtained, an organomercurial or a compound that did not contain mercury, depended on whether the initially formed organomercury compound was stable or unstable under the experimental conditions.

Ziegler was stung by Bergmann's mention^{70b} of Ziegler's three-membered cyclic C₂Hg intermediate pictured in his paper, protesting that the expression, "Quecksilberdreiring" (three-membered mercury ring) had never been used any place in his paper. (True enough, but he did show formula **24** in his paper,⁶⁹ and it even appeared in the present paper.⁷¹) Obviously irked, he did not write kindly about Bergmann, accusing him of speculation unsupported by experiment. On looking over some of Bergmann's papers published during that time, one is left with the impression that Ziegler was right.

Schlenk and Bergmann had found that alkali metals induced the isomerization of *cis*-stilbene to the *trans* isomer.⁷² Ziegler, claiming to have discovered this isomerization independently before this publication appeared, investigated this phenomenon.⁷³ It was found that even traces of the stilbene disodium or dilithium adducts catalyzed this isomerization.⁷³ It was suggested that sodium or lithium was transferred from the alkali-metal adducts, in which it was thought that the alkali metal was only loosely bound, to the *cis*-stilbene. The resulting dimetal adduct transferred alkali metal in its turn. When *trans*-stilbene was regenerated in this way, it accumulated in the equilibrium mixture, since *cis*-stilbene was more reactive in alkali-metal addition. The dimeric 1,1-diphenylethylene/sodium adduct (C₆H₅)₂C(Na)CH₂CH₂C(Na)(C₆H₅)₂ also catalyzed the *cis*- to *trans*-stilbene isomerization. The rate of this process was so fast that, as Ziegler said, one was reminded of ionic reactions. (Of course, being electron transfer processes, they are very fast.)

Ziegler carried out other studies on organoalkali-metal chemistry, but the observations discussed here are for the most part those which had some connection with Schlenk's chemistry.

In our discussion of Schlenk's career, we left him at his Habilitation in Munich and went on to survey his contributions to organic and organometallic chemistry. We now return to a consideration of the development of his career. His Habilitation, completed in 1909, was devoted to triarylmethyl radicals. Subsequently, he became Privatdozent. Through his work on triarylmethyl free radicals he had become quite visible, and a call to the University of Jena as Professor Extraordinarius (Associate Professor) came in 1913. In Jena Schlenk's organoalkali-metal chemistry came into full bloom. Here he also prepared the first stable diradical **25**.^{22c}



With these outstanding accomplishments in radical and organometallic chemistry Schlenk was recognized as a rising star. This led to a call to Vienna as full professor and Director of the Chemical Institute II of the University of Vienna in 1918.

A story about Schlenk as a lecturer is related by Thomas Tidwell in ref 21:

"Schlenk had a reputation for his lectures with demonstrations and on 15 January 1921, he made a presentation at the gala opening of the new "Hörsaal" for the Chemical Institute II at the Vienna University before a large audience that included Albert Einstein. The title of the lecture was

(70) (a) Bergmann, E. *Ber. Dtsch. Chem. Ges.* **1930**, *63*, 1617. (b) Bergmann, E. *Ber. Dtsch. Chem. Ges.* **1930**, *63*, 2593.

(71) Ziegler, K. *Ber. Dtsch. Chem. Ges.* **1931**, *64*, 445.

(72) Schlenk, W.; Bergmann, E. *Justus Liebigs Ann. Chem.* **1928**, *463*, 110.

(73) Ziegler, K.; Wollschitt, H. *Justus Liebigs Ann. Chem.* **1930**, *479*, 123.

“Applications of Electricity in Chemistry.” As related by his son Hermann he had obtained a new electrical apparatus but ignored warnings not to use this for the actual demonstration and received a tremendous electrical discharge, which could be seen going in one finger and out the other hand. Schlenk was thrown to the floor, but revived and finished the lecture.”

Another move came in 1921 when Schlenk was chosen to be the successor of Emil Fischer, who had died in 1919, as Professor of Chemistry and Director of the Chemical Laboratory of the Friedrich Wilhelm University of Berlin. In Berlin he continued his organosodium research, assisted by Ernst Bergmann, who had been a Schlenk student and subsequently, an Assistant after his Habilitation. He did, however, venture, if only briefly, into other areas. In 1923, interested in the mechanism of the catalytic hydrogenation of unsaturated organic compounds, he looked into the possibility of one of the then currently discussed mechanisms, a route involving labile metal hydride intermediates. He chose nickel because of previous work with this metal by others. Using (not surprisingly) an organometallic approach, Schlenk and Weichselfelder treated 0.17 g of anhydrous NiCl_2 with approximately 0.15 mol of $\text{C}_6\text{H}_5\text{MgBr}$ in diethyl ether with agitation at 14 °C.⁷⁴ The reaction mixture immediately became brown. During the course of the reaction purified hydrogen was admitted from a gas buret; H_2 absorption was rapid, taking up 4H per Ni. The product was a black solid. Decomposition of a dry sample of the latter by addition of alcohol and measurement of the evolved hydrogen established the formula NiH_2 . This solid was found to be the most active hydrogenation catalyst known in terms of rate and activity at room temperature. However, it had a fatal flaw: even traces of air immediately “killed” its activity at room temperature. This was not Schlenk’s only work with the Grignard reagent.

Schlenk had married Mathilde von Hacke in 1905. The couple had three sons, Wilhelm Jr. (1907–1975), Fritz (1909–1998), and Hermann (1914–2003), all of whom became Ph.D. chemists. With Wilhelm Jr. Schlenk published an important paper in organomagnesium chemistry on the equilibrium shown in eq 28,



the so-called “Schlenk Equilibrium”.⁷⁵ This discovery led to a better understanding of the constitution of the Grignard reagents. Curiously, it was Fritz who obtained his Ph.D. in 1934 under his father’s guidance; Wilhelm Jr. obtained his Ph.D. at the Technische Hochschule of Berlin with Robert Pschorr in 1929, and his Ph.D. dissertation included his work on Grignard reagents. Wilhelm Jr. published three more papers on organomagnesium chemistry in the *Berichte* as sole author in 1931: on the nature of Grignard reagent solutions, on the preparation of dialkyl- and diarylmagnesium compounds, and on the preparation of ether-free organomagnesium halides.

Schlenk was active in the German Chemical Society. He became its Vice President in 1922 and its President from 1926 to 1928.

(74) (a) Schlenk, W.; Weichselfelder, T. *Ber. Dtsch. Chem. Ges.* **1923**, *56*, 2230. This was an ingeniously devised experiment which must be read in detail for full appreciation of Schlenk’s superb experimental skill. Weichselfelder continued research in this area in Berlin, apparently independently. (b) Weichselfelder, T. *Justus Liebigs Ann. Chem.* **1926**, *447*, 64. (c) Weichselfelder, T. *Ber. Dtsch. Chem. Ges.* **1929**, *62*, 769.

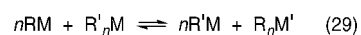
(75) Schlenk, W.; Schlenk, W., Jr. *Ber. Dtsch. Chem. Ges.* **1929**, *62*, 920.

Even before 1933, but certainly after Hitler’s ascension to power in Germany, Schlenk’s life became difficult. He made no secret of his beliefs, which were not in line with those of the National Socialists, and he did not abandon his Jewish friends and colleagues. He became persona non grata in Berlin, the capital. In 1935 he was removed from his chair at the University of Berlin and transferred to the University of Tübingen. There he became Professor of Chemistry and Director of the Chemistry Institute. Tübingen was glad to have him, and during the 7½ years he spent there he was held in high regard. He was busy with teaching, administration, and research, as well as with work on the second volume of his textbook of advanced organic chemistry. (The first had been completed in Berlin in 1932.) With the start of World War II in 1939 things became difficult in the Chemistry Institute. A severe shortage of funds developed. Schlenk had finished the second volume of his textbook in 1939 and had started on a third. The demands on Schlenk’s time were such that he did no further research. He had published his last paper in 1933 (the last one on organoalkali-metal chemistry in 1931). No publications resulted from his years in Tübingen. One last blow came in 1942 when he was expelled from the German Chemical Society (GDCh.). He died during the war in 1943.⁷⁶

The reaction of diorganomercurials with alkali metals is rarely used these days for the preparation of organoalkali-metal compounds. It served Schlenk and Holtz well and was still used in the 1930s, but then the better preparative routes of Ziegler, Wittig, Gilman and Morton (see Part 1) were developed and these became the methods of choice.

IV. Preparation of Organoalkali-Metal Compounds by the Transmetalation Reaction

Another procedure for the preparation of organoalkali-metal compounds is the transmetalation reaction, in which there is substituent exchange between an organoalkali-metal compound and an organic derivative of another metal, usually a heavy metal (mercury, tin, lead, antimony, bismuth, selenium, tellurium), and in a few cases silicon and even phosphorus and iodine (eq 29).



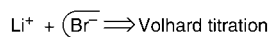
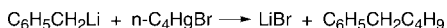
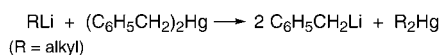
As indicated, and as expected, these are equilibrium reactions. When R and R’ are very similar, e.g., propyl and butyl, the equilibrium constant is close to 1 and the reaction is not synthetically useful. However, the reaction in eq 29 will proceed far to the right, i.e., the equilibrium constant will be large, when R’ is more electronegative than R: i.e., when R’ can more easily accommodate a partial negative charge. Thus the reaction in eq 29 will be synthetically useful when R is alkyl and R’ is an unsaturated group such as aryl, alkynyl, allyl, or vinyl or one that contains electronegative atoms such as halogen, oxygen, and nitrogen.⁷⁷

In 1917, it was Schlenk and Holtz²⁰ who reported the first examples of applications of the transmetalation reaction to the preparation of organoalkali-metal compounds (vide supra). The reaction of ethyllithium with dimethylmercury in petroleum ether

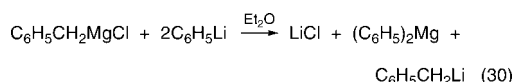
(76) The death notice, published in *Ber. Dtsch. Chem. Ges.* **1943**, *76A*, 59, promised that an obituary would be published in the *Berichte*, but one never appeared, before or after the end of the war. Note ref 21 in the present essay. A rather late recognition of Schlenk’s contributions to the area of organolithium chemistry came with the establishment, in 1997, by the German Chemical Society and the Chemetall Company of the Arfvedson-Schlenk Prize for outstanding contributions to lithium chemistry.

(77) In organic compounds the electronegativity of a carbon atom depends on its hybridization: $\text{C}(\text{sp}^3)$, 2.48; $\text{C}(\text{sp}^2)$, 2.75; $\text{C}(\text{sp})$, 3.29.

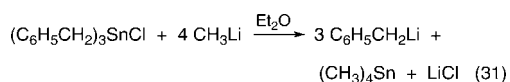
Scheme 13



(eq 18) had been expected to give methyllithium as the only insoluble product. However, here both organic substituents were alkyl groups and the product, as found out later by Weiss,⁴⁶ contained ethyl as well as methyl groups: on the average, it was $(\text{CH}_3)_{0.75}(\text{C}_2\text{H}_5)_{0.25}\text{Li}_4$. More favorable was the preparation of phenyllithium by the reaction of ethyllithium with diphenylmercury (eq 19), which proceeded rapidly far to the right since the more electronegative phenyl group was involved. Phenyllithium was isolated in good purity as a white, microcrystalline powder. Franz Hein and his co-workers at the University of Leipzig, during the course of their thorough studies of the electrochemistry of organoalkali-metal–diethylzinc and triethylaluminum systems, prepared phenyllithium as well as benzylolithium (the latter from dibenzylmercury) by transmetalation.⁷⁸ Ziegler et al. used the $\text{RLi}/(\text{C}_6\text{H}_5\text{CH}_2)_2\text{Hg}$ reaction in an analytical procedure for RLi solutions (Scheme 13).⁶³ The detour shown in Scheme 13 had to be taken because an alternate procedure, the alkyllithium/*n*-butyl bromide reaction, was a slow one with an unfavorable equilibrium constant. An alternate route to benzylolithium was developed by Ziegler and Derch (eq 30).⁷⁹



This procedure also was used for the conversion of *i*-C₃H₇MgCl to *i*-C₃H₇Li, a reagent whose present preparation by the direct reaction of isopropyl chloride with lithium metal was at that time not successful. Benzylolithium was prepared by Gilman and Rosenberg by the reaction of phenyllithium with benzyltriphenyltin (prepared by an organomagnesium route⁸⁰). A more practical starting material is tribenzyltin chloride, which is readily prepared by the reaction of benzyl chloride with metallic tin in boiling water. Its reaction with phenyllithium provides 3 molar equiv of benzylolithium per tin (eq 31).⁸¹ An organoantimony route to benzylolithium, the reaction of tribenzylstibine with 3 molar equiv. of ethyllithium in benzene also was reported.⁸² Benzylolithium is not soluble in benzene and precipitated as a lemon-yellow solid.



Many Ar_mM/alkyllithium exchange reactions, which produced ArLi reagents in moderate to high yield, have been reported,

(78) Hein, F.; Petzchner, E.; Wagler, K.; Segitz, F. A. Z. *Anorg. Allg. Chem.* **1924**, 141, 161.

(79) Ziegler, K.; Derch, F. *Ber. Dtsch. Chem. Ges.* **1931**, 64, 448 (preliminary notice in ref 66).

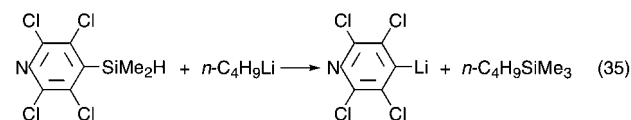
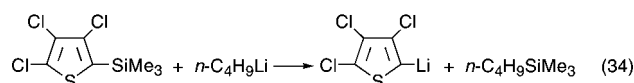
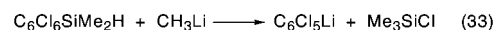
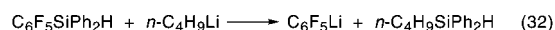
(80) Gilman, H.; Rosenberg, S. D. *J. Org. Chem.* **1959**, 24, 2063.

(81) Seyferth, D.; Suzuki, R.; Murphy, C. J.; Sabet, C. R. *J. Organomet. Chem.* **1964**, 2, 431.

(82) Talalaeva, T. V.; Kocheshkov, K. A. *Izv. Akad. Nauk SSSR, Otdel. Khim. Nauk* **1953**, 290; *Chem. Abstr.* **1954**, 48, 6389.

principally by Gilman and his co-workers⁸³ and by Kocheshkov in the USSR.⁸⁴ Since other routes to aryllithiums (ArX + Li; ArBr + RLi) are more practical, preparation of aryllithiums by transmetalation is not synthetically useful. Gilman investigated such reactions when he was studying relative reactivities of series of various organometallic compounds with various reagents under varying conditions (in James Flack Norris style research), trying to gain mechanistic insight. Reaction of aryl and mixed aryl compounds of mercury, tin, lead, antimony, and bismuth, usually with *n*-butyl- or ethyllithium, were studied.

Perhalophenyl- and perhaloheterocyclic lithium compounds have been prepared by lithium/silicon transmetalation (eqs 32–35).^{85,86} The reaction temperatures must be kept low (–70 °C) in order to avoid secondary lithium-halogen exchange reactions. Transmetalations involving silicon compounds occur only when the substituent on silicon is very electronegative, as in the examples noted above and in alkylnylsilanes. Pentafluoro- and pentachlorophenyllithium, however, are more readily prepared by lithium-halogen exchange.



The transmetalation reaction found its most useful applications in the preparation of unsaturated and functionally substituted organolithium reagents. New alkyl- and aryl-substituted vinylic lithium reagents could be prepared by the reaction of lithium metal with a substituted vinylic bromide⁸⁷ and, later, by the lithium–halogen exchange reaction between the vinylic bromide and 2 molar equiv of *tert*-butyllithium.⁸⁸ However, vinylolithium itself is not readily prepared by such procedures, and the transmetalation reactions of the easily prepared vinyltin compounds with phenyl- and *n*-butyllithium serve excellently in its preparation.⁸⁹ With tetravinyltin as starting material, when

(83) A selection: (a) Gilman, H.; Bebb, R. L. *J. Am. Chem. Soc.* **1939**, 61, 109. (b) Gilman, H.; Yablunsky, H. L.; Svigoon, A. C. *J. Am. Chem. Soc.* **1939**, 61, 1170. (c) Gilman, H.; Jones, R. G. *J. Am. Chem. Soc.* **1940**, 62, 2357. (d) Gilman, H.; Moore, F. W. *J. Am. Chem. Soc.* **1940**, 62, 3206. (e) Gilman, H.; Jones, R. G. *J. Am. Chem. Soc.* **1941**, 63, 1439; 1441. (f) Gilman, H.; Moore, F. W. *J. Am. Chem. Soc.* **1941**, 63, 2482. (g) Gilman, H.; Yale, H. L. *J. Am. Chem. Soc.* **1950**, 72, 8. (h) Gilman, H.; Rosenberg, S. D. *J. Org. Chem.* **1959**, 24, 2063.

(84) (a) Talalaeva, T. V.; Kocheshkov, K. A. *Izv. Akad. Nauk SSSR, Otdel. Khim. Nauk* **1953**, 126, 290; *Chem. Abstr.* **1954**4832856389. (b) Talalaeva, T. V.; Kocheshkov, K. A. *Dokl. Akad. Nauk SSSR* **1951**, 77, 621; *Chem. Abstr.* **1951**4510191. (c) Zasosov, V. A.; Kocheshkov, K. A. *Sbornik. Statei. Obshch. Khim., Akad. Nauk SSSR* **1953**, 1, 285; *Chem. Abstr.* **1955**48913.

(85) Fearon, F. W. G.; Gilman, H. *J. Organomet. Chem.* **1967**, 10 (409), 535.

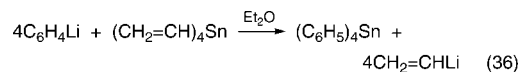
(86) Smith, M. R., Jr.; Gilman, H. *J. Organomet. Chem.* **1972**, 37, 35.

(87) Braude, E. A.; Coles, J. A. *J. Chem. Soc.* **1951**, 2078, 2085.

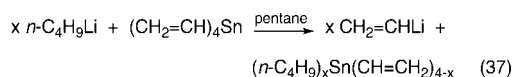
(88) Corey, E. J.; Beames, D. J. *J. Am. Chem. Soc.* **1972**, 94, 7210.

(89) (a) Seyferth, D.; Weiner, M. A. *Chem. Ind. (London)* **1959**, 402. (b) Seyferth, D.; Weiner, M. A. *J. Am. Chem. Soc.* **1961**, 83, 3583.

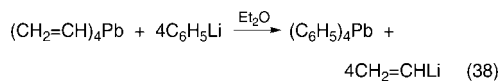
phenyllithium is the organolithium reagent used in a 4:1 molar ratio, the reaction shown in eq 36 takes place.



Tetraphenyltin has a very low solubility in diethyl ether (which may be decreased further by cooling the system when the reaction is complete); therefore, a reasonably pure ether solution containing a high yield of vinyl lithium results. (The vinyl lithium solution may contain some LiBr from the phenyllithium preparation.) Vinyltriphenyltin, which is more easily prepared than tetra vinyltin, also has been used as the vinyl group source. This procedure serves excellently when reactions of vinyl lithium with electrophiles are intended. Vinyl lithium is stable in diethyl ether at room temperature; therefore, the precautions required with ether solutions of ethyl- and *n*-butyllithium are not needed. If solid samples of vinyl lithium or solutions of this reagent that do not contain any impurities are desired, the reaction shown in eq 37



has proven useful. In pentane the equilibrium is such that the reaction does not go to completion and for synthetic purposes the optimum value of *x* is 2.0–2.5. In this solvent *n*-butyllithium and the tin compounds are soluble while vinyl lithium is not. Thus, pure samples can be obtained by filtration under an inert atmosphere and thorough washing with pentane. This procedure was used when the ¹H NMR spectrum of vinyl lithium in diethyl ether solution was obtained.⁹⁰ As expected, the reaction of tetra vinyllead with 4 molar equiv of phenyllithium in diethyl ether gave vinyl lithium and insoluble tetraphenyllead, both in high yield (eq 38).^{16c}



cis- and *trans*-propenyl lithium were prepared by reaction of 4 molar equiv of phenyllithium in diethyl ether with tetra-*cis*-propenyl- and tetra-*trans*-propenyltin, respectively.⁹¹ Since the conversion of (*cis*-CH₃CH=CH)₄Sn to the propenyl lithium was not complete, in order to perform ¹H NMR measurements, samples of the two lithium reagents were prepared by the reaction of *trans*-propenyltrimethyltin with 1 molar equiv of methyl lithium and of *cis*-propenyltrimethyltin with 2 molar equiv of methyl lithium. This approach resulted in clean ¹H NMR spectra in each case and showed that the propenyltin to propenyl lithium transmetalation occurred with retention of geometric configuration^{91,92} and that each isomeric propenyl lithium was configurationally stable in solution (in agreement with earlier cited work of Braude, Curtin, and Nesmeyanov). Each isomeric propenyl lithium reacted with electrophiles with retention of configuration (Scheme 14 shows these reactions for *trans*-CH₃CH=CHLi; a similar scheme can be written for the *cis* isomer). Since the transmetalations noted above appeared to indicate that they were equilibrium processes, this question was investigated by carrying out both reactions in the reverse as well as in the forward direction, in each case quenching the reaction mixture with trimethylchlorosilane. The results of these experiments are given in Table 3. It is clear that these are

Scheme 14

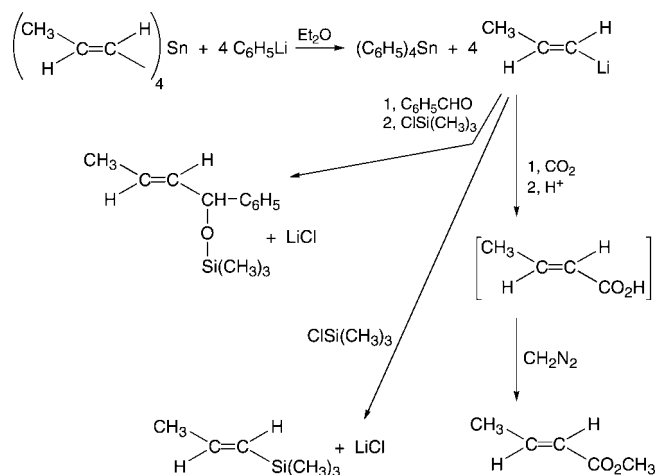
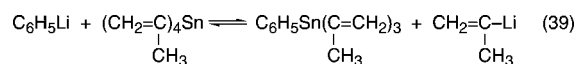


Table 3. Transmetalation Equilibria, Tetrapropenyltin Isomers

<i>cis</i> -CH ₃ CH=CH) ₄ Sn + 4C ₆ H ₅ Li ⇌ (C ₆ H ₅) ₄ Sn + 4 <i>cis</i> -CH ₃ CH=CHLi			
reacn	% (C ₆ H ₅) ₄ Sn	% <i>cis</i> -CH ₃ CH=CHLi ^a	% C ₆ H ₅ Li ^a
forward	50–56	49	29
reverse	51	46	25
<i>trans</i> -CH ₃ CH=CH) ₄ Sn + 4C ₆ H ₅ Li ⇌ (C ₆ H ₅) ₄ Sn + 4 <i>trans</i> -CH ₃ CH=CHLi			
reacn	% (C ₆ H ₅) ₄ Sn	% <i>trans</i> -CH ₃ CH=CHLi ^a	% C ₆ H ₅ Li ^a
forward	70–81	61	not detd
reverse	79	69	20

^a Yield of trimethylsilyl derivative.

equilibrium processes.⁹³ The existence of such an equilibrium was shown strikingly by the reaction of tetra isopropenyltin [CH₂=C(CH₃)₂]₄Sn, with 4 mol equiv of phenyllithium in diethyl ether.⁹¹ No tetraphenyltin precipitated, and only a low equilibrium yield of isopropenyl lithium was present. A study of both forward [(isopropenyl)₄Sn + 4C₆H₅Li and reverse [(C₆H₅)₄Sn + 4(isopropenyl)Li] indicated that the equilibrium involved is best written as shown in eq 39.



Other vinylic lithium reagents prepared using organotin precursors include *trans*-β-styryllithium (eq 40),⁹⁴ *trans*-(CH₃)₃SiCH=CHLi,⁹⁵ EtOCH=CHLi,⁹⁶ and THP-OCH₂CH=CHLi (THP = tetrahydropyranyl),⁹⁷ all prepared by the acetylene → vinylic tin → vinylic lithium process shown in eq 40, and CH₂=C(F)Li⁹⁸ and perfluorovinyl lithium (eq 41).⁹⁹ Addition of (CH₃)₃SnBr to such a solution of CF₂=CFLi gave (CH₃)₃SnCF=CF₂ in 64% yield. In contrast to vinyl lithium,

(93) For reviews on vinyl- and propenyl lithium chemistry see: (a) Seyferth, D.; Weiner, M. A.; Vaughan, L. G.; Raab, G.; Welch, D. E.; Cohen, H. M.; Alleston, D. L. *Bull. Soc. Chim. Fr.* **1963**, 1364 (in English). (b) Seyferth, D. *Rec. Chem. Progr.* **1965**, 26, 86.

(94) Seyferth, D.; Vaughan, L. G.; Suzuki, R. *J. Organomet. Chem.* **1964**, 1, 437.

(95) Seyferth, D.; Vick, S. C. *J. Organomet. Chem.* **1978**, 144, 1.

(96) (a) Ficini, J.; Falou, S.; Touzin, A.-M.; d'Angel, J. *Tetrahedron Lett.* **1977**, 3589. (b) Wollenberg, R. H.; Albizzati, K. F.; Peries, R. *J. Am. Chem. Soc.* **1977**, 99, 7365.

(97) Corey, E. J.; Wollenberg, R. H. *J. Org. Chem.* **1975**, 40, 2265.

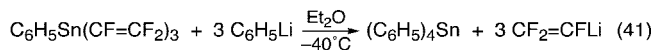
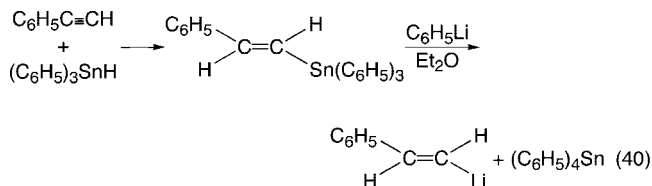
(98) Mathews, D. P.; Wald, P. P.; Sabol, J. S.; McCarthy, J. R. *Tetrahedron Lett.* **1994**, 35, 5177.

(99) (a) Seyferth, D.; Wada, T.; Raab, G. *Tetrahedron Lett.* **1960**, 22, 20. (b) Seyferth, D.; Welch, D. E.; Raab, G. *J. Am. Chem. Soc.* **1962**, 84, 4266.

(90) Johnson, C. S.; Weiner, M. A.; Waugh, J. S.; Seyferth, D. *J. Am. Chem. Soc.* **1961**, 83, 1306.

(91) Seyferth, D.; Vaughan, L. G. *J. Am. Chem. Soc.* **1964**, 86, 883.

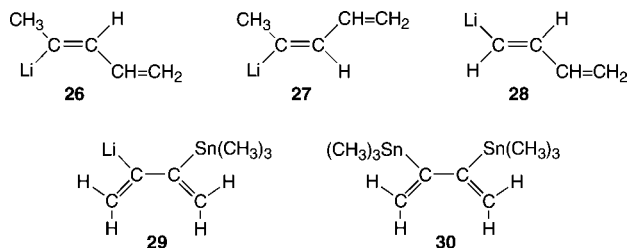
(92) Seyferth, D.; Vaughan, L. G. *J. Organomet. Chem.* **1963**, 1, 201.



perfluorovinyl lithium is not very stable in diethyl ether solution. Its solutions, even at -40°C , are dark brown and at 0°C no longer contained any active lithium reagent. Small-scale attempts to prepare concentrated solutions of $\text{CF}_2=\text{CFLi}$ in ether or pentane for ^{19}F NMR spectroscopic studies always resulted in rapid decomposition and occasional violent explosions. Possibly (but unproven), β -elimination to give difluoroacetylene occurred.

Attempts to prepare 1,2-dilithioethylene by transmetalation were unsuccessful. However, *trans*-($n\text{-C}_4\text{H}_9$)₃SnCH=CHSn($n\text{-C}_4\text{H}_9$)₃ was treated successively with 1 molar equiv each of $n\text{-C}_4\text{H}_9\text{Li}$, an electrophile, *n*-butyllithium, and a second electrophile (Scheme 15; the overall yield was 63%).⁹⁵

Li/Sn transmetalation has served in the synthesis of lithium derivatives of 1,3-dienes. Prepared from the respective trialkyltin derivatives were **26** and **27**,^{100a} **28**,^{100b} and **29**.^{100c,d} Lithium



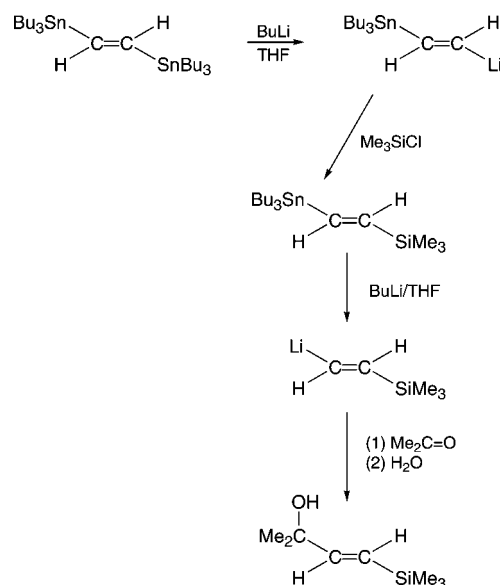
reagent **29** and its bis(trimethyltin) precursor **30** are of particular interest. Both trimethyltin groups of **30** can be replaced by lithium, either directly from **30** or in two steps, via **29**. The chemistry involved in these conversions turned out to be rather complicated. After it had been sorted out by chemical and spectroscopic studies, the conclusion was that the first step, reaction of **30** with 1 equiv of CH_3Li in THF, occurred readily at -78°C . The second step, conversion of **29** to a dilithium reagent, was slower and required a higher temperature, -50°C . The dilithium reagent formed was not the expected 2,3-dilithio-1,3-butadiene; rather, it was an isomerized product, $\text{LiCH}_2\text{C}\equiv\text{CCH}_2\text{Li}$.^{100d} A two-step procedure, formation of **29** and its reaction with $(\text{CH}_3)_3\text{SiCl}$, followed by Li/Sn exchange of the product and addition of a second equivalent of trimethylchlorosilane, served to give 2,3-bis(trimethylsilyl)-1,3-butadiene.

(100) (a) Piers, E.; Morton, H. E. *J. Org. Chem.* **1980**, *45*, 4263. (b) Wender, P. A.; Sieburth, S. M.; Petraitis, J. J.; Singh, S. K. *Tetrahedron* **1981**, *37*, 3967. (c) Reich, H. J.; Yelm, K. E.; Reich, I. L. *J. Org. Chem.* **1984**, *49*, 3438. (d) Reich, H. J.; Reich, I. L.; Yelm, K. E.; Holladay, J. E.; Gschneider, D. *J. Am. Chem. Soc.* **1993**, *115*, 6625. (e) Westmijze, H.; Ruitenbergh, K.; Meijer, J.; Vermeer, P. *Tetrahedron Lett.* **1982**, *23*, 2797.

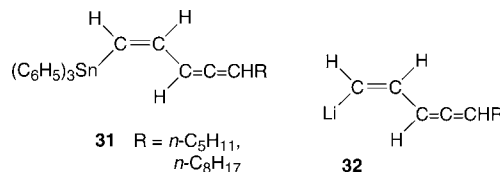
(101) (a) Barros, S. M.; Comasseto, J. V.; Berriet, J. *Tetrahedron Lett.* **1989**, *30*, 7353. (b) Zeni, G.; Lütke, D. S.; Panatieri, R. B.; Braga, A. L. *Chem. Rev.* **2006**, *106*, 1032. (c) Reich, H. J.; Willis, W. W.; Clark, P. D. *J. Org. Chem.* **1981**, *46*, 2775.

(102) Allylic lithium reagents are ambident nucleophiles: i.e., they can form the new C–C or C–element bond on reaction with an electrophile at either terminal carbon atom (α or γ). For this reason I write them as shown for allyllithium itself or as $\text{Li}(\text{CH}_2\text{CHCHR})$ in the case of a monosubstituted reagent. This says nothing about their solid-state and solution structures.

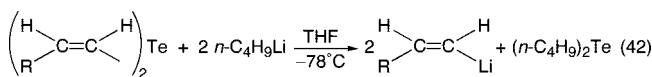
Scheme 15



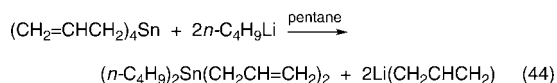
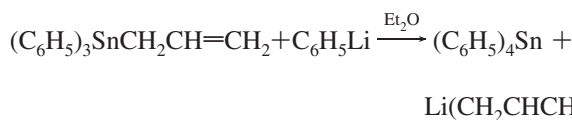
diene. Of interest also is the reaction of **31** with $n\text{-C}_4\text{H}_9\text{Li}$ in diethyl ether at -55°C to form the lithium reagent **32**.^{100e}



In addition to vinylic tin and lead compounds, vinylic tellurium^{101a,b} and selenium^{101c} compounds have served as precursors for vinylic lithium reagents (eq 42).

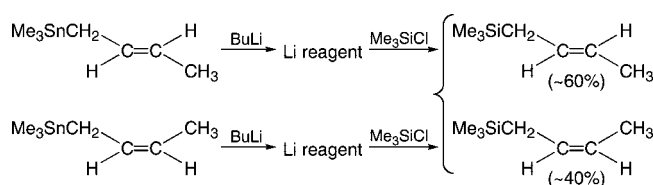


Allyllithium, $\text{Li}(\text{CH}_2\text{CHCH}_2)$, and diverse substituted allylic lithium reagents¹⁰² also can be prepared by the transmetalation reaction using allylic tin or lead compounds as starting materials. The same procedures that were developed for the preparation of vinyl lithium in ether solution or as the solid were found to be applicable to the preparation in good yield of allyllithium in ether solution or as the pure solid (eq 43 and 44).¹⁰³ Allyltriphenyltin, which can be prepared very easily in high yield by the Barbier procedure, is a better starting material than tetraallyltin, whose preparation is more difficult. In eq 43 it is tetraphenyltin that is the poorly soluble component; in pentane (eq 44) it is allyllithium. Solid allyllithium, a white solid, is violently pyrophoric on exposure to air.

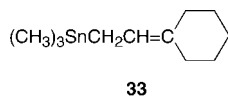


(103) (a) Seyferth, D.; Weiner, M. A. *J. Org. Chem.* **1959**, *24*, 1395. (b) Seyferth, D.; Weiner, M. A. *J. Org. Chem.* **1961**, *26*, 4797.

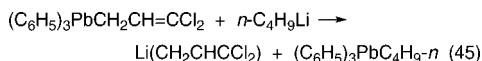
Scheme 16



Various methyl-substituted allylic lithium reagents were prepared by Li/Sn transmetalation. Methallyllithium, $\text{Li}(\text{CH}_2\text{C}(\text{CH}_3)\text{CH}_2)$, was prepared in diethyl ether solution by reaction of phenyllithium with methallyltriphenyltin.¹⁰³ Both *cis*- and *trans*-crotyltrimethyltin reacted with *n*-butyl- or methyl lithium to give crotyllithium, $\text{Li}(\text{CH}_2\text{CHCHCH}_3)$, in high yield.¹⁰⁴ In each case, reaction of the resulting lithium reagent solution with trimethylchlorosilane gave an approximately 3:2 mixture of *trans*- and *cis*-crotyltrimethylsilane (Scheme 16).¹⁰⁴ Since a ca. 3:2 mixture of *trans*- and *cis*-crotyllithium resulted, irrespective of the configuration of the starting crotyltrimethyltin that was used, the applications of crotyllithium in synthetic chemistry do not require the use of isomerically pure crotyltin starting material. It was found convenient to use crotyltriphenyltin, prepared by the Barbier procedure, as a mixture of *cis* and *trans* isomers in a 1:1 reaction with phenyllithium in ether. Because these transmetalation reactions are equilibrium processes, a catalytic amount of methyl- or *n*-butyllithium is sufficient to cause isomerization of pure *trans*- and *cis*-crotyltrimethyltin in ether solution to a 3:2 mixture of *trans*- and *cis*-crotyllithium in ether solution to a 3:2 mixture of *trans*- and *cis*-crotyltrimethyltin. In another study, four substituted allyltrimethyltin compounds, $(\text{CH}_3)_3\text{SnCH}_2\text{CH}=\text{CHC}_6\text{H}_{13-n}$, (30/70 *cis*/*trans*), $(\text{CH}_3)_3\text{SnCH}_2\text{CH}=\text{CHC}_6\text{H}_5$ (*trans* isomer), $(\text{CH}_3)_3\text{SnCH}_2\text{C}(\text{CH}_3)=\text{CHC}_2\text{H}_5$ and **33**, all prepared from



$(\text{C}_6\text{H}_5)_3\text{P}=\text{CHCH}_2\text{Sn}(\text{CH}_3)_3$ by the Wittig synthesis, were converted to the respective allylic lithium reagent by reaction with methyl lithium in THF/Et₂O solution.¹⁰⁵ These substituted lithium reagents as well as crotyllithium are of interest, since they can react with electrophiles to form the new C–C or C–element bond at the α (CH_2) or the γ terminus of the allyl group. Scheme 17 shows as an example the α,γ ratios observed in the products of some reactions of $\text{Li}(\text{CH}_2\text{CHCH}_6\text{H}_5)$. The *gem*-dihaloallyllithiums $\text{Li}(\text{CH}_2\text{CHCX}_2)$ also are ambident reagents, forming the new bond at either the α - or the γ -carbon atom, sometimes giving a mixture of products of both α and γ addition. *gem*-Dichloroallyllithium¹⁰⁶ was prepared by reaction of *n*-butyllithium with 3,3-dichloroallyltriphenyllead in THF–hexane medium at $-95\text{ }^\circ\text{C}$ (eq 45).



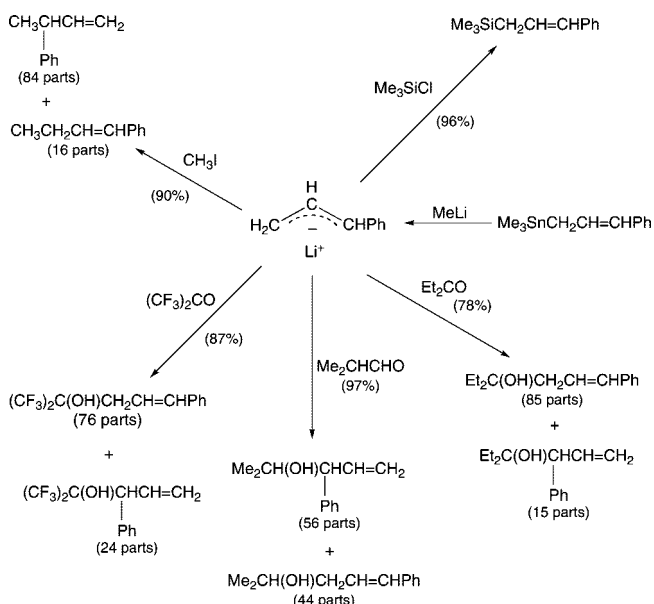
At the extremes, its reaction with $(\text{CH}_3)_2\text{C}=\text{O}$ gave, after

(104) (a) Seyferth, D.; Jula, T. F. *J. Organomet. Chem.* **1967**, 8, P13. (b) Seyferth, D.; Jula, T. F. *J. Organomet. Chem.* **1974**, 66, 195.

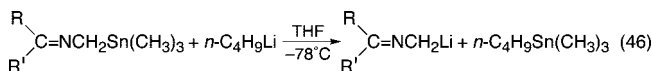
(105) (a) Seyferth, D.; Wursthorn, K. R.; Mammarella, R. E. *J. Org. Chem.* **1977**, 42, 3104. (b) Seyferth, D.; Mammarella, R. E. *J. Organomet. Chem.* **1979**, 177, 53.

(106) (a) Seyferth, D.; Murphy, G. J.; Woodruff, R. A. *J. Organomet. Chem.* **1974**, 66, C29. (b) Seyferth, D.; Murphy, G. J.; Woodruff, R. A. *J. Organomet. Chem.* **1977**, 141, 71. (c) Seyferth, D.; Murphy, G. J.; Woodruff, R. A. *J. Am. Chem. Soc.* **1974**, 96, 5011. (d) Seyferth, D.; Murphy, G. J.; Mauzé, B. *J. Am. Chem. Soc.* **1977**, 99, 5317.

(107) (a) Seyferth, D.; Wursthorn, K. R. *J. Organomet. Chem.* **1977**, 137, C17. (b) Seyferth, D.; Wursthorn, K. R. *J. Organomet. Chem.* **1979**, 182, 456.

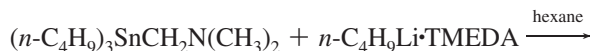
Scheme 17. Reactions of Phenylallyllithium, $\text{Li}(\text{CH}_2\text{CHCH}_6\text{H}_5)$ 

hydrolytic workup, $(\text{CH}_3)_2\text{C}(\text{OH})\text{CCl}_2\text{CH}=\text{CH}_2$ as the sole product, while only $(\text{CF}_3)_2\text{C}(\text{OH})\text{CH}_2\text{CH}=\text{CCl}_2$ was obtained in its reaction with $(\text{CF}_3)_2\text{C}=\text{O}$. (*gem*-Difluoroallyl)lithium, prepared by reaction of *n*-butyllithium with $(\text{CH}_3)_2\text{SnCH}_2\text{CH}=\text{CF}_2$ in THF at $-95\text{ }^\circ\text{C}$,¹⁰⁸ showed similar ambident reactivity. Another allylic lithium reagent, $\text{Li}[(\text{CH}_3)_3\text{Si}(\text{Cl})\text{CCH}_2]$, was prepared by Li/Pb transmetalation from $(\text{C}_6\text{H}_5)_3\text{PbCH}_2\text{CH}=\text{C}(\text{Cl})\text{Si}(\text{CH}_3)_3$ and *n*-butyllithium in THF at $-90\text{ }^\circ\text{C}$.¹⁰⁹ Of interest are the (2-azaallyl)lithium reagents, generated by Pearson et al.¹¹⁰ by Li/Sn transmetalation (eq 46), which were found to undergo inter- or intramolecular $[\pi_4s + \pi_2s]$ cycloaddition with olefins and acetylenes.



Alkenyltin compounds in which the C=C bond is separated from the tin atom by more than one CH_2 group do not undergo Li/Sn metalation. Thus, $(n\text{-C}_4\text{H}_9)_2\text{SnCH}_2\text{CH}_2\text{CH}=\text{CH}_2$ and $(n\text{-C}_4\text{H}_9)_2\text{Sn}(\text{CH}_2\text{CH}_2\text{CH}_2\text{CH}=\text{CH}_2)_2$ did not react with *n*-butyllithium in diethyl ether.¹¹¹

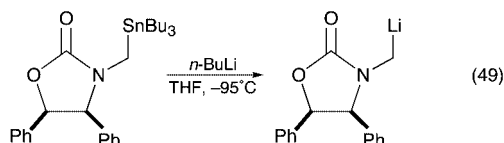
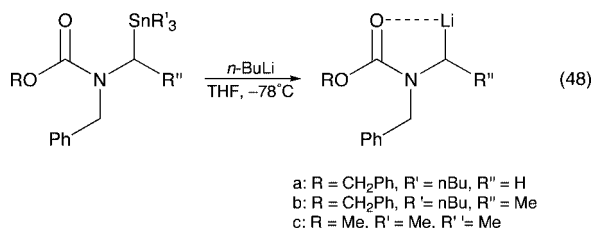
A useful and widely used application of the transmetalation reaction, specifically of Li/Sn exchange, has been in the preparation of functionally substituted organolithium reagents. It was Donald Peterson's 1967 communication which opened up this new application of the Li/Sn transmetalation reaction. The reaction of (dimethylaminomethyl)tri-*n*-butyltin with the *n*-butyllithium *N,N,N'*-tetramethylethylenediamine (TMEDA) complex (vide infra) was reported to give (dimethylaminomethyl)lithium in high yield (eq 47).¹¹²



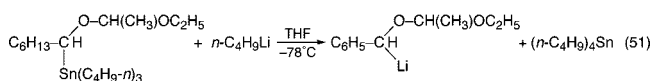
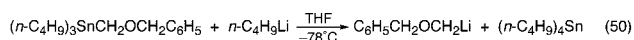
Using aminomethyltin derivatives with different substituents on the nitrogen atom, Peterson established the generality of this reaction.¹¹³ This Li/Sn exchange could be applied to more

(108) (a) Seyferth, D.; Simon, R. M.; Sepelak, D. J.; Klein, H. A. *J. Org. Chem.* **1980**, 45, 2273. (b) Seyferth, D.; Simon, R. M.; Sepelak, D. J.; Klein, H. A. *J. Am. Chem. Soc.* **1983**, 105, 4634.

complicated aminomethyltin compounds (eqs 48 and 48.).¹¹⁴



Because of their synthetic utility, α -aminoalkyllithium reagents have received more detailed study in recent years. Of interest is that there are cases where the attempted Li/Sn transmetalation is not successful for thermodynamic reasons, i.e., when *n*-butyllithium is more stable than the desired α -aminoalkyllithium compound, and whatever the mechanism may be (vide infra), the reaction does not proceed in the forward direction.¹¹⁵ α -Alkoxyalkyllithium reagents are of interest for their applications in synthetic organic chemistry. These also are readily prepared by Li/Sn transmetalation. Thus, Clark Still in 1978 reported reactions such as those shown in eqs 50 and 51.^{116a} The yields of the α -alkoxyalkyl-



lithium reagents were 98+%. Still carried out some experiments to probe why the equilibria appeared to favor such reagents to such an extent but reached no useful conclusion. The α -alkoxyalkyllithium reagents produced in such reactions were found to be configurationally stable.^{116b} The synthesis of α -alkoxyalkyllithium reagents (and their subsequent use in synthesis) was made more generally useful by a new general preparation of α -alkoxyalkyltin starting materials by Corey and Eckrich (Scheme 18).¹¹⁷ The yields of C=O addition products of benzaldehyde varied with the R group in the ROCH₂Sn compounds used: R = *tert*-C₄H₉, 95%; R = C₆H₅CH₂, 86%; R = CH₃OCH₂CH₂, 82; R = C₆H₅, 78; R = CH₃, 65.

(109) Seyferth, D.; Mammarella, R. E. *J. Organomet. Chem.* **1978**, *156*, 279.

(110) Pearson, W. H.; Szura, D. P.; Postich, M. J. *J. Am. Chem. Soc.* **1992**, *114*, 1329.

(111) Seyferth, D.; Weiner, M. A. *J. Am. Chem. Soc.* **1962**, *84*, 361.

(112) Peterson, D. J. *J. Organomet. Chem.* **1970**, *21*, P63.

(113) (a) Peterson, D. J. *J. Organomet. Chem.* **1971**, *66*, 209. (b) Peterson, D. J. *J. Am. Chem. Soc.* **1971**, *93*, 4027. (c) Peterson, D. J. *J. Am. Chem. Soc.* **1975**, *97*, 159.

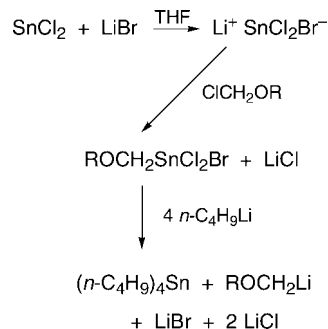
(114) (a) Pearson, W. H.; Lindbeck, A. C. *J. Org. Chem.* **1989**, *54*, 5654. (b) Pearson, W. H.; Lindbeck, A. C. *J. Am. Chem. Soc.* **1991**, *113*, 8546.

(115) Klein, R.; Gawley, R. E. *J. Am. Chem. Soc.* **2007**, *120*, 4126, and references cited therein.

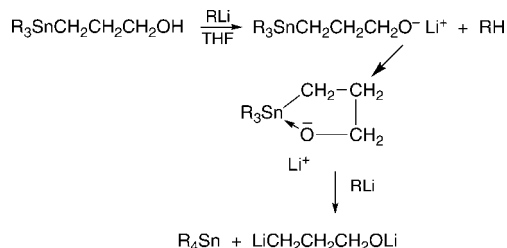
(116) (a) Still, W. C. *J. Am. Chem. Soc.* **1978**, *100*, 1481. (b) Still, W. C.; Sreekumar, C. *J. Am. Chem. Soc.* **1980**, *102*, 1201.

(117) Corey, E. J.; Eckrich, T. M. *Tetrahedron Lett.* **1983**, *24*, 3163.

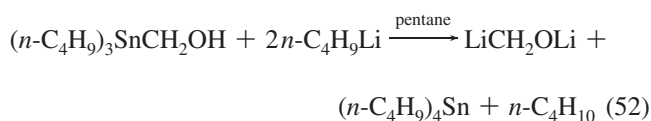
Scheme 18



Scheme 19

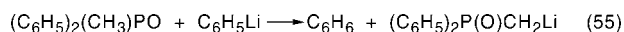
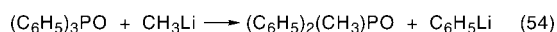
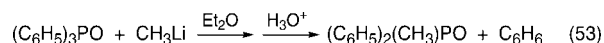


The reaction of 2 molar equiv of *n*-butyllithium with hydroxymethyltri-*n*-butyltin gave the novel dilithio reagent LiCH₂OLi (eq 52).¹¹⁸



Its reaction with benzaldehyde, followed by hydrolytic workup, afforded (C₆H₅CH(OH)CH₂OH; with *n*-octyl chloride, 1-nonanol was the product. As expected, the vinylic tin compounds (*n*-C₄H₉)₃SnCH=CHCH₂OH reacted with 2 molar equiv of *n*-butyllithium at -25 °C in pentane to give LiCH=CHCH₂OLi. Unexpectedly, the saturated (*n*-C₄H₉)₃SnCH₂CH₂CH₂OH reacted in the same manner (at -30 °C in THF), giving LiCH₂CH₂CH₂OLi.¹¹⁸ Although the authors did not comment on this observation, it is possible that in the latter reaction the attack by *n*-butyllithium at the tin atom is facilitated by an Sn-alkoxide ion interaction (Scheme 19). It is known that nucleophilic displacement reactions at a group 14 atom are facilitated by formation of a pentacoordinate intermediate.

The (*n*-C₄H₉)₃CH₂CH₂CH₂OH/2 *n*-butyllithium reaction is a deprotonation/transmetalation sequence. A transmetalation/deprotonation (metalation) sequence is the reaction course when 1 molar equiv of methylithium is added to triphenylphosphine oxide or sulfide.¹¹⁹ The reaction of methylithium with (C₆H₅)₃PO, with hydrolytic workup, is shown in eq 53. A detailed study of the reaction showed that it proceeded in two steps: (1) transmetalation (eq 54) and (2) metalation (eq 55).

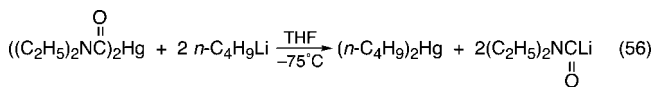


Hydrolysis gave benzene and the initially observed (C₆H₅)₂(CH₃)PO, but the lithium reagent could be intercepted with other electrophiles, e.g., (C₆H₅)₃SnCl, to give (C₆H₅)₂P(O)CH₂Sn(C₆H₅)₃. The two steps occurred at competi-

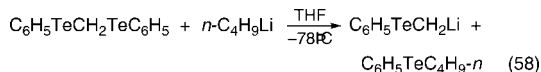
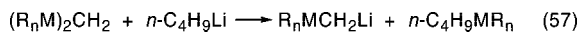
(118) Meyer, N.; Seebach, D. *Chem. Ber.* **1980**, *113*, 1290.

tive rates in the case of CH_3Li , but when the less reactive CH_3MgBr was used, the two steps could be studied separately.^{119b} In THF solution at room temperature only the transmetalation reaction occurred, giving $(\text{C}_6\text{H}_5)_2(\text{CH}_3)\text{PO}$ and $\text{C}_6\text{H}_5\text{MgBr}$. When this reaction mixture was heated at reflux, metalation, giving C_6H_6 and $(\text{C}_6\text{H}_5)_2\text{P}(\text{O})\text{CH}_2\text{MgBr}$, occurred. The $(\text{C}_6\text{H}_5)_3\text{PS}/\text{CH}_3\text{Li}$ reaction did not take place in diethyl ether, but addition of THF resulted in formation of a deep red solution of $(\text{C}_6\text{H}_5)_2\text{P}(\text{S})\text{CH}_2\text{Li}$.^{119c}

As a further example of the utility of the transmetalation reaction in organic synthesis is Schöllkopf and Gerhart's preparation of diethylcarbomoyllithium (eq 56).¹²⁰ Addition of a ketone to the reaction mixture gave the expected $(\text{C}_2\text{H}_5)_2\text{NC}(\text{O})\text{C}(\text{OH})\text{R}_2$.

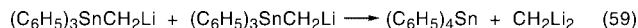


A number of organolithium reagents containing an organometallic or organometalloidal substituent have been prepared. A useful, general procedure for the preparation of such compounds was developed by Dieter Seebach, who applied it to the preparation of (α -phenylselenomethyl)-^{121,122} and (α -phenyltelluromethyl)lithium reagents.¹²³ This protocol involved the preparation of a starting material containing two or more of the organometallic or organometalloidal groups in question and displacing one of them with an organolithium reagent (eq 57). Thus, reaction of 1 molar equiv of *n*-butyllithium with $(\text{C}_6\text{H}_5\text{Se})_3\text{CCH}_3$ in THF at -78°C gave $(\text{C}_6\text{H}_5\text{Se})_2(\text{CH}_3)\text{CLi}$, while $(\text{C}_6\text{H}_5\text{Se})_2\text{CH}_2$ gave $\text{C}_6\text{H}_5\text{SeCH}_2\text{Li}$. $(\text{C}_6\text{H}_5\text{Te})_2\text{CH}_2$ reacted in a similar manner (eq 58). Such Li/Se transmetalation has been used to prepare α -lithioalkylsilanes from $\text{RSeCH}(\text{R}')\text{Si}(\text{CH}_3)_3$ selenides.¹²⁴



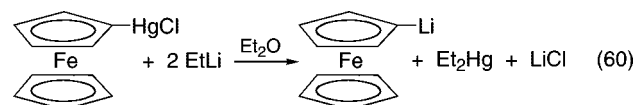
This general procedure has been used by Thomas Kauffmann and his co-workers at the University of Münster to prepare some novel group 14 and group 15 substituted organolithium compounds. Thus, reaction of $[(\text{C}_6\text{H}_5)_3\text{Sn}]_2\text{CH}_2$ with $\text{C}_6\text{H}_5\text{Li}$ in THF at -70°C gave $(\text{C}_6\text{H}_5)_4\text{Sn}$ and $(\text{C}_6\text{H}_5)_3\text{SnCH}_2\text{Li}$.¹²⁵ A curious feature of this reaction was that when the $(\text{C}_6\text{H}_5)_3\text{SnCH}_2\text{Li}$ reagent solution was hydrolyzed, the yield of $(\text{C}_6\text{H}_5)_3\text{SnCH}_3$, the expected hydrolysis product of the lithium reagent, was only 36%, while a 116% yield of tetraphenyltin was reported. A possible explanation for this could be a destructive self-reaction

(eq 59) which increases the yield of tetraphenyltin while diminishing the $(\text{C}_6\text{H}_5)_3\text{SnCH}_2\text{Li}$ yield.

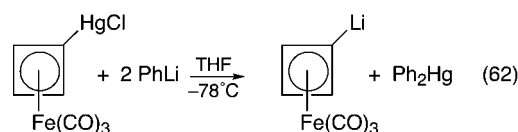
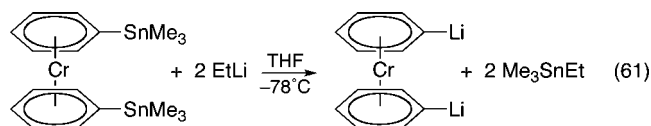


In the organolead series,¹²⁶ reaction of $[(\text{C}_6\text{H}_5)_3\text{Pb}]_2\text{CH}_2$ with $\text{C}_6\text{H}_5\text{Li}$ in THF at -70°C gave $(\text{C}_6\text{H}_5)_3\text{PbCH}_2\text{Li}$ in nearly quantitative yield. This reagent was fairly stable in solution to 20°C . In a similar manner, $[(\text{C}_6\text{H}_5)_3\text{Pb}]_3\text{CH}$ could be converted to $[(\text{C}_6\text{H}_5)_3\text{Pb}]_2\text{CHLi}$ by reaction with phenyllithium. Reaction of phenyllithium with $[(\text{C}_6\text{H}_5)_3\text{Pb}]_2\text{CHGe}(\text{C}_6\text{H}_5)_3$ and with $[(\text{C}_6\text{H}_5)_3\text{Pb}]_2\text{CHAsPh}_2$ provided the mixed reagents $(\text{C}_6\text{H}_5)_3\text{PbCH}(\text{Li})\text{Ge}(\text{C}_6\text{H}_5)_3$ and $(\text{C}_6\text{H}_5)_3\text{PbCH}(\text{Li})\text{As}(\text{C}_6\text{H}_5)_2$, respectively. These examples are given to show how broad and varied the possibilities for synthesis of multimetal organometallic compounds are. In group 15, $(\text{C}_6\text{H}_5)_2\text{AsCH}_2\text{Li}$,¹²⁷ $(\text{C}_6\text{H}_5)_2\text{-SbCH}_2\text{Li}$,¹²⁸ and $(\text{C}_6\text{H}_5)_2\text{BiCH}_2\text{Li}$ ¹²⁹ have been prepared by such Li/Sn transmetalation.

Transition-metal-containing organolithium reagents can be prepared by a number of standard procedures, including transmetalation. The first reported preparation of ferrocenyl-lithium was effected by Li/Hg exchange (eq 60).¹³⁰



1,1'-Dilithiodibenzenechromium, free of the monolithiated species usually obtained as a byproduct in the direct lithiation of dibenzenechromium, could be prepared by the reaction shown in eq 61.¹³¹ ((Chloromercurio)cyclobutadiene)iron tricarbonyl underwent Li/Hg exchange with phenyllithium at -78°C to give the useful monolithio derivative (eq 62).¹³² Another



transition-metal complex that contains a substituted cyclobutadiene ligand, **27**, was of interest. As in the case of *trans*-($n\text{-C}_4\text{H}_9$)₃SnCH=CHSn(C₄H₉-*n*)₃, even in the presence of an excess of phenyllithium, only one Li/Sn exchange occurred with **27**.

(119) (a) Seyferth, D.; Welch, D. E.; Heeren, J. K. *J. Am. Chem. Soc.* **1963**, *85*, 642. (b) Seyferth, D.; Welch, D. E.; Heeren, J. K. *J. Am. Chem. Soc.* **1964**, *86*, 1100. (c) Seyferth, D.; Welch, D. E. *J. Organomet. Chem.* **1964**, *2*, 1.

(120) Schöllkopf, U.; Gerhart, F. *Angew. Chem., Int. Ed. Engl.* **1967**, *6*, 805.

(121) (a) Seebach, D.; Büttner, G. *Angew. Chem., Int. Ed. Engl.* **1969**, *8*, 451. (b) Seebach, D.; Peletier, N. *Chem. Ber.* **1972**, *105*, 511.

(122) See also: (a) Dumont, W.; Bayet, P.; Krief, A. *Angew. Chem., Int. Ed. Engl.* **1974**, *13*, 804. (b) Anciaux, A.; Eman, A.; Dumont, W.; Krief, A. *Tetrahedron Lett.* **1975**, 1617. (c) Van Ende, D.; Dumont, W.; Krief, A. *Angew. Chem., Int. Ed. Engl.* **1975**, *14*, 700. (d) Reich, H. J.; Bowe, M. D. *J. Am. Chem. Soc.* **1990**, *112*, 8994.

(123) Seebach, D.; Beck, A. K. *Chem. Ber.* **1975**, *108*, 314.

(124) Dumont, W.; Krief, A. *Angew. Chem., Int. Ed. Engl.* **1976**, *15*, 161.

(125) Kauffmann, T.; Kriegsmann, R.; Altepeter, B.; Steinseifer, F. *Chem. Ber.* **1982**, *115*, 1810.

(126) (a) Kauffmann, T.; Kriegsmann, R.; Rensing, A.; König, R.; Steinseifer, F. *Chem. Ber.* **1985**, *118*, 370. (b) Kauffmann, T.; Rensing, A. *Chem. Ber.* **1985**, *118*, 380. (c) Rensing, A.; Echsler, K.-J.; Kauffmann, T. *Tetrahedron Lett.* **1980**, *21*, 2807.

(127) Kauffmann, T.; Altepeter, B.; Klas, N.; Kriegsmann, R. *Chem. Ber.* **1985**, *118*, 2353.

(128) Kauffmann, T.; Jousen, R.; Klas, N.; Vahrenhous, A. *Chem. Ber.* **1983**, *116*, 473.

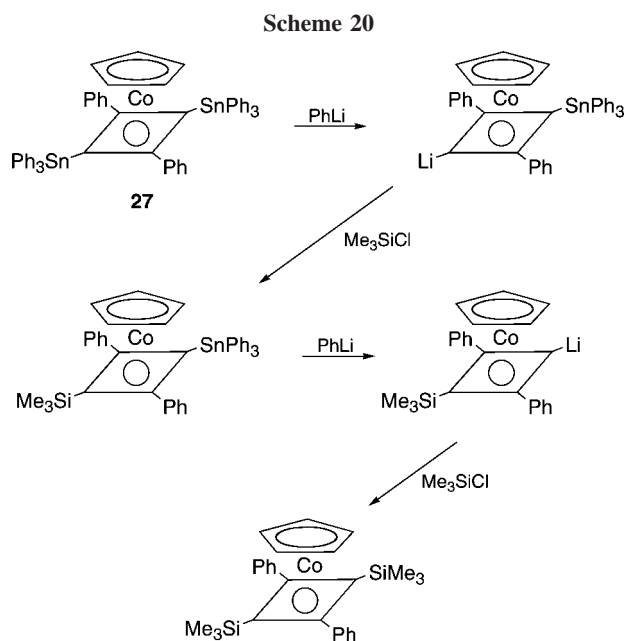
(129) (a) Steinseifer, F.; Kauffmann, T. *Angew. Chem., Int. Ed. Engl.* **1980**, *19*, 723. (b) Kauffmann, T.; Steinseifer, F.; Klas, N. *Chem. Ber.* **1985**, *118*, 1039.

(130) (a) Seyferth, D.; Helling, J. F. *Chem. Ind. (London)* **1961**, 1568. (b) Seyferth, D.; Hoffmann, H. P.; Burton, R.; Helling, J. F. *Inorg. Chem.* **1962**, *1*, 227.

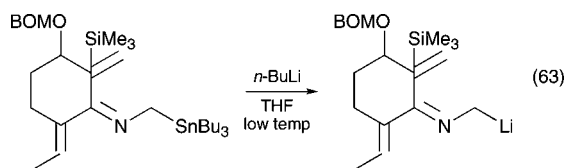
(131) Elschenbroich, C.; Schmidt, E.; Metz, B.; Massa, W.; Wolcadlo, S.; Burghaus, O. *Z. Anorg. Allg. Chem.* **1999**, *625*, 875.

(132) Dieck, H. Ph.D. Dissertation, University of Texas at Austin, Austin, TX, 1968.

However, the two triphenyltin substituents could be displaced in a stepwise manner¹³³ (Scheme 20).



There are many other examples of the application of the transmetalation reaction, most of them involving Li/Sn exchange, to be found in the later literature. (Two very useful reviews are available.)¹³⁴ This is still an active field, and the transmetalation reaction continues to be useful, especially to the synthetic organic chemist. The example shown in eq 63 is a recent one.¹³⁵ It should, however, be emphasized that if the vinylic bromide and the allylic chloride or bromide are available, the low-temperature lithium/halogen exchange reaction, whose use avoids the necessity of preparing an organometallic starting material, is the more practical route to the desired unsaturated organolithium reagent.



The question of the mechanism of the Li/Sn transmetalation reaction has been studied in some detail by Hans Reich¹³⁶ (Figure 10) and his students at the University of Wisconsin.¹³⁷ There were three possibilities: (1) direct S_N2 nucleophilic substitution by the organolithium reagent, $R^{\delta-}Li^{\delta+}$, at the metal atom, (2) reaction via a four-center transition state, and (3)



Figure 10. Hans J. Reich, courtesy of Professor Reich; reproduced by permission.

reaction proceeding by way of a pentacoordinate intermediate. (e.g., $Li^+[C_6H_5Sn(CH=CH_2)_4]^-$ in the case of the phenyllithium/tetraphenyltin reaction). The existence of the well-known “ate” complexes,¹³⁸ principally through the work of Hein and Wittig, made the last one a reasonable possibility and some workers (e.g., Kauffmann) discussed (without proof) the transmetalation reactions being studied in terms of “ate” complex intermediates. It was Reich who presented convincing evidence for the intermediacy of pentacoordinate stannate species in the Li/Sn transmetalation reaction on the basis of kinetic, stereochemical, and NMR spectroscopic studies.

In one approach the rate of the coupling reaction of phenyllithium with *n*-butyl iodide in THF solution was measured in the presence of varying concentrations of methylphenyltin compounds, $(CH_3)_n(C_6H_5)_{4-n}Sn$.^{137a} Tetramethyltin and trimethylphenyltin had practically no effect on the rate. With an increasing number of phenyl substituents the rate was depressed in the order $(CH_3)_2(C_6H_5)_2Sn < CH_3(C_6H_5)_3Sn$, as shown in Figure 11. This was ascribed to the formation of pentacoordinate “ate” complexes, $[(CH_3)_2(C_6H_5)_3Sn]Li$ and $[CH_3(C_6H_5)_4Sn]Li$, respectively, which tie up phenyllithium,¹³⁹ thus decreasing the

(133) Seyferth, D.; Vick, S. C. *J. Organomet. Chem.* **1977**, *139*, 209.

(134) (a) Pereyre, M.; Quintard, J.-P.; Rahm, A. *Tin in Organic Synthesis*, Butterworths: London, 1987, Chapter 9, pp 149–182. (b) Schlosser, M. In *Organometallics in Synthesis-A Manual*; Schlosser, M., Ed., Wiley: Chichester, U.K., 2002; pp 155–170, including 8.5 pages of tables of examples.

(135) Pearson, W. H.; Aponick, A. *Org. Lett.* **2006**, *8*, 1661.

(136) Hans J. Reich (b Danzig, 1943) B.Sc. 1964, University of Alberta; Ph.D. 1968 University of California at Los Angeles, doctoral research with D.J. Cram; postdoctoral work 1968–1969 with J. D. Roberts at the California Institute of Technology, 1969–1970 with R. B. Woodward at Harvard University; at Wisconsin since 1970. Prolific and outstanding contributions to organolithium chemistry with creative application of NMR spectroscopy; organochalcogen, especially organoselenium, chemistry, hypercoordinate iodine compounds, organosilicon chemistry. Winner in 2007 of the Arfvedson-Schlenk Prize for outstanding work in lithium chemistry; cf.: *Angew. Chem., Int. Ed.* **2007**, *46*, 8542.

(137) (a) Reich, H. J.; Phillips, N. H. *Pure Appl. Chem.* **1987**, *59*, 1021. (b) Reich, H. J.; Borst, J. P.; Coplien, M. B.; Phillips, N. H. *J. Am. Chem. Soc.* **1992**, *114*, 6577. (c) Reich, H. J.; Phillips, N. H. *J. Am. Chem. Soc.* **1986**, *108*, 2102. (d) Also extensive studies on Li/Se, Li/Te, and Li/I transmetalation were carried out. The conclusion arrived at was that RLi/organochalcogen or RLi/RI “ate” complexes can be involved as intermediates. These studies will not be discussed here. See, for example: Reich, H. J.; Gudmundsson, B. O.; Green, D. P.; Bevan, M. J.; Reich, I. L. *Helv. Chim. Acta* **2002**, *85*, 3748.

(138) (a) Tochtermann, W. *Angew. Chem.* **1966**, *78*, 355. (b) Wittig, G. *Angew. Chem.* **1958**, *70*, 65.

(139) In a similar manner, $Li[(C_6H_5)_6Sb]$ in solution is in equilibrium with C_6H_5Li and $(C_6H_5)_5Sb$, giving a system in which there is a slow release of phenyllithium if there is something present with which it can react: Wittig, G.; Benz, E. *Tetrahedron* **1960**, *10*, 37.

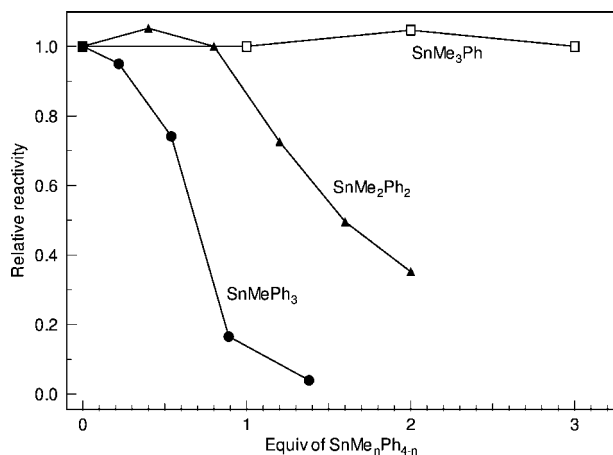
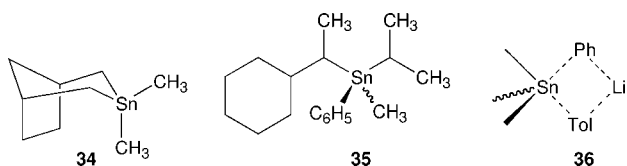


Figure 11. Effect of added $(\text{CH}_3)_3\text{SnC}_6\text{H}_5$, $(\text{CH}_3)_2\text{Sn}(\text{C}_6\text{H}_5)_2$, and $\text{CH}_3\text{Sn}(\text{C}_6\text{H}_5)_3$ on the rate of the $\text{C}_6\text{H}_5\text{Li} + n\text{-C}_4\text{H}_9\text{I}$ coupling reaction (slightly modified since original publication in *Pure Appl. Chem.* 1987, 59, 1022 and Phillips, N. Ph.D. Thesis, University of Wisconsin, 1988; reproduced by permission of International Union of Pure and Applied Chemistry).

rate of the $\text{C}_6\text{H}_5\text{Li}/n\text{-C}_4\text{H}_9\text{I}$ coupling reaction. Using a new sophisticated NMR procedure, which is carried out with an achiral compound and which did not require a configuration assignment, in which the rate of the isotope exchange between CD_3Li in diethyl ether and **34** was measured, a second-order rate profile was found which was compatible with a mechanism involving retention of configuration at the tin atom, but not with inversion.^{137b} Since a cyclic stannane might show stereochemistry different from that of an acyclic stannane, further experiments were carried out with compound **35** that had been kinetically enriched to a 6:1 diastereomer ratio. Here the results of experiments in which *p*-tolyllithium was the organolithium reagent that was used were found to be solvent-dependent: retention in diethyl ether but in THF with epimerization of configuration at tin. It was concluded that in THF the Li/Sn exchange occurred via a long-lived, pseudorotating pentacoordinate stannate intermediate, while in diethyl ether a tightly bound four-center transition state or intermediate, **36**, was involved.



Convincing ¹¹⁹Sn NMR evidence was provided for the presence in finite concentration of pentacoordinate “ate” complexes such as $\text{Li}[(\text{CH}_3)_5\text{Sn}]$ in THF/HMPA (HMPA = $(\text{Me}_2\text{N})_3\text{PO}$) solutions.^{137a} In THF alone a 3:2 $\text{CH}_3\text{Li}/(\text{CH}_3)_4\text{Sn}$ mixture showed only the signal due to $(\text{CH}_3)_4\text{Sn}$ at 0 ppm. As the polar HMPA was added and its concentration was increased by further additions, a new signal was observed at -277 ppm which kept increasing in intensity while that due to tetramethyltin decreased (Figure 12). When the HMPA concentration was 0.9 M, the $(\text{CH}_3)_4\text{Sn}$ signal had disappeared. Analysis of the ¹H-coupled ¹¹⁹Sn NMR spectrum showed that the tin signal was split equally by 15 protons (Figure 12). Similar experiments involving mixtures of mixed methylphenyltin compounds and methyl- or phenyllithium gave similar results. Thus pentacoordinate organotin species of type $\text{Li}[\text{R}'\text{R}_4\text{Sn}]$ can be involved as intermediates in Li/Sn transmetalation reactions. In solvents

less polar than HMPA, such as THF and diethyl ether, which usually are used, they are at best transient intermediates. In diethyl ether, on the basis of the stereochemical results noted above, a four-center transition state could be involved. The kinetics of some *n*-butyllithium/ α -aminoalkyltin compound transmetalations were studied by Klein and Gawley using the rapid injection NMR procedure (¹¹⁹Sn NMR in this case).¹¹⁵ The effect of solvent on the rate was significant: too fast to measure in THF, too slow in diethyl ether, and usually of a convenient rate in 40/60 $\text{Et}_2\text{O}/\text{THF}$.

V. Increasing the Scope of Organolithium Reagent Applicability: Organolithium Derived Superbases

An important, much practiced application of the simple alkyl and, less frequently, aryl derivatives of the alkali metals, based on the fact that they are strong bases, is their use in deprotonation of diverse weakly acidic organic and organometallic compounds, the Schorigin reaction (eq 64).



The new organoalkali-metal compounds which are formed in such reactions are then useful reagents in subsequent organic or organometallic syntheses. Since its discovery by Schorigin in 1908,⁷ thousands of examples of this reaction, commonly termed “metalation reaction” or “metal–hydrogen exchange reaction”, have been published.¹⁴⁰ A large variety of strong base reagents has been used in such metalation reactions: inorganic bases, in particular alkali-metal amides, and organometallic bases such as *n*-alkylsodium and -potassium reagents, $(\text{C}_6\text{H}_5)_3\text{CNa}$ and $(\text{C}_6\text{H}_5)_3\text{CK}$, as well as alkyllithium reagents.

At the present time the three isomeric butyllithium reagents, *n*-butyl-, *sec*-butyl-, and *tert*-butyllithium, commercially available in hydrocarbon solution, are the reagents of choice. However, the application of these compounds is somewhat limited in that they are not sufficiently basic to deprotonate extremely weakly acidic compounds such as benzene and ethylene. The basic properties of organolithium compounds can be enhanced by using them in donor solvents, such as diethyl ether and THF (at low temperature).¹⁴⁰ Very much stronger organolithium bases can be obtained, it was found, when a 1:1 mixture of *n*-butyllithium and a chelating tertiary diamine such as *N,N,N',N'*-tetramethylethylenediamine (TMEDA) is used.¹⁴¹ Such N-chelated organoalkali-metal compounds were discovered at the ESSO Research and Engineering Laboratories in Linden, NJ, in 1960 and reported in a U.S. patent in 1969.¹⁴² Their preparation was reported in a later patent.¹⁴³ Two patents, covering very similar chemistry, had been awarded earlier to Gert G. Eberhardt of Sun Oil Company in Philadelphia.¹⁴⁴

(140) Reviews: (a) Gilman, H.; Morton, J. W., Jr. *Org. React.* **1954**, *8*, 258. (b) Mallan, J. M.; Bebb, R. L. *Chem. Rev.* **1969**, *69*, 693. (c) Wakefield, B. J. *The Chemistry of Organolithium Compounds*; Pergamon: Oxford, U.K., 1974; Chapter 3, pp 26–50. (d) Reference, pp 185–284, including 63 pages of tables containing representative examples.

(141) (a) *Polyamine-Chelated Alkali Metal Compounds*; Langer, A. W., Jr., Ed.; American Chemical Society: Washington, DC, 1974; *Advances in Chemistry Series 130* (general reference). (b) Langer, A. W., Jr. *Trans. New York Acad. Sci., Ser. II*, **1965**, *27*, 741. (c) Eberhardt, G. G.; Butte, W. A., Jr. *J. Org. Chem.* **1964**, *29*, 2928.

(142) Langer, A. W., Jr. U.S. Patent 3,451,988, June 24, 1969. Filed Oct 25, 1966 (composition and uses for polymerization).

(143) Langer, A. W., Jr. U.S. Patent 3,769,345, Oct. 30, 1973. Filed Dec. 13, 1967 (method for preparing organolithium amine complexes).

(144) (a) Eberhardt, G. G. U.S. Patent 3,206,519, Sept 14, 1965. Filed Nov. 19, 1963 (preparation of alkyl aromatic hydrocarbons). (b) Eberhardt, G. G.; Butte, W. A., Jr. U.S. Patent 3,321,479, May 23, 1967. Filed Mar. 14, 1966. (preparation of organolithium amine complexes).

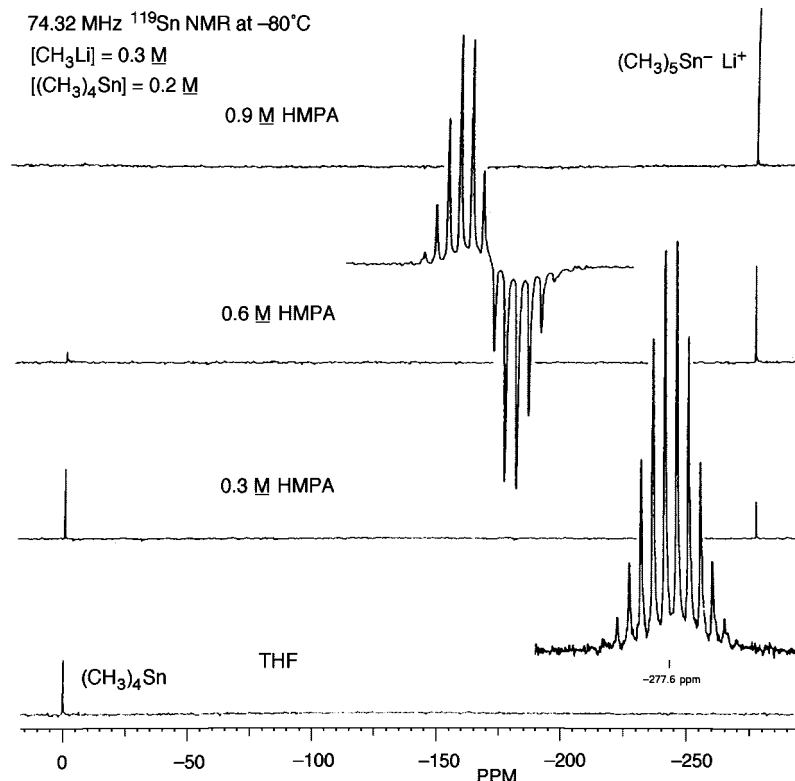


Figure 12. Effect of different concentrations of HMPA on the ^{119}Sn NMR spectrum of a 1:1 $\text{CH}_3\text{Li}/(\text{CH}_3)_4\text{Sn}$ mixture in THF at -80°C (J. Am. Chem. Soc. 1986, 108, 2102).

However, as Langer noted in his chapter in ref 141a for the first of these,^{144a} “Claims lost to 3,451,988 and 3,458,586” (both Langer patents) and for the second^{144b} “Claims lost to 3,769,345” (also a Langer patent). Presumably, this was the result of litigation involving ESSO, Sun Oil, and the U.S. Patent Office.

The alkyllithium–TMEDA combination was found to be a superbases in its reactivity. Not only did $n\text{-C}_4\text{H}_9\text{Li}$ –TMEDA lithiate toluene to benzylolithium and propene to allyllithium and $sec\text{-C}_4\text{H}_9\text{Li}$ –TMEDA lithiate 1-butene to crotyllithium, but also $n\text{-C}_4\text{H}_9\text{Li}$ –TMEDA lithiated benzene to give phenyllithium.¹⁴⁵ All of these organolithium reagents were formed in high yield as TMEDA complexes. This might, in some cases, be a disadvantage since, if acid hydrolytic workup was not possible, the separation of TMEDA might be a problem. Also, in the case of the lithiation of toluene, 1–5% of nuclear metalated byproducts (meta and para isomers) were present. This is not a problem with benzylolithium prepared by the transmetalation reaction. Other $n\text{-C}_4\text{H}_9\text{Li}$ –chelating tertiary diamine reagents were prepared, but the TMEDA complex was the most reactive. The main industrial interest in these $\text{C}_4\text{H}_9\text{Li}$ –diamine complexes derived from the fact that they are excellent initiators for the homo- and copolymerization of ethylene, styrene, and 1,3-dienes,^{141b,146} but their outstanding utility as bases stronger than n -butyllithium alone soon was recognized.

The most powerful basic alkali-metal-derived systems are obtained by adding 1 or 2 molar equiv of a sodium or potassium alkoxide, preferably one that is soluble, to the alkyllithium solution. Such mixed reagents are called “superbases”.

As reported in Part 1 of this essay,¹ such superbases originally were discovered accidentally in 1946 by Avery A. Morton at the Massachusetts Institute of Technology during his search for

an effective organosodium initiator for 1,3-diene polymerization (see pp 16–17 of ref 1). Most of the polymerization studies were done with the system obtained by mixing n -amylsodium, a lower α -olefin such as 1-propene, and isopropyl alcohol. The olefin and i -PrOH reacted with n -amylsodium to give a reagent containing an allylsodium compound and sodium isopropoxide (as well as NaCl from the n -amylsodium preparation). This was a very potent polymerization initiator (“ALFIN catalyst”).¹⁴⁷ However, more pertinent to the present discussion, Morton also found that addition of sodium isopropoxide or, better, potassium isopropoxide, to a suspension of n -amylsodium in alkane medium increased the already high basicity of n -amylsodium: more rapid reactions gave higher yields of metalation product.¹⁴⁸ The most spectacular observation made was that $n\text{-C}_5\text{H}_{11}\text{Na}/i\text{PrONa}$ could metalate ethylene directly to give vinylsodium.^{148b} Morton’s discovery of the “alkoxide effect” was never cited by the later workers, who apparently rediscovered the alkoxide effect some 20 years later. Perhaps they were too focused on organolithium chemistry to recognize that the concept had been discovered earlier in organosodium chemistry by Morton.

The story continues in the mid 1960s when three research groups independently rediscovered the “alkoxide effect”. In all three cases alkyllithium reagents, usually n -butyl-, sec -butyl-, and $tert$ -butyllithium, were “activated” by the addition of 1 molar equiv or more of a potassium or sodium alkoxide. The three groups reported such systems almost at the same time:

(147) Morton, A. A.; Patterson, G. H.; Donovan, J. J.; Little, E. L. *J. Am. Chem. Soc.* **1946**, *68*, 93.

(148) (a) Morton, A. A.; Holden, M. E. *T. J. Am. Chem. Soc.* **1947**, *69*, 1675. (b) Morton, A. A.; Marsh, F. D.; Coombs, R. D.; Lyons, A. L.; Penner, S. E.; Ramsden, H. E.; Baker, V. B.; Little, E. L.; Letsinger, R. L. *J. Am. Chem. Soc.* **1950**, *72*, 3785. (c) Morton, A. A.; Claff, C. E., Jr. *J. Am. Chem. Soc.* **1954**, *76*, 4935. (d) Morton, A. A.; Claff, C. E., Jr.; Collins, F. W. *J. Org. Chem.* **1955**, *20*, 428. (e) Morton, A. A.; Eisenmann, J. L. *J. Org. Chem.* **1958**, *23*, 1469.

(145) Smith, W. N. In ref 141a, Chapter 2, pp 23–55.

(146) Kamiński, C. W. In ref 141a, Chapter 7, pp 163–176.

C. F. Wofford of the Phillips Petroleum Company in Bartlesville, OK,¹⁴⁹ Lubomir Lochmann and his colleagues at the Institute of Macromolecular Science of the Czechoslovak Academy of Sciences in Prague,¹⁵⁰ and Manfred Schlosser of the University of Heidelberg.¹⁵¹ It was 3 years later when Wofford, together with Henry Hsieh, published details of the work done at the Phillips Petroleum Company laboratories.¹⁵²

The Wofford patent¹⁴⁹ was concerned with the polymerization of 1,3-dienes and styrenes using organolithium-derived initiators. One claim specifically cites a mixture of *n*-butyllithium and potassium *tert*-butoxide. Also claimed were mixtures of *n*-butyllithium with a potassium phenoxide, a potassium alkylmercaptide, potassium stearate, and potassium di-*n*-butylamide. The publication that followed up on the patent¹⁵² was devoted to alkyllithium/metal alkoxide polymerization initiator systems, the main finding being that they dramatically increased the rate of polymerization and also the vinyl content of polybutadiene. It was suggested that the propagation center in the polymerization reaction involved a dynamic equilibrium between carbon–metal and oxygen–metal bonds in which polymer–M species (M = K, Rb, Cs) and lithium alkoxides were formed.

The first paper in this area was published by the Czech group in 1964.¹⁵³ It was shown that the combination *n*-C₄H₉Li/*tert*-C₄H₉OLi was more efficient in initiating the anionic polymerization of methyl methacrylate than were *n*-C₄H₉Li and *tert*-C₄H₉OLi when used separately. (The effects of adding lithium alkoxides to *n*-butyllithium on the rates of initiation, propagation, and polymerization of styrene and butadiene also were investigated later by other workers.¹⁵⁴) This finding was ascribed to the formation of a complex between the two components.¹⁵⁵ Lochmann and his co-workers investigated the interaction of alkyllithiums with lithium alkoxides by thermometric titration and infrared spectroscopy, finding that 1:1 complexes were formed between *t*-C₄H₉OLi and *n*-butyl-, *tert*-butyl-, and isopropyllithium.¹⁵⁶ These could be isolated as white, crystalline, hydrocarbon-soluble solids. No structural evidence was obtained. Subsequent work showed the *n*-C₄H₉Li · *tert*-C₄H₉OLi complex

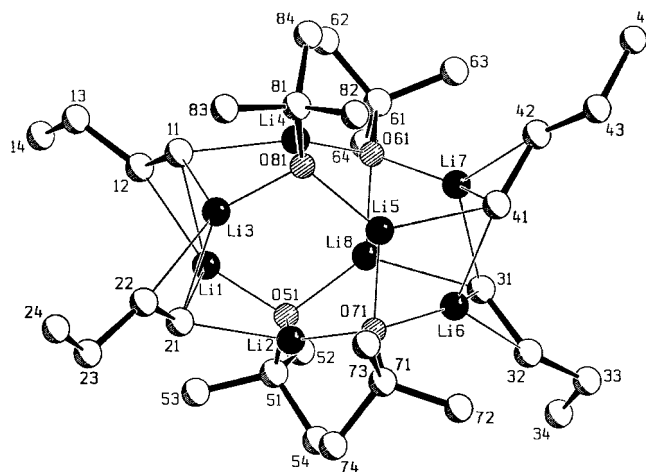


Figure 13. Solid-state structure of the *n*-C₄H₉Li · *tert*-C₄H₉OLi complex (*Angew. Chem., Int. Ed. Engl.* 1990, 29, 308; copyright Wiley-VCH Verlag GmbH & Co. KGaA, reproduced with permission).

to be tetrameric in benzene solution.¹⁵⁷ Some years later, Gernot Boche, Lochmann, and co-workers at the University of Marburg determined the solid-state structure of the *n*-C₄H₉Li · *tert*-C₄H₉OLi complex by X-ray diffraction (Figure 13).¹⁵⁸ The complex is a tetramer of complicated structure.

The results of the study of the *n*-C₄H₉Li/*tert*-C₄H₉OLi system led Lochmann and his co-workers to their investigation of the interaction of *n*-butyllithium with sodium and potassium *tert*-alkoxides. Sodium or potassium *tert*-butoxide or *tert*-pentoxide usually were used in combination with *n*-butyllithium, but other combinations have been reported. As described in ref 150 the procedure is very simple:

“To a suspension of 0.0643 mole of sodium *tert*-butoxide (purified by double sublimation) in 10 ml of dry heptane 90 ml of 0.930 M *n*-butyllithium in heptane (i.e., 0.0837 mole) at 0°C in about 15 min. is added under stirring. After the addition of *n*-butyllithium is started the alkoxide first partly dissolves (the formation of the intermediate association product); at normal temperature a complete solution may be observed. By the addition of more *n*-butyllithium the separation of *n*-butylsodium in the form of a white powder occurs. To complete the reaction the mixture is stirred 1 hr at 0°C and 1 hr at 30–40°C. The precipitate is sucked off, washed with heptane and dried for 5 hours at 50°C/1 mm Hg; yield 91.3%.”

The *n*-C₄H₉Na was essentially pure: Anal. Calcd: Na, 28.70. Found: Na, 28.73, 28.90; Li, only 0.07. Its reaction with CO₂ gave, as expected, valeric acid. The filtrate was shown by IR spectroscopy to contain *n*-C₄H₉Li · *tert*-C₄H₉OLi, which Lochmann et al. had studied earlier.¹⁵¹

A similar procedure was used to prepare *n*-octylsodium and *n*-dodecylsodium from the respective alkyllithium reagent. This procedure was used in situ to metalate triphenylmethane to triphenylmethyllithium.¹⁵⁰ Similar experiments with the *n*-C₄H₉Li/*t*-C₄H₉OK system were less straightforward, but a later study by Lochmann and Lim provided a useful preparation of *n*-butylpotassium.¹⁵⁹ Instead of potassium *tert*-butoxide, the

(149) Wofford, C. F. U.S. Patent 3,294,768, Dec 27, 1966, assigned to Phillips Petroleum Company; filed Nov. 14, 1963; British Patent GB 1,029,445, Nov 5, 1966, assigned to Phillips Petroleum Company.

(150) (a) Lochmann, L.; Pospíšil, J.; Lim, D. *Tetrahedron Lett.* **1966**, 257 (submitted Nov 1965). (b) Czech Patent 132,254, 1965, filing date Dec. 30, 1964. (c) Lubomir Lochmann (b. Prague, 1926). M.Sc. at Czech Technical University in Prague, 1949. Industry (organic synthesis), 1955–1960. In 1961 joined the Institute of Macromolecular Chemistry of the Czechoslovak Academy of Sciences in Prague. Ph.D., 1968; D.Sc., 1998 from the Institute. Visiting Scientist, 1992 and 1993 at Cornell Univ. with J. M. J. Fréchet. Research in the areas of polymer chemistry (anionic polymerization) and organoalkali-metal chemistry.

(151) (a) Schlosser, M. J. *Organomet. Chem.* **1967**, 8, 9. (b) Manfred Schlosser (b. 1934) Chemistry study at the University of Heidelberg; Ph.D. in organic chemistry (with Prof. Georg Wittig in 1960). Habilitation in Heidelberg in 1966, after which he was a group leader in the German Cancer Research Center in Heidelberg. Since 1971 professor of chemistry at the University of Lausanne in Switzerland. Research activities principally in area of organoalkali-metal chemistry, also organofluorine chemistry (synthetic and mechanistic studies).

(152) (a) Hsieh, H. L.; Wofford, C. F. *J. Polym. Sci., Part A-1* **1969**, 7, 449. (b) Wofford, C. F.; Hsieh, H. L. *J. Polym. Sci., Part A-1* **1969**, 7, 461.

(153) Trekoval, J.; Lim, D. *J. Polym. Sci., Part C* **1964**, 333.

(154) (a) Roovers, J. E. L.; Bywater, S. *Trans. Faraday Soc.* **1966**, 62, 1876. (b) Hsieh, H. L. *J. Polym. Sci., Part A-1* **1970**, 8, 533.

(155) T. L. Brown and co-workers had found that ethyllithium solubilized the normally insoluble lithium ethoxide in benzene and suggested that a complex was formed by interaction between the ethyllithium hexamer, in which the lithium atoms are Lewis acid sites, and the Lewis base, C₂H₅OLi, via the oxygen atom lone electron pairs: Brown, T. L.; Dickerhoof, D. W.; Bafus, D. A. *J. Am. Chem. Soc.* **1962**, 84, 1371.

(156) Lochmann, L.; Pospíšil, J.; Vodnansky, J.; Trekoval, J.; Lim, D. *Collect. Czech. Chem. Commun.* **1965**, 30, 2187.

(157) Halaska, V.; Lochmann, L. *Collect. Czech. Chem. Commun.* **1973**, 38, 1780.

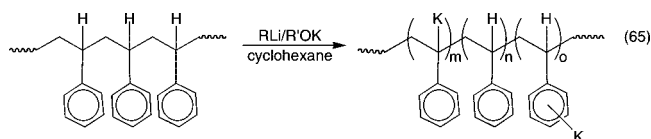
(158) Marsch, M.; Harms, K.; Lochmann, L.; Boche, G. *Angew. Chem., Int. Ed. Engl.* **1990**, 29, 308.

(159) Lochmann, L.; Lim, D. *J. Organomet. Chem.* **1971**, 28, 153.

hydrocarbon-soluble potassium (–)-(1*R*)-menthoxide was used in the reaction with *n*-butyllithium. A reagent ratio of 1:1 was the optimum, giving good yields of relatively pure *n*-C₄H₉K as a light brown solid. *n*-Butylpotassium thus prepared is less thermally stable than *n*-butylsodium, decomposing slowly in the solid state at room temperature. The in situ *n*-C₄H₉Li/*t*-C₄H₉OK reagent system was found to be a very reactive metalation agent, as had been reported originally.¹⁵⁰

The use of hydrocarbon-soluble metal alkoxides represented a significant improvement. Potassium *tert*-butoxide is not soluble in hydrocarbons. Its replacement by potassium alkoxides such as Me₂EtCOK, MeEt₂COK, Et₃COK, and the potassium menthoxide noted above, all of which are soluble in hydrocarbons, resulted in generally faster rates of reaction and in higher product yields when they were used in metalation reactions.

Lochmann and his co-workers continued their studies of anionic polymerization, mainly of methacrylate esters, and in the mid-1980s to 1990s published a number of papers on the more organometallic aspects of the RLi/ROM systems. The metalation of aromatic compounds was investigated more broadly. It was found that C₆H₅K is the main product of the reaction of the *n*-butyllithium/potassium *tert*-pentoxide reagent with benzene. Phenylpotassium of greatest purity (K:Li = 12) was obtained when a large excess of benzene was used.¹⁶⁰ Using soluble potassium alkoxide/*n*-butyllithium and 2-ethylhexyllithium combinations it was possible to dimetalate benzene.¹⁶¹ They also were used with good advantage in the metalation of alkylbenzenes¹⁶² and of phenol, thiophenol, and *o*-cresol.¹⁶³ Of particular interest is the polymetalation of polystyrene in a controlled manner by 2-ethylhexyllithium/potassium *tert*-pentoxide in cyclohexane.¹⁶⁴ Both benzylic and nuclear metalation sites were present (eq 65), as derivatization with trimethylchlorosilane showed.



The alkyllithium/potassium *tert*-pentoxide combination, which forms the alkylpotassium compound, reacted with alkyl and aryl bromides and iodides to give coupled products.¹⁶⁵ Three processes take place (Scheme 21). In the example shown, the major product was *n*-C₁₂H₂₆, but some *n*-C₁₆H₃₄ also was formed. When the alkyl groups of the lithium reagent and the halide were the same, a good yield of the coupled product, R–R, was obtained. When bromobenzene was the halide used, *n*-butylbenzene was the major product; only a very low yield of biphenyl was obtained.

A further improvement of the generation and utilization of *n*-butylsodium and *n*-butylpotassium was reported by Paul Schleyer and co-workers at the University of Erlangen.^{166,167} It was found that combining two activation procedures, addition

of 1 equiv of the metal *tert*-butoxide and a chelating tertiary diamine such as TMEDA, gave far superior sodium and potassium superbases. Thus, addition at 0 °C of TMEDA to a suspension of *n*-C₄H₉Na in hexane (obtained after removing by filtration the solution of *t*-C₄H₉OLi obtained in the *n*-C₄H₉Li + *t*-C₄H₉ONa reaction) immediately gave a clear solution.¹⁶⁶ By adjustment of the TMEDA to hexane ratio, *n*-butylsodium solutions in the 1–4 M range could be obtained. When the mixture was cooled to –78 °C, a white solid believed to be a [*n*-C₄H₉Na]·*x*TMEDA complex precipitated (it redissolved when the mixture was warmed). At 0 °C, it was stable in hexane. However, at 25 °C the *n*-C₄H₉Na/TMEDA in hexane solution decomposed in an exothermic metalation of the TMEDA. THF also dissolves solid *n*-butylsodium. The resulting solutions are stable at –78 °C, but at –40 °C the sodium alkyl deprotonates THF. The reactivity of the *n*-C₄H₉Na/TMEDA/hexane system was reported to be similar to that of *n*-C₄H₉Li·TMEDA.

n-Butylpotassium was prepared by a similar procedure, using in this case the more soluble potassium *tert*-pentoxide and a reaction temperature of –50 °C.¹⁶⁷ The *n*-C₄H₉K, isolated as a white powder, was suspended in hexane; subsequent addition of TMEDA at –50 °C gave a clear solution. Because the potassium reagent readily attacks TMEDA, the temperature had to be kept below –40 °C. THF also dissolved *n*-C₄H₉K, but the temperature of such solutions had to be maintained below –50 °C. The *n*-C₄H₉K/TMEDA/hexane system has high metalation power. It metalated toluene at –30 °C in less than 1 min, giving red crystalline C₆H₅CH₂K·TMEDA·0.5C₆H₅CH₃. For synthetic purposes, it was found sufficient to prepare a mixture of *n*-C₄H₉Li, *t*-C₄H₉OK, and TMEDA in hexane or pentane at temperatures below –40 °C. This system enabled, as the authors claimed, “the first successful direct metallation of ethylene” to give vinylpotassium, CH₂=CHK.¹⁶⁸ Unfortunately, the authors overlooked the earlier report by Morton and co-workers describing the direct metalation of ethylene to give vinylsodium, CH₂=CHNa, in good yield, using the *n*-C₅H₁₁Na/NaOP*r*-i combination. Checked, hence reliable, directions for the preparation of *n*-C₄H₉Li·TMEDA in hexane, *n*-C₄H₉Li·*t*-C₄H₉OK in THF, and *n*-C₄H₉Li·*t*-C₄H₉OM·TMEDA in hexane or pentane (M = Na, K) have been given by Brandsma and Verkruijssje.¹⁶⁹

The ¹H, ¹³C, and ²³Na NMR spectra of *n*-C₄H₉Na solutions in THF-*d*₈ at –75 °C suggested that only one modification of

(160) Lochmann, L. *Collect. Czech. Chem. Commun.* **1987**, 52, 2710.

(161) Lochmann, L.; Fossatelli, M.; Brandsma, L. *Recl. Trav. Chim. Pays-Bas* **1990**, 109, 529.

(162) (a) Lochmann, L.; Trekoval, J. *J. Organomet. Chem.* **1987**, 326, 1. (b) Lochmann, L.; Petránek, J. *Tetrahedron Lett.* **1991**, 32, 1483.

(163) Andringa, H.; Verkruijssje, H. D.; Brandsma, L.; Lochmann, L. *J. Organomet. Chem.* **1990**, 393, 307.

(164) Lochmann, L.; Fréchet, J. M. J. *Macromolecules* **1996**, 29, 1767.

(165) Lochmann, L.; Trekoval, J. *Collect. Czech. Chem. Commun.* **1986**, 51, 1439. For more detailed studies, see: (a) Lochmann, L. *J. Organomet. Chem.* **1989**, 376, 1. (b) Lochmann, L. *J. Organomet. Chem.* **1989**, 364, 281. (c) Brandsma, L.; Mal'kina, A. G.; Lochmann, L.; Schleyer, P. v. R. *Recl. Trav. Chim. Pays-Bas* **1994**, 113, 529.

(166) Schade, C.; Bauer, W.; Schleyer, P. v. R. *J. Organomet. Chem.* **1985**, 295, C25.

(167) Pi, R.; Bauer, W.; Brix, B.; Schade, C.; Schleyer, P. v. R. *J. Organomet. Chem.* **1986**, 306, C1.

(168) Brandsma, L.; Verkruijssje, H. D.; Schade, C.; Schleyer, P. v. R. *J. Chem. Soc., Chem. Commun.* **1986**, 260. Parsons et al., who used Morton's procedure with some modification, reported vinylsodium yields of 43–45%: Parsons, T. D.; Silverman, M. B.; Ritter, D. M. *J. Am. Chem. Soc.* **1957**, 79, 5091.

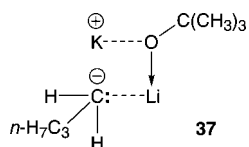
(169) Brandsma, L.; Verkruijssje, H. D. *Preparative Polar Organometallic Chemistry 1*; Springer: Berlin, 1987; pp 18–19. This book is an excellent guide to the preparation and use of organolithium, -sodium, and -potassium reagents.

n-butylsodium is present.¹⁶⁶ This probably is a monomer, since a cryoscopic molecular weight determination of *n*-octylsodium in THF gave a degree of aggregation, *n*, of 0.9 ± 0.1 at 50.7 mM concentration.¹⁶⁷ Similar NMR studies (¹H, ¹³C) of *n*-C₄H₉K in THF-*d*₈ at -60 °C also indicated the presence of monomeric species.¹⁶⁷

Organometallic and organic chemists are interested in the RLi/R'OM and RLi/R''OM/TMEDA superbases systems because they are so effective in deprotonating very weak organic acids. However, the RLi/R'OM systems resulted from the research of polymer chemists and in applications in polymerization these systems also shine. The rate of polymerization of butadiene initiated by *n*-butyllithium is greatly increased in the presence of an alkali-metal alkoxide.¹⁷⁰

In addition to the RLi·R'OM reagents there also is the 2RLi/KH system reported by Eberhardt,¹⁷¹ which also appears to be a superbases. Thus, when it was present in 1 mol % quantity it catalyzed the reaction of alkylbenzenes with ethylene. In one example, such a reaction of ethylene with ethylbenzene in hexane in an autoclave at 135 °C gave a product mixture containing 70% 1-ethylindane and 30% 3-phenylpentane. With toluene the product mixture obtained contained 15% indane and 84% propylbenzene. The initial intermediates without doubt were C₆H₅CH(K)CH₃ and C₆H₅CH₂K. Such deprotonation could not have been effected with *n*-butyllithium alone. A stoichiometric reaction of ethylbenzene and the 2:1 *n*-C₄H₉Li/KH reagent gave a bright red solid as expected for the α-potassium derivative of ethylbenzene.

Manfred Schlosser's approach, begun at the University of Heidelberg and since 1971 continued in Switzerland at the University of Lausanne, has been different from the organoalkali-metal chemistry discussed above. In his initial experiment¹⁵¹ Schlosser added an equimolar amount of potassium *tert*-butoxide to a solution of *n*-butyllithium in hexane. Reaction of the resulting mixture after only a short time with solid CO₂ gave, after acidic workup, benzoic acid in 77% yield. *n*-Butyllithium alone gave benzoic acid in less than 1% yield after a 3 h reaction period. Such activation was attributed to a complex that Schlosser wrote as **37**. This appeared to be a very strongly basic



and very reactive system; thus, Schlosser began an extensive investigation of the scope of its applicability, beginning with triphenyl- and diphenylmethane, toluene, *p*-methoxytoluene, and allylbenzene as substrates. Schlosser pursued this observation, finding that the *n*-C₄H₉Li/*t*-C₄H₉OK system readily metalated hydrocarbons of low acidity in the p*K*_a range 35–50.¹⁷² In a study of the various possible variants of the RLi/R'OK procedure Schlosser and Strunk examined the reactions with cumene of two series of reagents, one in which RLi was varied while R'OK was *t*-C₄H₉OK (RLi = CH₃Li, *n*-C₄H₉Li, C₂H₅CH(CH₃)Li, and (CH₃)₃CLi) and the other in which RLi was held constant as *n*-C₄H₉Li with R'OK varied (R' = *n*-C₃H₇, (C₂H₅)₂CH, (C₂H₅)₃C, and an oxime derivative, (C₂H₅)₂NO), in pentane at

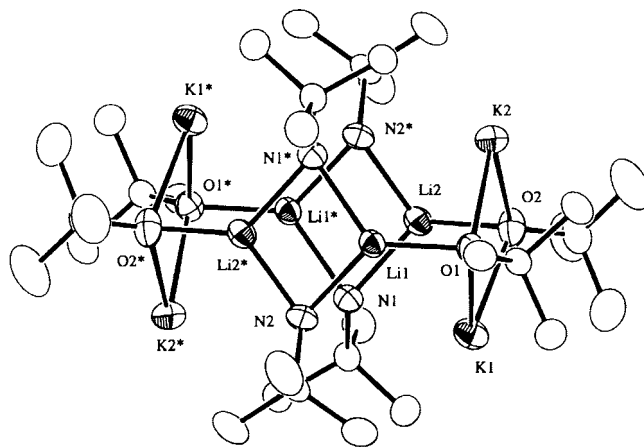
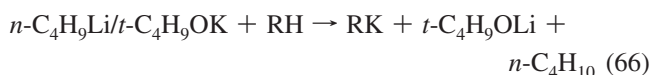


Figure 14. Solid-state structure of the $[[\{t\text{-C}_4\text{H}_9\text{NH}\}_4\{t\text{-C}_4\text{H}_9\text{O}\}_4\text{Li}_4\text{K}_4 \cdot (\text{C}_6\text{H}_6)_3](\text{C}_6\text{H}_6)]$ complex (Angew. Chem., Int. Ed. 2001, 40, 3246; copyright Wiley-VCH Verlag GmbH & Co. KGaA, reproduced with permission).

25 °C and in THF at -50 °C. The *n*-C₄H₉Li/(CH₃)₃COK combination seemed to be the most powerful and selective metalating agent tested, and as the authors concluded, "...it should be considered as the first choice whenever a very potent metalating agent is needed". Schlosser's system is different from the others in that it uses the organolithium reagent and the potassium alkoxide in a 1:1 molar ratio in THF at -50 °C, conditions under which the resulting reagent is soluble. The *n*-C₄H₉Li/*t*-C₄H₉OK reagent is indefinitely stable in THF at -75 °C, at least for a while at -50 °C.¹⁷³ In its reactions the products usually are the potassium derivatives of the hydrocarbons that were metalated and lithium *tert*-butoxide (eq 66). If the lithium derivative is desired instead, reaction of the potassium compound that was produced with anhydrous LiBr effects this transformation. Thus, in one example, allylpotassium was converted to allyllithium.¹⁷⁴



The development of superbases and of superbases chemistry remains an active area of research today. Some information about the structure of superbases systems is beginning to become available. See, for instance, the remarkable solid-state structure in Figure 14 of $[[\{t\text{-C}_4\text{H}_9\text{NH}\}_4\{t\text{-C}_4\text{H}_9\text{O}\}_4\text{Li}_4\text{K}_4 \cdot (\text{C}_6\text{H}_6)_3](\text{C}_6\text{H}_6)]$, prepared by reaction of *t*-C₄H₉NHLi and *t*-C₄H₉OK with an excess of benzene, which was reported by Mulvey and co-workers in 2001.¹⁷⁵ As Mulvey said about the superbasicity area, "A forest of literature has grown around...superbasicity focusing mainly on its exploitation in organic synthesis and, to a lesser extent, in polymerization." The "forest" continues to flourish and grow.

VI. Concluding Remarks

This concludes the discussion of the historical aspects of the synthesis of organoalkali-metal compounds. Unavoidably, some discussion of their reactivity and applications also had to be

(170) Reviews: (a) Lochmann, L.; Trekoval, J. *Collect. Czech. Chem. Commun.* **1988**, 53, 76. (b) Lochmann, L. *Eur. J. Inorg. Chem.* **2000**, 1115.

(171) Eberhardt, G. G. *J. Org. Chem.* **1964**, 29, 643.

(172) Schlosser, M.; Strunk, S. *Tetrahedron Lett.* **1984**, 25, 741. A reference list of 16 Schlosser papers on such metalations is given in this paper.

(173) Leroux, F.; Schlosser, M.; Zohar, E.; Marek, I. In *The Chemistry of Organolithium Compounds*; Rappaport, Z., Marek, I., Eds.; Wiley: Chichester, U.K., 2004; Part 1, pp 457–459.

(174) Schlosser, M.; Hartmann, J. *Angew. Chem., Int. Ed. Engl.* **1973**, 12, 439.

(175) Kennedy, A. R.; MacLellan, J. G.; Mulvey, R. E. *Angew. Chem., Int. Ed.* **2001**, 40, 3245.

included. However, this essay was not meant to deal with the reactions of the organoalkali-metal compounds—that is too vast an area and involves in large part relatively recent history. Nor will I deal with the mechanisms of organoalkali-metal reactions. Again, this is relatively recent history and we have already had a sampling of their reactions that can involve polar processes, four-center transition states, hypercoordinate intermediates, and electron-transfer processes. What remains to be covered are the historical aspects dealing with the structure of organoalkali-metal compounds in the solid state, their constitution in solution, in low-temperature matrices, and in the gas phase, and their bonding. This I hope to do in Part 3 of this essay.

Acknowledgment. I am indebted to Professor Irina Beletskaya of Moscow State University for biographical information about P. P. Schorigin, to Professor Mikhail Egorov, Director of the Zelinsky Institute of Organic Chemistry, for the photograph in this essay, and to Dr. Michael Wischnath, Director of the Archive of the University of Tübingen, for biographical information about Wilhelm Schlenk and the photograph in this issue. Their assistance is very much appreciated. As usual, my thanks to Professor Arnold L. Rheingold for the cover figures.

OM801047N

Communications

Synthesis, Structures, and Photoluminescent Properties of Cyclometalated Platinum(II) Complexes bearing Upper-Rim Phosphinated Calix[4]arenes

Siu-Wai Lai,* Queenie K.-W. Chan, Jie Han, Yong-Gang Zhi, Nianyong Zhu, and Chi-Ming Che*

Department of Chemistry, HKU-CAS Joint Laboratory on New Materials, and Open Laboratory of Chemical Biology of the Institute of Molecular Technology for Drug Discovery and Synthesis, The University of Hong Kong, Pokfulam Road, Hong Kong SAR, People's Republic of China

Received October 9, 2008

Summary: A series of upper-rim diphosphinated calixarene receptors bearing various R and R' substituents at the lower rim (L^n ; $n = 1-5$) were synthesized, and their reactions with $[Pt(Thpy)(HThpy)Cl]$ afforded the phosphorescent platinum(II)-modified calixarene receptors $[(PtThpyCl)_2L^n]$. The structure of $[(PtThpy(CH_3CN))_2L^1](ClO_4)_2$ and $[(PtThpyCl)_2L^5]$ were determined by X-ray crystallographic analysis, and the photophysical properties of $[(PtThpyCl)_2L^n]$ were investigated.

Calixarenes¹ have been extensively documented as ion carriers, chemical sensors, and models for in vivo reactions of enzymes.² Functionalization at the upper rim of calixarenes has expanded this class of molecules into transition-metal-bearing derivatives through metal–ligand coordination,^{3,4} which enables the signaling properties conferred by transition-metal complexes

to be incorporated into the calixarene systems. Signaling responses toward targeted guests involving calixarene receptors are commonly analyzed by NMR titration experiments⁵ and electrochemistry,⁶ yet reporting means using emission measurements have predominantly focused on $[Ru(bpy)_3]^{2+}$ -bearing molecules.^{7,8} Examples of optical sensors with luminescent metal complexes integrated into the framework of calixarenes are sparse.^{2d,9}

The square-planar geometry of platinum(II) complexes confers photophysical and photochemical properties that are different from those of octahedral $[Ru^{II}(bpy)_3]^{2+}$ derivatives due to the open Pt(II) coordination sites. Intrusion of guest molecules induces changes in its local environment, leading to a profound impact upon the photoluminescent properties.¹⁰ There is a growing interest in employing Pt(II) luminophores as a signaling moiety in the development of biomolecular chemosensors. Previous reports on cyclometalated platinum(II) complexes bearing Thpy ligands ($HThpy = 2-(2'-thienyl)pyridine$) revealed that they exhibit intriguing photoluminescent properties (visible emission, long emission lifetime) which are sensitive to the local environment.¹¹ These properties are advantageous to the development of luminescent sensors.

* To whom correspondence should be addressed. E-mail: swlai@hku.hk (S.-W.L.); cmche@hku.hk (C.-M.C.). Fax: (+852) 2857 1586.

(1) (a) Gutsche, C. D. In *Calixarenes*; The Royal Society of Chemistry: Cambridge, U.K., 1989. (b) Gutsche, C. D. In *Calixarenes Revisited, Monographs in Supramolecular Chemistry*; Stoddart, J. F., Ed.; The Royal Society of Chemistry: Cambridge, U.K., 1998. (c) *Calixarenes 2001*; Asfari, Z., Böhmer, V., Harrowfield, J., Vicens, J., Eds.; Kluwer Academic: Dordrecht, The Netherlands, 2001.

(2) (a) Ikeda, A.; Shinkai, S. *Chem. Rev.* **1997**, *97*, 1713–1734. (b) Molenveld, P.; Engbersen, J. F. J.; Reinhoudt, D. N. *Chem. Soc. Rev.* **2000**, *29*, 75–86. (c) Bakirci, H.; Koner, A. L.; Dickman, M. H.; Kortz, U.; Nau, W. M. *Angew. Chem., Int. Ed.* **2006**, *45*, 7400–7404. (d) Lo, H.-S.; Yip, S.-K.; Wong, K. M.-C.; Zhu, N.; Yam, V. W.-W. *Organometallics* **2006**, *25*, 3537–3540.

(3) (a) Wieser, C.; Dieleman, C. B.; Matt, D. *Coord. Chem. Rev.* **1997**, *165*, 93–161. (b) Steyer, S.; Jeunesse, C.; Armspach, D.; Matt, D.; Harrowfield, J. In *Calixarenes 2001*; Asfari, Z., Böhmer, V., Harrowfield, J., Vicens, J., Eds.; Kluwer Academic: Dordrecht, The Netherlands, 2001; pp 513–535. (c) Roundhill, D. M. *Prog. Inorg. Chem.* **1995**, *43*, 533–592. (d) Xu, W.; Vittal, J. J.; Puddephatt, R. J. *Inorg. Chem.* **1997**, *36*, 86–94. (e) Staffilani, M.; Hancock, K. S. B.; Steed, J. W.; Holman, K. T.; Atwood, J. L.; Juneja, R. K.; Burkhalter, R. S. *J. Am. Chem. Soc.* **1997**, *119*, 6324–6335. (f) Harvey, P. D. *Coord. Chem. Rev.* **2002**, *233–234*, 289–309. (g) Eisler, D. J.; Puddephatt, R. J. *Inorg. Chem.* **2006**, *45*, 7295–7305. (h) Puddephatt, R. J. *Can. J. Chem.* **2006**, *84*, 1505–1514.

(4) (a) Jacoby, D.; Floriani, C.; Chiesi-Villa, A.; Rizzoli, C. *J. Chem. Soc., Dalton Trans.* **1993**, 813–814. (b) Beer, P. D.; Drew, M. G. B.; Leeson, P. B.; Lyssenko, K.; Ogden, M. I. *J. Chem. Soc., Chem. Commun.* **1995**, 929–930. (c) Vézina, M.; Gagnon, J.; Villeneuve, K.; Drouin, M.; Harvey, P. D. *Chem. Commun.* **2000**, 1073–1074. (d) Gagnon, J.; Drouin, M.; Harvey, P. D. *Inorg. Chem.* **2001**, *40*, 6052–6056. (e) Dalbavie, J.-O.; Regnouf-de-Vains, J.-B.; Lamartine, R.; Perrin, M.; Lecocq, S.; Fenet, B. *Eur. J. Inorg. Chem.* **2002**, 901–909. (f) Jeunesse, C.; Armspach, D.; Matt, D. *Chem. Commun.* **2005**, 5603–5614. (g) Kim, S.; Kim, J. S.; Kim, S. K.; Suh, I.-H.; Kang, S. O.; Ko, J. *Inorg. Chem.* **2005**, *44*, 1846–1851.

(5) Beer, P. D.; Drew, M. G. B.; Heseck, D.; Shade, M.; Szemes, F. *Chem. Commun.* **1996**, 2161–2162.

(6) (a) Beer, P. D.; Heseck, D.; Kingston, J. E.; Smith, D. K.; Stokes, S. E.; Drew, M. G. B. *Organometallics* **1995**, *14*, 3288–3295. (b) Beer, P. D.; Heseck, D.; Nam, K. C.; Drew, M. G. B. *Organometallics* **1999**, *18*, 3933–3943.

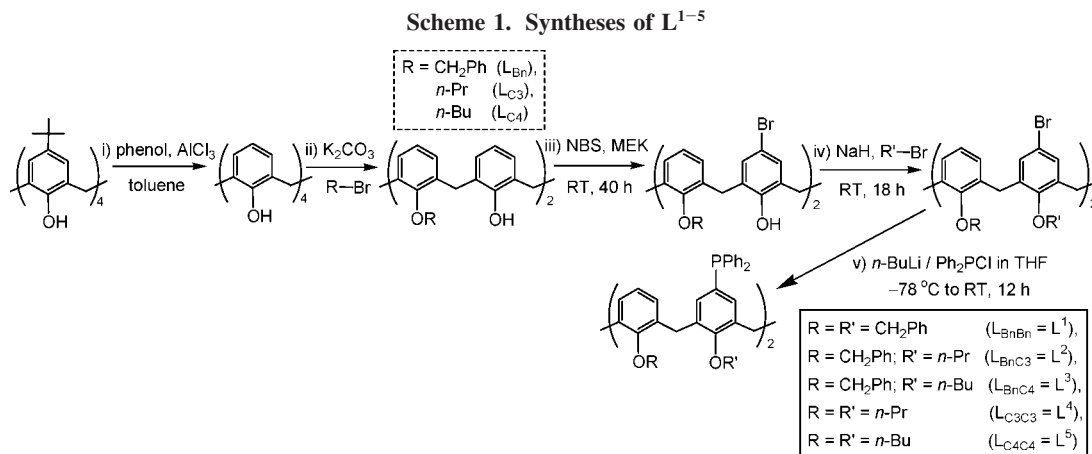
(7) (a) Szemes, F.; Heseck, D.; Chen, Z.; Dent, S. W.; Drew, M. G. B.; Goulden, A. J.; Graydon, A. R.; Grieve, A.; Mortimer, R. J.; Wear, T.; Weightman, J. S.; Beer, P. D. *Inorg. Chem.* **1996**, *35*, 5868–5879. (b) Beer, P. D.; Timoshenko, V.; Maestri, M.; Passaniti, P.; Balzani, V. *Chem. Commun.* **1999**, 1755–1756. (c) Beer, P. D.; Cadman, J. *Coord. Chem. Rev.* **2000**, *205*, 131–155. (d) Beer, P. D.; Szemes, F.; Passaniti, P.; Maestri, M. *Inorg. Chem.* **2004**, *43*, 3965–3975.

(8) Grigg, R.; Holmes, J. M.; Jones, S. K.; Norbert, W. D. J. A. *J. Chem. Soc., Chem. Commun.* **1994**, 185–187.

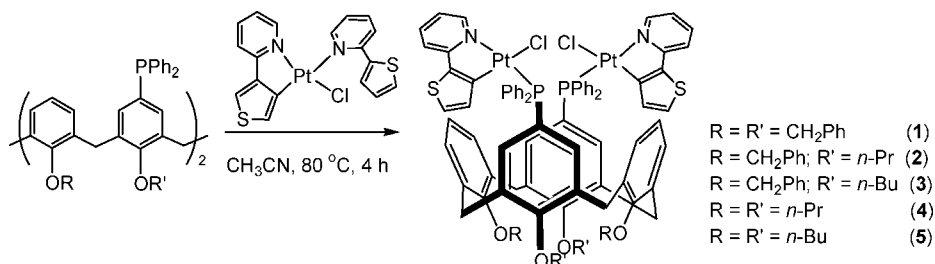
(9) (a) Beer, P. D. *Acc. Chem. Res.* **1998**, *31*, 71–80. (b) Keefe, M. H.; Benkstein, K. D.; Hupp, J. T. *Coord. Chem. Rev.* **2000**, *205*, 201–228.

(10) (a) Liu, H.-Q.; Cheung, T.-C.; Che, C.-M. *Chem. Commun.* **1996**, 1039–1040. (b) Wu, L.-Z.; Cheung, T.-C.; Che, C.-M.; Cheung, K.-K.; Lam, M. H. W. *Chem. Commun.* **1998**, 1127–1128. (c) Wong, K.-H.; Chan, M. C.-W.; Che, C.-M. *Chem. Eur. J.* **1999**, *5*, 2845–2849. (d) Che, C.-M.; Zhang, J.-L.; Lin, L.-R. *Chem. Commun.* **2002**, 2556–2557. (e) Che, C.-M.; Fu, W.-F.; Lai, S.-W.; Hou, Y.-J.; Liu, Y.-L. *Chem. Commun.* **2003**, 118–119.

(11) (a) Lai, S.-W.; Chan, M. C. W.; Peng, S.-M.; Che, C.-M. *Angew. Chem., Int. Ed.* **1999**, *38*, 669–671. (b) Lai, S.-W.; Chan, M. C. W.; Cheung, K.-K.; Peng, S.-M.; Che, C.-M. *Organometallics* **1999**, *18*, 3991–3997.



Scheme 2. Synthesis of [Pt(Thpy)]⁺-Incorporated Diphosphinated Calixarene Receptors, 1–5



In this work, a series of upper-rim diphosphinated calixarene receptors bearing various R and R' substituents at the lower rim were synthesized (Scheme 1), and their subsequent reactions with [Pt(Thpy)(HThpy)Cl] resulted in coordination of cyclometalated Pt(II) luminophores, [Pt(Thpy)]⁺, at the upper rim of the calixarenes, giving phosphorescent platinum(II)-modified calixarene receptors (Scheme 2).

25,26,27,28-Tetrahydroxycalix[4]arene was prepared by the reaction of *p*-*tert*-butylcalix[4]arene with phenol and AlCl₃ (step i in Scheme 1),¹² and its reaction with benzyl bromide, 1-iodopropane, or 1-iodobutane (R-Br; step ii in Scheme 1) in the presence of 1 equiv of K₂CO₃ in acetonitrile afforded dibenzoyloxy- (L_{Bn}), dipropoxy- (L_{C3}), or dibutoxycalix[4]arene (L_{C4}), respectively.¹³ Bromination was carried out at the para positions of hydroxylated aromatic rings using *N*-bromosuccinimide (NBS) and methyl ethyl ketone (MEK) (step iii in Scheme 1).¹⁴ This was followed by further reaction with benzyl

or alkyl bromide (R'-Br; step iv in Scheme 1) to afford various R and R' substituents at the lower rim of the calixarene ligand.¹⁵ Phosphination using Ph₂PCL at the upper rim of the calixarenes afforded L¹⁻⁵ (step v in Scheme 1).¹⁵

The reaction of L¹⁻⁵ with [Pt(Thpy)(HThpy)Cl]^{11b} in a 1:1 molar ratio in acetonitrile under reflux for 4 h gave [(PtThpyCl)₂Lⁿ] (1–5), which are isolated as orange solids in moderate to high yields (Scheme 2). Complexes 1–5 were characterized using ¹H, ¹⁹⁵Pt, ¹³C{¹H}, and ³¹P{¹H} NMR spectroscopy, ESI or FAB mass spectrometry, and X-ray crystallography (Supporting Information). They are air- and moisture-stable at room temperature.

The ¹H NMR spectra of 1–5 show signals consistent with their chemical formulation; the peak integration shows that the ratio of hydrogens for [Pt(Thpy)]⁺:Lⁿ is 2:1. The ¹H NMR spectra feature characteristic doublets at δ 2.87–3.05 and 4.15–4.40 due to the AB spin system of ArCH₂Ar in the calixarene ligand. Typically broad ¹⁹⁵Pt satellites at ~9.61 ppm were observed for 1–5. The ³¹P{¹H} NMR spectra of 1–5 reveal one singlet at δ 17.43–18.83 with ¹⁹⁵Pt satellites due to one-bond coupling (¹J_{PtP} = 4226–4232 Hz). This is comparable to that of [Pt(Thpy)PPh₃Cl] (Supporting Information) at δ 18.62 with ¹J_{PtP} = 4236 Hz, revealing that the phosphorus atoms in [(PtThpyCl)₂L¹⁻⁵] and [Pt(Thpy)PPh₃Cl] are in similar environments. The ¹⁹⁵Pt NMR spectra of 1–5 exhibit a doublet of peaks at ca. δ -4250 with ¹J_{PtP} coupling constants of 4220–4232 Hz. The ¹³C{¹H} NMR spectra of 1–5 are well resolved with peaks at δ 117.0–161.0 corresponding to the aryl protons in the [Pt(Thpy)]⁺ and Lⁿ (n = 1–5) moieties. Their ESI or FAB mass spectra show the [(PtThpy)₂LⁿCl]⁺ molecular ion. The

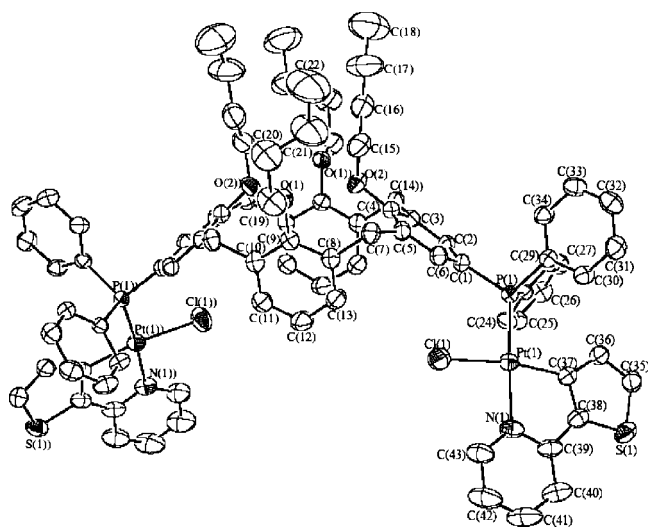


Figure 1. Perspective view of [(PtThpy)₂L⁵] (30% probability ellipsoids).

(12) Percec, V.; Bera, T. K.; De, B. B.; Sanai, Y.; Smith, J.; Holerca, M. N.; Barboiu, B.; Grubbs, R. B.; Fréchet, J. M. J. *J. Org. Chem.* **2001**, *66*, 2104–2117.

(13) van Loon, J.-D.; Arduini, A.; Coppi, L.; Verboom, W.; Pochini, A.; Ungaro, R.; Harkema, S.; Reinhoudt, D. N. *J. Org. Chem.* **1990**, *55*, 5639–5646.

(14) Shimizu, S.; Shirakawa, S.; Sasaki, Y.; Hirai, C. *Angew. Chem., Int. Ed.* **2000**, *39*, 1256–1259.

(15) Takenaka, K.; Obora, Y.; Jiang, L. H.; Tsuji, Y. *Organometallics* **2002**, *21*, 1158–1166.

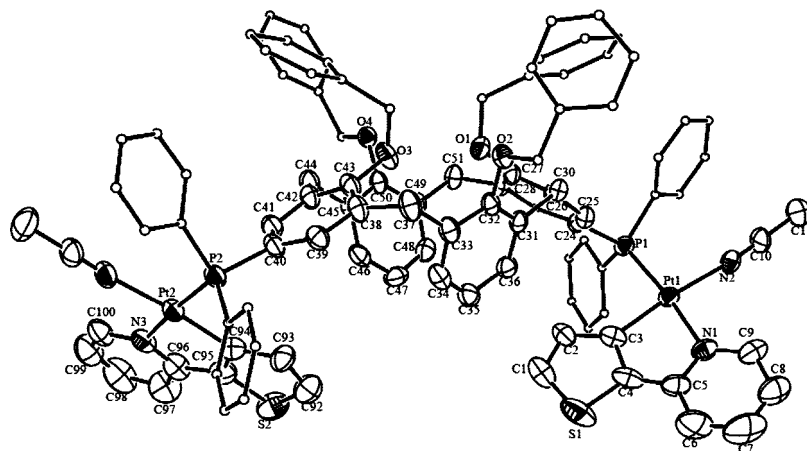


Figure 2. Perspective view of the cation in $[(\text{PtThpy}(\text{CH}_3\text{CN}))_2\text{L}^1](\text{ClO}_4)_2$ (30% probability ellipsoids).

high-resolution ESI-MS of $[(\text{PtThpyCl})_2\text{L}^4]$ in acetonitrile reveals peak clusters centered at m/z 1706.4 corresponding to $[(\text{PtThpy})_2\text{L}^4\text{Cl}]^+$, plus additional peaks centered at m/z 856.2 with a peak separation of 0.5 mass unit, which is attributed to $[(\text{PtThpy})_2\text{L}^4(\text{CH}_3\text{CN})]^{2+}$ (Figure S2 in the Supporting Information).

Crystals of $[(\text{PtThpyCl})_2\text{L}^5]$ were obtained by layering of *n*-hexane into a dichloromethane solution. However, upon layering of *n*-hexane into a dichloromethane solution of $[(\text{PtThpyCl})_2\text{L}^1]$ in the presence of LiClO_4 in acetonitrile, crystals of $[(\text{PtThpy}(\text{CH}_3\text{CN}))_2\text{L}^1](\text{ClO}_4)_2$ were obtained. As depicted in the crystal structures (Figures 1 and 2), the platinum atom adopts an approximately square planar geometry. The N–Pt–C angle of $\sim 80.6^\circ$ is typical for related complexes.^{11b} The Pt–N (2.087–2.124 Å) and Pt–C (~ 2.01 Å) distances of the $[(\text{PtThpy})^+]$ units agree with those reported for $[(\text{PtThpy})\text{PPh}_3\text{Cl}]$ (2.118(6) and 1.987(8) Å, respectively). For $[(\text{PtThpy}(\text{CH}_3\text{CN}))_2\text{L}^1]^{2+}$, the $\text{N}\equiv\text{CCH}_3$ groups are nearly linear (Pt–N–C = 174° ; N–C–C = 178°), whereas the Pt–NCCH₃ distances of 2.069(9) and 2.094(8) Å are slightly longer than that of 1.996(14) Å in $[(\text{Pt}(\text{trpy})\text{MeCN})]^{2+}$ (trpy = 2,2':6',2''-terpyridine),¹⁶ due to the trans effect of the thienyl carbanion (Figure 2). The Pt–P–C(calixarene) angles of $111.3(3)$ – $119.8(1)^\circ$ allow good separation between the two phenyl rings in PPh₂ and the $[(\text{PtThpy})^+]$ moiety, in order to avoid steric repulsion. The bond lengths and angles are consistent with those observed for metal complexes featuring such calix[4]arene scaffolds.¹⁵ The four *n*-BuO (Figure 1) or Ph₂CO moieties (Figure 2) remain at the lower rim to afford modified calixarenes in the cone conformation, and the four oxygen atoms are directed toward the cavity of the calixarenes. There are weak intermolecular interactions including $\text{PhCH}_2\cdots\text{CH}(\text{Thpy})$ (2.698–2.886 Å), $(\text{L}^5)\text{Ar}_2\text{CH}_2\cdots\text{CH}(\text{Ph}_2\text{P})$ (2.771 Å), and $(\text{L}^5)\text{HC}\cdots\text{HC}(\text{Ph}_2\text{P})$ (2.852 Å) in the crystal structure of $[(\text{PtThpyCl})_2\text{L}^5]$ (Figure 1). Similarly, there are intermolecular interactions between the $[(\text{PtThpy}(\text{CH}_3\text{CN}))_2\text{L}^1]^{2+}$ cations as well as between the $[(\text{PtThpy}(\text{CH}_3\text{CN}))_2\text{L}^1]^{2+}$ and perchlorate ions in the crystal structure of $[(\text{PtThpy}(\text{CH}_3\text{CN}))_2\text{L}^1](\text{ClO}_4)_2$. These weak interactions include $\text{CH}_3\text{CN}\cdots\text{HC}(\text{Ph}_2\text{P})$ (2.627 Å), $\text{NCCH}_3\cdots\text{OClO}_3$ (2.648 Å), $\text{PhCH}_2\cdots\text{OClO}_3$ (2.497 Å), and $(\text{pyridyl})\text{CH}\cdots\text{OClO}_3$ (2.486 Å).

The UV–visible absorption and emission properties of **1–5** have been studied and are listed in the Supporting Information. As examples, the absorption spectra of **3** and **4** in acetonitrile are depicted in Figures 3 and S3 (Supporting Information),

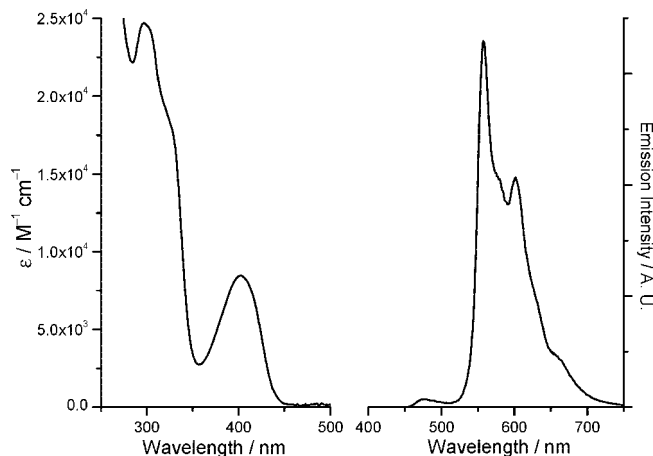


Figure 3. Absorption (left) and emission (right; $\lambda_{\text{ex}} = 400$ nm, concentration 1.55×10^{-5} M) spectra of **3** in acetonitrile at 298 K.

respectively. The high-energy, intense absorption bands with λ_{max} at 295–300 nm ($\epsilon = 23\,800$ – $29\,400$ $\text{M}^{-1} \text{cm}^{-1}$) are attributed to spin-allowed intraligand ^1L : $\pi(\text{Thpy}) \rightarrow \pi^*(\text{Thpy})$ and $\pi(\text{L}^n) \rightarrow \pi^*(\text{L}^n)$ transitions. The moderately intense low-energy band with λ_{max} at 402–406 nm ($\epsilon = 8200$ – 9600 $\text{M}^{-1} \text{cm}^{-1}$) is assigned to spin-allowed metal-to-ligand charge transfer $^1\text{MLCT}$: $\text{Pt}(5\text{d}) \rightarrow \pi^*(\text{Thpy})$ transition,^{11b} which closely resembles the $^1\text{MLCT}$ absorption of $[(\text{Pt}(\text{Thpy})\text{PPh}_3\text{Cl})]$ with λ_{max} at 398 nm ($\epsilon = 3800$ $\text{M}^{-1} \text{cm}^{-1}$). Solvatochromic effects for the absorption spectrum of **4** were investigated. The high-energy absorption maximum slightly shifts from 293 nm ($\epsilon = 29\,100$ $\text{M}^{-1} \text{cm}^{-1}$) in MeOH to 302 nm ($\epsilon = 31\,600$ $\text{M}^{-1} \text{cm}^{-1}$) in THF, whereas the low-energy band with λ_{max} at 398 nm ($\epsilon = 10\,000$ $\text{M}^{-1} \text{cm}^{-1}$) in MeOH is red-shifted to 402 nm ($\epsilon = 9400$ $\text{M}^{-1} \text{cm}^{-1}$) in CH_3CN and 409 nm ($\epsilon = 9900$ $\text{M}^{-1} \text{cm}^{-1}$) in THF.

The emission spectra of **3** and **4** in acetonitrile at 298 K exhibit a low-energy structured emission with peak maxima at ~ 558 and 602 nm (Figures 3 and S3). The microsecond emission lifetimes (~ 1.20 – 1.43 μs) of **1–5** in dichloromethane solutions indicate the emissions to be phosphorescence. Similar emission properties of analogous $[(\text{PtThpy})^+]$ complexes^{11b} and of $[(\text{PtThpy})\text{PPh}_3\text{Cl}]$ ¹⁷ have been reported. In comparison with the absorption data, solvatochromic effects on the emission energy of **4** is minor, as the emission λ_{max} does not alter upon

(16) Büchner, R.; Field, J. S.; Haines, R. J.; Cunningham, C. T.; McMillin, D. R. *Inorg. Chem.* **1997**, *36*, 3952–3956.

(17) Kulikova, M. V.; Balashev, K. P.; Kvam, P. I.; Songstad, J. *Russ. J. Gen. Chem.* **1999**, *69*, 1521–1527.

changing the solvent from dichloromethane to acetonitrile. Instead, the lifetime increases from 0.77 μs in CH_3CN to 2.09 μs in DMSO, and the emission quantum yield increases from 0.0074 in CH_3CN to 0.045 in CH_3OH . The emission data reveal that the emissive excited state is largely ^3IL in nature, although mixing with $^3\text{MLCT}$ cannot be excluded.

The solid-state emission spectra of **1–5** at 298 K show structured emission bands with peaks at ~ 559 , 580, and 603 nm, which become more resolved with slightly blue-shifted λ_{max} to 557 nm upon cooling to 77 K. Importantly, the emission lifetimes of solid samples of **1–5** significantly increase to 13.9–21.2 μs at 77 K. The emission spectra of **1–5** in butyronitrile glassy solution show vibronically resolved peaks at 550–655 nm and emission lifetimes of 42.1–44.1 μs . The significant temperature dependence for the emission lifetimes of solid samples of **1–5** is consistent with the d–d excited states being responsible for the nonradiative decay of the emission.

To examine the effects of auxiliary ligands upon the emission properties of $[\text{PtThpy}]^+$ luminophores, we synthesized $[\text{Pt}(\text{Thpy})\text{PPh}_3(\text{CH}_3\text{CN})\text{ClO}_4$ (**6**) by reacting $[\text{Pt}(\text{Thpy})\text{PPh}_3\text{Cl}]$ with AgClO_4 in acetonitrile. The low-energy $^1\text{MLCT}$ absorption band of **6** at 389 nm ($\epsilon = 2400 \text{ M}^{-1} \text{ cm}^{-1}$) is blue-shifted from that (398 nm; $\epsilon = 3800 \text{ M}^{-1} \text{ cm}^{-1}$) in $[\text{Pt}(\text{Thpy})\text{PPh}_3\text{Cl}]$ (Supporting Information). Interestingly, the emission λ_{max} values of $[\text{Pt}(\text{Thpy})\text{PPh}_3\text{Cl}]$ and **6** in acetonitrile solutions are virtually the same. However, both the emission quantum yield and lifetime of **6** remarkably increase to 0.17 and 26.2 μs , respectively, from $[\text{Pt}(\text{Thpy})\text{PPh}_3\text{Cl}]$ ($\Phi = 0.020$; $\tau = 6.8 \mu\text{s}$). Similar phenomena were observed when $[(\text{PtThpyCl})_2\text{L}^4]$ (**4**) was treated with AgClO_4 in acetonitrile; namely, a blue-shifted $^1\text{MLCT}$ absorption band (402 to 390 nm) and substantial enhancement in emission quantum yield (0.0074 to 0.21) and lifetime (0.77 to 28.9 μs) were detected. We postulate that the increased cationic charge on the $[\text{Pt}(\text{Thpy})\text{PPh}_3]^+$ luminophore, upon replacing the coordinated chloride ligand by acetonitrile, causes an increase in the

energy of the d–d excited state, which consequently leads to increases in the emission intensity and lifetime.

In conclusion, we have prepared phosphorescent platinum(II)-modified calixarene receptors by coordination of $[\text{Pt}(\text{Thpy})]^+$ moieties by the pendant phosphine groups at the upper rim of calix[4]arenes. The electronic and spectroscopic properties of the $[\text{Pt}(\text{Thpy})]^+$ units can be systematically varied by changing the bidentate cyclometalated ligands. Furthermore, the chloride and acetonitrile ligands in $[(\text{PtThpyCl})_2\text{L}^5]$ and $[\{\text{PtThpy}(\text{CH}_3\text{CN})\}_2\text{L}^1](\text{ClO}_4)_2$, respectively, would allow modification of the platinum(II)-incorporated calixarene receptors by ligand substitution reactions. All these can significantly affect the mixed $^3\text{MLCT}/^3\text{IL}$ emissive excited states, together with the deactivating d–d states, leading to a new class of luminescent calix[4]arene-based sensory molecules. Our studies on the binding reactions of $[(\text{PtThpyCl})_2\text{L}^n]$ with neutral and anionic hydrophobic analytes are in progress.

Acknowledgment. We are grateful for financial support from the Research Grant Council of the Hong Kong SAR, People's Republic of China (HKU 7030/06P), The University of Hong Kong (URC-administered Seed Funding Grant 200411159082), and the National Natural Science Foundation of China/Research Grants Council Joint Research Scheme (N_HKU 752/08). We thank Dr. Kwan-Ming Ng for performing high-resolution ESI-MS experiments and for helpful discussions.

Supporting Information Available: Text, figures, tables, and CIF files giving experimental details, spectroscopic data, crystallographic data, and selected photophysical spectra. This material is available free of charge via the Internet at <http://pubs.acs.org>.

OM800969Z

Gilman-Type versus Lipshutz-Type Reagents: Competition in Lithiocuprate Chemistry

Joanna Haywood, James V. Morey, and Andrew E. H. Wheatley*

Department of Chemistry, University of Cambridge, Lensfield Road, Cambridge CB2 1EW, U.K.

Ching-Yuan Liu

Advanced Elements Chemistry Laboratory, The Institute of Physical and Chemical Research, RIKEN, 2-1 Hirosawa, Wako-shi, Saitama 351-0198, Japan, and Organization for Frontier Research in Pharmaceutical Sciences, Hokuriku University, Kanagawa-machi, Kanazawa 920-1181, Japan

Shuji Yasuie and Jyoji Kurita

Faculty of Pharmaceutical Sciences, Hokuriku University, Kanagawa-machi, Kanazawa 920-1181, Japan

Masanobu Uchiyama*

Advanced Elements Chemistry Laboratory, The Institute of Physical and Chemical Research, RIKEN, 2-1 Hirosawa, Wako-shi, Saitama 351-0198, Japan

Paul R. Raithby

Department of Chemistry, University of Bath, Claverton Down, Bath BA2 7AY, U.K.

Received November 19, 2008

Summary: *CuCN* reacts with *RLi* and *TMPLi* (*TMP* = 2,2,6,6-tetramethylpiperidide) to give Gilman-type cuprates *R(TMP)CuLiⁿL* (*R* = Ph, *n* = 3, *L* = THF **2**; *R* = Me, *n* = 1, *L* = TMEDA **3**). **3** and **3**LiCN have been tested in directed ortho cupration with data suggesting enhanced efficiency for Lipshutz-type **3**LiCN; competition between Lipshutz- and Gilman-type formulations is rationalized by DFT methods.

It has recently been established that amido ligand components of homoleptic cuprates can act as bases in the directed ortho cupration (DoC) of functionalized arenes.¹ The nontransferable and potentially chiral nature of amido ligands in heteroleptic cuprates is already theoretically established,² and it is this which has formed the basis of their deployment in synthetic chemistry.³ Whereas homoleptic bis(alkyl)cuprates have been the focus of both synthetic applications and structural investigations,⁴ structure studies on heteroleptic organo(amido)cuprates are harder to come by.⁵ It is only lately that Davies et al. reported the first isolation and solid-state characterization of an organo(amido)cuprate,⁶ the head-to-tail dimeric structure of MesCu(NBn₂)Li

(Bn = benzyl) confirming theoretical expectations.⁷ In spite of the observation of a complex Schlenk equilibrium, the dimeric MesCu(NBn₂)Li system showed negligible signs of deaggregation in solution. While a deaggregated organo(amido)cuprate has been established in solution—a monomeric π -complex between *n*-butyl{(*R*)-*N*-methyl-1-phenyl-2-(1-pyrrolidinyl)ethanimido}cuprate and cyclohexanone being invoked in the Cu-mediated 1,4-alkylation of α,β -unsaturated ketones⁸—such a species has not hitherto been isolated.

In seeking to extend the field of directed aromatic deprotonation using heterobimetallic reagents,⁹ we have probed the utility of both Gilman- and Lipshutz-type¹⁰ organo(amido)cuprates in DoC reactions and found that the latter type represent substantially more effective substrates.¹ During the course of this work, we established that the treatment of CuCN with 2 equiv of TMPLi afforded the isolable Lipshutz-type complex (TMP)₂Cu(CN)Li₂·THF (**1**), which revealed a dimeric formulation in the solid state, fundamental to the integrity of which was (i) the ability of [TMP][−] to act as an intermetal bridge between Cu and Li and (ii) the retention of [CN][−] in the dimer core (Scheme 1). We next sought to investigate whether the retention of cyanide (Lipshutz characteristics) occurred in heteroleptic organo(amido)cuprates since metallo intermediates,

* To whom correspondence should be addressed. Fax: Int +44-1223-336362 (A.E.H.W.); Int +81-48-467-2879 (M.U.). E-mail: aehw2@cam.ac.uk (A.E.H.W.); uchi_yama@riken.jp.

(1) Usui, S.; Hashimoto, Y.; Morey, J. V.; Wheatley, A. E. H.; Uchiyama, M. *J. Am. Chem. Soc.* **2007**, *129*, 15102.

(2) Yamanaka, M.; Nakamura, E. *J. Am. Chem. Soc.* **2005**, *127*, 4697.

(3) (a) Lipshutz, B. H.; Sengupta, S. *Org. React.* **1992**, *41*, 135. (b) *Modern Organocopper Chemistry*; Krause, N., Ed.; Wiley-VCH: Weinheim, Germany, 2002. (c) *Compounds of Groups 12 and 11 (Zn, Cd, Hg, Cu, Ag, Au)*; O'Neil, I., Ed.; Georg Thieme: Stuttgart, Germany, 2004; Science of Synthesis, Vol. 3.

(4) E.g.: (a) Bertz, S. H.; Chopra, A.; Eriksson, M.; Ogle, C. A.; Seagle, P. *Chem. Eur. J.* **1999**, *5*, 2680. (b) Henze, W.; Vyater, A.; Krause, N.; Gschwind, R. M. *J. Am. Chem. Soc.* **2005**, *127*, 17335.

(5) Gschwind, R. M. *Chem. Rev.* **2008**, *108*, 3029.

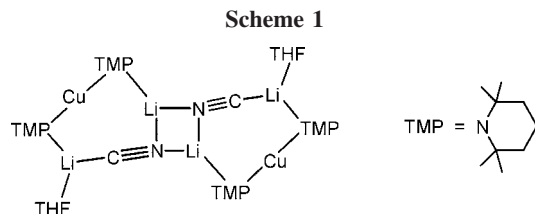
(6) Davies, R. P.; Hornauer, S.; Hitchcock, P. B. *Angew. Chem., Int. Ed.* **2007**, *46*, 5191.

(7) (a) Dieter, R. K.; Tokles, M. *J. Am. Chem. Soc.* **1987**, *109*, 2040. (b) Dieter, R. K.; Hanks, T. W. *Organometallics* **1992**, *11*, 3549. (c) Rossiter, B. E.; Eguchi, M.; Miao, G.; Swingle, N. M.; Hernandez, A. E.; Vickers, D.; Fluckiger, E.; Patterson, R. G.; Reddy, K. V. *Tetrahedron* **1993**, *49*, 965.

(8) Eriksson, J.; Davidsson, O. *Organometallics* **2001**, *20*, 4763.

(9) Mulvey, R. E.; Mongin, F.; Uchiyama, M.; Kondo, Y. *Angew. Chem., Int. Ed.* **2007**, *46*, 3802, and references cited therein.

(10) (a) Lipshutz, B. H.; Wilhelm, R. S.; Floyd, D. M. *J. Am. Chem. Soc.* **1981**, *103*, 7672. (b) Lipshutz, B. H.; Wilhelm, R. S.; Kozlowski, J. A. *Tetrahedron* **1984**, *40*, 5005. (c) Lipshutz, B. H.; Kozlowski, J. A.; Wilhelm, R. S. *J. Org. Chem.* **1984**, *49*, 3943. (d) Lipshutz, B. H. *Synthesis* **1987**, 325. (e) Lipshutz, B. H.; Sharma, S.; Ellsworth, E. L. *J. Am. Chem. Soc.* **1990**, *112*, 4032.



putatively of the type $R(\text{TMP})\text{Cu}(\text{CN})\text{Li}_2$, have recently been shown to be proficient DoC reagents.¹ Notably, recent theoretical work has suggested the importance of the seven-membered $\text{X}_2\text{Cu}(\text{CN})\text{Li}_2$ metallacycle in the chemistry of cyanide-containing higher order cuprates.¹¹ Interestingly, however, whereas several reports of cyanide-containing lower order cuprates exist,¹² the only fully characterized higher order cuprates to incorporate cyanide are homoleptic. Whereas metallacycle formation was noted in **1**,¹ the poor bridging ability of *t*Bu groups combined with the presence of strong Lewis base incurs ion separation in $[(t\text{Bu})_2\text{Cu}]^-[(\text{CN})\{\text{Li}(\cdot\text{THF})\cdot\text{PMDETA}\}_2]^+$,¹³ while in $(2\text{-Me}_2\text{NCH}_2\text{C}_6\text{H}_4)_2\text{Cu}(\text{CN})\{\text{Li}(\cdot 2\text{THF})\}_2$ the bridging ligands favor polymerization instead.¹⁴ Herein we present the preliminary structural results obtained when organo(cyano)cuprates are treated with a lithium amide. Data suggest that, in contrast to the 2:1 reaction of lithium amide with CuCN, the 1:1 reaction of $\text{RCu}(\text{CN})\text{Li}$ ($R = \text{alkyl, aryl}$) with a lithium amide results in the expulsion of LiCN, that Gilman-type products compete with the corresponding Lipshutz-type species, and that solvent interactions prevent aggregation.

The recently reported synthesis and isolation of **1** resulted from the treatment of CuCN with excess TMPLi, after which the solvent was removed and replaced by toluene for recrystallization.¹ The homoleptic product was shown to effect DoC of the representative substrate *N,N*-diisopropylbenzamide with the TMP ligand acting as a base, enabling homocoupling to give a 2,2-biaryl through oxidation by PhNO_2 . Conversely, the synthesis of heterocoupled $2\text{-RC}_6\text{H}_4\text{C}(\text{O})\text{NiPr}_2$ ($R = \text{Me, Ph}$) was enabled by the use of the corresponding putative heteroleptic cuprates $\text{R}(\text{TMP})\text{Cu}(\text{CN})\text{Li}_2$. In seeking to probe the identity of the aryl cuprate ($R = \text{Ph}$), we sequentially treated a slurry of CuCN in THF with THF stock solutions of PhLi and TMPLi (1 equiv each). The resulting solution was concentrated prior to storage at -30°C , after which colorless plates of **2** were obtained (Scheme 2). However, importantly, whereas the spectroscopic analysis of bulk **1** supplied evidence for the inclusion of cyanide (clearly seen at δ 167.1 by ^{13}C NMR spectroscopy and 2104.1 cm^{-1} by IR spectroscopy—replaced by a strong signal at 2129.2 cm^{-1} upon hydrolysis),¹⁵ comparable analysis of bulk **2** demonstrated the complete absence of both the ^{13}C NMR resonance and the infrared stretching modes attributable to cyanide. Instead, ^1H NMR spectroscopy yielded signals suggesting the presence of phenyl, TMP, and THF in a

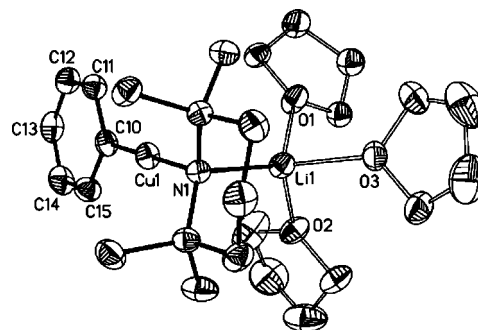
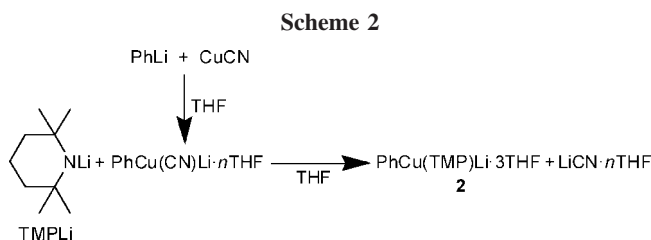


Figure 1. Structure of **2** at the 40% probability level with H atoms and disorder omitted. Selected bond lengths (Å): C10–Cu1 = 1.903(2), N1–Cu1 = 1.9116(18), N1–Li1 = 2.188(4).



1:1:3 ratio and therefore pointing to a Gilman-type formulation. This was confirmed crystallographically, with **2** depositing in the triclinic crystal system $P\bar{1}$, and the crystal structure (Figure 1) revealing the monomeric complex $\text{PhCu}(\mu\text{-TMP})\text{Li}\cdot 3\text{THF}$ in which the copper center adopts a near-linear geometry ($\text{N1-Cu1-C10} = 176.36(8)^\circ$) and the amide acts as an intermetal bridge ($\text{Cu1-N1-Li1} = 87.04(12)^\circ$). While such behavior has been seen in the metallacyclic $\text{M}(\mu\text{-R})(\mu\text{-N})\text{Li}$ cores of related aluminates¹⁶ and zincates,^{9,17} and equivocally in manganates,¹⁸ the motif seen here, in which essentially linear geometry at Cu^{19} prevents the formation of a four-membered metallacycle, bears close comparison to homoleptic **1** ($\text{Cu-N-Li} = 91.12(13), 94.92(14)^\circ$)¹ and $(\text{Ph}_2\text{N})_2\text{Cu}(\text{Ph}_2\text{N})\text{Li}_2\cdot 2\text{OEt}_2$ ($\text{Cu-N-Li} = 88.3(2)^\circ$ in a six-membered ring),²⁰ heteroleptic $\text{MesNHCu}(\text{PhNH})\text{Li}\cdot\text{DME}$ ($\text{Cu-N-Li} = 105.9(4), 107.2(5)^\circ$ in an eight-membered ring),²⁰ and the aryl(amido)cuprate $\text{MesCu}(\text{NBn}_2)\text{Li}$ ($\text{Cu-N-Li} = 89.96^\circ$).⁶ The observation of a terminal Cu-Ph interaction (1.903(2) Å) is highly unusual. While this interaction is known from other fields of organo-copper chemistry,²¹ the only precedents in lithiocuprate chem-

(16) (a) Naka, H.; Uchiyama, M.; Matsumoto, Y.; Wheatley, A. E. H.; McPartlin, M.; Morey, J. V.; Kondo, Y. *J. Am. Chem. Soc.* **2007**, *129*, 1921. (b) García-Alvarez, J.; Hevia, E.; Kennedy, A. R.; Klett, J.; Mulvey, R. E. *Chem. Commun.* **2007**, 2402.

(17) (a) Clegg, W.; Dale, S. H.; Hevia, E.; Honeyman, G. W.; Mulvey, R. E. *Angew. Chem., Int. Ed.* **2006**, *45*, 2370. (b) Uchiyama, M.; Matsumoto, Y.; Nobuto, D.; Furuyama, T.; Yamaguchi, K.; Morokuma, K. *J. Am. Chem. Soc.* **2006**, *128*, 8748. (c) Kondo, Y.; Morey, J. V.; Morgan, J. M.; Raithby, P. R.; Nobuto, D.; Uchiyama, M.; Wheatley, A. E. H. *J. Am. Chem. Soc.* **2007**, *129*, 12734. (d) Clegg, W.; García-Alvarez, J.; García-Alvarez, P.; Graham, D. V.; Harrington, R. W.; Hevia, E.; Kennedy, A. R.; Mulvey, R. E.; Russo, L. *Organometallics* **2008**, *27*, 2654.

(18) García-Alvarez, J.; Kennedy, A. R.; Klett, J.; Mulvey, R. E. *Angew. Chem., Int. Ed.* **2007**, *46*, 1105.

(19) Power, P. P.; Ruhlandt-Senge, K.; Shoner, S. C. *Inorg. Chem.* **1991**, *30*, 5013.

(20) Reiss, P.; Fenske, D. *Z. Anorg. Allg. Chem.* **2000**, *626*, 1317. (21) (a) Gambarotta, S.; Strologo, S.; Floriani, C.; Chiesi-Villa, A. *Organometallics* **1984**, *3*, 1444. (b) Dattelbaum, A. M.; Martin, J. D. *Polyhedron* **2006**, *25*, 349. (c) Fischer, R.; Gorls, H.; Westerhausen, M. *Organometallics* **2007**, *26*, 3269.

(22) (a) Hope, H.; Olmstead, M. M.; Power, P. P.; Sandell, J.; Xu, X. *J. Am. Chem. Soc.* **1985**, *107*, 4337. (b) Davies, R. P.; Hornauer, S. *Eur. J. Inorg. Chem.* **2005**, 51.

(11) (a) Nakamura, E.; Mori, S. *Angew. Chem., Int. Ed.* **2000**, *39*, 3750. (b) Mori, S.; Nakamura, E.; Morokuma, K. *J. Am. Chem. Soc.* **2000**, *122*, 7294.

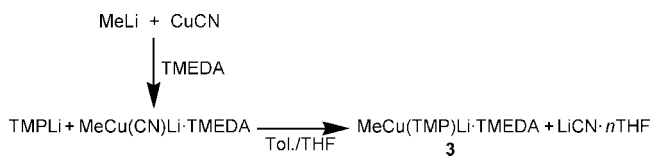
(12) (a) Hwang, C.-S.; Power, P. P. *J. Am. Chem. Soc.* **1998**, *120*, 6409. (b) Hwang, C.-S.; Power, P. P. *J. Am. Chem. Soc.* **1999**, *18*, 697. (c) Eaborn, C.; Hill, M. S.; Hitchcock, P. B.; Smith, J. D. *Organometallics* **2000**, *19*, 5780. (d) Bosold, F.; Marsch, M.; Harms, K.; Boche, G. *Z. Kristallogr. New Cryst. Struct.* **2001**, *216*, 143. (e) Eaborn, C.; El-Hamruni, S. M.; Hill, M. S.; Hitchcock, P. B. *Dalton Trans.* **2002**, n/a, 3975. (f) Davies, R. P.; Hornauer, S. *Eur. J. Inorg. Chem.* **2005**, 51.

(13) Boche, G.; Bosold, F.; Marsch, M.; Harms, K. *Angew. Chem., Int. Ed.* **1998**, *37*, 1684.

(14) Kronenburg, C. M. P.; Jastrzebski, J. T. B. H.; Spek, A. L.; van Koten, G. *J. Am. Chem. Soc.* **1998**, *120*, 9688.

(15) See the Supporting Information.

Scheme 3



istry are the longer 1.925(10) and 1.916 Å (mean) bonds noted in the ion separates $[\text{Ph}_2\text{Cu}]^-[\text{Li}\cdot 2(12\text{-crown-4})]^+$ and $\{[\text{Ph}_2\text{Cu}]^-\}_2\{(\text{Cu}\cdot 2\text{PPh}_3)\{(\text{CN})\text{Li}\}_2\cdot 5\text{THF}\}_2^{2+}$,²² while the remaining reported terminal Cu–Ar bonds in this area feature kinetically protective Mes,²³ C₆H₃-2,6-Mes₂,²⁴ or C₆H₃-2,6-Trip₂ (Trip = C₆H₂-2,4,6-*i*Pr₃).^{12a,b} Consistent with the high level of external solvation of the alkali metal (O–Li1 range 2.041(4)–2.067(4) Å), N1–Li1 is, at 2.188(4) Å, relatively long (viz. 1.982(5) and 1.995(4) Å in **1** and 1.969(10) Å in MesCu(NBn₂)Li).^{1,6}

The ability of the putative cuprate Me(TMP)Cu(CN)Li₂ to achieve the heterocoupled product 2-MeC₆H₄C(O)NiPr₂ led us to probe the identity of the heterometallic species isolable from a MeLi/CuCN/TMPLi mixture. Accordingly, a slurry of CuCN in THF was sequentially treated with etherate solutions of MeLi and TMPLi (1 equiv each). Concentration of the resulting solution gave an oil, the storage of which at –30 °C failed to yield any isolable material. However, a surprising modification of the protocol led to greater success. Thus, a stock solution of TMPLi (1 equiv) in dry toluene was added to a slurry containing equimolar MeLi and CuCN in dry TMEDA at –78 °C. The resulting cream-colored slurry changed color from medium yellow to pale yellow and was left to reach 0 °C, whereupon the introduction of THF gave a solution. The storage of this mixture at –30 °C for 24 h produced colorless needles (Scheme 3). As for **2**, ¹³C NMR and infrared spectroscopy again clearly showed the complete absence of cyanide. ¹H NMR spectroscopy in C₆D₆ showed signals attributable to only Me, TMP, and TMEDA, with the respective integrations (1:1:1) suggesting a Gilman-type cuprate akin to **2**, namely MeCu(μ-TMP)-Li·TMEDA (**3**). The most notable spectroscopic feature of this formulation is the cuprated methyl group, and this was plainly observable by both ¹H and ¹³C NMR methods at δ –0.07 and –11.0, respectively.

X-ray crystallography confirmed the proposed formulation of **3**, with the crystals depositing in the orthorhombic system *Pm**cn*. For each molecule of MeCu(μ-TMP)Li·TMEDA there resides one unit of lattice THF, though analysis suggests that this is largely removed in vacuo during isolation.¹⁵ The structure demonstrates a monomer in spite of a reduction in the coordination state of the alkali metal from distorted tetrahedral in **2** to essentially trigonal planar in **3** (sum of angles at Li1 359.9°; Figure 2). The TMEDA–Li interactions are 2.120(11) and 2.081(9) Å. However, in response to the decreased group 1 metal coordination state, the lithium–amide distance is, at 1.992(9) Å, rather short for a N–Li bond²⁵ and significantly less than the analogous interaction in **2**. The angles at both the intermetal amide bridge (Cu1–N1–Li1 = 92.1(3)°) and the copper atom (178.2(2)°) are comparable to those in **2**. However, both bonds to copper are extended in **3** relative to those in **2** (N1–Cu1 = 1.942(4) Å and C1–Cu1 = 1.927(5) Å). As with that of the Cu–Ph bond in **2**, the characterization of a Cu–Me interaction in the solid state is, in itself, unusual. Homoleptic

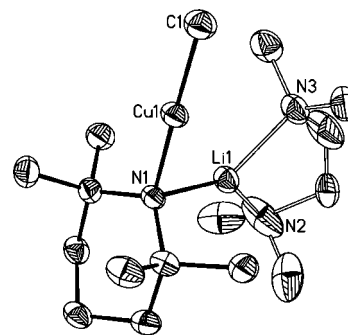


Figure 2. Structure of **3** at the 40% probability level with TMEDA disorder and lattice THF and H atoms omitted. Selected bond lengths (Å) and angles (deg): C1–Cu1 = 1.927(5), N1–Cu1 = 1.942(4), N1–Li1 = 1.992(9); Cu1–N1–Li1 = 92.1(3), N1–Li1–N2 = 139.2(5), N1–Li1–N3 = 133.6(5).

dimethylcuprate ions have been noted in $[\text{Me}_2\text{Cu}]^-[\text{Li}\cdot n\text{L}]^+$ ($n = 2$, L = 12-crown-4, C–Cu = 1.935(8) Å; $n = 3$, L = DME, mean C–Cu = 1.933 Å)^{22,26} and, of the alkyl(phosphido)cuprates $\text{RCu}\{\mu\text{-P}(t\text{Bu})_2\}\text{Li}\cdot 3\text{THF}$ (R = Me, *n*Bu, *s*Bu, *t*Bu), the methyl homologue has been fully characterized (C–Cu = 1.940(4) Å).²⁷

We have previously shown that Gilman-type cuprates represent inferior DoC substrates when they are compared to their Lipshutz-type analogues.¹ Accordingly, we conducted experiments that proved the importance of LiCN inclusion in amidocuprate chemistry by revealing the ortho iodination of benzonitrile in 74% yield employing (TMP)₂CuLi·LiCN but complete failure of the reaction if (TMP)₂CuLi·LiI is used instead. To further test this idea, here we have treated *N,N*-diisopropylbenzamide both with preisolated **3** and solutions containing **3** and LiCN and, thereafter, with I₂.¹⁵ Data reveal that iodination proceeds in both cases but affords only 37% 2-iodo-*N,N*-diisopropylbenzamide when employing preisolated **3**. This improved to 89% using a solution from which **3** had deposited at –30 °C (and which logically therefore contained LiCN) prior to its redissolution at ambient temperature. Having noted this discrepancy, we sought to probe the nature of the relationship between Lipshutz- and Gilman-type species theoretically (B3LYP method, SVP basis set for Cu and 6-31+G* basis set for other atoms).¹⁵ The calculation of a negative Δ*E* value of –3.5 kcal/mol suggests that in the presence of an excess of etherate solvent (Me₂O) the modeled heteroleptic (methyl/dimethylamido) Lipshutz-type cuprate Me(Me₂N)Cu(CN)-Li₂·2OMe₂ (viz. **1**) exists in facile equilibrium with its Gilman-type analogue MeCu(NMe₂)Li·3OMe₂ (viz. the tris(THF) solvate **2**, Scheme 4a). Of particular interest is the theoretical observation that the corresponding homoleptic bis(amido)cuprate (Me₂N)₂Cu(CN)Li₂·2OMe₂ dominates the modeled equilibrium between itself and the Gilman-type species Me₂NCu-(NMe₂)Li·3OMe₂ (Δ*E* = +9.1 kcal/mol, Scheme 4b). Not only are these data consistent with our previous isolation and characterization of **1**,¹ but the computed ability of Me(Me₂N)Cu(CN)Li₂·2OMe₂ to dissociate accounts for the tandem observations that a solution containing **3** and LiCN gives a high synthetic yield of 2-iodo-*N,N*-diisopropylbenzamide yet deposits Gilman-type **3**.

(23) Davies, R. P.; Hornauer, S. *Chem. Commun.* **2007**, 304.

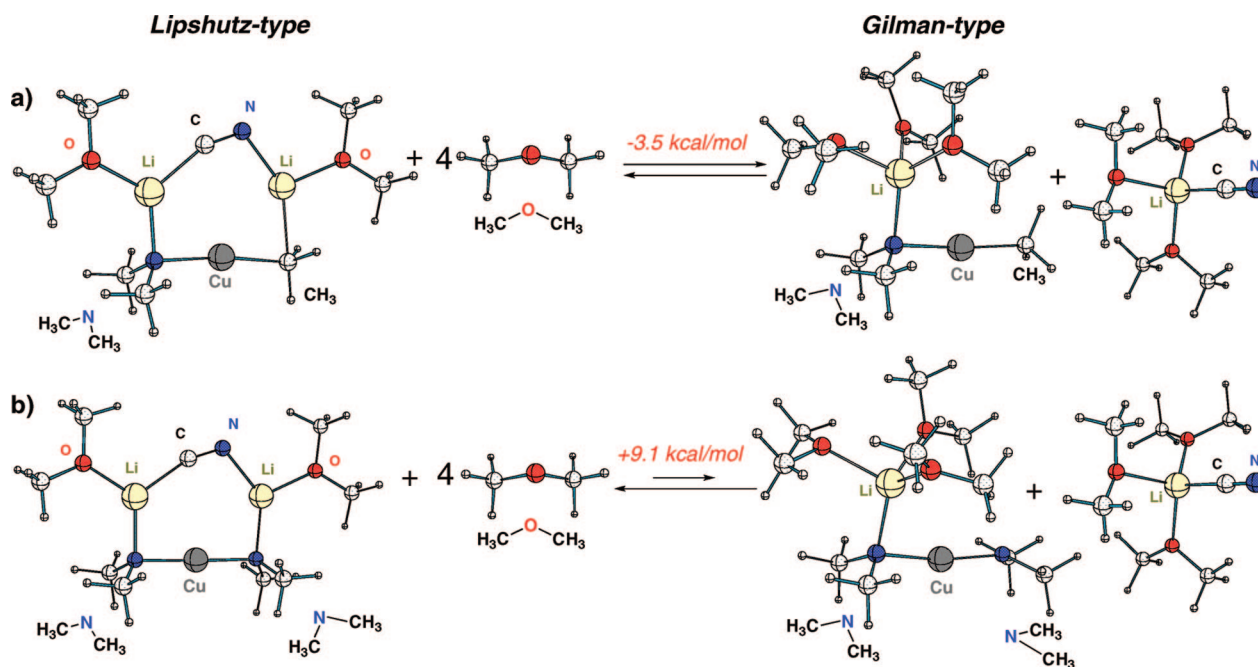
(24) (a) Niemeyer, M. *Organometallics* **1998**, *17*, 4649. (b) Hwang, C.-S.; Power, P. P. *Bull. Korean Chem. Soc.* **2003**, *24*, 605.

(25) Gregory, K.; Schleyer, P. v. R.; Snaith, R. *Adv. Inorg. Chem.* **1991**, *37*, 47.

(26) John, M.; Auel, C.; Behrens, C.; Marsch, M.; Harms, K.; Bosold, F.; Gschwind, R. M.; Rajamohanam, P. R.; Boche, G. *Chem. Eur. J.* **2000**, *6*, 3060.

(27) Martin, S. F.; Fishpaugh, J. R.; Power, J. M.; Giolando, D. M.; Jones, R. A.; Nunn, C. M.; Cowley, A. H. *J. Am. Chem. Soc.* **1988**, *110*, 7226.

Scheme 4



In summary, the isolation of **2** and **3** allows the first direct observation of organo(amido)cuprate monomers. In line with previous work on organo(amido)cuprates,⁶ the structures suggest a predilection for crystallization of the Gilman-type species $\text{RCu}(\text{amido})\text{Li}$ with the concomitant exclusion of LiCN . These data are in contrast with the recent isolation and characterization of a homoleptic Lipshutz-type bis(amido)cuprate and offer an explanation for cyanide retention therein and the previous observation of a seven-membered $\text{N}_2\text{Cu}(\text{CN})\text{Li}_2$ metallacycle. Hence, the crystal structures of **2** and **3** suggest that the ability of a cuprate structure to exhibit $\text{Li}(\mu\text{-CN})\text{Li}$ bonding must be combined with a high affinity for intermetal bridging in *both* of the Cu-bonded ligands in order to achieve the theoretically expected $\text{X}_2\text{Cu}(\text{CN})\text{Li}_2$ Lipshutz-type metallacycle.^{11a} DFT studies rationalize these data and, moreover, suggest the facile interconversion of Lipshutz- and Gilman-type structures in etherate solvent of heteroleptic alkyl(amido)cuprates. This behavior explains the crystallographic observation of **2** and **3**. Moreover, calculations point to the contrasting tendency for homoleptic bis(amido)cuprates to favor LiCN inclusion, as

observed previously by ourselves.¹ Finally, conscious that Gilman-type complexes are inefficient DoC substrates but that the putative cuprate $\text{Me}(\text{TMP})\text{Cu}(\text{CN})\text{Li}_2$ is an effective DoC reagent,¹ we have tested both preisolated **3** and solutions containing **3** and LiCN and have noted the enhanced reactivity of the Lipshutz-type species in the DoC of a representative benzamide.

Acknowledgment. This work was supported by the U.K. EPSRC (J.V.M., J.H.) and Hoansha and KAKENHI (Young Scientist (A), Houga, and Priority Area No. 452 and 459) (M.U.). The calculations were performed on the RIKEN Super Combined Cluster (RSCC).

Supporting Information Available: Text, figures, and tables giving synthetic and spectroscopic data and crystallographic data for **1**, **2**, and **3** and a CIF file giving crystal data for **3**. This material is available free of charge via the Internet at <http://pubs.acs.org>.

OM801101U

First Example of a Hydrated Monoorganotin Cation: Synthesis and Structure of $[\{\text{PhSn}(\text{H}_2\text{O})_3(\mu\text{-OH})_2\}][\{1,5\text{-C}_{10}\text{H}_6\text{-}(\text{SO}_3)_2\}_2]$

Vadapalli Chandrasekhar* and Puja Singh

Department of Chemistry, Indian Institute of Technology Kanpur, Kanpur-208016, India

Received October 9, 2008

Summary: The reaction of Ph_2SnO with naphthalene-1,5-disulfonic acid tetrahydrate affords, through a Sn–aryl bond cleavage process, the first example of a hydrated monoorganotin cation, $[\{\text{PhSn}(\text{H}_2\text{O})_3(\mu\text{-OH})_2\}][\{1,5\text{-C}_{10}\text{H}_6\text{-}(\text{SO}_3)_2\}_2]$. The structural elucidation of the latter showed that it contained a tetracationic dinuclear unit where the two tin atoms are bridged by two hydroxide ligands and each tin is hydrated with three molecules of water. Intermolecular hydrogen-bonding interactions between the water molecules and the disulfonate anions result in a pillared three-dimensional network.

Organotin oxides, hydroxides, and oxide hydroxides are versatile starting materials for the preparation of a number of organostannoxane assemblies.¹ Despite their widespread use in organotin chemistry, there have not been many efforts to understand the mechanism of formation of these organotin oxides/hydroxides/oxide hydroxides,² although it is generally agreed that one possible means of their generation involves hydrolysis of hydrated organotin cations. Our approach to understand this problem has been to discover synthetic routes to assemble hydrated organotin cations and to hydrolyze them in a controlled manner. In the reactions of organotin oxides with arylsulfonic acids we were able to isolate the hydrated diorganotin cations $[\text{Bu}_2\text{Sn}(\text{H}_2\text{O})_4]^{2+}[\text{2,5-Me}_2\text{-C}_6\text{H}_3\text{-SO}_3]^-_2$ (**1a**)^{3a} and $[\{\text{Bu}_2\text{Sn}(\text{H}_2\text{O})_3(\text{L})\text{Sn}(\text{H}_2\text{O})_3\text{Bu}_2\}]^{2+}[\text{L}]^{2-} \cdot 2\text{MeOH} \cdot 2\text{H}_2\text{O}$ (**1b**; L = 1,5-C₁₀H₆-(SO₃)₂)^{3b}. We were able to show that a direct hydrolysis of the former with pyridine leads to the 2D stannoxane polymer $[\{\text{Bu}_2\text{Sn}(\mu\text{-OH})(\text{O}_3\text{-SC}_6\text{H}_3\text{-2,5-Me}_2)\}_2]_n$.^{4a} On the other hand, by a variation of reaction conditions we recently isolated the dinuclear compound $[(\text{Phen})(\text{NO}_3)_2\text{Me}_2\text{Sn}(\mu\text{-OH})\text{SnMe}_2(\text{NO}_3)(\text{Phen})][\text{NO}_3]$, where the two tin centers are bridged by a single hydroxide ligand.^{4b} All of these pertain to diorganotin compounds, and there has not been a single example of a hydrated monoorganotin cation thus far. The main difficulty for this gap lies in finding appropriate synthetic procedures. The reaction of $\text{BuSn}(\text{O})(\text{OH})$ with various sulfonic acids has been investigated previously. In all the cases the main

product isolated is the dodecanuclear football-shaped cage $[(\text{RSn})_{12}\text{O}_{14}(\text{OH})_6]^{2+}[\text{R}'\text{SO}_3]^-_2$.⁵ We have tried to approach the synthesis of hydrated monoorganotin cations in a different way. Recently there has been interest in the use of Sn–C bond cleavage reactions among aryl- and alkyltin compounds as viable synthetic procedures for preparing organostannoxane compounds.⁶ Although most of these reactions occur with carboxylic/phosphonic/phosphinic acids, recent reports from our laboratory^{3b} and that of Beckmann⁷ suggested that Sn–C bond cleavage reactions can also occur in the reactions of organotin precursors with sulfonic acids. Spurred by this, we investigated the reaction of Ph_2SnO with naphthalene-1,5-disulfonic acid tetrahydrate. In this reaction we were able to isolate, by a Sn–aryl bond cleavage process, the first example of a hydrated monoorganotin cation, $[\text{PhSn}(\text{H}_2\text{O})_3(\mu\text{-OH})_2][1,5\text{-C}_{10}\text{H}_6\text{-}(\text{SO}_3)_2]_2$ (**2**). The structural elucidation of the latter showed that it contained a tetracationic dinuclear core where the two tin atoms are bridged by two hydroxide ligands and each tin is coordinated with three molecules of water (Figure 1). Compound **2** represents an unprecedented example of a hydrated monoorganotin cation that is formed presumably by the hydrolysis of the putative $[\text{PhSn}(\text{H}_2\text{O})_5]^{3+}$ species. In comparison to the case for monoorganotin cations, cationic diorganotin compounds are more well-known.⁸

In comparison to Sn–alkyl bonds, Sn–aryl bonds are more prone to cleavage during reactions with protic acids. In view of this, we have investigated the reaction of Ph_2SnO with naphthalene-1,5-disulfonic acid with a view to isolate Sn–Ph cleaved products. Accordingly, the reaction of Ph_2SnO with naphthalene-1,5-disulfonic acid tetrahydrate (LH₂), in a mixture of toluene and methanol (5:3) at room temperature for 4 days, afforded colorless crystals (32% yield)⁹ which were identified as $[\text{PhSn}(\text{H}_2\text{O})_3(\mu\text{-OH})_2][1,5\text{-C}_{10}\text{H}_6\text{-}(\text{SO}_3)_2]_2$, (**2**) (Scheme 1). The latter crystallized as its water solvate, **2**·3H₂O. The ¹¹⁹Sn

(5) (a) Chandrasekhar, V.; Boomishankar, R.; Gopal, K.; Sasikumar, P.; Singh, P.; Steiner, A.; Zacchini, S. *Eur. J. Inorg. Chem.* **2006**, 4129. (b) Eyechenne-Baron, C.; Ribot, F.; Sanchez, C. *J. Organomet. Chem.* **1998**, 567, 137. (c) Eyechenne-Baron, C.; Ribot, F.; Steunou, N.; Sacher, C.; Fayon, F.; Biesemans, M.; Martins, J. C.; Willem, R. *Organometallics* **2000**, 19, 1940.

(6) (a) Chandrasekhar, V.; Gopal, K.; Sasikumar, P.; Thirumoorthi, R. *Coord. Chem. Rev.* **2005**, 249, 1745. (b) Chandrasekhar, V.; Sasikumar, P.; Thilagar, P. *Organometallics* **2007**, 26, 4386. (c) Xie, Y. P.; Yang, J.; Ma, J. F.; Zhang, L. P.; Song, S. Y.; Su, Z. M. *Chem. Eur. J.* **2008**, 14, 4093. (d) Zheng, G. L.; Ma, J. F.; Su, Z. M.; Yan, L. K.; Yang, J.; Li, Y. Y.; Liu, J. F. *Angew. Chem.* **2004**, 116, 2463; *Angew. Chem., Int. Ed.* **2004**, 43, 2409. (e) Song, S. Y.; Ma, J. F.; Yang, J.; Gao, L. L.; Su, Z. M. *Organometallics* **2007**, 26, 2125. (f) Ma, C.; Sun, J.; Zhang, R. *J. Mol. Struct.* **2007**, 833, 203. (g) Zhang, R.; Zhang, Q.; Shi, Y.; Ma, C. *J. Organomet. Chem.* **2006**, 691, 1668. (h) Prabusankar, G.; Jousseau, B.; Toupan, T.; Allouchi, H. *Angew. Chem., Int. Ed.* **2006**, 45, 1255, and references therein.

(7) Beckmann, J.; Dakternieks, D.; Duthie, A.; Mitchell, C. *Appl. Organomet. Chem.* **2004**, 18, 54.

(8) Kašná, B.; Dostál, L.; Čiřářová, I.; Roman, J. *Organometallics* **2007**, 26, 4080, and references therein.

* To whom correspondence should be addressed. E-mail: vc@iitk.ac.in. Tel: (+91) 512-259-7259. Fax: (+91) 521-259-0007/7436.

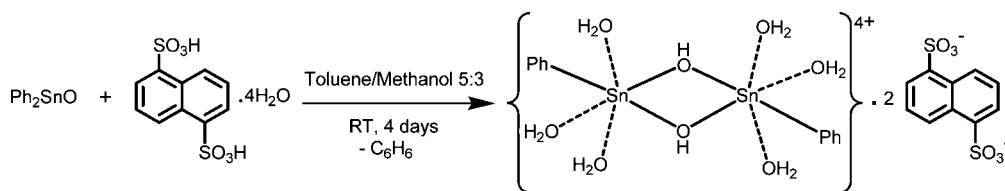
(1) (a) Davies, A. G. *Organotin Chemistry*, Wiley-VCH: Weinheim, Germany, 2004. (b) Chandrasekhar, V.; Gopal, K.; Thilagar, P. *Acc. Chem. Res.* **2007**, 40, 420. (c) Chandrasekhar, V.; Nagendran, S.; Baskar, V. *Coord. Chem. Rev.* **2002**, 235, 1. (d) Beckmann, J.; Jurkschat, K. *Coord. Chem. Rev.* **2001**, 215, 267. (e) Jain, V. K. *Coord. Chem. Rev.* **1994**, 135/136, 809. (f) Holmes, R. R. *Acc. Chem. Res.* **1989**, 22, 190.

(2) (a) Beckmann, J.; Henn, M.; Jurkschat, K.; Schürmann, M. *Organometallics* **2002**, 21, 192, and references therein. (b) Heinrich, P.; Hans, R. *J. Organomet. Chem.* **1989**, 364, 57. (c) Heinrich, P.; Hans, R. *J. Organomet. Chem.* **1989**, 368, 173. (d) Heinrich, P.; Hans, R. *J. Organomet. Chem.* **1989**, 373, 173.

(3) (a) Chandrasekhar, V.; Boomishankar, R.; Singh, S.; Steiner, A.; Zacchini, S. *Organometallics* **2002**, 21, 4575. (b) Chandrasekhar, V.; Boomishankar, R.; Steiner, A.; Bickley, J. F. *Organometallics* **2003**, 22, 3342.

(4) (a) Chandrasekhar, V.; Singh, P.; Gopal, K. *Organometallics* **2007**, 26, 2833. (b) Chandrasekhar, V.; Singh, P. *Organometallics* **2008**, 27, 4083.

Scheme 1. Synthesis of 2



NMR spectrum of $2 \cdot 3\text{H}_2\text{O}$ in $(\text{CD}_3)_2\text{SO}$ solution displayed a single peak at -577 ppm, consistent with the presence of a hexacoordinated tin ($1\text{C},5\text{O}$) in solution.¹⁰

The ESI-MS spectrum of $2 \cdot 3\text{H}_2\text{O}$ revealed a highest observable peak at m/z 1136.70 corresponding to the dimeric species $\{[\text{PhSn}(\text{H}_2\text{O})_3(\mu\text{-OCH}_3)\text{Sn}(\text{H}_2\text{O})_3\text{Ph}] + 2\text{L}\} + \text{H}^+$, indicating that the dinuclear structure found in the solid state is retained in solution, although the bridging hydroxide ligand is replaced with methoxide. The fragmentation pattern reveals the presence of other fragments, also including mononuclear species (see Figure S3 in the Supporting Information). ESI-MS analysis also indicates that the reaction of Ph_2SnO with 1,5-naphthalenedisulfonic acid proceeds through a disproportionation pathway. Accordingly, the ESI-MS spectrum of the crude sample obtained in this reaction, prior to recrystallization, showed peaks corresponding to triorganotin cationic species in addition to those identified for monoorganotin species (see Figure S4 in the Supporting Information).

Thermogravimetric analysis of $2 \cdot 3\text{H}_2\text{O}$ reveals a sequential loss of water molecules followed by loss of the naphthalenedisulfonate. The final char yield at around 550 °C is quite substantial and is about 36.8% (see Figure S5 in the Supporting Information).

The compound $2 \cdot 3\text{H}_2\text{O}$ contains the tetracationic dinuclear tin complex $\{[\text{PhSn}(\mu\text{-OH})(\text{H}_2\text{O})_3]_2\}^{4+}$. The four positive charges present on the complex are compensated by the presence of two naphthalene-1,5-disulfonate anions (Figure 1, Scheme 1). The dimeric core of the tetracation of $2 \cdot 3\text{H}_2\text{O}$, shown in Figure 1, consists of two centrosymmetrically related tin centers. Each tin is hexacoordinate in a distorted-octahedral geometry. The coordination environment around each tin consists of one phenyl substituent and three molecules of water. Two such tin centers are bridged to each other by two hydroxide ligands, leading to the formation of a central $[\text{Sn}_2(\mu\text{-OH})_2]$ unit. Unlike the case for diorganotin compounds, the occurrence of discrete dimeric $[\text{Sn}_2(\mu\text{-OH})_2]$ motifs is not very common among monoorganotin compounds. Previous instances of dimeric monoorganotin compounds containing $[\text{Sn}_2(\mu\text{-OH})_2]$ units include $[\text{R}_2\text{Sn}(\text{OH})\text{Cl}_2(\text{H}_2\text{O})]$ ($\text{R} = \text{Et}, ^t\text{Bu}, ^i\text{Bu}, ^i\text{Pr}, \text{Me}$), $[\{2,6\text{-P}(\text{O})(\text{OEt})_2\text{-4-}^t\text{Bu-C}_6\text{H}_2\}\text{SnF}_2\text{OH}]_2$, etc. and have been reviewed recently.¹⁰

Selected bond distance/angle data for $2 \cdot 3\text{H}_2\text{O}$ are given below Figure 1. The trans angles around each tin are as follows: $\text{O}1\text{-Sn}1\text{-C}1 = 171.49(10)^\circ$, $\text{O}2\text{-Sn}1\text{-O}1^* = 159.97(8)^\circ$, and

$\text{O}3\text{-Sn}1\text{-O}4 = 167.45(10)^\circ$. The Sn–O distances involving the central four-membered $[\text{Sn}_2(\mu\text{-OH})_2]$ motif are as follows: $\text{Sn}1\text{-O}1 = 2.044(2)$ Å and $\text{Sn}1\text{-O}1^* = 2.106(2)$ Å. These distances are shorter in comparison to those found among similar structural units of diorganotin compounds: $[\text{Bu}_2\text{SnOH}(\text{OTf})(\text{H}_2\text{O})_2]$ (2.116(3) Å), $[\text{Bu}_2\text{SnOH}(\text{OTf})(\text{H}_2\text{O})_2]$ (2.113(4) Å), and $[(S)\text{-2PB}_2\text{SnOH}(\text{OTf})(\text{H}_2\text{O})_2]$ (2.114(7) Å) ($(S)\text{-2PB} = (S)\text{-2-phenylbutyl}$).¹¹ Interestingly, in **2** the coordinated water molecules (O2, O3, and O4) are bound more firmly to the tin center ($\text{Sn}1\text{-O}2 = 2.087(2)$ Å, $\text{Sn}1\text{-O}3 = 2.130(2)$ Å, $\text{Sn}1\text{-O}4 = 2.109(2)$ Å; see caption of Figure 1) in comparison to those in $[\text{Bu}_2\text{Sn}(\text{H}_2\text{O})_4]^{2+}$ [2,5-Me₂-C₆H₃-SO₃][−] (2.271(3) Å)^{3a} or $\{[\text{Bu}_2\text{Sn}(\text{H}_2\text{O})_3(1,5\text{-C}_{10}\text{H}_6\text{-SO}_3)_2]\text{Sn}(\text{H}_2\text{O})_3\text{Bu}_2\}^{2+}$ [1,5-C₁₀H₆-(SO₃)₂]^{2−} · 2MeOH · 2H₂O (2.20(6) Å).^{3b} The shorter Sn–O distances found in $2 \cdot 3\text{H}_2\text{O}$ may be due to the increased Lewis acidic character of the tin centers owing to the tetracationic nature of the complex as well as the presence of a phenyl substituent on each tin.

The crystal structure of $2 \cdot 3\text{H}_2\text{O}$ reveals the presence of extensive and strong intermolecular hydrogen-bonding interactions (see Table S1 in the Supporting Information). The asymmetric unit of $2 \cdot 3\text{H}_2\text{O}$ contains three coordinated and three noncoordinated water molecules. Hydrogen-bonding interactions between all of these water molecules and the disulfonate anions glue four dimeric units together (Figure 2a). These interactions extend the supramolecular structure along the crystallographic *ab* plane to form a two-dimensional sheet (Figure 2a; for an extended view see Figure S2a in the Supporting Information). This sheet is single-layered, in contrast to the triple-layered 2D sheets found in **1b**.^{3b} All the four-membered $[\text{Sn}_2(\mu\text{-OH})_2]$ units are present in a parallel arrangement along the crystallographic *b* axis (Figure S2b). Adjacent 2D sheets of $2 \cdot 3\text{H}_2\text{O}$ are connected to each other through naphthyl groups of the anion. These *naphthyl pillars* are responsible for taking the structure into a final three-dimensional assembly (Figure 2b). The interlayer distance in this assembly is 8.90 Å and may be compared with that found in **1b** (11.5 Å). The *free space* present in the 3D assembly is occupied by the phenyl substituents present on tin atoms and is therefore unavailable for other guest molecules.

In conclusion, we have been able to isolate the first example of a hydrated monoorganotin cation through an Sn–aryl bond cleavage involving the reaction of Ph_2SnO with naphthalene-1,5-disulfonic acid. In view of the possibility

(9) Synthesis of $2 \cdot 3\text{H}_2\text{O}$: Ph_2SnO (0.11 g, 0.37 mmol) and naphthalene-1,5-disulfonic acid tetrahydrate (0.14 g, 0.37 mmol) were taken up in a mixture of toluene and methanol (5:3), and this mixture was stirred for 4 days at room temperature. The mixture was filtered, and the filtrate was allowed to evaporate at room temperature. Blocklike crystals of $2 \cdot 3\text{H}_2\text{O}$ were obtained after a few weeks. Yield: 0.07 g (32%, for isolated crystals). Mp: 250 °C dec. Anal. Calcd for $\text{C}_{16}\text{H}_{24}\text{O}_{13}\text{S}_2\text{Sn}$ (607.97 g): C, 31.58, H, 3.98. Found: C, 31.62, H, 4.03. IR (KBr, cm^{-1}): 3434 (br, $\nu(\text{H}_2\text{O})$), 1205 (s, $\nu(\text{SO}_3)$ asym str), 1043 (s, $\nu(\text{SO}_3)$ sym str), 996 (s, $\nu(\text{SO}_3)$ ionic), 609 (m, $\nu(\text{C-S})$). ¹H NMR (500 MHz, $(\text{CD}_3)_2\text{SO}$): δ 7.33–7.40 (m, 5H, phenyl CH), 8.83 (d, 2H, naphthyl CH), 7.90 (d, 2H, naphthyl CH), 7.49–7.51 (m, 2H, naphthyl CH). ¹¹⁹Sn NMR (500 MHz, $(\text{CD}_3)_2\text{SO}$): δ −577 (s).

(10) Chandrasekhar, V.; Singh, P.; Gopal, K. *Appl. Organomet. Chem.* **2007**, *21*, 483.

(11) Sakamoto, K.; Ikeda, H.; Akashi, H.; Fukuyama, T.; Orita, A.; Otera, J. *Organometallics* **2000**, *19*, 3242.

(12) Crystal data for **2**: size $0.2 \times 0.2 \times 0.1$ mm³; triclinic; space group $P\bar{1}$; $a = 10.495(5)$ Å, $b = 10.796(5)$ Å, $c = 11.583(5)$ Å; $\alpha = 72.431(5)^\circ$, $\beta = 76.672(5)^\circ$, $\gamma = 61.853(5)^\circ$; $V = 1097.1(9)$ Å³; $T = 153(2)$ K; $Z = 2$; $D_{\text{calcd}} = 1.838$ Mg m^{−3}; θ range $2.20\text{--}25.00^\circ$; 5681 reflections collected; 3798 independent reflections ($R_{\text{int}} = 0.0149$); $R_1 = 0.0241$, $wR_2 = 0.0623$ (for $I > 2\sigma(I)$); $R_1 = 0.0252$, $wR_2 = 0.0636$ (for all data); GOF = 1.071. The structure was solved and refined by full-matrix least squares on F^2 using the SHELXTL software package.¹³ All the hydrogens of the water molecules and the hydrogen of the hydroxyl group were located from the difference map and refined.

(13) Sheldrick, G. M. SHELXTL version 6.14; Bruker AXS Inc., Madison, WI, 2003.

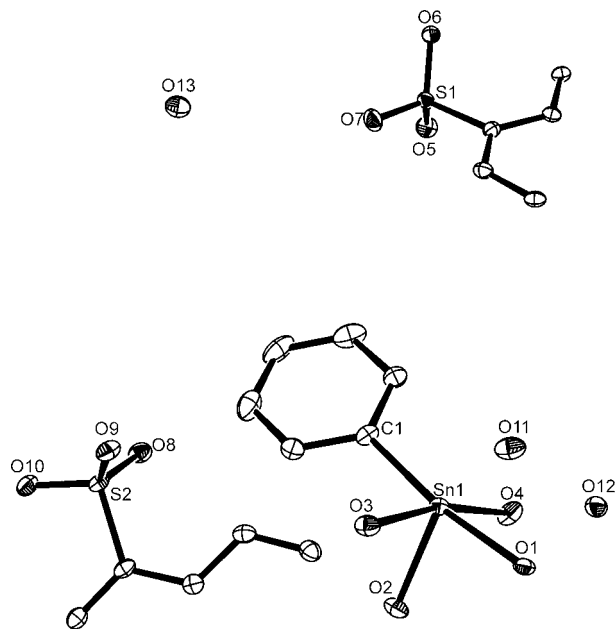


Figure 1. ORTEP representation of asymmetric unit of $2 \cdot 3\text{H}_2\text{O}$ showing 50% probability displacement ellipsoids. Hydrogen atoms have been omitted for clarity. Selected bond distances (Å) and bond angles (deg) are as follows: Sn1–O1 = 2.044(2), Sn1–O2 = 2.087(2), Sn1–O3 = 2.130(2), Sn1–O4 = 2.109(2), Sn1–C1 = 2.103(3), O1–H101 = 0.689(5); O1–Sn1–C1 = 171.49(10), O1–Sn1–O2 = 87.87(9), O1–Sn1–O1* = 72.45(10), O1–Sn1–O4 = 83.40(10), O1–Sn1–O3 = 88.02(9), O2–Sn1–C1 = 99.73(10), O2–Sn1–O1* = 159.97(8), O2–Sn1–O4 = 86.73(10), O2–Sn1–O3 = 83.80(10), O3–Sn1–O4 = 167.45(10), O1*–Sn1–O4 = 94.49(9), O1*–Sn1–O3 = 91.62(9), C1–Sn1–O3 = 96.56(11), C1–Sn1–O4 = 93.14(11), C1–Sn1–O1* = 100.16(10), Sn1–O1–Sn1* = 107.55(10). See Figure S1 in the Supporting Information for a complete atom-labeling scheme.

that pentaquo cations such as $[\text{ArSn}(\text{H}_2\text{O})_5]^{3+}$ are involved in the formation of $[\text{PhSn}(\text{H}_2\text{O})_3(\mu\text{-OH})_2][\text{C}_{10}\text{H}_6\text{-1,5-(SO}_3)_2]_2$, it would be interesting to find out synthetic routes for the preparation of stable members of this family. In addition to being interesting examples possessing rich hydrogen bonding, compounds such as $[\text{ArSn}(\text{H}_2\text{O})_5]^{3+}[\text{X}]^{3-}$ would also be valuable precursors for the preparation of novel organostannoxanes by controlled hydrolysis reactions. We are currently exploring these possibilities.

Acknowledgment. We are thankful to the Department of Science and Technology (DST), New Delhi, for financial support, including support for the CCD X-ray diffractometer

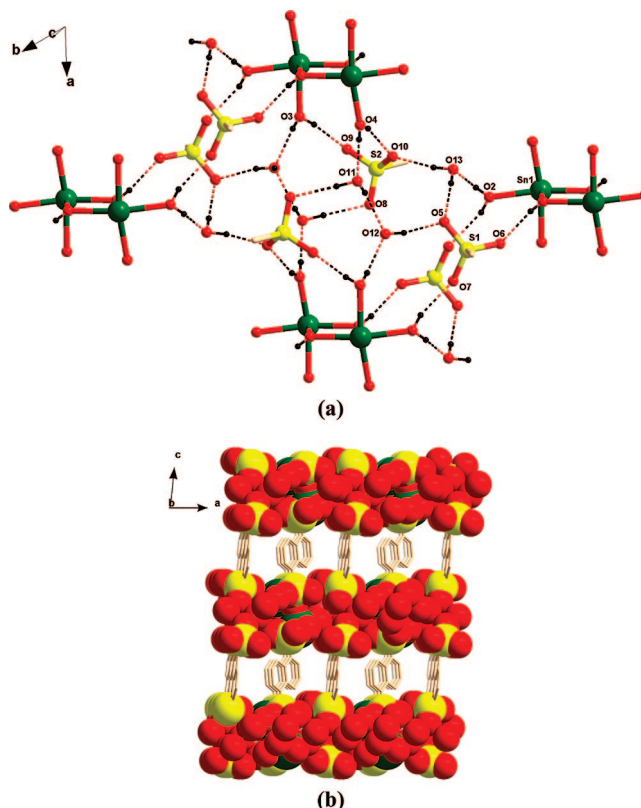


Figure 2. (a) View of a section of the 2D sheet of $2 \cdot 3\text{H}_2\text{O}$ along the ab plane. Four dimeric units are glued together through intermolecular H-bonding interactions. Phenyl groups have been omitted for clarity. For metric parameters see Table S1 in the Supporting Information. (b) View of the three-dimensional pillared structure of $2 \cdot 3\text{H}_2\text{O}$ along the b axis. Adjacent sheets (shown in the space-filling model) are linked together by “naphthyl” groups of naphthalene-1,5-disulfonate anions.

facility at IIT-Kanpur. P.S. thanks the Council of Scientific and Industrial Research of India for a Senior Research Fellowship. V.C. is grateful to the DST for a J. C. Bose National fellowship. V.C. is a Lalit Kapoor chair professor.

Supporting Information Available: A CIF file giving crystallographic data for $2 \cdot 3\text{H}_2\text{O}$ and figures, tables, and text giving additional views of $2 \cdot 3\text{H}_2\text{O}$, ESI-MS spectra of $2 \cdot 3\text{H}_2\text{O}$, ESI-MS spectra of crude product **2a**, a thermogravimetric curve for $2 \cdot 3\text{H}_2\text{O}$, and additional experimental details. This material is available free of charge via the Internet at <http://pubs.acs.org>.

OM800972M

Zincocenes as Mild Cyclopentadienyl Transfer Reagents toward Rhodium(I) Olefin Precursors. Facile Synthesis of $(\eta^5\text{-Cp}')\text{Rh}(\text{olefin})_2$ Compounds

Ana Cristina Esqueda, Salvador Conejero, Celia Maya, and Ernesto Carmona*

Instituto de Investigaciones Químicas, Departamento de Química Inorgánica, CSIC, and Universidad de Sevilla, Avda. Américo Vespucio 49, 41092 Sevilla, Spain

Received October 30, 2008

Summary: The Rh(I) cyclopentadienyl olefin compounds $[(\eta^5\text{-C}_5\text{Me}_4\text{R})\text{Rh}(\text{olefin})_2]$ ($\text{R} = \text{CMe}_3, \text{SiMe}_3, \text{SiMe}_2\text{CMe}_3$; olefin = $\text{C}_2\text{H}_4, \text{C}_2\text{H}_3\text{SiMe}_3$) are readily prepared from the corresponding $[\text{RhCl}(\text{olefin})_2]_2$ and zincocene, $[\text{Zn}(\text{C}_5\text{Me}_4\text{R})_2]$, precursors. The new compounds undergo hydrogen/deuterium exchange at the olefinic sites in deuterated benzene, at a rate dependent on the cyclopentadienyl substituents.

Cyclopentadienyl complexes of the transition metals are among the most widely used compounds in organometallic chemistry and catalysis,¹ the cyclopentadienyl fragment being a reliable ligand that has provided very important results in these fields of research. Both the parent cyclopentadienyl (Cp) and substituted cyclopentadienyls (Cp'), in particular pentamethylcyclopentadienyl, are often used, but recently, substituted Cp' ligands with bulky substituents are gaining importance, as they permit kinetic stabilization of otherwise unstable species, enhance the regioselectivity of some catalytic reactions, and can even act as suitable ligands for atomic layer deposition.² Generally their synthesis requires the use of cyclopentadienyl derivatives of the s elements, although various other reagents may be used and, for instance, Cp transfer from $\text{ZrCp}_2(\text{NBu}')_2$ (thf) to iridium has been reported.³

Rhodium cyclopentadienyls of the type $(\eta^5\text{-Cp}')\text{Rh}(\text{olefin})_2$ ⁴ and related compounds have a distinguished history as key precursors in important organometallic transformations such as hydrosilylation,⁵ C–H bond activation,⁶ and alkane borylation.⁷ Along with their iridium counterparts, they are often generated in a two-step process,⁸ which involves formation of $[(\eta^5\text{-Cp}')\text{RhCl}_2]_2$ dimers,⁹ followed by reduction to the desired M(I) derivatives.⁸ Even though the synthesis of the M(III) dimers⁹ is a general, high-yield procedure, utilization of commercial M(III) chlorides, e.g. $\text{RhCl}_3 \cdot 3\text{H}_2\text{O}$, and the generation of HCl as a byproduct thwart its use for Cp' ligands with substituents

prone to hydrolytic cleavage: e.g., the widely employed silyl-substituted cyclopentadienyls $\text{C}_5\text{H}_4\text{SiMe}_3, \text{C}_5\text{Me}_4\text{SiMe}_3, \text{C}_5\text{Me}_4\text{-SiMe}_2\text{Bu}'$, and others.¹⁰ Indeed, as part of this work, attempts to obtain $[(\eta^5\text{-C}_5\text{Me}_4\text{SiMe}_3)\text{RhCl}_2]_2$ have yielded instead the $\text{C}_5\text{Me}_4\text{H}$ derivative $[(\eta^5\text{-C}_5\text{Me}_4\text{H})\text{RhCl}_2]_2$.

Since zinc organometallics ZnR_2 ($\text{R} = \text{alkyl, aryl}$) are mild hydrocarbyl transfer reagents,¹¹ we have considered the possibility of using zincocenes, ZnCp'_2 , as also mild, Cp' transfer reagents. A variety of zincocenes may be generated from ZnCl_2 and the appropriate MCp' reagent ($\text{M} = \text{alkali metal}$).¹² Hence, the synthetic methodology herein reported appears to enjoy wide applicability using common $[\text{RhCl}(\text{olefin})_2]_2$ precursors. Moreover, ZnCp'_2 reagents need not be isolated. Reaction of the Rh(I) complex with in situ formed ZnCp'_2 (from ZnCl_2 and KCp' , 5 h, 20 °C) provides the desired compounds in good isolated yields.

To test our hypothesis, we first mixed $\text{Zn}(\text{C}_5\text{Me}_5)_2$ ^{12a} and $[\text{RhCl}(\text{C}_2\text{H}_4)_2]_2$ ¹³ in THF, at 0 °C, and allowed them to react at room temperature for 12 h, to obtain $(\eta^5\text{-C}_5\text{Me}_5)\text{Rh}(\text{C}_2\text{H}_4)_2$ ^{4c} in good yields (>85%). Next, the new compound $(\eta^5\text{-C}_5\text{Me}_4\text{Bu}')\text{Rh}(\text{C}_2\text{H}_4)_2$ (**1**) was prepared by a similar procedure using $\text{Zn}(\text{C}_5\text{Me}_4\text{Bu}')_2$ ^{12c,d} (Scheme 1) and was isolated in ca. 80% yield, following extraction with pentane of the crude

(5) (a) Duckett, S. B.; Haddleton, D. M.; Jackson, S. A.; Perutz, R. N.; Poliakoff, M.; Upmacis, R. K. *Organometallics* **1988**, *7*, 1526. (b) Duckett, S. B.; Perutz, R. N. *J. Chem. Soc., Chem. Commun.* **1991**, 28. (c) Perutz, R. N.; Haddleton, D. M.; Duckett, S. B.; Belt, S. T. *Organometallics* **1989**, *8*, 748. (d) Fernandez, M. J.; Bailey, P. M.; Bentz, P. O.; Ricci, J. S.; Koetzle, T. F.; Maitlis, P. M. *J. Am. Chem. Soc.* **1984**, *106*, 5458. (e) Duckett, S. B.; Perutz, R. N. *Organometallics* **1992**, *11*, 90. (f) Nikonov, G. J. *Adv. Organomet. Chem.* **2005**, *53*, 217. (g) Vyboishchikov, S. F.; Nikonov, G. I. *Organometallics* **2007**, *26*, 4160.

(6) See for example: (a) Jones, W. D.; Feher, F. J. *J. Am. Chem. Soc.* **1984**, *106*, 1650. (b) Jones, W. D. *Inorg. Chem.* **2005**, *44*, 4475. (c) Periana, R. A.; Bergman, R. G. *J. Am. Chem. Soc.* **1986**, *108*, 7332. (d) Periana, R. A.; Bergman, R. G. *J. Am. Chem. Soc.* **1986**, *108*, 7336. (e) Arndtsen, B. A.; Bergman, R. G.; Mobley, T. A.; Peterson, T. H. *Acc. Chem. Res.* **1995**, *28*, 154.

(7) (a) Chen, H.; Schlecht, S.; Semple, T. C.; Hartwig, J. F. *Science* **2000**, *287*, 1995. (b) Hartwig, J. F.; Cook, K. S.; Hapke, M.; Incarvito, C. D.; Fan, Y.; Webster, C. E.; Hall, M. B. *J. Am. Chem. Soc.* **2005**, *127*, 2538. (c) Hartwig, J. F. In *Activation and Functionalization of C–H Bonds*; Goldberg, K. I.; Goldman, A. S., Eds.; American Chemical Society: Washington, DC, 2004; ACS Symposium Series 885.

(8) (a) Lenges, C. P.; White, P. S.; Brookhart, M. *J. Am. Chem. Soc.* **1999**, *121*, 4385. (b) Lenges, C. P.; Brookhart, M. *Angew. Chem., Int. Ed.* **1999**, *38*, 3533. (c) Daugulis, O.; Brookhart, M. *Organometallics* **2004**, *23*, 527.

(9) White, C.; Yates, A.; Maitlis, P. M.; Heinekey, D. M. *Inorg. Synth.* **1992**, *29*, 228.

(10) (a) Horacek, H.; Gyepes, R.; Cisarova, I.; Polasek, M.; Varga, V.; Mach, K. *Collect. Czech. Chem. Commun.* **1996**, *61*, 1307. (b) Evans, W. J.; Davis, B. L.; Ziller, J. W. *Inorg. Chem.* **2001**, *40*, 6341. (c) Hitchcock, P. B.; Kerton, F. M.; Lawless, G. A. *J. Am. Chem. Soc.* **1998**, *120*, 10264.

(11) Elschenbroich, C. *Organometallics*, 3rd ed.; Wiley-VCH: Weinheim, Germany, 2006.

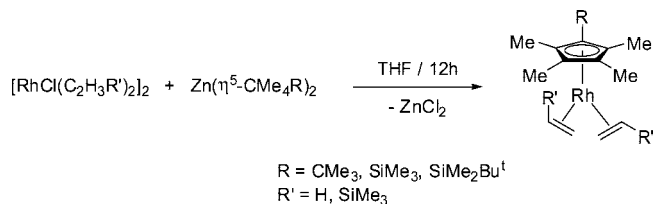
* To whom correspondence should be addressed. E-mail: guzman@us.es.

(1) (a) Deck, P. A. *Coord. Chem. Rev.* **2006**, *250*, 1032, and references therein. (b) Scheirs, J.; Kaminsky, W. *Metallocene-Based Polyolefins*; Wiley: Chichester, U.K., 2000; Vols. 1 and 2. (c) Togni, A.; Hayashi, T. *Ferrocenes*; Verlag Chemie: Weinheim, Germany, 1995.

(2) (a) Choukroun, R.; Wolff, F.; Lorber, C.; Donnadieu, B. *Organometallics* **2003**, *22*, 2245. (b) Yu, Y.; Bond, A. D.; Leonard, P. W.; Vollhardt, K. P. C.; Whitener, G. D. *Angew. Chem., Int. Ed.* **2006**, *45*, 1794. (c) Hatanpää, T.; Ritala, M.; Leskelä, M. *J. Organomet. Chem.* **2007**, *692*, 5256. (d) Dutta, B.; Solari, E.; Gauthier, S.; Scopelliti, R.; Severin, K. *Organometallics* **2007**, *26*, 4791. (e) Zhang, H.-J.; Demerseman, B.; Toupet, L.; Xi, Z.; Bruneau, C. *Adv. Synth. Catal.* **2008**, *350*, 1601. (f) Janiak, C.; Schumann, H. *Adv. Organomet. Chem.* **1991**, *23*, 291. (g) Ruspic, C.; Moss, J. R.; Schürmann, M.; Harder, S. *Angew. Chem., Int. Ed.* **2008**, *47*, 2121.

(3) Holland, P. L.; Andersen, R. A.; Bergman, R. G. *Organometallics* **1998**, *17*, 433.

(4) See for example: (a) King, R. B. *Inorg. Chem.* **1963**, *2*, 528. (b) Cramer, R. J. *J. Am. Chem. Soc.* **1964**, *86*, 217. (c) Moseley, K.; Kang, J. W.; Maitlis, P. M. *J. Chem. Soc. A* **1970**, 2875.

Scheme 1. Synthesis of (η^5 -Cp')Rh(olefin)₂ Compounds 1–6 using Zincoenes as Cyclopentadienyl Transfer Reagents


reaction product. ¹H NMR signals for the Cp' ring are found with δ 1.38 (Bu^t), 1.46 (α -Me), and 1.67 (β -Me), while the C₂H₄ ligands give rise to broad resonances at 1.52 and 1.98 ppm. In the ¹³C{¹H} NMR spectrum the ethylene carbon nuclei resonate at δ 44.3 and couple with ¹⁰³Rh ($J = 14$ Hz), whereas the quaternary ring carbon nuclei appear at δ 110.2 (CBu^t) and 99.3 and 93.8 (β -CMe and α -CMe) and exhibit coupling constants to rhodium of ca. 4–5 Hz. The structure of **1** has been determined by X-ray crystallography and will be reported elsewhere.

The procedure employed for the generation of **1** is general and can be applied to the synthesis of related complexes with 1,3-dienes, e.g. CH₂=C(Me)C(R)=CH₂ (R = H, Me), or the alkenylsilane CH₂=CHSiMe₃, as well as to that of the analogous derivatives of the silyl-substituted cyclopentadienyls C₅Me₄SiMe₃ and C₅Me₄SiMe₂Bu^t. As briefly noted earlier, attempts to obtain (η^5 -C₅Me₄SiMe₃)Rh(C₂H₄)₂ by reaction of RhCl₃·3H₂O with C₅Me₄(SiMe₃)H, followed by reduction with zinc powder,⁸ were thwarted by the generation in the first step of [(η^5 -C₅Me₄H)RhCl₂]₂, as a result of hydrolytic cleavage of the C–SiMe₃ bond of the Cp' ring. All attempted reactions behave well and give corresponding products in high yields. For comparison with recent work,⁸ we concentrate here on the C₂H₄ and C₂H₃SiMe₃ derivatives of the above Cp' ligands.

Accordingly, the vinylsilane complex (η^5 -C₅Me₄Bu^t)Rh(CH₂=CHSiMe₃)₂ (**2**) can be obtained as indicated in Scheme 1 but using [RhCl(C₂H₃SiMe₃)₂]₂ as the starting material, while the related (η^5 -C₅Me₄SiMe₂R)Rh(olefin)₂ derivatives **3–6** are formed from the appropriate Rh(I) olefin and ZnCp'₂^{12c} precursors (R = SiMe₃, R' = H (**3**), SiMe₃ (**4**); R = SiMe₂Bu^t, R' = H (**5**), SiMe₃ (**6**)). The bis(ethene) compounds **3** and **5** feature spectroscopic data similar to those of **1**, suggesting a similar structure, subsequently confirmed for **3** by X-ray crystallography (Figure 1). Despite the presence of Me and SiMe₃ ring substituents of different inductive effects, coordination of the Cp' ring is symmetrical, with Rh–C distances in the range 2.26–2.29 Å. Rh–C distances to the C₂H₄ ligands of ca. 2.12 Å are comparable to literature values for Rh–C₂H₄ compounds,^{8c,14} as are the C=C bond lengths of the coordinated ethene molecules (ca. 1.41 Å).

The bis(vinylsilane) derivatives **2** and **4** are produced as a major isomer (>95%), and the same applies to (η^5 -C₅Me₄SiMe₂Bu^t)Rh(CH₂=CHSiMe₃)₂ (**6**). This major isomer

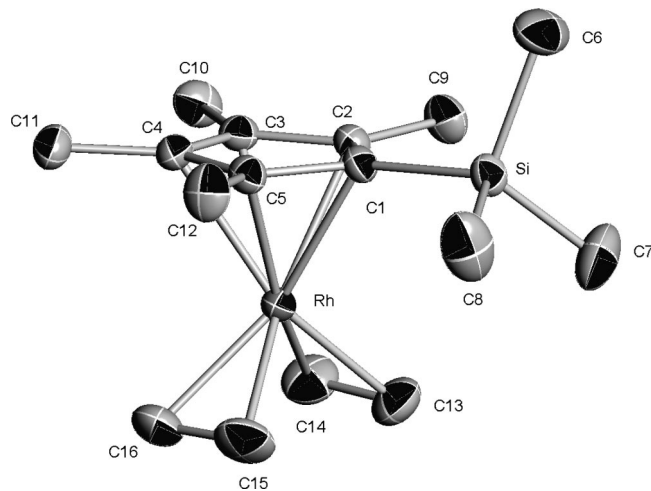
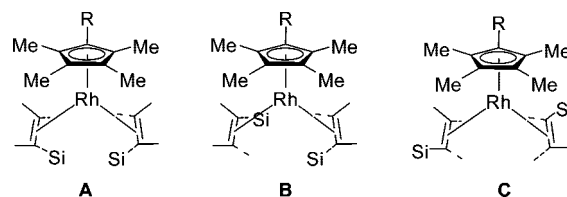


Figure 1. ORTEP view of complex **3** (50% thermal ellipsoids).

contains equivalent olefins but inequivalent ring α and β sites. Thus, for **2** the olefin ligands yield two complex multiplets at 2.34 (2 H, H $_{\beta}$) and 1.19 ppm (4 H, H $_{\alpha}$ and H $_{\beta}$), together with a shielded singlet at 0.08 ppm (18H) due to the SiMe₃ substituent. The methyl substituents of the C₅Me₄Bu^t ring appear at 1.98, 1.72, 1.59, and 1.57 ppm. Thus, while the two olefin ligands of these compounds are equivalent by NMR spectroscopy, the two α -Me and the two β -Me rings are not equivalent. These data rule out structures such as **A**, which possess a plane of symmetry, and are consistent with structures **B** and **C** (that would actually interconvert by internal rotation around the Rh–olefin bonds). Despite the lack of rotational symmetry of the Cp' ring caused by the R substituents, fast rotation of the ring creates an effective C₂ axis responsible for the equivalency by NMR of the olefin ligands of these molecules.^{8a,15} Steric repulsions between olefin and cyclopentadienyl substituents probably favor **B**, in which the two bulky SiMe₃ groups point away from the Cp' ring.



To complete the characterization of new compounds by chemical methods, incorporation of deuterium from C₆D₆ into the olefinic sites of vinylsilane derivatives **2**, **4**, and **6** has been investigated. Hydrogen/deuterium exchange reactions between different carbon centers are of much current importance, since they may provide relevant mechanistic information and allow the preparation of deuterium-labeled organic molecules.¹⁶ Hydrogen/deuterium exchange reactions at the olefinic sites of

(12) (a) Blom, R.; Boersma, J.; Budzelaar, P. H. M.; Fischer, B.; Haalan, A.; Volden, H. V.; Weidlein, J. *Acta Chem. Scand.* **1986**, *A40*, 113. (b) Burkey, D. J.; Hanusa, T. P. *J. Organomet. Chem.* **1996**, *512*, 165. (c) Fernández, R.; Resa, I.; del Río, D.; Carmona, E. *Organometallics* **2003**, *22*, 381. (d) Fernández, R.; Griirane, A.; Resa, I.; Rodríguez, A.; Carmona, E.; Álvarez, E.; Gutiérrez-Puebla, E.; Monge, A.; López del Amo, J. M.; Limbach, H.-H.; Lledós, A.; Masseras, F.; del Río, D., Submitted for publication.

(13) Cramer, R. *Inorg. Synth.* **1974**, *15*, 14.

(14) (a) Nicasio, M. C.; Paneque, M.; Pérez, P. J.; Pizzano, A.; Poveda, M. L.; Rey, L.; Sirol, S.; Taboada, S.; Trujillo, M.; Monge, A.; Ruiz, C.; Carmona, E. *Inorg. Chem.* **2000**, *39*, 180. (b) Day, V. M.; Stults, B. R.; Reimer, K. J.; Shaver, A. *J. Am. Chem. Soc.* **1974**, *96*, 1227.

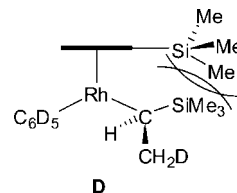
(15) (a) Cramer, R.; Reddy, G. S. *Inorg. Chem.* **1973**, *12*, 346. (b) Hauptman, E.; Sabo-Etienne, S.; White, P. S.; Brookhart, M.; Garner, J. M.; Fagan, P. J.; Calabrese, J. C. *J. Am. Chem. Soc.* **1994**, *116*, 8038.

(16) For recent examples see: (a) Santos, L. L.; Mereiter, K.; Paneque, M.; Slugovc, C.; Carmona, E. *New J. Chem.* **2003**, *27*, 107. (b) Yung, C. M.; Skaddan, M. B.; Bergman, R. G. *J. Am. Chem. Soc.* **2004**, *126*, 13033. (c) Feng, Y.; Lail, M.; Barakat, K. A.; Cundari, T. R.; Gunnoe, T. B.; Petersen, J. L. *J. Am. Chem. Soc.* **2005**, *127*, 14174. (d) Tenn, W. J., III.; Young, K. J. H.; Bhalla, G.; Oxgaard, J.; Goddard, W. A., III.; Periana, R. A. *J. Am. Chem. Soc.* **2005**, *127*, 14172. (e) Corberán, R.; Sanaú, M.; Peris, E. *J. Am. Chem. Soc.* **2006**, *128*, 3974. (f) Hanson, S. K.; Heinekey, D. M.; Goldberg, K. I. *Organometallics* **2008**, *27*, 1454. (g) Atzrdot, J.; Derdan, V.; Fey, T.; Zimmermann, J. *Angew. Chem., Int. Ed.* **2007**, *46*, 7744.

(η^5 -Cp')Rh(olefin)₂ compounds have long been known¹⁷ and have been studied recently by Brookhart and co-workers for (η^5 -C₅Me₅)Rh(CH₂=CHSiMe₃)₂.^{8a} In C₆D₆ the ¹H NMR signal of the α olefinic protons of the latter compound undergoes a 50% decrease in intensity in ca. 115 min at 50 °C, while the β -hydrogens require 250 min for their intensity to become half of the original values. The exchange is faster than for the related (η^5 -C₅Me₅)Rh(C₂H₄)₂, investigated by Jones and co-workers,^{17b} indicating more facile access to the unsaturated, 16-electron [(η^5 -C₅Me₅)Rh(olefin)] species that permits H/D exchange by activation of C₆D₆, followed by successive, reversible insertion and reductive elimination steps (for mechanistic details and reaction intermediates, see eq 3 in ref 8a).

Replacing C₅Me₅ by C₅Me₄Bu^t increases the electron-donating properties of the Cp' ligand, whereas the opposite is expected for C₅Me₄SiMe₃, according to average ν (CO) values for a large series of (Cp^R)₂Zr(CO)₂ complexes.¹⁸ As judged by corresponding $\Delta\nu$ values, the change is not very large and to a first approximation can be neglected. Larger differences in the steric effects of the cyclopentadienyl ligands are, however, to be expected, and they may be understood by consideration of their respective solid angles.^{19a} The value reported for C₅Me₅ is 187°, and since substituent effects are additive,^{19a} solid angles of 197 and 194° can be estimated for C₅Me₄Bu^t and C₅Me₄SiMe₃, respectively. Hence, H/D substitution at the vinylic sites of **2** and **4** should be faster than for the C₅Me₅ complex analogue. Accordingly, the half-lives for deuterium incorporation into the α sites of **2** and **4** are ca. 10 min (150 min for the C₅Me₅ derivative^{8a}) but, interestingly, while deuterium incorporation into the β sites of **2** is also faster (50 vs 250 min), it is slower for the SiMe₃-substituted complex **4** (ca. 550 min for 50% incorporation of deuterium). This implies that the secondary alkyl intermediate **D**, which permits H/D exchange at β -olefinic positions, is sterically more hindered for the C₅Me₄SiMe₃ complex **4** than for the C₅Me₄Bu^t analogue **2**. This could be due to C–SiMe₃ bonds being longer than C–CMe₃ bonds (covalent radius values for C_{sp}², C_{sp}³, and Si are 0.73, 0.76, and 1.11 Å, respectively²⁰), which may force the ring and alkyl SiMe₃ substituents in **D** to occupy the same region of space. In

fact, in a study of (η^5 -C₅H₃R₂)Fe(CO)(PR'₃)I complexes, for R = Bu^t, SiMe₃,^{19b} it has been found that bulk solid angles are a poor measure of the steric demands of the ligands at certain points in space. In accord with this assumption, the half-life for the exchange of the α and β hydrogens of (η^5 -C₅Me₄SiMe₂Bu^t)Rh(CH₂=CHSiMe₃)₂ (**6**) is comparable to that of **4** (15 min for the α proton and 550 min for the β proton at 50 °C).



In summary, a convenient, facile synthesis of (η^5 -Cp')Rh(olefin)₂ compounds has been developed using corresponding zincocenes, ZnCp'₂, as the cyclopentadienyl transfer reagents. This avoids low-yield procedures involving insoluble alkali-metal MCp' derivatives^{4a} or undesirable TICp' salts,^{5a–c} and allows the preparation of compounds with silyl-substituted rings that cannot be obtained by other established methods.⁸ The new compounds described exhibit the expected reactivity in C₆D₆-assisted H/D exchange processes.

Acknowledgment. Financial support from the Spanish Ministerio de Educación y Ciencia (MEC) (Project No. CTQ2007-62814) and Consolider-Ingenio 2010 (No. CSD2007-00006) (FEDER support), the Junta de Andalucía (Project Nos. FQM-3151 and FQM-672) is gratefully acknowledged. A.C.E. thanks the CONACYT for a research grant (Ref. No. 229340).

Supporting Information Available: Text and figures giving detailed procedures for the synthesis and characterization of complexes **1–6** and a CIF file giving crystallographic data of **3**. This material is available free of charge via the Internet at <http://pubs.acs.org>.

OM801046D

(17) (a) Seiwel, L. P. *J. Am. Chem. Soc.* **1974**, *96*, 7134. (b) Jones, W. D.; Duttweiler, R. P. J.; Feher, F. J.; Hessell, E. T. *New J. Chem.* **1989**, *13*, 725.

(18) Zachmanoglou, C. E.; Docrat, A.; Bridgewater, B. M.; Parkin, G.; Brandow, C. G.; Bercaw, J. E.; Jardine, C. N.; Lyall, M.; Green, J. C.; Keister, J. B. *J. Am. Chem. Soc.* **2002**, *124*, 9525.

(19) (a) White, D.; Coville, N. J. *J. Adv. Organomet. Chem.* **1994**, *36*, 95. (b) White, D.; Carlton, L.; Coville, N. J. *J. Organomet. Chem.* **1992**, *440*, 15.

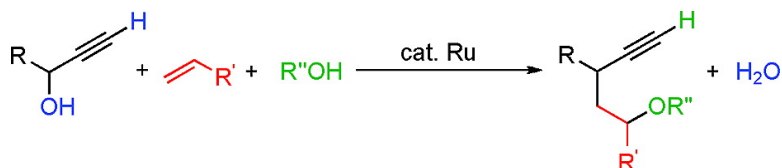
(20) Cordero, B.; Gomez, V.; Platero-Plats, A. E.; Reves, M.; Echeverria, J.; Cremades, E.; Barragan, F.; Alvarez, S. *Dalton Trans.* **2008**, 2832.

Ruthenium-Catalyzed Oxypropargylation of Alkenes

Yoshihiro Yamauchi, Yoshihiro Miyake, and Yoshiaki Nishibayashi

Organometallics, 2009, 28 (1), 48-50 • DOI: 10.1021/om801092a • Publication Date (Web): 26 November 2008

Downloaded from <http://pubs.acs.org> on May 6, 2009



More About This Article

Additional resources and features associated with this article are available within the HTML version:

- Supporting Information
- Links to the 1 articles that cite this article, as of the time of this article download
- Access to high resolution figures
- Links to articles and content related to this article
- Copyright permission to reproduce figures and/or text from this article

[View the Full Text HTML](#)



Ruthenium-Catalyzed Oxypropargylation of Alkenes

Yoshihiro Yamauchi, Yoshihiro Miyake, and Yoshiaki Nishibayashi*

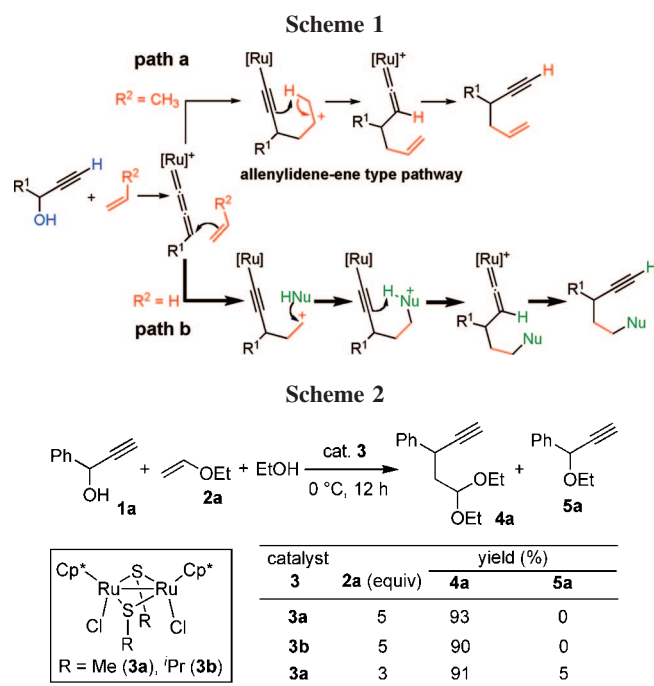
Institute of Engineering Innovation, School of Engineering, The University of Tokyo, Yayoi, Bunkyo-ku, Tokyo 113-8656, Japan

Received November 17, 2008

Summary: The ruthenium-catalyzed oxypropargylation of alkenes with propargylic alcohols and simple alcohols has been found via ruthenium–allenylidene complexes as key intermediates. As a synthetic application, an intramolecular cyclization using this method has been developed to give the corresponding anti-1-alkoxy-3-ethynylindanes in high to excellent yields with a high diastereoselectivity.

Functionalization of alkenes is one of the most attractive subjects in organic synthesis. A variety of reactions such as epoxidation, dihydroxylation, aminohydroxylation, hydroboration, hydrosilylation, cyclopropanation, and carbonylation, including their asymmetric versions, have been known for the introduction of new functional groups into alkene substrates.¹ We have recently disclosed the ruthenium-catalyzed carbon–carbon bond forming process between propargylic alcohols and alkenes which proceeded via an allenylidene²–ene type process (Scheme 1, path a).³ Here, if the selective capture of in situ produced reactive carbocation intermediates by other nucleophiles is possible, this may lead to a new method for heterofunctionalization of alkenes (Scheme 1, path b). In fact, we have now found that the ruthenium-catalyzed oxypropargylation of alkenes with propargylic alcohols and simple alcohols gave the corresponding functionalized compounds in high to excellent yields with a complete selectivity. Preliminary results are described here.

Treatment of 1-phenyl-2-propyn-1-ol (**1a**) with 5 equiv of ethyl vinyl ether (**2a**) in the presence of 2.5 mol % of [Cp*₂RuCl(μ₂-SMe)]₂ (Cp* = η⁵-C₅Me₅; **3a**) in ethanol at 0 °C for 12 h gave 5,5-diethoxy-3-phenyl-1-pentyne (**4a**) in 93% isolated yield (Scheme 2). Use of a complex bearing a sterically more demanding moiety, [Cp*₂RuCl(μ₂-SⁱPr)]₂ (**3b**), had no effect on the yield of **4a**. The reaction with 3 equiv of **2a** proceeded smoothly, **4a** being obtained in 91% isolated yield together with a small amount of propargylic ether (**5a**). Separately, we confirmed that no reaction occurred at all when



other catalysts such as the monoruthenium complex [CpRuCl(PPh₃)₂] and *p*-toluenesulfonic acid were used in place of **3**. In addition, no reaction took place at all when propargylic alcohols bearing an internal alkyne moiety were used as substrates.

Typical results of reactions of other propargylic alcohols with **2a** under the same reaction conditions are shown in Table 1. The presence of a substituent such as a fluoro, chloro, methoxy, or methyl group at the *para* position of the benzene ring of **1** did not have much effect on the yield of **4** (Table 1, runs 1–5). Reactions of propargylic alcohols bearing a methyl group at the *meta* and *ortho* positions of the benzene ring of **1** with **2a** proceeded smoothly to give the corresponding oxypropargylated products in excellent yields (Table 1, runs 6 and 7). Use of a 2-furyl, 1-naphthyl, or vinylic group in place of the phenyl group gave a similar yield of **4** (Table 1, runs 8–10). Separately, we confirmed that compounds **4** were readily transformed into the corresponding 4-pentynals in quantitative yields.⁵ On the other hand, the reaction of 1-cyclohexyl-2-propyn-1-ol with **2a** afforded only the corresponding propargylic ether (**5b**) in 99% yield. In addition to ethanol, other alcohols such as ⁿPrOH and ⁱPrOH are revealed to be available as nucleophiles (Table 1, runs 11 and 12). The reaction with *n*-butyl vinyl ether (**2b**) gave the corresponding product in 92% yield as a mixture of two diastereoisomers (Table 1, run 13). Reactions of **1a** with substituted vinylic ethers such as 1-ethoxy-1-propene (**2c**),

(5) See the Supporting Information for experimental details.

* To whom correspondence should be addressed. E-mail: ynishiba@sogo.t.u-tokyo.ac.jp.

(1) For a review, see: *Catalytic Heterofunctionalization*; Togni, A., Grützmacher, H., Eds.; Wiley-VCH: Weinheim, Germany, 2001.

(2) For recent reviews, see: (a) Bruneau, C.; Dixneuf, P. H. *Angew. Chem., Int. Ed.* **2006**, *45*, 2176. (b) *Metal Vinylidenes and Allenylidenes in Catalysis*; Bruneau, C., Dixneuf, P. H., Eds.; Wiley-VCH: Weinheim, Germany, 2008.

(3) (a) Nishibayashi, Y.; Inada, Y.; Hidai, M.; Uemura, S. *J. Am. Chem. Soc.* **2003**, *125*, 6060. (b) Nishibayashi, Y.; Yoshikawa, M.; Inada, Y.; Hidai, M.; Uemura, S. *J. Am. Chem. Soc.* **2004**, *126*, 16066. (c) Daini, M.; Yoshikawa, M.; Inada, Y.; Uemura, S.; Sakata, K.; Kanao, K.; Miyake, Y.; Nishibayashi, Y. *Organometallics* **2008**, *27*, 2046. (d) Fukamizu, K.; Miyake, Y.; Nishibayashi, Y. *J. Am. Chem. Soc.* **2008**, *130*, 10498.

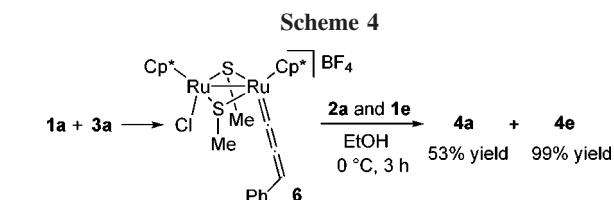
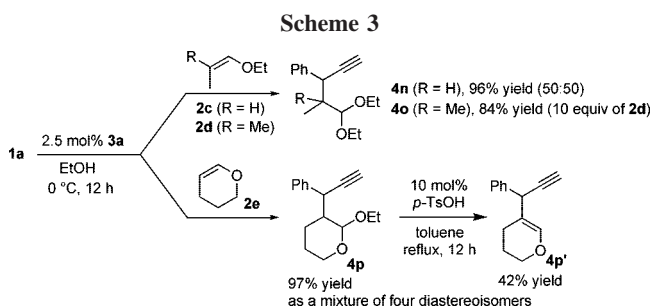
(4) For the preparation of a variety of chalcogenolate-bridged diruthenium complexes, including X-ray analysis and their catalytic activity toward the propargylic substitution reactions, see: (a) Nishibayashi, Y.; Imajima, H.; Onodera, G.; Hidai, M.; Uemura, S. *Organometallics* **2004**, *23*, 26. (b) Nishibayashi, Y.; Imajima, H.; Onodera, G.; Inada, Y.; Hidai, M.; Uemura, S. *Organometallics* **2004**, *23*, 5100.

Table 1. Ruthenium-Catalyzed Oxypropargylation of Vinyl Ethers (2)^a

run	R ¹ (1)	R ² (2)	R ³ OH	yield of 4 (%) ^b	ratio of diastereoisomers
1	Ph (1a)	Et (2a)	EtOH	93 (4a)	
2	<i>p</i> -FC ₆ H ₄ (1b)	Et (2a)	EtOH	88 (4b)	
3	<i>p</i> -ClC ₆ H ₄ (1c)	Et (2a)	EtOH	93 (4c)	
4	<i>p</i> -MeOC ₆ H ₄ (1d)	Et (2a)	EtOH	92 (4d)	
5	<i>p</i> -MeC ₆ H ₄ (1e)	Et (2a)	EtOH	94 (4e)	
6	<i>m</i> -MeC ₆ H ₄ (1f)	Et (2a)	EtOH	98 (4f)	
7	<i>o</i> -MeC ₆ H ₄ (1g)	Et (2a)	EtOH	98 (4g)	
8	2-furyl (1h)	Et (2a)	EtOH	86 (4h)	
9	1-naphthyl (1i)	Et (2a)	EtOH	97 (4i)	
10	Ph ₂ C=CH (1j)	Et (2a)	EtOH	95 (4j)	
11	Ph (1a)	Et (2a)	^t PrOH	95 (4k)	50:50
12	Ph (1a)	Et (2a)	^t PrOH	90 (4l)	53:47
13	Ph (1a)	^t Bu (2b)	EtOH	92 (4m)	50:50

^a All reactions of **1** (0.20 mmol) with **2** (1.00 mmol) were carried out in the presence of **3a** (0.005 mmol) at 0 °C for 12 h in R³OH (2 mL).

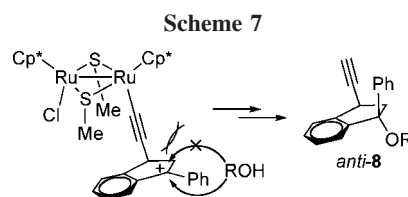
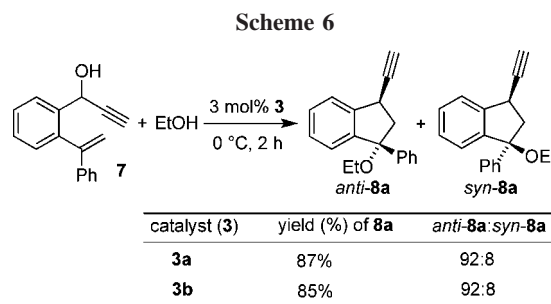
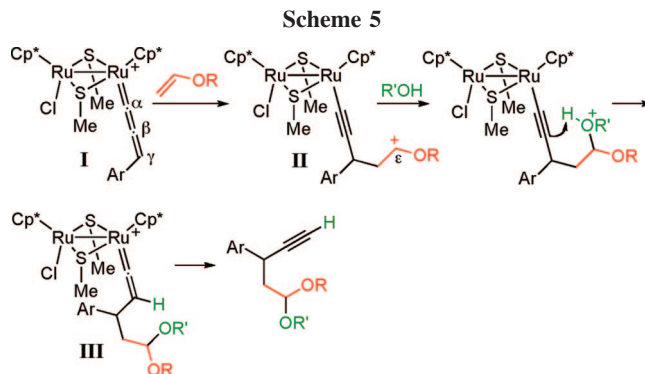
^b Isolated yield.



1-ethoxy-2-methyl-1-propene (**2d**), and 3,4-dihydro-2*H*-pyran (**2e**) proceeded smoothly to give the corresponding products (**4n–p**) in excellent yields (Scheme 3). Interestingly, **4p** was easily converted into the corresponding 1,4-enyne (**4p'**) in 42% yield. On the other hand, no oxypropargylation occurred when other alkenes such as styrene were used in place of **2**.

In order to obtain some information on the reaction pathway, the following stoichiometric and catalytic reactions were investigated. Treatment of the allenylidene complex **6**,⁷ which was separately prepared from the reaction of **3a** with **1a**, with excess amounts of **2a** and **1e** in ethanol gave **4a** in 53% yield together with **4e** in 99% yield (Scheme 4). On the other hand, the reaction of **1a** with **2a** in the presence of 5 mol % of **6** proceeded smoothly to give **4a** in 89% yield. These results indicate that allenylidene complexes are surely key intermediates for this oxypropargylation.

On the basis of these findings, a proposed reaction pathway is shown in Scheme 5. At present, we consider that the attack of a vinyl ether on the electron-deficient γ -carbon of **I** occurs



to give the corresponding alkynyl complex **II**, followed by the attack of an alcohol on the cationic ϵ -carbon of **II** to afford the corresponding oxypropargylated product via the ruthenium–vinylidene complex **III**. As described in our previous reports,⁸ we believe that the synergistic effect⁹ in the diruthenium complexes is quite important for the promotion of this catalytic reaction.

Next, we investigated the intramolecular version of this oxypropargylation. The reaction of a propargylic alcohol bearing an alkene moiety (**7**) in the presence of 3 mol % of **3a** in ethanol at 0 °C for 2 h gave 1-ethoxy-3-ethynyl-1-phenylindane (**8a**) in 87% isolated (97% GLC) yield as a mixture of two diastereoisomers, the *anti* isomer being the major species (*anti-8a*:*syn-8a* = 92:8) (Scheme 6). The molecular structure of the major isomer (*anti-8a*) was confirmed by X-ray analysis.⁵ The complex **3b** could be similarly employed, **8a** being obtained in 85% isolated yield with a similar diastereoselectivity. Intramolecular cyclization of **7** was carried out in a variety of alcohols in place of ethanol. Typical results are shown in Table 2. In all cases, the corresponding 1-alkoxy-3-ethynylindanes (**8**) were obtained in high to excellent yields with a high diastereoselectivity (Table 2, runs 2–5).

This intramolecular cyclization seems to proceed mainly through such a transition state as shown in Scheme 7. The attack of an alcohol on the reactive intermediate from the opposite

(6) The molecular structure of a diastereoisomer of **4p** was confirmed by X-ray analysis. See the Supporting Information for experimental details.

(7) Nishibayashi, Y.; Milton, M. D.; Inada, Y.; Yoshikawa, M.; Wakiji, I.; Hidai, M.; Uemura, S. *Chem. Eur. J.* **2005**, *11*, 1433.

(8) For recent examples, see: (a) Yamauchi, Y.; Onodera, G.; Sakata, K.; Yuki, M.; Miyake, Y.; Uemura, S.; Nishibayashi, Y. *J. Am. Chem. Soc.* **2007**, *129*, 5175. (b) Matsuzawa, H.; Miyake, Y.; Nishibayashi, Y. *Angew. Chem., Int. Ed.* **2007**, *46*, 6488. (c) Yamauchi, Y.; Yuki, M.; Tanabe, Y.; Miyake, Y.; Inada, Y.; Uemura, S.; Nishibayashi, Y. *J. Am. Chem. Soc.* **2008**, *130*, 2908.

(9) Ammal, S. C.; Yoshikai, N.; Inada, Y.; Nishibayashi, Y.; Nakamura, E. *J. Am. Chem. Soc.* **2005**, *127*, 9428.

Table 2. Ruthenium-Catalyzed Intramolecular Oxypropargylation (7)^a

run	ROH	time (h)	yield of 8 (%) ^b	<i>anti</i> - 8 : <i>syn</i> - 8 ^c
1	EtOH	2	87 (8a)	92:8
2	MeOH	2	81 (8b)	96:4
3	ⁿ PrOH	3	91 (8c)	96:4
4	ⁱ PrOH	3	78 (8d)	95:5
5	ⁿ BuOH	3	95 (8e)	92:8

^a All reactions of **7** (0.20 mmol) in ROH (2.5 mL) were carried out in the presence of **3a** (0.006 mmol) at 0 °C. ^b Isolated yield. ^c Determined by ¹H NMR.

site of the ruthenium–alkynyl moiety may lead to the formation of *anti*-**8**. Namely, the steric bulkiness of the ruthenium–alkynyl moiety may inhibit the formation of *syn*-**8**.

In summary, we have found the ruthenium-catalyzed oxypropargylation of alkenes with propargylic alcohols and simple alcohols via ruthenium–allenylidene complexes as key inter-

mediates. As a synthetic application, an intramolecular cyclization has been developed to give the corresponding *anti*-1-alkoxy-3-ethynylindanes in high to excellent yields with a high diastereoselectivity. The methodology described in this paper provides a novel synthetic approach to heterofunctionalization of alkenes. Further work is currently in progress to broaden its synthetic applicability to natural products and pharmaceuticals.

Acknowledgment. This work was supported by Grants-in-Aid for Scientific Research for Young Scientists (S) (No. 19675002) and for Scientific Research on Priority Areas (No. 18066003) from the Ministry of Education, Culture, Sports, Science and Technology of Japan. Y.N. thanks the Mazda Science and Technology Foundation and the Iwatani Naoji Foundation.

Supporting Information Available: Text, figures, tables, and CIF files giving experimental procedures, spectroscopic data, and X-ray data. This material is available free of charge via the Internet at <http://pubs.acs.org>.

OM801092A

Articles

Switching on the Phosphorescence of Pyrene by Cycloplatination

Jian Hu,[‡] John H. K. Yip,^{*,‡} Dik-Lung Ma,[†] Kwok-Yin Wong,[†] and Wai-Hong Chung[†]

Department of Chemistry, National University of Singapore, 3 Science Drive 3, Singapore, 117543, and
 Department of Applied Biology and Chemical Technology, The Hong Kong Polytechnic University,
 Hung Hom, Kowloon, Hong Kong SAR, People's Republic of China

Received May 8, 2008

1-Diphenylphosphinopyrene (1-PyP) and 1,6-bis(diphenylphosphino)pyrene (1,6-PyP) can be metalated at C5 and C10 to give cyclometalated complexes $[M(L)(1-PyP-H)]^+$ and $[M_2(L)_2(1,6-PyP)]^{2+}$ ($M = Pd$ or Pt , $L =$ diphosphines). The $\pi \rightarrow \pi^*$ transitions of the pyrenyl ring are strongly perturbed by the PPH_2 groups at C1/6, while the perturbation of the metal ions at C5/10 is weak. The phosphorescence of the pyrenyl ring is strongly enhanced by the heavy atom effect of the Pt ion up to a quantum yield of 1.5×10^{-2} . Direct coordination of the Pt ion to the pyrenyl ring is needed for enhancement of the phosphorescence.

Introduction

Pyrene has been commonly used as a fluorescent probe because of its intense fluorescence,¹ excimeric formation,^{1,2} and fluorescence anisotropy.³ Most of the applications of pyrene focus on its lowest energy singlet state (S_1), but the corresponding triplet excited state (T_1) and its phosphorescence have rarely been harnessed in chemical sensing and photochemical reactions.^{4a} A major obstacle is the low quantum yield of T_1 formation, as the $S_1 \rightarrow T_1$ intersystem crossing is spin-forbidden. Furthermore, because of the strong exchange interactions, the S_1 and T_1 states are widely separated, resulting in a large Franck–Condon barrier for the intersystem crossing. Heavy atoms with their large spin–orbit coupling are capable of

enhancing the phosphorescence by mixing the spin parentage of the excited states.^{1,5} Many studies focused on the external (intermolecular) heavy atom effect of metal ions, solvent molecules, or surfactants.^{4b,6} However, a more direct, effective way to induce the emission is to attach heavy metal atoms covalently to the organic ring.^{4a,7} Recently, Gray et al. have demonstrated gold(I) ion can induce the phosphorescence of pyrene.⁸ Our recent work showed that both Au(I) and Pt(II) ions can increase Φ_p up to 3.9×10^{-3} , and the effect of the metal ions is additive and position-dependent. For example, our results showed that 1,8-dimetalated pyrenes are less phosphorescent than the 1,6-metalated isomers.⁹

Bromopyrenes or their corresponding lithiated pyrenes were employed in the syntheses of the Au(I) and Pt(II) complexes.^{8–10} A major limitation of this method is that bromination of pyrene happens only at the C1, C3, C6, and C8 positions, and consequently only these positions have been metalated so far.

* To whom correspondence should be addressed. E-mail: chmyiphk@nus.edu.sg. Fax: 65-67791691.

[‡] National University of Singapore.

[†] The Hong Kong Polytechnic University.

(1) Birks, J. B. *Photophysics of Aromatic Molecules*; Wiley-Interscience: London, 1970.

(2) (a) Winnik, F. M. *Chem. Rev.* **1993**, *93*, 587. (b) Yang, R.-H.; Chan, W.-H.; Lee, A. W. M.; Xia, P.-F.; Zhang, H.-K.; Li, K. A. *J. Am. Chem. Soc.* **2003**, *125*, 2884. (c) Langenegger, S. M.; Häner, R. *Chem. Commun.* **2004**, 2792. (d) Nishizawa, S.; Kato, Y.; Teramae, N. *J. Am. Chem. Soc.* **1999**, *121*, 9463. (e) Bodenant, B.; Fages, F.; Delville, M.-H. *J. Am. Chem. Soc.* **1998**, *120*, 7511. (f) Kim, S. K.; Lee, S. H.; Lee, J. Y.; Lee, J. Y.; Bartsch, R. A.; Kim, J. S. *J. Am. Chem. Soc.* **2004**, *124*, 16499. (g) Moon, S.-Y.; Youn, N. J.; Park, S. M.; Chang, S.-K. *J. Org. Chem.* **2005**, *70*, 2394. (h) Martínez, R.; Espinosa, A.; Tárraga, A.; Molina, P. *Org. Lett.* **2005**, *7*, 5869. (i) Fujimoto, K.; Muto, Y.; Inouye, M. *Chem. Commun.* **2005**, 4780. (j) Okamoto, A.; Ichiba, T.; Saito, I. *J. Am. Chem. Soc.* **2004**, *126*, 8364. (k) Rogers, C. W.; Wolf, M. O. *Angew. Chem., Int. Ed.* **2002**, *41*, 1898. (l) Matkovich, K. M.; Thorne, L. M.; Wolf, M. O.; Pace, T. C. S.; Bohne, C.; Patrick, B. O. *Inorg. Chem.* **2006**, *45*, 4610.

(3) (a) Shyamala, T.; Sankararaman, S.; Mishra, A. K. *Chem. Phys.* **2006**, *330*, 469. (b) Sigman, M. E.; Read, S.; Barbas, J. T.; Ivanov, I.; Hagaman, E. W.; Buchanan, A. C., III; Dabestani, R.; Kidder, M. K.; Britt, P. F. *J. Phys. Chem. A* **2003**, *107*, 3450. (c) Sharma, J.; Tleugabulova, D.; Czardybon, W.; Brennan, J. D. *J. Am. Chem. Soc.* **2006**, *128*, 5496.

(4) (a) Pomestchenko, I. E.; Luman, C. R.; Hissler, M.; Ziessel, R.; Castellano, F. N. *Inorg. Chem.* **2003**, *42*, 1394. (b) Omary, M. A.; Kassab, R. M.; Haneline, M. R.; Elbjerrami, O.; Gabbai, F. P. *Inorg. Chem.* **2003**, *42*, 2176.

(5) (a) Kessinger, M.; Michl, J. *Excited States and Photochemistry of Organic Molecules*; Wiley-VCH: New York, 1995. (b) Suzuki, H. *Electronic Absorption Spectra and Geometry of Organic Molecules: an Application of Molecular Orbital Theory*; Academic Press: New York, 1967. (c) Turro, N. J. *Modern Molecular Photochemistry*; Benjamin: Menlo Park, NJ, 1978.

(6) (a) Blatt, E.; Launikonis, A.; Mau, A. W.-H.; Sasse, W. H. F. *Aust. J. Chem.* **1987**, *40*, 1. (b) Humphry-Baker, R.; Moroi, Y.; Gratzel, M. *Chem. Phys. Lett.* **1978**, *58*, 207. (c) Ramamurthy, V.; Caspar, J. V.; Eaton, D. F.; Kuo, E. W.; Corbin, D. R. *J. Am. Chem. Soc.* **1992**, *114*, 3882. (d) Mohamed, A. A.; Rawashdeh-Omary, M. A.; Omary, M. A.; Fackler, J. P., Jr. *Dalton Trans.* **2005**, 2597. (e) Burress, C.; Elbjerrami, O.; Omary, M. A.; Gabbai, F. P. *J. Am. Chem. Soc.* **2005**, *127*, 12166.

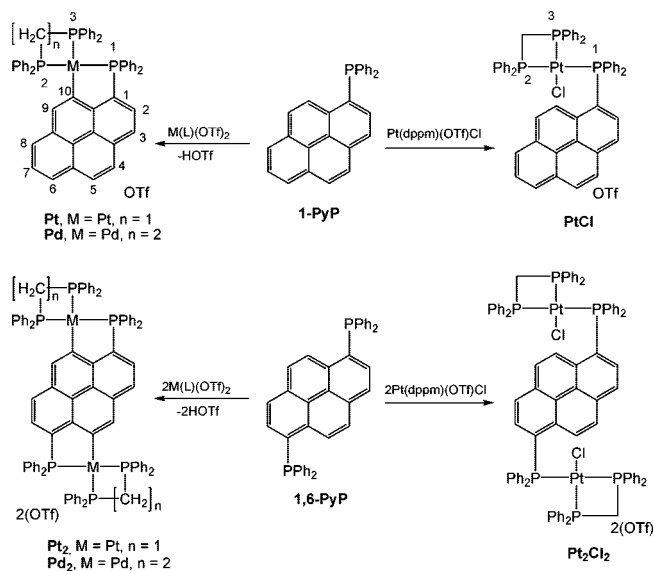
(7) (a) Che, C.-M.; Chao, H.-Y.; Miskowski, V. M.; Li, Y.; Cheung, K.-K. *J. Am. Chem. Soc.* **2001**, *123*, 4985. (b) Hong, X.; Cheung, K.-K.; Guo, C.-X.; Che, C.-M. *J. Chem. Soc., Dalton Trans.* **1994**, 1867. (c) Li, D.; Hong, X.; Che, C.-M.; Lo, W.-C.; Peng, S.-M. *Chem. Soc., Dalton Trans.* **1993**, 2929. (d) Chao, H.-Y.; Lu, W.; Li, Y.; Chan, M. C. W.; Che, C.-M.; Cheung, K.-K.; Zhu, N. *J. Am. Chem. Soc.* **2002**, *124*, 14696. (e) Osawa, M.; Hoshino, M.; Akita, M.; Wada, T. *Inorg. Chem.* **2005**, *44*, 1157.

(8) Partyka, D. V.; Esswein, A. J.; Zeller, M.; Hunter, A. D.; Gray, T. G. *Organometallics* **2007**, *26*, 3279.

(9) Heng, W. Y.; Hu, J.; Yip, J. H. K. *Organometallics* **2007**, *26*, 6760.

(10) (a) Yam, V. W.-W.; Choi, S. W.-K.; Cheung, K.-K. *J. Chem. Soc., Dalton Trans.* **1996**, 3411. (b) Weisemann, C.; Schmidtberg, G.; Brune, H.-A. *J. Organomet. Chem.* **1989**, *365*, 403.

Scheme 1



Our previous studies showed that Pt(II) ions can be anchored on an anthracene ring via facile cyclometalation between PtL(OTf)₂ [L = bis(diphenylphosphino)methane (dppm)] and 9,10-bis(diphenylphosphino)anthracene.^{11a} Demonstrated in this work is how cyclometalation allows C5 and C10 to be metalated. Our method started with the syntheses of the ligands 1-diphenylphosphinopyrene (1-PyP) and 1,6-bis(diphenylphosphino)pyrene (1,6-PyP), which possess PPh₂ groups at C1/C6 (Scheme 1). Coordination of Pd(dppe)(OTf)₂ (dppe = bis(diphenylphosphino)ethane) and Pt(dppm)(OTf)₂ to the phosphines would direct the attack of the metal ions at the C–H bonds at the C5 and C10 positions, leading to the cyclometalated complexes [Pt(dppm)(1-PyP-H)](OTf) (**Pt**), [Pd(dppe)(1-PyP-H)](OTf) (**Pd**), [Pt₂(dppm)₂(1,6-PyP-H₂)](OTf)₂ (**Pt₂**), and [Pd₂(dppe)₂(1,6-PyP-H₂)](OTf)₂ (**Pd₂**) (Scheme 1). Like many cyclometalated complexes,¹¹ the present complexes are emissive. The complexes [Pt(dppm)Cl(1-PyP)](OTf) (**PtCl**) and [Pt₂(dppm)₂Cl₂(1,6-PyP)](OTf) (**Pt₂Cl₂**), which consist of dangling Pt ions, were also prepared for comparison. Our results not only showed drastic enhancement of the phosphorescence by internal heavy atom effect but also provide insights into the interactions between the metal ions and pyrene.

Experimental Section

General Methods. All syntheses were carried out in a dry N₂ atmosphere using standard Schlenk techniques unless otherwise stated. All reagents and HPLC grade solvents for syntheses were

(11) (a) Hu, J.; Lin, R.; Yip, J. H. K.; Wong, K.-Y.; Ma, D.-L.; Vittal, J. J. *Organometallics* **2007**, *26*, 6533. (b) Kui, S. C. F.; Chui, S. S.-Y.; Che, C.-M.; Zhu, N. *J. Am. Chem. Soc.* **2006**, *128*, 8297. (c) Kui, S. C. F.; Sham, I. H. T.; Cheung, C. C. C.; Ma, C.-W.; Yan, B.; Zhu, N.; Che, C.-M.; Fu, W.-F. *Chem.-Eur. J.* **2007**, *13*, 417. (d) Yip, J. H. K.; Suwarno, Vittal, J. J. *Inorg. Chem.* **2000**, *39*, 3537. (e) Williams, J. A. G.; Beeby, A.; Davies, E. S.; Weinstein, J. A.; Wilson, C. *Inorg. Chem.* **2003**, *42*, 8609. (f) Ma, B.; Djurovich, P. I.; Thompson, M. E. *Coord. Chem. Rev.* **2005**, *249*, 1501. (g) Adachi, C.; Baldo, M. A.; Forrest, S. R.; Lamansky, S.; Thompson, M. E.; Kwong, R. C. *Appl. Phys. Lett.* **2001**, *78*, 1622. (h) Song, D.; Wu, Q.; Hook, A.; Kozin, I.; Wang, S. *Organometallics* **2001**, *20*, 4683. (i) Bai, D.-R.; Wang, S. *Organometallics* **2006**, *25*, 1517. (j) Ionkin, A. S.; Marshall, W. J.; Wang, Y. *Organometallics* **2005**, *24*, 619. (k) Koo, C.-K.; Lam, B.; Leung, S.-K.; Lam, M. H.-W.; Wong, W.-Y. *J. Am. Chem. Soc.* **2006**, *128*, 16434. (l) Koo, C.-K.; Ho, Y.-M.; Chow, C.-F.; Lam, M. H.-W.; Lau, T.-C.; Wong, W.-Y. *Inorg. Chem.* **2007**, *46*, 3603. (m) Fernández, S.; Forniés, J.; Gil, B.; Gómez, J.; Lalinde, E. *Dalton Trans.* **2003**, 822.

used as received. Solvents used for spectroscopic measurements were purified according to the literature procedures. 1-Bromopyrene¹² and 1,6-dibromopyrene⁹ were prepared according to literature methods. Bis(diphenylphosphino)methane (dppm), 1,2-bis(diphenylphosphino)ethane (dppe), and chlorodiphenylphosphine were obtained from Aldrich. Pt(dppm)Cl₂ and Pd(dppe)Cl₂ was prepared by substitution of MeCN by dppe from PtCl₂(MeCN)₂ and PdCl₂(MeCN)₂, respectively.¹³ Pt(dppm)(OTf)₂ and Pd(dppe)(OTf)₂ were prepared *in situ* based on modified literature procedures.¹³

Physical Measurements. NMR experiments were performed on a Bruker ACF 300 spectrometer. All chemical shifts (δ) are reported in ppm and coupling constants (J) in Hz. ¹H NMR chemical shifts are relative to SiMe₄, and the resonance of residual protons of solvents was used as an internal standard. ³¹P{¹H} NMR chemical shifts were relative to 85% H₃PO₄. The UV–vis absorption and emission spectra of the complexes were recorded on a Shimadzu UV-1601 UV–visible spectrophotometer and a Perkin-Elmer LS50B luminescence spectrophotometer, respectively. Emission lifetime measurements were performed with a Quanta Ray DCR-3 pulsed Nd:YAG laser system (excitation wavelength = 355 nm, pulse width = 8 ns). The decays were analyzed by means of DataStation software v2.3. The emission quantum yields were measured with rhodamine 101 perchlorate as standard. Error limits were estimated as follows: λ (± 1 nm); τ ($\pm 10\%$); Φ ($\pm 10\%$). Deaerated solutions used for emission spectra and lifetime measurements were obtained by four freeze–pump–thaw cycles. Elemental analyses of the complexes were carried out at the Chemical, Molecular and Materials Analysis Centre (CMMAC), National University of Singapore.

Synthesis of 1-(Diphenylphosphino)pyrene (1-PyP). The compound was synthesized following literature methods.¹⁴ 1-Bromopyrene (6.26 g, 22.3 mmol) was dissolved in 150 mL of freshly distilled diethyl ether, and the solution was kept at 0 °C. Butyl lithium (16.7 mL of 1.6 M solution in hexane, 26.7 mmol) was added dropwise to the solution, and the mixture was stirred for 10 min before addition of chlorodiphenylphosphine (4.00 mL, 22.3 mmol). The resulting mixture was stirred for 12 h at room temperature. A pale yellow solid was filtered and washed with water and diethyl ether; it was then dried under vacuum and stored under N₂. Yield: 6.00 g, 70%. ¹H NMR (CDCl₃, 300 MHz, δ /ppm): 8.77 (dd, ³J_{H–H} = 9 Hz, ⁴J_{H–P} = 5 Hz, 1H, H₁₀), 8.21–8.18 (m, 2H, H₆ and H₈), 8.12–7.99 (m, 5H, H_{3,4,5,7,9}), 7.56 (dd, ³J_{H–H} = 8 Hz, ³J_{H–P} = 4 Hz, 1H, H₂) and 7.35–7.34 (m, 10H, phenyl). ³¹P{¹H} NMR (CDCl₃, 121.5 MHz, δ /ppm): –13.85 (s).

Synthesis of 1,6-Bis(diphenylphosphino)pyrene (1,6-PyP). 1,6-Dibromopyrene (3.38 g, 9.39 mmol) was suspended in freshly distilled diethyl ether (100 mL) and kept at 0 °C. Butyl lithium (14.1 mL of 1.6 M solution in hexane, 22.56 mmol) was then added dropwise to the suspension, which was then stirred for 10 min before the addition of chlorodiphenylphosphine (4.14 g, 9.39 mmol). The resulting mixture was stirred for 12 h at room temperature. The pale yellow solid obtained was then filtered and washed with water, methanol, and diethyl ether. The product was further purified by column chromatography on silica gel with CH₂Cl₂ as the eluent. It was dried under vacuum and stored under N₂. Yield: 4.00 g, 75%. Melting point: 278–282 °C. Anal. Calcd (%) for C, 84.20; H, 4.95. Found (%): C, 84.35; H, 5.01. ¹H NMR (CDCl₃, 300 MHz, δ /ppm): 8.81 (dd, ³J_{H–H} = 9 Hz, ⁴J_{H–P} = 5 Hz, 2H, H_{5,10}), 8.07–8.01 (m, 4H, H_{3,8} and H_{4,9}), 7.56 (dd, ³J_{H–H} = 8 Hz, ³J_{H–P} = 4 Hz, 2H,

(12) Vyas, P. V.; Bhatt, A. K.; Ramachandraiah, G.; Bedekar, A. V. *Tetrahedron Lett.* **2003**, *44*, 4085.

(13) (a) Davies, J. A.; Hartley, F. R.; Murray, S. G. *J. Chem. Soc., Dalton Trans.* **1979**, *11*, 1705. (b) Fallis, S.; Anderson, G. K.; Rath, N. P. *Organometallics* **1991**, *10*, 3180.

(14) (a) Müller, T. E.; Green, J. C.; Mingos, D. M. P.; Mcpartlin, C. M.; Whittingham, C.; Williams, D. J.; Woodroffe, T. M. *J. Organomet. Chem.* **1998**, *551*, 313. (b) Yip, J. H. K.; Prabhavathy, J. *Angew. Chem., Int. Ed.* **2001**, *40*, 2159.

(H_{2,7}), 7.35–7.34 (m, 20H, phenyl). ³¹P{¹H} NMR (CDCl₃, 121.5 MHz, δ/ppm): –13.72 (s). EI-MS: *m/z*(relative abundance) 570.2(10%) [M]⁺, 385(40%) [M – PPh₂]⁺.

Synthesis of [Pt(dppm)(1-PyP-H)](OTf) (Pt). Pt(dppm)Cl₂ (228 mg, 0.35 mmol) and AgOTf (180 mg, 0.70 mmol) were mixed in CH₂Cl₂(40 mL)/CH₃CN(20 mL) and stirred for 1 day in the dark. The resulting mixture was filtered, and 1-PyP (135 mg, 0.35 mmol) was added to the filtrate. The mixture was stirred for 1 day, followed by filtration. The filtrate was concentrated to ~5 mL by rotaevaporation, followed by adding of excess diethyl ether to precipitate the pale yellow product, which was filtered, washed with diethyl ether, and dried under vacuum. The product was purified by recrystallization from a CH₂Cl₂/Et₂O solution. Yield: 0.19 g, 50%. Anal. Calcd (%) for C₅₄H₄₀F₃O₃P₃PtS: C, 58.22; H, 3.62. Found (%): C, 57.88; H, 3.35. ¹H NMR (CDCl₃, 300 MHz): δ/ppm 8.32–7.81 (unresolved m, 9H, pyrenyl H's), 7.58–7.16 (m, 30H, phenyl rings), 5.20–5.13 (m, 2H, CH₂). ³¹P{¹H} NMR (CDCl₃, 121.5 MHz): δ/ppm 44.41 (dd, P1), –25.93 (dd, P2), –33.23 (dd, P3); ¹J_{P1–Pt} = 2800 Hz, ¹J_{P2–Pt} = 2419 Hz, ¹J_{P3–Pt} = 1442 Hz; ²J_{P1–P2} = 362 Hz, ²J_{P1–P3} = 15 Hz, ²J_{P2–P3} = 42 Hz. ESI-MS (*m/z*): 964.5 [M – OTf]⁺.

Synthesis of [Pd(dppe)(1-PyP-H)](OTf) (Pd). AgOTf (179 mg, 0.696 mmol) was added to a 30 mL CH₂Cl₂ solution of Pd(dppe)Cl₂ (182 mg, 0.316 mmol). The mixture was stirred for 21 h, and AgCl was removed by filtration. To the filtrate was added 1-PyP (122 mg, 0.316 mmol), and the mixture was stirred for 1 day. The resulting mixture was filtered and concentrated. Addition of excess Et₂O precipitated the pale yellow product. Single crystals suitable for X-ray diffraction were grown by slow diffusion from CH₂Cl₂/Et₂O. Yield: 0.28 g, 85%. Anal. Calcd (%) for C₅₅H₄₂F₃O₃P₂S: C, 63.56; H, 4.07. Found (%): C, 63.25; H, 4.19. ¹H NMR (CDCl₃, 300 MHz): unresolved multiplets, 8.18–7.19 (4H), 7.96–7.81 (6H), 7.66–7.53 (7H), 7.43–7.37 (5H), 7.30–7.19 (16H); 2.78–2.58 (m, 4H, PCH₂CH₂P). ³¹P{¹H} NMR (CDCl₃, 121.5 MHz): δ/ppm 58.81 (P1), 55.51 (P2), 41.45 (P3). ABX system, ²J_{P1–P2} = 333 Hz, ²J_{P1–P3} = 30 Hz, ²J_{P2–P3} = 30 Hz. ESI-MS (*m/z*): 889.4 [M – OTf]⁺.

Synthesis of [Pt₂(dppm)₂(1,6-PyP-H₂)](OTf)₂ (Pt₂). AgOTf (95 mg, 0.370 mmol) was added into a 50 mL CH₂Cl₂ solution of Pt(dppm)Cl₂ (120 mg, 0.185 mmol), and the mixture was stirred for 6 h in the dark. The resulting mixture was filtered, and 1,6-PyP (53 mg, 0.093 mmol) was added to the filtrate. The mixture was stirred for 36 h, and the product was then precipitated by adding Et₂O to the concentrated reaction solution. The product was purified by recrystallization from CH₂Cl₂/Et₂O by slow diffusion. Yield: 152 mg, 94%. Anal. Calcd (%) for C₉₂H₇₀F₆O₆P₆Pt₂S₂·2CH₂Cl₂: C, 51.42; H, 3.40. Found (%): C, 51.45; H, 3.52. ¹H NMR (CD₃CN, 300 MHz): δ/ppm 8.29–8.25, 8.06–8.00, 7.96–7.89, 7.61–7.16, unresolved multiples; 5.10–5.03 (m, 4H, CH₂). ³¹P{¹H} NMR (CD₃CN, 121.5 MHz, δ/ppm): 46.50 (dd, P1), –24.46 (dd, P2), –31.92 (dd, P3); ¹J_{P1–Pt} = 2812 Hz, ¹J_{P2–Pt} = 2418 Hz, ¹J_{P3–Pt} = 1434 Hz; ²J_{P1–P2} = 347 Hz, ²J_{P1–P3} = 15 Hz, ²J_{P2–P3} = 42 Hz. ESI-MS (*m/z*): 863.8 [M – 2OTf]²⁺.

Synthesis of [Pd₂(dppe)₂(1,6-PyP-H₂)](OTf)₂ (Pd₂). AgOTf (197 mg, 0.767 mmol) was added to a 30 mL CH₂Cl₂ solution of Pd(dppe)Cl₂ (201 mg, 0.349 mmol), and the mixture was stirred for 1 day in the dark. Subsequently, the resulting mixture was filtered. 1,6-PyP (101 mg, 0.177 mmol) was added to the filtrate, and the mixture was stirred for 36 h. The resulting solution was concentrated to ~5 mL, and excess Et₂O was added to precipitate the product as a pale yellow solid. The product was purified by recrystallization from CH₂Cl₂/Et₂O. Yield: 0.32 g, 96%. Anal. Calcd (%) for C₉₄H₇₄F₆O₆P₆Pd₂S₂: C, 60.17; H, 3.97. Found (%): C, 59.70; H, 4.22. ¹H NMR (CD₂Cl₂, 300 MHz): 8.06–8.00 (m, 2H, H_{2,7} of pyrenyl ring), 7.89–7.83 (m, 8H, Ph), 7.73–7.67 (m, 2H, H_{3,8} of pyrenyl ring), 7.65–7.60 (m, 4H, Ph on P1), 7.55–7.51 (m, 8H, Ph), 7.44–7.35 (m, 8H, Ph), 7.28–7.18 (m, 34H, H_{4,9} of pyrenyl ring, Ph), 2.61–2.46 (m, 8H, CH₂). ³¹P{¹H} NMR (CD₂Cl₂, 121.5

MHz): δ/ppm 58.83 (P1), 55.57 (P2), 42.09 (P3). ABX system, ²J_{P1–P2} = 333 Hz, ²J_{P1–P3} = 30 Hz, ²J_{P2–P3} = 30 Hz. ESI-MS (*m/z*): 789.8 [M – 2OTf]²⁺.

[Pt(dppm)Cl(1-PyP)]OTf (PtCl). To a solution of AgOTf (107 mg, 0.416 mmol) in a mixture of CH₃CN (25 mL) and CH₂Cl₂ (25 mL) was added Pt(dppm)Cl₂ (271 mg, 0.417 mmol). The mixture was stirred for 2 h in the dark, followed by filtration. 1-PyP (161 mg, 0.416 mmol) was added to the filtrate, and the solution was stirred for 1 h before being filtered. The filtrate was concentrated by rotaevaporation, and excess Et₂O was added to precipitate the pale yellow product. Single crystals suitable for X-ray diffraction were obtained from CH₂Cl₂/Et₂O. Yield: 110 mg, 86%. Anal. Calcd (%) for C₅₄H₄₁ClF₃O₃P₃PtS·CH₂Cl₂: C, 53.47; H, 3.51. Found (%): C, 53.79; H, 3.40. ¹H NMR (CDCl₃, 300 MHz): δ/ppm 8.68 (dd, ³J_{H–H} = 9 Hz, ³J_{H–P} = 1.7 Hz, 1H, H₁₀ of pyrene ring), 8.35–7.94 (m, 10H, unresolved), 7.75–7.69 (m, 2H unresolved), 7.49–7.21 (m, 26H, unresolved), 5.23–4.99 (m, 2H, CH₂). ³¹P{¹H} NMR (CDCl₃, 121.5 MHz): 17.72 (dd, P1), –52.34 (dd, P2), –54.07 (dd, P3); ¹J_(P1–Pt) = 2345 Hz, ¹J_(P2–Pt) = 2090 Hz, ¹J_(P3–Pt) = 3031 Hz; ²J_(P1–P2) = 423 Hz, ²J_(P1–P3) = 23 Hz, ²J_(P2–P3) = 65 Hz. ESI-MS (*m/z*): 1001.3(100%) [M – OTf]⁺.

[Pt(dppm)Cl₂(1,6-PyP)](OTf)₂ (Pt₂Cl₂). It was prepared by the same procedure for PtCl, except that 0.5 equiv of 1,6-PyP was used instead of 1-PyP. Yield: 0.39 g, 90%. Anal. Calcd (%) for C₉₂H₈₂Cl₂F₆O₆P₆Pt₂S₂: C, 52.66; H, 3.94. Found (%): C, 52.46; H, 3.58. ¹H NMR (CD₂Cl₂/CD₃CN, 300 MHz): δ/ppm 8.77 (m, 2H, pyrenyl H's), 8.17 (m, 2H, pyrenyl H's), 7.82–7.74 (m, 4H, Ph), 7.60–7.29 (m, 60H, Ph and pyrenyl H's), 4.79–4.72 (m, 4H, CH₂). ³¹P{¹H} NMR (CD₂Cl₂/CD₃CN, 121.5 MHz): δ/ppm 18.76 (dd, P1), –50.88 (dd, P2), –53.07 (dd, P3); ²J_(P1–P2) = 403 Hz, ¹J_(P1–P3) = 40 Hz, ²J_(P2–P3) = 65 Hz. ESI-MS (*m/z*): 900.7 (30%) [M – 2(OTf)]²⁺, 1185.0 (100%) [M – Pt(dppm)Cl – 2(OTf)]⁺.

X-ray Crystallography. The diffraction experiments were carried out on a Bruker AXS SMART CCD 3-circle diffractometer with a sealed tube at 23 °C using graphite-monochromated Mo Kα radiation (λ = 0.71073 Å). The software used were SMART^{15a} for collecting frames of data, indexing reflection, and determination of lattice parameters; SAINT^{15a} for integration of intensity of reflections and scaling; SADABS^{15b} for empirical absorption correction; and SHELXTL^{15c} for space group determination, structure solution, and least-squares refinements on F². The crystals were mounted at the end of glass fibers and used for the diffraction experiments. Anisotropic thermal parameters were refined for the rest of the non-hydrogen atoms. The hydrogen atoms were placed in their ideal positions.

Results and Discussion

Synthesis. The ligands 1-(diphenylphosphino)pyrene (1-PyP) and 1,6-bis(diphenylphosphino)pyrene (1,6-PyP) were prepared by lithiation of 1-bromopyrene and 1,6-dibromopyrene, respectively, followed by the reaction with PPh₂Cl. The monophosphine ligand 1-PyP underwent facile cyclometalation with Pt(dppm)(OTf)₂ and Pd(dppe)(OTf)₂ to give mononuclear complexes [Pt(dppm)(1-PyP-H)](OTf) (Pt) and [Pd(dppe)(1-PyP-H)](OTf) (Pd), respectively. Similarly, the reactions of the diphosphine ligand 1,6-PyP with Pt(II) and Pd(II) gave the doubly cyclometalated complexes [Pt₂(dppm)₂(1,6-PyP-H₂)](OTf)₂ (Pt₂) and Pd₂(dppe)₂(1,6-PyP-H₂)](OTf)₂ (Pd₂), respectively (Scheme 1). The complexes were fully characterized by ESI-MS, ³¹P{¹H} NMR, and X-ray crystallography. The dangling complexes PtCl and Pt₂Cl₂ were prepared by reacting Pt(dppm)(OTf)Cl with the phosphines. The complexes decompose slowly in diluted CH₂Cl₂ solution, as adventitious chloride ions in the solvent can react with the Pt ions to form the stable *cis*-Pt(dppm)Cl₂.

Structures. The complexes were all characterized by single-crystal X-ray diffractions. The structures of Pt·CH₂Cl₂, Pd, Pt₂,

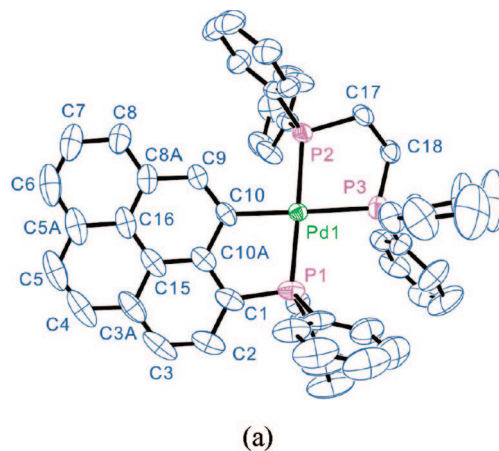
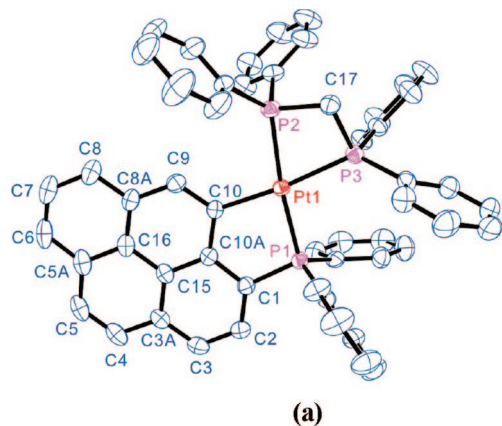


Figure 1. ORTEP diagram of $\text{Pt} \cdot \text{CH}_2\text{Cl}_2$ (50% thermal ellipsoids). H atoms, the anion, and solvent molecule are omitted for clarity.

$\text{Pd}_2 \cdot 3\text{CH}_2\text{Cl}_2$, $\text{PtCl} \cdot \text{CH}_2\text{Cl}_2$, and $\text{Pt}_2\text{Cl}_2 \cdot 2\text{CH}_3\text{CN}$ are depicted in Figures 1–6, respectively (see Supporting Information for selected bond lengths and angles). The structures are in accordance with the ESI-MS and $^1\text{P}\{^1\text{H}\}$ NMR data. For $\text{Pt} \cdot \text{CH}_2\text{Cl}_2$ and Pd , the metal ion is bonded to the C10 of the pyrenyl ring. On the other hand, the dicyclopalladated Pt_2 and $\text{Pd}_2 \cdot 3\text{CH}_2\text{Cl}_2$ have two metal centers attached to the C5 and C10 of the pyrenyl ring.

For the cyclometalated complexes, all structures consist of five-membered chelate rings formed between the metal ions and the pyrenyl ring. The formation of the chelate rings can be one of the driving forces for the facile cyclometalation. Both bimetallic cations of Pt_2 and Pd_2 display an approximate C_{2h} symmetry. For all complexes, the metal centers show distorted square-planar coordination and are coplanar with the pyrenyl rings.

The $\text{Pt}-\text{C}(2.051(3)-2.055(4) \text{ \AA})$ and $\text{Pt}-\text{P}(2.2596(8)-2.3323(8) \text{ \AA})$ bond lengths of Pt and Pt_2 are normal.^{11a} For Pt_2 , the $\text{Pt}(1)-\text{P}(3)$ (2.3262(12) \AA) bond is longer than the other $\text{Pt}-\text{P}$ bonds (2.2848(12)–2.3169(12) \AA). This is in accordance with the fact that P(3) and P(3A) are *trans* to the strongly σ -donating carbanions. Pd and Pd_2 have identical $\text{Pd}-\text{C}$ bond lengths (2.080(5) \AA). The bonds are significantly longer than those found in related cyclopalladated complexes, in which the $\text{Pd}-\text{C}$ bonds (1.934(14)–2.017(4) \AA) were assumed to have partial multiple-bond character on account of significant $\text{Pd}-\text{C}$ bond shortening compared to the sum of covalent radii (2.05–2.08 \AA) of carbon (0.77 \AA) and palladium (1.31 \AA).^{16,17} The partial multiple bonding was attributed to the $\text{Pd}(\text{II})$ -to-aryl π back-donation. In this work, the auxiliary ligands on $\text{Pd}(\text{II})$ are tertiary phosphines (dppe) instead of halogens, acetates, or acetylacetonate, as found in those complexes with shorter $\text{Pd}-\text{C}$ bonds, and the stronger σ -donating and π -accepting abilities of the *trans* phosphine ligands may account for the lengthening of $\text{Pd}-\text{C}$ bonds. Similar lengthening of the $\text{Pd}-\text{C}$ bond due to the

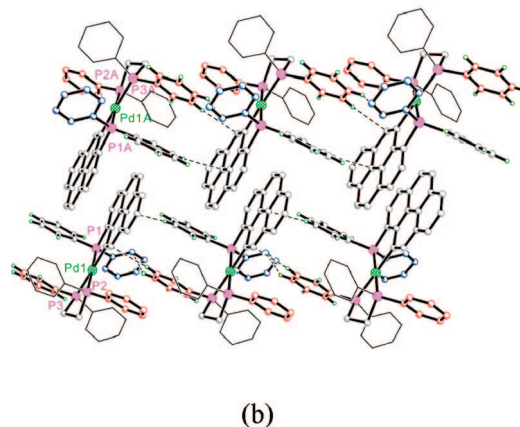


Figure 2. (a) ORTEP diagram of Pd (50% thermal ellipsoids). H atoms and the anion are omitted for clarity. (b) Packing diagram showing the $\pi-\pi$ stacking and edge-to-face interactions. The thermal ellipsoids are large presumably due to the high temperature (293 K) for data collection.

presence of *trans* phosphine ligands was reported.¹⁸ The $\text{Pd}-\text{P}$ bond lengths (2.2978(13)–2.3424(13) \AA) are normal.

No $\pi-\pi$ stacking between pyrenyl rings is observed in the crystal of $\text{Pt} \cdot \text{CH}_2\text{Cl}_2$. On the other hand, the cations of Pd aggregate into dimers via $\pi-\pi$ stacking of pyrenyl rings (Figure 2b), as they are parallel and partially overlap with an interplanar distance of 3.566 \AA . In addition, there are possible phenyl(edge)-to-pyrenyl(face) $\text{CH} \cdots \pi$ interactions between neighboring ions: one of the phenyl rings of dppe of a cation is directed toward the pyrenyl ring of an adjacent ion, and the distance between the phenyl H atoms and the centroid of the pyrenyl ring ($d(\text{CH} \cdots \pi)$) is 2.724 \AA , which is typical for the secondary hydrogen bonding.

(15) (a) SMART & SAINT Software Reference Manuals, Version 4.0; Siemens Energy & Automation, Inc., Analytical Instrumentation: Madison, WI, 1996. (b) Sheldrick, G. M. SADABS: a Software for Empirical Absorption Corrections; University of Göttingen: Germany, 2001. (c) SHELXTL Reference Manual, Version 5.03; Siemens Energy & Automation, Inc., Analytical Instrumentation: Madison, WI, 1996.

(16) (a) Churchill, M. R.; Wasserman, H. J.; Young, G. J. *Inorg. Chem.* **1980**, *19*, 762. (b) Selbin, J.; Abboud, K.; Watkins, S. F.; Gutierrez, M. A.; Fronczek, F. R. *J. Organomet. Chem.* **1983**, *241*, 259. (c) Navarro-Ranninger, C.; Zamora, F.; López-Solera, I.; Monge, A.; Masaguer, J. R. *J. Organomet. Chem.* **1996**, *505*, 149. (d) Vila, J. M.; Pereira, M. T.; Ortigueira, J. M.; Torres, M. L.; Califano, S.; Lata, D.; Fernández, J. J.; Fernández, A. *J. Organomet. Chem.* **1998**, *556*, 31.

(17) (a) Caygill, G. B.; Steel, P. J. *J. Organomet. Chem.* **1987**, *327*, 115. (b) Vila, J. M.; Gayoso, M.; Pereira, M. T.; Romar, A.; Fernández, J. J. *J. Organomet. Chem.* **1991**, *401*, 385. (c) Vila, J. M.; Gayoso, M.; Pereira, M. T.; Rodriguez, M. C.; Ortigueira, J. M.; Thornton-Pett, M. J. *J. Organomet. Chem.* **1992**, *426*, 267. (d) Vila, J. M.; Gayoso, M.; Fernández, A.; Bailey, N. A.; Adams, H. *J. Organomet. Chem.* **1993**, *448*, 233. (e) Fuchita, Y.; Yoshinaga, K.; Hanaki, T.; Kawano, H.; Kinoshita-Nagaoka, J. *J. Organomet. Chem.* **1999**, *580*, 273. (f) Phillips, I. G.; Steel, P. J. *J. Organomet. Chem.* **1991**, *410*, 1991. (g) Vila, J. M.; Gayoso, M.; Fernández, A.; Ortigueira, J. M.; Fernández, A.; Bailey, N. A.; Adams, H. *J. Organomet. Chem.* **1994**, *471*, 259. (h) Vila, J. M.; Gayoso, M.; Pereira, M. T.; Torres, M. L.; Fernández, J. J.; Fernández, A.; Rivero, B. E. *J. Organomet. Chem.* **1996**, *510*, 51.

(18) (a) Vila, J. M.; Gayoso, M.; López-Torres, M.; Fernández, J. J.; Fernández, A.; Ortigueira, J. M.; Bailey, N. A.; Adams, H. *J. Organomet. Chem.* **1996**, *511*, 129. (b) Vila, J. M.; Gayoso, M.; Pereira, M. T.; Ortigueira, J. M.; López-Torres, M.; Castineiras, A.; Suarez, A.; Fernández, J. J.; Fernández, A. *J. Organomet. Chem.* **1997**, *547*, 297.

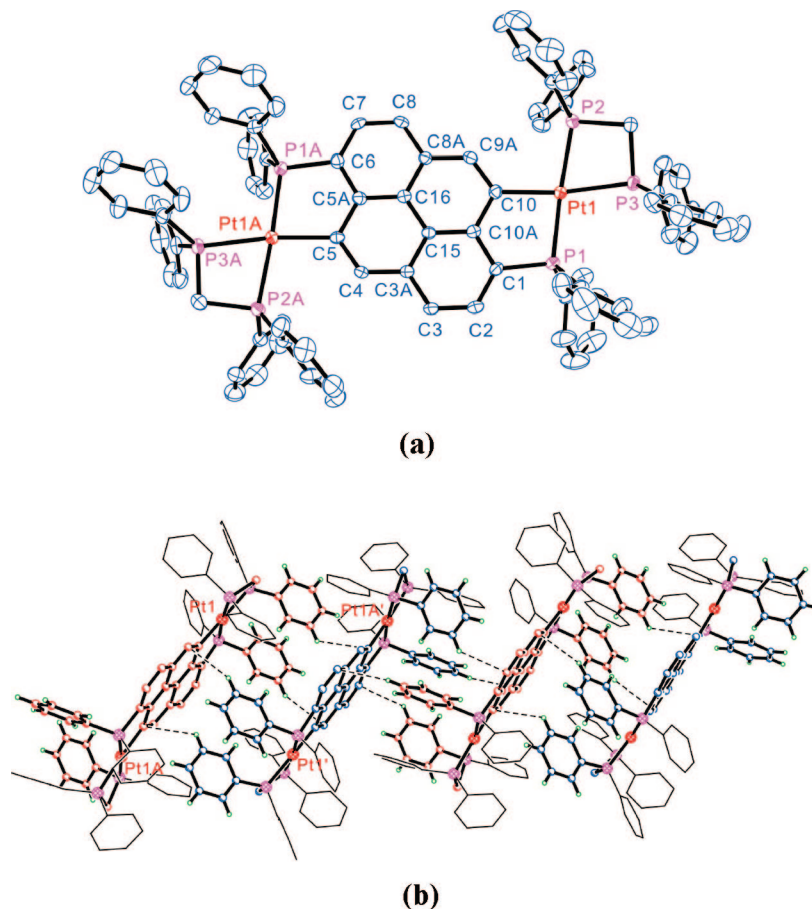


Figure 3. (a) ORTEP diagram of Pt_2 (50% thermal ellipsoids). (b) Packing diagram showing edge-to-face interactions between the phenyl and the pyrenyl rings. H atoms and anions are omitted for clarity.

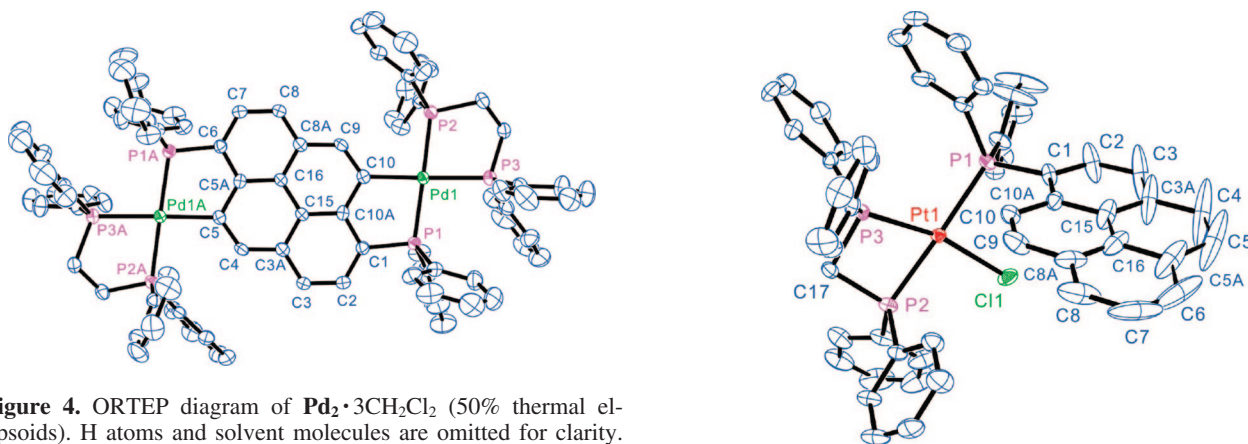


Figure 4. ORTEP diagram of $\text{Pd}_2 \cdot 3\text{CH}_2\text{Cl}_2$ (50% thermal ellipsoids). H atoms and solvent molecules are omitted for clarity.

Due to the steric hindrance of the bulky phenyl groups on the P atoms, no π - π stacking of pyrenyl rings is observed in the crystals of Pt_2 and $\text{Pd}_2 \cdot 3\text{CH}_2\text{Cl}_2$; however, inspection of the packing of the cations reveals extensive $\text{CH} \cdots \pi$ interactions. Figure 3b shows the crystal packing of Pt_2 . The cations are aligned with their pyrenyl rings being parallel to each other. Four phenyl rings are sandwiched between the pyrenyl rings, forming edge-to-face $\text{CH} \cdots \pi$ interactions with $d(\text{CH} \cdots \pi)$ of 2.807–2.873 Å. Similar $\text{CH} \cdots \pi$ interactions are observed in the crystal of $\text{Pd}_2 \cdot 3\text{CH}_2\text{Cl}_2$.

The molecular structure of $\text{PtCl} \cdot \text{CH}_2\text{Cl}_2$ (Figure 5) shows a Pt ion coordinated to one Cl^- and three P atoms, one from 1-PyP and the other two from dppm. The Pt ion has a distorted square-

Figure 5. ORTEP plot of $\text{PtCl} \cdot \text{CH}_2\text{Cl}_2$. H atoms, anion, and solvent molecule are omitted for clarity. Thermal ellipsoids are shown at 30% probability.

planar geometry, and the Pt–Cl (2.3411(12) Å)¹⁹ and Pt–P bond lengths are normal. The Pt(1)–P(3) bond (2.2437(11) Å) is shorter than the other two Pt–P bonds (Pt(1)–P(1) 2.3619(11) Å, Pt(1)–P(2) 2.2971(12) Å) because P(3) is *trans* to a weak σ -donor Cl^- , whereas the other two are *trans* to each other. The torsional angle between the Pt ion and the pyrene plane is 127.50°.

The structure of $\text{Pt}_2\text{Cl}_2 \cdot 2\text{CH}_3\text{CN}$ (Figure 6) shows two Pt ions, each coordinated to one Cl^- ion and three P atoms from

(19) Ho, K.-C.; McLaughlin, M.; McPartlin, M.; Robertson, G. *Acta Crystallogr.* **1982**, *B32*, 421.

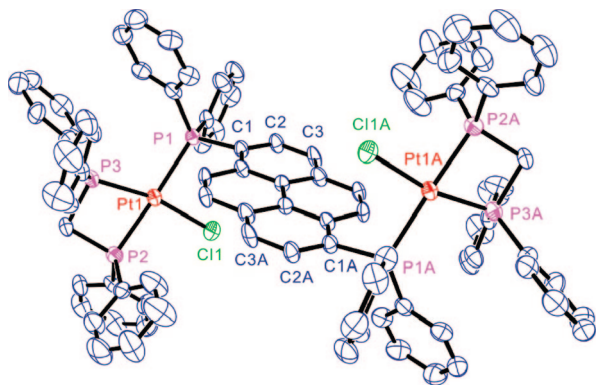


Figure 6. Molecular diagram of $\text{Pt}_2\text{Cl}_2 \cdot 2\text{CH}_3\text{CN}$ (50% thermal ellipsoids). H atoms, anions, and solvent molecules are omitted for clarity.

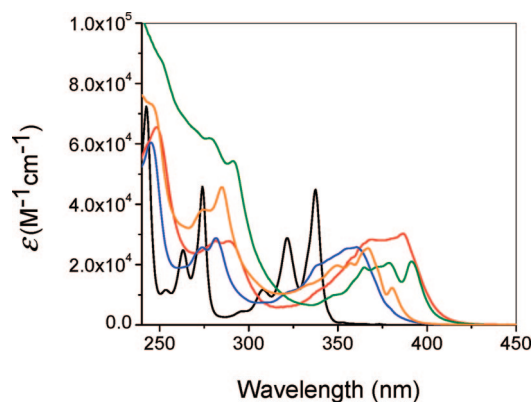


Figure 7. UV-vis absorption spectra of 1,6-PyP (red), 1-PyP (blue), Pt_2Cl_2 (green), PtCl (orange), and pyrene (black) in CH_2Cl_2 .

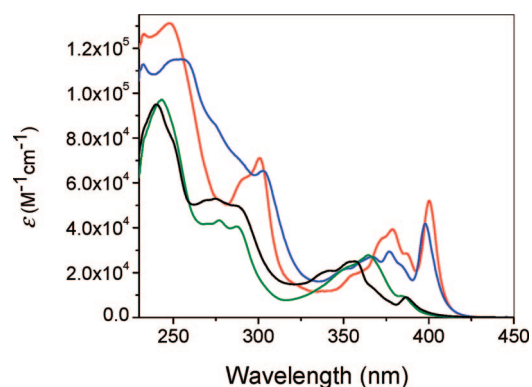


Figure 8. UV-vis absorption spectra of Pt_2 (red), Pd_2 (blue), Pt (green), and Pd (black).

1,6-PyP and dppm. The two metal centers adapt an *anti*-orientation. The Pt(II) ion has a distorted square-planar geometry. The bond lengths and angles are very similar to those of $\text{PtCl} \cdot \text{CH}_2\text{Cl}_2$. The Pt(1)–P(3) bond (2.242(2) Å) is shorter than the other two Pt–P bonds (Pt(1)–P(1) 2.366(2) Å, Pt(1)–P(2) 2.300(2) Å). The torsional angle between the Pt ion and the pyrene plane is 122.12°.

The ^{31}P and ^1H NMR spectra of the complexes are in accord with their X-ray crystal structures. A detailed discussion of the NMR spectroscopy of the complexes is given in the Supporting Information.

Electronic Spectroscopy. The UV-vis absorption spectra of the complexes and the ligands are shown in Figures 7 and 8, and the spectral data summarized in Table 2.

The absorption spectrum of pyrene displays four vibronic bands, $^1\text{L}_b$, $^1\text{L}_a$, $^1\text{B}_b$, and $^1\text{B}_a$, peaked at 352, 337, 274, and 243 nm. The $^1\text{L}_a$, $^1\text{B}_b$, and $^1\text{B}_a$ bands are very intense ($\epsilon_{\text{max}} = 4\text{--}8 \times 10^4 \text{ M}^{-1} \text{ cm}^{-1}$),^{5a} but the $^1\text{L}_b$ band is very weak ($\epsilon_{\text{max}} = 500 \text{ M}^{-1} \text{ cm}^{-1}$) because the corresponding transition is pseudoparity forbidden.^{1,20} The absorption spectra of the complexes and the ligands show three or four intense bands. Although the bands are broader and their vibronic features not resolved, their positions and intensity suggest that they are mainly pyrene-centered. Accordingly, they are labeled as I, II, III, and IV in correspondence to the $^1\text{B}_a$, $^1\text{B}_b$, $^1\text{L}_a$, and $^1\text{L}_b$ bands of pyrene, respectively.

The absorption bands become broadened in the spectra of 1-PyP and 1,6-PyP (Figure 7). Notably, bands III of 1-PyP and 1,6-PyP show red-shifts of 1900 and 3800 cm^{-1} , respectively. In addition, band IV of 1,6-PyP appears as a peak at 390 nm.

The absorption bands of PtCl and Pt_2Cl_2 (Figure 7) have similar energies and shapes to those of the corresponding ligands; especially the energies of bands III of the complexes and the ligands are very close. Notably, bands IV of the two complexes are very intense (PtCl : $\lambda_{\text{max}} = 380 \text{ nm}$, $\epsilon_{\text{max}} = 1.23 \times 10^4 \text{ M}^{-1} \text{ cm}^{-1}$; Pt_2Cl_2 : $\lambda_{\text{max}} = 391 \text{ nm}$, $\epsilon_{\text{max}} = 2.10 \times 10^4 \text{ M}^{-1} \text{ cm}^{-1}$).

Pt and Pd have very similar absorption spectra (Figure 8); the bands of Pt are only slightly red-shifted by 300–600 cm^{-1} from those of Pd . In addition, the energies of the absorptions are close to those of 1-PyP and PtCl . Bands IV of the complexes (Pt : $\lambda_{\text{max}} = 384 \text{ nm}$, $\epsilon_{\text{max}} = 9.6 \times 10^3 \text{ M}^{-1} \text{ cm}^{-1}$, Pd : $\lambda_{\text{max}} = 387 \text{ nm}$, $\epsilon_{\text{max}} = 9.0 \times 10^3 \text{ M}^{-1} \text{ cm}^{-1}$) appear as shoulders in the tails of bands III and are close to that of PtCl ($\lambda_{\text{max}} = 380 \text{ nm}$, $\epsilon_{\text{max}} = 1.23 \times 10^4 \text{ M}^{-1} \text{ cm}^{-1}$) in energy.

Analogous to Pd and Pt complexes, there is a high resemblance between the absorption spectra of Pt_2 and Pd_2 (Figure 8). Both spectra show four intense bands, I (230–270 nm), II (280–320 nm), III (340–390 nm), and IV (390–400 nm), of similar energy and intensity. Interestingly, band IV is more intense than band III. Furthermore, the intensities of bands IV of the binuclear complexes are higher than those of the mononuclear complexes and 1,6-PyP. Notably, the absorption energies of Pt_2 , Pd_2 , and 1,6-PyP are rather close.

The absorption bands of all the complexes are not sensitive to the polarity of the solvent, as no significant difference is observed when the solvent is changed from CH_2Cl_2 to CH_3CN . This is consistent with the fact that the transitions are mainly ligand centered. The metal-to-ligand charge-transfer transitions ($\epsilon \approx 10^3 \text{ M}^{-1} \text{ cm}^{-1}$) cannot be located, probably being covered by the intense ligand-centered transition.

Perturbations of Substituents. A substituent can perturb the frontier orbitals of pyrene by its inductive effect, its π -accepting/donating ability, or hyperconjugation. The four absorption bands of pyrene arise from electronic transitions from the HOMO–1 (b_{2g}) and the HOMO (b_{3g}) to the LUMO (a_u) and the LUMO+1 (b_{1u}). The HOMO \rightarrow LUMO ($^1\text{A}_g \rightarrow ^1\text{B}_{3u}$) transition gives rise to the $^1\text{L}_a$ band, while the HOMO–1 \rightarrow LUMO ($^1\text{A}_g \rightarrow ^1\text{B}_{2u}$) and HOMO \rightarrow LUMO+1 transitions lead to two degenerate $^1\text{B}_{2u}$ states, which mix strongly, resulting in a high-energy $^1\text{B}_b$ state and a $^1\text{L}_b$ state that is lower in energy than the $^1\text{L}_a$ state. However, the $^1\text{L}_b$ band is very weak due to the forbidden nature of the corresponding transition. Our recent study demonstrated that substituting pyrene with Au(I) or Pt(II) ions at C1, C6, or C8 led to red-shifts of the absorptions and an increase in the intensity of the $^1\text{L}_b$ band up to $2.2\text{--}33 \times 10^3 \text{ M}^{-1} \text{ cm}^{-1}$.⁹ The

(20) (a) Clar, E. *Spectrochim. Acta* **1950**, *4*, 116. (b) Yoshinaga, T.; Hiratsuka, H.; Tanzaki, Y. *Bull. Chem. Soc. Jpn.* **1977**, *50*, 3096.

Table 1. Crystallographic Data of the Complexes

	Pt•CH ₂ Cl ₂	Pd	Pt ₂	Pd ₂ •3CH ₂ Cl ₂	PtCl•CH ₂ Cl ₂	Pt ₂ Cl ₂ •2CH ₃ CN
formula	C ₅₅ H ₄₂ F ₃ O ₃ P ₃ PdS	C ₅₅ H ₄₂ F ₃ O ₃ P ₃ PdS	C ₉₂ H ₇₀ F ₆ O ₆ P ₆ Pt ₂ S ₂	C ₉₇ H ₈₀ Cl ₁₆ F ₆ O ₆ P ₆ Pd ₂ S ₂	C ₅₅ H ₄₂ F ₃ O ₃ P ₃ PtS	C ₉₆ H ₇₈ Cl ₃ F ₆ N ₂ O ₆ P ₆ Pt ₂ S ₂
cryst size (mm ³)	0.44 × 0.40 × 0.20	0.32 × 0.20 × 0.14	0.20 × 0.20 × 0.10	0.60 × 0.24 × 0.10	0.46 × 0.14 × 0.10	0.14 × 0.10 × 0.10
cryst system	monoclinic	triclinic	triclinic	triclinic	triclinic	triclinic
space group	P2 ₁ /n	P1	P1	P1	P1	P1
lattice param	a = 13.5802(6) Å, b = 17.440(4) Å, c = 21.2316(9) Å	a = 9.3873(4) Å, b = 14.5499(6) Å, c = 17.6888(7) Å	a = 15.5793(7) Å, b = 16.7840(7) Å, c = 19.0982(8) Å	a = 9.5118(10) Å, b = 15.8255(16) Å, c = 16.5373(17) Å	a = 11.0345(5) Å, b = 13.3791(6) Å, c = 17.3341(8) Å	a = 10.9217(5) Å, b = 13.3248(7) Å, c = 16.9365(9) Å
α	90°	85.375(1)°, β = 82.711(1)°, γ = 80.332(1)°	110.538(1)°, β = 110.094(1)°, γ = 98.770(1)°	74.366(2)°, β = 2321.7(4)	94.656(1)°, β = 100.037(1)°, γ = 97.473(1)°	α = 69.566(1)°, β = 86.911(2)°, γ = 81.616(1)°
V (Å ³)	4818.0(4)	2358.10(17)	4135.1(3)	2321.7(4)	2484.3(2)	2285.0(2)
Z	4	2	2	1	2	1
density(calc) (g/cm ³)	1.653	1.464	1.627	1.524	1.651	1.585
absorp coeff (mm ⁻¹)	3.224	0.596	3.614	3.774	3.181	3.334
F(000)	2384	1060	2004	1080	1228	1082
total no. of reflns	34 091	31 433	54 307	30 829	17 711	16 330
index ranges	-17 ≤ h ≤ 16, -15 ≤ k ≤ 22, -27 ≤ l ≤ 24	-12 ≤ h ≤ 2, -18 ≤ k ≤ 8, -22 ≤ l ≤ 22	-20 ≤ h ≤ 20, -21 ≤ k ≤ 24, -24 ≤ l ≤ 24	-12 ≤ h ≤ 12, -20 ≤ k ≤ 20, -21 ≤ l ≤ 21	-14 ≤ h ≤ 12, -17 ≤ k ≤ 15, -22 ≤ l ≤ 22	-14 ≤ h ≤ 13, -17 ≤ k ≤ -17, -21' l ≤ 17
2θ range for data collection (deg)	3.90 to 55.00	2.84 to 55.00	2.54 to 55.00	2.64 to 55.00	3.08 to 55.00	3.30 to 54.94
indep reflns	11 067 (R _{int} = 0.0281)	10 813 (R _{int} = 0.0500)	18 948 (R _{int} = 0.0606)	10 660 (R _{int} = 0.0630)	11 338 (R _{int} = 0.0219)	10 410 (R _{int} = 0.0504)
no. of params varied	634	595	1027	577	694	545
final R indices	R1 = 0.0302, wR2 = 0.0772	R1 = 0.0716, wR2 = 0.1704	R1 = 0.0418, wR2 = 0.0767	R1 = 0.0592, wR2 = 0.1318	R1 = 0.0410, wR2 = 0.1040	R1 = 0.0653, wR2 = 0.1431
goodness of fit (GOF)	1.057	1.113	0.982	1.042	1.038	1.026
largest diff peak and hole (e Å ⁻³)	1.363 and -0.887	1.160 and -0.810	1.356 and -0.623	0.927 and -0.685	1.777 and -0.934	2.157 and -1.175

latter is due to the uplifting of the degeneracy of the ¹B_{2u} states and mixing of the ¹L_a and ¹L_b states due to lowering of symmetry. The red-shift of the ¹L_a band is particularly pronounced and can be used to gauge the extent of the perturbations, as it is closely related to a change in the energy gap between the HOMO and the LUMO.

The red-shifts of band III, which corresponds to the ¹L_a band of the unperturbed system, displayed by 1-PyP (1900 cm⁻¹) and 1,6-PyP (3800 cm⁻¹) indicate strong perturbation of the PPh₂ group. The perturbation is additive with respect to the number of PPh₂ groups, as shown by the fact that the absorption of 1,6-PyP is shifted two times more than that of 1-PyP. The perturbations can arise from the donation of the lone pair and/or the inductive effect of the P atom. However, the absorption spectra of PtCl and Pt₂Cl₂ do not show significant shifts from their corresponding ligands. As the lone-pairs of the PPh₂ groups are donated to the metal ions in the complexes, the result suggests that the lone-pair donation does not play a significant role in perturbing the pyrenyl rings in the ligands. The perturbation of the PPh₂ group possibly comes from pyrene(ππ)-to-P(dπ) back-bonding and/or σ*(P-C)-π*(pyrenyl) interactions. It is known that σ*(Si-C)-π*(pyrenyl) interactions are responsible for the red-shift of the absorptions of trimethylsilyl-substituted pyrenes.²¹

The high resemblance between the spectra of Pt and Pd, and Pt₂ and Pd₂, is rather unexpected, as one would expect that given the different electronic properties of the two metals, the extent of their perturbations should be different. The energies of the other four bands of Pt₂ and Pd₂ are surprisingly close to those of PtCl and PdCl, respectively, suggesting that for the cyclometalated complexes the perturbation of the metal ions at C5/C10 is weaker than that of the coordinated PPh₂ groups at C1/6. It was shown that the extent of perturbations of a substituent is proportional to the square of the LCAO coefficient (c_{vi}²) of the carbon atom at the point of attachment.^{5a} A semiempirical calculation on pyrene shows that the c_{vi}² at C1 and C6 (0.12) are larger than that at C5 and C10 (0.08 in the HOMO), while similar carbon atoms have similar c_{vi}² values in the LUMO. This could be one of the reasons for the perturbation of the coordinated PPh₂ groups at C1/6 being stronger than that of the metal ions at C5/10. That the bands III (¹L_a) of Pt₂ and Pd₂ are very close in energy to those of Pd₂ and Pd suggests that the pyrenyl ring is not strongly perturbed by the metal-ligand π interactions. Nonetheless, the drastic increase in the intensity of band IV in the cyclometalated complexes indicates a lowering of the symmetry of the pyrene ring due to the metal-pyrene interactions.

Luminescence. Room-temperature emission spectra of de-aerated MeCN solutions of the complexes are shown in Figures 9 (PtCl and Pt₂Cl₂), 10 (Pd and Pd₂), and 11 (Pt and Pt₂), and the emission data are shown in Table 3.

The dangling complexes show fluorescence around 410 nm. Pt₂Cl₂ (Φ_f ≈ 10⁻³) is more emissive than PtCl (Φ_f ≈ 10⁻⁵). Comparing the emission with that of pyrene suggests it arises from the electronic transition from the lowest singlet excited state S₁ (¹L_b) to the ground state S₀. Pt₂Cl₂ shows a very weak emission around 650 nm (Φ_p < 10⁻⁵), which could be phosphorescence from the lowest triplet excited state T₁ (³L_b) to S₀.

Pd and Pd₂ display S₁ → S₀ fluorescence at 400 and 429 nm, respectively. The emissions are weak, with quantum yields (Φ_f) of 6.6 × 10⁻⁵ and 6.3 × 10⁻⁵ for Pd and Pd₂, respectively.

(21) Maeda, H.; Inoue, Y.; Ishida, H.; Mizuno, K. *Chem. Lett.* **2001**, 22, 1224.

Table 2. Electronic Absorption Spectral Data of the Complexes, 1,6-PyP, 1-PyP, and Pyrene

compound	λ_{\max}/nm (ϵ , $\times 10^4 \text{ M}^{-1} \text{ cm}^{-1}$)			
	bands			
	I	II	III	IV
Pt	243 (9.72)	277 (4.33), 288 (4.05)	352 ^{sh} (2.24), 365 (2.78)	384 (0.96)
Pd	240 (9.50)	275 (5.29), 287 ^{sh} (4.98)	342 (2.09), 357 (2.50), 365 ^{sh} (1.45)	387 (0.90)
Pt₂	247 (13.11)	301 (7.11)	356 ^{sh} (1.93), 373 (3.54), 379 (3.93), 386 (2.86)	400 (5.21)
Pd₂	252 (11.51)	303 (6.54)	352 (2.18), 367 (2.70), 377 (2.94), 383 (2.38)	398 (4.18)
PtCl	238 (7.70)	274 (3.82) 285 (4.57)	350 (1.97), 357 (2.05) 367 (2.54)	380 (1.23)
Pt₂Cl₂	250 ^{sh} (8.86)	278 (6.19), 291 (5.43)	365 (1.91), 379 (2.06)	391 (2.10)
1-PyP	245 (6.05)	274 (2.57), 282 (2.88)	337 ^{sh} (1.92), 360 (2.58)	^a
1,6-PyP	249 (6.55)	282 (2.79), 289 (2.78)	370 (2.83)	~390
pyrene	243 (7.24) (¹ B _a)	254 (1.16), 264 (2.48), 274 (4.58) (¹ B _b)	297 (0.45), 308 (1.17), 322 (2.88), 337 (4.48) (¹ L _a)	352 (0.08), 357 (0.05), 364 (0.04), 373 (0.03) (¹ L _b)

^a Band IV is covered by band III.

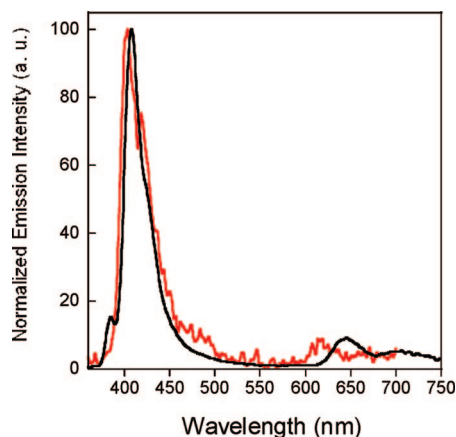


Figure 9. Emission spectra of **PtCl** (red) and **Pt₂Cl₂** (black) in deaerated CH₃CN solution at room temperature. Excitation wavelength = 320 nm. Filter: 350 nm cutoff.

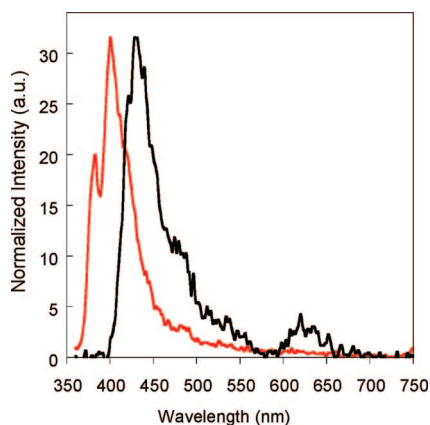


Figure 10. Emission spectra of **Pd** (red) and **Pd₂** (black) in deaerated CH₃CN solution at room temperature. Excitation wavelength = 320 nm. Filter: 350 nm cutoff.

A weak red emission at ~620 nm (quantum yield $\Phi_p < 10^{-5}$) is also observed for the deaerated solutions of **Pd₂**. Due to the low intensity of the emission, its lifetime, which lies in the microsecond domain, cannot be determined accurately. But the large Stokes shift and energy of the emission suggest it is the $T_1 \rightarrow S_0$ phosphorescence.

Replacing the Pd ion with its heavy congener greatly enhances phosphorescence. Both **Pt** and **Pt₂** show dual emissions in degassed solutions with a weak fluorescence at 370–450 nm

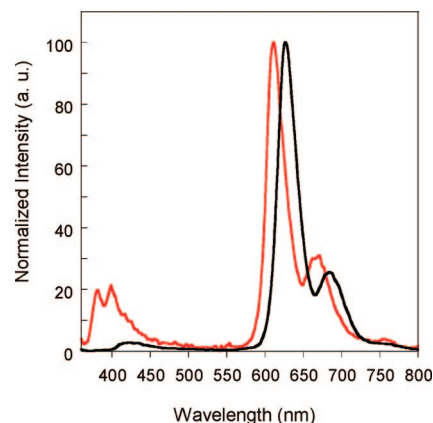


Figure 11. Emission spectra of deaerated MeCN solutions of **Pt** (red) and **Pt₂** (black) at room temperature. Excitation wavelength = 320 nm. Filter: 350 nm cutoff.

and strong red phosphorescence peaking at 611 nm (**Pt**) and 627 nm for (**Pt₂**), which corresponds to a $T_1 \rightarrow S_0$ transition. The phosphorescence has a vibronic shoulder, which is separated from the peak by $\sim 1350 \text{ cm}^{-1}$, as expected for pyrenyl-centered emission. Similar vibronic emissions are commonly observed for π -conjugated compounds and ligands. The spin-forbidden nature of the red emission is supported by its relatively long lifetime of 31.3 μs for **Pt** and 63.7 μs for **Pt₂** and the large Stokes shift from the corresponding bands IV ($\sim 9500 \text{ cm}^{-1}$). The large energy separation between the fluorescence and the phosphorescence ($\sim 9000 \text{ cm}^{-1}$) is consistent with the strong exchange interactions in excited state, which is mainly ligand-centered. Oxygen can quench the phosphorescence: in the aerated solutions, the intensity of the phosphorescence decreases; the phosphorescence returns upon deaeration. This observation lends further support to the triplet parentage of the red emission because oxygen is an efficient quencher for triplet emission. The fluorescence of **Pt** ($\Phi_f = 3.2 \times 10^{-4}$) is more intense than that of **Pt₂** ($\Phi_f = 7.9 \times 10^{-5}$), while the former is less phosphorescent than the latter. Φ_p of **Pt** (4.4×10^{-3}) is close to that of diaurated and diplatinated pyrenes that contain two Pt(PET₃)₂Br groups at the C1 and C6/C8 positions ($\Phi_p = 3.9 \times 10^{-3}$),⁹ but Φ_p (1.5×10^{-2}) of **Pt₂** is highest among all the metalated pyrenes. No excimeric emission is observed for all the complexes even at high concentrations ($> 10^{-3} \text{ M}$). Possibly formation of excimer is sterically hindered by the bulky phosphine ligands.

Intersystem crossing between singlet and triplet $\pi\pi^*$ excited states is very inefficient, as there is little change in the angular

Table 3. Emission Data of the Complexes

complex	fluorescence λ_{\max} (nm)	Φ_f	phosphorescence λ_{\max} (nm)	Φ_p	phosphorescence lifetime (μ s)
Pt	398	3.2×10^{-4}	611	4.4×10^{-3}	31.3
Pd	400	6.6×10^{-5}			
Pt₂	420	7.9×10^{-5}	627	1.5×10^{-2}	63.7
Pd₂	429	6.3×10^{-5}	620	$<10^{-5}$	^a
PtCl	404	10^{-5b}			
Pt₂Cl₂	408	10^{-5b}	650	$<10^{-5}$	^a

^a The intensity of the emission is too weak for accurate lifetime determination. ^b The quantum yields cannot be determined accurately, as the complexes tend to dissociate at concentration $\leq 10^{-5}$ M.

momentum. The relatively strong phosphorescence displayed by the Pt complexes is due to the heavy atom effect of the metal ion, which increases the rate of $S_1 \rightarrow T_1$ intersystem crossing. It should be noted that not only the metal ions but also P and Cl in the complexes are conventionally considered as heavy atoms. However, our results show that the effect of the metal ions is dominating. With its large spin-orbit coupling, the Pt ion can enhance phosphorescence by mixing the spin parentage of the singlet and triplet excited states. The Hamiltonian operator of the spin-orbit perturbation H_{SO} is given as equation 1, where Z and r are the atomic number of the heavy atom and the distance between the nucleus of the atom and the chromophore, and \mathbf{l}_i and \mathbf{s}_i are angular momentum and spin operators, respectively.²²

$$H_{SO} = \sum_i \frac{Ze^2}{4m^2c^2r^3} \mathbf{l}_i \mathbf{s}_i \quad (1)$$

It is clear from eq 1 that the spin-orbit coupling increases with the atomic number of the perturbing atom. This explains the fact that the phosphorescence of the Pt complexes is much stronger than that of the Pd complexes (Z of Pt and Pd are 78 and 46, respectively). Furthermore, the effect is additive, as it increases with the number of heavy atoms. This accounts for the fact that the phosphorescence of **Pt₂** is stronger than that of **Pt**, and **Pd₂** displays weak phosphorescence despite the weak spin-orbit coupling of the metal. Equation 1 also shows that the heavy atom effect decreases rapidly with the distance r ; however, only very weak phosphorescence is observed for **Pt₂Cl₂** despite the fact that the dangling Pt ions are not very far from the pyrenyl ring, as the shortest distance between the metal ions and the carbon atoms of the ring is only ~ 3.391 Å. This suggests that the metal-ligand orbital (σ and π) interactions are crucial to the manifestation of the heavy atom effect.

Although the lifetime of the phosphorescence of the Pt complexes is much longer than that of fluorescence, it is very much shorter than that of pyrene (~ 0.44 s).²³ This is again due to the spin-orbit coupling of the Pt ions, which introduces singlet character into the triplet excited state T_1 , making the $T_1 \rightarrow S_0$ transition less spin-forbidden.

Conclusion

By comparing the electronic spectra of the cyclometalated and dangling complexes, we deduce that the pyrenyl rings in these complexes are mainly perturbed by the PPh₂ group at C1/6. A surprising result is the similarity between the spectra of **Pt** and **Pd** or **Pt₂** and **Pd**. This suggests weak π interactions between the metal ions and the pyrenyl ring. On the other hand, the forbidden 1L_b band is intensified, mostly likely due to increased mixing between 1L_a and 1L_b states. The phosphorescence of pyrene can be switched on by the heavy atom effect. The quantum yield can be as high as 1.5×10^{-2} , as in the case of **Pt₂**. Finally, our study demonstrated that direct bonding of the metal ions to the pyrenyl ring is needed for efficient enhancement of the phosphorescence.

Acknowledgment. J.H.K.Y. would like to thank National University of Singapore for financial support and Miss Tan Geok Kheng and Professor Kop Lip Lin for solving the X-ray crystal structures.

Supporting Information Available: CIF files of the crystal structures and selected bond lengths and angles, and NMR spectra of the complexes. This material is available free of charge via the Internet at <http://pubs.acs.org>.

OM800410M

(23) (a) Kellogg, R. E.; Wyeth, N. C. *J. Chem. Phys.* **1966**, *45*, 3156. (b) Kropp, J. L.; Dawson, W. R.; Windsor, M. W. *J. Phys. Chem.* **1969**, *73*, 1747.

(22) Lower, S. K.; El-Sayed, M. A. *Chem. Rev.* **1966**, *66*, 199.

Synthesis, Characterization, and Polymerization of a Neutral Tantalacarborane Sandwich Complex Derived from a Pentaanionic Exo-Polyhedrally Linked Bis(C₂B₁₀-carborane) Ligand

Zhu Yinghui,^{*,†} Lee Cjin Nong,[†] Li Chuan Zhao,[†] Effendi Widjaja,[†] Chong Siow Hwei,[†] Wang Cun,[†] Joel Tan,[†] Martin Van Meurs,[†] Narayan S. Hosmane,[‡] and John A. Maguire[§]

Institute of Chemical and Engineering Sciences, 1, Pesek Road, Jurong Island, Singapore 627833, Department of Chemistry and Biochemistry, Northern Illinois University, DeKalb, Illinois 60115-2862, and Department of Chemistry, Southern Methodist University, Dallas, Texas 75275-0314

Received June 5, 2008

Tetramethyldisilazane-bridged *closo*-carborane compounds, [(*closo*-1-R-1,2-C₂B₁₀H₁₀)Me₂Si]₂NH (R = Me (**1**), Ph (**2**)), and their tantalum complexes, [(*closo*-2-R-2,3-C₂B₁₀H₁₀)Me₂Si]₂N]Ta(V) (R = Me (**3**), Ph (**4**)), have been prepared and characterized. Compounds **3** and **4** were found to be active catalysts for the polymerization of ethylene in the presence of the cocatalyst MAO to produce two morphologically different polyethylenes with high molecular weight.

1. Introduction

It is well-known that metallocene complexes, such as sandwich and half-sandwich group 4 compounds, play important roles in ethylene polymerization, due to their ability to produce stereospecific polymers.^{1–7} The design and synthesis of structurally unique metallocenes are still attracting a great deal of attention.^{6,7} Such complexes can be used as “single site” catalysts for homo- or copolymerization of polar olefins, such as styrene, methyl methacrylate (MMA), vinyl chloride, etc., to produce functionalized polymers.^{6,7} It is well recognized that the *nido*-carborane dianions [R₂C₂B₉H₉]²⁻, [R₂C₂B₄H₄]²⁻, and [R₂C₂B₁₀H₁₀]²⁻ (R = H, alkyl, or aryl groups) (Figure 1)^{8–10} are isolable with the cyclopentadienides, in that they have six π electrons delocalized on the C₂B₃ or C₂B₄ open faces of the dianions that can coordinate metals in an η^5 or η^6 fashion. Because of this similarity and the high catalyst activity of activated metallocenes, the design and synthesis of stable carborane ligands for use in transition-metal complexes, with the possibility of high catalytic activity, has been an ongoing area of research.^{11–14} It was found that carboranyl trianionic

ligands coordinated to group 4 compounds (Figure 2a) are active precatalysts for olefin polymerization.^{13,14} Herein we report the syntheses of tetramethyldisilazane-bridged *closo*-carboranes, a novel pentaanionic precursor, and its conversion to a neutral tantalum(V) metallacarborane (Figure 2b). The tantalacarboranes were found to be active precatalysts for olefin polymerization.

2. Experimental Section

2.1. General Methods. All operations were carried out under an argon atmosphere using standard Schlenk techniques or in a glovebox. The solvents diethyl ether, *n*-hexane, and tetrahydrofuran (THF) were dried with sodium. All other reagents were purchased from Sigma-Aldrich Pte. Ltd. or Katchem Spolo. s.r.o. and used as received. 1,3-Dichloro-1,1,3,3-tetramethyldisilazane¹⁵ and Cl₄-TaN(SiMe₃)₂¹⁶ were prepared according to literature methods. Elemental analyses were measured in a Euro EA elemental analyzer and melting points determined by a Büchi melting point analyzer. ¹H, ¹³C, and ¹¹B NMR were recorded on a Bruker Advance 400 MHz spectrometer. Chemical shifts were measured in ppm relative to a TMS standard (¹H, 400.2 MHz; ¹³C, 100.6 MHz; ¹¹B, 128.4 MHz). Near-infrared (IR) spectra were measured using a Bio-Rad spectrophotometer with KBr pellets. Far-infrared spectra were measured using a Bruker FT-IR Vertex 70 spectrophotometer with THF film. Molecular weights and molecular weight distributions of the polymers were determined by means of gel-permeation chromatography (GPC; Polymer Laboratories, PC-GPC-220) at 160 °C, using 1,2,4-trichlorobenzene stabilized with 0.0125% BHT as eluent with a column set of 2 \times PLgel 10 μ m MIXED-B (300 \times 7.5 mm). The weight average molecular weight and polydispersity index (*M_w* and *M_w*/*M_n*, respectively) were calculated on the basis of polystyrene standards: flow rate 1.0 mL/min, injected volume 200 μ L. The Scanning electron microscopy (SEM) images were obtained

* To whom correspondence should be addressed. Tel: +65 6796 3801 (3700). Fax: +65 6316 6182. E-mail: zhu_yinghui@ices.a-star.edu.sg.

[†] Institute of Chemical and Engineering Sciences.

[‡] Northern Illinois University.

[§] Southern Methodist University.

(1) Alt, H. G.; Koppl, A. *Chem. Rev.* **2000**, *100*, 1205–1221, and references therein.

(2) Hopf, A.; Kaminsky, W. *Catal. Commun.* **2002**, *3*, 459–464.

(3) Corradini, P.; Guerra, G.; Cavallo, L. *Acc. Chem. Res.* **2004**, *37*, 231–241.

(4) Miller, S. A.; Bercaw, J. E. *Organometallics* **2006**, *25*, 3576–3592.

(5) Silanes, I.; Mercero, J. M.; Ugalde, J. M. *Organometallics* **2006**, *25*, 4483–4490.

(6) Luo, Y.; Baldamus, J.; Hou, Z. *J. Am. Chem. Soc.* **2004**, *126*, 13910–13911.

(7) Jensen, T. R.; Yoon, S. C.; Dash, A. K.; Luo, L.; Marks, T. J. *J. Am. Chem. Soc.* **2003**, *125*, 14482–14494.

(8) Hosmane, N. S.; Maguire, J. A.; Zhu, Y. *Main Group Met. Chem.* **2006**, *5*, 251–265, and references therein.

(9) Xie, Z. *Acc. Chem. Res.* **2003**, *36*, 1–9, and references therein.

(10) Chui, K.; Yang, Q.; Mak, T. C. W.; Xie, Z. *Organometallics* **2000**, *19*, 1391–1401.

(11) Zhu, Y.; Vyakaranam, K.; Maguire, J. A.; Quintana, W.; Teixidor, F.; Vinas, C.; Hosmane, N. S. *Inorg. Chem. Commun.* **2001**, *4*, 486–489.

(12) Zhu, Y.; Maguire, J. A.; Hosmane, N. S. *Inorg. Chem. Commun.* **2002**, *5*, 296–299.

(13) Zhu, Y.; Zhong, Y.; Keith, C.; Maguire, J. A.; Hosmane, N. S. *J. Organomet. Chem.* **2005**, *690*, 2802–2808.

(14) Zhu, Y.; Shirley, L. P. S.; Fethi, C.; Keith, C.; Richard, A. K. *J. Organomet. Chem.* **2005**, *690*, 6284–6291.

(15) Bacque, E.; Pillot, J.-P.; Birot, M.; Dunogues, J. *J. Organomet. Chem.* **1994**, *481*, 167–172.

(16) Bernd, W.; Juergen, W.; Milius, Wolfgang, M. *Z. Anorg. Allg. Chem.* **1998**, *624*, 98–102.

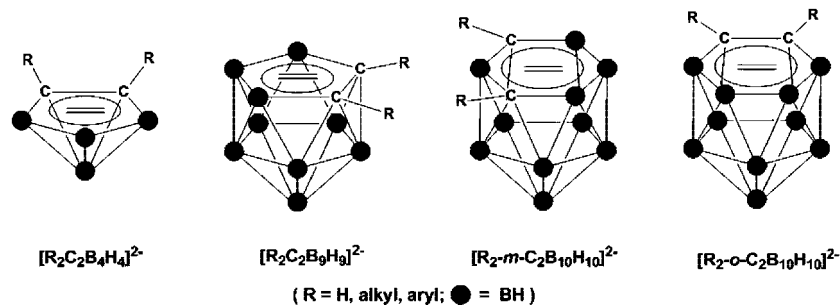
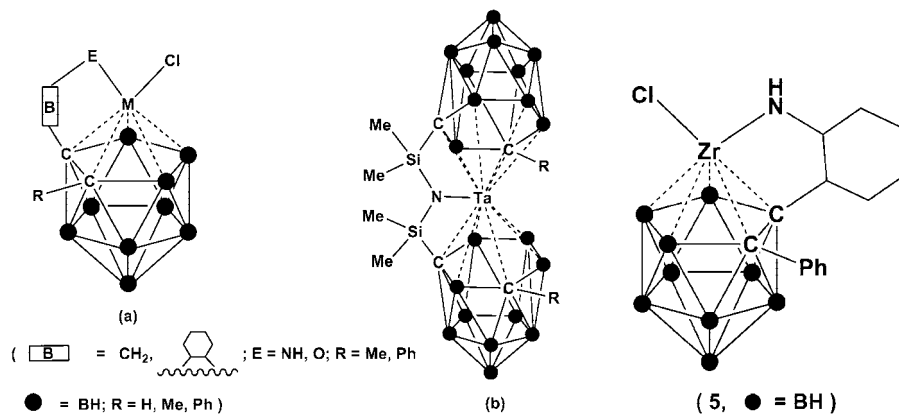
Figure 1. *nido*-Carborane-derived ligands.

Figure 2. Carboranyl trianion (a), pentaanionic coordinated Ta(V) complex (b), and 5.

on a JSM-6700F field-emission microscope. The Raman scattering spectra were measured at room temperature using a JY Horiba LabRAM Raman microscope. The high-resolution MS was measured on a Thermo Finnigan MAT XP95 analyzer using the EI-HR model (70 eV, source temperature 150 °C).

2.2. Synthesis of [(*closo*-1-Me-1,2- $C_2B_{10}H_{10}$) Me_2Si_2]NH (1). A 1.59 g (10.05 mmol) sample of *closo*-1-Me-1,2- $C_2B_{10}H_{11}$ was dissolved in 30 mL of THF to produce a clear solution, which was cooled to -78 °C. A 6.35 mL (10.16 mmol) amount of *n*-BuLi solution (1.6 M in hexane) was slowly added to the THF solution at -78 °C with syringe. After addition, the mixture was stirred at -78 °C for 30 min before being warmed to room temperature spontaneously and the reaction continued for 4 h. The solution was then cooled to -10 °C and added dropwise to a solution of $HN(SiMe_2Cl)_2$ (1.01 g, 4.99 mmol) in 10 mL of THF. After addition, the solution was warmed to room temperature spontaneously for 2 h followed by heating to 80 °C for 10 h. The mixture was then cooled to room temperature and concentrated to about 5 mL under reduced pressure. The resulting light brown residue was purified by thin-layer chromatography (TLC; SiO_2) and developed with a mixed solvent of pentane and ethyl ether (10/1 v/v). The main product was collected and dried under high vacuum to give a colorless solid of **1**: yield 1.14 g (2.56 mmol), 51.2% (mp 87–89 °C). Anal. Calcd for $C_{10}H_{39}B_{20}NSi_2$ (**1**): C, 26.94; H, 8.82; N, 3.14. Found: C, 26.90; H, 8.80; N, 3.10. 1H NMR (THF- d_8 , ppm): δ 0.04 (s, 12H, 4 \times Si- CH_3); 1.13–3.20 (m, 20H, 2 \times $C_2B_{10}H_{10}$); 2.02 (s, 6H, 2 \times C_{cage} - CH_3). ^{13}C NMR (THF- d_8 , ppm): δ 1.65 (Si- CH_3); 26.65 (C_{cage} - CH_3); 62.92 and 70.32 (C_{cage}). ^{11}B NMR (THF- d_8 , ppm): δ = -2.39 (1B, $^1J_{BH}$ = 148 Hz); -6.96 (1B, $^1J_{BH}$ = 154 Hz); -9.47 (2B, $^1J_{BH}$ = 155 Hz); -10.51 (2B, $^1J_{BH}$ = 74 Hz); -11.29 (2B, $^1J_{BH}$ = 122 Hz); -12.77 (2B, $^1J_{BH}$ = 174 Hz). ^{29}Si NMR (THF- d_8 , ppm): δ -107.93 (s). IR (KBr pellet, cm^{-1} , vs = very strong, s = strong, m = middle, w = weak, br = broad): ν 3272 (br, vs), 2963 (s, s), 2521 (ν_{BH} , s, m), 2296 (s, w), 2229 (s, w), 1642 (s, vs), 1509 (s, s), 1449 (s, s), 1413 (s, vs), 1315 (s, m), 1255 (s, w), 1180 (s, w), 1128 (s, w), 1068 (s, w), 938 (s, vs), 865 (s, w), 784 (s, m), 604 (br, s), 550 (s, m), 454 (s, m).

2.3. Synthesis of [(*closo*-1-Ph-1,2- $C_2B_{10}H_{10}$) Me_2Si_2]NH (2). A procedure similar to that used in the preparation of **1** was used to prepare [(*closo*-1-Ph-1,2- $C_2B_{10}H_{10}$) Me_2Si_2]NH (**2**). After purification, complex **2** (mp 103–105 °C) was obtained in 42.1% yield from the reaction of 2.21 g (10.03 mmol) of *closo*-1-Ph-1,2- $C_2B_{10}H_{11}$, 6.35 mL of *n*-BuLi (1.6 M in hexane), and $HN(SiMe_2Cl)_2$ (1.00 g, 4.94 mmol) in 10 mL of THF. Anal. Calcd for $C_{20}H_{43}B_{20}NSi_2$ (**2**): C, 42.17; H, 7.60; N, 2.46. Found: C, 42.09; H, 7.64; N, 2.41. 1H NMR (THF- d_8 , ppm): δ 0.13 (s, 12H, 4 \times Si- CH_3); 1.20–3.61 (m, 20H, 2 \times $C_2B_{10}H_{10}$); 6.83–7.74 (m, 10H, 2 \times C_{cage} - C_6H_5). ^{13}C NMR (THF- d_8 , ppm): δ 1.05 (Si- CH_3); 60.30 and 66.90 (C_{cage}); 126.84, 128.15, 130.53, and 133.42 (C_{cage} - C_6H_5). ^{11}B NMR (THF- d_8 , ppm): δ -2.86 (1B, $^1J_{BH}$ = 144 Hz); -4.67 (1B, $^1J_{BH}$ = 151 Hz); -8.99 (3B, $^1J_{BH}$ = 160 Hz); -10.81 (3B, $^1J_{BH}$ = 147 Hz); -12.75 (2B, $^1J_{BH}$ = 152 Hz). ^{29}Si NMR (THF- d_8 , ppm): δ -113.75 (s). IR (KBr pellet, cm^{-1}): ν 3374 (br, vs), 3068 (s, s), 2962 (s, s), 2582 (ν_{BH} , s, m), 1957 (s, w), 1637 (s, s), 1497 (s, m), 1448 (s, m), 1403 (s, m), 1261 (s, s), 1218 (s, m), 1196 (s, m), 1162 (s, w), 1081 (s, s), 1021 (s, m), 957 (s, s), 857 (s, s), 803 (s, s), 755 (s, m), 730 (s, m), 691 (s, s), 562 (s, m), 455 (s, m).

2.4. Synthesis of [(*closo*-2-Me-2,3- $C_2B_{10}H_{10}$) Me_2Si_2]N]Ta^V (3). In a glovebox, **1** (1.11 g, 2.49 mmol), 3.00 g (23.41 mmol) of dry naphthalene and 0.30 g (13.05 mmol) of fresh-cut sodium were suspended in 40 mL of dry THF, followed by addition of 1.60 mL of *n*-BuLi (1.6 M in hexane, 2.56 mmol). The reaction mixture was stirred at room temperature for 2 weeks. Tantalum(V) chloride ($TaCl_5$; 0.90 g, 2.51 mmol) was added, and the reaction was continued for 1 week. After filtering, solvent and naphthalene were removed under reduced pressure and a yellow-brown solid was obtained. The crude product was then purified by recrystallization from CH_2Cl_2 /pentane to give 0.33 g of pale yellow solid [(*closo*-2-Me-2,3- $C_2B_{10}H_{10}$) Me_2Si_2]N]Ta^V (**3**) in 21.2% yield. Mp: 178–179 °C. Anal. Calcd for $C_{10}H_{38}B_{20}NSi_2Ta$ (**3**): C, 19.19; H, 6.12; N, 2.24. Found: C, 19.09; H, 6.20; N, 2.13. MS: m/z 626.76 ($[M + H]^+$). 1H NMR (THF- d_8 , ppm): δ 0.18 (s (br), 12H, 4 \times Si- CH_3); 1.14–3.29 (m, 20H, 2 \times $C_2B_{10}H_{10}$); 1.94 (s, 6H, 2 \times C_{cage} - CH_3).

Table 1. Results of Ethylene Polymerization by 3^a

run	temp (°C)	ethylene pressure (atm)	[Al]/[Ta]	activity ^b	wt % of fibrous PE ^c
1	25	5	100	13	2.54
2	25	10	200	37	7.06
3	25	10	1000	29	9.74
4	50	5	100	18	8.53
5	50	10	100	1500	13.22
6	50	10	200	2470	21.72
7	50	10	1000	2055	26.44

^a Polymerization time = 30 min. ^b Activity in units of kg of PE/(mol of Ta) h atm). ^c wt % = weight percent of fibrous polyethylene in products.

¹³C NMR (THF-*d*₈, ppm): δ 0.15 (Si-CH₃); 24.24 (C_{cage}-CH₃); 66.08 and 69.18 (C_{cage}). ¹¹B NMR (THF-*d*₈, ppm): δ -1.25 (1B, ¹J_{BH} = 136 Hz); -4.92 (1B, ¹J_{BH} = 123 Hz); -9.19 (4B, ¹J_{BH} = 68 Hz); -10.44 (4B, ¹J_{BH} = 110 Hz). ²⁹Si NMR (THF-*d*₈, ppm): δ -110.92 (s). IR (KBr pellet, cm⁻¹): ν 3410 (br, vs), 2594 (ν_{BH}, s, m), 1634 (s, s), 1384 (s, w), 1261 (s, w), 1098 (br, w), 802 (s, m), 623 (br, s), 417 (s, w).

2.5. Synthesis of [(*closo*-2-Ph-2,3-C₂B₁₀H₁₀)Me₂Si₂N]Ta^V (4). A procedure similar to that used in the preparation of **3** was used to prepare [(*closo*-2-Ph-2,3-C₂B₁₀H₁₀)Me₂Si₂N]Ta^V (**4**). After purification, complex **4** (mp 154–156 °C) was obtained in 31.7% yield from the reaction of **2** (1.43 g, 2.50 mmol), 3.00 g (23.41 mmol) of n-BuLi (1.6 M in hexane), and 0.90 g (2.51 mmol) of TaCl₅ in 40 mL of THF. Anal. Calcd for C₂₀H₁₂B₂₀NSi₂Ta (4): C, 32.03; H, 5.65; N, 1.87. Found: C, 32.15; H, 5.64; N, 1.71. MS: *m/z* 749.90 ([M]⁺). ¹H NMR (THF-*d*₈, ppm): δ 0.16 (s, 12H, 4 × Si-CH₃); 1.27–3.70 (m, 20H, 2 × C₂B₁₀H₁₀); 6.72–7.64 (m, 10H, 2 × C_{cage}-C₆H₅). ¹³C NMR (THF-*d*₈, ppm): δ 0.18 (Si-CH₃); 66.89 and 69.94 (C_{cage}); 126.05, 126.88, 128.27, and 129.24 (C_{cage}-C₆H₅). ¹¹B NMR (THF-*d*₈, ppm): δ -2.88 (1B, ¹J_{BH} = 154 Hz); -4.76 (1B, ¹J_{BH} = 153 Hz); -9.09 (2B, ¹J_{BH} = 148 Hz); -10.99 (4B, ¹J_{BH} = 175 Hz); -12.92 (2B, ¹J_{BH} = 249 Hz). ²⁹Si NMR (THF-*d*₈, ppm): δ -108.20 (s). IR (KBr pellet, cm⁻¹): ν 3420 (br, s), 2950 (s, s), 2870 (s, s), 2521 (ν_{BH}, s, m), 1638 (s, s), 1489 (s, m), 1450 (s, m), 1375 (s, m), 1256 (s, s), 1097 (s, s), 1031 (s, m), 958 (s, m), 803 (s, m), 698 (s, m), 609 (s, w).

2.6. Evaluation of Catalytic Activity. The polymerization of ethylene, catalyzed by **3** (1.603 × 10⁻⁷ mol), was carried out for 30 min in 80 mL of toluene in the presence of the cocatalyst methylaluminoxane (MAO) in a Parr reactor. The argon pressure inside the predried reactor was reduced by high vacuum, followed by applied ethylene pressure. The reactor was adjusted to the optimized 50 °C and 10 atm. The ratio [Al]/[Ta] was selected as 200. As seen in Table 1, these conditions afforded the maximum catalytic activity. After 30 min, the reaction was quenched with 20 mL of a 10% HCl solution of MeOH. The toluene-insoluble polymers were collected by filtration and washed with copious amounts of MeOH and hexane, followed by drying under reduced pressure to produce 0.43 g of fibrous PE. The toluene filtrate was then precipitated by the addition of 200 mL of MeOH, collected by filtration, washed with MeOH (4 × 30 mL) and hexane (2 × 30 mL), and dried at 60 °C to a constant weight to give 1.55 g of powdery PE. A procedure similar to that described for **3** (above) was used to evaluate the ethylene polymerization using **4** as a catalyst. The results were essentially the same as found for **3**, except that the weight percent of the fibrous PE was 11.35 instead of the value of 21.72 found for **3**. Polymerization results are summarized in Table 2.

3. Results and Discussion

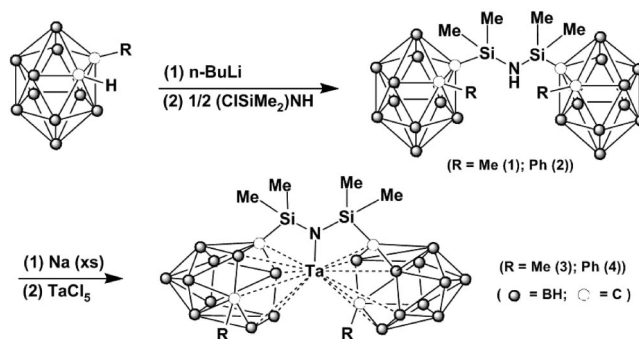
3.1. Synthesis and Characterization of Tetramethyldisilazane-Bridged *closo*-Carboranes and Derived Neutral Tantalum(V) Complexes. The reaction of 1,3-dichloro-1,1,3,3-tetramethyldisilazane with a twofold excess of the lithium salt

Table 2. Results of Ethylene Polymerization by 3–5

cat.	activity ^b	polymer ^a	
		<i>M</i> _w (10 ³ mol) ^d	<i>M</i> _w / <i>M</i> _n
3	2470 ^c	583.3	4.7
4	975	269	2.7
5	185 (47) ^e	47.9 (32.8) ^e	3.4 (1.8) ^e

^a Results for **3** were obtained under polymerization conditions of catalyst and cocatalyst: [Al]/[Ta] = 200, solvent toluene, *T* = 50 °C, *P*_{ethylene} = 10 atm, polymerization time 30 min. ^b Activity in units of kg of PE/(mol of Ta) h atm). ^c Calculated from all polymer, including fibrous and powdery polyethylene. ^d The molecular weight and molecular weight distribution of the polymers produced from the precipitate of toluene filtrate, powdery PE, were determined by means of gel-permeation chromatography (GPC: Polymer Laboratories, PC-GPC-220) at 160 °C using 1,2,4-trichlorobenzene stabilized with 0.0125% BHT as eluent. ^e Literature results for **5**¹⁴ were obtained under polymerization conditions of catalyst and cocatalyst: [Al]/[Zr] = 2000, solvent toluene, *T* = 50 °C, *P*_{ethylene} = 1.5 bar, polymerization time 2 h.

Scheme 1. Synthesis of the Tetramethyldisilazane-Bridged *closo*-Carboranes and Tantalum(V) Complexes



of the carborane monoanions [*closo*-1-R-1,2-C₂B₁₀H₁₀]⁻ (R = Me, Ph) led to the formation of the tetramethyldisilazane-bridged dicarborane pentaanionic precursors [(*closo*-1-R-1,2-C₂B₁₀H₁₀)Me₂Si₂NH] (R = Me (**1**), Ph (**2**)) in yields of 51.2% and 42.1% for **1** and **2**, respectively (Scheme 1). The ¹H, ¹³C, and ¹¹B NMR spectra of **1** and **2** show normal group resonances that are consistent with substituted *closo*-C₂B₁₀H₁₀ cages, as described in Scheme 1.¹⁷ The IR spectra of **1** and **2** show the expected absorption band of ν_{BH} at 2521 and 2582 cm⁻¹, respectively. Compounds **1** and **2** were converted to their pentaanions by treatment with *n*-BuLi and Na in the presence of naphthalene as electron-transfer reagent in THF.

The in situ synthesized “constrained geometry” pentaanionic ligands were metalated with tantalum(V) chloride to form the neutral carboranyl tantalum(V) complexes [(*closo*-2-R-2,3-C₂B₁₀H₁₀)Me₂Si₂N]Ta(V) (R = Me (**3**), Ph (**4**)) in 21.2% and 31.7% yields, respectively. The ¹H and ¹³C NMR spectra of **3** and **4** show normal group resonances, as described in the proposed structures. The near-IR spectra of **3** and **4** exhibit typical B–H absorptions at about 2594 and 2527 cm⁻¹. To verify the formation of the Ta–N bond, Cl₄TaN(SiMe₃)₂ was synthesized¹⁶ and its Raman spectrum was used for comparison (Figure 3). In the Raman spectrum of Cl₄TaN(SiMe₃)₂, no resonances in the region of 500–1200 cm⁻¹, where peaks for TaCl₅ should be seen, were observed. However, both Cl₄TaN(SiMe₃)₂ and **3** exhibited complicated absorption patterns in other regions. According to the literature,¹⁸ the strong

(17) (a) Gomez, F. A.; Hawthorne, M. F. *J. Org. Chem.* **1992**, *57*, 1384–1390. (b) Xie, Z.; Wang, S.; Zhou, Z.-Y.; Mak, T. C. W. *Organometallics* **1999**, *18*, 1641–1652.

(18) Kravchenko, V. V.; Zaitseva, M. G.; Kopylov, V. M.; Petrov, K. I. *J. Struct. Chem.* **1987**, *27*, 549–555.

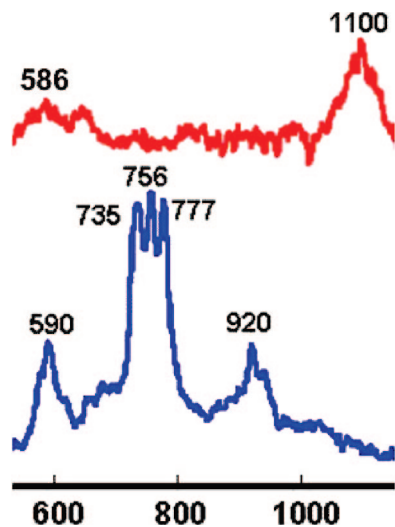


Figure 3. Raman spectra of $\text{TaCl}_4(\text{NSiMe}_3)$ (red) and **3** (blue).

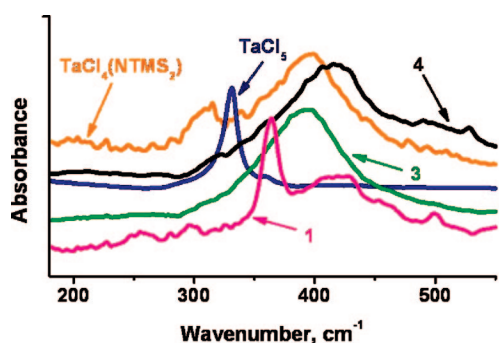


Figure 4. Far-IR spectra of TaCl_5 , $\text{TaCl}_4(\text{NSiMe}_3)$, **1**, **3**, and **4**.

absorptions at 1100 cm^{-1} ($\text{Cl}_4\text{TaN}(\text{SiMe}_3)_2$) and 920 cm^{-1} (**3**) may be assigned to $\nu_{\text{Si-N}}$ resonances. The peaks at 586 and 590 cm^{-1} found in **3** are tentatively attributed to the Ta–N resonances; there are no other reports regarding the location of the typical absorption of Ta–N bond in Raman analysis. The other absorptions of **3** at 735, 756, and 777 cm^{-1} may be caused by B–Ta, C–B, and Si–C_{cage} resonances.

In addition, the far-IR spectra of compounds **3** and **4** were compared to those of $\text{Cl}_4\text{TaN}(\text{SiMe}_3)_2$, TaCl_5 , and **1** (Figure 4). As can be seen from the figure, compounds **3**, **4**, and $\text{Cl}_4\text{TaN}(\text{SiMe}_3)_2$ show strong absorptions at 397, 416, and 400 cm^{-1} , respectively, which are consistent with reported $\nu_{\text{Ta-N}}$ absorptions.¹⁹ On the other hand, neither TaCl_5 nor **1** shows such absorptions (see Figure 4). These results clearly indicate the presence of a Ta–N bond in **3** and **4**.

3.2. Catalytic Evaluation of Carboranyl Pentaanionic Coordinated Tantalum(V) Complexes. In order to evaluate the catalytic activities of the novel neutral tantalum(V) complexes, compounds **3** and **4** have been investigated as precatalysts for ethylene polymerization in the presence of the cocatalyst MAO. Different conditions of reaction temperature, ethylene pressure, and the $[\text{Al}]/[\text{Ta}]$ ratio have been examined for compound **3**, and the results are given in Table 1. It was found that a temperature of $50\text{ }^\circ\text{C}$ with $[\text{Al}]/[\text{Ta}] = 200$ and $P_{\text{ethylene}} = 10\text{ atm}$ gave the highest catalytic activity ($2470\text{ kg of PE}/(\text{mol of Ta h atm})$); these conditions were selected for the comparison of the catalytic activities of **3** and **4** (Table 2).

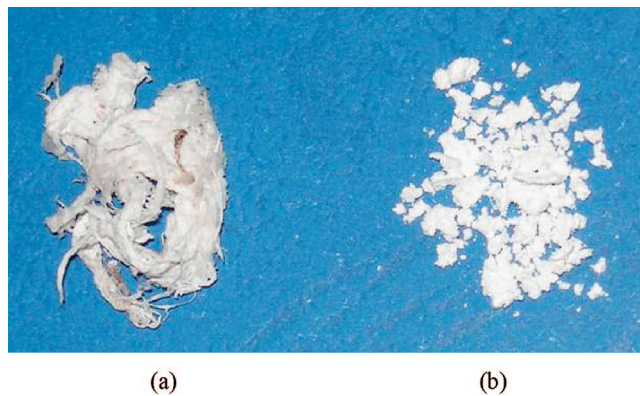


Figure 5. Polyethylene (PE) from catalyst **3** with cocatalyst MAO: (a) fibrous PE; (b) powdery PE.

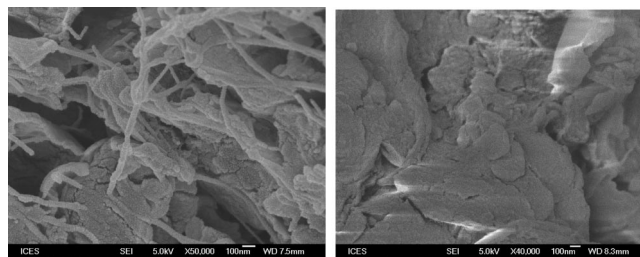


Figure 6. SEM images of PE from **3**: (a) fibrous PE; (b) powdery PE.

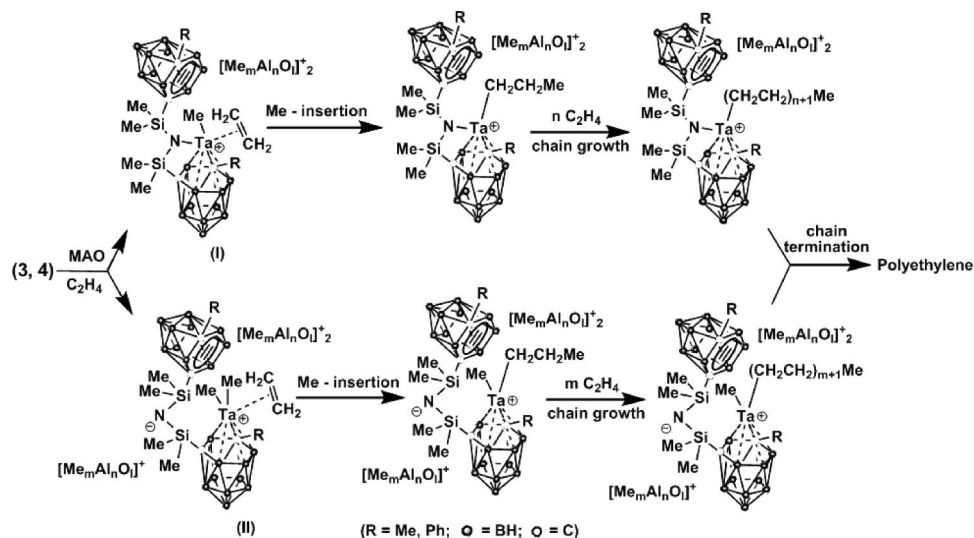
As can be seen from Table 2, under these conditions, compound **4** exhibited a much lower activity ($975\text{ kg of PE}/(\text{mol of Ta h atm})$). However, both are substantially higher than the value of $185\text{ kg of PE}/(\text{mol of Zr h atm})$ found for the carboranyl trianion, $[\text{nido-RR}'\text{C}_2\text{B}_9\text{H}_9]^{3-}$, coordinated zirconocarborane *closo*-1-Zr(Cl)-2-Ph-3-(2'- σ (H)-N-cyclohexyl)-2,3- η^5 -C₂B₉H₉ (**5**, Figure 2),¹⁴ under the same conditions (see Table 2). Interestingly, morphologically different polyethylenes, one fibrous and the other powdery (Figure 5), have been produced from a one-pot polymerization reaction with **3** and the cocatalyst MAO. The fibrous polyethylene possesses a viscometric molecular weight of 5.7×10^6 , much higher than that of the powdery polyethylene (Table 1). The morphologically different PEs show different T_m values (based on DSC analysis) of 135 and $127\text{ }^\circ\text{C}$ for fibrous polyethylene and powdery polyethylene, respectively. Interestingly, they show dramatically different images in SEM analysis (Figure 6). Microscale rods comprising nanoscale particles are found for fibrous PE SEM images, which are not seen in the powdery PE. The catalytic activities of **3** and **4** compare favorably with those of other reported η^5 -coordinated *nido*-carboranyl metallocenes such as *closo*-1-Zr(Me)(η^5 -C₅Me₅)-2,3- η^5 -C₂B₉H₁₁ (activity $72\text{ kg of PE}/(\text{mol of Zr h atm})$),²⁰ *closo*-1-TiCl₂-3-(π - η^2 -N,N'-dimethylaminomethyl)- η^5 -C₂B₉H₁₁ (activity $85\text{ kg of PE}/(\text{mol of Ti h atm})$)²¹ and σ -bonded *closo*-carboranyl metallocenes such as $\{[\eta^5\text{-}\sigma\text{-Me}_2\text{C}(\text{C}_9\text{H}_6)(\text{C}_2\text{B}_{10}\text{H}_{10})]\text{ZrCl}(\mu\text{-Cl})_{1.5}\}_2\{\text{Li}(\text{THF})_2\}$ (activity $2730\text{ kg of PE}/(\text{mol of Zr h atm})$).²² The mechanism for the neutral carboranyl tantalum(V)/MAO catalytic process is not known. However, the results suggest that two pathways might occur, one leading to the fibrous PE and the other to the powdery PE. A tentative polymerization scheme is shown in Scheme 2. In

(20) Crowther, D. J.; Baenziger, N. C.; Jordan, R. F. *J. Am. Chem. Soc.* **1991**, *113*, 1455–1457.

(21) Kim, D.-H.; Won, J. H.; Kim, S.-J.; Ko, J.; Kim, S. H.; Cho, S.; Kang, S. O. *Organometallics* **2001**, *20*, 4298–4300.

(19) Bradley, D. C.; Hursthouse, M. B.; Malik, K. M. A.; Nielson, A. J.; Vuru, G. B. C. *J. Chem. Soc., Dalton Trans.* **1984**, 1069–1072.

Scheme 2. Proposed Ethylene Polymerization by 3 and 4



keeping with other MAO-assisted schemes, the precursor **3** or **4** could react with MAO, leading to a metal–ligand bond rupture; either a N–Ta or a (η^6 -C₂B₄)–Ta bond could be broken to form catalytically active species (**I**, **II**) upon coordination with the ethylene monomer. For individual processes, the single-site polymerization mechanism of the conventional Ziegler–Natta catalysts may be operable.^{2–4} At this point it is impossible to predict which metal–ligand bond is broken or whether the two possible paths could lead to morphologically different forms of PE. More detailed mechanistic studies are currently underway in our laboratory, using FT-IR and NMR spectroscopy.

4. Conclusion

The novel carborane-based pentaanionic precursors [(*closo*-1-R-1,2-C₂B₁₀H₁₀)Me₂Si]₂NH (R = Me, Ph) and their derived neutral tantalum(V) complexes have been synthesized and characterized. The complexes [(*closo*-2-R-2,3-C₂B₁₀H₁₀)Me₂-

Si]₂N]Ta(V) (R = Me, Ph) were found to be active catalysts for the polymerization of ethylene in the presence of cocatalyst, MAO, to produce morphologically different polyethylenes in a single reaction.

Acknowledgment. We gratefully acknowledge financial support by the Institute of Chemical and Engineering Sciences (ICES) in Singapore, through grants from the Robert A. Welch Foundation (No. N-1322 to J.A.M.) and the National Science Foundation (No. CHE-0601023 to N.S.H.), and through the second research prize from the Alexander von Humboldt Foundation (to N.S.H.).

OM800516X

(22) Wang, H.; Wang, Y.; Li, H.-W.; Xie, Z. *Organometallics* **2001**, *20*, 5110–5118.

How to Stabilize η^3 -Silapropargyl/Alkynylsilyl Complex of $[\text{CpL}_2\text{M}]^+(\text{L} = \text{CO}, \text{PMe}_3, \text{or PF}_3 \text{ and } \text{M} = \text{W or Mo})$: Theoretical Prediction

Mausumi Ray,[†] Yoshihide Nakao,[†] Hirofumi Sato,[†] Hiroyuki Sakaba,[§] and Shigeyoshi Sakaki^{*†,‡,‡}

Department of Molecular Engineering, Graduate School of Engineering, Kyoto University
Kyotodaigaku-Katsura, Nishikyo-ku, Kyoto 615-8510, Japan, Fukui Institute for Fundamental Chemistry,
Nishihiraki-cho Takano, Kyoto 606-8103, Japan, and Department of Chemistry, Graduate School of
Science, Tohoku University, Aoba-ku, Sendai 980-8578, Japan

Received July 1, 2008

We theoretically investigated here how to stabilize a new transition metal η^3 -silapropargyl/alkynylsilyl complex $\text{CpL}_2\text{M}(\eta^3\text{-R}^2\text{SiCCR}^1)$ ($\text{M} = \text{W or Mo}$; $\text{L} = \text{CO}, \text{PMe}_3, \text{or PF}_3$; $\text{Cp} = \text{C}_5\text{H}_5$; $\text{R}^1 = \text{H}, \text{Me}, \text{tBu}, \text{or CF}_3$; $\text{R}^2 = \text{H}, \text{Me}, \text{or F}$) which is an interesting silicon analogue of a transition metal η^3 -propargyl complex. Though this complex was experimentally proposed as an intermediate in the synthesis of a tungsten acetylide–silylene complex $\text{Cp}(\text{CO})_2\text{W}(\text{CCtBu})(\text{SiPh}_2)$, it has not been synthesized yet. From theoretical computations with DFT method, we wish to propose that the combination of electron-withdrawing CF_3 on C, σ -electron-withdrawing/ π -electron-donating F on Si, Mo center, and CO is the best to stabilize the η^3 -silapropargyl/alkynylsilyl form. However, the combination of bulky tBu on C, either H or Me on Si, W center, and PMe_3 is the best to stabilize the acetylide–silylene form, which is also an interesting species. The reasons are discussed herein.

Introduction

As is well-known, silicon compounds are much different from carbon analogues even if their compositions are similar to each other; for instance, a silicon analogue of acetylene is very reactive and takes a trans-bent structure, as recently reported.^{1–5,6b,12} Because of significantly large differences between carbon and silicon compounds, silicon analogues of various carbon compounds have drawn a lot of interest.^{1–16}

Transition metal η^3 -propargyl/allenyl complex has been one of the research targets in recent organometallic chemistry, coordination chemistry, and catalytic chemistry because of its interesting geometry and reactivity.^{17,18} In this regard, many important results have been reported on their synthesis and characterization.^{17–20} However, transition metal η^3 -silapropargyl/alkynylsilyl complex, which is one of the silicon analogues of the η^3 -propargyl/allenyl complex, has not yet been synthesized, to our best knowledge, though it is expected to be of considerable interest.

* To whom correspondence should be addressed. E-mail: sakaki@moleng.kyoto-u.ac.jp.

[†] Department of Molecular Engineering, Graduate School of Engineering, Kyoto University Kyotodaigaku-Katsura.

[‡] Fukui Institute for Fundamental Chemistry.

[§] Department of Chemistry, Graduate School of Science, Tohoku University.

(1) (a) Sekiguchi, A.; Ichinohe, M.; Kinjo, R. *Bull. Chem. Soc. Jpn.* **2006**, *6*, 825. (b) Frenking, G.; Krapp, A.; Nagase, S.; Takagi, N.; Sekiguchi, A. *ChemPhysChem* **2006**, *7*, 799. (c) Sekiguchi, A.; Rei, K.; Masaaki, I. *Science* **2004**, *305*, 1755. (d) Sekiguchi, A.; Ziegler, S.; Robert, W.; Josef, M. *J. Am. Chem. Soc.* **1986**, *108*, 4241.

(2) (a) Weidenbruch, M. *Angew. Chem., Int. Ed.* **2005**, *44*, 514. (b) Weidenbruch, M. *J. Organomet. Chem.* **2002**, *646*, 39.

(3) Jutzi, P. *Angew. Chem., Int. Ed.* **2000**, *39*, 3797.

(4) (a) Power, P. P. *Chem. Comm.* **2003**, *17*, 2091, and references therein. (b) Power, P. P. *Organometallics* **2007**, *26*, 4362.

(5) (a) Takagi, N.; Nagase, S. *Eur. J. Inorg. Chem.* **2002**, *11*, 2775. (b) Takagi, N.; Nagase, S. *Chem. Lett.* **2001**, *10*, 966. (c) Kobayashi, K.; Takagi, N.; Nagase, S. *Organometallics* **2001**, *20*, 234. (d) Takagi, N.; Nagase, S. *Organometallics* **2001**, *20*, 5498. (e) Nagase, S.; Kobayashi, K.; Takagi, N. *J. Organomet. Chem.* **2000**, *611*, 264. (f) Kobayashi, K.; Nagase, S. *Organometallics* **1997**, *16*, 2489.

(6) (a) Clabo, D. A.; Schaefer, H. F. *J. Chem. Phys.* **1986**, *84*, 1664. (b) Thies, B. S.; Grev, R. S.; Schaefer, H. F. *Chem. Phys. Lett.* **1987**, *140*, 355. (c) Colegrove, B. T.; Schaefer, H. F. *J. Phys. Chem.* **1990**, *94*, 5593. (d) Colegrove, B. T.; Schaefer, H. F. *J. Am. Chem. Soc.* **1991**, *113*, 1557. (e) Grev, R. S. *Adv. Organomet. Chem.* **1991**, *33*, 125. (f) Grev, R. S.; Schaefer, K. F. *J. Chem. Phys.* **1992**, *97*, 7990.

(7) (a) Cordonnier, M.; Bogey, M.; Demuynck, C.; Destombes, J.-L. *J. Chem. Phys.* **1992**, *97*, 7984. (b) Bogey, M.; Bolvin, H.; Demuynck, C.; Destombes, J. L. *Phys. Rev. Lett.* **1991**, *66*, 413.

(8) (a) Koseki, S.; Gordon, M. S. *J. Phys. Chem.* **1988**, *92*, 364. (b) Koseki, S.; Gordon, M. S. *J. Phys. Chem.* **1989**, *93*, 118.

(9) Lischka, H.; Kohler, H.-J. *J. Am. Chem. Soc.* **1983**, *105*, 6646.

(10) Binkley, J. S. *J. Am. Chem. Soc.* **1984**, *106*, 603.

(11) Kalcher, J.; Sax, A.; Olbrich, G. *Int. J. Quantum Chem.* **1984**, *25*, 543.

(12) Kohler, H.-J.; Lischka, H. *Chem. Phys. Lett.* **1984**, *112*, 33.

(13) Wiberg, N.; Niedermayer, W.; Fischer, G.; Nöth, H.; Suter, M. *Eur. J. Inorg. Chem.* **2002**, 1066.

(14) Kutzelnig, W. *Angew. Chem., Int. Ed. Engl.* **1984**, *23*, 272.

(15) Coolidge, M. B.; Hrovat, D. A.; Borden, W. T. *J. Am. Chem. Soc.* **1992**, *114*, 2354.

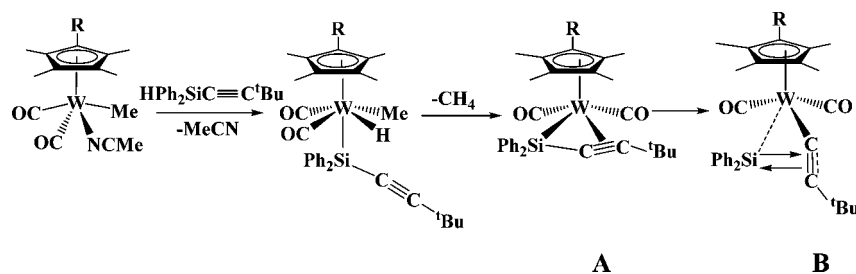
(16) Doherty, S.; Corrigan, G. F.; Carty, A. G.; Sappa, E. *Adv. Organomet. Chem.* **1995**, *37*, 39.

(17) Tsuji, J.; Mandai, T. *Angew. Chem., Int. Ed. Engl.* **1995**, *34*, 2589.

(18) (a) Casey, C. P.; Yi, C. S. *J. Am. Chem. Soc.* **1992**, *114*, 6597. (b) Casey, C. P.; Selmecky, A. D.; Nash, J. R.; Yi, C. S.; Powell, D. R.; Hayashi, R. K. *J. Am. Chem. Soc.* **1996**, *118*, 6698. (c) Casey, C. P.; Nash, J. R.; Yi, C. S.; Selmecky, A. D.; Chung, S.; Powell, D. R.; Hayashi, R. K. *J. Am. Chem. Soc.* **1996**, *118*, 6698. (d) Casey, C. P.; Bolter, T. M.; Kraft, S.; Guzei, I. A. *J. Am. Chem. Soc.* **2002**, *124*, 13215.

(19) Chen, J. T. *Coord. Chem. Rev.* **1999**, *190/192*, 1143, and references therein.

(20) (a) Shuchart, C. E.; Richard, W. R.; Wojcicki, A. *J. Organomet. Chem.* **1992**, *424*, 185. (b) Blosser, P. W.; Gallucci, J. C.; Wojcicki, A. *J. Am. Chem. Soc.* **1993**, *115*, 2994. (c) Blosser, P. W.; Schimpff, D. G.; Gallucci, J. C.; Wojcicki, A. *Organometallics* **1993**, *12*, 1993. (d) Graham, J. P.; Wojcicki, A.; Bursten, B. E. *Organometallics* **1999**, *18*, 837. (e) Wojcicki, A. *Inorg. Chem. Commun.* **2002**, *5*, 82, and references therein.

Scheme 1. Formation of Cp*(CO)₂W(CC^tBu)(SiPh₂) **B** via Cp*(CO)₂W(η³-Ph₂SiCC^tBu) **A**

Recently, tungsten η^3 -sila-propargyl/alkynylsilyl complex Cp*(CO)₂W(η^3 -Ph₂SiCC^tBu) **A** (Cp* = C₅Me₅) was experimentally proposed as an intermediate in the synthesis of tungsten acetylide–silylene complex Cp*(CO)₂W(CC^tBu)(SiPh₂) **B**, as shown in Scheme 1.^{21–23} However, **A** has not been isolated yet, though the similar tungsten η^3 -silaallyl complex Cp*(CO)₂W(η^3 -Me₂SiCHCMe₂), which is a silicon analogue of the transition metal η^3 -allyl complex, was recently isolated.²⁴ We also theoretically investigated the geometries and the bonding natures of Cp(CO)₂W(η^3 -H₂SiCCH) **1** (Cp = C₅H₅) and Cp(CO)₂W(CCH)(SiH₂) **2**, where **1** and **2** were employed as models of **A** and **B**, respectively.²² In this work, we found that **1** was slightly less stable than **2**. This computational result strongly suggests that one can successfully synthesize the transition metal η^3 -sila-propargyl/alkynylsilyl complex with the appropriate metal center, ligand, and substituents on Si and C atoms.

Our theoretical studies on the tungsten η^3 -sila-propargyl/alkynylsilyl complex Cp(CO)₂W(η^3 -H₂SiCCH) **1**²² and tungsten η^3 -silaallyl/vinylsilyl complex Cp(CO)₂W(η^3 -H₂SiCHCH₂)²⁵ demonstrated their interesting bonding natures; for instance, the nonbonding π -orbitals ($\varphi_{n\pi}$) of η^3 -H₂SiCCH and η^3 -H₂SiCHCH₂ groups are similar to those of the η^3 -propargyl and η^3 -allyl groups, respectively, but their π -orbitals (φ_{π}) are significantly different from those of the η^3 -propargyl and η^3 -allyl groups; in other words, the electronic structure of η^3 -H₂SiCCH group is intermediate between those of η^3 -sila-propargyl and alkynylsilyl groups and that of η^3 -H₂SiCHCH₂ group is intermediate between those of η^3 -silaallyl and vinylsilyl groups. These theoretical results indicate that the transition metal η^3 -sila-propargyl/alkynylsilyl complex provides a new interesting category of transition metal silicon compounds. Thus, its synthesis is challenging and its experimental characterization is interesting.

In this work, we theoretically investigated the η^3 -sila-propargyl/alkynylsilyl complex CpL₂M(η^3 -R₂SiCCR¹) (**1** for M = W and **3** for M = Mo; L = CO, PMe₃, or PF₃; Cp = C₅H₅, R¹ = H, Me, ^tBu, or CF₃; R² = H, Me, or F) and the acetylide–silylene complex CpL₂M(CCR¹)(SiR²)₂ (**2** for M = W and **4** for M = Mo) with DFT, MP2 to MP4(SDTQ), and

CCSD(T) methods. We also investigated the conversion reactions of **1** and **3** to **2** and **4**, respectively. Our main purposes here are to present a theoretical prediction on how to stabilize the transition metal η^3 -sila-propargyl/alkynylsilyl complex and to clarify how and why the stabilities, electronic structures, and bonding natures of **1** and **3** depend on the substituents of Si and C, ligands, and metal center.

Computational Details

CpL₂M(η^3 -R₂SiCCR¹) and CpL₂M(CCR¹)(SiR²)₂ are neutral and take closed-shell singlet spin state.²⁶ Their geometries were optimized with the density functional theory (DFT). Here, we employed B3PW91 functional^{27,28} for the exchange–correlation term because the geometry of Cp(CO)₂W(CC^tBu)(SiH₂) was well optimized with this functional compared to B3LYP functional^{27,29} (see Supporting Information Table S1). We ascertained that each equilibrium geometry did not exhibit any imaginary frequency and each transition state possessed only one imaginary frequency in which geometry changes were consistent with the reaction. Energy was evaluated with DFT, MP2 to MP4(SDTQ), and CCSD(T) methods, where the DFT-optimized geometry was employed.

Three kinds of basis set systems, Basis Set System-I (BS-I), Basis Set System-II (BS-II), and Basis Set System-III (BS-III) were employed in this work. In BS-I, core electrons of W and Mo were replaced with effective core potentials (ECPs)³⁰ and their valence electrons were represented with (341/321/21) and (341/321/31) basis sets,³⁰ respectively. cc-pVDZ basis sets³¹ were used for Si, C, and O, and 6–31G basis set was used for H.³² This BS-I was employed for geometry optimization. In BS-II, valence electrons of W and Mo were represented with (541/541/111/1) and (541/541/211/1) basis sets,^{30,33,34} respectively, where their core electrons were

(21) Sakaba, H.; Yoshida, M.; Kabuto, C.; Kabuto, K. *J. Am. Chem. Soc.* **2005**, *127*, 7276.

(22) Ray, M.; Nakao, Y.; Sato, H.; Sakaba, H.; Sakaki, S. *J. Am. Chem. Soc.* **2006**, *128*, 11927.

(23) The complex **B** of Scheme 1 contains strong charge transfer interactions between acetylide and silylene moieties, as discussed previously in our work.²² As a result, the silylene moiety considerably changes its direction toward the acetylide moiety and the bonding interaction between metal and silylene becomes weak. These features indicate that the bonding nature of this complex is intermediate between those of pure acetylide silylene complex and pure silacyclopentenyl complex. Here, we use the name of “acetylide–silylene complex” because there is no appropriate name for such species, where we placed an endash “–” between words of acetylide and silylene to represent the presence of bonding interaction between them.

(24) Sakaba, H.; Watanabe, S.; Kabuto, C.; Kabuto, K. *J. Am. Chem. Soc.* **2003**, *125*, 2842.

(25) Ray, M.; Nakao, Y.; Sato, H.; Sakaki, S. *Organometallics* **2007**, *26*, 4413.

(26) The proton NMR chemical shifts and spectrum shape indicate that Cp*(CO)₂W(CC^tBu)(SiPh₂) takes closed shell singlet state.²¹ Though Cp*(CO)₂W(η^3 -R₂SiCCR¹) has not been synthesized, proton NMR chemical shifts and spectrum shape of the similar Cp*(CO)₂W(η^3 -Me₂SiCHCMe₂) indicate that this complex takes closed-shell singlet state, too.²⁴

(27) (a) Becke, A. D. *Phys. Rev. A* **1988**, *38*, 3098. (b) Becke, A. D. *J. Chem. Phys.* **1993**, *98*, 5648.

(28) (a) Perdew, J. P. In *Electronic Structure of Solids '91*; Ziesche, P., Eschrig, H., Eds.; Akademik Verlag: Berlin, 1991; p 11. (b) Perdew, J. P.; Chevary, J. A.; Vosko, S. H.; Jackson, K. A.; Pederson, M. R.; Singh, D. J.; Fiolhais, C. *Phys. Rev. B* **1992**, *46*, 6671. (c) Perdew, J. P.; Chevary, J. A.; Vosko, S. H.; Jackson, K. A.; Pederson, M. R.; Singh, D. J.; Fiolhais, C. *Phys. Rev. B* **1993**, *48*, 4978. (d) Perdew, J. P.; Burke, K.; Wang, Y. *Phys. Rev. B* **1996**, *54*, 16533.

(29) (a) Lee, C.; Yang, W.; Parr, R. G. *Phys. Rev. B* **1988**, *37*, 785. (b) Miehlich, B.; Savin, A.; Stoll, H.; Preuss, H. *Chem. Phys. Lett.* **1989**, *157*, 200.

(30) Hay, P. J.; Wadt, W. R. *J. Chem. Phys.* **1985**, *82*, 299.

(31) (a) Dunning Jr, T. H. *J. Chem. Phys.* **1989**, *90*, 1007. (b) Woon, D. E.; Dunning, T. H., Jr. *J. Chem. Phys.* **1993**, *98*, 1358.

(32) (a) Ditchfield, R.; Hehre, W. J.; Pople, J. A. *J. Chem. Phys.* **1971**, *54*, 724. (b) Hehre, W.; Ditchfield, R.; Pople, J. A. *J. Chem. Phys.* **1972**, *56*, 2257.

(33) Couty, M.; Hall, M. B. *J. Comput. Chem.* **1996**, *17*, 1359.

(34) Ehlers, A. W.; Böhme, D. S.; Gobbi, A.; Höllwarth, A.; Jonas, V.; Kähler, K. F.; Stegmann, R.; Veldkamp, A.; Frenking, G. *Chem. Phys. Lett.* **1993**, *208*, 111.

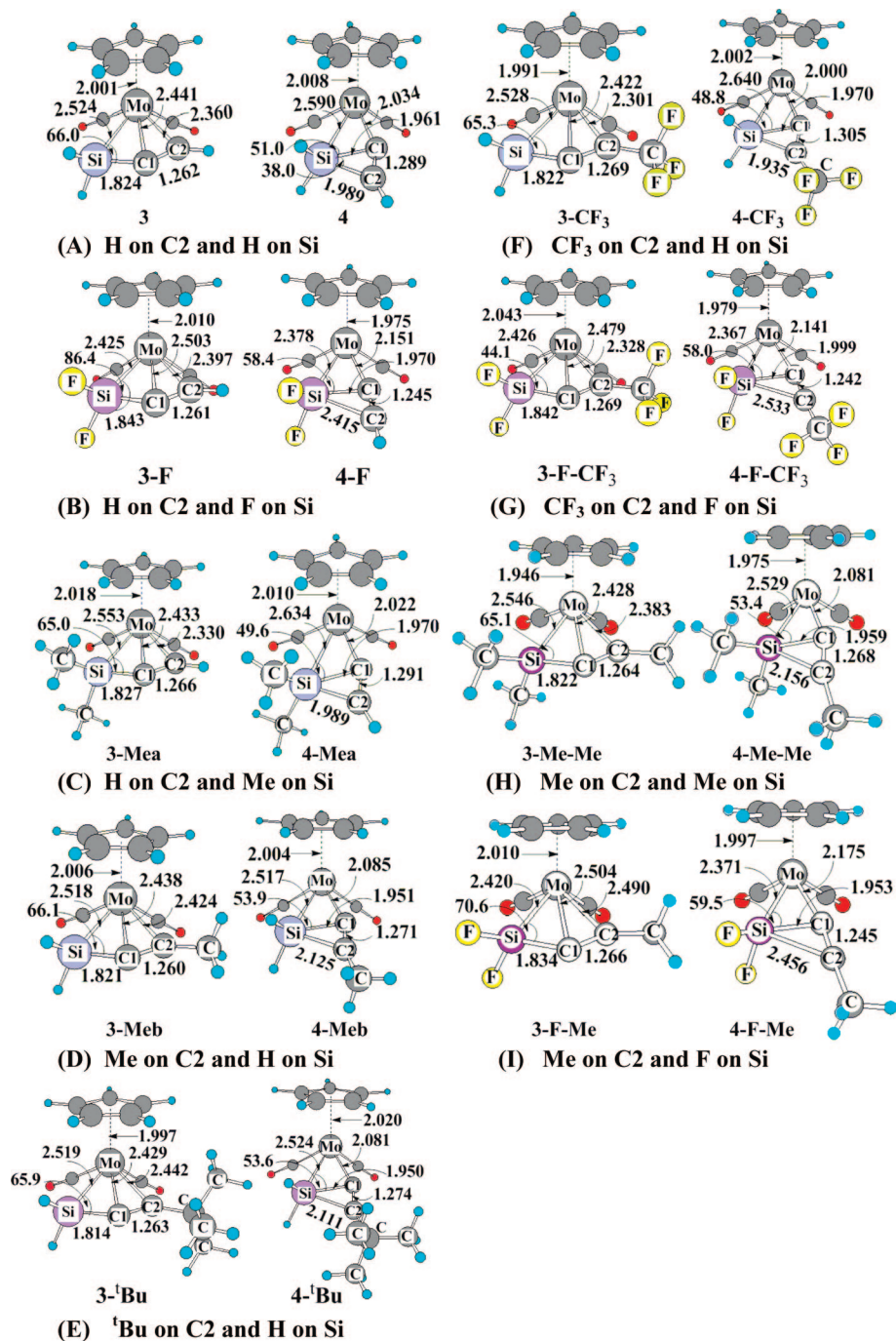


Figure 1. DFT(B3PW91)/BS-I optimized geometries of $\text{Cp}(\text{CO})_2\text{Mo}(\eta^3\text{-R}_2\text{SiCCR}^1)$ and $\text{Cp}(\text{CO})_2\text{Mo}(\text{CCR}^1)(\text{SiR}^2_2)$, where $\text{R}^1 = \text{H, Me, } ^t\text{Bu, or CF}_3$ and $\text{R}^2 = \text{H, F, or Me}$. See Supporting Information Figure S1 for geometries of tungsten complexes. Bond lengths are in angstroms and bond angles are in degrees.

replaced with the same ECPs as those of BS-I. For the other atoms, the same basis sets as those of BS-I were employed. This BS-II was used to evaluate energy changes. In BS-III, valence electrons of W and Mo were represented by (311111/22111/411/11) basis sets with Stuttgart–Dresden–Bonn (SDB) ECPs.^{35,36} For the other atoms, cc-pVTZ basis sets were used,³⁷ where the f polarization function was excluded to save CPU time. This BS-III was used to check if BS-II presents reliable energy change. Zero-point energy (ZPE), thermal energy, and entropy change were calculated with

the DFT/BS-I method at 298 K and 1 atm, where the assumptions of rigid rotator and harmonic oscillator were employed to evaluate partition functions of rotation and vibration movements and the assumption of ideal gas was employed to evaluate partition function of translation movement. Solvation effects (toluene; $\epsilon = 2.379$) were taken into consideration with polarizable continuum model (PCM),³⁸ where optimized geometries in gas-phase were employed.

Gaussian 03 program package (revision C.02)³⁹ was used for all of these computations.

(35) Andrae, D.; Haeussermann, U.; Dolg, M.; Stoll, H.; Preuss, H. *Theor. Chim. Acta.* **1990**, *77*, 123.

(36) Martin, J. M. L.; Sundermann, A. *J. Chem. Phys.* **2001**, *114*, 3408.

(37) (a) Dunning, T. H., Jr. *J. Chem. Phys.* **1989**, *90*, 1007. (b) Woon, D. E., Jr. *J. Chem. Phys.* **1993**, *98*, 1358.

(38) (a) Miertuš, S.; Scrocco, E.; Tomasi, J. *Chem. Phys.* **1981**, *55*, 117.

(b) Miertuš, S.; Tomasi, J. *Chem. Phys.* **1982**, *65*, 239. (c) Cossi, M.; Barone, V.; Cammi, R.; Tomasi, J. *Chem. Phys. Lett.* **1996**, *255*, 327.

Table 1. Relative Stability (ΔE)^a (in kcal/mol unit) of $\text{Cp}(\text{CO})_2\text{M}(\eta^3\text{-H}_2\text{SiCCH})$ to $\text{Cp}(\text{CO})_2\text{M}(\text{CCH})(\text{SiH}_2)$ (M = W or Mo) Calculated with Various Computational Methods

method	M = W ^b	M = Mo
DFT	-4.9 (-4.0) ^c	-1.9 (-0.9) ^c
MP2	+0.4	+4.1
MP3	-1.4	+2.5
MP4(DQ)	-0.1	+3.5
MP4(SDQ)	-0.9	+2.7
MP4(SDTQ)	-0.6	+2.9
CCSD(T)	-0.7	+2.9

^a The ΔE value is energy difference between $\text{Cp}(\text{CO})_2\text{M}(\text{CCH})(\text{SiH}_2)$ and $\text{Cp}(\text{CO})_2\text{M}(\eta^3\text{-H}_2\text{SiCCH})$. The BS-II was employed. ^b ref 22 ^c In parentheses are the ΔE value between $\text{Cp}^*(\text{CO})_2\text{M}(\eta^3\text{-H}_2\text{SiCCH})$ and $\text{Cp}^*(\text{CO})_2\text{M}(\text{CCH})(\text{SiH}_2)$.

Table 2. Relative Stability (ΔE)^a (in kcal/mol unit) of $\text{CpL}_2\text{M}(\eta^3\text{-R}^2\text{SiCCR}^1)$ to $\text{CpL}_2\text{M}(\text{CCR}^1)(\text{SiR}^2_2)$ (M = W or Mo, L = CO, PMe_3 , or PF_3)

R ¹ on C2	R ² on Si	L	M = W	M = Mo
^t Bu	H	CO	-5.2	-2.3
H	H	CO	-4.9	-1.9
		PMe_3	-14.3	-6.7
		PF_3	-5.6	-2.4
H	Me	CO	-4.2	-0.7
CF_3	H	CO	-4.1	-0.7
Me	F	CO	-4.0	-1.8
Me	H	CO	-3.5	-0.4
Me	Me	CO	-2.5	+0.4
H	F	CO	-2.0	+0.1
CF_3	F	CO	+1.1	+2.6

^a The ΔE value is energy difference between $\text{CpL}_2\text{M}(\text{CCR}^1)(\text{SiR}^2_2)$ and $\text{CpL}_2\text{M}(\eta^3\text{-R}^2\text{SiCCR}^1)$. The DFT(B3PW91)/BS-II method was employed. Its positive value represents that $\text{CpL}_2\text{M}(\eta^3\text{-R}^2\text{SiCCR}^1)$ is more stable than $\text{CpL}_2\text{M}(\text{CCR}^1)(\text{SiR}^2_2)$.

Results and Discussion

In this article, we wish to investigate first the relative stability of $\text{Cp}(\text{CO})_2\text{M}(\eta^3\text{-H}_2\text{SiCCH})$ to $\text{Cp}(\text{CO})_2\text{M}(\text{CCH})(\text{SiH}_2)$, make comparison between molybdenum and tungsten complexes, and then discuss ligand and substituent effects on the relative stability of $\text{CpL}_2\text{M}(\eta^3\text{-R}^2\text{SiCCR}^1)$ to $\text{CpL}_2\text{M}(\text{CCR}^1)(\text{SiR}^2_2)$.

Geometries and Relative Stabilities of $\text{Cp}(\text{CO})_2\text{M}(\eta^3\text{-H}_2\text{SiCCH})$ and $\text{Cp}(\text{CO})_2\text{M}(\text{CCH})(\text{SiH}_2)$ (M = W or Mo). Because geometries of $\text{Cp}(\text{CO})_2\text{W}(\eta^3\text{-H}_2\text{SiCCH})$ **1** and $\text{Cp}(\text{CO})_2\text{W}(\text{CCH})(\text{SiH}_2)$ **2** were previously discussed in our theoretical study,²² we wish to focus on the differences in geometry between the tungsten and molybdenum complexes here. Several geometrical parameters are moderately different between them (see Figure 1 and Supporting Information Figure S1 for their geometries): For instance, the Mo-Cp (center of the Cp ring) distance is moderately shorter than the W-Cp distance by 0.039 Å in $\text{Cp}(\text{CO})_2\text{M}(\eta^3\text{-H}_2\text{SiCCH})$ and by 0.043 Å in $\text{Cp}(\text{CO})_2\text{M}(\text{CCH})(\text{SiH}_2)$, indicating that the Mo-Cp interaction is moderately stronger than the W-Cp interaction probably because the donation from Cp to M becomes stronger upon switching W to Mo, as shown by the smaller electron population of Cp in **3** than in **4** (see Table S2 in Supporting Information). The Mo-C1 and Mo-C2 distances in $\text{Cp}(\text{CO})_2\text{Mo}(\eta^3\text{-H}_2\text{SiCCH})$ **3** are moderately longer than the W-C1 and W-C2 distances of the tungsten analogue **1** by 0.017 Å and 0.051 Å, respectively, though atomic radius of molybdenum is smaller than that of tungsten. The Mo-Si distance of $\text{Cp}(\text{CO})_2\text{Mo}(\text{CCH})(\text{SiH}_2)$ **4** is moderately shorter than the W-Si distance of the tungsten analogue **2** by 0.026 Å, whereas the Mo-C1 and Si-C2 distances of **4** are moderately longer than the W-C1 and Si-C2 distances of **2** by 0.020 Å and 0.032 Å, respectively. These geometrical differences suggest that the Mo-(η^3 -

H_2SiCCH) bond of **3** and Mo-C1 and Si-C2 bonding interactions of **4** are moderately weaker than the corresponding interactions of the tungsten analogues, respectively. The Wiberg bond indices are consistent with the above results; The Mo-C1 and Mo-C2 bond indices of **3** are moderately smaller than the W-C1 and W-C2 bond indices of **1** by 0.041 and 0.052, respectively, and the Mo-C1 and Si-C2 bond indices of **4** are moderately smaller than the W-C1 and Si-C2 bond indices of **2** by 0.081 and 0.049, respectively; see Supporting Information Table S3 for details of Wiberg bond index. These differences relate to the relative stabilities of the η^3 -silapropargyl/alkynylsilyl and acetylide-silylene forms,²³ as will be discussed below.

Relative stability of the η^3 -silapropargyl/alkynylsilyl form (**1** for M = W and **3** for M = Mo) to the acetylide-silylene form (**2** for M = W and **4** for M = Mo) is represented by the energy difference (ΔE) between these two forms, as shown in Table 1, where a positive ΔE value means that the η^3 -silapropargyl/alkynylsilyl form is more stable than the acetylide-silylene form. It is noted that the relative stability of the η^3 -silapropargyl/alkynylsilyl form is larger in the Mo complex than in the W complex; for instance, the ΔE value increases from -4.9 to -1.9 kcal/mol at the DFT level and from -0.7 to 2.9 kcal/mol at the CCSD(T) level upon going from the W complex to the Mo complex. The effect of Cp* on the relative stability of **1** to **2** was investigated because Cp* was used in the experiment; see Supporting Information Figure S2 for the geometries of the Cp* complexes.²¹ The difference of ΔE value between Cp and Cp* complexes is not large (about 1 kcal/mol); the ΔE value is -4.9 (-4.0) kcal/mol in the W complexes and -1.9 (-0.9) kcal/mol in the Mo complexes, as shown in Table 1, where in parenthesis and out of parenthesis are ΔE values for Cp* and Cp, respectively. Thus, we employed Cp instead of Cp* to save CPU time.

It is necessary to examine whether or not the DFT method presents reliable results about the relative stability of the η^3 -silapropargyl/alkynylsilyl form to the acetylide-silylene form, because only the DFT method can be applied to large complexes bearing ^tBu, CF_3 , PMe_3 , and PF_3 . The MP4(SDQ), MP4(SDTQ), and CCSD(T) methods present similar ΔE values in both W and Mo complexes, as shown in Table 1, suggesting that these methods present reliable results here. On the other hand, the DFT method presents more negative ΔE value than the other methods in the W complex. In the Mo complex, the DFT method presents negative ΔE value but the other methods present positive value. In other words, the DFT method underestimates the stability of the η^3 -silapropargyl/alkynylsilyl form. However, the change of ΔE value due to switching W to Mo is similar by a shift across such different levels as DFT, MP4(SDTQ), and CCSD(T); for instance, the ΔE value increases by 3.0, 3.5, and 3.6 kcal/mol in the DFT, MP4(SDTQ), and CCSD(T) methods, respectively, upon switching W to Mo. Thus, it is suggested that though the DFT method underestimates the stability of the η^3 -silapropargyl/alkynylsilyl form, the DFT method is useful to discuss how and why the stabilities of the η^3 -silapropargyl/alkynylsilyl and acetylide-silylene forms depend on the central metal, ligands, and substituents.

We also examined basis set effects by comparing the ΔE value among the DFT/BS-I, DFT/BS-II, and DFT/BS-III methods. Though the ΔE value is slightly different among these calculations, the difference is not large and the trend is the same in all the calculations with BS-I, BS-II, and BS-III, indicating that BS-II is useful to discuss the central metal, ligand, and

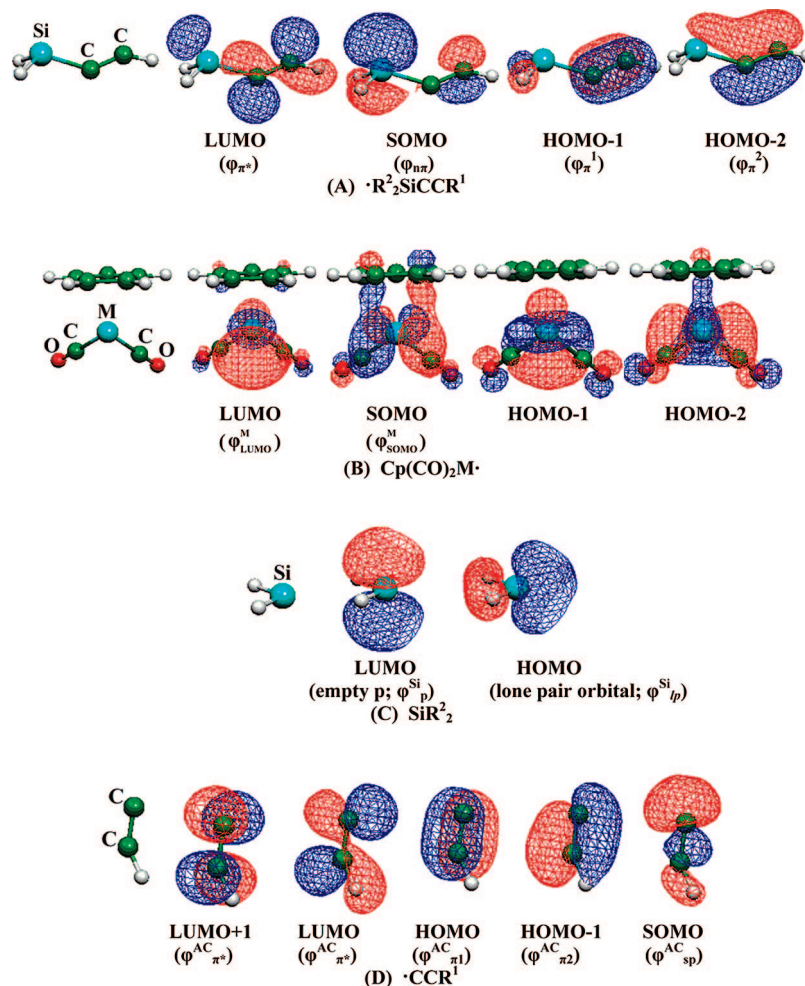


Figure 2. Several important Kohn–Sham orbitals in the fragments, $\cdot\text{R}^2\text{SiCCR}^1$, $\text{Cp}(\text{CO})_2\text{M}\cdot$, SiR^2 , and $\cdot\text{CCR}^1$.

substituent effects; see Supporting Information Table S4 for the DFT/BS-I and DFT/BS-III computational results.

Substituent Effects on Geometries and Relative Stabilities of $\text{Cp}(\text{CO})_2\text{M}(\eta^3\text{-R}^2\text{SiCCR}^1)$ and $\text{Cp}(\text{CO})_2\text{M}(\text{CCR}^1)(\text{SiR}^2)$ ($\text{M} = \text{W}$ or Mo , $\text{R}^1 = \text{H}$, Me , ^tBu , or CF_3 , and $\text{R}^2 = \text{H}$, Me , or F). Significantly large changes are observed in geometry when σ -electron-withdrawing/ π -electron-donating F is introduced on Si, as shown in Figure 1 and Supporting Information Figure S1: In $\text{Cp}(\text{CO})_2\text{Mo}(\eta^3\text{-F}_2\text{SiCCH})$ **3-F**, the Mo–Si distance becomes moderately shorter than that of **3**, indicating that the Mo–Si bonding interaction becomes stronger in **3-F** than in **3**. In $\text{Cp}(\text{CO})_2\text{Mo}(\text{CCH})(\text{SiF}_2)$ **4-F**, the Si–C2 distance is considerably longer and the Mo–Si distance is somewhat shorter than those of **4**. Also, the direction of SiF_2 considerably shifts toward the Mo center in **4-F** compared to that of **4**, in which the lone pair orbital of SiH_2 expands toward the C1 atom. These geometrical differences between **4** and **4-F** suggest that the acetylide–silylene interaction is considerably weaker in **4-F** than in **4**, whereas the Mo– SiR^2 and Mo– CCR^1 interactions become stronger by the introduction of F on Si. The Wiberg bond index supports these suggestions: The Mo–Si bond index of **3-F** is moderately larger than that of **3** by 0.049, while the Mo–Si bond index is somewhat larger by 0.182 and the Si–C2 bond index is considerably smaller by 0.383 in **4-F** than those of **4**. The Mo–Cp distance slightly lengthens upon going to **3-F** from **3** by 0.009 Å but somewhat shortens upon going to **4-F** from **4** by 0.033 Å, indicating that the Mo–Cp interaction little changes in **3-F** but becomes somewhat stronger in **4-F** by F on Si. This is because the donation of Cp to Mo

becomes stronger in **4-F** but slightly in **3-F**. The population changes are consistent with this discussion; see Table S2 and page S8 in the Supporting Information for populations and explanation of the M–Cp distance. The similar geometry changes by the introduction of F on Si are observed in the tungsten analogues (see Supporting Information Figure S1). The introduction of F on Si somewhat increases the stability of the η^3 -silylpropargyl/alkynylsilyl form by 2.9 and 2.0 kcal/mol in both of W and Mo complexes, respectively, as shown in Table 2, which is consistent with the changes in geometry and Wiberg bond index; remember the considerably longer Si–C2 distance and considerably smaller Si–C2 bond index in **4-F** than in **4**.

However, introduction of Me on Si induces moderate changes in geometries of **3** and **4**. The Mo–Si distance becomes moderately longer but the Mo–C2 distance becomes moderately shorter in **3-Mea** and the Mo–Si distance becomes moderately longer in **4-Mea**. The Wiberg bond indices also support these geometry changes; see Scheme S1 of Supporting Information. The Mo–Cp distance becomes somewhat longer in **3-Mea** by 0.017 Å but little in **4-Mea**. These results are consistent with population changes; see Table S2 in Supporting Information for population changes and explanation. Though these geometry changes are not clearly related to the relative stability of the η^3 -silylpropargyl/alkynylsilyl form, the Me on Si slightly increases the stability of the η^3 -silylpropargyl/alkynylsilyl form by 0.7 and 1.2 kcal/mol in the W and Mo complexes, respectively.

Table 3. Orbital Energies^a (in eV unit) of Several Important Orbitals of Fragments $\cdot R^2SiCCR^1$, $\cdot CCR^1$, SiR^2 , and $\cdot Cp(L)_2M$

R ¹	R ²	R ² SiCCR ¹			CCR ¹		
		φ_{π^*}	$\varphi_{n\pi}$ (SOMO)	φ_{π}	$\varphi_{\pi^*}^{AC}$	φ_{π}^{AC}	φ_{sp}^{AC} (SOMO)
H	H	-0.9 (3.5)	-6.0 (-9.1)	-8.8 (-12.3)	-0.9 (3.5)	-8.9 (-12.0)	-10.3 (-14.0)
Me	H	-0.4 (3.8)	-5.7 (-8.7)	-8.2 (-11.4)	-0.2 (4.0)	-8.2 (-11.1)	-9.3 (-14.9)
^t Bu	H	-0.5 (3.7)	-5.6 (-8.7)	-8.1 (-11.3)	-0.4 (3.8)	-8.0 (-10.9)	-9.0 (-13.3)
CF ₃	H	-1.9 (2.5)	-6.6 (-9.7)	-9.5 (-13.5)	-2.2 (1.9)	-9.7 (-12.9)	-10.9 (-16.4)
H	Me	-0.5 (3.7)	-5.1 (-8.2)	-8.3 (-12.0)	-1.0 (3.3)	-8.9 (-11.8)	-10.2 (-14.0)
H	F	-1.6 (2.5)	-6.8 (-10.6)	-9.4 (-12.9)	-0.8 (3.5)	-8.9 (-11.8)	-10.3 (-13.8)
CF ₃	F	-2.7 (1.6)	-7.3 (-11.2)	-10.0 (-14.1)	-2.2 (1.9)	-9.7 (-12.9)	-10.9 (-16.4)
SiR ²							
R ²		φ_{sp}^{Si}				φ_{sp}^{Si}	
H		-5.9 (-8.4)				-3.2 (0.3)	
Me		-5.1 (-7.6)				-2.2 (1.3)	
F		-8.1 (-11.2)				-2.4 (0.1)	
Cp(L) ₂ M [•]							
		φ_{LUMO}^M	φ_{SOMO}^M	HOMO-1		HOMO-2	
M = W							
L = CO		-2.8 (0.6)	-5.3 (-7.9)	-5.7 (-8.2)		-5.8 (-8.0)	
L = PMe ₃		-1.3 (1.5)	-3.2 (-5.2)	-3.6 (-5.9)		-3.9 (-6.1)	
L = PF ₃		-3.2 (0.2)	-5.9 (-8.8)	-6.1 (-9.0)		-6.4 (-9.1)	
M = Mo							
L = CO		-2.5 (0.6)	-5.5 (-8.2)	-5.8 (-8.8)		-6.0 (-8.5)	
L = PMe ₃		-1.1 (1.6)	-3.6 (-6.0)	-3.8 (-6.5)		-3.9 (-6.7)	
L = PF ₃		-2.9 (0.2)	-6.1 (-9.0)	-6.3 (-9.4)		-6.6 (-9.6)	

^a BS-II calculation. DFT and HF energies are presented without and in parenthesis, respectively.

Introduction of electron-donating Me on C2 moderately increases the Mo–C2 distance in **3-Meb** and the Mo–C1 distance in **4-Meb**, but little changes the Si–C1 distance in **3-Meb** and the Mo–Cp distances in **3-Meb** and **4-Meb**; see Figure 1. The similar geometry changes are induced by introduction of bulky ^tBu on C2 except for the Mo–Cp distance which slightly shortens in **3-^tBu** and moderately lengthens in **4-^tBu**; see **3-^tBu** and **4-^tBu** in Figure 1; see Table S2 and page S8 in Supporting Information for populations and explanation. Introduction of electron-withdrawing CF₃ on C2 moderately decreases the Mo–C2 and Mo–Cp distances in **3-CF₃** and the Mo–C1 and Mo–Cp distances in **4-CF₃**. These changes are reversed from those induced by Me and ^tBu, as expected. The Wiberg bond indices are consistent with the geometry changes by the introduction of Me, ^tBu, and CF₃ on C2; see Supporting Information Scheme S1. The introduction of Me on C2 moderately and CF₃ on C2 even more moderately increases the stability of the η^3 -silapropargyl/alkynylsilyl form by 1.4 (1.5) kcal/mol and 0.8 (1.2) kcal/mol, respectively, but the introduction of the bulky ^tBu on C2 slightly decreases the stability of the η^3 -silapropargyl/alkynylsilyl form by 0.3 (0.4) kcal/mol, though both Me and ^tBu on C2 induces similar geometry changes, where values of W and Mo complexes are presented without and with parenthesis, respectively.

The largest stability of the η^3 -silapropargyl/alkynylsilyl form is observed in the combination of Mo center, CF₃ on C2, and F on Si (see Table 2).⁴⁰ However, the largest stability of the acetylide–silylene form is observed in the combination of W center, ^tBu on C2, and either H or Me on Si.

We evaluated equilibrium constant (K_p) between the η^3 -silapropargyl/alkynylsilyl and acetylide–silylene forms to incorporate the entropy and thermal energy in the discussion. Both

of the K_p and ΔE values present the same trend about the relative stability; see Supporting Information Table S5. Thus, we wish to discuss the relative stability based on the ΔE value, hereafter.

Why Does the σ -Electron-Withdrawing/ π -Electron-Donating F on Si Increase the Stability of the η^3 -Silapropargyl/Alkynylsilyl Form but the Electron-Donating Me on Si so Little Influence It? Prior to starting discussion on the reason, we wish to summarize the bonding natures of the η^3 -silapropargyl/alkynylsilyl and acetylide–silylene forms, which were discussed in our previous work.²² Several important molecular orbitals of the η^3 -silapropargyl/alkynylsilyl group are shown in Figure 2A. The SOMO is a nonbonding π orbital ($\varphi_{n\pi}$) which is somewhat localized on Si. The HOMO-1 is a π -bonding orbital (φ_{π^1}) perpendicular to the SiCC plane. The HOMO-2 is in-plane π -bonding orbital (φ_{π^2}). Both are largely localized on the CC moiety. The LUMO is antibonding π^* orbital (φ_{π^*}). In Cp(CO)₂M, the SOMO (φ_{SOMO}^M) mainly consists of a d orbital of M which forms bonding interactions with Cp and CO ligands (Figure 2B). The HOMO-1 and HOMO-2 are nonbonding d orbital of M. The LUMO (φ_{LUMO}^M) mainly consists of d orbital of M. The $\varphi_{n\pi}$ mainly participates in covalent interaction with the φ_{SOMO}^M of Cp(CO)₂M[•] and the φ_{π^2} mainly participates in charge-transfer (CT) interaction with the φ_{SOMO}^M of Cp(CO)₂M[•]. In the acetylide–silylene form, the M-silylene interaction is not very strong because the silylene moiety tends to form silacyclopropenyl group by changing its direction toward the acetylide moiety.²² Though the silacyclopropenyl group is not completely formed,^{22,23} two kinds of CT interactions are strongly formed between acetylide and silylene moieties; one is the CT from the lone pair (φ_{sp}^{Si}) of silylene to the π^* ($\varphi_{\pi^*}^{AC}$) of acetylide and the other is the CT from the π (φ_{π}^{AC}) of acetylide to the empty p (φ_{sp}^{Si}) of silylene (Figure 2, parts C and D).^{22,23}

The introduction of F on Si weakens both CT interactions, as follows: The F substituent lowers the φ_{sp}^{Si} energy of silylene by 2.2 eV through its σ -electron-withdrawing nature, as shown in Table 3, to weaken the CT from silylene to acetylide, where DFT(B3PW91)/BS-II-calculated orbital energies are presented. Also, the F substituent raises the φ_{sp}^{Si} energy of silylene by 0.8

(39) Pople, J. A. et al. *Gaussian 03, Revision C.02*, Gaussian Inc.: Wallingford, CT, 2004. See Reference S1 of Supporting Information for complete reference of Gaussian 03.

(40) Introduction of Me on C2 more increases the stability of the η^3 -silapropargyl/alkynylsilyl form than that of CF₃, when H is bound with Si. However, introduction of CF₃ increases the stability more than that of Me, when F is bound with Si. We could not find the clear reason.

eV through its π -electron-donating nature (see Table 3), which weakens the CT from acetylide to silylene. As a result, the acetylide–silylene interaction is considerably weakened by the introduction of F on Si.

$$\Delta E_{\text{cov}} = \sqrt{(\epsilon_A - \epsilon_B)^2 + 4\beta^2} \quad (1)$$

$$\Delta E_{\text{cov}}^{\text{approx}} = |\epsilon_A - \epsilon_B| + \frac{\beta^2}{|\epsilon_A - \epsilon_B|} \quad (2)$$

The introduction of F on Si, however, strengthens the $\text{M}-(\eta^3\text{-R}_2\text{SiCCR}^1)$ bonding interaction, which is interpreted in terms of the valence orbital energy of the $\eta^3\text{-R}_2\text{SiCCR}^1$ group. As shown in Table 3, the $\varphi_{\text{n}\pi}$ energy of $\cdot\text{R}_2\text{SiCCR}^1$ becomes lower by 0.8 eV by the introduction of F on Si. The $\text{M}-(\eta^3\text{-R}_2\text{SiCCR}^1)$ bond energy was successfully discussed with eqs 1 and 2,^{25,41} where ϵ_A and ϵ_B are orbital energies of SOMOs of two fragments and β is resonance integral. Equation 1 is derived on the basis of simple Hückel MO method and eq 1 is simplified to eq 2 when the $|\epsilon_A - \epsilon_B|$ value is much larger than the $|\beta|$ value. These equations indicate that the A–B bond energy becomes larger as the SOMO energy difference increases when the β value does not change. Note that the β value is also an important factor to determine the bond strength. The β value between $\text{Cp}(\text{CO})_2\text{M}\cdot$ and $\cdot\text{R}_2\text{SiCCR}^1$ depends on the overlap between the valence orbital of $\text{Cp}(\text{CO})_2\text{M}\cdot$ and that of $\cdot\text{R}_2\text{SiCCR}^1$. Because the valence orbital of $\cdot\text{R}_2\text{SiCCR}^1$ is mainly determined by the SiCC flame, it is likely that the β value does not depend very much on the substituents R^1 and R^2 . This suggests that the energy difference between the $\varphi_{\text{SOMO}}^{\text{M}}$ and $\varphi_{\text{n}\pi}$ must be examined as an important factor to discuss how much the bond energy depends on R^1 and R^2 . The $\varphi_{\text{SOMO}}^{\text{M}}$ energy of $\text{Cp}(\text{CO})_2\text{M}\cdot$ is higher than the $\varphi_{\text{n}\pi}$ energy of $\cdot\text{R}_2\text{SiCCR}^1$ (see Table 3). Thus, the $\text{M}-(\eta^3\text{-R}_2\text{SiCCR}^1)$ bond energy becomes larger as the $\varphi_{\text{n}\pi}$ energy of $\cdot\text{R}_2\text{SiCCR}^1$ becomes lower. The σ -electron-withdrawing F on Si lowers the $\varphi_{\text{n}\pi}$ energy of $\cdot\text{R}_2\text{SiCCR}^1$ and increases the energy gap between $\varphi_{\text{n}\pi}$ and $\varphi_{\text{SOMO}}^{\text{M}}$, which leads to strengthening of the $\text{M}-(\eta^3\text{-R}_2\text{SiCCR}^1)$ bonding interaction. From these results, it should be concluded that the F on Si stabilizes the η^3 -silapropargyl/alkynylsilyl form and destabilizes the acetylide–silylene form.

Though both Me and F on Si increase the stability of the η^3 -silapropargyl/alkynylsilyl form, the effect of the Me is considerably smaller than that of the F. The Me on Si raises the $\varphi_{\text{n}\pi}$ energy of $\cdot\text{R}_2\text{SiCCR}^1$ by 0.4 eV, which leads to decrease of the energy difference between SOMOs of $\text{Cp}(\text{CO})_2\text{M}\cdot$ and $\cdot\text{R}_2\text{SiCCR}^1$. Thus, the $\text{M}-(\eta^3\text{-R}_2\text{SiCCR}^1)$ bonding interaction becomes weak by introduction of Me on Si. Also, the Me on Si raises the $\varphi_{\text{Si}}^{\text{ip}}$ and $\varphi_{\text{Si}}^{\text{p}}$ energies of SiMe_2 by 0.8 and 1.0 eV, respectively, relative to those of SiH_2 (Table 3), which strengthens the CT from silylene to acetylide but weakens the CT from acetylide to silylene. It is likely that the CT from acetylide to silylene is more important than the CT from silylene to acetylide because singlet silylene is electron-withdrawing. This suggests that the acetylide–silylene interaction becomes weak by the Me on Si. Thus, the Me on Si weakens both of the $\text{M}-(\eta^3\text{-R}_2\text{SiCCR}^1)$ and acetylide–silylene interactions. As a result, the Me on Si does not influence very much the relative stability of the η^3 -silapropargyl/alkynylsilyl form to the acetylide–silylene form.

Comparison Between W and Mo Centers. We wish to explain the reason why the Mo center favors the η^3 -silapropargyl/alkynylsilyl form but the W center favors the acetylide–silylene form. The $\varphi_{\text{SOMO}}^{\text{M}}$ and doubly occupied d orbitals of $\text{Cp}(\text{CO})_2\text{M}\cdot$ exist at lower energies but the $\varphi_{\text{LUMO}}^{\text{M}}$ (–2.5 eV) exists at higher energy than those of the W analogue, as shown in Table 3. Because the $\varphi_{\text{sp}}^{\text{AC}}$ energy of $\cdot\text{CCR}^1$ is lower than the $\varphi_{\text{SOMO}}^{\text{M}}$ energy of $\text{Cp}(\text{CO})_2\text{M}\cdot$ (Table 3), the SOMO energy difference is larger in the W complex (5.0 eV) than in the Mo complex (4.8 eV). Because, the $\varphi_{\text{n}\pi}$ energy of $\cdot\text{R}_2\text{SiCCR}^1$ is lower than the $\varphi_{\text{SOMO}}^{\text{M}}$ energy of $\text{Cp}(\text{CO})_2\text{M}\cdot$ (Table 3), the SOMO energy difference between $\cdot\text{R}_2\text{SiCCR}^1$ and $\text{Cp}(\text{CO})_2\text{M}\cdot$ is larger in the W complex (0.7 eV) than in the Mo complex (0.5 eV). Moreover, the second term of eq 1 more contributes to the M–L bond energy in the third row transition metal complex than in the second row transition metal complex, because the $|\beta|$ value becomes larger upon going from the second row transition metal to the third row one. As a result, the W–C1 and W–($\eta^3\text{-R}_2\text{SiCCR}^1$) bonding interactions are stronger than the Mo–C1 and Mo–($\eta^3\text{-R}_2\text{SiCCR}^1$) bonding interactions, respectively. In the η^3 -silapropargyl/alkynylsilyl form, not only the covalent M–($\eta^3\text{-R}_2\text{SiCCR}^1$) interaction but also the charge-transfer (CT) from the φ_{π^2} of $\cdot\text{R}_2\text{SiCCR}^1$ to the $\varphi_{\text{LUMO}}^{\text{M}}$ of $\text{Cp}(\text{CO})_2\text{M}\cdot$ participates in energy stabilization. Because the φ_{π^2} of $\cdot\text{R}_2\text{SiCCR}^1$ is largely localized in the CC moiety (see Figure 2A), the M–(CC) interaction is formed by this CT. Because the $\varphi_{\text{LUMO}}^{\text{M}}$ energy of $\text{Cp}(\text{CO})_2\text{W}\cdot$ (–2.8 eV) is lower than that of $\text{Cp}(\text{CO})_2\text{Mo}\cdot$ (–2.5 eV), this CT interaction is stronger in the W complex than in the Mo complex. Thus, both of the M–CCR¹ and M–($\eta^3\text{-R}_2\text{SiCCR}^1$) bonding interactions are stronger in the W complex than in the Mo complex. The above simple discussion does not present the clear explanation, and therefore, we must inspect the bonding interaction in more detail.

It is noted that the $\varphi_{\text{sp}}^{\text{AC}}$ energy of $\cdot\text{CCR}^1$ is much lower than the $\varphi_{\text{n}\pi}$ energy of $\cdot\text{R}_2\text{SiCCR}^1$ by 4.3 eV (Table 3); in other words, the SOMO energy difference between $\cdot\text{CCR}^1$ and $\text{Cp}(\text{CO})_2\text{M}\cdot$ is much larger than that between $\cdot\text{R}_2\text{SiCCR}^1$ and $\text{Cp}(\text{CO})_2\text{M}\cdot$. Thus, the M–CCR¹ bond energy increases upon going from Mo to W because the $\varphi_{\text{SOMO}}^{\text{M}}$ energy of $\text{Cp}(\text{CO})_2\text{W}\cdot$ (–5.3 eV) is higher than that of $\text{Cp}(\text{CO})_2\text{Mo}\cdot$ (–5.5 eV), and its increment is almost proportional to the SOMO energy difference between $\text{Cp}(\text{CO})_2\text{M}\cdot$ and $\cdot\text{CCR}^1$, as presented by eq 2. Alternatively, the M–($\eta^3\text{-R}_2\text{SiCCR}^1$) bond energy increases upon going from Mo to W to a lesser extent than the increment of the SOMO energy difference between $\text{Cp}(\text{CO})_2\text{M}\cdot$ and $\cdot\text{R}_2\text{SiCCR}^1$. In this case, the second term of eq 1 more contributes to the M–($\eta^3\text{-R}_2\text{SiCCR}^1$) bond energy than the M–CCR¹ bond energy. In other words, the M–CCR¹ bond energy increases upon going from Mo to W to a greater extent than does the M–($\eta^3\text{-R}_2\text{SiCCR}^1$) bond energy. This means that the Mo center is more favorable for stabilization of the η^3 -silapropargyl/alkynylsilyl form than the W center.

Why Do Me, 'Bu, and CF₃ on C Influence the Relative Stability of the η^3 -Silapropargyl/Alkynylsilyl Form to the Acetylide–Silylene Form? The frontier orbital energies of $\cdot\text{CCR}^1$ and $\cdot\text{R}_2\text{SiCCR}^1$ become higher by introduction of Me on C2 (see Table 3), which leads to decrease of the energy difference between their valence orbitals and the $\varphi_{\text{SOMO}}^{\text{M}}$ of $\text{Cp}(\text{CO})_2\text{M}\cdot$. However, the frontier orbital energies of $\cdot\text{CCR}^1$ and $\cdot\text{R}_2\text{SiCCR}^1$ become lower by introduction of CF₃ on C2, which leads to increase of the energy difference between their valence orbitals and the $\varphi_{\text{SOMO}}^{\text{M}}$ of $\text{Cp}(\text{CO})_2\text{M}\cdot$. Thus, Me on C2 weakens both M–CCR¹ and M–($\eta^3\text{-R}_2\text{SiCCR}^1$) bonds but

(41) (a) Sakaki, S.; Biswas, B.; Sugimoto, M. *Organometallics* **1998**, *17*, 1278. (b) Biswas, B.; Sugimoto, M.; Sakaki, S. *Organometallics* **1999**, *18*, 4015. (c) Sakaki, S.; Kai, S.; Sugimoto, M. *Organometallics* **1999**, *18*, 4825. (d) Sumimoto, M.; Iwane, N.; Takahama, T.; Sakaki, S. *J. Am. Chem. Soc.* **2004**, *126*, 10457.

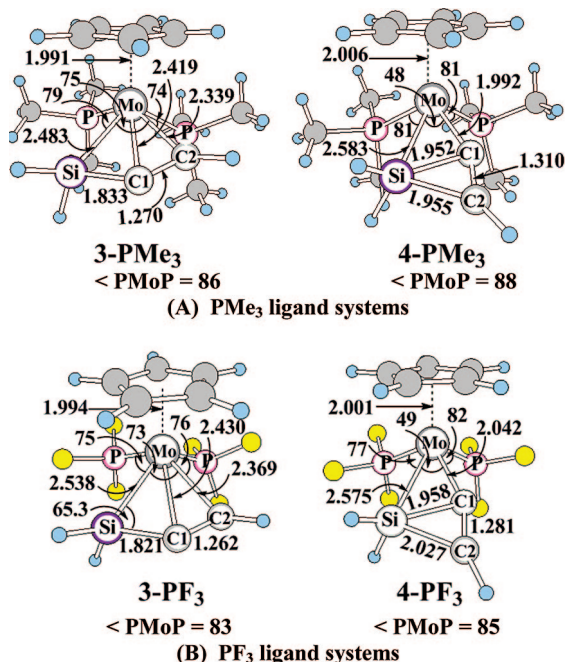


Figure 3. DFT(B3PW91)/BS-I optimized geometries of $\text{CpL}_2\text{Mo}(\eta^3\text{-H}_2\text{SiCCH})$ and $\text{CpL}_2\text{Mo}(\text{CCH})(\text{SiH}_2)$, where $L = \text{PMe}_3$ or PF_3 . See Supporting Information Figure S3 for geometries of the tungsten analogues. Bond lengths are in angstroms and bond angles are in degrees.

CF_3 on C2 strengthens both of them. As a result, Me and CF_3 do not change the relative stability of the η^3 -silapropargyl/alkynylsilyl form very much. We could not find a clear reason why the Me on C2 moderately and the CF_3 on C2 even more moderately increase the stability of the η^3 -silapropargyl/alkynylsilyl form.⁴²

Though the electronic effects are similar between Me and $t\text{Bu}$ (Table 3), they induce the reverse effect on the stability of the η^3 -silapropargyl/alkynylsilyl form (Table 2), as discussed above, indicating that not the electronic factor but the steric factor plays important role here. It is likely that the bulky substituent on C2 tends to take a more distant position from the Cp. Thus, the bulky substituent such as $t\text{Bu}$ prefers the acetylide-silylene form to the η^3 -silapropargyl/alkynylsilyl form, because the $t\text{Bu}$ on C2 is more distant from the Cp in the acetylide-silylene form than in the η^3 -silapropargyl/alkynylsilyl form.

Ligand Effects on Geometries and Relative Stabilities of $\text{CpL}_2\text{M}(\eta^3\text{-H}_2\text{SiCCH})$ and $\text{CpL}_2\text{M}(\text{CCH})(\text{SiH}_2)$ ($M = \text{W}$ or Mo and $L = \text{CO}$, PMe_3 , or PF_3). Use of electron-donating PMe_3 in place of CO moderately decreases the Mo-Si, Mo-C1, and Mo-C2 distances and even more moderately the Mo-Cp distance in **3- PMe_3** and moderately decreases the Mo-C1 and Si-C2 distances in **4- PMe_3** (Figure 3). These results suggest that the $\text{M}-(\eta^3\text{-R}_2\text{SiCCR}^1)$ bond becomes stronger in **3- PMe_3** than in **3** and the Mo-CCR¹ bond and the acetylide-silylene interaction become stronger in **4- PMe_3** than in **4**. Electron-withdrawing PF_3 induces opposite geometry changes to those

of PMe_3 except for the Mo-C1 distance in **3- PF_3** , as follows: Use of PF_3 in place of CO moderately increases the Mo-Si distance but moderately decreases the Mo-C1 and Mo-Cp distances in **3- PF_3** , whereas it moderately increases the Mo-C1 and Si-C2 distances and moderately decreases the Mo-Cp distance in **4- PF_3** ; see Supporting Information page S8 for the discussion of the M-Cp distance. These results suggest that the $\text{M}-(\eta^3\text{-R}_2\text{SiCCR}^1)$ bond becomes moderately weaker in **3- PF_3** than in **3** and the Mo-CCR¹ bond and the acetylide-silylene interaction become moderately weaker in **4- PF_3** than in **4**. These suggestions are also supported by the Wiberg bond index; see Supporting Information Scheme S1.

PMe_3 considerably decreases the stability of the η^3 -silapropargyl/alkynylsilyl form by 9.4 and 4.8 kcal/mol in the W and Mo complexes, respectively, as shown in Table 2, and PF_3 slightly decreases it in both W and Mo complexes, in contrast to the opposite geometry changes to those of PMe_3 .

PMe_3 considerably destabilizes the $\varphi_{\text{SOMO}}^{\text{M}}$ energy of $\text{CpL}_2\text{M}\cdot$ ($M = \text{W}$ or Mo ; $L = \text{CO}$, PMe_3 , or PF_3) by about 2.0 eV compared to CO (Table 3). However, PF_3 moderately stabilizes the $\varphi_{\text{SOMO}}^{\text{M}}$ energy by 0.6 eV. Though PMe_3 and PF_3 induce opposite electronic effects to each other, both of them increase the stability of the acetylide-silylene form. This result suggests that not electronic factor but steric factor plays important role here, as follows: Because PF_3 and PMe_3 are larger than CO, the coordination structure around metal center becomes more congested by coordination of PMe_3 and PF_3 . Also, the coordination structure of the η^3 -silapropargyl/alkynylsilyl complex is more congested than that of the acetylide-silylene complex; for instance, the SiMC2 angle is about 75° in the η^3 -silapropargyl/alkynylsilyl form but the SiMC1 angle is about 50° in the acetylide-silylene form. Thus, PF_3 and PMe_3 prefer the less congested acetylide-silylene form.

From these results, it is concluded that among these three ligands, CO should be used to stabilize the η^3 -silapropargyl/alkynylsilyl form and PMe_3 should be used to stabilize the acetylide-silylene form.

Conversion Reaction of $\text{Cp}(\text{CO})_2\text{Mo}(\eta^3\text{-H}_2\text{SiCCH})$ to $\text{Cp}(\text{CO})_2\text{Mo}(\text{CCH})(\text{SiH}_2)$. We wish to mention the conversion reaction of $\text{Cp}(\text{CO})_2\text{Mo}(\eta^3\text{-H}_2\text{SiCCH})$ **3** to $\text{Cp}(\text{CO})_2\text{Mo}(\text{CCH})(\text{SiH}_2)$ **4** because the experimental conditions to isolate **3** depend on the activation barrier of this conversion reaction. This reaction occurs through the transition state **TS₃₋₄**, as shown in Figure 4. In **TS₃₋₄**, the Si-C1 and Mo-C2 bonds of **3** are going to be broken like those of the tungsten analogue.²² The geometry changes in the imaginary frequency, which are displayed by arrows in Figure 4, are consistent with this conversion reaction.

The CCSD(T) and DFT methods present similar activation barrier (E_a) but the MP4(SDTQ) method presents larger barrier than the CCSD(T) and DFT methods (see Supporting Information Table S6). The barrier moderately fluctuates around MP2 and MP3, and somewhat increases upon going to MP4(SDTQ) from MP4(SDQ). Thus, it is concluded that the DFT- and CCSD(T)-calculated activation barriers are reliable for both W and Mo complexes. The activation barrier of the conversion reaction of **3** to **4** is 13.2 (14.1) kcal/mol, where values without parenthesis and with parenthesis are DFT- and CCSD(T)-calculated E_a values, respectively. This activation barrier is moderately smaller than that of the tungsten complex, which is 15.3 (15.8) kcal/mol.²² This difference is interpreted in terms of the $\text{M}-(\eta^3\text{-R}_2\text{SiCCR}^1)$ bond, as follows: In the transition state, the Si-C1 bond is being broken and the C2 is moving away from the Mo center, as shown in Figure 4. The origin of

(42) The small energy gap between the frontier orbital of $\text{Cp}(\text{CO})_2\text{M}\cdot$ and those of $\cdot\text{CCR}^1$ and $\cdot\text{R}_2\text{SiCCR}^1$ leads to the large stability of the η^3 -silapropargyl/alkynylsilyl form; see discussion of Mo and W centers. Thus, Me on C2 increases the stability of the η^3 -silapropargyl/alkynylsilyl form. However, CF_3 on C2 moderately increases the stability of the η^3 -silapropargyl/alkynylsilyl form, against the above expectation. It is likely that the CT from acetylide to silylene becomes weak by CF_3 on C2, which moderately increases the stability of the η^3 -silapropargyl/alkynylsilyl form.

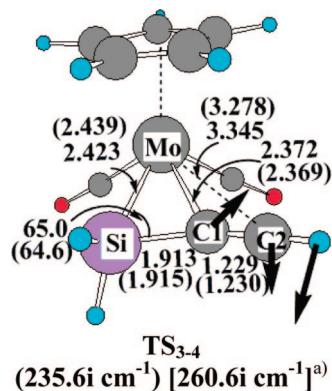


Figure 4. DFT(B3PW91)/BS-I optimized geometry of transition state in conversion reaction of $\text{Cp}(\text{CO})_2\text{Mo}(\eta^3\text{-H}_2\text{SiCCH})$ **3** to $\text{Cp}(\text{CO})_2\text{Mo}(\text{CCH})(\text{SiH}_2)$ **4**. Bond lengths are in angstroms and bond angles are in degrees. In parentheses are parameters for tungsten analogue. (a) Imaginary frequencies for molybdenum and tungsten analogues are given in parenthesis and bracket, respectively. Arrows represent important movement of atoms in imaginary frequency.

the activation barrier is the weakening of the Si–C1 bond and the Mo–(C1–C2) coordinate bond. Because the Si–C1 bond weakening occurs in both W and Mo complexes, the difference in E_a between W and Mo complexes arises from the weakening of the M–(C1–C2) coordinate bond. Because the φ_π of $\cdot\text{R}^2\text{SiCCR}^1$ is largely localized on the C1C2 moiety (Figure 2), as discussed above, the C1C2 moiety forms the CT with the $\varphi_{\text{LUMO}}^{\text{M}}$ of $\text{Cp}(\text{CO})_2\text{M}\cdot$. The Mo–(C1–C2) coordinate bond is moderately weaker than the W–(C1–C2) bond because the $\varphi_{\text{LUMO}}^{\text{M}}$ energy of $\text{Cp}(\text{CO})_2\text{M}\cdot$ (–2.5 eV) is higher than that of the W analogue (–2.8 eV). As a result, the Mo–C2 bond breaking induces smaller energy loss than the W–C2 bond breaking in the transition state.

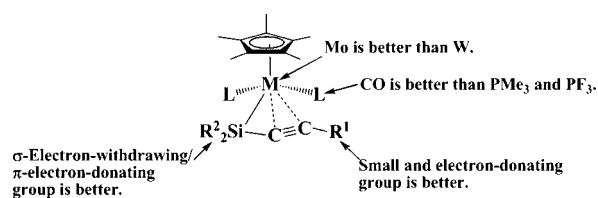
These moderate activation barriers suggest that the isolation of the η^3 -silapropargyl/alkynylsilyl form should be tried at low temperature in both of Mo and W complexes.

Conclusions

The relative stability of the η^3 -silapropargyl/alkynylsilyl complex $\text{CpL}_2\text{M}(\eta^3\text{-R}^2\text{SiCCR}^1)$ (**1** for M = W and **3** for M = Mo; L = CO, PMe_3 , or PF_3 ; Cp = C_5H_5 , R^1 = H, Me, $t\text{Bu}$, or CF_3 , R^2 = H, Me, or F) to the acetylide–silylene complex $\text{CpL}_2\text{M}(\text{CCR}^1)(\text{SiR}^2_2)$ (**2** for M = W and **4** for M = Mo) was theoretically investigated. Computational results are summarized in Scheme 2. From these computational results, we wish to predict that the combination of electron-withdrawing CF_3 on C, σ -electron-withdrawing/ π -electron-donating F on Si, Mo center, and CO is the best to stabilize the η^3 -silapropargyl/alkynylsilyl form and the combination of bulky $t\text{Bu}$ on C, either H or Me on Si, W center, and PMe_3 is the best to stabilize the acetylide–silylene form.

The conversion reaction of $\text{Cp}(\text{CO})_2\text{Mo}(\eta^3\text{-H}_2\text{SiCCH})$ **3** to $\text{Cp}(\text{CO})_2\text{Mo}(\text{CCH})(\text{SiH}_2)$ **4** occurs with moderate activation

Scheme 2. How to Stabilize $\text{CpL}_2\text{M}(\eta^3\text{-R}^2\text{SiCCR}^1)$



barrier, suggesting that the isolation of the η^3 -silapropargyl/alkynylsilyl form should be tried at low temperature.

From this theoretical study, we wish to predict that the synthesis of the η^3 -silapropargyl/alkynylsilyl complex will succeed in the near future by employing Mo as the metal center with Cp and CO ligands and introducing σ -electron-withdrawing/ σ -electron-donating group on Si and σ -electron-withdrawing group on C.⁴³

Acknowledgment. This work was financially supported by Grant-in-Aids on basic research (No. 1835005), Priority Areas for “Molecular Theory for Real Systems” (No. 461), and NAREGI project from the Ministry of Education, Science, Sports, and Culture. Some of theoretical calculations were performed with SGI workstations of Institute for Molecular Science (Okazaki, Japan).

Supporting Information Available: The complete reference of Gaussian 03 (1 page). DFT/BS-I optimized geometries of $\text{Cp}(\text{CO})_2\text{W}(\eta^3\text{-R}^2\text{SiCCR}^1)$ and $\text{Cp}(\text{CO})_2\text{W}(\text{CCR}^1)(\text{SiR}^2_2)$, where R^1 = H, Me, $t\text{Bu}$, or CF_3 , and R^2 = H, F, or Me (1 page). DFT/BS-I optimized geometries of $\text{Cp}^*(\text{CO})_2\text{M}(\eta^3\text{-H}_2\text{SiCCH})$ and $\text{Cp}^*(\text{CO})_2\text{M}(\text{CCH})(\text{SiH}_2)$, where M = W or Mo (1 page). DFT/BS-I optimized geometries of $\text{CpL}_2\text{W}(\eta^3\text{-H}_2\text{SiCCH})$ and $\text{CpL}_2\text{W}(\text{CCH})(\text{SiH}_2)$, where L = PMe_3 or PF_3 (1 page). Effects of functional on the structural parameters of $\text{Cp}(\text{CO})_2\text{W}(\text{CC}^t\text{Bu})(\text{SiH}_2)$ **2- $t\text{Bu}$** (1 page). Natural population of Cp and M in $\text{Cp}(\text{CO})_2\text{M}(\eta^3\text{-R}^2\text{SiCCR}^1)$ and $\text{Cp}(\text{CO})_2\text{M}(\text{CCR}^1)(\text{SiR}^2_2)$ (1 page). Wiberg bond indices in $\text{CpL}_2\text{M}(\eta^3\text{-R}^2\text{SiCCR}^1)$ and $\text{CpL}_2\text{M}(\text{CCR}^1)(\text{SiR}^2_2)$ (2 page). The DFT/BS-I and DFT/BS-III calculated reaction energy in conversion reaction of $\text{Cp}(\text{CO})_2\text{M}(\eta^3\text{-R}^2\text{SiCCR}^1)$ to $\text{Cp}(\text{CO})_2\text{M}(\text{CCR}^1)(\text{SiR}^2_2)$ (1 page). The DFT/BS-II calculated free energy change (ΔG), equilibrium constant (K_p) in conversion reaction of $\text{Cp}(\text{CO})_2\text{M}(\eta^3\text{-R}^2\text{SiCCR}^1)$ to $\text{Cp}(\text{CO})_2\text{M}(\text{CCR}^1)(\text{SiR}^2_2)$ and discussion (2 pages). Activation barrier calculated with different computational methods in conversion reaction of $\text{Cp}(\text{CO})_2\text{M}(\eta^3\text{-H}_2\text{SiCCH})$ to $\text{Cp}(\text{CO})_2\text{M}(\text{CCH})(\text{SiH}_2)$ (1 page). Cartesian coordinates and total energies of important species including transition states (11 pages). This material is available free of charge via the Internet at <http://pubs.acs.org>.

OM8006163

(43) In the synthesis of $\text{Cp}^*(\text{CO})_2\text{W}(\text{CC}^t\text{Bu})(\text{SiPh}_2)$, NMR spectra indicate that at low temperature several monomeric species are equilibrated with a dimer complex $[\text{Cp}^*(\text{CO})_2\text{W}(\text{Me}_2\text{SiCC}^t\text{Bu})]_2$. $\text{Cp}^*(\text{CO})_2\text{W}(\eta^3\text{-Me}_2\text{SiCC}^t\text{Bu})$ is one of the plausible candidates of such monomeric species. This result strongly suggests that the η^3 -silapropargyl/alkynylsilyl form can be synthesized by reasonable choices of metal center and substituents. See footnote 4 of ref 21.

Probing the Dynamics and Reactivity of a Stereochemically Nonrigid Cp*Ru(H)(κ^2 -P,Carbene) Complex

Matthew A. Rankin,[†] Darren F. MacLean,[†] Robert McDonald,[‡] Michael J. Ferguson,[‡] Michael D. Lumsden,^{†,§} and Mark Stradiotto^{*,†}

Department of Chemistry, Dalhousie University, Halifax, Nova Scotia, Canada B3H 4J3, X-Ray Crystallography Laboratory, Department of Chemistry, University of Alberta, Edmonton, Alberta, Canada T6G 2G2, and Atlantic Region Magnetic Resonance Center, Dalhousie University, Halifax, Nova Scotia, Canada B3H 4J3

Received August 6, 2008

The ability of the coordinatively saturated, 18-electron Cp*(H)Ru=CHR complex **1** to serve as a masked source of the coordinatively unsaturated Cp*Ru-CH₂R species **2** via reversible α -hydride elimination was surveyed. The rate constant for this dynamic process (300 K, C₆D₆) was measured to be $59 \pm 1 \text{ s}^{-1}$, on the basis of data obtained from selective inversion NMR experiments. Exposure of **1** to an atmosphere of CO or to an equivalent of either PMe₃ or PH₂Ph afforded the corresponding **2**·L adduct (L = CO, 98%; PMe₃, 93%; PH₂Ph, 67%). Treatment of **1** with Ph₂SiH₂, PhSiH₃, Ph₂SiClH, or PhSiClH₂ afforded the corresponding net Si–H addition product, **3a–d** (82–94%); an NMR spectroscopic investigation of the analogous reaction of **1** with Ph₂SiD₂ provided evidence in support of a reaction mechanism involving previously undocumented Si–H addition across the Ru=C unit in **1** in the formation of **3a**. Addition of Jutzi's acid (H(OEt)₂B(C₆F₅)₄) to **1** resulted in the quantitative formation of **4** (the N-C-H cyclometalated variant of [Cp*Ru(κ^2 -2-NMe₂-3-P'Pr₂-indene)]⁺B(C₆F₅)₄[−]). In monitoring the progress of the reaction of **1** with excess catecholborane (HBcat), evidence for the formation of the B–H addition product **5i** was obtained en route to the isolable (Bcat)Ru=C species (**5**, 54%). Conversely, no intermediates were observed in the reaction of **1** with mesitylborane (MesBH₂) leading to the Cp*Ru(P,N) complex **6** (81%), which features a tethered borane fragment and a Ru–H–B bridge. Crystallographic characterization data are provided for **2**·PMe₃, **3a**, **3b**, **3d**, **5**, and **6**.

Introduction

Coordinatively unsaturated (η^5 -C₅R₅)RuL_{*n*} (η^5 -C₅H₅ = Cp; η^5 -C₅Me₅ = Cp*) complexes represent appealing targets of inquiry, owing to their unique reactivity properties.¹ Significant research effort continues to be directed toward documenting the stoichiometric reactivity of these and other coordinatively unsaturated complexes, both as a means of augmenting our understanding of the substrate transformations that can occur within the coordination sphere of (η^5 -C₅R₅)RuL_{*n*} species and as an initial step toward the development of new metal-catalyzed reactivity.^{1i,2} In this context, one facet of our research program is focused on the synthesis and reactivity of Cp*Ru complexes derived from donor-substituted indene ligands.³ We have reported previously on our efforts to prepare the formally

zwitterionic, coordinatively unsaturated species Cp*Ru(κ^2 -3-P'Pr₂-2-NMe₂-indenide); in the absence of additional coligands, this zwitterion rapidly rearranges to the Cp*Ru(H)(κ^2 -P,C) hydridocarbene complex **1** via double geminal C–H bond activation involving a ligand NMe group.^{3f,g} Notably, a spectroscopic investigation of **1** employing 1D- and 2D-EXSY NMR techniques provided evidence for the first documented interconversion of Ru(H)=CH (in **1**) and Ru–CH₂ (in the unobserved intermediate **2**) fragments by way of reversible α -hydride elimination (Scheme 1).^{3g,4} Further indirect support for the viability of **2** was obtained via isolation of the adduct **2**·P_hPh₂ upon treatment of **1** with P_hPh₂. Intrigued by these preliminary observations, we became interested in obtaining rate data for this reversible α -hydride elimination process, as well as in exploring further the extent to which the intermediate **2** might play a role in the chemistry observed for the stereochemically

* To whom correspondence should be addressed. Fax: 1-902-494-1310. Tel: 1-902-494-7190. E-mail: mark.stradiotto@dal.ca.

[†] Department of Chemistry, Dalhousie University.

[‡] University of Alberta.

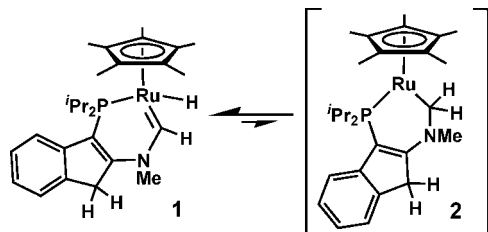
[§] Atlantic Region Magnetic Resonance Center, Dalhousie University.

(1) For selected recent reports and reviews, see: (a) Ito, M.; Ikariya, T. *Chem. Commun.* **2007**, 5134. (b) Ito, M.; Sakaguchi, A.; Kobayashi, C.; Ikariya, T. *J. Am. Chem. Soc.* **2007**, *129*, 290. (c) Palacios, M. D.; Puerta, M. C.; Valerga, P.; Lledós, A.; Veilly, E. *Inorg. Chem.* **2007**, *46*, 6958. (d) Ikariya, T.; Murata, K.; Noyori, R. *Org. Biomol. Chem.* **2006**, *4*, 393. (e) Bruneau, C.; Renaud, J.-L.; Demerseman, B. *Chem.–Eur. J.* **2006**, *12*, 5178. (f) Trost, B. M.; Frederiksen, M. U.; Rudd, M. T. *Angew. Chem., Int. Ed.* **2005**, *44*, 6630. (g) Jiménez-Tenorio, M.; Puerta, M. C.; Valerga, P. *Eur. J. Inorg. Chem.* **2004**, 17. (h) Nagashima, H.; Kondo, H.; Hayashida, T.; Yamaguchi, Y.; Gondo, M.; Masuda, S.; Miyazaki, K.; Matsubara, K.; Kirchner, K. *Coord. Chem. Rev.* **2003**, *245*, 177. (i) Glaser, P. B.; Tilley, T. D. *J. Am. Chem. Soc.* **2003**, *125*, 13640. (j) Davies, S. G.; McNally, J. P.; Smallridge, A. J. *Adv. Inorg. Chem.* **1990**, *30*, 1.

(2) For some prominent examples featuring alternative Ru complexes, see: (a) Gunanathan, C.; Ben-David, Y.; Milstein, D. *Science* **2007**, *317*, 790. (b) Grubbs, R. H. *Angew. Chem., Int. Ed.* **2006**, *45*, 3760. (c) Chauvin, Y. *Angew. Chem., Int. Ed.* **2006**, *45*, 3741. (d) Noyori, R. *Angew. Chem., Int. Ed.* **2002**, *41*, 2008.

(3) (a) Rankin, M. A.; Hesp, K. D.; Schatte, G.; McDonald, R.; Stradiotto, M. *Chem. Commun.* **2008**, 250. (b) Lundgren, R. J.; Rankin, M. A.; McDonald, R.; Stradiotto, M. *Organometallics* **2008**, *27*, 254. (c) Rankin, M. A.; MacLean, D. F.; Schatte, G.; McDonald, R.; Stradiotto, M. *J. Am. Chem. Soc.* **2007**, *129*, 15855. (d) Rankin, M. A.; Schatte, G.; McDonald, R.; Stradiotto, M. *J. Am. Chem. Soc.* **2007**, *129*, 6390. (e) Lundgren, R. J.; Rankin, M. A.; McDonald, R.; Schatte, G.; Stradiotto, M. *Angew. Chem., Int. Ed.* **2007**, *46*, 4732. (f) Rankin, M. A.; McDonald, R.; Ferguson, M. J.; Stradiotto, M. *Organometallics* **2005**, *24*, 4981. (g) Rankin, M. A.; McDonald, R.; Ferguson, M. J.; Stradiotto, M. *Angew. Chem., Int. Ed.* **2005**, *44*, 3603.

Scheme 1. Interconversion of 1 and 2 via Reversible α -Hydride Elimination



nonrigid 18-electron complex **1**. Herein we report on the results of these investigations, including studies documenting the reactivity of **1** with L-donor (L = CO, PR₃) and E-H (E = B, Si, P) containing substrates.

Results and Discussion

Selective Inversion NMR Experiments. Well-documented reversible α -hydride elimination phenomena involving alkyl-metal species are rare in comparison to analogous β -hydride elimination reactions,^{4,5} and to the best of our knowledge the interconversion of **1** and **2** represents the only spectroscopically characterized reversible α -hydride elimination process involving ruthenium. Expanding on our previous qualitative examination of this chemical exchange process by use of 1D- and 2D-EXSY ¹H NMR experiments,^{3f,g} we turned our attention to obtaining quantitative rate data. The rate constant for exchange of the Ru(H)=CH and Ru(H)=CH environments in **1** ($59 \pm 1 \text{ s}^{-1}$, 300 K) was measured by use of selective inversion ¹H NMR techniques, employing the program CIFIT for data analysis.⁶ This rate can be compared with α -hydride elimination rates reported by Schrock and co-workers^{5b} for molybdenum complexes (10^2 – 10^3 s^{-1} , ca. 295 K), as well as Threlkel and Bercaw^{5c} for a niobium complex (15.7 s^{-1} , 305 K).

Reactions with L-Donor Substrates. Exposure of **1** to either an atmosphere of CO or an equivalent of PMe₃ resulted in the quantitative (³¹P NMR) conversion to **2**·CO or **2**·PMe₃ in 98% and 93% isolated yield, respectively (Scheme 2). Solution NMR data fully support the structural formulation provided for these complexes, and in the case of **2**·PMe₃, the connectivity was confirmed on the basis of data obtained from a single-crystal X-ray diffraction study. An ORTEP diagram of **2**·PMe₃ is presented in Figure 1, while crystallographic data and selected interatomic distances for each of the crystallographically characterized compounds reported herein are collected in Tables 1 and 2, respectively. In keeping with **2**·PPh₂, the Ru–CN

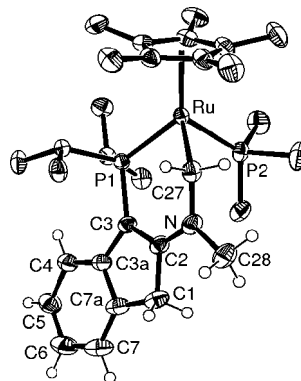
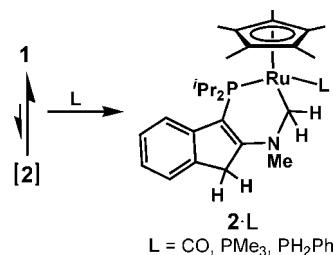


Figure 1. ORTEP diagram for **2**·PMe₃, shown with 50% displacement ellipsoids and with the atomic numbering scheme depicted; selected H-atoms have been omitted for clarity.

Scheme 2. Reactions Involving 1 and CO, PMe₃, and PH₂Ph



(2.118(2) Å) and RuC–N (1.477(2) Å) distances in **2**·PMe₃ are lengthened significantly relative to those found in **1** (1.886(2) and 1.374(3) Å),^{3f,g} thereby supporting the description of **2**·PMe₃ as being a base-stabilized adduct of the purported alkylruthenium intermediate, **2**. The planarity at nitrogen ($\sum \text{angles at N} = 358.5^\circ$) and the contracted N–C2 distance (1.347(2) Å) in **2**·PMe₃ are indicative of π -conjugation involving the nitrogen lone pair and the adjacent indene fragment. The apparent reactivity of **2** with CO differs from that of a related cyclometalated L_nRu(H)=CHR complex reported by Caulton and co-workers,⁷ for which uptake of 2 equiv of CO is observed to give the corresponding L_n(CO)Ru(CO)-CH₂R complex. Efforts to prepare related **2**·L adducts by using PPh₃, 4-dimethylaminopyridine, PhCN, MeCN, PhNH₂, acetone, or benzophenone at ambient temperature resulted in the incomplete consumption of **1** (³¹P NMR), while heating of these reaction mixtures (60 °C) led to decomposition.

Given the apparent propensity of **1** (and/or **2**) for E–H bond activation (*vide infra*), we turned our attention to phosphine substrates featuring P–H substituents. In an effort to probe possible P–H bond activation processes in the previously reported adduct **2**·PPh₂,^{3f,g} we prepared **2**·PDPPh₂ and periodically monitored the position of the isotopic label by use of ¹H and ²H NMR methods. However, after 96 h in benzene or C₆D₆, no scrambling of the deuterium label was noted. Furthermore, no P–H bond activation chemistry was observed upon treatment of **1** with an equivalent of PH₂Ph; quantitative formation of **2**·PH₂Ph was observed (³¹P NMR), and in turn this complex was isolated as an analytically pure solid in 67% yield (Scheme 2).

(4) For recent discussions of M-alkyl/M-alkylidene and related equilibria in late metal chemistry, see: (a) Álvarez, E.; Paneque, M.; Petronilho, A. G.; Poveda, M. L.; Santos, L. L.; Carmona, E.; Mereiter, K. *Organometallics* **2007**, *26*, 1231. (b) Kuznetsov, V. F.; Abdur-Rashid, K.; Lough, A. J.; Gusev, D. G. *J. Am. Chem. Soc.* **2006**, *128*, 14388. (c) Salem, H.; Ben-David, Y.; Shimon, L. J. W.; Milstein, D. *Organometallics* **2006**, *25*, 2292. (d) Clot, E.; Chen, J.; Lee, D.-H.; Sung, S. Y.; Appelhans, L. N.; Faller, J. W.; Crabtree, R. H.; Eisenstein, O. *J. Am. Chem. Soc.* **2004**, *126*, 8795. (e) Carmona, E.; Paneque, M.; Poveda, M. L. *Dalton Trans.* **2003**, 4022. (f) Caulton, K. G. *J. Organomet. Chem.* **2001**, *617*–618, 56.

(5) Reports providing quantitative rate data for reversible α -hydride elimination processes are scarce: (a) Morton, L. A.; Wang, R.; Yu, X.; Campana, C. F.; Guzei, I. A.; Yap, G. P. A.; Xue, Z.-L. *Organometallics* **2006**, *25*, 427. (b) Schrock, R. R.; Seidel, S. W.; Mösch-Zanetti, N. C.; Shih, K.-Y.; O'Donoghue, M. B.; Davis, W. M.; Reiff, W. M. *J. Am. Chem. Soc.* **1997**, *119*, 11876. (c) Threlkel, R. S.; Bercaw, J. E. *J. Am. Chem. Soc.* **1981**, *103*, 2650.

(6) (a) Bain, A. D. *Prog. Nucl. Magn. Reson.* **2003**, *43*, 63. (b) Bain, A. D.; Cramer, J. A. *J. Magn. Res. A* **1996**, *118*, 21. (c) Bain, A. D.; Cramer, J. A. *J. Magn. Res. A* **1993**, *103*, 217. (d) Bain, A. D.; Cramer, J. A. *J. Phys. Chem.* **1993**, *97*, 2884.

(7) Ingleson, M. J.; Yang, X.; Pink, M.; Caulton, K. G. *J. Am. Chem. Soc.* **2005**, *127*, 10846.

Table 1. Crystallographic Data for 2·PMe₃, 3a, 3b, 3d, 5, and 6

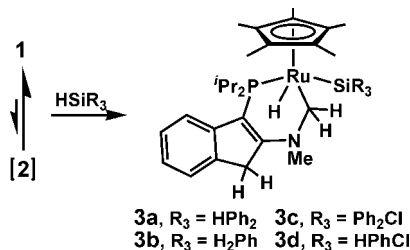
	2·PMe ₃	3a	3b	3d	5	6
empirical formula	C ₃₀ H ₄₉ N ₁ P ₂ Ru ₁	C ₃₉ H ₅₂ N ₁ P ₁ Si ₁ Ru ₁	C ₃₃ H ₄₈ N ₁ P ₁ Si ₁ Ru ₁	C ₃₃ H ₄₇ Cl ₁ N ₁ P ₁ Si ₁ Ru ₁	C ₃₃ H ₄₃ B ₁ N ₁ O ₂ P ₁ Ru ₁	C ₃₆ H ₅₃ B ₁ N ₁ P ₁ Ru ₁
fw	586.71	694.95	617.85	653.30	628.53	642.64
cryst dimens	0.62 × 0.57 × 0.40	0.32 × 0.22 × 0.03	0.35 × 0.33 × 0.13	0.38 × 0.28 × 0.28	0.53 × 0.16 × 0.15	0.52 × 0.39 × 0.08
cryst syst	monoclinic	monoclinic	triclinic	monoclinic	triclinic	monoclinic
space group	P2 ₁ /c	P2 ₁ /n	P $\bar{1}$	P2 ₁ /c	P $\bar{1}$	P2 ₁ /n
a (Å)	14.8499(10)	10.4510(17)	9.1971(12)	9.2240(13)	8.7547(8)	13.7723(9)
b (Å)	10.6117(7)	32.927(4)	9.4967(13)	9.8579(14)	10.0788(9)	15.3271(11)
c (Å)	19.3093(13)	11.0385(16)	18.536(3)	35.255(5)	19.0325(16)	15.9948 (11)
α (deg)	90	90	85.730(2)	90	80.9990(11)	90
β (deg)	106.1644(8)	114.777(10)	80.573(2)	95.641(2)	78.3360(11)	97.8006(10)
γ (deg)	90	90	76.799(2)	90	70.1735(11)	90
V (Å ³)	2922.5(3)	3448.8(9)	1553.7(4)	3190.2(8)	1540.1(2)	3345.1(4)
Z	4	4	2	4	2	4
ρ _{calcd} (g cm ⁻³)	1.333	1.338	1.323	1.360	1.355	1.276
μ (mm ⁻¹)	0.665	0.564	0.616	0.685	0.591	0.541
range of transn	0.7769–0.6834	0.9833–0.8402	0.9242–0.8132	0.8313–0.7807	0.9166–0.7449	0.9580–0.7662
2θ limit (deg)	54.98	50.00	52.84	54.88	55.04	54.94
	−19 ≤ h ≤ 19	−12 ≤ h ≤ 0	−11 ≤ h ≤ 11	−11 ≤ h ≤ 11	−11 ≤ h ≤ 11	−17 ≤ h ≤ 17
	−13 ≤ k ≤ 13	−39 ≤ k ≤ 0	−11 ≤ k ≤ 11	−12 ≤ k ≤ 12	−13 ≤ k ≤ 13	−19 ≤ k ≤ 19
	−25 ≤ l ≤ 25	−11 ≤ l ≤ 13	−23 ≤ l ≤ 23	−45 ≤ l ≤ 45	−24 ≤ l ≤ 24	−20 ≤ l ≤ 20
total data collected	24934	6366	12356	26737	13302	28881
indep reflns	6703	6022	6350	7263	6931	7631
R _{int}	0.0140	0.0721	0.0346	0.0320	0.0183	0.0293
obsd reflns	6262	3623	5202	6773	6262	6530
data/restraints/params	6703/0/313	6022/0/399	6350/0/353	7263/1/353	6931/0/358	7631/0/377
goodness-of-fit	1.083	1.020	1.068	1.395	1.072	1.066
R ₁ [<i>F</i> _o ² ≥ 2σ(<i>F</i> _o ²)]	0.0241	0.0672	0.0379	0.0642	0.0282	0.0287
wR ₂ [<i>F</i> _o ² ≥ −3σ(<i>F</i> _o ²)]	0.0657	0.1407	0.0919	0.1499	0.0732	0.0746
largest peak, hole (e Å ⁻³)	0.729, −0.319	0.518, −0.515	0.978, −0.388	1.553, −1.208	0.696, −0.206	0.616, −0.201

Table 2. Selected Interatomic Distances (Å) and Angles (deg) for 2·PMe₃, 3a, 3b, 3d, 5, and 6

	2·PMe ₃ ^a	3a ^b	3b ^b	3d ^{b,d}	5 ^g	6 ^{g,h}
Ru–P	2.2842(4)	2.315(2)	2.3243(8)	2.339(1)	2.2427(5)	2.3172(5)
Ru–X	2.2806(4)	2.377(2)	2.3445(9)	2.332(1)	2.048(2)	
Ru–H*	1.51(6)	1.44(3)	1.44(3) ^e	1.57(2) ^e		1.74(2)
X–H	1.46(6)	1.44(3) ^e				1.09(2)
Ru–H*···X	1.84(6)	1.89(3)	2.10 ^f			1.38(2)
Ru–CN	2.118(2)	2.141(7)	2.167(3)	2.158(5)	1.896(2)	
C–NMe	1.477(2)	1.472(8)	1.454(4)	1.463(6)	1.371(2)	1.510(2)
N–CH ₃	1.460(2)	1.464(8)	1.458(4)	1.458(6)	1.470(2)	1.487(2)
N–C2	1.347(2)	1.342(9)	1.339(4)	1.332(7)	1.380(2)	1.451(2)
P–C3	1.806(2)	1.782(7)	1.804(3)	1.800(5)	1.820(2)	1.813(2)
ΣN–C angles	358.5	359.3	359.7	359.5	359.8	328.5

^a X = P2. ^b X = Si. ^c The second Si–H distance is 1.45(3). ^d Si–C1 2.139(2). ^e Distance restrained during refinement. ^f Measured in the final refined structure; Si–H added at calculated position. ^g X = B. ^h Ru–N 2.226(2).

Reactions with Silanes. Encouraged by the rich reaction chemistry exhibited by Cp^{*}RuL_m complexes with organosilanes,⁸ the reactivity of **1** with Si–H-containing substrates was examined (Scheme 3). In preliminary experiments employing Ph₃SiH or Et₃SiH, no reaction was observed at ambient temperature, while heating of these reaction mixtures (60 °C) resulted in decomposition. Similarly, only partial consumption

Scheme 3. Reactions Involving **1** and Silanes

of **1** was observed in reactions employing Me₂PhSiH at ambient temperature, and attempts to conduct the reaction at higher temperatures resulted in decomposition. However, upon treatment with Ph₂SiH₂ or PhSiH₃, compound **1** was transformed cleanly into **3a** or **3b** (³¹P NMR), thereby allowing for the isolation of these complexes as analytically pure solids in 92% and 94% yield, respectively. For each of **3a** and **3b**, solution NMR data supported their identity as compounds formally arising from net Si–H addition across the Ru=C unit in **1**, or alternatively via Si–H oxidative addition to the reactive intermediate **2**. The observed ²J_{SiH} values in **3a** (22.9 Hz) and **3b** (7.8 Hz) point to an unsymmetrical Ru–H···Si interaction in each of these complexes in solution.^{8a,e} Such interactions were also observed in the solid state; ORTEP diagrams for **3a** and **3b** are presented in Figures 2 and 3. The relevant interatomic distances in each of these silane addition products compare well with those of 2·PMe₃ (*vide supra*), including the observation of a Ru–CN distance that is in keeping with a bond order of unity. Although we are hesitant to comment definitively with regard to the position of hydride ligands bridging Ru and Si, both **3a** and **3b** appear to feature Si centers that contain Si–H fragments (1.46(6) Å in **3a**; 1.44(3) and 1.45(3) Å in **3b**) as well as Ru–H···Si contacts (1.84(6) Å in **3a**; 1.89(3) Å in **3b**). Despite the apparent existence of such Ru–H···Si interactions, no chemical exchange was observed between the Ru–H and the Si–H environments within **3a** or **3b** on the basis of EXSY ¹H NMR experiments.⁹

The chlorosilanes Ph₂SiClH and PhSiClH₂ were also observed to react cleanly upon addition to **1**, affording the corresponding

(8) For selected reports and reviews, see: (a) Lachaize, S.; Sabo-Etienne, S. *Eur. J. Inorg. Chem.* **2006**, 2115. (b) Osipov, A. L.; Vyboishchikov, S. F.; Dorogov, K. Y.; Kuzmina, L. G.; Howard, J. A. K.; Lemenovskii, D. A.; Nikonov, G. I. *Chem. Commun.* **2005**, 3349. (c) Osipov, A. L.; Gerdov, S. M.; Kuzmina, L. G.; Howard, J. A. K.; Nikonov, G. I. *Organometallics* **2005**, *24*, 587. (d) Takao, T.; Amako, M.; Suzuki, H. *Organometallics* **2001**, *20*, 3406. (e) Corey, J. Y.; Braddock-Wilking, J. *Chem. Rev.* **1999**, *99*, 175. (f) Shelby, Q. D.; Lin, W.; Girolami, G. S. *Organometallics* **1999**, *18*, 1904. (g) Lemke, F. R.; Galat, K. J.; Youngs, W. J. *Organometallics* **1999**, *18*, 1419. (h) Tobita, H.; Kurita, H.; Ogino, H. *Organometallics* **1998**, *17*, 2850. (i) Wada, H.; Tobita, H.; Ogino, H. *Organometallics* **1997**, *16*, 3870. (j) Mitchell, G. P.; Tilley, T. D. *J. Am. Chem. Soc.* **1997**, *119*, 11236. (k) Campion, B. K.; Heyn, R. H.; Tilley, T. D. *Chem. Commun.* **1992**, 1201. (l) Campion, B. K.; Heyn, R. H.; Tilley, T. D. *Organometallics* **1992**, *11*, 3918. (m) Straus, D. A.; Zhang, C.; Quimbata, G. E.; Grumbine, S. D.; Heyn, R. H.; Tilley, T. D.; Rheingold, A. L.; Geib, S. J. *J. Am. Chem. Soc.* **1990**, *112*, 2673. (n) Straus, D. A.; Tilley, T. D.; Rheingold, A. L.; Geib, S. J. *J. Am. Chem. Soc.* **1987**, *109*, 5872. (o) References 1i and 3a,c,d herein.

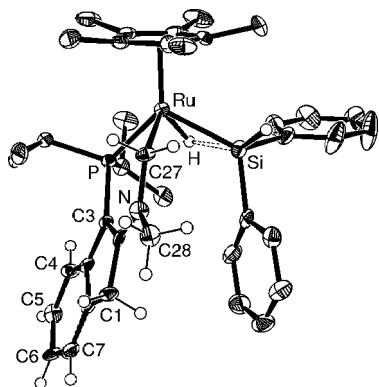


Figure 2. ORTEP diagram for **3a**, shown with 50% displacement ellipsoids and with the atomic numbering scheme depicted; selected H-atoms have been omitted for clarity.

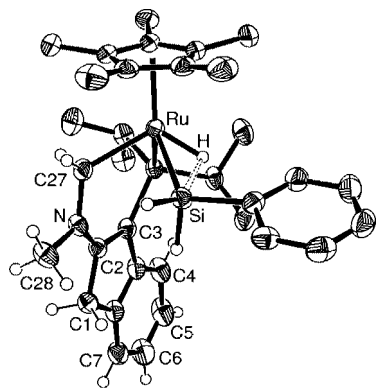


Figure 3. ORTEP diagram for **3b**, shown with 50% displacement ellipsoids and with the atomic numbering scheme depicted; selected H-atoms have been omitted for clarity.

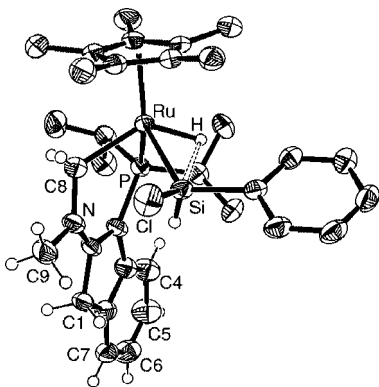
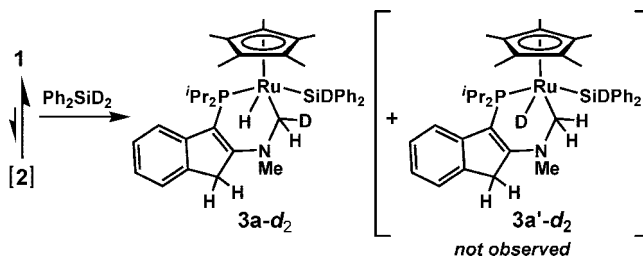


Figure 4. ORTEP diagram for **3d**, shown with 50% displacement ellipsoids and with the atomic numbering scheme depicted; selected H-atoms have been omitted for clarity.

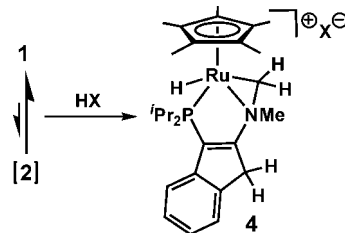
Si-H addition products **3c** and **3d** (respectively) in 87% and 82% isolated yield (Scheme 3). Complex **3d** forms as a mixture of two diastereomers (ca. 80:20 on the basis of NMR data), and single-crystal X-ray diffraction data obtained from a sample of **3d** allowed for the solid state characterization of one of these diastereomers; an ORTEP diagram of **3d** is presented in Figure 4. The salient structural features of **3d** compare well with those of **3a** and **3b** ($\text{Ru}-\text{H}\cdots\text{Si}$ 2.10 Å in **3d**), as well as those found within related Cp*Ru chlorosilyl complexes.^{8b,c,k}

(9) Chemical exchange of Ru-H and the Si-H environments in $\text{L}_n\text{Ru}(\text{H})(\text{SiHPh}_2)$ species has been observed previously: Gusev, D. G.; Nadasdi, T. T.; Caulton, K. G. *Inorg. Chem.* **1996**, *35*, 6772.

Scheme 4. Reaction Involving **1** and Ph_2SiD_2



Scheme 5. Reaction Involving **1** and $\text{H}(\text{OEt}_2)_2\text{B}(\text{C}_6\text{F}_5)_4$ (HX)



With an interest in probing the mechanistic pathway leading to the formation of **3a**, compound **1** in benzene or C_6D_6 was treated with 1 equiv of Ph_2SiD_2 , and the progress of the reaction was monitored by use of NMR techniques (Scheme 4). While ^{31}P NMR data confirmed the clean formation of the anticipated addition product within 2 h, data obtained from ^1H and ^2H NMR experiments provided evidence for deuteration exclusively at the Si-H and the RuC-H positions, as in **3a-d2**.¹⁰ These observations are inconsistent with simple Si-H oxidative addition to the reactive intermediate **2** (in which deuteration at Ru-H and Si-H would be anticipated in the first-formed product, as in **3a'-d2**), and are in keeping with net Si-H addition across the Ru=C unit in **1**. We cannot unequivocally discount the possibility that **3a'-d2** is the unobserved kinetic product in this reaction, which in turn rearranges rapidly to **3a-d2** via preferential C-D reductive elimination followed by C-H oxidative addition. Nonetheless, the transformation of **1** into **3a** appears to represent the first documented net addition of an Si-H bond across a Ru=C linkage.¹¹ Continued monitoring of **3a-d2** by use of NMR methods over the course of two weeks revealed partial deuterium incorporation at the NMe, Si-H, RuC-H, and Ru-H positions. While the conversion of Ru=C species into complexes featuring Ru-R and Ru-H linkages has been observed under catalytic hydrogenation conditions,¹² no reaction was observed upon exposure of **1** to an atmosphere of H_2 at ambient temperature. However, treatment of **1** with Jutzi's acid¹³ ($\text{H}(\text{OEt}_2)_2\text{B}(\text{C}_6\text{F}_5)_4$) resulted in the quantitative formation of the known compound **4** (the cyclometalated variant of $[\text{Cp}^*\text{Ru}(\kappa^2\text{-}2\text{-NMe}_2\text{-}3\text{-}P\text{-Pr}_2\text{-indene})]^+\text{B}(\text{C}_6\text{F}_5)_4^-$; Scheme 5).^{3f,g}

Reactions with Boranes. There is considerable interest in studying the stoichiometric reactivity of late metal complexes

(10) Compound **3a-d2** is formed as ca. 1:1 mixture of diastereomers. Selected diagnostic NMR data for **3a-d2** in benzene: ^1H NMR: δ 3.78 (d, $J = 6.0$ Hz, Ru-C(H)(D)-N), 3.19 (d, $J = 3.0$ Hz, Ru-C(D)(H)-N), 2.39 (NMe), 2.38 (NMe), -11.49 (d, $^2J_{\text{PH}} = 29.0$ Hz, Ru-H), -11.50 (d, $^2J_{\text{PH}} = 28.5$ Hz, Ru-H). ^2H NMR: δ 5.31 (br, Si-D), 3.77 (br, Ru-C(D)), 3.17 (br, Ru-C(D)). $^{13}\text{C}\{^1\text{H}\}$ NMR: δ 46.4 (NMe), 46.3 (NMe). $^{31}\text{P}\{^1\text{H}\}$ NMR: δ 47.9, 47.8.

(11) The addition of Si-H across Ru=C may represent an elementary reaction step in hydrosilylation chemistry employing Ru=C precatalysts: (a) Menozzi, C.; Dalko, P. I.; Cossy, J. *J. Org. Chem.* **2005**, *70*, 10717. (b) Maifeld, S. V.; Tran, M. N.; Lee, D. *Tetrahedron Lett.* **2005**, *46*, 105. (c) Aricó, C. S.; Cox, L. R. *Org. Biomol. Chem.* **2004**, *2*, 2558.

(12) (a) Schmidt, B. *Eur. J. Org. Chem.* **2004**, 1865. (b) Louie, J.; Bielawski, C. W.; Grubbs, R. H. *J. Am. Chem. Soc.* **2001**, *123*, 11312.

(13) Jutzi, P.; Müller, C.; Stammler, A.; Stammler, H.-G. *Organometallics* **2000**, *19*, 1442.

with B–H-containing substrates, both in terms of the development of metal–ligand bonding concepts and as a means of advancing our mechanistic understanding of prominent catalytic transformations such as the hydroboration of unsaturated substrates and the dehydrogenative borylation of hydrocarbons.^{14,15} Treatment of **1** with ca. 2.4 equiv of catecholborane (HBcat) in benzene at ambient temperature resulted in the consumption of the starting complex after 0.5 h, along with the initial formation of one major phosphorus-containing product ($\delta^{31}\text{P} = 54.8$, **5i**; ca. 85% of the reaction mixture) and three minor phosphorus-containing products ($\delta^{31}\text{P} = 72.2$, 71.8 (**5**), and 70.9; totaling ca. 15% of the reaction mixture). Carrying out analogous reactions in C_6D_6 allowed for the further *in situ* NMR characterization of **5i**; ^1H and ^{13}C NMR studies confirmed that this Ru–H species ($\delta^1\text{H} = -12.05$, $^2J_{\text{PH}} = 23.5$ Hz) does not feature a Ru=CH linkage as in **1**, and both the ^1H and ^{11}B NMR ($\delta^{11}\text{B} = 21.3$) spectra of **5i** were not significantly altered when decoupled from the other nucleus. On the basis of these and other NMR spectroscopic data, we tentatively assign **5i** as a Ru–boryl addition product (Scheme 6) that is structurally analogous to the Ru–silyl species **3a–d**. While continued monitoring (^{11}B and ^{31}P NMR) over the course of 6 days revealed the slow conversion of **5i** to **5**, the reappearance of **1** was also noted (**5i**:**5** of ca. 5:30:2). As such, an additional 0.6 equiv of HBcat was added to the reaction mixture, which promoted the quantitative conversion to **5** after a total reaction time of 16 days; compound **5** was isolated as an analytically pure powder in 54% yield. Efforts to accelerate the conversion of **5i** to **5** by heating such reaction mixtures at 60 °C resulted in formation of a complex mixture of phosphorus-containing products. ^1H and ^{13}C NMR data confirmed the absence of a Ru–H fragment and the existence of a Ru=CH linkage in **5**, thereby supporting the structural formulation presented in Scheme 6. The connectivity in **5** was further confirmed by use of X-ray diffraction techniques; an ORTEP diagram of **5** is presented in Figure 5. Notably, the Ru–B distance in **5** (2.048(2) Å) is shorter than related distances observed in the only other crystallographically characterized Ru–Bcat complexes, Ru(Bcat)₂(PPh₃)₂(CO)₂ (2.100(3) and 2.095(4) Å) and Ru(Bcat)₂(PPh₃)₂(CO)(CN-*p*-tolyl) (2.093(3) and 2.086(3) Å).¹⁶ In keeping with the structural features of the parent carbeneruthenium complex **1** (*vide supra*),^{3f,g} the planarity at nitrogen ($\Sigma_{\text{angles at N}} = 359.8^\circ$) and the relatively short Ru–C27 (Ru=C, 1.896(2) Å), N–C27 (RuC–N, 1.371(2) Å; cf. N–CH₃, 1.470(2) Å), and N–C2 (1.380(2) Å) distances in **5** point to significant π -bonding interactions along the Ru–C–N fragment and extending through

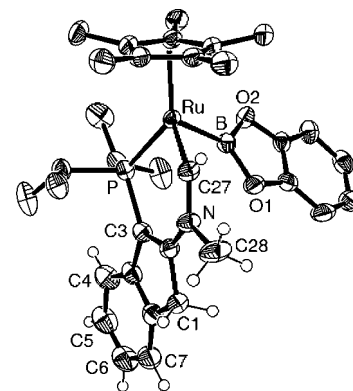
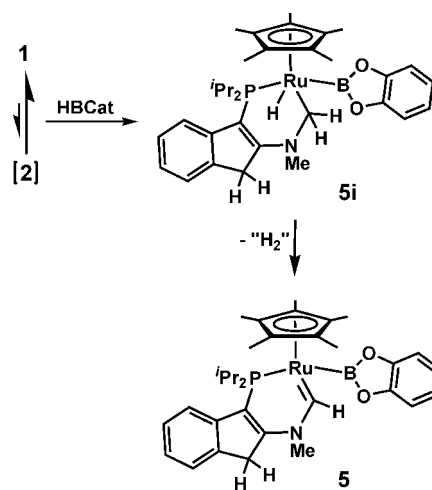


Figure 5. ORTEP diagram for **5**, shown with 50% displacement ellipsoids and with the atomic numbering scheme depicted; selected H-atoms have been omitted for clarity.

Scheme 6. Reaction Involving 1 and Catecholborane (HBcat)



to the carbocyclic backbone of the indene ligand. In the absence of additional data we are not able to comment definitively as to whether **5i** arises from B–H addition to **1** or **2**, nor are we able to provide mechanistic insights regarding the apparent dehydrogenation of **5i** to give **5**. However, the requirement of excess HBcat to promote the formation of **5**, along with the observation that **1** is initially consumed and then is re-formed during the course of this reaction, points to a potentially complex reaction scenario involving the net metathesis of Ru–B/H, B–H, and H–H bonds.^{14g} By comparison, compound **1** was not observed to react with pinacolborane (HBpin) under similar conditions at ambient temperature, and heating of such reaction mixtures at 60 °C for 7 days led to decomposition (^{31}P NMR).

Addition of 1 equiv of mesitylborane (MesBH_2) to a solution of **1** in benzene resulted in the quantitative conversion (^{31}P NMR) to a new phosphorus-containing product (**6**) over the course of 0.5 h (Scheme 7). Compound **6** was isolated in 81% yield and characterized initially by use of NMR techniques; ^1H NMR and ^{13}C NMR data confirmed the presence of Ru–H ($\delta^1\text{H} = -11.27$), N–CH₂, and BMe₃ fragments in **6**, in the absence of resonances attributable to a Ru=C(H) fragment. While these preliminary spectroscopic observations point to the possible identity of this complex as being a B–H addition product analogous to **5i** (i.e., **6i**), the crystallographic charac-

(14) (a) Braunschweig, H.; Kollann, C.; Rais, D. *Angew. Chem., Int. Ed.* **2006**, *45*, 5254. (b) Aldridge, S.; Coombs, D. L. *Coord. Chem. Rev.* **2004**, *248*, 535. (c) Crudden, C. M.; Edwards, D. *Eur. J. Org. Chem.* **2003**, 4695. (d) Braunschweig, H.; Colling, M. *Coord. Chem. Rev.* **2001**, 223, 1. (e) Piers, W. E. *Angew. Chem., Int. Ed.* **2000**, *39*, 1923. (f) Braunschweig, H. *Angew. Chem., Int. Ed.* **1998**, *37*, 1786. (g) Irvine, G. J.; Lesley, M. J. G.; Marder, T. B.; Norman, N. C.; Rice, C. R.; Robins, E. G.; Roper, W. R.; Whittell, G. R.; Wright, L. J. *Chem. Rev.* **1998**, *98*, 2685. (h) Beletskaya, I.; Pelter, A. *Tetrahedron* **1997**, *53*, 4957.

(15) For selected reports pertaining to Cp'RuL_n complexes, see: (a) Hesp, K. D.; Rankin, M. A.; McDonald, R.; Stradiotto, M. *Inorg. Chem.* **2008**, *47*, 7471. (b) Kawano, Y.; Hashiva, M.; Shimoji, M. *Organometallics* **2006**, *25*, 4420. (c) Saito, T.; Kuwata, S.; Ikariya, T. *Chem. Lett.* **2006**, 35, 1224. (d) Kuan, S. L.; Leong, W. K.; Goh, L. Y.; Webster, R. D. *Organomet. Chem.* **2006**, *691*, 907. (e) Murphy, J. M.; Lawrence, J. D.; Kawamura, K.; Incarvito, C.; Hartwig, J. F. *J. Am. Chem. Soc.* **2006**, *128*, 13684. (f) Kuan, S. L.; Leong, W. K.; Goh, L. Y.; Webster, R. D. *Organometallics* **2005**, *24*, 4639. (g) Merle, N.; Frost, C. G.; Koicok-Köhn, G.; Willis, M. C.; Weller, A. S. *J. Organomet. Chem.* **2005**, *690*, 2829. (h) Merle, N.; Koicok-Köhn, G.; Mahon, M. F.; Frost, C. G.; Ruggerio, G. D.; Weller, A. S.; Willis, M. C. *Dalton Trans.* **2004**, 3883. (i) Waltz, K. M.; Hartwig, J. F. *J. Am. Chem. Soc.* **2000**, *122*, 11358. (j) Hartwig, J. F.; Bhandari, S.; Rablen, P. R. *J. Am. Chem. Soc.* **1994**, *116*, 1839.

(16) Rickard, C. E. F.; Roper, W. R.; Williamson, A.; Wright, L. J. *Organometallics* **2000**, *19*, 4344.

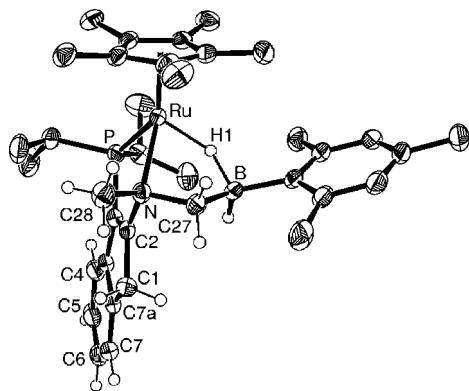
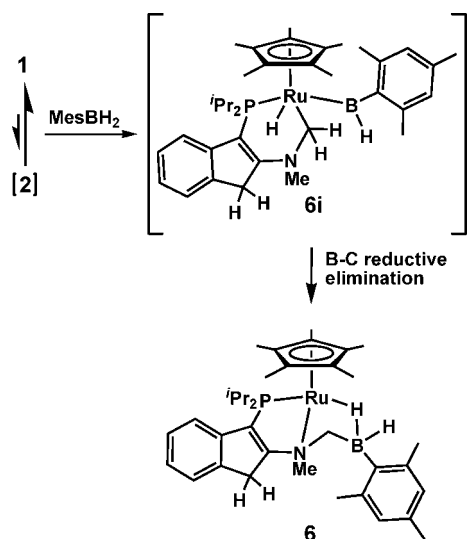


Figure 6. ORTEP diagram for **6**, shown with 50% displacement ellipsoids and with the atomic numbering scheme depicted; selected H-atoms have been omitted for clarity.

Scheme 7. A Possible Mechanistic Pathway in the Reaction Involving **1 and Mesitylborane (MesBH₂)**



terization of **6** allowed for the definitive characterization of this complex as the 18-electron species depicted in Scheme 7. An ORTEP diagram of **6** is presented in Figure 6. Compound **6** is comprised of a Cp*RuH fragment supported by an unusual κ^2 -P,N ligand featuring a tethered borane fragment that forms a Ru–H–B bridge.¹⁷ While the formation of **6** can be viewed as arising from initial B–H addition to either **1** or **2** to give the unobserved intermediate **6i**, which in turn could rearrange to **6** via B–C reductive elimination (by analogy with **5i** and **5**), alternative Ru–C/H–B σ -bond metathesis reaction sequences involving the putative alkylruthenium complex **2** cannot be ruled out.

Summary and Conclusions

The rate of α -hydride elimination in **1** and the reactivity properties of this stereochemically nonrigid 18-electron complex with L-donor (L = CO, PR₃) and E–H (E = B, Si, P) containing

substrates were documented. Exposure of **1** to an atmosphere of CO or to an equivalent of either PMe₃ or Ph₂Ph afforded the corresponding **2**·L adduct, thereby providing what can be viewed as indirect support for the ability of **1** to serve as a masked source of the unobserved alkylruthenium complex **2**. However, we cannot rule out reaction mechanisms leading to **2**·L involving L-addition to alternative, coordinatively unsaturated reactive intermediates derived from **1**, including those generated via Ru–P dissociation. In examining the reactivity of **1** with Si–H-containing substrates, products of net Si–H addition were observed. While such addition products could in principle arise via addition to either **1** or **2**, a deuterium labeling study employing Ph₂SiD₂ provided evidence in support of a reaction mechanism involving previously undocumented Si–D addition across the Ru=C unit in **1**. Interesting and divergent reactivity was noted with B–H-containing substrates. Complex **1** was observed to react with catecholborane (HBcat) to give a first-formed B–H addition product that underwent net dehydrogenation to give an isolable (Bcat)Ru=C species. In contrast, no intermediates were observed in the reaction of **1** with mesitylborane (MesBH₂); the product of this B–C bond forming reaction corresponds to a Cp*Ru(P,N) complex featuring a Ru–H–B bridge to a tethered borane fragment. Although further mechanistic studies are required in order to comment definitively regarding the possible intermediacy of **2** in the observed reactivity of **1**, the studies documented herein serve to underscore the potentially interesting reaction chemistry that may be derived from late metal complexes that exhibit reversible α -hydride elimination.

Experimental Section

General Considerations. All manipulations were conducted in the absence of oxygen and water under an atmosphere of dinitrogen, either by use of standard Schlenk methods or within an mBraun glovebox apparatus, utilizing glassware that was oven-dried (130 °C) and evacuated while hot prior to use. Celite (Aldrich) was oven-dried for 5 days and then evacuated for 24 h prior to use. The nondeuterated solvents diethyl ether, benzene, and pentane were deoxygenated and dried by sparging with dinitrogen gas, followed by passage through a double-column solvent purification system purchased from mBraun Inc. Diethyl ether was purified over two alumina-packed columns, while benzene and pentane were purified over one alumina-packed column and one column packed with copper-Q5 reactant. All solvents used within the glovebox were stored over activated 4 Å molecular sieves. Purification of MeCN was achieved by refluxing over CaH₂ for 4 days under dinitrogen, followed by distillation. All deuterated solvents (Cambridge Isotopes) and liquid silane reagents (Aldrich and Strem) were degassed by using three repeated freeze–pump–thaw cycles and then dried over 4 Å molecular sieves for 24 h prior to use. Ph₂Ph (Aldrich) was stored over 4 Å molecular sieves for 24 h prior to use. Pinacolborane (HBpin; Aldrich) was degassed by using three repeated freeze–pump–thaw cycles prior to use. Compound **1** (unpublished FTIR (NaCl) data for **1**: ν (Ru–H): 1937 cm⁻¹),^{3f,g} H(OEt₂)₂B(C₆F₅)₄,¹³ and MesBH₂¹⁸ were prepared employing literature procedures. Hydrogen (99.999%, UHP grade) and carbon monoxide gases (99.5%, chemically pure grade) were obtained from Air Liquide and were used as received. All purchased and prepared solid reagents were dried *in vacuo* for 24 h prior to use. Otherwise, all other commercial reagents were obtained from Aldrich and were used as received. Unless otherwise stated NMR characterization

(17) For some other crystallographically characterized complexes featuring a Ru–H–B bridging motif, see: (a) Alcaraz, G.; Clot, E.; Helmstedt, U.; Vendier, L.; Sabo-Etienne, S. *J. Am. Chem. Soc.* **2007**, *129*, 8704. (b) Lachaize, S.; Essalah, K.; Montiel-Palma, V.; Vendier, L.; Chaudret, B.; Barthelat, J.-C.; Sabo-Etienne, S. *Organometallics* **2005**, *24*, 2935. (c) Montiel-Palma, V.; Lumbierres, M.; Donnadiou, B.; Sabo-Etienne, S.; Chaudret, B. *J. Am. Chem. Soc.* **2002**, *124*, 5624. (d) Baker, R. T.; Calabrese, J. C.; Westcott, S. A.; Marder, T. B. *J. Am. Chem. Soc.* **1995**, *117*, 8777. (e) References 15a–d and 15f–h herein.

(18) (a) Smith, K.; Pelter, A.; Jin, Z. *Angew. Chem., Int. Ed.* **1994**, *33*, 851. (b) Pelter, A.; Smith, K.; Buss, D.; Jin, Z. *Heteroat. Chem.* **1992**, *3*, 275.

data were collected at 300 K on a Bruker AV-500 spectrometer operating at 500.1 (^1H), 125.8 (^{13}C), 99.4 (^{29}Si), 160.5 (^{11}B), and 202.5 (^{31}P) MHz with chemical shifts reported in parts per million downfield of SiMe_4 (for ^1H , ^{13}C , and ^{29}Si), 85% H_3PO_4 in water (for ^{31}P), or $\text{BF}_3 \cdot \text{OEt}_2$ (for ^{11}B). ^1H , ^{11}B , and ^{13}C NMR chemical shift assignments are given on the basis of data obtained from ^{13}C -DEPT, ^1H - ^1H COSY, ^1H - ^{13}C HSQC, ^1H - ^{13}C HMBC, and ^1H - ^{11}B HSQC NMR experiments. ^{29}Si NMR chemical shift assignments and coupling constant data are given on the basis of data obtained from ^1H - ^{29}Si HMBC/HMQC (including J-HMBC¹⁹) and ^1H -coupled ^1H - ^{29}Si HMQC experiments. The rate constant for reversible α -hydride elimination in **1** was measured in C_6D_6 according to the procedure of Bain.^{6a} Both selective inversion and nonselective ^1H NMR experiments were performed, using a total of 20 different delays. For the selective experiment, the $\text{Ru}(\text{H})=\text{CH}$ signal was inverted using a 1.5 ms Gaussian pulse; a relaxation delay of 7 s was used for both experiments. Data were analyzed by using the program CIFIT.^{6b-d} IR data were collected on a Bruker VECTOR 22 FT-IR instrument. Elemental analyses were performed by Canadian Microanalytical Service Ltd., Delta, British Columbia.

Synthesis of 2·CO. Within a glovebox, a 250 mL glass reaction flask was charged with **1** (0.094 g, 0.18 mmol), benzene (5 mL), and a magnetic stirbar. After the vessel was sealed with a PTFE cap, the resulting bright orange solution was removed from the glovebox, connected to a Schlenk line, and degassed via three repeated freeze-pump-thaw cycles. An atmosphere of CO was then introduced to the vessel. The bomb was then resealed after 0.25 h, and the solution was stirred magnetically for 48 h. After this time period, the solution was brownish-yellow and ^{31}P NMR data collected on an aliquot of this reaction mixture indicated quantitative conversion to **2·CO**. Upon removal of solvent and other volatile materials *in vacuo*, followed by trituration with pentane (2×1.5 mL), **2·CO** was isolated as an analytically pure, tan powder (0.097 g, 0.018 mmol, 98%). Anal. Calcd for $\text{C}_{28}\text{H}_{40}\text{PNORu}$: C 62.41; H 7.49; N 2.60. Found: C 62.43; H 7.64; N 2.46. ^1H NMR (C_6D_6): δ 7.55 (d, $^3J_{\text{HH}} = 8.0$ Hz, 1H, C4-H or C7-H), 7.27 (t, $^3J_{\text{HH}} = 7.5$ Hz, 1H, C5-H or C6-H), 7.12 (d, $^3J_{\text{HH}} = 7.0$ Hz, 1H, C7-H or C4-H), 6.99 (t, $^3J_{\text{HH}} = 7.5$ Hz, 1H, C6-H or C5-H), 3.85 (m, 1H, N-C(H_a)(H_b)-Ru), 3.38–3.28 (m, 2H, P(CHMe_aMe_b) and N-C(H_a)(H_b)-Ru), 3.20–2.95 (m, 2H, C(H_a)(H_b)), 2.78 (s, 3H, NMe), 2.00 (m, 1H, P(CHMe_cMe_d)), 1.70 (s, 15 H, C₅Me₅), 1.36 (d of d, $^3J_{\text{PH}} = 11.5$ Hz, $^3J_{\text{HH}} = 7.0$ Hz, 3H, P(CHMe_cMe_d)), 1.10–0.98 (m, 9H, P(CHMe_aMe_b) and P(CHMe_cMe_d)). $^{13}\text{C}\{^1\text{H}\}$ NMR (C_6D_6): δ 209.0 (d, $^2J_{\text{PC}} = 18.7$ Hz, CO), 168.8 (d, $^2J_{\text{PC}} = 12.8$ Hz, C2), 149.8 (C3a or C7a), 136.2 (d, $J_{\text{PC}} = 7.9$ Hz, C7a or C3a), 126.8 (C5 or C6), 123.0 (C4 or C7), 119.5 (C6 or C5), 119.1 (C7 or C4), 95.1 (C₅Me₅), 89.9 (d, $^1J_{\text{PC}} = 48.2$ Hz, C3), 43.7 (NMe), 40.4 (d, $^3J_{\text{PC}} = 6.9$ Hz, C1), 39.3 (d, $^2J_{\text{PC}} = 15.1$ Hz, N-CH₂-Ru), 27.8 (d, $^1J_{\text{PC}} = 21.4$ Hz, P(CHMe_cMe_d)), 24.5 (d, $^1J_{\text{PC}} = 32.7$ Hz, P(CHMe_aMe_b)), 21.3 (d, $^2J_{\text{PC}} = 7.0$ Hz, P(CHMe_cMe_d)), 20.1 (P(CHMe_aMe_b)), 19.3 (d, $^2J_{\text{PC}} = 2.9$ Hz, P(CHMe_aMe_b)), 19.0 (d, $^2J_{\text{PC}} = 6.7$ Hz, P(CHMe_aMe_b)), 10.3 (C₅Me₅). $^{31}\text{P}\{^1\text{H}\}$ NMR (C_6D_6): δ 55.3. FTIR (NaCl; cm^{-1}) $\nu(\text{CO})$: 1897.

Synthesis of 2·PMe₃. A solution of PMe_3 (1.0 M in toluene, 0.10 mL, 0.10 mmol) was added via Eppendorf micropipette to a glass vial containing a bright orange solution of **1** (0.052 g, 0.10 mmol) in benzene (4 mL). The vial was then sealed with a PTFE-lined cap and stirred magnetically for 22 h. During this time period, the solution lightened gradually in color to golden yellow. ^{31}P NMR data collected on an aliquot of this solution indicated quantitative conversion to **2·PMe₃**. The solvents and other volatile materials were then removed *in vacuo*, which left an oily yellow-orange residue. After the solid was triturated with pentane (2×1.5 mL), the residual solvent was removed *in vacuo*, which left **2·PMe₃** as a yellow powder (0.056 g, 0.095 mmol, 93%). Anal. Calcd for

$\text{C}_{30}\text{H}_{49}\text{P}_2\text{NRu}$: C 61.39; H 8.42; N 2.39. Found: C 61.13; H 8.52; N 2.34. ^1H NMR (C_6D_6): δ 7.23 (d, $^3J_{\text{HH}} = 8.0$ Hz, 1H, C4-H or C7-H), 7.26 (t, $^3J_{\text{HH}} = 7.0$ Hz, 1H, C5-H or C6-H), 7.14 (m, 1H, C7-H or C4-H), 6.92 (t, $^3J_{\text{HH}} = 7.0$ Hz, 1H, C6-H or C5-H), 3.90 (m, 1H, N-C(H_a)(H_b)-Ru), 3.10 (m, 1H, P(CHMe_aMe_b)), 3.13–2.99 (m, 3H, N-C(H_a)(H_b)-Ru and C(H_a)(H_b)), 2.83 (s, 3H, NMe), 2.14 (m, 1H, P(CHMe_cMe_d)), 1.62 (s, 15 H, C₅Me₅), 1.36 (d of d, $^3J_{\text{PH}} = 10.0$ Hz, $^3J_{\text{HH}} = 7.0$ Hz, 3H, P(CHMe_cMe_d)), 1.11 (d of d, $^3J_{\text{PH}} = 16.5$ Hz, $^3J_{\text{HH}} = 6.5$ Hz, 3H, P(CHMe_aMe_b)), 1.07–1.02 (m, 12H, PMe_3 and P(CHMe_cMe_d)), 0.97 (d of d, $^3J_{\text{PH}} = 14.5$ Hz, $^3J_{\text{HH}} = 7.0$ Hz, 3H, P(CHMe_aMe_b)). $^{13}\text{C}\{^1\text{H}\}$ NMR (C_6D_6): δ 167.6 (d, $^2J_{\text{PC}} = 13.1$ Hz, C2), 151.1 (C3a or C7a), 135.7 (d, $J_{\text{PC}} = 6.8$ Hz, C7a or C3a), 127.0 (C5 or C6), 122.3 (C4 or C7), 119.0 (C7 or C4), 118.7 (C6 or C5), 91.1 (d, $^1J_{\text{PC}} = 38.5$ Hz, C3), 90.4 (C₅Me₅), 45.9 (NMe), 44.0 (d of d, $^2J_{\text{PC}} = 17.4$ Hz, $^2J_{\text{PC}} = 14.2$ Hz, N-CH₂-Ru), 41.5 (d, $^3J_{\text{PC}} = 6.7$ Hz, C1), 31.0 (d of d, $^1J_{\text{PC}} = 23.0$ Hz, $^3J_{\text{PC}} = 3.6$ Hz, P(CHMe_cMe_d)), 24.9 (d, $^1J_{\text{PC}} = 26.0$ Hz, P(CHMe_aMe_b)), 22.5 (d, $^1J_{\text{PC}} = 22.8$ Hz, PMe_3), 21.8 (d, $^2J_{\text{PC}} = 7.2$ Hz, P(CHMe_cMe_d)), 21.1 (d, $^2J_{\text{PC}} = 3.9$ Hz, P(CHMe_aMe_b)), 20.5 (P(CHMe_cMe_d)), 20.1 (d, $^2J_{\text{PC}} = 9.9$ Hz, P(CHMe_aMe_b)), 10.7 (C₅Me₅). $^{31}\text{P}\{^1\text{H}\}$ NMR (C_6D_6): δ 54.0 (d, $^2J_{\text{PP}} = 38.5$ Hz), 5.9 (d, $^2J_{\text{PP}} = 38.5$ Hz). A crystal of **2·PMe₃** suitable for single-crystal X-ray diffraction studies was grown from an undisturbed concentrated pentane solution over the course of 4 days at ambient temperature.

Synthesis of 2·PH₂Ph. Phenylphosphine (0.022 mL, 0.20 mmol) was added via Eppendorf micropipette to a glass vial containing a magnetically stirred solution of **1** (0.10 g, 0.20 mmol) in benzene (6 mL). The vial was sealed with a PTFE-lined cap and magnetic stirring was initiated. Over the course of several minutes, the reaction mixture evolved from bright orange to yellow. After 0.5 h, ^{31}P NMR data collected on an aliquot of this crude reaction mixture indicated the quantitative formation of **2·PH₂Ph**. The benzene solvent and other volatile materials were removed *in vacuo*, yielding an oily yellow solid. The residue was treated with pentane (2×2 mL), after which the yellow supernatant solution was carefully removed via a Pasteur pipet, leaving a yellow solid. The pentane solution was stored at -35 °C in order to induce precipitation. After 24 h, a microcrystalline yellow solid that had formed was isolated by transferring the supernatant solution to a new glass vial; this solution was concentrated *in vacuo* in order to induce further precipitation. After repeating this procedure, the isolated solids were combined and dried *in vacuo*, yielding **2·PH₂Ph** as an analytically pure, pale yellow powder (0.083 g, 0.13 mmol, 67%). Anal. Calcd for $\text{C}_{33}\text{H}_{47}\text{P}_2\text{NRu}$: C 63.83; H 7.64; N 2.26. Found: C 63.81; H 7.64; N 1.93. ^1H NMR (C_6D_6): δ 7.60 (d, $^3J_{\text{HH}} = 8.0$ Hz, 1H, C4-H or C7-H), 7.32–7.22 (m, 3H, 2 P-aryl Hs and aryl H), 7.15 (m, 1H, aryl H), 7.11–7.05 (m, 3H, P-aryl Hs), 6.97 (t, $^3J_{\text{HH}} = 7.0$ Hz, 1H, C5-H or C6-H), 5.56 (d of d, $^1J_{\text{PH}} = 312.6$ Hz, $^2J_{\text{HH}} = 5.5$ Hz, 1H, P(H_a)(H_b)), 5.12 (d of d of d, $^1J_{\text{PH}} = 328.1$ Hz, $^3J_{\text{PH}} = 7.5$ Hz, $^2J_{\text{HH}} = 5.5$ Hz, 1H, P(H_a)(H_b)), 3.82 (m, 1H, N-C(H_a)(H_b)-Ru), 3.51 (m, 1H, P(CHMe_aMe_b)), 3.11 (m, 1H, N-C(H_a)(H_b)-Ru), 3.05–2.94 (m, 2H, C(H_a)(H_b)), 2.33 (s, 3H, NMe), 2.13 (m, 1H, P(CHMe_cMe_d)), 1.66 (s, 15 H, C₅Me₅), 1.36 (d of d, $^3J_{\text{PH}} = 10.0$ Hz, $^3J_{\text{HH}} = 7.0$ Hz, 3H, P(CHMe_cMe_d)), 1.17–1.09 (m, 6H, P(CHMe_aMe_b) and P(CHMe_cMe_d)), 0.99 (d of d, $^3J_{\text{PH}} = 14.5$ Hz, $^3J_{\text{HH}} = 6.5$ Hz, 3H, P(CHMe_aMe_b)). $^{13}\text{C}\{^1\text{H}\}$ NMR (C_6D_6): δ 167.7 (d, $^2J_{\text{PC}} = 12.6$ Hz, C2), 151.8 (C3a or C7a), 136.0 (d, $J_{\text{PC}} = 7.0$ Hz, C7a or C3a), 134.0 (d of d, $^1J_{\text{PC}} = 35.0$ Hz, $^3J_{\text{PC}} = 3.1$ Hz, P-aryl C), 133.1 (d, $J_{\text{PC}} = 8.7$ Hz, 2 P-aryl CHs), 128.4 (P-aryl CH), 128.3–128.0 (2 P-aryl CHs, obscured by C_6D_6), 127.0 (C5 or C6), 122.5 (aryl CH), 118.9 (C4 or C7), 118.8 (aryl CH), 90.0 (C₅Me₅), 88.4 (d, $^1J_{\text{PC}} = 42.0$ Hz, C3), 45.7 (NMe), 42.6 (d of d, $^2J_{\text{PC}} = 17.1$ Hz, $^2J_{\text{PC}} = 13.8$ Hz, N-CH₂-Ru), 40.9 (d, $^3J_{\text{PC}} = 6.9$ Hz, C1), 29.5 (d of d, $^1J_{\text{PC}} = 21.4$ Hz, $^3J_{\text{PC}} = 3.3$ Hz, P(CHMe_cMe_d)), 26.7 (d, $^1J_{\text{PC}} = 28.8$ Hz, P(CHMe_aMe_b)), 21.2 (d, $^2J_{\text{PC}} = 7.0$ Hz, P(CHMe_cMe_d)), 20.4–20.2 (m, P(CHMe_aMe_b) and either

(19) Meissner, A.; Sørensen, O. W. *Magn. Reson. Chem.* **2001**, *39*, 49.

P(CHMe_aMe_b) or P(CHMe_cMe_d), 19.2 (²J_{PC} = 7.5 Hz, P(CHMe_cMe_d) or P(CHMe_aMe_b)), 10.4 (C₅Me₅). ³¹P{¹H} NMR (C₆D₆): δ 54.6 (d, ²J_{PP} = 40.5 Hz), 8.9 (d, ²J_{PP} = 40.5 Hz).

Synthesis of 3a. To a glass vial containing a solution of **1** (0.088 g, 0.17 mmol) in benzene (6 mL) was added Ph₂SiH₂ (0.032 mL, 0.17 mmol) via Eppendorf micropipette. The vial was then sealed with a PTFE-lined cap and the solution mixed manually by inversion several times. After 4 h, ³¹P NMR data collected on an aliquot of this solution indicated the quantitative formation of **3a**. Within this time period, the color of the solution changed from bright orange to yellow. The benzene solvent and other volatiles were then removed *in vacuo*, yielding an oily orange-yellow solid. After the residue was triturated with pentane (1.5 mL) and the pentane was removed *in vacuo*, **3a** was isolated as an analytically pure, light yellow-orange powder (0.11 g, 0.16 mmol, 92%). Anal. Calcd for C₃₉H₅₂PNSiRu: C 67.39; H 7.55; N 2.02. Found: C 67.52; H 7.49; N 1.93. ¹H NMR (C₆D₆): δ 7.90–7.88 (m, 2H, Si-aryl Hs), 7.64–7.62 (m, 2H, Si-aryl Hs), 7.36 (d, ³J_{HH} = 8.0 Hz, 1H, C4–H or C7–H), 7.26–7.23 (m, 3H, 2 Si-aryl Hs and either C5–H or C6–H), 7.15–7.11 (m, 2H, Si-aryl Hs), 7.03 (d, ³J_{HH} = 7.0 Hz, 1H, C7–H or C4–H), 6.94–6.90 (m, 3H, 2 Si-aryl Hs and either C6–H or C5–H), 5.28 (d, *J* = 1.5 Hz, 1H, Si–H), 3.80 (m, 1H, N–C(H_a)(H_b)–Ru), 3.30 (m, 1H, P(CHMe_aMe_b)), 3.22 (d of d, *J* = 5.0 Hz, *J* = 3.0 Hz, 1H, N–C(H_a)(H_b)–Ru), 2.66 (m, 1H, C(H_a)(H_b)), 2.39 (s, 3H, NMe), 2.22–2.16 (m, 2H, P(CHMe_cMe_d) and C(H_a)(H_b)), 1.45–1.40 (m, 18H, C₅Me₅ and P(CHMe_aMe_b)), 1.26 (d of d, ³J_{PH} = 11.5 Hz, ³J_{HH} = 7.0 Hz, 3H, P(CHMe_cMe_d)), 1.20 (d of d, ³J_{PH} = 17.0 Hz, ³J_{HH} = 7.0 Hz, 3H, P(CHMe_aMe_b)), 0.89 (d of d, ³J_{PH} = 15.5 Hz, ³J_{HH} = 7.0 Hz, 3H, P(CHMe_cMe_d)), –11.49 (d, ²J_{PH} = 28.7 Hz, 1H, Ru–H). ¹³C{¹H} NMR (C₆D₆): δ 168.6 (d, ²J_{PC} = 8.4 Hz, C2), 149.9 (C3a or C7a), 145.7 (Si-aryl C), 145.6 (Si-aryl C), 136.4 (2 Si-aryl CHs), 136.1 (d, *J*_{PC} = 8.7 Hz, C7a or C3a), 135.3 (2 Si-aryl CHs), 128.2 (Si-aryl CH), 127.4 (Si-aryl CH), 127.3 (Si-aryl CH), 126.8 (Si-aryl CH), 126.7 (C5 or C6), 126.6 (2 Si-aryl CHs), 122.5 (C4 or C7), 119.1 (C6 or C5), 118.2 (C7 or C4), 95.4 (C₅Me₅), 86.3 (d, ¹J_{PC} = 52.0 Hz, C3), 46.4 (NMe), 40.4 (d, ³J_{PC} = 7.2 Hz, C1), 38.9 (d, ²J_{PC} = 15.3 Hz, N–CH₂–Ru), 30.5 (d, ¹J_{PC} = 21.3 Hz, P(CHMe_cMe_d)), 25.3 (d, ¹J_{PC} = 37.0 Hz, P(CHMe_aMe_b)), 21.3 (d, ²J_{PC} = 7.4 Hz, P(CHMe_cMe_d)), 20.4 (P(CHMe_aMe_b)), 20.3 (P(CHMe_aMe_b)), 19.5 (d, ²J_{PC} = 5.7 Hz, P(CHMe_aMe_b)), 9.5 (C₅Me₅). ³¹P{¹H} NMR (C₆D₆): δ 47.7. ²⁹Si{¹H} NMR (C₆D₆): δ 32.8 (¹H–²⁹Si HMBC/HMQC), ¹J_{SiH} = 178.5 Hz (¹H-coupled ¹H–²⁹Si HMQC), ²J_{SiH} = 22.9 Hz (¹H-coupled ¹H–²⁹Si HMQC). FTIR (NaCl; cm^{–1}) ν(Ru–H, Si–H): 2066–1954 (overlapping). A crystal of **3a** suitable for single-crystal X-ray diffraction studies was grown from a concentrated Et₂O solution at –35 °C.

Synthesis of 3b. A protocol analogous to that described for **3a** was used: a mixture of **1** (0.097 g, 0.19 mmol) and PhSiH₃ (0.024 mL, 0.19 mmol) in benzene (5 mL) afforded **3b** quantitatively within 0.5 h (³¹P NMR), which was isolated as an analytically pure, light yellow powder (0.11 g, 0.18 mmol, 94%). Anal. Calcd for C₃₃H₄₈PNSiRu: C 64.05; H 7.82; N 2.26. Found: C 63.71; H 7.93; N 2.11. ¹H NMR (C₆D₆): δ 8.06 (d, ³J_{HH} = 6.5 Hz, 2H, Si-aryl Hs), 7.48 (d, ³J_{HH} = 8.0 Hz, 1H, C4–H or C7–H), 7.30 (t, ³J_{HH} = 7.5 Hz, 2H, Si-aryl Hs), 7.25 (t, ³J_{HH} = 8.0 Hz, 1H, C5–H or C6–H), 7.21 (t, ³J_{HH} = 7.0 Hz, 1H, Si-aryl H), 7.12 (d, ³J_{HH} = 7.0 Hz, 1H, C7–H or C4–H), 6.97 (t, ³J_{HH} = 7.0 Hz, 1H, C6–H or C5–H), 4.44 (apparent t, *J* = 5.0 Hz, 1H, Si(H_a)(H_b)), 4.23 (m, 1H, Si(H_a)(H_b)), 3.92 (apparent t, *J* = 9.0 Hz, 1H, N–C(H_a)(H_b)–Ru), 3.28 (m, 1H, P(CHMe_aMe_b)), 3.23–3.16 (m, 2H, C(H_a)(H_b) and N–C(H_a)(H_b)–Ru), 3.03–2.98 (m, 4H, C(H_a)(H_b) and NMe), 2.12 (m, 1H, P(CHMe_cMe_d)), 1.43 (s, 15H, C₅Me₅), 1.35 (d of d, ³J_{PH} = 11.5 Hz, ³J_{HH} = 7.0 Hz, 3H, P(CHMe_cMe_d)), 1.17–1.08 (m, 6H, P(CHMe_aMe_b)), 0.99 (d of d, ³J_{PH} = 15.0 Hz, ³J_{HH} = 7.0 Hz, 3H, P(CHMe_cMe_d)), –11.72 (apparent d of t, *J* = 30.3 Hz, *J* = 4.5 Hz, 1H, Ru–H). ¹³C{¹H} NMR (C₆D₆): δ 167.1 (d, ²J_{PC} =

11.7 Hz, C2), 149.9 (C3a or C7a), 143.7 (Si-aryl C), 136.2 (d, *J*_{PC} = 8.4 Hz, C7a or C3a), 136.1 (2 Si-aryl CHs), 127.7 (Si-aryl CH), 127.5 (2 Si-aryl CHs), 126.8 (C5 or C6), 122.9 (C4 or C7), 119.5 (C6 or C5), 118.7 (C7 or C4), 95.0 (C₅Me₅), 87.9 (d, ¹J_{PC} = 47.4 Hz, C3), 48.0 (NMe), 40.2 (d, ³J_{PC} = 6.8 Hz, C1), 38.9 (d, ²J_{PC} = 16.0 Hz, N–CH₂–Ru), 29.6 (d, ¹J_{PC} = 21.5 Hz, P(CHMe_cMe_d)), 24.0 (d, ¹J_{PC} = 36.1 Hz, P(CHMe_aMe_b)), 21.5 (d, ²J_{PC} = 7.5 Hz, P(CHMe_cMe_d)), 20.6 (P(CHMe_cMe_d)), 19.7 (d, ²J_{PC} = 5.8 Hz, P(CHMe_aMe_b)), 18.8 (P(CHMe_aMe_b)), 9.6 (C₅Me₅). ³¹P{¹H} NMR (C₆D₆): δ 51.2. ²⁹Si{¹H} NMR (C₆D₆): δ 8.7 (¹H–²⁹Si HMBC/HMQC), ¹J_{SiH} = 188.8 Hz, 170.6 Hz (¹H-coupled ¹H–²⁹Si HMQC), ²J_{SiH} = 7.8 Hz (¹H-coupled ¹H–²⁹Si HMQC). FTIR (NaCl; cm^{–1}) ν(Ru–H, Si–H): 2070–1982 (overlapping). A crystal of **3b** suitable for single-crystal X-ray diffraction studies was grown from a concentrated MeCN solution at ambient temperature.

Synthesis of 3c. A protocol analogous to that described for **3a** was used: a mixture of **1** (0.026 g, 0.051 mmol) and Ph₂SiCH (0.010 mL, 0.051 mmol) in benzene (3 mL) afforded **3c** quantitatively within 12 h (³¹P NMR), which was isolated as an analytically pure, pale yellow powder (0.032 g, 0.044 mmol, 87%). Anal. Calcd for C₃₉H₅₁PNSiClRu: C 64.21; H 7.05; N 1.92. Found: C 64.39; H 7.17; N 1.55. ¹H NMR (C₆D₆): δ 8.22–8.18 (m, 2H, Si-aryl Hs), 7.76–7.72 (m, 2H, Si-aryl Hs), 7.24–7.15 (m, 4H, 3 Si-aryl Hs and either C4–H or C7–H), 7.06 (t, ³J_{HH} = 7.0 Hz, 1H, C5–H or C6–H), 6.42 (d, ³J_{HH} = 7.0 Hz, 1H, C7–H or C4–H), 6.85 (t, ³J_{HH} = 7.0 Hz, 1H, C6–H or C5–H), 6.76–6.73 (m, 3H, Si-aryl Hs), 4.00–3.97 (m, 2H, N–C(H_a)(H_b)–Ru), 3.27 (br m, 1H, P(CHMe_aMe_b)), 2.89 (s, 3H, NMe), 2.49 (m, 1H, C(H_a)(H_b)), 2.14 (m, 1H, P(CHMe_cMe_d)), 1.75 (m, 1H, C(H_a)(H_b)), 1.47 (s, 15H, C₅Me₅), 1.41 (d of d, ³J_{PH} = 16.0 Hz, ³J_{HH} = 7.0 Hz, 3H, P(CHMe_aMe_b)), 1.24–1.14 (m, 6H, P(CHMe_cMe_d) and P(CHMe_aMe_b)), 0.84 (d of d, ³J_{PH} = 15.0 Hz, ³J_{HH} = 7.0 Hz, 3H, P(CHMe_cMe_d)), –11.58 (d, ²J_{PH} = 29.0 Hz, 1H, Ru–H). ¹³C{¹H} NMR (C₆D₆): δ 168.7 (d, ²J_{PC} = 11.9 Hz, C2), 149.1 (C3a or C7a), 147.8 (Si-aryl C), 145.6 (Si-aryl C), 136.3 (d, *J*_{PC} = 9.4 Hz, C7a or C3a), 135.3 (2 Si-aryl CHs), 133.8 (2 Si-aryl CHs), 128.1 (C5 or C6, obscured by C₆D₆), 127.2 (2 Si-aryl CHs), 126.6 (Si-aryl CH), 126.5 (Si-aryl CH), 125.9 (2 Si-aryl CHs), 122.4 (C4 or C7), 119.3 (C6 or C5), 117.7 (C7 or C4), 97.8 (C₅Me₅), 45.9 (NMe), 39.9 (d, ³J_{PC} = 7.5 Hz, C1), 38.2 (d, ²J_{PC} = 15.2 Hz, N–CH₂–Ru), 31.2 (d, ¹J_{PC} = 21.6 Hz, P(CHMe_cMe_d)), 25.7 (d, ¹J_{PC} = 36.7 Hz, P(CHMe_aMe_b)), 22.1 (d, ²J_{PC} = 7.2 Hz, P(CHMe_cMe_d)), 21.5 (P(CHMe_aMe_b) and P(CHMe_cMe_d)), 20.0 (d, ²J_{PC} = 5.3 Hz, P(CHMe_aMe_b)), 9.7 (C₅Me₅). ³¹P{¹H} NMR (C₆D₆): δ 42.6. ²⁹Si{¹H} NMR (C₆D₆): δ 60.9 (¹H–²⁹Si HMBC), ²J_{SiH} not detected by J-HMBC nor ¹H-coupled ¹H–²⁹Si HMQC. FTIR (NaCl; cm^{–1}) ν(Ru–H): 1968.

Synthesis of 3d. A protocol analogous to that described for **3a** was used: a mixture of **1** (0.10 g, 0.20 mmol), PhSiClH₂ (0.026 mL, 0.20 mmol), and benzene (6 mL) afforded **3d** quantitatively within 0.5 h (³¹P NMR), which was isolated as an analytically pure, pale yellow powder (0.10 g, 0.16 mmol, 82%). Complex **3d** forms as a mixture of diastereomers (80:20) on the basis of NMR data. Anal. Calcd for C₃₃H₄₇PNSiClRu: C 60.66; H 7.26; N 2.14. Found: C 60.43; H 7.30; N 2.14. **Major diastereomer of 3d:** ¹H NMR (C₆D₆): δ 8.29 (d, ³J_{HH} = 7.5 Hz, 2H, Si-aryl Hs), 7.36–7.31 (m, 3H, 2 Si-aryl CHs and aryl H), 7.22–7.18 (m, 2H, Si-aryl CH and aryl H), 7.10 (d, ³J_{HH} = 7.0 Hz, 1H, C4–H or C7–H), 6.94 (t, ³J_{HH} = 7.0 Hz, 1H, C5–H or C6–H), 5.51 (d, *J* = 4.5 Hz, 1H, Si–H), 4.06 (apparent t, *J* = 10.0 Hz, 1H, N–C(H_a)(H_b)–Ru), 3.64 (d of d, *J* = 9.0 Hz, *J* = 4.0 Hz, N–C(H_a)(H_b)–Ru), 3.24–3.12 (m, 5H, NMe and C(H_a)(H_b) and P(CHMe_aMe_b)), 3.04 (m, 1H, C(H_a)(H_b)), 2.07 (m, 1H, P(CHMe_cMe_d)), 1.51 (s, 15H, C₅Me₅), 1.28 (d of d, ³J_{PH} = 12.0 Hz, ³J_{HH} = 7.5 Hz, 3H, P(CHMe_cMe_d)), 1.05 (d of d, ³J_{PH} = 17.0 Hz, ³J_{HH} = 7.0 Hz, 3H, P(CHMe_aMe_b)), 0.96 (d of d, ³J_{PH} = 15.0 Hz, ³J_{HH} = 7.0 Hz, 3H, P(CHMe_cMe_d)), 0.77 (d of d, ³J_{PH} = 16.0 Hz, ³J_{HH} = 7.0 Hz, 3H, P(CHMe_aMe_b)),

–11.72 (d of d, $J = 31.5$ Hz, $J = 4.0$ Hz, 1H, Ru–H). $^{13}\text{C}\{^1\text{H}\}$ NMR (C_6D_6): δ 168.0 (d, $^2J_{\text{PC}} = 11.4$ Hz, C2), 149.5 (C3a or C7a), 144.6 (Si-aryl C), 136.3 (d, $J_{\text{PC}} = 8.8$ Hz, C7a or C3a), 136.0 (2 Si-aryl CHs), 128.4 (Si-aryl CH), 127.3 (2 Si-aryl CHs), 126.8 (aryl CH), 123.0 (C4 or C7), 119.6 (C6 or C5), 119.6 (aryl CH), 96.8 (C_5Me_5), 87.0 (d, $^1J_{\text{PC}} = 49.7$ Hz, C3), 46.6 (NMe), 40.2 (d, $^3J_{\text{PC}} = 7.0$ Hz, C1), 38.8 (d, $^2J_{\text{PC}} = 16.0$ Hz, N- CH_2 -Ru), 29.5 (d, $^1J_{\text{PC}} = 22.1$ Hz, P(CHMe $_c$ Me $_d$)), 23.8 (d, $^1J_{\text{PC}} = 36.9$ Hz, P(CHMe $_a$ Me $_b$)), 21.6 (d, $^2J_{\text{PC}} = 7.5$ Hz, P(CHMe $_c$ Me $_d$)), 20.7 (P(CHMe $_c$ Me $_d$)), 19.4 (d, $^2J_{\text{PC}} = 5.3$ Hz, P(CHMe $_a$ Me $_b$)), 18.0 (P(CHMe $_a$ Me $_b$)), 9.6 (C_5Me_5). $^{31}\text{P}\{^1\text{H}\}$ NMR (C_6D_6): δ 47.0. $^{29}\text{Si}\{^1\text{H}\}$ NMR (C_6D_6): δ 55.1 (^1H - ^{29}Si HMBC/HMQC), $^1J_{\text{SiH}} = 216.4$ Hz (^1H -coupled ^1H - ^{29}Si HMQC), $^2J_{\text{SiH}} = 4.3$ Hz (J-HMBC). Selected NMR features for the **minor diastereomer of 3d**: ^1H NMR (C_6D_6): δ 5.80 (s, 1H, Si–H), 2.64 (s, 3H, NMe), 1.47 (s, 15H, C_5Me_5), –10.97 (d, $^2J_{\text{PH}} = 29.0$ Hz, 1H, Ru–H). $^{13}\text{C}\{^1\text{H}\}$ NMR (C_6D_6): δ 96.4 (C_5Me_5), 46.2 (NMe), 40.9 (d, $^3J_{\text{PC}} = 7.0$ Hz, C1), 37.7 (d, $^2J_{\text{PC}} = 15.3$ Hz, N- CH_2 -Ru), 9.7 (C_5Me_5). $^{31}\text{P}\{^1\text{H}\}$ NMR (C_6D_6): δ 46.8. $^{29}\text{Si}\{^1\text{H}\}$ NMR (C_6D_6): δ 56.2 (^1H - ^{29}Si HMBC/HMQC), $^1J_{\text{SiH}} = 203.7$ Hz (^1H -coupled ^1H - ^{29}Si HMQC), $^2J_{\text{SiH}}$ not detected by J-HMBC. Slow evaporation of a concentrated pentane solution of **3d** provided a crystal suitable for single-crystal X-ray diffraction analysis, which was found to contain only one of the two diastereomers. FTIR (NaCl; cm^{-1}) ν (Ru–H, Si–H): 2090–1955 (overlapping).

Reaction of 1 with H(OEt) $_2$ B(C $_6$ F $_5$) $_4$. Treatment of **1** (0.010 g, 0.020 mmol) in benzene (6 mL) with H(OEt) $_2$ B(C $_6$ F $_5$) $_4$ (0.032 g, 0.039 mmol) resulted in the separation of a brown-yellow oil. After the vial contents were stirred magnetically for a total of 10 min, the mixture was allowed to settle for 1 h. The clear benzene supernatant was decanted away from the oil via pipet, and the oil was dried *in vacuo* and washed with pentane to give a pale yellow solid. The solid was then treated with THF- d_8 , and NMR features of this product were found to be consistent with the previously characterized **4**.^{3f,g}

Formation of 5i and Synthesis of 5. To a glass vial containing a magnetically stirred solution of **1** (0.084 g, 0.16 mmol) in benzene (6 mL) was added catecholborane (0.040 mL, 0.38 mmol) via Eppendorf micropipette, and the vial was then sealed with a PTFE-lined cap. Analysis of ^{31}P NMR collected on an aliquot of the reaction mixture after 0.5 h revealed the complete consumption of **1**, along with the formation of one major phosphorus-containing product (δ $^{31}\text{P} = 54.8$ (**5i**), ca. 85% of the reaction mixture) and three minor phosphorus-containing products (δ $^{31}\text{P} = 72.2$, 71.8 (**5**), and 70.9, totaling ca. 15% of the reaction mixture). A smaller scale reaction conducted in C_6D_6 allowed for the *in situ* characterization of **5i** (data provided below). Continued monitoring of the reaction mixture (^{31}P NMR) over the course of 6 days revealed the slow conversion of **5i** to **5**, along with the reappearance of **1** (**5i**:**1** of ca. 5:30:2). Additional catecholborane was added to the reaction mixture (0.010 mL, 0.094 mmol), and after a total reaction time of 16 days, the quantitative conversion to **5** was detected spectroscopically (^{31}P NMR). The reaction mixture was concentrated *in vacuo*, which afforded an oily orange solid. The residue was triturated with pentane (2 \times 1.5 mL) and then washed with Et $_2$ O (2 \times 1.5 mL) and pentane (1.5 mL). After removal of solvents and other volatile materials *in vacuo*, **5** was isolated as an orange powder (0.056 g, 0.088 mmol, 54%). Anal. Calcd for $\text{C}_{33}\text{H}_{43}\text{PNB}_2\text{Ru}$: C 63.02; H 6.90; N 2.23. Found: C 62.86; H 6.88; N 2.24. **NMR data for 5i**: ^1H NMR (C_6D_6): δ 7.61 (d, $^3J_{\text{HH}} = 8.0$ Hz, 1H, C4–H or C7–H), 7.30 (t, $^3J_{\text{HH}} = 8.0$ Hz, 1H, C5–H or C6–H), 7.24 (d, $^3J_{\text{HH}} = 7.5$ Hz, 1H, C7–H or C4–H), 7.02 (t, $^3J_{\text{HH}} = 7.0$ Hz, 1H, C6–H or C5–H), 6.82–6.79 (m, 2H, BO-aryl Hs), 6.76–6.73 (m, 2H, BO-aryl Hs), 3.81 (apparent t, $J = 10.0$ Hz, 1H, N-C(H_a)(H_b)-Ru), 3.41 (m, 1H, P(CHMe $_a$ Me $_b$)), 3.23–3.16 (m, 2H, N-C(H_a)(H_b)-Ru and C1(H_a)(H_b)), 2.94 (m, 1H, C1(H_a)(H_b)), 2.32 (s, 3H, NMe), 2.09 (m, 1H, P(CHMe $_c$ Me $_d$)), 1.71 (s, 15H, C_5Me_5), 1.40 (d of d,

$^3J_{\text{PH}} = 11.5$ Hz, $^3J_{\text{HH}} = 7.0$ Hz, 3H, P(CHMe $_c$ Me $_d$)), 1.14–1.06 (m, 6H, P(CHMe $_a$ Me $_b$)), 0.99 (d of d, $^3J_{\text{PH}} = 15.0$ Hz, $^3J_{\text{HH}} = 7.0$ Hz, 3H, P(CHMe $_c$ Me $_d$)), –12.05 (d, $^2J_{\text{PH}} = 23.5$ Hz, 1H, Ru–H). $^{13}\text{C}\{^1\text{H}\}$ NMR (C_6D_6): δ 168.5 (d, $^2J_{\text{PC}} = 12.5$ Hz, C2), 151.2 (2 BO-aryl C), 150.2 (C3a or C7a), 136.3 (d, $J_{\text{PC}} = 8.1$ Hz, C7a or C3a), 126.8 (C5 or C6), 122.8 (C4 or C7), 120.7 (2 BO-aryl CH), 119.4 (C7 or C4), 119.3 (C6 or C5), 110.2 (2 BO-aryl CH), 96.6 (C_5Me_5), 88.6 (d, $^1J_{\text{PC}} = 45.7$ Hz, C3), 42.8 (NMe), 40.4 (d, $^3J_{\text{PC}} = 6.5$ Hz, C1), 37.3 (d, $^2J_{\text{PC}} = 15.3$ Hz, N- CH_2 -Ru), 28.1 (d, $^1J_{\text{PC}} = 23.4$ Hz, P(CHMe $_c$ Me $_d$)), 23.1 (d, $^1J_{\text{PC}} = 34.3$ Hz, P(CHMe $_a$ Me $_b$)), 21.5 (d, $^2J_{\text{PC}} = 7.5$ Hz, P(CHMe $_c$ Me $_d$)), 20.2 (P(CHMe $_c$ Me $_d$)), 19.4 (d, $^2J_{\text{PC}} = 6.4$ Hz, P(CHMe $_a$ Me $_b$)), 18.8 (P(CHMe $_a$ Me $_b$)), 10.2 (C_5Me_5). $^{31}\text{P}\{^1\text{H}\}$ NMR (C_6D_6): δ 54.8. $^{11}\text{B}\{^1\text{H}\}$ NMR (C_6D_6): δ 21.3 (br). **NMR data for 5**: ^1H NMR (C_6D_6): δ 11.96 (d, $J = 2.5$ Hz, 1H, Ru=CH), 7.54 (d, $^3J_{\text{HH}} = 7.5$ Hz, 1H, C4–H or C7–H), 7.24 (d, $^3J_{\text{HH}} = 7.0$ Hz, 1H, C7–H or C4–H), 7.19 (m, 1H, C5–H or C6–H), 7.09 (t, $^3J_{\text{HH}} = 7.5$ Hz, 1H, C6–H or C5–H), 6.89 (apparent d of d, $J = 6.0$ Hz, $J = 3.5$ Hz, 2H, BO-aryl Hs), 6.70 (apparent d of d, $J = 5.5$ Hz, $J = 3.0$ Hz, 2H, BO-aryl Hs), 3.37–3.12 (m, 2H, C(H_a)(H_b)), 3.10 (s, 3H, NMe), 3.03 (m, 1H, P(CHMe $_a$ Me $_b$)), 2.00 (s, 15H, C_5Me_5), 1.59 (m, 1H, P(CHMe $_c$ Me $_d$)), 1.11–1.01 (m, 6H, P(CHMe $_a$ Me $_b$) and P(CHMe $_c$ Me $_d$)), 0.94 (d of d, $^3J_{\text{PH}} = 16.0$ Hz, $^3J_{\text{HH}} = 7.5$ Hz, 3H, P(CHMe $_c$ Me $_d$)), 0.66 (d of d, $^3J_{\text{PH}} = 15.0$ Hz, $^3J_{\text{HH}} = 7.0$ Hz, 3H, P(CHMe $_a$ Me $_b$)). $^{13}\text{C}\{^1\text{H}\}$ NMR (C_6D_6): δ 251.1 (d, $^2J_{\text{PC}} = 16.2$ Hz, Ru=C), 159.9 (d, $^2J_{\text{PC}} = 10.2$ Hz, C2), 151.0 (2 BO-aryl C), 147.9 (C3a or C7a), 137.3 (d, $J_{\text{PC}} = 6.8$ Hz, C7a or C3a), 127.1 (C5 or C6), 123.1 (C4 or C7), 122.8 (C6 or C5), 121.8 (C7 or C4), 120.2 (2 BO-aryl CH), 110.1 (2 BO-aryl CH), 105.6 (d, $^1J_{\text{PC}} = 39.8$ Hz, C3), 98.7 (C_5Me_5), 48.9 (NMe), 41.0 (d, $^3J_{\text{PC}} = 6.3$ Hz, C1), 33.6 (d, $^1J_{\text{PC}} = 19.1$ Hz, P(CHMe $_c$ Me $_d$)), 24.8 (d, $^1J_{\text{PC}} = 34.2$ Hz, P(CHMe $_a$ Me $_b$)), 19.7 (d, $^2J_{\text{PC}} = 4.9$ Hz, P(CHMe $_c$ Me $_d$)), 19.5 (d, $^2J_{\text{PC}} = 5.0$ Hz, P(CHMe $_c$ Me $_d$)), 18.5–18.3 (m, P(CHMe $_a$ Me $_b$)), 11.3 (C_5Me_5). $^{31}\text{P}\{^1\text{H}\}$ NMR (C_6D_6): δ 71.8. $^{11}\text{B}\{^1\text{H}\}$ NMR (C_6D_6): δ 53.2 (br). Slow evaporation of a concentrated pentane solution of **5** provided a crystal suitable for single-crystal X-ray diffraction analysis.

Synthesis of 6. Mesitylborane (0.016 g, 0.12 mmol) was added to a glass vial containing a bright orange solution of **1** (0.060 g, 0.12 mmol) in benzene (6 mL). After the vial was sealed with a PTFE-lined cap, the solution was shaken manually several times. ^{31}P NMR data collected on an aliquot of this solution indicated quantitative conversion to **6** within 0.5 h; after this time period the solution was dull orange. The benzene solvent and other volatile materials were removed *in vacuo*, which left an oily orange solid. The residue was triturated with pentane (2 \times 1.5 mL) and then washed with pentane (1 mL). After removal of trace amounts of pentane *in vacuo*, **6** was isolated as a yellow-orange powder (0.061 g, 0.095 mmol, 81%). Anal. Calcd for $\text{C}_{36}\text{H}_{53}\text{PNBRu}$: C 67.24; H 8.31; N 2.18. Found: C 66.95; H 8.46; N 2.11. ^1H NMR (C_6D_6): δ 7.52 (d, $^3J_{\text{HH}} = 7.5$ Hz, 1H, C4–H or C7–H), 7.24 (t, $^3J_{\text{HH}} = 7.5$ Hz, 1H, C5–H or C6–H), 7.17–7.10 (m, 2H, aryl Hs), 7.01 (s, 2H, B-aryl Hs), 4.33–4.24 (m, 2H, N-C(H_a)(H_b)-B), 3.39 (m, 1H, C(H_a)(H_b)), 3.03 (m, 1H, P(CHMe $_a$ Me $_b$)), 2.88 (m, 1H, C(H_a)(H_b)), 2.62 (s, 6H, B-aryl *o*-Me), 2.59 (s, 3H, NMe), 2.35 (s, 3H, B-aryl *p*-Me), 2.25 (m, 1H, P(CHMe $_c$ Me $_d$)), 1.37 (d, $J = 1.5$ Hz, 15H, C_5Me_5), 1.33 (d of d, $^3J_{\text{PH}} = 10.0$ Hz, $^3J_{\text{HH}} = 7.0$ Hz, 3H, P(CHMe $_c$ Me $_d$)), 1.24 (d of d, $^3J_{\text{PH}} = 16.0$ Hz, $^3J_{\text{HH}} = 7.0$ Hz, 3H, P(CHMe $_a$ Me $_b$)), 1.17 (d of d, $^3J_{\text{PH}} = 17.0$ Hz, $^3J_{\text{HH}} = 7.0$ Hz, 3H, P(CHMe $_a$ Me $_b$)), 0.90 (d of d, $^3J_{\text{PH}} = 16.0$ Hz, $^3J_{\text{HH}} = 7.0$ Hz, 3H, P(CHMe $_c$ Me $_d$)), –11.27 (br s, 1H, Ru–H–B). $^{13}\text{C}\{^1\text{H}\}$ NMR (C_6D_6): δ 178.1 (d, $^2J_{\text{PC}} = 21.0$ Hz, C2), 145.8 (B-aryl C), 145.0 (d, $J_{\text{PC}} = 3.9$ Hz, C3a or C7a), 142.6 (*o*-B-aryl C), 142.1 (d, $J_{\text{PC}} = 3.2$ Hz, C7a or C3a), 136.1 (d, $^1J_{\text{PC}} = 22.4$ Hz, C3), 133.3 (*p*-B-aryl C), 128.8 (B-aryl CHs), 126.7 (C5 or C6), 125.1 (aryl CH), 125.0 (aryl CH), 122.7 (C4 or C7), 82.5 (C_5Me_5), 67.7 (br m, N- CH_2 -B), 57.2 (NMe), 29.8 (d, $^3J_{\text{PC}} = 8.8$ Hz, C1), 26.4 (d, $^1J_{\text{PC}}$

= 20.4 Hz, P(CHMe_cMe_d), 25.9 (2 B-aryl *o*-Me), 24.5 (d, ¹J_{PC} = 25.7 Hz, P(CHMe_aMe_b)), 21.3 (B-aryl *p*-Me), 20.6 (d, ²J_{PC} = 5.8 Hz, P(CHMe_cMe_d)), 20.0 (d, ²J_{PC} = 6.9 Hz, P(CHMe_eMe_d)), 19.5–19.3 (m, P(CHMe_aMe_b)), 11.0 (C₅Me₅). ³¹P{¹H} NMR (C₆D₆): δ 67.1. ¹¹B{¹H} NMR (C₆D₆): δ -18.3 (br). FTIR (NaCl; cm⁻¹) ν(B–H): 2297. Slow evaporation of a C₆D₆ solution of **6** provided a suitable crystal for single-crystal X-ray diffraction studies.

Crystallographic Characterization of 2·PMe₃, 3a, 3b, 3d, 5, and 6. Crystallographic data were obtained at 193(±2) K on a Bruker PLATFORM/SMART 1000 CCD diffractometer (except for **3a**, for which data were collected by using a Siemens P4/RA diffractometer) using graphite-monochromated Mo Kα (λ = 0.71073 Å) radiation, employing samples that were mounted in inert oil and transferred to a cold gas stream on the diffractometer. Programs for diffractometer operation, data collection, and data reduction (including SAINT and SADABS) were supplied by Bruker. Gaussian integration was employed as the absorption correction method for **3a, 3b, 3d,** and **5**, while SADABS was used for **2·PMe₃** and **6**. For **3a, 3b, 3d,** and **5**, the structure was solved by use of direct methods, while for **2·PMe₃** and **6**, a Patterson search/structure expansion was employed. Refinements were carried out by use of full-matrix least-squares procedures (on *F*²) with *R*₁ based on *F*_o² ≥ 2σ(*F*_o²) and *wR*₂ based on *F*_o² ≥ -3σ(*F*_o²). Anisotropic displacement parameters were employed throughout for the non-hydrogen atoms. The B–H, Si–H (except for in **3d**), and Ru–H positions were located in the Fourier difference map and refined freely, with the exception that the Ru–H distance in **3d** was restrained to be 1.60(2) Å. Otherwise, all hydrogen atoms

were added at calculated positions and refined by use of a riding model employing isotropic displacement parameters based on the isotropic displacement parameter of the attached atom. Additional crystallographic information is provided in the deposited CIF. All thermal ellipsoid plots were generated by use of ORTEP-3 for Windows version 1.074.²⁰

Acknowledgment. The Natural Sciences and Engineering Research Council (NSERC) of Canada (including a Discovery Grant for M.S. and a Postgraduate Scholarship for M.A.R.), the Canada Foundation for Innovation, the Nova Scotia Research and Innovation Trust Fund, and Dalhousie University are acknowledged for their generous support of this work. We also thank the Atlantic Region Magnetic Resonance Center (Dalhousie University) for assistance in the acquisition of NMR data, as well as Professor Alex Bain (McMaster University) for advice regarding selective inversion NMR experiments and for providing the CIFIT program used in the ensuing data analysis.

Supporting Information Available: Single-crystal X-ray diffraction data in CIF format for **2·PMe₃, 3a, 3b, 3d, 5,** and **6** are available free of charge via the Internet at <http://pubs.acs.org>.

OM800761C

(20) Farrugia, L. J. *ORTEP-3* for Windows version 1.074. *J. Appl. Crystallogr.* **1997**, *30*, 565.

Metal-Organic Frameworks from Dipodal and Tripodal Silicon-Centered Tetrahedral Ligands

Zhongqiang Liu, Charlotte L. Stern, and Joseph B. Lambert*

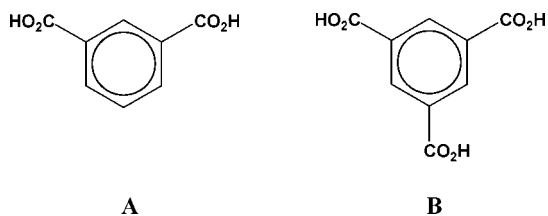
Department of Chemistry, Northwestern University, Evanston, Illinois 60208-3113

Received July 17, 2008

Six metal-organic frameworks from organic systems with tetrahedral geometry have been prepared and their crystal structures solved. The organic portions contain different central atoms ($M = S, C, Si$), a common binding group (4-carboxyphenyl), and a sterically variable series of nonbinding groups ($H, =O, CF_3$, phenyl, and tolyl). Five of these systems are dipodal, with two carboxyphenyl groups, and one is tripodal, with three. Dipodal systems with small, nonbinding groups produced two-dimensional, layered structures with medium void percentages. The nonbinding groups are positioned away from the voids. Dipodal systems with large (aryl), nonbinding groups produced three-dimensional networks with larger void percentages. The nonbinding aryl groups are directed into the voids, where they line the surfaces. The single tripodal case produced a two-dimensional, layered structure with a high void percentage. The pore sizes and shapes are tailored by and for the nonbinding groups.

Introduction

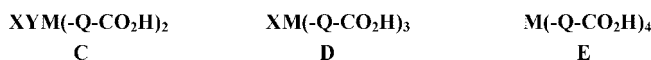
Metal-organic frameworks (MOFs) are a class of porous solids based on a lattice of metal ions connected by organic bridges.^{1,2} Choice of the two constituents largely dictates pore size and shape. MOFs often exhibit favorable storage properties of small molecules such as nitrogen, carbon dioxide, or hydrogen. In the present study, the focus is on the nonbinding portions of the organic constituent. Although numerous di- and tricarboxylic acids with aromatic centers have been examined (**A** and **B** are prototypes³), fewer examples have been prepared



in which the carboxylic acid groups are attached to a saturated, tetrahedral center, and these centers are usually carbon.^{4–7}

In tetrahedral systems, the central atom M is attached through spacers Q to two carboxylic acid groups for binding with the metal, so-called dipodal (“two-footed”) systems (**C**). Tripodal

systems contain three binding groups (**D**), and tetrapodal groups contain four (**E**). The groups X and Y are nonbinding. These



materials may form one-, two-, or three-dimensional frameworks, depending on the mode of binding with the metal ions. We previously reported two MOFs from tetrapodal systems.⁸ We report herein the synthesis and characterization of several MOFs constructed from di- and tripodal building blocks. We utilize silicon as the core atom (M) because of the ease of synthesis, but we also examine other core atoms (carbon, sulfur). We incorporate *para*-phenylene as the spacer Q between the core atom M and the carboxylic acid functionality, for reasons of synthetic convenience and to expand the size of the organic portion.

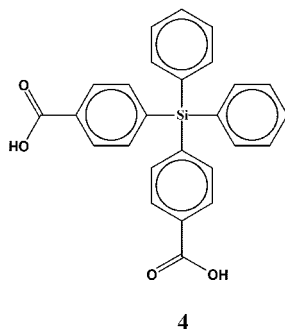
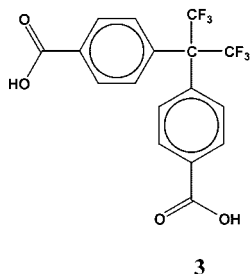
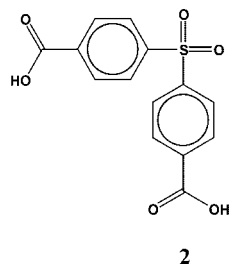
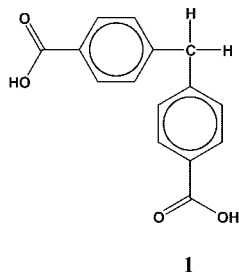
In contrast to our previously studied tetrapodal systems **E**,⁸ di- and tripodal systems (**C** and **D**) have one or two organic substituent (X and Y) that cannot bind with the metal. Such systems also contrast with many examples of the planar genre, e.g., **A** and **B**, which lack appended nonbinding substituents. Nonbinding groups may be positioned either away from or into any void within the crystalline MOF. Consequently, they play a strategic role in the design and realization of molecular voids. In this study, we have prepared MOFs with a variety of nonbinding substituents to explore their role in the properties of pores within crystals.

Results

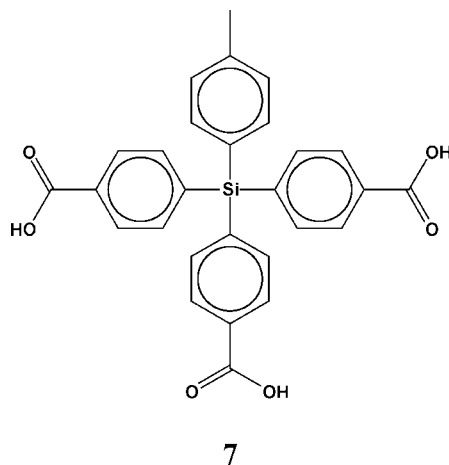
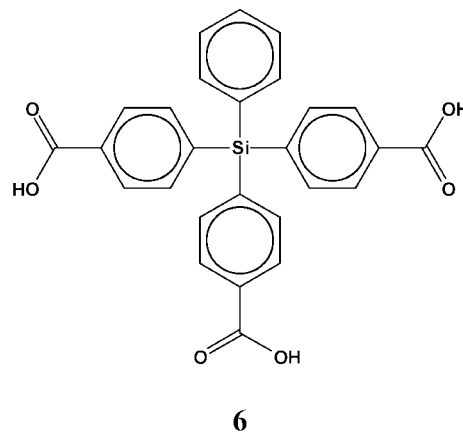
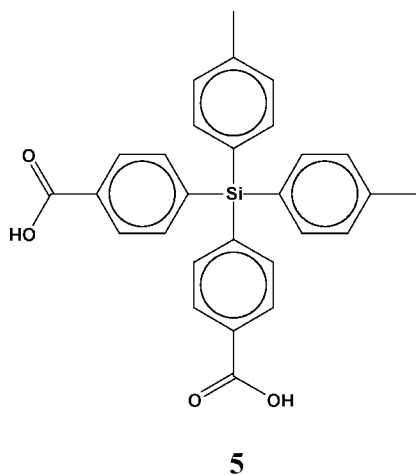
The organic constituents that we examined were the dipodal **1–5** and the tripodal **6** and **7**. Molecules **1–3** were

* Corresponding author. E-mail: jlambert@northwestern.edu.
 (1) Hupp, J. T.; Poeppelmeier, K. R. *Science* **2005**, *309*, 2008–2009.
 (2) Ockwig, N. W.; Delgado-Friedrichs, O.; O’Keeffe, M.; Yaghi, O. M. *Acc. Chem. Res.* **2005**, *38*, 176–182.
 (3) (a) Chui, S. S. Y.; Lo, S. M. F.; Charmont, J. P. H.; Orpen, A. G.; Williams, I. D. *Science* **1999**, *283*, 1148–1150. (b) Eddaoudi, M.; Kim, J.; Wachter, J. B.; Chae, H. K.; O’Keeffe, M.; Yaghi, O. M. *J. Am. Chem. Soc.* **2001**, *123*, 4368–4369.
 (4) Yaghi, O. M.; Richardson, D. A.; Li, G.; Davis, E.; Groy, T. L. *Mater. Res. Soc. Symp. Proc.* **1995**, *371*, 15–19.
 (5) Pan, L.; Sander, M. B.; Huang, X.; Li, J.; Smith, M.; Bittner, E.; Bockrath, B.; Johnson, J. K. *J. Am. Chem. Soc.* **2004**, *126*, 1308–1309.
 (6) Zou, R.-Q.; Zhong, R.-Q.; Du, M.; Kiyobayashi, M.; Xu, Q. *Chem. Commun.* **2007**, 2467–2469.
 (7) Gándara, F.; Gomez-Lor, B.; Gutiérrez-Puebla, E.; Iglesias, M.; Monge, M. A.; Proserpio, D. M.; Snejko, N. *Chem. Mater.* **2008**, *20*, 72–76.

(8) Lambert, J. B.; Liu, Z.; Liu, C. *Organometallics* **2008**, *27*, 1464–1469.
 (9) Speck, S. B. *J. Org. Chem.* **1953**, *18*, 1689–1700.
 (10) Milligan, R. J.; Delano, C. B.; Aponyi, T. J. *J. Macromol. Sci. Chem.* **1976**, *A10*, 1461–1477.
 (11) Cazacu, M.; Marcu, M.; Vlad, A.; Rusu, G. I.; Avadenei, M. *J. Organomet. Chem.* **2004**, *689*, 3005–3011.
 (12) Dybtssev, D. N.; Chun, H.; Yoon, S. H.; Kim, D.; Kim, K. *J. Am. Chem. Soc.* **2004**, *126*, 32–33.



commercially available, and **4** and **6** were prepared according to the literature.^{9–11} The new syntheses of **5** and **7** are presented in the Experimental Section.



did not yield diffraction data of sufficient quality to give a good structure. High-quality crystal structures were obtained for the other six MOFs, details of which are given in the Experimental Section and in the Supporting Information.

Pore volumes after removal of unbound solvent were calculated from the crystallographic data by Platon, which determines the volume within the total potential solvent area (TPSA) for a rolling guest molecule with a specified probe radius, e.g., 1.2 Å for H₂O, 1.65 Å for CO₂, 1.8 Å for N₂, 2.35 Å for 1-propanol, and 2.5 Å for isobutane. The probe radius is set at an extremely small value (0.1 Å) to assess the total possible void in the crystal. Table 1 presents the calculated pore volumes as a function of the probe radius of theoretical guest molecules with radii from 0.1 to 2.5 Å.

Thermogravimetric analysis was carried out on **2-Cd**, **3-Zn**, **4-Zn**, **5-Zn**, and **6-Zn**. Plots of temperature versus mass are provided in the Supporting Information.

Discussion

Pore Volume Analysis. The dipodal systems with the smallest nonbinding side groups (**1-Zn** with H and **2-Cd** with =O) exhibit modest TPSA-0.1 volumes (ca. 40%), a measure of the total void volume (Table 1). The dipodal **3-Zn** has a somewhat larger nonbinding side group (CF₃) and exhibits a

Both zinc nitrate and cadmium nitrate were used to provide the metal ions in the MOFs. We were able to isolate Zn MOFs from six organic ligands (**1-Zn**, **3-Zn**, **4-Zn**, **5-Zn**, **6-Zn**, and **7-Zn**) and a Cd MOF from one (**2-Cd**). Crystals of **7-Zn**

slightly smaller TPSA-0.1 volume (36.6%), similar to that of the previously reported **3-Cu**.⁵ The recently reported **3-Zn(2)**⁶ has the smallest volume in the table (ca. 31%). Although both **3-Zn** and **3-Zn(2)** have space group C2/c,

Table 1. Volume within the Total Potential Solvent Area (TPSA) Available to Probe Molecules as a Function of Probe Radius, Expressed as a Percentage (%) of the Total Crystal Volume^a

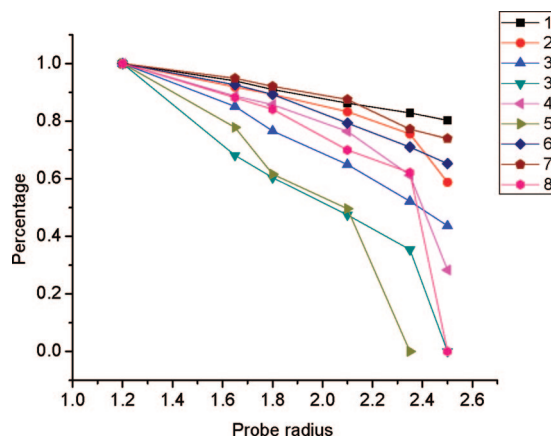
system	radius, Å							ratio ^b
	0.1	1.2	1.65	1.80	2.10	2.35	2.5	
1-Zn	42.0	23.3	21.9	21.2	20.1	19.3	18.7	0.55
2-Cd	40.4	23.3	21.4	20.8	19.4	17.6	13.7	0.58
3-Zn	36.6	9.4	8.0	7.2	6.1	4.9	4.1	0.26
3-Zn(2)^c	30.8	0.0	0.0	0.0	0.0	0.0	0.0	0.00
3-Cu^d	39.5	11.6	7.9	7.0	5.5	4.1	0.0	0.29
4-Zn	48.9	30.1	26.7	25.8	23.0	18.4	8.5	0.62
5-Zn	46.4	23.4	18.2	14.4	11.6	0.0	0.0	0.50
6-Zn	55.2	42.0	38.9	37.5	33.3	29.8	27.4	0.76
Ge-Zn^e	58.7	46.4	44.0	42.7	40.6	35.8	34.3	0.79
Mn-For^f	48.3	34.6	30.5	29.1	24.2	21.5	0.0	0.72

^a Calculated by Platon (version 230608) with grid 0.1 Å for probe 0.1 Å and grid 0.2 Å for all other probe radii. ^b Ratio of TPSA(1.2)/TPSA(0.1). ^c Crystallographic data from ref 6. ^d Crystallographic data from ref 5. ^e Crystallographic data from ref 8. ^f Crystallographic data from ref 12.

the beta angles differ (90.7° vs 92.5°) and the zinc clusters are different. The TPSA-0.1 volume percentages for all the MOFs constructed from **3** are less than 40%. The medium-sized, nonbinding CF₃ group clearly does not lead to enhancement of the total void volume, compared with the structures **1** and **2** with smaller nonbinding groups. Dipodal systems with large (aromatic) nonbinding side groups [**4-Zn** (phenyl) and **5-Zn** (tolyl)] exhibit higher TPSA-0.1 volumes (>45%). Thus larger nonbinding groups do not lower the void volume. On the contrary, they increase the available TPSA-0.1 volume, possibly by assisting efficient arrangement of the framework backbone to generate more void volume. Such hypotheses must be examined in light of the framework structure. The tripodal system **6-Zn** and the previously reported tetrahedral system **Ge-Zn**⁸ have the largest calculated TPSA-0.1 volumes in the table (>55%), which may be rationalized in terms of the framework structure (vide infra).

The total free volume as measured by TPSA-0.1 serves as a measure of the overall porosity of the crystal. Details of the crystal structure, however, may result in obstructions that prevent a probe molecule from entering portions of the voids. A water molecule, with a kinetic radius of 1.2 Å, is regarded as one of the smallest guest molecules. The calculated percentages for the TPSA-1.2 volumes diminished from the TPSA-0.1 volumes for all samples, by elimination of voids that can be accessed only by probes with radii less than 1.2 Å. The final column in Table 1 gives the ratio of TPSA-1.2 to TPSA-0.1. Among the dipodal systems, the MOFs with the medium nonbinding CF₃ group (**3**) exhibit the largest percentage decrease, 70–100% according to the final column. The MOFs **3-Zn** and **3-Cu**⁵ have TPSA-1.2 volumes representing about 10% of the crystal, and the MOF **3-Zn(2)**⁶ has no available void (0%). In the last crystal, the unit cell cannot hold even a single water molecule. All other MOFs exhibited good accessibility for guests with the size of a water molecule. The remaining dipodal systems (**1-Zn**, **2-Cd**, **4-Zn**, and **5-Zn**) have TPSA-1.2 volumes representing 23–30% of the crystal, indicating decreased availability by about 40–50% from TPSA-0.1 according to the final column. The tripodal (**6-Zn**) and the tetrahedral (**Ge-Zn**)⁸ systems exhibited TPSA-1.2 volumes that represent 42–46% of the crystals, a decrease of only ca. 25%.

Crystal selectivity to probe molecules may be indicated by changes in the TPSA volumes as the probe molecules become larger. As expected, the TPSA percentages decrease with larger probe radii, but not in the same fashion for all systems. The MOF **5-Zn** is entirely closed (and **3-Zn** and **3-Cu** mostly) to a

**Figure 1.** Ratio of TPSA with variable guest probe radius to TPSA-1.2. The numbers 1–6 correspond to the MOF numbers; 3' is **3-Cu**, 7 is **Ge-Zn**, and 8 is **Mn-For**.

molecule with probe radius 2.35 Å such as 1-propanol, but the MOFs **1-Zn**, **2-Cd**, **4-Zn**, **6-Zn**, **Ge-Zn**, and **Mn-For** are still open to it. At probe radius 2.5 Å such as for isobutane, the voids in **4-Zn** and **Mn-For** are mostly closed off, but **1-Zn**, **2-Cd**, **6-Zn**, and **Ge-Zn** are still reasonably open. In fact, **1-Zn** is remarkably nonselective throughout the entire range of probe sizes, and **2-Cd**, **6-Zn**, and **Ge-Zn** show only modest selectivity. Although **3-Zn** and **3-Cu** do show selectivity, the overall amount of crystal void is always small (ca. 0–10%). The MOF **Mn-For** shows selectivity only above 2.35 Å. MOFs **4-Zn** and **5-Zn** show both high selectivity and high crystal voids. These observations are summarized in Figure 1, in which accessibility is represented by the ratio of the TPSA for a given probe radius to the TPSA-1.2. The relatively level lines at the top indicate poor selectivity for **1-Zn**, **6-Zn**, and **Ge-Zn** (7 in the plot), and the relatively steep lines indicate high selectivity for **4-Zn** and **5-Zn**, as well as **3-Zn**, **3-Cu** (3' in the plot), and (for a single point) **Mn-For** (8 in the plot). Predictions based on crystallographic voids may not translate into gas sorption, because of crystalline instability on removal of nonbound solvent.^{13,14} These predictive trends are being tested by the experimental determination of porosity and gas sorption.

Influence of the Nonbinding Substituents on the Reticulated Structures. The two structures with the smallest nonbinding substituents, H in **1-Zn** and =O in **2-Cd**, have very similar reticulated structures. Although the smallest repeating unit for **1-Zn** is a trizinc cluster and that for **2-Cd** is a dicadmium structure (Figure 2), the reticulated structures in both cases are composed of two-dimensional layers with large, square, solvent-filled channels (Figure 3).¹⁵ For both systems, the nonbinding side chains (atoms in this case) are pointed away from the channels: H of CH₂ for **1-Zn** (not depicted in Figure 3, left) and O of SO₂ for **2-Cd** (shown in red in Figure 3, right). These small atomic substituents do not have to be directed into the void channels but can be accommodated within the layers. The depiction in Figure 4 displays the inner surfaces in blue and the outer surfaces in gray.

The square channels depicted in Figures 3 and 4 have approximate dimensions 7.6 × 8.2 Å for **1-Zn** and 5.9 × 5.9 Å for **2-Cd**. The channels in both cases are reasonably accessible

(13) Yaghi, O.; O'Keefe, M.; Kanatzidis, M. J. *Solid State Chem.* **2000**, 152, 1–2.

(14) Barbour, L. J. *Chem. Commun.* **2006**, 1163–1168.

(15) Zhuang, W. J.; Sun, C.-Y.; Jin, L.-P. *Polyhedron* **2007**, 26, 1123–1132.

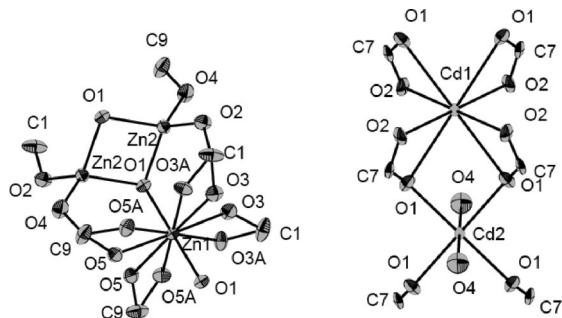


Figure 2. Trinuclear zinc-oxo cluster of **1-Zn** (left) and the dinuclear cadmium-oxo cluster of **2-Cd** (right) with 50% probability level thermal ellipsoids.

to probes with radii between 1.2 and 2.5 Å (Table 1), although the large size of the channel openings suggests low selectivity, at least in this range (Figure 1). These respectable void sizes are tempered by the layered structure of these MOFs. Heating could delaminate such structures and lead to void inaccessibility or even destruction of the channels.

Trifluoromethyl, as represented in **3**, is the next larger nonbinding substituent. The tetrazinc cluster of the smallest repeating unit in **3-Zn** (Figure 5, left) leads to a three-dimensional reticulated structure (Figure 5, right). The structure contains a small, square pore (ca. 3.5 × 3.5 Å) formed by phenylene rings from two distinct smallest repeating units. The trifluoromethyl groups in green are directed away from the pore into a larger (ca. 5.1 × 5.1 Å) square that appears to be mostly filled. The small size of the pore resulted in the smallest TPSA values of MOFs in the present study for the entire range 1.2–2.5 Å (Table 1). MOF **3-Cu**⁵ is similar, but MOF **3-Zn(2)**⁶ has a very different structure without voids. The structure of the recently reported **3-In** is rather like the layered structures of **1-Zn** and **2-Cd**, but the trifluoromethyl groups still are directed away from any void.⁷

Molecules **4** and **5** introduce relatively bulky nonbinding substituents with phenyl and tolyl, respectively. In their zinc complexes, **4-Zn** contains a tetrazinc cluster and **5-Zn** a classical pinwheel dizinc cluster (Figure 6). These clusters lead to the reticulated structures illustrated in Figure 7. The long, narrow channels (3.6 × 15.2 Å) in **4-Zn** (left) clearly are lined by the nonbinding phenyl substituents. The narrow (2.6 × 5.2 Å) channels of **5-Zn** (right) extend from one cyan-colored zinc cluster vertically to the next Zn cluster below it. These channels also are lined by the tolyl groups. Consequently, these larger substituents limit the size and define the properties of the resulting channels, in contrast with the channels observed in the MOFs from **1–3**. Nonetheless, both **4-Zn** and **5-Zn** are porous solids (Table 1) with 23–30% void volume for a probe of radius 1.2 Å, the largest observed among those discussed so far. Moreover, they slowly close off as the probe radius increases (Figure 1). The slit-like channel of **4-Zn** and the worm-hole-like channel of **5-Zn** are visualized with van der Waals surfaces in Figure 8.

Molecule **6** is tripodal and carries a single nonbinding phenyl ring. It forms a tetrazinc cluster (Figure 9, left) that translates into a two-dimensional array (Figure 9, right) resembling the (6,3)-connected network of AB₂ compounds such as CdI₂ (see Experimental Section for details). Figure 9 (right) depicts the planar array viewed along the *a* axis, but the channel is best viewed along the *b* axis (see the Experimental Section). The resulting channels are visualized in Figure 10 (left). This reticulated structure is the most porous of those examined here

(Table 1, 42% void volume for TPSA-1.2). This relatively large void shows little selectivity according to Figure 1.

Conclusions

Carboxylic acid functionalities arranged around tetrahedral centers react with metal ions to produce solids possessing framework structures with significant voids. Dipodal systems with small to medium, nonbinding side groups attached to carbon or sulfur central atoms [**1-Zn** (–H), **2-Cd** (=O), **3-Zn** (–CF₃)] form structures (Figures 3 and 5) with low to medium void volumes exemplified by TPSA-1.2 values of ca. 10–23%. Dipodal systems with larger (aromatic), nonbinding side groups on silicon central atoms (**4-Zn** [phenyl] and **5-Zn** [tolyl]) form three-dimensional networks (Figure 7) with medium to high porosity (TPSA-1.2 of 23–30%). The tripodal system **6-Zn** with three carboxyphenyl groups and one nonbinding phenyl group possesses a two-dimensional framework (Figure 9) with the largest observed porosity (TPSA-1.2 of 42%). These results suggest that increased porosity may be achieved by larger nonbinding side groups. In **1-Zn** (H), **2-Cd** (=O), and **3-Zn** (–CF₃), the small substituents are directed away from the voids into occupied regions of the two- or three-dimensional arrays (Figures 3 and 5). The pairs of large phenyl (**4-Zn**) and tolyl (**5-Zn**) groups apparently cannot meld into the innards of the reticulated structure, so they are thrust into the voids, where they serve more or less as linings (Figures 7 and 8). The substituents both limit the size of the voids and provide a hydrocarbon and π-electron-rich surface.

The network found in **6-Zn** is a metal-organic analogue of the crystal structure of the (6,3)-connected AB₂ system cadmium diiodide, in which the octahedral (hexacoordinate) tetrazinc-oxo subcluster of **6-Zn** simulates the geometry around cadmium and the tetrahedral (tricoordinate) silicon subcluster simulates the geometry around iodine.

Experimental Section

Di(4-tolyl)di(4-carboxyphenyl)silane (5) and (4-Tolyl)tri(4-carboxyphenyl)silane (7). A 250 mL, round-bottomed flask containing a stirring bar was charged with 1.55 g (4 mmol) of tetra(4-tolyl)silane,¹⁶ 90 mL of pyridine, and 30 mL of water. The mixture was heated to mild reflux, and KMnO₄ (6.3 g, 40 mmol) was added in portions. The mixture was refluxed for several hours until the dark purple solution became light yellow. The flask was cooled to room temperature, and the byproduct MnO₂ was removed by vacuum filtration. The filtrate was concentrated on a hot plate to about 15 mL, and concentrated HCl was added until the pH was 1. The resulting solid was subjected to repetitive column chromatography (hexane/ethyl acetate/methanol) to produce pure di(4-carboxyphenyl)di(4-tolyl)silane (**5**) and tri(4-carboxyphenyl)(4-tolyl)silane (**7**) in yields of about 10% each. Di(4-tolyl)di(4-carboxyphenyl)silane: ¹H NMR (acetone-*d*₆) δ 8.07 (d, 4H), 7.66 (d, 4H), 7.41 (d, 4H), 7.29 (d, 4H), 2.36 (s, 6H); ¹³C NMR (acetone-*d*₆) δ 167.2, 140.8, 139.6, 136.4, 132.5, 129.6, 128.9, 21.3. (4-Tolyl)tri(4-carboxyphenyl)silane: ¹H NMR (acetone-*d*₆) δ 8.10 (d, 6H), 7.72 (d, 6H), 7.47 (d, 2H), 7.32 (d, 2H), 2.39 (s, 3H); ¹³C NMR (acetone-*d*₆) δ 166.8, 140.6, 139.3, 136.5, 132.3, 129.4, 129.1, 20.9.

Preparation of the Metal-Organic Frameworks. The following procedure illustrates the synthesis for one example. The other procedures are very similar and can be found elsewhere.¹⁷

(16) Lambert, J. B.; Zhao, Y.; Stern, C. *J. Phys. Org. Chem.* **1997**, *10*, 229–232.

(17) Liu, Z., Ph.D. Dissertation, Northwestern University, Evanston, IL, 2005.

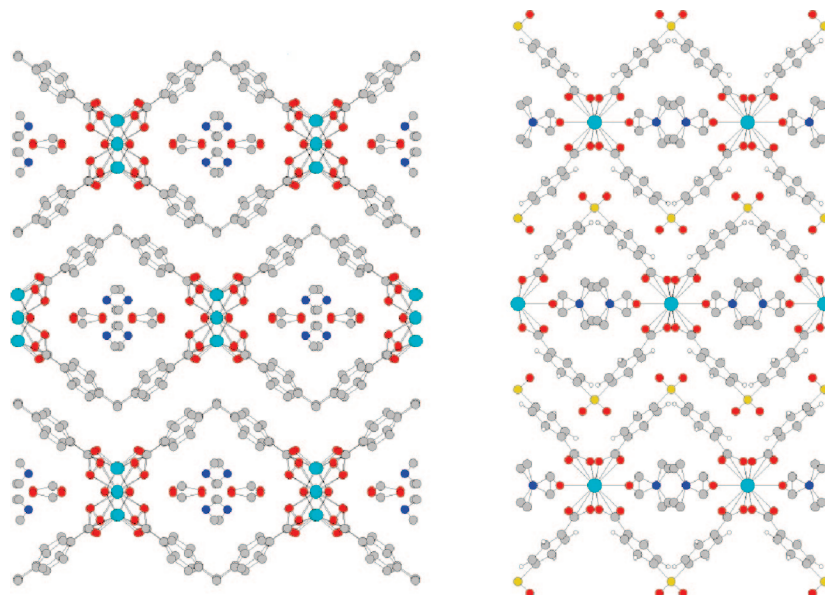


Figure 3. (Left) View along the *c* axis of the framework of **1-Zn**: Zn (cyan), O (red), C (gray), and N (blue). The solvent dimethylformamide is not chemically bound to the framework. (Right) View along the (Cd–Cd) *c* axis of the framework of **2-Cd**: Zn (cyan), O (red), C (gray), N (blue), and S (yellow).

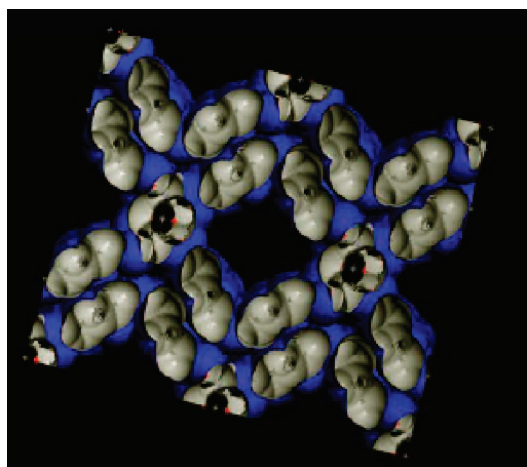


Figure 4. Calculated van der Waals surfaces for two layers of the reticulated structure of **1-Zn**. The central black zone constitutes the channel. The blue and gray colors respectively represent the inner (toward the void) and outer (toward the framework) van der Waals surfaces.

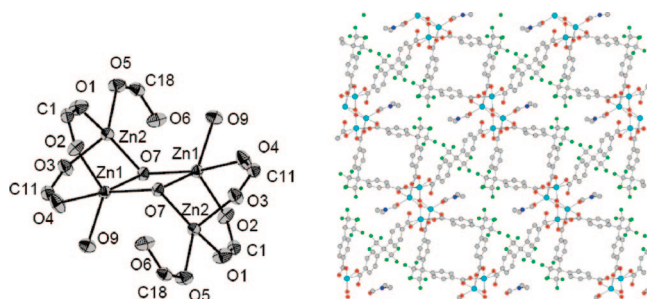


Figure 5. (Left) Tetranuclear zinc-oxo cluster of **3-Zn** with 50% probability level thermal ellipsoids. (Right) View along the *b* axis of the framework of **3-Zn**: Zn (cyan), O (red), C (gray), N (blue), and F (green).

Tri(4-carboxyphenyl)phenylsilane-zinc (6-Zn). To a 20 mL vial were added 27 mg (0.06 mmol) of tri(4-carboxyphenyl)phenylsilane and 60 mg (0.2 mmol) of zinc nitrate hexahydrate.

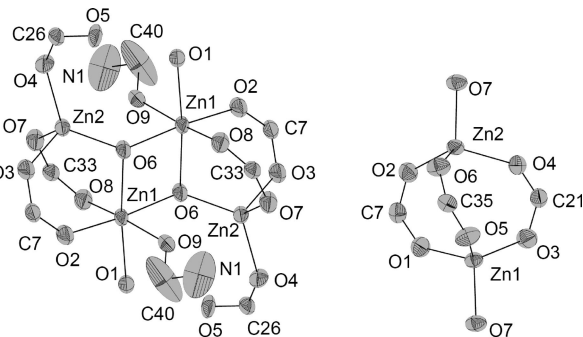


Figure 6. (Left) Tetranuclear zinc-oxo cluster of **4-Zn** with 50% probability level thermal ellipsoids. (Right) Dinuclear zinc-oxo cluster of **5-Zn** with 50% probability level thermal ellipsoids.

Dimethylformamide (DMF, 4.5 mL), ethanol (4.5 mL), and water (3.6 mL) were added to dissolve the organic ligand and the salt. The mixture was shocked by ultrasonic sound for 10 min. The solution was filtered through fritted glass (fine) into three 4 mL vials, which were sealed with Teflon-lined caps. These vials were placed in an oil bath. The bath was heated slowly to 75 °C, held at that temperature for three days, and then cooled to room temperature. Colorless crystals were collected and dried under vacuum (10 Torr) for three days at room temperature, with an overall yield of 20%.

Elemental Analyses. Di(4-carboxyphenyl)methane-zinc (**1-Zn**). Anal. after the sample was dried at room temperature under vacuum (0.1 Torr) for 24 h: calcd for $(C_{15}H_{10}O_4)(Zn_3(OH)_2)(C_3H_7NO)_2(H_2O)_{1.5}$: C, 47.42%, H, 4.31%, N, 3.07%; found: C, 47.25%, H, 3.91%, N, 3.17%. Di(4-carboxyphenyl)sulfone-cadmium (**2-Cd**). Anal. after the sample was dried at room temperature under vacuum (0.1 Torr) for 24 h: calcd for $(C_{14}H_8O_6S)Cd(C_3H_7NO)(H_2O)_{0.5}$: C, 40.94%, H, 3.23%, N, 2.81%; found: C, 40.98%, H, 3.08%, N, 2.83%. 2,2-Di(carboxyphenyl)-1,1,1,3,3,3-hexafluoropropane-zinc (**3-Zn**). Anal. after the sample was dried at room temperature under vacuum (0.1 Torr) for 24 h: calcd for $(C_{17}H_8F_6O_4)_3(Zn_4(OH)_2)(C_3H_7NO)_2(C_2H_6O)_3$: C, 43.22%, H, 3.34%, N, 1.60%; found: C, 43.58%, H, 3.60%, N, 1.82%. Anal. after the sample was dried at 150 °C under vacuum (0.1 Torr) for 4 h: calcd for $(C_{17}H_8F_6O_4)_3(Zn_4(OH)_2)(C_3H_7NO)_{0.5}$: C, 41.96%, H, 1.98%, N, 0.47%; found: C, 42.21%, H, 1.96%, N, 0.19%. Di(4-

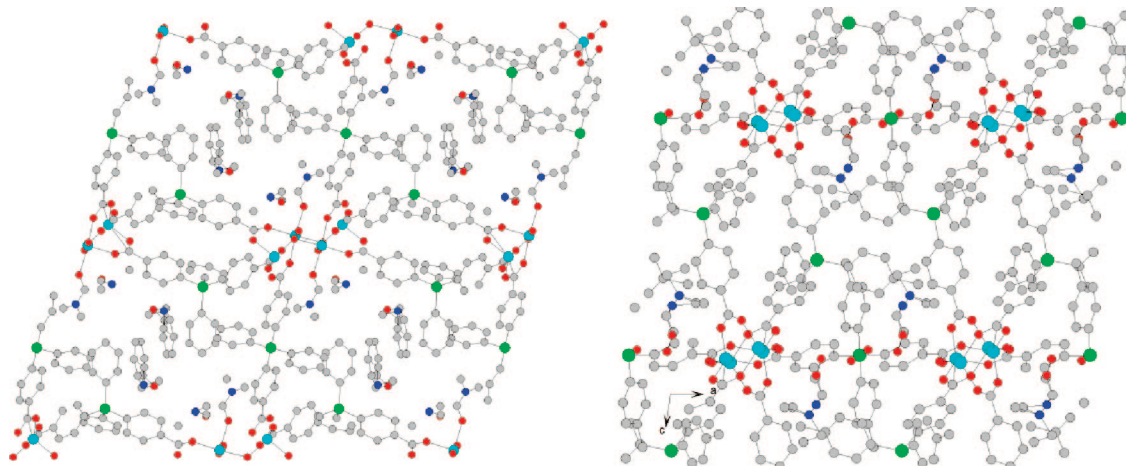


Figure 7. (Left) View along the *b* axis of the framework of **4-Zn**: Zn (cyan), O (red), C (gray), N (blue), and Si (green). (Right) View along the *b* axis of the framework of **5-Zn**: Zn (cyan), O (red), N (blue), C (gray), and Si (green).

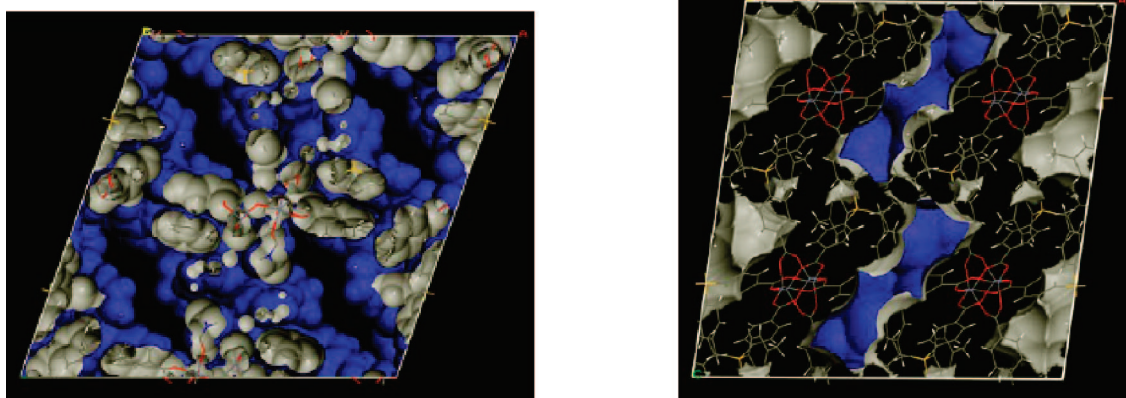


Figure 8. (Left) Depiction of the pores in **4-Zn**. (Right) Depiction of the pores in **5-Zn**. The central black zones constitute the channels. The blue and gray colors respectively represent the inner (toward the void) and outer (toward the framework) calculated van der Waals surfaces.

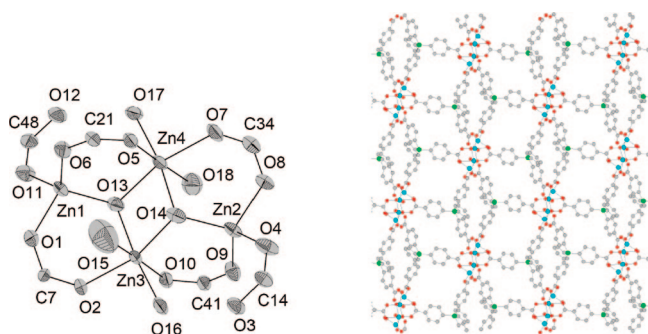


Figure 9. (Left) Tetranuclear zinc-oxo cluster of **6-Zn** with 50% probability level thermal ellipsoids. (Right) View along the *a* axis of the framework of **6-Zn**: Zn (cyan), O (red), C (gray), and Si (green).

carboxyphenyl)diphenylsilane-zinc (**4-Zn**). Anal. after the sample was dried at room temperature under vacuum (0.1 Torr) for 24 h: calcd for $(C_{26}H_{18}O_4Si)_3(Zn_4(OH)_2)(C_3H_7NO)_{0.1}(C_6H_6)_{0.5}$: C, 60.67%, H, 3.74%, N, 0.01%; found: C, 61.03%, H, 3.61%, N, 0.35%. Di(4-carboxyphenyl)di(4-tolyl)silane-zinc (**5-Zn**). Anal. after the sample was dried under vacuum (10 Torr) at room temperature for 3 days: calcd for $(C_{28}H_{22}O_4Si)_3(Zn_4(OH)_2)(C_3H_7NO)(C_2H_6O)_{0.5}(H_2O)$: C, 60.01%, H, 4.58%, N, 0.80%; found: C, 59.96%, H, 4.42%, N, 1.01%. Anal. after the sample was dried at room temperature under vacuum (0.1 Torr) for 24 h: calcd for $(C_{28}H_{22}O_4Si)_3(Zn_4(OH)_2)(C_3H_7NO)_{0.5}$: C, 60.99%, H, 4.28%, N, 0.42%; found: C, 60.93%,

H, 4.39%, N, 0.43%. Tri(4-carboxyphenyl)phenylsilane-zinc (**6-Zn**). Anal. after the sample was dried at room temperature under a vacuum of 0.1 Torr for 24 h: calcd for $(C_{27}H_{17}O_6Si)_2(Zn_4(OH)_2)(C_3H_7NO)(H_2O)$: C, 51.96%, H, 3.44%, N, 1.06%; found: C, 51.70%, H, 3.29%, N, 1.21%. Anal. after the crystals were dried under vacuum (0.1 Torr) at 150 °C for 4 h: calcd for $(C_{27}H_{17}O_6Si)_2(Zn_4(OH)_2)$: C, 52.88%, H, 2.96%, N, 0.0%; found: C, 52.62%, H, 2.90%, N, 0.19%.

Single-Crystal Structures. Crystals were mounted using oil (Infinite V8512) on a glass fiber. Measurements were made on a CCD area detector with graphite-monochromated MoK α radiation. The structures were solved by direct methods and expanded using Fourier techniques. Non-hydrogen atoms were refined anisotropically. Hydrogen atoms were included at calculated positions but were not refined, except as noted in the following. Some crystallographic parameters are collected in Table 2, and further details are given elsewhere¹⁷ and in the Supporting Information.

Crystal Structure of 1-Zn. Molecular Formula. The two hydrogen atoms (H8 and H16) on the methylene carbon were refined isotropically. The hydrogen atoms on the unbound, disordered solvent DMF and the water molecules were not included. The molecular formula, based on the three-zinc portion, was obtained as follows. The three Zn atoms are attached to four organic portions, each of which contributes $C_{15}H_{10}O_4$ to the molecular formula but is shared by two trizinc clusters. The total formula for this portion of the structure therefore is $Zn_3C_{30}H_{20}O_8$. The two bound hydroxides contribute a pair of oxygens, but the attached hydrogens were not

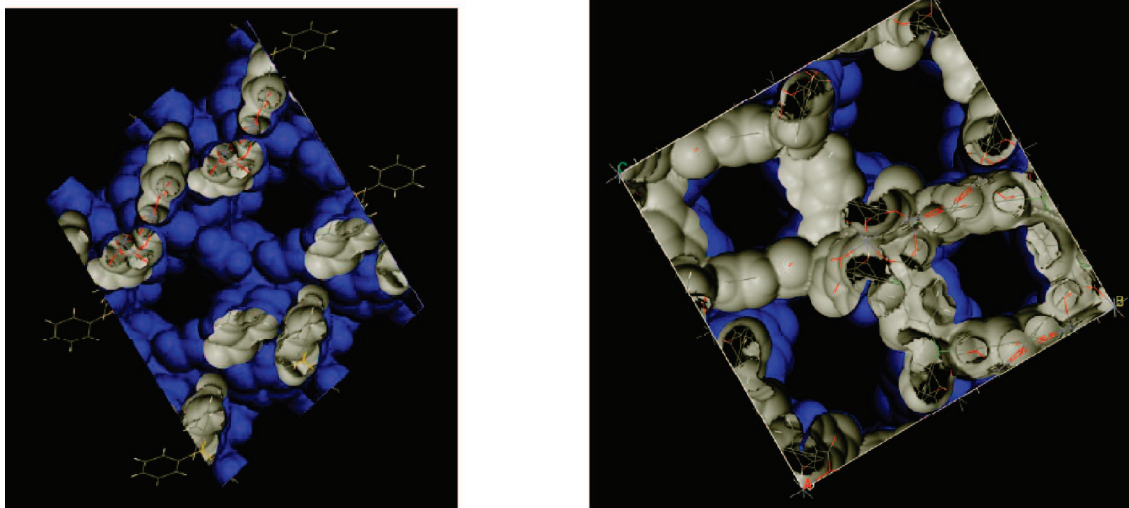


Figure 10. (Left) Depiction of the pores in **6-Zn**. (Right) Depiction of the pores in the zinc cluster of $\text{Ge}(\text{C}_6\text{H}_4\text{CO}_2\text{H})_4$ from ref 8. The central black zones constitute the channels. The blue and gray colors respectively represent the inner (toward the void) and outer (toward the framework) calculated van der Waals surfaces.

Table 2. Crystallographic Parameters

	1-Zn	2-Cd	3-Zn	4-Zn	5-Zn	6-Zn
cryst syst	monoclinic	monoclinic	monoclinic	monoclinic	monoclinic	tri- clinic
space group	$C/2c$	$C2/m$	$P2/n$	$C/2c$	$C/2c$	$P\bar{1}$
a , Å	16.2	11.7	17.9	33.4	27.1	10.0
b , Å	21.8	22.7	7.5	9.6	12.1	17.1
c , Å	12.1	7.7	23.8	32.3	28.0	24.0
α , deg	90	90	90	90	90	87.8
β , deg	129.7	124.8	92.5	109.5	97.6	79.7
γ , deg	90	90	90	90	90	75.5
volume, Å ³	3291.5	1675.4	3189.7	9858.3	9104.0	3898.9
Z	4	4	4	8	8	4
maximum transmission	0.8498	0.7469	0.9741	0.9296	0.9052	0.7404
min. transmn	0.4698	0.5104	0.6211	0.6917	0.6415	0.5517
final R1 ($I > 2\sigma(I)$)	0.0544	0.0605	0.0407	0.0713	0.0589	0.0656
final wR1 ($I > 2\sigma(I)$)	0.1511	0.1462	0.1024	0.2097	0.1875	0.1927

included, bringing the formula to $\text{Zn}_3\text{C}_{30}\text{H}_{20}\text{O}_{10}$. The hydrogen atoms of the unbound solvent molecules, DMF (C_3NO) and water, were not included, bringing the total molecular formula to $\text{Zn}_3\text{C}_{33}\text{H}_{20}\text{NO}_{12}$, which was calculated and reported (per three Zn atoms).

Reticulated Structure. The zinc cluster substructure of **1-Zn** has the formula $\text{Zn}_3(\text{RCO}_2)_4(\text{OH})_2$, with two types of zinc atoms (Figure 2, left). Hexacoordinate Zn1 is bound to four disordered oxygen atoms (O3, O5) of two pairs of carboxylate ions (C1, C9) and to two oxygen atoms (O1) from two identical hydroxide ions. Tetracoordinate Zn2 is bound to two oxygen atoms (O2, O4) from two carboxylate ions (C1, C9) and to two oxygen atoms (O1) from two identical hydroxide ions. Thus carboxyl groups C1 and C9 bridge between Zn1 and Zn2. The trizinc cluster contains two identical Zn2 atoms. The hydroxide ion O1 is tricoordinate and bridges to all three zinc atoms (Zn1, Zn2, Zn2). Each carboxylate group is attached through the phenylene spacer to the CH_2 group, which in turn is attached through the second phenylene spacer to another trizinc cluster. The constituents reticulate to form two-dimensional layers with large solvent-filled channels (Figure 3, left), in a superstructure very similar to that of **2-Cd** (Figure 3, right). The size of the channel is roughly 7.6×8.2 Å, slightly larger than that of **2-Cd**. The distance between benzene rings from adjacent layers is about 3.76 Å, which suggests some aromatic π - π stacking.

Crystal Structure of 2-Cd. Molecular Formula. Hydrogen atoms of the bound DMF molecule were not included. Based on a two-cadmium portion, the organic molecule is present four times and is shared by two dicadmium clusters. It contributes

$\text{Cd}_2\text{C}_{28}\text{H}_{16}\text{O}_{12}\text{S}_2$ to the molecular formula. The two bound DMF molecules contribute $\text{C}_6\text{N}_2\text{O}_2$ to give the calculated and reported formula of $\text{Cd}_2\text{C}_{34}\text{H}_{16}\text{N}_2\text{O}_{14}\text{S}_2$ (per two Cd atoms).

Reticulated Structure. The cadmium cluster substructure of the sulfone **2** has the general formula $\text{Cd}_2(\text{RCO}_2)_4(\text{DMF})_2$, with two types of Cd (Figure 2, right). Octacoordinate Cd1 is bound to eight oxygen atoms (four O1 and four O2) from four identical, bidentate carboxylate ions (C7), and hexacoordinate Cd2 is bound to four oxygen atoms (O1) from four identical, monodentate carboxylate ions (C7) and to two oxygen atoms (O4) from two solvent DMF molecules. Thus O1 bridges between Cd1 and Cd2. Each carboxylate group is bound through the phenylene spacer to the sulfone group, which is bound through its second phenylene substituent to another cadmium cluster. Repetition of these arrangements creates two-dimensional layers with large channels filled with disordered solvent (Figure 3, right). The sulfonyl groups are packed above and below the Cd cluster. The size of the channel is roughly 5.9×5.9 Å. The distance between benzene rings from adjacent layers is about 3.75 Å, which suggests some aromatic π - π stacking.

Crystal Structure of 3-Zn. Molecular Formula. Hydrogen atoms of the unbound, disordered solvent ethanol molecule and of the two bound hydroxide anions were not included. The molecular formula, based on a four-zinc portion, was obtained as follows. The four Zn atoms are attached to six carboxyl groups of six organic molecules. Each of these organic molecules contributes $\text{C}_{17}\text{H}_8\text{F}_6\text{O}_4$ but is shared by two tetrazinc clusters. Consequently, this portion of the molecular formula is $\text{Zn}_4\text{C}_{51}\text{H}_{24}\text{F}_{18}\text{O}_{12}$ (for example, for C, $17(6/2) = 51$). The two bound hydroxide groups increase the

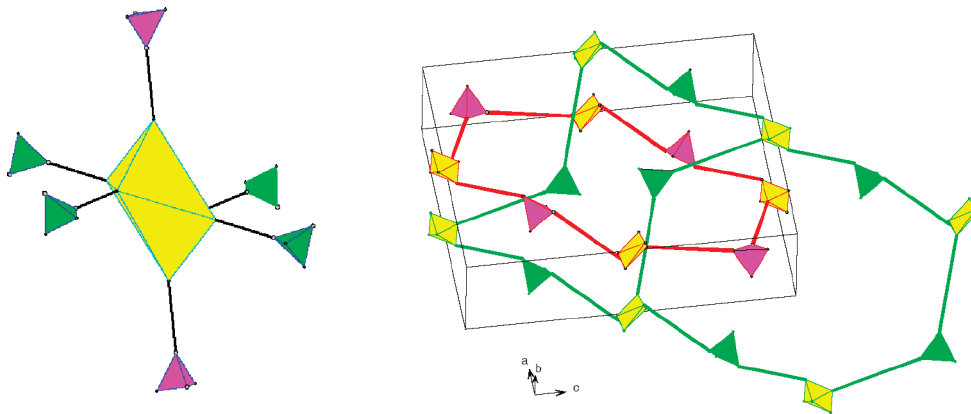


Figure 11. (Left) Zinc-oxo cluster of **3-Zn** simplified to a hexacoordinated antiprismatic octahedron (yellow) bound to four tetrahedra via carboxylate ions (C1 or C11, green) and to two tetrahedra via carboxylate ions (C18, purple). (Right) Two interpenetrating strands within a unit cell.

formula to $Zn_4C_{51}H_{24}F_{18}O_{14}$. The two bound DMF molecules add $C_6H_{14}N_2O_2$, bringing the formula to $Zn_4C_{57}H_{38}F_{18}N_2O_{16}$. On the basis of Zn_4 , there is an unbound, disordered, half-occupied ethanol molecule. The methylene carbon lies on an inversion center and is counted only a single time for each pair of ethanol molecules. The resulting contribution to the molecule formula is $C_{1.5}O$ (methyl twice, oxygen twice, methylene once, for C_3O_2 per Zn_8 , divided by two for half-occupancy, without hydrogen atoms). The final molecular formula, calculated and reported, is $Zn_4C_{58.5}H_{38}F_{18}N_2O_{17}$ (per four Zn atoms).

Reticulated Structure. The zinc complex of **3** crystallizes with a tetranuclear zinc cluster substructure (Figure 5, left) with the general formula $Zn_4(RCO_2)_6(OH)_2(DMF)_2$. Each carboxylate group is attached via a phenylene spacer (R) to the central atom C of **3**, not represented in the figure. There are two distinct zinc atoms. Pentacoordinate Zn1 is attached to two oxygen atoms (O2, O4) from two different carboxylate groups (C1, C11), two oxygen atoms from two identical hydroxide ions (O7), and one oxygen atom (O9) from the solvent dimethylformamide (DMF). Tetracoordinate Zn2 is attached to three oxygen atoms (O1, O3, O5) from three different carboxylate groups (C1, C11, C18) and one oxygen atom from hydroxide (O7). There are two of each type of Zn in the repeating structure. The two hydroxide ions (O7) are tridentate, bonding with two Zn1 atoms and one Zn2 atom. Four carboxylate groups (two each of C1 and C11) are bidentate and bridge between Zn1 and Zn2. Two carboxylate groups (C18) are monodentate and bond only to Zn2. The metal and organic constituents reticulate to form a porous framework (Figure 5, right). The framework contains a molecular square (ca. 3.5×3.5 Å) composed of two tetrazinc clusters and two molecules of **3**. The framework also contains a larger cyclic structure (ca. 5.1×5.1 Å) composed of four tetrazinc clusters and four molecules of **3**. The framework topology may be reduced conceptually by viewing the zinc-oxo cluster as a hexacoordinate antiprism (the four zinc atoms as a unit are bound to six carboxylate groups). In the same sense, **3** is a bidentate tetrahedron with the CF_3 groups providing the other two unbound groups on the tetrahedron. Figure 11 (left) illustrates one antiprism or octahedron bound to six tetrahedra. Repetition of this building block in three dimensions produces the framework, which is complicated by the presence of two identical, interpenetrating strands (Figure 11, right). The octahedra and tetrahedra of one strand are connected by green lines, and those of the other strand by red lines in the figure.

Crystal Structure of 4-Zn. Molecular Formula. Hydrogen atoms of the unbound, disordered solvent benzene, DMF, and water molecules and of the bound hydroxide ions and water molecules were not included. On the basis of a tetrazinc cluster, there are six organic molecules ($SiC_{26}H_{18}O_4$), each shared between two zinc clusters. Their contribution to the molecular formula therefore is

$Zn_4Si_3C_{78}H_{54}O_{12}$. The oxygen atoms from the two bound hydroxide ions and two bound water molecules bring the formula to $Zn_4Si_3C_{78}H_{54}O_{16}$. The DMF molecule depicted in Figure 6 (left) as bound to Zn1 brings the total to $Zn_4Si_3C_{81}H_{54}NO_{17}$. One disordered solvent position is shared by one full DMF and one full water molecule, contributing C_3NO_2 and bringing the total to $Zn_4Si_3C_{84}H_{54}N_2O_{19}$. Another disordered solvent position is shared by one benzene and one DMF molecule, each with half-occupancy [$1/2(C_3NO + C_6) = C_{4.5}N_{0.5}O_{0.5}$], for a grand total of $Zn_4Si_3C_{88.5}H_{54}N_{2.5}O_{19.5}$, which was calculated and reported (per four Zn atoms).

Reticulated Structure. The tetrazinc cluster substructure of **4-Zn** has the general formula $Zn_2(RCO_2)_6(OH)_2(H_2O)_2(DMF)_2$ with two types of zinc atoms (Figure 6, left). Hexacoordinate Zn1 is bound to two oxygen atoms (O2, O8) of two different carboxylate ions (C7, C33), two identical hydroxide ions (O6), one water molecule (O1), and the oxygen atom (O9) of a molecule of bound DMF solvent. Tetracoordinate Zn2 is bound to three oxygen atoms (O3, O2, O7) from three carboxylate ions (C7, C26, C33) and to one hydroxide ion (O6). The tridentate hydroxide ions O6 bridge to two Zn1 and one Zn2 atom to complete the tetrazinc cluster. There are two types of carboxylate ions. Two pairs of bidentate carboxylate ions (C7, C33) bridge between Zn1 and Zn2, and two monodentate carboxylate ions C26 bind to each Zn2. The tetrazinc cluster as a whole may be considered to be an octahedron bound to six carboxylate ions. The zinc-oxo clusters and the bidentate organic molecules reticulate to form the framework of Figure 7 (left). The topology may be simplified by representing the zinc-oxo cluster as an octahedral antiprism and the organic molecule as a dipodal tetrahedron. The octahedron is connected to three pairs of carboxylate ions (C7, C26, C33). Figure 12 (left) shows the zinc-oxo subunit as a yellow octahedron connected to six organic tetrahedra. The octahedron is connected via two monodentate carboxylate ions to purple tetrahedra and via four bidentate carboxylate ions to green tetrahedra. Figure 12 (right) extends the model to include the bridging of the dipodal organic molecules to pairs of octahedra.

Crystal Structure of 5-Zn. Molecular Formula. Hydrogen atoms of the unbound, disordered solvent DMF and water molecules and of the one bound hydroxide ion were not included. The two Zn atoms are connected to three organic molecules ($SiC_{28}H_{22}O_4$), each of which is shared by two dizinc clusters. Their contribution to the molecular formula is $Zn_2Si_{1.5}C_{42}H_{33}O_6$. The bound hydroxide ion, without its hydrogen, brings the formula to $Zn_2Si_{1.5}C_{42}H_{33}O_7$. The two disordered DMF molecules and the one disordered water molecule were allotted quarter occupancy, contributing respectively $C_{1.5}N_{0.5}O_{0.5}$ and $O_{0.25}$, bringing the formula to $Zn_2Si_{1.5}C_{43.5}H_{33}N_{0.5}O_{7.75}$. The methyl carbons C14, H28, and C42 with their attached hydrogens are disordered over two sites and were half-

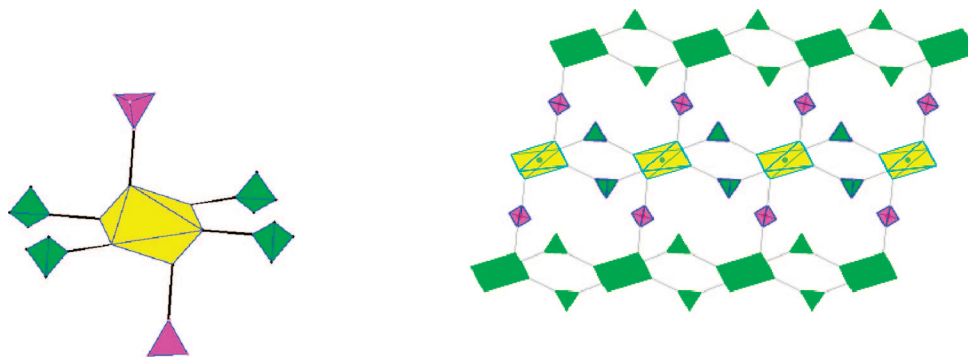


Figure 12. (Left) Octahedral yellow zinc-oxo cluster of **4-Zn** connected to six organic tetrahedra, distinguished by differences in the denticity of the attached carboxylate ions. The octahedron is connected via bidentate carboxylates to two purple tetrahedra, via bidentate carboxylates to two green carboxylates, and via monodentate carboxylates to two green carboxylates. (Right) Each purple organic tetrahedron is bridged between a yellow and a green octahedron, and each green tetrahedron is bridged between green octahedra. This view is along the *b* axis.

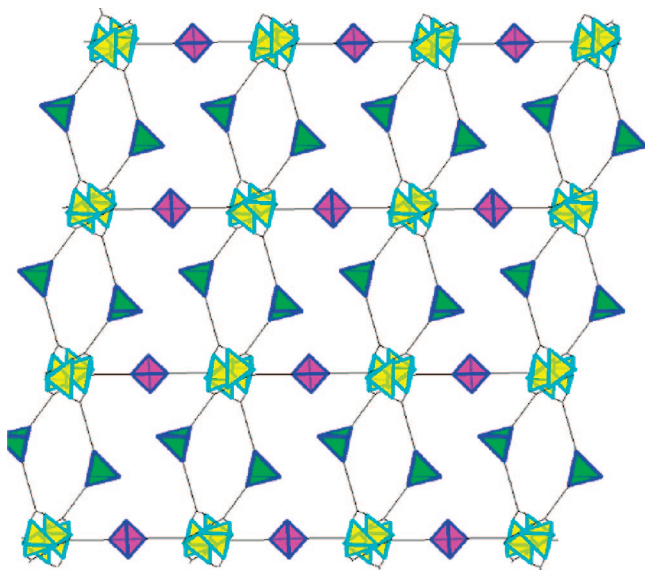


Figure 13. Pairs of dizinc clusters of **5-Zn** are represented by series of yellow octahedra, and silicon ligands are represented by purple and green tetrahedra.

occupied, reducing the atom count by $C_{1.5}H_{4.5}$ (half of three methyl groups), resulting in the calculated and reported formula of $Zn_2Si_{1.5}C_{42}H_{28.5}N_{0.5}O_{7.75}$ (per two Zn atoms).

Reticulated Structure. The zinc substructure cluster of **5-Zn** with general formula $Zn_2(RCO_2)_3(OH)$ contains two tetracoordinate zinc atoms that are bridged in a bidentate fashion via oxygen atoms (O1, O3, O5 and O2, O4, O6) to the same three carboxylate ions (C7, C21, C35) in a pinwheel structure and to a single hydroxide ion (O7) that bridges between Zn1 and Zn2 of adjacent clusters (Figure 6, right). The dizinc cluster and the connected organic portions reticulate to form the porous framework illustrated in Figure 7 (right). The topology of this framework may be understood by representing each pinwheel as a pair of parallel triangles and the dipodal silicon ligand as a tetrahedron with two arms (Figure 13). A pair of dizinc clusters constitutes an octahedron bound to six tetrahedra. Repetition of the interconnected octahedra and tetrahedra results in the reticulated framework.

Crystal Structure of 6-Zn. Molecular Formula. Hydrogen atoms of the bound hydroxide ions and water molecules were not included. Based on a cluster of four Zn atoms, there are six organic portions, each shared by three tetrazinc clusters. Each organic molecule contributes $SiC_{27}H_{17}O_6$. For the tetrazinc cluster, these numbers are multiplied by 6/3, to give a molecular formula of $Zn_4Si_2C_{54}H_{34}O_{12}$. To these are added four water molecules and two

hydroxide ions without hydrogens, to give $Zn_4Si_2C_{54}H_{34}O_{18}$. This formula corresponds to the calculated formula of molecular weight 1288.5. Refinements were carried out on this unit by squeezing out 2.5 DMF molecules of solvation. The DMF atoms, $(C_3H_7NO)_{2.5}$, then were reinstated after refinement to give the reported formula of $Zn_4Si_2C_{61.5}H_{51.5}N_{2.5}O_{20.5}$, with the reported molecular weight of 1471 (per four Zn atoms).

Reticulated Structure. The zinc-oxo substructure of **6-Zn** (Figure 9, left) has the overall formula $Zn_4(RCO_2)_6(OH)_2(H_2O)_4$, in which four distinct zinc atoms lie in the same plane. Tetracoordinate Zn1 and Zn2 are bound to one oxygen atom each (Zn1 to O1, O6, O11 and Zn2 to O4, O8, O9) of three different carboxylate ions (C7, C21, C48 for Zn1 and C14, C34, C41 for Zn2) and to one hydroxide ion (O13 for Zn1 and O14 for Zn2). Hexacoordinate Zn3 and Zn4 are bound to one oxygen atom each (Zn3 to O2, O10 and Zn4 to O5, O7) of two different carboxylate ions (C7, C41 for Zn3 and C21, C34 for Zn4), to two hydroxide ions (O13, O14 for both Zn3 and Zn4), and to two water molecules (O15, O16 for Zn3 and O17, O18 for Zn4). The water molecules are monodentate, but the hydroxide ions are tridentate (O13 bridging Zn1, Zn3, Zn4 and O14 bridging Zn2, Zn3, Zn4). Four carboxylate ions are bridging: C7 between Zn1 and Zn3, C21 between Zn1 and Zn4, C34 between Zn2 and Zn4, C41 between Zn2 and Zn3. Two carboxylate ions are monodentate: C14 to Zn2, C48 to Zn1. Connection of the zinc-oxo clusters through the silicon bridges to other zinc-oxo clusters builds up the framework (Figure 9, right). As each cluster is bound to six carboxylate ions, it mimics the geometry of a twisted prism or octahedron. The framework topology may be simplified by representing the zinc cluster as an octahedron (yellow in Figure 14, left) and the organic ligand as a tricoordinate tetrahedron (purple and green in Figure 14, left). This network strongly resembles that of cadmium iodide (CdI_2),¹⁸ which is a typical infinite, two-dimensional, (6,3)-connected network for AB_2 compounds.¹⁹ In the structure of CdI_2 (Figure 14, right), each cadmium cation is octahedrally coordinated to six iodide anions, and each iodide anion is coordinated to three cadmium cations. In **6-Zn**, the octahedral zinc-oxo cluster corresponds to cadmium and the tricoordinate organic ligand to iodide. The layers of the two structures also exhibit resemblances. In the CdI_2 network each cadmium ion is directly above and below cadmium ions on adjacent layers. In the framework of **6-Zn** the substructures are similarly arranged. Both structures have internal channels. For **6-Zn** the channel is best seen when viewed along the *b* axis (Figure 15). Two sides of the channel are formed by the zinc-oxo clusters and two sides by the phenylene group between silicon and a carboxylate

(18) Palosz, B. S. E. *J. Appl. Crystallogr.* **1989**, 22, 622–623.

(19) Partin, D. E.; O'Keefe, M. *J. Solid State Chem.* **1991**, 95, 176–183.

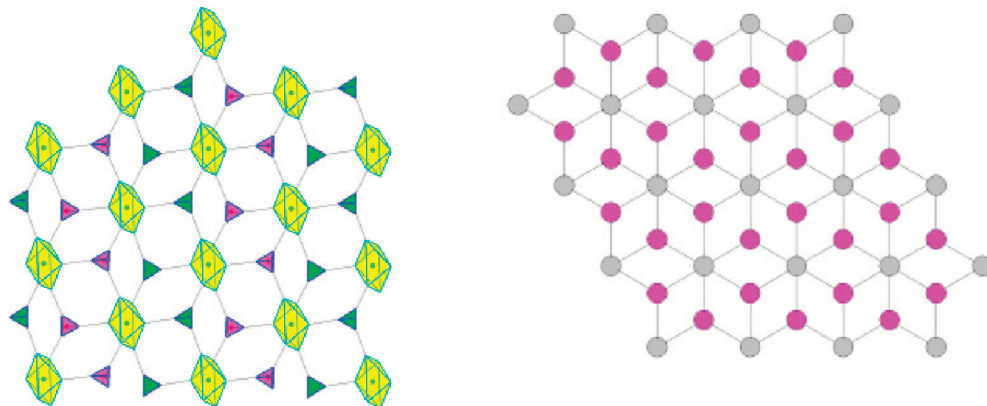


Figure 14. (Left) Octahedral yellow zinc-oxo cluster of **6-Zn** attached to six tricoordinate organic ligands (purple and green), viewed along the *a* axis. (Right) Lattice of CdI_2 , viewed along the *c* axis with hexacoordinate cadmium (gray) bound to tricoordinate iodide (purple).¹⁸

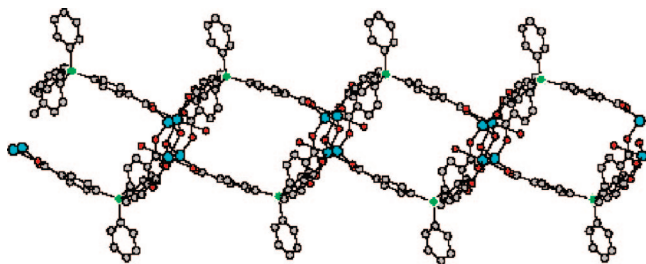


Figure 15. Primary channel in **6-Zn**, as viewed along the *b* axis: Zn (cyan), O (red), C (gray), and Si (green).

group. The channel has a cross section of approximately 8.5×8.5 Å. The noncoordinating phenyl ring attached to silicon is stored inside a bowl-shaped region formed by three zinc clusters and four complete organic molecules. An orthogonal view may be seen along the *a* axis in Figure 9, right.

Thermogravimetric Analysis. Samples of **2-Cd**, **3-Zn**, and **6-Zn** were dried at room temperature for 3 days under vacuum (10 Torr). Samples of **4-Zn** and **5-Zn** were dried at room temperature for 24 h under vacuum (0.1 Torr). The crystalline materials became white powders, which were subjected to TGA under ambient atmosphere. Solvent content consequently was quite different from the materials used for X-ray crystallography. The mass loss observed for **3-Zn** between 150 and 220 °C was 13.5%. This loss

is consistent with a decrease from three molecules of ethanol to zero and from 2.5 molecules of DMF to one. The difference in numbers of unbound solvent molecules between the TGA and X-ray results is caused by the drying procedures. The mass loss for **2-Cd** of 14.6% between 220 and 300 °C corresponds to the loss of two molecules of DMF within a solid that retains one molecule of water. The mass losses for **4-Zn** of 3.4% between about 50 and 350 °C and for **5-Zn** of only 2.2% between about 50 and 170 °C are too small to interpret in terms of particular molecules lost. The mass loss for **6-Zn** of 9.3% between 40 and 200 °C corresponds to the loss of one molecule of DMF and of one molecule of water. The results for all these cases indicate the presence of various solvent molecules bound loosely in voids without covalent bonding, capable of being expelled just through heating.

Acknowledgment. This work was supported by the National Science Foundation, grant no. CHE-0349412.

Supporting Information Available: Crystal data for **1-Zn**, **2-Cd**, **3-Zn**, **4-Zn**, **5-Zn**, and **6-Zn**. Description of void calculations by Platon. Further depictions of the reticulated structures. Thermogravimetric plots for **2-Cd**, **3-Zn**, **4-Zn**, **5-Zn**, and **6-Zn**. This material is available free of charge via the Internet at <http://pubs.acs.org>.

OM800678G

$(\eta^5\text{-C}_4\text{H}_4\text{S})\text{Cr}(\text{CO})_3$ and $(\eta^5\text{-C}_4\text{H}_4\text{Se})\text{Cr}(\text{CO})_3$: A DFT Investigation of the Ground-State Singlet and Triplet Surfaces. New Insights into the Mechanism of C–S or C–Se Insertion Reactions

Mohammed A. H. Alamiry,[†] Peter Brennan, Anthony Coleman,[‡] Conor Long,* and Mary T. Pryce

School of Chemical Sciences, Dublin City University, Dublin 9, Ireland

Received August 13, 2008

The singlet and triplet surfaces for the interaction of thiophene or selenophene with a chromium tricarbonyl unit were calculated using the B3LYP/LanL2DZ+p model chemistry. The singlet surfaces confirm that the $(\eta^5\text{-C}_4\text{H}_4\text{E})\text{Cr}(\text{CO})_3$ (E = S or Se) are the lowest energy species. The $(\eta^1(\text{C}2)\text{-C}_4\text{H}_4\text{E})\text{Cr}(\text{CO})_3$ and $(\kappa^2(\text{E},\text{C})\text{-C}_4\text{H}_4\text{E})\text{Cr}(\text{CO})_3$ species were also located in shallow energy minima. Reaction path modeling on the singlet surfaces provided activation energies for the endothermic insertion process of 172 and 160 kJ mol⁻¹ for E = S or Se, respectively. The activation energy for the insertion process on the triplet surfaces is on the order of 70 kJ mol⁻¹. A novel $\eta^3(\text{E},\text{C},\text{C})\text{-}\eta^1(\text{C})$ -coordinated species was located as a transition state between the insertion species and $(\eta^5\text{-C}_4\text{H}_4\text{E})\text{Cr}(\text{CO})_3$ on the singlet surfaces and an intermediate on the triplet surface for E = S.

Introduction

Hydrodesulfurization (HDS) is an important large-scale process to remove sulfur-containing compounds from fossil fuels.¹ Recent concerns regarding the environmental impact of the oxides of sulfur in the atmosphere and the need to improve combustion efficiencies have resulted in more stringent control of the acceptable level of sulfur in fuels.² The current HDS technology will need to be improved in order to meet the new regulatory standards, with a resurgent interest in improving the catalytic systems used in the HDS process. Currently these rely on heterogeneous catalysts based on alumina-supported transition metals and their sulfides. Some model studies have focused on removal of benzothiophenes and their derivatives because benzothiophenes represent a particular difficulty for the HDS process due to their thermodynamic stability. Thiophene exhibits a wide range of coordination modes to metal atoms including $\eta^1(\text{S})$, $\eta^1(\text{C})$, $\eta^2(\text{C},\text{C})$, $\eta^2(\text{C}-\text{S})$, $\eta^4(\text{C})$, and η^5 . Studying the chemical properties of such complexes can provide important insights into the possible mechanism or mechanisms of the heterogeneous HDS process as it relates to thiophenes. In addition, modern theoretical methods can also provide information on the structure and energy of intermediates and transition states in the chemistry of S–C bond activation, which is a key reaction step in the HDS process.

The oxidative insertion of a metal atom into the S–C bond of thiophenes has been investigated by *ab initio* methods.^{3,4} Studies have indicated that the initial coordination of the thiophene ligand controls the direction of subsequent reactions

to produce either the oxidative insertion product or the C–H activation product.⁵ The mapping of the potential energy surface for the thiophene–metal interaction is essential for a more complete description of the thiophene activation chemistry. For instance recent DFT calculations on the thiophene–Pt interaction⁵ showed that the initial coordination of the thiophene ligand to the C=C double bond leads to the kinetically favored insertion product. The C–S bond activation in thiophene by $(\eta^5\text{-C}_5\text{Me}_5)\text{RhP}(\text{Me}_3)$ has also been modeled using DFT methods. These studies have found two isomeric transition states in which the coordinated thiophene ligand tilts either toward the C₅Me₅ ligand or toward the PMe₃ ligand.⁶ The transition states connect to the insertion product and two isomeric $\eta^2(\text{S},\text{C})$ -coordinated species, which in turn connect to $\eta^1(\text{S})$ - and $\eta^2(\text{C},\text{C})$ -coordinated species. Thus it appears that $\eta^1(\text{S})$ and $\eta^2(\text{C},\text{C})$ represent the initial coordination modes for the thiophene ligand to the sterically demanding rhodium center.

We have chosen the $(\eta^5\text{-C}_4\text{H}_4\text{E})\text{Cr}(\text{CO})_3$ system as the starting point for our investigations into the E–C insertion process (E = S or Se). Unlike the molybdenum complex the chromium complex is accessible using published synthetic procedures.⁷ In this system, the insertion reaction is an intramolecular process where the initial coordination mode of the thiophene or selenophene ligand is well defined. We believe that the $(\eta^5\text{-C}_4\text{H}_4\text{E})\text{Cr}(\text{CO})_3$ system is an excellent model for both experimental and theoretical investigations.

We have recently reported the photochemical properties of $(\eta^5\text{-C}_4\text{H}_4\text{Se})\text{Cr}(\text{CO})_3$ using both time-resolved and matrix isolation methods.⁸ This work confirmed that insertion of the Cr atom into the Se–C bond occurs under photolytic conditions. The insertion product $(\kappa^2(\text{Se},\text{C})\text{-C}_4\text{H}_4\text{Se})\text{Cr}(\text{CO})_3$ is remarkably

* Corresponding author. E-mail: conor.long@dcu.ie.

[†] Present address: Molecular Photonics Laboratory, School of Natural Sciences, Bedson Building, University of Newcastle, Newcastle upon Tyne NE1 7RU, U.K.

[‡] Present address: Stratingh Institute for Chemistry, University of Groningen, Nijenborgh 4, 9747 AG, Groningen, The Netherlands.

(1) Ito, E.; van Veen, J. A. R. *Catal. Today* **2006**, *116*, 446–460.

(2) Light-Duty Diesel Tier 2 Amendments. In EPA420-F-06-027, U.S. Environmental Protection Agency, 2006.

(3) Atesin, T. A.; Jones, W. D. *Organometallics* **2008**, *27*, 53–60.

(4) Sargent, A. L.; Titus, E. P. *Organometallics* **1998**, *17*, 65–77.

(5) Dong, L.; Duckett, S. B.; Ohman, K. F.; Jones, W. D. *J. Am. Chem. Soc.* **1992**, *114*, 151–160.

(6) Atesin, T. A.; Jones, W. D. *Organometallics* **2008**, *27*, 3666–3670.

(7) Angelici, R. J. *Bull. Soc. Chim. Belg.* **1995**, *104*, 265–282.

(8) Brennan, P.; George, M. W.; Jina, O. S.; Long, C.; McKenna, J.; Pryce, M. T.; Sun, X.-Z.; Khuong, Q.; Vuong, K. Q. *Organometallics* **2008**, *27*, 3671–3680.

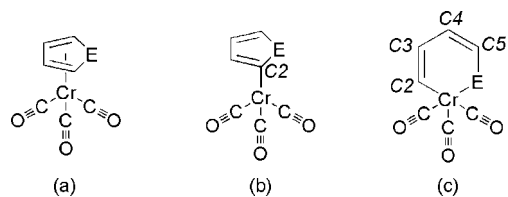


Figure 1. Three coordination modes for thiophene or selenophene to the chromium tricarbonyl fragment: (a) $(\eta^5\text{-C}_4\text{H}_4\text{E})\text{Cr}(\text{CO})_3$, (b) $(\eta^1(\text{C}2)\text{-C}_4\text{H}_4\text{E})\text{Cr}(\text{CO})_3$, and (c) the insertion species $(\kappa^2(\text{E},\text{C})\text{-C}_4\text{H}_4\text{E})\text{Cr}(\text{CO})_3$ (E = S or Se).

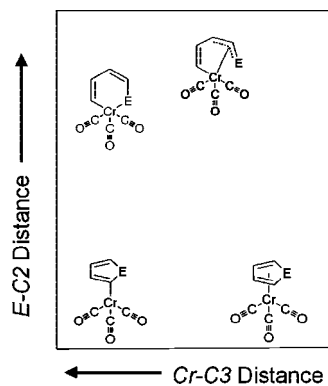


Figure 2. Range of coordination modes for the interaction between thiophene (E = S) or selenophene (E = Se) and the chromium tricarbonyl fragment depending on the coordinate system used in the relaxed potential energy scans.

stable, and this is attributed to a ground-state triplet character. We have now undertaken a more detailed investigation of the potential energy surfaces for the interaction of a chromium tricarbonyl fragment with either thiophene or selenophene on both the singlet and triplet surfaces. The initial coordination mode to the metal is η^5 , and the singlet $(\eta^5\text{-C}_4\text{H}_4\text{E})\text{Cr}(\text{CO})_3$ species provides convenient energy and geometry references. The results of these calculations are presented here.

Results

In the previous matrix isolation investigation,⁸ a number of photoproducts were observed following visible and UV/vis irradiation of $(\eta^5\text{-C}_4\text{H}_4\text{Se})\text{Cr}(\text{CO})_3$. These included the $(\kappa^2(\text{Se},\text{C})\text{-C}_4\text{H}_4\text{Se})\text{Cr}(\text{CO})_3$ and $(\eta^1(\text{C})\text{-C}_4\text{H}_4\text{Se})\text{Cr}(\text{CO})_3$ species (Figure 1).^{9–13} In the work reported here the insertion and η^1 - and η^5 -species were used to define the coordinate system of the surfaces used for a series of relaxed scan calculations. Calculations on both the triplet and singlet surfaces located $(\eta^5\text{-C}_4\text{H}_4\text{E})\text{Cr}(\text{CO})_3$, $(\eta^1(\text{C}2)\text{-C}_4\text{H}_4\text{E})\text{Cr}(\text{CO})_3$, and the insertion species $(\kappa^2(\text{E},\text{C})\text{-C}_4\text{H}_4\text{E})\text{Cr}(\text{CO})_3$ (E = S or Se), and these species provided the initial parameters for the subsequent surface calculations. Attempts to locate $\eta^2(\text{C},\text{C})$, $\eta^2(\text{E},\text{C})$, or $\eta^1(\text{E})$ species failed. However a novel $\eta^3(\text{E},\text{C},\text{C})\text{-}\eta^1(\text{C})$ species was located on the triplet surfaces (top right structure in Figure 2, E = S or Se).

(9) White, C. J.; Angelici, R. J.; Choi, M. G. *Organometallics* **1995**, *14*, 332–340.

(10) Ganter, C.; Brassat, L.; Ganter, B. *Chem. Ber. Recl.* **1997**, *130*, 659–662.

(11) Calvarin, G.; Berar, J. F.; Weigel, D. *Acta Crystallogr., Sect. A* **1978**, *34*, S304–S304.

(12) Novi, M.; Guanti, G.; Dellerba, C. *J. Heterocycl. Chem.* **1975**, *12*, 1055–1059.

(13) Lumbroso, H.; Segard, C.; Roques, B. *J. Organomet. Chem.* **1973**, *61*, 249–260.

Selected calculated bond lengths for the complexes located in this study are presented in Table 1.

The potential energy surfaces were obtained from calculations in which the E to C2 distance was varied between the limits of the insertion species and those of the $(\eta^1(\text{C}2)\text{-C}_4\text{H}_4\text{E})\text{Cr}(\text{CO})_3$ species (E = S or Se). This parameter formed one axis. The second axis mapped the change in the Cr to C3 distance from that in the insertion species to that in $(\eta^5\text{-C}_4\text{H}_4\text{E})\text{Cr}(\text{CO})_3$. Thus the $(\eta^5\text{-C}_4\text{H}_4\text{E})\text{Cr}(\text{CO})_3$ species appear toward the bottom right-hand side of the grid, the $(\eta^1(\text{C}2)\text{-C}_4\text{H}_4\text{E})\text{Cr}(\text{CO})_3$ toward the bottom left-hand side, and the insertion species $(\kappa^2(\text{E},\text{C})\text{-C}_4\text{H}_4\text{E})\text{Cr}(\text{CO})_3$ toward the top left-hand side (Figure 2). Using these coordinate axes it is possible to map most coordination modes of the heteroligands. Relaxed potential energy calculations were performed for each selected value of E–C2 and Cr–C3. Both the triplet and singlet surfaces were explored in these calculations. The gas-phase structures were optimized in redundant internal coordinates without further geometric constraints.¹⁴

Singlet PE Surface of $(\eta^5\text{-C}_4\text{H}_4\text{S})\text{Cr}(\text{CO})_3$. The relaxed potential energy surface obtained for the singlet thiophene system is presented in Figure 3. It is clear from this surface that $(\eta^5\text{-C}_4\text{H}_4\text{S})\text{Cr}(\text{CO})_3$ is the most stable species and was assigned a reference energy of 0 kJ mol⁻¹. In the η^5 -species the thiophene ligand is nonplanar. The sulfur atom lies out of the plane defined by the remaining four carbon atoms. The S–C2–C3–C4 dihedral angle is 12.57° (see Figure 1 for atom-numbering system). The energy of the $(\eta^1(\text{C}2)\text{-C}_4\text{H}_4\text{S})\text{Cr}(\text{CO})_3$ species is 67 kJ mol⁻¹ greater than that of $(\eta^5\text{-C}_4\text{H}_4\text{S})\text{Cr}(\text{CO})_3$. The thiophene ligand is essentially planar in this complex with a S–C2–C3–C4 dihedral angle of 0.66°. The structures of both singlet and triplet $(\kappa^2(\text{S},\text{C})\text{-C}_4\text{H}_4\text{S})\text{Cr}(\text{CO})_3$ are compared in Figure 4. The Cr–S–C5–C4 dihedral angle is 31° on the singlet surface, and the energy is approximately 140 kJ mol⁻¹ higher than the singlet $(\eta^5\text{-C}_4\text{H}_4\text{S})\text{Cr}(\text{CO})_3$ species.

Attempts to locate transition states on this surface using synchronous transit-guided quasi-Newton (STQN) methods failed. This is because the surfaces contain many local stationary points. A more successful method of mapping the reaction pathways involved superimposing the results of relaxed potential energy scans in which only one internuclear vector was varied on the appropriate surface. For example, the energy change involved in the insertion process was obtained from relaxed potential energy scans where the Cr–C3 distance was varied between the limits calculated for $(\eta^5\text{-C}_4\text{H}_4\text{S})\text{Cr}(\text{CO})_3$ and $(\kappa^2(\text{S},\text{C})\text{-C}_4\text{H}_4\text{S})\text{Cr}(\text{CO})_3$. The path taken for the insertion process is represented by the dashed curve in Figure 3 and the associated energy change in Figure 5. The transition state lies some 30 kJ mol⁻¹ above $(\kappa^2(\text{S},\text{C})\text{-C}_4\text{H}_4\text{S})\text{Cr}(\text{CO})_3$ and 172 kJ mol⁻¹ above $(\eta^5\text{-C}_4\text{H}_4\text{S})\text{Cr}(\text{CO})_3$. The dissociation energy for a single S–C bond is on the order of 370 kJ mol⁻¹.¹⁵ The transition state for this process was located and optimized using the Berny algorithm (Opt = TS in Gaussian 03),¹⁴ and its position on the surface is indicated by a filled diamond in Figure 3. The structure of the transition state showing the $\eta^3(\text{S},\text{C},\text{C})\text{-}\eta^1(\text{C})$ coordination mode is presented in Figure 6.

Triplet PE Surface of $(\eta^5\text{-C}_4\text{H}_4\text{S})\text{Cr}(\text{CO})_3$. The energies of the triplet $(\eta^5\text{-C}_4\text{H}_4\text{S})\text{Cr}(\text{CO})_3$ and $(\eta^1(\text{C}2)\text{-C}_4\text{H}_4\text{S})\text{Cr}(\text{CO})_3$ species are similar and lie some 129 kJ mol⁻¹ above that of the singlet $(\eta^5\text{-C}_4\text{H}_4\text{S})\text{Cr}(\text{CO})_3$ species based on calculations using

(14) Peng, C. Y.; Ayala, P. Y.; Schlegel, H. B.; Frisch, M. J. *J. Comput. Chem.* **1996**, *17*, 49–56.

(15) *Handbook of Chemistry and Physics*, 89th ed.; CRC Press: London, 2008.

Table 1. Calculated Energies and Selected Bond Lengths (Å) (B3LYP/LanL2DZ+p) for Complexes in This Study^a

compound	mult. ^b	energy (au)	E-C2	Cr-C4	C2-C3	C3-C4	C4-C5	C5-E	Cr-E	Cr-C2	Cr-CO (av)	CrC-O (av)
(η^5 -C ₄ H ₄ S)Cr(CO) ₃	s	-591.155050073	1.84553	2.27358	1.40601	1.44422	1.40601	1.40601	1.84553	2.22829	1.83457	1.18913
(η^1 (C2)-C ₄ H ₄ Se)Cr(CO) ₃	s	-591.129354305	1.82969	2.59046	1.40367	1.44660	1.37324	1.80783	2.96446	2.13951	1.82634	1.18926
(κ^2 (S,C)-C ₄ H ₄ S)Cr(CO) ₃	s	-591.112568251	3.33511	2.78185	1.40010	1.44328	1.38931	1.77825	2.30325	2.13951	1.82634	1.18926
(η^3 (S,C,C)- η^1 (C)-C ₄ H ₄ S)Cr(CO) ₃	s, TS	-591.123278724	3.07408	2.46178	1.40818	1.44315	1.41863	1.71223	2.43318	1.88009	1.88780	1.17882
(η^5 -C ₄ H ₄ S)Cr(CO) ₃	t	-591.110026919	1.77325	2.23872	1.41505	1.43930	1.42585	1.77717	2.94173	2.46062	1.87644	1.18433
(η^1 (C2)-C ₄ H ₄ S)Cr(CO) ₃	t	-591.110026916	1.83521	3.19530	1.41036	1.45315	1.36989	1.81582	2.97180	2.17798	1.89229	1.18528
(κ^2 (S,C)-C ₄ H ₄ S)Cr(CO) ₃	t	-591.113985067	3.19728	3.57824	1.39409	1.43681	1.37664	1.77734	2.33403	1.95621	1.95249	1.17290
(η^3 (S,C,C)- η^1 (C)-C ₄ H ₄ S)Cr(CO) ₃	t, TS	-591.116318618	2.79295	2.46976	1.37921	1.45844	1.40236	1.75663	2.33335	2.06417	1.89990	1.17737
(η^5 -C ₄ H ₄ Se)Cr(CO) ₃	s	-590.280146112	1.95670	2.26574	1.40745	1.44432	1.40745	1.95670	2.63230	2.23308	1.83472	1.18713
(η^1 (C2)-C ₄ H ₄ Se)Cr(CO) ₃	s	-590.253338851	1.92207	2.60894	1.37397	1.44736	1.40451	1.94230	2.96242	2.11783	1.82704	1.18923
(η^3 (Se,C,C)- η^1 (C)-C ₄ H ₄ Se)Cr(CO) ₃	s	-590.235685842	3.44935	3.15059	1.39763	1.44620	1.38888	1.90448	2.40846	1.93906	1.86996	1.17912
(η^5 -C ₄ H ₄ Se)Cr(CO) ₃	t	-590.232653126	1.96174	2.26835	1.41518	1.43781	1.41496	1.96161	2.99430	2.32691	1.88038	1.18384
(η^1 (C2)-C ₄ H ₄ Se)Cr(CO) ₃	t	-590.234188077	1.95103	3.24925	1.40834	1.45209	1.37217	1.92978	2.89451	2.13633	1.88922	1.18533
(η^3 (Se,C)-C ₄ H ₄ Se)Cr(CO) ₃	t, TS	-590.229094552	2.42727	3.88842	1.38670	1.42175	1.37859	1.72066	2.19291	1.91005	1.93506	1.17548

^a Full details of structural parameters are available in the Supporting Information. ^b Multiplicity s = singlet, t = triplet, TS = transition state.

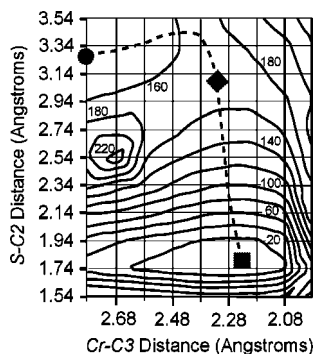


Figure 3. Singlet energy surface for the thiophene to Cr(CO)₃ interaction. The location of (η^5 -C₄H₄S)Cr(CO)₃ is indicated with a solid square, (κ^2 (S,C)-C₄H₄S)Cr(CO)₃ with a solid circle, and the (η^3 (S,C,C)- η^1 (C)-C₄H₄S)Cr(CO)₃ transition state with a solid diamond. Contour lines are drawn at 20 kJ mol⁻¹ intervals.

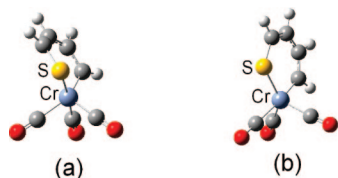


Figure 4. Comparison of the structures of (a) the singlet (κ^2 (S,C)-C₄H₄S)Cr(CO)₃ showing the nonplanar metallacycle and (b) the triplet (κ^2 (S,C)-C₄H₄S)Cr(CO)₃ chromathiabenzene complex.

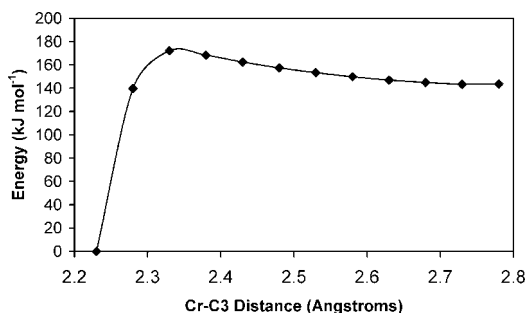


Figure 5. Plot of the energy versus Cr-C3 bond distance ranging from 2.28185 Å in (η^5 -C₄H₄S)Cr(CO)₃ to 2.73185 Å in (κ^2 (S,C)-C₄H₄S)Cr(CO)₃, indicating an activation barrier of 172 kJ mol⁻¹ for the insertion process on the singlet surface. The barrier for the return reaction is approximately 30 kJ mol⁻¹.

the reparametrized B3LYP* functional coupled with the TZVP basis set (see Experimental Section). The triplet insertion species (κ^2 (S,C)-C₄H₄S)Cr(CO)₃ also has an energy close to that of the triplet (η^5 -C₄H₄S)Cr(CO)₃ species, approximately 120 to 140

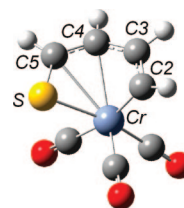


Figure 6. Structure obtained from a transition-state search on the reaction path between the (η^5 -C₄H₄S)Cr(CO)₃ and (κ^2 (S,C)-C₄H₄S)Cr(CO)₃ on the triplet surface using the Bery algorithm. The (η^3 (S,C,C)- η^1 (C)) coordination mode is indicated by explicit bonds to the chromium atom.

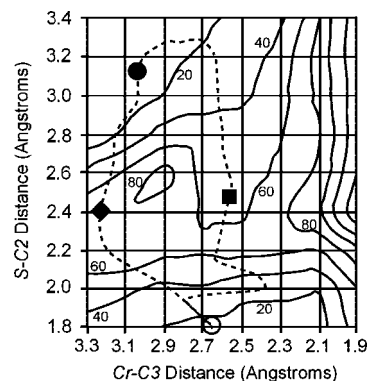


Figure 7. Triplet surface for the thiophene to Cr(CO)₃ interaction. The energy contours are indicated at 20 kJ mol⁻¹ intervals. The (η^1 (C2)-C₄H₄S)Cr(CO)₃ energy is set at an arbitrary 0 kJ mol⁻¹. Two paths joining (κ^2 (S,C)-C₄H₄S)Cr(CO)₃ (filled circle) and (η^1 (C2)-C₄H₄S)Cr(CO)₃ (open circle) are indicated by dashed curves. Path 1 passes through a (η^2 (S,C2)-C₄H₄S)Cr(CO)₃ transition state (solid diamond), and path 2 involves the formation of an intermediate species (η^3 (S,C5,C4)- η^1 (C2)-C₄H₄S)Cr(CO)₃ (solid square); see Figure 1 for numbering system.

kJ mol⁻¹ above that of the singlet (η^5 -C₄H₄S)Cr(CO)₃. In the case of the triplet species the structure can be described as a thiochromabenzene species where the chromium, sulfur, and the four cyclic carbon atoms lie in the same plane (Figure 4).

The triplet potential energy surface was obtained by varying the S-C2 and Cr-C3 bond lengths and optimizing the remaining structural parameters (Figure 7). The transformation from the insertion species to (η^5 -C₄H₄S)Cr(CO)₃ or (η^1 (C2)-C₄H₄S)Cr(CO)₃ was explored by conducting two separate relaxed energy scans each starting with the insertion species (solid circle). The first involved reduction of the S-C2 distance (via the η^2 (S,C) transition state and intermediate, route 1). The second reduced the Cr-C3 distance and reached the (η^1 (C2)-

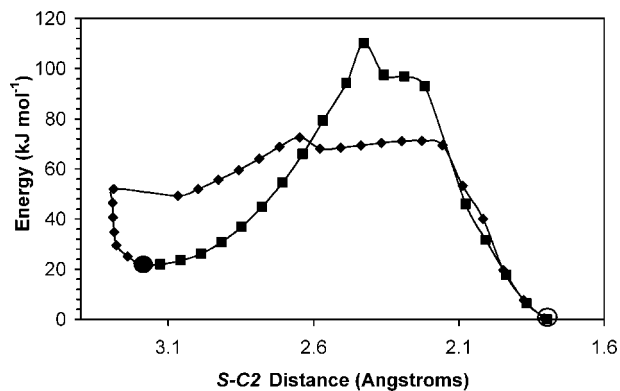


Figure 8. Comparison of the energy change in moving from the insertion species ($\kappa^2(\text{S},\text{C}2)\text{-C}_4\text{H}_4\text{S})\text{Cr}(\text{CO})_3$ (marked with a solid circle) to the $(\eta^1(\text{C}2)\text{-C}_4\text{H}_4\text{S})\text{Cr}(\text{CO})_3$ (open circle) on the triplet surface. Squares indicate the energy change obtained in the relaxed scan where the $\text{S-C}2$ bond length is reduced, while the diamonds indicate the energy change where the $\text{Cr-C}3$ distance is reduced.

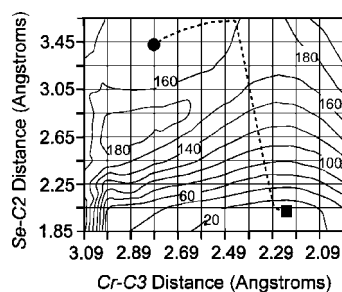


Figure 9. Singlet potential energy surface for the selenophene to $\text{Cr}(\text{CO})_3$ interaction. Contour lines are drawn at 20 kJ mol^{-1} intervals. The dashed line indicates the path taken in a relaxed scan in which the $\text{Cr-C}3$ distance is varied between the value in $(\kappa^2(\text{Se},\text{C})\text{-C}_4\text{H}_4\text{Se})\text{Cr}(\text{CO})_3$ (indicated with a solid circle) to that in $(\eta^5\text{-C}_4\text{H}_4\text{Se})\text{Cr}(\text{CO})_3$ (indicated by the solid square).

$\text{C}_4\text{H}_4\text{S})\text{Cr}(\text{CO})_3$ via a $\eta^3(\text{S},\text{C}2,\text{C}3)\text{-}\eta^1(\text{C}4)$ transition state and intermediate (route 2). The energy changes for these routes are presented in Figure 8. It is clear that route 2 is energetically favored. Both routes terminate at the $(\eta^1(\text{C}2)\text{-C}_4\text{H}_4\text{S})\text{Cr}(\text{CO})_3$ species, represented by the open circle in Figures 7 and 8. It should also be noted that route 2 involves an initial expansion of the $\text{S-C}2$ interatomic distance.

Singlet Surface of $(\eta^5\text{-C}_4\text{H}_4\text{Se})\text{Cr}(\text{CO})_3$. The singlet energy surface for the $(\eta^5\text{-C}_4\text{H}_4\text{Se})\text{Cr}(\text{CO})_3$ system was constructed in a similar manner to that of the thiophene system and is presented in Figure 9. The lowest energy species is $(\eta^5\text{-C}_4\text{H}_4\text{Se})\text{Cr}(\text{CO})_3$, and its energy is set to 0 kJ mol^{-1} . The $(\eta^1(\text{C}2)\text{-C}_4\text{H}_4\text{Se})\text{Cr}(\text{CO})_3$ and $(\kappa^2(\text{Se},\text{C})\text{-C}_4\text{H}_4\text{Se})\text{Cr}(\text{CO})_3$ species lie at 70 and 126 kJ mol^{-1} , respectively. The activation barrier to the insertion process was estimated by conducting a relaxed scan of the $\text{Cr-C}3$ distance and allowing all other geometric parameters to optimize without constraints. The energy change is presented in Figure 10. These results indicate an activation energy of approximately 160 kJ mol^{-1} for the $(\eta^5\text{-C}_4\text{H}_4\text{Se})\text{Cr}(\text{CO})_3$ to $(\kappa^2(\text{Se},\text{C})\text{-C}_4\text{H}_4\text{Se})\text{Cr}(\text{CO})_3$ reaction. The measured bond dissociation energy for a single selenium-carbon bond is 238 kJ mol^{-1} .¹⁶

Triplet Surface of $(\eta^5\text{-C}_4\text{H}_4\text{Se})\text{Cr}(\text{CO})_3$. The triplet energy surface of $(\eta^5\text{-C}_4\text{H}_4\text{Se})\text{Cr}(\text{CO})_3$ is presented in Figure 11. The

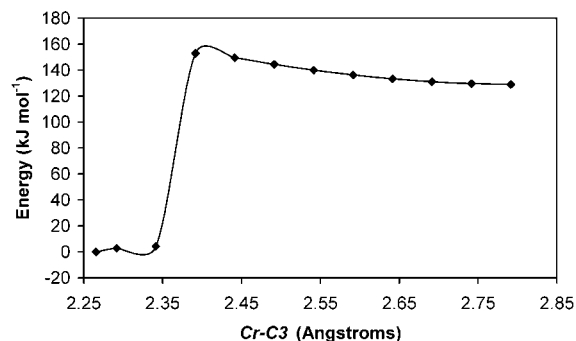


Figure 10. Plot of the energy change upon expanding the $\text{Cr-C}3$ distance from that in $(\eta^5\text{-C}_4\text{H}_4\text{Se})\text{Cr}(\text{CO})_3$ to that in $(\kappa^2(\text{Se},\text{C})\text{-C}_4\text{H}_4\text{Se})\text{Cr}(\text{CO})_3$ on the singlet surface.

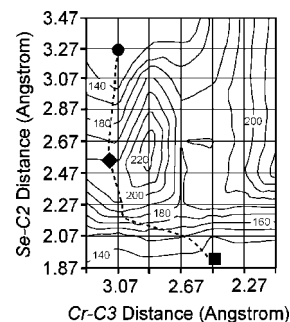


Figure 11. Triplet potential energy for the selenophene $\text{Cr}(\text{CO})_3$ interaction. Contour lines are drawn at 10 kJ mol^{-1} intervals and set relative to the energy of the singlet $(\eta^5\text{-C}_4\text{H}_4\text{Se})\text{Cr}(\text{CO})_3$ species. The location of the triplet $(\kappa^2(\text{Se},\text{C})\text{-C}_4\text{H}_4\text{Se})\text{Cr}(\text{CO})_3$ is indicated with a solid circle, and the location of triplet $(\eta^5\text{-C}_4\text{H}_4\text{Se})\text{Cr}(\text{CO})_3$ with a solid square. The dashed line indicates the path of the relaxed scan where the $\text{Se-C}2$ distance is varied, and the solid diamond indicates the location of the triplet $\eta^2(\text{Se},\text{C})$ transition state.

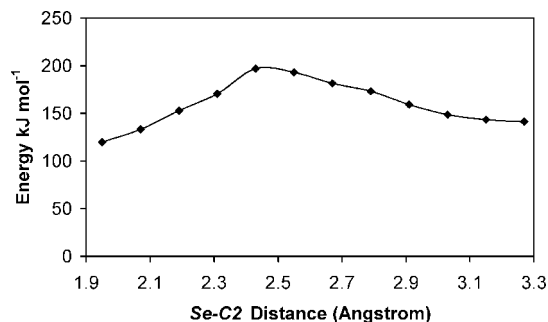


Figure 12. Plot of the energy change when the $\text{Se-C}2$ distance is varied between the distance in $(\eta^5\text{-C}_4\text{H}_4\text{Se})\text{Cr}(\text{CO})_3$ and that in $(\kappa^2(\text{Se},\text{C})\text{-C}_4\text{H}_4\text{Se})\text{Cr}(\text{CO})_3$ on the triplet surface. The transition state lies some 77 kJ mol^{-1} above $(\eta^5\text{-C}_4\text{H}_4\text{Se})\text{Cr}(\text{CO})_3$ and 57 kJ mol^{-1} above $(\kappa^2(\text{Se},\text{C})\text{-C}_4\text{H}_4\text{Se})\text{Cr}(\text{CO})_3$.

energy of this surface is calibrated relative to the energy of the singlet $(\eta^5\text{-C}_4\text{H}_4\text{Se})\text{Cr}(\text{CO})_3$ species set at 0 kJ mol^{-1} . A relaxed scan in which the $\text{Se-C}2$ distance was varied between that in $(\eta^5\text{-C}_4\text{H}_4\text{Se})\text{Cr}(\text{CO})_3$ and $(\kappa^2(\text{Se},\text{C})\text{-C}_4\text{H}_4\text{Se})\text{Cr}(\text{CO})_3$ is superimposed upon this surface. This is indicated by a dashed curve that joins the $(\eta^5\text{-C}_4\text{H}_4\text{Se})\text{Cr}(\text{CO})_3$ species to $(\kappa^2(\text{Se},\text{C})\text{-C}_4\text{H}_4\text{Se})\text{Cr}(\text{CO})_3$ via an $(\eta^2(\text{Se},\text{C})\text{-C}_4\text{H}_4\text{Se})\text{Cr}(\text{CO})_3$ transition state. The energy change involved in this process is presented in Figure 12, which shows an activation barrier of 77 kJ mol^{-1} . Attempts to calculate the reaction path via an $\eta^3(\text{Se},\text{C},\text{C})\text{-}\eta^1(\text{C})$ transition state or intermediate similar to that obtained for the thiophene system failed. The energies of the $(\eta^5\text{-C}_4\text{H}_4\text{S})\text{Cr}(\text{CO})_3$ and $(\eta^5\text{-C}_4\text{H}_4\text{Se})\text{Cr}(\text{CO})_3$ species are

Table 2. Comparison of the Singlet and Triplet Energies for Various Complexes at the B3LYP*/TZVP Model Chemistry^a

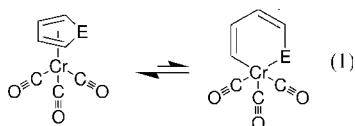
complex	multiplicity	energy (au)	ΔE (kJ mol ⁻¹)	comment
$(\eta^5\text{-C}_4\text{H}_4\text{Se})\text{Cr}(\text{CO})_3$	singlet	-3931.29845	119.4	singlet lower than triplet
$(\eta^5\text{-C}_4\text{H}_4\text{Se})\text{Cr}(\text{CO})_3$	triplet	-3931.25298		
$(\text{C,Se-C}_4\text{H}_4\text{Se})\text{Cr}(\text{CO})_3$	singlet	-3931.254574	8.5	triplet lower than singlet
$(\text{C,Se-C}_4\text{H}_4\text{Se})\text{Cr}(\text{CO})_3$	triplet	-3931.257818		

^a All energies were corrected for zero-point energy.

$\text{C}_4\text{H}_4\text{Se})\text{Cr}(\text{CO})_3$ and $(\kappa^2(\text{Se,C})\text{-C}_4\text{H}_4\text{S})\text{Cr}(\text{CO})_3$ on the singlet and triplet surfaces were calculated at the B3LYP*/TZVP level. The triplet $(\eta^5\text{-C}_4\text{H}_4\text{Se})\text{Cr}(\text{CO})_3$ lies 119.4 kJ mol⁻¹ above that of the singlet, while the energies of the singlet and triplet $(\kappa^2(\text{Se,C})\text{-C}_4\text{H}_4\text{Se})\text{Cr}(\text{CO})_3$ species are similar, the triplet energy being slightly (8.5 kJ mol⁻¹) lower than the singlet (Table 2).

Discussion

It is clear from the calculations on the singlet surfaces that the $(\eta^5\text{-C}_4\text{H}_4\text{E})\text{Cr}(\text{CO})_3$ species lie at the bottom of a deep energy well. All other coordination modes for the heteroligand have significantly higher energies. The singlet surfaces are somewhat smoother than those of the triplet. While the $(\eta^1(\text{C}2)\text{-C}_4\text{H}_4\text{E})\text{Cr}(\text{CO})_3$ and $(\kappa^2(\text{E,C})\text{-C}_4\text{H}_4\text{E})\text{Cr}(\text{CO})_3$ both exist in shallow minima (E = S or Se), the energy barriers for their reaction to the $(\eta^5\text{-C}_4\text{H}_4\text{E})\text{Cr}(\text{CO})_3$ are small. Thus in the case of the insertion process the equilibrium lies very much in favor of the $(\eta^5\text{-C}_4\text{H}_4\text{E})\text{Cr}(\text{CO})_3$ species (reaction 1).



Calculations indicate that the insertion process passes through a $(\eta^3(\text{E,C,C})\text{-}\eta^1(\text{C})\text{-C}_4\text{H}_4\text{E})\text{Cr}(\text{CO})_3$ transition state. This is an unusual coordination mode for this class of ligand. The electron count on the chromium atom remains at 18 in this transition state if the heteroatom is considered to be a 3 + 2 electron donor. The insertion species $(\kappa^2(\text{E,C})\text{-C}_4\text{H}_4\text{E})\text{Cr}(\text{CO})_3$ is formally a 16-electron species where the heteroatom acts as a three-electron donor. The range of Cr–C3 distances required to map the $(\eta^5\text{-C}_4\text{H}_4\text{E})\text{Cr}(\text{CO})_3$ to $(\kappa^2(\text{E,C})\text{-C}_4\text{H}_4\text{E})\text{Cr}(\text{CO})_3$ reaction is smaller on the singlet surface than on the triplet. This is because on the singlet surface the Cr atom remains out of the plane defined by the heteroatom and the cyclic carbon atoms in the insertion species. The calculated dihedral angle Cr–S–C5–C6 is 31° in the singlet $(\kappa^2(\text{S,C})\text{-C}_4\text{H}_4\text{S})\text{Cr}(\text{CO})_3$, considerably larger than the equivalent angle measured for a thiaplatinacycle complex (12.0(1)°).¹⁷ This facilitates the reaction to regenerate $(\eta^5\text{-C}_4\text{H}_4\text{E})\text{Cr}(\text{CO})_3$ and explains why the singlet surfaces appear to be smoother than the triplet.

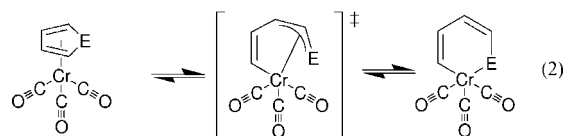
In the course of the matrix isolation experiments on the $(\eta^5\text{-C}_4\text{H}_4\text{Se})\text{Cr}(\text{CO})_3$ system, visible photolysis produced $(\kappa^2(\text{Se,C})\text{-C}_4\text{H}_4\text{Se})\text{Cr}(\text{CO})_3$.⁸ The insertion species appeared to be inert toward reaction with CO or N₂. This was explained by proposing a triplet character for this species and that its reaction with small molecules was therefore “spin blocked”. Consequently the relative energies of the insertion species on both the singlet and triplet surfaces are important for a full description of the insertion process and how it might be promoted in this system.

This was estimated by two methods. The first method was used for the thiophene system. This involved calculating the energy of $(\kappa^2(\text{S,C})\text{-C}_4\text{H}_4\text{S})\text{Cr}(\text{CO})_3$ on both the singlet and triplet surfaces relative to the appropriate $(\eta^5\text{-C}_4\text{H}_4\text{S})\text{Cr}(\text{CO})_3$ species at the B3LYP/LANL2DZ+p model chemistry. The energy difference between the $(\eta^5\text{-C}_4\text{H}_4\text{S})\text{Cr}(\text{CO})_3$ species on the singlet and triplet surfaces was then calculated using the B3LYP*/TZVP model chemistry. This energy difference was then used to calibrate the energy of the triplet surface. This approach indicates that the energies of the singlet and triplet $(\kappa^2(\text{S,C})\text{-C}_4\text{H}_4\text{S})\text{Cr}(\text{CO})_3$ species are very similar, although it should be acknowledged that error associated with these calculations could be considerably greater than the calculated energy difference of 20 kJ mol⁻¹.

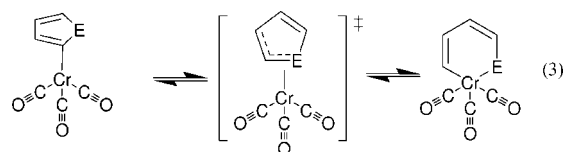
The second method was used for the selenophene system. Here the energies of the singlet and triplet $(\eta^5\text{-C}_4\text{H}_4\text{Se})\text{Cr}(\text{CO})_3$ and the singlet and triplet $(\kappa^2(\text{Se,C})\text{-C}_4\text{H}_4\text{Se})\text{Cr}(\text{CO})_3$ were estimated using the B3LYP*/TZVP model chemistry (Table 2). Again the results of these calculations confirm that the energies of the singlet and triplet $(\kappa^2(\text{Se,C})\text{-C}_4\text{H}_4\text{Se})\text{Cr}(\text{CO})_3$ are similar (within 8.5 kJ mol⁻¹). Here the calculations suggest that the triplet energy is slightly lower than the singlet, but again the energy difference is within the expected error (Table 2).

The structure of the triplet $(\kappa^2(\text{E,C})\text{-C}_4\text{H}_4\text{E})\text{Cr}(\text{CO})_3$ species is very likely to be the main reason for its stability relative to the triplet $(\eta^5\text{-C}_4\text{H}_4\text{E})\text{Cr}(\text{CO})_3$. The planarity of the metallating system permits π -conjugation, producing a chromathia-benzene or chromaselenabenzene compound with a formal 16-electron count on the chromium atom.

The reaction of $(\eta^5\text{-C}_4\text{H}_4\text{E})\text{Cr}(\text{CO})_3$ to form $(\kappa^2(\text{E,C})\text{-C}_4\text{H}_4\text{E})\text{Cr}(\text{CO})_3$ on the singlet surface is highly endothermic, and the equilibrium lies on the side of the $(\eta^5\text{-C}_4\text{H}_4\text{E})\text{Cr}(\text{CO})_3$ species. The transition state on this reaction path has an $\eta^3(\text{E,C,C})\text{-}\eta^1(\text{C})$ structure (reaction 2, E = S or Se).

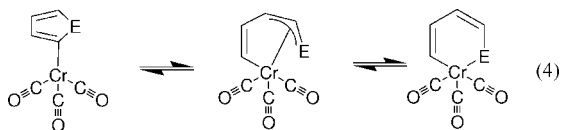


On the triplet surface two reaction pathways were found joining $(\eta^1(\text{C}2)\text{-C}_4\text{H}_4\text{S})\text{Cr}(\text{CO})_3$ with $(\kappa^2(\text{S,C})\text{-C}_4\text{H}_4\text{S})\text{Cr}(\text{CO})_3$, one passing through an $(\eta^2(\text{S,C})\text{-C}_4\text{H}_4\text{Se})\text{Cr}(\text{CO})_3$ transition state (reaction 3; E = S) and the other involving an $(\eta^3(\text{E,C,C})\text{-}\eta^1(\text{C})\text{-C}_4\text{H}_4\text{E})\text{Cr}(\text{CO})_3$ intermediate species (reaction 4; E = S).



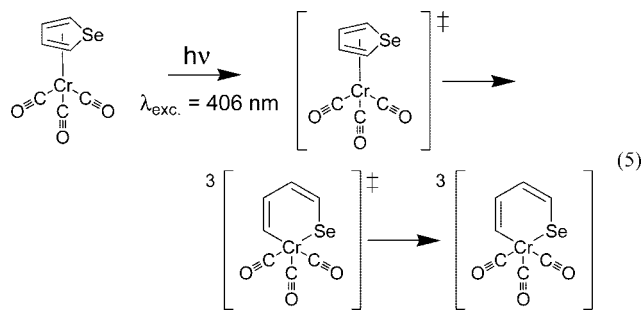
For the selenium system, only one route was found on the triplet surface joining $(\eta^1(\text{C}2)\text{-C}_4\text{H}_4\text{Se})\text{Cr}(\text{CO})_3$ with $(\kappa^2(\text{Se,C})\text{-C}_4\text{H}_4\text{Se})\text{Cr}(\text{CO})_3$ (reaction 3; E = Se), and this involved a

(17) Chantson, J.; Gorls, H.; Lotz, S. *J. Organomet. Chem.* **2003**, 687, 39–45.



$\eta^2(\text{Se},\text{C})$ transition state. A relaxed scan starting with the $(\kappa^2(\text{Se},\text{C})\text{-C}_4\text{H}_4\text{Se})\text{Cr}(\text{CO})_3$ and reducing the $\text{Cr}\text{-C}3$ distance passed through a $\eta^3(\text{Se},\text{C},\text{C})\text{-}\eta^1(\text{C})$ intermediate but failed to connect to either $(\eta^5\text{-C}_4\text{H}_4\text{Se})\text{Cr}(\text{CO})_3$ or $(\eta^1(\text{C}2)\text{-C}_4\text{H}_4\text{Se})\text{Cr}(\text{CO})_3$.

It is evident from these calculations that the processes to produce the insertion species are more favorable on the triplet surfaces rather than the singlet. This explains why in the matrix isolation experiments evidence was obtained for the formation of the triplet $(\kappa^2(\text{Se},\text{C})\text{-C}_4\text{H}_4\text{Se})\text{Cr}(\text{CO})_3$ under photochemical conditions (reaction 5).⁸



Concluding Comments

The results of the singlet surface calculations confirm that insertion of a chromium tricarbonyl unit into a $\text{E}\text{-C}$ bond is a highly endothermic process ($\text{E} = \text{S}$ or Se) and is achieved via a novel $\eta^3(\text{E},\text{C},\text{C})\text{-}\eta^1(\text{C})$ transition state. This further demonstrates how the mechanism of the insertion process is influenced by the initial coordination mode of the heterocyclic ligand to the metal center. On the triplet surface the $\eta^3(\text{S},\text{C},\text{C})\text{-}\eta^1(\text{C})$ species exists as an intermediate joining $(\kappa^2(\text{S},\text{C})\text{-C}_4\text{H}_4\text{S})\text{Cr}(\text{CO})_3$ and $(\eta^5\text{-C}_4\text{H}_4\text{S})\text{Cr}(\text{CO})_3$, while in the case of the selenophene analogue the equivalent reaction involves an $\eta^2(\text{Se},\text{C})$ transition state. The insertion species $(\kappa^2(\text{E},\text{C})\text{-C}_4\text{H}_4\text{E})\text{Cr}(\text{CO})_3$ ($\text{E} = \text{S}$ or Se) exhibit a remarkable stability on the triplet surface, and this is confirmed by recent matrix isolation and time-resolved infrared studies.⁸ The authors are grateful for the comments of one reviewer who indicated that chromium sulfide is a poor HDS catalyst and that this may be a reflection of the high energy of the insertion product on the singlet surface similar to that observed in this investigation.

Experimental Section

DFT methods were used, which employed a three-parameter hybrid functional (B3)¹⁸ and the Lee–Yang–Parr correlation functional (LYP), i.e., the B3LYP functional.¹⁹ All calculations were performed using the Gaussian 03 package,²⁰ using HP dual Xeon processor workstations. It is known that the B3LYP functional

tends to underestimate the energy of high-spin states relative to low-spin states.^{21,22} Consequently, Reiher has proposed that a reduction in the exact exchange parameter from 0.2 to 0.15 provides a more reliable estimate of the energy difference between spin states in organometallic systems and called this modified functional B3LYP*.²³ For estimates of the energy difference between the singlet and triplet $(\eta^5\text{-C}_4\text{H}_4\text{E})\text{Cr}(\text{CO})_3$ species, the B3LYP* functional coupled with a triple- ζ basis set with polarization functions was used (TZVP). For calculations to map either the singlet or triplet surfaces the standard B3LYP functional was used coupled with a double- ζ basis set^{24–27} augmented with an f-function on the chromium²⁸ and d-functions on the S or Se atoms (LANL2-DZ+p).²⁹ These model chemistries represent a compromise between accuracy in measuring energy differences between species with different multiplicities and the computational cost of the large number of optimization cycles to map the singlet or especially the triplet surfaces. Initial geometries were obtained from molecular mechanics calculations, and the final geometries of species located at local energy minima were optimized using tight convergence criteria. Zero-point energy corrections were applied to species at stationary points. A listing of internal parameters is provided in the Supporting Information.

Acknowledgment. C.L. wishes to thank DCU for the award of a Senior Research Fellowship to support this work.

Supporting Information Available: This material is available free of charge via the Internet at <http://pubs.acs.org>.

OM8007794

(19) Lee, C. T.; Yang, W. T.; Parr, R. G. *Phys. Rev. B* **1988**, *37*, 785–789.

(20) Frisch, M. J.; Trucks, G. W.; Schlegel, H. B.; Scuseria, G. E.; Robb, M. A.; Cheeseman, J. R.; Montgomery, J. J. A.; Vreven, T.; Kudin, K. N.; Burant, J. C.; Millam, J. M.; Iyengar, S. S.; Tomasi, J.; Barone, V.; Mennucci, B.; Cossi, M.; Scalmani, G.; Rega, N.; Petersson, G. A.; Nakatsuji, H.; Hada, M.; Ehara, M.; Toyota, K.; Fukuda, R.; Hasegawa, J.; Ishida, M.; Nakajima, T.; Honda, Y.; Kitao, O.; Nakai, H.; Klene, M.; Li, X.; Knox, J. E.; Hratchian, H. P.; Cross, J. B.; Adamo, C.; Jaramillo, J.; Gomperts, R.; Stratmann, R. E.; Yazyev, O.; Austin, A. J.; Cammi, R.; Pomelli, C. J.; Ochterski, W.; Ayala, P. Y.; Morokuma, K.; Voth, G. A.; Salvador, P.; Dannenberg, J. J.; Zakrzewski, V. G.; Dapprich, S.; Daniels, A. D.; Strain, M. C.; Farkas, O.; Malick, D. K.; Rabuck, A. D.; Raghavachari, K.; Foresman, J. B.; Ortiz, J. V.; Cui, Q.; Baboul, A. G.; Clifford, S.; Cioslowski, J.; Stefanov, B. B.; Liu, G.; Liashenko, A.; Piskorz, P.; Komaromi, I.; Martin, R. L.; Fox, D. J.; Keith, T.; Al-Laham, M. A.; Peng, C. Y.; Nanayakkara, A.; Challacombe, M.; Gill, P. M. W.; Johnson, B.; Chen, W.; Wong, M. W.; Gonzalez, C.; Pople, J. A. *Gaussian 03, Revision C.02*; Gaussian, Inc.: Wallingford, CT, 2004.

(21) Reiher, M.; Salomon, O.; Hess, B. A. *Theor. Chem. Acc.* **2001**, *107*, 48–55.

(22) Reiher, M.; Salomon, O.; Sellmann, D.; Hess, B. A. *Chem.—Eur. J.* **2001**, *7*, 5195–5202.

(23) Salomon, O.; Reiher, M.; Hess, B. A. *J. Chem. Phys.* **2002**, *117*, 4729–4737.

(24) Dunning, T. H., Jr.; Hay, P. J. In *Modern Theoretical Chemistry*; Schaefer, H. F., Ed.; Plenum: New York, 1976; Vol. 3, pp 1–28.

(25) Hay, P. J.; Wadt, W. R. *J. Chem. Phys.* **1985**, *82*, 270–283.

(26) Hay, P. J.; Wadt, W. R. *J. Chem. Phys.* **1985**, *82*, 299–310.

(27) Wadt, W. R.; Hay, P. J. *J. Chem. Phys.* **1985**, *82*, 284–298.

(28) Ehlers, A. W.; Bohme, M.; Dapprich, S.; Gobbi, A.; Hollwarth, A.; Jonas, V.; Kohler, K. F.; Stegmann, R.; Veldkamp, A.; Frenking, G. *Chem. Phys. Lett.* **1993**, *208*, 111–114.

(29) Hollwarth, A.; Bohme, M.; Dapprich, S.; Ehlers, A. W.; Gobbi, A.; Jonas, V.; Kohler, K. F.; Stegmann, R.; Veldkamp, A.; Frenking, G. *Chem. Phys. Lett.* **1993**, *208*, 237–240.

(18) Becke, A. D. *J. Chem. Phys.* **1993**, *98*, 5648–5652.

Aggregation and Reactivity of Organozincate Anions Probed by Electropray Mass Spectrometry

Konrad Koszinowski* and Petra Böhler

Department Chemie und Biochemie, Ludwig-Maximilians-Universität München, Butenandtstr. 5–13, 81377 München, Germany

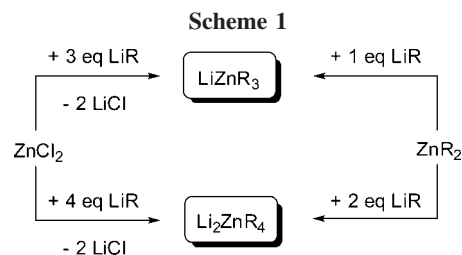
Received July 23, 2008

Electropray ionization (ESI) of mixtures of organolithium compounds and zinc chloride in tetrahydrofuran produced manifold mono- and polynuclear organozincate anions. Formation of the latter is strongly favored by the incorporation of chloride ligands, which apparently adopt bridging binding modes. Analysis of $\text{Li}^n\text{Bu}/\text{ZnCl}_2$ solutions at different concentrations showed that the relative ESI signal intensities for anions in different aggregation states closely correlate with their expected equilibria in solution. Moreover, the uni- and bimolecular gas-phase reactivity of the mass-selected anionic organozincates was studied. Upon collision-induced dissociation, most of these complexes lose a neutral metal fragment, and only the tributylzincates ZnBu_3^- react by elimination of alkenes. The tributylzincate complexes were also found to undergo ion–molecule reactions with formic acid. The relative rates for these proton-transfer processes decrease in the series Zn^nBu_3^- , Zn^sBu_3^- , and Zn^tBu_3^- , and they also decrease if the butyl groups are substituted for chloride ligands. These trends fully agree with the known solution-phase chemistry of organozinc compounds.

1. Introduction

Lithium organozincate complexes LiZnR_3 and Li_2ZnR_4 ($\text{R} = \text{organyl}$)¹ form in the reactions of ZnCl_2 and ZnR_2 with LiR (Scheme 1). These organozincate complexes show a higher nucleophilic reactivity than diorganyl zinc compounds ZnR_2 ,^{2,3} while still preserving the high chemoselectivity characteristic of organozinc compounds.^{4,5} Because of this combination of favorable properties, organozincates are valuable reagents in organic synthesis. As such, their applications range from halogen-zinc exchange,^{6–9} carbozincation,⁸ and Michael-type reactions^{8,10} to the initiation of anionic polymerizations¹¹ and epoxide ring openings.⁸

Despite this practical importance, many facets of organozincate chemistry are only poorly understood. First of all, the formulas LiZnR_3 and Li_2ZnR_4 refer to the overall composition of the reactive mixtures but do not necessarily reflect the stoichiometry of the actual species present in solution. Hein and Schramm performed cryoscopic measurements on solutions of diethylzinc and ethyllithium in benzene and observed the formation of aggregates with high molecular weights.¹² Toppet,



Slinckx, and Smets could establish by NMR spectroscopy that the addition of tetrahydrofuran (thf) to such solutions resulted in deaggregation.¹³ NMR-spectroscopic measurements by Seitz and co-workers revealed that mixtures of dimethylzinc and methyllithium in thf contain complexes of $\text{LiZn}(\text{CH}_3)_3$ and $\text{Li}_2\text{Zn}(\text{CH}_3)_4$ stoichiometries,¹⁴ whereas only $\text{Li}_2\text{Zn}(\text{CH}_3)_4$ and $\text{Li}_3\text{Zn}(\text{CH}_3)_5$ appear to exist in diethyl ether at low temperatures.¹⁵ More recently, Uchiyama and co-workers used a combination of spectroscopic techniques to characterize the zincate complexes present in thf solutions of $\text{Li}_2\text{Zn}(\text{CH}_3)_4$, $\text{Li}_2\text{Zn}(\text{CH}_3)_3(\text{CN})$, and $\text{Li}_2\text{Zn}(\text{CH}_3)_3(\text{SCN})$.⁸ Their results point to the presence of tetracoordinate organozincate species.⁸ In addition to controlling the aggregation of organozincates, the solvent presumably also has a key influence on their dissociation equilibria. For the related lithium organocuprate complexes, solvent-separated ion pairs are known to prevail in thf.¹⁶ In contrast, contact ion pairs predominate in diethylether, which has poorer coordinating capabilities.¹⁶ A similar situation may

* To whom correspondence should be addressed. E-Mail: Konrad.Koszinowski@cup.uni-muenchen.de.

(1) Linton, D. J.; Schooler, P.; Wheatley, A. E. H. *Coord. Chem. Rev.* **2001**, *223*, 53.

(2) Maclin, K. M.; Richey, H. G., Jr. *J. Org. Chem.* **2002**, *67*, 4602.

(3) Uchiyama, M.; Nakamura, S.; Ohwada, T.; Nakamura, M.; Nakamura, E. *J. Am. Chem. Soc.* **2004**, *126*, 10897.

(4) Knochel, P.; Singer, R. D. *Chem. Rev.* **1993**, *93*, 2117.

(5) Knochel, P.; Perea, J. J. A.; Jones, P. *Tetrahedron* **1998**, *54*, 8275.

(6) Harada, T.; Katsuhira, T.; Hattori, K.; Oku, A. *J. Org. Chem.* **1993**, *58*, 2958.

(7) Kondo, Y.; Fujinami, M.; Uchiyama, M.; Sakamoto, T. *J. Chem. Soc., Perkin Trans. 1* **1997**, 799.

(8) Uchiyama, M.; Kameda, M.; Mishima, O.; Yokoyama, N.; Koike, M.; Kondo, Y.; Sakamoto, T. *J. Am. Chem. Soc.* **1998**, *120*, 4934.

(9) Uchiyama, M.; Furuyama, T.; Kobayashi, M.; Matsumoto, Y.; Tanaka, K. *J. Am. Chem. Soc.* **2006**, *128*, 8404.

(10) Isobe, M.; Kondo, S.; Nagasawa, N.; Goto, T. *Chem. Lett.* **1977**, 679.

(11) Kobayashi, M.; Matsumoto, Y.; Uchiyama, M.; Ohwada, T. *Macromolecules* **2004**, *37*, 4339.

(12) Hein, F.; Schramm, H. *Z. Phys. Chem.* **1930**, *A151*, 234.

(13) Toppet, S.; Slinckx, G.; Smets, G. *J. Organomet. Chem.* **1967**, *9*, 205.

(14) Seitz, L. M.; Little, B. F. *J. Organomet. Chem.* **1969**, *18*, 227.

(15) Seitz, L. M.; Brown, T. L. *J. Am. Chem. Soc.* **1966**, *88*, 4140.

(16) John, M.; Auel, C.; Behrens, C.; Marsch, M.; Harms, K.; Bosold, F.; Gschwind, R. M.; Rajamohanam, P. R.; Boche, G. *Chem. Eur. J.* **2000**, *6*, 3060.

be expected in the case of lithium organozincates although only few examples of solvent-separated ion pairs have been reported for these.¹⁷

In order to obtain further insight into the nature of organozincate complexes in thf solution, we employed electrospray-ionization (ESI) mass spectrometry. In contrast to NMR spectroscopy and cryoscopy, ESI mass spectrometry selectively probes the charged components present in solution and thus seems particularly well-suited for the detection of solvent-separated organozincate complexes. Moreover, mass spectrometry provides a straightforward means to establish the stoichiometry of ionic species (for potential complications due to fragmentation during the ionization process, see below). Thanks to these assets, ESI mass spectrometry has recently become one of the chief methods to characterize ionic species in organometallic chemistry.^{18,19} While so far, most studies have focused on cations, Lipshutz and co-workers already in 1999 successfully used ESI mass spectrometry for the identification of organometallate complexes, namely organocuprates.²⁰

Besides taking advantage of its analytical power, we also used mass spectrometry to characterize the reactivity of ionic species. Gas-phase experiments on mass-selected ions have substantially contributed to our current understanding of organometallic reactivity.^{19–29} Such experiments neglect solvent effects but have the great advantage of excluding complex equilibria, which can severely complicate reactivity studies in solution. With respect to organometallate complexes, O'Hair and co-workers have extensively investigated the uni- and bimolecular gas-phase reactivity of organomagnesates³⁰ and their heavier homologues,³¹ as well as of organocuprates^{32,33} and -argentates,³² all prepared from gaseous precursors. We have performed similar gas-phase experiments on organozincate complexes extracted directly from solution and compare the obtained gas-phase data with the trends known for the corresponding solution chemistry. Such a comparison promises to reveal to what extent the system's intrinsic reactivity probed in the gas phase does correlate with its reactivity in solution and under which circumstances gas-phase data can be used for predictions on solution chemistry.

In the present study, we have investigated organozincates prepared by the transmetalation of ZnCl₂ (as well as of ZnBr₂ and ZnI₂) with organolithium compounds LiR. We not only

consider homoleptic organozincate complexes, but also include mixed organochlorozincates, such as ZnRCl₂⁻ and ZnR₂Cl⁻. These species are likely intermediates in the formation of homoleptic organozincates starting from ZnCl₂ and LiR (Scheme 1). Among the different organozincates studied, we particularly focus on those bearing butyl groups. LiZnⁿBu₃ and Li₂ZnⁿBu₄ are arguably the organozincates most commonly used for synthetic applications,^{7,9,11} and it will be interesting to see whether the complexes ZnⁿBu_nCl_{3-n}⁻ differ in their reactivity from their counterparts ZnⁿBu_nCl_{3-n}⁻ and ZnⁿBu_nCl_{3-n}⁻ (1 ≤ n ≤ 3). To answer this question, we probed the bimolecular gas-phase reactivity of these species toward methyl iodide and formic acid as prototypical examples of carbon electrophiles and proton donors, respectively.

2. Experimental Section

2.1. Materials and General Synthetic Methods. Tetrahydrofuran was distilled from potassium/benzophenone. ZnCl₂ was dried by repeatedly heating it under high vacuum until it melted. Solutions of organolithium compounds LiR in alkanes were used as purchased. Their exact concentrations were determined by titration with 1,3-diphenyl-2-propanone tosylhydrazone.³⁴ Standard Schlenk techniques were applied in all cases.

2.2. Preparation of LiR/ZnCl₂ and 2 LiR/ZnCl₂ Solutions. To a solution of dry ZnCl₂ in thf, 1 or 2 equiv., respectively, of the organolithium compound LiR were added under argon. The resulting solution (c = 0.1 mol L⁻¹) was stirred at room temperature for 24 h and then diluted to 1 ≤ c ≤ 50 mmol L⁻¹ before analysis by ESI mass spectrometry.

2.3. Preparation of 4 LiR/ZnCl₂ Solutions.⁹ To a solution of dry ZnCl₂ in thf cooled down to -78 °C, 4 equiv. of the organolithium compound LiR were added under argon. The resulting solution (c = 0.1 mol L⁻¹) was allowed to warm up to 0 °C and was stirred at this temperature for 2 h. The solution was diluted to c = 50 mmol before analysis by ESI mass spectrometry.

2.4. ESI Mass Spectrometry. Samples of the thf solutions of the lithium organozincate complexes were transferred into a gastight syringe and administered into the ESI source of a TSQ 7000 multistage mass spectrometer (Thermo-Finnigan) by means of a syringe pump (Harvard apparatus). Typical flow rates ranged from 5 to 20 μL min⁻¹. Particular care was taken to exclude or minimize contact of the organometallic samples with air. Traces of moisture or oxygen in the inlet system were eliminated by extensively flushing it with dry thf before adding the organometallic sample.

The sample solution entered the ESI source via a fused-silica tube (0.10 mm inner diameter). Stable electrospray conditions were usually achieved for ESI voltages ranging from 3.0 to 4.3 kV with nitrogen as a sheath gas (2.5 bar). The spray then passed through a heated capillary held at 60 °C. This relatively low temperature yielded acceptable signal intensities while preventing excessive fragmentation of the potentially labile organozincate complexes. Furthermore, the potential difference between the heated capillary and the following electrooptic lens was kept low to avoid strong acceleration of the ions and unwanted fragmentations due to energetic collisions with gas molecules present in the ESI source region. Similar ESI conditions were maintained for all experiments to ensure direct comparability.

The m/z ratios of the ions were established by scanning the first quadrupole mass filter. The ions then passed an octopole and a second quadrupole mass filter before reaching the detector.

In response to the comments of one of the reviewers, we repeated the ESI-mass spectrometric analysis of a solution of LiⁿBu/ZnCl₂. This experiment was not performed with the TSQ 7000 instrument

(17) Westerhausen, M.; Wieneke, M.; Ponikvar, W.; Nöth, H.; Schwarz, W. *Organometallics* **1998**, *17*, 1438.

(18) Plattner, D. A. *Int. J. Mass Spectrom.* **2001**, *207*, 125.

(19) Chen, P. *Angew. Chem.* **2003**, *115*, 2938; *Angew. Chem. Int. Ed.* **2003**, *42*, 2832.

(20) Lipshutz, B. H.; Keith, J.; Buzard, D. J. *Organometallics* **1999**, *18*, 1571.

(21) Armentrout, P. B.; Beauchamp, J. L. *J. Am. Chem. Soc.* **1981**, *103*, 784.

(22) Squires, R. R. *Chem. Rev.* **1987**, *87*, 623.

(23) Hanratty, M. A.; Beauchamp, J. L.; Illies, A. J.; van Koppen, P.; Bowers, M. T. *J. Am. Chem. Soc.* **1988**, *110*, 1.

(24) Schwarz, H. *Acc. Chem. Res.* **1989**, *22*, 282.

(25) Eller, K.; Schwarz, H. *Chem. Rev.* **1991**, *91*, 1121.

(26) Freiser, B. S. *Acc. Chem. Res.* **1994**, *27*, 353.

(27) Schröder, D.; Schwarz, H. *Angew. Chem.* **1995**, *107*, 2126; *Angew. Chem., Int. Ed. Engl.* **1995**, *34*, 1973.

(28) Armentrout, P. B. *Acc. Chem. Res.* **1995**, *28*, 430.

(29) Schröder, D.; Shaik, S.; Schwarz, H. *Acc. Chem. Res.* **2000**, *33*, 139.

(30) O'Hair, R. A. J.; Vrkic, A. K.; James, P. F. *J. Am. Chem. Soc.* **2004**, *126*, 12173.

(31) Jacob, A. P.; James, P. F.; O'Hair, R. A. J. *Int. J. Mass Spectrom.* **2006**, *255/256*, 45.

(32) James, P. F.; O'Hair, R. A. J. *Org. Lett.* **2004**, *6*, 2761.

(33) Rijs, N.; Khairallah, G. N.; Waters, T.; O'Hair, R. A. J. *J. Am. Chem. Soc.* **2008**, *130*, 1069.

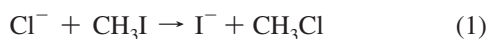
(34) Lipton, M. F.; Sorensen, C. M.; Sadler, A. C.; Shapiro, R. H. *J. Organomet. Chem.* **1980**, *186*, 155.

but instead with a quadrupole ion trap mass spectrometer (LTQ, Finnigan). The ESI conditions in this additional experiment were similar to those applied in the rest of the work.

2.5. Gas-Phase Reactivity Studies. For probing the uni- or bimolecular gas-phase reactivity of an organozincate ion of a particular m/z ratio, the first quadrupole mass filter was used to mass-select this ion. The mass-selected ion then passed the octopole, to which volatile substrates could be added via a needle valve and a home-built inlet system. The inlet system could be evacuated in order to avoid contamination of the substrates with air. For studying the unimolecular reactivity of a mass-selected ion in a collision-induced dissociation (CID), argon (Linde, 99.998% purity) was used as collision gas. For the bimolecular reactions of the organozincate ions with methyl iodide and formic acid, these substrates were purified by repeated freeze–pump–thaw cycles. The m/z ratios of the product ions formed by CID or ion–molecule reactions were then established by scanning the second quadrupole mass filter before the ions reached the detector. The vacuum chamber of the mass spectrometer was held at $T \approx 343$ K, and we assume that this temperature also describes the distribution of the internal energy of the neutral reactants.

The collision energy $E_{\text{LABORATORY}}$ could be controlled by changing the voltage offset of the octopole V_{oct} . To determine the true zero point in $E_{\text{LABORATORY}}$, we varied V_{oct} while measuring the absolute signal intensity (so-called potential-retardation analysis). The derivative of the obtained curve with respect to V_{oct} then yielded the kinetic energy distribution of the ions with a maximum at the true zero point in $E_{\text{LABORATORY}}$. These energy distributions were Gaussian-shaped with typical full widths at half-maximum of 1.6 ± 0.3 eV. The zero point in $E_{\text{LABORATORY}}$ for the different measurements was constant within ± 0.3 eV. Note that these potential-retardation analyses were not performed for the organozincate ions themselves but for CH_3O^- , Cl^- , Br^- , PhO^- , and Na(OPh)_2^- , because higher and more stable signal intensities could be achieved for these anions (by ESI of methanolic solutions of their sodium salts). As the instrumental parameters applied in the potential-retardation analyses were very similar to those used for the investigation of the organozincate ions, we assume that the latter had kinetic energy distributions comparable to those observed for CH_3O^- , Cl^- , Br^- , PhO^- , and Na(OPh)_2^- .

For CID experiments, typically three different values for V_{oct} were applied, corresponding to low (1.5 eV), medium (~ 12 eV), and high (~ 20 eV) collision energies $E_{\text{LABORATORY}}$. These energies cannot be easily converted to collision energies in the center-of-mass frame because multiple collisions are likely at the typical argon pressure applied ($p(\text{Ar}) \approx 0.6$ mtorr in the 18 cm-long interaction region as measured with a Convectron). The ion–molecule reactions of organozincate ions with methyl iodide and formic acid were studied at a collision energy of $E_{\text{LABORATORY}} = 0$ eV and pressures in the range of $0.1 \leq p \leq 0.5$ mtorr (uncorrected reading of the Convectron). The lower limit of this range roughly corresponds to single-collision conditions. Each reaction was studied at three or more different pressures under pseudofirst order conditions (excess of the neutral substrate). In addition, the well-known³⁵ ion–molecule reactions of the anions and CH_3O^- , HS^- , Cl^- , and Br^- with methyl iodide were considered for comparison. As expected, in all cases the formation of I^- was observed and thus indicated the occurrence of a nucleophilic substitution, as demonstrated in eq 1 for Cl^- .



The relative rate constants determined for the reactions of CH_3O^- , HS^- , Cl^- , and Br^- with methyl iodide show the same trend as data obtained from a selected-ion flow-tube study performed at room temperature³⁵ but are not in quantitative agreement with the latter

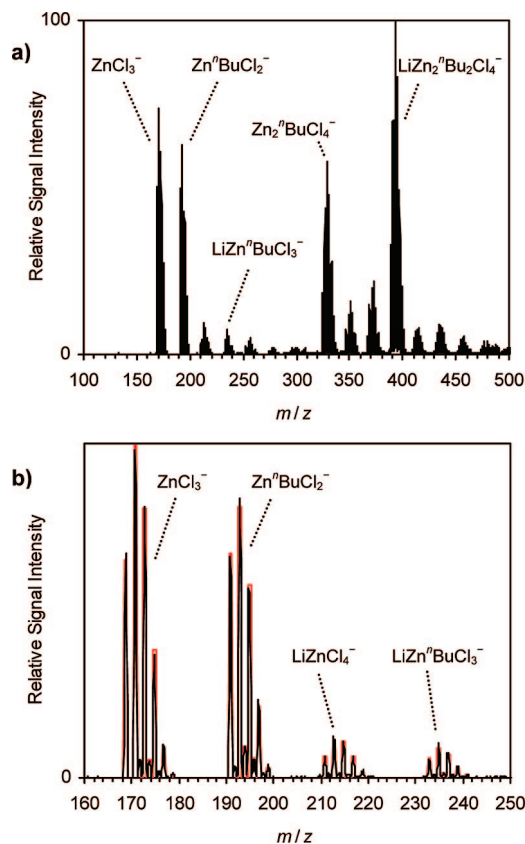


Figure 1. Anion-mode ESI mass spectrum of a 10-mMolar solution of $\text{Li}^n\text{Bu}/\text{ZnCl}_2$ in thf. (a) Overview. (b) Comparison of observed (black) and expected isotopic patterns (red) for the low mass range.

(Table S1 of the Supporting Information). Possible reasons for this disagreement could be the deviation in temperature between the two experiments or the absence of an inert bath gas in the present study. In general, both the rather broad kinetic energy distribution of the ions and the errors inherent in the measurement of the pressure are likely to limit the accuracy of the relative rate constants that can be obtained with our commercial instrument.

3. Results

3.1. Solutions of $\text{Li}^n\text{Bu}/\text{ZnCl}_2$ **3.1.1. $\text{Li}^n\text{Bu}/\text{ZnCl}_2$.** Anion-mode ESI of a 10-mMolar solution of $\text{Li}^n\text{Bu}/\text{ZnCl}_2$ in thf yielded rich mass spectra (Figure 1a). Besides the purely inorganic zincate complex ZnCl_3^- , organozincate ions were observed at higher m/z ratios. A first indication of their identity is given by their exact m/z ratios. While $m/z = 168.8$ observed for $^{64}\text{Zn}^{35}\text{Cl}_3^-$ clearly reflects the large mass defects of zinc and chlorine, these are apparently compensated for in the case of the ion at $m/z = 191.0$. This ion therefore must contain several hydrogen atoms and thus most likely bears a butyl group. Hence, the assignment as $^{64}\text{Zn}^n\text{Bu}^{35}\text{Cl}_2^-$ is straightforward.

In addition to this mononuclear species, the polynuclear complexes LiZnCl_4^- , $\text{LiZn}^n\text{BuCl}_3^-$, $\text{Zn}_2^n\text{BuCl}_4^-$, and $\text{LiZn}_2^n\text{Bu}_2\text{Cl}_4^-$ were found in the m/z range probed. For all of these ions, the measured isotopic patterns fully agree with those calculated for the expected zincates based on the natural abundances of the different isotopes (see Figure 1b for the low mass range).³⁶ The identities of the organozincates were further

(35) Gronert, S.; DePuy, C. H.; Bierbaum, V. M. *J. Am. Chem. Soc.* **1991**, *113*, 4009.

(36) Isotope patterns can be conveniently calculated with the help of web-based resources, such as: Yan, J. Isotope Pattern Calculator v4.0 (<http://www.geocities.com/junhuayan/pattern.htm>).

Table 1. Fragmentation Reactions of Mass-Selected Organozincate Anions

entry	parent ion		fragment ion ^a		neutral fragment(s)		figure
	<i>m/z</i>	assignment ^b	<i>m/z</i>	assignment ^b	Δm	assignment	
1	191	⁶⁴ Zn ⁿ Bu ³⁵ Cl ₂ ⁻	35	³⁵ Cl ⁻	156	⁶⁴ Zn ⁿ Bu ³⁵ Cl	S1
2a	235	Li ⁶⁴ Zn ⁿ Bu ³⁵ Cl ₂ ³⁷ Cl ⁻	77	Li ³⁵ Cl ⁻	158	⁶⁴ Zn ⁿ Bu ³⁷ Cl	S2
b			193	⁶⁴ Zn ⁿ Bu ³⁵ Cl ³⁷ Cl ⁻	42	Li ³⁵ Cl	
3	327	⁶⁴ Zn ₂ ⁿ Bu ³⁵ Cl ₃ ³⁷ Cl ⁻	171	⁶⁴ Zn ³⁵ Cl ₂ ³⁷ Cl ⁻	156	⁶⁴ Zn ⁿ Bu ³⁵ Cl	S3
4a	393	Li ⁶⁴ Zn ₂ ⁿ Bu ₂ ³⁵ Cl ₂ ³⁷ Cl ₂ ⁻	37	³⁷ Cl ⁻	356	Li ⁶⁴ Zn ₂ ⁿ Bu ₂ ³⁵ Cl ₂ ³⁷ Cl	S4
b			77	Li ³⁵ Cl ⁻	316	⁶⁴ Zn ₂ ⁿ Bu ₂ ³⁷ Cl ₂	
c			171	⁶⁴ Zn ³⁵ Cl ₂ ³⁷ Cl ⁻	222	Li ⁶⁴ Zn ⁿ Bu ₂ ³⁷ Cl	
d			215	Li ⁶⁴ Zn ³⁵ Cl ₂ ³⁷ Cl ₂ ⁻	178	⁶⁴ Zn ⁿ Bu ₂	
e			235	Li ⁶⁴ Zn ⁿ Bu ³⁵ Cl ₂ ³⁷ Cl ⁻	158	⁶⁴ Zn ⁿ Bu ³⁷ Cl	
5	193	⁶⁴ Zn ⁿ Bu ³⁵ Cl ³⁷ Cl ⁻	35	³⁵ Cl ⁻	158	⁶⁴ Zn ⁿ Bu ³⁷ Cl	S7
6	191	⁶⁴ Zn ⁿ Bu ³⁵ Cl ₂ ⁻	35	³⁵ Cl ⁻	156	⁶⁴ Zn ⁿ Bu ³⁵ Cl	S8
7a	351	⁶⁴ Zn ⁶⁶ Zn ⁿ Bu ₂ ³⁵ Cl ₂ ³⁷ Cl ⁻	173	⁶⁶ Zn ³⁵ Cl ₂ ³⁷ Cl ⁻	178	⁶⁴ Zn ⁿ Bu ₂	S9
b			193	⁶⁶ Zn ⁿ Bu ³⁵ Cl ₂ ⁻	158	⁶⁴ Zn ⁿ Bu ³⁷ Cl	
8a	333	⁶⁴ Zn ⁶⁶ Zn ⁿ Bu ₂ (OH) ³⁵ Cl ³⁷ Cl ⁻	155	⁶⁶ Zn(OH) ³⁵ Cl ³⁷ Cl ⁻	178	⁶⁴ Zn ⁿ Bu ₂	S10
b			195	⁶⁶ Zn ⁿ Bu ³⁵ Cl ³⁷ Cl ⁻	138	⁶⁴ Zn ⁿ Bu(OH)	
9	149	⁶⁴ Zn(CH ₃) ₃ ³⁵ Cl ₂ ⁻	35	³⁵ Cl ⁻	114	⁶⁴ Zn(CH ₃) ₃ ³⁵ Cl	S12
10	287	⁶⁴ Zn ⁶⁶ Zn(CH ₃) ₃ ³⁵ Cl ₃ ³⁷ Cl ⁻	173	⁶⁶ Zn ³⁵ Cl ₂ ³⁷ Cl ⁻	114	⁶⁴ Zn(CH ₃) ₃ ³⁵ Cl	S13
11	309	Li ⁶⁴ Zn ⁶⁶ Zn(CH ₃) ₂ ³⁵ Cl ₃ ³⁷ Cl ⁻	79	Li ³⁵ Cl ³⁷ Cl ⁻	230	⁶⁴ Zn ⁶⁶ Zn(CH ₃) ₂ ³⁵ Cl ₂	S14
b			171	⁶⁴ Zn ³⁵ Cl ₂ ³⁷ Cl ⁻	138	Li ⁶⁶ Zn(CH ₃) ₂ ³⁵ Cl	
c			193	Li ⁶⁴ Zn(CH ₃) ₃ ³⁵ Cl ₂ ³⁷ Cl ⁻	116	⁶⁶ Zn(CH ₃) ₃ ³⁵ Cl	
d			215	Li ⁶⁶ Zn ³⁵ Cl ₃ ³⁷ Cl ⁻	94	⁶⁴ Zn(CH ₃) ₂	
12	219	⁶⁴ Zn(C ₄ H ₉ S) ³⁵ Cl ³⁷ Cl ⁻	37	³⁷ Cl ⁻	182	⁶⁴ Zn(C ₄ H ₉ S) ³⁵ Cl	S16
13	213	⁶⁴ Zn ⁿ Bu ₂ ³⁵ Cl ⁻	35	³⁵ Cl ⁻	178	⁶⁴ Zn ⁿ Bu ₂	S19
14	213	⁶⁴ Zn ⁿ Bu ₂ ³⁵ Cl ⁻	35	³⁵ Cl ⁻	178	⁶⁴ Zn ⁿ Bu ₂	S20
15	213	⁶⁴ Zn ⁿ Bu ₂ ³⁵ Cl ⁻	35	³⁵ Cl ⁻	178	⁶⁴ Zn ⁿ Bu ₂	S21
16	129	⁶⁴ Zn(CH ₃) ₂ ³⁵ Cl ⁻	35	³⁵ Cl ⁻	94	⁶⁴ Zn(CH ₃) ₂	S23
17	265	⁶⁴ Zn(C ₄ H ₉ S) ₂ ³⁵ Cl ⁻	35	³⁵ Cl ⁻	230	⁶⁴ Zn(C ₄ H ₉ S) ₂	S25
18a	235	⁶⁴ Zn ⁿ Bu ₃ ⁻	179	⁶⁴ ZnH ⁿ Bu ₂ ⁻	56	C ₄ H ₈	S26
b			123	⁶⁴ ZnH ₂ ⁿ Bu ⁻	112	2 C ₄ H ₈	
19a	235	⁶⁴ Zn ⁿ Bu ₃ ⁻	179	⁶⁴ ZnH ⁿ Bu ₂ ⁻	56	C ₄ H ₈	S27
b			123	⁶⁴ ZnH ₂ ⁿ Bu ⁻	112	2 C ₄ H ₈	
20a	267	⁶⁴ Zn ⁿ Bu ₂ (ⁿ BuOO) ⁻	33	HOO ⁻	234	⁶⁴ Zn ⁿ Bu ₂ , C ₄ H ₈	S29
b			67	⁶⁴ ZnH ₃ ⁻	200	2 C ₄ H ₈ , C ₄ H ₈ O ₂	
c			71	C ₄ H ₇ O ⁻	196	⁶⁴ Zn ⁿ Bu ₂ , H ₂ O	
d			73	C ₃ H ₅ O ₂ ⁻	194	⁶⁴ Zn ⁿ Bu ₂ , CH ₄	
e			89	ⁿ BuOO ⁻	178	⁶⁴ Zn ⁿ Bu ₂	
f			123	⁶⁴ Zn ⁿ BuH ₂	144	C ₄ H ₈ , C ₄ H ₈ O ₂	
g			211	⁶⁴ ZnH ⁿ Bu(OO ⁿ Bu) ⁻	56	C ₄ H ₈	
21a	235	⁶⁴ Zn ⁿ Bu ₃ ⁻	179	⁶⁴ ZnH ⁿ Bu ₂ ⁻	56	C ₄ H ₈	S31
b			123	⁶⁴ ZnH ₂ ⁿ Bu ⁻	112	2 C ₄ H ₈	
22a	111	⁶⁴ Zn(CH ₃) ₂ (OH) ⁻	17	OH ⁻	94	⁶⁴ Zn(CH ₃) ₂	S33
b			95	⁶⁴ Zn(CH ₃)O ⁻	16	CH ₄	
23	313	⁶⁴ Zn(C ₄ H ₉ S) ₃ ⁻	83	C ₄ H ₉ S ⁻	230	⁶⁴ Zn(C ₄ H ₉ S) ₂	S35

^a For isotopic or isotopologue fragment ions, respectively, observed at neighboring *m/z* ratios only one major component is listed. ^b Only one major isotopologue is given. In several cases, additional isotopologues will significantly contribute to the signal intensity of the observed ion.

confirmed by CID experiments, which gave the expected fragment ions: mononuclear ZnⁿBuCl₂⁻ produced Cl⁻ as ionic fragment (Table 1, entry 1, and Figure S1 of the Supporting Information), and the polynuclear species mainly formed LiCl₂⁻ and/or zincate ions (Table 1, entries 2–4, and Figures S2–S4 of the Supporting Information).

The observed signal intensities exhibited a clear dependence on the concentration. At *c*(LiⁿBu/ZnCl₂) = 1 mmol L⁻¹, ZnCl₃⁻ predominates, whereas at higher concentrations the polynuclear complexes Zn₂ⁿBuCl₄⁻ and LiZn₂ⁿBu₂Cl₄⁻ prevail (Figure 2). The predominance of the purely inorganic ZnCl₃⁻ at low concentrations possibly results from the partial decomposition of the organometallic species by residual traces of moisture and/or oxygen. The effect of such contaminants should be most pronounced for low concentrations *c*(LiⁿBu/ZnCl₂).

3.1.2. LiⁿBu/ZnCl₂ and LiⁿBu/ZnCl₂. Anion-mode ESI of solutions of LiⁿBu/ZnCl₂ and LiⁿBu/ZnCl₂ in thf gave results similar to those obtained for LiⁿBu/ZnCl₂. Besides ZnCl₃⁻, the direct analogues of ZnⁿBuCl₂⁻ and LiZn₂ⁿBu₂Cl₄⁻ were observed (Figures S5 and S6 of the Supporting Information). In addition, the complexes Zn₂ⁿBu₂Cl₃⁻ and Zn₂ⁿBu₂Cl₃⁻ were found, whose counterpart did not show considerable signal intensity for the case of LiⁿBu/ZnCl₂. The identities of ZnⁿBuCl₂⁻, ZnⁿBuCl₂⁻,

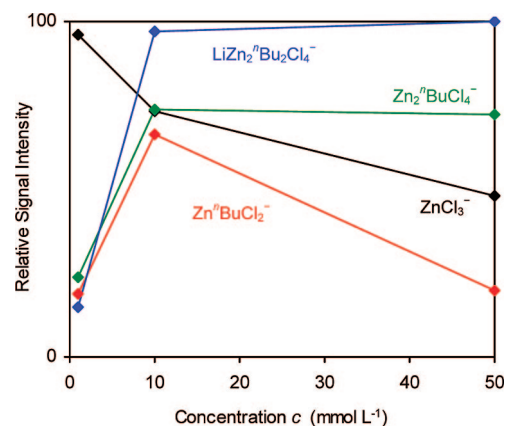


Figure 2. Relative signal intensities of zincate complexes produced by anion-mode ESI of 1-, 10-, and 50-mmolar solutions of LiⁿBu/ZnCl₂ in thf.

and Zn₂ⁿBu₂Cl₃⁻ were corroborated by CID (Table 1, entries 5–7, and Figures S7 and S9 of the Supporting Information). CID also helped to establish the composition of Zn₂ⁿBu₂(OH)Cl₂⁻ (Table 1, entry 8, and Figure S10 of the

Supporting Information). The formation of $\text{Zn}(\text{OH})\text{Cl}_2^-$ upon fragmentation, eq 2, proves the identity of this unexpected complex.



$\text{Zn}_2^{\text{t}}\text{Bu}_2(\text{OH})\text{Cl}_2^-$ possibly originates from partial hydrolysis by traces of moisture. As one reviewer pointed out, an alternative genesis of $\text{Zn}_2^{\text{t}}\text{Bu}_2(\text{OH})\text{Cl}_2^-$ might involve ether cleavage of thf by the $\text{Li}^{\text{t}}\text{Bu}$ reagent. $\text{Li}^{\text{t}}\text{Bu}$ cleaves ethers much faster than $\text{Li}^{\text{n}}\text{Bu}$,³⁷ which would explain why no significant analogous hydroxo complexes were found for the $\text{Li}^{\text{n}}\text{Bu}/\text{ZnCl}_2$ solutions. To investigate this possibility further, we repeated the analysis of thf solutions of $\text{Li}^{\text{t}}\text{Bu}/\text{ZnCl}_2$, but this time prepared the solutions by addition of the organolithium reagent at $-78\text{ }^\circ\text{C}$, followed by warming-up to $0\text{ }^\circ\text{C}$. This lower temperature is known to significantly reduce the rate of ether cleavage,³⁷ whereas the transmetalation reaction does occur under these conditions.⁹ We still observed the formation of $\text{Zn}_2^{\text{t}}\text{Bu}_2(\text{OH})\text{Cl}_2^-$, which suggests that it does not originate exclusively from ether cleavage.

3.1.3. $\text{LiCH}_3/\text{ZnCl}_2$. The preparation and analysis of methylzincate complexes proved to be more difficult than the investigation of other organozincates. Solutions of $\text{LiCH}_3/\text{ZnCl}_2$ in thf tended to form precipitates rather easily and yielded relatively low anion-mode ESI signal intensities. Apparently, methylzincate complexes exhibit a particularly high sensitivity toward residual water and/or oxygen contaminations. Nevertheless, the mass spectra obtained show the expected mononuclear $\text{Zn}(\text{CH}_3)\text{Cl}_2^-$, together with ZnCl_3^- , as well as the polynuclear complexes $\text{Zn}_2(\text{CH}_3)\text{Cl}_4^-$ and $\text{LiZn}_2(\text{CH}_3)_2\text{Cl}_4^-$ (Figure S11 of the Supporting Information). $\text{Zn}(\text{CH}_3)\text{Cl}_2^-$ produced Cl^- as ionic fragment upon CID (Table 1, entry 9, and Figure S12 of the Supporting Information); $\text{Zn}_2(\text{CH}_3)\text{Cl}_4^-$ and $\text{LiZn}_2(\text{CH}_3)_2\text{Cl}_4^-$ predominantly yielded zincate species (Table 1, entries 10 and 11, and Figures S13 and S14 of the Supporting Information).

3.1.4. $\text{Li}(\text{C}_4\text{H}_3\text{S})/\text{ZnCl}_2$. Anion-mode ESI of a 1:1 mixture of zinc chloride and 2-lithiothiophene ($\text{Li}(\text{C}_4\text{H}_3\text{S})$) in thf gave $\text{Zn}(\text{C}_4\text{H}_3\text{S})\text{Cl}_2^-$ as a base peak together with small amounts of ZnCl_3^- and complexes at higher m/z ratios, which were not investigated in more detail (Figure S15 of the Supporting Information). Like the other ZnRCl_2^- species studied, $\text{Zn}(\text{C}_4\text{H}_3\text{S})\text{Cl}_2^-$ formed Cl^- and an organozinc chloride species upon CID (Table 1, entry 12, Figure S16 of the Supporting Information).

3.2. Solutions of 2 LiR/ZnCl_2 . **3.2.1. 2 $\text{Li}^{\text{n}}\text{Bu}/\text{ZnCl}_2$, 2 $\text{Li}^{\text{t}}\text{Bu}/\text{ZnCl}_2$, and 2 $\text{Li}^{\text{i}}\text{Bu}/\text{ZnCl}_2$.** The anion-mode ESI mass spectra of 50-mMolar solutions of 2 $\text{Li}^{\text{n}}\text{Bu}/\text{ZnCl}_2$, 2 $\text{Li}^{\text{t}}\text{Bu}/\text{ZnCl}_2$, and 2 $\text{Li}^{\text{i}}\text{Bu}/\text{ZnCl}_2$ in thf all showed almost exclusively dibutylzincates ZnBu_2Cl^- (Figures 3, S17, and S18 of the Supporting Information). Upon CID, these complexes simply fragmented into Cl^- and ZnBu_2 (Table 1, entries 13–15, and Figures S19 and S21 of the Supporting Information).

3.2.2. 2 $\text{LiCH}_3/\text{ZnCl}_2$. Anion-mode ESI of a solution of 2 $\text{LiCH}_3/\text{ZnCl}_2$ in thf yielded the expected $\text{Zn}(\text{CH}_3)_2\text{Cl}^-$ complex (Figure S22), but only at rather low signal intensity. The higher signal intensity observed for $\text{Zn}(\text{CH}_3)\text{Cl}_2^-$ as well as the presence of significant amounts of ZnCl_3^- both indicate partial decomposition of $\text{Zn}(\text{CH}_3)_2\text{Cl}^-$ and related species. Like its butyl analogues, $\text{Zn}(\text{CH}_3)\text{Cl}_2^-$ fragmented into Cl^- and diorganylzinc upon CID (Table 1, entry 16, and Figure S23 of the Supporting Information). Besides the mononuclear zincates mentioned, the

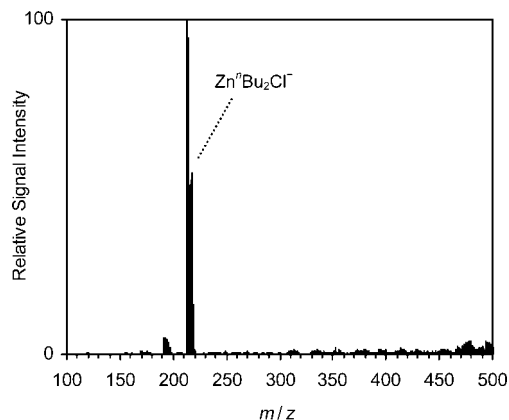


Figure 3. Anion-mode ESI mass spectrum of a 50-mMolar solution of 2 $\text{Li}^{\text{n}}\text{Bu}/\text{ZnCl}_2$ in thf.

polynuclear species $\text{LiZn}_2(\text{CH}_3)_2\text{Cl}_4^-$ was detected as well. This complex was also present in $\text{LiCH}_3/\text{ZnCl}_2$ solutions in thf (see above).

3.2.3. 2 $\text{Li}(\text{C}_4\text{H}_3\text{S})/\text{ZnCl}_2$. The anion-mode ESI mass spectrum of a solution of 2 $\text{Li}(\text{C}_4\text{H}_3\text{S})/\text{ZnCl}_2$ in thf showed $\text{Zn}(\text{C}_4\text{H}_3\text{S})_2\text{Cl}^-$ as base peak (Figure S24 of the Supporting Information). As expected, CID of this complex produced Cl^- as ionic fragment (Table 1, entry 17, and Figure S25 of the Supporting Information). Interestingly, in addition to $\text{Zn}(\text{C}_4\text{H}_3\text{S})_2\text{Cl}^-$, small amounts both of $\text{Zn}(\text{C}_4\text{H}_3\text{S})\text{Cl}_2^-$ and $\text{Zn}(\text{C}_4\text{H}_3\text{S})_3^-$ were detected. The simultaneous presence of these two complexes points to a partial disproportionation of $\text{Zn}(\text{C}_4\text{H}_3\text{S})_2\text{Cl}^-$ according to eq 3.



3.3. Solutions of 4 LiR/ZnCl_2 . **3.3.1. 4 $\text{Li}^{\text{n}}\text{Bu}/\text{ZnCl}_2$.** Initial attempts to detect $\text{Zn}^{\text{n}}\text{Bu}_3^-$ in 10-mMolar thf solutions of 3 $\text{Li}^{\text{n}}\text{Bu}/\text{ZnCl}_2$ prepared at room temperature did not prove successful. Instead of $\text{Zn}^{\text{n}}\text{Bu}_3^-$, mainly $\text{Zn}^{\text{n}}\text{Bu}_2\text{Cl}^-$ was observed, and thus indicated an incomplete transmetalation. In order to bring the transmetalation to completion, we therefore employed 4 equiv. of $\text{Li}^{\text{n}}\text{Bu}$ and also increased the concentration to $c(4 \text{Li}^{\text{n}}\text{Bu}/\text{ZnCl}_2) = 50 \text{ mmol L}^{-1}$ to minimize the potential problem of partial decomposition by traces of water and/or oxygen. Moreover, we prepared the thf solutions of 4 $\text{Li}^{\text{n}}\text{Bu}/\text{ZnCl}_2$ at $-78\text{ }^\circ\text{C}$ and kept them at $0\text{ }^\circ\text{C}$, following the procedure reported by Uchiyama et al.⁹ The thus prepared solutions contained substantial amounts of analyte (20.5 mg/mL), which accumulated in the ESI source and usually caused complete clogging within 30 min or less.

The anion-mode ESI mass spectrum of a 50-mMolar solution of 4 $\text{Li}^{\text{n}}\text{Bu}/\text{ZnCl}_2$ in thf indeed showed $\text{Zn}^{\text{n}}\text{Bu}_3^-$ as base peak (Figure 4). Upon CID, this species lost up to two molecules of C_4H_8 , thereby producing the mono- and dihydrido zincates $\text{ZnH}^{\text{n}}\text{Bu}_2^-$ and $\text{ZnH}_2^{\text{n}}\text{Bu}^-$ (Table 1, entry 18, and Figure S26 of the Supporting Information). $\text{ZnH}^{\text{n}}\text{Bu}_2^-$ also directly appeared in the anion-mode ESI mass spectrum of 4 $\text{Li}^{\text{n}}\text{Bu}/\text{ZnCl}_2$ in thf (Figure 4). Probably, the $\text{ZnH}^{\text{n}}\text{Bu}_2^-$ observed here originated from unwanted fragmentation of $\text{Zn}^{\text{n}}\text{Bu}_3^-$ during the ESI process despite the mild conditions applied. Alternatively, such a fragmentation reaction could have occurred already in solution.

In addition, the anion-mode ESI mass spectrum showed small amounts of $\text{LiZn}^{\text{n}}\text{Bu}_4^-$. The low signal intensity did not permit a corroboration of this assignment by a CID experiment, but

(37) Gilman, H.; Haubein, A. H.; Hartzfeld, H. *J. Org. Chem.* **1954**, *19*, 1034.

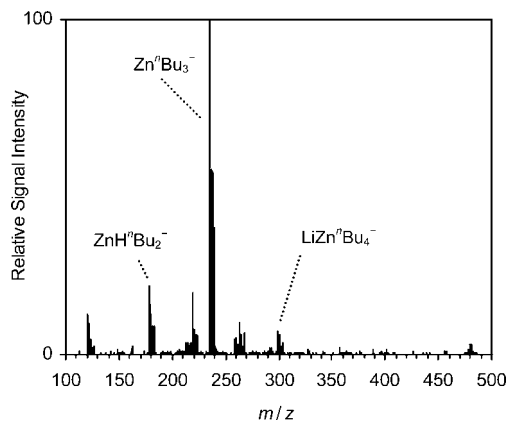


Figure 4. Anion-mode ESI mass spectrum of a 50-mMolar solution of 4 LiⁿBu/ZnCl₂ in thf.

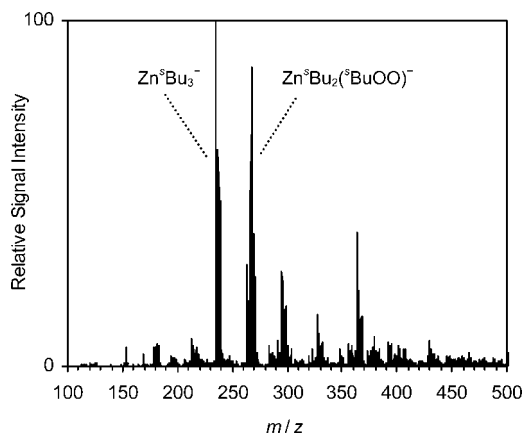


Figure 5. Anion-mode ESI mass spectrum of a 50-mMolar solution of Li^sBu/ZnCl₂ in thf.

the exact m/z ratios observed point to the presence of a high number of hydrogen atoms (see above). Therefore, the assignment as LiZnⁿBu₄⁻ seems plausible.

3.3.2. 4 Li^sBu/ZnCl₂. Anion-mode ESI of a 50-mMolar solution of 4 Li^sBu/ZnCl₂ in thf yielded the expected triorganozincate Zn^sBu₃⁻ (Figure 5). In perfect analogy to its ZnⁿBu₃⁻ counterpart, this complex eliminated up to two molecules of C₄H₈ when subjected to CID (Table 1, entry 19, and Figure S27 of the Supporting Information). We also found evidence for the related LiZnⁿBu₄⁻ ion. While again, the only low signal intensity was not sufficient for a conclusive CID experiment, the isotopic pattern and the exact m/z ratios observed are compatible with this assignment (Figure S28 of the Supporting Information).

In addition, the anion-mode ESI mass spectrum of the 4 LiⁿBu/ZnCl₂ solution showed a number of other species, most prominently a group of ions in the range $267 \leq m/z \leq 271$. The measured isotopic pattern strongly suggests a mononuclear zincate, and the exact m/z ratios indicate the presence of a similar number of hydrogen atoms as in ZnⁿBu₃⁻. Moreover, the ratio between the signal intensities of the ion at $m/z = 267$ and its putative ¹³C isotopologue at $m/z = 268$, $I(267):I(268) = 100:13$, is consistent with the presence of twelve carbon atoms. A structural assignment compatible with these findings is given by the butylperoxy zincate Zn^sBu₂(OO^sBu)⁻. CID fully confirmed this assignment in that it produced the anions HOO⁻,

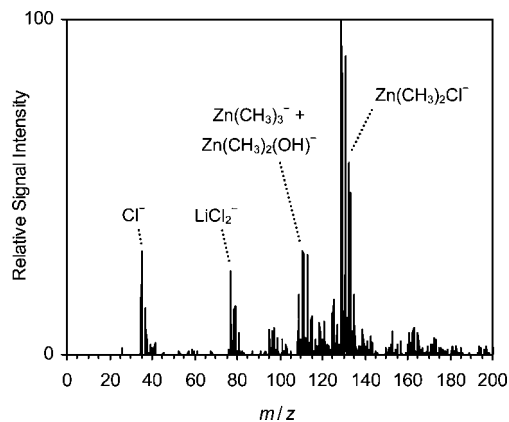


Figure 6. Anion-mode ESI mass spectrum of a 50-mMolar solution of 4 LiCH₃/ZnCl₂ in thf.

C₄H₇O⁻, and C₃H₅O₂⁻ (Table 1, entry 20, and Figure S29 of the Supporting Information), which are known to form in the fragmentation of the related 'BuOO⁻ anion³⁸ and which would not be expected for a simple dioxygen adduct, i.e., (O₂)ZnⁿBu₃⁻. Other fragmentation processes observed produced the butylperoxide anion ^sBuOO⁻ and hydrido zincates (Table 1, entry 20).

3.3.3. 4 LiⁿBu/ZnCl₂. Solutions of 4 LiⁿBu/ZnCl₂ in thf much resembled their 4 LiⁿBu/ZnCl₂ and 4 LiⁿBu/ZnCl₂ counterparts and mainly produced ZnⁿBu₃⁻ upon anion-mode ESI (Figure S30 of the Supporting Information). CID of this species again led to the elimination of up to two molecules of C₄H₈ and the formation of hydrido zincates (Table 1, entry 21, and Figure S31 of the Supporting Information). The hydrido zincate ZnHⁿBu₂⁻ also directly appeared in the anion-mode ESI mass spectrum. In addition, ZnⁿBu₂Cl⁻ was observed as well.

3.3.4. 4 LiCH₃/ZnCl₂. The detection of Zn(CH₃)₃⁻ proved particularly challenging. Anion-mode ESI of 50-mMolar solutions of 4 LiCH₃/ZnCl₂ in thf gave rather low and unstable signal intensities. The main peak observed corresponds to Zn(CH₃)₂Cl⁻ (Figure 6), indicating incomplete transmetalation and/or partial decomposition of Zn(CH₃)₃⁻. Besides smaller amounts of Cl⁻ and LiCl₂⁻, the mass spectrum also shows peaks in the range $109 \leq m/z \leq 115$. The ratio $m/z = 109$ is the one expected for ⁶⁴Zn(CH₃)₃⁻ but the experimental isotopic pattern is not consistent with that calculated for pure Zn(CH₃)₃⁻. A careful analysis revealed the presence of two different zincate species with partially overlapping isotopic patterns. We observed that the peak at $m/z = 109$ was absent in the beginning of a measurement. The remaining peaks then displayed an isotopic pattern characteristic of (mononuclear) zinc (Figure S32 of the Supporting Information). CID of the ion with $m/z = 111$ produced ionic fragments at $m/z = 17$ and 95 (Table 1, entry 22, and Figure S33 of the Supporting Information). These dissociation processes can be rationalized by assuming the presence of Zn(CH₃)₂(OH)⁻, which can eliminate Zn(CH₃)₂ or CH₄, eqs 4a and 4b, respectively.



Zn(CH₃)₂(OH)⁻ presumably forms by partial hydrolysis. If any, the first part of the solution sampled should be prone to contamination by residual traces of moisture in the inlet system of the ESI source. The assignment as Zn(CH₃)₂(OH)⁻ thus seems in line with the decline of its signal intensity during the measurement and the emergence of intact Zn(CH₃)₃⁻. The observed isotopic pattern in the range $109 \leq m/z \leq 115$ can be

(38) Schalley, C. A.; Schröder, D.; Schwarz, H.; Möbus, K.; Boche, G. *Chem. Ber./Recueil* **1997**, *130*, 1085.

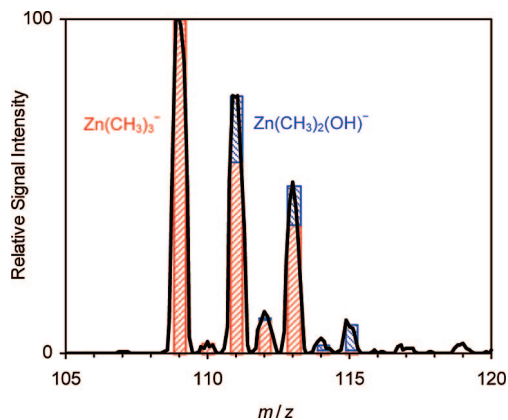


Figure 7. Detail of the anion-mode ESI mass spectrum of a 50-mMolar solution of 4 LiCH₃/ZnCl₂ in thf (black) together with the expected isotopic patterns for Zn(CH₃)₃⁻ (red) and Zn(CH₃)₂(OH)⁻ (blue) in a ratio of 5.0:1.0.

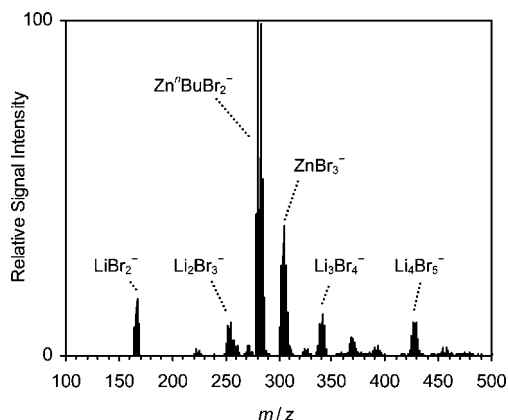


Figure 8. Anion-mode ESI mass spectrum of a 1-mMolar solution of 2 LiⁿBu/ZnBr₂ in thf.

fully explained by the simultaneous presence of Zn(CH₃)₃⁻ and Zn(CH₃)₂(OH)⁻, as illustrated in Figure 7. The recorded isotopic pattern can be exactly reproduced assuming a 5:1 mixture of Zn(CH₃)₃⁻ and Zn(CH₃)₂(OH)⁻. Unfortunately, though, the signal intensity of the former was too low for a CID experiment.

3.3.5. 4 Li(C₄H₉S)/ZnCl₂. Anion-mode ESI of a 50-mMolar solution of 4 Li(C₄H₉S)/ZnCl₂ in thf gave almost exclusively Zn(C₄H₉S)₃⁻ (Figure S34 of the Supporting Information). Upon CID, this species lost Zn(C₄H₉S)₂ to produce C₄H₉S⁻ (Table 1, entry 23, and Figure S35 of the Supporting Information).

3.4. Transmetalation of ZnBr₂ and ZnI₂. In order to assess the effect of the halide anion X⁻ from the reactant zinc salt ZnX₂, we also briefly studied the transmetalation reactions of ZnBr₂ and ZnI₂ with 2 equiv. of LiⁿBu. Anion-mode ESI of the respective thf solutions produced the mononuclear organozincate complexes ZnⁿBuBr₂⁻ and ZnⁿBuI₂⁻ (Figures 8 and 9). Polynuclear organozincates were absent, whereas a manifold of lithium halide clusters Li_nX_{n+1}⁻ were observed. Diorganozincate complexes ZnⁿBu₂X⁻ were not detected either, which might be due to the rather low concentrations of the organometallic species (*c*(LiⁿBu) = 2 mmol L⁻¹) and their partial decomposition by traces of moisture/and or oxygen.

3.5. Cation-Mode ESI Mass Spectra. The cation-mode ESI mass spectra of thf solutions of various lithium organozincate complexes uniformly yielded Li(thf)₃⁺ in high signal intensities (Figure 10). Besides, smaller amounts of Li(thf)₂⁺, Li(thf)₄⁺, and Li₂Cl(thf)₄⁺, but no zinc-containing complexes were detected.

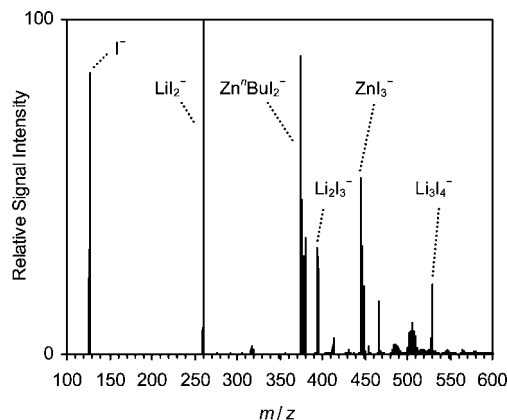


Figure 9. Anion-mode ESI mass spectrum of a 1-mMolar solution of 2 LiⁿBu/ZnI₂ in thf.

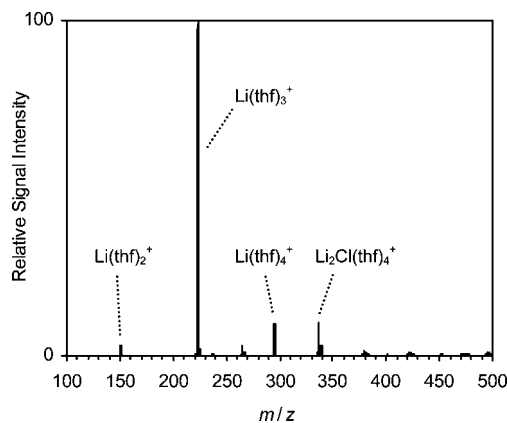


Figure 10. Cation-mode ESI mass spectrum of a 10-mMolar solution of LiCH₃/ZnCl₂ in thf.

Table 2. Relative Rate Constants and Branching Ratios of the Ion-molecule Reactions between Organozincate Ions and Formic Acid

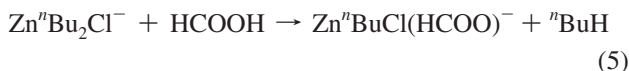
reactant ion	<i>k</i> _{rel} ^a	product channel	branching ratio
Zn ⁿ Bu ₂ Cl ⁻	10 ± 5	Zn ⁿ Bu(HCOO)Cl ⁻ + ⁿ BuH	100
Zn ⁿ Bu ₂ Cl ⁻	<5	Zn ⁿ Bu(HCOO)Cl ⁻ + ⁿ BuH	100
Zn ⁿ Bu ₃ ⁻	100	HCOO ⁻ + Zn ⁿ Bu ₂ + ⁿ BuH	20 ± 20
		Zn ⁿ Bu ₂ (HCOO) ⁻ + ⁿ BuH	80 ± 20
Zn ⁿ Bu ₃ ⁻	35 ± 15	HCOO ⁻ + Zn ⁿ Bu ₂ + ⁿ BuH	20 ± 20
		Zn ⁿ Bu ₂ (HCOO) ⁻ + ⁿ BuH	80 ± 20
Zn ⁿ Bu ₃ ⁻	15 ± 5	Zn ⁿ Bu ₂ (HCOO) ⁻ + ⁿ BuH	100

^a Relative rate constants normalized to *k*_{rel}(ZnⁿBu₃⁻) = 100.

3.6. Gas-Phase Reactivity Studies. 3.6.1. Reactions with Methyl Iodide. Upon exposure of the mass-selected organozincate complexes ZnR_nCl_{3-n}⁻ (R = ⁿBu, ^sBu, and ^tBu) to gaseous methyl iodide, only traces of I⁻ ions were detected. The negligibly low intensity of the I⁻ signal did not show a correlation with the applied pressure *p*(CH₃I). Therefore, the traces of I⁻ observed probably did not originate from ion-molecule reactions between the organozincate ions and methyl iodide but rather from unknown background processes. On the basis of a comparison with well-studied ion-molecule reactions involving methyl iodide (see Experimental Section), we can estimate an upper limit for the efficiency of the reactions between the organozincate ions and methyl iodide of <1% (less than one in hundred collisions is productive).

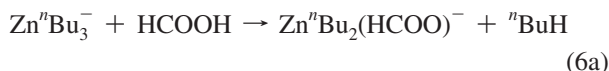
3.6.2. Reactions with Formic Acid. The monobutylzincate complexes ZnⁿBuCl₂⁻, ZnⁿBuCl₂⁻, and ZnⁿBuCl₂⁻ did not react with gaseous formic acid to a measurable extent. In contrast, exposure of mass-selected ⁶⁴ZnⁿBu₂³⁵Cl⁻ (*m/z* = 213) to gaseous

HCOOH resulted in the formation of $^{64}\text{Zn}^n\text{Bu}^{35}\text{Cl}(\text{HCOO})^-$ ($m/z = 201$, Figure S36 of the Supporting Information). The product assignment was confirmed by monitoring the reaction of the mass-selected isotopologue at $m/z = 215$ (corresponding to a mixture of $^{66}\text{Zn}^n\text{Bu}_2^{35}\text{Cl}^-$ and $^{64}\text{Zn}^n\text{Bu}_2^{37}\text{Cl}^-$), which indeed yielded the expected product ion shifted to $m/z = 203$ (Figure S37 of the Supporting Information). The amount of $\text{Zn}^n\text{BuCl}(\text{HCOO})^-$ detected (relative to reactant $\text{Zn}^n\text{Bu}_2\text{Cl}^-$) showed a clear correlation with the applied pressure $p(\text{HCOOH})$ as one expects for a bimolecular reaction between $\text{Zn}^n\text{Bu}_2\text{Cl}^-$ and HCOOH. The reaction can be understood as a combination of proton transfer and ligand exchange, eq 5.



An analogous, but slower reaction was observed for $\text{Zn}^n\text{Bu}_2\text{Cl}^-$ (Figure S38 of the Supporting Information), whereas no product could be detected in the case of $\text{Zn}^n\text{Bu}_2\text{Cl}^-$.

The reaction of Zn^nBu_3^- with formic acid produced $\text{Zn}^n\text{Bu}_2(\text{HCOO})^-$ together with smaller amounts of HCOO^- , eqs 6a and 6b, respectively (Figure S39 of the Supporting Information).



Equation 6a constitutes the analogue of eq 5, and similar to that case, the product assignment was corroborated by analyzing the reaction of a second isotopologue (Figure S40 of the Supporting Information). In the other reaction channel, eq 6b, a proton is transferred as well but here the formate anion does not bind to the zinc species. The analogous reactions also occurred in the case of Zn^nBu_3^- (Figure S41 of the Supporting Information) with a similar branching ratio between the two product channels. For Zn^nBu_3^- , only the reaction analogous to eq 6a was observed (Figure S42 of the Supporting Information).

Although the mass spectrometer used in the present work is not ideal for the quantitative analysis of ion–molecule reactions (see Experimental Section), it can be used to determine approximate relative rate constants. A comparison of the obtained data shows that Zn^nBu_3^- exhibits the highest reactivity of the organozincate complexes studied (Table 2). We could not directly measure the absolute rate of this reaction, but a comparison with measurements of well-known ion–molecule reactions (see Experimental Section) suggests that it apparently approaches the collision rate.

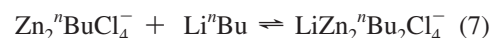
4. Discussion

4.1. Stoichiometry of Organozincate Complexes. As we have demonstrated, ESI mass spectrometry can be used to detect a manifold of different organozincate complexes present in thf solutions. This finding strongly suggests that these lithium organozincates at least partly form separated ion pairs in thf. ESI mass spectrometry thus provides complementary information to reported NMR-spectroscopic studies, which did not detect free organozincate anions. In NMR-spectroscopic analyses of solutions of n $\text{LiCH}_3/\text{ZnCl}_2$ ($n = 3$ and 4)⁸ and 4 $\text{Li}^n\text{Bu}/\text{ZnCl}_2$ in thf,⁹ a single organozinc species was observed in each case. Presumably, the equilibration between contact and separated ion pairs proceeds too fast to be resolved by NMR spectroscopy,

despite the low temperatures applied in the reported experiments. Similarly, other equilibration processes might occur faster than the NMR time scale as well, thus explaining why the ESI mass spectra obtained for the solutions of lithium organozincates show a higher diversity than the corresponding NMR spectra. Lipshutz and co-workers made an analogous observation for thf solutions of related lithium organocuprates.²⁰

The suggested presence of separated lithium organozincates is fully corroborated by the observation of solvated lithium ions $\text{Li}(\text{thf})_n^+$ in the cation-mode ESI mass spectra. Thus, the lithium organozincates in thf behave similarly to lithium organocuprates, which are known to form solvent-separated ion pairs in this solvent as well.¹⁶ The driving force for the solvation of lithium organozincates clearly is the coordination of Li^+ by the strong donor thf. The relative strength of this interaction becomes evident from the fact that even the tetracoordinate complex $\text{Li}(\text{thf})_4^+$ is sufficiently stable to survive the ESI process (for the absolute Li^+ affinity of the related dimethylether, compare ref 39), whereas no solvated organozincates could be detected. The Lewis-base thf obviously does not bind strongly to the anionic organozincate species.

Previous studies have shown that thf not only profoundly affects the ion-pairing behavior of lithium organometallates, but that it also has a key influence on the aggregation of lithium organozincates.¹³ Our present results allow us to address this question in more detail. For solutions of $\text{Li}^n\text{Bu}/\text{ZnCl}_2$ in thf, we found that the signal intensities of $\text{Zn}_2^n\text{BuCl}_4^-$ and $\text{LiZn}_2^n\text{Bu}_2\text{Cl}_4^-$ increased at higher concentrations (Figure 2). This increase apparently reflects a shift of the equilibrium toward higher aggregation states, eq 7.



The depletion of $\text{Zn}^n\text{BuCl}_2^-$ observed when increasing the concentration from $c(\text{Li}^n\text{Bu}/\text{ZnCl}_2) = 10$ to 50 mmol L^{-1} is fully in line with this explanation. This consistency gives us confidence that the observed trends reflect the true properties of the solution chemistry and are not just artifacts from the ESI process, such as, e.g., the well-known formation of salt clusters not present in the solution phase.⁴⁰ Nevertheless, two caveats must be considered:

(1) The relative ESI signal intensities measured for two different ions do not necessarily correlate linearly with their relative concentrations in solution. While it seems likely that structurally similar ions display comparable ESI response factors, it is largely unknown how structurally more diverse ions behave.

(2) Labile complexes possibly do not survive the ESI process but instead may at least partly undergo fragmentation reactions. In the present context, such unwanted fragmentations could potentially lead to a discrimination against the detection of some of the polynuclear organozincates (see below).

Because of these ambiguities, a rigorous quantitative comparison of the signal intensities observed for the different organozincate complexes is not indicated. At a qualitative level, a comparison of the different organozincates detected reveals many similarities (Table 3). Mononuclear organozincate complexes $\text{ZnR}_n\text{Cl}_{3-n}^-$ ($1 \leq n \leq 3$) were found in all cases and

(39) More, M. B.; Glending, E. D.; Ray, D.; Feller, D.; Armentrout, P. B. *J. Phys. Chem.* **1996**, *100*, 1605.

(40) Pleasance, S.; Thibault, P.; Sim, P. G.; Boyd, R. K. *Rapid Commun. Mass Spectrom.* **1991**, *5*, 307.

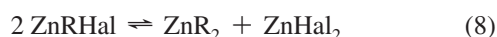
Table 3. Organozincate complexes observed in significant quantities.

complex	ratio R:Zn	R = ⁿ Bu	ⁱ Bu	^t Bu	CH ₃	C ₄ H ₉ S
Zn ₂ RCl ₄ ⁻	0.5	+			+	
ZnRCl ₂ ⁻	1	+	+	+	+	+
LiZnRCl ₃ ⁻	1	+				
Zn ₂ R ₂ Cl ₃ ⁻	1		+	+		
LiZn ₂ R ₂ Cl ₄ ⁻	1	+	+	+	+	
ZnR ₂ Cl ⁻	2	+	+	+	+	+
ZnR ₃ ⁻	3	+	+	+	+	+

irrespective of the organyl R, and analogous complexes ZnRBr₂⁻ and ZnRI₂⁻ (R = ⁿBu) were observed when ZnBr₂ and ZnI₂, respectively, were used as Zn(II) source. Complexes of these types thus appear to be common components of mmolar mixtures of organolithium compounds and zinc halides in thf. While the homoleptic lithium organozincates Li⁺ZnR₃⁻ and (Li⁺)₂(ZnR₄²⁻) have been well-known for relatively long time,¹ their heteroleptic counterparts Li⁺ZnRHal₂⁻ and Li⁺ZnR₂Hal⁻ have received only very little attention.⁴¹ The present results demonstrate the existence of these species and point to the role of the halide ions present, which bind to the zinc center and thereby may also influence the reactivity of the organozinc reagent. In this context, it is interesting to note that the addition of LiCl has a marked influence on the reactivity of organozinc⁴² and organomagnesium compounds.^{43,44}

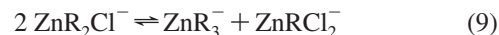
With respect to polynuclear organozincates, the situation is more complex. No polynuclear thiophenylzincates of significant abundance were observed. This finding comes somewhat as a surprise because one might expect the sulfur atom of the thiophenyl group to engage easily in coordinative binding to a second metal center. In contrast, polynuclear complexes were detected in significant abundance for all of the alkylzincates investigated. A more careful analysis reveals, however, that only those polynuclear complexes form readily that bear one alkyl group or less per zinc atom. Apparently, a minimum number of chloride ligands is thus essential for the stability of aggregated organozincates in thf. For the synthetically most important lithium organozincates LiZnR₃ and Li₂ZnR₄, the presence of higher aggregates therefore seems unlikely at mmolar solutions in thf. While the ESI source used in the present work did not permit to probe solutions with *c* > 50 mmol L⁻¹, Uchiyama et al. successfully analyzed 1-molar solutions of 4 LiⁿBu/ZnCl₂ in thf and observed the LiZnⁿBu₄⁻ complex (the authors did not mention the detection of other ions).⁹ This ion represents the direct counterpart of the LiZnⁿBu₄⁻ and LiZnⁿBu₄⁻ species found in the present work. The results of Uchiyama et al. thus indicate that solutions of lithium organozincates Li₂ZnR₄ in thf contain complexes in low aggregation states even at high concentrations.

Besides equilibria between different aggregation states, Schlenk-type equilibria may operate for organozincates complexes as well. Only little is known about such Schlenk equilibria for neutral organozinc compounds, eq 8.



Whereas earlier studies found the equilibrium to lie almost exclusively on the left for Zn(CH₃)I and ZnEtI in thf,⁴⁵ recent work has shown that Lewis acids can considerably facilitate

disproportionation.⁴⁶ For the dialkylzincates ZnR₂Cl⁻ investigated in the present study, we did not observe significant amounts of ZnR₃⁻ and ZnRCl₂⁻ along with the ZnR₂Cl⁻ species. Assuming similar ESI response factors for the ZnR_nCl_{3-n}⁻ complexes, we therefore conclude that the anionic Schlenk-type equilibria for dialkylzincates, eq 9, strongly favor the ZnR₂Cl⁻ species.



In the case of the dithiophenylzincate complex Zn(C₄H₉S)₂Cl⁻, however, the simultaneous presence of this ion, Zn(C₄H₉S)₃⁻, and Zn(C₄H₉S)Cl₂⁻ suggests that the disproportionation occurs to a significant extent. In no instance have we found evidence for an analogous disproportionation of ZnRCl₂⁻ species.

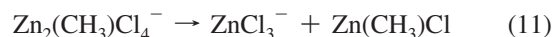
In addition to the organozincate complexes listed in Table 3, a few oxygen-containing organozincates were detected as well. Presumably, these species originated from the reactions with contaminants, which were most likely present in the diluted solutions and/or the inlet system of the ESI source (for their possible formation by ether cleavage, see above). The complexes Zn₂ⁿBu₂(OH)Cl₂⁻ and Zn(CH₃)₂(OH)⁻ probably result from hydrolysis reactions. In contrast, the butylperoxy species ZnⁿBu₂(ⁿBuOO)⁻ must form in a reaction with dioxygen. The fact that neither its ZnⁿBu(ⁿBuOO)Cl⁻ nor its Zn(ⁿBuOO)Cl₂⁻ analogue were observed indicates that it probably originates from the direct reaction between ZnⁿBu₃⁻ and dioxygen, eq 10a, rather than from the addition of preformed ⁿBuOO⁻ anion to ZnⁿBu₂, eq 10b.



4.2. Unimolecular Fragmentation Reactions in the Gas Phase. The different fragmentation reactions found for organozincate complexes can be divided into two categories:

- (1) fragmentation by elimination of a neutral metal fragment and
- (2) fragmentation by elimination of an alkene.

The first type of fragmentation is particularly favorable for polynuclear organozincates. In the case of Zn₂(CH₃)Cl₄⁻, e.g., the dissociation reaction occurred already at *E*_{LABORATORY} = 1.5 eV (Figure S13 of the Supporting Information), eq 11. This facile fragmentation implies that some of the Zn₂(CH₃)Cl₄⁻ complexes most likely already dissociate during the ESI process (see above).



In this and similar fragmentation reactions, the neutral metal fragment is relatively stable and the resulting ion can well accommodate the negative charge. The ability of the ionic fragment to delocalize the negative charge indeed appears to be the major factor in determining the outcome of a dissociation reaction. Because of the high electronegativity of chlorine, ZnCl₃⁻ can better stabilize the negative charge than Zn(CH₃)Cl₂⁻, which therefore does not form upon CID of Zn₂(CH₃)Cl₄⁻. The other polynuclear organozincate complexes investigated also preferentially eliminate ZnRCl or, if possible, ZnR₂ species rather than ZnCl₂ (Table 1). The mononuclear organozincates ZnRCl₂⁻ and ZnR₂Cl⁻ exhibit exactly the same

(41) Habeeb, J. J.; Osman, A.; Tuck, D. G. *J. Organomet. Chem.* **1980**, *185*, 117.

(42) Ochiai, H.; Jang, M.; Hirano, K.; Yorimitsu, H.; Oshima, K. *Org. Lett.* **2008**, *10*, 2681.

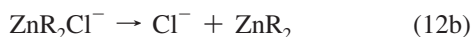
(43) Krasovskiy, A.; Knochel, P. *Angew. Chem.* **2004**, *116*, 3396; *Angew. Chem., Int. Ed.* **2004**, *43*, 3333.

(44) Krasovskiy, A.; Straub, B. F.; Knochel, P. *Angew. Chem.* **2006**, *118*, 165; *Angew. Chem., Int. Ed.* **2006**, *45*, 159.

(45) Evans, D. F.; Fazakerley, G. V. *J. Chem. Soc. A* **1971**, 182.

(46) Blake, A. J.; Shannon, J.; Stephens, J. C.; Woodward, S. *Chem. Eur. J.* **2007**, *13*, 2462.

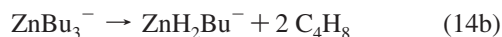
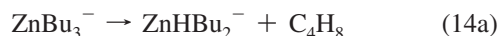
tendency and exclusively yield Cl^- when subjected to CID, eqs 12a and 12b.



Obviously, Cl^- is much more stable than the carbanions R^- formed alternatively. For the triorganylzincates ZnR_3^- , formation of R^- cannot be avoided, however, if again a metal fragment is to be eliminated, eq 13.



In the case of trithiophenylzincate $\text{Zn}(\text{C}_4\text{H}_3\text{S})_3^-$, this reaction does occur, which can be ascribed to the relatively good stabilization of the resulting carbanion with a sulfur atom in α -position to the negative charge. In contrast, the tributylzincates ZnBu_3^- do not undergo this type of fragmentation but upon CID instead release one or even two butene molecules, eq 14a and 14b, respectively.



Most probably, these reactions proceed as β -hydride eliminations. This reaction type is quite common for metal compounds that bear alkyl groups with β -hydrogen atoms, although it is less well-established for the specific case of zinc organyls. A recent study on the gas-phase pyrolysis of diethylzinc concluded that β -hydride eliminations do not play a major role for that system except for photolytic processes.⁴⁷ The present findings suggest a different situation for the anionic tributylzincates.

4.3. Bimolecular Gas-Phase Reactivity. The present data on the gas-phase reactivity of organozincate anions can be directly compared with the results that O'Hair and co-workers reported for organomagnesates $\text{Mg}(\text{CH}_3)_2\text{X}_2^-$ ($\text{X} = \text{Cl}$ and CH_3COO)³⁰ and organocuprates, such as $\text{Cu}(\text{CH}_3)_2^-$.^{32,33} Whereas the organozincate complexes ZnBuCl_2^- complexes fail to react with formic acid, gaseous $\text{Mg}(\text{CH}_3)_2\text{Cl}_2^-$ even reacts with much weaker proton donors, such as water and methanol.³⁰ Moreover, ZnBu_2Cl^- and ZnBu_3^- do not react with methyl iodide to a significant extent, while $\text{Cu}(\text{CH}_3)_2^-$ undergoes coupling.³² Thus, gaseous organozincates display a more moderate reactivity than their organomagnesate and organocuprate counterparts. This trend is fully in line with the solution-phase chemistry of organozinc, -magnesium, and -copper compounds, of which the former are well-known as the mildest and most chemoselective reagents.^{4,5}

Further insight can be gained from a comparison of the gas-phase reactivity of the different organozincate complexes probed. The reactions between the $\text{ZnBu}_n\text{Cl}_{3-n}^-$ anions and formic acid clearly show that the substitution of chloride ligands for butyl groups increases the nucleophilic reactivity of the organozincate. This trend parallels the situation in solution, where diorganylzinc compounds ZnR_2 are known to be more reactive than organozinc halides ZnRHal .⁴⁸ In the case of the *n*-butylzincates, the rate constant for the gas-phase reaction of the triorganyl species Zn^nBu_3^- with formic acid is approximately $10\times$ higher than that of the $\text{Zn}^n\text{Bu}_2\text{Cl}^-$ complex. A similar difference was observed for their *s*-butyl analogues (Table 2). In addition, the reactivity of the organozincate complexes also depends on

the nature of the butyl groups. Both for the ZnBu_3^- and for the ZnBu_2Cl^- series, the *n*-butylzincates are more reactive toward formic acid than their *s*-butyl counterparts, which in turn are more reactive than the *t*-butyl species. The low reactivity of the *t*-butylzincates is particularly interesting, given their importance in synthetic applications. While at first sight it might seem contradictory that a lower reactivity should be beneficial for synthetic applications, it is exactly this tolerance of functional groups and superior chemoselectivity, which make organozincates so valuable. The rather slow gas-phase reactions of the *t*-butylzincates toward formic acid help us to understand why $\text{Li}_2\text{Zn}^n\text{Bu}_4$ can be used for the initiation of the living polymerization of *N*-isopropylacrylamide in aqueous solution.¹¹ Thus, the reactivity of the organozincate complexes probed in the gas phase once more closely mimics their chemistry in solution.

5. Conclusions

Anion-mode ESI mass spectrometry of mixtures of organolithium compounds and zinc chloride in thf resulted in the detection of a manifold of organozincate ions. Besides mononuclear species of the types ZnRCl_2^- , ZnR_2Cl^- , and ZnR_3^- , polynuclear complexes, such as $\text{LiZn}_2\text{R}_2\text{Cl}_4^-$ were detected as well. Concentration-dependence studies suggested that the observed species can be directly related to equilibria between different aggregation states in solution. ESI mass spectrometry thus offers unique possibilities to probe the exact molecular composition of solvent-separated organozincate anions present in thf solutions.

The observation of ZnRCl_2^- and ZnR_2Cl^- complexes shows that not only organolithium compounds but also chloride ions are effective in binding to the zinc center and formation of zincate species. We are currently investigating the implications of this finding for understanding the high reactivity of recently developed LiCl-containing organozinc and organomagnesium reagents. Chloride ligands moreover apparently enable the formation of polynuclear complexes by adopting bridging-mode bonds. The availability of chloride ions therefore has a crucial effect on the aggregation equilibria in thf solutions. In contrast, bromide and iodide ions do not seem to promote the formation of polynuclear zincate complexes in a comparable manner. In the case of a mixture of 2-lithiothiophene and ZnCl_2 , we also found evidence for the operation of Schlenk equilibria and the disproportionation of $\text{Zn}(\text{C}_4\text{H}_3\text{S})_2\text{Cl}^-$ in solution.

In addition, we investigated the uni- and bimolecular gas-phase reactivity of the organozincate complexes extracted from solution. Upon energetic collisions, the organozincate anions preferentially lose neutral metal fragments. This fragmentation channel is energetically inaccessible in the case of the tributylzincates ZnBu_3^- , which instead expel butene to yield hydrido-zincate species. Presumably, this reaction corresponds to a β -hydride elimination. Trialkylzincates ZnR_3^- thus appear to be interesting model systems to study β -hydride eliminations of organozinc compounds, for which this reaction type is not as well established as for other organometallics.

The gaseous butylzincate complexes are less reactive toward methyl iodide and formic acid than related magnesate and cuprate anions. This trend exactly mirrors the situation in solution. Moreover, we found that the reactivity is further reduced when going from the tributylzincates ZnBu_3^- to di- and monobutylzincates ZnBu_2Cl^- and ZnBuCl_2^- , respectively. Very similarly, organozinc halides ZnRHal in solution are less reactive than diorganylzinc species ZnR_2 . The fact that such important features of organozinc chemistry known from solution are preserved in the gas phase suggests that these features

(47) Kim, Y. S.; Won, Y. S.; Hagelin-Weaver, H.; Omenetto, N.; Anderson, T. J. *Phys. Chem. A* **2008**, *112*, 4246.

(48) Knochel, P. *Synlett* **1995**, 393.

constitute intrinsic properties of organozinc compounds and that gas-phase methods can contribute to their elucidation. With respect to the question of why *t*-butylzincates have proven particularly useful in synthetic applications, our results show that *t*-butylzincate anions are significantly less reactive toward the proton donor formic acid than their *s*- and *n*-butyl analogues. This lower tendency to accept protons should render *t*-butylzincates more tolerant toward hydroxy groups and thus adds to their outstanding chemoselectivity.

Acknowledgment. Dedicated to Professor Helmut Schwarz on the occasion of his 65th birthday. We thank Prof. Ulrich Koszinowski for generously making his TSQ 7000 mass

spectrometer available to us. We gratefully acknowledge support by Prof. Herbert Mayr, Prof. Thomas Carell, the Munich Center for Integrated Protein Science CIPS^M, the Fonds der Chemischen Industrie, and the Deutsche Forschungsgemeinschaft (SFB 749).

Supporting Information Available: Table giving the relative rate constants of ion–molecule reactions used for calibration and figures showing additional mass spectra. This material is available free of charge via the Internet at <http://pubs.acs.org>.

OM8007037

Synthesis and Structural Analysis of (Cyclopentadienyl)(pyrrolide)titanium(IV) Complexes and Their Use in Catalysis for Olefin Polymerization

Irfan Saeed, Shohei Katao, and Kotohiro Nomura*

Graduate School of Materials Science, Nara Institute of Science and Technology (NAIST), 8916-5 Takayama, Ikoma, Nara 630-0101, Japan

Received July 28, 2008

$\text{Cp}^*\text{TiCl}_2(\text{L})$ [$\text{L} = \text{C}_4\text{H}_4\text{N}$ (**1**), 2,5- $\text{Me}_2\text{C}_4\text{H}_2\text{N}$ (**2**), 2,4- $\text{Me}_2\text{C}_4\text{H}_2\text{N}$ (**3**), 2,4- Me_2 -3-Et C_4HN (**4**)], $\text{Cp}^*\text{TiCl}(\text{2,4-Me}_2\text{-3-EtC}_4\text{HN})_2$ (**5**), and $\text{Cp}^*\text{Ti}(\text{C}_4\text{H}_4\text{N})_3$ (**6**) were prepared by treating Cp^*TiCl_3 with the corresponding lithium salts in toluene or *n*-hexane. The structures of **3–6** determined by X-ray crystallography indicate that the complexes have a distorted tetrahedral geometry around Ti, and the nitrogen atom binds to Ti in an η^1 fashion. The dimethyl analogues $\text{Cp}^*\text{TiMe}_2(\text{L})$ [$\text{L} = \text{C}_4\text{H}_4\text{N}$ (**7**), 2,5- $\text{Me}_2\text{C}_4\text{H}_2\text{N}$ (**8**)] could be prepared by adopting a route that involves *in situ* generation of $\text{Cp}^*\text{Ti}(\text{Cl})\text{Me}_2$, prepared by the reaction of Cp^*TiCl_3 with 2.0 equiv of MeLi in Et_2O , and the subsequent treatment with the corresponding lithium salts. The Cp analogues $\text{CpTiCl}_2(\text{L})$ [$\text{L} = \text{C}_4\text{H}_4\text{N}$ (**9**), 2,5- $\text{Me}_2\text{C}_4\text{H}_2\text{N}$ (**10**), 2,4- $\text{Me}_2\text{C}_4\text{H}_2\text{N}$ (**11**), 2,4- Me_2 -3-Et C_4HN (**12**)] were also prepared by treating CpTiCl_3 with the corresponding lithium salts in Et_2O or *n*-hexane. The crystallographic analyses of **9–11** indicate that the dimethylpyrrolide ligand in **10** coordinates to Ti in η^5 mode, whereas the nitrogen atom in the pyrrolide ligand (in complexes **9** and **11**) binds to Ti in an η^1 fashion (σ bonding in addition to π donation). These complexes (**1–4**, **7–12**) exhibited moderate catalytic activities for ethylene polymerization in the presence of methylaluminoxane (MAO), and the activities were highly affected by the substituent on the pyrrolide ligand. In the polymerization using a series of dichloro complexes, the Cp^* -pyrrolide analogue **1** exhibited the highest catalytic activity, and an increase in the steric bulk led to the decrease in activity, whereas the activity of the Cp analogues increased upon increasing the steric bulk in the pyrrolide ligand. The dimethyl complexes (**7**, **8**) exhibited notable catalytic activities in the presence of MAO, and the activities increased in the presence of $^i\text{Bu}_3\text{Al}[\text{Ph}_3\text{C}][\text{B}(\text{C}_6\text{F}_5)_4]$ cocatalyst in place of MAO. The resultant polymers possessed unimodal molecular weight distributions. These complexes also exhibited moderate catalytic activities for syndiospecific styrene polymerization, and the activities of the Cp^* analogues increased at high temperature.

Introduction

The design and synthesis of efficient transition metal complex catalysts that precisely control olefin coordination polymerization attract considerable attention in the fields of catalysis, organometallic chemistry, and polymer chemistry.^{1–7} *Non-bridged* half-metallocene type group 4 transition metal complexes of the type $\text{Cp}'\text{M}(\text{L})\text{X}_2$ ($\text{Cp}' =$ cyclopentadienyl group; $\text{M} = \text{Ti}, \text{Zr}, \text{Hf}$; $\text{L} =$ anionic ligand such as OAr, NR_2 , $\text{N} = \text{CR}_2$, $\text{N} = \text{PR}_3$, etc.; $\text{X} =$ halogen, alkyl) have been considered as one of the promising candidates for new efficient catalysts,^{6–8} because these complex catalysts exhibit unique characteristics for the production of new polymers^{6,9–20} that are not prepared (or very difficult to prepare) by conventional Ziegler–Natta

catalysts, as well as by ordinary metallocene type¹ and/or “constrained geometry” (linked Cp-amide) type catalysts.^{1d,2} Moreover, their syntheses are generally simplified (one or two steps in high yields), and the ligand modifications sterically and/or electronically should be easier especially than those in the ordinary linked half-metallocene type complexes.⁶ We already demonstrated that the half-titanocenes containing an aryloxo ligand of the type $\text{Cp}'\text{TiCl}_2(\text{OAr})$ ($\text{Cp}' =$ substituted cyclopentadienyl; OAr = aryloxo) not only exhibited notable catalytic activities for olefin polymerization⁸ but also displayed unique characteristics especially for copolymerization of ethylene with α -olefin,^{9,10} vinylcyclohexane,¹¹ 2-methyl-1-pentene,¹² styrene,^{13,14} and cyclic olefins such as norbornene,¹⁵ cyclopentene,¹⁶ and cyclohexene.¹⁷ It was revealed that an efficient catalyst for desired (co)polymerization can be modified by simple replace-

* Corresponding author. Tel: +81-743-72-6041. Fax: +81-743-72-6049. E-mail: nomurak@ms.naist.jp.

(1) (a) Brintzinger, H. H.; Fischer, D.; Mühlaupt, R.; Rieger, B.; Waymouth, R. M. *Angew. Chem., Int. Ed. Engl.* **1995**, *34*, 1143. (b) Kaminsky, W. *Macromol. Chem. Phys.* **1996**, *197*, 3903. (c) Kaminsky, W.; Arndt, M. *Adv. Polym. Sci.* **1997**, *127*, 143. (d) Suhm, J.; Heinemann, J.; Wörner, C.; Müller, P.; Stricker, F.; Kressler, J.; Okuda, J.; Mühlaupt, R. *Macromol. Symp.* **1998**, *129*, 1.

(2) McKnight, A. L.; Waymouth, R. M. *Chem. Rev.* **1998**, *98*, 2587.

(3) (a) Britovsek, G. J. P.; Gibson, V. C.; Wass, D. F. *Angew. Chem., Int. Ed.* **1999**, *38*, 429. (b) Gibson, V. C.; Spitzmesser, S. K. *Chem. Rev.* **2003**, *103*, 283. (c) Bolton, P. D.; Mountford, P. *Adv. Synth. Catal.* **2005**, *347*, 355.

(4) *Frontiers in Metal-Catalyzed Polymerization* (special issue): Gladysz, J. A. *Chem. Rev.* **2000**, *100* (4). For example: (a) Ittel, S. D.; Johnson, L. K.; Brookhart, M. *Chem. Rev.* **2000**, *100*, 1169. (b) Alt, H. G.; Köppl, A. *Chem. Rev.* **2000**, *100*, 1205. (c) Chen, E. Y.-X.; Marks, T. J. *Chem. Rev.* **2000**, *100*, 1391.

(5) (a) Coates, G. W.; Hustad, P. D.; Reinartz, S. *Angew. Chem., Int. Ed.* **2002**, *41*, 2236. (b) Domski, G. J.; Rose, J. M.; Coates, G. W.; Bolig, A. D.; Brookhart, M. *Prog. Polym. Sci.* **2007**, *32*, 30.

(6) Nomura, K.; Liu, J.; Padmanabhan, S.; Kitiyanan, B. *J. Mol. Catal. A* **2007**, *267*, 1. References including list of reported complexes are cited therein.

(7) Stephan, D. W. *Organometallics* **2005**, *24*, 2548.

ment of both the cyclopentadienyl fragment (Cp') and anionic ancillary donor ligands (L).⁶ More recently, we demonstrated that these catalysts are also effective in introducing functional groups into polyolefins in an efficient manner.^{18,19}

Pyrrolyl ligands and their derivatives are considered to be isoelectronic with the cyclopentadienyl fragments (Cp'), but these ligands are known to show an η^5 (π fashion) versus η^1 (σ fashion bound only via nitrogen) coordination mode, depending upon the substituents and/or other factors.^{20–22} Several examples concerning synthesis and structural analysis of titanium complexes containing pyrrolides such as Cp₂Ti(η^1 -C₄H₄N)₂,^{20a} Cp*₂Ti(η^1 -C₄H₄N),^{20g} (η^5 -C₄Me₄N)₂TiCl₂,^{20b} (η^5 -C₄Me₄N)TiCl₃,^{20b} (η^5 -C₄H₄N)Ti(SPh)₃,^{20b}

(η^5 -C₄H₄N)TiCl₂(SPh),^{20b} and CpTi(η^5 -C₄Me₄N)Cl₂^{20b} have been reported in the literature. Moreover, reports regarding group 4 transition metal complexes of pyrrolide-containing chelate ligands (pyrrole-imine, etc.) and their use as olefin polymerization catalysts have also appeared.²³ Examples concerning highly selective trimerization of ethylene to 1-hexene using a catalyst system consisting of CrCl₃, pyrrole, and MAO^{24a,b} and considerable advancement in the presence of a series of pyrrole-based ligands are also known.^{24c–f} More recently, pyrrolide ligands have been used in the design of single-component vanadium catalysts for ethylene polymerization,^{21h} as well as for cationic rare earth metal-catalyzed styrene polymerization.²⁵ Despite the various above-mentioned examples, synthesis and structural analysis of half-titanocenes containing a series of (substituted) pyrrolides, especially detailed study concerning a relationship between the ligand substituents and the structure (η^1 or η^5 , etc.) and/or the catalytic activity, have never been explored.²⁶ Therefore, in this paper, we introduce the synthesis and structural analysis of half-titanocenes containing a series of (substituted) pyrrolide ligands of the type Cp'TiX₂(L) [Cp' = Cp*, Cp, L = C₄H₄N, 2,5-Me₂C₄H₂N, 2,4-Me₂C₄H₂N, 2,4-Me₂-3-EtC₄HN, X = Cl, Me]. We have also explored the effect of ligand substituents toward catalytic activity in ethylene polymerization and syndiospecific styrene polymerization in the presence of methylaluminoxane (MAO) cocatalyst.²⁷

Results and Discussion

1. Synthesis and Structural Analysis of Cp*TiCl₂(L) [L = C₄H₄N, 2,5-Me₂C₄H₂N, 2,4-Me₂C₄H₂N, 2,4-Me₂-3-EtC₄HN], Cp*TiCl₂(2,4-Me₂-3-EtC₄HN)₂, and Cp*Ti(C₄H₄N)₃. The general scheme for the synthesis of Cp*TiCl₂(L) [L = C₄H₄N (**1**), 2,5-

(21) Selected recent examples for synthesis and some reactions with vanadium, niobium, tantalum, and molybdenum complexes containing pyrrolide ligands: (a) Tayebani, M.; Conoci, S.; Feghali, K.; Yap, G. P. A.; Gambarrota, S. *Organometallics* **2000**, *19*, 4568. (b) Aharonian, G.; Gambarrota, S.; Yap, G. P. A. *Organometallics* **2002**, *21*, 4257. (c) Gao, G.; Korobkov, I.; Gambarrota, S. *Inorg. Chem.* **2004**, *43*, 1108. (d) Hock, A. S.; Schrock, R. R.; Hoveyda, A. H. *J. Am. Chem. Soc.* **2006**, *128*, 16373. (e) Singh, R.; Schrock, R. R.; Müller, P.; Hoveyda, A. H. *J. Am. Chem. Soc.* **2007**, *129*, 12654. (f) Krcijmann, T.; Arndt, S.; Schrock, R. R.; Müller, P. *Organometallics* **2007**, *26*, 5702. (g) Vidyaratne, I.; Crewdson, P.; Lefebvre, E.; Gambarrota, S. *Inorg. Chem.* **2007**, *46*, 8836. (h) Jabri, A.; Korobkov, I.; Gambarrota, S.; Duchateau, R. *Angew. Chem., Int. Ed.* **2007**, *46*, 6119. (i) Ilango, S.; Vidjayacoumar, B.; Gambarrota, S.; Gorelsky, S. *Inorg. Chem.* **2008**, *47*, 3265.

(22) Bonding geometry of pyrrolyl in Zr complexes: Dias, A. R.; Ferreira, A. P.; Veiros, L. F. *Organometallics* **2003**, *22*, 5114.

(23) As related examples, synthesis of group 4 metal complexes containing iminopyrrole or aminopyrrole ligands, see: (a) Male, N. A. H.; Thornton-Pett, M.; Bochmann, M. *J. Chem. Soc., Dalton Trans.* **1997**, 2487. (b) Dawson, D. M.; Walker, D. A.; Thornton-Pett, M.; Bochmann, M. *J. Chem. Soc., Dalton Trans.* **2000**, 459. (c) Matsuo, Y.; Mashima, K.; Tani, K. *Chem. Lett.* **2000**, 1114. (d) Yoshida, Y.; Matsui, S.; Takagi, Y.; Mitani, M.; Nakano, T.; Tanaka, H.; Kashiwa, N.; Fujita, T. *Organometallics* **2001**, *20*, 4793. (e) Huang, J.-H.; Chi, L.-S.; Yu, R.-C.; Jiang, G. J.; Yang, W.-T.; Lee, G.-H.; Pen, S.-M. *Organometallics* **2001**, *20*, 5788. (f) Tsurugi, H.; Matsuo, Y.; Yamagata, T.; Mashima, K. *Organometallics* **2004**, *23*, 2797. (g) Yasumoto, T.; Yamagata, T.; Mashima, K. *Organometallics* **2005**, *24*, 3375. (h) Tsurugi, H.; Mashima, K. *Organometallics* **2006**, *25*, 5210.

(24) (a) Manyik, R. M.; Walker, W. E.; Wilson, T. P. (Union Carbide Corporation) US 3300458, 1967. (b) Manyik, R. M.; Walker, W. E.; Wilson, T. P. *J. Catal.* **1977**, *47*, 197. (c) Reagan, W. K. (Phillips Petroleum Company) EP0417477, 1991. (d) Freeman, J. W.; Buster, J. L.; Knudsen, R. D. (Phillips Petroleum Company) US 5,856,257, 1999. (e) Salo, V. B.; Guan, Z. *Organometallics* **2003**, *22*, 5033. (f) Ruther, T. H.; Braussaud, N.; Cavell, K. J. *Organometallics* **2001**, *20*, 1247.

(25) Nishiura, M.; Mashiko, T.; Hou, Z. *Chem. Commun.* **2008**, 2019.

(26) Synthesis and structural analysis of *ansa*-cyclopentadienyl pyrrolyl titanium complexes: Seo, W. S.; Cho, Y. J.; Yoon, S. C.; Park, J. T.; Park, Y. J. *Organomet. Chem.* **2001**, *640*, 79.

(27) Synthesis and polymerization study of ethylene with some of the complexes in this paper were reported in the patent: Etheron, B. P.; Nagy, S. (Occidental Chemical Corporation) US5539124, 1994.

(8) Selected examples (except introduced below), see: (a) Shah, S. A. A.; Dorn, H.; Voigt, A.; Roesky, H. W.; Parisini, E.; Schmidt, H. -G.; Noltemeyer, M. *Organometallics* **1996**, *15*, 3176. (b) Richter, J.; Edelman, F. T.; Noltemeyer, M.; Schmidt, H. -G.; Schmulinson, M.; Eisen, M. S. *J. Mol. Catal. A* **1998**, *130*, 149. (c) Doherty, S.; Errington, R. J.; Jarvis, A. P.; Collins, S.; Clegg, W.; Elsegood, M. R. *J. Organometallics* **1998**, *17*, 3408. (d) Sita, L. R.; Babcock, R. *Organometallics* **1998**, *17*, 5228. (e) Stephan, D. W.; Stewart, J. C.; Guérin, F.; Spence, R. E. v. H.; Xu, W.; Harrison, D. G. *Organometallics* **1999**, *18*, 1116. (f) Vollmerhaus, R.; Shao, P.; Taylor, N. J.; Collins, S. *Organometallics* **1999**, *18*, 2731. (g) Antiñolo, A.; Carrillo-Hermosilla, F.; Corrochano, A.; Fernández-Baeza, J.; Lara-Sanchez, A. R.; Ribeiro, M.; Lanfranchi, M.; Otero, A.; Pellinghelli, M. A.; Portela, M. F.; Santos, J. V. *Organometallics* **2000**, *19*, 2837. (h) Jayaratne, K. C.; Sita, L. R. *J. Am. Chem. Soc.* **2000**, *122*, 958. (i) Sinnema, P.-J.; Spaniol, T. P.; Okuda, J. *J. Organomet. Chem.* **2000**, *598*, 179. (j) McMeeking, J.; Gao, X.; Spence, R. E. v. H.; Brown, S. J.; Jeremic, D. *USP 6114481*, 2000. (k) Kretschmer, W. P.; Dijkhuis, C.; Meetsma, A.; Hesses, B.; Teuben, J. H. *Chem. Commun.* **2002**, 608. (l) Nomura, K.; Fujii, K. *Organometallics* **2002**, *21*, 3042. (m) Huang, J.; Lian, B.; Qian, Y.; Zhou, W.; Chen, W.; Zheng, G. *Macromolecules* **2002**, *35*, 4871. (n) Nomura, K.; Fujii, K. *Macromolecules* **2003**, *36*, 2633. (o) Mahanthappa, M. K.; Cole, A. P.; Waymouth, R. M. *Organometallics* **2004**, *23*, 836. (p) Tamm, M.; Randoll, S.; Bannenberg, T.; Herdtweck, E. *Chem. Commun.* **2004**, 876. (q) Ishino, H.; Takemoto, S.; Hirata, K.; Kanaizuka, Y.; Hidai, M.; Nabika, M.; Seki, Y.; Miyatake, T.; Suzuki, N. *Organometallics* **2004**, *23*, 454. (r) Yasumoto, T.; Yamagata, T.; Mashima, K. *Organometallics* **2005**, *24*, 3375. (s) Tamm, M.; Randoll, S.; Herdtweck, E.; Kleigrew, N.; Kehr, G.; Erker, G.; Rieger, B. *Dalton Trans.* **2006**, 459. (t) Zhang, H.; Katao, S.; Nomura, K.; Huang, J. *Organometallics* **2007**, *26*, 5967.

(9) (a) Nomura, K.; Naga, N.; Miki, M.; Yanagi, K.; Imai, A. *Organometallics* **1998**, *17*, 2152. (b) Nomura, K.; Naga, N.; Miki, M.; Yanagi, K. *Macromolecules* **1998**, *31*, 7588.

(10) (a) Nomura, K.; Oya, K.; Komatsu, T.; Imanishi, Y. *Macromolecules* **2000**, *33*, 3187. (b) Nomura, K.; Oya, K.; Imanishi, Y. *J. Mol. Catal. A* **2001**, *174*, 127.

(11) Nomura, K.; Itagaki, K. *Macromolecules* **2005**, *38*, 8121.

(12) (a) Nomura, K.; Itagaki, K.; Fujiki, M. *Macromolecules* **2005**, *38*, 2053. (b) Itagaki, K.; Fujiki, M.; Nomura, K. *Macromolecules* **2007**, *40*, 6489.

(13) (a) Nomura, K.; Komatsu, T.; Imanishi, Y. *Macromolecules* **2000**, *33*, 8122. (b) Nomura, K.; Okumura, H.; Komatsu, T.; Naga, N. *Macromolecules* **2002**, *35*, 5388.

(14) (a) Zhang, H.; Nomura, K. *J. Am. Chem. Soc.* **2005**, *127*, 9364. (b) Zhang, H.; Nomura, K. *Macromolecules* **2006**, *39*, 5266.

(15) (a) Nomura, K.; Tsubota, M.; Fujiki, M. *Macromolecules* **2003**, *36*, 3797. (b) Wang, W.; Tanaka, T.; Tsubota, M.; Fujiki, M.; Yamanaka, S.; Nomura, K. *Adv. Synth. Catal.* **2005**, *347*, 433. (c) Nomura, K.; Wang, W.; Fujiki, M.; Liu, J. *Chem. Commun.* **2006**, 2659.

(16) Liu, J.; Nomura, K. *Adv. Synth. Catal.* **2007**, *349*, 2235.

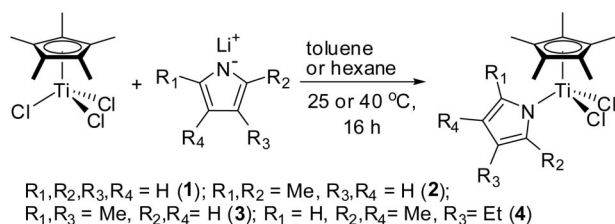
(17) Wang, W.; Fujiki, M.; Nomura, K. *J. Am. Chem. Soc.* **2005**, *127*, 4582.

(18) (a) Nomura, K.; Liu, J.; Fujiki, M.; Takemoto, A. *J. Am. Chem. Soc.* **2007**, *129*, 14170. (b) Nomura, K.; Kitiyanan, B. *Curr. Org. Synth.* **2008**, *5*, 217.

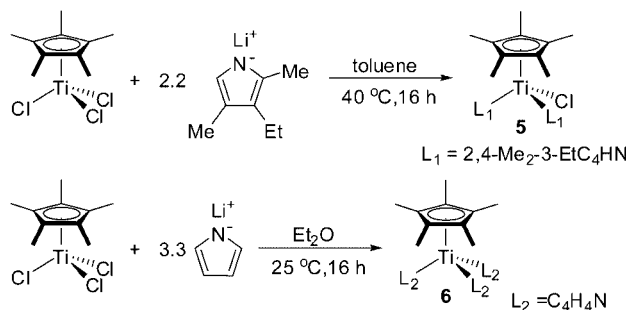
(19) Liu, J.; Nomura, K. *Macromolecules* **2008**, *41*, 1070.

(20) Examples for synthesis of titanium and zirconium complexes containing pyrrolyl or carbazolyl ligands: (a) Bynum, R. V.; Hunter, V. W. E.; Rogers, R. D.; Atwood, J. L. *Inorg. Chem.* **1980**, *19*, 2368. (b) Dias, A. R.; Galvão, A. M.; Galvão, A. C.; Salema, M. S. *J. Chem. Soc., Dalton Trans.* **1997**, 1055. (c) Riley, P. N.; Fanwick, P. E.; Rothwell, I. P. *J. Chem. Soc., Dalton Trans.* **2001**, 181. (d) Tanski, J. M.; Parkin, G. *Organometallics* **2002**, *21*, 587. (e) Novak, A.; Blake, A. J.; Wilson, C.; Love, J. B. *Chem. Commun.* **2002**, 2796. (f) Nygren, C. L.; Bragg, M. E. T.; Turner, J. F. C. *Acta Crystallogr.* **2004**, *C60*, m4. (g) Spannenberg, A.; Burlakov, V. V.; Arndt, P.; Klahn, M.; Rosenthal, U. *Z. Kristallogr. NCS* **2007**, *222*, 192.

Scheme 1



Scheme 2



$\text{Me}_2\text{C}_4\text{H}_2\text{N}$ (**2**), 2,4- $\text{Me}_2\text{C}_4\text{H}_2\text{N}$ (**3**), 2,4- $\text{Me}_2\text{-3-EtC}_4\text{HN}$ (**4**) is depicted in Scheme 1. $\text{Cp}^*\text{TiCl}_2[\text{C}_4\text{H}_4\text{N}]$ (**1**) could be prepared in 36% yield by treatment of Cp^*TiCl_3 with 1.5 equiv of LiNC_4H_4 , prepared by treating pyrrole with $n\text{BuLi}$ (1 equiv), in toluene at 40 °C, and **1** was isolated as deep brown microcrystals from the chilled hexane solution (−20 °C). The same reaction at room temperature gave a lower yield of **1**, and the yield was also low if the same reaction was conducted at high temperatures (50–95 °C). The observed trend is similar to the observed facts in the synthesis of $\text{Cp}^*\text{TiCl}_2[\text{N}(\text{Me})(\text{cyclohexyl})]$,^{8m} and optimization of the reaction conditions (temperature, equiv of lithium salts, etc.) was thus necessary probably due to gradual decomposition of the lithium salt in the reaction solution. A mixture of **1** and unidentified product was obtained when the reaction was conducted in Et_2O at room temperature (25 °C), and an attempt at isolation of **1** from the mixture was not successful. Use of the potassium salt (prepared by the reaction of pyrrole derivative with $\text{KN}(\text{SiMe}_3)_2$ in a hexane/toluene mixture)²⁸ instead of $\text{LiC}_4\text{H}_4\text{N}$ did not result in any significant improvements in the yields. An attempted synthesis by the reaction of Cp^*TiCl_3 with pyrrole in the presence of NEt_3 was not successful either. Therefore, the conditions described above (with the lithium salt in toluene at 40 °C) seem to be suited for isolation of **1**.

The Cp^* analogues containing dimethylpyrrolides (**2**, **3**) could also be prepared in moderate yields (39% and 29%, respectively) by adopting the same procedure as that for **1**. In contrast, an attempted synthesis of the 2,4- $\text{Me}_2\text{-3-EtC}_4\text{HN}$ analogue (**4**) under the same conditions resulted in the formation of bis(pyrrolide) complex $\text{Cp}^*\text{TiCl}_2(2,4\text{-Me}_2\text{-3-EtC}_4\text{HN})_2$ (**5**, Scheme 2), probably due to the higher nucleophilicity of $\text{Li}(2,4\text{-Me}_2\text{-3-EtC}_4\text{HN})$ than those for the lithium dimethylpyrrolides. The desired monopyrrolide complex (**4**) could be synthesized by adopting mild conditions; the reaction of Cp^*TiCl_3 with 1.1 equiv of $\text{Li}(2,4\text{-Me}_2\text{-3-EtC}_4\text{HN})$ in hexane at room temperature (25 °C) afforded **4** in 44% yield. All three chlorine atoms in Cp^*TiCl_3 could be replaced with pyrrolide ligands when Cp^*TiCl_3 was treated with 3.3 equiv of $\text{LiC}_4\text{H}_4\text{N}$ in Et_2O at room temperature; $\text{CpTi}(\text{C}_4\text{H}_4\text{N})_3$ (**6**) could be thus obtained in 76% yield (Scheme 2).

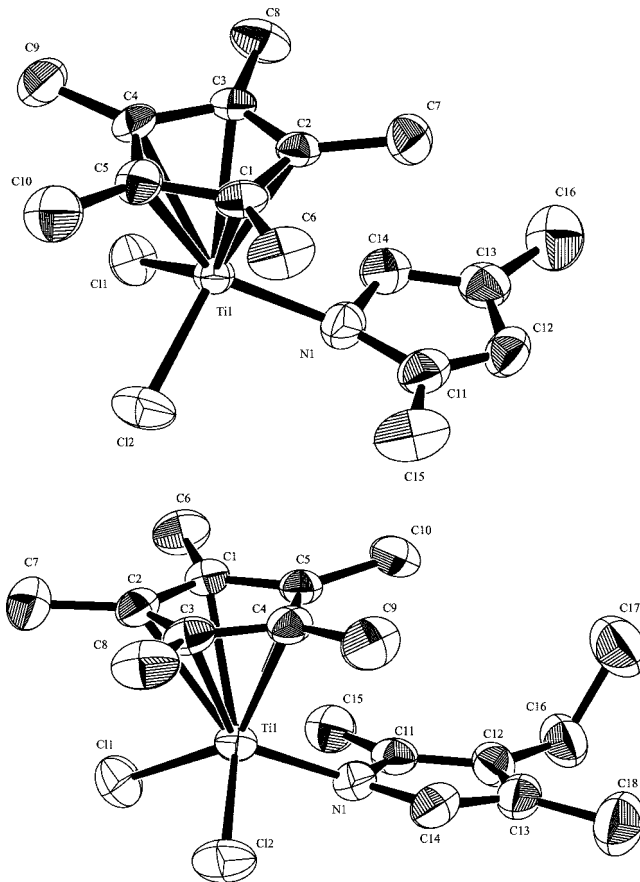


Figure 1. ORTEP drawings of $\text{Cp}^*\text{TiCl}_2(2,4\text{-Me}_2\text{C}_4\text{H}_2\text{N})$ (**3**, top) and $\text{Cp}^*\text{TiCl}_2(2,4\text{-Me}_2\text{-3-EtC}_4\text{HN})$ (**4**, bottom). Thermal ellipsoids are drawn at the 50% probability level, and H atoms are omitted for clarity.

All the complexes (**1**–**6**) were identified on the basis of ^1H and ^{13}C NMR spectra and elemental analysis, and the structures of **3**–**6** were determined by X-ray crystallography, as described below. Resonances ascribed to protons in pyrrole were observed at 6.17 and 6.84 ppm in the ^1H NMR spectrum of **1**, and the resonance is rather close to those in free pyrrole (6.26 and 6.76 ppm). The results would thus suggest that the pyrrolide ligand in **1** forms a Ti–N σ bond in η^1 fashion. The ^1H NMR spectra of the other Cp^* analogues (**2**–**4**) also showed similar resonances, suggesting that the N atom in these complexes (**2**–**4**) also binds to titanium similarly, as also seen by their crystal structures (for **3**, **4**, Figure 1).

Structures of $\text{Cp}^*\text{TiCl}_2(2,4\text{-Me}_2\text{C}_4\text{H}_2\text{N})$ (**3**) and $\text{Cp}^*\text{TiCl}_2(2,4\text{-Me}_2\text{-3-EtC}_4\text{HN})$ (**4**) were determined by X-ray crystallography (Figure 1), and selected bond lengths and the angles are summarized in Table 1. These complexes have a distorted tetrahedral geometry around the titanium metal center, and the Ti–N bond distances [1.969(4) and 1.965(2) Å for **3** and **4**, respectively] are close to that in the Cp-carbazole analogue $\text{CpTi}(\eta^1\text{-C}_{12}\text{H}_8\text{N})\text{Cl}_2$ [1.969(3) Å]^{20c} but shorter than those in $\text{Cp}_2\text{Ti}(\eta^1\text{-C}_4\text{H}_4\text{N})_2$ [2.070(5), 2.100(4) Å],^{20a} $\text{Cp}^*_2\text{Ti}(\eta^1\text{-C}_4\text{H}_4\text{N})$ [2.096(4) Å],^{20g} and Ti complexes containing bis(pyrrolide-imine) chelate ligands [2.033(2)–2.049(3) Å].^{23c} In contrast, the Ti–N bond distances are apparently longer than those in $(1,3\text{-Me}_2\text{C}_5\text{H}_3)\text{TiCl}_2[\text{N}(2,6\text{-Me}_2\text{C}_6\text{H}_3)(\text{SiMe}_3)]$ [1.898(2) Å],^{8k} $\text{Cp}^*\text{TiCl}_2[\text{N}(\text{Me})(\text{cyclohexyl})]$ [1.870(3) Å],^{8m} and $\text{Cp}^*\text{TiCl}_2(\text{N} = \text{CPh}_2)$ [1.827(2) Å],²⁹ but the distance is shorter than the estimated value (2.02 Å) for a titanium–nitrogen single bond according to Pauling's covalent radii.³⁰ These results thus

(28) Heldt, I.; Behrens, U. *Z. Anorg. Allg. Chem.* **2005**, *631*, 749.

Table 1. Selected Bond Distances and angles for $\text{Cp}^*\text{TiCl}_2(2,4\text{-Me}_2\text{C}_4\text{H}_2\text{N})$ (**3**) and $\text{Cp}^*\text{TiCl}_2(2,4\text{-Me}_2\text{-3-EtC}_4\text{HN})$ (**4**)^a

	3	4
Bond Distances (Å)		
Ti(1)–Cl(1)	2.2639(19)	2.2548(12)
Ti(1)–Cl(2)	2.2458(19)	2.2578(11)
Ti(1)–N(1)	1.969(4)	1.965(2)
Ti(1)–C(1)	2.346(6)	2.346(3)
Ti(1)–C(2)	2.337(5)	2.394(4)
Ti(1)–C(3)	2.345(5)	2.404(3)
Ti(1)–Cp	2.032	2.034
Bond Angles (deg)		
Cl(1)–Ti(1)–Cl(2)	103.63(7)	103.57(4)
Cl(1)–Ti(1)–N(1)	101.32(12)	102.06(9)
Cl(2)–Ti(1)–N(1)	102.81(17)	101.81(9)
Cp–Ti(1)–Cl(1)	113.72(9)	114.17(6)
Cp–Ti(1)–Cl(2)	114.47(9)	113.87(6)
Cp–Ti(1)–N(1)	118.89(16)	119.32(10)

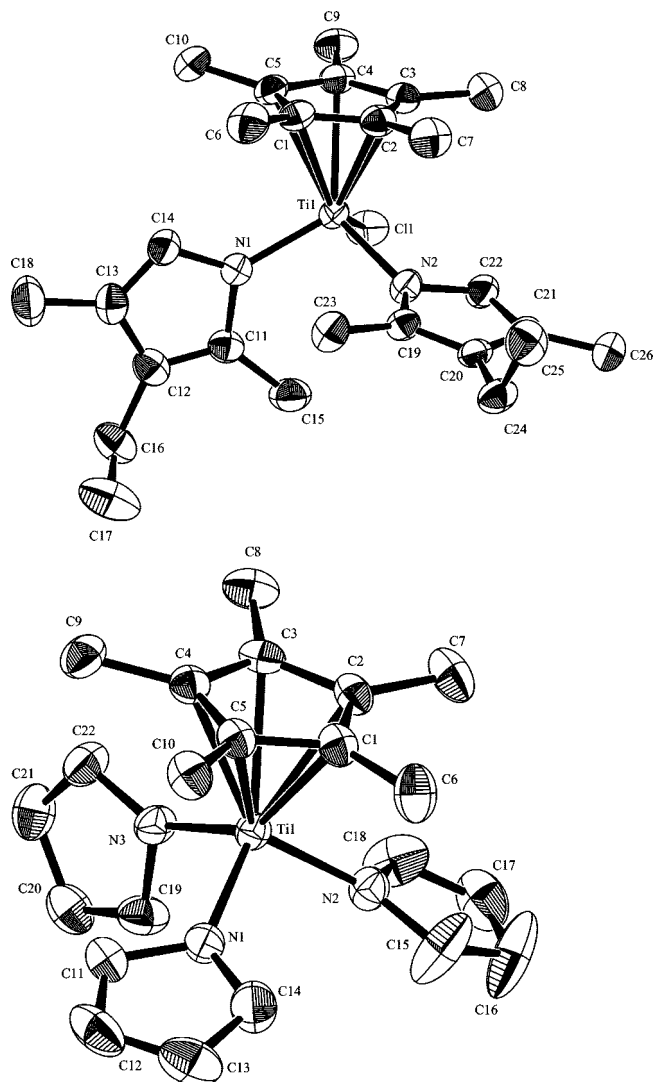
^a Detailed analysis results are shown in the Supporting Information.**Table 2.** Selected Bond Distances and Angles for $\text{Cp}^*\text{TiCl}(2,4\text{-Me}_2\text{-3-EtC}_4\text{HN})_2$ (**5**) and $\text{Cp}^*\text{Ti}(\text{C}_4\text{H}_4\text{N})_3$ (**6**)^a

$\text{Cp}^*\text{TiCl}(2,4\text{-Me}_2\text{-3-EtC}_4\text{HN})_2$ (5)			
Bond Distances (Å)			
Ti(1)–Cl(1)	2.2679(8)	Ti(1)–C(2)	2.356(2)
Ti(1)–N(1)	1.9601(17)	Ti(1)–C(3)	2.3572(18)
Ti(1)–N(2)	1.9790(14)	Ti(1)–Cp	2.064
Ti(1)–C(1)	2.410(2)		
Bond Angles (deg)			
Cl(1)–Ti(1)–N(1)	104.65(6)	Cp–Ti(1)–Cl(1)	112.97(3)
Cl(1)–Ti(1)–N(2)	100.76(6)	Cp–Ti(1)–N(1)	117.87(5)
N(1)–Ti(1)–N(2)	101.11(6)	Cp–Ti(1)–N(2)	117.24(5)
$\text{Cp}^*\text{Ti}(\text{C}_4\text{H}_4\text{N})_3$ (6)			
Bond Distances (Å)			
Ti(1)–N(1)	1.990(2)	Ti(1)–C(2)	2.364(3)
Ti(1)–N(2)	2.000(2)	Ti(1)–C(3)	2.387(3)
Ti(1)–N(3)	1.964(2)	Ti(1)–Cp	2.042
Ti(1)–C(1)	2.352(3)		
Bond Angles (deg)			
N(1)–Ti(1)–N(2)	102.64(11)	Cp–Ti(1)–N(1)	115.49(9)
N(1)–Ti(1)–N(3)	101.96(11)	Cp–Ti(1)–N(2)	116.66(9)
N(2)–Ti(1)–N(3)	102.18(11)	Cp–Ti(1)–N(3)	115.76(10)

^a Detailed analysis results are shown in the Supporting Information.

suggest that both the titanium and nitrogen form a σ bond in addition to π donation from the nitrogen, although the π donation from nitrogen to Ti may be weak compared to the complexes exemplified above (such as anilide,^{8k} amide,^{8m} and ketimide²⁹). The pyrrolide rings are oriented almost parallel to the Cp* ring in both complexes, as indicated by small dihedral angles of 8.3° (**3**) and 7.7° (**4**).

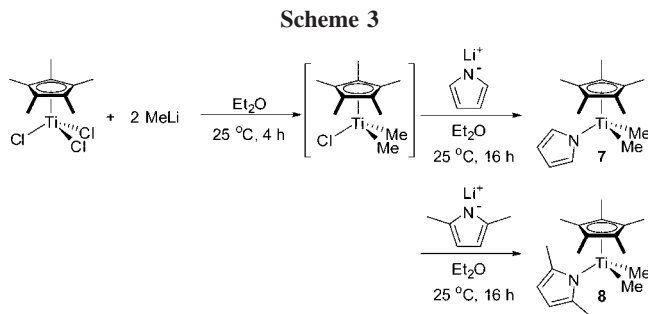
The structures of $\text{Cp}^*\text{TiCl}(2,4\text{-Me}_2\text{-3-EtC}_4\text{HN})_2$ (**5**) and $\text{Cp}^*\text{Ti}(\text{C}_4\text{H}_4\text{N})_3$ (**6**) are shown in Figure 2, and selected bond distances and angles are summarized in Table 2. These complexes have a distorted tetrahedral geometry around Ti, and all nitrogen atoms in the pyrrolide ligands bind to Ti through σ donation in addition to π donation from the nitrogen, which is supported by the Ti–N bond lengths [**5**, 1.960(17) and 1.979(14); **6**, 1.990(2), 2.000(2), and 1.964(2) Å], although, as described above, the π donation from N seems rather weak. In the case of the bis(pyrrolide) complex (**5**), one of the pyrrolide ligand has a perpendicular orientation to the Cp* ring (dihedral angle = 87.8°) and the ethyl and one methyl group positioned

**Figure 2.** ORTEP drawings of $\text{Cp}^*\text{TiCl}(2,4\text{-Me}_2\text{-3-EtC}_4\text{HN})_2$ (**5**, top) and $\text{Cp}^*\text{Ti}(\text{C}_4\text{H}_4\text{N})_3$ (**6**, bottom). Thermal ellipsoids are drawn at the 50% probability level, and H atoms are omitted for clarity.

away from the Cp* ring, whereas the other pyrrolide ligand is located parallel to the Cp* ring (dihedral angle = 13.9°). Similarly, one of the pyrrolide rings in the tris(pyrrolide) analogue (**6**) is perpendicular (dihedral angle = 89.5°) to that of the Cp*, whereas the remaining two pyrrolide ligands are inclined at dihedral angles of 16.9° and 19.5°. The Ti–N bond distances for two pyrrolide ligands in **5** were slightly different; the pyrrolide ligand positioned parallel to the Cp* possessed a longer Ti–N bond length [1.9790(14) Å] than that in the pyrrolide ligand perpendicular to the Cp* ring [1.9601(17) Å]. This tendency would be pronounced in the case of tris(pyrrolide) complex **6**, and the bond distance in the pyrrolide rings bearing a parallel spatial orientation relative to the Cp* ring was longer [1.990(2) and 2.000(2) Å] than that in the pyrrolide ring perpendicular to the Cp* ring [1.964(2) Å].

2. Synthesis and Structural Analysis of $\text{Cp}^*\text{TiMe}_2(\text{C}_4\text{H}_4\text{N})$ and $\text{Cp}^*\text{TiMe}_2(2,5\text{-Me}_2\text{C}_4\text{H}_2\text{N})$. Although an attempt to isolate the dimethyl complex $\text{Cp}^*\text{TiMe}_2[\text{C}_4\text{H}_4\text{N}]$ (**7**), by treating Cp^*TiMe_3 with pyrrole (in Et_2O at 25 °C), which was the procedure for preparation of half-hafnocene dimethyl complexes containing pyrrolide-imine chelate ligand,^{23g} was not successful, complex **7** could be successfully prepared in 66% yield by adopting an alternative route that involves *in situ*

(29) Nomura, K.; Yamada, J.; Wang, W.; Liu, J. *J. Organomet. Chem.* **2007**, *692*, 4675.(30) Pauling, L. *The Nature of the Chemical Bond*, 3rd ed.; Cornell University Press: Ithaca, NY, 1960.



generation of $\text{Cp}^*\text{Ti}(\text{Cl})\text{Me}_2$, prepared by the reaction of Cp^*TiCl_3 with 2.0 equiv of MeLi in Et_2O and subsequent treatment with $\text{Li}(\text{C}_4\text{H}_4\text{N})$ (Scheme 3). The 2,5-dimethylpyrrolide analogue, $\text{Cp}^*\text{TiMe}_2(2,5\text{-Me}_2\text{C}_4\text{H}_2\text{N})$ (**8**), was also prepared according to the same procedure in 67% yield. These complexes were identified on the basis of ^1H and ^{13}C NMR spectra and elemental analyses, and their structures were determined by X-ray crystallography (Figure 3).

Complex **8** showed four magnetically nonequivalent protons in the ^1H NMR spectrum (in C_6D_6) at room temperature; specifically two sets of signals due to each proton (e.g., the resonance ascribed to Ti-Me was observed as two singlets at 0.69 and 1.39 ppm) were observed. No significant changes in the spectra were seen at various temperatures (-50 to 50 $^\circ\text{C}$), and two singlets corresponding to each type of proton displayed different integration values. The results may be explained by assuming the existence of **8** as two species [η^1 and η^5 mode of coordination of the ligand, or orientation of the pyrrolide ring (parallel or perpendicular)], but we have no firm evidence to explain the observed facts. The former assumption may be more appropriate as the speculation, because the pyrrolide ligand in the Cp-dichloro analogue $\text{Cp}^*\text{TiCl}_2(2,5\text{-Me}_2\text{C}_4\text{H}_2\text{N})$ coordinates to Ti in an η^5 mode, confirmed by X-ray crystallography.

Single crystals of **7** were grown from a chilled, concentrated Et_2O solution in a freezer (-20 $^\circ\text{C}$), and the structure could be thus determined by X-ray crystallography (Figure 3). Selected bond distances and the angles are summarized in Table 3. The complex also has a distorted tetrahedral geometry around titanium, and the Ti-N bond distance [2.002(15) \AA] is somewhat longer than those in the (mono, di) chloro complexes **3–5** (1.96–1.98 \AA). The Ti-C bond lengths in Ti-Me are 2.091(2) and 2.094(2) \AA , which are comparable with those in $\text{Cp}^*\text{TiMe}_2(\text{O}-2,6\text{-}^i\text{Pr}_2\text{C}_6\text{H}_3)$ [2.101(3) \AA]³¹ and those in the related complexes. The dihedral angle between the cyclopentadienyl ring and pyrrolide ring (20.6 $^\circ$) is close to those in **5** and **6** (13.9–19.5 $^\circ$). Complex **8** also has a distorted tetrahedral geometry around titanium, and the 2,5-dimethylpyrrolide ligand exhibits an η^1 mode of coordination. The Ti-N bond distance [2.009(5) \AA] is comparable to that in the pyrrolide complex **7** [2.002(15) \AA], while it is somewhat longer than those in the (mono, di) chloro complexes **3–5** (1.96–1.98 \AA). The Ti-C bond lengths in Ti-Me are 2.115(7) and 2.184(7) \AA , which are comparable with those in $\text{Cp}^*\text{TiMe}_2(\text{O}-2,6\text{-}^i\text{Pr}_2\text{C}_6\text{H}_3)$ [2.101(3) \AA]³¹ and those in the related complexes. The Cp-Ti distance [2.053 \AA] is slightly longer than that in complex **7** [2.037 \AA]. The C(11)-Ti(1)-C(12) bond angle [87.2(3) $^\circ$] was significantly smaller than in the pyrrolide counterpart **7** [102.10(8) $^\circ$] and dichloro complexes **3** and **4** [103.63(7) $^\circ$ and 103.57(4) $^\circ$, respectively].

3. Synthesis and Structural Analysis of $\text{Cp}^*\text{TiCl}_2(\text{L})$ [L = $\text{C}_4\text{H}_4\text{N}$, 2,5-Me₂C₄H₂N, 2,4-Me₂C₄H₂N, 2,4-Me₂-3-EtC₄H₂N]. The Cp-dichloro analogues $\text{Cp}^*\text{TiCl}_2(\text{C}_4\text{H}_4\text{N})$ (**9**), 2,5-Me₂C₄H₂N (**10**), 2,4-Me₂C₄H₂N (**11**), and 2,4-Me₂-3-EtC₄H₂N (**12**) could

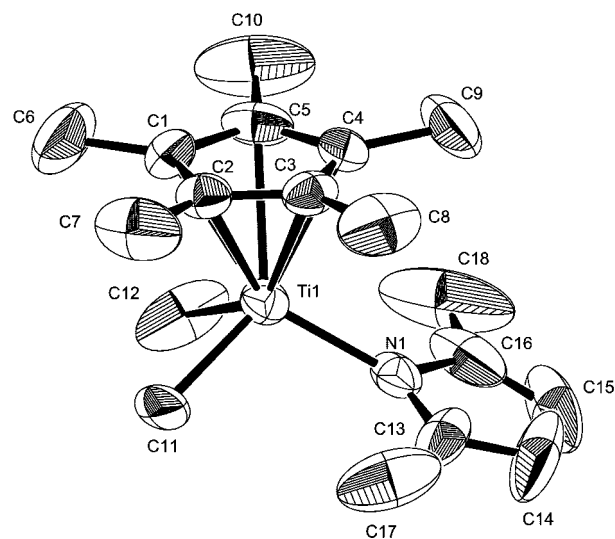
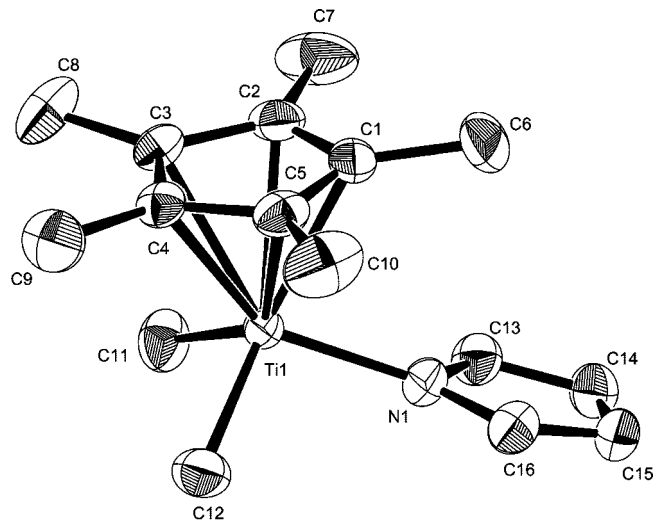


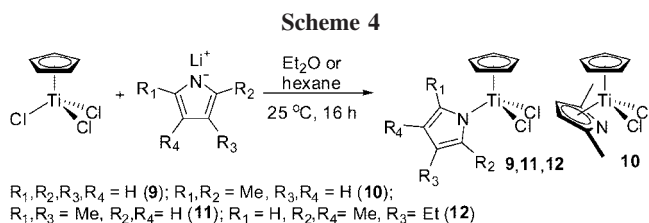
Figure 3. ORTEP drawings of $\text{Cp}^*\text{TiMe}_2(\text{C}_4\text{H}_4\text{N})$ (**7**, top) and $\text{Cp}^*\text{TiMe}_2(2,5\text{-Me}_2\text{C}_4\text{H}_2\text{N})$ (**8**, bottom). Thermal ellipsoids are drawn at the 50% probability level, and H atoms are omitted for clarity.

Table 3. Selected Bond Distances and Angles for $\text{Cp}^*\text{TiMe}_2(\text{C}_4\text{H}_4\text{N})$ (**7**) and $\text{Cp}^*\text{TiMe}_2(2,5\text{-Me}_2\text{C}_4\text{H}_2\text{N})$ (**8**)^a

	7	8
Bond Distances (\AA)		
Ti(1)-N(1)	2.002(15)	2.009(5)
Ti(1)-C(11)	2.091(2)	2.115(7)
Ti(1)-C(12)	2.184(2)	2.184(7)
Ti(1)-C(1)	2.351(19)	2.399(6)
Ti(1)-C(2)	2.353(18)	2.383(6)
Ti(1)-C(3)	2.381(17)	2.359(5)
Ti(1)-Cp	2.037	2.053
Bond Angles (deg)		
C(11)-Ti(1)-C(12)	102.10(8)	87.2(3)
N(1)-Ti(1)-C(11)	103.20(7)	105.7(2)
N(1)-Ti(1)-C(12)	102.47(7)	108.2(2)
Cp-Ti(1)-N(1)	113.42(6)	121.45(16)
Cp-Ti(1)-C(11)	114.40(6)	113.7(2)
Cp-Ti(1)-C(12)	119.16(5)	115.0(2)

^a Detailed analysis results are shown in the Supporting Information.

be prepared by treating Cp^*TiCl_3 with 1.1 equiv of the corresponding lithium pyrrolide in Et_2O or *n*-hexane (Scheme 4). The dimethylpyrrolide analogues (**10**, **11**) could also be prepared (yields 63% and 68%, respectively) if the reactions were



conducted in *n*-hexane, and the same reactions in Et₂O resulted in the production of unidentified impurities, which were difficult to separate.

The structures of **9** and **11** determined by X-ray crystallography are shown in Figure 4, and selected bond lengths and the angles are summarized in Table 4. These complexes have a distorted tetrahedral geometry around Ti, and the nitrogen atom in the pyrrolide ligand binds to Ti as seen in the Cp* analogues **1–6**. The Ti–N bond lengths [**9**, 1.968(13); **11**, 1.956(19) Å] are close to those in the Cp* analogues; the same trend was seen in the Ti–Cl bond distances. In contrast, orientation of the pyrrolide ring relative to Cp' is strongly affected by the nature of the cyclopentadienyl fragment; for example, the pyrrolide ring is almost perpendicular to Cp (dihedral angle = 88.3°) in complex **11**, whereas the dihedral angle in Cp* analogue **3** is 8.3°. The corresponding dihedral angle in **9** is

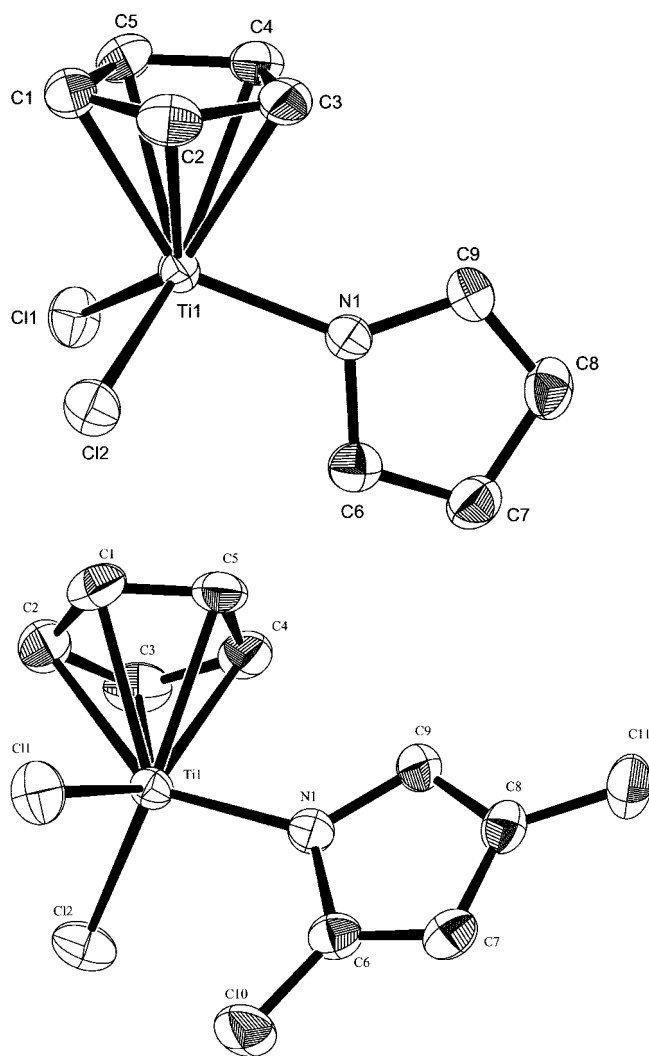


Figure 4. ORTEP drawings of CpTiCl₂(2,4-Me₂C₄H₂N) (**9**, top) and CpTiCl₂(2,4-Me₂C₄H₂N) (**11**, bottom). Thermal ellipsoids are drawn at the 50% probability level, and H atoms are omitted for clarity.

Table 4. Selected Bond Distances and Angles for CpTiCl₂(C₄H₄N) (**9**) and CpTiCl₂(2,4-Me₂C₄H₂N) (**11**)^a

	9	11
Bond Distances (Å)		
Ti(1)–Cl(1)	2.258(7)	2.2444(4)
Ti(1)–Cl(2)	2.252(13)	2.2561(4)
Ti(1)–N(1)	1.956(19)	1.9681(13)
Ti(1)–C(1)	2.346(2)	2.3541(18)
Ti(1)–C(2)	2.306(2)	2.3458(17)
Ti(1)–C(3)	2.334(3)	2.3431(18)
Ti(1)–Cp	2.018	2.021
Bond Angles (deg)		
Cl(1)–Ti(1)–Cl(2)	101.77(3)	102.335(19)
Cl(1)–Ti(1)–N(1)	103.90(6)	104.28(4)
Cl(2)–Ti(1)–N(1)	104.22(10)	106.31(3)
Cp–Ti(1)–Cl(1)	116.52(4)	115.35(3)
Cp–Ti(1)–Cl(2)	116.45(6)	114.37(2)
Cp–Ti(1)–N(1)	112.37(9)	113.04(4)

^a Detailed analysis results are shown in the Supporting Information.

79.3°, and the value is somewhat close to that in **11** rather than those in **3** (8.3°) or **7** (20.6°).

The X-ray structure of complex **10**, containing a 2,5-dimethylpyrrolide ligand, is shown in Figure 5, and selected bond distances and the angles are summarized in Table 5. Note that the pyrrolide ligand in **10** coordinates to Ti in an η⁵ mode. The outcome of this coordination mode is observed in the relative positions of the two five-membered rings, which are located at a dihedral angle of 57.9°. Moreover, the Cl(1)–Ti–Cl(2) bond angle is rather small [94.71(3)°] compared with those of other complexes [101–104°]. The η⁵ mode of this bonding also has a significant effect on the C–C bond lengths of the nitrogen heterocyclic ligand. The C–C bond distances (involving carbon directly bonded with nitrogen) in complex **9** are 1.323(3) and 1.359(4) Å, which are close to a typical C=C bond (1.34 Å), implying that the ring carbons remain intact during complex formation and coordination to Ti mainly occurs through nitrogen, as mentioned above. In contrast, the C–C bond distances (involving carbon adjacent to nitrogen) in complex **10** undergo a significant elongation [1.400(4) and 1.410(4) Å], thus indicating the involvement of ring carbons in coordination to Ti.

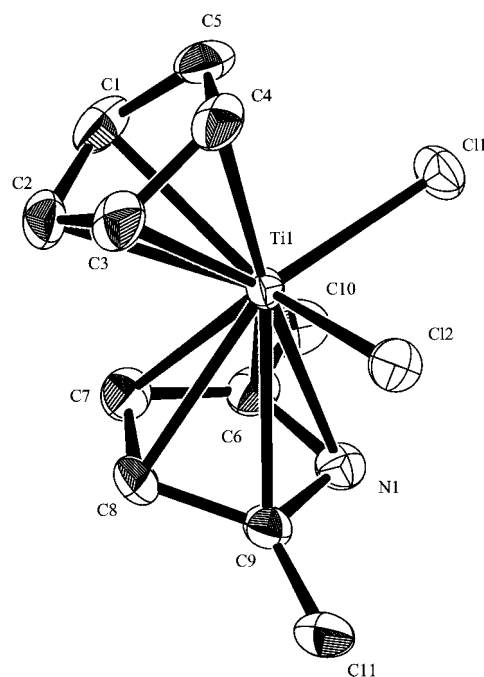


Figure 5. ORTEP drawing of CpTiCl₂(2,5-Me₂C₄H₂N) (**10**). Thermal ellipsoids are drawn at the 50% probability level, and H atoms are omitted for clarity.

Table 5. Selected Bond Distances and angles for CpTiCl₂(2,5-Me₂C₄H₂N) (10)^a

Bond Distances (Å)			
Ti(1)–Cl(1)	2.3495(9)	Ti(1)–N(1)	2.421(2)
Ti(1)–Cl(2)	2.3378(9)	Ti(1)–C(6)	2.396(3)
Ti(1)–C(1)	2.358(3)	Ti(1)–C(7)	2.379(3)
Ti(1)–C(2)	2.391(3)	Ti(1)–Cp	2.064
Ti(1)–C(3)	2.372(3)	Ti(1)–pyrrole	2.087
Bond Angles (deg)			
Cl(1)–Ti(1)–Cl(2)	94.71(3)	Cp–Ti(1)–pyrrole	130.72(5)
Cp–Ti(1)–Cl(1)	107.28(6)	pyrrole–Ti(1)–Cl(1)	105.71(4)
Cp–Ti(1)–Cl(2)	106.39(5)	pyrrole–Ti(1)–Cl(2)	106.24(5)

^a Detailed analysis results are shown in the Supporting Information.

The ¹H and ¹³C NMR spectra also suggest an η⁵-coordination of the 2,5-dimethylpyrrolide ligand, since the ring protons (6.82 ppm) and carbons (127.97 and 147.95 ppm) are considerably different from those of the free ligand (¹H NMR: 5.75 ppm; ¹³C NMR: 105.78 and 126.18 ppm). Moreover, resonances ascribed to protons in the pyrrolide were highly affected by the temperature measured, as shown in Figure 6. The results may be explained by assuming the presence of an equilibrium between η¹ and η⁵ coordination of the pyrrolide ligand (or rotation of the ring) in **10**. As described in the Introduction, pyrrolyl ligands and their derivatives generally show an η⁵ (π fashion) versus η¹ (σ fashion bound only via nitrogen) coordination mode, depending upon the nature of the substituents and/or other factors.^{20–22} Although we do not have a clear reason why the 2,5-dimethylpyrrolide ligand in **10** coordinates to Ti in an η⁵ mode, whereas the pyrrolide ligand in other complexes coordinates to Ti in an η¹ fashion, the results presented here should be important not only for a basic understanding of group 4 transition metal complexes containing pyrrolides but also for designing efficient catalyst precursors for precise olefin polymerization.

4. Polymerization of Ethylene and Styrene by Cp'TiCl₂(L) [Cp' = Cp*, Cp; L = C₄H₄N, 2,5-Me₂C₄H₂N, 2,4-Me₂C₄H₂N, 2,4-Me₂-3-EtC₄H₂N]–MAO Catalyst Systems. Ethylene polymerizations using the Cp*-pyrrolide complexes (**1–4**, **7**, and **8**) and the Cp-pyrrolide analogues

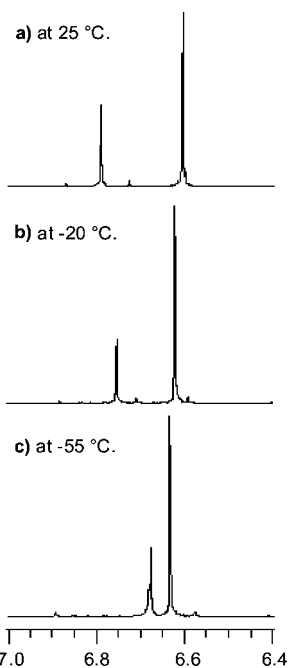
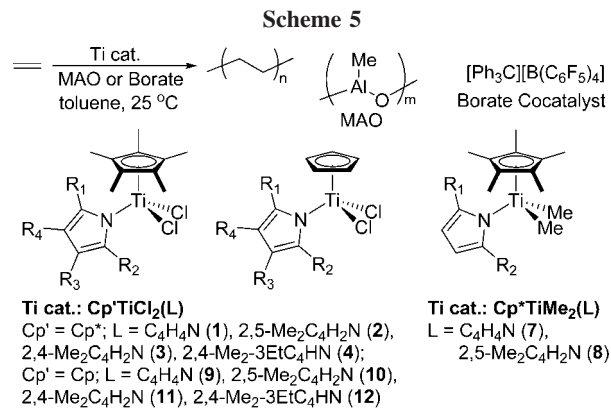


Figure 6. ¹H NMR spectra (in CDCl₃, extended at 6.4–7.0 ppm) of CpTiCl₂(2,5-Me₂C₄H₂N) (**10**) at various temperature [at (a) 25 °C, (b) –20 °C, (c) –55 °C].



(**9–12**) were conducted at 25 °C in toluene in the presence of methylaluminoxane (MAO). The polymerizations using the dimethyl analogues (**7**, **8**) were also conducted in the presence of [Ph₃C][B(C₆F₅)₄]. The results are summarized in Table 6. MAO white solids prepared by removing AlMe₃ and toluene from the commercially available samples (PMAO-S, 6.8 wt % in toluene, Tosoh Finechem Co.) were chosen, because they were effective in the preparation of high molecular weight ethylene/α-olefin copolymers with unimodal molecular weight distributions when Cp*TiCl₂(O-2,6-*i*-Pr₂C₆H₃) was used as the catalyst precursor.^{9b}

It turned out that the Ti dichloro complexes (**1–4**, **9–12**) exhibited moderate catalytic activities for ethylene polymerization in the presence of MAO, and the activities were affected by the substituent on the pyrrolide ligand. The catalytic activities of Cp*TiCl₂(L) increased in the order L = C₄H₄N (**1**, 5400–5940 kg PE/mol Ti · h) > 2,4-Me₂-3-EtC₄H₂N (**4**, 1860, 1950), 2,4-Me₂C₄H₂N (**3**, 1740) > 2,5-Me₂C₄H₂N (**2**, 1500). Complex **1** exhibited the highest activity among the Cp* analogues, and an increase in the steric bulk led to a decrease in the activity. In contrast, the activity of the Cp analogues increased upon increasing the steric bulk in the pyrrolide ligand, since the activity of CpTiCl₂(L) increased in the order 2,4-Me₂-3-EtC₄H₂N (**12**, 1410 kg PE/mol Ti · h) > 2,4-Me₂C₄H₂N (**11**, 930) > 2,5-Me₂C₄H₂N (**10**, 750) > C₄H₄N (**9**, 330). The latter trend by the Cp analogues seems similar to that of Cp'TiCl₂(O-2,6-*i*-Pr₂C₆H₃)^{6,9} as well as that of ordinary metallocenes,²⁹ in which introduction of electron-donating substituents would stabilize the catalytically active species, leading to higher activity.

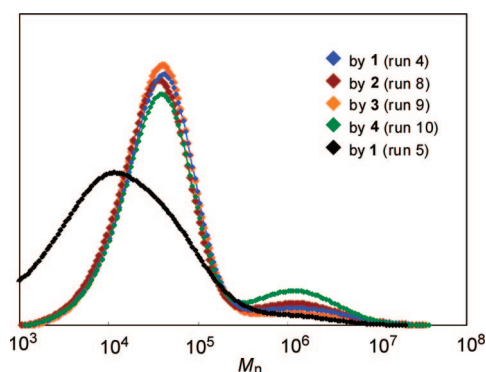
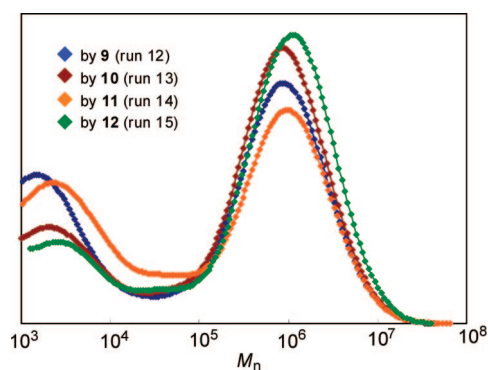
GPC traces for the resultant polyethylenes prepared by the Cp* analogues and by the Cp analogues are shown in Figures 7 and 8. The resultant polymers prepared by the Cp* analogues possessed rather low molecular weights ($M_n = (2.07–2.28) \times 10^4$) and contained a small amount of high molecular weight polymers (Figure 7), and the ratio of the high molecular weight polymer increased in that prepared by **4**. The molecular weight of the resultant polyethylene was more affected by the Al/Ti molar ratio, because the distribution became broad if the amount of MAO charged increased (run 5). The trend observed here seems somewhat similar to that observed in the ethylene polymerization using substituted zirconocenes,³² in which an increase in the steric bulk of Cp*(Cp')ZrCl₂ led to a decrease in both the activity and the molecular weight in the resultant polymers due to the steric crowding. In contrast, the Cp analogues afforded high molecular weight polyethylene with rather broad distributions ($M_n = (2.79–4.42) \times 10^5$, $M_w/M_n =$

(32) Influence of cyclopentadienyl fragment in ethylene polymerization by substituted zirconocenes: Möhring, P. C.; Coville, N. J. *J. Organomet. Chem.* **1991**, 479, 1.

Table 6. Ethylene Polymerization by Cp*TiCl₂(L) [Cp* = Cp*; L = C₄H₄N (1), 2,5-Me₂C₄H₂N (2), 2,4-Me₂C₄H₂N (3), 2,4-Me₂-3-EtC₄H₂N (4): Cp* = Cp; L = C₄H₄N (9), 2,5-Me₂C₄H₂N (10), 2,4-Me₂C₄H₂N (11), 2,4-Me₂-3-EtC₄H₂N (12)]-MAO and Cp*TiMe₂(L) [L = C₄H₄N (7), 2,5-Me₂C₄H₂N (8)]-[Ph₃C][B(C₆F₅)₄] Catalyst Systems^a

run	catalyst Cp*; L	amount (μmol)	MAO (mmol)	polymer yield (mg)	activity ^b	M _n ^c × 10 ⁻³	M _w /M _n ^c
1	Cp*; C ₄ H ₄ N (1)	0.2	1.0	54	1620		
2	Cp*; C ₄ H ₄ N (1)	0.2	2.0	93	2790		
3	Cp*; C ₄ H ₄ N (1)	0.2	3.0	183	5490		
4	Cp*; C ₄ H ₄ N (1)	0.2	3.0	185	5550	22.7 ^d	2.4
5	Cp*; C ₄ H ₄ N (1)	0.2	4.0	198	5940	6.77	8.0
6	Cp*; C ₄ H ₄ N (1)	0.1	3.0	90	5400		
7	Cp*; C ₄ H ₄ N (1)	0.1	3.0	93	5580		
8	Cp*; 2,5-Me ₂ C ₄ H ₂ N (2)	0.2	3.0	50	1500	20.7	2.4
9	Cp*; 2,4-Me ₂ C ₄ H ₂ N (3)	0.2	3.0	58	1740	22.8 ^d	2.3
10	Cp*; 2,4-Me ₂ -3-EtC ₄ H ₂ N (4)	0.2	3.0	65	1950	940	2.1
						21.8	2.3
11	Cp*; 2,4-Me ₂ -3-EtC ₄ H ₂ N (4)	0.2	3.0	62	1860		
12	Cp*TiMe ₂ (C ₄ H ₄ N) (7)	0.2	— ^e	323	9690		
13	Cp*TiMe ₂ (C ₄ H ₄ N) (7)	0.2	— ^e	334	10020	112	2.5
14	Cp*TiMe ₂ (C ₄ H ₄ N) (7)	0.2	3.0	199	5970	17.3 ^f	2.2
15	Cp*TiMe ₂ (C ₄ H ₄ N) (7)	0.2	3.0	196	5880		
16	Cp*TiMe ₂ (2,5-Me ₂ C ₄ H ₂ N) (8)	0.2	— ^e	270	8100	160	2.8
17	Cp*TiMe ₂ (2,5-Me ₂ C ₄ H ₂ N) (8)	0.2	— ^e	263	7890	146	3.0
18	Cp*TiMe ₂ (2,5-Me ₂ C ₄ H ₂ N) (8)	0.2	3.0	154	4620	12.6 ^f	2.9
19	Cp*TiMe ₂ (2,5-Me ₂ C ₄ H ₂ N) (8)	0.2	3.0	149	4470		
20	Cp; C ₄ H ₄ N (9)	0.2	3.0	11	330	336	4.3
						2.18	2.2
21	Cp; 2,5-Me ₂ C ₄ H ₂ N (10)	0.2	3.0	25	750	312	4.5
						2.61	2.1
22	Cp; 2,4-Me ₂ C ₄ H ₂ N (11)	0.2	3.0	31	930	442	3.5
						2.91	3.6
23	Cp; 2,4-Me ₂ -3-EtC ₄ H ₂ N (12)	0.2	3.0	47	1410	279	5.8
						3.17	1.7

^a Reaction conditions: toluene total 30 mL, ethylene 6 atm, 10 min, 25 °C, 100 mL scale autoclave, d-MAO (prepared by removing AlMe₃ and toluene from commercially available MAO). ^b Activity = kg PE/mol Ti · h. ^c GPC data in *o*-dichlorobenzene vs polystyrene standards. ^d Trace amount of high molecular weight polymer was also obtained in the GPC trace. ^e Conditions: [tBuAl]/[Ti] = 250, [[Ph₃C][B(C₆F₅)₄]]/[Ti] = 3.0. ^f Peak ascribed to high molecular weight was also seen in tiny trace amount.

**Figure 7.** GPC traces of polyethylene prepared by MAO catalyst systems. Detailed conditions and results are shown in Table 6.**Figure 8.** GPC traces of polyethylene prepared by MAO catalyst systems. Detailed conditions and results are shown in Table 6.

3.49–5.83) containing a certain amount of low molecular weight polymers (Figure 8), and a decrease in the steric bulk in the pyrrolide ligand led to an increase in the ratio of oligomers (runs 20, 21, by **9** and **10**) along with a decrease in the catalytic activity.

The results shown here are promising, because the activities observed here (especially of the dichloro Cp* analogues) were higher than those observed with Cp*TiCl₂[N(2,6-Me₂C₆H₃)(SiMe₃)] (902 kg PE/mol Ti · h using 2.0 μmol of catalyst for 30 min).^{8k} Complex **1** exhibited the highest activity (5550 kg PE/mol Ti · h; run 4) among the present dichloro complexes, and this catalyst performance surpassed the activity of the complexes containing substituted amides as anionic ancillary ligands, Cp*TiCl₂[N(Me)(R)] [R = Me, Et, cyclohexyl] (180–4540 kg PE/mol Ti · h using 0.5–2.0 μmol of the catalyst).^{8m}

Ethylene polymerizations using the dimethyl complexes (**7** and **8**) were also carried out in the presence of MAO and [Ph₃C][B(C₆F₅)₄] as cocatalysts. The pyrrolide-containing complex **7** in conjunction with MAO cocatalyst exhibited comparable catalytic activity (5970 kg PE/mol Ti · h) to its dichloro counterpart **1** (5550 kg PE/mol Ti · h), and the M_n value in the resultant polymer was close to that prepared by **1**–MAO catalyst with unimodal distribution (run 4 vs 14, Figure 9a).³³ Note that significant increase in the catalytic activity (10020 kg PE/mol Ti · h) was observed upon employing [Ph₃C][B(C₆F₅)₄] as cocatalyst along with ^tBu₃Al as scavenger, and the resultant polymer possessed higher M_n values than that prepared by **7**–MAO catalyst with unimodal molecular weight distribution (run 13, Figure 9a). The unimodal molecular weight distributions in the resultant polymer suggest that these polymerizations proceeded with a single catalytically active species. These facts

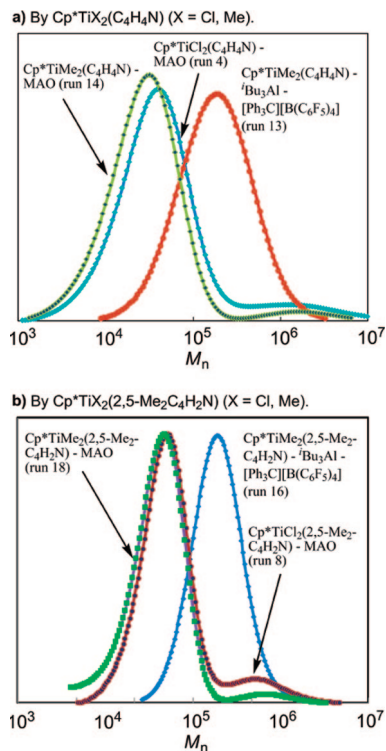


Figure 9. GPC traces of polyethylene prepared by (a) $\text{Cp}^*\text{TiMe}_2(\text{C}_4\text{H}_4\text{N})$ (**7**), (b) $\text{Cp}^*\text{TiMe}_2(2,5\text{-Me}_2\text{C}_4\text{H}_2\text{N})$ (**8**)–MAO or $\text{Bu}_3\text{Al}/[\text{Ph}_3\text{C}][\text{B}(\text{C}_6\text{F}_5)_4]$ catalyst systems. Detailed conditions and results are shown in Table 6.

strongly suggest that dissociation of the pyrrolide ligand (pyrrolide transfer to Al) should not take place under these conditions. The observed difference in the M_n values by MAO or borate would suggest that the major chain transfer pathway in the polymerization using **7** (or **1**)–MAO catalyst would be the chain transfer to Al, and the assumption should be in good agreement with the above facts seen in the polymerization using **1**–MAO catalyst (effect of Al/Ti molar ratio, runs 4, 5).³³

It should also be noted that remarkable enhancement in the catalytic activity of **8** (4620 kg PE/mol Ti·h) in comparison with **2** (1500 kg PE/mol Ti·h) was observed, and further

improvement in the activity (8100 kg PE/mol Ti·h) has been accomplished by using $[\text{Ph}_3\text{C}][\text{B}(\text{C}_6\text{F}_5)_4]/\text{Bu}_3\text{Al}$ in place of MAO as the cocatalyst. The resultant polymers prepared by **8**–borate catalyst possessed high molecular weights with unimodal molecular weight distributions ($M_n = (1.46\text{--}1.60) \times 10^5$, $M_w/M_n = 2.75\text{--}2.96$, runs 16, 17, Figure 9b). The fact that use of borate cocatalyst leads to superior catalytic performance in the present case seems promising, because we previously reported that catalytic activities of $\text{Cp}^*\text{TiCl}_2(\text{O-2,6-}^i\text{Pr}_2\text{C}_6\text{H}_3)/\text{MAO}$ and $\text{Cp}^*\text{TiCl}_2(\text{O-2,6-}^i\text{Pr}_2\text{C}_6\text{H}_3)/[\text{Ph}_3\text{C}][\text{B}(\text{C}_6\text{F}_5)_4]/\text{Bu}_3\text{Al}$ systems were almost identical.^{9b} The results also suggest that these polymerizations (by the dimethyl analogue) proceeded with single catalytically active species without dissociation of the pyrrolide ligand under these conditions.³³

Since we previously demonstrated that the efficient catalyst precursors for ethylene polymerization using half-titanocenes containing aryloxo,^{13a} anilide,^{8k} and amide^{8m} ligands could be tuned to the efficient catalyst precursors for syndiospecific styrene polymerization by simple modification of the cyclopentadienyl fragment (Cp'), we thus conducted styrene polymerizations using the Cp^* -pyrrolide analogues (**1**–**4**) and the Cp -pyrrolide analogues (**9**–**12**) in toluene in the presence of methylaluminoxane (MAO). The results are summarized in Table 7. As reported previously,^{13,14} the resultant polymer consisted of a mixture of atactic polystyrene produced by MAO itself (acetone-soluble fraction) and syndiotactic polystyrene (acetone-insoluble fraction) produced by the catalyst.

It turned out that the catalytic activity (calculated based on polymer yield of syndiotactic polystyrene and the amount of Ti employed) of $\text{Cp}^*\text{TiCl}_2(\text{C}_4\text{H}_4\text{N})$ (**1**) increased at high temperature (runs 25–30), as seen in styrene polymerization using $\text{Cp}^*\text{TiCl}_2(\text{O-2,6-}^i\text{Pr}_2\text{C}_6\text{H}_3)$ MAO catalyst.³⁴ The activity of 3170 kg sPS/mol Ti·h was thus attained at 80 °C (run 30). The resultant polymers possessed rather high molecular weights with unimodal molecular weight distributions, but the M_w/M_n values in the resultant polymer prepared at high temperature became large (the distribution became broad), probably due to decomposition of the catalytically active species. The observed catalytic activities of (**2**–**4**)–MAO catalysts at 80 °C were lower than that of the **1**–MAO catalyst (run 30 vs runs 31–33), probably due to increase in the steric bulk.

Table 7. Styrene Polymerization by $\text{Cp}'\text{TiCl}_2(\text{L})$ [$\text{Cp}' = \text{Cp}^*$; $\text{L} = \text{C}_4\text{H}_4\text{N}$ (**1**), 2,5-Me₂C₄H₂N (**2**), 2,4-Me₂C₄H₂N (**3**), 3-Et-2,4-Me₂C₄H₂N (**4**), and $\text{Cp}' = \text{Cp}$; $\text{L} = \text{C}_4\text{H}_4\text{N}$ (**9**), 2,5-Me₂C₄H₂N (**10**), 2,4-Me₂C₄H₂N (**11**), 3-Et-2,4-Me₂C₄H₂N (**12**)]–MAO Catalyst Systems^a

run	catalyst Cp' ; L	temp/°C	polymer yield/mg ^b	activity ^c	$M_n^c \times 10^{-5}$	M_w/M_n^d
24	Cp^* ; C ₄ H ₄ N (1)	25	32	191		
25	Cp^* ; C ₄ H ₄ N (1)	25	35	210	12.2	1.8
26	Cp^* ; C ₄ H ₄ N (1)	40	55	330	8.12	1.6
27	Cp^* ; C ₄ H ₄ N (1)	50	221	1330	2.72	4.8
28	Cp^* ; C ₄ H ₄ N (1)	60	328	1970	1.85	3.2
29	Cp^* ; C ₄ H ₄ N (1)	70	335	2010	1.76	3.2
30	Cp^* ; C ₄ H ₄ N (1)	80	529	3170	1.58	3.7
31	Cp^* ; 2,5-Me ₂ C ₄ H ₂ N (2)	80	231	1390	1.69	3.3
32	Cp^* ; 2,4-Me ₂ C ₄ H ₂ N (3)	80	251	1510	2.85	3.4 ^e
33	Cp^* ; 2,4-Me ₂ -3-EtC ₄ H ₂ N (4)	80	287	1720	2.72	4.9
34	Cp ; C ₄ H ₄ N (9)	25	81	486	13.8	1.5 ^e
35	Cp ; C ₄ H ₄ N (9)	40	192	1150	13.9	1.5 ^e
36	Cp ; C ₄ H ₄ N (9)	60	142	852		
37	Cp ; C ₄ H ₄ N (9)	80	42	252		
38	Cp ; 2,5-Me ₂ C ₄ H ₂ N (10)	40	31	186	18.1	1.3
					0.7	1.5
39	Cp ; 2,4-Me ₂ C ₄ H ₂ N (11)	40	201	1210	12.6	1.5
					0.4	1.3
40	Cp ; 2,4-Me ₂ -3-EtC ₄ H ₂ N (12)	40	195	1170	16.3	1.4 ^e

^a Reaction conditions: complex 1.0 μmol , styrene 10 mL, styrene + toluene 30 mL, 10 min, 100 mL scale autoclave, d-MAO = 3.0 mmol (prepared by removing AlMe_3 and toluene from commercially available MAO). ^b Acetone-insoluble fraction. ^c Activity = kg sPS/mol Ti·h. ^d GPC data in *o*-dichlorobenzene vs polystyrene standards. ^e Low molecular weight polymers were contaminated in small amount.

It also turned out that the activities of CpTiCl₂(C₄H₄N) (**9**)–MAO catalyst were dependent upon the polymerization temperature, and the activity was high if the polymerization was conducted at 40 °C (run 35). The resultant polymers possessed high molecular weights with unimodal molecular weight distributions but a containing small amount of low molecular weight polymers (which is apparently different from the atactic polymer contaminated by preparing with MAO itself). The activities by **11,12**–MAO catalysts (runs 39, 40) were similar to that of **9**, but low activity was observed if **10** (where the pyrrolide ligand has an η⁵ coordination confirmed by X-ray crystallography) was used as the catalyst precursor. The resultant polymers prepared by (**9**–**12**)–MAO catalysts consisted of high and low molecular weight polymers, suggesting that several (at least two) catalytically active species were present in the reaction mixture under these conditions.

Concluding Remarks

In summary, we have established a route for systematic synthesis of various half-titanocenes containing pyrrolides and its ring-substituted derivatives as anionic ancillary ligands of the types Cp*TiCl₂(L) [L = C₄H₄N (**1**), 2,5-Me₂C₄H₂N (**2**), 2,4-Me₂C₄H₂N (**3**), 2,4-Me₂-3-EtC₄H₂N (**4**)], Cp*TiCl(2,4-Me₂-3-EtC₄H₂N)₂ (**5**), Cp*Ti(C₄H₄N)₃ (**6**), Cp*TiMe₂(L) [L = C₄H₄N (**7**), 2,5-Me₂C₄H₂N (**8**)], and CpTiCl₂(L) [L = C₄H₄N (**9**), 2,5-Me₂C₄H₂N (**10**), 2,4-Me₂C₄H₂N (**11**), 2,4-Me₂-3-EtC₄H₂N (**12**)]. These complexes were identified based on elemental analysis and NMR spectra, and the structures of **3**–**11** were determined by X-ray crystallographic analysis. Most of these complexes have a distorted tetrahedral geometry around Ti, and pyrrolide ligands coordinate to Ti through the nitrogen atom in an η¹ fashion, whereas the 2,5-dimethylpyrrolide ligand in **10** has a η⁵-coordination mode, confirmed by X-ray crystallography. The complexes **1**–**4** and **9**–**12** exhibited moderate catalytic activities for ethylene polymerization in the presence of MAO, and the activities were affected by the substituent on the pyrrolide ligand. Complex **1** exhibited the highest activity among the Cp* analogues, and an increase in the steric bulk led to a decrease in the activity, whereas the activity of the Cp analogues increased upon increasing the steric bulk in the pyrrolide ligand. The dimethyl complexes **7** and **8** exhibited higher catalytic activities, and notable increases were observed if these polymerizations were conducted in the presence of borate cocatalyst [Ph₃C][B(C₆F₅)₄]. The resultant polymers prepared by (**7,8**)–cocatalyst systems possessed high molecular weights with unimodal distributions, strongly suggesting that these polymerizations proceeded with a single catalytically active species without dissociation of the pyrrolide ligand. The dichloro complexes were also effective for syndiospecific styrene polymerization, and the activity was more affected by the polymerization temperature than the substituents in the pyrrolides. The results presented here are promising not only from the viewpoint of basic understanding of the chemistry of pyrrolide-containing half-titanocenes but from the standpoint of designing efficient transition metal catalysts for olefin polymerization.

(33) In the ethylene polymerizations using the dichloro (**1, 2**) and the dimethyl (**7, 8**) analogues in the presence of MAO, a tiny trace amount of high molecular weight polymer was also observed in the GPC trace, although ratios in the dimethyl analogues (**7, 8**) were extremely low. As commented by reviewers, this may be speculated as due to a probable dissociation of the pyrrolide ligand (pyrrolide transfer from Ti to Al), and this may be a reason for the bimodal molecular weight distribution in the resultant polyethylene.

(34) Byun, D.-J.; Fudo, A.; Tanaka, A.; Fujiki, M.; Nomura, K. *Macromolecules* **2004**, *37*, 5520.

Experimental Section

General Procedures. All experiments were carried out under a nitrogen atmosphere in a Vacuum Atmospheres drybox unless otherwise specified. All chemicals used were of reagent grade and were purified by the standard purification procedures. Anhydrous grade tetrahydrofuran, diethyl ether, hexane, dichloromethane, and toluene (Kanto Kagaku Co. Ltd.) were transferred into bottles containing molecular sieves (mixture of 3 Å and 4 Å 1/16, and 13X) under a nitrogen stream in the drybox and were used without further purification. Reagent grade pyrrole, 2,4-dimethylpyrrole, 2,5-dimethylpyrrole, 2,4-dimethyl-3-ethylpyrrole, CpTiCl₃, and Cp*TiCl₃ were purchased from Wako Chemical Co., Ltd., and were used as received. [Ph₃C][B(C₆F₅)₄] (Asahi Glass Co., Ltd.) of reagent grade was used as received and stored in the drybox. Ethylene for polymerization was of polymerization grade (purity >99.9%, Sumitomo Seika Co., Ltd.) and was used as received, and styrene of reagent grade (Kanto Kagaku Co. Ltd.) was stored in a freezer after passing through an alumina short column under nitrogen flow in the drybox. Elemental analyses were performed by using a PE2400II Series (Perkin-Elmer Co.). Some analysis runs were employed twice to confirm the reproducibility in independent analysis/synthesis runs.

All ¹H and ¹³C NMR spectra were recorded on a JEOL JNM-LA400 spectrometer (399.65 MHz, ¹H; 100.40 MHz, ¹³C). All deuterated NMR solvents were stored over molecular sieves under a nitrogen atmosphere, and all chemical shifts are given in ppm and are referenced to residual solvent peaks. ¹³C NMR spectra for polyethylene and polystyrene were recorded on a JEOL JNM-LA400 spectrometer with proton decoupling. The pulse interval was 5.2 s, the acquisition time was 0.8 s, the pulse angle was 90°, and the number of transients accumulated was ca. 6000.

The molecular weights and molecular weight distributions of the polyethylene samples were measured at 145 °C by gel permeation chromatography (Waters 150 CV) using *o*-dichlorobenzene as the solvent and calibration with standard polystyrene samples (measured at Sumitomo Chemical Co., Ltd.). Molecular weights and molecular weight distributions for the polystyrene samples were measured by gel permeation chromatography (Tosoh HLC-8121GPC/HT) with a polystyrene gel column (TSK gel GMHHR-H HT × 2, 30 cm × 7.8 mm i.d.), ranging from <10² to <2.8 × 10⁸ MW at 140 °C using *o*-dichlorobenzene containing 0.05 wt/v % 2,6-di-*tert*-butyl-*p*-cresol as the solvent. The molecular weight was calculated by a standard procedure based on the calibration with standard polystyrene samples.

Synthesis of Li(C₄H₄N). Li(C₄H₄N) was prepared according to the following procedure. Into a *n*-hexane (50 mL) solution containing pyrrole (2.01 g, 0.03 mol) precooled at –20 °C (in the freezer) was added slowly in small portions *n*-hexane solution containing *n*-BuLi (18.9 mL of 1.58 mol/L solution, 0.03 mol). Immediate formation of voluminous white precipitates was observed. The stirred mixture was then warmed slowly to room temperature and was stirred for 4 h. The resultant precipitates were thus collected on a glass filter and were adequately washed with *n*-hexane twice and dried under vacuum. Yield: 89%. ¹H NMR (THF-*d*₈): δ 6.00 (br, 2H, NCH), 6.77 (br, 2H, NCHC H). ¹³C NMR (THF-*d*₈): δ 105.01, 134.03.

Lithium salts of 2,5-dimethylpyrrole, 2,4-dimethylpyrrole, and 3-ethyl-2,4-dimethylpyrrole were prepared similarly, and their NMR data are summarized as follows.

Li(2,5-Me₂C₄H₂N). ¹H NMR (THF-*d*₈): δ 2.36 (s, 6H, Me), 5.67 (s, 2H, NCHC H). ¹³C NMR (THF-*d*₈): δ 17.96, 105.01, 134.03.

Li(2,4-Me₂C₄H₂N). ¹H NMR (THF-*d*₈): δ 2.21 (s, 3H, Me), 2.38 (s, 3H, Me), 5.70 (s, 1H, CH), 6.46 (s, 1H, CH). ¹³C NMR (THF-*d*₈): δ 13.68, 18.07, 107.60, 117.44, 124.48, 136.34.

Li(3-Et-2,4-Me₂C₄H₂N). ¹H NMR (THF-*d*₈): δ 1.18 (t, 3H, *J* = 7.7 Hz, Me), 2.20 (s, 3H, Me), 2.38 (s, 3H, Me), 2.58 (q, 2H, *J* = 7.7 Hz, CH₂), 6.47 (s, 1H, NCHC H). ¹³C NMR (THF-*d*₈): δ 12.37, 16.01, 17.91, 20.27, 115.79, 119.94, 123.20, 132.16.

Synthesis of Cp*TiCl₂(C₄H₄N) (1). Into a sealed tube equipped with a Kontes three-way bulb, containing a toluene solution (10 mL) of Cp*TiCl₃ (289 mg, 1.0 mmol), was added lithium pyrrolide [LiN(C₄H₄), 88 mg, 1.5 mmol] at -20 °C. The stirred reaction mixture was then warmed slowly to room temperature, and the tube was then placed into an oil bath preheated at 40 °C; the mixture was stirred overnight. To the solution was then added CH₂Cl₂ (1 mL), and the mixture was then filtered through a Celite pad. The filter cake was washed with toluene, and the combined filtrate and wash were taken to dryness under reduced pressure to give a dark brown residue. The residue was washed with cold *n*-hexane (3 mL), and the brown residue, the hexane-insoluble part, was dissolved in a minimum amount of CH₂Cl₂/hexane. The chilled solution (-20 °C) afforded deep brown microcrystals. Yield: 115 mg (36%). ¹H NMR (CDCl₃): δ 2.24 (15H, C₅Me₅), 6.17 (s, 2H, NCH-CH), 6.84 (s, 2H, NCH-CH). ¹³C NMR (CDCl₃): δ 13.36, 110.31, 127.58, 136.23. Anal. Calcd for C₁₄H₁₉Cl₂N₂Ti: C, 52.53; H, 5.98; N, 4.38. Found: C, 52.21; H, 5.83; N, 4.25.

Cp*TiCl₂(2,5-Me₂C₄H₂N) (2). The synthetic procedure of **2** was the same as that for **1** except that the lithium salt of 2,5-dimethylpyrrole (152 mg, 1.5 mmol) was used in place of LiN(C₄H₄). Yield: 136 mg (39%). ¹H NMR (CDCl₃): δ 2.16 (s, 15H, C₅Me₅), 2.28 (s) and 2.29 (s) (6H, Me), 5.80 (s, 2H, NCCH). ¹³C NMR (CDCl₃): δ 13.38, 13.71, 19.01, 111.82, 134.06. Anal. Calcd for C₁₆H₂₃Cl₂N₂Ti: C, 55.20 or 51.75 (+TiC); H, 6.66; N, 4.02. Found: C, 53.74; H, 6.66; N, 3.71.

Cp*TiCl₂(2,4-Me₂C₄H₂N) (3). The synthetic procedure of **3** was the same as that for **1** except that lithium 2,4-dimethylpyrrolide (152 mg, 1.5 mmol) was used in place of LiN(C₄H₄). Yield: 101 mg (29%). ¹H NMR (CDCl₃): δ 2.03 (s, 3H, Me), 2.19 (s, 15H, C₅Me₅), 2.23 (s, 3H, Me), 5.77 (s, 1H), 6.43 (s, 1H). ¹³C NMR (CDCl₃): δ 12.15, 13.24, 17.13, 113.85, 121.92, 124.05, 135.27, 137.58. Anal. Calcd for C₁₆H₂₃Cl₂N₂Ti: C, 55.20; H, 6.66; N, 4.02. Found: C, 54.96; H, 6.82; N, 3.93.

Cp*TiCl₂(3-Et-2,4-Me₂C₄H₂N) (4). The synthetic procedure of **4** was the same as that for **1** except that lithium 3-ethyl-2,4-dimethylpyrrolide (142 mg, 1.1 mmol) was used in place of LiN(C₄H₄) and the reaction was carried out in hexane at room temperature (25 °C). Yield: 166 mg (44%). ¹H NMR (CDCl₃): δ 1.07 (t, 3H, *J* = 7.7 Hz, CH₃CH₂-), 1.95 (3H, Me), 2.10 (s, 15H, C₅Me₅), 2.14 (s, 3H, Me), 2.38 (q, 2H, *J* = 7.7 Hz, CH₃CH₂-), 6.46 (s, 1H, CH). ¹³C NMR (CDCl₃): δ 12.28, 13.21, 13.33, 16.31, 18.32, 122.85, 132.20, 135.45, 139.07, 147.54. Anal. Calcd for C₁₈H₂₇Cl₂N₂Ti: C, 57.47 or 54.28 (+TiC); H, 7.23; N, 3.72. Found: C, 56.78; H, 7.29; N, 3.46.

Cp*TiCl₂(3-Et-2,4-Me₂C₄H₂N)₂ (5). The synthetic procedure of **5** was the same as that for **1** except that lithium 3-ethyl-2,4-dimethylpyrrolide (282 mg, 2.2 mmol) was used in place of LiN(C₄H₄). The resultant solids were dissolved in a minimum amount of *n*-hexane, and the chilled solution afforded deep brown microcrystals. Yield: 148 mg (32%). ¹H NMR (CDCl₃): δ 0.96 (t, 6H, *J* = 7.7 Hz, CH₃CH₂-), 1.79 (s, 6H, Me), 2.00 (s, 6H, Me), 2.17 (s, 15H, MeCp*), 2.24 (q, 4H, *J* = 7.7 Hz, CH₃CH₂), 6.72 (s, 2H, CH). ¹³C NMR (CDCl₃): δ 10.38, 13.13, 13.22, 15.12, 17.47, 119.15, 121.30, 124.31, 131.67, 132.14. Anal. Calcd for C₂₆H₃₉Cl₂N₂Ti: C, 67.46 or 64.86 (+TiC); H, 8.49; N, 6.05. Found: C, 66.37; H, 8.44; N, 5.89.

Cp*TiCl(C₄H₄N)₃ (6). The synthetic procedure of **6** was the same as that for **1** except that 3.3 equiv of lithium pyrrolide (241 mg, 3.3 mmol) was used, and the reaction was conducted in Et₂O at room temperature (25 °C). Yield: 290 mg (76%). ¹H NMR (CDCl₃): δ 2.19 (s, 15H, MeCp*), 6.06 (6H, NCH), 6.69 (s, 6H, NCHCH). ¹³C NMR (CDCl₃): δ 12.81, 108.70, 120.77, 132.63. Anal. Calcd for C₂₂H₂₇N₃Ti: C, 69.29; H, 7.14; N, 11.02. Found: C, 69.02; H, 7.11; N, 10.85.

Synthesis of Cp*TiMe₂(C₄H₄N) (7). Into a cooled Et₂O solution (10 mL) containing Cp*TiCl₃ (289 mg, 1.0 mmol) was added in small

portions an Et₂O solution of MeLi (1.83 mL of 1.09 M in 5 mL of ether, 2.0 mmol) over a period of 30 min at -20 °C. The stirred reaction mixture was then warmed slowly to room temperature and was stirred for 4 h. The reaction mixture was then cooled to -20 °C, and LiN(C₄H₄) (73 mg, 1.0 mmol) was added. The reaction mixture was warmed slowly to room temperature (25 °C) and was stirred overnight. To the mixture was then added CH₂Cl₂ (1.0 mL), and the mixture was then evaporated *in vacuo*. The resultant solid residue was then extracted with toluene, and the resultant brown, oily residue was dissolved in a minimum amount of Et₂O. The chilled solution (-20 °C) placed in the freezer afforded reddish-yellow microcrystals over a period of ca. 10 days. Yield: 184 (66%). ¹H NMR (C₆D₆): δ 1.13 (s, 6H, Ti-Me), 1.82 (s, 15H, C₅Me₅), 6.57 (s, 2H, NCH-CH-), 6.94 (s, 2H, NCH-CH-). ¹³C NMR (C₆D₆): δ 11.67, 67.17, 109.68, 124.83, 124.91. Anal. Calcd for C₁₆H₂₅N₂Ti: C, 68.82; H, 9.02; N, 5.02. Found: C, 68.64; H, 9.29; N, 4.84.

Cp*TiMe₂(2,5-Me₂C₄H₂N) (8). The synthetic procedure of **8** was the same as that for **7** except that the lithium salt of 2,5-dimethylpyrrole (101 mg, 1.0 mmol) was used in place of lithium pyrrolide. Yield: 206 mg (67%). ¹H NMR (C₆D₆): δ 0.69 and 1.39 (s, 6H, Ti-Me), 1.64 and 1.69 (s, 15H, C₅Me₅), 2.16 and 2.20 (s, 6H, Me), 5.68 and 5.77 (s, 2H). ¹³C NMR (C₆D₆): δ 11.96, 12.49, 17.56, 18.28, 41.74, 64.45, 110.56, 110.99, 123.34, 137.67. The resonance due to each carbon was observed as two sets most probably due to the existence of **8** as two different species in solution. Anal. Calcd for C₁₈H₂₉N₂Ti: C, 70.35 or 66.44 (+TiC); H, 9.51; N, 4.56. Found: C, 67.53; H, 9.38; N, 4.31.

Synthesis of CpTiCl₂(C₄H₄N) (9). Into a chilled Et₂O solution (10 mL) containing CpTiCl₃ (219 mg, 1.0 mmol) was added the lithium salt of pyrrole (80 mg, 1.1 mmol) in small portions at -20 °C. The reaction mixture was stirred overnight at room temperature (25 °C). To the mixture was then added CH₂Cl₂ (1 mL), and the solution was then placed in a rotary evaporator *in vacuo* to remove solvent (Et₂O, etc.). The resultant residue was then dissolved in toluene and filtered through a Celite pad, and removal of toluene *in vacuo* afforded a dark brown solid. The solid was then dissolved in a minimum amount of CH₂Cl₂/hexane, and the chilled solution (-20 °C) afforded dark brown microcrystals. Yield: 165 mg (66%). ¹H NMR (CDCl₃): δ 6.08 (s, 2H, NCH), 7.03 (s, 5H, Cp), 7.56 (s, 2H). ¹³C NMR (CDCl₃): δ 108.35, 121.51, 130.46. Anal. Calcd for C₉H₉Cl₂N₂Ti: C, 43.25 or 38.44 (+TiC); H, 3.63; N, 5.60. Found: C, 42.94; H, 3.72; N, 5.51.

Synthesis of CpTiCl₂(2,5-Me₂C₄H₂N) (10). The synthetic procedure for **10** was the same as that for **9** except that the lithium salt of 2,5-dimethylpyrrole was used in place of lithium pyrrolide and the reaction was carried out in *n*-hexane. Yield: 175 mg (63%). ¹H NMR (CDCl₃): δ 2.43 (s, 6H, Me), 6.63 (s, 5H, Cp), 6.82 (s, 2H, CH). ¹³C NMR (CDCl₃): δ 18.72, 122.69, 127.97, 147.95. Anal. Calcd for C₁₁H₁₃Cl₂N₂Ti: C, 47.52 or 43.20 (+TiC); H, 4.71; N, 5.04. Found: C, 46.15; H, 4.57; N, 4.62.

Synthesis of CpTiCl₂(2,4-Me₂C₄H₂N) (11). The synthetic procedure for **11** was the same as that for **9** except that the lithium salt of 2,4-dimethylpyrrole was used in place of lithium pyrrolide and the reaction was carried out in *n*-hexane. Yield: 188 mg (68%). ¹H NMR (CDCl₃): δ 2.06 (s, 3H, Me), 2.49 (s, 3H, Me), 5.83 (s, 1H, CH), 6.80 (s, 5H, Cp), 6.89 (s, 1H, CH). ¹³C NMR (CDCl₃): δ 12.36, 17.71, 115.81, 121.60, 125.25, 128.46, 143.65. Anal. Calcd for C₁₁H₁₃Cl₂N₂Ti: C, 47.52 or 43.20 (+TiC); H, 4.71; N, 5.04. Found: C, 46.29; H, 4.54; N, 4.73.

Synthesis of CpTiCl₂(3-Et-2,4-Me₂C₄H₂N) (12). The synthetic procedure for **12** was the same as that for **9** except that the lithium salt of 3-ethyl-2,4-dimethylpyrrole was used in place of lithium pyrrolide and the reaction was carried out in Et₂O. Yield: 230 mg (75%). ¹H NMR (CDCl₃): δ 1.11 (t, 3H, *J* = 7.7 Hz, CH₃CH₂-), 2.03 (3H, Me), 2.27 (s, 3H, Me), 2.50 (q, 2H, *J* = 7.7 Hz, CH₃CH₂-), 6.65 (s, 5H, Cp), 7.05 (s, 1H, CH). ¹³C NMR (CDCl₃): δ 12.61, 13.09, 17.06, 19.03, 120.90, 124.30, 140.83, 143.92, 153.11.

Table 8. Crystal Data and Structure Refinement Parameters for Cp*TiCl₂(2,4-Me₂C₄H₂N) (3), Cp*TiCl₂(2,4-Me₂-3-EtC₄H₃N) (4), Cp*TiCl₂(2,4-Me₂-3-EtC₄H₃N)₂ (5), Cp*Ti(C₄H₄N)₃ (6), Cp*TiMe₂(C₄H₄N) (7), Cp*TiMe₂(2,5-Me₂C₄H₂N) (8), CpTiCl₂(C₄H₄N) (9), CpTiCl₂(2,5-Me₂C₄H₂N) (10), and CpTiCl₂(2,4-Me₂C₄H₂N) (11)^a

	3	4	5	6	7	8	9	10	11
formula	C ₁₆ H ₂₃ Cl ₂ N ₂ Ti	C ₁₈ H ₂₇ NCl ₂ Ti	C ₂₆ H ₃₉ ClN ₂ Ti	C ₂₂ H ₂₇ TiN ₃	C ₁₆ H ₂₅ TiN	C ₁₈ H ₂₉ TiN	C ₉ H ₉ TiCl ₂ N	C ₁₁ H ₁₃ TiCl ₂ N	C ₁₁ H ₁₃ Cl ₂ N ₂ Ti
fw	348.17	376.22	462.96	381.38	279.28	307.33	249.98	278.04	278.04
cryst color, habit	black, block	black, block	brown, block	red, block	yellow, block	red, block	black, block	red, block	black, block
cryst size (mm)	0.40 × 0.10 × 0.08	0.20 × 0.20 × 0.15	0.40 × 0.25 × 0.15	0.18 × 0.15 × 0.10	0.35 × 0.25 × 0.25	0.22 × 0.20 × 0.10	0.40 × 0.40 × 0.35	0.40 × 0.25 × 0.15	0.65 × 0.35 × 0.32
cryst syst	orthorhombic	monoclinic	triclinic	triclinic	monoclinic	orthorhombic	monoclinic	monoclinic	monoclinic
space group	P2 ₁ 2 ₁ 2 ₁ (#19)	P2 ₁ /n (#14)	P1̄ (#2)	P1̄ (#2)	P2 ₁ /n (#14)	Pbca (#61)	C2/c (#15)	P2 ₁ /n (#14)	P2 ₁ /n (#14)
a (Å)	7.4447(3)	8.2632(6)	8.9914(4)	8.3120(5)	6.8203(3)	9.0942(5)	20.6144(8)	8.0616(3)	7.8925(2)
b (Å)	15.0333(6)	7.0964(5)	9.1605(4)	10.8070(6)	26.8547(11)	12.9222(9)	9.5226(4)	15.7344(6)	9.2764(3)
c (Å)	15.3365(6)	33.568(3)	18.0910(10)	11.6816(9)	8.6868(4)	30.1231(14)	13.8562(5)	11.4488(4)	16.8923(6)
V (Å ³)	1716.43(12)	1951.9(2)	1292.92(11)	998.44(11)	1588.07(11)	3540.0(3)	2086.60(14)	1361.23(8)	1236.67(7)
Z value	4	4	2	2	4	8	8	4	4
D _{calcd} (g/cm ³)	1.347	1.280	1.189	1.268	1.168	1.153	1.591	1.357	1.493
F ₀₀₀	728.00	792.00	496.00	404.00	600.00	1328.00	1008.00	568.00	568.00
no. of reflns measd	16 422	14 515	12 827	9872	14 926	21 541	10 084	13 175	11 211
no. of observations	1391	2235	4883	2359	2580	1270	2178	2756	2384
no. of variables	204	226	310	262	188	210	127	161	149
R1	0.0429	0.0412	0.0392	0.0424	0.0329	0.0571	0.0408	0.0557	0.0250
wR2	0.1050	0.1011	0.1379	0.1028	0.1132	0.0664	0.1814	0.1136	0.0758
goodness of fit	1.013	0.997	1.001	1.001	1.003	1.057	1.005	1.000	1.009

^a Detailed conditions are shown in the Supporting Information.

Crystallographic Analysis. All measurements were made on a Rigaku RAXIS-RAPID imaging plate diffractometer with graphite-monochromated Mo K α radiation. The selected crystal collection parameters are listed in Table 8, and the detailed results are described in the reports attached below. All structures were solved by direct methods and expanded using Fourier techniques,³⁵ and the non-hydrogen atoms were refined anisotropically. Hydrogen atoms were included but not refined. All calculations for complexes **1–12** were performed using the Crystal Structure^{36,37} crystallographic software package.

Polymerization of Ethylene Using MAO as Cocatalyst. Ethylene polymerizations were conducted in toluene by using a 100 mL scale autoclave. Solvent (29.0 mL) and MAO as a white solid (174 mg, 3.0 mmol), prepared by removing toluene and AlMe₃ from commercially available MAO (PMAO-S, Tosoh Finechem Co.), were charged into the autoclave in the drybox, and the apparatus was placed under ethylene atmosphere (1 atm). After the addition of a toluene solution (1.0 mL) containing a prescribed amount of **1** via a syringe, the reaction apparatus was pressurized to 5 atm (total 6 atm), and the mixture was stirred magnetically for 10 min. After the above procedure, ethylene was purged, and the mixture was then poured into MeOH (150 mL) containing HCl (10 mL). The resultant polymer was collected on a filter paper by filtration and was adequately washed with MeOH and then dried *in vacuo*.

Polymerization of Ethylene Using Borate as Cocatalyst. A typical procedure for polymerization of ethylene by Cp*TiMe₂(L) [L = C₄H₄N (**7**), 2,5-Me₂C₄H₂N (**8**)]–[Ph₃C][B(C₆F₅)₄] catalyst systems is as follows. Toluene (28 mL) and t-Bu₃Al (50 μ mol) were added into the autoclave in the drybox, and the reaction apparatus was then replaced and filled with ethylene (1 atm) at 25 °C. A toluene solution

(1.0 mL) containing **7** (0.2 μ mol) was then added, immediately followed by addition of a toluene solution (1.0 mL) containing [Ph₃C][B(C₆F₅)₄] (0.6 μ mol). The reaction apparatus was then immediately pressurized to 5 atm (total ethylene pressure 6 atm), and the mixture was magnetically stirred for 10 min. After the reaction, the remaining ethylene was purged upon cooling in the ice bath, and the mixture was then poured into MeOH (150 mL) containing HCl (5 mL). The resultant polymer was collected on a filter paper by filtration, was adequately washed with MeOH, and then was dried *in vacuo*.

Syndiospecific Polymerization of Styrene. Toluene (19 mL), styrene (10 mL), and the MAO solid (174 mg, 3.0 mmol) were added into the autoclave (100 mL scale stainless steel) in the drybox, and the reaction apparatus was then replaced and filled with nitrogen at the given temperature. A toluene solution (1.0 mL) containing a prescribed amount of **1** was then added into the autoclave. The mixture was magnetically stirred for 10 min, and the mixture was then poured into MeOH (150 mL) containing HCl (5 mL). The resultant polymer was collected on a filter paper by filtration and was adequately washed with MeOH and then dried *in vacuo*. According to a previous report,^{13,14} the resultant polymer mixture was separated into two fractions, and atactic polystyrene prepared only by MAO itself was extracted with acetone; syndiotactic polystyrene prepared by **1**–MAO catalyst was isolated as the acetone-insoluble fraction.

Acknowledgment. The present research is partly supported by a Grant-in-Aid for Scientific Research (B) from the Japan Society for the Promotion of Science (JSPS, No.18350055), and I.S. expresses his thanks to the JSPS for a postdoctoral fellowship (No. 07061). The authors also thank Tosoh Finechem Co. for donating MAO, and Sumitomo Chemicals for GPC analysis of polyethylene.

Supporting Information Available: Crystal structure determinations, reports for **3–11**; the crystallographic data are also given as CIF files. These materials are available free of charge via the Internet at <http://pubs.acs.org>.

OM800713T

(35) Beurskens, P. T.; Admiraal, G.; Beurskens, G.; Bosman, W. P.; de Delder, R.; Israel, R.; Smits, J. M. M. *DIRDIF94; The DIRDIF94 program system*; Technical report of the crystallography laboratory; University of Nijmegen: The Netherlands, 1994.

(36) *Crystal Structure 3.6.0*, Crystal Structure Analysis Package; Rigaku and Rigaku/MS: The Woodlands, TX, 2000–2004.

(37) Watkin, D. J.; Prout, C. K.; Carruthers, J. R.; Betteridge, P. W. *CRYSTALS Issue 10*; Chemical Crystallography Laboratory: Oxford, UK, 1996.

Quantitative Determination of the Regioselectivity of Nucleophilic Addition to η^3 -Propargyl Rhenium Complexes and Direct Observation of an Equilibrium between η^3 -Propargyl Rhenium Complexes and Rhenacyclobutenes

Charles P. Casey,* Timothy M. Boller, Joseph S. M. Samec, and John R. Reinert-Nash

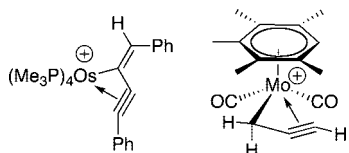
Department of Chemistry, University of Wisconsin–Madison, Madison, Wisconsin 53706

Received July 31, 2008

PMe_3 adds selectively to the central carbon of the η^3 -propargyl complex $[\text{C}_5\text{Me}_5(\text{CO})_2\text{Re}(\eta^3\text{-CH}_2\text{C}\equiv\text{CCMe}_3)][\text{BF}_4]$ (**1-t-Bu**) to form the metallacyclobutene $[\text{C}_5\text{Me}_5(\text{CO})_2\text{Re}(\text{CH}_2\text{C}(\text{PMe}_3)=\text{CCMe}_3)][\text{BF}_4]$ (**7**). The rate of rearrangement of the metallacyclobutene **7** to η^2 -alkyne complex $[\text{C}_5\text{Me}_5(\text{CO})_2\text{Re}(\eta^2\text{-Me}_3\text{PCH}_2\text{C}\equiv\text{CCMe}_3)][\text{BF}_4]$ (**8**) is independent of phosphine concentration, consistent with a dissociative mechanism proceeding via η^3 -propargyl complex **1-t-Bu**. The rate of this rearrangement is 480 times slower than the rate of exchange of PMe_3 with the labeled metallacyclobutene **7-d₉**. This rate ratio provides an indirect measurement of the regioselectivity for addition of PMe_3 to the central carbon of η^3 -propargyl complex **1-t-Bu** to give **7** compared to addition to a terminal carbon to give **8**. The addition of PPh_3 to **1-t-Bu** gives the metallacyclobutene $[\text{C}_5\text{Me}_5(\text{CO})_2\text{Re}(\text{CH}_2\text{C}(\text{PPh}_3)=\text{CCMe}_3)][\text{BF}_4]$ (**11**). Low-temperature ^1H NMR spectra provide evidence for an equilibrium between metallacyclobutene **11** and η^3 -propargyl complex **1-t-Bu** ($K_{\text{eq}} \approx 44 \text{ M}^{-1}$ at -46°C and $\Delta G^\circ(0^\circ\text{C}) = -1.2 \pm 0.2 \text{ kcal mol}^{-1}$).

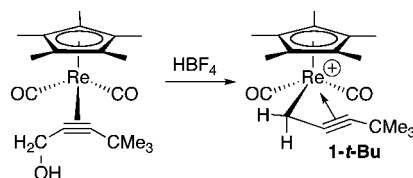
Introduction

η^3 -Propargyl transition metal complexes, the triple-bond analogues of the very well studied η^3 -allyl complexes, are becoming increasingly important in synthetic chemistry.¹ The first stable η^3 -propargyl complex, $[(\text{Me}_3\text{P})_4\text{Os}(\eta^3\text{-PhC}\equiv\text{CC}=\text{CHPh})][\text{PF}_6]$, was reported by Werner in 1985,² and the first isolated η^3 -propargyl complex not having an *exo*-double bond, $[(\text{C}_6\text{Me}_5\text{H})\text{Mo}(\text{CO})_2(\eta^3\text{-CH}_2\text{C}\equiv\text{CH})][\text{BF}_4]$, was reported by Kryvich in 1991.³



We first synthesized η^3 -propargyl rhenium complexes by hydride abstraction from alkyne complexes and later developed a regioselective synthesis via protonation of propargyl alcohol complexes (Scheme 1).⁴ Other methods for the synthesis of isolable η^3 -propargyl complexes include halide abstraction from

Scheme 1



η^1 -propargyl or η^1 -allenyl metal halide complexes,⁵ reaction of metal halides with propargyl nucleophiles,⁶ reaction of propargyl ether complexes with Lewis acids,⁷ rearrangement of η^1 -homopropargyl metal complexes,⁸ and oxidative addition of propargyl halides or tosylates to metal complexes.^{6,9}

^1H and ^{13}C NMR spectroscopic data and X-ray crystallographic structures suggest that η^3 -propargyl complexes are best represented as a combination of η^3 -propargyl and η^3 -allenyl resonance structures (Figure 1).¹ Crystallographic data show that all three carbons are within bonding distance of the metal (2.2–2.5 Å), with the central carbon often nearest to the metal center. The $\text{CR}_2=\text{C}$ bond length is substantially longer (1.34–1.40

* Corresponding author. E-mail: casey@chem.wisc.edu.

(1) Reviews: (a) Chen, J.-T. *Coord. Chem. Rev.* **1999**, 190–192, 1143. (b) Kurosawa, H.; Ogoshi, S. *Bull. Chem. Soc. Jpn.* **1998**, 71, 973. (c) Doherty, S.; Corrigan, J. F.; Carty, A. J.; Sappa, E. *Adv. Organomet. Chem.* **1995**, 37, 39. (d) Wojcicki, A. *New J. Chem.* **1994**, 18, 61.

(2) Gotzig, J.; Otto, H.; Werner, H. *J. Organomet. Chem.* **1985**, 287, 247.

(3) (a) Krivykh, V. V.; Taits, E. S.; Petrovskii, P. V.; Struchov, Y. T.; Yanovski, A. I. *Mendeleev Commun.* **1991**, 103. (b) Gusev, O. V.; Krivykh, V. V.; Rubezhov, A. Z. *Organomet. Chem. USSR* **1991**, 4, 233.

(4) (a) Casey, C. P.; Yi, C. S. *J. Am. Chem. Soc.* **1992**, 114, 6597. (b) Casey, C. P.; Selmezy, A. D.; Nash, J. R.; Yi, C. S.; Powell, D. R.; Hayashi, R. K. *J. Am. Chem. Soc.* **1996**, 118, 6698.

(5) (a) Blosser, P. W.; Schimpff, D. G.; Gallucci, J. C.; Wojcicki, A. *Organometallics* **1993**, 12, 1993. (b) Huang, T.-M.; Chen, J.-T.; Lee, G.-H.; Wang, Y. *J. Am. Chem. Soc.* **1993**, 115, 1170. (c) Huang, T.-M.; Hsu, R.-H.; Yang, C.-S.; Chen, J.-T.; Lee, G.-H.; Wang, Y. *Organometallics* **1994**, 13, 3657. (d) Ogoshi, S.; Tsutsumi, K.; Kurosawa, H. *J. Organomet. Chem.* **1995**, 493, C19. (e) Baize, M. W.; Blosser, P. W.; Plantevin, V.; Schimpff, D. G.; Gallucci, J. C.; Wojcicki, A. *Organometallics* **1996**, 15, 164.

(6) (a) Blosser, P. W.; Gallucci, J. C.; Wojcicki, A. *J. Am. Chem. Soc.* **1993**, 115, 2994. (b) Gordon, G. J.; Whitby, R. J. *J. Chem. Soc., Chem. Commun.* **1997**, 1045.

(7) Weng, W.; Arif, A. M.; Gladysz, J. A. *Angew. Chem., Int. Ed. Engl.* **1993**, 32, 891.

(8) Stang, P. J.; Crittall, C. M.; Arif, A. M. *Organometallics* **1993**, 12, 4799.

(9) Nishida, T.; Ogoshi, S.; Tsutsumi, K.; Fukunishi, Y.; Kurosawa, H. *Organometallics* **2000**, 19, 4488.

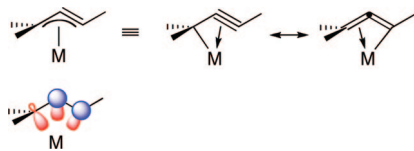
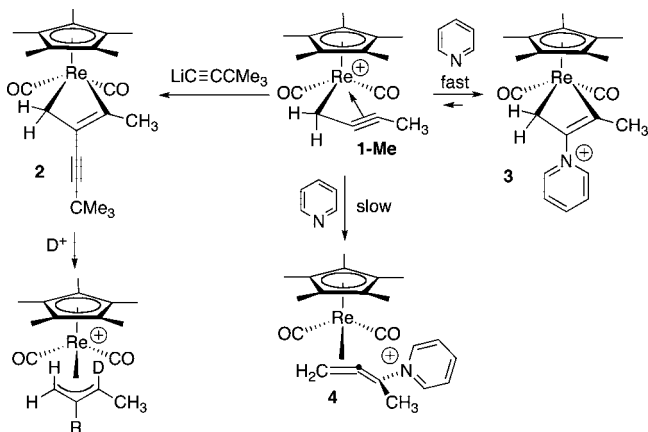


Figure 1. Resonance structures for η^3 -propargyl complexes.

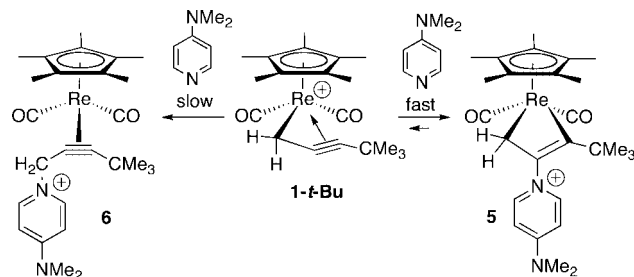
Å) than in free allenes, and the C≡CR bond length is longer than in free acetylenes. The CR₂-C≡CR angle varies from 145° to 155°, implying substantial strain about the central carbon. This strain may be responsible for the highly reactive nature of η^3 -propargyl complexes.

Scheme 2



In contrast to η^3 -allyl metal complexes, which are usually attacked by nucleophiles at a terminal carbon, η^3 -propargyl metal complexes are selectively attacked by nucleophiles at the center carbon.¹ Nucleophiles have been observed to attack each of the three carbon centers of η^3 -propargyl rhenium complexes. We found that while kinetic addition of nucleophiles occurs at the center carbon of the η^3 -propargyl ligand to give rhenacyclobutene complexes, this addition is sometimes reversible and can be followed by addition at either of the other two metal-bound carbon atoms to give η^2 -allene or η^2 -alkyne complexes.^{4a,10,11} The methyl-substituted η^3 -propargyl complex [C₅Me₅(CO)₂Re(η^3 -CH₂C≡CMe)] [BF₄] (**1-Me**) reacted irreversibly with carbon nucleophiles such as malonates and acetylides to give metallacyclobutenes (Scheme 2); protonation of the metallacyclobutenes led to η^3 -allyl complexes. At low temperature, nitrogen nucleophiles added to the central propargyl carbon to produce the metastable metallacyclobutene complexes. Upon warming, the nitrogen nucleophile dissociated from the rhenacyclobutenes and then readded to the resulting η^3 -propargyl complex at one of the terminal sites to give either an η^2 -allene or an η^2 -alkyne complex. For example, **1-Me** reacted with pyridine at -40 °C to give rhenacyclobutene **3**, which rearranged to η^2 -allene complex **4** at room temperature (Scheme 2). 4-Dimethylaminopyridine added to the central carbon of the *tert*-butyl-substituted **1-*t*-Bu** below -40 °C to give the rhenacyclobutene complex **5**, which rearranged to η^2 -alkyne complex **6** at room temperature; apparently, attack at the *t*-Bu-substituted

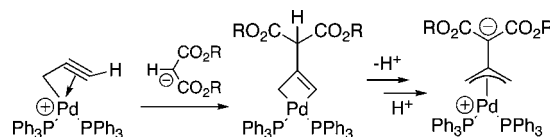
Scheme 3



carbon to give an allene complex was prevented by steric hindrance (Scheme 3).

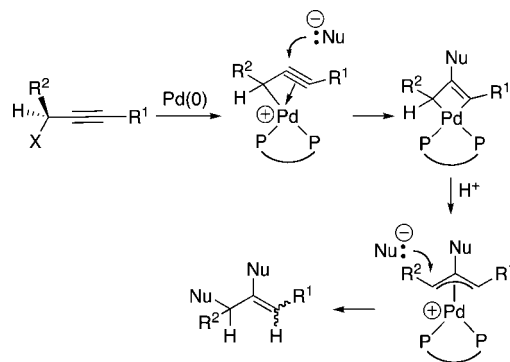
In some cases, nucleophilic additions to η^3 -propargyl complexes have led to η^3 -allyl complexes, consistent with initial kinetic attack at the center carbon of the η^3 -propargyl ligand followed by protonation of the metallacyclobutene intermediate.^{12,6} In other cases, nucleophilic additions to η^3 -propargyl complexes have led to η^3 -trimethylenemethane complexes, consistent with initial kinetic attack at the center carbon of the η^3 -propargyl ligand followed by protonation of the metallacyclobutene intermediate and deprotonation at the atom α to the central allyl carbon (Scheme 4).¹³

Scheme 4



Tsuji pioneered the development of palladium-catalyzed reactions for addition of two nucleophiles to propargyl substrates.¹⁴ For example, the reactions of carbon nucleophiles with propargyl carbonates produce double nucleophilic addition products where nucleophiles have added to both the central and a terminal carbon of the propargyl unit. We have proposed that these double nucleophilic additions occur by oxidative addition to produce an η^3 -propargyl intermediate, which then undergoes addition of the first nucleophile to the central propargyl carbon to produce a metallacyclobutene; this is followed by protonation of the metallacyclobutene to generate an η^3 -allyl complex that is attacked by a second nucleophile (Scheme 5).¹⁰

Scheme 5

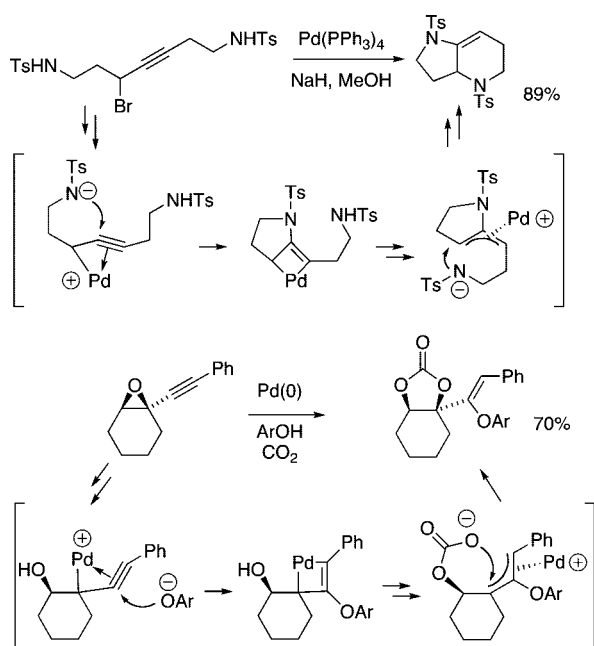


(10) Casey, C. P.; Nash, J. R.; Yi, C. S.; Selmecey, A. D.; Chung, S.; Powell, D. R.; Hayashi, R. K. *J. Am. Chem. Soc.* **1998**, *120*, 722.

(11) The Pd-catalyzed reaction of propargyl halides with thiols gives mixtures of propargyl and allenyl sulfides. These reactions have been proposed to occur by attack of nucleophiles at the terminal carbons of an η^3 -propargyl intermediate. However, kinetic attack at the central propargyl carbon might be reversible. Tsutsumi, K.; Yabukami, T.; Fujimoto, K.; Kawase, T.; Morimoton, T.; Kakiuchi, K. *Organometallics* **2003**, *22*, 2996.

Ohno has imaginatively constructed bicyclic heterocycles by palladium-catalyzed domino cyclization of propargyl bromides.¹⁵ Yoshida has devised a clever palladium-catalyzed three-component coupling of propargylic oxiranes, phenols, and

Scheme 6



carbon dioxide.¹⁶ Both of these processes involve double nucleophilic addition to propargyl substrates (Scheme 6).¹⁷

Because rhenacyclobutenes are the only observed kinetic product of nucleophilic attack on η^3 -propargyl rhenium complexes, it was not possible to quantitatively measure the regioselectivity from product ratios. Here we report an indirect method for the quantitative determination of this regioselectivity. We also report the first direct observation of an equilibrium between an η^3 -propargyl metal complex and a metallacyclobutene.

Results

Both the rate and the regioselectivity of the addition of nucleophiles to the central carbon of η^3 -propargyl rhenium complexes are so high that it is not possible to directly measure how much faster attack at the center carbon is than attack at one of the terminal carbons. Since the rhenacyclobutene is the only observed initial product and neither an η^2 -alkyne complex nor an η^2 -allene complex is initially seen, estimates of >20 can be placed on the regioselectivity. In some cases, the initially formed metallacyclobutene rearranged to a thermodynamically more stable η^2 -alkyne complex ($\Delta G^\circ \leq -2.3$ kcal mol⁻¹). The reaction was complete before the cold sample was inserted into the precooled NMR probe; this requires a $t_{1/2}$ of less than a minute at -50 °C and $\Delta G^\ddagger(0.02$ M ligand) ≤ 14.7 kcal mol⁻¹, $\Delta G^\ddagger(1.0$ M ligand) ≤ 12.9 kcal mol⁻¹.

(12) Tsai, F.-Y.; Hsu, R.-H.; Huang, T.-M.; Chen, J.-T.; Lee, G.-H.; Wang, Y. *J. Organomet. Chem.* **1996**, 520, 85.

(13) (a) Baize, M. W.; Furilla, J. L.; Wojcicki, A. *Inorg. Chim. Acta* **1994**, 223, 1. (b) Baize, M. W.; Plantevin, V.; Gallucci, J. C.; Wojcicki, A. *Inorg. Chim. Acta* **1995**, 235, 1. (c) Su, C.-C.; Chen, J.-T.; Lee, G.-H.; Wang, Y. *J. Am. Chem. Soc.* **1994**, 116, 4999. (d) Plantevin, V.; Blosser, P. W.; Gallucci, J. C.; Wojcicki, A. *Organometallics* **1994**, 13, 3651.

(14) (a) For reviews, see: Tsuji, J.; Mandai, T. *Angew. Chem., Int. Ed. Engl.* **1995**, 34, 2589. (b) Ohno, H. *Chem. Pharm. Bull.* **2005**, 53, 1211.

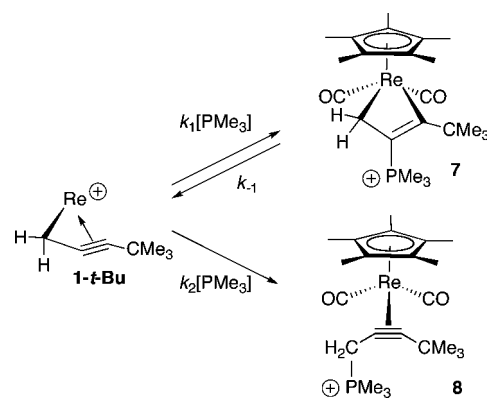
(15) Ohno, H.; Okanao, A.; Kosaka, S.; Tsukamoto, K.; Ohata, M.; Ishihara, K.; Maeda, H.; Tanaka, T.; Fujii, N. *Org. Lett.* **2008**, 10, 1171.

(16) Yoshida, M.; Murao, T.; Sugimoto, K.; Ihara, M. *Synlett* **2007**, 575.

(17) Another interesting synthetic application that involves propargyl complexes is the palladium-catalyzed deoxygenation of propargyl formates. Radinov, R.; Hutchings, S. D. *Tetrahedron Lett.* **1999**, 40, 8955.

Indirect Determination of Regioselectivity of Attack of Phosphines. The relative rates of nucleophilic addition to the center and terminal carbons can be measured indirectly by comparing the rates of exchange of nucleophiles with the metallacyclobutene adducts and of rearrangement of the metallacyclobutene to an η^2 -alkyne complex (eqs 1–4, Scheme 7, and Figure 2). The difference between the barriers for exchange and rearrangement is also the difference between the barriers for attack at the central and terminal carbons. This method assumes a dissociative mechanism for nucleophilic exchange with the metallacyclobutene that proceeds via an η^3 -propargyl intermediate.

Scheme 7



$$\text{Rate}(\text{exchange}) = k_{-1}[7] \quad (1)$$

$$\text{Rate}(\text{rearrangement}) = k_{-1}[7](k_2[\text{PMe}_3]/\{k_1[\text{PMe}_3] + k_2[\text{PMe}_3]\}) = k_{-1}[7](k_2/\{k_1 + k_2\}) \quad (2)$$

$$\text{Rate}(\text{rearrangement})/\text{Rate}(\text{exchange}) = k_2/\{k_1 + k_2\} \quad (3)$$

$$\text{Rate}(\text{rearrangement})/\text{Rate}(\text{exchange}) \approx k_2/k_1 \text{ when } k_1 \gg k_2 \quad (4)$$

We chose to study the exchange and rearrangement kinetics of $[\text{C}_5\text{Me}_5(\text{CO})_2\text{Re}(\text{CH}_2\text{C}(\text{PMe}_3)=\text{CCMe}_3)][\text{BF}_4]$ (**7**) since this metallacyclobutene is relatively stable and had been fully characterized by X-ray crystallography.¹⁰ In addition, **7** had been found to slowly rearrange at room temperature to a single product, the η^2 -alkyne complex $[\text{C}_5\text{Me}_5(\text{CO})_2\text{Re}(\eta^2\text{-Me}_3\text{-}$

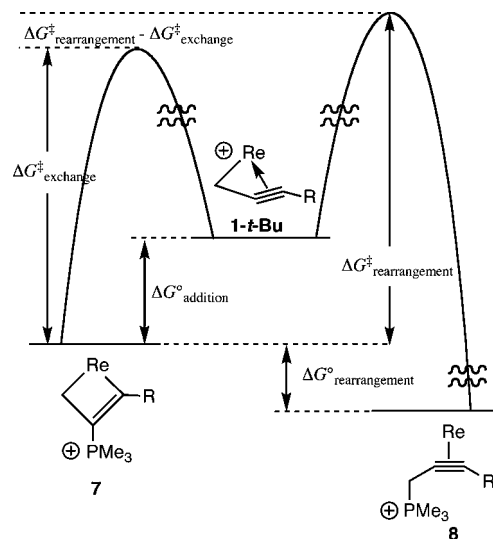


Figure 2. Free energy diagram for nucleophilic addition to η^3 -propargyl complex **1-t-Bu**.

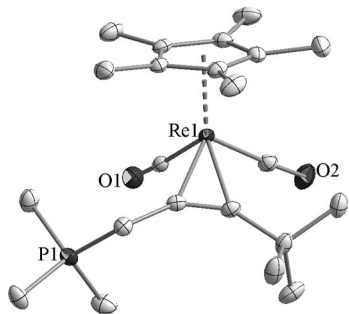
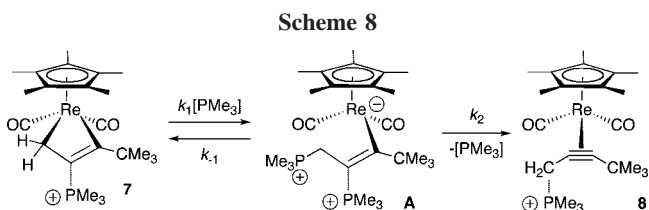


Figure 3. X-ray structure of $[\text{C}_5\text{Me}_5(\text{CO})_2\text{Re}(\eta^2\text{-Me}_3\text{PCH}_2\text{C}\equiv\text{CCMe}_3)]^+$.

$\text{PCH}_2\text{C}\equiv\text{CCMe}_3][\text{BF}_4]$ (**8**),¹⁰ which was further characterized in the current work by X-ray diffraction (Figure 3). The rearrangement product, η^2 -alkyne complex **8**, results from nucleophilic addition to the less crowded terminal CH_2 carbon of the intermediate η^3 -propargyl complex **1-t-Bu** and not to the more sterically hindered *tert*-butyl-substituted carbon to form an η^2 -allene isomer.

Since our method for determining relative regioselectivity depends on the assumption that rearrangement of metallacyclobutene **7** to η^2 -alkyne complex **8** proceeds by phosphine dissociation to generate an η^3 -propargyl intermediate, we needed to establish the rate law for the rearrangement. This was particularly necessary since associative mechanisms are conceivable. For example, phosphine attack might occur at the terminal carbon of **7** to give intermediate **A**, which could then undergo loss of phosphine to generate **8** (Scheme 8). Alkyl and vinyl $\text{CpRe}(\text{CO})_2\text{R}^-$ anions are well-known stable species.¹⁸ The dissociative mechanism of Scheme 7 and the associative mechanism of Scheme 8 are readily distinguished by their kinetic independence or dependence on $[\text{PR}_3]$.



The rate of rearrangement of metallacyclobutene complex **7** was studied in the presence and absence of added PMe_3 . Two yellow CD_3CN solutions¹⁹ of **7** were prepared in resealable NMR tubes, and excess PMe_3 was condensed into one. The rate of rearrangement of **7** to **8** was monitored by ^1H NMR spectroscopy at 64 °C. First-order rate law fits were obtained. The rate in the absence of added PMe_3 ($k_{\text{rearr}} = (8.2 \pm 0.1) \times 10^{-4} \text{ s}^{-1}$) and in the presence of 0.29 M added PMe_3 ($k_{\text{rearr}} = (7.9 \pm 0.1) \times 10^{-4} \text{ s}^{-1}$) were very similar. The failure to observe a rate enhancement in the presence of added PMe_3 rules out an associative mechanism for the rearrangement of metallacyclobutene complex **7** to η^2 -alkyne complex **8**.²⁰

(18) (a) Casey, C. P.; Vosejпка, P. C.; Askham, F. R. *J. Am. Chem. Soc.* **1990**, *112*, 3713. (b) Casey, C. P.; Vosejпка, P. C.; Gavney, J. A., Jr. *J. Am. Chem. Soc.* **1990**, *112*, 4083.

(19) Phosphine reactions in CD_2Cl_2 were problematic at elevated temperatures due to nucleophilic attack of PMe_3 on the solvent.

(20) The intriguing possibility of an associative mechanism for rearrangement of a metallacyclobutene was explored by studying rearrangements involving 1,2-bis(diphenylphosphino)ethane ligands, where the associative mechanism would be more likely with the possibility of intramolecular attack by a second phosphine. Even with diphos ligands, the dissociative mechanism is strongly favored. See Supporting Information.

The deuterium-labeled metallacyclobutene $[\text{C}_5\text{Me}_5(\text{CO})_2\text{Re}(\text{CH}_2\text{C}[\text{P}(\text{CD}_3)_3]=\text{CCMe}_3)][\text{BF}_4]$ (**7-d₉**) was prepared by addition of $\text{P}(\text{CD}_3)_3$ to **1-t-Bu**. The kinetics of the exchange of a 4.5-fold excess of $\text{P}(\text{CH}_3)_3$ with 0.1 M **7-d₉** were studied by ^1H NMR spectroscopy at 10 °C in CD_3CN by monitoring the appearance of the $\text{P}(\text{CH}_3)_3$ resonance of the exchanged metallacyclobutene **7** (Figure 4). Data analysis gave $k_{\text{exch}} = (4.9 \pm 0.5) \times 10^{-5} \text{ s}^{-1}$ and $\Delta G^\ddagger_{10 \text{ °C}} = 22.4 \text{ kcal}\cdot\text{mol}^{-1}$.

Since exchange of phosphine with **7** is much faster than rearrangement to **8**, it was not possible to measure both rates at the same temperature. We therefore measured the rate of rearrangement of **7** to **8** by ^1H NMR spectroscopy in CD_3CN between 35 and 65 °C. A linear Eyring plot of $\ln[k/T]$ versus $1/T$ gave $\Delta H^\ddagger = 30.1 \pm 0.9 \text{ kcal}\cdot\text{mol}^{-1}$, $\Delta S^\ddagger = 16.0 \pm 0.9 \text{ eu}$, and $\Delta G^\ddagger_{10 \text{ °C}} = 25.6 \text{ kcal}\cdot\text{mol}^{-1}$. Extrapolation of the rearrangement rate to 10 °C gave $k_{\text{rearr}} = 1.02 \times 10^{-7} \text{ s}^{-1}$.

The rate of exchange of PMe_3 with metallacyclobutene **7** is therefore 480 times faster than the rearrangement of **7** to **8** at 10 °C ($k_{\text{exch}}/k_{\text{rearr}} = [4.9 \times 10^{-5} \text{ s}^{-1}] \div [1.0 \times 10^{-7} \text{ s}^{-1}] = 480$). Inspection of Figure 2 reveals that this is also the rate difference between attack of PMe_3 at the center carbon and the CH_2 terminal carbon of η^3 -propargyl complex **1-t-Bu**. This rate difference corresponds to a 3.2 $\text{kcal}\cdot\text{mol}^{-1}$ difference in free energy of activation ($\Delta\Delta G^\ddagger_{10 \text{ °C}} = 25.6 - 22.4 \text{ kcal}\cdot\text{mol}^{-1}$).

Regioselectivity of addition of PMePh_2 to 1-t-Bu was also determined indirectly by comparing the rates of rearrangement and exchange of rhenacyclobutene $[\text{C}_5\text{Me}_5(\text{CO})_2\text{Re}(\text{CH}_2\text{-C}[\text{PMePh}_2]=\text{CCMe}_3)][\text{BF}_4]$ (**9**). Addition of PMePh_2 to η^3 -propargyl complex **1-t-Bu** at -88 °C led to complete conversion to the rhenacyclobutene **9**, which had characteristic ^1H NMR resonances at δ 0.11 (d, $J = 12.6 \text{ Hz}$, CHH), 1.49 (d, $J = 12.2 \text{ Hz}$, CHH), and 2.39 (d, $J_{\text{PH}} = 12.2 \text{ Hz}$, PCH_3). The reaction of excess PMe_3 with PPh_2Me -substituted metallacyclobutene **9** led to exchange and formation of the more stable PMe_3 -substituted metallacyclobutene **7**. The rate constant for exchange at -40 °C was determined by ^1H NMR spectroscopy: $k = 5.85 \times 10^{-4} \text{ s}^{-1}$, $\Delta G^\ddagger = 16.9 \text{ kcal}\cdot\text{mol}^{-1}$.

Upon warming to room temperature, **9** rearranged to η^2 -alkyne complex $[\text{C}_5\text{Me}_5(\text{CO})_2\text{Re}(\eta^2\text{-Ph}_2\text{MePCH}_2\text{C}\equiv\text{CCMe}_3)][\text{BF}_4]$ (**10**), which had characteristic ^1H NMR resonances at δ 2.45 (d, $J_{\text{PH}} = 13.1 \text{ Hz}$, PCH_3), 4.15 (t, $J = 16.1 \text{ Hz}$, CHH), and 4.72 (t, $J = 15.8 \text{ Hz}$, CHH). The rate of rearrangement of **9** to **10** at -15 °C was measured by ^1H NMR spectroscopy: $k = 3.27 \times 10^{-5} \text{ s}^{-1}$, $\Delta G^\ddagger(-15 \text{ °C}) = 20.3 \text{ kcal}\cdot\text{mol}^{-1}$. The difference between this barrier for rearrangement and the barrier for exchange ($\Delta\Delta G^\ddagger = 20.3 - 16.9 = 3.4 \text{ kcal}\cdot\text{mol}^{-1}$) is similar to the difference in barriers for exchange and rearrangement of PMe_3 -substituted metallacyclobutene **7** and implies a regioselective preference of 960 for addition of PMePh_2 to the center propargyl carbon of **1-t-Bu**.

More Rapid Dissociation of PPh_3 than PMe_3 from Metallacyclobutenes. Previously, we had reported that the addition of PPh_3 to **1-t-Bu** gave the metallacyclobutene complex $[\text{C}_5\text{Me}_5(\text{CO})_2\text{Re}(\text{CH}_2\text{C}(\text{PPh}_3)=\text{CCMe}_3)][\text{BF}_4]$ (**11**), which subsequently rearranged to alkyne complex $[\text{C}_5\text{Me}_5(\text{CO})_2\text{Re}(\eta^2\text{-Ph}_3\text{PCH}_2\text{C}\equiv\text{CCMe}_3)][\text{BF}_4]$ (**12**). In repeating this work, we monitored the reaction of **1-t-Bu** (0.030 M) with PPh_3 (0.063 M) in CD_2Cl_2 by ^1H NMR spectroscopy and found that metallacyclobutene **11** was formed at -78 °C with characteristic low-frequency doublets for the metal-bound CH_2 group at δ 0.14 and 1.1 ($^2J = 12 \text{ Hz}$). When the sample was warmed to -20 °C, the conversion of metallacyclobutene **11** to alkyne complex **12** was observed by ^1H NMR spectroscopy to be 80% complete within 2 h ($\Delta G^\ddagger \approx 18.9(5) \text{ kcal}\cdot\text{mol}^{-1}$). Upon warming to 25

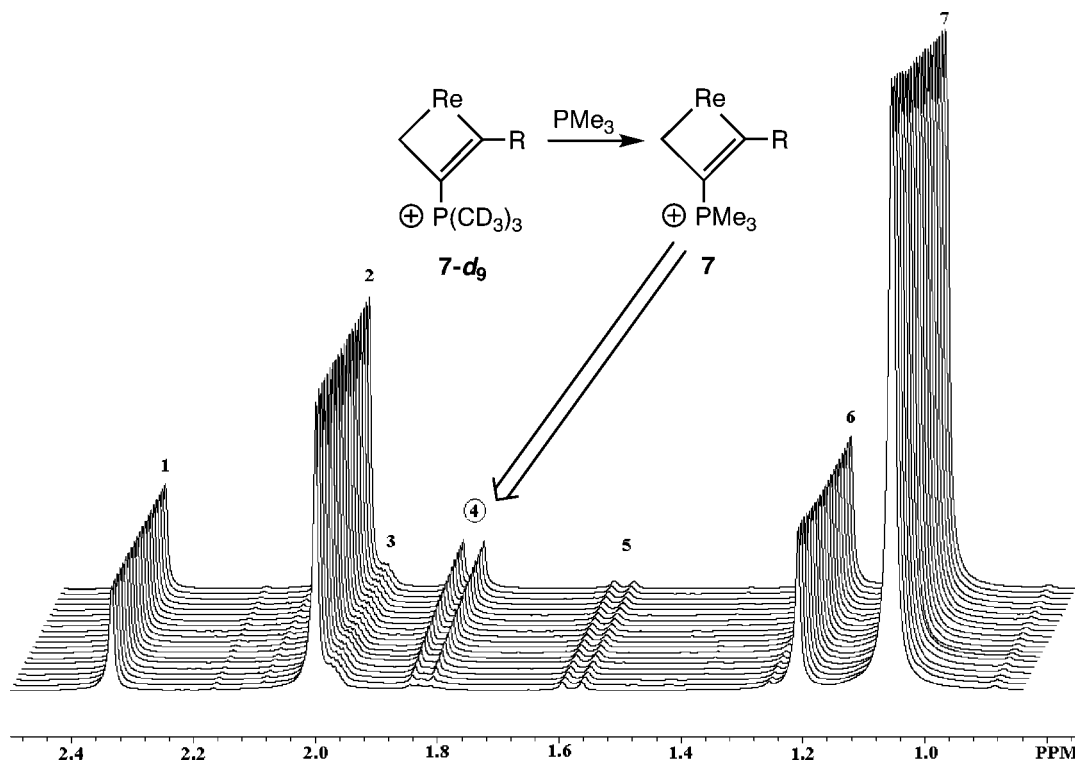
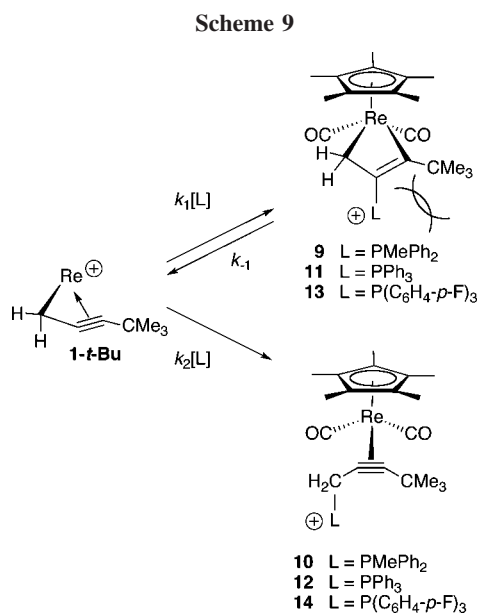


Figure 4. Elapsed time ^1H NMR spectra for exchange at 10°C in CD_3CN : $7\text{-}d_9 + \text{P}(\text{CH}_3)_3$ approaches equilibrium with $7 + \text{P}(\text{CD}_3)_3$. Peak 4, $\text{P}(\text{CH}_3)_3$ of 7 . Other peaks: peak 2, Cp^* of 7 ; 5, CH of 7 ; 6, $t\text{Bu}$ of 7 ; 7, excess $\text{P}(\text{CH}_3)_3$; 1, toluene standard; 3, CD_3CN .



$^\circ\text{C}$, only η^2 -alkyne complex **12** was observed by ^1H NMR spectroscopy (Scheme 9). Note that this rate of rearrangement conflicts with the previously reported slow rearrangement of the metallacycle **11** to η^2 -alkyne complex **12** over 2 days at room temperature in CD_2Cl_2 .¹⁰

The much more rapid rearrangement of the PPh_3 -substituted rhenacyclobutene **9** than the PMe_3 -substituted rhenacyclobutene **7** ($\Delta\Delta G^\ddagger \approx 6.7(5) \text{ kcal} \cdot \text{mol}^{-1}$) implies a correspondingly more rapid dissociation of phosphine from their respective rhenacyclobutenes and can be attributed in part to the greater leaving group ability of the much less nucleophilic PPh_3 group. In addition, the particularly unfavorable steric interaction between the large PPh_3 and the bulky *tert*-butyl group is relieved upon PPh_3 dissociation. The much less congested methyl-substituted

metallacyclobutene $[\text{C}_5\text{Me}_5(\text{CO})_2\text{Re}(\text{CH}_2\text{C}(\text{PPh}_3)=\text{CCH}_3)][\text{BF}_4]$ does not rearrange to either an η^2 -alkyne or η^2 -allene complex even upon extended heating at $50\text{--}60^\circ\text{C}$. Only eventual decomposition is observed.

Observation of Equilibrium between η^3 -Propargyl Complex **1-t-Bu and PPh_3 -Substituted Metallacyclobutene **11**.** Upon close examination of the low-temperature ^1H NMR spectra, it became apparent that the formation of metallacyclobutene **11** did not go to completion and that an equilibrium was established with the η^3 -propargyl complex **1-t-Bu**. After PPh_3 (0.063 M in CD_2Cl_2) was added to a yellow solution of η^3 -propargyl complex **1-t-Bu** (0.030 M in CD_2Cl_2) at -78°C , ^1H NMR spectroscopy at -88°C showed a tiny resonance at δ 3.41 (CHH) characteristic of **1-t-Bu** in addition to intense resonances for the metallacyclobutene **11** (δ 0.14, CHH). Upon increasing the temperature to -66°C , the amount of η^3 -propargyl complex **1-t-Bu** increased and a 9.6:1 equilibrium mixture of **11/1-t-Bu** was observed ($K_{\text{eq}} = [\mathbf{11}]/[\mathbf{1-t-Bu}][\text{PPh}_3] \approx 280 \text{ M}^{-1}$). At -56°C , the amount of the η^3 -propargyl complex increased further, and a 4.5:1 equilibrium mixture of **11/1-t-Bu** was observed ($K_{\text{eq}} \approx 100 \text{ M}^{-1}$). When the sample was recooled to -66°C , the ratio of **11:1-t-Bu** reverted to 9.6:1. At -46°C , the ratio of **11:1-t-Bu** dropped to 1.9:1 ($K_{\text{eq}} \approx 44 \text{ M}^{-1}$). When the temperature was lowered to -66°C , the ratio of **11:1-t-Bu** increased to 10.8:1 ($K_{\text{eq}} \approx 310 \text{ M}^{-1}$). Thus, as the temperature increases, the equilibrium shifts toward η^3 -propargyl complex **1-t-Bu** and free PPh_3 at the expense of the adduct rhenacyclobutene **11** (Figure 5).

When the sample was warmed to -34°C , the ratio of **11:1-t-Bu** fell to 1.1:1 ($K_{\text{eq}} \approx 25 \text{ M}^{-1}$) and some conversion to η^2 -alkyne complex $[\text{C}_5\text{Me}_5(\text{CO})_2\text{Re}(\eta^2\text{-Ph}_3\text{PCH}_2\text{C}\equiv\text{CCMe}_3)][\text{BF}_4]$ (**12**) (16% after 10 min) was seen ($\Delta G^\ddagger \approx 17.5(5) \text{ kcal} \cdot \text{mol}^{-1}$).²¹ At -23.5°C , a 1:2 ratio of **11:1-t-Bu** ($K_{\text{eq}} \approx 11 \text{ M}^{-1}$) was seen along with 56% conversion to the thermodynamically stable η^2 -alkyne complex **12** after 10 min ($\Delta G^\ddagger \approx$

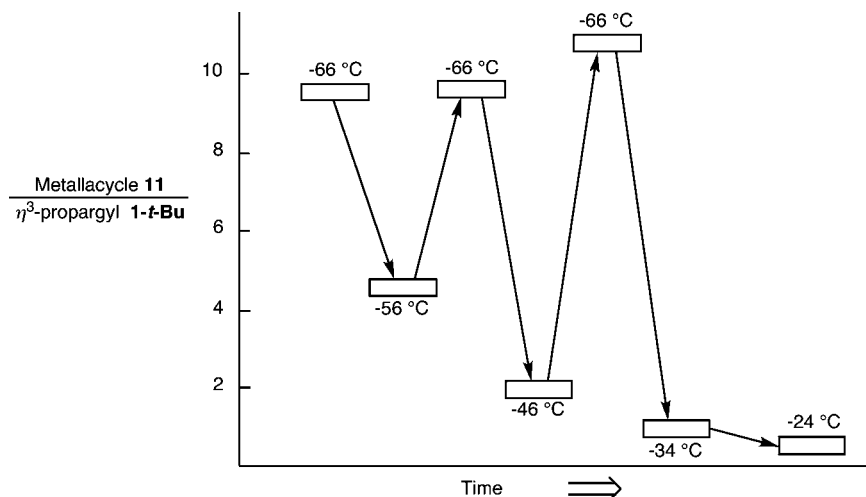


Figure 5. Ratio of rhenacyclobutene **11** to η^3 -propargyl complex **1-t-Bu** as temperature is raised and lowered.

17.8(5) kcal mol⁻¹.²¹ After 1 h at room temperature, complete conversion to **12** was seen. When this solution of η^2 -alkyne complex **12** was recooled to -66 °C, no change in the NMR spectrum was seen, demonstrating that the formation of the thermodynamically stable η^2 -alkyne complex is irreversible.

Additional measurements of the equilibrium between the rhenacyclobutene and the η^3 -propargyl complex carried out using lower concentrations of the PPh₃ (0.042 M in CD₂Cl₂) and the same concentration of η^3 -propargyl complex **1-t-Bu** (0.03 M in CD₂Cl₂) gave similar values for the equilibrium constants. At -66 °C, a 4.5:1 equilibrium mixture of rhenacyclobutene **11**: η^3 -propargyl complex **1-t-Bu** was observed by ¹H NMR spectroscopy ($K_{\text{eq}} \approx 260 \text{ M}^{-1}$). At -46 °C, a 1:1 mixture of **11**/**1-t-Bu** was seen ($K_{\text{eq}} \approx 35 \text{ M}^{-1}$). A van't Hoff plot of all the equilibrium data gave $\Delta H^\circ = -8.0 \pm 1 \text{ kcal} \cdot \text{mol}^{-1}$, $\Delta S^\circ = -25 \pm 3 \text{ eu}$, and $\Delta G^\circ(0 \text{ }^\circ\text{C}) = -1.2 \pm 0.2 \text{ kcal} \cdot \text{mol}^{-1}$.

Equilibrium between η^3 -Propargyl Complex **1-t-Bu and Other Phosphine-Substituted Metallacyclobutenes.** The more nucleophilic phosphine PMePh₂ formed the more stable metallacyclobutene **9**, and the less nucleophilic phosphine P(C₆H₄-*p*-F)₃ formed the less stable metallacyclobutene **13**.

Addition of PMePh₂ (0.05 M in CD₂Cl₂) to η^3 -propargyl complex **1-t-Bu** (0.030 M in CD₂Cl₂) at -88 °C led to complete conversion to rhenacyclobutene **9**. Neither η^3 -propargyl complex **1-t-Bu** nor the stable η^2 -alkyne complex **10** was observed by ¹H NMR spectroscopy below -24 °C. However, upon warming to -13 °C, ¹H NMR spectroscopy showed small amounts of the η^3 -propargyl complex **1-t-Bu** (8%) and of η^2 -alkyne complex **10** (17% after 10 min and increasing amounts at longer times). When the temperature was raised to 8 °C, the amount of η^3 -propargyl complex **1-t-Bu** remained relatively constant (8%) while the amount of rhenacyclobutene complex **9** decreased and the amount of η^2 -alkyne complex **10** increased.

At lower than stoichiometric concentrations of PMePh₂ (0.011 M in CD₂Cl₂) compared to **1-t-Bu** (0.030 M in CD₂Cl₂), a relatively constant 0.43:1 ratio of rhenacyclobutene complex **9** to η^3 -propargyl complex **1-t-Bu** was seen between -88 and -56 °C. Too little free PMePh₂ was present to be observed. When the temperature was increased to -24 °C, some dissociation of PMePh₂ from the metallacycle occurred and the ratio of **9**:**1-t-Bu** decreased to 0.32:1 ($K_{\text{eq}} \approx 80 \text{ M}^{-1}$, $\Delta G(-24 \text{ }^\circ\text{C}) \approx -2.2$

kcal · mol⁻¹).²² When the solution was recooled to -66 °C, the ratio reverted to 0.43:1. When the solution was warmed to -2 °C, the ratio dropped to 0.2:1 ($K_{\text{eq}} \approx 50 \text{ M}^{-1}$, $\Delta G^\circ(-2 \text{ }^\circ\text{C}) \approx -2.1 \text{ kcal} \cdot \text{mol}^{-1}$) and some rearrangement to the thermodynamically stable η^2 -alkyne complex **10** was observed (6% after 5 min). Upon further increasing the temperature to 9 °C, the ratio of **9**:**1-t-Bu** dropped to 0.1:1 ($K_{\text{eq}} \approx 25 \text{ M}^{-1}$, $\Delta G^\circ(9 \text{ }^\circ\text{C}) \approx -1.8 \text{ kcal} \cdot \text{mol}^{-1}$). After 15 min at 9 °C, all the PMePh₂ was consumed and only propargyl complex **1-t-Bu** and η^2 -alkyne complex **10** were observed. A plot of ΔG versus temperature allowed extrapolation to $\Delta G^\circ(0 \text{ }^\circ\text{C}) \approx -2.0 \text{ kcal} \cdot \text{mol}^{-1}$.

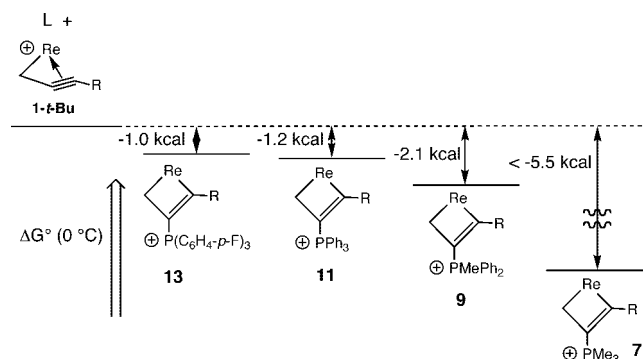


Figure 6. Thermodynamics of rhenacyclobutene formation.

Addition of the less nucleophilic phosphine P(C₆H₄-*p*-F)₃ (0.05 M in CD₂Cl₂) to η^3 -propargyl complex **1-t-Bu** (0.030 M in CD₂Cl₂) at -80 °C led to slow conversion (ΔG^\ddagger (metallacycle formation) $\approx 14.2(8) \text{ kcal} \cdot \text{mol}^{-1}$)²¹ to the rhenacyclobutene [C₅Me₅(CO)₂Re(CH₂C[P(C₆H₄-*p*-F)₃]=CCMe₃)] [BF₄] (**13**), which had characteristic ¹H NMR resonances at δ 0.05 (CHH) and 0.70 (CMe₃). After 2 h, a 1.3:1 equilibrium mixture of **13**/**1-t-Bu** was observed ($K_{\text{eq}} = [\mathbf{13}]/[\mathbf{1-t-Bu}][\text{PAr}_3] \approx 38 \text{ M}^{-1}$). When the solution was warmed to -70 °C, the ratio dropped to 0.56:1 ($K_{\text{eq}} \approx 14 \text{ M}^{-1}$). Upon further increasing the temperature to -60 °C, the ratio of **13**:**1-t-Bu** dropped to 0.2:1 ($K_{\text{eq}} \approx 4.6 \text{ M}^{-1}$). Conversion to the η^2 -alkyne complex [C₅Me₅(CO)₂Re[η^2 -(*p*-F-C₆H₄)₃PCH₂C≡CCMe₃]] [BF₄] (**14**) began at -30 °C and was complete at -20 °C ($\Delta G^\ddagger \approx 17.2(8) \text{ kcal} \cdot \text{mol}^{-1}$).²¹

(22) Because the free phosphine was difficult to observe directly, its concentration was estimated by subtracting the concentration of rhenacyclobutene complex and η^2 -alkyne complex from the initial phosphine concentration. Errors in estimation are considerable, and only very approximate equilibrium constants were obtained.

(21) These approximate ΔG^\ddagger values are obtained from the approximate rates. If rate estimates are off by a factor of 3 at 0 °C, ΔG^\ddagger would be off by 0.6 kcal · mol⁻¹.

Additional measurements of the equilibrium between the **13** and **1-t-Bu** were carried out using a higher concentration of the $P(C_6H_4-p-F)_3$ (0.10 M in CD_2Cl_2), and the same concentration of **1-t-Bu** (0.03 M in CD_2Cl_2) gave similar values for the equilibrium constants. [At $-80^\circ C$, 4.3:1 **13:1-t-Bu**, $K_{eq} \approx 54 M^{-1}$; at $-70^\circ C$, 1.7:1 **13:1-t-Bu**, $K_{eq} \approx 20 M^{-1}$; at $-60^\circ C$, 0.7:1 **13:1-t-Bu**, $K_{eq} \approx 7.6 M^{-1}$.] A van't Hoff plot gave $\Delta H^\circ = -7.2 \pm 0.5 \text{ kcal} \cdot \text{mol}^{-1}$, $\Delta S^\circ = -30 \text{ eu} \pm 4$, and $\Delta G^\circ(0^\circ C) = -1.0 \pm 0.2 \text{ kcal} \cdot \text{mol}^{-1}$.

The equilibrium between PMe_3 -substituted metallacycle **7** and η^3 -propargyl complex **1-t-Bu** lay too far on the side of the metallacycle to be directly observable. A limit on the equilibrium constant can be estimated from the fact that none of **1-t-Bu** was detectable by 1H NMR spectroscopy of 0.1 M solutions of **7**, and 2% of **1-t-Bu** would have been readily detected. This requires $K_{eq} \geq 25\,000 M^{-1}$ and $\Delta G^\circ(0^\circ C) \leq -5.5 \text{ kcal} \cdot \text{mol}^{-1}$. Figure 5 summarizes the thermodynamic information of the equilibrium between rhenacyclobutenes and η^3 -propargyl complex **1-t-Bu**.

Discussion

Thermodynamics of Rhenacyclobutene Formation. It is surprising that the metallacyclobutene complexes and η^3 -propargyl complex **1-t-Bu** are so similar in thermodynamic stability. For PPh_3 , PPh_2Me , and $P(C_6H_4-p-F)_3$, both species were observable in solution and K_{eq} could be measured directly. For PMe_3 , η^3 -propargyl complex **1-t-Bu** was not directly observable, and a limit of $\Delta G^\circ \leq -5.5 \text{ kcal} \cdot \text{mol}^{-1}$ was placed on the stability of the metallacycle. The stability of the metallacycles follows the same order as the nucleophilicity of the phosphines. Steric effects are also important in determining the stability of the metallacycles, as shown by the fact that the metallacycle formed by addition of PPh_3 to Me-substituted η^3 -propargyl complex **1-Me** is much more kinetically stable than the metallacycle **11** formed by addition of PPh_3 to *t*-Bu-substituted **1-t-Bu**.

Kinetics of Exchange and Rearrangement. The kinetics of exchange of phosphines with the metallacycles proceed by a kinetically first-order dissociative mechanism and were measured only for metallacycles **7** and **9**. The barrier for exchange of PMe_3 with PPh_2Me -substituted metallacycle **9** was 5.5 kcal lower than the barrier for PMe_3 exchange with deuterium-labeled metallacycle **7-d₉**. This activation energy difference parallels the thermodynamic stability of the metallacycles and the leaving group ability of the phosphines.

Crude measurements of the rates of rearrangement of all the metallacycles to η^2 -alkyne complexes were made for all the metallacycles. The barriers for rearrangement also paralleled the thermodynamic stability of the metallacycles and the leaving group ability of the metallacycles [ΔG^\ddagger for PMe_3 (25.6) > PPh_2Me (20.3) > PPh_3 (~18) > $P(C_6H_4-p-F)_3$ (~17)].

Regioselectivity of metallacyclobutene formation was too high to be measured directly for all of the phosphines studied. The regioselectivity of PMe_3 addition to **1-t-Bu** was carefully determined by an indirect method: comparison of the rate of exchange of PMe_3 with deuterium-labeled metallacycle **7-d₉** with the rate of rearrangement of metallacycle **7** to η^2 -alkyne complex **8** (Figure 7). The regioselectivity for addition of PMe_3 to the central carbon of **1-t-Bu** was 480:1 ($\Delta\Delta G^\ddagger = 3.2 \text{ kcal} \cdot \text{mol}^{-1}$). Similarly, a similar regioselectivity ($\Delta\Delta G^\ddagger = 3.4 \text{ kcal} \cdot \text{mol}^{-1}$) for addition of PPh_2Me to the central carbon of **1-t-Bu** was estimated from the rate of exchange of PMe_3 with rhenacyclobutene **9** and from the rate of rearrangement of **9** to **10**.

DFT computational studies of rhenium η^3 -propargyl complexes were undertaken to better understand the regioselective addition of nucleophiles to the central propargyl carbon.

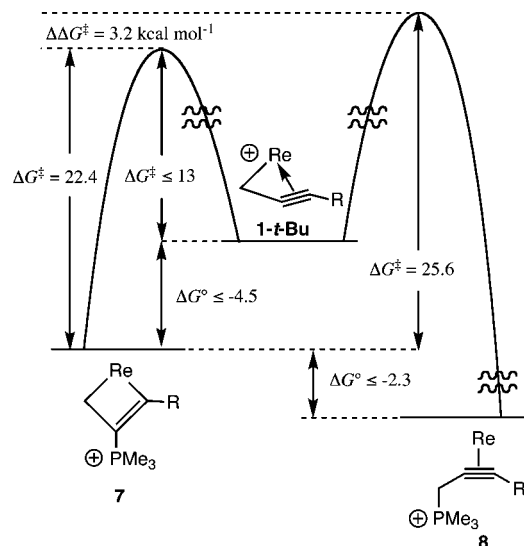


Figure 7. Free energy diagram for reaction of PMe_3 with **1-t-Bu**.

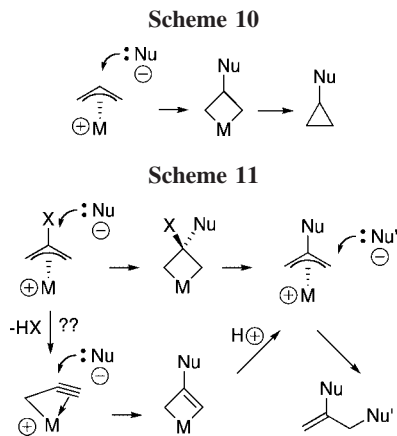
Discussions of nucleophilic addition to η^3 -propargyl complexes usually involve comparisons with well-studied η^3 -allyl complexes.

Transition metal η^3 -allyl complexes usually undergo nucleophilic addition to a terminal carbon,²³ although an increasing number of cases of attack at the central carbon have been reported. The most direct evidence for attack at the central carbon of η^3 -allyl complexes comes from isolation of metallacyclobutenes.²⁴ Formation of cyclopropanes in the reaction of nucleophiles with η^3 -allyl complexes is best explained by attack at the central carbon followed by reductive elimination (Scheme 10).²⁵ η^3 -Allyl complexes having a leaving group such as Cl or OR at the central carbon sometimes react with nucleophiles to give products in which the substituent at the central carbon is replaced by a nucleophile and another nucleophile adds to the

(23) (a) Trost, B. M.; Verhoeven, T. R. In *Comprehensive Organometallic Chemistry*; Wilkinson, G., Stone, F. G. A., Abel, E. W., Eds.; Pergamon: Oxford, UK, 1982; Vol. 8, Chapter 57. (b) Tsujii, J. *Tetrahedron* **1986**, *42*, 4361. (c) Trost, B. M.; Van Vranken, D. L. *Chem. Rev.* **1996**, *96*, 395. (d) Trost, B. M.; Crawley, M. L. *Chem. Rev.* **2003**, *103*, 2921. (e) Trost, B. M. *J. Org. Chem.* **2004**, *69*, 5813.

(24) (a) Ephritikhine, M.; Green, M. L. H.; Mackenzie, R. E. *J. Chem. Soc., Chem. Commun.* **1976**, 619. (b) Ephritikhine, M.; Francis, B. R.; Green, M. L. H.; Mackenzie, R. E.; Smith, M. J. *J. Chem. Soc., Dalton Trans.* **1977**, 1131. (c) Adam, G. J. A.; Davies, S. G.; Ford, K. A.; Ephritikhine, M.; Todd, P. F.; Green, M. L. H. *J. Mol. Catal.* **1980**, *8*, 15. (d) Periana, R. A.; Bergman, R. G. *J. Am. Chem. Soc.* **1984**, *106*, 7272. (e) McGhee, W. D.; Bergman, R. G. *J. Am. Chem. Soc.* **1985**, *107*, 3388. (f) Periana, R. A.; Bergman, R. G. *J. Am. Chem. Soc.* **1986**, *108*, 7346. (g) Tjaden, E. B.; Stryker, J. M. *J. Am. Chem. Soc.* **1990**, *112*, 6420. (h) Wakefield, J. B.; Stryker, J. M. *J. Am. Chem. Soc.* **1991**, *113*, 7057. (i) Tjaden, E. B.; Stryker, J. M. *Organometallics* **1992**, *11*, 16. (j) Tjaden, E. B.; Schwiebert, K. E.; Stryker, J. M. *J. Am. Chem. Soc.* **1992**, *114*, 1100. (k) Schwiebert, K. E.; Stryker, J. M. *Organometallics* **1993**, *12*, 600. (l) Tjaden, E. B.; Stryker, J. M. *J. Am. Chem. Soc.* **1993**, *115*, 2083. (m) Review of metallacyclobutenes: Jennings, P. W.; Johnson, L. L. *Chem. Rev.* **1994**, *94*, 2241.

(25) (a) Hegedus, L. S.; Darlington, W. H.; Russell, C. E. *J. Org. Chem.* **1980**, *45*, 5193. (b) Carfagna, C.; Maniani, L.; Musco, A.; Sallase, G.; Santi, R. *J. Org. Chem.* **1991**, *56*, 3924. (c) Carfagna, C.; Galarini, R.; Musco, A.; Santi, R. *Organometallics* **1991**, *10*, 3956. (d) Hoffmann, H. M. R.; Otte, A. R.; Wilde, A. *Angew. Chem., Int. Ed. Engl.* **1992**, *31*, 234. (e) Wilde, A.; Otte, A. R.; Hoffmann, H. M. R. *J. Chem. Soc., Chem. Commun.* **1993**, 615. (f) Formica, M.; Musco, A.; Pontellini, R.; Linn, K.; Mealli, C. *J. Organomet. Chem.* **1993**, *448*, C6. (g) Carfagna, C.; Galarini, R.; Linn, K.; López, J. A.; Mealli, C.; Musco, A. *Organometallics* **1993**, *12*, 3019. (h) Hoffmann, H. M. R.; Otte, A. R.; Wilde, A.; Menzer, S.; Williams, D. J. *Angew. Chem., Int. Ed. Engl.* **1995**, *34*, 100. (i) Satake, A.; Nakata, T. *J. Am. Chem. Soc.* **1998**, *120*, 10391. (j) Satake, A.; Koshino, H.; Nakata, T. *Chem. Lett.* **1999**, 49. (k) Tjaden, E. B.; Stryker, J. M. *J. Am. Chem. Soc.* **1990**, *112*, 6420. (l) Grigg, R.; Korders, M. *Eur. J. Org. Chem.* **2001**, *4*, 707.



terminal carbon (Scheme 11).²⁶ These reactions have been suggested to proceed by an unusual addition of a nucleophile to the central carbon followed by elimination of the leaving group from the central carbon to give a substituted η^3 -allyl complex, which is then attacked at a terminal carbon by a second nucleophile. However, an alternative mechanism involves elimination of HX from the η^3 -allyl complex to produce an η^3 -propargyl complex, which then undergoes “normal” addition of a nucleophile to the central carbon to produce a metallacyclobutene; protonation of the metallacyclobutene can then produce an η^3 -allyl complex, which is then attacked at a terminal carbon by a second nucleophile.

Several computational studies of η^3 -allyl compounds have addressed the regioselectivity issue and provided insight into the importance of ligand substitution, conformational preference, and the question of orbital control versus charge control.²⁷ Most studies have focused on η^3 -allyl palladium and platinum complexes.²⁸

Green has reported extended Hückel molecular orbital calculations (EHMO) on the neutral η^3 -propargyl molybdenum complex $C_5H_5(\eta^2-HC\equiv CH)Mo(\eta^3-CH_2C\equiv CH)$.²⁹ Although the regiochemistry of nucleophilic addition was not commented upon, the EHMO results indicated a significant difference in calculated atomic charges between the center (positive) and terminal (negative) carbons, which might form the basis of a charge-controlled explanation of addition of nucleophiles to the

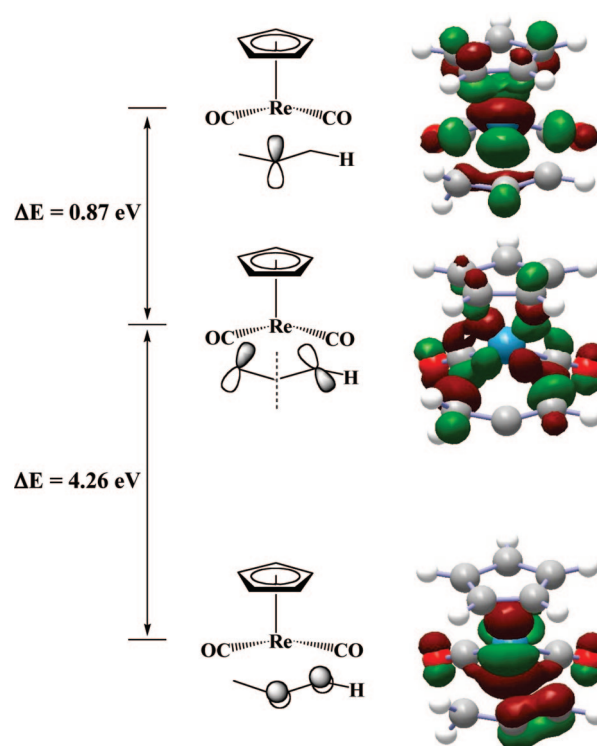


Figure 8. HOMO, LUMO, and LUMO+1 of $[C_5H_5(CO)_2Re(\eta^3-CH_2C\equiv CH)]^+$ (**B**).

center carbon. Wojcicki and Bursten reported³⁰ calculations of the model η^3 -propargyl complex $[(PH_3)_3Pt(\eta^3-CH_2C\equiv CH)]^+$ using the Fenske–Hall (FH) molecular orbital method and later DFT calculations³¹ and concluded that nucleophilic addition to the central η^3 -propargyl carbon was charge controlled.

Since no analogous theoretical studies of mid-transition metal η^3 -propargyl compounds were available, we carried out DFT calculations on the model complex $[C_5H_5(CO)_2Re(\eta^3-CH_2C\equiv CH)]^+$ (**B**) using B3LYP/LANL2DZ,³² available in the Gaussian 94³³ and Gaussian 98³⁴ packages. The molecular orbitals of the η^3 -propargyl fragment may be described as the simple combination of π -systems for its allyl and ethylene fragments. DFT calculations gave an accurate picture of the frontier molecular orbitals (FMOs) for **B** and provided insight into the regioselectivity of nucleophilic additions. The energy diagram and the molecular orbitals of the HOMO, LUMO, and LUMO+1 of **B** are shown in Figure 8.

If kinetic addition of nucleophiles to **B** were orbital controlled, the LUMO of **B** should have a significant coefficient on the central carbon. Since the LUMO calculated for **B** has a node at the center carbon and is concentrated on the terminal carbons, the observed nucleophilic attack at the central carbon is not orbital controlled. If nucleophilic attack at the η^3 -fragment were charge controlled,

(30) Graham, J. P.; Wojcicki, A.; Bursten, B. E. *Organometallics* **1999**, *18*, 837.

(31) Hall, M. B.; Fenske, R. F. *Inorg. Chem.* **1972**, *11*, 768.

(32) Density functional theory (DFT) has been established as an excellent method for calculations involving organometallic compounds. (a) Ziegler, T. *Chem. Rev.* **1991**, *91*, 651. (b) Ziegler, T. *Can. J. Chem.* **1995**, *73*, 743.

(33) Frisch, M. J.; Trucks, G. W.; Schlegel, H. B.; Gill, P. M. W.; Johnson, B. G.; Robb, M. A.; Cheeseman, J. R.; Keith, T.; Petersson, G. A.; Montgomery, J. A.; Raghavachari, K.; Al-Laham, M. A.; Zakrzewski, V. G.; Ortiz, J. V.; Foresman, J. B.; Cioslowski, J.; Stefanov, B. B.; Nanayakkara, A.; Challacombe, M.; Peng, C. Y.; Ayala, P. Y.; Chen, W.; Wong, M. W.; Adres, J. L.; Replogle, E. S.; Gomperts, R.; Martin, R. L.; Fox, D. J.; Binkley, J. S.; Defrees, D. J.; Baker, J.; Stewart, J. P.; Head-Gordon, M.; Gonzalez, C.; Pople, J. A. *Gaussian 94, Revision E.2*; Gaussian, Inc.: Pittsburgh, PA, 1995.

(26) (a) Ohe, K.; Matsuda, H.; Morimoto, T.; Ogoshi, S.; Chatani, N.; Murai, S. *J. Am. Chem. Soc.* **1994**, *116*, 4125. (b) Castaño, A. M.; Aranyos, A.; Szabó, K. J.; Bäckvall, J.-E. *Angew. Chem., Int. Ed. Engl.* **1995**, *34*, 2551. (c) Tsai, F.-Y.; Chen, H.-W.; Chen, J.-T.; Lee, G.-H.; Wang, Y. *Organometallics* **1997**, *16*, 822. (d) Aranyos, A.; Szabó, K. J.; Castaño, A. M.; Bäckvall, J.-E. *Organometallics* **1997**, *16*, 1058. (e) Organ, M. G.; Miller, M. *Tetrahedron Lett.* **1997**, *38*, 8181. (f) Organ, M. G.; Miller, M.; Konstantinou, Z. *J. Am. Chem. Soc.* **1998**, *120*, 9283. (g) Kadota, J.; Komori, S.; Fukumoto, Y.; Murai, S. *J. Org. Chem.* **1999**, *64*, 7523. (h) Kadota, J.; Katsuragi, H.; Fukumoto, Y.; Murai, S. *Organometallics* **2000**, *19*, 979. (i) Organ, M. G.; Arvanitis, E. A.; Hynes, S. J. *J. Org. Chem.* **2003**, *68*, 3918.

(27) (a) Suzuki, T.; Fujimoto, H. *Inorg. Chem.* **1999**, *38*, 370. (b) Sakaki, S.; Takeuchi, K.; Sugimoto, M.; Kurosawa, H. *Organometallics* **1997**, *16*, 2995. (c) Aranyos, A.; Szabó, K. J.; Castaño, A. M.; Bäckvall, J.-E. *Organometallics* **1997**, *16*, 1058. (d) Ward, T. R. *Organometallics* **1996**, *15*, 2836. (e) Carfagna, C.; Galarini, R.; Linn, K.; Lopez, J. A.; Mealli, C.; Musco, A. *Organometallics* **1993**, *12*, 3019. (f) Curtis, M. D.; Eisenstein, O. *Organometallics* **1984**, *3*, 887. (g) Davies, S. G.; Green, M. L. H.; Mingos, D. M. P. *Tetrahedron* **1978**, *34*, 3047.

(28) (a) Kollmar, M.; Goldfuss, B.; Reggelin, M.; Rominger, F.; Helmchen, G. *Chem.-Eur. J.* **2001**, *7*, 4913. (b) Delbecq, F.; Lapouge, C. *Organometallics* **2000**, *19*, 2716. (c) Branchadell, V.; Moreno-Mañas, M.; Pajuelo, F.; Pleixats, R. *Organometallics* **1999**, *18*, 4934. (d) Biswas, B.; Sugimoto, M.; Sakaki, S. *Organometallics* **1999**, *18*, 4015. (e) Hagelin, H.; Åkermark, B.; Norrby, P. O. *Chem.-Eur. J.* **1999**, *5*, 902.

(29) Carfagna, C.; Deeth, R. J.; Green, M.; Mahon, M. F.; McInnes, J. M.; Pellegrini, S.; Woolhouse, C. B. *J. Chem. Soc., Dalton Trans.* **1995**, 3975.

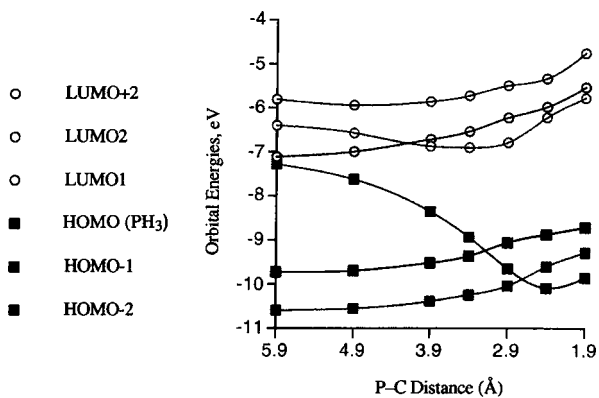


Figure 9. Walsh orbital diagram for approach of PH_3 to the center carbon of **B**.

the charge on the central carbon of the η^3 -propargyl unit should be more positive than that on the terminal carbons. The natural charges computed by the natural population analysis³⁵ subset of the DFT calculation show a greater positive charge on the center carbon and support the hypothesis that the observed kinetic addition to the central carbon is charge controlled (Figure 8).³⁶

The attack of a nucleophile at the central carbon of an η^3 -propargyl complex can be envisioned as attack at LUMO+1, which has a major contribution from the central carbon. Thus, an incoming nucleophile could interact with the slightly higher energy LUMO+1 orbital to avoid steric repulsions at the C_1 and C_3 positions, resulting in a preference for central attack. A linear synchronous transit calculation (LST) was performed to approximate addition of the model nucleophile PH_3 to the central propargyl carbon of **B** to give the model metallacyclobutene complex $[\text{C}_5\text{H}_5(\text{CO})_2\text{Re}(\text{CH}_2\text{C}(\text{PH}_3)=\text{CH})]^+$. Along the reaction coordinate, a rapid decrease in energy of the HOMO (lone pair of PH_3) was observed as the lone pair develops a bonding interaction, and an inversion of the LUMO and LUMO+1 orbitals was observed as the nucleophile approaches (Figure 9). This implies that while charge controls the site of nucleophilic attack, the accessible energy and nodal properties of LUMO+1 allow the attack to proceed smoothly. An exclusive LUMO orbital control argument can be made for the observed η^2 -alkyne and η^2 -allene rearrangement products arising from nucleophilic attack at the terminal carbons.

A similar DFT study of $[(\text{PH}_3)_2\text{Pd}(\eta^3\text{-CH}_3\text{CHC}\equiv\text{CH})]^+$ was performed by Delbecq, Sinou, and co-workers.³⁷ Similar to the results reported here for a rhenium cation, they found that the central propargylic carbon was most positive, that the LUMO

had a node at the central carbon, and that nucleophilic attack at the central carbon involved interaction with LUMO+1. Their conclusion that regioselective attack at the central carbon resulted from a combination of charge control and the availability of a low-lying orbital centered on the middle propargylic carbon is similar to that reported here.

Experimental Section

Rate of Rearrangement of 7 to 8. A CD_3CN solution of **7** (26 mg, 0.04 mmol, 0.085 M) containing toluene as an internal integration standard ($10\ \mu\text{L}$, $8.5\ \mu\text{mol}$) was monitored by ^1H NMR spectroscopy at $64.5\ ^\circ\text{C}$ over 1.5 h. A plot of $\ln[\mathbf{7}]$ versus time was linear to over 3 half-lives ($R^2 > 0.98$) and gave $k_{\text{rearr}} = 7.25 \times 10^{-4}\ \text{s}^{-1}$, $t_{1/2} = 16\ \text{min}$, and $\Delta G^\ddagger = 24.7\ \text{kcal}\cdot\text{mol}^{-1}$.

Measurements were repeated on similarly prepared samples of **7** over the temperature range $35\text{--}55\ ^\circ\text{C}$, and the resulting rates of rearrangement were used in an Eyring plot of k_{obs} versus $1/T$: $k_{\text{obs}}(35\ ^\circ\text{C}) = 9.2 \times 10^{-6}\ \text{s}^{-1}$; $k_{\text{obs}}(44\ ^\circ\text{C}) = 3.1 \times 10^{-5}\ \text{s}^{-1}$; $k_{\text{obs}}(54\ ^\circ\text{C}) = 1.7 \times 10^{-4}\ \text{s}^{-1}$ [see Figure 1-S in the Supporting Information for Eyring plot]. These data provided $\Delta H^\ddagger = 30.1 \pm 0.9\ \text{kcal}\cdot\text{mol}^{-1}$, $\Delta S^\ddagger = 16.0 \pm 0.9\ \text{eu}$, and were used to calculate $\Delta G^\ddagger_{10\ ^\circ\text{C}} = 25.6\ \text{kcal}\cdot\text{mol}^{-1}$, $k_{\text{rearr}} = 1.02 \times 10^{-7}\ \text{s}^{-1}$, $t_{1/2} \approx 78\ \text{days}$.

$[\text{C}_5\text{Me}_5(\text{CO})_2\text{Re}(\text{CH}_2\text{C}(\text{P}(\text{CD}_3)_3)=\text{CCMe}_3)][\text{BF}_4]$ (7-d₉**).** An excess of $\text{P}(\text{CD}_3)_3$ was condensed onto a frozen CH_2Cl_2 solution of **1-t-Bu** (28.2 mg, 0.05 mmol) at $77\ \text{K}$. A pale yellow-green solution was obtained upon brief mixing at room temperature. Volatile material was evaporated to give **7-d₉** in quantitative yield as an off-white flaky powder. ^1H NMR (CD_3CN , 360 MHz, $-20\ ^\circ\text{C}$): δ 0.086 (d, $J = 12.2\ \text{Hz}$, CHH), 1.01 (s, CMe_3), 1.40 (dd, $J = 12.3, 1.1\ \text{Hz}$, CHH), 1.85 (s, C_5Me_5).

Rate of Exchange of $\text{P}(\text{CH}_3)_3$ with 7-d₉. Excess $\text{P}(\text{CH}_3)_3$ was condensed onto a frozen ($77\ \text{K}$) CD_3CN solution of **7-d₉** (30 mg, 0.047 mmol, 0.107 M) containing toluene ($10\ \mu\text{L}$, $8.5\ \mu\text{mol}$) as an internal standard for NMR integration. The sample was melted, thoroughly mixed at $-78\ ^\circ\text{C}$, and transferred to a NMR spectrometer probe precooled to $-20\ ^\circ\text{C}$. Integration showed that its initial concentration of $\text{P}(\text{CH}_3)_3$ was 0.55 M (5 equiv relative to **7-d₉**). The NMR probe was warmed to $10\ ^\circ\text{C}$ (thermocouple calibration), and the appearance of the $\text{P}(\text{CH}_3)_3$ ^1H NMR resonance of **7** (δ 1.79) was monitored versus toluene internal standard. The reaction was monitored for 1.5 half-lives, with a late data point acquired after 3 half-lives [see Figure 2-S in the Supporting Information for kinetic plot]. Exponential fit of the concentration versus time data ($R^2 > 0.98$) gave a calculated equilibrium concentration for **7** (0.0979 M) and $k_{\text{exch}} = (4.9 \pm 0.5) \times 10^{-5}\ \text{s}^{-1}$, $t_{1/2} = 3.9\ \text{h}$, and $\Delta G^\ddagger = 22.1\ \text{kcal}\cdot\text{mol}^{-1}$.

Acknowledgment. Financial support was provided by the National Science Foundation (CHE-0209476). Grants from the NSF (CHE-9629688) and NIH (I S10 RR04981-01) for the purchase of NMR spectrometers are acknowledged. We thank Dr. Douglas R. Powell for assistance with X-ray crystallography, Dr. Charles Fry for assistance with NMR spectrometry, and Professor Frank A. Weinhold for assistance with computations.

Supporting Information Available: General experimental information, experimental procedures, additional free energy diagrams for reactions of phosphines with **1-t-Bu₃**, information on rearrangement of diphosphine-substituted metallacyclobutenes, selected computational output for $[\text{C}_5\text{H}_5(\text{CO})_2\text{Re}(\eta^3\text{-CH}_2\text{C}\equiv\text{CH})]^+$ (**B**), X-ray crystallographic data for **8-Cl** and $\{\text{C}_5\text{Me}_5(\text{CO})_2\text{Re}[\eta^2\text{-}(\text{Ar}_2\text{PCH}_2\text{CH}_2\text{PPh}_2)\text{CH}_2\text{C}\equiv\text{CCMe}_3]\}[\text{BF}_4] \cdot 2\text{CH}_2\text{Cl}_2$ (**18-CH₂Cl₂**). This material is available free of charge via the Internet at <http://pubs.acs.org>.

(34) Frisch, M. J.; Trucks, G. W.; Schlegel, H. B.; Scuseria, G. E.; Robb, M. A.; Cheeseman, J. R.; Zakrzewski, V. G.; Montgomery, J. A., Jr.; Stratmann, R. E.; Burant, J. C.; Dapprich, S.; Millam, J. M.; Daniels, A. D.; Kudin, K. N.; Strain, M. C.; Farkas, O.; Tomasi, J.; Barone, V.; Cossi, M.; Cammi, R.; Mennucci, B.; Pomelli, C.; Adamo, C.; Clifford, S.; Ochterski, J.; Petersson, G. A.; Ayala, P. Y.; Cui, Q.; Morokuma, K.; Malick, D. K.; Rabuck, A. D.; Raghavachari, K.; Foresman, J. B.; Cioslowski, J.; Ortiz, J. V.; Baboul, A. G.; Stefanov, B. B.; Liu, G.; Liashenko, A.; Piskorz, P.; Komaromi, I.; Gomperts, R.; Martin, R. L.; Fox, D. J.; Keith, T.; Al-Laham, M. A.; Peng, C. Y.; Nanayakkara, A.; Challacombe, M.; Gill, P. M. W.; Johnson, B.; Chen, W.; Wong, M. W.; Andres, J. L.; Gonzalez, C.; Head-Gordon, M.; Replege, E. S.; Pople, J. A. *Gaussian 98, Revision A.9*; Gaussian, Inc.: Pittsburgh, PA, 1998.

(35) (a) Glendenning, E. D.; Badenhop, J. K.; Reed, A. E.; Carpenter, J. E.; Weinhold, F. *NBO 4.0*; Theoretical Chemistry Institute, University of Wisconsin: Madison, WI, 1996. (b) Reed, A. E.; Weinstock, R. B.; Weinhold, F. *J. Chem. Phys.* **1985**, *83*, 735.

(36) The Mulliken charges show a similar trend, with the central carbon being most positive: $\text{CH}_2(+.091)\text{--C}(+0.357)\text{--CH}(+0.005)$.

(37) Labrosse, J.-R.; Lhoste, P.; Delbecq, F.; Sinou, D. *Eur. J. Org. Chem.* **2003**, 2813.

Radical Coupling of Iodocarbonyl Compounds with Butenylindium Generated by Transmetalation between Cyclopropylmethylstannane and Indium Halides

Makoto Yasuda, Kensuke Kiyokawa, Kenji Osaki, and Akio Baba*

Department of Applied Chemistry, Center for Atomic and Molecular Technologies, Graduate School of Engineering, 2-1 Yamadaoka, Suita, Osaka 565-0871, Japan

Received September 19, 2008

The reaction of cyclopropylmethylstannane **1** with α -iodocarbonyl compounds **2** in the presence of either InBr_3 or InCl_3 gave the C–C coupling products **3**. Various types of iodocarbonyl compounds such as esters, amides, and ketones were applied to this system to afford the corresponding cyclopropylethyl-substituted carbonyls **3**. Transmetalation between cyclopropylmethylstannane and indium halides afforded butenylindium dihalide and dibutenylindium halide, as confirmed by NMR spectroscopy. The reactivity of dibutenylindium halide was greater than that of monobutenyl species. The active species, dibutenylindium halide, was stabilized by complexation using DPPE, and its structure was analyzed using X-ray crystallography. The solid state of the complex shows a linear structure with a core $(-\text{Cl}-\text{In}-\text{Cl}-\text{In}-\text{P}-\text{C}-\text{C}-\text{P}-\text{In}-)$ _n with five-coordinated indium centers. The reaction between **1** and **2**, mediated by indium halides, proceeded in a radical manner. The *in situ*-generated alkylindium species and a small amount of oxygen, which can be supplied by atmospheric air, initiated the radical reaction.

Introduction

Cyclopropylmethylstannane has the potential to introduce a cyclopropyl ring to organic molecules through C–C bond formation. Although some examples using cyclopropylmethylstannane were reported by Young, only ring-opening reactions took place with inorganic reagents such as SO_2 , Brønsted acid, or iodine.¹ The lack of a suitable activation method creates difficulty in the control of cyclopropylmethylstannane for carbon–carbon bond formation. There are some examples of starting from a butenylmetal species instead of a cyclopropylmethyl compound to introduce cyclopropylmethyl groups in organic compounds. For example, there is the reaction of butenylstannane with acetals, acid chlorides, and aldehydes in the presence of Lewis acids to form cyclopropylmethylated products.^{2,3} *In situ*-generated butenylgallium, -indium, and -aluminum from butenyl Grignard reagents with metal halides are assumed, and they couple with α -halocarbonyls in the presence of Et_3B as a radical initiator.⁴ However, the reaction using cyclopropylmethylstannane for introduction of the cyclopropyl ring through C–C bond formation has never been reported as far as we know.

In this paper, we report a radical coupling of cyclopropylmethylstannane with α -halocarbonyl compounds mediated by indium halides. In this system, no additional radical initiator

was required. Effective transmetalation between the stannane and indium halides gives the butenylindium species, as confirmed by NMR spectroscopy and X-ray analysis. The use of the stannane is advantageous because it allows smooth and clean transmetalation, and the byproduct, halostannane, had no effect on the reaction system.

Results and Discussion

Reaction of Cyclopropylmethylstannane **1 with α -Iodocarbonyl **2a**.** The reaction of cyclopropylmethylstannane **1** with phenyl 2-iodoacetate **2a** in the presence of 0.5 equiv of InBr_3 gave the corresponding coupling product **3a** in 73% yield in toluene and a nitrogen-flowing flask (Table 1, entry 1). Although a trace amount of the ring-opening product, which was not precisely identified,⁵ was observed, the effective introduction of a cyclopropyl group was accomplished. Without additives, there was no reaction (entry 2). Some solvents, such as Et_2O or MeCN , gave lower yields, and no reaction was observed in THF, probably due to strong solvent coordination (entries 4–6). Exposure to air improved the yield of **3a** (entry 7). The other indium halides, InCl_3 or InI_3 , gave lower yields (entries 8 and 9). GaCl_3 also gave a high yield of **3a** (entry 10), but AlCl_3 afforded phenyl 4-iodohexanoate in 41% yield with a trace amount of **3a** (entry 11). In the reaction using $\text{BF}_3 \cdot \text{OEt}_2$ as an additive, a low yield of **3a** was obtained and the rearranged species, butenylstannane, was confirmed after the reaction (entry 12).¹ When ZnCl_2 , TiCl_4 , ZrCl_4 , HfCl_4 , or SnCl_2 was used as additive, satisfactory yields were not obtained (entries 13–17). The loading of a catalytic amount of galvinoxyl suppressed the reaction (entry 18), and thus the reaction proceeds via a radical mechanism.

Investigation of Active Species. To gain a thorough understanding of the active species, the relationship between the

* Corresponding author. E-mail: baba@chem.eng.osaka-u.ac.jp.

(1) (a) Lucke, A. J.; Young, D. J. *J. Org. Chem.* **2005**, *70*, 3579–3583. (b) Lucke, A. J.; Young, D. J. *Tetrahedron Lett.* **1991**, *32*, 807–810.

(2) (a) Sugawara, M.; Yoshida, J. *Chem. Commun.* **1999**, 505–506. (b) Sugawara, M.; Yoshida, J. *Tetrahedron* **2000**, *56*, 4683–4689.

(3) (a) Peterson, D. J.; Robbins, D. *Tetrahedron Lett.* **1972**, *13*, 2135–2138. (b) Peterson, D. J.; Robbins, D.; Hansen, J. R. *J. Organomet. Chem.* **1974**, *73*, 237–250. (c) Herndon, J. W.; Harp, J. J. *Tetrahedron Lett.* **1992**, *33*, 6243–6246. (d) Ueno, Y.; Ohta, M.; Okawara, M. *Tetrahedron Lett.* **1982**, *23*, 2577–2580. (e) Nicolaou, K. C.; Claremon, D. A.; Barnette, W. E.; Seitz, S. P. *J. Am. Chem. Soc.* **1979**, *101*, 3704–3706.

(4) Usugi, S.-i.; Tsuritani, T.; Yorimitsu, H.; Shinokubo, H.; Oshima, K. *Bull. Chem. Soc. Jpn.* **2002**, *75*, 841–845.

(5) (a) Sakurai, H.; Inai, T.; Hosomi, A. *Tetrahedron Lett.* **1977**, *18*, 4045–4048. (b) Hatanaka, Y.; Kuwajima, I. *Tetrahedron Lett.* **1986**, *27*, 719–722.

Table 1. Optimization of Reaction Conditions^a

entry	additive	solvent	yield, %
1	InBr ₃	toluene	73
2	none	toluene	0
3	InBr ₃	CH ₂ Cl ₂	76
4	InBr ₃	Et ₂ O	42
5	InBr ₃	MeCN	17
6	InBr ₃	THF	0
7 ^b	InBr ₃	toluene	79
8	InCl ₃	toluene	50
9	InI ₃	toluene	57
10	GaCl ₃	toluene	71
11	AlCl ₃	toluene	<5 ^c
12	BF ₃ ·OEt ₂	toluene	9
13	ZnCl ₂	toluene	0
14	TiCl ₄	toluene	13
15	ZrCl ₄	toluene	0
16	HfCl ₄	toluene	0
17	SnCl ₂	toluene	0
18	InBr ₃ ^d	toluene	<5

^a All entries were carried out at room temperature in solvent (1 mL) with 1.0 mmol of **1**, 1.0 mmol of **2a**, and 0.5 mmol of additive. ^b Exposure to air (15 min). ^c Phenyl 4-iodohexanoate was formed (41% yield). ^d Addition of galvinoxyl (0.1 mmol).

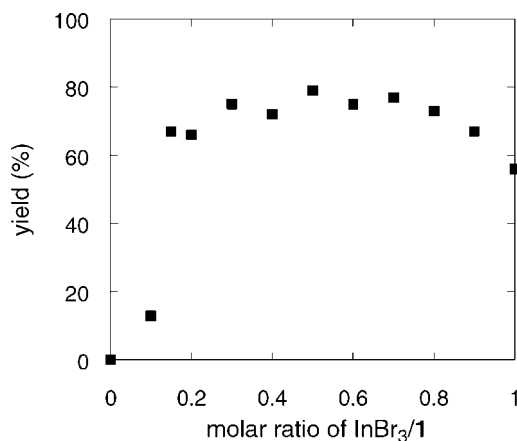


Figure 1. Relationship between amount of InBr₃ and the yield of **3a** in the reaction of **1** (1 mmol) with **2a** (1 mmol) at rt for 4.5 h.

loading ratio of InBr₃/1 and the product yield was investigated in the reaction of **1** with **2a**, and the results are shown in Figure 1. As the ratio InBr₃/1 increased from 0.1 to 0.5, higher yields of **3a** were obtained, and ca. 0.5 equiv of InBr₃ afforded the highest yield. It was curious that ca. 0.3 equiv of InBr₃ also gave a relatively high yield, while the yield was reduced when 1.0 equiv of InBr₃ was used. These results suggest generation of different active species as a result of varying the ratio of InBr₃/1.

As confirmation of the conclusion demonstrated by the results in Figure 1, we examined the three types of mixtures of InBr₃ and **1** with the ratios of 1/1, 1/2, and 1/3 (= InBr₃/1) using NMR spectroscopy (Figure 2). The 1/1 mixture of InBr₃/1 gave two types of butenyl-substituted species that were assumed to be butenylindium dibromide **4** and dibutenylindium bromide **5** generated by transmetalation (spectrum a). One species that is reasonable for dibutenylindium bromide **5** was observed when mixed at a ratio of 1/2 (InBr₃/1) (spectrum b). No other highly substituted species were found from the 1/3 mixture (InBr₃/1), and only dibutenylindium species **5** and unreacted **1** were

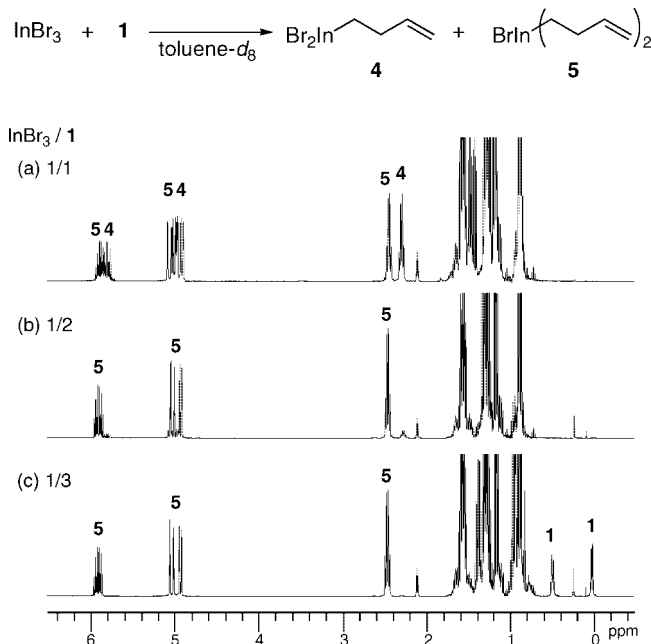


Figure 2. ¹H NMR spectra of the reaction mixtures of InBr₃ and **1** with (a) 1/1, (b) 1/2, and (c) 1/3 ratios in toluene-*d*₈.

observed (spectrum c). The mass spectrum of the 1/2 mixture of InBr₃/1 gave the molecular ion corresponding to the dibutenylindium species [calculated for (C₈H₁₄In), 225.0134; found for *m/z*, 225.0134]. The dibutenyl species **5** was more reactive than **4**, as evidenced by more rapid consumption of **5** than of **4** when iodoester **2a** was added to a mixture that included both **4** and **5** (see Supporting Information). The amount of **4** remained nearly constant until **5** was completely consumed. Both butenyl groups on **5** were transferred to the product prior to transfer of the butenyl group on **4**. The amount of the monobutenyl species **4** was decreased after **5** had disappeared (see Supporting Information). The result that loading 1.0 equiv of InBr₃ resulted in low efficiency, as shown in Figure 1, is consistent with the greater production of the less reactive monosubstituted indium species. Transmetalation of allylic stannane or hydrostannane with indium halides is widely reported,^{6,7} but this is the first example where transmetalation of cyclopropylmethylstannane results in a homoallylic building block.⁸

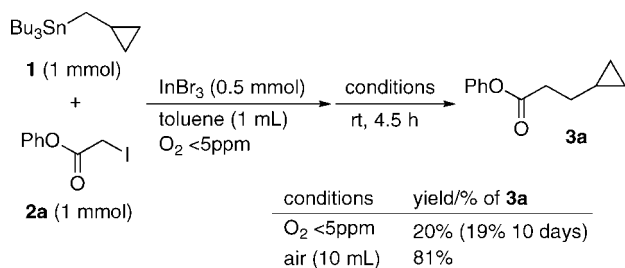
Reaction Mechanism. To investigate the effect of air on the coupling reaction shown in Table 1, the InBr₃-mediated reaction of **1** with **2a** was performed in a nitrogen-filled glovebox (O₂ < 5 ppm), as shown in Scheme 1. The reaction gave **3a** in 20% yield after 4.5 h (19% yield even after 10 days). On the other hand, loading 10 mL of air through a syringe into the mixture of **1**, **2a**, and InBr₃ prepared in the glovebox gave **3a** in 81% yield after stirring for 4.5 h. These results suggest that oxygen plays an important role in the generation of radical species like

(6) (a) Yasuda, M.; Miyai, T.; Shibata, I.; Baba, A.; Nomura, R.; Matsuda, H. *Tetrahedron Lett.* **1995**, *36*, 9497–9500. (b) Miyai, T.; Inoue, K.; Yasuda, M.; Baba, A. *Synlett* **1997**, 699–700. (c) Inoue, K.; Shimizu, Y.; Shibata, I.; Baba, A. *Synlett* **2001**, 1659–1661. (d) Miyai, T.; Inoue, K.; Yasuda, M.; Shibata, I.; Baba, A. *Tetrahedron Lett.* **1998**, *39*, 1929–1932. (e) Inoue, K.; Yasuda, M.; Shibata, I.; Baba, A. *Tetrahedron Lett.* **2000**, *41*, 113–116. (f) Inoue, K.; Sawada, A.; Shibata, I.; Baba, A. *Tetrahedron Lett.* **2001**, *42*, 4661–4663. (g) Baba, A.; Shibata, I. *Chem. Rec.* **2005**, *5*, 323–335.

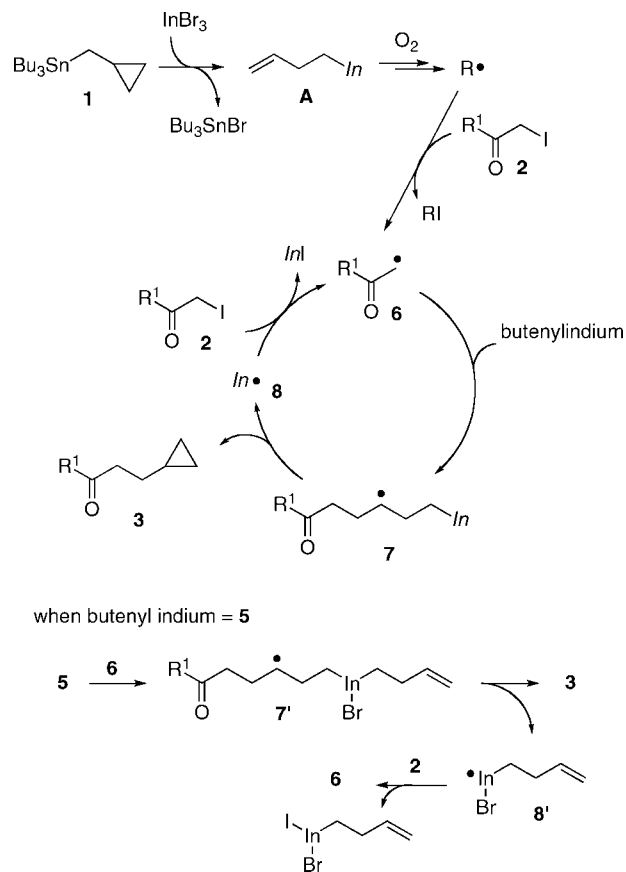
(7) Marshall, J. A.; Hinkle, K. W. *J. Org. Chem.* **1995**, *60*, 1920–1921.

(8) We examined the transmetalation of **1** with AlCl₃ but observed only butenylstannane as a rearranged product. GaCl₃ gave butenylgallium species in the reaction with **1**, and further studies are now in progress.

Scheme 1. Effect of Air on the Coupling Reaction



Scheme 2. Plausible Reaction Mechanism



the O_2 – Et_3B system.⁹ In our system, use of another radical initiator is not necessary, as exposure to air is sufficient to initiate the coupling reaction. The *in situ*-generated butenylindium species acts as a radical initiator as well as an alkylating reagent. The conventional experimental bench procedure (not in a glovebox) using a nitrogen-flow system may have adequate oxygen to accelerate the reaction system.

A plausible reaction mechanism is shown in Scheme 2. Transmetalation between 1 and InBr_3 gives butenylindium species A (other butenyl group and/or ligands are omitted on In). Oxygen-assisted radical initiation abstracts iodine from the iodocarbonyl compound 2.⁹ The generated acylmethyl radical 6 is trapped by butenylindium to give the radical species 7. Species 7 cyclizes with elimination of the indium radical 8,

(9) (a) Nozaki, K.; Oshima, K.; Utimoto, K. *J. Am. Chem. Soc.* **1987**, *109*, 2547–2549. (b) Miura, K.; Ichinose, Y.; Nozaki, K.; Fugami, K.; Oshima, K.; Utimoto, K. *Bull. Chem. Soc. Jpn.* **1989**, *62*, 143–147. (c) Yorimitsu, H.; Nakamura, T.; Shinokubo, H.; Oshima, K.; Omoto, K.; Fujimoto, H. *J. Am. Chem. Soc.* **2000**, *122*, 11041–11047. (d) Ollivier, C.; Renaud, P. *Chem. Rev.* **2001**, *101*, 3415–3434. (e) Yorimitsu, H.; Oshima, K. In *Radicals in Organic Synthesis*; Renaud, P.; Sibi, M. P. Eds.; Wiley-VCH: Weinheim, 2001; Vol. 1, Chapter 1.2.

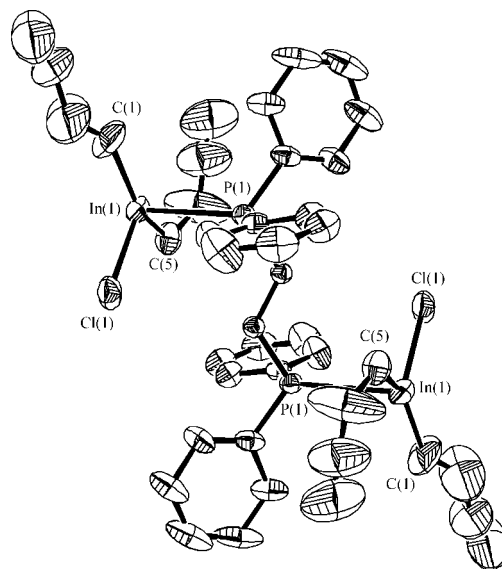
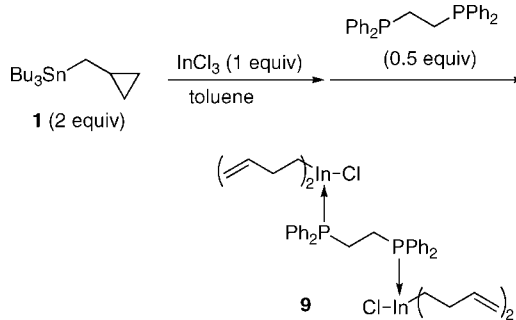


Figure 3. ORTEP drawing of molecular structure of dibutenylindium chloride–DPPE complex 9 (all hydrogens are omitted for clarity).

Scheme 3. Isolation of Butenylindium Species



which abstracts iodine from 2, and the acylmethyl radical 6 is regenerated. When the radical species 6 is trapped by dibutenylindium bromide 5, the resulting indium radical, butenylindium(II) bromide 8', is generated via 7'. The species 8' abstracts the iodine of 2 to give 6 and butenylbromoindium(III) iodide. Because the formed butenylbromoindium(III) iodide is close to radical 6, fast coupling between them takes place effectively.¹⁰ This mechanism is consistent with the observation that both butenyl groups on dibutenylindium bromide 5 are preferentially consumed over the butenyl group on 4. Species 7 could abstract an iodine from 2 to afford an iodinated compound, which then cyclizes into product 3.¹¹ However, this mechanism does not explain the rate difference between the butenyl groups on 5 and 4. Another interesting point is that the byproduct halostannane is not likely to affect the reaction system, and transmetalation starting from tin compounds is quite effective.

X-ray Analysis of Butenylindium Generated by Transmetalation. Complexation of the active species in the reaction system by various ligands was examined to prove that butenylindium species were generated using X-ray analysis of

(10) It might also be explainable that the iodoindium species has a high reactivity toward the carbonyl compound. The halogens on the indium center dramatically affect the reactivity of oxy-functionalized compounds; for example: Nishimoto, Y.; Yasuda, M.; Baba, A. *Org. Lett.* **2007**, *9*, 4931–4934. The iodine might supply high reactivity in this case.

(11) A halogen substitution reaction using alkylindium species toward haloalkenes was reported: Nomura, R.; Miyazaki, S.-i.; Matsuda, H. *J. Am. Chem. Soc.* **1992**, *114*, 2738–2740.

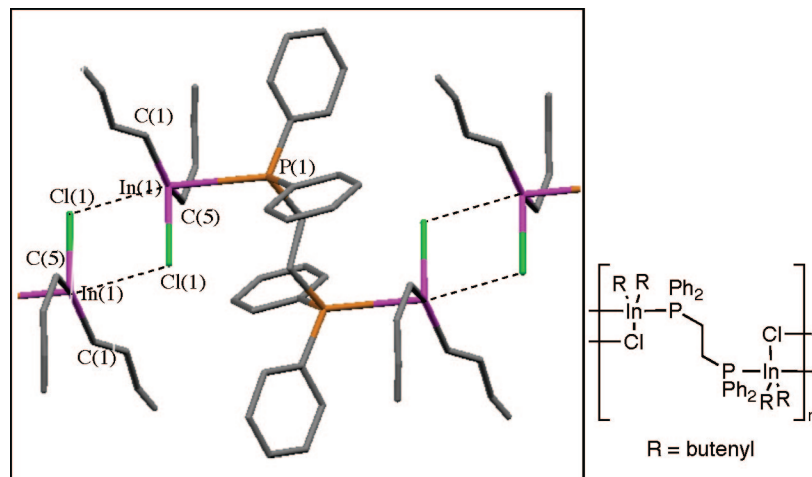


Figure 4. Molecular structure and its intermolecular contacts of dibutenylindium chloride–DPPE complex **9** (all hydrogens are omitted for clarity). Selected bond angles (deg) and lengths (Å): C(1)–In(1)–C(5) 146.6(3), C(1)–In(1)–Cl_{eq}(1) 106.5(3), C(5)–In(1)–Cl_{eq}(1) 105.93(17), P(1)–In(1)–Cl_{ax}(1) 169.95(2), P(1)–In(1)–Cl_{eq}(1) 88.73(3), In(1)–C(1) 2.145(11), In(1)–C(5) 2.148(6), In(1)–P(1) 2.9264(11), In(1)–Cl_{eq}(1) 2.5011(17), In(1)–Cl_{ax}(1) 2.9899(13).

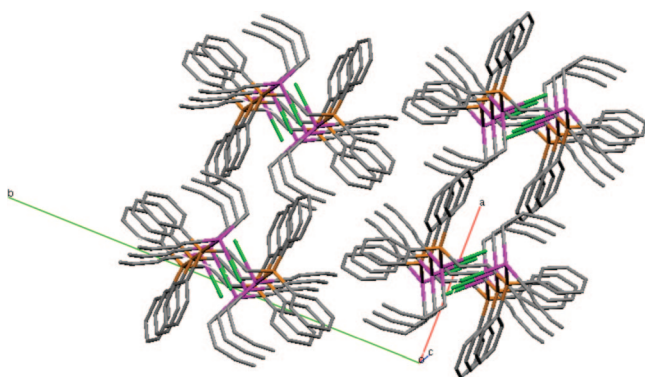


Figure 5. Packing structure of dibutenylindium chloride–DPPE complex **9** (all hydrogens are omitted for clarity).

isolated compounds. Among various ligands and indium sources employed, DPPE and InCl₃ gave a crystal of dibutenylindium complex **9** that was suitable for X-ray analysis, as shown in Scheme 3.

The ORTEP drawing of the indium complex **9** and its intermolecular contacts are shown in Figures 3 and 4. The five-coordinated indium centers had two butenyl groups, a phosphorus in DPPE, and two chlorines. Each chlorine binds two indium centers by bridging.¹² Although DPPE is often used as a bidentate ligand, each phosphine moiety in **9** independently coordinates to different indium centers. The indium center exhibited a distorted trigonal bipyramidal structure with bond angles of C–In–C (146.6°) and C–In–Cl (106.5° and 105.9°), the sum of which was 359°. P–In–Cl exhibited bond angles of 169.95° and 88.73°. The lengths of the two In–C bonds were 2.145 and 2.148 Å. The lengths of the other three bonds around the indium, In–P, In–Cl_{eq}, and In–Cl_{ax}, were 2.926, 2.501, and 2.990 Å, respectively. This is the first example of X-ray crystallographic analysis of a butenylindium species.

Because two In–Cl moieties interact with each other and the phosphines in DPPE independently coordinate to indium centers, the packing structure is clearly linear with a core (–Cl–In–

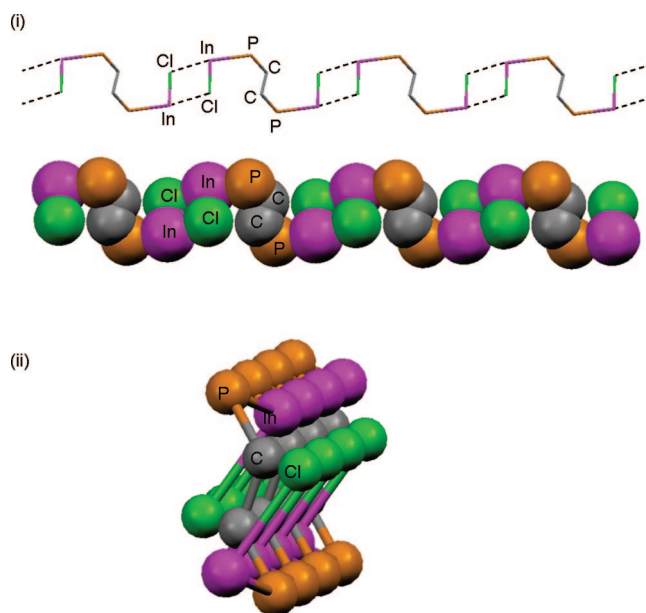
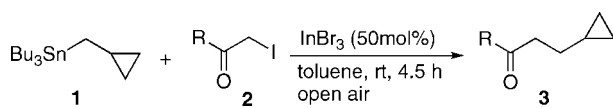


Figure 6. Part of a linear shaped structure of dibutenylindium chloride–DPPE complex **9** (In, P, and carbons of DPPE are shown only for clarity). Views along the *a* axis and *c* axis (with a slight deviation) are shown in (i) and (ii), respectively.

Cl–In–P–C–C–P–In–), as shown in Figures 5 and 6. The unit has a length of ca. 10 Å. The view along the *c* axis of the linear structure exhibits three types of atoms (P, In, Cl) in a linear arrangement at close distances. This arrangement appears promising for new materials, although applications of this compound have not yet been investigated.

Synthesis of Cyclopropylethyl Carbonyl Compounds 3. Table 2 shows the scope and limitations of using the reaction system for various substrates. The reactions were carried out with exposure to air through the CaCl₂ drying tube. Primary iodoesters **2a–d** (entries 1–4) effectively gave the corresponding coupling products, the cyclopropylethyl carbonyl compounds **3a–d**. Although the *tert*-butyl ester **2e** gave a low yield, in the absence of air, the yield increased to 53% (entry 5).¹³ The coupling also proceeded with secondary substrates **2f–h** in moderate to high yields (entries 6–8). A high yield was obtained for the reaction with iodolactone **2i** (entry 9). The reaction with

(12) (a) Schachner, J. A.; Lund, C. L.; Burgess, I. J.; Quail, J. W.; Schatte, G.; Müller, J. *Organometallics* **2008**, *27*, 4703–4710. (b) Schachner, J. A.; Lund, C. L.; Quail, J. W.; Müller, J. *Organometallics* **2005**, *24*, 4483–4488.

Table 2. Reaction of **1** with α -Iodocarbonyl Compounds **2**^a

entry	iodocarbonyl	yield/ % (under N ₂) ^c
1	2a	3a 79 (64)
2 ^b	2b	3b 71 (56)
3	2c	3c 66 (62)
4	2d	3d 68 (50)
5	2e	3e 11 (53)
6	2f	3f 48 (46)
7	2g	3g 47 (79)
8	2h	3h 65 (47)
9	2i	3i 80 (98)
10	2j	3j <5 (<5)
11 ^{b,d}	2k	15 (30)
12 ^{b,d}	2k	3k 54 (62)
13	2l	3l 71 (67)

^a All entries were carried out at room temperature in solvent (1 mL) with 1.0 mmol of **1**, 1.0 mmol of **2**, and 0.5 mmol of InBr₃. Tin compound **1** was added to the mixture of **2** and InBr₃ in toluene.

^b Iodocarbonyl **2** was added to the mixture of **1** and InBr₃ in toluene that had been previously stirred at room temperature for 30 min. ^c Reactions were carried out on the bench using a nitrogen-flowing flask. ^d Reactions were carried out at 100 °C.

the tertiary iodoester **2j** resulted in a low yield (entry 11). Instead of iodoesters, iodoamide **2k** and iodoketone **2l** gave the corresponding products in satisfactory yields (entries 12 and 13). A conventional reaction procedure, which used a nitrogen-flow flask on the bench whereby a very small amount of oxygen was introduced, gave yields that were nearly identical to those obtained under air, although in some cases lower yields were obtained.

Conclusion

This paper describes the transmetalation of cyclopropylmethylstannane with indium halides to give dibutenylindium halide and butenylindium dihalide. This transmetalation can be applied to the reactions with iodocarbonyls to give coupling products that bear cyclopropyl groups. This reaction does not

require a radical initiator. Open air conditions sometimes accelerated the radical reaction pathway. The generated dibutenylindium species was stabilized by a phosphine ligand, and the resulting complex was analyzed using X-ray crystallography. The butenylindium species was used as an alkylating reagent without a radical initiator. Transmetalation starting from the stannane proceeded in an effective and clean manner for the synthesis of interesting cyclopropylated carbonyl compounds.

Experimental Section

General Procedures. IR spectra were recorded as thin films or as solids in KBr pellets on a HORIBA FT-720 spectrophotometer. ¹H and ¹³C NMR spectra were obtained with a 400 and 100 MHz spectrometer, respectively, with TMS as internal standard. ¹¹⁹Sn NMR spectra were obtained with a 150 MHz spectrometer with Me₄Sn as external standard. Mass spectra were recorded on a JEOL JMS-DS303. All reactions were carried out under nitrogen. Column chromatography was performed on silica gel (Merck C60). Recycle GPC was performed with CHCl₃ as the eluent. Bulb-to-bulb distillation (Kugelrohr) was accomplished in a Sibata GTO-250RS at the oven temperature and pressure indicated. Yields were determined by GLC or ¹H NMR using internal standards.

Materials. Dehydrated toluene, dichloromethane, Et₂O, acetonitrile, and THF were purchased and used as obtained. The additives examined in Table 1 were also purchased from commercial sources. Cyclopropylmethylstannane **1** was prepared as previously described.^{1a} All iodocarbonyls **2a–l** were prepared according to the known method.¹⁴ The spectral data of **2d**,¹⁵ **2e**,¹⁶ **2g**,¹⁷ **2h**,¹⁴ **2i**,¹⁸ **2k**,¹⁹ and **2l**²⁰ were in excellent agreement with the reported data. The spectral data of **2c** were in an excellent agreement with those obtained for the commercially available product. The synthetic procedure and spectral data of the other iodocarbonyls **2a**, **2b**, **2f**, and **2j** are shown below. All other reagents were commercially available.

Cyclopropylmethyltributylstannane (1).²¹ To tributyltin methoxide (330 mmol) was added poly(methylhydrosiloxane) (330 mmol), and the mixture was stirred for 8 h at room temperature. The resultant mixture was purified by distillation under reduced pressure to give Bu₃SnH (85.9 g, 89%).²² To hexachloroacetone (600 mmol) was added triphenylphosphine (110 mmol) at 0 °C, and the suspension was stirred vigorously for 5 min. To the suspension was slowly added 1-cyclopropylmethanol (100 mmol) for 25 min. The mixture was warmed to room temperature and stirred for 3 h before flash distillation to collect a volatile product, chlorocyclopropylmethane (7.9 g, 88%).^{1a} To a solution of *n*-butyllithium (1.6 M in hexane, 47 mL) in THF (80 mL) at 0 °C was slowly added diisopropylamine (75 mmol), and the mixture was stirred for 20 min. To the mixture was slowly added Bu₃SnH (75 mmol) for 30 min, and the mixture was stirred for 15 min to generate Bu₃SnLi. 1-Chloro-1-cyclopropylmethane (70 mmol) was slowly added to the mixture for 30 min, which was warmed to room temperature. After stirring for 16 h KF(aq) (10%, 200 mL)

(14) Loiseau, F.; Simone, J.-M.; Carcache, D.; Bobal, P.; Neier, R. *Monatsh. Chem.* **2007**, *138*, 121–129.

(15) Curran, D. P.; Tamine, J. *J. Org. Chem.* **1991**, *56*, 2746–2750.

(16) Neu, H.; Kihlberg, T.; Långström, B. *J. Labelled Compd. Radiopharm.* **1997**, *39*, 509–524.

(17) Kihara, N.; Ollivier, C.; Renaud, P. *Org. Lett.* **1999**, *1*, 1419–1422.

(18) Denmark, S. E.; Yang, S.-M. *J. Am. Chem. Soc.* **2004**, *126*, 12432–12440.

(19) Hlavinka, M. L.; Greco, J. F.; Hagadorn, J. R. *Chem. Commun.* **2005**, 5304–5306.

(20) Yin, G.; Zhou, B.; Meng, X.; Wu, A.; Pan, Y. *Org. Lett.* **2006**, *8*, 2245–2248.

(21) H^A and H^B are defined as hydrogens that are *cis* and *trans* to RCH-cyclopropyl, respectively.

(22) Hayashi, K.; Iyoda, J.; Shiihara, I. *J. Organomet. Chem.* **1967**, *10*, 81–94.

(13) The conditions without air employed on the bench might have enough oxygen during the experimental process. A very small amount of oxygen resulted in high efficiency in this case.

was poured into the mixture. EtOAc (200 mL) was added, and the organic layer was washed using saturated NaCl(aq) (200 mL) and H₂O (200 mL). After drying with MgSO₄ the solvent was evaporated and the residue was purified by column chromatography (hexane) on silica gel and distillation under reduced pressure to give the product (9.4 g, 37%): bp 78 °C/0.07 mmHg; ¹H NMR (400 MHz, CDCl₃) 1.49 (m, 6H, 2'-H₂ × 3), 1.31 (tq, *J* = 7.2, 7.2 Hz, 6H, 3'-H₂ × 3), 0.96–0.69 (m, 18H, 4'-H₃ × 3, 1'-H₂ × 3, 1-H₂ and SnCH₂CH), 0.46 (m, 2H, H^A × 2), –0.04 (m, 2H, H^B × 2); ¹³C NMR (100 MHz, CDCl₃) 29.4 (t, C-2', d, ²*J*_{Sn-C} = 19.7 Hz), 27.5 (t, C-3', d, ³*J*_{Sn-C} = 52.4 Hz), 15.0 (t, C-1, d, ¹*J*_{119Sn-C} = 307.2, ¹*J*_{117Sn-C} = 293.3 Hz), 13.8 (q, C-4'), 9.2 (d, SnCH₂CH, d, ²*J*_{Sn-C} = 19.7 Hz), 9.0 (t, C-1', d, ¹*J*_{119Sn-C} = 312.1, ¹*J*_{117Sn-C} = 299.0 Hz), 8.3 (t, two methylene groups in cyclopropyl ring, d, ³*J*_{Sn-C} = 34.4 Hz); ¹¹⁹Sn NMR (150 MHz, CDCl₃) –15.6; IR (neat) 2958, 2924, 1462 cm⁻¹; MS (EI, 70 eV) *m/z* 291 (39), 289 (86), 288 (31), 287 (59), 285 (28), 235 (57), 233 (57), 231 (37), 179 (94), 178 (29), 177 (100), 176 (34), 175 (70), 173 (22), 121 (31), 119 (24); HRMS (EI, 70 eV) calcd for (C₁₂H₂₇¹²⁰Sn) 291.1135 (M – CH₂C₃H₅), found for *m/z* 291.1104 and calcd for (C₁₂H₂₅¹²⁰Sn) 289.0978 (M – Bu), found for *m/z* 289.1048. Anal. Calcd for C₁₆H₃₄Sn: C, 55.68; H, 9.93. Found: C, 55.47; H, 9.91.

Phenyl 2-Iodoacetate (2a). To a stirred solution of sodium iodide (135 mmol) in acetone (150 mL) was added phenyl bromoacetate (45 mmol). The mixture was stirred for 3 h, and then acetone was evaporated. Ethyl acetate (200 mL) was added, and the organic layer was washed by Na₂S₂O₃(aq) (10%, 200 mL) and water (2 × 200 mL) and then dried (MgSO₄). The solvent was evaporated and the residue was purified by recrystallization to give the product (10.5 g, 90%): mp 65–67 °C; ¹H NMR (400 MHz, CDCl₃) 7.40 (dd, *J* = 8.0, 8.0 Hz, 2H, *m*), 7.25 (t, *J* = 8.0 Hz, 1H, *p*), 7.11 (d, *J* = 8.0 Hz, 2H, *o*), 3.90 (s, 2H, 2-H₂); ¹³C NMR (100 MHz, CDCl₃) 167.5 (s, C-1), 150.5 (s, C-*i*), 129.5 (d, C-*m*), 126.2 (d, C-*p*), 120.9 (d, C-*o*), –6.0 (t, C-2); IR (KBr) 1736 (C=O) cm⁻¹; MS (EI, 70 eV) *m/z* 262 (M⁺, 8), 94 (100); HRMS (EI, 70 eV) calcd for (C₈H₇IO₂) 261.9491 (M⁺), found for *m/z* 261.9475. Anal. Calcd for C₈H₇IO₂: C, 36.67; H, 2.69; I, 48.43. Found: C, 36.68; H, 2.63; I, 48.70.

Benzyl 2-Iodoacetate (2b). To a stirred solution of sodium iodide (30 mmol) in acetone (60 mL) was added benzyl 2-chloroacetate (30 mmol). The mixture was stirred for 3 h, and then acetone was evaporated. Ethyl acetate (200 mL) was added, and the organic layer was washed by Na₂S₂O₃(aq) (10%, 100 mL) and water (100 mL × 2) and then dried (MgSO₄). The solvent was evaporated, and the residue was purified by distillation under reduced pressure to give the product (6.7 g, 80%): bp 75 °C/0.1 mmHg; ¹H NMR (400 MHz, CDCl₃) 7.40–7.30 (m, 5H, Ar), 5.15 (s, 2H, C₆H₅CH₂), 3.71 (s, 2H, 2-H₂); ¹³C NMR (100 MHz, CDCl₃) 168.5 (s, C-1), 135.0 (s, C-*i*), 128.5 (d), 128.4 (d, C-*p*), 128.2, (d), 67.7 (t, C₆H₅CH₂), –5.5 (t, C-2); IR (neat) 1732 (C=O) cm⁻¹; MS (EI, 70 eV) *m/z* 276 (M⁺, 0.04), 149 (C₆H₅CH₂OCOCH₂⁺, 89), 107 (C₆H₅CH₂O⁺, 100), 91 (C₆H₅CH₂⁺, 90); HRMS (EI, 70 eV) calcd for (C₉H₉IO₂) 275.9647 (M⁺), found for *m/z* 275.9655. Anal. Calcd for C₉H₉IO₂: C, 39.16; H, 3.29; I, 45.97. Found: C, 39.07; H, 3.16; I, 45.96.

Benzyl 2-Iodopropanoate (2f). To a stirred solution of benzyl alcohol (110 mmol) and pyridine (120 mmol) in CH₂Cl₂ (80 mL) at 0 °C was slowly added a solution of 2-bromopropionyl bromide (120 mmol) in CH₂Cl₂ (20 mL) for 25 min.²³ The mixture was warmed to room temperature, stirred for 12 h, and then quenched by water (200 mL). Chloroform (200 mL) was added, and the organic layer was washed by 1 M HCl aq (200 mL) and saturated NaHCO₃(aq) (200 mL) and then dried (MgSO₄). The solvent was evaporated, and the residue was purified by distillation under reduced pressure to give the bromoester (24.0 g, 87%), bp 78 °C/

0.05 mmHg. The spectral data of the obtained bromoester (benzyl 2-bromopropanoate) were in excellent agreement with the reported data.²⁴ To a stirred solution of sodium iodide (100 mmol) in acetone (100 mL) was added benzyl 2-bromopropanoate (50 mmol). The mixture was stirred for 8 h, and then the solvent was evaporated. Ethyl acetate (200 mL) was added, and the organic layer was washed by Na₂S₂O₃ (aq) (10%, 100 mL) and water (100 mL × 2) and then dried (MgSO₄). The solvent was evaporated, and the residue was purified by distillation under reduced pressure to give the product (12.4 g, 82%): bp 84 °C/0.06 mmHg; ¹H NMR (400 MHz, CDCl₃) 7.42–7.30 (m, 5H, Ar), 5.17 (m, 2H, C₆H₅CH₂), 4.51 (q, *J* = 7.2 Hz, 1H, 2-H), 1.97 (d, *J* = 7.2 Hz, 3H, 3-H₃); ¹³C NMR (100 MHz, CDCl₃) 171.6 (s, C-1), 135.2 (s, *i*), 128.5 (d), 128.4 (d, *p*), 128.2 (d), 67.4 (t, C₆H₅CH₂), 23.2 (q, C-3), 12.8 (d, C-2); IR (neat) 1736 (C=O) cm⁻¹; MS (CI, 200 eV) *m/z* 291 (M + 1, 13), 91 (C₆H₅CH₂⁺, 100); HRMS (CI, 200 eV) calcd for (C₁₀H₁₂IO₂) 290.9882 (M + 1), found for *m/z* 290.9894. Anal. Calcd for C₁₀H₁₁IO₂: C, 41.40; H, 3.82; I, 43.75. Found: C, 41.63; H, 3.78; I, 43.92.

Phenyl 2-Iodo-2-methylpropanoate (2j). To a stirred solution of phenol (110 mmol) and sulfuric acid (95%, 0.3 mL) in toluene (65 mL) was added 2-bromo-2-methylpropionyl bromide (110 mmol). The mixture was heated to reflux for 5 h and then cooled to room temperature and quenched by water (200 mL). Ethyl acetate (200 mL) was added, and the organic layer was washed by KOH(aq) (10%, 200 mL) and water (200 mL) and then dried (MgSO₄). The solvent was evaporated, and the residue was purified by distillation under reduced pressure to give the bromoester (21.6 g, 81%), bp 63 °C/0.04 mmHg. The spectral data of the obtained bromoester were in excellent agreement with the reported data.²⁵ To a stirred solution of sodium iodide (160 mmol) in acetone (80 mL) was added phenyl 2-bromo-2-methylpropanoate (40 mmol). The mixture was heated to reflux for 14 h and then cooled to room temperature, and acetone was evaporated. Ethyl acetate (200 mL) was added, and the organic layer was washed by Na₂S₂O₃(aq) (10%, 100 mL) and water (100 mL × 2) and then dried (MgSO₄). The solvent was evaporated, and the residue was purified by distillation under reduced pressure to give the product (8.72 g, 75%): bp 100 °C/0.6 mmHg; ¹H NMR (400 MHz, CDCl₃) 7.40 (dd, *J* = 8.0, 8.0 Hz, 2H, *m*), 7.25 (t, *J* = 8.0 Hz, 1H, *p*), 7.13 (d, *J* = 8.0 Hz, 2H, *o*), 2.20 (s, 6H, 3-H₃ and 2-Me); ¹³C NMR (100 MHz, CDCl₃) 171.9 (s, C-1), 150.7 (s, *i*), 129.4 (d, *m*), 126.0 (d, *p*), 120.8 (d, *o*), 33.5 (q, C-3 and 2-Me); IR (neat) 1747 (C=O) cm⁻¹; MS (EI, 70 eV) *m/z* 290 (M⁺, 28), 197 (COC(CH₃)₂I⁺, 48), 169 (C(CH₃)₂I⁺, 100), 163 (C₆H₅OCOC(CH₃)₂⁺, 76), 135 (64), 94 (85), 70 (COC(CH₃)₂⁺, 28), 69 (22), 41 (38); HRMS (EI, 70 eV) calcd for C₁₀H₁₁IO₂ 289.9804 (M⁺), found for *m/z* 289.9822. Anal. Calcd for C₁₀H₁₁IO₂: C, 41.40; H, 3.82; I, 43.75. Found: C, 41.65; H, 3.68; I, 43.59.

Procedure for Optimization of Coupling of Cyclopropylmethylstannane 1 and Iodocarbonyls 2 (Table 1). According to the next paragraph, the reactions were employed under the conditions noted in text.

General Procedure for InBr₃-Mediated Coupling of Cyclopropylmethylstannane 1 and Iodocarbonyls 2 (Table 2). To a suspension of InBr₃ (0.5 mmol) and iodocarbonyls 2 (1 mmol) in toluene (1 mL) was added (cyclopropylmethyl)tributylstannane 1 (1 mmol) with a CaCl₂ drying tube that was exposed to air. The reaction mixture was stirred at rt for 4.5 h. The mixture was quenched by addition of NH₄F(aq) (10%, 10 mL) and extracted with diethyl ether (3 × 10 mL). The collected organic layer was dried over MgSO₄ and concentrated *in vacuo*. The procedures used for further purification of the new compounds are shown in the

(24) DeGraw, J. I.; Christie, P. H.; Kisliuk, R. L.; Gaumont, Y.; Sirotnak, F. M. *J. Med. Chem.* **1990**, *33*, 212–215.

(25) Schick, H.; Ludwig, R.; Kleiner, K.; Kunath, A. *Tetrahedron* **1995**, *51*, 2939–2946.

(23) Kakiya, H.; Nishimae, S.; Shinokubo, H.; Oshima, K. *Tetrahedron* **2001**, *57*, 8807–8815.

Product Data section. The reactions under nitrogen were performed using the same operation.

NMR Study of Transmetalation between 1 and 2 (Figure 2). Three mixtures with different ratios of $\text{InBr}_3/\mathbf{1}$ ($= 1/1, 1/2,$ and $1/3$) were prepared in toluene- d_8 . After mixing for ca. 2 h, the mixtures were transferred into NMR tubes, and the resulting spectra are shown in Figure 2.

Product Data. The spectral data of **3e**,²⁶ **3f**,⁴ **3i**,⁴ **3k**,⁴ and **3l**⁴ were in excellent agreement with the reported data. Spectral data for the products **3a**, **3b**, **3c**, **3d**, **3g**, **3h**, and **3j** are shown below.

Phenyl 3-Cyclopropylpropanoate (3a).²¹ According to the general procedure, this compound was prepared from **1** and **2a** to give the product as a colorless liquid after chromatography (hexane). Further purification was performed by distillation under reduced pressure. Bp 90 °C/0.07 mmHg; ¹H NMR (400 MHz, CDCl_3) 7.38 (dd, $J = 8.0, 7.2$ Hz, 2H, *m*), 7.22 (t, $J = 7.2$ Hz, 1H, *p*), 7.08 (d, $J = 8.0$ Hz, 2H, *o*), 2.66 (t, $J = 7.2$ Hz, 2H, 2- H_2), 1.66 (dt, $J = 7.2, 7.2$ Hz, 2H, 3- H_2), 0.81 (ttt, $J = 8.0, 7.2, 5.6$ Hz, 1H, $\text{COCH}_2\text{CH}_2\text{CH}$), 0.49 (ddd, $J = 8.0, 5.6, 4.8$ Hz, 2H, $\text{H}^A \times 2$), 0.13 (ddd, $J = 5.6, 5.6, 4.8$ Hz, 2H, $\text{H}^B \times 2$); ¹³C NMR (100 MHz, CDCl_3) 172.1 (s, C-1), 150.7 (s, C-*i*), 129.3 (d, C-*m*), 125.7 (d, C-*p*), 121.5 (d, C-*o*), 34.5 (t, C-2), 30.0 (t, C-3), 10.4 (d, $\text{COCH}_2\text{CH}_2\text{CH}$), 4.5 (t, two methylene groups in cyclopropyl ring); IR (neat) 1759 (C=O) cm^{-1} ; MS (EI, 70 eV) m/z 190 (M^+ , 37), 97 ($\text{COCH}_2\text{CH}_2\text{C}_3\text{H}_5^+$, 34), 94 (100), 69 ($\text{CH}_2\text{CH}_2\text{C}_3\text{H}_5^+$, 44), 55 ($\text{CH}_2\text{C}_3\text{H}_5^+$, 24); HRMS (EI, 70 eV) calcd for ($\text{C}_{12}\text{H}_{14}\text{O}_2$) 190.0994 (M^+), found for m/z 190.1000.

Benzyl 3-Cyclopropylpropanoate (3b).²¹ According to the general procedure, this compound was prepared from **1** and **2b** to give the product as a colorless liquid after chromatography (hexane/EtOAc = 95/5). Further purification was performed by distillation under reduced pressure. Bp 77 °C/0.2 mmHg; ¹H NMR (400 MHz, CDCl_3) 7.41–7.28 (m, 5H, Ar), 5.12 (s, 2H, $\text{C}_6\text{H}_5\text{CH}_2$), 2.46 (t, $J = 7.2$ Hz, 2H, 2- H_2), 1.54 (dt, $J = 7.2, 7.2$ Hz, 2H, 3- H_2), 0.70 (ttt, $J = 8.0, 5.6, 7.2$ Hz, 1H, $\text{COCH}_2\text{CH}_2\text{CH}$), 0.40 (ddd, $J = 8.0, 5.6, 4.0$ Hz, 2H, $\text{H}^A \times 2$), 0.05 (ddd, $J = 5.6, 5.6, 4.0$ Hz, 2H, $\text{H}^B \times 2$); ¹³C NMR (100 MHz, CDCl_3) 173.5 (s, C-1), 136.1 (s, C-*i*), 128.5 (d), 128.2 (d), 128.1 (d, C-*p*), 66.1 (t, $\text{C}_6\text{H}_5\text{CH}_2$), 34.4 (t, C-2), 30.4 (t, C-3), 10.4 (d, $\text{COCH}_2\text{CH}_2\text{CH}$), 4.4 (t, two methylene groups in cyclopropyl ring); IR (neat) 1736 (C=O) cm^{-1} ; MS (EI, 70 eV) m/z 204 (M^+ , 0.71), 104 (61), 91 ($\text{C}_6\text{H}_5\text{CH}_2^+$, 100); HRMS (EI, 70 eV) calcd for $\text{C}_{13}\text{H}_{16}\text{O}_2$ 204.1150 (M^+), found for m/z 204.1139. Anal. Calcd for $\text{C}_{13}\text{H}_{16}\text{O}_2$: C, 76.44; H, 7.90. Found: C, 76.52; H, 7.71.

Ethyl 3-Cyclopropylpropanoate (3c).²¹ According to the general procedure, this compound was prepared from **1** and **2c** to give the product as a colorless liquid after chromatography (hexane/EtOAc = 94/6). Further purification was performed by distillation under reduced pressure. Bp 90 °C/20 mmHg; ¹H NMR (400 MHz, CDCl_3) 4.13 (q, $J = 7.2$ Hz, 2H, $\text{CH}_3\text{CH}_2\text{OCO}$), 2.39 (t, $J = 7.2$ Hz, 2H, 2- H_2), 1.53 (dt, $J = 7.2, 7.2$ Hz, 2H, 3- H_2), 1.26 (t, $J = 7.2$ Hz, 3H, $\text{CH}_3\text{CH}_2\text{OCO}$), 0.71 (m, 1H, $\text{COCH}_2\text{CH}_2\text{CH}$), 0.43 (ddd, $J = 8.0, 5.6, 4.0$ Hz, 2H, $\text{H}^A \times 2$), 0.05 (m, 2H, $\text{H}^B \times 2$); ¹³C NMR (100 MHz, CDCl_3) 173.7 (s, C-1), 60.1 (t, $\text{CH}_3\text{CH}_2\text{OCO}$), 34.5 (t, C-2), 30.1 (t, C-3), 14.2 (q, $\text{CH}_3\text{CH}_2\text{OCO}$), 10.4 (d, $\text{COCH}_2\text{CH}_2\text{CH}$), 4.3 (t, two methylene groups in cyclopropyl ring); IR (neat) 1739 (C=O) cm^{-1} ; MS (EI, 70 eV) m/z 142 (M^+ , 15), 114 ($\text{CH}_3\text{CH}_2\text{OCOCH}_2\text{CH}_2\text{CH}^+$, 70), 113 ($\text{OCOCH}_2\text{CH}_2\text{C}_3\text{H}_5^+$, 20), 99 ($\text{CH}_2\text{OCOCH}_2\text{CH}_2\text{C}_3\text{H}_5^+$, 32), 97 ($\text{COCH}_2\text{CH}_2\text{C}_3\text{H}_5^+$, 64), 96 (21), 88 (96), 73 ($\text{CH}_3\text{CH}_2\text{OCO}^+$, 42), 71 (27), 70 (32), 69 ($\text{CH}_2\text{CH}_2\text{C}_3\text{H}_5^+$, 100), 68 (88), 67 (22), 61 (36), 60 (88), 55 ($\text{CH}_2\text{C}_3\text{H}_5^+$, 71), 54 (27), 42 (22), 41 (C_3H_5^+ , 74), 39 (31); HRMS (EI, 70 eV) calcd for ($\text{C}_8\text{H}_{14}\text{O}_2$) 142.0994 (M^+), found for m/z 142.1010.

Allyl 3-Cyclopropylpropanoate (3d).²¹ According to the general procedure, this compound was prepared from **1** and **2d** to give the product as a colorless liquid after chromatography (hexane/EtOAc = 94/6). Further purification was performed by distillation under reduced pressure. Bp: 120 °C/30 mmHg; ¹H NMR (400 MHz, CDCl_3) 5.93 (ddt, $J = 17.6, 10.4, 5.6$ Hz, 1H, $\text{CH}_2\text{CHCH}_2\text{OCO}$), 5.32 (ddd, $J = 17.6, 3.2, 1.6$ Hz, 1H, $\text{CH}_2\text{CH}=\text{CHH}$), 5.24 (ddd, $J = 10.4, 3.2, 1.6$ Hz, 1H, $\text{CH}_2\text{CH}=\text{CHH}$), 4.58 (ddd, $J = 5.6, 1.6, 1.6$ Hz, 2H, $\text{CH}_2\text{CHCH}_2\text{OCO}$), 2.44 (t, $J = 7.2$ Hz, 2H, 2- H_2), 1.63 (dt, $J = 7.2, 7.2$ Hz, 2H, 3- H_2), 0.72 (ttt, $J = 8.0, 5.6, 7.2$ Hz, 1H, $\text{COCH}_2\text{CH}_2\text{CH}$), 0.43 (ddd, $J = 8.0, 5.6, 4.0$ Hz, 2H, $\text{H}^A \times 2$), 0.06 (ddd, $J = 5.6, 5.6, 4.0$ Hz, 2H, $\text{H}^B \times 2$); ¹³C NMR (100 MHz, CDCl_3) 173.4 (s, C-1), 132.3 (d, $\text{CH}_2\text{CHCH}_2\text{OCO}$), 118.1 (t, $\text{CH}_2\text{CHCH}_2\text{OCO}$), 65.0 (t, $\text{CH}_2\text{CHCH}_2\text{OCO}$), 34.4 (t, C-2), 30.1 (t, C-3), 10.5 (d, $\text{COCH}_2\text{CH}_2\text{CH}$), 4.4 (t, two methylene groups in cyclopropyl ring); IR (neat) 1739 (C=O), 1651 (C=C) cm^{-1} ; MS (CI, 200 eV) m/z 155 ($\text{M} + 1$, 100); HRMS (CI, 200 eV) calcd for ($\text{C}_9\text{H}_{15}\text{O}_2$) 155.1072 ($\text{M} + 1$), found for m/z 155.1080.

Phenyl 3-Cyclopropyl-2-methylpropanoate (3g).²¹ According to the general procedure, this compound was prepared from **1** and **2f** to give the product as a colorless liquid after chromatography (hexane/EtOAc = 94/6). Further purification was performed by distillation under reduced pressure. Bp: 95 °C/0.15 mmHg; ¹H NMR (400 MHz, CDCl_3) 7.38 (dd, $J = 8.0, 7.2$ Hz, 2H, *m*), 7.22 (t, $J = 7.2$ Hz, 1H, *p*), 7.08 (d, $J = 8.0$ Hz, 2H, *o*), 2.81 (tq, $J = 7.2, 7.2$ Hz, 1H, 2-H), 1.69 (ddd, $J = 14.4, 7.2, 7.2$ Hz, 1H, 3- HH), 1.53 (ddd, $J = 14.4, 7.2, 7.2$ Hz, 1H, 3- HH), 1.34 (d, $J = 7.2$ Hz, 3H, 2-Me), 0.82 (m, 1H, $\text{COCH}(\text{CH}_3)\text{CH}_2\text{CH}$), 0.50 (m, 2H, $\text{H}^A \times 2$), 0.13 (m, 2H, $\text{H}^B \times 2$); ¹³C NMR (100 MHz, CDCl_3) 175.1 (s, C-1), 150.7 (s, *i*), 129.3 (d, *m*), 125.5 (d, *p*), 121.4 (d, *o*), 40.2 (d, C-2), 38.6 (t, C-3), 16.9 (q, 2-Me), 8.8 (d, $\text{COCH}(\text{CH}_3)\text{CH}_2\text{CH}$), 4.6 (t, $\text{COCH}(\text{CH}_3)\text{CH}_2\text{CH}^A\text{H}_2$), 4.4 (t, $\text{COCH}(\text{CH}_3)\text{CH}_2\text{CH}^B\text{H}_2$); IR (neat) 1759 (C=O) cm^{-1} ; MS (EI, 70 eV) m/z 204 (M^+ , 28), 111 ($\text{COCH}(\text{CH}_3)\text{CH}_2\text{C}_3\text{H}_5^+$, 54), 94 (88), 83 ($\text{CH}(\text{CH}_3)\text{CH}_2\text{C}_3\text{H}_5^+$, 70), 55 ($\text{CH}_2\text{C}_3\text{H}_5^+$, 100); HRMS (EI, 70 eV) calcd for ($\text{C}_{13}\text{H}_{16}\text{O}_2$) 204.1150 (M^+), found for m/z 204.1145. Anal. Calcd for $\text{C}_{13}\text{H}_{16}\text{O}_2$: C, 76.44; H, 7.90. Found: C, 76.15; H, 7.74.

Ethyl 3-Cyclopropyl-2-methylpropanoate (3h).²¹ According to the general procedure, this compound was prepared from **1** and **2h** to give the product as a colorless liquid after chromatography (hexane/EtOAc = 94/6). Further purification was performed by distillation under reduced pressure. Bp: 100 °C/10 mmHg; ¹H NMR (400 MHz, CDCl_3) 4.13 (q, $J = 7.2$ Hz, 2H, $\text{CH}_3\text{CH}_2\text{OCO}$), 2.53 (tq, $J = 7.2, 7.2$ Hz, 1H, 2-H), 1.53 (ddd, $J = 14.4, 7.2, 7.2$ Hz, 1H, 3- HH), 1.37 (ddd, $J = 14.4, 7.2, 7.2$ Hz, 1H, 3- HH), 1.26 (t, $J = 7.2$ Hz, 3H, $\text{CH}_3\text{CH}_2\text{OCO}$), 1.18 (d, $J = 7.2$ Hz, 3H, 2-Me), 0.69 (m, 1H, $\text{COCH}_2\text{CH}_2\text{CH}$), 0.43 (m, 2H, $\text{H}^A \times 2$), 0.04 (m, 2H, $\text{H}^B \times 2$); ¹³C NMR (100 MHz, CDCl_3) 176.8 (s, C-1), 60.1 (t, $\text{CH}_3\text{CH}_2\text{OCO}$), 40.1 (d, C-2), 38.7 (t, C-3), 17.0 (q, 2-Me), 14.2 (q, $\text{CH}_3\text{CH}_2\text{OCO}$), 8.9 (d, $\text{COCH}(\text{CH}_3)\text{CH}_2\text{CH}$), 4.5 (t, $\text{COCH}(\text{CH}_3)\text{CH}_2\text{CH}^A\text{H}_2$), 4.2 (t, $\text{COCH}(\text{CH}_3)\text{CH}_2\text{CH}^B\text{H}_2$); IR (neat) 1736 (C=O) cm^{-1} ; MS (EI, 70 eV) m/z 156 (M^+ , 14), 128 ($\text{CH}_3\text{CH}_2\text{OCOCH}(\text{CH}_3)\text{CH}_2\text{CH}^+$, 70), 102 (65), 87 (36), 83 ($\text{CH}(\text{CH}_3)\text{CH}_2\text{C}_3\text{H}_5^+$, 48), 74 (100), 55 ($\text{CH}_2\text{C}_3\text{H}_5^+$, 91), 41 (C_3H_5^+ , 25); HRMS (EI, 70 eV) calcd for ($\text{C}_9\text{H}_{16}\text{O}_2$) 156.1150 (M^+), found for m/z 156.1139.

Phenyl 3-Cyclopropyl-2,2-dimethylpropanoate (3j).²¹ According to the general procedure, this compound was prepared from **1** and **2j** to give the product as a colorless liquid after chromatography (hexane/EtOAc = 94/6) and recycle GPC. ¹H NMR (400 MHz, CDCl_3) 7.38 (dd, $J = 8.0, 7.2$ Hz, 2H, *m*), 7.22 (t, $J = 7.2$ Hz, 1H, *p*), 7.08 (d, $J = 8.0$ Hz, 2H, *o*), 1.63 (d, $J = 7.2$ Hz, 2H, 3- H_2), 1.36 (s, 6H, 2-Me₂), 0.79 (ttt, $J = 8.0, 7.2, 4.8$ Hz, 1H, $\text{COC}(\text{CH}_3)_2\text{CH}_2\text{CH}$), 0.50 (ddd, $J = 8.0, 5.6, 4.0$ Hz, 2H, $\text{H}^A \times 2$), 0.13 (ddd, $J = 5.6, 4.8, 4.0$ Hz, 2H, $\text{H}^B \times 2$); ¹³C NMR (100 MHz, CDCl_3) 176.5 (s, C-1), 151.0 (s, *i*), 129.3 (d, *m*), 125.5 (d, *p*), 121.4 (d, *o*), 45.4 (t, C-3), 43.4 (s, C-2), 25.3 (q, 2-Me₂), 7.0

(26) Orsini, F.; Pelizzoni, F.; Ricca, G. *Tetrahedron* **1984**, *40*, 2781–2787.

(d, $\text{COC}(\text{CH}_3)_2\text{CH}_2\text{CH}$), 4.5 (t, two methylene groups in cyclopropyl ring); IR (neat) 1751 ($\text{C}=\text{O}$) cm^{-1} ; MS (EI, 70 eV) m/z 218 (M^+ , 3), 125 ($\text{COC}(\text{CH}_3)_2\text{CH}_2\text{C}_3\text{H}_5^+$, 50), 97 ($\text{C}(\text{CH}_3)_2\text{CH}_2\text{C}_3\text{H}_5^+$, 84), 96 (28), 94 (84), 81 (30), 55 ($\text{CH}_2\text{C}_3\text{H}_5^+$, 100); HRMS (EI, 70 eV) calcd for ($\text{C}_{14}\text{H}_{18}\text{O}_2$) 218.1307 (M^+), found for m/z 218.1367. Anal. Calcd for $\text{C}_{14}\text{H}_{18}\text{O}_2$: C, 77.03; H, 8.31. Found: C, 76.76; H, 8.29.

Dibutenylindium Chloride–DPPE Complex (9). To a suspension of InCl_3 (0.5 mmol) in toluene (1 mL) was added (cyclopropylmethyl)tributylstannane (**1**; 1 mmol) at rt. The mixture was stirred for 2 h, and then 1,2-bis(diphenylphosphino)ethane (0.25 mmol) was loaded. The mixture was stirred for 1 h, and then the volatiles were evaporated to give a viscous liquid, which was then washed by hexane to give the product as a white solid (95 mg, 42%). The product was recrystallized from dichloromethane/hexane for X-ray analysis. The data obtained from the measurement was good ($R_{\text{int}} = 0.056$), and the analysis was completed to optimize the structure. Although some level A alerts still remain, this structure should be justified because of the excellent level of the data and structure refinement. ^1H NMR (400 MHz, CDCl_3) 7.47–7.31 (m, 20H, Ar), 5.89 (ddt, $J = 16.8, 9.6, 6.4$ Hz, 4H, 3-H \times 4), 4.95 (dd,

$J = 16.8, 1.6$ Hz, 4H, 4-*HH* \times 4), 4.88 (dd, $J = 9.6, 1.6$ Hz, 4H, 4-*HH* \times 4), 2.38 (dt, $J = 7.2, 6.4$ Hz, 8H, 2- H_2 \times 4), 2.36 (m, 4H, $\text{PCH}_2\text{CH}_2\text{P}$), 1.11 (t, $J = 7.2$ Hz, 8H, 1- H_2 \times 4); ^{13}C NMR (100 MHz, CDCl_3) 142.7 (C-3), 132.8 (*o*, d, $^2J_{\text{P-C}} = 15.6$ Hz), 132.3 (*i*), 130.2 (*p*), 129.0 (*m*, d, $^3J_{\text{P-C}} = 8.2$ Hz), 113.1 (C-4), 30.9 (C-2), 21.9 ($\text{PCH}_2\text{CH}_2\text{P}$, d, $^1J_{\text{P-C}} = 9.8$ Hz), 20.4 (C-1).

Acknowledgment. This work was supported by Grants-in-Aid for Scientific Research on Priority Areas (No. 18065015, “Chemistry of Concerto Catalysis” and No. 20036036, “Synergistic Effects for Creation of Functional Molecules”) and for Scientific Research (No. 19550038) from the Ministry of Education, Culture, Sports, Science and Technology, Japan.

Supporting Information Available: Results of NMR experiment of the reaction of varying **2a** and crystallographic data for **9**. This material is available free of charge via the Internet at <http://pubs.acs.org>.

OM8009156

Platinum(II) Complexes Featuring Chiral Diphosphines and N-Heterocyclic Carbene Ligands: Synthesis and Evaluation as Cycloisomerization Catalysts

Delphine Brissy,[†] Myriem Skander,[†] Pascal Retailleau,[†] Gilles Frison,[‡] and Angela Marinetti^{*,†}

Institut de Chimie des Substances Naturelles, CNRS UPR 2301, 1, Avenue de la Terrasse, 91198 Gif-sur-Yvette, France, and Laboratoire des Mécanismes Réactionnels, Département de Chimie, Ecole Polytechnique and CNRS, 91128 Palaiseau Cedex, France

Received August 1, 2008

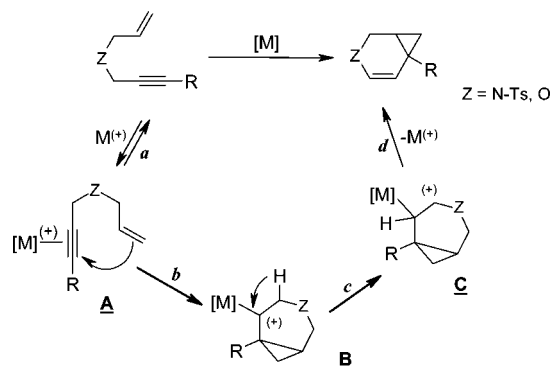
Square-planar platinum(II) complexes that combine chiral diphosphines and NHC ligands have been obtained in high yields from (NHC)Pt⁽⁰⁾(dvtms) complexes, via an oxidative addition/ligand exchange sequence. The use of suitable carbene–diphosphine pairs allows axially chiral, configurationally stable platinum complexes to be isolated. The Pt(II) complexes have been evaluated as precatalysts for the cycloisomerization reaction of an allyl propargylamine derivative. Their catalytic properties have been examined as a function of structural variations on both the diphosphine and the NHC units. For axially chiral species possible epimerization pathways have been envisioned and the inversion barriers have been estimated through computational studies.

Introduction

Transition metal-promoted enyne cycloisomerizations have emerged as powerful synthetic tools that convert simple starting materials into diverse cyclic products of increased complexity.¹ The conversion of 1,6-enynes into bicyclo[4.1.0]heptenes shown in Scheme 1 belongs to this class. These last reactions are known to be promoted by highly electrophilic metal species such as Pt(II) halides² and complexes,³ Pt(IV) halides,⁴ Au(I) salts⁵ and complexes,⁶ and cationic Ir(I) complexes.⁷ Allyl propargyl ethers and amine derivatives are common substrates whose cycloisomerizations afford 3-oxa- or 3-azabicyclo[4.1.0]hept-4-ene derivatives, respectively.

The PtCl₂-catalyzed process was first reported by Fürstner,^{2a,8} who also proposed a mechanistic pathway based on the

Scheme 1. Cycloisomerization of 1,6-Enynes into Bicyclo[4.1.0]heptenes: Postulated Mechanism



electrophilic activation of the alkyne via its Pt π -complex **A** (Scheme 1). The platinum-coordinated alkyne displays carbocationic character and undergoes nucleophilic attack by the tethered alkene following a 6-*endo-dig* cyclization mode. The resulting metal-stabilized bicyclic carbocation **B**⁹ evolves then to **C** by hydride migration. The final step involves formation of the double bond of the bicyclic product and concomitant elimination of the Pt(II) catalyst. This postulated mechanistic pathway was supported later by theoretical studies from Soriano.^{10a}

According to the mechanistic proposal above, the observed rearrangement mainly results from the peculiar “ π -acidic” properties of platinum(II)^{1d} and its high affinity for the π -system of the acetylenic substrate. The whole catalytic cycle involves a single platinum–substrate bond, changing from π - to σ -bonds in the successive elementary steps, and consequently, simulta-

* Corresponding author. E-mail: angela.marinetti@icsn.cnrs-gif.fr.

[†] Institut de Chimie des Substances Naturelles.

[‡] Département de Chimie, Ecole Polytechnique and CNRS.

(1) (a) Aubert, C.; Buisine, O.; Malacria, M. *Chem. Rev.* **2002**, *102*, 813–834. (b) Bruneau, C. *Angew. Chem., Int. Ed.* **2005**, *44*, 2328–2334. (c) Zhang, L.; Sun, J.; Kozmin, S. A. *Adv. Synth. Catal.* **2006**, *348*, 2271–2296. (d) Fürstner, A.; Davies, P. W. *Angew. Chem., Int. Ed.* **2007**, *46*, 3410–3449. (e) Jiménez-Núñez, E.; Echavarren, A. M. *Chem. Commun.* **2007**, 333–346.

(2) (a) Fürstner, A.; Szillat, H.; Stelzer, F. *J. Am. Chem. Soc.* **2000**, *122*, 6785–6786. (b) Nevado, C.; Ferrer, C.; Echavarren, A. M. *Org. Lett.* **2004**, *6*, 3191–3194. (c) Cho, E. J.; Kim, M.; Lee, D. *Org. Lett.* **2006**, *8*, 5413–5416. (d) Hercouet, A.; Berrée, F.; Lin, C. H.; Toupet, L.; Carboni, B. *Org. Lett.* **2007**, *9*, 1717–1720.

(3) Ferrer, C.; Raducan, M.; Nevado, C.; Claverie, C. K.; Echavarren, A. M. *Tetrahedron* **2007**, *63*, 6306–6316.

(4) Blum, J.; Beer-Kraft, H.; Badrich, Y. *J. Org. Chem.* **1995**, *60*, 5567–5569.

(5) Nieto-Oberhuber, C.; Munoz, M. P.; Bunuel, E.; Nevado, C.; Cardenas, D. J.; Echavarren, A. M. *Angew. Chem., Int. Ed.* **2004**, *43*, 2402–2406.

(6) (a) Lee, S. I.; Kim, S. M.; Kim, S. Y.; Chung, Y. K. *Synlett* **2006**, 2256–2260. (b) Lee, S. I.; Kim, S. M.; Choi, M. R.; Kim, S. Y.; Chung, Y. K. *J. Org. Chem.* **2006**, *71*, 9366–9372. (c) Kim, S. M.; Park, J. H.; Choi, S. Y.; Chung, Y. K. *Angew. Chem., Int. Ed.* **2007**, *46*, 6172–6175.

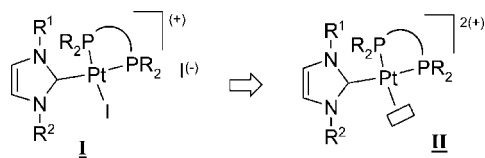
(7) Shibata, T.; Kobayashi, Y.; Maekawa, S.; Tshida, N.; Takagi, K. *Tetrahedron* **2005**, *61*, 9018–9024.

(8) Fürstner, A.; Stelzer, F.; Szillat, H. *J. Am. Chem. Soc.* **2001**, *123*, 11863–11869.

(9) This molecular entity can also be considered as a metal carbene species. For a detailed discussion see ref 1d.

(10) (a) Soriano, E.; Ballesteros, P.; Marco-Contelles, J. *Organometallics* **2005**, *24*, 3172–3181. (b) Soriano, E.; Marco-Contelles, J. *J. Org. Chem.* **2005**, *70*, 9345–9353. (c) Soriano, E.; Ballesteros, P.; Marco-Contelles, J. *J. Org. Chem.* **2004**, *69*, 8018–8023.

neous coordination of the alkyne and the alkene to the metal center is not required. It is thus conceivable that platinum complexes bearing modifiable ligands could be used as catalysts instead of platinum salts, provided that even a single coordination site would be available for substrate coordination. This working hypothesis led us to design precatalysts made of square-planar platinum(II) complexes bearing three strongly bound ligands,¹¹ including chiral diphosphines, and a halide as the only arguably labile group. Complexes **I** had been targeted, where an N-heterocyclic carbene (NHC) and a chelating diphosphine ligands are combined. They are expected to generate the tricoordinate species **II** as a potential catalyst. Their successful use as well-defined, phosphine-modified platinum precatalysts for the enantioselective cycloisomerization of 1,6-enynes has been mentioned in our preliminary communication.¹²



We report here extensive synthetic and structural studies on complexes **I**, as well as comparative tests showing the effects of the phosphine and carbene ligands on the catalytic behavior of **I** in a model cycloisomerization reaction. Theoretical investigations of the structural features of complexes **I** and **II** are also reported.

Results and Discussion

Synthesis and Structural Characterizations of Platinum(II) Complexes. With the aim of building tetracoordinated platinum(II) precatalysts for the cycloisomerization reactions shown in Scheme 1, we have targeted the mixed NHC/diphosphine complexes **I** as potentially suitable species. The choice of NHC ligands is a result of the high stability of their transition metal complexes and their excellent properties as supporting ligands in homogeneous catalysis,^{13,14} while chelating diphosphines have been selected mainly because the diverse array of commercially available chiral compounds would offer the opportunity to develop an asymmetric version of these cycloisomerizations.

For the preparation of the mixed NHC/diphosphine platinum complexes **I** we have investigated a new sequence, which starts from the (NHC)Pt⁰(dvtms) complexes (dvtms = divinyltetramethyldisiloxane, compounds **1** and **2** in Schemes 2–4) introduced by Markó et al.^{14d} We reasoned that these stable and easily available Pt(0) compounds could represent versatile starting materials for the generation of Pt(II) derivatives through oxidative addition reactions. The labile alkene was expected to be then displaced rather easily by strongly coordinating ligands such as phosphines.

In order to check the approach, iodine was envisioned as a suitable reactant for the oxidation step and PPh₃ as a representa-

(11) Platinum(II) complexes bearing three phosphorus ligands have been used previously in enantioselective diene cycloisomerizations: (a) Kerber, W. D.; Gagné, M. R. *Org. Lett.* **2005**, *7*, 3379–3381. (b) Feducia, J. A.; Campbell, A. N.; Doherty, M. Q.; Gagné, M. R. *J. Am. Chem. Soc.* **2006**, *128*, 13290–13297. (c) Feducia, J. A.; Gagné, M. R. *J. Am. Chem. Soc.* **2008**, *130*, 592–599.

(12) Brissy, D.; Skander, M.; Retailleau, P.; Marinetti, A. *Organometallics* **2007**, *26*, 5782–5785.

(13) (a) Herrmann, W. A.; Köcher, C. *Angew. Chem., Int. Ed.* **1997**, *36*, 2163–2187. (b) Herrmann, W. A. *Angew. Chem., Int. Ed.* **2002**, *41*, 1291–1309.

Scheme 2. Synthesis of the Triphenylphosphine/NHC Platinum(II) Complex **3**

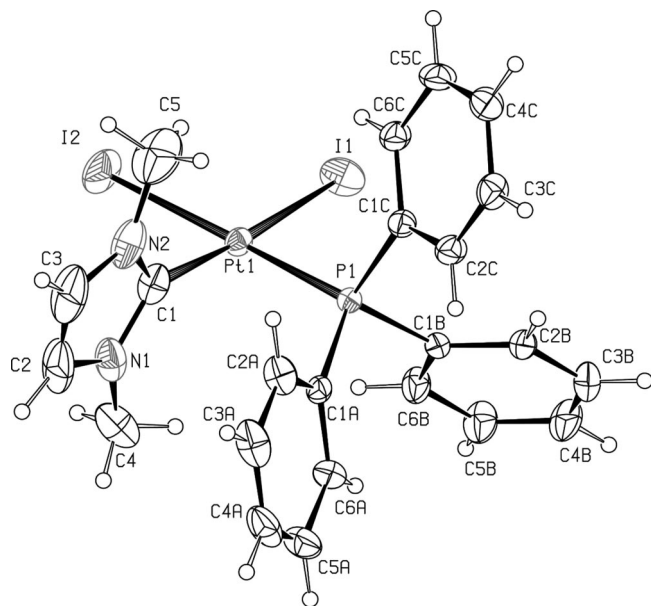
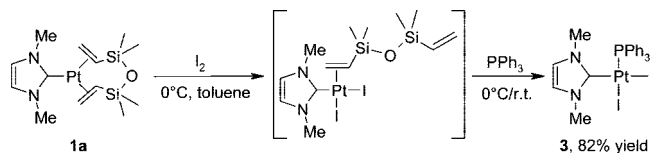


Figure 1. ORTEP drawing of the *cis*-(NHC)(triphenylphosphine)-PtI₂ complex **3**. Selected bond lengths [Å]: Pt–P = 2.2439(15), Pt–C(1) = 1.984(8), Pt–I(1) = 2.6517(7), Pt–I(2) = 2.6482(6), C(1)–N(1) = 1.351(11), C(1)–N(2) = 1.345(10). Selected bond angles [deg]: P–Pt–C(1) = 91.4(2), C(1)–Pt–I(2) = 84.8(2), I(1)–Pt–I(2) = 90.79(2), I(1)–Pt–P = 92.95(4). Torsion angle between the N–C(19)–N and P–Pt–I(2) mean planes: 89.1°.

tive phosphorus ligand. The (NHC)Pt(dvtms) complex **1a** was reacted in toluene at 0 °C successively with I₂ and 1 equiv of triphenylphosphine (Scheme 2). The anticipated oxidation of Pt(0) into Pt(II) took place and the expected NHC/phosphine complex **3** was isolated in 82% yield after column chromatography.

Most notably, a single isomer of complex **3** was isolated, where the carbene and phosphine ligands occupy mutually *cis*-

(14) Pt(0)–NHC complexes have been involved so far in alkene and alkyne hydrosilylation. (a) Markó, I. E.; Stérin, S.; Buisine, O.; Mignani, G.; Branlard, P.; Tinant, B.; Declercq, J.-P. *Science* **2002**, *298*, 204–206. (b) Sprengers, J. W.; Mars, M. J.; Duin, M. A.; Cavell, K. J.; Elsevier, C. J. *J. Organomet. Chem.* **2003**, *679*, 149–152. (c) Buisine, O.; Berthon-Gelloz, G.; Brière, J.-F.; Stérin, S.; Mignani, G.; Branlard, P.; Tinant, B.; Declercq, J.-P.; Markó, I. E. *Chem. Commun.* **2005**, 3856–3858. (d) Berthon-Gelloz, G.; Buisine, O.; Brière, J.-F.; Michaud, G.; Stérin, S.; Mignani, G.; Tinant, B.; Declercq, J.-P.; Chapon, D.; Markó, I. E. *J. Organomet. Chem.* **2005**, *690*, 6156–6168. (e) De Bo, G.; Berthon-Gelloz, G.; Tinant, B.; Markó, I. E. *Organometallics* **2006**, *25*, 1881–1890. (f) Poyatos, M.; Maise-François, A.; Bellemin-Lapponnaz, S.; Gade, L. H. *Organometallics* **2006**, *25*, 2634–2641. (g) Berthon-Gelloz, G.; Schumers, J.-M.; De Bo, G.; Markó, I. E. *J. Org. Chem.* **2008**, *73*, 4190–4197, hydroboration and diboration reactions. (h) Lillo, V.; Mata, J.; Segarra, A. M.; Peris, E.; Fernandez, E. *Chem. Commun.* **2007**, 2184–2186. (i) Lillo, V.; Mata, J.; Ramirez, J.; Peris, E.; Fernandez, E. *Organometallics* **2006**, *25*, 5829–5831, while Pt(II)–NHC complexes have been reported to display catalytic activity in the CH activation of methane. (j) Ahrens, S.; Strasser, T. *Inorg. Chim. Acta* **2006**, *359*, 4789–4796, in alkynes hydroarylation. (k) Biffis, A.; Tubaro, C.; Buscemi, G.; Basato, M. *Adv. Synth. Catal.* **2008**, *350*, 189–196, as well as in the reductive cyclization of diynes and enynes. (l) Jung, I. G.; Seo, J.; Lee, S. I.; Choi, S. Y.; Chung, Y. K. *Organometallics* **2006**, *25*, 4240–4242.

Table 1. Platinum(II)–Diphosphine Complexes Bearing Symmetrical Imidazolylidene Ligands

compd	R ¹	diphosphine	yield	³¹ P NMR: δ (¹ J _{P–Pt}) [² J _{P–P}]
1	4a	(<i>R,R</i>)-MeDuPhos	84%	64.7 (2169 Hz) 63.7 (3229 Hz) [6 Hz]
2	5a	(<i>R</i>)-Binap	47%	6.2 (2293 Hz) 5.1 (3370 Hz) [21 Hz]
3	6a	(<i>R,R</i>)-Et-FerroTANE	95%	29.4 (3104 Hz) 26.4 (2191 Hz) [10 Hz]
4	7a	(<i>S,S</i>)-Chiraphos	84%	37.8 (2170 Hz) 37.3 (3232 Hz) [17 Hz]
5	7b	(<i>S,S</i>)-Chiraphos	96%	38.4 (2140 Hz) 37.0 (3255 Hz) [16 Hz]
6	7c	(<i>S,S</i>)-Chiraphos	70%	37.1 (2216 Hz) 34.9 (3278 Hz) [16 Hz]

positions. The *cis*-arrangement of **3** was supported by ³¹P NMR data showing a signal at δ 8.5 ppm, with ¹J_{Pt–P} couplings of 3695 Hz. The ¹J_{Pt–P} coupling constant value lies in the range usually observed in platinum(II) complexes when iodide and phosphorus ligands are in *trans* relative positions.¹⁵

The molecular structure of **3** was then reliably assessed by single-crystal X-ray diffraction study. The corresponding ORTEP drawing is depicted in Figure 1.

The crystal structure shows a square-planar coordination of the metal center. The heterocyclic carbene is perpendicular to the plane encompassing the four ligands (torsion angle = 89.1°). The Pt–C(1) bond length amounts to 1.984 Å and is in the expected range for Pt–imidazolylidene bonds.¹⁶

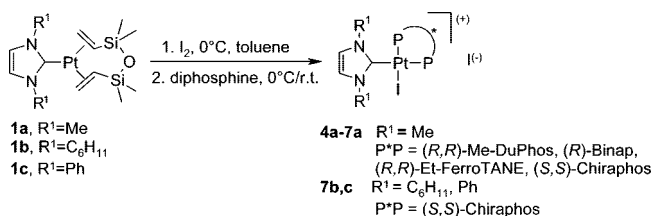
The formation of the *cis*-isomer of **3** as the unique product is consistent with the higher thermodynamic stability of *cis*-configured carbene/phosphine complexes of platinum, highlighted recently by Huynh,¹⁷ although a kinetic preference for the *cis*-isomer cannot be ruled out either.¹⁸

In order to achieve partial characterization of the intermediate olefin complex (Scheme 2), the oxidative addition of iodine to complex **1a** was monitored by ¹H NMR in toluene-*d*₈. The observed intermediate results from addition of I₂ and concomitant displacement of one of the coordinated olefin moieties: NMR signals for both the Pt-coordinated {δ 4.4–4.6 (m, 2H), 5.33 (d, ³J_{H–H} = 15 Hz, ³J_{H–Pt} = 62 Hz, 1H)} and unbound vinyl groups {δ 5.74 (dd, ³J_{H–H} = 20.0 Hz, ²J_{H–H} = 4.0 Hz, 1H), 5.95 (dd, ³J_{H–H} = 15.0 Hz, ²J_{H–H} = 4.0 Hz, 1H), 6.15 (dd, ³J_{H–H} = 20.0 Hz, ³J_{H–H} = 15.0 Hz, 1H) ppm} of the divinylsiloxane moiety have been observed. The pairs of enantiotopic methyl groups on silicon display two separate signals each, at δ 0.16 (s, 3H), 0.17 (s, 3H), 0.40 (s, 3H), and 0.45 (s, 3H) ppm. The imidazolylidene ligand displays non-equivalent N-Me (δ 3.86 and 3.89 ppm) and CH groups at δ 6.96 and 7.00 (³J_{H–H} = 2.0 Hz) ppm. A structurally related (NHC)Pt(olefin)Cl₂ complex has been reported recently by Nolan.¹⁹

The reaction sequence above involving iodine oxidative addition to a Pt(0)-NHC complex and subsequent complexation of a phosphorus ligand was then performed by using symmetrically substituted carbenes and chiral chelating diphosphines (Scheme 3).

In a first series of experiments the (*N,N*-dimethylimidazolylidene)Pt⁰ complex **1a** was oxidized with iodine and then

Scheme 3. Synthesis of the Imidazolylidene/Chiral Diphosphine Platinum(II) Complexes 4–7



combined with the commercially available diphosphines (*R,R*)-Me-DuPhos, (*R*)-Binap, (*R,R*)-Et-FerroTane, and (*S,S*)-Chiraphos (entries 1–4 in Table 1). Then, the *N,N*-dicyclohexyl- and *N,N*-diphenylimidazolylidene platinum(0) complexes were used as starting materials for the reaction with (*S,S*)-Chiraphos (entries 5 and 6). The corresponding cationic, diphosphine-containing complexes **4–7** were obtained in moderate to good yields as solids that separate directly from the reaction mixture. If necessary, additional purification of the final product was performed by column chromatography.

In their ³¹P NMR spectra (see Table 1) these square-planar complexes display typical patterns: two nonequivalent phosphorus centers generate an AB system with ²J_{P–P} = 6 to 18 Hz, while ¹⁹⁵Pt–³¹P couplings split the signals again into satellites. The ¹J_{P–Pt} couplings allow reliable assignment of the ³¹P NMR signals to *cis*- and *trans*-phosphorus atoms, as larger couplings (>3000 Hz) are expected for phosphorus atoms *trans* to the halide ligand.

An X-ray diffraction study has been performed on the (*N,N'*-dicyclohexylimidazolylidene)Pt[(*S,S*)-Chiraphos] complex **7b** (Figure 2). The platinum center displays a perfect square-planar coordination of the four ligands, and the Pt–C(1) bond distance (2.063 Å) is similar to that found in other platinum(II)–NHC complexes. In chelate complexes, (*S,S*)-Chiraphos is known to preferentially adopt a δ -conformation since this allows the methyl groups to occupy pseudoequatorial positions.²⁰ The same preferred conformation of the diphosphine backbone has been noticed in complex **7b**. The higher steric hindrance is thus displayed in the bottom-left and upper-right quadrants of the coordination sphere of platinum (see sketch in Figure 2). Accordingly, the carbene ligand deviates from the expected arrangement, perpendicular to the coordination plane (90° dihedral angle, see Figure 1), to a tilt angle of 73.9° (dihedral angle between the P(1)–Pt–P(2) and N(1)–C(1)–N(2) mean planes) so as to minimize steric interactions between the bulky cyclohexyl group and the phosphine in the hindered bottom-left region. A similar distortion of the coordinated carbene from an orthogonal disposition was noticed in the crystal structure of a ((*R,R*)-Me-DuPhos)Pt(NHC)I₂ complex.¹²

The same synthetic procedure as above was then applied to the preparation of complexes **8** from the unsymmetrically substituted imidazolylidene-platinum(0) complexes **2a–k** (R¹ ≠ R²) and (*S,S*)-Chiraphos (Scheme 4). Square-planar complexes of this series featuring unsymmetrical carbene ligands are

(15) Favez, R.; Roulet, R.; Pinkerton, A. A.; Schwarzenbach, D. *Inorg. Chem.* **1980**, *19*, 1356–1365.

(16) (a) McGuinness, D. S.; Cavell, K. J.; Yates, B. F.; Skelton, B. W.; White, A. H. *J. Am. Chem. Soc.* **2001**, *123*, 8317–8328. (b) Han, Y. H.; Huynh, H. V.; Tan, G. K. *Organometallics* **2007**, *26*, 4612–4617. (c) Fantasia, S.; Petersen, J. L.; Jacobsen, H.; Cavallo, L.; Nolan, S. P. *Organometallics* **2007**, *26*, 5880–5889.

(17) Slow conversion of *trans*-configured carbene/phosphine platinum(II) complexes into the thermodynamically favoured *cis*-isomers was observed: see ref 16b.

(18) For a detailed discussion on the mechanism and stereochemical outcome of ligand substitution on square-planar platinum complexes, see: Cross, R. J. *Chem. Soc. Rev.* **1985**, *14*, 197–223.

(19) Fantasia, S.; Jacobsen, H.; Cavallo, L.; Nolan, S. P. *Organometallics* **2007**, *26*, 3286–3288.

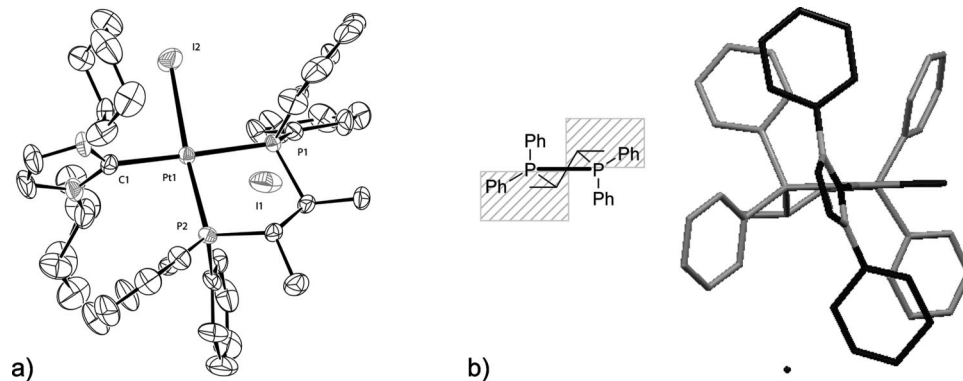
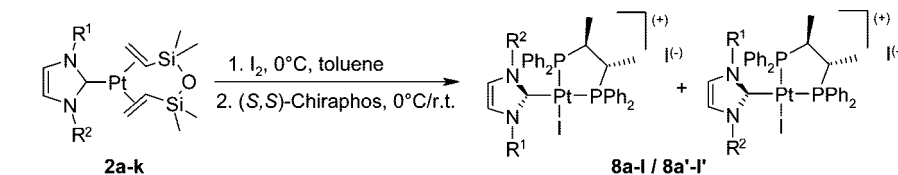


Figure 2. (a) ORTEP view of the (*N,N'*-dicyclohexylimidazolylidene)Pt[(*S,S*)-Chiraphos] I_2 complex **7b**. Selected bond distances (\AA): Pt–C(1) = 2.062(9), C(1)–N(1) = 1.346(12), C(1)–N(2) = 1.336(12), Pt–P(1) = 2.286(2), Pt–P(2) = 2.236(2), Pt–I(2) = 2.6364(9). Selected bond angles (deg): P(1)–Pt–P(2) = 85.40(8), P(2)–Pt–C(1) = 95.2(3), C(1)–Pt–I(2) = 89.5(2), P(1)–Pt–I(2) = 89.91(6), N(1)–C(1)–N(2) = 104.7(8). (b) Schematic drawings of the (*S,S*)-Chiraphos complex highlighting the δ -conformation of the carbon backbone and the tilt angle of the imidazole ring with respect to the coordination plane.

Scheme 4. Synthesis of [(*S,S*)-chiraphos]Pt(II) Complexes **8** Bearing Unsymmetrical NHC Ligands



Comp	R ¹ , R ²	yield	Epimers ratio ^a	Comp	R ¹ , R ²	yield	Epimers ratio ^a
8a,a' ¹²	Me, Ph	84%	1:1	8g,g'	CH ₂ Ph, Ph	63%	1:1
8b,b'	Me, CH ₂ Ph	90%	1:1	8h,h'	CH ₂ Ph, Cy	56%	1:1
8c,c'	Me, <i>t</i> -Bu	89%	1:1	8i,i'	NaphCH ₂ , Cy	76%	1:1
8d,d'	Me, 2,6-(<i>i</i> Pr) ₂ C ₆ H ₃	71%	80:20 ^b	8j,j'	NaphCH ₂ , <i>t</i> -Bu	53%	91:9
8e,e'	Me, Mes	72%	95:5 ^b	8k,k'	Me, (<i>S</i>)-CH(Me)Ph	93%	70:30
8f,f'	CH ₂ Ph, <i>t</i> -Bu	80%	91:9	8l,l'	Me, (<i>R</i>)-CH(Me)Ph	92%	77:23

^a The absolute axial configuration of the single epimers has not been assigned, except for **8i,i'**. ^b Kinetic products ratio

expected to display axial chirality^{21,22} and, consequently, to generate diastereomeric pairs if rotation of the NHC ligand around the Pt–C bond is prevented by either steric hindrance or a multiple-bond character of the Pt–C bond.

Complexes **8a–l** have been obtained indeed as mixtures of epimers with opposite axial configurations. Assignment of the axial configurations has been done for **8i,i'** by X-ray diffraction studies on complex **8i'**. As shown in Figure 3, complex **8i'** displays an *R* configuration. The axial configuration of the other complexes **8** has not been assigned so far.

Reactions in Scheme 4 proceed with good diastereoselectivity only for Pt(0) complexes bearing very bulky imidazolylidene ligands. Thus for instance, use of the NHC ligand bearing a *t*-Bu and a CH₂Ph substituent on the nitrogen atoms affords the

corresponding epimeric complexes **8j** and **8j'** in a 91:9 ratio, while the analogous complexes **8h,h'**, bearing the less hindered *N*-cyclohexyl substituent, are formed in 1:1 ratio. The absolute axial configuration of complexes **8j,j'** could not be unambiguously determined by crystallography. Nevertheless, based on the structural assignment for **8i'**, and by comparing the ¹H NMR data of these closely related complexes, we could tentatively assume that the major epimer **8j** displays an *S* axial configuration.²³ This is consistent with the expected trend by which, in the favored epimer **8j**, the bulkier *tert*-butyl substituent lies in the nonhindered upper-left quadrant of the (*S,S*)-Chiraphos platinum(II) complex.

The configurational stability of complexes **8a,a'** has been checked by ¹H NMR on enriched mixtures of **8a+8a'**: samples with **8a:8a'** ratios of 9:2 and 3:7, respectively, have been obtained by fractional crystallization. No interconversion of the epimers was observed, neither at room temperature nor after heating at 50 °C for 20 h.²⁴

(20) (a) Brunkan, N. M.; White, P. S.; Gagné, M. R. *Angew. Chem., Int. Ed.* **1998**, *37*, 1579–1582. (b) Brunner, H.; Winter, A.; Breu, J. *J. Organomet. Chem.* **1998**, *553*, 285–306.

(21) For examples of axially chiral, square-planar complexes bearing NHC ligands see: (a) Enders, D.; Gielen, H.; Breuer, K. *Tetrahedron: Asymmetry* **1997**, *8*, 3571–3574. (b) Enders, D.; Gielen, H.; Runsink, J.; Breuer, K.; Brode, S.; Boehn, K. *Eur. J. Inorg. Chem.* **1998**, *91*, 3–919. (c) Enders, D.; Gielen, H. *J. Organomet. Chem.* **2001**, *617–618*, 70–80. (d) Bolm, C.; Kesselgruber, M.; Raabe, G. *Organometallics* **2002**, *21*, 707–710. (e) Faller, J. W.; Fontaine, P. P. *Organometallics* **2006**, *25*, 5887–5893.

(22) The axis of chirality is represented by the carbene–Pt bond, whereas the two perpendicular planes contain this axis and either the two nitrogen atoms of the NHC ligand, for the first one, or the P and iodine atoms, for the second (see Figure 3).

(23) The N-CH₂ groups of complexes **8i** and **8i'** display typical ¹H NMR patterns made of two doublets. These doublets display a significantly larger $\Delta\delta$ shift for complex **8i** (1.94 ppm) than for **8i'** (0.61 ppm). The corresponding signals for complex **8j** have $\Delta\delta = 1.95$ ppm. Thus, it is tentatively assumed that **8j** displays the same structural features as **8i**, i.e., an *S* axial configuration.

(24) Single epimers of analogous, configurationally stable, NHC–Pt complexes containing Me-DuPHOS or Me-BPE as the bidentate chiral phosphine have been characterized previously: see ref 12.

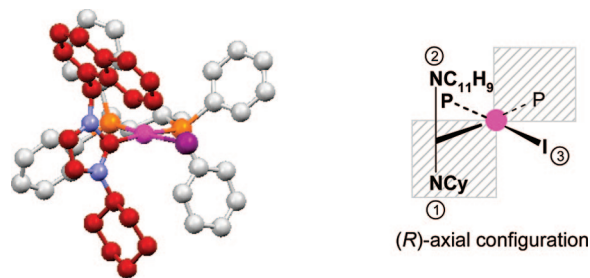


Figure 3. View of complex **8i'** from X-ray data.

In light of these data, an unexpected behavior was observed however for complexes **8e,e'** and **8d,d'**, which contain the bulky *N*-mesityl-*N*-methylimidazolyliene and *N*-(2,6-diisopropylphenyl)-*N*-methylimidazolyliene ligands, respectively. Complexes **8e,e'** were isolated as a 9:1 mixture of two compounds, which were tentatively assigned as the expected epimers with opposite axial configurations (72% total yield). When this mixture was stirred at room temperature in CDCl₃, slow isomerization was observed by ¹H NMR, which was then completed by heating at about 50 °C for 48 h. The final equilibrium mixture contains the isomeric derivative **8e'** as the major component, in 85% relative amount. In a similar way, the initial 7:3 mixture of complexes **8d+8d'** was slowly converted into pure **8d'** at room temperature in CDCl₃ solutions. The apparent facile isomerization of **8e** into **8e'**, or **8d** into **8d'**,²⁵ markedly contrasts with the observed configurational stability of complexes **8a,a'** and cannot be easily rationalized at present.

Catalysis and Computational Studies. As already mentioned in the Introduction, the NHC-diphosphine-Pt(II) complexes **I** have been designed as potential catalysts for a definite class of enyne cycloisomerization reactions, those proceeding through simple activation of the alkyne moiety by π -complexation on platinum. Thus, the cycloisomerization of the 1,6-enyne **9**, bearing a nitrogen-containing tether, into the 3-azabicyclo[4.1.0]-heptene **10**^{2a} has been selected as the test reaction to evaluate the catalytic activity of complexes **I**.²⁶ To the best of our knowledge, no enantioselective synthesis of the bicyclic derivative **10** has been reported so far, although analogous asymmetric cycloisomerization reactions promoted by Ir complexes⁷ have been described recently.

The standard protocol for catalytic reactions involves the use of a 9:1 toluene/dichloromethane mixture as the solvent,²⁷ a 4 mol % amount of catalyst, and heating at 90 °C for about 20 h. The catalytically active species have been generated from the Pt(II) complexes **4–7** by addition of AgBF₄ as a suitable halide scavenger. Conversion rates (from ¹H NMR) and enantioselectivities are given in Table 2. The enantiomeric excesses of **10** were measured by HPLC on samples that may contain some residual starting material, **9**.

In a preliminary screening, the relative efficiencies of various chiral diphosphines have been evaluated by comparing the catalytic behavior of the Pt complexes **4a–7a** bearing an *N,N'*-dimethylimidazolyliene ligand (entries 1–4 in Table 2). Clean reactions were usually observed, with the expected bicycle **10** being the only product. The highest catalytic activity and enantioselectivity levels were obtained with the Chiraphos

(25) Unfortunately, crystals of **8e'** or **8d'** suitable for X-ray diffraction studies could not be obtained.

(26) (a) For previous examples of enyne cycloisomerization reactions promoted by ligand-modified platinum(II) see ref 3. (b) Fürstner, A.; Davies, P. W.; Gress, T. *J. Am. Chem. Soc.* **2005**, *127*, 8244–8245.

(27) Addition of a small amount of dichloromethane is required to produce, initially, a homogeneous solution of the catalyst.

Scheme 5. Cycloisomerization Studies with Chiral Pt(II) Catalysts: Test Reaction

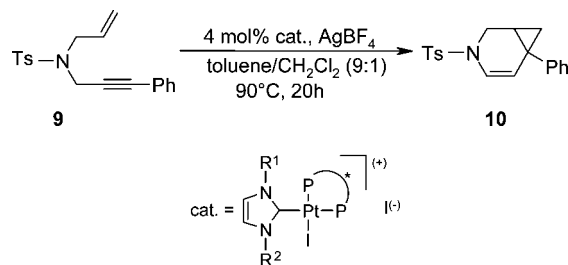


Table 2. Cycloisomerization Reactions Promoted by Chiral Pt Catalysts 4–7

entry	cat.	R ¹ , R ²	diphosphine	conv [%] ^a	ee [%] ^b
1	4a	Me	(<i>R,R</i>)-MeDuPhos	59	7
2	5a	Me	(<i>R</i>)-Binap	67	12
3	6a	Me	(<i>R,R</i>)-Et-FerroTANE	56	28
4	7a	Me	(<i>S,S</i>)-Chiraphos	100	58
5	7b	C ₆ H ₁₁	(<i>S,S</i>)-Chiraphos	91	64
6	7c	Ph	(<i>S,S</i>)-Chiraphos	15	36

^a By ¹H NMR of the crude reaction mixture. ^b HPLC: Chiracel OD, hexane/*i*PrOH, 99:1.

complex **7a** (entry 4), which gave total conversion and a 58% enantiomeric excess.

Following this preliminary screening, Chiraphos was selected as the preferred chiral diphosphine, and a second series of experiments was performed then with platinum complexes in which Chiraphos is combined with other symmetrically substituted NHC moieties (entries 5–7). Substitution of the nitrogen atoms by phenyl groups (complex **7c**) decreased both the catalytic activity and enantioselectivity (entry 6). The use of an imidazolyliene ligand bearing bulky cyclohexyl substituents afforded an active catalyst, **7b**, and allowed the enantiomeric excesses to be slightly improved from 58% to 64% (entry 5).

We next surveyed the catalytic properties of the (*S,S*)-Chiraphos complexes **8**, featuring unsymmetrically substituted NHC ligands, disregarding the fact that they have been isolated mainly as epimeric mixtures. Representative results are given in Table 3.

It appears that the nature of the nitrogen substituents of the imidazolyliene moiety modulates to some extent the enantioselectivity of the cycloisomerization reaction above. Carbenes bearing the rather bulky cyclohexyl or *tert*-butyl groups, combined with benzyl and 1-naphthylmethyl groups, respectively, allowed the highest enantioselectivities to be attained, with enantiomeric excesses up to 74% (entries **5** and **8**). The chiral induction did not improve significantly when complexes **8k** and **8l** were used, which display an additional stereogenic center on the nitrogen substituent (entries 9 and 10 vs 2).

All together these results show that the carbene ligands modulate to some extent both the yields and enantioselectivities of the cycloisomerization reaction promoted by the chiraphos-Pt complexes **7** and **8**. As an additional evidence of the essential role of the carbene ligand, it must be mentioned that a PtI₂(Chiraphos) complex afforded only trace amounts of the expected 3-azabicyclo[4.1.0]heptene, in the reaction conditions of Scheme 5.

When surveying the catalytic properties of the Pt complexes **8** made of *N,N'*-unsymmetrically substituted carbenes, a major question arose about the suitability of using the diastereomeric mixtures above as precatalysts. This procedure may be considered as convenient and adequate only if the epimeric platinum complexes interconvert during the catalytic cycle. Thus, to gain

Table 3. Cycloisomerization Reactions Promoted by Chiral (NHC)Pt-[(*S,S*)-Chiraphos] Complexes **8** (Scheme 5)

	Pre-catalyst	R ¹ , R ²	conv [%]	ee [%]
1	8a,a'	Me, Ph	90	57
2	8b,b'	Me, CH ₂ Ph	60	58
3	8c,c'	Me, <i>t</i> -Bu	91	62
4	8d,d'	Me, 2,6-di(<i>i</i> Pr) ₂ C ₆ H ₃	90	60
5	8f,f'	CH₂Ph, <i>t</i>-Bu	100	73
6	8g,g'	CH ₂ Ph, Ph	100	48
7	8h,h'	CH ₂ Ph, Cy	100	70
8	8i,i'	NaphCH₂, Cy	91	74
9	8k,k'	Me, (<i>S</i>)-CH(Me)Ph	70	42
10	8l,l'	Me, (<i>R</i>)-CH(Me)Ph	81	61

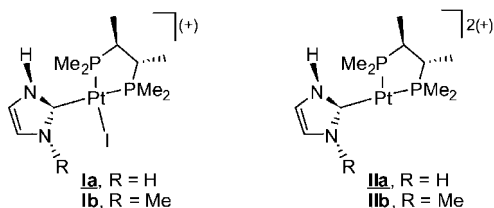
insight into the configurational stability of the axially chiral platinum catalysts above during the cycloisomerization reaction, we compared the behavior of mixtures of the epimeric complexes **8i,i'** at different isomer ratios. Only minor variations of the enantiomeric excess have been observed, which cannot be ascribed to the catalytic activity of distinct epimeric catalysts. Thus, for instance, catalysts made from 1:1 and >95:5 mixtures of **8i+8i'** afforded the cyclization product **10** in 74% and 72% ee, respectively, in parallel experiments.

Thus, we came to the conclusion that the axial configuration of the platinum complexes **8i,i'** is likely to be lost during the cycloisomerization reaction. This is not inconsistent with the assessed configurational stability of the starting square-planar complexes **8**, since transient tricoordinated Pt complexes are expected to be involved in the process as the catalytically active species (see Introduction). Such tricoordinated complexes might display much lower epimerization barriers than the corresponding tetracoordinated species, due to peculiar isomerization mechanisms. This has been assessed through the experimental and theoretical studies above.

The epimerization process has been evidenced as follows: the iodide ligand has been removed from complex **8i'** (single diastereomer) by addition of 2 equiv of AgBF₄ in CH₂Cl₂ at room temperature. After about 10 min, an excess of KI was added and the mixture was stirred overnight. Monitoring the mixture by ¹H NMR showed the presence of a 60:40 mixture of the two epimeric complexes **8i,i'**.

A DFT study was carried out in order to enlighten and compare the structures and epimerization barriers of the tetracoordinated and tricoordinated platinum(II) complexes **I** and **II**, bearing a chelating diphosphine and an imidazolylidene ligand.²⁸ Calculations were carried out using simplified structures displaying the two-carbon bridge of (*S,S*)-Chiraphos. Methyl groups have been used as phosphorus substituents and the imidazolylidene ligands bear either two hydrogen atoms or a methyl group and a hydrogen atom as the N-substituents (Figure 4).

The optimized structures for complexes **Ia** and **IIa** are displayed in Figure 5. The calculated bond angles for the square-planar complex **Ia**, i.e., P–Pt–P = 85.7°, P–Pt–I = 90.9°, I–Pt–C = 87.0°, and C–Pt–P = 96.4°, fit well with the

**Figure 4.** Calculated models of complexes **I** and **II**.

experimental values reported above for complex **7b** (P–Pt–P = 85.4°, P–Pt–I = 89.9°, I–Pt–C = 89.5°, and C–Pt–P = 95.2°). Furthermore, as in the crystal structure, the heterocyclic carbene is perpendicular to the P–Pt–P plane. This indicates that, in the absence of steric repulsion, the N- and P-substituents do not affect the geometrical features of these complexes.

The tricoordinated dicationic complex **IIa** adopts a T-shaped coordination with only minor variations of the bond angles with respect to complex **Ia**. Thus, for instance, the C–Pt–P bond angle increases by only 6.0° after removal of the iodide ligand, showing a very small shift of the carbene moiety from its initial position. The perpendicular conformation of the imidazolylidene ligand is also maintained, reflecting, as in **Ia**, a better electronic interaction between the ligand and the metal fragment in this arrangement.

We next considered the epimerization process, which could follow different pathways (Table 4). The conversion of complex (*R*)-**I** (or (*R*)-**II**) into complex (*S*)-**I** (or (*S*)-**II**) could take place through rotation of the carbene ligand around the Pt–C axis via **TS1**. Other possible epimerization pathways for complexes **I** and **II** involve a tetrahedral (**TS2**) and a Y-shaped achiral (**TS3**) transition state, respectively.²⁹

For the epimerization processes of the tetracoordinated complexes **Ia,b**, our calculations reveal that rotation around the Pt–C bound axis is a low-energy-demanding process for carbene with low steric hindrance, i.e., with hydrogens as the N-substituents. The transition state **TS1** requires indeed only 15.6 kJ/mol free energy from **Ia**. The other pathway from **Ia**, which involves passage through a transient tetrahedral Pt(II) (**TS2**), has a much higher free energy barrier of 170.8 kJ/mol. This path is thus unlikely and has not been considered from **Ib**. Inclusion of steric hindrance with a *N*-methyl substituted carbene greatly increases the barrier to reach **TS1**. Indeed steric interaction between the *N*-methyl group and either the phosphine or the iodide ligand leads to transition states located respectively 61.7 and 74.6 kJ/mol higher in energy than **Ib**. It is noticeable that the iodide group induces a slightly more pronounced steric effect than the PMe₂ moiety. These results suggest that rotation around the Pt–C axis, and thus the epimerization process, could be easily prevented by the use of *N,N'*-disubstituted carbenes,

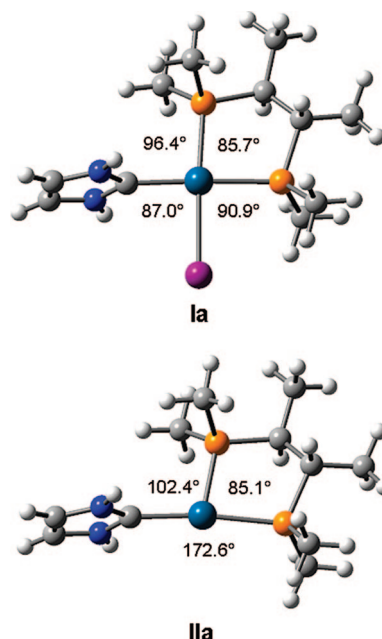
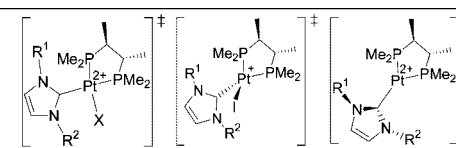
**Figure 5.** Geometrical structures of complexes **Ia** and **IIa**.

Table 4. Activation Free Energy Calculated at the B3LYP/6-31G(d,p)/LANL2DZ Level for the Epimerization Pathways for Complexes Ia,b and IIa,b (energies in kJ/mol)



	R ¹	R ²	X	TS1	TS2	TS3
Ia	H	H	I ⁻	15.6	170.8	-
Ib	H	Me	I ⁻	74.6	-	-
IIa	H	H	∅	29.0	-	17.9
IIb	H	Me	∅	27.7	-	18.3
IIIb	Me	H	∅	51.5	-	18.3

in agreement with the above experimental results indicating the configurational stability of complexes **I**.

The same trend is observed for the tricoordinated, T-shaped complexes **IIa,b**, revealing the possibility of preventing rotation around the Pt–C bond axis by using bulky N-substituted carbenes. Indeed, moving from **IIa** (R¹ = R² = H) to **IIIb** (R¹ = Me, R² = H) induces an increase of the barrier from 29.0 to 51.5 kJ/mol to reach **TS1** when the methyl substituent is *cis* to the phosphine. We did however notice that (i) the increase is lower than that observed when moving from **Ia** to **Ib**, reflecting the possibility for the tricoordinated complexes to slightly open the C–Pt–P bond angle (C–Pt–P bond angles of 102.8° and 114.2° in **Ib-TS1** and **IIIb-TS1**, respectively, for R¹ = Me), and (ii) steric hindrance is not observed when the methyl substituent is located *trans* to the phosphine (R² = Me). These results indicate that epimerization through rotation of the carbene moiety is easier for the tricoordinated complexes **II** than for tetracoordinated complexes **I**; an increase of the steric bulk of the phosphorus and/or the carbene substituents could nevertheless block this path. However, an alternative epimerization pathway can be envisioned for complexes **II** that involves a Y-shaped transition state **TS3** and swinging of the carbene ligand between two contiguous coordination sites. This is expected to be a low-energy pathway, irrespective of the nature and steric bulk of the carbene and phosphorus substituents. Our calculations confirm this hypothesis, **TS3** being located at ~18 kJ/mol from both **IIa** and **IIIb**.

Thus, the above computations afford some rationale to the observed easy epimerization of the tricoordinated platinum(II) complexes that are generated from **8** after removal of the halide ligand.

Conclusions

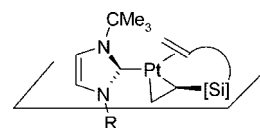
A general synthetic approach to platinum(II) complexes bearing both an NHC and a phosphine or a diphosphine ligand has been developed. The method involves oxidative addition of I₂ to the easily available (NHC)Pt⁰(dvtms) complexes. When combining (*S,S*)-Chiraphos and unsymmetrically substituted carbenes, epimeric mixtures of axially chiral complexes of the general formula (NHC)Pt(Chiraphos)⁺I⁻ have been isolated, most of which display configurational stability. Experiments and DFT calculations suggest that epimerization of these tetracoordinated square-planar complexes is precluded mainly by the steric hindrance between the imidazolylidene N-substituent and the phosphine or the iodide ligands, which prevents rotation of the carbene around the Pt–C bond.

The Pt(II) complexes above represent suitable precatalysts for the enantioselective cycloisomerization reaction of *N*-allyl-*N*-(3-phenylpropyn-2-yl)-4-methylbenzenesulfonamide into the corresponding 3-azabicyclo[4.1.0]hept-4-ene. Tuning of the phosphine–NHC pair allows modulation of the catalytic properties and enantiomeric excesses up to 74% to be attained in this model reaction. These results support the postulated mechanism, which involves tricoordinated platinum complexes as the catalytically active species. Experiments and DFT calculations indicate that, in the case of unsymmetrically substituted NHC complexes, the T-shaped tricoordinated intermediates can easily epimerize through a Y-shaped transition state, allowing swinging of the carbene between the two available coordination sites. This epimerization process is broadly insensitive to the steric hindrance of the ligands.

Experimental Section

All reactions were run under an argon atmosphere, by using standard techniques for manipulating air-sensitive compounds. Anhydrous CH₂Cl₂ was obtained by filtration through drying columns. Toluene and all reagents were of commercial quality and were used without further purification. Flash column chromatography was performed using 40–63 mesh silica. Nuclear magnetic resonance spectra (¹H, ¹³C, ³¹P) were recorded on either Bruker AV 500 or AV 300 spectrometers. Optical rotations were determined with a JASCO P-1010 polarimeter. HPLC was performed at a column temperature of 20 °C on a Waters 2695 Separations Module equipped with a diode array UV detector.

Starting Materials: (NHC)Pt⁰(dvtms) Complexes. Imidazolium salts have been prepared either by alkylation of 1-substituted imidazoles with alkyl halides or from primary amines, glyoxal, and formaldehyde according to the reported methods.³⁰ The Pt(0) complexes **1** and **2** have been prepared by the synthetic procedure described by Markó,^{14d} which involves reaction of an imidazolium salt (1 equiv) with 1 equiv of the Karstedt's catalyst (Pt₂(dvtms)₃) (2% Pt in xylene solution) in xylene, in the presence of *t*-BuOK (1.4 equiv) at 0 °C to rt for several hours. Complexes **1a**, **1b**, **1d**,^{14d} and **2a**¹² are known compounds. Spectral data for the Pt(0) complexes **1c** and **2b–k** are reported hereafter. Complexes **2c**, **2f**, and **2j**, bearing *N*-*t*-Bu-substituted imidazolylidenes, display two separate series of NMR signals. This has been tentatively assigned to the presence of noninterconverting (or slowly interconverting) isomers due to hindered rotation of the NHC ligand around the Pt–C axis, combined with the metallacyclopropane-like character of the olefin–metal bonds, which differentiates the two faces of the coordination plane (see X-ray data in ref 14d).



(1,3-Diphenylimidazol-2-ylidene)(1,3-divinyltetramethyldisiloxane)platinum(0) (1c). Complex **1c** was obtained in 20% yield (60 mg, 0.1 mmol) from 1,3-diphenylimidazolium chloride (130 mg, 0.5 mmol), after purification by chromatography with an 8:2 heptane/ethyl acetate mixture as the eluent (*R*_f = 0.4). ¹H NMR (300 MHz, CDCl₃): δ -0.61 (s, 6H, SiMe), 0.21 (s, 6H, SiMe), 1.5–1.7 (4H, H₂C=CHSi), 1.93 (dd, *J* = 9.6 Hz, *J* = 1.8 Hz, ²*J*_{H–Pt} = 50 Hz, 2H, H₂C=CHSi), 7.3 (6H), 7.43 (s, ⁴*J*_{H–Pt} = 11.1 Hz, 2H, NCH=), 7.5 (4H); ¹³C NMR (75 MHz, CDCl₃) δ -2.8 (Me), 1.4 (Me), 33.8 (¹*J*_{C–Pt} = 122 Hz, H₂C=CHSi), 41.5 (¹*J*_{C–Pt} = 163 Hz, H₂C=CHSi), 122.3 (³*J*_{C–Pt} = 38 Hz, NCH=), 124.6, 127.8, 128.6, 140.8 (C) ppm.

(1-Benzyl-3-methylimidazol-2-ylidene)(1,3-divinyltetramethyldisiloxane)platinum(0) (2b). Complex **2b** was obtained in 78% yield (73 mg, 0.13 mmol) from 1-benzyl-3-methylimidazolium

iodide³¹ (50 mg, 0.17 mmol), after purification by chromatography with an 8:2 heptane/ethyl acetate mixture as the eluent ($R_f = 0.4$). Colorless oil; ¹H NMR (300 MHz, CDCl₃) δ -0.06 (s, 6H, SiMe), 0.58 (s, 6H, SiMe), 2.0–2.3 (4H, H₂C=CHSi), 2.49 (br d, $J = 10.5$ Hz, ²J_{H-Pt} = 52.8 Hz, 2H, H₂C=CHSi), 3.82 (s, ⁴J_{H-Pt} = 2.7 Hz, 3H, NMe), 5.40 (s, ⁴J_{H-Pt} = 5.4 Hz, 2H, NCH₂Ph), 7.16 (d, ³J = 2.1 Hz, ⁴J_{H-Pt} = 11.7 Hz, 1H, NCH=), 7.28 (d, ³J = 2.1 Hz, ⁴J_{H-Pt} = 12.0 Hz, 1H, NCH=), 7.4 (2H, Ph), 7.5–7.6 (3H, Ph); ¹³C NMR (75 MHz, CDCl₃) δ -1.9 (SiMe), 1.5 (SiMe), 34.5 (¹J_{C-Pt} = 118 Hz, H₂C=CHSi), 36.9 (³J_{C-Pt} = 45.0 Hz, NMe), 40.3 (¹J_{C-Pt} = 158 Hz, H₂C=CHSi), 53.3 (³J_{C-Pt} = 42 Hz, NCH₂Ph), 120.5 (³J_{C-Pt} = 36 Hz, NCH=), 122.5 (³J_{C-Pt} = 37 Hz, NCH=), 127.5, 127.8, 128.7, 136.8(C_{Ph}), 184.7 (Pt=C) ppm.

(1-*tert*-Butyl-3-methylimidazol-2-ylidene)(1,3-divinyltetramethyldisiloxane) platinum(0) (2c). Complex **2c** was obtained in 41% yield (42 mg, 0.08 mmol) from 1-*tert*-butyl-3-methylimidazolium iodide³¹ (58 mg, 0.2 mmol) after purification by chromatography with 9:1 heptane/ethyl acetate as the eluent. Due to hindered rotation of the carbene moiety, complex **2c** is formed as a 1:1 mixture of isomers. White solid; ¹H NMR (300 MHz, CDCl₃) δ -0.28 (s, 6H, SiMe), -0.27 (s, 6H, SiMe), 0.33 (s, 12H, SiMe), 1.56 (s, 9H, CMe₃), 1.6 (s, 9H, CMe₃), 1.6–2.0 (8H), 2.14 (d, $J = 9.9$ Hz, ²J_{H-Pt} = 52 Hz, 2H, H₂C=CHSi), 2.28 (d, $J = 11.1$ Hz, ²J_{H-Pt} = 54 Hz, 2H, H₂C=CHSi), 3.45 (s, ⁴J_{H-Pt} = 5.1 Hz, 3H, NMe), 3.50 (s, ⁴J_{H-Pt} = 5.1 Hz, 3H, NMe), 6.96 (d, ³J = 2.1 Hz, ⁴J_{H-Pt} = 10 Hz, 1H, NCH=), 6.97 (d, ³J = 2.1 Hz, ⁴J_{H-Pt} = 11 Hz, 1H, NCH=), 7.20 (d, ³J = 2 Hz, 1H, NCH=), 7.21 (d, ³J = 2 Hz, 1H, NCH=) ppm.

(1-(2,6-Diisopropylphenyl)-3-methylimidazol-2-ylidene)(1,3-divinyltetramethyldisiloxane)platinum(0) (2d). Complex **2d** was obtained in 34% yield (87 mg, 0.14 mmol) from 1-(2,6-diisopropylphenyl)-3-methylimidazolium chloride (0.15 mg, 0.41 mmol),^{30c} after purification by chromatography with 95:5 heptane/ethyl acetate as the eluent ($R_f = 0.3$). ¹H NMR (300 MHz, CDCl₃) δ -0.41 (s, 6H, SiMe), 0.25 (s, 6H, SiMe), 1.06 (d, ³J = 6.9 Hz, 6H, CHMe₂), 1.19 (d, ³J = 6.6 Hz, 6H, CHMe₂), 1.5–2.1 (6H, H₂C=CHSi), 2.75 (m, 2H, CHMe₂), 3.71 (s, NMe), 7.02 (d, ³J = 1.8 Hz, ⁴J_{H-Pt} = 11 Hz, 1H, NCH=), 7.14 (d, ³J = 7.7 Hz, 2H), 7.18 (d, ³J = 1.8 Hz, ⁴J_{H-Pt} = 10 Hz, 1H, NCH=), 7.32 (t, ³J = 7.7 Hz, 1H); ¹³C NMR (75 MHz, CDCl₃) δ -1.8 (SiMe), 1.5 (SiMe), 22.2 (Me), 26.2 (Me), 28.1 (CHMe₂), 34.7 (¹J_{C-Pt} = 110 Hz, H₂C=CHSi), 37.4 (NMe), 40.4 (¹J_{C-Pt} = 159 Hz, H₂C=CHSi), 120.9 (CH), 123.4 (CH), 124.8 (CH), 129.3 (CH), 146.0 (C) ppm.

(1-Mesityl-3-methylimidazol-2-ylidene)(1,3-divinyltetramethyldisiloxane)platinum(0) (2e). Complex **2e** was obtained in quantitative yield (130 mg, 0.22 mmol) from 1-mesityl-3-methylimidazolium iodide³² (72 mg, 0.22 mmol), after purification by chromatography with 9:1 heptane/ethyl acetate as the eluent ($R_f = 0.2$). ¹H NMR (300 MHz, CDCl₃) δ -0.66 (s, 6H, SiMe), 0.23 (s, 6H, SiMe), 1.6–1.9 (4H, H₂C=CHSi), 2.03 (6H, Me), 2.20 (d, $J = 11$ Hz, ²J_{H-Pt} = 51.6 Hz, 2H, H₂C=CHSi), 2.22 (3H, Me), 3.67

(s, 3H, NMe), 6.84 (s, 2H), 6.95 (d, ³J = 1.8 Hz, ⁴J_{H-Pt} = 10 Hz, 1H, NCH=), 7.20 (d, ³J = 1.8 Hz, ⁴J_{H-Pt} = 10 Hz, 1H, NCH=); ¹³C NMR (75 MHz, CDCl₃) δ -2.4 (SiMe), 1.4 (SiMe), 17.9 (Me), 20.9 (Me), 34.7 (¹J_{C-Pt} = 118 Hz, H₂C=CHSi), 37.2 (NMe), 40.3 (¹J_{C-Pt} = 162 Hz, H₂C=CHSi), 121.8 (NCH=), 122.7 (NCH=), 128.8 (CH), 135.1 (C), 138.5 (C) ppm.

(1-Benzyl-3-*tert*-butylimidazol-2-ylidene)(1,3-divinyltetramethyldisiloxane)platinum(0) (2f). Complex **2f** was obtained in 31% yield (104 mg, 0.17 mmol) from 1-benzyl-3-*tert*-butylimidazolium chloride (140 mg, 0.56 mmol), after purification by chromatography with 9:1 heptane/ethyl acetate as the eluent. Colorless oil. Due to hindered rotation of the carbene moiety, complex **2f** is formed as a 1:1 mixture of isomers. ¹H NMR (300 MHz, CDCl₃) δ -0.47 (s, 6H, SiMe), -0.29 (s, 6H, SiMe), 0.27 (s, 6H, SiMe), 0.30 (s, 6H, SiMe), 1.59 (s, 9H, CMe₃), 1.62 (s, 9H, CMe₃), 1.7–2.3 (12H, H₂C=CHSi), 5.13 (s, 2H, NCH₂Ph), 5.25 (s, 2H, NCH₂Ph), 6.81 (d, ³J = 1.8 Hz, 1H, NCH=), 6.88 (d, ³J = 1.8 Hz, 1H, NCH=), 7.1 (4H), 7.2–7.3 (8H); ¹³C NMR (75 MHz, CDCl₃, selected data) δ -2.6 (SiMe), -2.5 (SiMe), -1.50 (SiMe), 30.6 (CMe₃), 30.7 (CMe₃), 32.8 (¹J_{C-Pt} = 123 Hz, H₂C=CHSi), 34.1 (¹J_{C-Pt} = 119 Hz, H₂C=CHSi), 43.2 (¹J_{C-Pt} = 169 Hz, H₂C=CHSi), 43.5 (¹J_{C-Pt} = 168 Hz, H₂C=CHSi), 54.3 (NCH₂), 54.4 (NCH₂), 58.2 (NCMe₃) ppm.

(1-Benzyl-3-phenylimidazol-2-ylidene)(1,3-divinyltetramethyldisiloxane)platinum(0) (2g). Complex **2g** was obtained in 53% yield (98 mg, 0.16 mmol) from 1-benzyl-3-phenylimidazolium bromide, after purification by chromatography with 8:2 heptane/ethyl acetate as the eluent ($R_f = 0.3$). ¹H NMR (300 MHz, CDCl₃) δ -0.67 (s, 6H, SiMe), 0.12 (s, 6H, SiMe), 1.5–2.1 (6H, H₂C=CHSi), 5.10 (s, 2H, NCH₂), 6.91 (d, ³J = 2.1 Hz, ⁴J_{H-Pt} = 11 Hz, 1H, NCH=), 7.0–7.2 (9H), 7.3–7.4 (2H); ¹³C NMR (75 MHz, CDCl₃, selected data) δ -2.6 (SiMe), 1.4 (SiMe), 34.4 (¹J_{C-Pt} = 121 Hz, H₂C=CHSi), 41.4 (¹J_{C-Pt} = 162 Hz, H₂C=CHSi), 53.8 (³J_{C-Pt} = 44.7 Hz, NMe), 120.9 (³J_{C-Pt} = 36.2 Hz, NCH=), 122.3 (³J_{C-Pt} = 37 Hz, NCH=), 136.4 (C), 140.6 (C), 185.1 (C–Pt) ppm.

(1-Benzyl-3-cyclohexylimidazol-2-ylidene)(1,3-divinyltetramethyldisiloxane)platinum(0) (2h). 1-Cyclohexylimidazole³³ was prepared from cyclohexylamine, glyoxal, and paraformaldehyde in dioxane/water in the presence of H₃PO₄ (63% yield after chromatography on silica gel with CH₂Cl₂/MeOH as the eluent). 1-Benzyl-3-cyclohexylimidazolium chloride was obtained in 96% yield by reacting 1-cyclohexylimidazole with benzyl chloride in dioxane at 100 °C. Complex **2h** was obtained in 39% yield (100 mg, 0.16 mmol) from 1-benzyl-3-cyclohexylimidazolium chloride (100 mg, 0.41 mmol), after purification by chromatography with 95:5 heptane/ethyl acetate as the eluent. ¹H NMR (300 MHz, CDCl₃) δ -0.24 (s, 3H, SiMe), 0.08 (s, 3H, SiMe), 0.33 (s, 6H, SiMe), 1.0–2.0 (14H), 2.18 (d, $J = 10.8$ Hz, ²J_{H-Pt} = 52.2 Hz, 2H, H₂C=CHSi), 4.4 (m, 1H, NCH), 5.10 (s, 2H, NCH₂), 6.91 (d, ³J = 1.5 Hz, ⁴J_{H-Pt} = 13 Hz, 1H, NCH=), 7.03 (d, ³J = 1.5 Hz, ⁴J_{H-Pt} = 12 Hz, 1H, NCH=), 7.1–7.3 (5H, Ph); ¹³C NMR (75 MHz, CDCl₃, selected data) δ -1.8 (SiMe), 1.4 (SiMe), 25.3 (CH₂), 25.4 (CH₂), 33.9 (CH₂), 34.0 (CH₂=CHSi), 40.7 (¹J_{C-Pt} = 162 Hz, CH₂=CHSi), 53.5 (NCH₂), 58.4 (NCH), 117.6 (NCH=), 120.7 (³J_{C-Pt} = 34 Hz, NCH=), 127.7, 128.6, 136.8 (C_{Ph}), 182.6 (C–Pt) ppm.

(1-Cyclohexyl-3-(1-naphthylmethyl)imidazol-2-ylidene)(1,3-divinyltetramethyldisiloxane)platinum(0) (2i). 1-Cyclohexyl-3-(1-naphthylmethyl)imidazolium bromide was obtained in 88% yield by reacting 1-cyclohexylimidazole with 1-(bromomethyl)naphthalene in dioxane at 100 °C. ¹H NMR (300 MHz, CDCl₃) δ 1.1–1.5 (3H), 1.6–1.9 (5H), 2.0–2.1 (2H), 4.32 (tt, ³J = 11.7, ³J = 4.0 Hz, 1H, NCH), 5.95 (s, 2H, NCH₂), 7.5–7.7 (4H), 7.84 (t, $J = 1.8$ Hz, 1H, NCH=), 7.84 (t, $J = 1.8$ Hz, 1H, NCH=), 8.0–8.2 (3H), 9.45 (t, $J = 1.8$ Hz, 1H, NCHN) ppm. Complex **2i** was obtained in

(28) For recent computational studies on the NHC–metal bond see: (a) Green, J. C.; Herbert, B. J. *Dalton Trans.* **2005**, 1214–1220. (b) Cavallo, L.; Correa, A.; Costabile, C.; Jacobsen, H. *J. Organomet. Chem.* **2005**, *690*, 5407–5413. (c) Jacobsen, H.; Correa, A.; Costabile, C.; Cavallo, L. *J. Organomet. Chem.* **2006**, *691*, 4350–4358, and references therein.

(29) The epimerization process could also be operative through dissociation/reassociation of the carbene ligand or be facilitated by dissociation of one arm of the diphosphine. These pathways are however unlikely due to the ability of these ligands to strongly bind the metal. The calculated dissociation energy of 329 and 241 kJ/mol for respectively the carbene and one phosphine of **1a** confirms this hypothesis.

(30) (a) Herrmann, W. A.; Köcher, C.; Goossen, L. J.; Artus, G. R. J. *Chem.–Eur. J.* **1996**, *2*, 1627–1636. (b) Chianese, A. R.; Crabtree, R. H. *Organometallics* **2005**, *24*, 4432–4436. (c) Jafarpour, L.; Stevens, E. D.; Nolan, S. P. *J. Organomet. Chem.* **2000**, *606*, 49–54.

(31) Chu, Y.; Deng, H.; Cheng, J.-P. *J. Org. Chem.* **2007**, *72*, 7790–7793.

(32) Nieto-Oberhuber, C.; Lopez, S.; Echavarren, A. M. *J. Am. Chem. Soc.* **2005**, *127*, 6178–6179.

(33) Gridnev, A. A.; Mihaltseva, I. M. *Synth. Commun.* **1994**, *24*, 1547–1556.

66% yield (119 mg, 0.17 mmol) from 1-cyclohexyl-3-(1-naphthylmethyl)imidazolium bromide (100 mg, 0.27 mmol), after purification by chromatography with 9:1 heptane/ethyl acetate as the eluent ($R_f = 0.4$). ^1H NMR (300 MHz, CDCl_3) δ -0.20 (s, 6H, SiMe), 0.35 (s, 6H, SiMe), 1.0–2.0 (14H), 2.38 (d, $J = 10.8$ Hz, $^2J_{\text{H-Pt}} = 53.4$ Hz, 2H, $\text{H}_2\text{C}=\text{CHSi}$), 4.44 (m, 1H, NCH), 5.53 (s, 2H, NCH_2), 6.78 (d, $^3J = 1.8$ Hz, $^4J_{\text{H-Pt}} = 12$ Hz, 1H, $\text{NCH}=\text{C}$), 6.96 (d, $^3J = 1.8$ Hz, $^4J_{\text{H-Pt}} = 10$ Hz, 1H, $\text{NCH}=\text{C}$), 7.2–7.5 (4H), 7.8–8.0 (3H); ^{13}C NMR (75 MHz, CDCl_3) δ -1.8 (SiMe), 1.5 (SiMe), 25.3 (CH_2), 25.4(CH_2), 33.9 (CH_2), 34.2 ($\text{CH}_2=\text{CHSi}$), 40.6 ($^1J_{\text{C-Pt}} = 162$ Hz, $\text{CH}_2=\text{CHSi}$), 51.6 (NCH_2), 58.5 (NCH), 117.4 ($\text{NCH}=\text{C}$), 120.6 ($\text{NCH}=\text{C}$), 123.5, 125.2, 126.0, 126.5, 127.1, 128.7, 128.9, 131.2 (C), 132.0 (C), 133.7 (C) ppm.

(1-tert-Butyl-3-(1-naphthylmethyl)imidazol-2-ylidene)(1,3-divinyltetramethyldisiloxane)platinum (2j). 1-tert-Butyl-3-(1-naphthylmethyl)imidazolium bromide was obtained in 93% yield by reacting 1-tert-butylimidazole with 1-(bromomethyl)naphthalene in dioxane at 100 °C. ^1H NMR (300 MHz, CDCl_3) δ 1.63 (s, 9H, CMe_3), 5.96 (s, 2H, NCH_2), 7.4–7.7 (5H), 7.79 (t, $J = 1.8$ Hz, 1H, $\text{NCH}=\text{C}$), 8.0–8.1 (2H), 8.2 (1H), 9.67 (1H, NCHN) ppm. Complex **2j** was obtained in 47% yield (130 mg, 0.20 mmol) from 1-tert-butyl-3-(1-naphthylmethyl)imidazolium bromide (150 mg, 0.43 mmol), after purification by chromatography with 9:1 heptane/ethyl acetate as the eluent ($R_f = 0.3$). Due to hindered rotation of the carbene moiety, complex **2c** is formed as a 1:1 mixture of isomers. Pale yellow oil; ^1H NMR (300 MHz, CDCl_3) δ -0.57 (s, 6H, SiMe), -0.25 (s, 6H, SiMe), 0.27 (s, 6H, SiMe), 0.32 (s, 6H, SiMe), 1.63 (s, 9H, CMe_3), 1.66 (s, 9H, CMe_3), 1.9–2.1 (8H), 2.28 (d, $J = 11.1$ Hz, $^2J_{\text{H-Pt}} = 52.8$ Hz, 2H, $\text{H}_2\text{C}=\text{CHSi}$), 2.40 (dd, $J = 8.1$ Hz, $J = 2.7$ Hz, $^2J_{\text{H-Pt}} = 54.6$ Hz, 2H, $\text{H}_2\text{C}=\text{CHSi}$), 5.55 (s, $^4J_{\text{H-Pt}} = 6.0$ Hz, 2H, NCH_2), 5.65 (s, $^4J_{\text{H-Pt}} = 5.7$ Hz, 2H, NCH_2), 6.70 (d, $^3J = 2.1$ Hz, $^4J_{\text{H-Pt}} = 10.8$ Hz, 1H, $\text{NCH}=\text{C}$), 6.74 (d, $^3J = 2.1$ Hz, $^4J_{\text{H-Pt}} = 10.2$ Hz, 1H, $\text{NCH}=\text{C}$), 7.1–7.2 (4H), 7.4–7.5 (6H), 7.8 (6H) ppm.

(1-Methyl-3-(1-phenylethyl)imidazol-2-ylidene)(1,3-divinyltetramethyldisiloxane) platinum(0) ((S)-2k, (R)-2k). (S)-1-(1-Phenylethyl)imidazole was prepared from (S)- α -methylbenzylamine (3 mmol), glyoxal (7.5 mmol), and paraformaldehyde (7.5 mmol) in the presence of H_3PO_4 . Yield: 430 mg, (83%) after chromatography on silica gel with 5:95 EtOH/ CH_2Cl_2 as the eluent. ^1H NMR (300 MHz, CDCl_3) δ 1.88 (d, $^3J = 6.9$ Hz, 3H, Me), 5.37 (q, $^3J = 6.9$ Hz, 1H, NCHMe), 6.95 (t, $J = 2$ Hz, 1H, $\text{NCH}=\text{C}$), 7.10 (t, $J = 2$ Hz, 1H, $\text{NCH}=\text{C}$), 7.15–7.20 (2H), 7.3–7.4 (3H), 7.61 (1H, NCHN) ppm. ((S)-1-methyl-3-(1-phenylethyl)imidazolium iodide was obtained in 66% yield by reaction of (S)-1-(1-phenylethyl)imidazole and MeI in acetonitrile at 80 °C. ^1H NMR (300 MHz, CDCl_3) δ 2.07 (d, $^3J = 6.9$ Hz, 3H, Me), 4.14 (s, 3H, Me), 5.86 (q, $^3J = 6.9$ Hz, 1H, NCHMe), 7.18 (1H), 7.37 (1H), 7.4–7.5 (5H), 10.3 (1H, NCHN). Complex (S)-**2k** was obtained in 78% yield (141 mg, 0.24 mmol) from (S)-1-methyl-3-(1-phenylethyl)imidazolium iodide, after purification by chromatography with 8:2 heptane/ethyl acetate as the eluent. (S)-**2k**: pale yellow oil; ^1H NMR (500 MHz, CDCl_3) δ -0.25 (s, 6H, SiMe), 0.35 (s, 6H, SiMe), 1.71 (d, $^3J = 7.0$ Hz, 3H, NCHMe), 1.8–2.1 (4H, $\text{H}_2\text{C}=\text{CHSi}$), 2.3 (br, 2H, $\text{H}_2\text{C}=\text{CHSi}$), 3.54 (3H, NMe), 5.86 (br, 1H, NCHMe), 6.87 (br, 1H, $\text{NCH}=\text{C}$), 7.01 (s, $^4J_{\text{H-Pt}} = 11.5$ Hz, 1H, $\text{NCH}=\text{C}$), 7.2–7.4 (5H, Ph); ^{13}C NMR (75 MHz, CDCl_3) δ -2.0 (SiMe), 1.4 (SiMe), 20.5 (NCHMe), 34.4 ($^1J_{\text{C-Pt}} = 117$ Hz, $\text{H}_2\text{C}=\text{CHSi}$), 36.8 ($^3J_{\text{C-Pt}} = 45.0$ Hz, NMe), 40.1 ($\text{H}_2\text{C}=\text{CHSi}$), 57.4 (NCHMe), 117.8 ($^3J_{\text{C-Pt}} = 36$ Hz, $\text{NCH}=\text{C}$), 122.5 ($^3J_{\text{C-Pt}} = 37$ Hz, $\text{NCH}=\text{C}$), 126.6, 127.6, 128.5, 140.9 (C_{Ph}), 183.5 ($\text{Pt}=\text{C}$) ppm. $[\alpha]_{\text{D}} = -116$ (c 0.6, CHCl_3). The enantiomeric complex (R)-**2k** was obtained by the same reaction starting from (R)-1-methyl-3-(1-phenylethyl)imidazolium iodide.

cis-(N,N'-Dimethylimidazolylidene)Pt(triphenylphosphine)diiodide (3). A solution of I_2 (25 mg, 0.1 mmol) in toluene (3 mL) was added at 0 °C to a solution of (N,N'-dimethylimidazolylidene) $\text{Pt}^0(\text{dvtms})$ complex **1a** (50 mg, 0.1 mmol) in 2

mL of toluene under argon. To the resulting mixture was then added at 0 °C a solution of PPh_3 (30 mg, 0.11 mmol) in toluene (1 mL). The reaction mixture was stirred at room temperature for 4 h. After evaporation of the solvent, the final product was purified by chromatography with a 1:1 heptane/ethyl acetate mixture as the eluent ($R_f = 0.2$). Yield of **3**: 66 mg (82%). Yellow solid. ^{31}P NMR (CDCl_3) δ 8.5 ($J_{\text{P-Pt}} = 3695$ Hz); ^1H NMR (300 MHz, CDCl_3) δ 3.50 (6H, NMe), 6.51 (s, $J_{\text{H-Pt}} = 10.2$ Hz, 2H, $\text{NCH}=\text{C}$), 7.2–7.6 (15H, Ph); ^{13}C NMR (75 MHz, CDCl_3) δ 37.5 (NMe), 121.7 ($\text{NCH}=\text{C}$), 128.1 (d, $J_{\text{C-Pt}} = 11$ Hz, CH), 130.8, 134.2 (d, $J_{\text{C-Pt}} = 10$ Hz, CH) ppm; MS (^{195}Pt) calcd for $\text{C}_{25}\text{H}_{25}\text{I}_2\text{N}_2\text{P}_2\text{PtNa}$ 829.9234, found 829.9274. Crystals suitable for X-ray diffraction studies were obtained from a $\text{CH}_2\text{Cl}_2/\text{Et}_2\text{O}$ solution.

Synthesis of the (Diphosphine)(NHC)PtI₂ Complexes. Typical Procedure: Synthesis of (N,N'-Dimethylimidazolylidene)-Pt((R,R)-MeDuPhos)I₂ (4a). A solution of I_2 (25 mg, 0.1 mmol) in toluene (4 mL) was added at 0 °C to a solution of (N,N'-dimethylimidazolylidene) $\text{Pt}^0(\text{dvtms})$ complex **1a** (50 mg, 0.1 mmol) in 3 mL of toluene under argon. The resulting mixture was then added at 0 °C to a solution of (R,R)-MeDuPhos in toluene (3 mL). The reaction mixture was stirred overnight at room temperature, during which time the desired product separated from the mixture as a pale yellow solid. Yield: 84% (72 mg). ^1H NMR (500 MHz, CDCl_3) δ 0.97 (dd, $^3J_{\text{H-Pt}} = 16.5$ Hz, $^3J = 7.0$ Hz, 3H, Me), 1.01 (dd, $^3J_{\text{H-Pt}} = 17.0$ Hz, $^3J = 7.0$ Hz, 3H, Me), 1.1–1.2 (m, 1H, CH_2), 1.21 (dd, $^3J_{\text{H-Pt}} = 19.0$ Hz, $^3J = 7.0$ Hz, 3H, Me), 1.46 (dd, $^3J_{\text{H-Pt}} = 19.0$ Hz, $^3J = 7.0$ Hz, 3H, Me), 1.8–2.0 (m, 2H, CH_2), 2.2–2.6 (5H), 2.7–2.8 (2H), 2.98 (m, 1H, PCHMe), 3.79 (s, 3H, NMe), 3.85 (m, 1H, PCHMe), 3.89 (s, 3H, NMe), 7.22 (s, 1H, $\text{NCH}=\text{C}$), 7.50 (s, 1H, $\text{NCH}=\text{C}$), 7.7–7.8 (3H), 7.99 (t, $J = 7.5$ Hz, 1H); ^{13}C NMR (125 MHz, CDCl_3) δ 14.1 (Me), 14.3 (Me), 16.8 (Me), 17.0 (Me), 35.7 (d, $J_{\text{C-Pt}} = 7.4$ Hz, CH_2), 36.0 (d, CH_2), 36.2 (CH_2), 37.4 ($J_{\text{C-Pt}} = 16$ Hz, CH_2), 38.0–38.5 ($\text{PCHMe} + \text{NMe}$), 39.3 ($J_{\text{C-Pt}} = 24$ Hz, N-Me), 41.2 (d, $^1J_{\text{C-Pt}} = 35$ Hz, PCHMe), 42.9 (d, $^1J_{\text{C-Pt}} = 35$ Hz, PCHMe), 123.9 (N- $\text{CH}=\text{C}$), 125.7 (N- $\text{CH}=\text{C}$), 132.8–133.5 (Ar) ppm; HRMS (^{195}Pt) calcd for $\text{C}_{21}\text{H}_{37}\text{I}_2\text{N}_2\text{P}_2\text{PtNa}$ 724.1022, found 724.1025. $[\alpha]_{\text{D}} = -15$ (c 0.5, CHCl_3).

(N,N'-Dimethylimidazolylidene)Pt((R)-Binapp)I₂ (5a). A pale yellow solid was obtained in 47% yield (54 mg). ^1H NMR (500 MHz, CDCl_3) δ 3.66 (s, 3H, NMe), 4.02 (s, 3H, NMe), 6.52 (d, $J = 8.5$ Hz, 1H), 6.7 (3H), 6.8 (2H), 6.9–7.1 (5H), 7.14 (2H), 7.21 (2H), 7.28 (2H), 7.3–7.4 (7H), 7.47 (d, $J = 10$ Hz, 1H), 7.5–7.7 (7H), 8.00 (dd, $J = 8.5$ Hz, $J = 2$ Hz, 1H), 8.14 (dd, $J = 10.5$ Hz, $J = 8.5$ Hz, 1H); ^{13}C NMR (125 MHz, CDCl_3 , selected data) δ 38.2 (N-Me), 38.9 (NMe) ppm; HRMS (^{195}Pt) calcd for $\text{C}_{49}\text{H}_{40}\text{I}_2\text{N}_2\text{P}_2\text{Pt}$ 1040.1359, found 1040.1292. $[\alpha]_{\text{D}} = +225$ (c 0.5, CHCl_3).

(N,N'-Dimethylimidazolylidene)Pt((R,R)-Et-FerroTane)I₂ (6a). **6a** was isolated as an orange oil that spontaneously separates from the crude reaction mixture and solidifies on standing (94 mg, 95% yield). ^1H NMR (500 MHz, CDCl_3) δ 0.61 (t, $^3J = 7.5$ Hz, 3H, Me), 0.78 (t, $^3J = 7.5$ Hz, 3H, Me), 1.1–1.3 (m, 4H, CH_2), 1.16 (t, $^3J = 7.5$ Hz, 3H, Me), 1.30 (t, $^3J = 7.5$ Hz, 3H, Me), 1.7 (m, 1H), 1.9 (m, 2H), 2.2 (m, 1H), 2.2–2.4 (m, 3H), 2.50 (m, $J_{\text{H-Pt}} = 38.5$ Hz, 1H), 2.6 (m, 1H), 2.75 (m, 1H), 2.95 (m, 1H, PCH), 3.77 (s, 3H, NMe), 3.97 (s, 3H, NMe), 4.14 (m, 1H), 4.24 (1H, CH_{Cp}), 4.36 (1H, CH_{Cp}), 4.64 (1H, CH_{Cp}), 4.66 (1H, CH_{Cp}), 4.70 (1H, CH_{Cp}), 4.84 (2H, CH_{Cp}), 4.94 (1H, CH_{Cp}), 7.42 (s, 1H, $\text{NCH}=\text{C}$), 7.54 (s, 1H, $\text{NCH}=\text{C}$); ^{13}C NMR (125 MHz, CDCl_3) δ 11.7 (d, $^3J_{\text{C-Pt}} = 9$ Hz, Me), 12.0 (d, $^3J_{\text{C-Pt}} = 15$ Hz, Me), 13.6 (d, $^3J_{\text{C-Pt}} = 13$ Hz, Me), 13.8 (d, $^3J_{\text{C-Pt}} = 13$ Hz, Me), 24.7 (d, $^2J_{\text{C-Pt}} = 5$ Hz, CH_2), 24.9 (d, $^2J_{\text{C-Pt}} = 2$ Hz, CH_2), 26.7 (CH_2), 26.8 (CH_2), 34.6 (d, $^2J_{\text{C-Pt}} = 17$ Hz, CH_2), 35.8 (d, $^2J_{\text{C-Pt}} = 16$ Hz, CH_2), 38.0, 38.2, 38.4 (PCH), 38.5 (NMe), 39.6 (NMe), 39.6 (d, $^1J_{\text{C-Pt}} = 38$ Hz, PCH), 42.4 (d, $^1J_{\text{C-Pt}} = 40$ Hz, PCH), 73.5–76.0 (CH_{Cp}), 124.6

(NCH=), 125.1 (NCH=) ppm; HRMS (^{195}Pt , ^{57}Fe) calcd for $\text{C}_{29}\text{H}_{44}\text{FeIN}_2\text{P}_2\text{Pt}$ 860.1005, found 860.0983. $[\alpha]_{\text{D}} = -203$ (c 0.5, CHCl_3).

(*N,N'*-Dimethylimidazolylidene)Pt((*S,S*)-Chiraphos) I_2 (**7a**). **7a** was obtained as a colorless solid that precipitates from the crude reaction mixture (81 mg, 84% yield). ^1H NMR (500 MHz, CDCl_3) δ 1.04–1.13 (6H, Me), 2.3 (m, 1H, PCH), 2.8 (m, 1H, PCH), 2.90 (s, 3H, NMe), 3.47 (s, 3H, NMe), 6.83 (s, 1H, NCH=), 7.1–7.8 (m, 19H), 7.9 (m, 2H); ^{13}C NMR (125 MHz, CDCl_3) δ 13.4 (d, $^2J_{\text{C-P}} = 16$ Hz, Me), 14.0 (d, $^2J_{\text{C-P}} = 16$ Hz, Me), 34.3 (dd, $^1J_{\text{C-P}} = 37$ Hz, $^2J_{\text{C-P}} = 12$ Hz, PCH), 36.9 (NMe), 37.0 (dd, $^1J_{\text{C-P}} = 38$ Hz, $^2J_{\text{C-P}} = 15$ Hz, PCH), 38.0 ($J_{\text{C-Pt}} = 25$ Hz, NMe), 123.9 ($J_{\text{C-Pt}} = 27$ Hz, NCH=), 124.0 ($J_{\text{C-Pt}} = 27$ Hz, NCH=) ppm; HRMS (^{195}Pt) calcd for $\text{C}_{33}\text{H}_{36}\text{IN}_2\text{P}_2\text{Pt}$ 844.1046, found 844.1021. $[\alpha]_{\text{D}} = +142$ (c 0.5, CHCl_3).

(*N,N'*-Dicyclohexylimidazolylidene)Pt((*S,S*)-Chiraphos) I_2 (**7b**). **7b** was isolated as a pale yellow solid that spontaneously separates from the crude reaction mixture (105 mg, 96% yield). The solid was recrystallized from a dichloromethane/ether mixture. ^1H NMR (500 MHz, CDCl_3) δ -0.14 (1H, NCH CH_2), 0.7–1.8 (m, 17H), 1.08 (dd, $^3J_{\text{H-P}} = 15$ Hz, $J = 7$ Hz, 3H, Me), 1.20 (dd, $^3J_{\text{H-P}} = 12.9$ Hz, $J = 6.9$ Hz, 3H, Me), 2.25 (m, 2H), 2.49 (d, $J = 12$ Hz, 1H), 3.03 (m, 1H), 3.91 (m, 1H, NCH), 4.23 (m, 1H, NCH), 6.88 (s, 1H, NCH=), 7.10 (s, 1H, NCH=), 7.1–7.2 (2H), 7.5–8.0 (18H); ^{13}C NMR (75 MHz, CDCl_3) δ 13.8 (d, $^2J_{\text{C-P}} = 17$ Hz, Me), 13.9 (d, $^2J_{\text{C-P}} = 17$ Hz, Me), 24.7 (CH_2), 25.0 (CH_2), 25.3 (CH_2), 25.6 (CH_2), 26.1 (CH_2), 31.1 (CH_2), 33.1 (CH_2), 33.5 (CH_2), 34.8 (dd, $^1J_{\text{C-P}} = 33$ Hz, $^2J_{\text{C-P}} = 10$ Hz, PCH), 37.2 (dd, $^1J_{\text{C-P}} = 40$ Hz, $^2J_{\text{C-P}} = 16$ Hz, PCH), 59.8 (NCH), 60.3 (NCH), 119.5 (d, $^4J_{\text{C-P}} = 5.7$ Hz, NCH=), 119.9 (d, $^4J_{\text{C-P}} = 5.6$ Hz, NCH=), 160.7 (dd, $^2J_{\text{C-P}} = 139$ Hz, $^2J_{\text{C-P}} = 10$ Hz, C=Pt) ppm; HRMS (^{195}Pt) calcd for $\text{C}_{43}\text{H}_{52}\text{IN}_2\text{P}_2\text{Pt}$ 980.2298, found 980.2073. $[\alpha]_{\text{D}} = +90$ (c 0.5, CHCl_3). Crystals suitable for X-ray diffraction studies have been grown from $\text{CH}_2\text{Cl}_2/\text{AcOEt}$.

(*N,N'*-Diphenylimidazolylidene)Pt((*S,S*)-Chiraphos) I_2 (**7c**). The synthesis of **7c** was performed at a 0.05 mmol scale. **7c** was obtained in 70% yield (38 mg) after chromatography on silica gel with 95:5 $\text{CH}_2\text{Cl}_2/\text{MeOH}$ as the eluent ($R_f = 0.3$). Colorless solid. ^1H NMR (500 MHz, CDCl_3) δ 0.83 (dd, $^3J_{\text{C-P}} = 15.0$ Hz, $J = 6.5$ Hz, 3H, Me), 0.94 (dd, $^3J_{\text{C-P}} = 12.5$ Hz, $J = 6.5$ Hz, 3H, Me), 1.90 (m, 1H, PCH), 2.33 (m, 1H, PCH), 6.9–7.0 (4H), 7.1 (4H), 7.2–7.4 (11H), 7.5–7.7 (6H), 7.7–7.8 (5H), 7.81 (d, 2H); ^{13}C NMR (125 MHz, CDCl_3 , selected data) δ 13.3 (d, $^2J_{\text{C-P}} = 16$ Hz, Me), 13.7 (br d, Me), 34.4 (br dd, PCH), 36.6 (br dd, PCH), 125.3 (NCH=), 125.5 (NCH=), 125.8 (CH), 126.6 (CH), 128.6–135.8, 138.0 (C), 138.7 (C) ppm; HRMS (^{195}Pt) calcd for $\text{C}_{43}\text{H}_{40}\text{IN}_2\text{P}_2\text{Pt}$ 968.1359, found 968.1266. $[\alpha]_{\text{D}} = +349$ (c 0.5, CHCl_3).

(1-Benzyl-3-methylimidazol-2-ylidene)Pt((*S,S*)-Chiraphos) I_2 (**8b,b'**). Complex **8** was obtained as a 1:1 mixture of epimers. It was isolated as a pale yellow solid that spontaneously separates from the crude reaction mixture (94 mg, 90% yield). ^{31}P NMR (121 MHz, CDCl_3) δ 38.1 (d, $J_{\text{P-P}} = 16$ Hz, $J_{\text{P-Pt}} = 2177$ Hz), 38.0 (d, $J_{\text{P-P}} = 16$ Hz, $J_{\text{P-Pt}} = 2169$ Hz), 37.7 (d, $J_{\text{P-P}} = 16$ Hz, $J_{\text{P-Pt}} = 3217$ Hz), 37.4 (d, $J_{\text{P-P}} = 16$ Hz, $J_{\text{P-Pt}} = 3225$ Hz); ^1H NMR (500 MHz, CDCl_3) δ 1.1–1.2 (Me), 2.34 (m, PCH), 2.93 (m, PCH), 2.98 (NMe), 3.11 (d, $^2J = 14.0$ Hz, CH_2Ph), 3.55 (NMe), 4.62 (d, $^2J = 14.0$ Hz, CH_2Ph), 5.19 (d, $^2J = 14.5$ Hz, CH_2Ph), 5.28 (d, $^2J = 14.5$ Hz, CH_2Ph), 6.44 (s), 6.63 (s), 6.87 (s), 7.0–8.0 (Ar) ppm; HRMS (^{195}Pt) calcd for $\text{C}_{39}\text{H}_{40}\text{IN}_2\text{P}_2\text{Pt}$ (M – I) 920.1359, found: 920.1282.

(1-*tert*-Butyl-3-methylimidazol-2-ylidene)Pt((*S,S*)-Chiraphos) I_2 (**8c,c'**). A 1:1 mixture of the diastereomeric **8c** and **8c'** was obtained after separation of the crude reaction mixture by column chromatography ($\text{CH}_2\text{Cl}_2/\text{EtOH}$, 98:2, $R_f = 0.2$). Yield: 90 mg, 89%. ^{31}P NMR (121 MHz, CDCl_3) δ 39.3 (d, $J_{\text{P-P}} = 15$ Hz, $J_{\text{P-Pt}} = 2165$ Hz), 37.1 (d, $J_{\text{P-P}} = 15$ Hz, $J_{\text{P-Pt}} = 3393$ Hz) and 37.0 (d, $J_{\text{P-P}} = 16$ Hz, $J_{\text{P-Pt}} = 2199$ Hz), 36.0 (d, $J_{\text{P-P}} = 16$ Hz, $J_{\text{P-Pt}} = 3310$ Hz); ^1H NMR

(500 MHz, CDCl_3) δ 1.1–1.4 (MeCH), 1.23 (s, CMe_3), 1.53 (s, CMe_3), 2.02 (m, CHMe), 2.22 (m, CHMe), 3.22 (s, NMe), 3.52 (CHMe), 3.60 (m, CHMe), 3.63 (s, NMe), 6.70 (NCH=), 7.00 (NCH=), 7.11 (NCH=), 7.19 (NCH=), 7.3–7.7 (Ph), 8.2 (Ph) ppm; HRMS (^{195}Pt) calcd for $\text{C}_{36}\text{H}_{42}\text{IN}_2\text{P}_2\text{Pt}$ (M – HI) 886.1516, found 886.1508.

(1-(2,6-Diisopropylphenyl)-3-methylimidazol-2-ylidene)Pt((*S,S*)-Chiraphos) I_2 (**8d,d'**). This compound was obtained in 71% yield (79 mg) as a yellow solid that separates from the reaction mixture. The solid contains a 8:2 mixture of **8d**+**8d'**. The filtrate contains small amounts of **8d**+**8d'**, with **8d'** being the major epimer. MS (ESI) m/z 991 (M – I + H, 86), 748 (100). Spectral data for **8d** (from the mixture): ^{31}P NMR (121 MHz, CDCl_3) δ 36.3 (d, $J_{\text{P-P}} = 16$ Hz, $J_{\text{P-Pt}} = 2110$ Hz), 32.0 (d, $J_{\text{P-P}} = 16$ Hz, $J_{\text{P-Pt}} = 3390$ Hz); ^1H NMR (500 MHz, CDCl_3 , selected data) δ 0.36 (d, $^3J = 7.0$ Hz, 3H, Me), 1.0 (6H, Me), 1.1–1.2 (6H, Me), 1.32 (d, $^3J = 5.5$ Hz, 3H, Me), 3.65 (3H, NMe) ppm.

Stirring of the **8d**+**8d'** mixture at room temperature for 48 h in CDCl_3 led to conversion of **8d** into **8d'** (>9:1). Spectral data for **8d'**: ^{31}P NMR (121 MHz, CDCl_3) δ 38.6 (d, $J_{\text{P-P}} = 17$ Hz, $J_{\text{P-Pt}} = 2182$ Hz), 36.6 (d, $J_{\text{P-P}} = 17$ Hz, $J_{\text{P-Pt}} = 3368$ Hz); ^1H NMR (500 MHz, CDCl_3) δ 0.27 (d, $^3J = 6.6$ Hz, 3H, Me), 0.49 (d, $^3J = 6.6$ Hz, 3H, Me), 0.72 (d, $^3J = 6.6$ Hz, 3H, Me), 0.86 (dd, $^3J_{\text{H-P}} = 12.9$ Hz, $^3J = 6.9$ Hz, 3H, Me), 0.95 (dd, $^3J_{\text{H-P}} = 14.7$ Hz, $^3J = 6.9$ Hz, 3H, Me), 1.01 (d, $^3J = 6.6$ Hz, 3H, Me), 1.8–2.0 (2H), 2.57 (m, 1H, PCHMe), 3.32 (s, 3H, NMe), 3.68 (m, 1H, CHMe $_2$), 6.77 (d, $^3J = 0.9$ Hz, 1H, NCH=), 6.92 (1H, NCH=), 6.9–7.8 (Ar); ^{13}C NMR (75 MHz, CDCl_3 , selected data) δ 13.6 (PCHMe), 21.9 (Me), 22.6 (Me), 25.4 (Me), 27.6 (Me), 28.0 (Me), 28.7 (Me), 39.7 (NMe) ppm. $[\alpha]_{\text{D}} = +135$ (c 0.5, CHCl_3).

(1-Mesityl-3-methylimidazol-2-ylidene)Pt((*S,S*)-Chiraphos) I_2 (**8e,e'**). This compound was obtained in 88% yield (94 mg) as a pale yellow solid that separates from the reaction mixture. The solid contains a 95:5 mixture of **8e**+**8e'**. MS (ESI) m/z 949 (M – I + H, 100%). Spectral data for **8e** (from the 95:5 mixture with **8e'**): ^{31}P NMR (121 MHz, CDCl_3) δ 39.4 (d, $J_{\text{P-P}} = 17$ Hz, $J_{\text{P-Pt}} = 2216$ Hz), 35.3 (d, $J_{\text{P-P}} = 17$ Hz, $J_{\text{P-Pt}} = 3373$ Hz); ^1H NMR (600 MHz, CDCl_3) δ 1.0–1.1 (6H, PCHMe), 1.25 (3H, Me), 1.95 (s, 3H, Me), 2.28 (2H, PCHMe), 2.35 (s, 3H, Me), 3.58 (s, 3H, NMe), 6.79 (s, 1H), 6.84 (s, 1H), 6.94 (s, 1H), 7.1–7.8 (20H, Ph), 7.94 (s, 1H); ^{13}C NMR (150 MHz, CDCl_3 , recorded at -20 °C) δ 13.5–13.9 (Me), 18.4 (Me), 21.1 (Me), 21.5 (Me), 33.9 (PCHMe), 35.3 (CHMe), 39.4 (NMe), 164.4 ($J_{\text{Pt-C}} = 153$ Hz, Pt=C) ppm. When the sample of **8e** (+**8e'**) was heated at 50 °C in CDCl_3 , clean conversion of **8e** into **8e'** was observed. After 48 h heating, a 15:85 mixture of **8e**+**8e'** was obtained. Spectral data for **8e'**: ^{31}P NMR (121 MHz, CDCl_3) δ 39.8 (d, $J_{\text{P-P}} = 17$ Hz, $J_{\text{P-Pt}} = 2161$ Hz), 36.4 (d, $J_{\text{P-P}} = 17$ Hz, $J_{\text{P-Pt}} = 3350$ Hz); ^1H NMR (300 MHz, CDCl_3) δ 0.88 (dd, $^3J_{\text{H-P}} = 14.7$ Hz, $J = 6.9$ Hz, 3H, Me), 1.00 (dd, $^3J_{\text{H-P}} = 12.9$ Hz, $^3J = 6.9$ Hz, 3H, Me), 1.19 (s, 3H, Me), 1.89 (m, 1H, PCHMe), 2.17 (s, 3H, Me), 2.35 (s, 3H, Me), 2.88 (m, 1H, PCHMe), 3.14 (s, 3H, NMe), 6.42 (s, 1H), 6.83 (s, 1H), 6.89 (s, 1H), 7.0–7.8 (Ar) ppm.

(1-Benzyl-3-*tert*-butylimidazol-2-ylidene)Pt((*S,S*)-Chiraphos) I_2 (**8f,f'**). The solid that separates from the reaction mixture was filtered and purified by filtration through a short silica gel column with $\text{CH}_2\text{Cl}_2/\text{EtOH}$ as the eluent. Yield: 87 mg (80%) of a 91:9 mixture of **8f**+**8f'**. Spectral data for the major epimer **8f** are the following: ^{31}P NMR (121 MHz, CDCl_3) δ 37.8 (d, $J_{\text{P-P}} = 16$ Hz, $J_{\text{P-Pt}} = 2198$ Hz), 36.0 (d, $J_{\text{P-P}} = 16$ Hz, $J_{\text{P-Pt}} = 3306$ Hz); ^1H NMR (500 MHz, CDCl_3) δ 1.11 (dd, $^3J_{\text{H-P}} = 15.0$ Hz, $J = 6.0$ Hz, 3H, Me), 1.23 (m, 3H, Me), 1.57 (s, 9H, CMe_3), 2.28 (m, 1H, PCHMe), 3.43 (d, $^2J = 14.0$ Hz, 1H, CH_2Ph), 3.55 (m, 1H, PCHMe), 5.74 (d, $^2J = 14.0$ Hz, 1H, CH_2Ph), 6.35 (s, 1H, NCH=), 7.12 (2H), 7.16 (s, 1H), 7.25 (3H), 7.4–7.8 (18H, Ph), 8.22 (2H, Ph); ^{13}C NMR (125 MHz, CDCl_3) δ 14.3 (d, $^2J_{\text{C-P}} = 17$ Hz, Me), 15.0 (d, $^2J_{\text{C-P}} = 20$ Hz, Me), 32.2 (CMe_3), 35.8 (dd, $^1J_{\text{C-P}} = 35$ Hz, $^2J_{\text{C-P}} = 13$ Hz,

PCH), 40.2 (dd, $^1J_{C-P} = 38$ Hz, $^2J_{C-P} = 14$ Hz, PCH), 54.8 (CH₂Ph), 59.3 (NCMe₃), 121.0 (NCH), 121.6 (NCH) ppm; HRMS (^{195}Pt) calcd for C₄₂H₄₆IN₂P₂Pt (M - I) 962.1829, found 962.1838. Minor epimer **8f'**: ^{31}P NMR (121 MHz, CDCl₃) δ 39.8 (d, $J_{P-P} = 15$ Hz), 37.6 (d, $J_{P-P} = 15$ Hz) ppm.

(1-Benzyl-3-phenylimidazol-2-ylidene)Pt((S,S)-Chiraphos))I₂ (8g,g'). A 1:1 mixture of **8g**+**8g'** was obtained after chromatography on a silica gel column with 98:2 CH₂Cl₂/EtOH as the eluent: 70 mg, 63% yield. ^{31}P NMR (121 MHz, CDCl₃, selected data) δ 39.2 (d, $J_{P-P} = 16$ Hz, $J_{P-Pt} = 2213$ Hz), 37.5 (d, $J_{P-P} = 16$ Hz, $J_{P-Pt} = 2190$ Hz), 37.2 (d, $J_{P-P} = 16$ Hz, $J_{P-Pt} = 3227$ Hz), 35.6 (d, $J_{P-P} = 16$ Hz, $J_{P-Pt} = 3278$ Hz); ^1H NMR (500 MHz, CDCl₃) δ 1.00 (dd, $^3J_{H-P} = 15.0$ Hz, $J = 6.5$ Hz, 2 Me), 1.04 (dd, $^3J_{H-P} = 12.5$ Hz, $J = 6.5$ Hz, Me), 1.10 (dd, $^3J_{H-P} = 13.0$ Hz, $J = 7.0$ Hz, Me), 2.01 (m, PCH), 2.22 (m, PCH), 2.37 (m, PCH), 3.07 (m, PCH), 3.28 (d, $^2J = 14.0$ Hz, CH₂Ph), 4.78 (d, $^2J = 14.0$ Hz, CH₂Ph), 5.53 (d, $^2J = 14$ Hz, CH₂Ph), 5.60 (d, $^2J = 14$ Hz, CH₂Ph); MS(ESI) *m/z* 982 (M - I, 100%).

(1-Benzyl-3-cyclohexylimidazol-2-ylidene)Pt((S,S)-Chiraphos))I₂ (8h,h'). This compound was obtained in 56% yield (62 mg) as a 1:1 mixture of diastereomers after column chromatography with CH₂Cl₂/EtOH as the eluent ($R_f = 0.3$). Colorless solid. ^{31}P NMR (121 MHz, CDCl₃) δ 38.8 (d, $J_{P-P} = 16$ Hz, $J_{P-Pt} = 2168$ Hz), 38.4 (d, $J_{P-P} = 16$ Hz, $J_{P-Pt} = 2152$ Hz), 37.8 (d, $J_{P-P} = 16$ Hz, $J_{P-Pt} = 3218$ Hz), 36.8 (d, $J_{P-P} = 16$ Hz, $J_{P-Pt} = 3250$ Hz); ^1H NMR (500 MHz, CDCl₃, selected data) δ -0.01 (br d, $J = 11$ Hz), 2.96 (m, PCH), 3.02 (d, $^2J = 14.0$ Hz, CH₂Ph), 3.12 (m, PCH), 3.98 (NCH), 4.32 (NCH), 4.64 (d, $^2J = 14.5$ Hz, CH₂Ph), 5.20 (d, $^2J = 14.5$ Hz, CH₂Ph), 5.31 (d, $^2J = 14.0$ Hz, 1H, CH₂Ph), 6.58 (s, 1H), 6.70 (s, 1H), 6.83 (s, 1H) ppm; HRMS (^{195}Pt) calcd for C₄₄H₄₈IN₂P₂Pt (M - I) 988.1985, found 988.1987.

(1-Cyclohexyl-3-(1-naphthylmethyl)imidazol-2-ylidene)Pt((S,S)-Chiraphos))I₂ (8i,i'). This compound was obtained in 76% yield (88 mg) as a 1:1 mixture of epimers. The yellow solid separates from the crude reaction mixture. Pure (*R_a*)-**8i'** was isolated by slow crystallization in CHCl₃. Spectral data for **8i'**: ^{31}P NMR (121 MHz, CDCl₃) δ 38.1 (d, $J_{P-P} = 16$ Hz, $J_{P-Pt} = 2157$ Hz), 36.3 (d, $J_{P-P} = 16$ Hz, $J_{P-Pt} = 3259$ Hz); ^1H NMR (500 MHz, CD₂Cl₂) δ -0.1 (br s, 1H), 0.98 (dd, $^3J_{H-P} = 15.0$ Hz, $J = 6.5$ Hz, 3H, Me), 1.05 (dd, $^3J_{H-P} = 12.5$ Hz, $J = 6.5$ Hz, 3H, Me), 0.9–1.1 (4H), 1.2 (m, 1H), 1.60–1.65 (2H), 1.79 (br d, $J \approx 12$ Hz, 1H), 2.28 (m, 1H, PCH), 2.52 (br d, $J \approx 12$ Hz, 1H), 2.61 (m, 1H, PCH), 3.98 (br, 1H, NCH), 5.00 (d, $^2J = 15.0$ Hz, 1H, CH₂Naph), 5.61 (d, $^2J = 14.5$ Hz, 1H, CH₂Naph), 6.44 (s, 1H), 6.74 (s, 1H), 6.91 (d, $J = 7.0$ Hz, 1H), 7.2–7.8 (Ar); ^{13}C NMR (125 MHz, CD₂Cl₂, selected data) δ 13.4–13.9 (CHMe), 25.4 (CH₂), 26.1 (CH₂), 26.6 (CH₂), 31.6 (CH₂), 33.8 (CH₂), 34.7 (PCHMe), 37.1 (PCHMe), 53.3 (NCH₂), 61.2 (NCH), 119.6 (NCH=), 122.4 (NCH=) ppm; HRMS (^{195}Pt) calcd for C₄₈H₅₀IN₂P₂Pt (M - I): 1038.2142. Found: 1038.2115. $[\alpha]_D = +18$ (c 0.5, CHCl₃). Crystals suitable for X-ray diffraction studies have been obtained from CHCl₃. **8i'** displays an (*R*)-axial configuration. A small amount of pure **8i** (3 mg) was isolated from the filtrate by crystallization. Spectral data for **8i**: ^{31}P NMR (121 MHz, CDCl₃) δ 37.6 (d, $J_{P-P} = 16$ Hz, $J_{P-Pt} = 2168$ Hz), 37.1 (d, $J_{P-P} = 16$ Hz, $J_{P-Pt} = 3220$ Hz); ^1H NMR (500 MHz, CDCl₃) δ 0.8–1.9 (16H), 2.4 (br m, 1H, PCH), 3.00 (br m, 1H, PCH), 3.65 (d, $^2J = 14.5$ Hz, 1H, CH₂Naph), 4.37 (1H, NCH), 5.62 (d, $^2J = 14.5$ Hz, 1H, CH₂Naph), 6.42 (s, 1H), 7.0–8.0 (Ar) ppm.

(1-tert-Butyl-3-(1-naphthylmethyl)imidazol-2-ylidene)Pt((S,S)-Chiraphos))I₂ (8j,j'). This complex was obtained in 53% yield (60 mg) as a 91:9 mixture of two epimers. The solid that separates from the reaction mixture was purified by column chromatography with 95:5 CH₂Cl₂/EtOH as the eluent. Pale yellow solid. Spectral data for the major epimer **8j** (from the mixture): ^{31}P NMR (121 MHz, CDCl₃) δ 37.4 (d, $J_{P-P} = 16$ Hz, $J_{P-Pt} = 2195$ Hz), 36.0 (d, $J_{P-P} = 16$ Hz, $J_{P-Pt} = 3298$ Hz); ^1H NMR (500 MHz, CDCl₃) δ

1.15 (dd, $^3J_{H-P} = 15.0$ Hz, $J = 6.5$ Hz, 3H, Me), 1.23 (dd, $^3J_{H-P} = 14$ Hz, $J = 7.0$ Hz, 3H, Me), 1.59 (9H, CMe₃), 2.34 (1H, PCH), 3.48 (1H, PCH), 4.05 (d, $^2J = 14.5$ Hz, 1H, CH₂Naph), 6.00 (d, $^2J = 14.5$ Hz, 1H, CH₂Naph), 6.24 (s, 1H), 6.99 (d, $J = 7.0$ Hz, 1H), 7.1–7.9 (Ar), 8.19 (2H); ^{13}C NMR (125 MHz, CDCl₃, selected data) δ 14.4 (d, $^2J_{C-P} = 16$ Hz, Me), 14.8 (d, $^2J_{C-P} = 13$ Hz, Me), 32.2 (CMe₃), 35.8 (dd, $^1J_{C-P} = 35$ Hz, $^2J_{C-P} = 11$ Hz, PCH), 39.7 (dd, $^1J_{C-P} = 40$ Hz, $^2J_{C-P} = 14$ Hz, PCH), 52.7 (CH₂Naph), 59.4 (CMe₃) ppm; HRMS (^{195}Pt) calcd for C₄₆H₄₈IN₂P₂Pt 1012.1985, found 1012.2053. Minor epimer **8j'**: ^{31}P NMR (121 MHz, CDCl₃) δ 40.2 (d, $J_{P-P} = 15$ Hz), 37.8 (d, $J_{P-P} = 15$ Hz) ppm.

((S)-1-Methyl-3-(1-phenylethyl)imidazol-2-ylidene)Pt((S,S)-Chiraphos))I₂ (8k,k'). This compound was obtained in 93% yield (98 mg of an orange solid that spontaneously separates from the reaction mixture) from (*S*)-**2k**, as a 70:30 mixture of two epimers. Spectral data for the major epimer **8k** (from the mixture): ^{31}P NMR (121 MHz, CDCl₃) δ 38.1 (d, $J_{P-P} = 16$ Hz, $J_{P-Pt} = 2162$ Hz), 37.8 (d, $J_{P-P} = 16$ Hz, $J_{P-Pt} = 3213$ Hz); ^1H NMR (500 MHz, CDCl₃, selected data) δ 1.04 (d, $^3J = 7.0$ Hz, 3H, MeCHPh), 1.1–1.2 (6H, Me), 2.38 (1H, PCH), 3.00 (s, 3H, NMe), 3.0 (1H, PCH), 5.70 (q, $^3J = 6.5$ Hz, 1H, NCHPh), 6.79 (s, 1H), 6.88 (s, 1H) ppm; HRMS (^{195}Pt) calcd for C₄₀H₄₂IN₂P₂Pt 934.1516, found 934.1490. Minor epimer **8k'**: ^{31}P NMR (121 MHz, CDCl₃) δ 38.5 (d, $J_{P-P} = 16$ Hz), 35.4 (d, $J_{P-P} = 16$ Hz) ppm; ^1H NMR (500 MHz, CDCl₃, selected data) δ 1.63 (d, $^3J = 7.0$ Hz, 3H, MeCHPh), 2.3 (1H, PCH), 2.8 (1H, PCH), 3.49 (s, 3H, NMe), 5.62 (br q, 1H, NCHPh) ppm.

((R)-1-Methyl-3-(1-phenylethyl)imidazol-2-ylidene)Pt((S,S)-Chiraphos))I₂ (8l,l'). This compound was obtained from (*R*)-**2k** in 90% yield (95 mg) as a yellow solid that separates from the reaction mixture. The solid contains a 77:23 mixture of **8l**+**8l'**. Spectral data for the major epimer **8l** (from the mixture): ^{31}P NMR (121 MHz, CDCl₃) δ 38.1 (d, $J_{P-P} = 16$ Hz, $J_{P-Pt} = 2150$ Hz), 36.5 (d, $J_{P-P} = 16$ Hz, $J_{P-Pt} = 3228$ Hz); ^1H NMR (500 MHz, CDCl₃, selected data) δ 0.88 (d, $^3J = 7.0$ Hz, 3H, MeCHPh), 1.0–1.3 (6H, Me), 2.13 (m, 1H, CHMe), 3.24 (m, CHMe), 3.57 (s, 3H, NMe), 5.33 (br q, NCHPh) ppm. Minor epimer **8l'**: ^{31}P NMR (121 MHz, CDCl₃) δ 38.1 (d, $J_{P-P} = 13$ Hz), 37.8 (d, $J_{P-P} = 13$ Hz); ^1H NMR (300 MHz, CDCl₃, selected data) δ 1.0–1.2 (6H, Me), 1.75 (d, $^3J = 7$ Hz, 3H, MeCHPh), 2.30 (m, 1H, CHMe), 3.00 (NMe), 5.66 (br q, 1H, NCHPh); HRMS (^{195}Pt) calcd for C₄₀H₄₂IN₂P₂Pt 934.1516, found 934.1464.

Enyne Cycloisomerization Reaction. *N*-Allyl-*N*-(3-phenylpropyn-2-yl)-4-methylbenzenesulfonamide was prepared as described.³⁴

The (NHC)(diphosphine)PtI₂ complex **I** (6.4×10^{-3} mmol) was dissolved in 0.5 mL of CH₂Cl₂. AgBF₄ (3 mg, 0.016 mmol), *N*-allyl-*N*-(3-phenylpropyn-2-yl)-4-methylbenzenesulfonamide **9** (52 mg, 0.16 mmol), and toluene (4.5 mL) were added successively. The resulting mixture was heated at 90 °C for 20 h. After evaporation of the solvents, conversion rates were measured by ^1H NMR on the crude mixture. 6-Phenyl-3-(toluene-4-sulfonyl)-3-aza-bicyclo[4.1.0]hept-4-ene, **10**,^{2a} was isolated by flash chromatography on a silica gel column (heptane/ethyl acetate, 90:10). Enantiomeric excesses were determined by HPLC: Chiralpak IC column, eluent hexane/methyl *tert*-butyl ether/2-propanol (75/20/5); flow 1 mL/min, retention times 20.0 and 21.4 min (major). Samples for HPLC may contain some residual starting material, which elutes with a retention time of 25.1 min under these conditions. **10**: $[\alpha]_D = -67$ (c 0.5, CHCl₃) for a 70% ee sample.

(34) Morimoto, T.; Fuji, K.; Tsutsumi, K.; Kakiuchi, K. *J. Am. Chem. Soc.* **2002**, *124*, 3806–3807.

Computational Methods. Calculations have been carried out with the Gaussian03 package of programs.³⁵ Full geometry optimizations for all compounds were carried out with the use of the B3LYP³⁶ density functional level of theory and with the following basis set. A 6-31G(d,p) basis set was employed for the first- (H), second- (C, N), and third-row (P) elements. The standard LANL2DZ small-core relativistic effective-core potential with a valence shell of double- ζ quality was used on platinum³⁷ and iodine.³⁸ The validity of this level of calculation

(35) Frisch, M. J.; Trucks, G. W.; Schlegel, H. B.; Scuseria, G. E.; Robb, M. A.; Cheeseman, J. R.; Montgomery, J. A.; Vreven, T.; Kudin, K. N.; Burant, J. C.; Millam, J. M.; Iyengar, S. S.; Tomasi, J.; Barone, V.; Mennucci, B.; Cossi, M.; Scalmani, G.; Rega, N.; Petersson, G. A.; Nakatsuji, H.; Hada, M.; Ehara, M.; Toyota, K.; Fukuda, R.; Hasegawa, J.; Ishida, M.; Nakajima, T.; Honda, Y.; Kitao, O.; Nakai, H.; Klene, M.; Li, X.; Knox, J. E.; Hratchian, H. P.; Cross, J. B.; Bakken, V.; Adamo, C.; Jaramillo, J.; Gomperts, R.; Stratmann, R. E.; Yazyev, O.; Austin, A. J.; Cammi, R.; Pomelli, C.; Ochterski, J. W.; Ayala, P. Y.; Morokuma, K.; Voth, G. A.; Salvador, P.; Dannenberg, J. J.; Zakrzewski, V. G.; Dapprich, S.; Daniels, A. D.; Strain, M. C.; Farkas, O.; Malick, D. K.; Rabuck, A. D.; Raghavachari, K.; Foresman, J. B.; Ortiz, J. V.; Cui, Q.; Baboul, A. G.; Clifford, S.; Cioslowski, J.; Stefanov, B. B.; Liu, G.; Liashenko, A.; Piskorz, P.; Komaromi, I.; Martin, R. L.; Fox, D. J.; Keith, T.; Al-Laham, M. A.; Peng, C. Y.; Nanayakkara, A.; Challacombe, M.; Gill, P. M. W.; Johnson, B.; Chen, W.; Wong, M. W.; Gonzalez, C.; Pople, J. A. *Gaussian 03, Revision D.02*; Gaussian, Inc.: Wallingford, CT, 2004.

(36) (a) Lee, C.; Yang, W.; Parr, R. G. *Phys. Rev. B* **1988**, *37*, 785–789. (b) Becke, A. D. *J. Chem. Phys.* **1993**, *98*, 5648–5652.

(37) Hay, P. J.; Wadt, W. R. *J. Chem. Phys.* **1985**, *82*, 270–283.

has been demonstrated before in studies on Pt(II) complexes.¹⁰ Each stationary point has been characterized with frequency analysis and shows the correct number of negative eigenvalues (0 for a local minimum and one for a transition state). The Gibbs free energy corresponding to a given pathway was deduced from the equation

$$\Delta G = \Delta E_{\text{elec}} + \Delta ZPE + \Delta E_{\text{T}} - T\Delta S \quad (1)$$

with ΔE_{elec} , ΔZPE , ΔE_{T} , and ΔS being the differences in the electronic energy, zero-point vibrational energy, thermal energy, and entropy between the products and the reactants, respectively.

Supporting Information Available: ¹³C NMR or ¹H NMR spectra for the new Pt(0) complexes **1** and **2**. ³¹P, ¹H, and ¹³C NMR spectra for the Pt(II) complexes **3–8**. X-ray crystallographic data (CIF files) for complexes **3a**, **7b**, and **8i'**. Chiral HPLC traces for the starting materials and products of the cycloisomerization reaction. Crystallographic data have been deposited with the Cambridge Crystallographic Data Centre as nos. CCDC-696746 (**3a**), CCDC-696747 (**7b**), and CCDC-696748 (**8i'**). Detailed optimized geometries and free energies for the calculated structures (Table 4). This material is available free of charge via the Internet at <http://pubs.acs.org>.

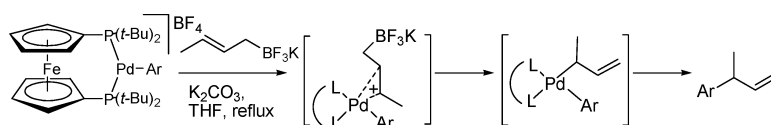
OM800743R

(38) Hay, P. J.; Wadt, W. R. *J. Chem. Phys.* **1985**, *82*, 284–298.

#-Selective Cross-Coupling Reactions of Potassium Allyltrifluoroborates with Haloarenes Catalyzed by a Pd(0)/D-*t*-BPF or Pd(0)/Josiphos ((*R,S*)-CyPF-*t*-Bu) Complex: Mechanistic Studies on Transmetalation and Enantioselection

Yasunori Yamamoto, Shingo Takada, Norio Miyaura, Tetsuji Iyama, and Hiroto Tachikawa
Organometallics, 2009, 28 (1), 152-160 • DOI: 10.1021/om800832r • Publication Date (Web): 24 November 2008

Downloaded from <http://pubs.acs.org> on April 10, 2009



More About This Article

Additional resources and features associated with this article are available within the HTML version:

- Supporting Information
- Access to high resolution figures
- Links to articles and content related to this article
- Copyright permission to reproduce figures and/or text from this article

[View the Full Text HTML](#)



ACS Publications
 High quality. High impact.

γ -Selective Cross-Coupling Reactions of Potassium Allyltrifluoroborates with Haloarenes Catalyzed by a Pd(0)/D-*t*-BPF or Pd(0)/Josiphos ((*R,S*)-CyPF-*t*-Bu) Complex: Mechanistic Studies on Transmetalation and Enantioselection

Yasunori Yamamoto,* Shingo Takada, and Norio Miyaura*

Division of Chemical Process Engineering, Graduate School of Engineering, Hokkaido University, Sapporo 060-8628, Japan

Tetsuji Iyama and Hiroto Tachikawa

Division of Materials Chemistry, Graduate School of Engineering, Hokkaido University, Sapporo 060-8628, Japan

Received August 27, 2008

Cross-coupling between bromoarenes and [(*E*)-CH₃CH=CHCH₂BF₃]*K* (**2a**) by a catalyst prepared from Pd(OAc)₂ and D-*t*-BPF selectively provided γ -coupling products via S_E2' substitution. Mechanistic study of transmetalation revealed a heretofore unknown process, namely, formation of a highly electrophilic [Pd(Ar)(D-*t*-BPF)]⁺ before transmetalation with **2a**. Thus, kinetic data in coupling of 4-substituted bromoarenes with **2a** showed a linear positive correlation ($\rho = -1.1$) accelerated by donating substituents. This rate-determining role of transmetalation was further confirmed by kinetic data between oxidative adducts [Pd(Ar)(Br)(D-*t*-BPF)] and **2a** that exhibited an analogous correlation with a negative ρ -value (-0.50). Theoretical study by density functional theory (DFT) calculation showed that transmetalation between [Ar-Pd]⁺ and **2a** via an S_E2' (open) transition state is a slightly lower energy process than an S_E2' (closed) process. Allylic substitutions with chiral catalysts are the current topics for enantioselective C–C bond formation, but the catalysts that are effective for allylic nucleophiles have remained unexplored. Among the ligands screened, (*R,S*)-CyPF-*t*-Bu was found to achieve 77–90% ee for representative para- and meta-substituted bromoarenes and 2-bromo-1-alkenes in refluxing aqueous tetrahydrofuran (THF) or MeOH. To obtain mechanistic information on enantioselection, the mode of substrate coordination to a cationic phenylpalladium intermediate was calculated, that is, the reaction stage directly preceding the stereodetermining insertion step by DFT calculation. A stable adduct between [Pd(CyPF-*t*-Bu)(Ph)]⁺ and **2a** located at the C–C double bond from its *re*-face yielding the experimentally observed *R*-product is preferred thermodynamically rather than the corresponding *si*-coordination.

Introduction

Transition-metal-catalyzed cross-coupling reactions have proved to be one of the most powerful methods for selective C–C bond formation.¹ Among the possible combinations of electrophiles and nucleophiles, reactions of allylic metals with aryl, alkenyl, and allyl electrophiles or with their reversed combination provide an important class of compounds because of the frequent occurrence of allylic fragments in natural products.² The coupling reactions of allylmagnesium,³ -zinc,⁴ -boron,⁵ -silicon,⁶ -tin,⁷ and -zirconium⁸ compounds with Ni and Pd catalysts have been extensively studied. Perfect control of the coupling position by phosphine ligands was first achieved by Hatanaka and Hiyama et al. using a combination of

allyltrifluorosilanes and haloarenes.^{6a,c} The coupling selectively occurred at the γ -carbon when using PPh₃ or bisphosphines possessing a large bite angle such as 1,4-bis(diphenylphosphino)butane (dppb), whereas bisphosphines possessing a relatively small angle such as 1,3-bis(diphenylphosphino)propane (dppp) underwent selective coupling at the α -carbon. Such an effect of phosphine ligands was also demonstrated in regioselective Stille coupling of aryl halides with Me₃SiCH₂CH=CHCH₂-SnBu₃ at the α - or γ -carbon.^{7g} There have been very few attempts to employ allylboron compounds, but boron reagents have various advantages, including availability, air and moisture stability, low toxicity, and easy removal of boron-derived byproducts. We have reported the efficiency of potassium allyltrifluoroborates for perfect γ -selective coupling with bro-

* To whom correspondence should be addressed. Tel/fax: +81-11-706-6561; e-mail: yasuyama@eng.hokudai.ac.jp (Y.Y.) and miyaura@eng.hokudai.ac.jp.

(1) For reviews, see: (a) *Boronic Acids*; Hall, D. G., Ed.; Wiley-VCH: Weinheim, Germany, 2005. (b) *Metal-Catalyzed Cross-Coupling Reactions*, 2nd ed.; de Meijere, A., Diederich, F., Eds.; Wiley-VCH: Weinheim, Germany, 2004. (c) *Cross-Coupling Reactions. A Practical Guide*; Miyaura, N., Ed.; Springer: Berlin, 2002. (d) *Handbook of Organopalladium Chemistry for Organic Synthesis*; Negishi, E.-I., Ed.; John Wiley & Sons: New York, 2002. (e) *Metal-Catalyzed Cross-Coupling Reactions*; Diederich, F., Stang, P. J., Eds.; Wiley-VCH: Weinheim, Germany, 1998.

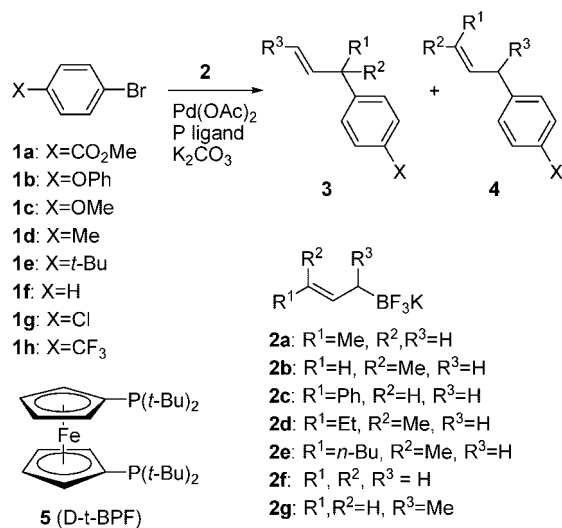
(2) (a) Heck, R. H. *J. Am. Chem. Soc.* **1968**, *90*, 5531. (b) Negishi, E.-I.; Chatterjee, S.; Matsushita, H. *Tetrahedron Lett.* **1981**, *22*, 3737. (c) Legros, J.-Y.; Flaud, J.-C. *Tetrahedron Lett.* **1990**, *31*, 7453. (d) Mareno-Mañas, M.; Pajuelo, F.; Pleixats, R. *J. Org. Chem.* **1995**, *60*, 2396. (e) Chung, K.-G.; Miyake, Y.; Uemura, S. *J. Chem. Soc., Perkin Trans. 1* **2000**, 2725. (f) Bouyssi, D.; Gerusz, V.; Balme, G. *Eur. J. Org. Chem.* **2002**, 2445. (g) Ikegami, R.; Koresawa, A.; Shibata, T.; Takagi, K. *J. Org. Chem.* **2003**, *68*, 2195. (h) Kayaki, Y.; Koda, T.; Ikariya, T. *Eur. J. Org. Chem.* **2004**, 4989. (i) Tsukamoto, H.; Sato, M.; Kondo, Y. *Chem. Commun.* **2004**, 1200.

moarenes and bromoalkenes⁹ and their asymmetric coupling with bromoarenes using (*R,S*)-CyPF-*t*-Bu as the chiral auxiliary.¹⁰ Such a selective γ -coupling was also achieved by Szabo and co-workers in the synthesis of allylboronic acids via cross-coupling between diboronic acid and allylic alcohols or vinylcyclopropanes.¹¹ The proposed mechanisms of those γ -selective coupling reactions of allylic nucleophiles were the S_E2' (open or closed) process reported for allylsilicon compounds^{6b} and the addition-elimination process reported for allylboronic acids,^{5a,11c,12,13} whereas formation of (π -allyl)palladium(II) intermediate, which predominates α -coupling, was ruled out.^{5a} In this paper, we report transmetalation and enantioselection mechanisms involved in cross-coupling between potassium (*E*)-crotyltrifluoroborate and bromoarenes catalyzed by a Pd(0)/*D-t*-BPF or Pd(0)/Josiphos ((*R,S*)-CyPF-*t*-Bu) complex. Formation of a cationic palladium(II) intermediate such as [ArPd]⁺ before transmetalation was proposed on the basis of results of kinetic and theoretical studies.

Results and Discussion

γ -Selective Coupling Catalyzed by Pd(0)/*D-t*-BPF. Reaction between potassium allyltrifluoroborates (**2**) and bromoarenes gave γ -coupling products in high yields with perfect regioselectivities for variously functionalized bromoarenes (Scheme 1).⁹ Air- and water-stable allyltrifluoroborates (**2**), synthesized by treatment of allylboronic acids or esters with KHF₂, were advantageous over triallylboranes and allylboronic acids or esters in preparation and handling of pure and water-stable crystalline materials.^{14,15} These K⁺ salts are highly insoluble in common organic solvents, but the reaction smoothly proceeded in aqueous

Scheme 1. γ -Selective Coupling Giving **3** (Table 1)



tetrahydrofuran (THF) or MeOH in the presence of a palladium catalyst prepared in situ from Pd(OAc)₂ and phosphine ligands. Since the reaction was very slow in the absence of a base, it was carried out in a basic solution as was previously reported in cross-coupling reactions of potassium aryl- and 1-alkenyltrifluoroborates.¹⁵ The use of K₂CO₃ (3 equivalents) in anhydrous THF gave the best results (85–99% yields), whereas the use of stronger bases, such as K₃PO₄ and KOH, resulted in lower yields (9–30%).

The yields and regioselectivities of the coupling position were highly sensitive to phosphine ligands employed for palladium acetate in the reaction of 4-bromoanisole with potassium (*E*)-crotyltrifluoroborate (**2a**) (Table 1). Monodentate PPh₃ and bidentate dppm and dppe possessing a relatively small bite angle resulted in a mixture of two isomers (entries 1–3), whereas bisphosphines that have a bite angle larger than dppp yielded a γ -coupling product (**3**) as the sole product (entries 4–8). This effect of bite angle was almost the same as that reported for allyltrifluorosilanes.^{6a,c} Although these catalysts suffered from low yields mainly because of formation of anisole derived by hydrogenolysis of bromoanisole, *D-t*-BPF¹⁶ was finally found to be the best ligand to achieve high yields and high γ -selectivities for 4-bromoanisole and methyl 4-bromobenzoate (entries 9–11). This ligand also worked well for a series of allylboronates including (*Z*)-crotyl- (**2b**), (*E*)-cinnamyl- (**2c**), (*E*)-3-methyl-2-pentenyl (**2d**), (*E*)-3-methyl-2-heptenyl (**2e**), allyl (**2f**),

(3) (a) Tsuji, T.; Yorimitsu, H.; Oshima, K. *Angew. Chem., Int. Ed.* **2002**, *41*, 4137. (b) Ohmiya, H.; Tsuji, T.; Yorimitsu, H.; Oshima, K. *Chem. Eur. J.* **2004**, *10*, 5640.

(4) (a) Peet, W. G.; Tam, W. *J. Chem. Soc., Chem. Commun.* **1983**, 853. (b) Campbell, J. B.; Firor, J. W.; Davenport, T. W. *Synth. Commun.* **1989**, *19*, 2265.

(5) (a) Nilsson, K.; Hallberg, A. *Acta Chem. Scand.* **1987**, *B41*, 569. (b) Miyaura, N.; Suzuki, A. *Chem. Rev.* **1995**, *95*, 2457. (c) Kalinin, V. N.; Denisov, F. S.; Bubnov, Y. N. *Mendeleev Commun.* **1996**, 202. (d) Fürstner, A.; Seidel, G. *Synlett* **1998**, 161. (e) Fürstner, A.; Leitner, A. *Synlett* **2001**, 290. (f) Occhiato, E. G.; Trabocchi, A.; Guarna, A. *J. Org. Chem.* **2001**, *66*, 2459. (g) Kotha, S.; Behera, M.; Shah, V. R. *Synlett* **2005**, 1877.

(6) (a) Hatanaka, Y.; Ebina, Y.; Hiyama, T. *J. Am. Chem. Soc.* **1991**, *113*, 7075. (b) Hatanaka, Y.; Goda, K.-i.; Hiyama, T. *Tetrahedron Lett.* **1994**, *35*, 1279. (c) Hatanaka, Y.; Goda, K.-i.; Hiyama, T. *Tetrahedron Lett.* **1994**, *35*, 6511. (d) Hiyama, T.; Matsushashi, H.; Fujita, A.; Tanaka, M.; Hirabayashi, K.; Shimizu, M.; Mori, A. *Organometallics* **1996**, *15*, 5762.

(7) (a) Kosugi, M.; Sasazawa, K.; Shimizu, Y.; Migita, T. *Chem. Lett.* **1977**, *6*, 301. (b) Trost, B. M.; Keinan, E. *Tetrahedron Lett.* **1980**, *21*, 2595. (c) Godschalk, J.; Stille, J. K. *Tetrahedron Lett.* **1980**, *21*, 2599. (d) Echavarren, A. M.; Stille, J. K. *J. Am. Chem. Soc.* **1987**, *109*, 5478. (e) Martorell, G.; García-Raso, A.; Saá, J. M. *Tetrahedron Lett.* **1990**, *31*, 2357. (f) Farina, V.; Krishnan, B. *J. Am. Chem. Soc.* **1991**, *113*, 9585. (g) Obora, Y.; Tsuji, Y.; Kobayashi, M. *J. Org. Chem.* **1995**, *60*, 4647. (h) Cotter, W. D.; Barbour, L.; McNamara, K. L.; Hechter, R.; Lachicotte, R. *J. Am. Chem. Soc.* **1998**, *120*, 11016.

(8) Hirano, K.; Yorimitsu, H.; Oshima, K. *Synlett* **2005**, 1787.

(9) Yamamoto, Y.; Takada, S.; Miyaura, N. *Chem. Lett.* **2006**, *35*, 704.

(10) Yamamoto, Y.; Takada, S.; Miyaura, N. *Chem. Lett.* **2006**, *35*, 1368.

(11) (a) Sebelius, S.; Olsson, V. J.; Szabó, K. *J. Am. Chem. Soc.* **2005**, *127*, 10478. (b) Olsson, V. J.; Sebelius, S.; Selander, N.; Szabó, K. *J. Am. Chem. Soc.* **2006**, *128*, 4588. (c) Sebelius, S.; Olsson, V. J.; Wallner, O. A.; Szabó, K. *J. Am. Chem. Soc.* **2006**, *128*, 8150. (d) Dutheil, G.; Selander, N.; Szabó, K. *Synthesis* **2008**, 2293.

(12) Miyaura, N.; Suzuki, A. *J. Organomet. Chem.* **1981**, *213*, C53.

(13) (a) Karabelas, K.; Westerlund, C.; Hallberg, A. *J. Org. Chem.* **1985**, *50*, 3896. (b) Karabelas, K.; Hallberg, A. *J. Org. Chem.* **1986**, *51*, 5286. (c) Karabelas, K.; Hallberg, A. *J. Org. Chem.* **1989**, *54*, 1773. (d) Albéniz, A. C.; Espinet, P.; López-Fernández, R. *Organometallics* **2006**, *25*, 5449.

(14) (a) Darses, S.; Genêt, J.-P. *Eur. J. Org. Chem.* **2003**, 4313. (b) Molander, G. A.; Ellis, N. *Acc. Chem. Res.* **2007**, *40*, 275. (c) Darses, S.; Genêt, J.-P. *Chem. Rev.* **2008**, *108*, 288.

(15) (a) Darses, S.; Genêt, J.-P.; Brayer, J.-L.; Demoute, J.-P. *Tetrahedron Lett.* **1997**, *38*, 4393. (b) Darses, S.; Michaud, G.; Genêt, J.-P. *Tetrahedron Lett.* **1998**, *39*, 5045. (c) Darses, S.; Michaud, G.; Genêt, J.-P. *Eur. J. Org. Chem.* **1999**, 1875. (d) Batey, R. A.; Thadani, A. N.; Smil, D. V. *Tetrahedron Lett.* **1999**, *40*, 4289. (e) Batey, R. A.; Thadani, A. N.; Smil, D. V. *Synthesis* **2000**, 990. (f) Batey, R. A.; Quach, T. D. *Tetrahedron Lett.* **2001**, *42*, 9099. (g) Molander, G. A.; Rivero, M. R. *Org. Lett.* **2002**, *4*, 107. (h) Thadani, A. N.; Batey, R. A. *Org. Lett.* **2002**, *4*, 3827. (i) Molander, G. A.; Katona, B. W.; Machrouhi, F. *J. Org. Chem.* **2002**, *67*, 8416. (j) Molander, G. A.; Bernardi, C. R. *J. Org. Chem.* **2002**, *67*, 8424. (k) Molander, G. A.; Biolatto, B. *J. Org. Chem.* **2003**, *68*, 4302. (l) Molander, G. A.; Yun, C.-S.; Ribagorda, M.; Bilatto, B. *J. Org. Chem.* **2003**, *68*, 5534. (m) Barder, T. E.; Buchwald, S. L. *Org. Lett.* **2004**, *6*, 2649. (n) Kabalka, G. W.; Dong, G.; Venkataiah, B. *Tetrahedron Lett.* **2004**, *45*, 5139. (o) Kabalka, G. W.; Dong, G.; Venkataiah, B. *Tetrahedron Lett.* **2005**, *46*, 763. (p) Molander, G. A.; Felix, L. A. *J. Org. Chem.* **2005**, *70*, 3950. (q) Kabalka, G. W.; Al-Masum, M. *Org. Lett.* **2006**, *8*, 11. (r) Molander, G. A.; Sommers, E. M.; Baker, S. R. *J. Org. Chem.* **2006**, *71*, 1563. (s) Molander, G. A.; Yokoyama, Y. *J. Org. Chem.* **2006**, *71*, 2493. (t) Molander, G. A.; Ham, J.; Seapy, D. G. *Tetrahedron* **2007**, *63*, 768.

(16) (a) Itoh, T.; Sato, K.; Mase, T. *Adv. Synth. Catal.* **2004**, *346*, 1859. (b) Itoh, T.; Mase, T. *Tetrahedron Lett.* **2005**, *46*, 3573.

Table 1. γ -Selective Coupling of Potassium Allyltrifluoroborates (**2**) with Haloarenes Giving **3** (Scheme 1)

entry	2	ArBr, X =	ligand	yield/% ^a (3/4)
1 ^b	2a	4-MeO	PPh ₃	42 (78/22)
2 ^b	2a	4-MeO	dppm	35 (78/22)
3 ^b	2a	4-MeO	dppe	17 (37/63)
4 ^b	2a	4-MeO	dppp	37 (>99/1)
5 ^b	2a	4-MeO	dppf	68 (>99/1)
6 ^b	2a	4-MeO	DPEphos	21 (>99/1)
7 ^b	2a	4-MeO	Xantphos	10 (>99/1)
8 ^b	2a	4-MeO	DBFphos	10 (>99/1)
9 ^b	2a	4-MeO	D- <i>t</i> -BPF	87 (>99/1)
10 ^c	2a	4-MeO	D- <i>t</i> -BPF	85 (>99/1)
11 ^c	2a	4-CO ₂ Me	D- <i>t</i> -BPF	99 (>99/1)
12 ^c	2b	4-CO ₂ Me	D- <i>t</i> -BPF	91 (>99/1)
13 ^c	2c	4-CO ₂ Me	D- <i>t</i> -BPF	99 (>99/1)
14 ^c	2d	4-CO ₂ Me	D- <i>t</i> -BPF	96 (>99/1)
15 ^c	2e	4-CO ₂ Me	D- <i>t</i> -BPF	99 (>99/1)
16 ^{c,d}	2f	4-CO ₂ Me	D- <i>t</i> -BPF	99 (-)
17 ^c	2g	4-CO ₂ Me	D- <i>t</i> -BPF	99 (<1/99) ^e

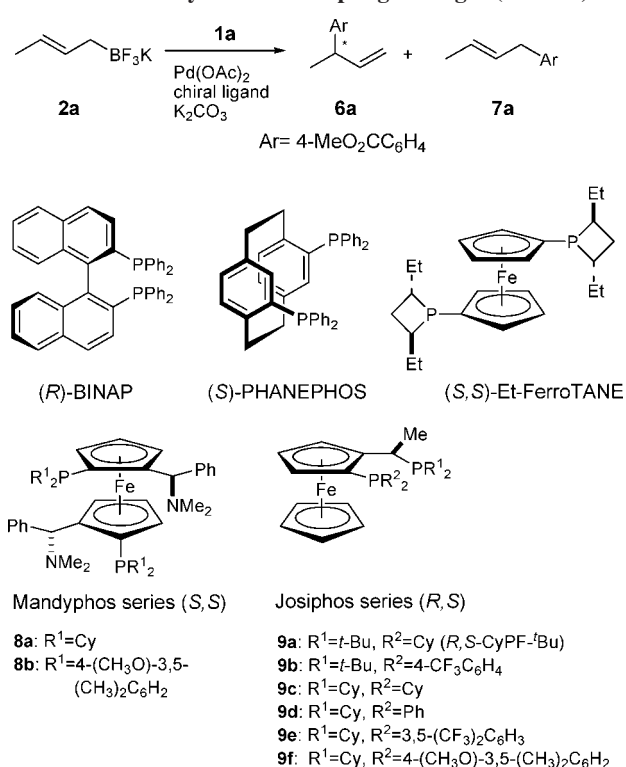
^a NMR yields for entries 1–8 and isolated yields for entries 9–17.

^b The reactions were conducted for 20 h at reflux in THF–H₂O (10/1) in the presence of Pd(OAc)₂ (3 mol %), a ligand (3 mol %), haloarene (0.5 mmol), **2** (0.75 mmol), and K₂CO₃ (1.5 mmol). ^c The reactions were conducted for 22 h at reflux in THF in the presence of Pd(OAc)₂ (3 mol %), a ligand (3.6 mol %), haloarene (1 mmol), **2** (2.5 mmol), and K₂CO₃ (3 mmol). ^d Walphos was used as ligand. ^e E/Z = 55/45.

and 1-methyl-2-propenylboronate (**2g**). Among these boronates chosen for investigating scope and limitations, it was interesting that **2d** and **2e** selectively gave a quaternary carbon (entries 14 and 15) and **2g** gave a linear 2-butenyl product via complete S_E2' substitution (entry 17). Our previous study also showed that other representative bromoarenes, including hindered 2,6-dimethyl derivatives and 2-bromo-1-alkenes, achieve γ -selectivities higher than 99%.⁹ Thus, such high yields and high γ -selectivity are characteristic for D-*t*-BPF, which has a large bite angle and steric hindrance and a strong electron-donating ability to the palladium(0) metal center.

Asymmetric Coupling Catalyzed by Pd(0)/(R,S)-CyPF-*t*-Bu. Transition-metal-catalyzed allylic substitutions with nucleophiles, especially their asymmetric versions using chiral catalysts, are the current topics.^{17–19} Several efficient chiral catalysts have been developed for those purposes and have considerably expanded the scope of enantioselective C–C and C–heteroatom bond formation. However, chiral catalysts for allylic nucleophiles have remained unexplored.

The regioselectivities of the coupling position (**6a**, **7a**) and enantioselectivities of **6a** were highly sensitive to phosphine ligands employed for palladium acetate in the reaction between potassium (*E*)-crotyltrifluoroborate (**2a**) and methyl 4-bromobenzoate (Scheme 2 and Table 2). The use of BINAP, Et-FerroTANE, PHANEPHOS, and other representative C₂ symmetric chiral phosphines resulted in the formation of two isomers

Scheme 2. Asymmetric Coupling Giving **6** (Table 2)**Table 2.** Asymmetric Coupling of Potassium Crotyltrifluoroborate (**2a**) with Methyl 4-Bromobenzoate (**1a**) (Scheme 2)^a

entry	ligand	yield/% ^b	6a/7a	% ee of 6a ^c
1	(<i>R</i>)-BINAP	86	68/32	3
2	(<i>S,S</i>)-Et-FerroTANE	84	31/69	12
3	(<i>S</i>)-PHANEPHOS	63	84/16	20 (<i>S</i>)
4	8a	98	93/7	31 (<i>R</i>)
5	8b	84	96/4	46 (<i>S</i>)
6	9a ((<i>R,S</i>)-CyPF- <i>t</i> -Bu)	96	92/8	63 (<i>R</i>)
7	9b	54	83/17	26 (<i>R</i>)
8	9c	73	99/1	10
9	9d	57	83/17	44 (<i>R</i>)
10	9e	64	14/86	5
11	9f	63	21/79	4
12 ^d	9a ((<i>R,S</i>)-CyPF- <i>t</i> -Bu)	93	95/5	82 (<i>R</i>)
13 ^e	9a ((<i>R,S</i>)-CyPF- <i>t</i> -Bu)	93	93/7	82 (<i>R</i>)

^a The reactions were conducted at reflux for 22 h in THF in the presence of Pd(OAc)₂ (3 mol %), a ligand (3.6 mol %), methyl 4-bromobenzoate (1 mmol), **2a** (2.5 mmol), and K₂CO₃ (3 mmol).

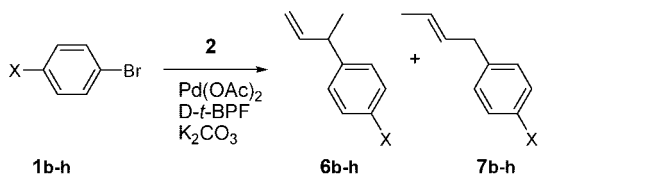
^b Isolated yields. ^c Enantiomer excess was determined by a chiral stationary column. ^d The reaction in THF–H₂O (1/4). ^e The reaction in MeOH–H₂O (1/9).

with low enantioselectivities (entries 1–3). On the other hand, the use of ferrocene-type ligands of Mandypfos and Josiphos series (**8** and **9**) is dominated by the formation of a γ -coupling product (**6**) (entries 4–11). Among the ligands screened, (*R,S*)-CyPF-*t*-Bu (**9a**) was finally found to be the best ligand to achieve 63% ee with 92% γ -selectivity in refluxing THF (entry 6). The absolute configuration of 3-(4-methoxycarbonylphenyl)-1-butene (**6a**) was established to be *R* ([α]_D – 12.68 (*c* 0.59, benzene)) by the specific rotation reported for (*S*)-isomer ([α]_D + 12 (*c* 0.9, CHCl₃)) and retention times of two enantiomers in high-performance liquid chromatography (HPLC) analysis.^{18d,19b} Allyltrifluoroborates (**2**) are highly insoluble in common organic solvents. Thus, addition of water to THF or MeOH resulted in significant improvement of yields and enantioselectivities because of the high solubility of **2a** in aqueous solvents (entries 12 and 13). The enantioselectivities thus achieved were in the

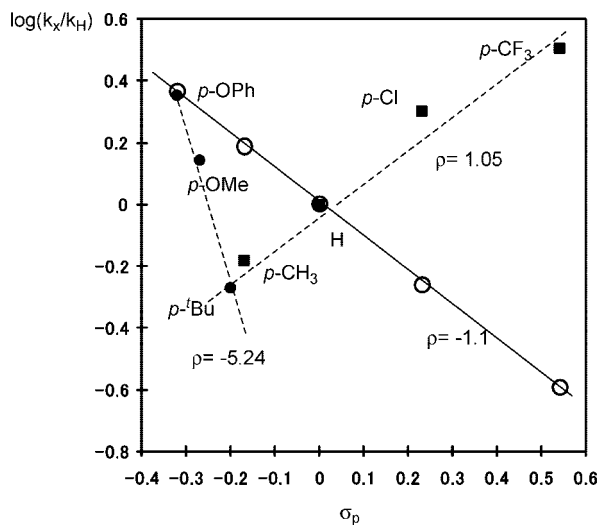
(17) (a) Hayashi, T. *J. Organomet. Chem.* **2002**, 653, 41. (b) Hayashi, T.; Tajika, M.; Tamao, K.; Kumada, M. *J. Am. Chem. Soc.* **1976**, 98, 3718. (c) Hayashi, T.; Konishi, M.; Fukushima, M.; Mise, T.; Kagotani, M.; Tajika, M.; Kumada, M. *J. Am. Chem. Soc.* **1982**, 104, 180. (d) Hayashi, T.; Konishi, M.; Fukushima, M.; Kanehira, K.; Hioki, T.; Kumada, M. *J. Org. Chem.* **1983**, 48, 2195.

(18) (a) van Zijl, A. W.; Arnold, L. A.; Minnaard, A. J.; Feringa, B. L. *Adv. Synth. Catal.* **2004**, 346, 413. (b) Tissot-Croset, K.; Alexakis, A. *Tetrahedron Lett.* **2004**, 45, 7375. (c) Yorimitsu, H.; Oshima, K. *Angew. Chem., Int. Ed.* **2005**, 44, 4435. (d) López, F.; van Zijl, A. W.; Minnaard, A. J.; Feringa, B. L. *Chem. Commun.* **2006**, 409.

(19) (a) RajanBabu, T. V.; Nomura, N.; Nandi, J. J. M.; Park, H.; Sun, X. *J. Org. Chem.* **2003**, 68, 8431. (b) Zhang, A.; RajanBabu, T. V. *Org. Lett.* **2004**, 6, 1515. (c) Park, H.; Kumareswaran, R.; RajanBabu, T. V. *Tetrahedron* **2005**, 61, 6352. (d) Shi, W.-J.; Xie, J.-H.; Zhou, Q.-L. *Tetrahedron: Asymmetry* **2006**, 16, 705.

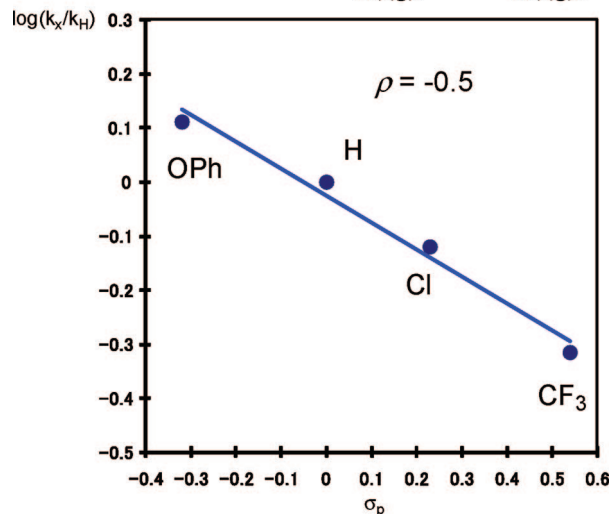
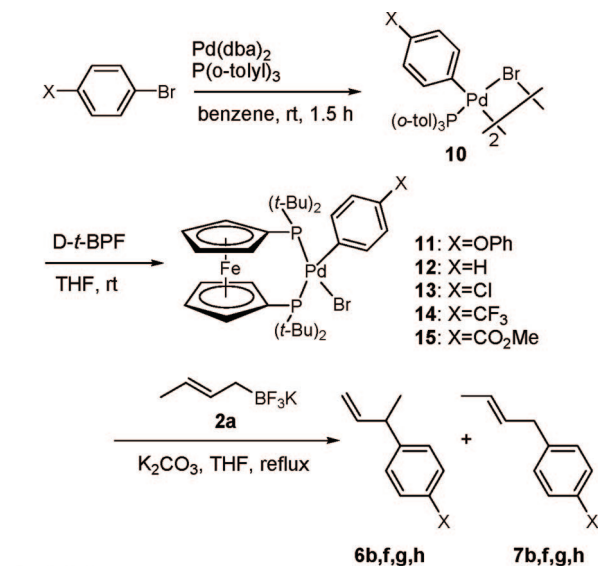
Scheme 3. Hammett Plot Based on Kinetic Data and σ Values in the Reaction between 1 and 2

b: X=OPh, c: X=OMe, d: X=Me, e: X= *t*-Bu, f: X= H, g: X= Cl, h: X= CF_3



range of 77–90% ee for representative para- and meta-substituted bromoarenes and 2-bromo-1-alkenes.¹⁰

Kinetic Studies on Transmetalation. The reaction between **2a** and para-substituted bromoarenes with $\text{Pd}(\text{OAc})_2/\text{D-}t\text{-BPF}$ in refluxing THF showed Hammett's correlations suggesting a rate-determining role of the transmetalation step (Scheme 3). There were two correlations when the relative rates were estimated by a competitive reaction of two bromoarenes for **2a** (dotted lines, ● and ■). The reactivity linearly was increased by donating groups having σ -values lower than -0.1 (●, $\rho = -5.24$) and withdrawing groups higher than 4-MeOC₆H₄Br (■, $\rho = 1.05$). This result was in sharp contrast to the single correlation ($\rho = -1.1$) to σ in a range of -0.3 to 0.5 when the initial rates were estimated by conversions of the independent runs for each bromoarene (solid line, O). Among the steps involved in the catalytic cycle of cross-coupling, oxidative addition exhibits a linear positive correlation accelerated by withdrawing groups as was observed in most cross-coupling reactions of arylboronic acids with haloarenes.²⁰ It is difficult to conclude that this is due to the rate-determining role of reductive elimination²¹ because there is no scrambling of the coupling position between γ -coupling products and thermally stable linear α -carbon coupling products. Thus, it is reasonable to conclude that the two correlations shown by the dotted lines were the result of a balance of the reverse effects of substituents on oxidative addition and transmetalation. The linear correlation

Scheme 4. Hammett Plot Based on Kinetic Data and σ Values in the Coupling between 11–15 and 2a

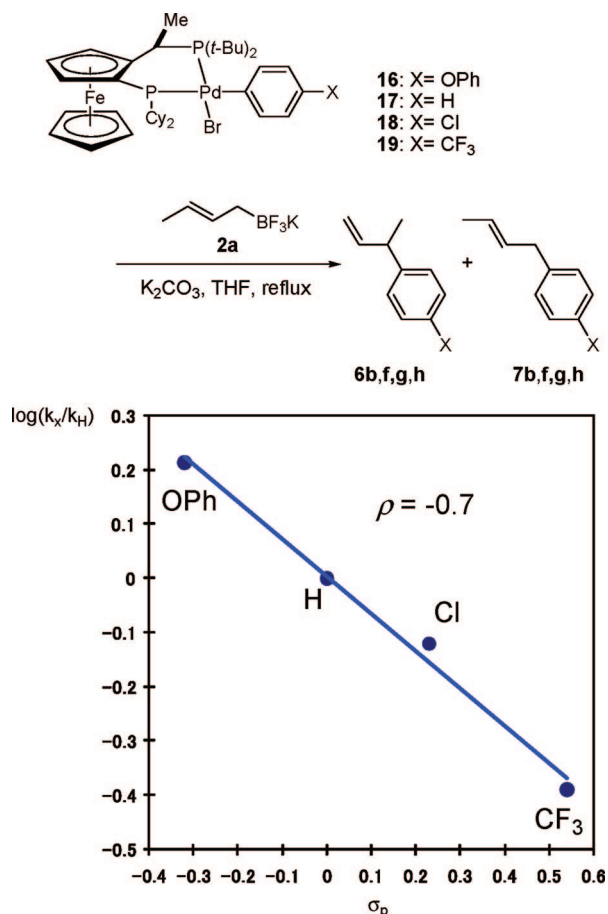
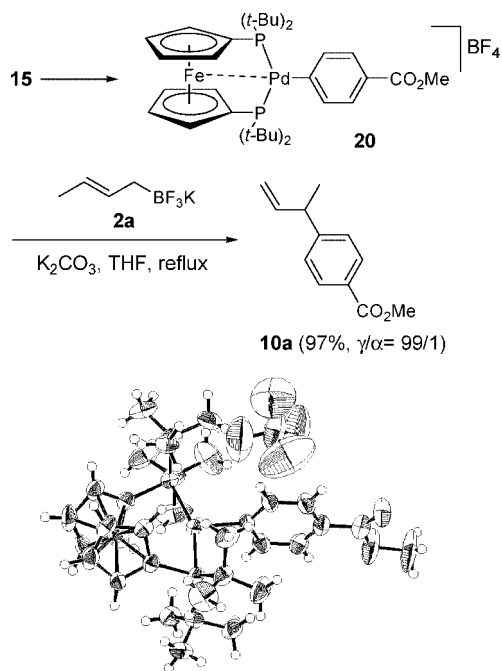
shown by a solid line is attributable to the electronic effect on transmetalation.

Five oxidative adducts of bromoarenes, **11–15** (X = OPh, H, Cl, CF_3 , CO_2Me), were synthesized by the method of Hartwig and co-workers²² as intermediates for transmetalation. The competitive reaction of (*E*)-crotyltri-fluoroborate (**2a**) with two oxidative adducts (**11–14**) in refluxing THF showed a single correlation with a small negative ρ -value (-0.50) (Scheme 4). The CyPF-*t*-Bu ligand used for asymmetric coupling is also dominated by the γ -coupling products for formation of a chiral secondary carbon. The reaction between (*E*)-crotylborate (**2a**) and four oxidative adducts (**16–19**, X = OPh, H, Cl, CF_3) of CyPF-*t*-Bu showed a single correlation with a small negative ρ -value (Scheme 5). The slope (-0.70) was almost the same as that of *D-}t\text{-BPF} ligand.*

A possible mechanism that accounts for the electronic effect of substituents is one proceeding through a cationic palladium(II) species by elimination of a bromine ligand before reaction with **2a**. The expected cationic palladium(II) species (**20**) was synthesized by treatment of **15** with AgBF_4 .^{22b} Indeed, the reaction between **2a** and **20** afforded perfect γ -selectivity (Scheme 6). The equilibrium formation of $[\text{Pd}(\text{Ar})(\text{D-}t\text{-BPF})]^+$ from $\text{Pd}(\text{Ar})(\text{D-}t\text{-BPF})(\text{Br})$ has been reported.^{22b}

(20) (a) Moriya, T.; Miyaura, N.; Suzuki, A. *Synlett* **1994**, 149. (b) Saito, S.; Oh-tani, S.; Miyaura, N. *J. Org. Chem.* **1997**, *62*, 8024. (c) Weissman, H.; Milstein, D. *Chem. Commun.* **1999**, 1901. (d) Zim, D.; Lando, V. R.; Dupont, J.; Montiro, A. L. *Org. Lett.* **2001**, *3*, 3049. (e) Liang, L.-C.; Chien, P.-S.; Huang, M.-H. *Organometallics* **2005**, *24*, 353.

(21) (a) Temple, J. S.; Riediker, M.; Schwartz, J. *J. Am. Chem. Soc.* **1982**, *104*, 1310. (b) Goliaszewski, A.; Schwartz, J. *J. Am. Chem. Soc.* **1984**, *106*, 5028. (c) Goliaszewski, A.; Schwartz, J. *Organometallics* **1985**, *4*, 417. (d) Bertani, R.; Berton, A.; Carturan, G.; Campostrini, R. *J. Organomet. Chem.* **1988**, *349*, 263.

Scheme 5. Hammett Plot Based on Kinetic Data and σ Values in the Reaction between 16–19 and 2a**Scheme 6. A Regiochemical Selectivity in the Coupling of Cationic Complex (20) with 2a**ORTEP drawing of (D-*t*-BPF)Pd(4-MeO₂CC₆H₄)(BF₄) (20)

Density Functional Theory (DFT) Calculations on the Energy Diagram of Oxidative Addition, Transmetalation, and Reductive Elimination Reactions. Results of theoretical studies on oxidative addition and reductive elimination of cross-

coupling reaction and Heck coupling reaction have been reported.^{23–27} The energy diagram of oxidative addition, Pd(PH₃)₂ (a) + Ph–Br (b) → TS_{oa} → Pd(PH₃)₂(Ph)(Br) (c), is given in Figure 1, while the structure of the transition state (TS_{oa}) is illustrated in Figure 2. The C–Br length of Ph–Br (b) at the initial separation is calculated to be 1.973 Å. At the transition state, the C–Br length of TS_{oa} is 2.239 Å, which is elongated by 0.266 Å by the interaction with Pd. TS_{oa} has a triangle form composed of a Br–Pd–Ph skeleton with an angle of 52.3° (∠Br–Pd–C). The bond lengths of Pd–Br and Pd–C of TS_{oa} are 2.774 and 2.136 Å, respectively. The activation energy at TS_{oa} is 10.2 kcal/mol relative to the initial separation (zero level) at the B3LYP/LANL2DZ level. The oxidative adduct, Pd(PH₃)₂(Ph)(Br), is 26.1 kcal/mol lower in energy than that of the initial separation, Pd(PH₃)₂ + Ph–Br. If the solvent effect is not considered, the energy level of c is slightly larger than that in THF (–21.2 kcal/mol). The formation of a cationic palladium(II) species (d) via substitution of the Pd–Br bond with H₂O takes place smoothly with a 13.6 kcal/mol energy barrier, whereas it is significantly large (100.4 kcal/mol) in the absence of a solvent effect indicating an important role of the solvent effect in this charge-separated system. The energy level of this state composed of (H₃P)Pd(Ph)⁺–OH₂ (d) and CH₃CH=CHCH₂BF₃[–] (e) is –12.6 kcal/mol lower than that of the initial state. The coordination of allylboronate (e) to a cationic palladium(II) complex (d) by the S_E2' (closed) transition state (f) is +2.0 kcal/mol higher than that by the S_E2' (open) state (g), though the former state (f', 10.4 kcal/mol) is 8 kcal/mol lower than the latter one (g', +18.4 kcal/mol) in the absence of a solvent effect. Thus, there is no large difference in energy levels between S_E2' closed and open coordination, whereas the S_E2' open process is slightly more stable than the S_E2' closed process in THF solvent. After TS_{tm}, the BF₃ group is substituted by a water molecule for formation of a strong Pd–C bond (h) with a 30 kcal/mol energy barrier. The structure of the transition state for transmetalation (TS_{tm}) is illustrated in Figure 2. If the solvent effect is not considered, the energy level of h becomes higher than zero level (+16.9 kcal/mol). The transition state of reductive elimination (TS_{re}) has a triangle structure composed of Pd and two carbon atoms of phenyl and allyl groups as shown in Figure 2. The energy of TS_{re} is 16.3 kcal/mol higher than

(22) (a) Paul, F.; Patt, J.; Hartwig, J. F. *Organometallics* **1995**, *14*, 3030. (b) Mann, G.; Shelby, Q.; Roy, A. H.; Hartwig, J. F. *Organometallics* **2003**, *22*, 2775.

(23) (a) Sumimoto, M.; Iwane, N.; Takahama, T.; Sakaki, S. *J. Am. Chem. Soc.* **2004**, *126*, 10457. (b) Braga, A. A.; Morgon, N. H.; Ujaque, G.; Maseras, F. *J. Am. Chem. Soc.* **2005**, *127*, 9298. (c) Goossen, L. J.; Koley, D.; Hermann, H. L.; Thiel, W. *J. Am. Chem. Soc.* **2005**, *127*, 11102. (d) Goossen, L. J.; Koley, D.; Hermann, H. L.; Thiel, W. *Organometallics* **2006**, *25*, 54. (e) Braga, A. A.; Ujaque, G.; Maseras, F. *Organometallics* **2006**, *25*, 3647. (f) Baraga, A. A. C.; Morgon, N. H.; Ujaque, G.; Lledós, A.; Maseras, F. *J. Organomet. Chem.* **2006**, *691*, 4459. (g) Sicre, C.; Braga, A. A. C.; Maseras, F.; Cid, M. M. *Tetrahedron* **2008**, *64*, 7437. (h) Huang, Y.-L.; Weng, C.-M.; Hong, F.-E. *Chem. Eur. J.* **2008**, *14*, 4426.

(24) (a) Goossen, L. J.; Koley, D.; Hermann, H. L.; Thiel, W. *Organometallics* **2005**, *24*, 2398. (b) Ahlquist, M.; Norrby, P.-O. *Organometallics* **2007**, *26*, 550. (c) Lam, K. C.; Marder, T. B.; Lin, Z. *Organometallics* **2007**, *26*, 758. (d) Fazaeli, R.; Ariafard, A.; Jamshidi, S.; Tabatabaie, E. S.; Pishro, K. A. *J. Organomet. Chem.* **2007**, *692*, 3984. (e) Li, Z.; Guo, Q.-X.; Liu, L. *Organometallics* **2008**, *27*, 4043.

(25) (a) Ananikov, V. P.; Musaev, D. G.; Morokuma, K. *J. Am. Chem. Soc.* **2002**, *124*, 2839. (b) Cárdenas, D. J.; Echavarran, A. M. *New J. Chem.* **2004**, *28*, 338. (c) Ananikov, V. P.; Musaev, D. G.; Morokuma, K. *Eur. J. Inorg. Chem.* **2007**, 5390.

(26) (a) Lee, M.-T.; Lee, H. M.; Hu, C.-H. *Organometallics* **2007**, *26*, 1317. (b) Surawatanawong, P.; Fan, Y.; Hall, M. B. *J. Organomet. Chem.* **2008**, *693*, 1552.

(27) (a) Nova, A.; Ujaque, G.; Maseras, F.; Lledós, A.; Espinet, P. *J. Am. Chem. Soc.* **2006**, *128*, 14571. (b) Álvarez, R.; Pérez, M.; Faza, O. N.; de Lera, A. R. *Organometallics* **2008**, *27*, 3378.

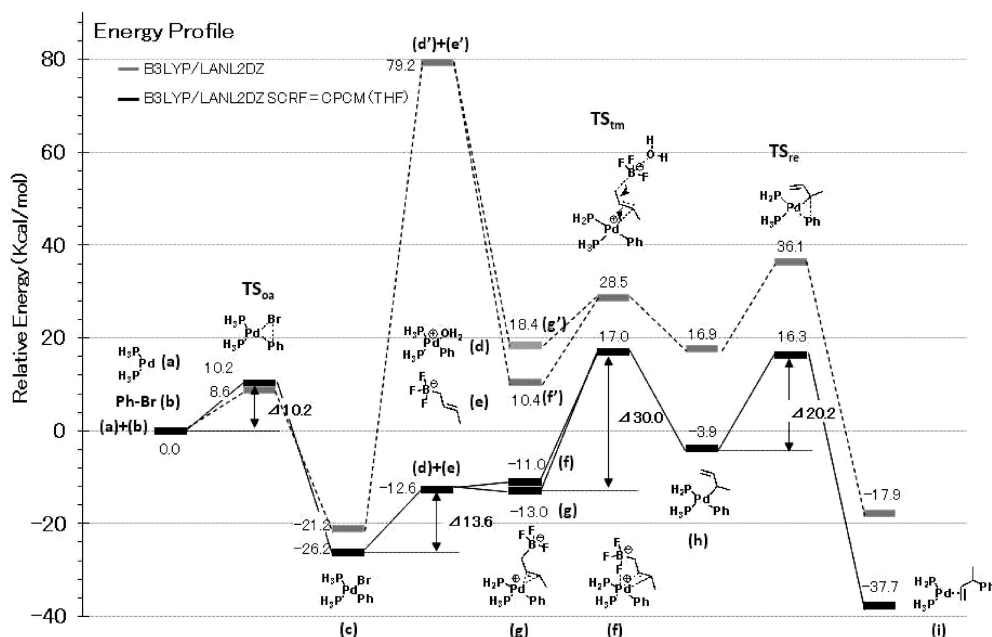


Figure 1. DFT calculation of transition state.

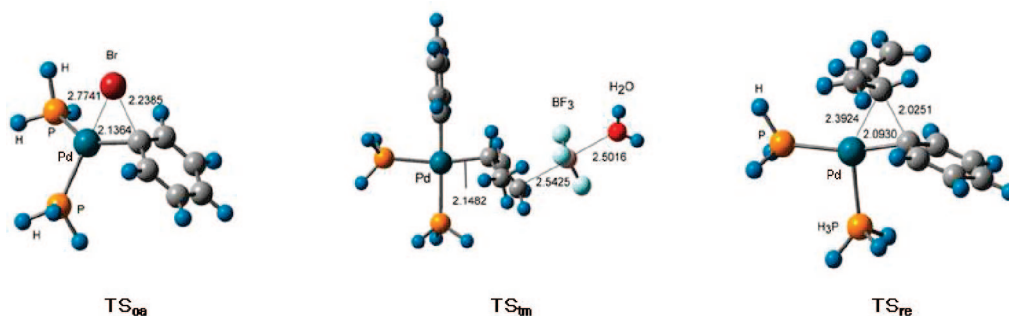


Figure 2. Optimized structures of TS_{oa} , TS_{tm} , and TS_{re} calculated at the B3LYP/LANL2DZ level.

zero level. In the final state for giving **i**, the bonding of the phenyl group (Ph) is changed from Pd to the carbon atom of allylic carbon, and the Pd atom interacts with the C=C double bond of $H_2C=CH(Ph)CH_3$ (**i**). The reaction energy is calculated to be -37.7 kcal/mol, which is large enough to proceed under thermal conditions.

Proposed Mechanism for Transmetalation. Transmetalation is a critical process involved in various metal-catalyzed bond-forming reactions, but the mechanistic features, including its kinetics, still remain unexplored. Intermediates before transmetalation between arylboronic acids and platinum(II) halides or palladium(II) halides were studied by Osakada²⁸ and Hartwig.²⁹ We reported the results of a kinetic study of transmetalation between para-substituted arylboronic acids and cationic $[Pd(Ph)(PPh_3)(dppe)]BF_4$ that showed a small negative ρ value (-0.54).³⁰ There have also been theoretical studies on transmetalation of arylboronic acids and diborons.²³ Among precedents for transmetalation between $Ar-Pd-X$ and allylfluorosilanes, an S_E2' (open) process involving a direct

interaction of the palladium metal center to the C=C double bond and an S_E2' (closed) process involving an F-chelation between Pd and Si atoms were proposed on the basis of the effects of phosphine ligands, the effect of F bases on α - and γ -coupling selectivity, and the stereochemistry in substitution of chiral allylsilane compounds.^{6b} On the other hand, the high-efficiency cationic palladium species for transmetalation has been demonstrated in the palladium-catalyzed bond-forming reactions of $ArB(OH)_2$ with ArN_2BF_4 or Ar_2IX ($X = BF_4, OTf$)³¹ and conjugate addition reactions of arylboronic acids to enones catalyzed by dicationic $[Pd(dppe)(PhCN)_2](BF_4)_2$.³⁰ The involvement of such a cationic species in Heck reaction between aryl triflates and 4-substituted styrenes was demonstrated by a kinetic study of substituents;³² however, it is not common in analogous coupling or addition reactions of organic halides.

All kinetic data suggested the formation of a cationic species (**22**) as the intermediate for transmetalation with allylborates

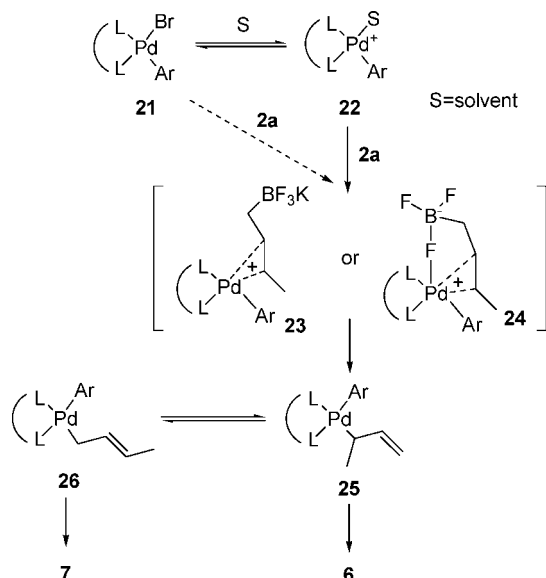
(28) (a) Osakada, K.; Onodera, H.; Nishihara, Y. *Organometallics* **2005**, *24*, 190. (b) Pantcheva, I.; Nishihara, Y.; Osakada, K. *Organometallics* **2005**, *24*, 3815. (c) Pantcheva, I.; Osakada, K. *Organometallics* **2006**, *25*, 1735. (d) Suzuki, Y.; Osakada, K. *Organometallics* **2006**, *25*, 3251.

(29) Stambuli, J. P.; Bühl, M.; Hartwig, J. F. *J. Am. Chem. Soc.* **2002**, *124*, 9346.

(30) Nishikata, T.; Yamamoto, Y.; Miyaura, N. *Organometallics* **2004**, *23*, 4317.

(31) (a) Kang, S.-K.; Lee, H.-W.; Jang, S.-B.; Ho, P.-S. *J. Org. Chem.* **1996**, *61*, 4720. (b) Sengupta, S.; Bhattacharyya, S. *J. Org. Chem.* **1997**, *62*, 3405. (c) Andrus, M. B.; Song, C. *Org. Lett.* **2001**, *3*, 3761. (d) Selvakumar, K.; Zapf, A.; Spanenberg, A.; Beller, M. *Chem. Eur. J.* **2002**, *8*, 3901. (e) Dai, M.; Liang, B.; Wang, C.; Chen, J.; Yang, Z. *Org. Lett.* **2004**, *6*, 221.

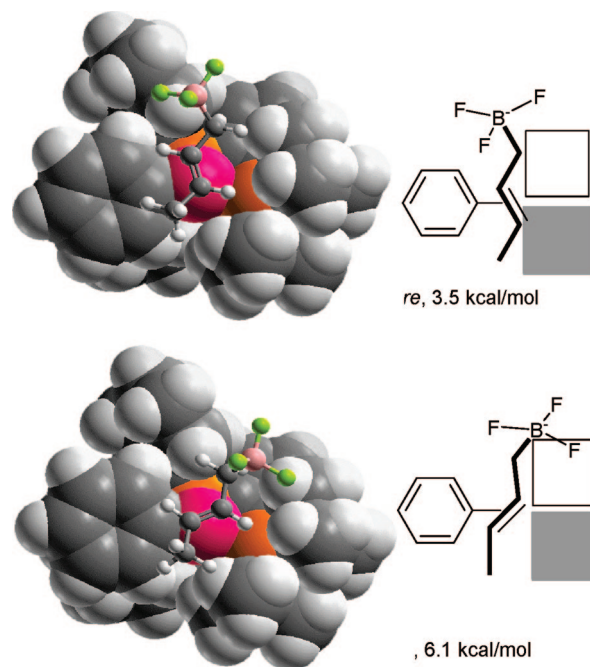
(32) (a) Ozawa, F.; Kubo, A.; Hayashi, T. *J. Am. Chem. Soc.* **1991**, *113*, 1417. (b) Cabri, W.; Candiani, I.; DeBernardinis, S.; Francalanci, F.; Penco, S. *J. Org. Chem.* **1991**, *56*, 5796. (c) Ozawa, F.; Kubo, A.; Matsumoto, Y.; Hayashi, T. *Organometallics* **1993**, *12*, 4188.

Scheme 7. Formation of a Cationic Palladium(II) Species (22) before Transmetalation with 2a

(2) when bulky and donating *D-t*-BPF was used as the ligand (Scheme 7). Since the reaction resulted in perfect γ -selectivities for all bromoarenes, the formation of an allylic π -complex intermediate before reductive elimination or an addition–elimination mechanism between Ar–Pd–X and the double bond of **2a** is ruled out. On the basis of these mechanistic precedents, our kinetic and theoretical calculation results, it was concluded that the formation of a π -complex (**23**) via coordination of the C–C double bond of **2a** to **22** is the most probable transition state that selectively gives γ -coupling products (**6**) via σ -allylpalladium(II) intermediates (**25**). A chelated cyclic complex (**24**) via coordination of F and a C–C double bond is another probable process, but the theoretical study indicated that the F chelation does not affect the stability of the transition state.

Enantioselection Mechanism in Asymmetric Coupling. The X-ray structure of [Pd(CyPF-*t*-Bu)(4-MeOC₆H₄)(NH₃)]OTf (**27**) reported by Shen and Hartwig is shown in Figure 3.³³ The molecular structure displays a slightly twisted square-planar coordination geometry for the palladium(II) atom ligated with two phosphorus atoms of (*R,S*)-CyPF-*t*-Bu, one carbon atom of the 4-methoxyphenyl group and one nitrogen atom of NH₃. There is a steric hindrance to pressure the right NH₃ upward and the left 4-methoxyphenyl group downward with respect to the P–Pd–P plane thus suggesting that the free space is accessible to reactants in the upper-right and lower-left quadrants. The dihedral angle between the P–Pd–P and C–Pd–N plane is 18.9° with anticlockwise rotation to the C–Pd–N plane. Such twisted structures suggesting free spaces accessible to the reactants have been reported for PdCl₂[(*R*)-binap]^{32c} and [Pd(PhCN)₂(chiraphos)](BF₄)₂³⁴ complexes.

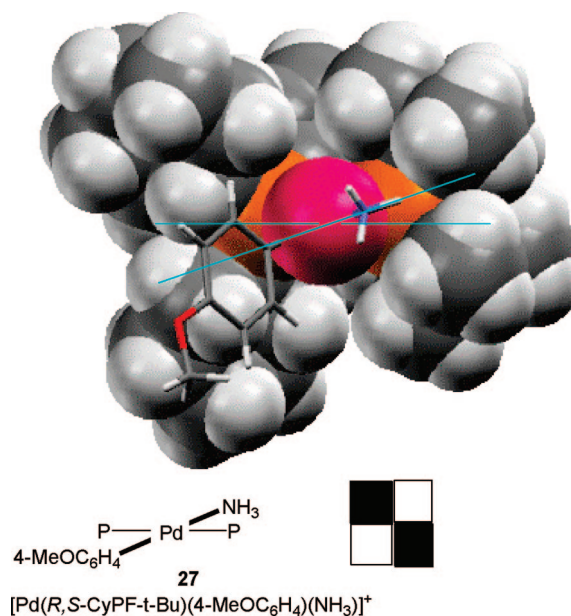
The minimum energy mode of substrate coordination to the cationic phenylpalladium intermediate was calculated, that is, the reaction stage directly preceding the stereodetermining insertion step by DFT calculation at the B3LYP/LANL2DZ level of theory. Two stable adducts between [Pd(CyPF-*t*-Bu)(Ph)]⁺ and **2a** located at the C–C double bond from its *re*-face (**28**) or *si*-face (**29**) via the S_E2' (open) process without F-chelation are shown in Scheme 8. Thus, reaction from the *re*-face yielding

Scheme 8. DFT Calculation of S_E2 (Open) Conformation at Minimum Energy Level

the experimentally observed enantiomer *R*-product is preferred thermodynamically (2.6 kcal/mol) over that of the *si*-face because of steric requirement between the methyl group of allylic moiety and the *t*-butyl group in the lower-right second quadrant. This is consistent with the experimental results shown in Table 2 suggesting a small energy difference (1–2 kcal/mol) between the two processes giving *R*- and *S*-enantiomers.

Experimental Section

General Procedure for γ -Selective Cross-Coupling (Table 1). A 20 mL flask charged with palladium acetate (0.015 mmol, 3 mol %), 1,1'-bis(di-*tert*-butylphosphino)ferrocene (*D-t*-BPF) (0.018 mmol), potassium allyltrifluoroborates (1.25 mmol), and K₂CO₃ (1.5

**Figure 3.** X-Ray structure of [Pd(*R,S*-CyPF-*t*-Bu)(4-MeOC₆H₄)(NH₃)]⁺ reported by Shen and Hartwig and possible free space accessible to reactants.(33) Shen, Q.; Hartwig, J. F. *J. Am. Chem. Soc.* **2006**, *128*, 10028.(34) Nishikata, T.; Yamamoto, Y.; Gridnev, I. D.; Miyaura, N. *Organometallics* **2005**, *24*, 5025.

mmol) was flush with nitrogen. THF (5 mL) and bromoarene (0.5 mmol) were added successively. After being refluxed for 22 h, the reaction mixture was treated with 1 N HCl (10 mL) at room temperature. Flash chromatography on silica gel gave the coupling product.

General Procedure for Asymmetric Cross-Coupling (Table 2). A flask charged with potassium (*E*)-2-butenyltrifluoroborate (2.5 mmol), Pd(OAc)₂ (3 mol %), 1-dicyclohexylphosphino-2-di-*tert*-butylphosphinoethylferrocene (CyPF-*t*-Bu) (3.6 mol %), and K₂CO₃ (3.0 mmol) was flushed with nitrogen. H₂O/MeOH (9/1, 5 mL) and bromoarene (1.0 mmol) were then added. The resulting mixture was stirred at 80 °C for 22 h. Isolated yields determined by chromatography on silica gel are shown in Table 2. Enantiomer excess was determined by a chiral stationary column.

Preparation of Palladium Complexes (Schemes 4 and 5). Pd₂(dba)₃·CHCl₃,³⁵ Pd[P(*o*-tolyl)₃]₂,³⁶ {Pd[P(*o*-tolyl)₃](Ph)(*μ*-Br)}₂,³⁶ (D-*t*-BPF)Pd(Ar)(Br) (Ar = C₆H₄-4-OPh (**11**), C₆H₅ (**12**), C₆H₄-4-Cl (**13**), C₆H₄-4-CF₃ (**14**), C₆H₄-4-CO₂Me (**15**)),^{22b} (CyPF-*t*-Bu)Pd(Ar)(Br) (Ar = C₆H₄-4-Oph (**16**), C₆H₅ (**17**), C₆H₄-4-Cl (**18**), C₆H₄-4-CF₃ (**19**)),³⁷ and [(D-*t*-BPF)Pd(C₆H₄-4-CO₂Me)](BF₄) (**20**)^{22b} were prepared according to published methods.

Pd(D-*t*-BPF)(Br)(4-PhOC₆H₄) (11**).** Crystallization from benzene/CH₂Cl₂/pentane; ¹H NMR (400 MHz, CDCl₃) δ 7.75 (d, *J* = 15.9 Hz, 1H), 7.54 (d, *J* = 8.0 Hz, 1H), 7.43–7.36 (m, 3H), 7.33 (t, *J* = 8.0 Hz, 1H), 7.10 (d, *J* = 15.9 Hz, 1H), 6.96 (d, *J* = 7.1 Hz, 2H), 5.57 (s, 4H), 4.33 (s, 4H), 1.42 (d, *J* = 7.1 Hz, 18H), 1.40 (d, *J* = 8.0 Hz, 18H); ³¹P NMR (162 MHz, CDCl₃) δ 23.75; HRMS *m/z*: calcd for C₃₈H₅₃FeO₂Pd 749.1956, found 749.1960.

Pd(D-*t*-BPF)(Br)(C₆H₅) (12**).** Crystallization from benzene/CH₂Cl₂/pentane; ¹H NMR (400 MHz, CDCl₃) δ 7.59 (d, *J* = 7.8 Hz, 2H), 7.16 (d, *J* = 7.4 Hz, 2H), 6.99 (t, *J* = 7.1 Hz, 1H), 5.54 (s, 4H), 4.33 (s, 4H), 1.40 (d, *J* = 7.4 Hz, 18H), 1.39 (d, *J* = 7.8 Hz, 18H); ³¹P NMR (162 MHz, CDCl₃) δ 20.71; HRMS *m/z*: calcd for C₃₂H₄₉FeP₂Pd 657.1694, found 657.1697; anal. calcd for C₃₃H₄₉FeP₂Pd: C, 52.09; H, 6.69; found: 48.73; H, 6.82.

Pd(D-*t*-BPF)(Br)(4-ClC₆H₄) (13**).** Crystallization from benzene/CH₂Cl₂/pentane; ¹H NMR (400 MHz, CDCl₃) δ 7.55 (d, *J* = 7.6 Hz, 2H), 7.19 (d, *J* = 7.1 Hz, 2H), 5.59 (s, 4H), 4.31 (s, 4H), 1.40 (d, *J* = 7.5 Hz, 18H), 1.38 (d, *J* = 7.6 Hz, 18H); ³¹P NMR (162 MHz, CDCl₃) δ 23.43; HRMS *m/z*: calcd for C₃₂H₄₈ClFeP₂Pd 691.1304, found 691.1307.

Pd(D-*t*-BPF)(Br)(4-CF₃C₆H₄) (14**).** Crystallization from benzene/CH₂Cl₂/pentane; ¹H NMR (400 MHz, CDCl₃) δ 7.75 (d, *J* = 15.9 Hz, 2H), 7.10 (d, *J* = 15.9 Hz, 2H), 5.63 (s, 4H), 4.34 (s, 4H), 1.40 (d, *J* = 7.1 Hz, 18H), 1.38 (d, *J* = 7.1 Hz, 18H); ³¹P NMR

(162 MHz, CDCl₃) δ 23.42; HRMS *m/z*: calcd for C₃₃H₄₈F₃FeP₂Pd 725.1568, found 725.1566.

Pd(D-*t*-BPF)(Br)(4-MeO₂CC₆H₄) (15**).** Crystallization from benzene/CH₂Cl₂/pentane; ¹H NMR (400 MHz, CDCl₃) δ 7.82 (d, *J* = 8.3 Hz, 2H), 7.77 (d, *J* = 8.3 Hz, 2H), 5.63 (s, 4H), 4.34 (s, 4H), 3.92 (s, 3H), 1.40 (d, *J* = 7.8 Hz, 18H), 1.38 (d, *J* = 7.3 Hz, 18H); ³¹P NMR (162 MHz, CDCl₃): 18.99; HRMS *m/z*: calcd for C₃₄H₅₁FeO₂P₂Pd 715.1749, found 715.1746; anal. calcd for C₃₄H₅₁FeO₂P₂Pd: C, 51.31; H, 6.46; found: 49.27; H, 6.53.

Pd(CyPF-*t*-Bu)(Br)(4-PhOC₆H₄) (16**).** Crystallization from CH₂Cl₂/pentane; ¹H NMR (400 MHz, CDCl₃) δ 7.97–7.84 (m, 2H), 7.38–7.24 (m, 4H), 7.15–7.09 (m, 1H), 7.07–6.90 (m, 2H), 5.89 (br s, 1H), 4.89 (s, 1H), 4.52 (s, 1H), 4.26 (s, 5H), 3.21–3.18 (m, 1H), 1.99 (t, *J* = 7.1 Hz, 3H), 1.70 (d, *J* = 11.7 Hz, 9H), 1.19 (d, *J* = 13.1 Hz, 9H), 2.61–0.86 (m, 22H); ³¹P NMR (162 MHz, CDCl₃): 74.22 (d, *J* = 35.1 Hz), 18.26 (br s); HRMS *m/z*: calcd for C₄₄H₆₁FeO₂P₂Pd 829.2582, found 829.2593.

Pd(CyPF-*t*-Bu)(Br)(C₆H₅) (17**).** Crystallization from CH₂Cl₂/pentane; ¹H NMR (400 MHz, CDCl₃) δ 7.50 (br s, 1H), 7.32 (br s, 2H), 6.89–6.84 (m, 2H), 4.89 (br s, 1H), 4.52 (s, 1H), 4.45 (s, 1H), 4.25 (s, 5H), 3.21–3.18 (m, 1H), 1.98 (t, *J* = 7.6 Hz, 3H), 1.66 (d, *J* = 12.2 Hz, 9H), 1.18 (d, *J* = 12.0 Hz, 9H), 2.63–0.86 (m, 22H); ³¹P NMR (162 MHz, CDCl₃) δ 73.51 (d, *J* = 36.6 Hz), 18.21 (br s); HRMS *m/z*: calcd for C₃₈H₅₇FeP₂Pd 737.2320, found 737.2328.

Pd(CyPF-*t*-Bu)(Br)(4-ClC₆H₄) (18**).** Crystallization from CH₂Cl₂/pentane; ¹H NMR (400 MHz, CDCl₃) δ 7.11 (d, *J* = 8.3 Hz, 2H), 6.89 (d, *J* = 7.8 Hz, 2H), 4.88 (br s, 1H), 4.53 (s, 1H), 4.47 (s, 1H), 4.25 (s, 5H), 3.19–3.16 (m, 1H), 1.98 (t, *J* = 7.6 Hz, 3H), 1.67 (d, *J* = 11.7 Hz, 9H), 1.18 (d, *J* = 13.2 Hz, 9H), 2.51–0.86 (m, 22H); ³¹P NMR (162 MHz, CDCl₃) δ 75.03 (d, *J* = 33.5 Hz), 18.44 (br s); HRMS *m/z*: calcd for C₃₈H₅₆ClFeP₂Pd 771.1930, found 771.1925.

Pd(CyPF-*t*-Bu)(Br)(4-CF₃C₆H₄) (19**).** Crystallization from CH₂Cl₂/pentane; ¹H NMR (400 MHz, CDCl₃) δ 7.35 (d, *J* = 7.8 Hz, 2H), 7.12 (d, *J* = 7.8 Hz, 2H), 4.89 (br s, 1H), 4.54 (s, 1H), 4.48 (s, 1H), 4.26 (s, 5H), 3.19–3.17 (m, 1H), 1.99 (t, *J* = 7.4 Hz, 3H), 1.66 (d, *J* = 12.7 Hz, 9H), 1.18 (d, *J* = 13.2 Hz, 9H), 2.69–0.87 (m, 22H); ³¹P NMR (162 MHz, CDCl₃) δ 77.56 (d, *J* = 32.6 Hz), 20.67 (br s); HRMS *m/z*: calcd for C₃₉H₅₆F₃FeP₂Pd 805.2194, found 805.2206.

Pd(D-*t*-BPF)(4-MeO₂CC₆H₄)(BF₄) (20**).** AgBF₄ (0.91 mmol) in THF (5 mL) was added to a solution of Pd(D-*t*-BPF)(Br)(4-MeO₂CC₆H₄) (0.70 mmol) in CH₂Cl₂ (35 mL). The suspension was stirred at room temperature for 1 h. The product was isolated by filtration. Recrystallization from THF gave brown needles (89%). ¹H NMR (400 MHz, CDCl₃) δ 7.82 (d, *J* = 7.8 Hz, 2H), 7.78 (d, *J* = 7.8 Hz, 2H), 5.41 (s, 4H), 4.30 (s, 4H), 3.92 (s, 3H), 1.39 (t, *J* = 7.3 Hz, 18H), 1.37 (d, *J* = 7.4 Hz, 18H); ³¹P NMR (162 MHz, CDCl₃) δ 21.27; ¹¹B NMR (128 MHz, CDCl₃) δ 6.50; HRMS *m/z*: calcd for C₃₄H₅₁FeO₂P₂Pd 715.1749, found 715.1755. The X-ray structure is shown in Scheme 6.

Kinetic Measurement of Coupling between Potassium Allyltrifluoroborates and *p*-Substituted Bromoarenes (Scheme 3). To a solution of Pd(OAc)₂ (0.015 mmol), D-*t*-BPF (0.018 mmol), potassium (*E*)-2-butenyltrifluoroborate (0.75 mmol), and K₂CO₃ (1.5 mmol) in THF (7 mL) was added *p*-substituted bromoarene (0.5 mmol) (*p*-PhOC₆H₄Br, *p*-MeC₆H₄Br, PhBr, *p*-ClC₆H₄Br, or *p*-CF₃C₆H₄Br). The mixture was stirred at 75 °C. The reaction progress was followed by gas chromatography (GC) analysis of the coupling product.

Competitive Reactions Using Pd(D-*t*-BPF)(Ar)(Br) or Pd(CyPF-*t*-Bu)(Ar)(Br) (Schemes 4 and 5). A 20 mL flask was charged with Pd(D-*t*-BPF)(Ph)(Br) (0.25 mmol), Pd(D-*t*-BPF)(Ar)(Br) (0.25 mmol Ar = *p*-PhOC₆H₄, *p*-ClC₆H₄, *p*-CF₃C₆H₄), potassium (*E*)-2-butenyltrifluoroborate (0.75 mmol), and K₂CO₃ (1.5 mmol) under nitrogen. THF (7 mL) was added, and the resulting

(35) Ukai, T.; Kawazura, H.; Ishii, Y.; Bonnet, J. J.; Ibers, J. A. *J. Organomet. Chem.* **1974**, *65*, 253.

(36) (a) Paul, F.; Patt, J.; Hartwig, J. F. *Organometallics* **1995**, *14*, 3030. (b) Widenhoefer, R. A.; Zhong, H. A.; Buchwald, S. L. *Organometallics* **1996**, *15*, 2745.

(37) Roy, A. H.; Hartwig, J. F. *J. Am. Chem. Soc.* **2003**, *125*, 8704.

(38) (a) Lee, C.; Parr, R. G.; Yang, W. *Phys. Rev. B* **1988**, *37*, 785. (b) Becke, A. D. *J. Chem. Phys.* **1993**, *98*, 5648. (c) Stephens, P. J.; Devlin, F. J.; Chabalowski, C. F.; Frisch, M. J. *J. Phys. Chem.* **1994**, *98*, 11623.

(39) Frisch, M. J.; Trucks, G. W.; Schlegel, H. B.; Scuseria, G. E.; Robb, M. A.; Cheeseman, J. R.; Montgomery, J. A., Jr.; Vreven, T.; Kudin, K. N.; Burant, J. C.; Millam, J. M.; Iyengar, S. S.; Tomasi, J.; Barone, V.; Mennucci, B.; Cossi, M.; Scalmani, G.; Rega, N.; Petersson, G. A.; Nakatsuji, H.; Hada, M.; Ehara, M.; Toyota, K.; Fukuda, R.; Hasegawa, J.; Ishida, M.; Nakajima, T.; Honda, Y.; Kitao, O.; Nakai, H.; Klene, M.; Li, X.; Knox, J. E.; Hratchian, H. P.; Cross, J. B.; Adamo, C.; Jaramillo, J.; Gomperts, R.; Stratmann, R. E.; Yazyev, O.; Austin, A. J.; Cammi, R.; Pomelli, C.; Ochterski, J. W.; Ayala, P. Y.; Morokuma, K.; Voth, G. A.; Salvador, P.; Dannenberg, J. J.; Zakrzewski, V. G.; Dapprich, S.; Daniels, A. D.; Strain, M. C.; Farkas, O.; Malick, D. K.; Rabuck, A. D.; Raghavachari, K.; Foresman, J. B.; Ortiz, J. V.; Cui, Q.; Baboul, A. G.; Clifford, S.; Cioslowski, J.; Stefanov, B. B.; Liu, G.; Liashenko, A.; Piskorz, P.; Komaromi, I.; Martin, R. L.; Fox, D. J.; Keith, T.; Al-Laham, M. A.; Peng, C. Y.; Nanayakkara, A.; Challacombe, M.; Gill, P. M. W.; Johnson, B.; Chen, W.; Wong, M. W.; Gonzalez, C.; Pople, J. A. *Gaussian 03*, revision B.04; Gaussian, Inc.: Pittsburgh, PA, 2003.

solution was heated to 75 °C. The relative rate was estimated by GC analysis of coupling products (a sum of products **6** and **7**).

Computational Details. All calculations were performed by means of the density functional theory method, the hybrid Becke3LYP functional with a hybrid Becke exchange functional, and a Lee–Yang–Parr correlation functional as implemented in Gaussian 03.^{39,40} The basis sets were described using an effective core potential (LANL2DZ) for all atoms.⁴¹ The structures at the stationary points were fully optimized at the B3LYP/LANL2DZ level of theory. Solvent effects on the energy diagram were included using self-consistent reaction field (SCRF) method using CPCM.⁴² Tetrahydrofuran (THF) was used as solvent throughout.

(40) (a) Wadt, W. R.; Hay, P. J. *J. Chem. Phys.* **1985**, *82*, 284. (b) Hay, P. J.; Wadt, W. R. *J. Chem. Phys.* **1985**, *82*, 299.

Acknowledgment. This work was supported by a Grant-in-Aid for Scientific Research in Priority Areas (no. 18064001, Synergy of Elements) and the Global COE Program (No. B01, Catalysis as the Basis for Innovation in Materials Science) from the Ministry of Education, Culture, Sports, Science, and Technology, Japan.

Supporting Information Available: Text describing experimental details, spectral and analytical data of the products, and X-ray data (PDF). This material is available free of charge via Internet at <http://pubs.acs.org>.

OM800832R

(41) (a) Barone, V.; Cossi, M. *J. Phys. Chem. A* **1998**, *102*, 1995. (b) Cossi, M.; Scalmani, G.; Rega, N.; Barone, V. *J. Comput. Chem.* **2003**, *24*, 669.

Elucidation of Heterocumulene Activation by a Nucleophilic-at-Metal Iridium(I) Carbene

Matthew T. Whited and Robert H. Grubbs*

Arnold and Mabel Beckman Laboratories of Chemical Synthesis, Division of Chemistry and Chemical Engineering, California Institute of Technology, Pasadena, California 91125

Received October 9, 2008

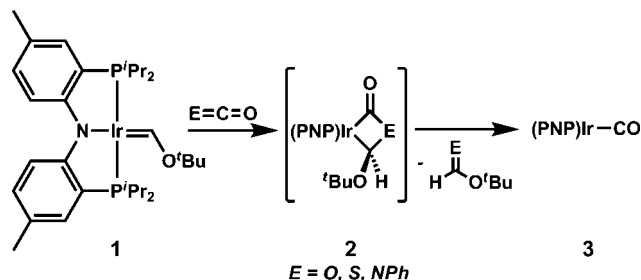
A carbene complex supported by the (PNP)Ir framework is shown to facilitate sulfur-atom transfer from CS₂ and PhNCS by an unusual multiple-bond metathesis pathway, and kinetically trapped intermediates are provided to support the proposed metal-initiated mechanism for heterocumulene activation. Experimental and theoretical studies on a series of (PNP)Ir–L complexes suggest that a high-lying, nucleophilic Ir(d₂) orbital mediates this unique reactivity. The combination of evidence indicates that square-planar Ir(I) carbenes of this type are best formulated as nucleophilic-at-metal carbenes, exhibiting reactivity initiated by a nucleophilic metal center rather than a nucleophilic or electrophilic carbene and providing products that are complementary to those typically observed for high-valent alkylidenes.

Introduction

The reactivity of transition metal–carbon multiple bonds has been the subject of intense investigation for many years, allowing the development of a host of transformations based on reactivity of the carbene unit.¹ In general, these transformations are dominated by carbon-based frontier orbitals.² Thus, metal–carbon multiple bonds are conventionally divided into two classes, where Fischer carbenes (coordinated singlet carbenes) are electrophilic at carbon and Schrock carbenes (coordinated triplet carbenes) are nucleophilic at carbon.

We have been investigating the reactivity of iridium species supported by Ozerov's PNP ligand (PNP = [N(2-P'Pr₂-4-Me-C₆H₃)₂]^{−3}) and recently reported an unusual transformation of carbon dioxide, carbonyl sulfide, and phenyl isocyanate, where atom and group transfer to a Fischer carbene at square-planar iridium(I) was effected by C=E bond cleavage (E = O, S, NPh).⁴ We proposed that these unique metathesis reactions were

Scheme 1. Decarbonylation of Heterocumulenes by Carbene 1



made possible by a nucleophilic iridium center, which could initiate atom and group transfer by attack of an electrophilic heterocumulene, cyclization to metallacycle **2**, and elimination of formate, thioformate, or formimidate to afford (PNP)Ir-CO (**3**, Scheme 1).

This formulation implies that the high d-electron count and coordinatively unsaturated nature of carbene **1** confer a degree of nucleophilicity to the iridium center that controls reactivity of the complex, contrasting previous reports of heterocumulene reactivity where the metal-bound carbenes act as nucleophiles and C–C bonds are formed.^{5,6} Such behavior would not be entirely unexpected in light of Roper's previous observation, which we have confirmed for our system,⁴ that heteroatom-substituted carbenes rarely exhibit electrophilic character when attached to electron-rich, late transition metals.^{2f} Additionally, Stone has reported that a square-planar carbene of iridium(I) performs the oxidative addition of dihydrogen, affording an

(5) Examples of more commonly observed nucleophilic reactivity between metal carbenes and heterocumulenes: (a) Schrock, R. R. *J. Am. Chem. Soc.* **1976**, *98*, 5399. (b) Klein, D. P.; Bergman, R. G. *J. Am. Chem. Soc.* **1989**, *111*, 3079. (c) Lee, S. K.; Cooper, N. J. *J. Am. Chem. Soc.* **1990**, *112*, 9419. (d) Mindaola, D. J.; Hillhouse, G. L. *J. Am. Chem. Soc.* **2002**, *124*, 9976.

(6) This behavior is more closely related to what is observed for Sadighi's structurally and electronically similar Cu(I)-boryl complexes: (a) Laitar, D. S.; Müller, P.; Sadighi, J. P. *J. Am. Chem. Soc.* **2005**, *127*, 17196. (b) Laitar, D. S.; Tsui, E. Y.; Sadighi, J. P. *J. Am. Chem. Soc.* **2006**, *128*, 11036.

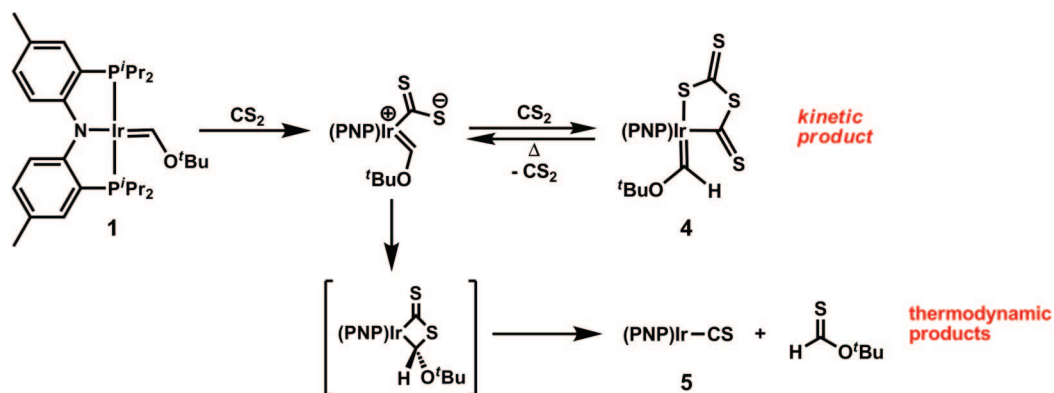
* Corresponding author. E-mail: rhg@caltech.edu.

(1) For leading references, see: (a) Fischer, E. O. *Pure Appl. Chem.* **1970**, *24*, 407. (b) Fischer, E. O. *Pure Appl. Chem.* **1978**, *50*, 857. (c) Cardin, D. J.; Cetinkaya, B.; Lappert, M. F. *Chem. Rev.* **1972**, *72*, 545. (d) Cotton, F. A.; Lukehart, C. M. *Prog. Inorg. Chem.* **1972**, *16*, 487. (e) Schrock, R. R. *Acc. Chem. Res.* **1979**, *12*, 99. (f) Schrock, R. R. *J. Chem. Soc., Dalton Trans.* **2001**, *18*, 2541. (g) Schrock, R. R. *Chem. Rev.* **2002**, *102*, 145. (h) Doyle, M. P. *Chem. Rev.* **1986**, *86*, 919. (i) Brookhart, M.; Studabaker, W. B. *Chem. Rev.* **1987**, *87*, 411. (j) Doetz, K. H.; Minatti, A. Fischer Type Carbene Complexes. In *Transition Metals for Organic Synthesis*; Beller, M., Bolm, C., Eds.; Wiley-VCH: Weinheim, 2004; Vol. 2, pp 397–425. (k) *Handbook of Metathesis*; Grubbs, R. H., Ed.; Wiley-VCH: Weinheim, 2003.

(2) (a) Nugent, W. A.; Mayer, J. M. *Metal-Ligand Multiple Bonds*; Wiley: New York, 1988. (b) Schrock, R. R. *J. Am. Chem. Soc.* **1975**, *97*, 6577. (c) Nugent, W. A.; McKinney, R. J.; Kasowski, R. V.; Van-Catledge, F. A. *Inorg. Chim. Acta* **1982**, *65*, L91. (d) Nakatsuji, H.; Ushio, J.; Han, S.; Yonezawa, T. *J. Am. Chem. Soc.* **1983**, *105*, 426. (e) Ushio, J.; Nakatsuji, H.; Yonezawa, T. *J. Am. Chem. Soc.* **1984**, *106*, 5892. (f) Block, T. F.; Fenske, R. F.; Casey, C. P. *J. Am. Chem. Soc.* **1976**, *98*, 441. (g) Gallop, M. A.; Roper, W. R. *Adv. Organomet. Chem.* **1986**, *25*, 121. (h) Taylor, T. E.; Hall, M. B. *J. Am. Chem. Soc.* **1984**, *106*, 1576. (i) Cundari, T. R.; Gordon, M. S. *J. Am. Chem. Soc.* **1991**, *113*, 5231.

(3) (a) Fan, L.; Foxman, B. M.; Ozerov, O. V. *Organometallics* **2004**, *23*, 326. (b) Ozerov, O. V.; Guo, C.; Papkov, V. A.; Foxman, B. M. *J. Am. Chem. Soc.* **2004**, *126*, 4792.

(4) Whited, M. T.; Grubbs, R. H. *J. Am. Chem. Soc.* **2008**, *130*, 5874.

Scheme 2. Reaction of Carbene **1** with Carbon Disulfide

iridium(III) dihydrido carbene.⁷ By analogy, the electron-rich metal center in our system might be expected to play a central role in substrate activation.

In this contribution, we report that reaction of **1** with CS_2 and PhNCS , which are isoelectronic to the heterocumulenes previously examined, allows observation and isolation of kinetically trapped intermediate species, supporting a mechanism of atom transfer that clearly requires a distinct mode of carbene reactivity. Additionally, we present experimental and theoretical studies suggesting that a high-lying, nucleophilic $\text{Ir}(d_2)$ orbital plays a critical role in initiating these unusual transformations. Taken together, our findings suggest a new strategy for the activation of heterocumulenes and other electrophiles across metal–ligand multiple bonds at late transition metals. Interestingly, these reactivity patterns are complementary to those observed for the nucleophilic alkylidenes of the high-valent early metals.^{2a,5a,8}

Results and Discussion

I. Reactivity with Carbon Disulfide. In light of the high driving force for the formation of carbonyl complex **3**, reaction of carbene **1** with heterocumulenes lacking oxygen was examined with the goal of stabilizing an intermediate species analogous to metallacycle **2**. However, in contrast to the reactivity observed with oxygen-containing heterocumulenes,⁴ dissolution of $(\text{PNP})\text{Ir}=\text{C}(\text{H})\text{O}^t\text{Bu}$ (**1**) in neat CS_2 did not afford $(\text{PNP})\text{Ir}-\text{CS}$ but instead yielded the unusual CS_2 head-to-tail dimer complex **4**, in which the iridium carbene unit remained intact (Scheme 2),^{9,10} as confirmed by X-ray diffraction analysis (Figure 1). The carbene proton retains a distinctive ^1H NMR shift (δ 15.5 ppm), consistent with an iridium–carbon multiple bond, but collapses from a triplet (in complex **1**) to a singlet (in complex **4**) due to the shifting of the C–H bond vector out

of the plane of the iridium–phosphorus bonds.¹¹ The carbene is observed by ^{13}C NMR at δ 266.7 ppm, shifted significantly downfield from the parent *tert*-butoxymethylidene (δ 210.0 ppm).¹² As a result of the change in metal oxidation state, the $\text{Ir}=\text{C}$ bond of **4** is slightly elongated (1.96 Å) relative to compound **1** (1.88 Å), and the $\text{C}(27)-\text{O}(1)$ bond is contracted by approximately the same amount (from 1.35 Å to 1.28 Å), indicating a decrease in metal–carbon multiple-bond character and concomitant increase in the effective carbon–oxygen bond order.

Heating a benzene solution of **4** (70 °C, 16 h) caused quantitative degradation to $(\text{PNP})\text{Ir}-\text{CS}$ (**5**) with concomitant expulsion of *tert*-butyl thioformate and CS_2 (Scheme 2), indicating the potential intermediacy of CS_2 dimer **4** in the sulfur-atom transfer process (and suggesting CO_2 dimers as possible intermediates in previously reported oxygen-atom transfer reactions).¹⁰ However, previous studies of the kinetics of CO_2 deoxygenation by **1** had shown a first-order rate dependence on CO_2 concentration, indicating that such a mechanism was not operative.⁴ Additionally, the connectivity of **4** is more consistent with intermediates typically invoked in heterocumulene disproportionation reactions.¹³ Thus, we were interested to see whether **4** was instead a kinetic product formed from the trapping of an intermediate species formed by reaction of **1** with CS_2 .

Slow addition of 1 equiv of CS_2 to a benzene solution of **1** resulted in the immediate and quantitative formation of thio-carbonyl complex **5** at ambient temperature, ruling out the intermediacy of **4** in the atom transfer reaction. Thus, as in our original assessment of the mechanism, we propose that reaction begins with nucleophilic attack by iridium at an electrophilic heterocumulene carbon. Depending on the concentration of CS_2 , two pathways are available for this intermediate, and it can either be trapped by a second molecule of CS_2 , affording **4**, or cyclize to the irida(dithio)lactone and decompose to give **5** and *tert*-

(7) Fraser, P. J.; Roper, W. R.; Stone, F. G. A. *J. Chem. Soc., Dalton Trans.* **1974**, 760.

(8) (a) Tebbe, F. N.; Parshall, G. W.; Reddy, G. S. *J. Am. Chem. Soc.* **1978**, *100*, 3611. (b) Pine, S. H.; Zahler, R.; Evans, D. A.; Grubbs, R. H. *J. Am. Chem. Soc.* **1980**, *102*, 3270.

(9) This binding motif for CS_2 has been observed previously: (a) Werner, H.; Kolb, O.; Feser, R.; Schubert, U. *J. Organomet. Chem.* **1980**, *191*, 283. (b) Cowie, M.; Dwight, S. K. *J. Organomet. Chem.* **1980**, *198*, C20. (c) Cowie, M.; Dwight, S. K. *J. Organomet. Chem.* **1981**, *214*, 233. (d) Mason, G.; Swepston, P. N.; Ibers, J. A. *Inorg. Chem.* **1983**, *22*, 411. (e) Carmona, E.; Galindo, A.; Monge, A.; Muñoz, M. A.; Poveda, M. L.; Ruiz, C. *Inorg. Chem.* **1990**, *29*, 5074. (f) George, D. S. A.; Hiltz, R. W.; McDonald, R.; Cowie, M. *Inorg. Chim. Acta* **2000**, *300*, 353.

(10) Though not observed for our system, an iridium-supported head-to-tail dimer of CO_2 has also been reported: Herskovitz, T.; Guggenberger, L. *J. Am. Chem. Soc.* **1976**, *98*, 1615.

(11) Similar behavior has been observed for phosphine-supported ruthenium carbenes: (a) Nguyen, S. T.; Johnson, L. K.; Grubbs, R. H.; Ziller, J. W. *J. Am. Chem. Soc.* **1992**, *113*, 3974. (b) Dias, E. L.; Nguyen, S. T.; Grubbs, R. H. *J. Am. Chem. Soc.* **1997**, *119*, 3887. (c) Schwab, P.; Grubbs, R. H.; Ziller, J. W. *J. Am. Chem. Soc.* **1996**, *118*, 100.

(12) Romero, P. E.; Whited, M. T.; Grubbs, R. H. *Organometallics* **2008**, *27*, 3422.

(13) (a) Chatt, J.; Chatt Kubota, M.; Leigh, G. J.; March, F. C.; Mason, R.; Yarrow, D. J. *J. Chem. Soc., Chem. Commun.* **1974**, 1033. (b) Fachinetti, G.; Floriani, C.; Chiesi-Villa, A.; Guastini, C. *J. Am. Chem. Soc.* **1979**, *101*, 1767. (c) Pasquali, M.; Floriani, C.; Chiesi-Villa, A.; Guastini, C. *Inorg. Chem.* **1980**, *19*, 3847. (d) Thewissen, D. H. M. W.; Van Gaal, H. L. M. *J. Organomet. Chem.* **1979**, *172*, 69. (e) Gibson, J. A. E.; Cowie, M. *Organometallics* **1984**, *3*, 984.

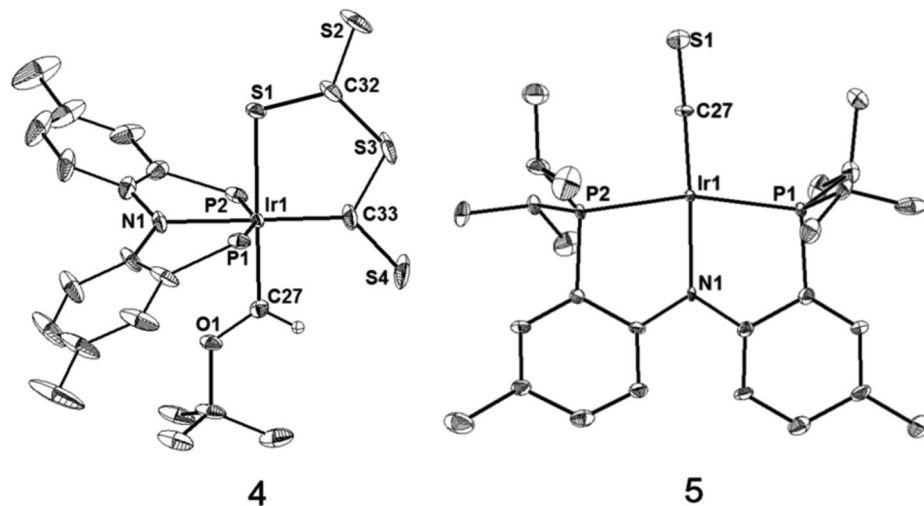


Figure 1. Displacement ellipsoid (30%) representation of complexes **4** (left) and **5** (right) with ^tPr phosphine substituents omitted from **4** for clarity. Relevant bond lengths (Å) and angles (deg), for **4**: Ir1–C27 1.960(4), Ir1–S1 2.397(1), Ir1–N1 2.119(4), Ir1–C33 1.998(5), Ir1–P1 2.350(1), Ir1–P2 2.357(1), C27–O1 1.281(5), S1–Ir1–C27 179.1(1), N1–Ir1–C33 178.5(2), P1–Ir1–P2 159.52(4). For **5**: Ir1–C27 1.82(2), Ir1–N1 2.04(1), Ir1–P1 2.298(3), Ir1–P2 2.290(3), N1–Ir1–C27 170.0(7), P1–Ir1–P2 164.2(1).

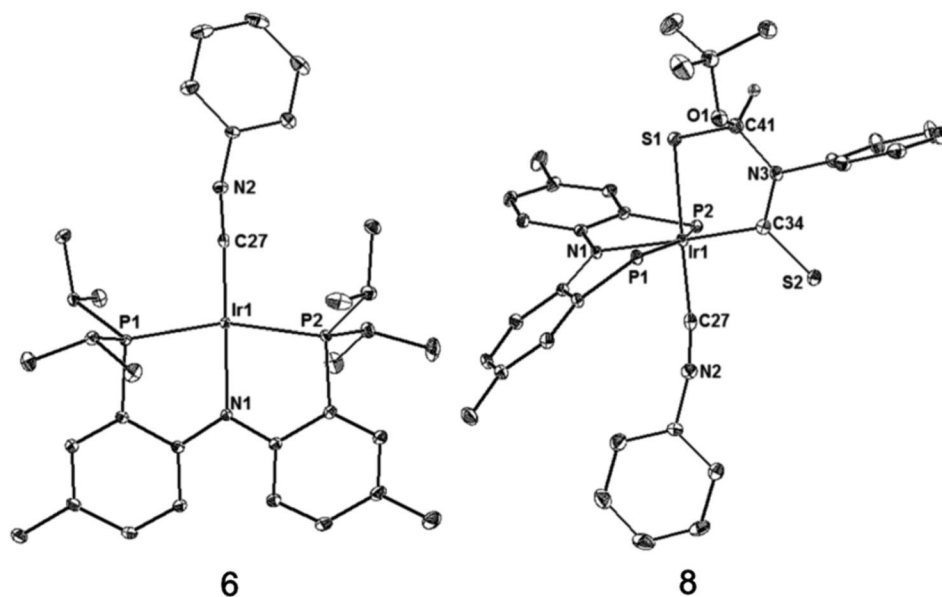


Figure 2. Displacement ellipsoid (30%) representation of complexes **6** (left) and **8** (right) with ^tPr phosphine substituents omitted from **8** for clarity. Relevant bond lengths (Å) and angles (deg), for **6**: Ir1–C27 1.852(1), Ir1–N1 2.071(9), Ir1–P1 2.2811(3), Ir1–P2 2.2877(3), C27–N2 1.197(1), N1–Ir1–C27 177.09(4), P1–Ir1–P2 162.16(1). For **8**: Ir1–C27 1.937(2), Ir1–S1 2.3648(5), Ir1–N1 2.155(2), Ir1–C34 2.049(2), Ir1–P1 2.3392(6), Ir1–P2 2.3533(6), C27–Ir1–S1 177.47(6), N1–Ir1–C34 177.42(6), P1–Ir1–P2 160.36(2).

butylthioformate as thermodynamic products (Scheme 2).¹⁴ Therefore, compound **4** can be viewed as a protected form of an intermediate species in the atom transfer reaction, supporting the view that atom and group transfers to carbene complex **1** are initiated by a nucleophilic metal rather than an electrophilic carbene ligand.^{15,16} This interpretation is also consistent with

(14) It is possible that the CS₂ adduct and dithiolactone shown in Scheme 2 are in equilibrium, but we currently have no evidence supporting this view.

(15) The reactivity of metal–ligand multiple bonds with carbon disulfide is typically initiated by nucleophilic ligands: (a) Mayr, A.; Lee, T.-Y. *Angew. Chem., Int. Ed.* **1993**, *32*, 1726. (b) Zuckerman, R. L.; Bergman, R. G. *Organometallics* **2000**, *19*, 4795.

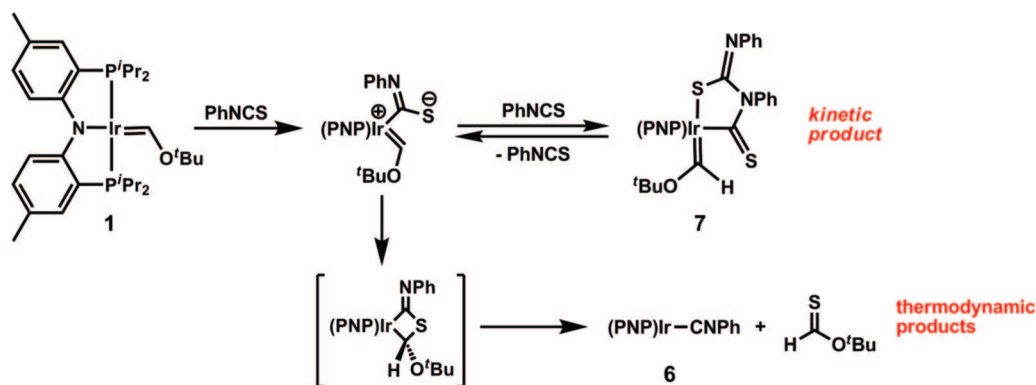
(16) The nucleophilicity of d⁸ metal complexes is well-known and has been extensively investigated: (a) Shriver, D. F. *Acc. Chem. Res.* **1970**, *3*, 231. (b) Werner, H. *Pure Appl. Chem.* **1982**, *54*, 177. (c) Pearson, R. G.; Figdore, P. E. *J. Am. Chem. Soc.* **1980**, *102*, 1541.

the observation that reductive condensations of CS₂ are generally promoted by nucleophilic, electron-rich metal centers.^{9a,e}

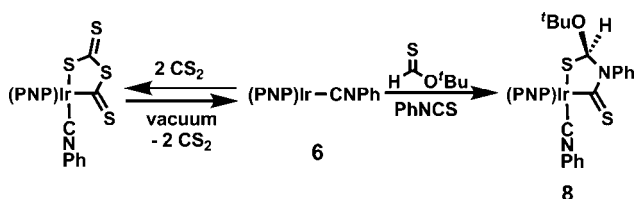
II. Reaction with Phenyl Isothiocyanate. The reactivity of **1** with isothiocyanates is considerably more complex, and depending on reaction conditions, several species were observed to form. In analogy to reaction with CS₂, slow addition of **1** resulted in quantitative sulfur-atom transfer to generate (PNP)Ir–CNPh (**6**, Figure 2) and *tert*-butyl thioformate (Scheme 3). Although metal-mediated desulfurization of isothiocyanates has been reported,^{16b,17} this process typically occurs by sulfur-atom transfer to a phosphine ligand and has not been observed for metal-bound carbenes.

(17) (a) Manuel, T. A. *Inorg. Chem.* **1964**, *3*, 1703. (b) Werner, H.; Juthani, B. *J. Organomet. Chem.* **1981**, *209*, 211.

Scheme 3. Reaction of Carbene 1 with Phenyl Isothiocyanate



Scheme 4. Nucleophilic Reactivity of Isocyanide Complex 6



In light of the reactivity observed for CS_2 , we were hopeful that exposure of **1** to an excess of PhNCS would allow the isolation of an iridium-supported PhNCS dimer similar to **4**. Addition of an excess (2–10 equiv) of PhNCS to concentrated solutions of **1** led to the formation of species **7**, for which the spectroscopic data proved nearly identical to those of CS_2 dimer **4**, particularly the distinctive shift of the carbene proton in ^1H NMR (δ 15.5 ppm). However, this apparent PhNCS dimer was observed to decompose quickly (1 h) to isocyanide complex **6**, indicating the more facile reversibility of PhNCS versus CS_2 condensation in these complexes.

In the presence of excess PhNCS and *tert*-butyl thioformate, compound **6** converts to a new, structurally unusual species **8**, in which the C_3 symmetry has been broken (Scheme 4). X-ray diffraction analysis of single crystals of **8** revealed the structural motif depicted in Figure 2, which results from the reductive condensation of PhNCS and *tert*-butyl thioformate. Based on the structure observed for complex **8** and the spectroscopic similarities between complexes **7** and **4**, we tentatively assign the connectivity of the unstable PhNCS dimer **7** as shown in Scheme 3. Although the isomeric metallacycle resulting from C–S bond formation is the more commonly observed product of isothiocyanate condensation (I in Figure 3),^{9e,13d} metallacycles such as **7**, which result from C–N bond formation, have been reported (II in Figure 3).^{13e,18}

Isocyanide complex **6** was also shown to react with large excesses of CS_2 , forming varying amounts of a species formulated as the $\text{C}_2\text{S}_4^{2-}$ adduct of the isocyanide complex analogous to CS_2 dimer **4** (observed by ^1H and ^{31}P NMR). Unlike **4**, which is stable in solution and the solid state at ambient temperature, this adduct is in equilibrium with isocya-

nide complex **6**, and application of vacuum causes quantitative regeneration of **6** (Scheme 4). Nevertheless, the analogies between the nucleophilic reactivity observed for $(\text{PNP})\text{Ir}-\text{CNPh}$ (**6**) and $(\text{PNP})\text{Ir}=\text{C}(\text{H})\text{O}^t\text{Bu}$ (**1**) highlight the isoelectronic relationship between these molecules and suggest that computational studies can illuminate the factors controlling reactivity of these types of molecules.

III. Computational Examination of $(\text{PNP})\text{Ir}-\text{L}$ Complexes. Having obtained experimental support for our proposed mechanism of nucleophilic attack by iridium to initiate atom and group transfer reactions from heterocumulenes, we turned our attention to computational methods to help elucidate the ground-state configuration of the carbene shown to effect these unusual transformations. Using the atomic coordinates determined from the crystal structure of **1**, density functional calculations were performed at the B3LYP/LACVP** level of theory. The molecular surfaces of the frontier orbitals produced by these calculations are represented in Figure 4 (HOMO–1, HOMO, and LUMO).

As predicted from simple molecular orbital considerations, the frontier orbitals represent the nonbonding $\text{Ir}(d_{z^2})$, iridium–carbene π , and iridium–carbene π^* orbitals. In contrast to the HOMO and LUMO, which are significantly delocalized over the molecule, the HOMO–1 is localized entirely on iridium, representing a prototypical d_{z^2} orbital. Based on the reactivity patterns observed previously and in this report, we propose that this high-lying, localized orbital is primarily responsible for the nucleophilic activation of heterocumulene substrates, leading to group transfer or reductive condensation.

Since $(\text{PNP})\text{Ir}=\text{C}(\text{H})\text{O}^t\text{Bu}$ (**1**), $(\text{PNP})\text{Ir}-\text{CO}$ (**3**), $(\text{PNP})\text{Ir}-\text{CS}$ (**5**), and $(\text{PNP})\text{Ir}-\text{CNPh}$ (**6**) are isoelectronic, DFT calculations were extended to this entire series of molecules.¹⁹ In fact, the gross ordering and shape of the orbitals remain constant throughout the series. However, the energies of the high-lying orbitals, particularly d_{z^2} (HOMO–1), vary across the series, reflecting to some degree the relative reactivities of the molecules.

As described above, carbene complex **1**, for which the HOMO–1 orbital is highest in energy (Table 1), forms the dimeric adduct **4** upon reaction with excess CS_2 . Isocyanide complex **6**, which possesses a d_{z^2} orbital close in energy to that calculated for **1**, reacts with CS_2 to generate the analogous dimeric adduct (Scheme 4). The carbonyl and thiocarbonyl complexes, which have significantly lower energy calculated d_{z^2} orbitals (Table 1), show no evidence for reactivity with neat

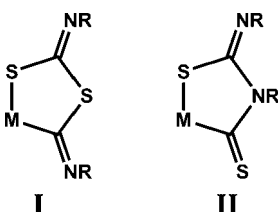


Figure 3. Common bonding motifs for isothiocyanate dimers.

(18) Itoh, K.; Matsuda, I.; Ueda, F.; Ishii, Y.; Ibers, J. A. *J. Am. Chem. Soc.* 1977, 99, 2118.

(19) Further details regarding calculations on **1**, **3**, **5**, and **6** are provided in the Supporting Information.

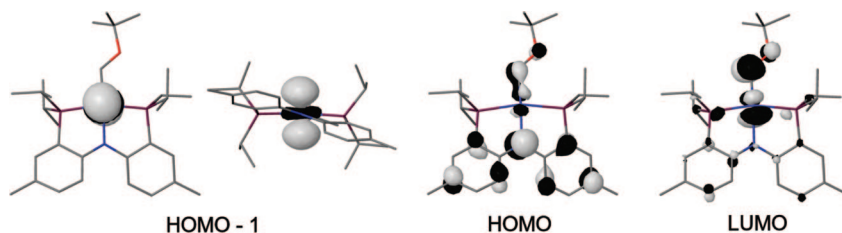


Figure 4. Molecular surfaces of frontier orbitals calculated for (PNP)Ir=C(H)O'Bu (1).

Table 1. Energies of Ir(d_z^2) Orbitals for (PNP)Ir–L Molecules

complex	energy of HOMO–1 (eV)
(PNP)Ir=C(H)O'Bu (1)	–4.62
(PNP)Ir–CNPh (6)	–4.80
(PNP)Ir–CO (3)	–4.99
(PNP)Ir–CS (5)	–5.22

CS₂ or PhNCS. Thus, as outlined in Table 1, the propensity of a (PNP)Ir–L complex to form a C₂S₄^{2–} adduct with CS₂ is correlated to the relative destabilization of the d_z^2 molecular orbital (HOMO–1), consistent with our proposed mechanism.

Conclusions

In conclusion, we have reported well-defined sulfur-atom transfer reactions from CS₂ and PhNCS to an iridium-supported Fischer carbene. These reactions represent, to the best of our knowledge, the first examples of sulfur-atom transfer from heterocumulenes across an M=C bond and appear to be facilitated by the nucleophilic character of the iridium center of complex **1**. Under suitable conditions, exposure of carbene **1** to these reagents allows observation of trapped kinetic adducts, which clearly require a metal-initiated mechanism, in contrast to the standard reactivity patterns observed for metal carbenes.² DFT calculations were performed on a series of (PNP)Ir–L molecules and highlight the importance of a high-lying, nucleophilic Ir(d_z^2) orbital in initiating this unusual heterocumulene reactivity.

Drawing from these experimental and theoretical results, we propose that complex **1** is best formulated as a nucleophilic-at-metal carbene. It is particularly beneficial to consider these findings in relation to the known reactivity of high-valent alkylidene complexes of the early metals. Schrock has reported that a tris(neopentyl)neopentylidene tantalum(V) complex reacts instantaneously with CO₂ to produce di-*tert*-butylallene and a polymeric tantalum oxide (Scheme 5)^{5a} and has proposed that this and related olefination reactions proceed by initial substrate coordination to the coordinatively unsaturated, highly electrophilic tantalum.²⁰ Subsequent group transfer releases olefin and attaches the strongly π -basic oxo ligand to the high-valent tantalum center. In contrast, we have reported that the square-planar iridium(I) carbene **1** attacks the electrophilic central

carbon of CO₂,⁴ ultimately oxygenating the carbene ligand and transferring a strongly π -acidic carbonyl to the electron-rich, d⁸ iridium center, providing a complementary reactivity pathway to the tantalum case (Scheme 5).

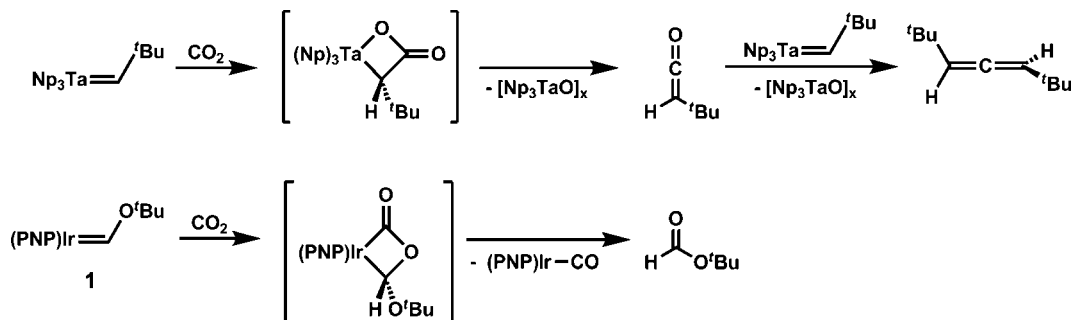
The carbene ligand of **1** ultimately acts as an electrophile in the reported reactions, consistent with the classical behavior of Fischer-type carbenes, but this only occurs after substrate activation by the electron-rich iridium center renders the heterocumulene more nucleophilic and the carbene more electrophilic. Thus, the coordinatively unsaturated nature of the carbene complex reveals a distinct pathway for the activation of multiple bonds via a metal- rather than ligand-initiated mechanism. These findings suggest that square-planar carbenes of the late transition metals may generally exhibit a strong propensity to activate electrophilic substrates toward atom and group transfer across metal–carbon multiple bonds, and the application of these types of transformations in catalytic processes is the subject of ongoing investigation.

Experimental Section

General Considerations. All manipulations were carried out using standard Schlenk or glovebox techniques under a dinitrogen atmosphere. Unless otherwise noted, solvents were deoxygenated and dried by thorough sparging with Ar gas followed by passage through an activated alumina column.²¹ (PNP)Ir=C(H)O'Bu (**1**) and (PNP)Ir–CO (**3**) were prepared according to literature procedure.⁴ Phenyl isothiocyanate was purchased from Aldrich and degassed in vacuo prior to use. Other reagents were purchased from commercial vendors and used without further purification. Elemental analyses were carried out at Desert Analytics, Tucson, AZ. NMR spectra were recorded at ambient temperature on Varian Mercury 300 and 500 MHz spectrometers. ¹H and ¹³C NMR chemical shifts were referenced to residual solvent. ³¹P NMR chemical shifts are reported relative to an external standard of 85% H₃PO₄. X-ray diffraction studies were carried out in the Beckman Institute Crystallographic Facility on a Bruker KAPPA APEX II diffractometer.

X-ray Crystallography Procedures. X-ray quality crystals were grown as indicated in the experimental procedures for each complex. The crystals were mounted on a glass fiber with Paratone-N oil. Structures were determined using direct methods with standard

Scheme 5. Contrasting CO₂ Reactivity of Schrock-Type and Nucleophilic-at-Metal Carbenes (Np = neopentyl)



Fourier techniques using the Bruker AXS software package. In some cases, Patterson maps were used in place of the direct methods procedure.

Computational Methods. Hybrid density functional theory calculations were performed for (PNP)Ir=C(H)O'Bu (**1**), (PNP)Ir-CO (**3**), (PNP)Ir-CS (**5**), and (PNP)Ir-CNPh (**6**) using the Jaguar package (version 7.5, release 110), employing the B3LYP functional and 6-31G** basis set.²² Iridium was represented with the LACVP** basis set.^{23,24} Atomic coordinates were imported from relevant single-crystal X-ray structures and subjected to geometry optimization.

Preparation of (PNP)Ir=C(H)O'Bu(C₂S₄) (4**).** To a stirring solution of (PNP)Ir=C(H)O'Bu (**1**) (50.0 mg, 0.0707 mmol) in pentane (5 mL) was added excess carbon disulfide (ca. 200 μ L), causing the immediate precipitation of a brown-orange solid. The solution was stirred for 15 min and the orange powder isolated by filtration. The powder was dissolved in a minimal amount of THF, and analytically pure red crystals of **4** were isolated by vapor diffusion of pentane into the concentrated THF solution (28.0 mg, 46%). ¹H NMR (C₆D₆): δ 15.55 (s, 1H, -C(H)O'Bu), 7.53 (dt, $J_1 = 8.4$ Hz, $J_2 = 2.4$ Hz, 2H, Ar-H), 6.73 (dd, $J_1 = 8.7$ Hz, $J_2 = 1.8$ Hz, 2H, Ar-H), 6.58 (m, 2H, Ar-H), 2.74 (m, 2H, -CH(CH₃)₂), 2.11 (s, 6H, Ar-CH₃), 2.09 (m, 2H, -CH(CH₃)₂), 1.11 (m, 12H, -CH(CH₃)₂), 0.91 (dvt, 6H, -CH(CH₃)₂), 0.77 (s, 9H, -C(CH₃)₃), 0.74 (dvt, 6H, -CH(CH₃)₂). ¹³C{¹H} NMR (CD₂Cl₂): δ 269.7 (Ir-CS₂), 266.7 (Ir-C(H)O'Bu), 236.8 (Ir-SCS₂). ³¹P{¹H} NMR (C₆D₆): δ 20.5 (s). Anal. Calcd for C₃₃H₅₀IrNOP₂S₄: C, 46.13; H, 5.87; N, 1.63. Found: C, 45.98; H, 5.81; N, 1.57.

Preparation of (PNP)Ir-CS (5**).** **Method A.** A resealable NMR tube was charged with compound **4** (24.0 mg, 0.0279 mmol) in THF (ca. 1 mL) and heated at 70 °C for 16 h, causing a slight lightening of the solution from brownish-red to pale red. NMR spectroscopy confirmed the presence of **5** as the sole component.

Method B. Compound **1** (31.1 mg, 0.0440 mmol) was dissolved in benzene (3 mL) and carbon disulfide (2.7 μ L, 0.045 mmol) added dropwise as a dilute solution in benzene (1 mL), causing a color change from purple to pale red. After 30 min, volatile components were removed in vacuo and the residues were crystallized by slow evaporation of pentane from a concentrated solution to afford brown-red crystals of analytically pure **5** (25.4 mg, 87%). ¹H NMR (C₆D₆): δ 7.58 (d, $J = 8.4$ Hz, 2H, Ar-H), 6.96 (br s, 2H, Ar-H), 6.78 (d, $J = 8.7$ Hz, 2H, Ar-H), 2.55 (m, 4H, -CH(CH₃)₂), 2.17 (s, 6H, Ar-CH₃), 1.42 (dvt, 12H, -CH(CH₃)₂), 1.15 (dvt, 12H, -CH(CH₃)₂). ¹³C{¹H} NMR (C₆D₆): δ 262.0 (Ir-CS). ³¹P{¹H} NMR (C₆D₆): δ 53.2 (s). Anal. Calcd for C₂₇H₄₀IrNP₂S: C, 48.78; H, 6.06; N, 2.11. Found: C, 48.52; H, 6.06; N, 2.03.

Preparation of (PNP)Ir-CNPh (6**).** Phenyl isothiocyanate (9.15 μ L, 0.0765 mmol) was added dropwise as a solution in benzene (1 mL) over 1 min to a stirring purple solution of compound **1** in benzene (5 mL), causing a gradual color change to red-orange over a period of 30 min. Volatiles were removed in vacuo to afford an orange powder, which was crystallized by slow evaporation of pentane from a concentrated solution to afford analytically pure **6** as orange crystals (40.0 mg, 72%). ¹H NMR (C₆D₆): δ 7.79 (d, $J = 8.7$ Hz, 2H, Ar-H), 7.33 (d, $J = 7.5$ Hz, 2H, Ar-H), 7.10–6.90 (m, 5H, Ar-H), 6.85 (d, $J = 8.1$ Hz, 2H, Ar-H), 2.38 (septet, ³J_{HH} = 3.0 Hz, -CH(CH₃)₂), 2.22 (s, 6H, Ar-CH₃), 1.35 (dvt, 12H, -CH(CH₃)₂), 1.14 (dvt, 12H, -CH(CH₃)₂). ¹³C{¹H} NMR (C₆D₆): δ 176.8 (t, ³J_{PC} = 9.3 Hz, Ir-CNPh). ³¹P{¹H} NMR (C₆D₆): δ 53.6

(s). Anal. Calcd for C₃₃H₄₅IrN₂P₂: C, 54.75; H, 6.27; N, 3.87. Found: C, 54.87; H, 6.20; N, 3.86.

Observation of Complex 7. Phenyl isothiocyanate (9.1 μ L, 0.076 mmol) was added in one portion to an NMR tube containing a solution of complex **1** (24.4 mg, 0.0345 mmol) in C₆D₆ (600 μ L), causing an immediate color change from dark purple to bright red. After 15 min, analysis of the solution by NMR revealed a mixture of complexes **7** and **1** (70:30). Spectral data for complex **7**: ¹H NMR (C₆D₆): δ 15.5 (s, 1H, Ir=C(H)O'Bu), 7.59 (d, $J = 8.4$ Hz, 2H, Ar-H), 7.53–7.35 (m, 4H, Ar-H), 7.29–7.19 (m, 4H, Ar-H), 6.81–6.63 (m, 6H, Ar-H), 3.01 (m, 2H, -CH(CH₃)₂), 2.19 (m, 2H, -CH(CH₃)₂), 2.13 (s, 6H, Ar-CH₃), 1.47–1.29 (m, 12H, -CH(CH₃)₂), 1.19 (dvt, 6H, -CH(CH₃)₂), 1.00 (dvt, 6H, -CH(CH₃)₂). ³¹P{¹H} NMR (C₆D₆): δ 18.8 (br s).

Preparation of Complex 8. Phenyl isothiocyanate (8.2 μ L, 0.069 mmol) was added dropwise as a solution in benzene (1 mL) over 1 min to a stirring purple solution of complex **1** (48.0 mg, 0.0679 mmol) in benzene (5 mL), causing a gradual color change to red-orange over a period of 30 min. After 2 h, additional phenyl isothiocyanate (ca. 100 μ L) was added as a solution in benzene (1 mL) to the stirring reaction, causing further lightening to bright orange. After 24 h, volatiles were removed in vacuo and the residues crystallized by slow evaporation of pentane from a concentrated solution to afford complex **8** as bright orange crystals (25.4 mg, 39%). ¹H NMR (C₆D₆): δ 7.68 (d, $J = 6.9$ Hz, 1H, Ar-H), 7.60 (m, 1H, Ar-H), 7.52 (m, 1H, Ar-H), 7.40 (m, 1H, Ar-H), 7.31–7.16 (m, 4H, Ar-H), 7.15–6.94 (m, 3H, Ar-H), 6.92–6.69 (m, 3H, Ar-H), 6.63 (m, 2H, Ar-H), 6.24 (s, 1H, -CH(O'Bu)), 3.96 (m, 1H, -CH(CH₃)₂), 3.45 (m, 1H, -CH(CH₃)₂), 2.67 (m, 1H, -CH(CH₃)₂), 2.48 (m, 1H, -CH(CH₃)₂), 2.18 (s, 3H, Ar-CH₃), 2.16 (s, 3H, Ar-CH₃), 1.97 (m, 3H, -CH(CH₃)₂), 1.80–1.45 (m, 9H, -CH(CH₃)₂), 1.38–0.98 (m, 12H, -CH(CH₃)₂), 0.90 (s, 9H, -C(CH₃)₃). ³¹P NMR (C₆D₆): δ 16.1 (d, ²J_{PP} = 361 Hz), 7.5 (d, ²J_{PP} = 361 Hz). Anal. Calcd for C₄₅H₆₀IrN₃OP₂S₂: C, 55.31; H, 6.19; N, 4.30. Found: C, 55.12; H, 6.15; N, 4.06.

Acknowledgment. We gratefully acknowledge the Moore Foundation (fellowship to M.T.W.) and BP (MC² program) for financial support. Larry Henling provided crystallographic assistance, and Dr. Ian Stewart aided with DFT calculations.

Supporting Information Available: Calculated surfaces and energies for frontier molecular orbitals of **1**, **3**, **5**, and **6**. Crystallographic details for complexes **4**, **5**, **6**, and **8** are provided in CIF format. This material is available free of charge via the Internet at <http://pubs.acs.org>.

OM8009766

(20) (a) The electrophilicity of the metal center in many alkylidene complexes is so pronounced that the M=C–H bond angle is contracted to allow an α -agostic interaction with the electron-deficient metal center: Schultz, A. J.; Williams, J. M.; Schrock, R. R.; Rupprecht, G. A.; Fellmann, J. A. *J. Am. Chem. Soc.* **1979**, *101*, 1593. (b) Schultz, A. J.; Brown, R. K.; Williams, J. M.; Schrock, R. R. *J. Am. Chem. Soc.* **1981**, *103*, 169. (c) Goddard, R. J.; Hoffmann, R.; Jemmis, E. D. *J. Am. Chem. Soc.* **1980**, *102*, 7667.

(21) Pangborn, A. B.; Giardello, M. A.; Grubbs, R. H.; Rosen, R. K.; Timmers, F. J. *Organometallics* **1996**, *15*, 1518.

(22) *Jaguar 7.5*; Schrodinger, LLC: New York, NY, 2008.

(23) (a) Becke, A. D. *Phys. Rev. A* **1988**, *38*, 3098. (b) Becke, A. D. *J. Chem. Phys.* **1993**, *98*, 5648. (c) Lee, C. T.; Yang, W. T.; Parr, R. G. *Phys. Rev. B* **1988**, *37*, 785. (d) Vosko, S. H.; Wilk, L.; Nusair, M. *Can. J. Phys.* **1980**, *58*, 1200.

(24) (a) Hay, P. J.; Wadt, W. R. *J. Chem. Phys.* **1985**, *82*, 270. (b) Wadt, W. R.; Hay, P. J. *J. Chem. Phys.* **1985**, *82*, 284.

Crystal Structure of TaCl(NMe₂)₄ and Its Reactions with Lithium Amides and Water. Indirect Observation of an Equilibrium among TaCl(NMe₂)₄, Ta(NMe₂)₅ and Ta₂(μ-Cl)₂(NMe₂)₆Cl₂

Shu-Jian Chen,[†] Hu Cai,^{†,‡} and Zi-Ling Xue*[†]

Department of Chemistry, University of Tennessee, Knoxville, Tennessee 37996–1600, and Department of Chemistry, Nanchang University, Nanchang 336000, China

Received April 24, 2008

Reactions of TaCl(NMe₂)₄ (**2**) with LiNR₂ (R = SiMe₃, Et), yielding Ta(NMe₂)₄(NR₂) (R = SiMe₃, **4**; Et, **7**), Ta(NMe₂)₅ (**1**), (Me₂N)₃TaN(SiMe₃)SiMe₂CH₂ (**5**), and Ta(NMe₂)₃(NEt₂)₂ (**8**), respectively, suggest the presence of an equilibrium among TaCl(NMe₂)₄ (**2**), Ta(NMe₂)₅ (**1**), and Ta₂(μ-Cl)₂(NMe₂)₆Cl₂ (**3**): $2 \mathbf{2} \rightleftharpoons \mathbf{1} + 0.5 \mathbf{3}$. New products Ta(NMe₂)₄(NR₂) have been characterized. Ta(NMe₂)₄(NEt₂) (**7**), Ta(NMe₂)₅ (**1**), and Ta(NMe₂)₃(NEt₂)₂ (**8**) are in a slow exchange: $2 \mathbf{7} \rightleftharpoons \mathbf{1} + \mathbf{8}$ with an equilibrium constant of $K_{\text{eq}} = 0.25(0.01)$ at 90 °C. The following are also reported: X-ray crystal structure and a one-step synthesis of TaCl(NMe₂)₄ (**2**), reaction of **2** with H₂O giving Ta₂(μ-Cl)₂(μ-O)(NMe₂)₆ (**9**), X-ray structure of **9**, and preparation of LiNEt₂ solid.

Introduction

Early transition metal amides are of intense interest as precursors to microelectronic materials.¹ They have been used in chemical vapor deposition (CVD) processes to make metal oxide thin films as gate insulators^{1a–d} and metal nitride (M–Si–N ternary) films as diffusion barriers.^{1e–g} Ta(NMe₂)₅ (**1**), a CVD precursor to Ta₂O₅ films,² was first reported by Bradley in 1962.³ TaCl(NMe₂)₄ (**2**), a precursor to Ta(NMe₂)₅ (**1**), was later prepared by Chisholm and co-workers using a metathesis reaction between Ta(NMe₂)₅ (**1**) and Ta₂(μ-Cl)₂(NMe₂)₆Cl₂ (**3**).⁴ Monochloride TaCl(NMe₂)₄ (**2**) is a precursor to amide, alkyl,⁴ silyl,⁵ guanidinate,⁶ and aminoxy³ derivatives. Such derivatives are often precursors to microelectronic materials or intermediates in the formation of these materials.³ The crystal structure of **2** remains unknown in large part because of its high solubility in many organic solvents.

Chisholm and co-workers reported the crystal structure of TaCl₂(NMe₂)₃ as a dimer Ta₂(μ-Cl)₂(NMe₂)₆Cl₂ (**3**).⁷ It is not clear if TaCl(NMe₂)₄ (**2**) is a monomer or dimer. In our current studies of the reactions of metal amides complexes with O₂^{3,5,8} and silanes,^{1g,9} we have prepared **2** through reaction of TaCl₅ with 4 equiv of LiNMe₂ and obtained crystals of **2** through sublimation at 85 °C. Its X-ray crystal structure revealed that it is a monomer in pseudo trigonal bipyramidal geometry with an axial Cl ligand. The reaction of TaCl(NMe₂)₄ (**2**) with LiN(SiMe₃)₂ yields Ta(NMe₂)₄[N(SiMe₃)₂] (**4**) as well as Ta(NMe₂)₅ (**1**) and (Me₂N)₃TaN(SiMe₃)SiMe₂CH₂ (**5**),¹⁰ suggesting an equilibrium among **2**, **1** and **3** (Scheme 1). **5** has been prepared from Ta₂(μ-Cl)₂(NMe₂)₆Cl₂ (**3**) and LiN(SiMe₃)₂.¹⁰ Additional studies revealed that the reaction of TaCl(NMe₂)₄ (**2**) with LiNEt₂ gave Ta(NMe₂)₄(NEt₂) (**7**), Ta(NMe₂)₅ (**1**) and Ta(NMe₂)₃(NEt₂)₂ (**8**). **7**, **1**, and **8** are involved in a slow exchange (Scheme 2). Our studies of **2** and its reactivities are reported here.

Results and Discussion

TaCl(NMe₂)₄ (**2**) had been prepared earlier from TaCl₅ in three steps.⁴ In the current work, it was prepared in one step in 66% yield from the reaction of TaCl₅ with 4 equiv of LiNMe₂. Our earlier, repeated attempts to grow crystals of **2** from its solution failed, either because of its high solubility in most solvents or because of the noncrystalline nature of its solid obtained from the solvents. Pale-yellow crystals of **2** were later obtained on a coldfinger during the sublimation of **2** at 85 °C from the reaction between TaCl₅ and 4 equiv of LiNMe₂. The

* To whom correspondence should be addressed. E-mail: xue@ion.chem.utk.edu.

[†] University of Tennessee.

[‡] Nanchang University.

(1) (a) Wallace, R. M.; Wilk, G. D. *Crit. Rev. Solid State Mater. Sci.* **2003**, *28*, 231. (b) Smith, R. C.; Ma, T.; Hoilien, N.; Tsung, L. Y.; Bevan, M. J.; Colombo, L.; Roberts, J.; Campbell, S. A.; Gladfelter, W. L. *Adv. Mater. Opt. Electron.* **2000**, *10*, 105. (c) Hendrix, B. C.; Borovik, A. S.; Xu, C.; Roeder, J. F.; Baum, T. H.; Bevan, M. J.; Visokay, M. R.; Chambers, J. J.; Rotondaro, A. L. P.; Bu, H.; Colombo, L. *Appl. Phys. Lett.* **2002**, *80*, 2362. (d) Son, K.-A.; Mao, A. Y.; Sun, Y.-M.; Kim, B. Y.; Liu, F.; Kamath, A.; White, J. M.; Kwong, D. L.; Roberts, D. A.; Vrtis, R. N. *Appl. Phys. Lett.* **1998**, *72*, 1187. (e) Raaijmakers, I. J. *Thin Solid Films* **1994**, *247*, 85. (f) Custer, J. S.; Smith, P. M.; Fleming, J. G.; Roherty-Osmun, E. *Inorganic Materials Synthesis*; Winter, C. H., Hoffman, D. M., Eds.; ACS Symposium Series; American Chemical Society: Washington, D.C., 1999; Vol. 727, p 86. (g) Liu, X.-Z.; Wu, Z.-Z.; Cai, H.; Yang, Y.-H.; Chen, T.-N.; Vallet, C. E.; Zuhf, R. A.; Beach, D. B.; Peng, Z.-H.; Wu, Y.-D.; Concolino, T. E.; Rheingold, A. L.; Xue, Z.-L. *J. Am. Chem. Soc.* **2001**, *123*, 8011.

(2) Chen, S.-J.; Zhang, X.-H.; Yu, X.; Qiu, H.; Yap, G. P. A.; Guzei, I. A.; Lin, Z.; Wu, Y.-D.; Xue, Z.-L. *J. Am. Chem. Soc.* **2007**, *129*, 14408.

(3) Bradley, D. C.; Thomas, I. M. *Can. J. Chem.* **1962**, *40*, 1355.

(4) Chisholm, M. H.; Tan, L.-S.; Huffman, J. C. *J. Am. Chem. Soc.* **1982**, *104*, 4879.

(5) Wu, Z.; Cai, H.; Yu, X.; Blanton, J. R.; Diminnie, J. B.; Pan, H.-J.; Xue, Z. *Organometallics* **2002**, *21*, 3973.

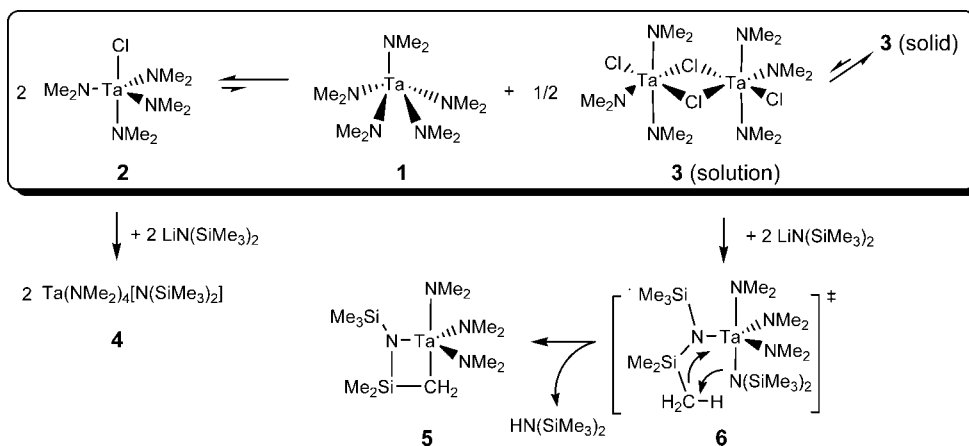
(6) Tin, M. K. T.; Thirupathi, N.; Yap, G. P. A.; Richeson, D. S. *J. Chem. Soc., Dalton Trans.* **1999**, 2947.

(7) Chisholm, M. H.; Huffman, J. C.; Tan, L.-S. *Inorg. Chem.* **1981**, *20*, 1859.

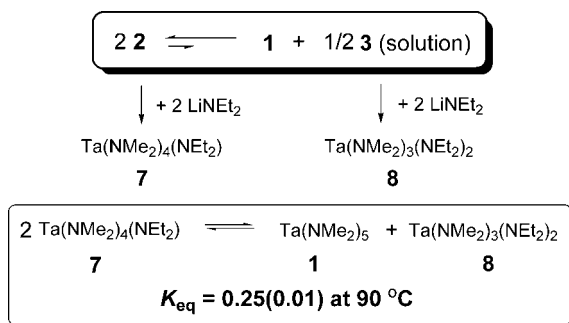
(8) Wang, R.-T.; Zhang, X.-H.; Chen, S.-J.; Yu, X.-H.; Wang, C.-S.; Beach, D. B.; Wu, Y.-D.; Xue, Z.-L. *J. Am. Chem. Soc.* **2005**, *127*, 5204.

(9) (a) Liu, X.-Z.; Wu, Z.-Z.; Peng, Z.-H.; Wu, Y.-D.; Xue, Z.-L. *J. Am. Chem. Soc.* **1999**, *121*, 5350. (b) Cai, H.; Chen, T.-N.; Wang, X.-P.; Schultz, A. J.; Koetzle, T. F.; Xue, Z.-L. *Chem. Comm.* **2002**, 230.

(10) Cai, H.; Yu, X.; Chen, T.; Chen, X.-T.; You, X.-Z.; Xue, Z. *Can. J. Chem.* **2003**, *81*, 1398.

Scheme 1. Equilibria among **2**, **1**, **3** (Solution), and **3** (Solid) as Well as Reaction of **2** with LiN(SiMe₃)₂ To Give **4**, **1**, and **5**

Scheme 2



crystals were carefully removed from the coldfinger, and one was cut into a suitable size for X-ray diffraction. The crystals of **2** were very sensitive to air, decomposing readily in paratone oil which was used to coat crystals for protection.

Crystal structure of Ta₂(μ-Cl)₂(NMe₂)₆Cl₂ (**3**),⁷ reported by Chrisolm and co-workers, displays a dimer, where two chlorides bridge two Ta atoms to give a four-member ring with two other chlorides and all amides as terminal ligands. In comparison, crystal structure of **2** reveals a monomer (Figure 1) as a distorted trigonal bipyramid. This suggests monomer is more thermally and sterically stable for the monochloride **2**. It should be noted that Ta(NMe₂)₅ (**1**) and Ta(NEt₂)₅ adopt a distorted square pyramidal and trigonal bipyramidal structure, respectively.¹¹ The chloride in TaCl(NMe₂)₄ (**2**) takes the axial position with a Ta–Cl bond length of 2.5077(13) Å, slightly

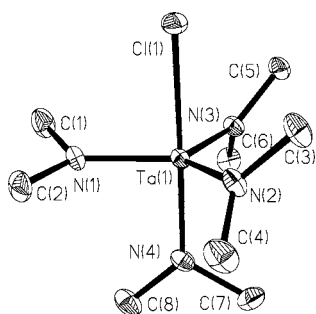


Figure 1. Crystal structure of TaCl(NMe₂)₄ (**2**). Selected bond lengths (Å) and angles (deg): Ta(1)–N(1) 1.951(4), Ta(1)–N(2) 1.974(4), Ta(1)–N(3) 1.988(3), Ta(1)–N(4) 2.008(4), Ta(1)–Cl(1) 2.5077(13), N(1)–Ta(1)–N(2) 122.05(17), N(1)–Ta(1)–N(3) 118.09(17), N(2)–Ta(1)–N(3) 119.46(14), N(1)–Ta(1)–N(4) 90.38(16), N(2)–Ta(1)–N(4) 92.14(18), N(3)–Ta(1)–N(4) 93.87(15), N(1)–Ta(1)–Cl(1) 88.58(11), N(2)–Ta(1)–Cl(1) 87.99(13), N(3)–Ta(1)–Cl(1) 87.06(11), N(4)–Ta(1)–Cl(1) 178.85(11).

longer than those of the axial Ta–Cl bond [2.454(4) Å] in (Me₂N)₃Ta(SiPh₂Bu^t)Cl⁵ and the terminal Ta–Cl bond in **3** [2.463(1) Å].⁷ In **2**, the axial Ta(1)–N(4) bond [2.008(4) Å] is longer than equatorial Ta–N bonds [1.974(4)–1.988(3) Å]. Such a difference was also observed in the structures of (Me₂N)₃Ta(SiPh₂Bu^t)Cl and (Me₂N)₃Ta[Si(SiMe₃)₃]Cl/(Me₂N)₃Ta[Si(SiMe₃)₃]Br.⁵ These Ta–N bond lengths are similar to those [1.965(5)–2.038(8) Å] in Ta(NMe₂)₅ (**1**).¹¹ The Cl(1)–Ta(1)–N(4) angle of 178.85(11)° shows that the two axial ligands are nearly linear. The angles of the axial chloride to equatorial N atoms are 87.06(11)–88.58(11)°, smaller than those of the axial N(4) to the N atoms [90.38(16)–93.87(15)°], probably as a result of the repulsion by bulkier axial -NMe₂ ligand.

Direct reaction of Ta(NMe₂)₅ with Me₃SiCl gave Ta₂(μ-Cl)₂(NMe₂)₆Cl₂ (**3**), rather than TaCl(NMe₂)₄ (**1**), because of the facile ligand redistribution and the lower solubility of **3**.⁷ Our studies further reveal that there is an equilibrium among TaCl(NMe₂)₄ (**2**), Ta(NMe₂)₅ (**1**), and Ta₂(μ-Cl)₂(NMe₂)₆Cl₂ (**3**) in toluene-*d*₈. In ¹H NMR at 23 °C, the equilibrium 2 **2** ⇌ **1** + 0.5 **3** is not directly observed.¹² Although **3** is not observed, its presence is inferred from the formation of **5** (Scheme 1) and HN(SiMe₃)₂, when LiN(SiMe₃)₂ is added to **2**. Reaction of **3** with LiN(SiMe₃)₂ is known to give **5** and HN(SiMe₃)₂, with Ta(NMe₂)₃[N(SiMe₃)₂]Cl as an intermediate.¹⁰ Other products from the reaction between TaCl(NMe₂)₄ (**2**) and LiN(SiMe₃)₂ at 23 °C are Ta(NMe₂)₄[N(SiMe₃)₂] (**4**), Ta(NMe₂)₅ (**1**) with a molar ratio of **4**: **1**: **5**: HN(SiMe₃)₂ ≈ 5: 1: 1: 1.

The observation that significant amounts of both **1** and **5** are yielded in the reaction of **2** with LiN(SiMe₃)₂ suggests that the reaction of **3** with LiN(SiMe₃)₂ is faster than that of **2** with LiN(SiMe₃)₂, thus shifting the equilibrium to the formation of **1** and **3**. In other words, although the concentration of **3** is below the ¹H NMR detection limit, its fast reaction with LiN(SiMe₃)₂ eventually increases concentrations of **1**, **5** and HN(SiMe₃)₂ to 20% of that of **4** at the end of the reaction. The indirect observation of the equilibrium 2 **2** ⇌ **1** + 0.5 **3** here is unusual.

(11) (a) Ta(NMe₂)₅ (**1**): Batsanov, A. S.; Churakov, A. V.; Howard, J. A. K.; Hughes, A. K.; Johnson, A. L.; Kingsley, A. J.; Neretin, I. S.; Wade, K. *J. Chem. Soc., Dalton Trans.* **1999**, 3867. (b) Ta(NEt₂)₅: Davies, H. O.; Jones, A. C.; McKinnell, E. A.; Raftery, J.; Muryn, C. A.; Afzaal, M.; O'Brien, P. *J. Mater. Chem.* **2006**, *16*, 2226.

(12) (a) Both ¹H and ¹³C -NMe₂ peaks of Ta(NMe₂)₅ (**1**) and TaCl(NMe₂)₄ (**2**) overlap in toluene-*d*₈. The presence of **1** in the equilibrium mixture could not be independently confirmed. (b) A small amount of Ta₂(μ-Cl)₂(μ-O)(NMe₂)₆ (**9**) is often present in the equilibrium mixture, and its -NMe₂ peak in ¹H NMR at 3.57 ppm is close to that of Ta₂(μ-Cl)₂(NMe₂)₆Cl₂ (**3**) at 3.56 ppm in toluene-*d*₈.

Reverse reaction in the equilibrium $2 \rightleftharpoons 1 + 0.5 \mathbf{3}$ (Scheme 1) was also observed. Mixing Ta(NMe₂)₅ (**1**) and 0.5 equiv of Ta₂(μ-Cl)₂(NMe₂)₆Cl₂ (**3**) in toluene-*d*₈ at 23 °C led to the formation of **2**, although the low solubility (1.5 mg/mL estimated by ¹H NMR) and slow dissolution of **3** in toluene-*d*₈ [**3** (solution) \rightleftharpoons **3** (solid), Scheme 1] at 23 °C make the formation of **2** slow. Heating the solution to 80 °C increases the solubility of **3** and makes the formation of TaCl(NMe₂)₄ (**2**) faster. After the formation of **2**, the solution showed no detectable amount of Ta₂(μ-Cl)₂(NMe₂)₆Cl₂ (**3**) by ¹H NMR,¹² indicating the equilibrium $2 \rightleftharpoons 1 + 0.5 \mathbf{3}$ (Scheme 1) is shifted exclusively to the left at 23 °C.

Ta(NMe₂)₄[N(SiMe₃)₂] (**4**) does not convert to **1** and (Me₂N)₃TaN(SiMe₃)SiMe₂CH₂ (**5**) in toluene-*d*₈ at 23 °C for a few days. Heating the solution at 86 °C for 24 h led to the decomposition of **4** to unknown species. The result rules out a pathway in which **4** is yielded initially in the reaction of TaCl(NMe₂)₄ (**2**) with LiN(SiMe₃)₂, and then it converts to **1** and **5**.

Reactions of TaCl(NMe₂)₄ (**2**) with LiN(SiMe₃)₂ was found to be complete in 4 h at 10 °C and in 2.5 h at 15 °C, respectively. Slow formation of **1** and **5** was observed in the process. Ta₂(μ-Cl)₂(NMe₂)₆Cl₂ (**3**) was not, however, detected during monitoring of the reaction, suggesting that the equilibrium $2 \rightleftharpoons 1 + 0.5 \mathbf{3}$ (Scheme 1) is shifted exclusively to the left. Reaction of **3** with LiN(SiMe₃)₂ further decreases the likeliness of the observation of **3** in the reaction.

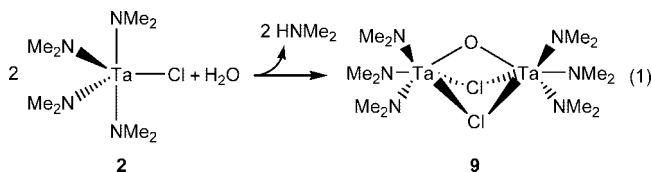
Reaction of TaCl(NMe₂)₄ (**2**) with 1 equiv of LiNEt₂ was also investigated. This reaction at 23 °C was found to yield Ta(NMe₂)₄(NEt₂) (**7**) as well as Ta(NMe₂)₃(NEt₂)₂ (**8**) and Ta(NMe₂)₅ (**1**) in a molar ratio of about 2.8:1:1 (Scheme 2). Ta(NMe₂)₃(NEt₂)₂ (**8**) has been reported earlier in a patent by Chen and co-workers.¹³ Ta(NMe₂)₄(NEt₂) (**7**) is a new product, and it was characterized by ¹H and ¹³C NMR and elemental analysis. **7** is a pale-yellow solid at 23 °C. One set of peaks were observed for both -NMe₂ and -NEt₂ ligands in ¹H and ¹³C NMR spectra. The structure of **7** is not clear. If it is trigonal bipyramidal, the NMR observations suggest there is perhaps a fast exchange of the axial and equatorial ligands in **7**.

We also found that there is an exchange among **7**, **1** and **8**: $2 \mathbf{7} \rightleftharpoons \mathbf{1} + \mathbf{8}$ (Scheme 2).

Two tests were conducted. In the first test, **1** was added to a mixture of **7** and **8** in toluene-*d*₈ at 23 °C, and peaks of **7** slowly grew up while peaks of **1** and **8** dropped. In the absence of **1**, no change was observed of a mixture of **7** and **8** in toluene-*d*₈ at 23 °C for 9 days. In a second test, a solution of Ta(NMe₂)₄(NEt₂) (**7**) in toluene-*d*₈ was monitored and found to yield Ta(NMe₂)₃(NEt₂)₂ (**8**) and Ta(NMe₂)₅ (**1**). The exchange $2 \mathbf{7} \rightleftharpoons \mathbf{1} + \mathbf{8}$ (Scheme 2) at 90 °C is faster, but it still took 4–5 days to reach an equilibrium with $K_{\text{eq}} = 0.25(0.01)$ at 90 °C. Given that the exchange of the products $2 \mathbf{7} \rightleftharpoons \mathbf{1} + \mathbf{8}$ (Scheme 2) is very slow, it is unlikely that this exchange would change the ratio of the three products (**7**: **1**: **8** = 2.8: 1: 1) from the reaction of TaCl(NMe₂)₄ (**2**) with 1 equiv of LiNEt₂. In other

words, the exchange of the starting materials $2 \rightleftharpoons 1 + 0.5 \mathbf{3}$ led to the observation of the three products **7**, **1** and **8** in this reaction.

The new complex Ta(NMe₂)₄[N(SiMe₃)₂] (**4**) was characterized by ¹H and ¹³C NMR and elemental analysis. Repeated attempts to obtain the crystal structure of **4** were not successful. Crystal-like solids gave poor reflections on an X-ray diffractometer.



Complex TaCl(NMe₂)₄ (**2**) in THF was found to react with

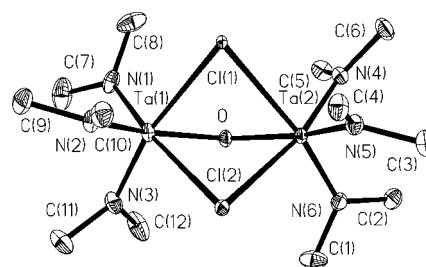
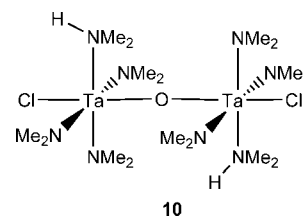


Figure 2. Crystal structure of Ta₂(μ-Cl)₂(μ-O)(NMe₂)₆ (**9**). Selected bond lengths (Å) and angles (deg): Cl(1)–Ta(1) 2.7571(15), Cl(1)–Ta(2) 2.8214(15), Cl(2)–Ta(2) 2.7128(17), Cl(2)–Ta(1) 2.7618(16), N(1)–Ta(1) 1.965(7), N(2)–Ta(1) 1.995(7), N(3)–Ta(1) 1.943(7), N(4)–Ta(2) 1.951(7), N(5)–Ta(2) 1.993(7), N(6)–Ta(2) 1.961(7), O–Ta(1) 1.931(5), O–Ta(2) 1.936(5), Ta(1)–Cl(1)–Ta(2) 73.92(4), Ta(2)–Cl(2)–Ta(1) 75.57(4), Ta(1)–O–Ta(2) 120.3(3), O–Ta(1)–Cl(1) 74.04(16), O–Ta(1)–Cl(2) 72.96(16).

H₂O (0.5 equiv in THF), yielding Ta₂(μ-Cl)₂(μ-O)(NMe₂)₆ (**9**) and HNMe₂ (eq 1). One -NMe₂ ligand in **2** was removed as HNMe₂ in the reaction, followed by dimerization to give **9**. The X-ray structure of **9** in Figure 2 reveals that, of the two bridging Ta–Cl–Ta bonds, Cl(1)–Ta(1) bond length [2.7571(15) Å] is smaller than that of the Cl(1)–Ta(2) bond [2.8214(15) Å]. However, both bridging Ta–Cl bond lengths [2.7128(17)–2.8214(15) Å] in **9** are longer than that of the terminal Ta–Cl bond [2.5077(13) Å]. The difference here is similar to those in Ta₂(μ-Cl)₂(NMe₂)₆Cl₂ (**3**)⁷ and Cl(Me₂N)₂Zr(μ-Cl)₂(μ-NMe₂)Zr(NMe₂)₂(THF).¹⁴ In **3**, the bridging Ta–Cl bonds [2.586(1) and 2.635(2) Å] are longer than that of the terminal Ta–Cl bond [2.463(1) Å].⁷ The bridging Zr–Cl bond lengths of 2.6130(12)–2.7214(12) Å in the Zr complex¹⁴ are also longer than that of the terminal Zr–Cl bond [2.4409(12) Å]. The Ta(1)–O–Ta(2) bond angle [120.3(3)°] is much larger than two Ta(1)–Cl–Ta(2) bond angles [73.92(4) and 75.57(4)°] in **9**.



Chisholm and co-workers have also reported a Ta dimeric complex Ta₂(μ-O)Cl₂(NMe₂)₆(HNMe₂)₂ (**10**) containing a single bridging oxo ligand.⁷ It is interesting to compare **9** with **10**. Complex **9** is a derivative of **10** without the HNMe₂ ligand.

(13) Chen, T.; Xu, C.; Baum, T. H. U.S. Patent 2005079290,2005, "Tantalum amide complexes for depositing tantalum-containing films, and method of making same." Preparation, NMR chemical shifts, and elemental analysis of Ta(NMe₂)₃(NEt₂)₂ (**8**) were given.

(14) Wu, Z.-Z.; Diminnie, J. B.; Xue, Z.-L. *Inorg. Chem.* **1998**, *37*, 2570.

(15) (a) Sheldrick, G. M. *SADABS, A Program for Empirical Absorption Correction of Area Detector Data*; University of Göttingen: Göttingen, Germany, 2000. (b) Sheldrick, G. M. *SHELXL-97, A Program for the Refinement of Crystal Structures*; University of Göttingen: Göttingen, Germany, 1997.

The Ta atoms in **10** adopt an octahedron coordination sphere using terminal chloride and HNMe₂ as ligands. Loss of lone pair electrons in HNMe₂ in **9** leads to the formation of the two bridging chloride ligands so that their lone pair electrons could be used to remediate electron deficiency in **9**. The Ta–O bond length of 1.928(6) Å in **10** is nearly identical to those [1.931(5) and 1.936(5) Å] in **9**. The Ta–O–Ta bond [174.3(3)°] in **10** is nearly linear, while that [120.3(3)°] in Ta₂(μ-Cl)₂(μ-O)(NMe₂)₆ (**9**) is, however, much smaller. The two Ta atoms in **9** are closer [Ta(1)-to-Ta(2) distance: 3.3545 Å] than those in, e.g., Ta₂(μ-Cl)₂(NMe₂)₆Cl₂ (**3**) [Ta(1)-to-Ta(2) distance: 4.1 Å]⁷ probably to accommodate one oxo and two bridging ligands. In addition to the smaller Ta–O–Ta bond angle in **9** (than in **10**), the Ta–Cl–Ta [73.92(4) and 75.57(4)°] bond angles in **9** are also much smaller than that [103.7(0)°] in Ta₂(μ-Cl)₂(NMe₂)₆Cl₂ (**3**).⁷ The Ta–N bond lengths [1.943(7)–1.995(7) Å] are close to those in, e.g., TaCl(NMe₂)₄ (**2**) [1.951(4) to 2.008(4) Å].

Experimental Section

General Procedures. All manipulations were carried out under a dry and oxygen-free nitrogen atmosphere with the use of glovebox or Schlenk techniques. All solvents were purified by distillation from potassium/benzophenone ketyl. Benzene-*d*₆ and toluene-*d*₈ were dried and stored over activated molecular sieves under nitrogen. TaCl₅ (Strem), LiNMe₂ (Aldrich), and LiN(SiMe₃)₂ (Aldrich) were used as received. ¹H and ¹³C NMR spectra were recorded on a Bruker AMX-400 Fourier transform spectrometer. Elemental analysis was conducted by Complete Analysis Laboratories, Inc., Parsippany, NJ.

Synthesis of LiNEt₂. HNEt₂ was dried over NaOH pellets at 23 °C for 24 h and then distilled at 72 °C under nitrogen. HNEt₂ (12.590 g, 0.172 mmol) in hexanes (30 mL) at 0 °C was treated with 1 equiv of *n*-BuLi (0.173 mmol, 108.0 mL, 1.6 M in hexane) over a period of 1 h. The mixture was stirred at 23 °C for additional 2.5 h. Volatiles were removed in vacuo to give white powders of LiNEt₂ (12.920 g, 0.163 mmol, 95% yield).

Synthesis of TaCl(NMe₂)₄ (2**).** Hexanes (100 mL) were added to a solid mixture of TaCl₅ (7.660 g, 21.38 mmol) and LiNMe₂ (4.363 g, 85.52 mmol) at –40 °C with vigorous stirring. The mixture was slowly warmed to 23 °C, and the solution was then refluxed at 72 °C for 22 h. The deep brown solution was filtered, and the residue was extracted with hexanes for 3 times (3 × 60 mL). Volatiles were removed from the filtrate in vacuo, and subsequent sublimation at 85 °C yielded 5.567 g (14.18 mmol, 66%) of yellow crystalline TaCl(NMe₂)₄ (**2**). ¹H NMR of **2** (benzene-*d*₆, 399.88 MHz, 23 °C) δ 3.24 (s, 24H, NMe₂). ¹³C NMR (benzene-*d*₆, 100.55 MHz, 23 °C) δ 45.93 (s, NMe₂). The crystals were used directly in the subsequent X-ray diffraction to be discussed below.

Synthesis of Ta(NMe₂)₄[N(SiMe₃)₂] (4**).** Toluene (20 mL) was added to a solid mixture of TaCl(NMe₂)₄ (**2**, 0.684 g, 1.74 mmol) and LiN(SiMe₃)₂ (0.291 g, 1.74 mmol) at –78 °C with vigorous stirring. The mixture was slowly warmed to 23 °C and stirred for 15 h. Volatiles were removed from the mixture in vacuo, and the residue was extracted with *n*-pentane. Filtration and crystallization yielded a pale-yellow solid of **4** (0.423 g, 0.817 mmol, 47% yield) at –32 °C. ¹H NMR of **4** (benzene-*d*₆, 399.79 MHz, 23 °C) δ 3.26 (s, 24H, NMe₂), 0.33 (s, 18H, SiMe₃). ¹³C NMR (benzene-*d*₆, 100.54 MHz, 23 °C) δ 48.28 (s, NMe₂), 5.17 (s, SiMe₃). Anal. calcd for C₁₄H₄₂N₅Si₂Ta: C, 32.48; H, 8.18. Found: C, 32.41; H, 8.13.

Synthesis of Ta(NMe₂)₄(NEt₂) (7**).** To TaCl(NMe₂)₄ (**2**, 2.330 g, 5.932 mmol) in *n*-pentane (15 mL) at 0 °C was added slowly 1 equiv of LiNEt₂ (0.460 g, 5.932 mmol) in Et₂O (15 mL). The solution was then stirred at 0–13 °C for 2 h. The solution was settled and filtered. Volatiles were removed from the filtrate in vacuo and *n*-pentane was added to the residue. The solution was concentrated and then put in a freezer (–32 °C) for crystallization.

A pale-yellow solid (0.700 g, 1.630 mmol, 27.5%) of Ta(NMe₂)₄(NEt₂) (**7**) was isolated in one day. ¹H NMR (benzene-*d*₆, 399.79 MHz, 23 °C) δ 3.49 (q, 4H, NCH₂CH₃), 3.28 (s, 24H, NCH₃), 1.12 (t, 6H, NCH₂CH₃). ¹³C NMR (benzene-*d*₆, 100.53 MHz, 23 °C) δ 47.57 (s, NCH₂CH₃), 46.60 (s, NCH₃), 17.01 (s, NCH₂CH₃). Anal. calcd for C₁₂H₃₄N₅Ta: C, 33.57; H, 7.98. Found: C 33.36, H 7.84.

Heating of Ta(NMe₂)₄[N(SiMe₃)₂] (4**) at 86 °C.** The solution of Ta(NMe₂)₄[N(SiMe₃)₂] (**4**) (16.7 mg, 0.0323 mmol) and bibenzyl (internal standard, 11.3 mg, 0.0620 mmol) in toluene (0.46 mL) in a Young tube was heated at 86 °C for 50 h. ¹H NMR spectrum of the solution revealed that **4** had decomposed to unknown species.

Indirect Observation of the Equilibrium among TaCl(NMe₂)₄ (2**), Ta(NMe₂)₅ (**1**), and Ta₂(μ-Cl)₂(NMe₂)₆Cl₂ (**3**).** TaCl(NMe₂)₄ (**2**, 35.7 mg, 0.0914 mmol), LiN(SiMe₃)₂ (15.3 mg, 0.0914 mmol), and bibenzyl (internal standard, 15.9 mg, 0.0872 mmol) were dissolved in toluene-*d*₈ in a Young tube. The reaction yielded Ta(NMe₂)₄[N(SiMe₃)₂] (**4**, 0.0592 mmol, 65% yield), Ta(NMe₂)₅ (**1**, 0.0123 mmol, 13% yield), **6** (0.0113 mmol, 12% yield), and HN(SiMe₃)₂ (0.0115 mmol, 13% yield), suggesting that there is an equilibrium as shown in Scheme 1.

Reaction of TaCl(NMe₂)₄ (2**) with 1 equiv of LiN(SiMe₃)₂ at 10 and 15 °C. Reaction at 10 °C.** LiN(SiMe₃)₂ (12.7 mg, 0.0760 mmol) and bibenzyl (internal standard, 20.4 mg, 0.112 mmol) were dissolved in toluene-*d*₈ in a Young tube and the solution was cooled to –78 °C. TaCl(NMe₂)₄ (**2**, 29.7 mg, 0.0760 mmol) was added at –78 °C, and the solution was then warmed to 10 °C. ¹H NMR was used to follow the reaction, and it revealed that the reaction was completed in 4 h.

Reaction at 15 °C. LiN(SiMe₃)₂ (12.7 mg, 0.0760 mmol) and bibenzyl (internal standard, 13.3 mg, 0.0729 mmol) were dissolved in toluene-*d*₈ in a Young tube and the solution was cooled to –78 °C. TaCl(NMe₂)₄ (**2**, 29.7 mg, 0.0760 mmol) was added at –78 °C, and the solution was then warmed to 15 °C. ¹H NMR was used to follow the reaction, and it revealed that the reaction was completed in 2.5 h.

The reaction at both 10 and 15 °C gave the same products Ta(NMe₂)₄[N(SiMe₃)₂] (**4**), Ta(NMe₂)₅ (**1**), **5**, and HN(SiMe₃)₂ in ratios of 4:1:1:1 and 3:1:1:1, respectively.

Reaction of TaCl(NMe₂)₄ (2**) with 1 equiv of LiNEt₂.** TaCl(NMe₂)₄ (**2**, 53.4 mg, 0.137 mmol) and LiNEt₂ (10.8 mg, 0.137 mmol) were mixed in benzene-*d*₆ (0.46 mL) in a Young tube and the solution was shaken for 10 min. The reaction yielded Ta(NMe₂)₄(NEt₂) (**7**), Ta(NMe₂)₃(NEt₂)₂ (**8**), and Ta(NMe₂)₅ (**1**) in a molar ratio 2.8:1:1.

Exchange of Ta(NMe₂)₄(NEt₂) (7**), Ta(NMe₂)₃(NEt₂)₂ (**8**), and Ta(NMe₂)₅ (**1**). Exchange at 23 °C.** Ta(NMe₂)₅ (**1**, 22.3 mg, 0.0556 mmol) was added to a mixture of Ta(NMe₂)₄(NEt₂) (**7**) and Ta(NMe₂)₃(NEt₂)₂ (**8**, total 19.3 mg; 26 mol% **7** and 74 mol% **8**) and bibenzyl (internal standard, 10.6 mg, 0.0576 mmol) in toluene-*d*₈ (0.46 mL). The solution was kept at 23 °C for over 160 h. ¹H NMR revealed that the peaks of **7** slowly grew up. A similar slow exchange was observed with a solution of **1** (8.7 mg, 0.0218 mmol), **7** and **8** (total 18.8 mg; 29 mol% **7** and 71 mol% **8**) and bibenzyl (internal standard, 10.3 mg, 0.0565 mmol) in toluene-*d*₈ (0.46 mL).

Exchange at 90 °C. A solution of **1** (9.1 mg, 0.0227 mmol), **7** and **8** (total 18.8 mg; 29 mol% **7** and 71 mol% **8**) and bibenzyl (internal standard, 10.0 mg, 0.0549 mmol) in toluene-*d*₈ (0.46 mL) was initially heated at 60 °C and then at 90 °C. The solution was monitored by ¹H NMR at 23 °C. The heating at 90 °C lasted about 4–5 days until no change in concentrations of the three complexes was observed. Since the exchange at 23 °C was very slow and the time needed for a ¹H NMR spectrum was short (about 10 min), cooling the solution to 23 °C for 10 min essentially “quenched” the exchange. In a second test, a solution of Ta(NMe₂)₄(NEt₂) (**7**, 12.3 mg, 0.0287 mmol) and bibenzyl (internal standard, 10.1 mg, 0.0554 mmol) in toluene-*d*₈ was heated at 90 °C. The solution was

periodically cooled to 23 °C to take ¹H NMR spectra. The heating was found to yield Ta(NMe₂)₃(NEt₂)₂ (**8**) and Ta(NMe₂)₅ (**1**) over a period of 4–5 days to reach an equilibrium.

When a mixture (19.9 mg total) of **7**, **8** and bibenzyl (internal standard, 10.5 mg, 0.0576 mmol) in toluene-*d*₈ (0.46 mL) was kept at 23 °C for 9 days, no change was observed.

Reactions of TaCl(NMe₂)₄ with H₂O. Ta₂(μ-Cl)₂(μ-O)(NMe₂)₆ (**9**) has been isolated from the reaction of TaCl(NMe₂)₄ (**2**) with 1 equiv of H₂O. To TaCl(NMe₂)₄ (**2**, 1.000 g, 2.546 mmol) in THF (10 mL) with vigorous stirring at –30 °C was added slowly 1 equiv of H₂O (46.0 μL) in 5 mL of THF. After temperature was raised to 23 °C, solution was stirred for additional 1 h. Volatiles were removed under reduced pressure and pale yellow residue was extracted with hexanes. Filtrate was concentrated for crystallization at –32 °C. Yellow crystals of **9** (0.463 g, 0.649 mmol, 51% yield) were collected in a few days. ¹H NMR of **9** (benzene-*d*₆, 399.87 MHz, 23 °C) δ 3.57 (s, 36H, 6NMe₂). ¹³C NMR (benzene-*d*₆, 100.56 MHz, 23 °C) δ 47.36 (s, 6NMe₂). Anal. calcd for C₁₂H₃₆N₆OCl₂Ta₂: C, 20.21; H, 5.09. Found: C, 20.14; H, 5.07.

Determination of X-Ray Crystal Structures of **2 and **9**.** The data were collected at –100 °C on a Bruker-AXS APEX diffractometer with a Kryoflex low temperature device, a CCD area

detector fitted with an upgraded Nicolet LT-2 low temperature device, and a graphite-monochromated Mo source (*K*_α radiation, 0.71073 Å). Suitable crystals were coated with paratone oil (Exxon) and mounted on loops under a stream of nitrogen at the data collection temperature. The structures were solved by direct methods. Non-hydrogen atoms were anisotropically refined. All hydrogen atoms were treated as idealized contributions. Empirical absorption correction was performed with SADABS.^{15a} In addition the global refinements for the unit cells and data reductions of the two structures were performed using the Saint program (version 6.02). All calculations were performed using SHELXTL (version 5.1) proprietary software package.^{15b}

Acknowledgment is made to the National Science Foundation (CHE-051692). We thank Tara Williams for assistance.

Supporting Information Available: Crystallographic data of **2** and **9**. This material is available free of charge via the Internet at <http://pubs.acs.org>.

OM800362T

Reaction of the Iridacyclopentadiene

$\text{Tp}^{\text{Me}_2}\text{Ir}(\text{C}(\text{R})=\text{C}(\text{R})\text{C}(\text{R})=\text{C}(\text{R}))(\text{H}_2\text{O})$ ($\text{R} = \text{CO}_2\text{Me}$) with Alkynes

Margarita Paneque,^{*,†} Manuel L. Poveda,^{*,†} Nuria Rendón,[†] and Kurt Mereiter[‡]

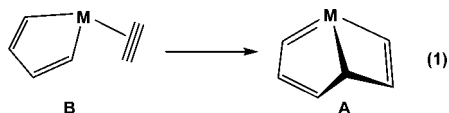
Instituto de Investigaciones Químicas and Departamento de Química Inorgánica, Consejo Superior de Investigaciones Científicas (CSIC) and Universidad de Sevilla, Avenida Américo Vespucio 49, Isla de la Cartuja, 41092 Sevilla, Spain, and Department of Chemistry, Vienna University of Technology, Getreidemarkt 9/164SC, A-1060 Vienna, Austria

Received February 8, 2008

The iridacyclopentadiene derivative $\text{Tp}^{\text{Me}_2}\text{Ir}(\text{C}(\text{R})=\text{C}(\text{R})\text{C}(\text{R})=\text{C}(\text{R}))(\text{H}_2\text{O})$ (**1**) (Tp^{Me_2} = hydrotris(3,5-dimethylpyrazolyl)borate, $\text{R} = \text{CO}_2\text{Me}$) reacts with an excess of $\text{MeC}\equiv\text{CMe}$ with formation of the iridacycloheptatriene $\text{Tp}^{\text{Me}_2}\text{Ir}(\text{C}(\text{Me})=\text{C}(\text{Me})\text{C}(\text{R})=\text{C}(\text{R})\text{C}(\text{R})=\text{C}(\text{R}))(\text{H}_2\text{O})$ (**3**) and the first metallabicyclo[3,2,0]heptatriene $\text{Tp}^{\text{Me}_2}\text{Ir}(\text{C}(\text{Me})\text{C}(\text{Me})=\text{C}(\text{R})\text{C}(\text{R})\text{C}(\text{R})=\text{C}(\text{R}))(\text{H}_2\text{O})$ (**4**). Both species are involved in the equilibrium $\mathbf{3} \rightleftharpoons \mathbf{4} + \text{H}_2\text{O}$, which has been studied as a function of temperature. By contrast, $\text{PhC}\equiv\text{CPh}$ gives only a compound related to **4**, namely, the species $\text{Tp}^{\text{Me}_2}\text{Ir}(\text{C}(\text{Ph})\text{C}(\text{Ph})=\text{C}(\text{R})\text{C}(\text{R})\text{C}(\text{R})=\text{C}(\text{R}))(\text{H}_2\text{O})$ (**5**), which does not react with water. Complex **1** incorporates two molecules of terminal alkynes such as $\text{HC}\equiv\text{CPh}$ and $\text{HC}\equiv\text{CCH}_2\text{CH}_2\text{OH}$ with formation of complex chelating alkenyl-allylic structures, and the same is true for $\text{Me}_3\text{SiC}\equiv\text{CPh}$ and $\text{Me}_3\text{SiC}\equiv\text{CSiMe}_3$, where the SiMe_3 groups are replaced by hydrogen atoms under the reaction conditions. In all these cases the two alkynes are added consecutively into one of the $\text{Ir}-\text{C}$ bonds of **1**. Finally, the reaction of **1** with $\text{HC}\equiv\text{CCO}_2\text{Me}$ gives a fully substituted cyclopentadiene with two of the substituents being metalated by the iridium center and in this case the two $\text{Ir}-\text{C}$ bonds of **1** are cleaved in the process. All the new compounds have been characterized by microanalysis, IR and NMR spectroscopies, and in some cases by X-ray diffraction analysis.

Introduction

In two recent theoretical papers¹ about the well-known process of cyclotrimerization of alkynes catalyzed by transition metal species,² it has been found that a metallabicyclo[3.2.0]heptatriene (**A**), the result of the internal coupling of the metallacyclopentadiene-alkyne complex **B** (eq 1), may be implicated as an active intermediate. Species **A** then undergoes



a structural opening to an unsaturated metallacycloheptatriene

(this can be formulated as a saturated bis(carbene) species depending on the system^{1a}), i.e., the expected product of the insertion of the alkyne into a $\text{M}-\text{C}$ bond of **B**, which eventually experiences reductive elimination to give a benzenoid nucleus.

In a recent paper³ we have shown that the iridacyclopentadiene $\text{Tp}^{\text{Me}_2}\text{Ir}(\text{C}(\text{R})=\text{C}(\text{R})\text{C}(\text{R})=\text{C}(\text{R}))(\text{H}_2\text{O})$ (**1**)⁴ (Tp^{Me_2} = hydrotris(3,5-dimethylpyrazolyl)borate, $\text{R} = \text{CO}_2\text{Me}$) reacts with dimethyl acetylenedicarboxylate ($\text{MeO}_2\text{CC}\equiv\text{CCO}_2\text{Me}$, DMAD) to give the iridacycloheptatriene $\text{Tp}^{\text{Me}_2}\text{Ir}(\text{C}(\text{R})=\text{C}(\text{R})\text{C}(\text{R})=\text{C}(\text{R})\text{C}(\text{R})=\text{C}(\text{R}))(\text{H}_2\text{O})$ (**2**) (eq 2). Surprisingly, and as described in the present contribution, the first example of a transition metal derivative with structure **A** is obtained when complex **1** is treated with 2-butyne ($\text{MeC}\equiv\text{CMe}$). In addition, the reactivity of **1** with other alkynes such as $\text{PhC}\equiv\text{CPh}$, $\text{Me}_3\text{SiC}\equiv\text{CSiMe}_3$, $\text{HC}\equiv\text{CPh}$, $\text{HC}\equiv\text{CCH}_2\text{CH}_2\text{OH}$, and $\text{HC}\equiv\text{CCO}_2\text{Me}$ is also reported herein. Part of this work has been the subject of a preliminary communication.⁵

Results and Discussion

Reaction of 1 with 2-Butyne. When $\text{Tp}^{\text{Me}_2}\text{Ir}(\text{C}(\text{R})=\text{C}(\text{R})\text{C}(\text{R})=\text{C}(\text{R}))(\text{H}_2\text{O})$ (**1**) is treated with an excess of $\text{MeC}\equiv\text{CMe}$,

(3) Paneque, M.; Posadas, C. M.; Poveda, M. L.; Rendón, N.; Santos, L. L.; Álvarez, E.; Salazar, V.; Mereiter, K.; Oñate, E. *Organometallics* **2007**, *26*, 3403.

(4) Álvarez, E.; Paneque, M.; Posadas, C. M.; Poveda, M. L.; Rendón, N.; Mereiter, K. *Chem.-Eur. J.* **2007**, *13*, 5160.

(5) Paneque, M.; Poveda, M. L.; Rendón, N.; Mereiter, K. *J. Am. Chem. Soc.* **2004**, *126*, 1610.

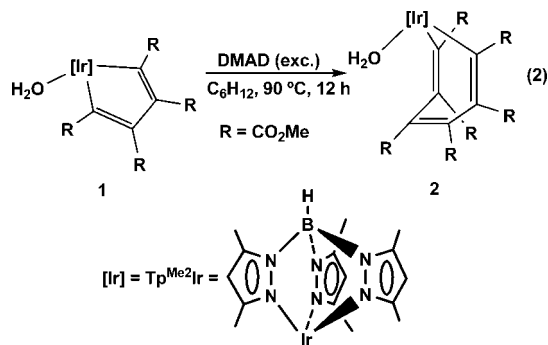
* To whom correspondence should be addressed. E-mail: paneque@iiq.csic.es.

[†] Universidad de Sevilla and Consejo Superior de Investigaciones Científicas.

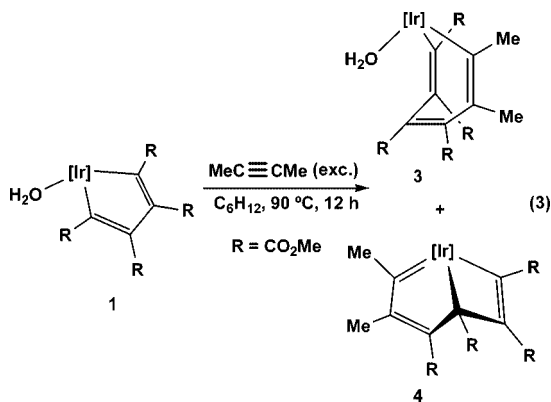
[‡] Vienna University of Technology.

(1) (a) Kirchner, K.; Calhorda, M. J.; Schmid, R.; Veiros, L. F. *J. Am. Chem. Soc.* **2003**, *125*, 11721. (b) Yamamoto, Y.; Arakawa, T.; Ogawa, R.; Itoh, K. *J. Am. Chem. Soc.* **2003**, *125*, 12143.

(2) (a) Collman, J. P.; Hegedus, L. S.; Norton, J. R.; Finke, R. G. *Principles and Applications of Organotransition Metal Chemistry*; University Science Books: Mill Valley, CA, 1987. (b) Kezuka, S.; Tanaka, S.; Ohe, T.; Nakaya, Y.; Takeuchi, R. *J. Org. Chem.* **2006**, *71*, 543. (c) Saito, S.; Yamamoto, Y. *Chem. Rev.* **2000**, *100*, 2901. (d) Grotjahn, D. B. In *Comprehensive Organometallic Chemistry II*; Abel, E. W., Stone, F. G. A., Wilkinson, G., Eds.; Pergamon: Oxford, 1995; Vol. 12, Chapter 7.3. (e) Cadierno, V.; García-Garrido, S. E.; Gimeno, J. *J. Am. Chem. Soc.* **2006**, *128*, 15094. (f) Kakeya, M.; Fujihara, T.; Kasaya, T.; Nagasawa, A. *Organometallics* **2006**, *25*, 4131, and reference ¹.



in C_6H_{12} at 90 °C, a mixture of the complexes **3** and **4** (whose proportion depends on the water concentration in the reaction media) is obtained in very high yield (eq 3).



3 is a yellow crystalline solid whose structure is related to that presented for **2** (see Introduction); that is, it is an iridacycloheptatriene that is formally formed by the insertion of $MeC\equiv CMe$ into one of the $Ir-C$ bonds of **1**. Complex **3** has been fully characterized by microanalysis, IR and NMR spectroscopies, and X-ray diffraction analysis. As expected, it exhibits NMR features quite similar to those found for **2**³ and will not be described in any detail here (see Experimental Section). Figure 1 shows a view of the molecular structure of complex **3**, while Tables 1 and 2 collect the crystal data and the relevant bond lengths and angles, respectively. As can be observed, the metallacycle features a boat structure with the central double $C=C$ bond pointing to the metal center, while the water ligand is hydrogen bonded to O(56) of the CO_2Me substituent at C(52), this carbon being the one bonded to the $-C(Me)=C(Me)-$ moiety (Figure 1; a second hydrogen bond is donated intermolecularly to O(65), not shown). The two $Ir-C(sp^2)$ bond distances exhibit similar and normal values (2.03 Å av),^{3,4,6} while, as expected, the $Ir-N$ (pyrazolyl) bond length *trans* to the hard H_2O ligand (2.03 Å) is shorter than the other two (2.14 Å av).^{3,4}

The other compound formed in eq 3 is complex **4**, a green crystalline solid that represents the first example of metallabicyclo-[3.2.0]heptatriene structure mentioned in the Introduction. Its $^{13}C\{^1H\}$ NMR spectrum features resonances at 275.1 and 20.5 ppm, which are assigned to the carbenic functionality and to the sp^3 carbon directly bonded to the iridium, respectively, while in the long-range $^1H-^{13}C$ HETCOR spectrum the cross-peaks found between the Me protons, derived from the added alkyne, and the carbenic carbon are in accord with the depicted structure. The conclusions of these spectroscopic solution studies find

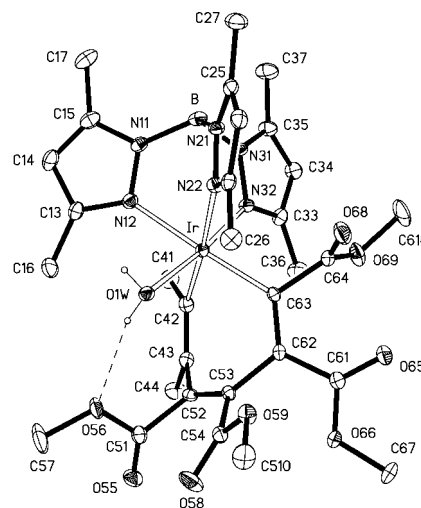


Figure 1. X-ray structure of complex **3** (30% displacement ellipsoids, hydrogen atoms omitted for clarity except for the water molecule $H_2O(1w)$).

additional support in the solid state structure deduced from the X-ray diffraction study carried out for complex **4** (Figure 2 and Tables 1 and 3). The bond distances $Ir-C(42)$ (1.91 Å), $Ir-C(63)$ (2.03 Å), and $Ir-C(53)$ (2.14 Å) are in the range expected for $Ir-carbene$,⁶ $Ir-alkenyl$, and $Ir-alkyl$ functionalities,^{3,4,6} although the latter bond is somewhat longer than normal $Ir-C(sp^3)$ bonds, probably due to ring strain. The $C-Ir-C$ bite angles are 66.0° and 81.8° for the four- and five-membered metallacycles, respectively, and finally, the $Ir-N$ (pyrazolyl) bond length of the one *trans* to the carbene (2.25 Å) is longer than the other two (2.16 Å each).

As already commented on, there is no precedent for the structure presented by complex **4** in transition metal chemistry, except for a related silicon compound stabilized by very bulky substituents.⁷ A tungsten complex with a similar bicyclic skeleton, but with a more complicated bonding pattern, can also be found in the literature.⁸ It is also worth mentioning that the parent pure organic compound [3.2.0]hepta-1,3,6-triene is not known but has been implicated in a number of chemical reactions as a highly unstable intermediate.⁹

Interestingly compounds **3** and **4** easily interconvert into each other. Thus, when **3** is dissolved in dry C_6D_6 , the solution turns green, and, on the other hand, **4** gives solutions in acetone- d_6 that become yellow when a little water is added. In both cases the interconversion is confirmed by 1H NMR spectroscopy. A quantitative study of the $3 \rightleftharpoons 4 + H_2O$ equilibrium has been carried out with D_2O (0.6 M in acetone- d_6) in the temperature range 40–70 °C, and the results are shown in graphic form in Figure 3 ($\Delta H = 6.5 \text{ kcal}\cdot\text{mol}^{-1}$, $\Delta S = 19.1 \text{ cal}\cdot\text{mol}^{-1}\cdot\text{K}^{-1}$).

Scheme 1 shows the proposed mechanism for the $3 \rightleftharpoons 4 + H_2O$ interconversion. Complex **3** loses the water ligand to give **C** (we prefer to formulate this intermediate as an unsaturated 16 e^- species rather than a 18 e^- bis(carbene)^{1a}), which then

(7) Kon, Y.; Ogasawara, J.; Sakamoto, K.; Kabuto, C.; Kira, M. *J. Am. Chem. Soc.* **2003**, *125*, 9310.

(8) (a) Agh-Atabay, N. M.; Davidson, J. L.; Douglas, G.; Muir, K. W. *J. Chem. Soc., Chem. Commun.* **1989**, 549. For a somewhat related iridacyclobutene resulting from a carbene insertion into a iridacyclopentadiene, see: (b) O'Connor, J. M.; Pu, L.; Woolard, S.; Chadha, R. K. *J. Am. Chem. Soc.* **1990**, *112*, 6731.

(9) (a) Breslow, R.; Washburn, W.; Bergman, R. G. *J. Am. Chem. Soc.* **1969**, *91*, 196. (b) Billups, W. E.; Saini, R. K.; Litosh, V. A.; Alemany, L. B.; Wilson, W. K.; Wiberg, K. B. *J. Org. Chem.* **2002**, *67*, 4436. (c) Bajorek, T.; Werstink, N. H. *Can. J. Chem.* **2005**, *83*, 1352.

(6) Ilg, K.; Paneque, M.; Poveda, M. L.; Rendón, N.; Santos, L. L.; Carmona, E.; Mereiter, K. *Organometallics* **2006**, *25*, 2230.

Table 1. Crystal Data and Data Collection and Refinement Details for 3·CHCl₃, 4·CH₂Cl₂, 8·solv, and 11·2CH₂Cl₂

	3·CHCl ₃	4·CH ₂ Cl ₂ ^a	8·solv ^b	11·2CH ₂ Cl ₂ ^c
formula	C ₃₁ H ₄₂ BIrN ₆ O ₉ ·CHCl ₃	C ₃₁ H ₄₀ BIrN ₆ O ₈ ·CH ₂ Cl ₂	C ₄₃ H ₄₆ BIrN ₆ O ₈	C ₃₅ H ₄₂ BIrN ₆ O ₁₂ ·2CH ₂ Cl ₂
mol wt	965.08	912.63	977.87	1111.61
color, habit	yellow prism	green prism	yellow prism	yellow fragment
symmetry, space group	orthorhombic, <i>P</i> 2 ₁ 2 ₁	triclinic, <i>P</i> $\bar{1}$	monoclinic, <i>C</i> 2/ <i>c</i>	triclinic, <i>P</i> $\bar{1}$
<i>a</i> , Å	14.5281(8)	11.0348(6)	39.850(2)	11.225(2)
<i>b</i> , Å	16.3834(9)	12.5531(7)	11.0782(6)	13.849(3)
<i>c</i> , Å	17.0149(9)	14.0159(8)	21.2993(12)	16.314(3)
α , deg	90	88.743(1)	90	80.248(4)
β , deg	90	75.343(1)	108.718(1)	76.248(4)
γ , deg	90	87.515(1)	90	70.208(4)
<i>V</i> , Å ³	4049.9(4)	1876.4(2)	8905.5(9)	2306.8(7)
<i>Z</i>	4	2	8	2
<i>D</i> _{calcd} , g cm ⁻³	1.583	1.615	1.459	1.600
μ , mm ⁻¹	3.550	3.755	3.055	3.189
θ range, deg	2.4–30	2.20–30	2.24–30	2.58–25
temp, K	173(2)	298(2)	173(2)	173(2)
no. of data collected	58 618	28 299	65 632	20 763
no. of unique data	11 754 (<i>R</i> _{int} = 0.062)	10 85 (<i>R</i> _{int} = 0.023)	12 906 (<i>R</i> _{int} = 0.030)	8093 (<i>R</i> _{int} = 0.061)
no. of params/restraints	488/5	441/0	573/283	540/205
<i>R</i> ₁ ^d (<i>F</i> ² > 2 σ (<i>F</i> ²))	0.0321	0.0246	0.0308	0.0779
<i>wR</i> ₂ ^e (all data)	0.0712	0.0650	0.0738	0.1454
diff Fourier peaks min./max., e Å ⁻³	−0.81/1.86	−0.43/0.86	−1.91/3.57	−1.67/1.46

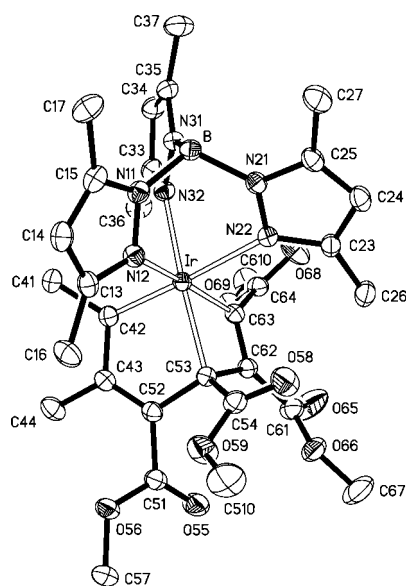
^a Solvent disordered and squeezed with the program PLATON (Spek, A. L., 2006) but contained in chemical formula and quantities thereof. ^b Solvent (essentially petroleum ether) disordered and squeezed with the program PLATON, but not contained in chemical formula and quantities thereof. ^c Solvent content idealized. ^d $R_1(F) = \sum |F_o| - |F_c| / \sum |F_o|$. ^e $wR_2(F^2) = \{\sum [w(F_o^2 - F_c^2)^2] / \sum [w(F_o^2)]\}^{1/2}$.

Table 2. Selected Bond Lengths (Å) and Angles (deg) for 3·CHCl₃

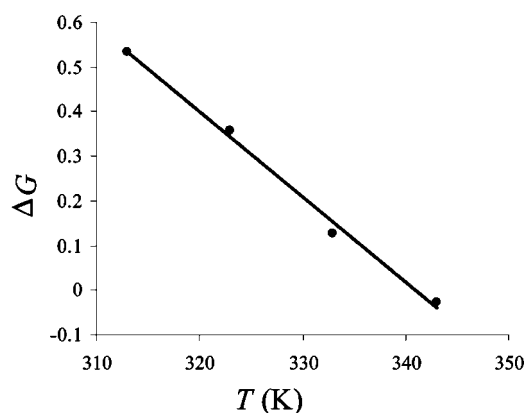
Ir–N(12)	2.135(3)	C(42)–C(43)	1.361(5)
Ir–N(22)	2.149(3)	C(43)–C(52)	1.470(5)
Ir–N(32)	2.030(3)	C(52)–C(53)	1.343(5)
Ir–C(42)	2.040(4)	C(53)–C(62)	1.490(5)
Ir–C(63)	2.022(4)	C(62)–C(63)	1.358(5)
Ir–O(1W)	2.135(3)		
N(12)–Ir–N(22)	84.4(1)	N(22)–Ir–O(1W)	85.3(1)
N(12)–Ir–N(32)	88.5(1)	N(32)–Ir–C(42)	88.1(2)
N(12)–Ir–C(42)	91.6(2)	N(32)–Ir–C(63)	91.5(1)
N(12)–Ir–C(63)	176.2(2)	N(32)–Ir–O(1W)	174.4(1)
N(12)–Ir–O(1W)	86.6(1)	C(42)–Ir–C(63)	92.2(2)
N(22)–Ir–N(32)	91.5(1)	C(42)–Ir–O(1W)	94.8(1)
N(22)–Ir–C(42)	175.9(2)	C(63)–Ir–O(1W)	93.2(1)
N(22)–Ir–C(63)	91.9(2)		

Table 3. Selected Bond Lengths (Å) and Angles (deg) for 4·CH₂Cl₂

Ir–N(12)	2.163(2)	C(42)–C(43)	1.438(4)
Ir–N(22)	2.245(2)	C(43)–C(52)	1.348(4)
Ir–N(32)	2.155(2)	C(52)–C(53)	1.506(4)
Ir–C(42)	1.905(3)	C(53)–C(62)	1.524(3)
Ir–C(53)	2.136(2)	C(62)–C(63)	1.337(3)
Ir–C(63)	2.025(2)		
N(12)–Ir–N(22)	85.4(1)	N(22)–Ir–C(63)	89.0(1)
N(12)–Ir–N(32)	87.5(1)	N(32)–Ir–C(42)	96.4(1)
N(12)–Ir–C(42)	89.6(1)	N(32)–Ir–C(53)	167.5(1)
N(12)–Ir–C(53)	104.8(1)	N(32)–Ir–C(63)	102.0(1)
N(12)–Ir–C(63)	168.4(1)	C(42)–Ir–C(53)	81.8(1)
N(22)–Ir–N(32)	83.1(1)	C(42)–Ir–C(63)	95.9(1)
N(22)–Ir–C(42)	175.0(1)	C(53)–Ir–C(63)	66.0(1)
N(22)–Ir–C(53)	99.8(1)		

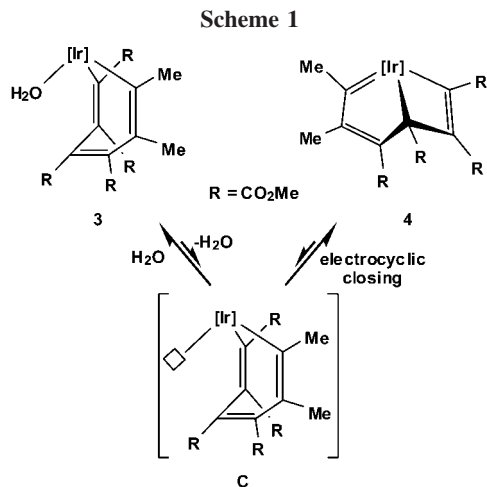
**Figure 2.** X-ray structure of complex 4 (30% displacement ellipsoids, hydrogen atoms omitted for clarity).

experiences ring contraction by regioselective attack of a *C*(CO₂Me) sp² carbon to the iridium to afford compound 4. There is no evidence for the formation of an isomeric species

**Figure 3.** ΔG versus *T* for the 3 ⇌ 4 + H₂O equilibrium.

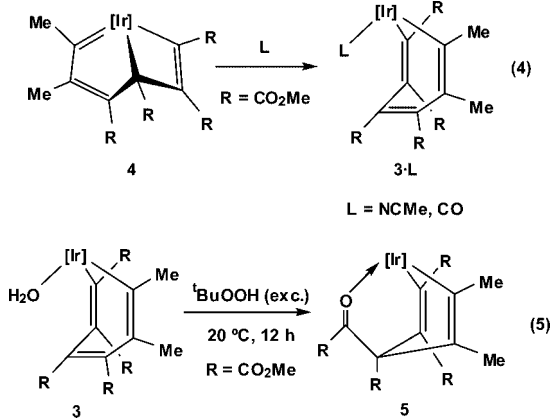
in which a $-\text{C}(\text{Me})=\text{C}(\text{Me})-$ unit is on the four-membered iridacycle, and this may be due, at least partially, to the stabilization that a donor substituent, like the methyl group, confers to the electrophilic carbene.¹⁰ In fact the iridacycloheptatriene 2,³ mentioned in the Introduction, in which all the substituents are CO₂Me, does not give a compound related to 4

(10) (a) Carmona, E.; Paneque, M.; Poveda, M. L. *Dalton Trans.* **2003**, 4022. (b) Carmona, E.; Paneque, M.; Santos, L. L.; Salazar, V. *Coord. Chem. Rev.* **2005**, 294, 1729.

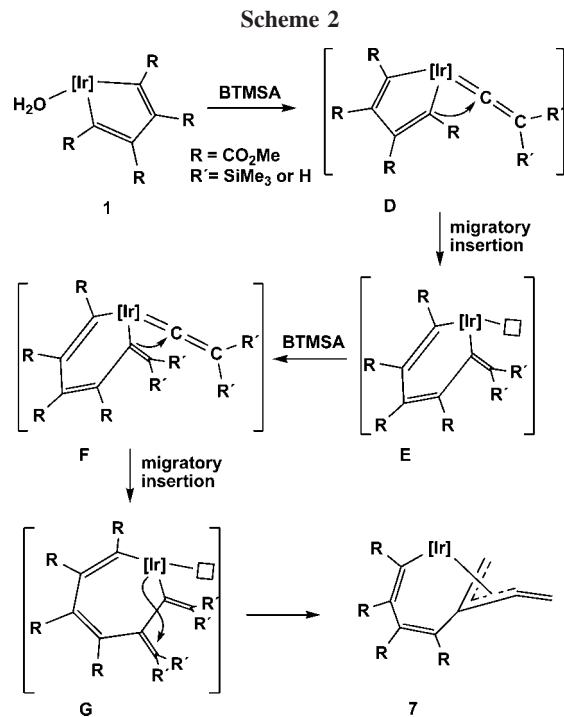
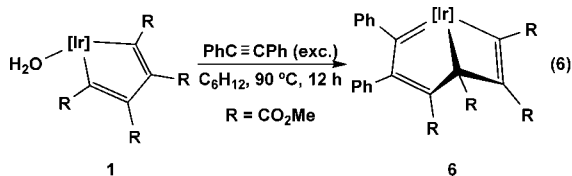


(under molecular sieves, in C_6D_6 , at 60°C , 48 h) even though that the water ligand is labile under these conditions.³ Finally and with respect to the formation of **3** and **4** from **1** and $\text{MeC}\equiv\text{CMe}$, the experimental data obtained are not sufficient to decide which species is formed in the first place, as this reaction is slower than the $\mathbf{3} \rightleftharpoons \mathbf{4} + \text{H}_2\text{O}$ equilibrium.

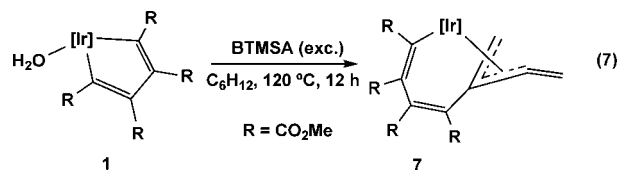
As expected,^{3,4} complex **4** reacts with other Lewis bases such as NCMe and CO with formation of the stable adducts $\mathbf{3}\cdot\text{L}$ (eq 4). Compound **3**, in a typical reaction of this kind of iridacyclopentadienes,³ is cleanly oxidized by tBuOOH to give the ketoester **5** (eq 5). The spectroscopic data of $\mathbf{3}\cdot\text{L}$ are similar to those obtained for **3** and will not be commented on, while for **5** the $^{13}\text{C}\{^1\text{H}\}$ NMR spectrum exhibits resonances at 209.1 and 77.5 ppm, assigned to the keto group bonded to Ir and to the quaternary aliphatic carbon, respectively.



Reaction of Complex 1 with $\text{PhC}\equiv\text{CPh}$. Complex **1** reacts with an excess of $\text{PhC}\equiv\text{CPh}$ to give the brown compound **6** in $\geq 80\%$ spectroscopic yield (eq 6). Its spectroscopic characteristics indicate that it is related to the already described bicyclic **4** and furthermore that the $\text{PhC}\equiv\text{CPh}$ molecule has been incorporated into the five-membered iridacycle. Complex **6** has no tendency to react with water, and it is recovered unaltered upon heating, in different solvents, at 90°C with an excess of added H_2O .



Reaction of Complex 1 with $\text{Me}_3\text{SiC}\equiv\text{CSiMe}_3$. When a solution of **1** in C_6H_{12} is heated (90°C , 12 h) in the presence of an excess of $\text{Me}_3\text{SiC}\equiv\text{CSiMe}_3$ (BTMSA), the chelating alkenyl-allylic species **7** is formed in ca. 75% spectroscopic yield (eq 7).



As can be observed, two alkyne moieties have been incorporated into one of the Ir–C bonds of **1** in the form of a 1,2,3- η^3 -butadienyl ligand¹¹ in such a way that all the SiMe_3 groups have been replaced, probably due to hydrolysis, by hydrogen atoms. In recent work carried out in this laboratory we have reported⁴ on compounds related to **7** but with normal allyl termini, i.e., without the $=\text{CH}_2$ substituent, and some years ago we also synthesized some 1,2,3- η^3 -butadienyl Ir(III) complexes containing the Tp^{Me_2} ligand.¹² Therefore the NMR spectroscopic characterization of **7** was straightforward, and the relevant data are collected in the Experimental Section.

For the formation of **7** we propose the mechanism shown in Scheme 2. First, the water molecule is displaced by a molecule of BTMSA, to give **D**, in which the alkyne has isomerized to a vinylidene ligand,¹³ a process that has been observed in the reaction of $\text{Tp}^{\text{Me}_2}\text{Ir}(\text{Ph})_2(\text{N}_2)$ with BTMSA.⁶ Then, a migratory

(11) Brisdon, B. J.; Walton, R. A. *Polyhedron* **1995**, *14*, 1259.

(12) Boutry, O.; Poveda, M. L.; Carmona, E. *J. Organomet. Chem.* **1997**, *528*, 143.

(13) (a) Werner, H. *J. Organomet. Chem.* **1994**, *475*, 45. (b) Werner, H.; Baum, M.; Schneider, D.; Windmueller, B. *Organometallics* **1994**, *13*, 1089. (c) Werner, H.; Lass, R. W.; Gevert, O.; Wolf, J. *Organometallics* **1997**, *16*, 4077. (d) Jiménez, M. V.; Sola, E.; Lahoz, F. J.; Oro, L. A. *Organometallics* **2005**, *24*, 2722. (e) Bustelo, E.; Carbó, J. J.; Lledós, A.; Mereiter, K.; Puerta, M. C.; Valerga, P. *J. Am. Chem. Soc.* **2003**, *125*, 3311. (f) De Angelis, F.; Sgamellotti, A.; Re, N. *Dalton Trans.* **2004**, 3225.

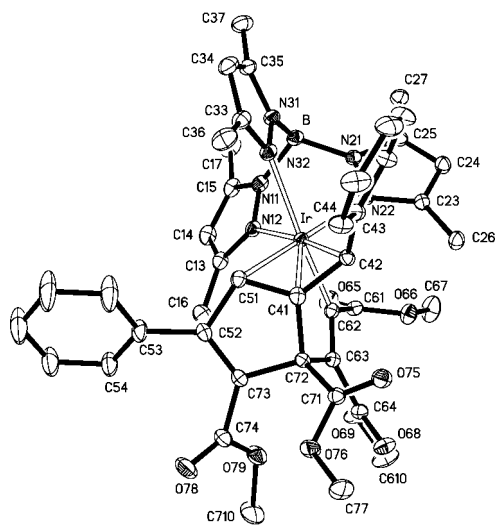


Figure 4. X-ray structure of complex **8** (30% displacement ellipsoids, hydrogen atoms omitted for clarity).

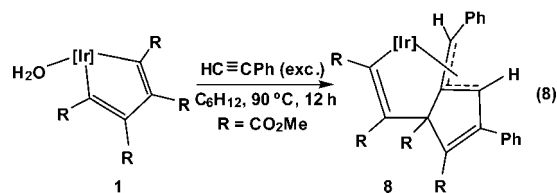
Table 4. Selected Bond Lengths (Å) and Angles (deg) for **8**·solv

Ir–N(12)	2.137(2)	C(41)–C(51)	1.410(3)
Ir–N(22)	2.087(2)	C(41)–C(72)	1.531(4)
Ir–N(32)	2.245(2)	C(51)–C(52)	1.482(4)
Ir–C(41)	2.111(3)	C(52)–C(73)	1.348(4)
Ir–C(42)	2.144(3)	C(62)–C(63)	1.346(4)
Ir–C(51)	2.286(3)	C(63)–C(72)	1.530(4)
Ir–C(62)	2.016(3)	C(72)–C(73)	1.531(3)
C(41)–C(42)	1.439(3)		
N(12)–Ir–N(22)	89.9(1)	N(32)–Ir–C(41)	111.7(1)
N(12)–Ir–N(32)	83.1(1)	N(32)–Ir–C(42)	98.9(1)
N(12)–Ir–C(41)	134.6(1)	N(32)–Ir–C(51)	90.0(1)
N(12)–Ir–C(42)	174.1(1)	N(32)–Ir–C(62)	170.7(1)
N(12)–Ir–C(51)	104.5(1)	C(41)–Ir–C(42)	39.5(1)
N(12)–Ir–C(62)	90.4(1)	C(41)–Ir–C(51)	37.1(1)
N(22)–Ir–N(32)	84.8(1)	C(41)–Ir–C(62)	77.6(1)
N(22)–Ir–C(41)	132.5(1)	C(42)–Ir–C(51)	70.0(1)
N(22)–Ir–C(42)	95.8(1)	C(42)–Ir–C(62)	88.3(1)
N(22)–Ir–C(51)	164.0(1)	C(51)–Ir–C(62)	98.1(1)
N(22)–Ir–C(62)	88.6(1)		

insertion reaction into an Ir–C bond of the metallacycle¹⁴ furnishes intermediate **E**, where the whole process is repeated to end up with species **G**. Finally, bond reorganization of the latter intermediate gives complex **7** (R' = H). Although it is clear that all the SiMe₃ groups are replaced by hydrogen atoms in the formation of **7**, it is not known when and how this occurs, but according to the literature, it probably takes place in the alkyne to vinylidene isomerization.¹³

Reaction of Complex 1 with HC≡CPh and Me₃SiC≡CPh. Complex **1** reacts with an excess of HC≡CPh, under the experimental conditions depicted in eq 8, with formation of a mixture of compounds, with one of them, compound **8**, clearly predominating (60% spectroscopic yield). **8** can be isolated by chromatography on silica gel, and its structural complexity has been ascertained by X-ray diffraction studies (Figure 4 and Tables 1 and 4).

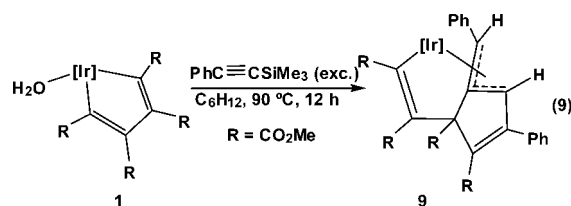
As can be observed, complex **8** is another chelating alkenyl-allylic species, in this case bicyclic, in which the allyl ligand has been formed by the coupling of two HC≡CPh molecules, with concomitant incorporation into the metallacycle **1**. The Ph



substituent of the allyl is positioned *anti* with respect to the C(R) group that is bonded to the central carbon of the η³-allyl moiety, and it has been found that it is slowly rotating in solution, at room temperature, on the NMR time scale. In the ¹³C{¹H} NMR spectrum, the carbon nuclei of the allylic ligand resonate at 39.0 (CHPh), 116.6 (C_q), and 60.5 (CH) ppm, respectively, while the aliphatic quaternary carbon, C(R), appears at δ 72.1. With respect to the solid state structure, the Ir–C(62) bond length of 2.02 Å corresponds well for an Ir–C(sp²) single bond,⁶ while the distances of the metal to the carbon atoms of the η³-allyl moiety are 2.11 Å (central) and 2.14 and 2.29 Å (termini), unexceptional for this kind of ligand.⁴

Scheme 3 shows a plausible, but highly speculative, mechanism for the formation of **8**. First, a molecule of alkyne regioselectively inserts into an Ir–C bond of **1** with formation of the unsaturated metallacycloheptatriene **H**. This species does not stabilize by addition of water or ring contraction (see the case of MeC≡CMe or PhC≡CPh) but reacts with another equivalent of HC≡CPh to give intermediate **I** via alkyne to vinylidene isomerization^{13e,13f} and regioselective migratory insertion of this ligand into the Ir–C(H)= bond. Finally, a ring contraction process will form the allyl ligand present in **8**.

Interestingly, when the reaction of **1** with an excess of Me₃SiC≡CPh is carried out under conditions similar to those employed for the synthesis of **8**, an isomer of this species, the chelating alkenyl-allyl **9** (eq 9), is obtained in ca. 60% isolated yield. They differ only in the stereochemistry of the CHPh terminus of the allyl moiety, and this is reflected by the similarity of the NMR data obtained for both complexes. For the case of **9** the *cisoid* disposition of the two hydrogen substituents of the allyl is clearly revealed by the NOESY spectrum (see Experimental Section). It is proposed that formation of **9** follows a

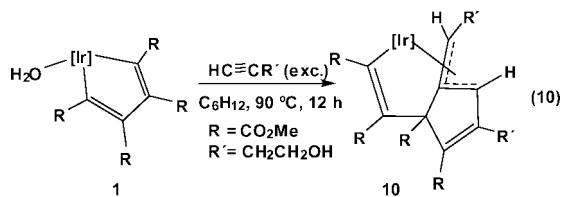


mechanism almost identical to that already advanced for **8** (Scheme 3) but with the SiMe₃ substituent forcing the different stereochemical outcome, perhaps at the formation stage of the intermediate related to **I**. Once again the SiMe₃ groups have been replaced by hydrogen atoms despite the “neutral” reaction conditions.

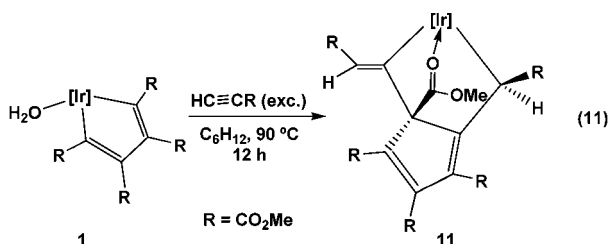
Reaction of Complex 1 with HC≡CCH₂CH₂OH and HC≡CCO₂Me. In the first case, complex **10**, an analogue of **8**, is obtained in ca. 60% isolated yield (eq 10), despite the different nature of the substituents on the alkyne, CH₂CH₂OH and Ph, respectively. Complex **10** has been fully characterized by NMR spectroscopy, and the corresponding data obtained are collected in the Experimental Section.

Finally, the reaction of **1** with an excess of HC≡CCO₂Me, in C₆H₁₂ at 90 °C, furnishes compound **11**, in ca. 50% isolated yield, whose molecular complexity has been revealed by X-ray diffraction analysis (eq 11). As can be observed, two molecules

(14) (a) Chin, C. S.; Lee, H. *Chem.–Eur. J.* **2004**, *10*, 4518. (b) Clark, G. R.; Johns, P. M.; Roper, W. R.; Wright, L. J. *Organometallics* **2006**, *25*, 1771. (c) O'Connor, J. M.; Hübner, K.; Merwin, R.; Gantzel, P. K.; Fong, B. S.; Adams, M.; Rheingold, A. L. *J. Am. Chem. Soc.* **1997**, *119*, 3631.



of the alkyne have been incorporated into complex **1** with formation of a fully substituted cyclopentadiene with two of the substituents being metalated by iridium. The NMR data obtained for **11** are in accord with the structure found in the solid state, and thus the carbon nuclei bonded to Ir resonate at 150.7 (sp^2) and 8.1 (sp^3) ppm in the $^{13}C\{^1H\}$ NMR spectrum, while the sp^3 carbon of the cyclopentadiene ring appears at δ 94.1. Figure 5 shows a view of a molecule of **11**, while structure data are contained in Tables 1 and 5. One of the three Ir–N(pyrazolyl) bond distances of **11**, specifically that *trans* to



the coordinated oxygen atom, is significantly shorter (2.02 Å) than the other two (2.15 Å *av*). The Ir–C(sp^3) and Ir–C(sp^2) bond lengths are 2.17 and 1.99 Å, respectively, typical values of these kinds of bonds.^{3,4,6} Due to the complex structure of **11**, it is not appropriate to propose a mechanism for its formation, although it is clear that the two alkyne molecules have not been incorporated consecutively into one of the Ir–C bonds of **1**, but instead one each into the two initially existing Ir–C bonds.

Conclusions

The reaction of iridacyclopentadiene $Tp^{Me_2}Ir(C(R)=C(R)-C(R)=C(R))(H_2O)$ (**1**) ($R = CO_2Me$) with an excess of $MeC\equiv CMe$ has allowed the synthesis of the first metallabicyclo-[3.2.0]heptatriene, a kind of structure recently invoked in the transition metal mediated catalytic cyclotrimerization of alkynes. This species readily reacts with Lewis bases, with formation of iridacycloheptatrienes, and for the case of H_2O , this process is reversible. A related bicyclic compound is obtained when **1** reacts with $PhC\equiv CPh$, and as in the case of $MeC\equiv CMe$, the entering alkyne is incorporated into the five-membered part of the bicyclic structure. By contrast, two molecules of alkyne add to **1** when the alkyne is of the terminal type or if it has $SiMe_3$ substituents (to be interchanged by hydrogens in the course of the reaction), giving complicated structures with a highly substituted η^3 -allyl ligand in most cases.

Experimental Section

General Procedures. Microanalyses were by the Microanalytical Service of the Instituto de Investigaciones Químicas (Sevilla, Spain). In our hands, compounds **6**, **9**, and **10** could not be purified satisfactorily. The presence of crystallization solvent in the remaining compounds was authenticated by NMR. Infrared spectra were obtained with a Bruker Vector 22 spectrometer. The NMR instruments were Bruker DRX-500, DRX-400, and DPX-300

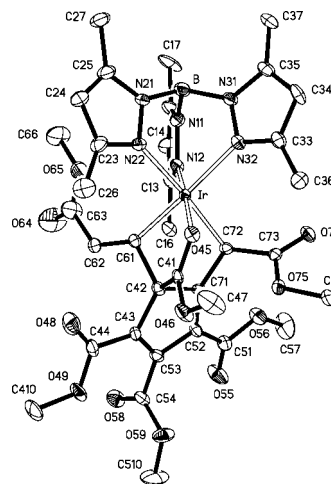
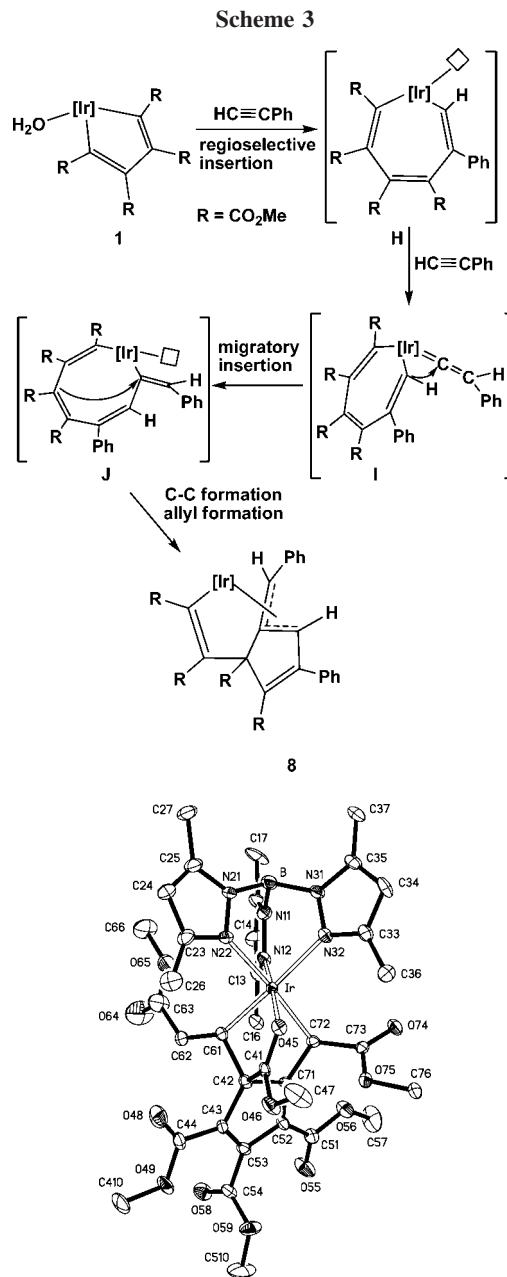


Figure 5. X-ray structure of complex **11** (30% displacement ellipsoids, hydrogen atoms omitted for clarity).

spectrometers. Spectra were referenced to external $SiMe_4$ (δ 0 ppm) using the residual protio solvent peaks as internal standards (1H NMR experiments) or the characteristic resonances of the solvent nuclei (^{13}C NMR experiments). Spectral assignments were made by means of routine one- and two-dimensional NMR experiments where appropriate. All manipulations were performed under dry, oxygen-free dinitrogen, following conventional Schlenk techniques.

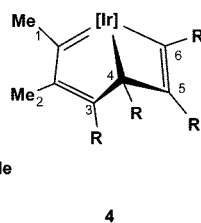
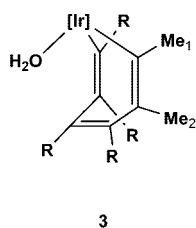
The metallacyclopentadiene $Tp^{Me_2}Ir(C(R)=C(R)C(R)=C(R))(H_2O)$ (**1**) was obtained as reported previously.⁴

Compounds 3 and 4. To a suspension of **1** in C_6H_{12} (0.6 g, 0.76 mmol; 8 mL) $MeC\equiv CMe$ (6 mL of a 0.5 M solution in C_6H_{12} , 3 mmol) was added, and the mixture was stirred at 90 °C for 12 h. Thereafter the green solution was taken to dryness and formation of compounds **3** and **4** (80% spectroscopic yield) was ascertained by 1H NMR. A pure mixture of **3** and **4** was isolated by column chromatography (silica gel), using a 1:1 mixture of hexane/ Et_2O as eluent (64% yield). Upon crystallization from pentane/ CH_2Cl_2 (1:1) at -20 °C, the mixture of yellow (compound **3**) and green

Table 5. Selected Bond Lengths (Å) and Angles (deg) for $11 \cdot 2\text{CH}_2\text{Cl}_2$

Ir–N(12)	2.023(10)	C(42)–C(61)	1.634(16)
Ir–N(22)	2.105(10)	C(42)–C(71)	1.510(16)
Ir–N(32)	2.199(10)	C(43)–C(53)	1.339(17)
Ir–O(45)	2.112(8)	C(52)–C(53)	1.452(16)
Ir–C(61)	1.991(12)	C(52)–C(71)	1.392(16)
Ir–C(72)	2.172(12)	C(61)–C(62)	1.290(14)
C(42)–C(43)	1.471(16)	C(71)–C(72)	1.453(15)
N(12)–Ir–N(22)	89.6(4)	N(22)–Ir–C(72)	175.9(5)
N(12)–Ir–N(32)	91.3(4)	N(32)–Ir–O(45)	93.1(4)
N(12)–Ir–O(45)	174.9(4)	N(32)–Ir–C(61)	173.1(5)
N(12)–Ir–C(61)	93.9(4)	N(32)–Ir–C(72)	102.6(4)
N(12)–Ir–C(72)	90.6(5)	O(45)–Ir–C(61)	81.9(4)
N(22)–Ir–N(32)	81.5(4)	O(45)–Ir–C(72)	86.0(4)
N(22)–Ir–O(45)	93.5(4)	C(61)–Ir–C(72)	81.9(5)
N(22)–Ir–C(61)	94.0(5)		

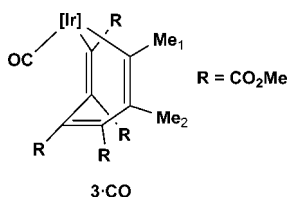
crystals (compound **4**) obtained was decanted from the mother liquor and dried in vacuo. **3** and **4** were carefully separated by hand to obtain pure samples of both compounds.



3: ^1H NMR (CD_3COCD_3 , 25 °C): δ 5.74, 5.71, 5.67 (s, 1 H each, 3 CH_{pz}), 3.82, 3.54, 3.47, 2.89 (s, 3 H each, 4 CO_2Me), 2.36, 2.33, 2.31, 2.08, 1.97, 1.96 (s, 3 H each, 6 Me_{pz}), 1.90 (s, 3 H, Me_2), 1.17 (s, 3 H, Me_1). $^{13}\text{C}\{^1\text{H}\}$ NMR (CD_3COCD_3 , 25 °C): δ 178.1, 175.0, 169.6, 166.0 (CO_2Me), 161.3, 147.6, 132.7, 126.2 (CCO_2Me), 154.6, 153.3, 151.0, 145.0, 144.4, 143.4 (C_{qppz}), 146.9, 125.9 (CMe), 107.8, 107.3, 106.9 (CH_{pz}), 53.1, 52.1, 51.6, 50.3 (CO_2Me), 29.2 (Me_1), 17.3 (Me_2), 16.4, 15.4, 13.3, 12.6, 12.4, 12.3 (Me_{pz}). IR (Nujol): $\nu(\text{OH})$ 3333 cm^{-1} . Anal. Calcd for $\text{C}_{31}\text{H}_{42}\text{BN}_6\text{O}_8\text{Ir} \cdot 0.5\text{CH}_2\text{Cl}_2$: C, 42.6; H, 4.8; N, 9.5. Found: C, 42.7; H, 4.7; N, 9.6.

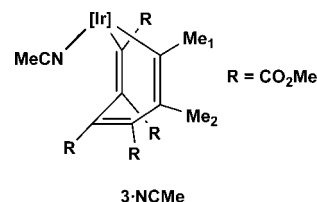
4: ^1H NMR (CDCl_3 , 25 °C): δ 5.81, 5.67, 5.63 (s, 1 H each, 3 CH_{pz}), 3.86, 3.71, 3.49, 3.34 (s, 3 H each, 4 CO_2Me), 2.57 (s, 3 H, Me_2), 2.46, 2.44, 2.42, 2.37, 1.80, 1.68 (s, 3 H each, 6 Me_{pz}), 1.04 (s, 3 H, Me_1). $^{13}\text{C}\{^1\text{H}\}$ NMR (CDCl_3 , 25 °C): δ 275.1 (C^1), 173.6, 172.2, 167.7, 163.0 (CO_2Me), 165.1, 162.1 (C^2 and C^3), 154.8, 151.9, 149.3, 143.8, 143.5 (1:1:1:1:2, C_{qppz}), 141.3, 135.4 (C^5 and C^6), 109.4, 107.7, 106.3 (CH_{pz}), 51.9, 51.2, 51.1, 50.8 (CO_2Me), 45.1 (Me_1), 20.4 (C^4), 15.0, 14.2, 14.0, 13.2, 12.8, 12.7 (Me_{pz}), 13.9 (Me_2). Anal. Calcd for $\text{C}_{31}\text{H}_{40}\text{BN}_6\text{O}_8\text{Ir} \cdot \text{CH}_2\text{Cl}_2$: C, 42.1; H, 4.6; N, 9.5. Found: C, 42.9; H, 4.7; N, 9.5.

Compound 3·CO. A solution of **4** in C_6H_{12} (0.05 g, 0.06 mmol; 3 mL) was placed in a Fischer-Porter vessel, and the stirred mixture was heated under 2 atm of CO at 90 °C for 12 h. Thereafter, the pale yellow solution was taken to dryness, and quantitative conversion into **3·CO** was ascertained by ^1H NMR. It was crystallized (pale yellow crystals) from its concentrated solutions in hexane/ CH_2Cl_2 (1:1) upon cooling at –20 °C. Alternatively, this compound can be prepared from **3** or from a mixture of **3** and **4**, following the method described above.



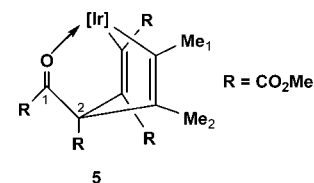
^1H NMR (CDCl_3 , 25 °C): δ 5.81, 5.78, 5.77 (s, 1 H each, 3 CH_{pz}), 3.86, 3.68, 3.63, 3.09 (s, 3 H each, 4 CO_2Me), 2.36, 2.34, 2.27, 2.19, 2.16 (s, 2:1:1:1:1, 6 Me_{pz}), 1.89 (s, 3 H, Me_2), 1.39 (s, 3 H, Me_1). $^{13}\text{C}\{^1\text{H}\}$ NMR (CDCl_3 , 25 °C): δ 173.6, 170.4, 167.3, 165.6 (CO_2Me), 165.3 (CO), 153.1, 152.6, 151.1, 144.3, 143.3 (1:1:1:2:1, C_{qppz}), 152.1, 145.4, 135.9, 126.6 (CCO_2Me), 141.8, 131.1 (CMe), 107.5, 106.9, 106.7 (CH_{pz}), 52.1, 51.9, 51.8, 50.7 (CO_2Me), 28.2 (Me_1), 16.9 (Me_2), 15.7, 14.3, 13.6, 13.0, 12.6, 12.5 (Me_{pz}). IR (Nujol): $\nu(\text{CO})$ 2046 cm^{-1} . Anal. Calcd for $\text{C}_{32}\text{H}_{40}\text{BN}_6\text{IrO}_9 \cdot \text{CH}_2\text{Cl}_2$: C, 43.5; H, 4.7; N, 9.4. Found: C, 44.0; H, 4.6; N, 9.6.

Compound 3·NCMe. A solution of **4** in CH_3CN (0.05 g, 0.06 mmol; 3 mL) was stirred at room temperature for 12 h. Thereafter the yellow solution was taken to dryness and quantitative conversion into **3·NCMe** was ascertained by ^1H NMR. This compound was purified by crystallization (yellow crystals) from hexane/ CH_2Cl_2 (1:1) at –20 °C. Alternatively, **3·NCMe** can be prepared from **3** or from a mixture of **3** and **4**, following the method described above.



^1H NMR (CDCl_3 , 25 °C): δ 5.76, 5.72, 5.67 (s, 1 H each, 3 CH_{pz}), 3.85, 3.64, 3.61, 3.05 (s, 3 H each, 4 CO_2Me), 2.37 (s, 3 H, NCMe), 2.35, 2.34, 2.22, 2.13, 2.09 (s, 2:1:1:1:1, 6 Me_{pz}), 1.89 (s, 3 H, Me_2), 1.26 (s, 3 H, Me_1). $^{13}\text{C}\{^1\text{H}\}$ NMR (CDCl_3 , 25 °C): δ 176.9, 172.8, 169.7, 165.9 (CO_2Me), 153.8 (1 CCO_2Me + 1 C_{qppz}), 151.8, 150.3, 144.0, 143.7, 142.8 (C_{qppz}), 150.0, 133.1, 123.5 (CCO_2Me), 145.9, 128.3 (CMe), 120.7 (MeCN), 107.2, 106.8, 106.6 (CH_{pz}), 52.0, 51.9, 51.7, 50.6 (CO_2Me), 29.5 (Me_1), 17.4 (Me_2), 16.3, 14.1, 13.6, 13.0, 12.8, 12.7 (Me_{pz}), 4.6 (MeCN). Anal. Calcd for $\text{C}_{33}\text{H}_{43}\text{BN}_7\text{O}_8\text{Ir} \cdot 0.5\text{CH}_2\text{Cl}_2$: C, 44.2; H, 4.8; N, 10.8. Found: C, 43.7; H, 4.8; N, 10.8.

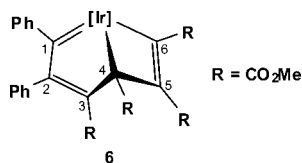
Compound 5. To a solution of **4** in CH_2Cl_2 (0.02 g, 0.024 mmol; 3 mL) was added an excess of $^t\text{BuOOH}$ (~0.05 mL, 0.53 mmol) and the mixture stirred at room temperature for 12 h. Thereafter the red solution was taken to dryness and the residue subjected to several cycles of adding Et_2O and evaporation in vacuo to eliminate the excess peroxide. Quantitative conversion into **5** was ascertained by ^1H NMR. Alternatively, **5** can be prepared from **3** or from a mixture of **3** and **4**, following the method described above.



^1H NMR (CDCl_3 , 25 °C): δ 5.80, 5.69, 5.67 (s, 1 H each, 3 CH_{pz}), 3.95, 3.83, 3.64, 3.23 (s, 3 H each, 4 CO_2Me), 2.45, 2.34, 1.94, 1.65, 1.61 (s, 1:2:1:1:1, 6 Me_{pz}), 1.96 (s, 3 H, Me_2), 1.52 (s, 3 H, Me_1). $^{13}\text{C}\{^1\text{H}\}$ NMR (CDCl_3 , 25 °C): δ 209.1 (C^1), 173.9, 171.5, 166.0, 164.9 (CO_2Me), 154.1, 152.1, 151.2, 144.2, 143.5 (1:1:1:1:2, C_{qppz}), 150.5, 114.9 (CMe), 160.8, 127.2 (CCO_2Me), 107.1, 106.9, 106.8 (CH_{pz}), 77.5 (C^2), 53.4, 52.3, 52.1, 50.8 (CO_2Me), 24.2 (Me_1), 16.5 (Me_2), 16.1, 13.6, 13.3, 12.7, 12.6, 12.1 (6 Me_{pz}). Anal. Calcd for $\text{C}_{31}\text{H}_{40}\text{BN}_6\text{O}_9\text{Ir} \cdot 0.5\text{CH}_2\text{Cl}_2$: C, 42.7; H, 4.6; N, 9.5. Found: C, 42.5; H, 4.8; N, 9.4.

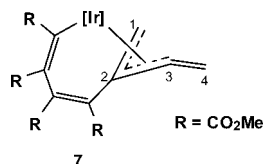
Compound 6. To a suspension of **1** in cyclohexane (0.6 g, 0.76 mmol; 8 mL) was added $\text{PhC}\equiv\text{CPh}$ (3.03 mmol, 0.540 g) and the resulting mixture stirred at 90 °C for 12 h. Thereafter the dark brown

solution was dried under vacuum, and the ^1H NMR spectrum of the residue revealed that **6** had been formed in 80% spectroscopic yield.



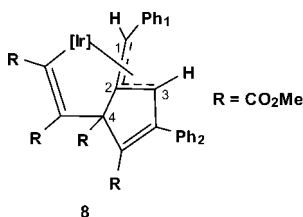
^1H NMR (CDCl_3 , 25 $^\circ\text{C}$): δ 7.96, 7.45, 7.31, 7.24, 6.87, 6.45 (d, t, t, t, d, 2:1:2:2:1:2, 10 CH_{ar}), 5.75, 5.65, 5.34 (s, 1 H each, 3 CH_{pz}), 3.56, 3.54, 3.30, 3.14 (s, 3 H each, 4 CO_2Me), 2.54, 2.45, 2.39, 2.38, 2.11, 1.06 (s, 3 H each, 6 Me_{pz}). $^{13}\text{C}\{^1\text{H}\}$ NMR (CDCl_3 , 25 $^\circ\text{C}$): δ 241.0 (C^1), 186.7 (C^2), 174.3, 171.8, 168.1, 162.6 (CO_2Me), 166.0 (C^3), 157.7, 140.4 (C_{qar}), 154.0, 153.8, 151.2, 144.0, 143.6, 143.3 (C_{qpz}), 140.2, 136.8 (C^5 and C^6), 129.0, 128.5, 127.4, 127.3, 127.2, 121.6 (1:2:2:2:2:1, CH_{ar}), 109.4, 108.3, 105.8 (CH_{pz}), 51.7, 51.2, 51.0, 50.4 (CO_2Me), 26.0 (C^4), 15.8, 15.0, 13.2, 13.0, 12.9, 12.8 (Me_{pz}).

Compound 7. To a suspension of **1** in cyclohexane (0.05 g, 0.063 mmol; 5 mL) was added $\text{Me}_3\text{SiC}\equiv\text{CSiMe}_3$ (28.6 μL , 0.126 mmol) and the suspension stirred at 120 $^\circ\text{C}$ for 24 h. After that, the solvent was removed under reduced pressure, and formation of compound **7** (~75% spectroscopic yield) was ascertained by ^1H NMR. This compound was purified by column chromatography on silica gel using hexane/ Et_2O (1:1 \rightarrow 1:3) mixtures as eluent (yellow microcrystalline solid). Yield: 58%. R_f = 0.12 [silica gel, hexane/ Et_2O (1:3)].



^1H NMR (CDCl_3 , 25 $^\circ\text{C}$): δ 5.89, 5.86, 5.49 (s, 1 H each, 3 CH_{pz}), 5.31, 4.52 (d, 1 H each, $^2J_{\text{HH}} = 1.6$ Hz, C^4H_2), 4.41, 3.54 (d, 1 H each, $^2J_{\text{HH}} = 1.6$ Hz, C^1H_2), 3.89, 3.77, 3.43, 2.82 (s, 3 H each, 4 CO_2Me), 2.43, 2.27, 2.15, 1.82 (s, 2:2:1:1, 6 Me_{pz}). $^{13}\text{C}\{^1\text{H}\}$ NMR (CDCl_3 , 25 $^\circ\text{C}$): δ 173.2, 169.0, 167.1, 164.5 (CO_2Me), 153.1, 152.4, 150.6, 144.4, 143.3, 143.3 (C_{qpz}), 147.1, 141.1, 131.8, 116.4 (CCO_2Me), 141.9 (C^3), 108.7, 106.6, 106.3 (CH_{pz}), 100.3 (C^4 , $^1J_{\text{CH}} = 160$ Hz), 86.1 (C^2), 52.8, 52.4, 51.9, 50.8 (CO_2Me), 27.5 (C^1 , $^1J_{\text{CH}} = 160$ Hz), 15.8, 15.4, 14.1, 12.9, 12.7, 12.6 (Me_{pz}). Anal. Calcd for $\text{C}_{31}\text{H}_{38}\text{BN}_6\text{O}_8\text{Ir}\cdot 0.5\text{CH}_2\text{Cl}_2$: C, 43.6; H, 4.5; N, 9.6. Found: C, 43.8; H, 4.8; N, 9.3.

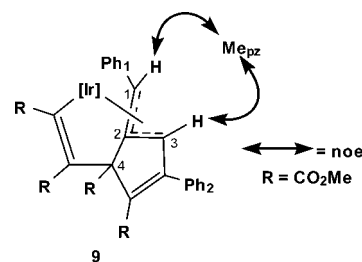
Compound 8. **1** was suspended in cyclohexane (0.4 g, 0.506 mmol; 8 mL), and $\text{PhC}\equiv\text{CH}$ (0.22 mL, 2.02 mmol) was added. The mixture was stirred at 90 $^\circ\text{C}$ for 12 h, and then the solvent was removed under reduced pressure. Formation of compound **8** (60% spectroscopic yield) was determined by ^1H NMR, and the crude product was purified by column chromatography on silica gel using a mixture of hexane/ Et_2O (1:1) as eluent (pale yellow crystals). Yield: 32%.



^1H NMR (CDCl_3 , 25 $^\circ\text{C}$): δ 7.41 (m, 2 H, 2 $\text{CH}_{\text{ar}}(\text{Ph}_2)$), 7.23 (m, 3 H, 3 $\text{CH}_{\text{ar}}(\text{Ph}_2)$), 7.02 (t, 2 H, 2 $\text{CH}_{\text{ar}}(\text{Ph}_1)$), 6.89 (br s, 3 H, 3 $\text{CH}_{\text{ar}}(\text{Ph}_1)$), 6.37 (s, 1 H, C^1H), 6.22 (s, 1 H, C^3H), 5.95, 5.66,

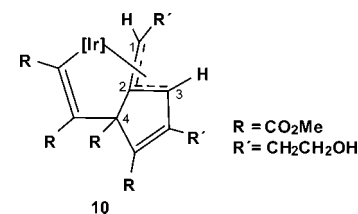
5.29 (s, 1 H each, 3 CH_{pz}), 3.97, 3.67, 3.59, 3.04 (s, 3 H each, 4 CO_2Me), 2.50, 2.41, 2.38, 2.34, 1.59, 0.83 (s, 3 H each, 6 Me_{pz}). $^{13}\text{C}\{^1\text{H}\}$ NMR (CDCl_3 , 25 $^\circ\text{C}$): δ 172.0, 171.2, 166.6, 164.9 (CO_2Me), 155.2, 155.1, 151.9, 144.3, 143.7, 143.2 (C_{qpz}), 151.8 (CPh_2), 145.3, 142.3, 125.1 (CCO_2Me), 141.5 ($\text{C}_{\text{qar}}(\text{Ph}_1)$), 135.0 ($\text{C}_{\text{qar}}(\text{Ph}_2)$), 130.0 (br, *o*, *o'*- $\text{CH}_{\text{ar}}(\text{Ph}_1)$), 128.9 (*o*, *o'*- $\text{CH}_{\text{ar}}(\text{Ph}_2)$), 128.7 (*p*- $\text{CH}_{\text{ar}}(\text{Ph}_2)$), 128.2, 128.0 (*m*, *m'*- $\text{CH}_{\text{ar}}(\text{Ph}_1)$) and *m*, *m'*- $\text{CH}_{\text{ar}}(\text{Ph}_2)$ respectively), 126.1 (*p*- $\text{CH}_{\text{ar}}(\text{Ph}_1)$), 116.6 (C^2), 108.8, 108.3, 106.8 (CH_{pz}), 72.1 (C^4), 60.5 (C^3 , $^1J_{\text{CH}} = 171$ Hz), 52.8, 51.7, 51.4, 50.7 (CO_2Me), 39.0 (C^1 , $^1J_{\text{CH}} = 151$ Hz), 16.9, 13.7, 13.5, 13.1, 12.9 (1:1:1:1:2, Me_{pz}). Anal. Calcd for $\text{C}_{43}\text{H}_{46}\text{BN}_6\text{O}_8\text{Ir}\cdot 0.5\text{CH}_2\text{Cl}_2$: C, 51.2; H, 4.6; N, 8.2. Found: C, 51.3; H, 4.7; N, 7.8.

Compound 9. **1** was suspended in cyclohexane (0.1 g, 0.126 mmol; 4 mL), and $\text{PhC}\equiv\text{CSiMe}_3$ (99.1 μL , 0.504 mmol) was added. The resulting mixture was stirred at 90 $^\circ\text{C}$ for 12 h, and the solvent was removed under vacuum. ^1H NMR monitoring of the crude of the reaction showed formation of compound **9** in 80% spectroscopic yield. This complex was purified by column chromatography on silica gel using a mixture of hexane/ Et_2O (1:1) as eluent. Yield: 58%.



^1H NMR (CDCl_3 , 25 $^\circ\text{C}$): δ 7.59 (br d, 2 H, 2 $\text{CH}_{\text{ar}}(\text{Ph}_1)$), 7.26 (m, 3 H, 3 $\text{CH}_{\text{ar}}(\text{Ph}_1)$), 6.91 (t, 1 H, 1 $\text{CH}_{\text{ar}}(\text{Ph}_2)$), 6.78 (t, 2 H, 2 $\text{CH}_{\text{ar}}(\text{Ph}_2)$), 6.74 (s, 1 H, C^3H), 6.47 (d, 2 H, 2 $\text{CH}_{\text{ar}}(\text{Ph}_2)$), 5.90 (s, 1 H, C^1H), 5.62, 5.60, 5.55 (s, 1 H each, 3 CH_{pz}), 3.86, 3.82, 3.43, 2.77 (s, 3 H each, 4 CO_2Me), 2.47, 2.43, 2.42, 2.12, 1.61, 1.07 (s, 3 H each, 6 Me_{pz}). $^{13}\text{C}\{^1\text{H}\}$ NMR (CDCl_3 , 25 $^\circ\text{C}$): δ 172.8, 168.9, 167.4, 163.9 (CO_2Me), 154.8, 154.6, 152.0, 143.9, 143.7, 143.7 (C_{qpz}), 144.0 (CPh_2), 143.0, 135.3, 127.7 (CCO_2Me), 140.3 ($\text{C}_{\text{qar}}(\text{Ph}_1)$), 137.1 ($\text{C}_{\text{qar}}(\text{Ph}_2)$), 130.1 (*o*, *o'*- $\text{CH}_{\text{ar}}(\text{Ph}_1)$), 129.1 (*m*, *m'*- $\text{CH}_{\text{ar}}(\text{Ph}_1)$), 127.4, 127.3 (*o*, *o'*, *m*, *m'*- $\text{CH}_{\text{ar}}(\text{Ph}_2)$), 126.8 (*p*- $\text{CH}_{\text{ar}}(\text{Ph}_1)$), 125.8 (*p*- $\text{CH}_{\text{ar}}(\text{Ph}_2)$), 118.0 (C^3 , $^1J_{\text{CH}} = 154$ Hz), 116.0 (C^2), 109.6, 106.7, 106.4 (CH_{pz}), 87.5 (C^4), 53.0, 52.6, 52.0, 50.8 (CO_2Me), 52.2 (C^1 , $^1J_{\text{CH}} = 158$ Hz), 15.0, 14.4, 13.5, 13.1, 12.9, 12.8 (Me_{pz}).

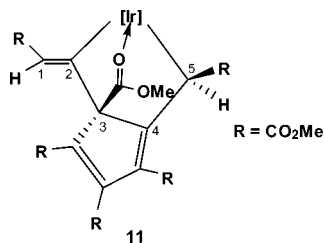
Compound 10. To a suspension of **1** in cyclohexane (0.1 g, 0.126 mmol; 8 mL) was added $\text{HC}\equiv\text{CCH}_2\text{CH}_2\text{OH}$ (28.7 μL , 0.379 mmol), and the mixture was stirred at 90 $^\circ\text{C}$ for 12 h. Thereafter the solvent was removed under reduced pressure, and the formation of compound **10** in ~85% spectroscopic yield was determined by ^1H NMR. This complex was purified by column chromatography on silica gel using $\text{Et}_2\text{O} \rightarrow \text{Et}_2\text{O}/\text{AcOEt}$ (1:1) as eluent. Yield: 56%.



R_f = 0.39 [silica gel, $\text{Et}_2\text{O}/\text{AcOEt}$ (1:3)]. ^1H NMR (CDCl_3 , 25 $^\circ\text{C}$): δ 6.20 (s, 1 H, C^3H), 5.82, 5.76, 5.64 (s, 1 H each, 3 CH_{pz}), 5.03 (dd, 1 H, $^3J_{\text{HH}} = 11.2$, 4 Hz, C^1H), 3.90, 3.80, (m, 1 H each, $\text{CCH}_2\text{CH}_2\text{OH}$), 3.84, 3.65, 3.57, 3.01 (s, 3 H each, 4 CO_2Me), 3.75, 3.60 (m, 1 H each, $\text{C}^1\text{CH}_2\text{CH}_2\text{OH}$), 3.24, 2.65 (ddd, dt, 1 H each, $^3J_{\text{HH}} = 14.9$, 9.5, 4.9 Hz; $^2J_{\text{HH}} = 13.5$, $^3J_{\text{HH}} = 5.2$ Hz, $\text{CCH}_2\text{CH}_2\text{OH}$), 2.38, 2.37, 2.32, 2.29, 2.25, 1.65 (s, 3 H each, 6 Me_{pz}), 1.65, 1.55

(m, 1 H each, $C^1CH_2CH_2OH$). Signals of the OH groups have not been located. $^{13}C\{^1H\}$ NMR ($CDCl_3$, 25 °C): δ 172.6, 171.9, 166.9, 165.3 (CO_2Me), 158.1 (CCH_2CH_2OH), 154.6, 153.8, 149.7, 144.4, 144.2, 143.2 (C_{qpz}), 144.5, 142.9, 127.0 (CCO_2Me), 116.8 (C^2), 110.2, 108.2, 106.6 (CH_{pz}), 71.3 (C^4), 63.3 ($C^1CH_2CH_2OH$, $^1J_{CH} = 141$ Hz), 61.7 (CCH_2CH_2OH , $^1J_{CH} = 145$ Hz), 58.2 (C^3 , $^1J_{CH} = 168$ Hz), 53.4, 51.5, 51.4, 50.6 (CO_2Me), 40.6 (C^1 , $^1J_{CH} = 147$ Hz), 34.5 ($C^1CH_2CH_2OH$, $^1J_{CH} = 126$ Hz), 33.6 (CCH_2CH_2OH , $^1J_{CH} = 128$ Hz), 17.0, 16.4, 15.2, 13.3, 12.8, 12.7 (Me_{pz}). IR (Nujol): ν (OH) 3439 (br) cm^{-1} .

Compound 11. To a suspension of **1** in cyclohexane (0.1 g, 0.126 mmol; 8 mL) was added $HC\equiv CCO_2Me$ (22.5 μL , 0.253 mmol), and the mixture was stirred at 90 °C for 12 h. The solvent was removed under reduced pressure, and 1H NMR monitoring of the crude of the reaction showed formation of complex **11** in ~85% spectroscopic yield. **11** was purified by crystallization from a pentane/ CH_2Cl_2 (1:1) mixture at -20 °C (bright yellow crystals). Yield: 54%.



1H NMR ($CDCl_3$, 25 °C): δ 5.92 (s, 1 H, C^1H), 5.82, 5.69, 5.61 (s, 1 H each, 3 CH_{pz}), 5.59 (s, 1 H, C^5H), 4.05, 3.95, 3.76, 3.70, 3.47, 2.50 (s, 3 H each, 6 CO_2Me), 2.45, 2.39, 2.34, 2.19, 1.98, 1.92 (s, 3 H each, 6 Me_{pz}). $^{13}C\{^1H\}$ NMR ($CDCl_3$, 25 °C): δ 183.3, 168.6, 165.4, 162.6, 161.5 (2:1:1:1:1, CO_2Me), 181.2 (C^4), 151.3, 128.9 (CCO_2Me), 150.7 (C^2), 152.4, 150.3, 144.5, 143.2, 142.1 (2:1:1:1:1, C_{qpz}), 123.0 (C^1 , $^1J_{CH} = 157$ Hz), 108.3, 107.7, 106.5 (CH_{pz}), 94.1 (C^3), 57.2, 52.6, 52.1, 51.8, 51.3, 50.4 (CO_2Me), 14.4, 13.0, 13.0, 12.7, 12.3 (1:1:1:2:1, Me_{pz}), 8.1 (C^5 , $^1J_{CH} = 139$ Hz). Anal. Calcd for $C_{35}H_{42}BN_6O_{12}Ir \cdot 0.5CH_2Cl_2$: C, 43.3; H, 4.4; N, 8.5. Found: C, 43.8; H, 4.2; N, 8.4.

X-ray Structure Determination. X-ray data of complexes **3**, **4**, **8**, and **11** in the form of the solvates **3**· $CHCl_3$, **4**· CH_2Cl_2 , **8**·solv

(solv = essentially petroleum ether), and **11**· $2CH_2Cl_2$ were collected on a Bruker Smart APEX CCD area detector diffractometer using graphite-monochromated Mo $K\alpha$ radiation ($\lambda = 0.71073$ Å) and 0.3° ω -scan frames covering complete spheres of the reciprocal space with $\theta_{max} = 25-30^\circ$. After data integration with the program SAINT+ corrections for absorption, $\lambda/2$ effects, and crystal decay were applied with the program SADABS.¹⁵ The structures were solved by direct methods, expanded by Fourier syntheses, and refined on F^2 with the program suite SHELX97.¹⁶ All non-hydrogen atoms were refined anisotropically using DELU restraints for the U_{ij} of **8**·solv and **11**· $2CH_2Cl_2$. Most H atoms were placed in calculated positions and thereafter treated as riding. A torsional parameter was refined for each pyrazole-bound methyl group. The water molecule in **3**· $CHCl_3$ was idealized and refined as a rigid group. The disordered solvents in **4**· CH_2Cl_2 and **8**·solv were squeezed with the program PLATON, and modest orientation disorder of one CO_2Me group in **4**· CH_2Cl_2 and a phenyl ring in **8**·solv was taken into account.¹⁷ Crystal data and experimental details are given in Table 1, the molecular structures of the Ir complexes are shown in Figures 1, 2, 4, and 5, and selected geometric data are reported in Tables 2–5.

Acknowledgment. Financial support from the Spanish Ministerio de Ciencia e Innovación (MICINN) (projects CTQ2007-62814 and CONSOLIDER-INGENIO2010, CSD2007-006, FEDER support, and HU2003-039) and from the Junta de Andalucía is gratefully acknowledged. N.R. thanks the MEC and the CSIC for research grants.

Supporting Information Available: Complete crystallographic data and technical details in CIF format for complexes **3**, **4**, **8**, and **11**. This material is available free of charge via the Internet at <http://pubs.acs.org>.

OM8001153

(15) Bruker programs: SMART, version 5.629; SAINT+, version 6.45; SADABS, version 2.10; SHELXTL, version 6.14; Bruker AXS Inc.: Madison, WI, 2003.

(16) Sheldrick, G. M. *SHELX97: Program System for Crystal Structure Determination*; University of Göttingen: Göttingen, Germany, 1997.

(17) Spek, A. L. *PLATON: A Multipurpose Crystallographic Tool*; University of Utrecht: Utrecht, The Netherlands, 2006.

Versatile Behavior of Conjugated Diynes with Zirconocene Reactive Species

Stéphane Bredeau,^{†,‡} Esteban Ortega,[†] Geneviève Delmas,[†] Philippe Richard,[†]
Roland Fröhlich,[‡] Bruno Donnadieu,[§] Gerald Kehr,[‡] Nadine Pirió,^{*,†} Gerhard Erker,[‡] and
Philippe Meunier^{*,†}

Institut de Chimie Moléculaire de l'Université de Bourgogne (ICMUB)-UMR CNRS 5260, 9, avenue Alain Savary, BP 47870, 21078 Dijon Cedex, France, Organisch-Chemisches Institut der Universität Münster, Corrensstrasse 40, 48149 Münster, Germany, and Laboratoire de Chimie de Coordination du CNRS, 205 route de Narbonne, 31077 Toulouse cedex 4, France

Received June 4, 2008

Thermal decomposition of Cp_2ZrPh_2 in the presence of the buta-1,3-diynes $\text{RC}\equiv\text{CC}\equiv\text{CR}$ ($\text{R} = \text{Ph}$, SiMe_3) can lead to seven- or five-membered metallacycles. In both cases a stable benzo-fused seven-membered zirconacyclocumulene arising from a 2-fold insertion of the triple bonds of the dialkyne in the in situ generated zirconocene benzyne is formed. In the case of $\text{Me}_3\text{SiC}\equiv\text{CC}\equiv\text{CSiMe}_3$ a second minor complex is isolated: a 3-alkynyl-substituted zirconaindene arising from a β monoinsertion of one acetylenic function of the conjugated diyne in the zirconocene benzyne. No stable 2-alkynyl-substituted zirconacycle was isolated. This α monoinsertion complex is an intermediate in the exchange of the metalated moiety with a main-group atom (e.g., antimony) in a zirconacyclocumulene, explaining the formation of a 2-alkynyl-substituted stibaindene. In the thermal decomposition of $\text{Cp}_2\text{Zr}(\text{Me})\text{SCH}_2\text{R}^4$ ($\text{R}^4 = \text{Ph}$, $p\text{-MeOC}_6\text{H}_4$) in the presence of $\text{PhC}\equiv\text{CC}\equiv\text{CPh}$, only the α monoinsertion of one triple bond of the diacetylenic reagent in the transient zirconathiirane is observed. The 2-alkynyl-substituted five-membered zirconathiolane is isolated as a bis-sulfonium zirconocene-ate dimer. X-ray diffraction studies corroborate the molecular structure of all these zirconacyclic complexes and stibacycle.

Introduction

The search for new pathways permitting carbon–carbon and carbon–heteroatom bond formation remains among the most important goals of modern chemistry. The use of group 4 transition metal assisted methodology is one efficient tool to reach this objective.¹ Some zirconocene-based reactions were developed by our group concerning the access to main-group heterocycles not easily available by other procedures.² Our investigations were focused on the reaction of the transient zirconocene benzyne **1** with unsaturated heteroatom-containing derivatives, acetylenic substrates for the most part. We reported the preparation of 2-phosphino-1-zirconaindenes **2**³ as well as benzo–zirconacyclohexadiene–phosphacyclobutenes **3**^{4,5} or

–silacyclobutenes **4**⁵ by the coupling reaction of the benzyne complex **1** with alkynylphosphanes and bis(alkynyl)phosphanes or –silanes, respectively (Scheme 1). In the case of P-tethered diynes, 3-(alkynylphosphino)zirconaindenes **5**⁵ were also formed as minor products.

Recently, we reported the reaction of zirconocene thioaldehydes **6** with (diphenylphosphino)acetylene, leading to the sulfur-bridged binuclear α -phosphinozirconathiolanes **7** (Scheme 2).⁶

These zirconacyclic complexes were converted on one hand into a variety of mono- (**A–C**), di- (**D, E**), or tricyclic (**F, G**) derivatives incorporating one or two group 14 or 15 elements when treated with HCl or dihalogenated main-group-element reagent (Chart 1).^{3,5,7}

In the course of discovering new zirconocene-mediated methodologies of synthetic use, it was demonstrated that the zirconocene fragment [Cp_2Zr] promoted the coupling of diynes with formation of zirconacyclic cumulenes.⁸ We have established in a previous contribution that reaction of 1,4-diphenylbuta-1,3-diyne with zirconocene benzyne **1** yielded quantitatively the stable seven-membered zirconacyclocumulene **8a** (Scheme 3).⁹ In contrast, the synthesis of a metallaindene complex with an alkynyl substituent in the β -position was

* To whom correspondence should be addressed. N.P.: e-mail, Nadine.Pirió@u-bourgogne.fr; tel, +33(0)3-8039-6106; fax, +33(0)3-8039-3682. P.M.: e-mail, Philippe.Meunier@u-bourgogne.fr; tel, +33(0)3-8039-6105; fax, +33(0)3-8039-3682.

[†] Institut de Chimie Moléculaire de l'Université de Bourgogne (ICMUB)-UMR CNRS 5260.

[‡] Organisch-Chemisches Institut der Universität Münster.

[§] Laboratoire de Chimie de Coordination du CNRS.

(1) Reviews and book contributions: (a) *Titanium and Zirconium in Organic Chemistry*; Marek, I., Ed.; Wiley-VCH: Weinheim, Germany, 2002. (b) Barluenga, J.; Rodríguez, F.; Álvarez-Rodrigo, L.; Fañanás, F. J. *Chem. Soc. Rev.* **2005**, 34, 76. (c) Meunier, P.; Pirió, N. In *Encyclopedia of Inorganic Chemistry*; King, R. B., Ed.; Wiley: Chichester, U.K., 2005, 4488. (d) Marek, I.; Chinkov, N.; Levin, A. *Synlett* **2006**, 4, 501. (e) Rosenthal, U.; Burlakov, V. V.; Bach, M. A.; Beweries, T. *Chem. Soc. Rev.* **2007**, 36, 719.

(2) Majoral, J.-P.; Meunier, P.; Igau, A.; Pirió, N.; Zablocka, M.; Skowronska, A.; Bredeau, S. *Coord. Chem. Rev.* **1998**, 145, 178–180.

(3) Miquel, Y.; Igau, A.; Donnadieu, B.; Majoral, J.-P.; Dupuis, L.; Pirió, N.; Meunier, P. *Chem. Commun.* **1997**, 729.

(4) Dupuis, L.; Pirió, N.; Meunier, P.; Igau, A.; Donnadieu, B.; Majoral, J.-P. *Angew. Chem., Int. Ed. Engl.* **1997**, 9, 987.

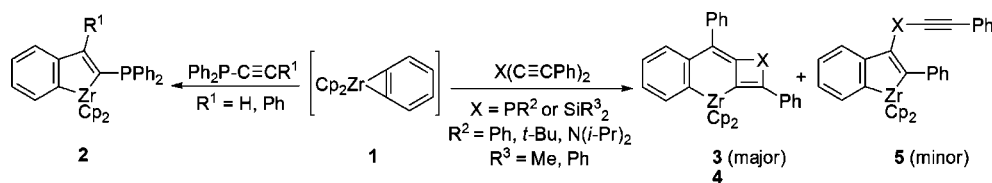
(5) Pirió, N.; Bredeau, S.; Dupuis, L.; Schütz, P.; Meunier, P.; Donnadieu, B.; Igau, A.; Majoral, J.-P. *Tetrahedron* **2004**, 1317.

(6) (a) Ortega, E.; Pirió, N.; Meunier, P.; Donnadieu, B. *Chem. Commun.* **2004**, 678. (b) Ortega, E.; Pirió, N.; Meunier, P.; Richard, P. *Acta Crystallogr., Sect. E* **2004**, E60 (2), m201.

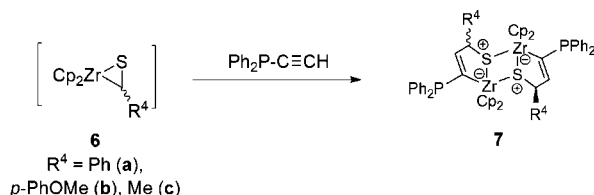
(7) Ortega, E. Ph.D. Thesis, University of Burgundy, Burgundy, France, 2003.

(8) (a) Rosenthal, U.; Pellny, P. M.; Kirchbauer, F. G.; Burlakov, V. V. *Acc. Chem. Res.* **2000**, 33, 119. (b) Rosenthal, U.; Burlakov, V. V.; Arndt, P.; Baumann, W.; Spannenberg, A. *Organometallics* **2005**, 24, 456.

Scheme 1. Reaction of Zirconocene Benzyne with Alkynylphosphanes and Bis(alkynyl)phosphanes or -silanes



Scheme 2. Reaction between Zirconocene Thioaldehydes and Alkynylphosphane



described starting from the benzyne tantalum carborane complex $(Et_2C_2B_4H_4)CpTa(\eta^2-C_6H_4)$ and $PhC\equiv CC\equiv CPh$.¹⁰ The present report aims at describing the extension of this latter reaction to another diyne (e.g., 1,4-bis(trimethylsilyl)buta-1,3-diyne) as well as to another low-valent zirconocene species (e.g., zirconocene thioaldehydes **6a,b** in Scheme 2).

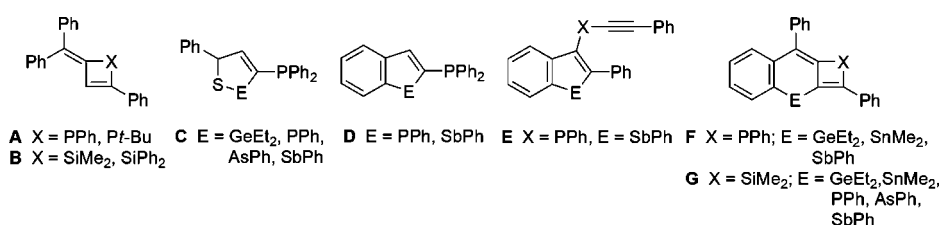
Results and Discussion

The above-mentioned reaction of **1** with 1,4-diphenylbuta-1,3-diyne provides the starting point for the current investigation. Thermolysis of Cp_2ZrPh_2 in the presence of $PhC\equiv CC\equiv CPh$ has been shown to produce only the seven-membered zirconacyclocumulene **8a** (no formation of the 3-alkynylzirconaindene **9a**) probably arising from the 2-fold insertion of the two carbon-carbon triple bonds of the diyne into the zirconium-carbon bond of the in situ generated complex **1** via the formation of the 2-alkynylzirconaindene intermediate **8'a** (Scheme 3). Such a two-step mechanism was already evidenced in the formation of the benzo-zirconacyclohexadiene-phosphacyclobutenes **3a-c** resulting from reaction of P-tethered diynes and diphenylzirconocene.⁵ Nevertheless, the postulated intermediate **8'a** was never observed in the reaction mixture. Therefore, a variable-temperature NMR study was realized. At ambient temperature only one bis(cyclopentadienyl)zirconium complex is formed quantitatively ($\delta_{H}(Cp)$ 5.62 ppm) corresponding to complex **8a**. In a $CDFCl_2/CDF_2Cl/CD_2Cl_2$ solvent mixture¹¹ at lower temperature (213 K) no chemical shift corresponding to the intermediate **8'a** is detected in the expected range for a Cp ring. The $8a \rightleftharpoons 8'a$ equilibration is probably too fast on the NMR time scale, indicating that in our case the 2-alkynylzirconaindene **8'a** represents a high-lying intermediate. This feature is probably due to the remarkable stability of complex **8a** as evidenced by DFT calculations reported elsewhere⁹ resulting directly from the interaction between the d_{xy} metal atomic orbital with one terminal σ orbital and with the in-plane π orbital of the cumulene.

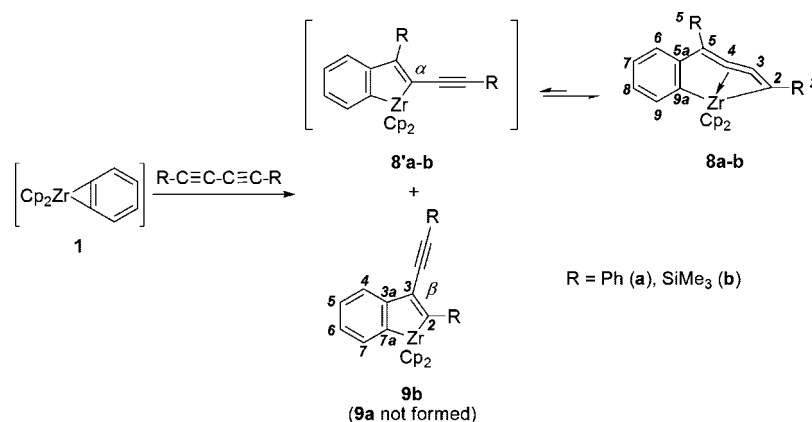
In order to gain a deeper understanding of the coupling reaction of buta-1,3-diyne with zirconocene benzyne **1**, the analogous reaction was performed with the more hindered 1,4-bis(trimethylsilyl)-1,3-butadiyne. A toluene solution of $Me_3SiC\equiv CC\equiv CSiMe_3$ and Cp_2ZrPh_2 heated up at 80 °C over 15 h led to the formation of two complexes as shown by the usual spectroscopic and analytical methods (Scheme 3).

The ¹H NMR spectrum of the crude product exhibits two cyclopentadienyl signals at 5.83 (minor) and 5.23 (major) ppm as well as two pairs of trimethylsilyl signals at 0.40, 0.33 (major) and 0.23, 0.19 (minor) ppm, allowing us to conclude that two bis(cyclopentadienyl)zirconium complexes are formed in a 10:5.2 ratio. The ²⁹Si NMR spectrum is in agreement with the formation of two zirconium complexes, as two pairs of chemical shifts at -24.1, -20.0 (minor) and -15.1, -12.3 (major) ppm are detected. The ¹³C NMR data are also consistent with a reaction yielding a pair of products. The mass spectrum (EI 70 eV) shows only one molecular ion peak $[M]^+$ at m/z 490, indicative of two mononuclear complexes with the same molecular formula. IR data are also instructive, as two characteristic absorption bands appeared at 1874 and 2126 cm^{-1} which can be assigned to a $>C=C=C=C<$ and $-C\equiv C-$ units, respectively. All these data are in agreement with a seven-membered zirconacyclocumulene as well as with a five-membered zirconacycle containing a pendant triple carbon-carbon bond. One might suppose that these two complexes are the expected zirconacyclocumulene **8b** and the intermediary species 2-alkynylzirconaindene **8'b**, arising respectively from the double and single insertion of the acetylenic function of the starting buta-1,3-diyne in the zirconium-carbon bond of the zirconocene benzyne **1** (Scheme 4). In order to displace this $8b \rightleftharpoons 8'b$ equilibration, some ¹H and ¹³C NMR experiments were carried out at higher temperature in toluene-*d*₈ ($T = 368$ K). However, the cyclopentadienyl resonances are not modified in terms of chemical shifts and ratios. Moreover, the respective proportions of the two complexes remain the same after 21 days of heating at 90 °C and 8 days more at 110 °C. Consequently, identification based only on spectroscopic data was uncertain. In order to complete the characterization of these zirconacycles, suitable crystals for X-ray diffraction study were obtained by recrystallization from pentane. Figures 1 and 2 show the ORTEP views of the two different complexes contained surprisingly in the same cell unit: the seven-membered zirconacyclocumulene **8b** and the five-membered zirconaindene **9b**. Important bond lengths and angles are also summarized. On one hand the solid-state structure shows that the compound **8b** has the expected

Chart 1. Diversity of Heterocycles Coming from Zirconacycles 3-7



Scheme 3. Reactivity of Zirconocene Benzyne with Conjugated Dienes



conjugated arrangement and is very similar to that of the previously described cyclic complex **8a**.⁹ Structural features for similar highly strained cyclic zirconacyclocumulenes already reported in the literature¹² closely resemble those in **8b**. The molecular structure reveals a characteristic bent-metalocene arrangement of the ligands around zirconium. The angle between the geometrical centers of both Cp rings and the zirconium is 131.8°.

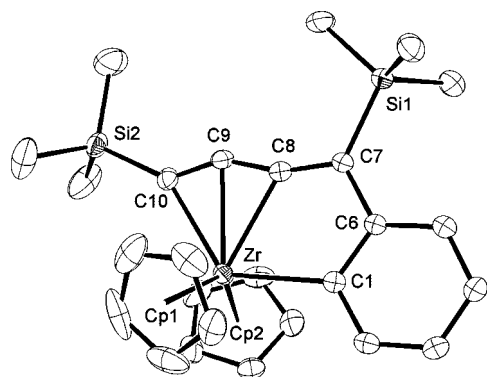


Figure 1. ORTEP view of **8b**. Selected bond lengths (Å) and angles (deg): Zr–C1 = 2.393(3), Zr–C10 = 2.454(3), Zr–C9 = 2.435(3), Zr–C8 = 2.430(3), C10–C9 = 1.275(5), C9–C8 = 1.327(5), C8–C7 = 1.338(5), C7–C6 = 1.477(4); Cp1–Zr–Cp2 = 131.8, C1–Zr–C10 = 127.43(11), C10–C9–C8 = 149.7(3), C9–C8–C7 = 160.8(3).

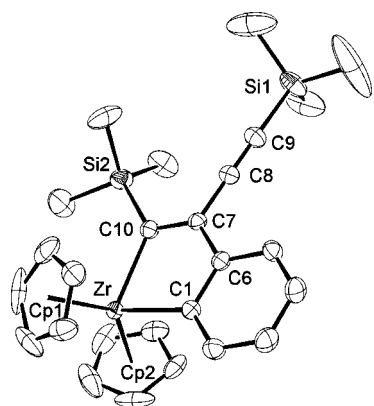


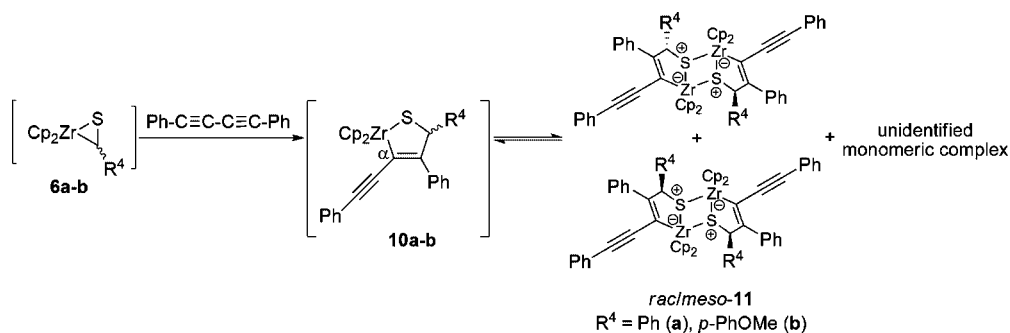
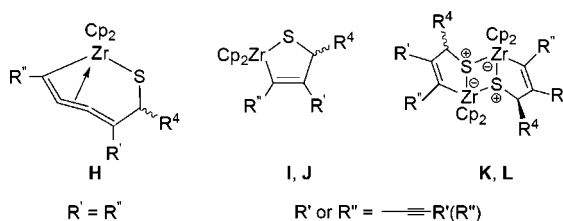
Figure 2. ORTEP view of **9b**. Selected bond lengths (Å) and angles (deg): Zr–C1 = 2.270(3), Zr–C10 = 2.276(3), C10–C7 = 1.369(4), C7–C6 = 1.488(5), C8–C9 = 1.199(5), C10–Si = 1.874(4), C9–Si = 1.839(4); Cp1–Zr–Cp2 = 137.4, C1–Zr–C10 = 79.03(12), C7–C8–C9 = 177.9(4), C8–C9–Si = 173.0(4), C10–C7–C8 = 121.4(3), C10–C7–C6 = 122.3(3), C6–C7–C8 = 116.3(3).

The four Zr–C(sp²) bond lengths are 2.454(3), 2.435(3), 2.430(3), and 2.393(3) Å for Zr–C10, Zr–C9, Zr–C8, and Zr–C1, respectively. The C1–Zr–C10 angle is relatively open at 127.43(11)°, pointing out that the zirconacycle is practically planar. The bond lengths for C10–C9, C9–C8, C8–C7, and C7–C6 are about 1.30 Å, indicating the same bond order. The angle values for C10–C9–C8 and C9–C8–C7 (149.7(3) and 160.8(3)°, respectively) are quite far from the theoretical value of 180°, but they agree with a deformed cumulene fragment in order to decrease the cyclic strain. These data corroborate the ones already described for **8a**. Indeed, the molecular structures of **8a** and **8b** closely resemble each other, differences coming only from the substituent of the starting 1,3-diyne (Ph versus SiMe₃). On the other hand, the molecular structure of the unforeseen 3-alkynyl-substituted zirconaindene **9b** is clearly evidenced. Similar to the structural features mentioned above for **8b**, the two zirconium–carbon(sp²) distances Zr–C10 and Zr–C1 and the angle values C10–Zr–C1 and Cp1–Zr–Cp2 clearly confirmed the bent character of **9b**. Moreover, the C8–C9 distance (1.199(5) Å) is representative of a triple carbon–carbon bond. The C7–C8–C9 (177.9(4)°) and C8–C9–Si (173.0(4)°) angles are in good agreement with a linear C≡CSiMe₃ unit. The molecular structure is comparable to that observed for the 3-(alkynylphosphino)stibaindene **E** (Chart 1) previously structurally characterized starting from **5a** by an exchange reaction with PhSbCl₂.⁵ Therefore, these results clearly demonstrated that, depending on the nature of the substituent of the acetylenic reagent, two types of zirconacycles are formed. On the basis of NMR experiments and X-ray diffraction studies, we can propose the mechanism outlined in Scheme 3 for the preparation of five- and seven-membered zirconacycles (**9a,b**, **8a,b**): (i) formation of the α-regioisomeric zirconacycles **8a,b** arising from the insertion reaction of one of the C≡C triple bonds of the buta-1,3-diyne into a Zr–C bond of the transient zirconocene benzyne **1** and (ii) rapid intramolecular insertion reaction of the second alkynyl group into a Zr–C bond of the intermediates **8'a,b** providing the highly stabilized seven-membered zirconacyclocumulenes **8a,b**. Nevertheless, due to the probably strong steric interaction between the trimethylsilyl group and zirconium (this interaction being lower in the case of the phenyl substituent), the β-regioisomeric zirconacycle **9b** is also formed. It is noteworthy that it is not possible to further transform this latter complex because of its regiochemistry. A

(9) Bredeau, S.; Delmas, G.; Pirio, N.; Richard, P.; Donnadiou, B.; Meunier, P. *Organometallics* **2000**, *19*, 4463.

(10) Boring, E.; Sabat, M.; Finn, M. G.; Grimes, R. N. *Organometallics* **1998**, *17*, 3865.

(11) Siegel, J. S.; Anet, F. A. L. *J. Org. Chem.* **1988**, *53*, 2629.

Scheme 4. Formation of Dimeric 2-Alkynylzirconathiolanes *rac*-/*meso*-11a,bChart 2. Predictable Products from Reaction of Conjugated Diynes and $\text{Cp}_2\text{Zr}(\eta^2\text{-RCHS})$ 

similar behavior was already reported in the case of intramolecular coupling of P-tethered diynes promoted by the zirconocene benzene.⁵

On the basis of the promising results we obtained with $\text{Ph}_2\text{PC}\equiv\text{CH}$ and zirconocene thioaldehydes **6a–c**,⁶ we focused our efforts on the preparation of functionalized chalcogenated heterocycles using buta-1,3-diyne. Indeed, considering the structural diversity of complexes obtained by the coupling reaction of various conjugated diynes with zirconocene benzene **1**, it was of interest to explore this chemistry with related reactive species such as **6a,b**. In that case, insertion reactions of buta-1,3-diyne in the Zr–C bond(s) could lead to the formation of various complexes: a thiazirconacyclocumulene (**H**) and/or five-membered alkynylthiazirconacycles (**I** and/or **J**) and/or sulfur-bridged binuclear alkynylzirconathiolanes (**K** and/or **L**) (Chart 2).

A toluene solution of 1,4-diphenylbuta-1,3-diyne and the zirconocene thioaldehyde precursor $\text{Cp}_2\text{Zr}(\text{Me})\text{SCH}_2\text{R}$,⁴ prepared from dimethylzirconocene and 1 equiv of the corresponding thiol (PhCH_2SH for **6a** and $p\text{-MeOC}_6\text{H}_4\text{CH}_2\text{SH}$ for **6b**), led to the precipitation of a mixture of two complexes after 24 h of stirring at 90 °C (Scheme 4). After washing with pentane, the major complexes *rac/meso*-**11a,b** were isolated in quite good yield (around 70%). NMR studies of these new zirconacycles were regarded as hard to manage, due to their poor solubility in any common solvent. Only ¹H NMR spectra could be measured. For the unidentified product in the reaction mixture, two Cp resonances representative of a monomeric complex were found in the spectra (5.48, 5.30 ppm (**a**) and 5.61, 5.54 ppm (**b**)). For the major complexes ¹H NMR spectra revealed the presence of four singlet resonances for the cyclopentadienyl ligands characteristic of a formation of a pair of dimers in a 1:1 ratio: e.g., 6.33, 6.24, 5.68, and 5.59 ppm for *rac*-/*meso*-**11a** and 6.36, 6.26, 5.85, and 5.73 ppm for *rac*-/*meso*-**11b**. Moreover, elementary analysis was consistent with a stoichiometric reaction between the corresponding transient zirconocene thioaldehydes **6a,b** and the diyne. The real structure of *rac*-/*meso*-**11a,b** was not yet clear even though we could obtain good crystals suitable for X-ray analysis, since two sulfur-bridged binuclear alkynylzirconathiolanes (**K** or **L**) were expected.

Finally the slow diffusion of pentane in a highly diluted dichloromethane solution of *rac*-/*meso*-**11b** afforded single crystals, and X-ray crystal structure analysis provided unequivocal evidence for the regio- and also stereochemical assignment. The molecular structure reveals two zirconathiolane units with an alkynyl group in an α position linked with each other by two Zr–S bonds. The Ortep view and a summary of pertinent bond lengths and angles are depicted in Figure 3. The molecule is centrosymmetric, with the center of symmetry at the center of the four-membered Zr–S–Zr–S ring. The two *p*-methoxyphenyl groups are in trans positions. The structural features of this *meso* diastereoisomeric complex are comparable to those of related sulfur-bridged zirconocene dimers.⁶ The complex *meso*-**11b** appears as a bis-sulfonium 2-alkynyl-substituted zirconocene-ate dimer: the two zirconium–sulfur distances Zr–S and Zr–S[#] (2.568(4) and 2.716(4) Å, respectively) and the large angle value C1–Zr–S[#] (131.21(8)°) are typical for five-coordinated $\text{Cp}_2\text{Zr}^{\text{IV}}$ complexes.¹³ In comparison to the intermediate complex **8'**, the major α -regioisomer **10** did not give a ring-enlarged seven-membered zirconacycle and evolved to a dimeric product that prevented the zirconacyclopentene from reacting with the second acetylenic function.

It is well established that five-membered zirconacycles are good building blocks for preparing heterocyclic molecules through the exchange reaction of a zirconium atom with transfer of the organic part to an electrophilic reagent. Therefore, interesting tricyclic derivatives incorporating two group 14 and/or 15 elements, **F** and **G** (Chart 1), were generated by a zirconium dihalogenated main group element exchange reaction starting from **3a** and **4a**,⁵ and we felt that zirconacyclocumulenes **8a,b** would provide a ready entry for the synthesis of new main-group heterocycles. Treatment of a toluene solution of **8a** with 1 equiv of phenylantimony dichloride gave the metalloid heterocycle **12** (eq 1). After extraction in pentane, the only byproduct of the reaction (Cp_2ZrCl_2) is removed by flash chromatography on silica. The stibacycle **12** was isolated in quite good yield after workup and characterized by usual spectroscopic and analytical methods. Although no relevant information could be retained from the ¹H NMR data, the ¹³C NMR clearly shows two singlets at 100.4 and 91.8 ppm in the expected range for a C≡C unit (classical acetylenic carbon resonances are in the 70–110 ppm range). Moreover, in the IR spectrum (KBr),

(12) (a) Hsu, D. P.; Davis, W. M.; Buchwald, S. L. *J. Am. Chem. Soc.* **1993**, *115*, 10394. (b) Rosenthal, U.; Ohff, A.; Baumann, W.; Kempe, R.; Tillack, A.; Burlakov, V. V. *Angew. Chem., Int. Ed. Engl.* **1994**, *33*, 1605. (c) Kempe, R.; Ohff, A.; Rosenthal, U. *Z. Kristallogr.* **1995**, *210*, 707. (d) Ashe, A. J., III; Al-Ahmad, S.; Kampf, J. *Organometallics* **1999**, *18*, 4234. (e) Pellny, P.-M.; Kirchbauer, F. G.; Burlakov, V. V.; Baumann, W.; Spannenberg, A.; Rosenthal, U. *J. Am. Chem. Soc.* **1999**, *121*, 8313. (f) Burlakov, V. V.; Ohff, A.; Lefeber, C.; Tillack, A.; Baumann, W.; Kempe, R.; Rosenthal, U. *Chem. Ber.* **1995**, *128*, 967.

(13) Majoral, J.-P.; Zablocka, M. *New J. Chem.* **2005**, *29*, 13.

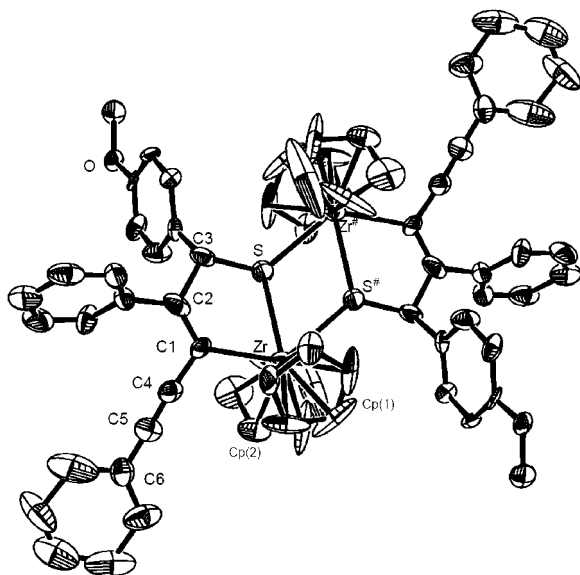


Figure 3. ORTEP view of *meso*-**11b**. Selected bond lengths (Å) and angles (deg): Zr–C1 = 2.348(13), Zr–S = 2.568(4), Zr–S# = 2.716(4), C4–C5 = 1.203(17); Cp(1)–Zr–Cp(2) = 128.86, C1–Zr–S = 70.1(3), S–Zr–S# = 61.12(6), C1–Zr–S# = 131.21(8).

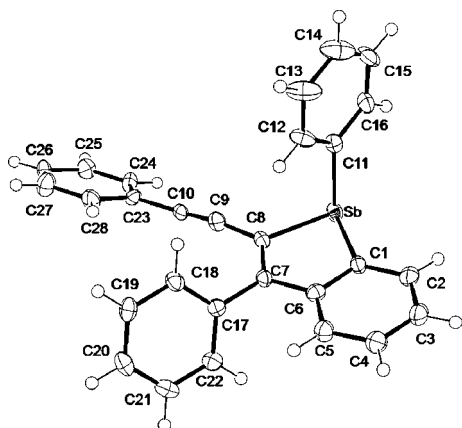
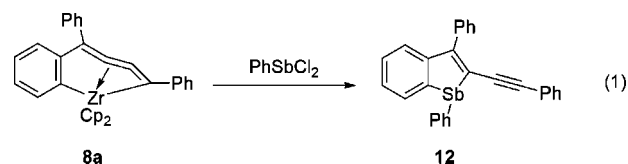


Figure 4. ORTEP view of **12**. Selected bond distances (Å) and angles (deg) for both independent molecules of **12**: Sb–C1 = 2.140(4) and 2.154(4), Sb–C8 = 2.164(4) and 2.154(4), Sb–C11 = 2.160(4) and 2.152(4); C8–Sb–C11 = 95.27(15) and 94.47(16), C1–Sb–C11 = 95.63(15) and 95.41(15), C1–Sb–C8 = 79.92(15) and 79.88(16).

one absorption is observed at 2174 cm^{-1} in the area characteristic of the stretching vibrations for free carbon–carbon triple bonds (2050–2200 cm^{-1}). Such information is in favor of the existence of a five-membered ring with a $\text{C}\equiv\text{C}$ unit and the loss of the original seven-membered metallacyclocumulene arrangement. Recrystallization of **12** from diethyl ether/pentane generates suitable single crystals for its X-ray crystal structure analysis. Elucidation of **12** as a 2-alkynyl-substituted stibaindene was achieved by X-ray diffraction studies. The ORTEP view and the relevant bond lengths and angles are shown in Figure 4. In the five-membered stibacyclic ring, the three Sb–C(sp²) distances are identical in length with those found in known tertiary stibines:¹⁴ e.g., 2.155 Å for Ph_3Sb and 2.129 Å for $(\text{C}_4\text{H}_5\text{S})_3\text{Sb}$. The stibaindene ring is planar and is orthogonal to the plane of the phenyl ring. More generally, the highly pyramidalized geometry around the antimony atom and the bond distances and angles within the ring system are all in

good agreement with those of other structurally characterized stibole derivatives.^{5,15} The solid-state structure of **12** confirms that the formation of **8** involves a consecutive insertion of the two carbon–carbon triple bonds of $\text{RC}\equiv\text{CC}\equiv\text{CR}$ into the zirconium bond of the transient zirconocene benzyne **1** via the 2-alkynylzirconaindene **8'**.



Conclusion

Zirconocene benzyne and thioaldehydes react with 1,4-diphenyl- and 1,4-bis(trimethylsilyl)buta-1,3-diynes to yield seven-membered and 2- or 3-alkynyl-substituted five-membered zirconacycles, demonstrating how the combination of the substituent on the diyne and the nature of the three-membered zirconacyclic species can lead to three reaction patterns. A two-step mechanism involving a double insertion of the two carbon–carbon triple bonds of the conjugated diynes into the zirconium–carbon bond of the transient zirconocene benzyne explains the formation of the 18-electron zirconacyclocumulenes (stabilization by interaction between the metal and the middle double bond). With a more hindered substituent, a further minor 3-alkynylzirconaindene arising from the simple β insertion of one of the triple bonds is provided. With zirconocene thioaldehydes, the simple α insertion of one of the acetylenic bonds leads to a 2-alkynylzirconothiolane which is preferentially stabilized by the formation of a coordination dimer. These results point out that the zirconacycles with an alkynyl group in a position α to the metal show ring expansion to seven-membered zirconacycles or bridged association to dimeric zirconacycles, whereas those with an alkynyl group in a β position are stable. This work also furnishes a novel path for the preparation of a functionalized stibaindene. Investigations are underway in our laboratory to further explore the use of zirconacyclic intermediates as vehicles for the preparation of new and attractive main-group compounds.

Experimental Section

General Remarks. All reactions were carried out under argon using Schlenk-type glassware or in a glovebox. Solvents, including deuterated solvents used for NMR spectroscopy, were dried and distilled prior to use. Mass spectra were determined by using a Kratos Concept IS spectrometer, while NMR spectra were measured using a Bruker DRX500 or Varian Unity Plus 600 NMR spectrometer. Most assignments were based on a series of 2D NMR experiments (chemical shifts are given in ppm relative to TMS for ¹H, ¹³C, and ²⁹Si nuclei). IR spectra were measured using a Nicolet 5 DXC FT IR spectrometer. Melting points were determined by differential scanning calorimetry (2010 DSC, DuPont/STA Instruments). Combustion analyses were performed by the analytical service of the ICMUB of the Université de Bourgogne or by the Organisch-Chemisches Institut der Universität Münster. Reagents

(14) (a) Adams, E. A.; Kolis, J. W.; Pennington, W. T. *Acta Crystallogr. Sect. C* **1990**, *46*, 917. (b) Vela, J.; Sharma, P.; Cabrera, A.; Alvarez, C.; Rosas, N.; Hernandez, S.; Toscano, A. *J. Organomet. Chem.* **2001**, *634*, 5.

(15) (a) Buchwald, S. L.; Fischer, R. A.; Foxman, B. M. *Angew. Chem., Int. Ed. Engl.* **1990**, *29*, 771. (b) Hsu, D. P.; Warner, B. P.; Fisher, R. A.; Davis, W. M.; Buchwald, S. L. *Organometallics* **1994**, *13*, 5160. (c) Yasuike, S.; Iida, T.; Yamaguchi, K.; Seki, I.; Kurita, J. *Tetrahedron Lett.* **2001**, *42*, 441.

Table 1. Crystallographic Data and Data Collection and Structure Refinement Details for **8b**, **9b**, *meso*-**11b**, and **12**

	8b, 9b	<i>meso</i> - 11b	12
formula	C ₅₂ H ₆₄ Si ₄ Zr ₂	C ₆₈ H ₅₆ O ₂ S ₂ Zr ₂	C ₂₈ H ₁₉ Sb
<i>M_r</i>	983.83	1151.68	477.18
<i>T</i> , K	198(2)	180(2)	110(2)
cryst syst	triclinic	monoclinic	triclinic
Sspace group	<i>P</i> $\bar{1}$	<i>P</i> 2 ₁ / <i>c</i>	<i>P</i> $\bar{1}$
<i>a</i> , Å	10.071(1)	12.748(2)	10.4651(2)
<i>b</i> , Å	16.353(1)	8.0431(15)	10.8893(3)
<i>c</i> , Å	16.588(1)	30.174(6)	18.5233(5)
α , deg	107.83(1)	90	85.015(1)
β , deg	98.08(1)	98.960(16)	83.552(1)
γ , deg	95.16(1)	90	81.445(1)
<i>V</i> , Å ³	2549.1(3)	3056.1(10)	2068.88(9)
<i>Z</i>	2	4	4
<i>F</i> (000)	1024	1184	952
<i>D</i> _{calcd} , g/cm ³	1.282	1.252	1.532
λ , Å	0.710 73	0.710 73	0.710 73
μ , mm ⁻¹	0.535	0.451	1.344
cryst size, mm ³	0.35 × 0.30 × 0.15		0.17 × 0.04 × 0.04
(<i>sin</i> θ)/ λ _{max} , Å ⁻¹	0.67	0.67	0.672
index ranges	-13 ≤ <i>h</i> ≤ 13 -21 ≤ <i>k</i> ≤ 21 -22 ≤ <i>l</i> ≤ 21	-14 ≤ <i>h</i> ≤ 14 -8 ≤ <i>k</i> ≤ 5 -33 ≤ <i>l</i> ≤ 33	-13 ≤ <i>h</i> ≤ 13 -14 ≤ <i>k</i> ≤ 13 -24 ≤ <i>l</i> ≤ 23
no. of rflns collected (RC)	27 654	16 419	15 609
no. of indep RC (IRC)	12 465 (<i>R</i> (int) = 0.055)	4369 (<i>R</i> (int) = 0.1520)	9372 (<i>R</i> (int) = 0.0505)
no. of IRC with <i>I</i> > 2σ(<i>I</i>) (IRCGT)	7723	2067	5762
refinement method	full-matrix least squares on <i>F</i> ²	full-matrix least squares on <i>F</i> ²	full-matrix least squares on <i>F</i> ²
no. of data/restraints/params	12 465/0/535	4369/10/336	9372/156/614
<i>R</i> for IRCGT	<i>R</i> ^{1a} = 0.0526, <i>wR</i> ^{2b} = 0.1127	<i>R</i> ^{1a} = 0.1005, <i>wR</i> ^{2b} = 0.2485	<i>R</i> ^{1a} = 0.045, <i>wR</i> ^{2b} = 0.072
<i>R</i> for IRC	<i>R</i> ^{1a} = 0.1052, <i>wR</i> ^{2b} = 0.1312	<i>R</i> ^{1a} = 0.1728, <i>wR</i> ^{2b} = 0.2791	<i>R</i> ^{1a} = 0.104, <i>wR</i> ^{2b} = 0.087
goodness of fit ^c	1.026	0.985	0.98
largest diff peak and hole, e Å ⁻³	0.580 and -0.468	0.872 and -0.831	0.737 and -0.997

^a *R*¹ = $\sum(|F_o| - |F_c|)/\sum|F_o|$. ^b *wR*² = $[\sum w(F_o^2 - F_c^2)^2/\sum w(F_o^2)^2]$ ^{1/2}. ^c Goodness of fit = $[\sum w(F_o^2 - F_c^2)^2/(N_o - N_c)]^{1/2}$.

were purchased from commercial suppliers and used without further purification, except for the thiols which were distilled and stored under an argon atmosphere. Cp₂ZrPh₂,¹⁶ Cp₂ZrMe₂,¹⁶ and PhS-bCl₂¹⁷ were prepared according to the literature procedures.

X-ray Crystal Structure Analysis. 8b and 9b. The data sets were collected at 198 K with a Nonius KappaCCD diffractometer ($\lambda = 0.710\ 73\ \text{\AA}$), equipped with a Nonius FR591 rotating anode generator. The structure was solved with direct methods and refined with full-matrix least-squares methods based on *F*² (SHELX97).¹⁸ An absorption correction was applied (SORTAV).¹⁹

meso-11b. Data were collected at 180 K on a Stoe Imaging Plate Diffraction System (IPDS) ($\lambda = 0.710\ 73\ \text{\AA}$), equipped with an Oxford Cryosystems Cryostream Cooler device. The final unit cell parameters were obtained by least-squares refinement of a set of 5000 reflections, and crystal decay was monitored by measuring 200 reflections by image. Any fluctuations of the intensity were observed over the course of the data collection. Numerical absorption corrections²⁰ were applied to the data. The structure was solved by direct methods using SIR92²¹ and refined by least-squares procedures on *F*² with the aid of SHELX97.¹⁸ All hydrogen atoms were located on a difference Fourier map and refined with a riding model, and all non-hydrogen atoms were anisotropically refined.

12. Single crystals were mounted in inert oil and transferred to the cold nitrogen stream (110 K) of a Nonius Kappa CCD diffractometer ($\lambda = 0.710\ 73\ \text{\AA}$). The structure was solved via a Patterson search program and refined with full-matrix least-squares methods based on *F*² (SHELX97)¹⁸ with the aid of the WINGX program.²² The phenylacetylene groups of both independent molecules present in the asymmetric unit are disordered over two positions. The occupancies converged to 0.5 (due to steric reasons, the same value is observed in both molecules). Hydrogen atoms were included using a riding model. Although all non-hydrogen atoms were anisotropically refined, restraints (ISOR) were applied to the *U*_{ij} values of the atoms of the disordered groups to approximate an isotropic behavior in order to prevent some atoms from becoming "nonpositive-definite".

Crystallographic data and data collection and structure refinement details for **8b**, **9b**, *meso*-**11b**, and **12** are given in Table 1. Crystallographic data (excluding structure factors) for the structures reported in this paper have been deposited with the Cambridge Crystallographic Data Centre as supplementary publication numbers CCDC-635422 (**8b, 9b**), CCDC-635391 (*meso*-**11b**), and CCDC-634729 (**12**). Copies of the data can be obtained, free of charge, on application to The Director, CCDC, 12 Union Road, Cambridge CB2 1EZ, U.K. (fax +44-1223-336033; e-mail deposit@ccdc.cam.ac.uk, or web http://www.ccdc.cam.ac.uk).

Temperature-Dependent ¹H and ¹³C NMR Spectra for Zirconacyclocumulene 8a. ¹H NMR (dichloromethane-*d*₂, 600 MHz, 213 K): δ 7.89 (d, *J*_{HH} = 7.6 Hz, 1H, 9-H), 7.73 (m, 2H, *o*-Ph²), 7.70 (m, 2H, *o*-Ph⁵), 7.49 (m, 2H, *m*-Ph²), 7.47 (m, 2H,

(16) Samuel, E.; Rausch, M. D. *J. Am. Chem. Soc.* **1973**, *95*, 6263.

(17) Wieber, M.; Wirth, D.; Fetzer, I. *Z. Anorg. Allg. Chem.* **1983**, *505*, 134.

(18) Sheldrick, G. M. SHELX97 (includes SHELXS97 and SHELXL97), Release 97-2, Programs For Crystal Structure Analysis; University of Göttingen, Göttingen, Germany, 1998.

(19) (a) Blessing, R. H. *Acta Crystallogr.* **1995**, *A51*, 33. (b) Blessing, R. H. *J. Appl. Crystallogr.* **1997**, *30*, 421.

(20) X-SHAPE (revision 1.01): A Crystal Optimisation for Numerical Correction; STOE and Cie, July 1996 (X SHAPE is based on the program HABITUS by Dr. Wolfgang Herrendorf, Institut für Anorganische Chemie, Universität Giessen).

(21) Altomare, A.; Cascarano, G.; Giacovazzo, G.; Guagliardi, A.; Burla, M. C.; Polidori, G.; Camalli, M. SIR92 Program for Automatic Solution of Crystal Structures by Direct Methods. *J. Appl. Crystallogr.* **1994**, *27*, 435.

(22) *International Tables for X-ray Crystallography*; Kynoch Press: Birmingham, U.K., 1994; Vol. IV.

(23) Burnett, M. N.; Johnson, C. K. ORTEP-III: Oak Ridge Thermal Ellipsoid Plot Program for Crystal Structure Illustrations; Oak Ridge National Laboratory Report ORNL-6895; Oak Ridge National Laboratory, Oak Ridge, TN, 1996. Windows implementation: Farrugia, L. *J. Appl. Crystallogr.* **1997**, *30*, 565.

(24) Farrugia, L. *J. Appl. Crystallogr.* **1999**, *32*, 837.

m-Ph⁵), 7.38 (m, 1H, *p*-Ph⁵), 7.36 (m, 1H, *p*-Ph²), 7.34 (d, $J_{\text{HH}} = 7.6$ Hz, 1H, 6-H), 7.04 (t, $J_{\text{HH}} = 7.6$ Hz, 1H, 7-H), 6.99 (t, $J_{\text{HH}} = 7.6$ Hz, 1H, 8-H), 5.58 (s, 10H, Cp) ppm. ¹H NMR (dichloromethane-*d*₂, 600 MHz, 298 K): δ 7.92 (m, 1H, 9-H), 7.76 (m, 2H, *o*-Ph²), 7.71 (m, 2H, *o*-Ph⁵), 7.51 (m, 2H, *m*-Ph²), 7.49 (m, 2H, *m*-Ph⁵), 7.40 (m, 1H, *p*-Ph⁵), 7.37 (m, 1H, *p*-Ph²), 7.35 (m, 1H, 6-H), 7.07 (m, 1H, 7-H), 7.04 (m, 1H, 8-H), 5.62 (s, 10H, Cp) ppm. ¹³C NMR (dichloromethane-*d*₂, 151 MHz, 213 K): δ 183.5 (9a), 163.3 (5a), 160.7 (2), 144.3 ($J_{\text{CH}} = 152$ Hz, 9), 140.6 (5), 138.8 (*i*-Ph⁵), 134.3 (*i*-Ph²), 132.4 ($J_{\text{CH}} = 164$ Hz, *o*-Ph²), 128.7 ($J_{\text{CH}} = 162$ Hz, *m*-Ph²), 128.5 ($J_{\text{CH}} = 163$ Hz, *o*-Ph⁵), 128.3 ($J_{\text{CH}} = 162$ Hz, *p*-Ph²), 128.2 ($J_{\text{CH}} = 162$ Hz, *m*-Ph⁵), 127.6 ($J_{\text{CH}} = 162$ Hz, *p*-Ph⁵), 124.0 ($J_{\text{CH}} = 156$ Hz, 6), 123.0 ($J_{\text{CH}} = 158$ Hz, 8), 122.5 ($J_{\text{CH}} = 159$ Hz, 7), 105.7 (Cp), n.o (3, 4) ppm [signals at 170.7, 111.6, and 86.1 from unidentified product]. ¹³C NMR (dichloromethane-*d*₂, 151 MHz, 298 K): δ 184.4 (9a), 164.2 (5a), 161.6 (2, from ghmbc), 144.7 (9), 141.8 (5), 140.0 (*i*-Ph⁵), 135.3 (*i*-Ph²), 132.9 (*o*-Ph²), 129.3 (*m*-Ph²), 129.1 (*o*-Ph⁵), 128.73 (*p*-Ph²), 128.71 (*m*-Ph⁵), 128.1 (*p*-Ph⁵), 125.0 (6), 123.9 (8), 123.3 (7), 106.6 (Cp), not obsd (3, 4) ppm (signals at 112.3 and 87.7 from unidentified product).

Preparation of Zirconacyclocumulene 8b and 3-Alkynylzirconaindene 9b. A solution of Cp₂ZrPh₂ (0.375 g, 1.0 mmol) and Me₃SiC≡C≡CSiMe₃ (0.194 g, 1.0 mmol) in 35 mL of toluene was heated at 80 °C for 15 h. After removal of the solvent in vacuo, the solid obtained was stirred with pentane to afford a yellow powder (0.40 g, 0.81 mmol, 81%), which was recrystallized from pentane to yield 0.35 g (0.71 mmol, 71%) of the seven- and five-membered zirconacycles **8b** and **9b** as yellow crystals. Mp 151.7 °C. Anal. Calcd for C₂₆H₃₂Si₂Zr: C, 63.48; H, 6.56. Found: C, 63.58; H, 6.56. IR (KBr): 2937, 2126, 1874, 1623, 1427, 1238, 1099, 1015, 840, 812 cm⁻¹. MS (70 eV): *m/z* (%): 490 (22) [M]⁺.

8b. ¹H NMR (toluene-*d*₈, 500 MHz, 298 K): δ 7.78 (m, 1H, 9-H), 7.61 (m, 1H, 6-H), 7.18 (m, 1H, 7-H), 7.08 (m, 1H, 8-H), 5.23 (s, 10H, Cp), 0.40 ($J_{\text{SiH}} = 6.7$ Hz, 9H, Me₃Si⁵), 0.33 ($J_{\text{SiH}} = 6.6$ Hz, 9H, Me₃Si²) ppm. ¹³C NMR (toluene-*d*₈, 126 MHz, 298 K): δ 190.9 (9a), 170.0 (5a), 163.8 (2), 156.0 (5), 144.1 (9), 126.3 (6), 123.6 (7), 123.4 (8), 106.0 (Cp), 1.38 (Me₃Si⁵), -0.40 (Me₃Si²), not obsd (3, 4) ppm. ²²Si{¹H} NMR (benzene-*d*₆, 39.8 MHz, 300 K): δ -15.1, -12.3 ppm.

9b. ¹H NMR (toluene-*d*₈, 500 MHz, 298 K): δ 7.98 (m, 1H, 7-H), 7.43 (m, 1H, 4-H), 7.18 (m, 1H, 5-H), 7.08 (m, 1H, 6-H), 5.83 (s, 10H, Cp), 0.23 ($J_{\text{SiH}} = 6.9$ Hz, 9H, Me₃SiC≡), 0.19 ($J_{\text{SiH}} = 6.3$ Hz, 9H, Me₃Si²) ppm. ¹³C NMR (toluene-*d*₈, 126 MHz, 298 K): δ 221.9 (2), 186.0 (7a), 138.9 (4), 127.2, 125.7 (5,6), 125.4 (7), 112.3 (Cp), 102.8 (-C≡), 93.9 (SiC≡), 0.70 (Me₃Si²), 0.10 (Me₃SiC≡), not obsd (3, 3a) ppm. ²²Si{¹H} NMR (benzene-*d*₆, 39.8 MHz, 300 K): δ -24.1, -20.0 ppm.

Preparation of Dimeric 2-Alkynylzirconathiolanes *rac*-/*meso*-11a,b. To a solution of dimethylzirconocene (1.20 g; 4.8 mmol) in toluene (15 mL) was added 1,4-diphenylbutadiyne (0.97 g; 4.8 mmol) followed by a stoichiometric amount of phenylmethanethiol (for **11a**: 0.56 mL, 4.8 mmol) or (4-methoxyphenyl) methanethiol (for **11b**: 0.67 mL, 4.8 mmol). The resulting solution

was stirred for 2 h at room temperature, and then it was heated to 90 °C for 24 h. A beige solid precipitated during the reaction. The mixture was cooled to room temperature and then concentrated in vacuo, and then pentane (20 mL) was added. The resulting solid product was washed with 5 × 10 mL of pentane and vacuum-dried to yield 1.86 g of *rac*-*meso*-**11a** (1.70 mmol, 71%) as a beige powder and 1.91 g of *rac*-*meso*-**11b** (1.66 mmol, 69%) as a beige powder.

***rac*-*meso*-11a.** Mp 145 °C dec. Anal. Calcd for C₆₆H₅₂S₂Zr₂: C, 72.61; H, 4.80; S, 5.87. Found: C, 72.54; H, 4.91; S, 5.83. MS (70 eV): *m/z* (%) 544 (65) [¹/₂M]⁺ (monomeric form). ¹H NMR (toluene-*d*₈, 500 MHz, 300 K): δ 7.42–7.32 (m, H_{arom}), 7.19–7.00 (m, H_{arom}), 6.96–6.89 (m, H_{arom}), 6.33, 6.24, 5.68, 5.59 (s, 40H, Cp), 5.34 (broad s, 4H, CHPh) ppm.

***rac*-*meso*-11b.** Mp 150 °C dec. Anal. Calcd for C₆₈H₅₆O₂S₂Zr₂: C, 70.91; H, 4.90; S, 5.57. Found: C, 70.88; H, 4.99; S, 5.49. MS (70 eV): *m/z* (%) 574 (67) [¹/₂M]⁺ (monomeric form). ¹H NMR (toluene-*d*₈, 500 MHz, 300 K): δ 7.46–7.09 (m, H_{arom}), 7.01–6.94 (m, H_{arom}), 6.36, 6.26, 5.85, 5.73 (s, 40H, Cp), 5.37 (broad s, 4H, CHPh), 3.22, 3.18 (s, 12H, OMe) ppm.

Preparation of Stibacycle 12. A solution of PhSbCl₂ (0.14 g, 0.34 mmol) in toluene was added dropwise to a solution of complex **8a** (0.17 g, 0.34 mmol) in toluene cooled to -30 °C. The reaction mixture was warmed slowly to room temperature and stirred for 15 h. After removal of the solvent in vacuo, the residue was extracted with pentane (2 × 10 mL) and purified by column chromatography (SiO₂, diethyl ether) to afford the expected compound as a yellow oil (0.14 g, 0.29 mmol, 87%), which was recrystallized from 10 mL of pentane to yield 0.09 g (0.19 mmol, 56%) of 2-phenylalkynylstibaindole **12** as yellow crystals. Anal. Calcd for C₂₈H₁₉Sb: C, 70.44; H, 3.98. Found: C, 70.36; H, 4.25. IR (KBr): 2174 cm⁻¹. MS (70 eV): *m/z* (%) 476 (27) [M]⁺. ¹H NMR (chloroform-*d*, 500 MHz, 298 K): δ 6.84–7.03 (m, H_{arom}), 7.16–7.27 (m, H_{arom}), 7.48–7.51 (m, H_{arom}), 7.59–7.64 (m, H_{arom}) ppm. ¹³C{¹H} NMR (chloroform-*d*, 125 MHz, 298 K): δ 163.5, 152.5, 146.8, 139.0, 138.4 (s, C_{quat}), 135.7, 134.9, 131.8, 129.62, 129.55, 129.51, 129.3, 129.0, 128.7, 128.60, 128.58, 128.4, 128.3 (s, CH_{arom} and Ph), 124.6 (s, C_{quat}), 100.4 (s, ≡C-Ph), 91.8 (s, C≡CPh) ppm.

Acknowledgment. Financial support from the Ministère de l'Éducation Nationale, de la Recherche et la Technologie (France), the CNRS (France), Conseil Régional de Bourgogne (France), Fonds der Chemischen Industrie, and the Deutsche Forschungsgemeinschaft (Germany) is gratefully acknowledged. We thank S. Royer for her helpful technical assistance.

Supporting Information Available: CIF files giving crystal data for **8b**, **9b**, *meso*-**11b**, and **12**. This material is available free of charge via the Internet at <http://pubs.acs.org>.

OM800512U

m-Terphenyl Anchored Palladium Diphosphinite PCP-Pincer Complexes That Promote the Suzuki–Miyaura Reaction Under Mild Conditions

Mark C. Lipke, Robert A. Woloszynek, Liqing Ma, and John D. Protasiewicz*

Department of Chemistry, Case Western Reserve University, Cleveland, Ohio 44106

Received July 3, 2008

Diphosphinite PCP-pincer pro-ligands anchored by a *meta*-terphenyl backbone were synthesized. These pro-ligands, [2,6-(2-Ph₂POC₆H₄)₂C₆H₃X] (**3a** X = I, **3b** X = Br) and [2,6-(2-ⁱPr₂POC₆H₄)₂C₆H₃X] (**4a** X = I, **4b** X = Br) upon reaction with Pd₂(dba)₃ yield PCP palladium pincer complexes [2,6-(2-Ph₂POC₆H₄)₂C₆H₃PdX] (**5a** X = I, **5b** X = Br) and [2,6-(2-ⁱPr₂POC₆H₄)₂C₆H₃PdX] (**6a** X = I, **6b** X = Br). The structures of **5a–b** and **6a–b** were determined by single crystal X-ray diffraction analyses. Complexes **5b** and **6b** were evaluated for their efficacy in promoting catalytic Suzuki–Miyaura CC coupling reactions. A variety of aryl bromides efficiently underwent CC coupling reactions with *p*-tolylboronic acid with high yields in the presence of either **5b** or **6b**. Compound **6b** also proved to be a very active pro-catalyst for the coupling of aryl chlorides with *p*-tolylboronic acid. Excellent to good yields (in some cases greater than 90%) were achieved even with electron rich or sterically hindered aryl chlorides.

Introduction

Since its introduction in 1979,¹ the Suzuki–Miyaura reaction has become very important to modern synthetic chemists.^{2–7} This catalytic CC coupling reaction between aryl halides and aryl boronic acids to form biaryls can occur under mild conditions and tolerates a wide variety of functional groups. In addition, boronic acids are of low toxicity and their reaction byproducts are easily separated from the desired product. As a result of its utility, much attention has been paid to improving methods and finding new applications for the Suzuki–Miyaura reaction.^{8,9} The development of better catalysts has received particularly significant attention.^{10,11} Complexes have ultimately been reported which show impressive catalytic activity in the Suzuki–Miyaura reaction at room temperature,^{12,13} when using hindered substrates,¹⁴ when using aryl chlorides,¹⁵ or with very low catalyst loadings.^{16,17}

Pincer ligand complexes have been recognized for their thermal and chemical stability since they were first reported in the 1970s.¹⁸ More recently, enormous attention has been paid to these terdentate complexes for the development of new palladium catalysts.^{19,20} Numerous palladium pincer complex variations have been tested for catalytic activity in a variety of CC coupling reactions. For example, palladium pincer complexes of 1,3-bis(2-pyridyloxy)benzene have been reported to have extremely high turnover numbers (TON = 8.4 × 10⁸) in Heck coupling reactions.²¹ Other researchers have used chiral substituents to create a chiral pocket around palladium for asymmetric catalysis.^{22–48} For example, enantiomeric excesses

* To whom correspondence should be addressed. E-mail: protasiewicz@case.edu.

- Miyaura, N.; Yamada, K.; Suzuki, A. *Tetrahedron Lett.* **1979**, 3437–3440.
- Yin, L. X.; Liebscher, J. *Chem. Rev.* **2007**, 107, 133–173.
- Weng, Z.; Teo, S.; Hor, T. S. A. *Acc. Chem. Res.* **2007**, 40, 676–684.
- Negishi, E.-i., Ed. *Handbook of Organopalladium Chemistry for Organic Synthesis*, Volume 2; John Wiley & Sons: New York, 2002.
- Negishi, E.-i., Ed. *Handbook of Organopalladium Chemistry for Organic Synthesis*, Volume 1; John Wiley & Sons: New York, 2002.
- Tsuji, J., Ed. *Perspectives in Organopalladium Chemistry for the XXI Century*; Elsevier Science: Amsterdam, 1999.
- Tsuji, J. *Palladium Reagents and Catalysts: Innovations in Organic Synthesis*; Wiley & Sons: Chichester, 1995.
- Suzuki, A. *J. Organomet. Chem.* **1999**, 576, 147–168.
- Miyaura, N.; Suzuki, A. *Chem. Rev.* **1995**, 95, 2457–2483.
- Kotha, S.; Lahiri, K.; Kashinath, D. *Tetrahedron* **2002**, 58, 9633–9695.
- Bellina, F.; Carpita, A.; Rossi, R. *Synthesis* **2004**, 2419–2440.
- Barder, T. E.; Walker, S. D.; Martinelli, J. R.; Buchwald, S. L. *J. Am. Chem. Soc.* **2005**, 127, 4685–4696.
- Old, D. W.; Wolfe, J. P.; Buchwald, S. L. *J. Am. Chem. Soc.* **1998**, 120, 9722–9723.

(14) Altenhoff, G.; Goddard, R.; Lehmann, C. W.; Glorius, F. *J. Am. Chem. Soc.* **2004**, 126, 15195–15201.

(15) Littke, A. F.; Fu, G. C. *Angew. Chem., Int. Ed.* **2002**, 41, 4176–4211.

(16) Bedford, R. B.; Hazelwood, S. L.; Limmert, M. E. *Chem. Commun.* **2002**, 2610–2611.

(17) Zapf, A.; Ehrentauf, A.; Beller, M. *Angew. Chem., Int. Ed.* **2000**, 39, 4153–4155.

(18) Moulton, C. J.; Shaw, B. L. *J. Chem. Soc., Dalton Trans.* **1976**, 10204.

(19) Albrecht, M.; van Koten, G. *Angew. Chem., Int. Ed.* **2001**, 40, 3750–3781.

(20) Singleton, J. T. *Tetrahedron* **2003**, 59, 1837–1857.

(21) Yoon, M. S.; Ryu, D.; Kim, J.; Ahn, K. H. *Organometallics* **2006**, 25, 2409–2411.

(22) Albrecht, M.; Kocks, B. M.; Spek, A. L.; van Koten, G. *J. Organomet. Chem.* **2001**, 624, 271–286.

(23) Gerisch, M.; Krumper, J. R.; Bergman, R. G.; Tilley, T. D. *J. Am. Chem. Soc.* **2001**, 123, 5818–5819.

(24) Williams, B. S.; Dani, P.; Lutz, M.; Spek, A. L.; Van Koten, G. *Helv. Chim. Acta* **2001**, 84, 3519–3530.

(25) Morales-Morales, D.; Cramer, R. E.; Jensen, C. M. *J. Organomet. Chem.* **2002**, 654, 44–50.

(26) Diez-Barra, E.; Guerra, J.; Lopez-Solera, I.; Merino, S.; Rodriguez-Lopez, J.; Sanchez-Verdu, P.; Tejada, J. *Organometallics* **2003**, 22, 541–547.

(27) Gerisch, M.; Krumper, J. R.; Bergman, R. G.; Tilley, T. D. *Organometallics* **2003**, 22, 47–58.

(28) Motoyama, Y.; Nishiyama, H. *Synlett* **2003**, 1883–1885.

(29) Lee, H. M.; Zeng, J. Y.; Hu, C.-H.; Lee, M.-T. *Inorg. Chem.* **2004**, 43, 6822–6829.

as high as 83% have been reported for asymmetric Michael reactions catalyzed by bispyrroloimidazolone NCN palladium pincer complexes.³⁴ In regard to the Suzuki–Miyaura reaction, palladium pincer complexes have recently been reported which act as effective catalysts for the coupling of aryl chlorides with aryl boronic acids.⁴⁹ Inspired by such developments, we set out to examine the catalytic properties of pincer complexes recently developed in our laboratories.

These particular pincer complexes are constructed upon a triaryl ring backbone (*m*-terphenyl). A *m*-terphenyl backbone was designed as it should yield more rigid pincer and nonplanar (globally) complexes, as compared to those anchored by *m*-xylyl and related frameworks (Chart 1, left).⁵⁰ Control of ligand dynamics is key to achieving well defined steric profiles and for projecting possible chirality. For nonplanar pincer ligands, a C₂-symmetric environment can be produced, but for many pincer complexes interconversion between two possible atropisomers can be facile (Chart 1, right). We have shown that *m*-terphenyl based pincer complexes maintain a nonplanar conformation.⁵¹ Herein we examine pincer complexes containing phosphinite groups and have evaluated their catalytic activity for the Suzuki–Miyaura reaction using a variety of aryl bromides and chlorides. The catalytic activity of these complexes at different reaction temperatures was also examined.

Results and Discussion

Synthesis of Diphosphinite Pro-Ligands. Compounds **1a** and **1b** were synthesized following standard procedures for

(30) Slagt, M. Q.; Stiriba, S.-E.; Kautz, H.; Gebbink, R. J. M. K.; Frey, H.; Van Koten, G. *Organometallics* **2004**, *23*, 1525–1532.

(31) Takenaka, K.; Uozumi, Y. *Adv. Synth. Catal.* **2004**, *346*, 1693–1696.

(32) Takenaka, K.; Uozumi, Y. *Org. Lett.* **2004**, *6*, 1833–1835.

(33) Medici, S.; Gagliardo, M.; Williams, S. B.; Chase, P. A.; Gladiali, S.; Lutz, M.; Spek, A. L.; van Klink, G. P. M.; van Koten, G. *Helv. Chim. Acta* **2005**, *88*, 694–705.

(34) Takenaka, K.; Minakawa, M.; Uozumi, Y. *J. Am. Chem. Soc.* **2005**, *127*, 12273–12281.

(35) Baber, R. A.; Bedford, R. B.; Betham, M.; Blake, M. E.; Coles, S. J.; Haddow, M. F.; Hursthouse, M. B.; Orpen, A. G.; Pilarski, L. T.; Pringle, P. G.; Wingad, R. L. *Chem. Commun.* **2006**, 3880–3882.

(36) Benito-Garagorri, D.; Becker, E.; Wiedermann, J.; Lackner, W.; Pollak, M.; Mereiter, K.; Kisala, J.; Kirchner, K. *Organometallics* **2006**, *25*, 1900–1913.

(37) Benito-Garagorri, D.; Bocokic, V.; Mereiter, K.; Kirchner, K. *Organometallics* **2006**, *25*, 3817–3823.

(38) Benito-Garagorri, D.; Mereiter, K.; Kirchner, K. *Eur. J. Inorg. Chem.* **2006**, 4374–4379.

(39) Gosiewska, S.; Huis in't Veld, M.; De Pater, J. J. M.; Bruijninx, P. C. A.; Lutz, M.; Spek, A. L.; Van Koten, G.; Klein Gebbink, R. J. M. *Tetrahedron: Asymmetry* **2006**, *17*, 674–686.

(40) Hao, X.-Q.; Gong, J.-F.; Du, C.-X.; Wu, L.-Y.; Wu, Y.-J.; Song, M.-P. *Tetrahedron Lett.* **2006**, *47*, 5033–5036.

(41) Motoyama, Y.; Shimozone, K.; Nishiyama, H. *Inorg. Chim. Acta* **2006**, *359*, 1725–1730.

(42) Soro, B.; Stoccoro, S.; Minghetti, G.; Zucca, A.; Cinellu, M. A.; Manassero, M.; Gladiali, S. *Inorg. Chim. Acta* **2006**, *359*, 1879–1888.

(43) Szabo, K. J. *Synlett* **2006**, 811–824.

(44) Wallner, O. A.; Olsson, V. J.; Eriksson, L.; Szabo, K. J. *Inorg. Chim. Acta* **2006**, *359*, 1767–1772.

(45) Yoon, M. S.; Ramesh, R.; Kim, J.; Ryu, D.; Ahn, K. H. *J. Organomet. Chem.* **2006**, *691*, 5927–5934.

(46) Aydin, J.; Kumar, K. S.; Sayah, M. J.; Wallner, O. A.; Szabo, K. J. *J. Org. Chem.* **2007**, *72*, 4689–4697.

(47) Debono, N.; Iglesias, M.; Sanchez, F. *Adv. Synth. Catal.* **2007**, *349*, 2470–2476.

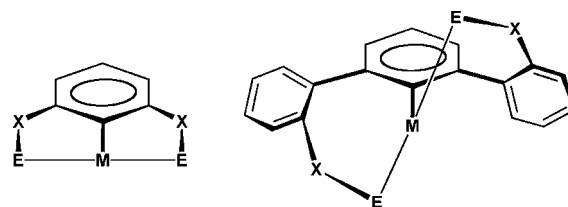
(48) Benito-Garagorri, D.; Kirchner, K. *Acc. Chem. Res.* **2008**, *41*, 201–213.

(49) Bolliger, J. L.; Blacque, O.; Frech, C. M. *Angew. Chem., Int. Ed.* **2007**, *46*, 6514–6517.

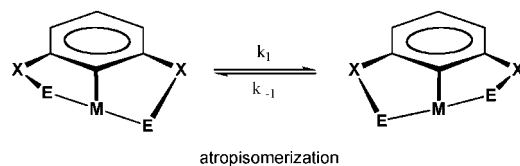
(50) Ma, L.; Woloszynek, R. A.; Chen, W.; Ren, T.; Protasiewicz, J. D. *Organometallics* **2006**, *25*, 3301–3304.

(51) Ma, L.; Imbesi, P. M.; Updegraff, J. B., III; Hunter, A. D.; Protasiewicz, J. D. *Inorg. Chem.* **2007**, *46*, 5220–5228.

Chart 1

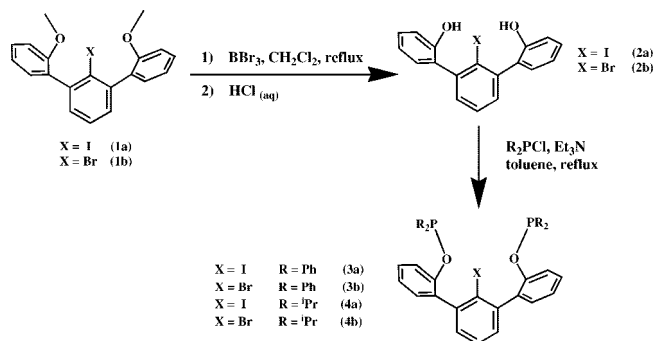


m-xylyl platform compared to 2,6-dibenzylphenyl platform



atropisomerization

Scheme 1



synthesis of *m*-terphenyls.^{52,53} Compound **1b** was obtained in 61% yield by use of bromine in place of iodine used in procedure for **1a**. The ¹H NMR spectra of **1a** and **1b** are consistent with characterization of **1a** reported in the literature.^{54–56}

Two isomers of **1a** and **1b** are indicated by two individual peaks near 3.8 ppm whose combined integrals indicate six protons relative to the signals for the eleven protons in the aromatic region. It is reasonable to ascribe these species as *syn*- and *anti*-isomers, resulting from different conformations of the flanking phenyl rings about the aryl-aryl bonds.

The dimethoxy-*m*-terphenyls, **1a–b** were converted to dihydroxy compounds **2a** and **2b** by demethylation promoted by BBr₃ (Scheme 1).⁵⁷ While it was reported that demethylation of the nonhalogenated analog, 2,2''-dimethoxy-*m*-terphenyl (**1c**, X = H, Scheme 1) required only one equivalent of BBr₃, full conversion of **1a–b** necessitated use of two equivalents of BBr₃. Workup with HCl followed by purification via precipitation from CH₂Cl₂ with hexanes gave **2a** and **2b** in 88 and 90% yields, respectively.

Diphosphinite pro-ligands **3a–b** and **4a–b** were synthesized from **2a–b** following procedures analogous to those reported for the syntheses of R₂POPh and 1,3-(R₂PO)₂Ph. Compounds **2a** and **2b** thus provided **3a** and **3b**, respectively, after a 3 h reflux in toluene with chlorodiphenylphosphine in the presence

(52) Saednya, A.; Hart, H. *Synthesis* **1996**, 1455–1458.

(53) Hart, H.; Harada, K.; Du, C. J. F. *J. Org. Chem.* **1985**, *50*, 3104–3110.

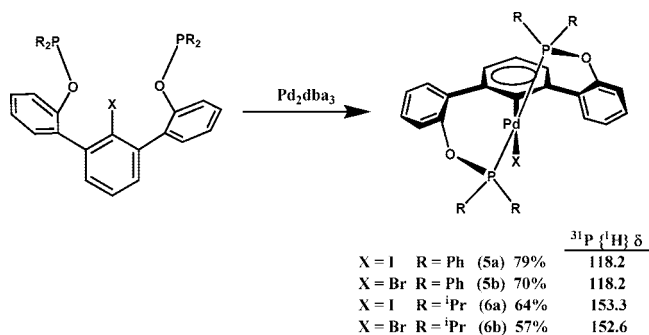
(54) Ionkin, A. S.; Marshall, W. J. *Heteroat. Chem.* **2003**, *14*, 360–364.

(55) Rabe, G. W.; Zhang-Pressé, M.; Riederer, F. A.; Yap, G. P. A. *Inorg. Chem.* **2003**, *42*, 3527–3533.

(56) Rabe, G. W.; Riederer, F. A.; Zhang-Pressé, M.; Rheingold, A. L. *Organometallics* **2007**, *26*, 5724–5726.

(57) Grewal, R. S.; Hart, H.; Vinod, T. K. *J. Org. Chem.* **1992**, *57*, 2721–2726.

Scheme 2. Synthesis of Palladium Pincer Complexes



of excess triethylamine. Compounds **4a–b** were synthesized in an analogous manner using chlorodiisopropylphosphine. Monitoring of the reaction progress by ³¹P and ¹H NMR spectroscopic analyses of reaction aliquots showed formation of both **4a** and **4b** required longer (20 h) reaction times compared to **3a–3b**.

Pro-ligands **3a–b** were isolated as sticky tan solids and **4a–b** were isolated as pale yellow oils. The ³¹P{¹H} NMR resonances of the diphosphinite ligands are in agreement with the reported values for similar phosphinite and diphosphinite ligands.^{58,59} Spectra of **3a** and **3b** both showed ³¹P{¹H} NMR resonances at δ 111.8, while **4a** and **4b** displayed peaks at δ 146.7 and 146.9, respectively. The susceptibility of these compounds to oxidation made complete purification difficult. Reports for related diphosphinite ligands indicated that further purification may not be required for the formation and isolation of complexes with palladium.⁵⁹ Diphosphinite pro-ligands **3a–b** and **4a–b** were thus used without further purification.

Synthesis of Diphosphinite Pincer Complexes. The pincer complexes **5a–b** and **6a–b** were readily synthesized from ligand precursors by reaction with 0.5 equivalents of Pd₂dba₃ (dba = dibenzylideneacetone) in benzene at room temperature (Scheme 2).⁴⁴ Reaction progress was monitored using ³¹P{¹H} NMR spectroscopy to observe the consumption of **3a–b** or **4a–b**. For the synthesis of **5a–b**, complete consumption of **3a–b** was observed after reacting for 1 h. The synthesis of **6a** and **6b**, however, required a 20 h reaction time for full reaction. The air stable palladium pincer complexes were readily purified by column chromatography. Complexes **5a–b** were easily purified by first eluting dibenzylideneacetone with 10% ethyl acetate in hexanes followed by elution of the desired complex with CHCl₃. Complexes **6a–b** required slightly more care to purify as these metal complexes eluted before dibenzylideneacetone with 10% ethyl acetate in hexanes.

All four metal complexes were characterized by ¹H, ¹³C{¹H}, and ³¹P{¹H} NMR spectroscopy and elemental analysis. As with similar diphosphinite complexes, a small downfield shift was observed for the phosphorus resonance of the metal complex relative to the free ligand.³⁵ This shift was 8–9 ppm for the bis(diphenylphosphinite) complexes **5a–b**. The bis(diisopropylphosphinite) complexes **6a–b** had a downfield shift of approximately 6 ppm relative to the starting ligands **4a–b**. The complexes were found to have high stability to air as they remained unchanged in solution after several days of exposure to air.

X-Ray Crystallographic Analyses. Single crystal X-ray diffraction analysis was used to determine the structures of the

palladium complexes. The structures of **5a–b** are shown in Figure 1 and **6a–b** in Figure 2. As expected, these diphosphinite complexes are structurally similar to [2,6-(2-Ph₂PCH₂-C₆H₄)₂C₆H₃PdBr] (**7**), a diphosphine *m*-terphenyl pincer complex that was reported previously.⁵⁰ Key bond lengths and angles about the palladium centers in **5a–b**, **6a–b**, and **7** are summarized in Table 1. The iodide analogs **5a** and **6a** differ slightly from their respective bromide counterparts **5b** and **6b** with regard to the Pd–X bond which is longer when X = I than when X = Br. Complexes **5a–b** are very similar to **7**.

Complexes **5a–b** and **7** exhibit pseudo square planar geometries around their Pd(II) centers and crystallographically imposed C₂ axes of symmetry passing through the C(1)–Pd–X bond. A twist angle, Φ, may be defined for the angle between the plane of the phenyl ring containing C1 and the plane containing palladium and the four atoms directly attached to it. Complex **7**, with Φ = 76.7°, has the highest twist angle of any reported pincer complex. Complex **5a** (Φ = 73.9°) and **5b** (Φ = 73.8°) are only slightly less twisted than **7**.

The structures of complex **6a–b** have a few notable differences compared to complexes **5a–b** and **7**. These differences arise from the steric effects of the relatively bulky isopropyl groups in **6a–b** that cause the geometry around the palladium atom in **6a–b** to deviate somewhat from planarity. Steric interactions between the isopropyl groups and the halogen atom force the halogen atom out of the plane containing C(1), P(1), P(2), and Pd. As a result, in **6a–b**, the C(1)–Pd–X bond angles are somewhat smaller than the 180° C(1)–Pd–X bond angles found in **5a–b**. Another slight difference between **6a–b** and **5a–b** is a 10% decrease in twist angle for complexes **6a–b** relative to **5a–b**. Even with these differences, the structures of **6a–b** are still quite similar to **5a–b** and **7**.

Suzuki–Miyaura CC Cross Coupling Reactions Using Complexes 5b and 6b. Preliminary screening of **5a–b** and **6a–b** as catalysts for the coupling of phenylboronic acid with several aryl bromides revealed that the iodide compounds, **5a** and **6a**, had nearly the same catalytic activity as their respective bromide counterparts, **5b** and **6b**. Examination of **5b** and **6b** for catalytic activity in Suzuki–Miyaura cross coupling reactions of *p*-tolylboronic acids with a variety of aryl bromides and chlorides was thus undertaken (Scheme 3). Experiments were conducted in refluxing 1,4-dioxane in the presence of excess Cs₂CO₃, and the products were isolated by filtering reaction mixtures through a thin pad of silica gel followed by evaporation of solvent under reduced pressure. This method proved successful in most cases to give the product in >95% purity as estimated by ¹H NMR spectroscopy.

Complex **5b** proved to be an excellent catalyst precursor for the coupling reaction between *p*-tolylboronic acid and a variety of aryl bromides (Table 2). These tests were carried out in refluxing 1,4-dioxane in the presence of Cs₂CO₃ with 1 mol% of the complex. After 1 h, desired coupling products were isolated in >88% yields for all aryl bromides which were screened. An isolated yield of 99% was obtained when electron-rich 2-bromoanisole was utilized as the reactant. Even sterically hindered 2-bromomesitylene underwent coupling to give the desired biphenyl product in 88% yield. The use of several different solvents and bases were explored with complex **5b** in an effort to enhance its performance under the reaction conditions. However, complex **5b** was unsuccessful in Suzuki–Miyaura CC coupling reactions utilizing aryl chlorides under a variety of conditions.

These studies showed that while complex **5b** was effective for coupling *p*-tolylboronic acid with aryl bromides, complex

(58) Bedford, R. B.; Hazelwood, S. L.; Horton, P. N.; Hursthouse, M. B. *Dalton Trans.* **2003**, 4164–4174.

(59) Bedford, R. B.; Draper, S. M.; Noelle Scully, P.; Welch, S. L. *New J. Chem.* **2000**, 24, 745–747.

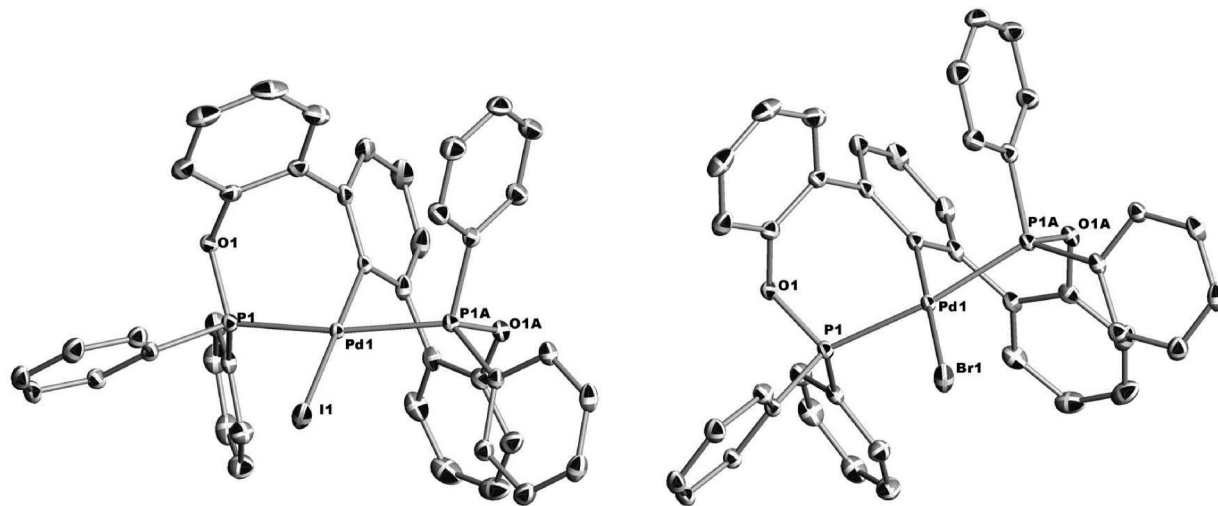


Figure 1. Ortep representations (50% probability ellipsoids) of the molecular structure of **5a** (left) and **5b** (right).

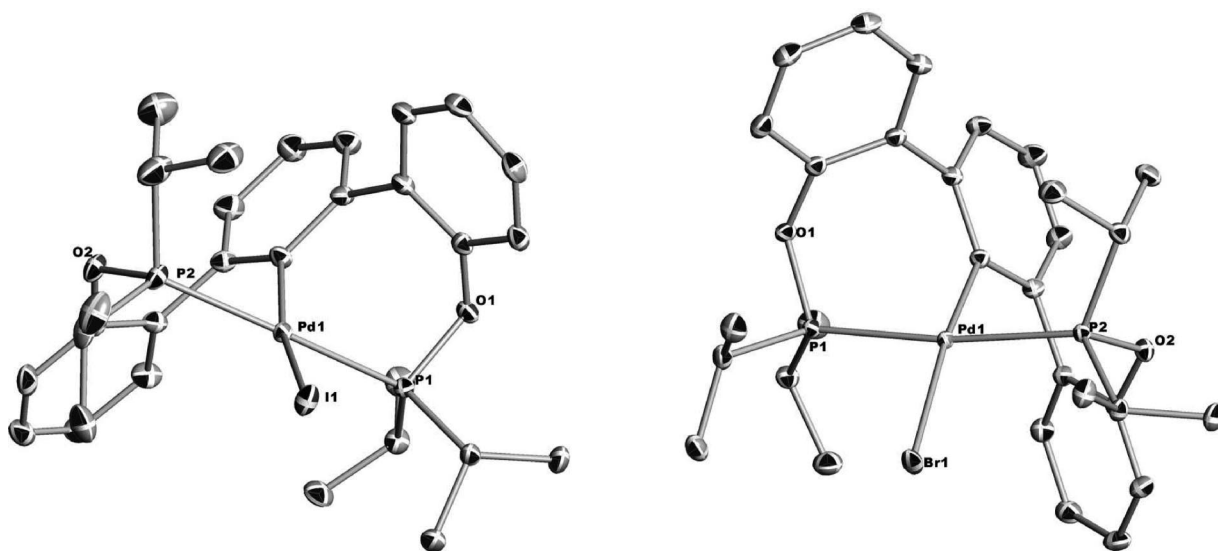
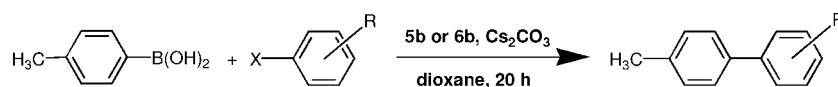


Figure 2. Ortep representations (50% probability ellipsoids) of the molecular structure of **6a** (left) and **6b** (right).

Table 1. Selected Bond Lengths and Angles

	7 ⁵⁰	5a	5b ⁵⁰	6a	6b
Pd–C(1) (Å)	2.067(4)	2.058(2)	2.063(3)	2.053(2)	2.0442(14)
Pd–P(1) (Å)	2.3071(7)	2.2808(4)	2.2824(5)	2.3365(5)	2.3023(4)
Pd–P(2) (Å)	2.3071(7)	2.2808(4)	2.2824(5)	2.3026(5)	2.3271(4)
Pd–X(Å)	2.5024(5)	2.6408(3)	2.4918(4)	2.6689(2)	2.51449(18)
C(1)–Pd–X	180.0°	180.0°	180.0°	165.90(6)°	168.20(4)°
P(1)–Pd–P(2)	169.48(4)°	167.53°	167.41(3)°	172.393(19)°	172.772(14)°
Twist Angle (Φ)	76.7°	73.9°	73.8°	66.8°	66.4°

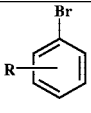
Scheme 3. Suzuki–Miyaura CC Coupling Reactions



6b was shown to promote the CC coupling reaction of *p*-tolylboronic acid to either aryl bromides or aryl chlorides. Complex **6b** was chosen for a more thorough evaluation of its catalytic properties because of its superior performance. Several aryl bromides and aryl chlorides were used as substrates for coupling with *p*-tolylboronic acid (Table 3). Unless otherwise noted, 1 mol% of complex **6b** was used. Reactions were carried out at three different reaction temperatures in order to determine catalytic activity under a variety of conditions. In refluxing 1,4-dioxane, the coupling

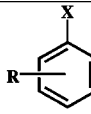
reaction proceeded in excellent yield for all substrates evaluated. The most noteworthy results are the coupling of the boronic acid with chloromesitylene in 86% yield and with 2-chloroanisole in 99% yield. Relatively few palladium complexes are capable of catalyzing the Suzuki–Miyaura reaction with sterically hindered or electron rich aryl chlorides.^{15,17,60} Furthermore, these yields are, to our knowledge, among the highest attained using PCP pincer complexes in the Suzuki–Miyaura reaction with such sterically hindered or electron rich aryl chlorides.^{49,60,61}

Table 2. Suzuki–Miyaura CC Coupling Reactions between Substituted Arylbromides and *p*-Tolylboronic Acid Promoted by **5b**

 R =	X	mol% 5b	Temperature (°C)	Yield (%) ^a
H	Br	1	100	99
2-methoxy	Br	1	100	99
2,4,6-trimethyl	Br	1	100	88

^a Isolated yield from 0.6 mmol aryl halide, 0.9 mmol *p*-tolylboronic acid, 1.8 mmol of Cs₂CO₃, 2 mL dioxane

Table 3. Suzuki–Miyaura CC Coupling Reactions between Substituted Arylhalides and *p*-Tolylboronic Acid Promoted by **6b**

 R =	X	mol% 6b	Temperature (°C)	Yield (%) ^a
H	Br	1	100	96
H	Br	1	75	98
H	Br	1	50	76 ^b
2-methyl	Br	1	100	98
2-methyl	Br	1	75	97
2-methyl	Br	1	50	45 ^b
2-methoxy	Br	1	100	99
2-methoxy	Br	1	75	96
2-methoxy	Br	1	50	36
2,4,6-trimethyl	Br	1	100	87
2,4,6-trimethyl	Br	1	75	77 ^b
2,4,6-trimethyl	Br	1	50	<10
H	Cl	1	100	89
H	Cl	1	75	68
H	Cl	2	75	79
2-methyl	Cl	1	100	93
2-methyl	Cl	1	75	61
2-methyl	Cl	2	75	62 ^b
2-methoxy	Cl	1	100	99
2-methoxy	Cl	1	75	82
2-methoxy	Cl	2	75	83 ^b
2-methoxy	Cl	0.5	75	52 ^b
4-methoxy	Cl	1	75	81
4-methoxy	Cl	2	75	83
2,4,6-trimethyl	Cl	1	100	86
2,4,6-trimethyl	Cl	1	75	68
2,4,6-trimethyl	Cl	2	75	69 ^b

^a Isolated yield from 0.6 mmol aryl halide, 0.9 mmol *p*-tolylboronic acid, 1.8 mmol of Cs₂CO₃, 2 mL dioxane. ^b Analysis of reaction products by protocol described in text complicated by presence of other impurities, and thus ¹H NMR spectroscopy was used to correct yields.

The same reactions were run at 75 °C while all other conditions remained the same. Of the aryl bromides, only bromomesitylene gave a significant decrease in coupling yield at this temperature. The aryl chlorides, on the other hand, all had significantly reduced yields at 75 °C. Peculiarly, electron rich 2-chloroanisole and 4-chloroanisole gave respectable yields for biaryl formation. Increasing the catalyst loading to 2 mol%, however, gave a notable increase in yield only for chlorobenzene and 2-chlorotoluene. Even with these substrates, the increase in yield was only slightly more than 10%. It is quite notable that the coupling reaction occurred when using aryl chlorides at 75 °C since pincer complexes usually do not catalyze such reactions using unactivated chloroarenes at temperatures below 100 °C (vide infra), though reaction temperatures as low as room

(60) Walker, S. D.; Barder, T. E.; Martinelli, J. R.; Buchwald, S. L. *Angew. Chem., Int. Ed.* **2004**, *43*, 1871–1876.

(61) Rosa, G. R.; Ebeling, G.; Dupont, J.; Monteiro, A. L. *Synthesis* **2003**, 2894–2897.

temperature have been achieved with other palladium complexes.^{14,15,62} An additional test was run at 75 °C was done with 2-chloroanisole using only 0.5 mol% of **6b** which gave a yield of 52% and thus a turnover number of 104.

Complex **6b** was tested for catalytic activity at a reaction temperature of 50 °C while maintaining all other conditions. At this temperature, desired coupling was not observed for any of the aryl chlorides used. Optimization of the reaction conditions was attempted by utilizing alternative bases and even aryl trihydroxyborates⁶³ as reactants, but all efforts were unsuccessful in attaining coupling at 50 °C with aryl chlorides as substrates. While yields were depressed, aryl bromides, with the exception of bromomesitylene, were successfully coupled at 50 °C.

Two different reaction mechanisms are conceivable for the coupling of aryl halides and aryl boronic acids by palladium pincer complexes and other related palladacycles. In one mechanism, the complex releases colloidal Pd(0) which might serve as the active catalyst by a Pd(0)/Pd(II) catalytic cycle. In the other mechanism, the complex remains intact and catalysis occurs via a Pd(II)/Pd(IV) catalytic cycle. For the majority of palladacycles, evidence suggests that the Pd(0)/Pd(II) catalytic cycle is followed.^{64–68} There have been, however, a small number of pincer complexes reported for which mechanistic tests suggest a Pd(II)/Pd(IV) catalytic cycle.⁴⁹

Observations on these catalysis reactions are consistent with a classical Pd(0)/Pd(II) catalytic cycle. Reaction mixtures begin turning yellow fairly soon after being heated in an oil bath. At 100 °C, color changes became evident within about 1 min. After reacting for 20 h, black precipitates were also clearly evident. At 75 °C, similar colorations developed more slowly and were apparent within 5 min. Similar black precipitates were also evident after 20 h. Reaction mixtures involving aryl chlorides at 50 °C slowly turned yellow, but no black precipitate was evident. When using aryl bromides at 50 °C, the reactions slowly turned yellow and some black precipitate was evident after 20 h.

As the more successful CC coupling reactions were also accompanied by the visual indicators often attributed to the formation of elemental palladium, it seems reasonable to ascribe the efficacy of compound **6b** to its ability to release Pd(0) in a beneficial way. A more definitive analysis involves using elemental mercury to amalgamate released palladium to remove participation of Pd(0) in the catalytic cycle.^{66–71} Catalytic CC coupling reactions between 2-chloroanisole or chlorobenzene with *p*-tolylboronic acid at 75 °C were thus attempted in the presence of a drop (ca. 120 mg) of mercury (99.999% purity). Analysis of such reaction mixtures showed no CC coupling product, indicating that the catalytic activity of complex **6b** is

(62) Navarro, O.; Kelly, R. A., III; Nolan, S. P. *J. Am. Chem. Soc.* **2003**, *125*, 16194–16195.

(63) Cammidge, A. N.; Goddard, V. H. M.; Gopee, H.; Harrison, N. L.; Hughes, D. L.; Schubert, C. J.; Sutton, B. M.; Watts, G. L.; Whitehead, A. J. *Org. Lett.* **2006**, *8*, 4071–4074.

(64) Beletskaya, I. P.; Cheprakov, A. V. *J. Organomet. Chem.* **2004**, *689*, 4055–4082.

(65) Dupont, J.; Consorti, C. S.; Spencer, J. *Chem. Rev.* **2005**, *105*, 2527–2571.

(66) Yu, K.; Sommer, W.; Richardson, J. M.; Weck, M.; Jones, C. W. *Adv. Synth. Catal.* **2005**, *347*, 161–171.

(67) Bergbreiter, D. E.; Osburn, P. L.; Frels, J. D. *Adv. Synth. Catal.* **2005**, *347*, 172–184.

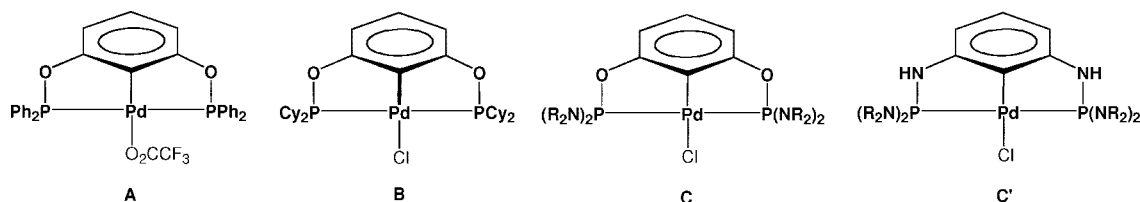
(68) Eberhard, M. R. *Org. Lett.* **2004**, *6*, 2125–2128.

(69) Widegren, J. A.; Finke, R. G. *J. Mol. Catal. A: Chem.* **2003**, *198*, 317–341.

(70) Phan, N. T. S.; Van Der Sluys, M.; Jones, C. W. *Adv. Synth. Catal.* **2006**, *348*, 609–679.

(71) Sommer, W. J.; Yu, K.; Sears, J. S.; Ji, Y.; Zheng, X.; Davis, R. J.; Sherrill, C. D.; Jones, C. W.; Weck, M. *Organometallics* **2005**, *24*, 4351–4361.

Chart 2



coupled somehow to the formation of colloidal Pd(0).⁶⁸ Heating (75 °C) solutions of **6b** alone or in the presence of mercury in dioxane for extended periods of time (16 h) provided no evidence of decomposition, attesting to the inherent thermal robustness of the compound. Solutions of **6b** heated in the presence of Cs₂CO₃, or a mixture of Cs₂CO₃ and Hg, however, became yellow colored and gave new species as indicated by the presence of new ³¹P NMR signals (62.2 and 52.6 ppm, respectively). These new resonances might suggest the presence of ¹Pr₂P(=O)OAr functionalities⁷² and oxidation of the ligand system in **6b**. One of several possible transformations of palladium phosphinite ligands involves hydrolysis.⁷³ At this time a fuller picture of the process leading to colloidal Pd(0) is not available, due to the obvious complexity of the reagents and additives all playing possible roles in transforming the precatalyst **6b** into its active form.

Regardless of mechanism, complex **6b** displays noteworthy activity as a precatalyst. Comparisons to some recent work on PCP diphosphinite pincer complexes (Chart 2) can be made. Complex **A** has shown good activity for promoting the coupling of bromobenzenes with phenyl boronic acid, but is only able to achieve effective conversions with the activated chloroarene, 4-chloronitrobenzene.⁵⁹ The closely related derivative **B** was also reported to utilize 4-chloronitrobenzene in coupling with phenylboronic acid at only 40 °C, albeit it at very low conversions (9–12%).⁷⁴ Compounds **C** and **C'** (NR₂ = piperidinyl) display impressive activities, and can couple even unactivated chloroarenes with phenylboronic acid with both high efficiency and rates at 100 °C.⁴⁹ This system is very interesting because no evidence for the participation of colloidal palladium was found, for example, by the lack of impact on catalysis by the addition of mercury.

The activity of complex **6b** might be attributed to the differently sized chelate rings, having 7 atoms versus 5 (see examples in Chart 2). It has been recently reported that in the Heck reaction involving the olefination of haloarenes, PCP pincer complex **E** outperforms complex **D** (Chart 3) and has a greater range of accessible substrates.^{75,76}

Conclusion

We have synthesized four diphosphinite palladium pincer complexes based on a *m*-terphenyl framework. The synthesis of the pincer ligands and complexes was accomplished using standard methods for the synthesis of diphosphinite pincer complexes. Single crystal X-ray diffraction methods were used

(72) Keglevich, G.; Tamas, A.; Parlagh, G.; Toke, L. *Heteroat. Chem.* **2001**, *12*, 38–41.

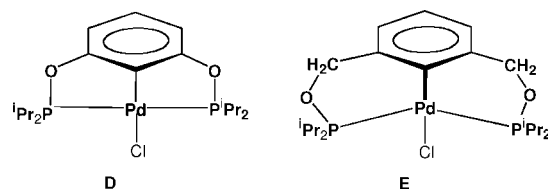
(73) Pryjomka, I.; Bartosz-Bechowski, H.; Ciunik, Z.; Trzeciak, A. M.; Ziolkowski, J. J. *Dalton Trans.* **2005**, 213–220.

(74) Gong, J.-F.; Zhang, Y.-H.; Song, M.-P.; Xu, C. *Organometallics* **2007**, *26*, 6487–6492.

(75) Morales-Morales, D.; Redon, R.; Yung, C.; Jensen, C. M. *Chem. Commun.* **2000**, 1619–1620.

(76) Naghipour, A.; Sabounchei, S. J.; Morales-Morales, D.; Canseco-Gonzalez, D.; Jensen, C. M. *Polyhedron* **2007**, *26*, 1445–1448.

Chart 3



to analyze the structures of these complexes. Complexes **5b** and **6b** were evaluated for their catalytic activity in the Suzuki–Miyaura coupling reaction between 4-tolylboronic acid and a variety of aryl halides. Complex **5b** proved to be excellent for promoting the CC coupling of 4-tolylboronic acid with aryl bromides, including bromomesitylene. Complex **6b** had even higher catalytic activity as it successfully promoted the CC coupling of the boronic acid with aryl chlorides in high yield and even at reduced temperatures. Mechanistic investigations using elemental mercury suggest that these pincer complexes may ultimately serve as precursors for the release of highly active colloidal Pd(0) as the actual catalytic species.

Experimental Section

General Procedures. All reactions, unless otherwise stated, were carried out utilizing Schlenk techniques or in an MBRAUN Labmaster 130 drybox under an atmosphere of dry N₂. Tetrahydrofuran (THF), diethyl ether, hexanes and *n*-pentane were purified prior to use by distillation from sodium/benzophenone ketyl under an atmosphere of dry N₂. Benzene (anhydrous) and toluene (Anhydrous, 99.9%) were purchased from Acros and used as received. Methylene chloride was passed through alumina and degassed prior to use. 1,4-Dioxane was dried over 4 Å molecular sieves and degassed immediately prior to use. Diphenylchlorophosphine (95% tech.) and diisopropylchlorophosphine (97%) were purchased from Acros and used without further purification. *para*-Tolylboronic acid was synthesized according to a literature procedure⁷⁷ and was purified by recrystallization from H₂O or by repeated rinsing with hexanes.

NMR data were recorded on a Varian Inova spectrometer operating at 400, 100, and 161.8 MHz for the ¹H, ¹³C{¹H}, and ³¹P{¹H} spectra, respectively, unless otherwise stated. ³¹P{¹H} NMR data are referenced to an external 85% H₃PO₄ standard, while the ¹H and ¹³C{¹H} NMR data are referenced using residual solvent signals.

2,6-(2-CH₃OC₆H₄)₂C₆H₃I (1a). A round-bottom flask was equipped with a reflux condenser and charged with a stirbar before the addition of 200 mL of THF. 1,3-Dichlorobenzene (5.00 g, 34.0 mmol) was added via syringe and the contents were cooled to –78 °C. With rapid stirring, *n*-BuLi (16.3 mL, 40.8 mmol) was added dropwise via syringe over 30 min during which the clear solution turned milky white in color. The contents were stirred at –78 °C for 2 h. To this was added a solution of 2-methoxyphenylmagnesium bromide (freshly prepared from 2-bromoanisole (22.3 g, 119 mmol)

(77) Norrild, J. C.; Eggert, H. *J. Am. Chem. Soc.* **1995**, *117*, 1479–1484.

Table 4. Selected Data Collection and Structure Solution Information

compound	5a	5b	6a	6b
Empirical formula	C ₄₂ H ₃₁ IO ₂ P ₂ Pd	C ₄₂ H ₃₁ BrO ₂ P ₂ Pd	C ₃₀ H ₃₉ IO ₂ P ₂ Pd	C ₃₀ H ₃₉ BrO ₂ P ₂ Pd
Formula weight	862.91	815.92	726.85	679.86
Temperature (K)	100	100	100	100 ^a
Wavelength (Å)	0.71073	0.71073	0.71073	0.71073
Crystal system	Orthorhombic	Orthorhombic	Monoclinic	Monoclinic
Space group	<i>Pbcn</i>	<i>Pbcn</i>	<i>P2(1)/n</i>	<i>P2(1)/n</i>
Unit cell dimensions	<i>a</i> = 15.1802(5) <i>b</i> = 11.6483(3) <i>c</i> = 19.6981(6) α = 90 β = 90 γ = 90	<i>a</i> = 14.9444(2) <i>b</i> = 11.6289(2) <i>c</i> = 19.7745(3) α = 90 β = 90 γ = 90	<i>a</i> = 9.1944(3) <i>b</i> = 16.2698(5) <i>c</i> = 19.5100(6) α = 90 β = 94.999(1) γ = 90	<i>a</i> = 9.2586(1) <i>b</i> = 16.0146(2) <i>c</i> = 19.3448(3) α = 90 β = 95.296(1) γ = 90
Volume (Å ³)	3483.1(2)	3436.55(9)	2907.4(2)	2856.06(6)
Z	4	4	4	4
Density (calcd. g/cm ³)	1.646	1.577	1.661	1.581
Absorption coeff. (mm ⁻¹)	1.548	1.833	1.836	2.187
<i>F</i> (000)	1712	1640	1456	1384
Crystal size (mm)	0.58 × 0.40 × 0.10	0.26 × 0.20 × 0.12	0.40 × 0.20 × 0.10	0.35 × 0.35 × 0.20
Crystal color and shape	Lt. brown plate	Lt. brown block	Lt. yellow block	Lt. yellow block
θ range data collection	2.71~33.17	3.03~33.14	1.63~28.32	1.65~27.5
Limiting indices	-23 < <i>h</i> < 23 -17 < <i>k</i> < 16 -30 < <i>l</i> < 30	-22 < <i>h</i> < 10 -8 < <i>k</i> < 17 -30 < <i>l</i> < 23	-12 < <i>h</i> < 12 -21 < <i>k</i> < 21 -25 < <i>l</i> < 25	-12 < <i>h</i> < 12 -20 < <i>k</i> < 16 -25 < <i>l</i> < 20
Reflections collected	78927	11657	48996	29738
Independent reflections	6639	6006	7198	6546
Refinement method	Full-matrix least-squares on <i>F</i> ²			
Data/restraints/parameters	78927/0/236	11657/0/235	48996/0/333	29738/0/333
Goodness-of-fit on <i>F</i> ²	1.150	1.018	1.102	1.068
Final <i>R</i> indices [<i>I</i> > 2 σ (<i>I</i>)] ^{a,b}	<i>R</i> 1 = 0.0288 <i>wR</i> 2 = 0.0594	<i>R</i> 1 = 0.0362 <i>wR</i> 2 = 0.0774	<i>R</i> 1 = 0.0228 <i>wR</i> 2 = 0.0542	<i>R</i> 1 = 0.0173 <i>wR</i> 2 = 0.0430
<i>R</i> indices (all data)	<i>R</i> 1 = 0.0465 <i>wR</i> 2 = 0.0720	<i>R</i> 1 = 0.0677 <i>wR</i> 2 = 0.0885	<i>R</i> 1 = 0.0239 <i>wR</i> 2 = 0.0550	<i>R</i> 1 = 0.0190 <i>wR</i> 2 = 0.0454

^a $R(F) = \frac{\sum ||F_o| - |F_c||}{\sum |F_o|}$. ^b $R_w(F^2) = \frac{[\sum \{w(F_o^2 - F_c^2)^2\} / \sum \{w(F_o^2)^2\}]^{0.5}}{w^{-1} = \sigma^2(F_o^2) + (aP)^2 + bP}$, where $P = [F_o^2 + 2 F_c^2]/3$ and *a* and *b* are constants adjusted by the program.

and Mg (4.96 g, 20.4 mmol) in 150 mL THF). The resulting solution was then warmed to room temperature before heating under reflux overnight. The contents were cooled to 0 °C before the addition of excess iodine (15.6 g, 61.5 mmol) which was added in portions under positive pressure of N₂. The mixture with iodine was stirred for 1 h. The contents were then poured into an aqueous Na₂SO₃ solution (5% by weight). The organics were extracted with diethyl ether, washed with 5% Na₂SO₃ (1 × 100 mL), brine (3 × 100 mL), collected and dried over MgSO₄. Rotary evaporation yielded an off-white solid which was recrystallized from ethanol to give 8.94 g (63%) of white solid. (Chemical shifts of two isomers are reported without further assigning to *syn*- or *anti*-) ¹H NMR (CDCl₃, 300 MHz): δ 3.81–3.83 (s, 6H), 6.97–7.00 (d, 2H, *J* = 8 Hz), 7.03–7.08 (t, 2H, *J* = 8 Hz), 7.17–7.27 (m, 4H), 7.38–7.46 (m, 3H).

2,6-(2-CH₃OC₆H₄)₂C₆H₃Br (1b). Compound **1b** was synthesized in a manner analogous to that outlined for **1a**. The 2,6-dichlorophenyllithium solution was prepared from 6.47 g of 1,3-dichlorobenzene (44.0 mmol) and 21.1 mL of *n*-BuLi (52.8 mmol) in 200 mL of THF. To this was added a freshly prepared solution of the Grignard reagent (prepared from 2-bromoanisole (28.8 g, 154 mmol) and Mg (6.42 g, 264 mmol) in 200 mL THF). After heating under reflux overnight, bromine (3.10 mL, 60.5 mmol) was added slowly via syringe. The crude product was obtained as for compound **1a**. Purification was accomplished by rinsing with *n*-pentane to yield 9.89 g (61%) of **1b** as a white powder. (Chemical shifts of two isomers are reported without further assigning to *syn*- or *anti*-) ¹H NMR (CDCl₃): δ 3.80–3.82 (s, 6H), 6.98–7.00 (d, 2H, *J* = 8 Hz), 7.04–7.05 (t, 2H, *J* = 8 Hz), 7.26 (t, 2H, *J* = 8 Hz), 7.27 (d, 2H, *J* = 8 Hz), 7.37–7.41 (m, 3H); ¹³C{¹H} NMR (CDCl₃): δ 55.61, 55.66, 110.91, 111.05, 120.21, 120.27, 126.45, 126.57, 129.12, 130.13, 130.22, 130.75, 131.02, 131.12, 131.27, 140.292, 156.57, 156.71. Elemental analysis calculated for C₂₀H₁₇O₂Br: C, 65.05; H, 4.65. Found: C, 64.81; H, 4.70.

2,6-(2-HOC₆H₄)₂C₆H₃I (2a). A round-bottom flask was charged with a stirbar, **1a** (2.00 g, 4.81 mmol), and CH₂Cl₂ (100 mL). The flask was equipped with a reflux condenser. A 1.0 M solution of BBr₃ (9.61 mL, 9.61 mmol) was added dropwise via syringe. The contents were then heated under reflux for 2 h. The solution turned slightly pink in color during this time. The solution was then cooled to room temperature and 3 mL concentrated HCl was slowly added via syringe with rapid stirring. The volatiles were removed via rotary evaporation to yield a pale yellow residue. This was taken up in 100 mL of ethyl acetate and filtered through a pad of silica gel. The filtrate was concentrated via rotary evaporation to yield a light orange solid. The crude solid was taken up in 5 mL CH₂Cl₂ and precipitated into hexanes. The precipitate was isolated by filtration, rinsed with hexanes and dried *in vacuo* to yield **2a** as a pale tan solid (1.64 g, 88%). mp 120–122 °C. (Chemical shifts of two isomers are reported without further assigning to *syn*- or *anti*-) ¹H NMR (CDCl₃): δ 4.75 (broad s, 2H), 6.90 (d, 1H, *J* = 8 Hz), 6.97–7.02 (m, 3H), 7.09–7.15 (m, 2H), 7.24–7.53 (m, 5H). ¹³C{¹H} NMR (CDCl₃): δ 107.6, 115.98, 116.00, 120.63, 120.67, 128.64, 129.00, 129.68, 129.95, 130.15, 130.21, 130.53, 131.81, 132.18, 143.65, 144.04, 151.98, 152.19.

2,6-(2-HOC₆H₄)₂C₆H₃Br (2b). Compound **2b** was synthesized and purified by a method analogous to that outlined for compound **2a**. The following quantities of starting materials were used: 4.00 g (10.8 mmol) **1b**, 21.7 mL (21.7 mmol) 1.0 M BBr₃ in CH₂Cl₂, and 75 mL CH₂Cl₂. Compound **2b** was isolated as a light tan solid (3.32 g, 90%). mp 134–136 °C. (Chemical shifts of two isomers are reported without further assigning to *syn*- or *anti*-) ¹H NMR (CDCl₃): δ 4.94 (broad s, 2H), 6.94 (d, 1H, *J* = 8 Hz), 6.99–7.05 (m, 3H), 7.17–7.22 (m, 2H), 7.28–7.51 (m, 5H). ¹³C{¹H} NMR (CDCl₃): 115.93, 120.66, 126.71, 127.74, 128.10, 128.22, 128.60, 129.66, 129.89, 130.35, 130.66, 131.50, 131.86, 139.42, 139.57, 152.29, 152.45.

2,6-(2-Ph₂POC₆H₄)₂C₆H₃I (3a). A three-neck round-bottom flask was charged with a stirbar and **2a** (0.325 g, 0.837 mmol) before being equipped with a reflux condenser. To this was added anhydrous toluene (40 mL) followed by chlorodiphenylphosphine (0.30 mL, 1.63 mmol). A pale yellow color was evident upon adding the chlorodiphenylphosphine. Excess triethylamine (0.36 mL, 2.51 mmol) was added and the solution became cloudy and pale pink in color. The contents were heated to reflux and the solution became homogeneous. After 3 h, a white precipitate had formed. A small aliquot was collected via syringe and concentrated *in vacuo* for ³¹P{¹H} and ¹H NMR analysis, which demonstrated complete consumption of the starting material by disappearance of the resonance assigned to the hydroxyl groups of **2a** in the ¹H NMR. The contents were cooled to room temperature. The solution was filtered through a thin pad of Celite in a dry box. The Celite was rinsed with additional toluene (2 × 10 mL). The combined organics were concentrated *in vacuo*, yielding a sticky yellow solid. The solid was dissolved in 10 mL of diethyl ether, filtered through Celite, and dried *in vacuo* to yield the desired diphosphinite ligand, **3a**, as a pale-yellow solid, which was not purified further (0.522 g, 82%). (Chemical shifts of two isomers are reported without further assigning to *syn*- or *anti*-) ¹H NMR (CDCl₃): δ 6.98 (d, 2H, *J* = 8 Hz), 7.07 (t, 1H, *J* = 4 Hz), 7.11 (d, 2H, *J* = 8 Hz), 7.23 (d, 2H, *J* = 8 Hz), 7.26–7.34 (broad m, 20H), 7.38 (t, 4H, *J* = 4 Hz). ³¹P{¹H} NMR (CDCl₃): δ 111.8.

2,6-(2-Ph₂POC₆H₄)₂C₆H₃Br (3b). Compound **3b** was synthesized and purified by a method analogous to that outlined for compound **3a**. The following quantities of starting materials were used: 0.500 mg (1.47 mmol) **2b**, 0.53 mL (2.87 mmol) chlorodiphenylphosphine, 0.36 mL (2.51 mmol) triethylamine, and 40 mL of anhydrous toluene. Compound **3b** was isolated as a pale-tan, sticky solid, which was not purified further (0.800 g, 77%). (Chemical shifts of two isomers are reported without further assigning to *syn*- or *anti*-) ¹H NMR (CDCl₃): δ 7.01 (d, 2H, *J* = 8 Hz), 7.08 (t, 1H, *J* = 4 Hz), 7.11 (d, 2H, *J* = 8 Hz), 7.24–7.34 (broad m, 22H), 7.38 (t, 4H, *J* = 4 Hz). ³¹P{¹H} NMR (CDCl₃): δ 111.8.

2,6-(2-ⁱPr₂POC₆H₄)₂C₆H₃I (4a). A three-neck round-bottom flask was charged with a stirbar and **2a** (0.300 g, 0.773 mmol) before being equipped with a reflux condenser. To this was added anhydrous toluene (30 mL) followed by chlorodiisopropylphosphine (0.24 mL, 1.5 mmol) which resulted in a light pink solution. Triethylamine (0.33 mL, 2.3 mmol) was then added, resulting in cloudiness that dissipated within 5 min. The contents were heated to reflux and the solution became homogeneous and clear after 30 min. After heating under reflux for 20 h, the contents were cooled to room temperature. A small aliquot was collected via syringe and concentrated *in vacuo* for ³¹P{¹H} and ¹H NMR analysis, which demonstrated complete consumption of the starting material by disappearance of the resonance assigned to the hydroxyl groups of **2a** in the ¹H NMR. Degassed petroleum ether (10 mL) was added and a white precipitate was evident after a few minutes of stirring. The contents were taken into the dry box and filtered through Celite. The filtrate was concentrated *in vacuo*, yielding a pale-brown oil, which was not purified further (0.308 g, 64%). (Chemical shifts of two isomers are reported without further assigning to *syn*- or *anti*-) ¹H NMR (CDCl₃, 300 MHz): δ 0.86–1.02 (m, 18H), 0.99–1.26 (m, 6H), 1.61–1.84 (m, 4H), 7.02 (t, 2H, *J* = 8 Hz), 7.12–7.15 (m, 2H), 7.20 (d, 2H, *J* = 8 Hz), 7.30–7.38 (m, 4H), 7.49 (t, 1H, *J* = 8 Hz). ³¹P{¹H} NMR (CDCl₃): δ 146.7.

2,6-(2-ⁱPr₂POC₆H₄)₂C₆H₃Br (4b). Compound **4b** was synthesized and purified by a method analogous to that outlined for compound **4a**. The following quantities of starting materials were used: 0.200 g (0.586 mmol) **2b**, 0.18 mL (1.14 mmol) of chlorodiisopropylphosphine, 0.25 mL (1.76 mmol) triethylamine, and 30 mL of anhydrous toluene. Compound **4b** was isolated as a pale-yellow oil, which was not purified further (0.289 g, 86%). (Chemical shifts of two isomers are reported without further

assigning to *syn*- or *anti*-) ¹H NMR (CDCl₃): δ 0.87–1.05 (m, 18H), 1.16–1.31 (m, 6H), 1.66–1.72 (m, 2H), 1.76–1.82 (m, 2H), 7.02 (t, 2H, *J* = 8 Hz), 7.11–7.14 (m, 2H), 7.20 (d, 2H, *J* = 8 Hz), 7.30–7.38 (m, 4H), 7.47–7.51 (t, 1H, *J* = 8 Hz). ³¹P{¹H} NMR (CDCl₃): δ 146.9.

2,6-(2-Ph₂POC₆H₄)₂C₆H₃PdI (5a). A flame dried, 20 mL screw cap vial was charged with a stir bar, **3a** (0.085 g, 0.11 mmol), and 0.051 g (0.056 mmol) Pd₂dba₃. Anhydrous benzene (5 mL) was added and the vial was sealed. The contents were stirred at room temperature and the reaction was monitored by ³¹P NMR analysis. After 1 h, complete consumption of the free ligand was shown by the disappearance of its ³¹P NMR resonance. The dark-purple solution was filtered through Celite. The resulting orange solution was concentrated via rotary evaporation to yield a pale orange solid. The crude product was purified by flash chromatography over silica gel. Dibenzylideneacetone was eluted first with 10% EtOAc/hexanes followed by **5a** which was eluted with chloroform. Rotary evaporation of the chloroform gave a pale orange solid which was rinsed with 5 mL diethyl ether, filtered and dried *in vacuo* to yield analytically pure **5a** as a pale-orange solid (0.077 g, 79%). X-ray quality crystals were grown from vapor diffusion of hexanes into a concentrated chloroform solution at –5 °C. ¹H NMR (CDCl₃): δ 6.21 (d, 2H, *J* = 8 Hz), 6.76 (d, 2H, *J* = 8 Hz), 6.81 (d, 2H, *J* = 8 Hz), 7.01 (t, 2H, *J* = 8 Hz), 7.04 (t, 1H, *J* = 8 Hz), 7.17–7.20 (m, 6H), 7.26–7.29 (m, 4H), 7.35–7.44 (m, 8H), 7.68–7.73 (m, 4H). ¹³C{¹H} NMR (CDCl₃): δ 121.6, 124.9, 125.2, 127.7 (virtual triplet, *J* = 5 Hz), 128.1 (virtual triplet, *J* = 5 Hz), 128.8, 128.9 (virtual triplet, *J* = 7 Hz), 130.1, 130.8, 131.4, 133.0 (virtual triplet, *J* = 7 Hz), 134.4 (virtual triplet, *J* = 22 Hz), 135.7, 143.2, 146.0, 151.6. ³¹P{¹H} NMR (CDCl₃): δ 118.2. Elemental analysis calcd for C₄₂H₃₁O₂P₂PdI: C, 58.46; H, 3.62. Found: C, 58.19; H, 3.65.

2,6-(2-Ph₂POC₆H₄)₂C₆H₃PdBr (5b). Complex **5b** was synthesized and purified by a method analogous to that outlined for complex **5a**. The following quantities of starting materials were used: 0.145 g (0.204 mmol) of **3b**, 0.093 g (0.102 mmol) Pd₂dba₃, and 10 mL of anhydrous benzene. Analytically pure **5b** was isolated as an off-white solid (0.1177 g, 70%). X-ray quality crystals were grown from vapor diffusion of hexanes into a concentrated chloroform solution at –5 °C. ¹H NMR (CDCl₃): δ 6.18 (d, 2H, *J* = 8 Hz), 6.75 (d, 2H, *J* = 8 Hz), 6.80 (d, 2H, *J* = 8 Hz), 6.99 (t, 2H, *J* = 8 Hz), 7.22 (t, 1H, *J* = 8 Hz), 7.14–7.16 (m, 6H), 7.26–7.29 (m, 4H), 7.35–7.46 (m, 8H), 7.72–7.77 (m, 4H). ¹³C{¹H} NMR (CDCl₃): δ 121.6, 124.8, 125.1, 127.7 (virtual triplet, *J* = 5 Hz), 128.0 (virtual triplet, *J* = 5 Hz), 128.8 (virtual triplet, *J* = 7 Hz), 130.1, 131.3, 132.9 (virtual triplet, *J* = 7 Hz), 133.3, 133.6, 134.2 (virtual triplet, *J* = 22 Hz), 135.6, 143.1, 145.9, 151.5. ³¹P{¹H} NMR (CDCl₃): δ 118.2. Elemental analysis calculated for C₄₂H₃₁O₂P₂PdBr: C, 61.82; H, 3.83. Found: C, 61.07; H, 3.78.

2,6-(2-ⁱPr₂POC₆H₄)₂C₆H₃PdI (6a). A flame dried, 20 mL screw cap vial was charged with stir bar, **4a** (0.160 g, 0.258 mmol), and 0.5 equivalents of Pd₂dba₃ (0.118 g, 0.129 mmol). Anhydrous benzene (15 mL) was then added and the vial was sealed. The contents were stirred at room temperature and the reaction was monitored by ³¹P{¹H} NMR analysis. After 20 h, ³¹P{¹H} NMR analysis showed the disappearance of the resonance of the free ligand. The solution was filtered and solvent was removed from the filtrate via rotary evaporation to yield a pale yellow solid. The crude product was purified by flash chromatography over silica gel (EtOAc:hexanes, 1:10). The product after evaporation of volatiles was rinsed with 5 mL diethyl ether, filtered and dried *in vacuo* to yield analytically pure **6a** as a light-orange solid (0.120 g, 64%). X-ray quality crystals were grown from vapor diffusion of hexanes into a concentrated chloroform solution at –5 °C. ¹H NMR (CDCl₃): δ 0.64–0.70 (m, 6H), 1.00–1.06 (m, 6H), 1.24–1.29 (m, 6H), 1.40–1.45 (m, 6H), 2.18–2.24 (m, 2H), 3.28–3.32 (m, 2H), 6.99 (d, 2H, *J* = 8 Hz), 7.07 (d, 2H, *J* = 8 Hz), 7.16 (t, 1H, *J* = 8 Hz), 7.21 (t, 2H, *J* = 8 Hz), 7.26–7.33 (m, 4H). ³¹P{¹H} NMR (CDCl₃):

δ 153.3. Elemental analysis calcd for $C_{30}H_{39}O_2P_2PdI$: C, 49.57; H, 5.41. Found: C, 49.63; H, 5.53.

2,6-[2-OP(*i*Pr)₂C₆H₄]₂C₆H₃PdBr (6b). Complex **6b** was synthesized and purified by a method analogous to that outlined for complex **6a**. The following quantities of starting materials were used: 0.285 g (0.497 mmol) **4b**, 0.228 g (0.249 mmol) Pd₂dba₃, and 10 mL of anhydrous benzene. Analytically pure **6b** was isolated as a white solid (0.192 g, 57%). X-ray quality crystals were grown from vapor diffusion of hexanes into a concentrated chloroform solution at -5 °C. ¹H NMR (CDCl₃): δ 0.65–0.71 (m, 6H), 0.98–1.04 (m, 6H), 1.26–1.32 (m, 6H), 1.40–1.45 (m, 6H), 2.13–2.19 (m, 2H), 3.04–3.11 (m, 2H), 6.98 (d, 2H, $J = 8$ Hz), 7.08 (d, 2H, $J = 8$ Hz), 7.14 (t, 1H, $J = 8$ Hz), 7.21 (t, 2H, $J = 8$ Hz), 7.26–7.33 (m, 4H). ¹³C{¹H} NMR (CDCl₃): δ 16.4, 16.6, 17.3 (virtual triplet, $J = 5$ Hz), 18.5, 27.4 (virtual triplet, $J = 14$ Hz), 29.9 (virtual triplet, $J = 10$ Hz), 122.1, 124.5, 124.9, 128.0, 129.3, 132.1, 136.6, 142.9, 144.2, 152.2. ³¹P{¹H} NMR (CDCl₃): δ 152.6. Elemental analysis calcd for $C_{30}H_{39}O_2P_2PdBr$: C, 52.98; H, 5.78. Found: C, 52.58; H, 5.76.

Typical Procedure for Suzuki–Miyaura CC Coupling Reactions. A 5 mL conical vial was charged with Cs₂CO₃ (0.586 g, 1.8 mmol), *p*-tolylboronic acid (0.122 g, 0.9 mmol), 0.6 mmol of aryl halide, and 1 mol% of either complex **5b** or **6b**. The vial was equipped with a magnetic spinvane and a reflux condenser before being filled with nitrogen. 1,4-Dioxane (2 mL) was added and the vial placed in an oil bath maintained at the desired reaction temperature. After 20 h the reaction was cooled to room temperature, diluted with diethyl ether, and filtered through a thin pad of silica gel. The silica gel was rinsed with 25 mL of additional diethyl ether. The combined organics were concentrated under reduced

pressure to yield the desired coupling product, typically of >95% purity as judged by ¹H NMR spectroscopy.

X-Ray Crystallographic Studies. The X-ray intensity data were measured at 100 K on a Bruker SMART Apex II CCD-based X-ray diffractometers system equipped with a Mo-target X-ray tubes ($\lambda = 0.71073$ Å) located at either Bruker AXS in Madison WI, (compounds **5a** and **5b**) or at Case Western Reserve University (compounds **6a** and **6b**). Data collection and solution parameters are summarized in Table 4. Further information is provided within the cif files supplied as Supporting Information. Crystals were mounted on a MiTeGen micromount using paratone-N which were then frozen. The frames were integrated with the Bruker SAINT build in APEX II software package using a narrow-frame integration algorithm, which also corrects for the Lorentz and polarization effects. Absorption corrections were applied using AXScale. The structures were solved and refined using the Bruker SHELXTL (Version 6.14) software. The positions of all non-hydrogen atoms were derived from the Direct Methods (TREF) solution. With all non-hydrogen atoms being anisotropic and all hydrogen atoms being isotropic the structure was refined to convergence by least-squares method on F², XSELL (Version 6.3.1), incorporated in SHELXTL (Version 6.14).

Acknowledgment. We acknowledge support from the ACS-PRF (PRF 44644-AC3) and Dr. Charles Campana (Bruker AXS) for crystallographic assistance.

Supporting Information Available: CIF files having full X-ray crystallographic data. This material is available free of charge via the Internet at <http://pubs.acs.org>.

OM800626B

Multimetallic Arrays: Symmetrical and Unsymmetrical Bi-, Tri-, and Tetrametallic Organometallic Complexes of Ruthenium(II) and Osmium(II)

Mairi J. Macgregor,[†] Graeme Hogarth,[‡] Amber L. Thompson,[†] and James D. E. T. Wilton-Ely^{*†}

Chemistry Research Laboratory, University of Oxford, Mansfield Road, Oxford OX1 3TA, U.K., and Department of Chemistry, University College London, 20 Gordon Street, London WC1H 0AJ, U.K.

Received July 20, 2008

The cationic complex $[\text{Ru}(\text{C}(\text{C}\equiv\text{CPh})=\text{CHPh})(\text{S}_2\text{CNC}_4\text{H}_8\text{NH}_2)(\text{CO})(\text{PPh}_3)_2]^+$ was prepared from the reaction of $[\text{Ru}(\text{C}(\text{C}\equiv\text{CPh})=\text{CHPh})\text{Cl}(\text{CO})(\text{BTD})(\text{PPh}_3)_2]$ (BTD = 2,1,3-benzothiadiazole) with the zwitterionic dithiocarbamate $\text{H}_2\text{NC}_4\text{H}_8\text{NCS}_2$ and characterized structurally. In situ generation of the metalladithiocarbamate $[\text{Ru}(\text{C}(\text{C}\equiv\text{CPh})=\text{CHPh})(\text{S}_2\text{CNC}_4\text{H}_8\text{NCS}_2)(\text{CO})(\text{PPh}_3)_2]$ followed by treatment with $[\text{Ru}(\text{C}(\text{C}\equiv\text{CPh})=\text{CHPh})\text{Cl}(\text{CO})(\text{BTD})(\text{PPh}_3)_2]$ yielded the symmetrical bimetallic complex $[\{\text{Ru}(\text{C}(\text{C}\equiv\text{CPh})=\text{CHPh})(\text{CO})(\text{PPh}_3)_2\}_2(\text{S}_2\text{CNC}_4\text{H}_8\text{NCS}_2)]$. The same product was also accessible by reaction of $\text{KS}_2\text{CNC}_4\text{H}_8\text{NCS}_2\text{K}$ with $[\text{Ru}(\text{C}(\text{C}\equiv\text{CPh})=\text{CHPh})\text{Cl}(\text{CO})(\text{BTD})(\text{PPh}_3)_2]$. This direct method also yielded the symmetrical bimetallic complexes $[\{\text{Ru}(\text{CH}=\text{CHR})(\text{CO})(\text{PPh}_3)_2\}_2(\text{S}_2\text{CNC}_4\text{H}_8\text{NCS}_2)]$ (R = Bu^t, CPh₂OH, C₆H₄Me-4, CO₂Me, CH₂OSiMe₂Bu^t) and a tetrametallic species when R = C₅H₄FeC₅H₅. The osmium analogues $[\{\text{Os}(\text{CR}^1=\text{CHR}^2)(\text{CO})(\text{PPh}_3)_2\}_2(\text{S}_2\text{CNC}_4\text{H}_8\text{NCS}_2)]$ (R¹ = C≡CPh, R² = Ph; R¹ = H, R² = C₆H₄Me-4) were also prepared by this method. The stepwise deprotonation and functionalization of $[\text{Ru}(\text{C}(\text{C}\equiv\text{CPh})=\text{CHPh})(\text{S}_2\text{CNC}_4\text{H}_8\text{NH}_2)(\text{CO})(\text{PPh}_3)_2]^+$ with NEt₃ and CS₂ was utilized in the generation of the unsymmetrical complexes $[\{\text{Ru}(\text{C}(\text{C}\equiv\text{CPh})=\text{CHPh})(\text{CO})(\text{PPh}_3)_2\}_2(\text{S}_2\text{CNC}_4\text{H}_8\text{NCS}_2)\{\text{Ru}(\text{CH}=\text{CHR})(\text{CO})(\text{PPh}_3)_2\}]$ (R = Bu^t, CPh₂OH, C₆H₄Me-4, CO₂Me, CH₂OSiMe₂Bu^t, C₅H₄FeC₅H₅) and the heterobimetallic variant $[\{\text{Ru}(\text{C}(\text{C}\equiv\text{CPh})=\text{CHPh})(\text{CO})(\text{PPh}_3)_2\}_2(\text{S}_2\text{CNC}_4\text{H}_8\text{NCS}_2)\{\text{Os}(\text{CH}=\text{CHC}_6\text{H}_4\text{Me-4})(\text{CO})(\text{PPh}_3)_2\}]$. The mixed carbonyl–thiocarbonyl complex $[\{\text{Ru}(\text{C}(\text{C}\equiv\text{CPh})=\text{CHPh})(\text{CO})(\text{PPh}_3)_2\}_2(\text{S}_2\text{CNC}_4\text{H}_8\text{NCS}_2)\{\text{Ru}(\text{C}(\text{C}\equiv\text{CPh})=\text{CHPh})(\text{CS})(\text{PPh}_3)_2\}]$ was also prepared by the same stepwise procedure. These are the first reported examples of alkenyl species bridged by a dithiocarbamate ligand. The similarly unprecedented linked bis(alkynyl)diruthenium complex $[\{\text{Ru}(\text{C}\equiv\text{CBu}^t)(\text{CO})(\text{PPh}_3)_2\}_2(\text{S}_2\text{CNC}_4\text{H}_8\text{NCS}_2)]$ was prepared by heating $[\{\text{Ru}(\text{CH}=\text{CHC}_6\text{H}_4\text{Me-4})(\text{CO})(\text{PPh}_3)_2\}_2(\text{S}_2\text{CNC}_4\text{H}_8\text{NCS}_2)]$ with excess HC≡CBu^t. The first molecular complex bearing all three group 8 metals, $[\{\text{Ru}(\text{C}(\text{C}\equiv\text{CPh})=\text{CHPh})(\text{CO})(\text{PPh}_3)_2\}_2(\text{S}_2\text{CNC}_4\text{H}_8\text{NCS}_2)\{\text{Os}(\text{CH}=\text{CHFc})(\text{CO})(\text{PPh}_3)_2\}]$, was achieved through the reaction of $[\text{Ru}(\text{C}(\text{C}\equiv\text{CPh})=\text{CHPh})(\text{S}_2\text{CNC}_4\text{H}_8\text{NH}_2)(\text{CO})(\text{PPh}_3)_2]^+$ with $[\text{Os}(\text{CH}=\text{CHFc})\text{Cl}(\text{CO})(\text{BTD})(\text{PPh}_3)_2]$ (Fc = C₅H₄FeC₅H₅, BTD = 2,1,3-benzothiadiazole). Further trimetallic species $[\{\text{Ru}(\text{C}(\text{C}\equiv\text{CPh})=\text{CHPh})(\text{CO})(\text{PPh}_3)_2\}_2(\text{S}_2\text{CNC}_4\text{H}_8\text{NCS}_2)_2\text{M}]$ (M = Ni, Pd, Pt, Zn) were prepared by the reaction of $[\text{Ru}(\text{C}(\text{C}\equiv\text{CPh})=\text{CHPh})(\text{S}_2\text{CNC}_4\text{H}_8\text{NH}_2)(\text{CO})(\text{PPh}_3)_2]^+$ with Ni(OAc)₂, PdCl₂(NCMe)₂, PtCl₂(NCPh)₂, and Zn(OAc)₂ in the presence of NEt₃ and CS₂.

Introduction

Many transition-metal dithiocarbamate complexes are known,¹ and a number of these have found use in applications as diverse as materials science, medicine, and agriculture. Their extensive metal-centered electrochemistry² and ability to stabilize a wide range of oxidation states have proved to be key factors in many applications. While polyfunctional variants of many ligands have been used to create multimetallic systems, this approach to dithiocarbamates has rarely been exploited.

Recent work to harness their versatility in the area of supramolecular design has illustrated their utility in this regard.³ Our recent contributions in this area have centered on the use

of a piperazine dithiocarbamate that exists as a zwitterion.⁴ This species can be used to coordinate to a first metal center, while retaining the potential to bond to a second on deprotonation and functionalization with CS₂ at the other end. A general strategy for the synthesis of homo- and heterobimetallic

* To whom correspondence should be addressed. E-mail: james.wilton-ely@chem.ox.ac.uk.

[†] University of Oxford.

[‡] University College London.

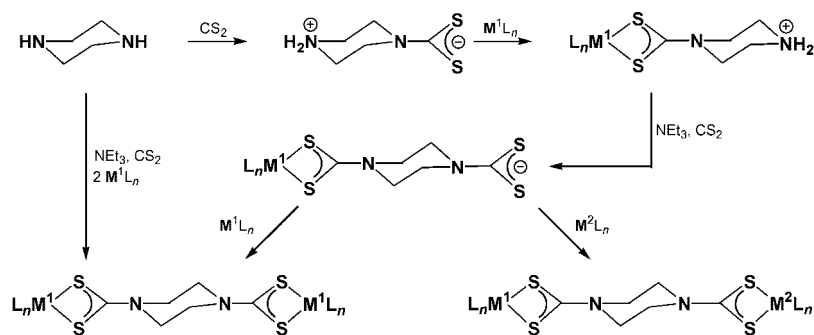
(1) Hogarth, G. *Prog. Inorg. Chem.* **2005**, *53*, 71–561.

(2) Bond, A. M.; Martin, R. L. *Coord. Chem. Rev.* **1984**, *54*, 23–98.

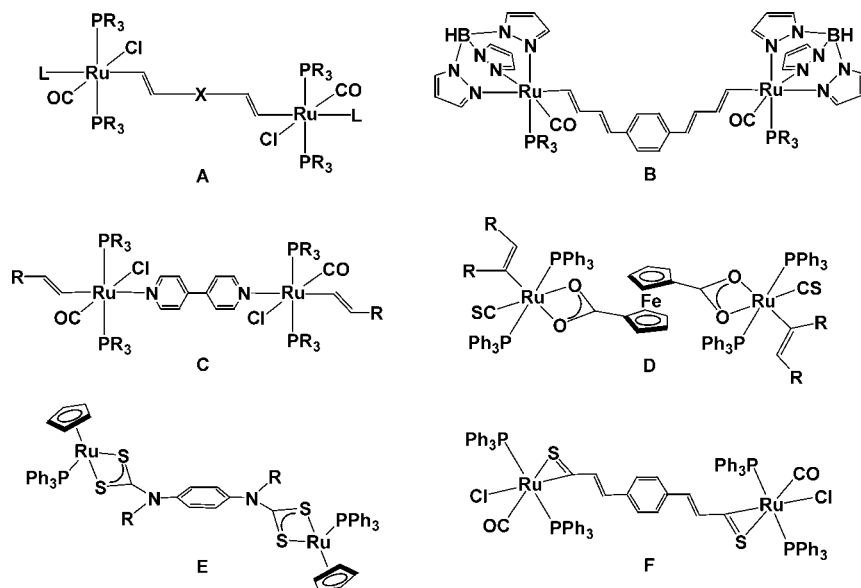
(3) (a) Beer, P. D.; Berry, N. G.; Cowley, A. R.; Hayes, E. J.; Oates, E. C.; Wong, W. W. H. *Chem. Commun.* **2003**, 2408–2409. (b) Wong, W. W. H.; Curiel, D.; Cowley, A. R.; Beer, P. D. *Dalton Trans.* **2005**, 359, 364. (c) Beer, P. D.; Cheetham, A. G.; Drew, M. G. B.; Fox, O. D.; Hayes, E. J.; Rolls, T. D. *Dalton Trans.* **2003**, 603, 611. (d) Beer, P. D.; Berry, N.; Drew, M. G. B.; Fox, O. D.; Padilla-Tosta, M. E.; Patell, S. *Chem. Commun.* **2001**, 199, 200. (e) Padilla-Tosta, M. E.; Fox, O. D.; Drew, M. G. B.; Beer, P. D. *Angew. Chem., Int. Ed.* **2001**, *40*, 4235–4239. (f) Fox, O. D.; Drew, M. G. B.; Beer, P. D. *Angew. Chem., Int. Ed.* **2000**, *39*, 135–140. (g) Vickers, M. S.; Cookson, J.; Beer, P. D.; Bishop, P. T.; Thiebaut, B. *J. Mater. Chem.* **2006**, *16*, 209–215. (h) Cookson, J.; Beer, P. D. *Dalton Trans.* **2007**, 1459, 1472.

(4) (a) Wilton-Ely, J. D. E. T.; Solanki, D.; Hogarth, G. *Eur. J. Inorg. Chem.* **2005**, 4027–4030. (b) Wilton-Ely, J. D. E. T.; Solanki, D.; Knight, E. R.; Holt, K. B.; Thompson, A. L.; Hogarth, G. *Inorg. Chem.*, in press.

Scheme 1. General Scheme for the Generation of Bimetallic Complexes



Scheme 2. Examples of Bimetallic Organotransition-Metal Compounds



complexes using a piperazine dithiocarbamate ligand is shown in Scheme 1.

A particularly intriguing aspect is the accessibility of heterobimetallic systems using this route. However, to date the metal units linked by such ligands⁵ have been simple coordination compounds, largely neglecting the bridging of organotransition-metal centers. Few bimetallic ruthenium complexes with alkenyl ligands are known, and almost all are symmetrical in nature.⁶ Some relevant examples of linked organometallics are shown in Scheme 2. Either the alkenyl ligand is utilized to bridge the metal centers (**A**, X = C₆H₄, C₆H₄C₆H₄, CH₂C(OR)-

C(OR)CH₂, (CH)₂, (CH)₄, (CH)₆; **B**),⁷ or the linker is a diamine (**C**), diisocyanide,^{7a} or a bidentate dicarboxylate (**D**) unit.⁸ Sulfur ligands are rarely used to link organometallic centers. An unusual example is that reported by Shaver,⁹ in which a diruthenium complex (**E**) is isolated from the reaction of 2 equiv of [CpRu(PPh₃)₂SH] with *p*-phenylenediisothiocyanate while reaction of [RuHCl(CS)(PPh₃)₃] with 1,4-diethynylbenzene followed by treatment of carbon monoxide yields a bridging thioacyl (**F**).⁸ Linked diosmium alkenyl complexes are extremely rare, with only two known examples derived from the double hydroosmiation of 1,3,5-triethynylbenzene.¹⁰

(5) Some metal complexes of piperazine bis(dithiocarbamates) have been reported: (a) Esmadi, F. T.; Irshaidat, T. Z. *Synth. React. Inorg. Met.-Org. Chem.* **2000**, *30*, 1347–1362. (b) Glidewell, C.; Johnson, I. L. *Polyhedron* **1988**, *7*, 1371–1375. (c) Siddiqi, K. S.; Zaidi, F. R.; Zaidi, S. A. A. *Synth. React. Inorg. Met.-Org. Chem.* **1980**, *10*, 569–578. (d) Marcotrigiano, G.; Pellacani, G. C.; Preti, C.; Tosi, G. *Bull. Chem. Soc. Jpn.* **1975**, *48*, 1018–1020. (e) Hulanicki, A.; Shishkova, L. *Chem. Anal. (Warsaw)* **1965**, *10*, 837–845. (f) Yin, H. D.; Ma, C. L.; Wang, Y.; Fang, H. X.; Shao, J. X. *Acta Chim. Sinica* **2002**, *60*, 897–903. (g) Yin, H.; Wang, C. *Appl. Organomet. Chem.* **2004**, *18*, 145–146. (h) Tian, L.; Shang, Z.; Yu, Q.; Li, D.; Yang, G. *Appl. Organomet. Chem.* **2004**, *18*, 253–254. (i) Yin, H. D.; Wang, C. H.; Xing, Q. *J. Chin. J. Struct. Chem.* **2004**, *23*, 490–493. (j) Yu, S.-Y.; Zhang, Z.-X.; Cheng, E. C.-C.; Li, Y.-Z.; Yam, V. W.-W.; Huang, H.-P.; Zhang, R. *J. Am. Chem. Soc.* **2005**, *127*, 17994–17995.

(6) Xia, H.; Wen, T. B.; Hu, Q. Y.; Wang, X.; Chen, X. X.; Shek, L. Y.; Williams, I. D.; Wong, K. S.; Wong, G. K. L.; Jia, G. *Organometallics* **2005**, *24*, 562–569.

(7) (a) Jia, G.; Wu, W. F.; Yeung, R. C. Y.; Xia, H. P. *J. Organomet. Chem.* **1997**, *539*, 53–59. (b) Liu, S. H.; Chen, Y.; Wan, K. L.; Wen, T. B.; Zhou, Z.; Lo, M. F.; Williams, I. D.; Jia, G. *Organometallics* **2002**, *21*, 4984–4992. (c) Liu, S. H.; Xia, H.; Wen, T. B.; Zhou, Z.; Jia, G. *Organometallics* **2003**, *22*, 737–743. (d) Liu, S. H.; Hu, Q. Y.; Xue, P.; Wen, T. B.; Williams, I. D.; Jia, G. *Organometallics* **2005**, *24*, 769–772. (e) Liu, S. H.; Xia, H.; Wan, K. L.; Yeung, R. C. Y.; Hu, Q. Y.; Jia, G. *J. Organomet. Chem.* **2003**, *683*, 331–336. (f) Xia, H.; Wen, T. B.; Hu, Q. Y.; Wang, X.; Chen, X.; Shek, L. Y.; Williams, I. D.; Wong, K. S.; Wong, G. K. L.; Jia, G. *Organometallics* **2005**, *24*, 562–569. (g) Maurer, J.; Sarkar, B.; Schwederski, B.; Kaim, W.; Winter, R. F.; Zálaiš, S. *Organometallics* **2006**, *25*, 3701–3712.

(8) Cowey, A.; Hector, A. L.; Hill, A. F.; White, A. J. P.; Williams, D. J.; Wilton-Ely, J. D. E. *T. Organometallics* **2007**, *26*, 6114–6125.

(9) Kovács, I.; Lebus, A.-M.; Shaver, A. *Organometallics* **2001**, *20*, 35–41.

(10) Xia, H.; Wen, T. B.; Hu, Q. Y.; Wang, X.; Chen, X.; Shek, L. Y.; Williams, I. D.; Wong, K. S.; Wong, G. K. L.; Jia, G. *Organometallics* **2005**, *24*, 562–569.

None of these methods is widely applicable to the preparation of unsymmetrical heterobimetallic organometallic complexes. This report applies the approach outlined in Scheme 1⁴ to the area of group 8 alkenyl chemistry.

Results and Discussion

A wide range of ruthenium alkenyl complexes¹¹ is readily accessible from hydrometalation of alkynes by the compounds [RuHCl(CO)L_{2/3}] (L = PⁱPr₃,¹² PPh₃¹³), and many aspects of the resulting alkenyl complexes have been explored in fundamental work by the groups of Werner,¹⁴ Esteruelas,¹⁵ Santos,¹⁶

Caulton,¹⁷ Hill,¹⁸ and others,¹⁹ as well as by ourselves.²⁰ The most convenient triphenylphosphine-stabilized alkenyl complexes to use as starting materials are those of the forms [Ru(CR¹=CHR²)Cl(CO)(PPh₃)₂]¹³ and [Ru(CR¹=CHR²)Cl(CO)-(BTD)(PPh₃)₂] (BTD = 2,1,3-benzothiadiazole),^{18a} where BTD is a labile ligand. A marked advantage of the latter is that it avoids contamination with tris(phosphine) material. Reaction of [Ru(C(C≡CPh)=CHPh)Cl(CO)(BTD)(PPh₃)₂] with the piperazine dithiocarbamate S₂CNC₄H₈NH₂ yielded the cation [Ru(C(C≡CPh)=CHPh)(S₂CNC₄H₈NH₂)(CO)(PPh₃)₂]Cl (**1**). The retention of the enynyl ligand was indicated by a broadened singlet resonance for H_β at 6.29 ppm in the ¹H NMR spectrum, while peaks for the piperazine protons were seen at 2.59 and 3.49 ppm. Resonances for the NH₂ protons were not generally observed and were assumed to be broad and/or obscured by other resonances. Three characteristic bands were visible in the solid-state infrared spectrum (KBr/Nujol) for the ν_{C=C}, ν_{CO}, and ν_{CS} absorptions at 2148, 1924, and 999 cm⁻¹, respectively. A mutually trans disposition of phosphines was indicated by a singlet in the ³¹P NMR spectrum at 38.0 ppm. A molecular ion at *m/z* 1018 and satisfactory elemental analysis confirmed the overall composition of the compound. The particularly advantageous spectroscopic features of the enynyl ligand (H_β in ¹H NMR, ν_{C=C} in IR) led to complex **1** being employed as the primary starting point for the multimetallic complexes described here. To complete the characterization of the compound, single crystals were grown and a structural study undertaken (Figure 1):

The geometry at the metal center is a slightly distorted octahedral arrangement with cis-interligand angles in the range 70.33(4)–93.16(14)°. The enynyl ligand is displaced by around 13° from the plane formed by the ruthenium center and the other donor atoms. Otherwise, the data associated with the enynyl ligand are comparable to those reported for previous examples.^{20a,b} The S₂CNC₂ unit of the dithiocarbamate ligand is almost coplanar, due to the well-established multiple-bond character of the C–N bond. The closest comparable structure is that of the bimetallic species [{(dppm)₂Ru }₂(S₂CNC₄H₈NCS₂)](BF₄)₂.^{4a}

(18) (a) Hill, A. F.; Melling, R. P. *J. Organomet. Chem.* **1990**, *396*, C22–C24. (b) Hill, A. F.; Harris, M. C. J.; Melling, R. P. *Polyhedron* **1992**, *11*, 781–787. (c) Harris, M. C. J.; Hill, A. F. *Organometallics* **1991**, *10*, 3903–3906. (d) Bedford, R. B.; Hill, A. F.; Thompsett, A. R.; White, A. J. P.; Williams, D. J. *Chem. Commun.* **1996**, 1059, 1060. (e) Hill, A. F.; White, A. J. P.; Williams, D. J.; Wilton-Ely, J. D. E. T. *Organometallics* **1998**, *17*, 4249–4258. (f) Cannadine, J. C.; Hill, A. F.; White, A. J. P.; Williams, D. J.; Wilton-Ely, J. D. E. T. *Organometallics* **1996**, *15*, 5409–5415. (g) Hill, A. F.; Ho, C. T.; Wilton-Ely, J. D. E. T. *Chem. Commun.* **1997**, 2207, 2208. (h) Hill, A. F.; Wilton-Ely, J. D. E. T. *J. Chem. Soc., Dalton Trans.* **1999**, 3501, 3510. (i) Cowley, A. R.; Hector, A. L.; Hill, A. F.; White, A. J. P.; Williams, D. J.; Wilton-Ely, J. D. E. T. *Organometallics* **2007**, *26*, 6114–6125.

(19) (a) El Guaoui, M.; Ros, J.; Solans, X.; Font-Bardía, M. *Inorg. Chim. Acta* **1995**, *231*, 181–186. (b) Matas, L.; Muniente, J.; Ros, J.; Alvarez-Larena, A.; Piniella, J. F. *Inorg. Chem. Commun.* **1999**, *2*, 364–367. (c) El Guaoui, M.; Yáñez, R.; Ros, J.; Alvarez-Larena, A.; Piniella, J. F. *Inorg. Chem. Commun.* **1999**, *2*, 288–291. (d) Torres, M. R.; Perales, A.; Loumhrari, H.; Ros, J. *J. Organomet. Chem.* **1990**, *385*, 379–386. (e) Matas, L.; Moldes, I.; Soler, J.; Ros, J.; Alvarez-Larena, A.; Piniella, J. F. *Organometallics* **1998**, *17*, 4551–4555. (f) Loumhrari, H.; Ros, J.; Torres, M. R.; Perales, A. *Polyhedron* **1990**, *9*, 907–911. (g) Maddock, S. M.; Rickard, C. E. F.; Roper, W. R.; Wright, L. J. *Organometallics* **1996**, *15*, 1793–1803. (h) Deshpande, S. S.; Gopinathan, S.; Gopinathan, C. J. *Organomet. Chem.* **1991**, *415*, 265–270. (i) Bedford, R. B.; Cazin, C. S. J. *J. Organomet. Chem.* **2000**, *598*, 20–23.

(20) (a) Wilton-Ely, J. D. E. T.; Wang, M.; Benoit, D.; Tocher, D. A. *Eur. J. Inorg. Chem.* **2006**, 3068–3078. (b) Wilton-Ely, J. D. E. T.; Pogorzelec, P. J.; Honarkhah, S. J.; Tocher, D. A. *Organometallics* **2005**, *24*, 2862–2874. (c) Wilton-Ely, J. D. E. T.; Honarkhah, S. J.; Wang, M.; Tocher, D. A. *Dalton Trans.* **2005**, 1930–1939. (d) Wilton-Ely, J. D. E. T.; Wang, M.; Honarkhah, S. J.; Tocher, D. A. *Inorg. Chim. Acta* **2005**, *358*, 3218–3226.

(11) For an overview of alkenyl chemistry of ruthenium(II), see: (a) Whittlesey, M. K. In *Comprehensive Organometallic Chemistry III*; Crabtree, R. H., Mingos, D. M. P., Bruce, M. I., Eds.; Elsevier: Oxford, U.K., 2006; Vol. 6. (b) Hill, A. F. In *Comprehensive Organometallic Chemistry II*; Abel, E. W., Stone, F. G. A., Wilkinson, G., Eds.; Pergamon Press: Oxford, U.K., 1995; Vol. 7.

(12) Werner, H.; Esteruelas, M. A.; Otto, H. *Organometallics* **1986**, *5*, 2295–2299.

(13) Torres, M. R.; Vegas, A.; Santos, A.; Ros, J. *J. Organomet. Chem.* **1986**, *309*, 169–177.

(14) (a) Jung, S.; Ilg, K.; Brandt, C. D.; Wolf, J.; Werner, H. *Eur. J. Inorg. Chem.* **2004**, 469–480. (b) Jung, S.; Brandt, C. D.; Wolf, J.; Werner, H. *Dalton Trans.* **2004**, 375, 383. (c) Werner, H.; Jung, S.; Gonzalez-Herrero, P.; Ilg, K.; Wolf, J. *Eur. J. Inorg. Chem.* **2001**, 1957–1961. (d) Jung, S.; Ilg, K.; Wolf, J.; Werner, H. *Organometallics* **2001**, *20*, 2121–2123. (e) Werner, H.; Stüer, W.; Jung, S.; Weberndörfer, B.; Wolf, J. *Eur. J. Inorg. Chem.* **2002**, 1076–1080. (f) Werner, H.; Stark, A.; Steinert, P.; Grunwald, C.; Wolf, J. *Chem. Ber.* **1995**, *128*, 49–62.

(15) (a) Esteruelas, M. A.; López, A. M.; Oñate, E. *Organometallics* **2007**, *26*, 3260–3263. (b) Bolano, T.; Castarlenas, R.; Esteruelas, M. A.; Oñate, E. *J. Am. Chem. Soc.* **2006**, *128*, 3965–3973. (c) Eguillar, B.; Esteruelas, M. A.; Oliván, M.; Oñate, E. *Organometallics* **2005**, *24*, 1428–1438. (d) Castarlenas, R.; Esteruelas, M. A.; Oñate, E. *Organometallics* **2001**, *20*, 3283–3292. (e) Castarlenas, R.; Esteruelas, M. A.; Oñate, E. *Organometallics* **2001**, *20*, 2294–2302. (f) Esteruelas, M. A.; García-Yebra, C.; Oliván, M.; Oñate, E.; Tajada, M. *Organometallics* **2000**, *19*, 5098–5106. (g) Castarlenas, R.; Esteruelas, M. A.; Oñate, E. *Organometallics* **2000**, *19*, 5454–5463. (h) Buil, M. L.; Esteruelas, M. A.; García-Yebra, C.; Gutiérrez-Puebla, E.; Oliván, M. *Organometallics* **2000**, *19*, 2184–2193. (i) Bohanna, C.; Buil, M. L.; Esteruelas, M. A.; Oñate, E.; Valero, C. *Organometallics* **1999**, *18*, 5176–5179. (j) Bohanna, C.; Callejas, B.; Edwards, A.; Esteruelas, M. A.; Lahoz, F. J.; Oro, L. A.; Ruiz, N.; Valero, C. *Organometallics* **1998**, *17*, 373–381. (k) Esteruelas, M. A.; Gómez, A. V.; López, A. M.; Oñate, E. *Organometallics* **1998**, *17*, 3567–3573. (l) Esteruelas, M. A.; Liu, F.; Oñate, E.; Sola, E.; Zeier, B. *Organometallics* **1997**, *16*, 2919–2928. (m) Buil, M. L.; Elipse, S.; Esteruelas, M. A.; Oñate, E.; Peinado, E.; Ruiz, N. *Organometallics* **1997**, *16*, 5748–5755. (n) Esteruelas, M. A.; Lahoz, F. J.; Oñate, E.; Oro, L. A.; Sola, E. *J. Am. Chem. Soc.* **1996**, *118*, 89–99. (o) Bohanna, C.; Esteruelas, M. A.; Herrero, J.; López, A. M.; Oro, L. A. *J. Organomet. Chem.* **1995**, *498*, 199–206. (p) Bohanna, C.; Esteruelas, M. A.; Lahoz, F. J.; Oñate, E.; Oro, L. A.; Sola, E. *Organometallics* **1995**, *14*, 4825–4831. (q) Bohanna, C.; Esteruelas, M. A.; Lahoz, F. J.; Oñate, E.; Oro, L. A. *Organometallics* **1995**, *14*, 4685–4696. (r) Crochet, P.; Esteruelas, M. A.; López, A. M.; Martínez, M.-P.; Oliván, M.; Oñate, E.; Ruiz, N. *Organometallics* **1998**, *17*, 4500–4509.

(16) (a) Gómez-Lor, B.; Santos, A.; Ruiz, M.; Echavarren, A. M. *Eur. J. Inorg. Chem.* **2001**, 2305–2310. (b) Castaño, A. M.; Echavarren, A. M.; López, J.; Santos, A. *J. Organomet. Chem.* **1989**, *379*, 171–175. (c) Montoya, J.; Santos, A.; Echavarren, A. M.; Ros, J. *J. Organomet. Chem.* **1990**, *390*, C57–C60. (d) Loumhrari, H.; Ros, J.; Torres, M. R.; Santos, A.; Echavarren, A. M. *J. Organomet. Chem.* **1991**, *411*, 255–261. (e) Montoya, J.; Santos, A.; López, J.; Echavarren, A. M.; Ros, J.; Romero, A. *J. Organomet. Chem.* **1992**, *426*, 383–398. (f) López, J.; Romero, A.; Santos, A.; Vegas, A.; Echavarren, A. M.; Nohedra, P. *J. Organomet. Chem.* **1989**, *373*, 249–258. (g) Echavarren, A. M.; López, J.; Santos, A.; Montoya, J. *J. Organomet. Chem.* **1991**, *414*, 393–400. (h) Torres, M. R.; Vegas, A.; Santos, A.; Ros, J. *J. Organomet. Chem.* **1987**, *326*, 413–421. (i) Torres, M. R.; Santos, A.; Ros, J.; Solans, X. *Organometallics* **1987**, *6*, 1091–1095. (j) Santos, A.; Lopez, J.; Matas, L.; Ros, J.; Galan, A.; Echavarren, A. M. *Organometallics* **1993**, *12*, 4215–4218.

(17) (a) Huang, D. J.; Renkema, K. B.; Caulton, K. G. *Polyhedron* **2006**, *25*, 459–468. (b) Marchenko, A. V.; Gérard, H.; Eisenstein, O.; Caulton, K. G. *New J. Chem.* **2001**, *25*, 1382–1388. (c) Marchenko, A. V.; Gérard, H.; Eisenstein, O.; Caulton, K. G. *New J. Chem.* **2001**, *25*, 1244–1255. (d) Coalter, J. N.; Streib, W. E.; Caulton, K. G. *Inorg. Chem.* **2000**, *39*, 3749–3756. (e) Pedersen, A.; Tilset, M.; Følting, K.; Caulton, K. G. *Organometallics* **1995**, *14*, 875–888.

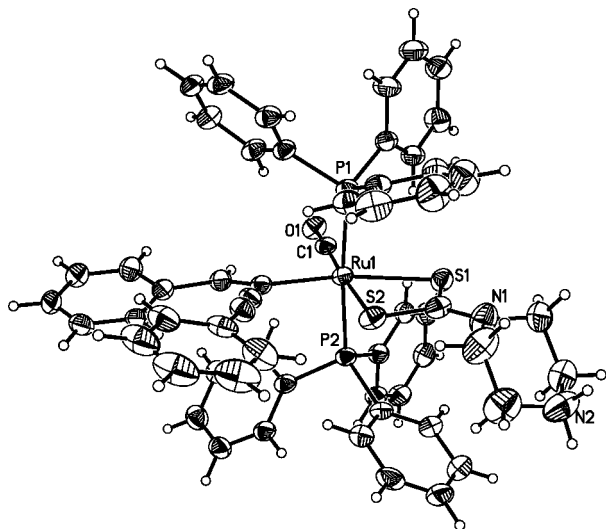


Figure 1. Molecular structure of the cation in compound **1**. Selected bond distances (Å) and angles (deg): Ru1–C1 = 1.831(5), Ru1–C12 = 2.109(5), Ru1–S2 = 2.466(1), Ru1–S1 = 2.508(1), O1–C1 = 1.166(6), S1–C2 = 1.707(5), S2–C2 = 1.697(6), N1–C2 = 1.354(7), C11–C12 = 1.351(7), C13–C14 = 1.215(7); S2–C2–S1 = 114.6(3), S2–Ru1–S1 = 70.33(4), C11–C12–Ru1 = 127.6(4), P1–Ru1–P2 = 173.73(4), C(13)–C(14)–C(15) = 169.9(6).

In both compounds the piperazine ring adopts a chair conformation. The Ru–S bond distances in compound **1** are slightly longer than those in the bimetallic examples, while the C–S and N–C distances are similar. However, the S2–Ru1–S1 angle of 70.33(4)° is smaller than that of 71.40(7)° in the previously reported complex.

Successive treatment of **1** with triethylamine, carbon disulfide, and [Ru(C(C≡CPh)=CHPh)Cl(CO)(BTD)(PPh₃)₂] led to generation of the ammonium moiety and conversion into the bimetallic complex [{Ru(C(C≡CPh)=CHPh)(CO)(PPh₃)₂]₂(S₂CNC₄H₈NCS₂)] (**2**), as shown in Scheme 3. The same product was obtained by reaction of the double salt KS₂CNC₄H₈NCS₂K with 2 equiv of [Ru(C(C≡CPh)=CHPh)Cl(CO)(BTD)(PPh₃)₂]. As might be expected, compound **2** was found to display spectroscopic features similar to those of **1** with a broadened alkenyl resonance at 6.32 ppm and peaks between 2.21 and 2.27 ppm for the piperazine protons in the ¹H NMR spectrum, reflecting the different environments of the axial and equatorial protons. Integration of the aromatic region confirmed the presence of two Ru(PPh₃)₂(enynyl) units to one piperazine. Absorptions were observed in the solid-state infrared spectrum at 2153 ($\nu_{C=C}$) and 1924 cm⁻¹ (ν_{CO}), further indicating retention of the enynyl and carbonyl ligands but failing to show any significant change from the same features in the precursor. A molecular ion in the FAB mass spectrum at *m/z* 1952 and good agreement of elemental analysis with the calculated values helped differentiate between compounds **1** and **2**.

Initially, the reaction mixture to transform **1** into **2** was stirred for 2 h. However, the presence of side products was observed and these were attributed to insertion of carbon disulfide into the Ru–C bond, a reaction which has some precedent.²¹ The reaction to form compound **2** is relatively rapid, and so best results were obtained using a method in which the reaction mixture was stirred only for 10 min before workup.

Further examples of symmetrical bimetallic species were prepared using the direct method outlined above. Reaction of 2 equiv of [Ru(CH=CHBu^t)Cl(CO)(PPh₃)₂] with KS₂CNC₄H₈NCS₂K (Scheme 4) led to the formation of [{Ru(CH=CHBu^t)(CO)(PPh₃)₂]₂(S₂CNC₄H₈NCS₂)] (**3**). A new carbonyl absorption was observed at 1908 cm⁻¹ in the solution infrared spectrum (CH₂Cl₂) and a new singlet in the ³¹P NMR spectrum at 40.4 ppm. The retention of the alkenyl ligand was evidenced by a singlet at 0.02 ppm for the methyl protons in the ¹H NMR spectrum along with a doublet resonance for H_β at 5.95 ppm (*J*_{HH} = 17.3 Hz). The piperazine protons gave rise to a broad series of multiplets between 1.99 and 2.60 ppm. This dynamic behavior, presumably as a result of flexing of the piperazine ring, could not be frozen out at low temperatures (-40 °C) and coalesced to some extent at elevated temperatures (+40 °C). High-molecular-weight complexes often fail to yield a molecular ion in the mass spectrum, and this was found to be the case with complex **3**: only fragmentations for loss of an alkenyl ligand and [M – alkenyl – PPh₃]⁺ were found at *m/z* 1631 and 1367, respectively. The formulation was supported by elemental analysis, which was found to be in good agreement with calculated values. The complex [{Ru(CH=CHC₆H₄Me-4)(CO)(PPh₃)₂]₂(S₂CNC₄H₈NCS₂)] (**4**) was prepared in an identical manner.

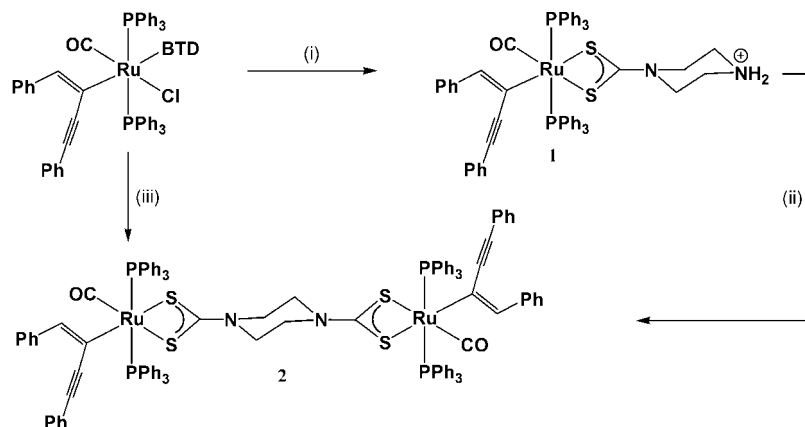
Having prepared examples with both mono- and disubstituted alkenyl ligands, we decided to explore complexes with alkenyl moieties derived from propargyl alcohols (Scheme 4). The species [Ru(CH=CHCPh₂OH)(BTD)Cl(CO)(PPh₃)₂] was obtained readily from the hydorruthenation of 1,1-diphenyl-2-propyn-1-ol by [RuHCl(CO)(BTD)(PPh₃)₂]. This went on to react in a manner similar to that for complex **4** to yield a colorless product formulated as [{Ru(CH=CHCPh₂OH)(CO)(PPh₃)₂]₂(S₂CNC₄H₈NCS₂)] (**5**) on the basis of spectroscopic and analytical data. Treatment of [Ru(CH=CHCO₂Me)Cl(CO)(PPh₃)₂] with 0.5 equiv of KS₂CNC₄H₈NCS₂K yielded [{Ru(CH=CHCO₂Me)(CO)(PPh₃)₂]₂(S₂CNC₄H₈NCS₂)] (**6**). The ester group was seen as a medium-intensity $\nu_{C=O}$ absorption at 1659 cm⁻¹, to lower frequency of the more intense carbonyl absorption at 1917 cm⁻¹ in the solution (CH₂Cl₂) infrared spectrum. The methyl protons were observed at 3.37 ppm in the ¹H NMR spectrum along with H_α and H_β at 9.47 (*J*_{HH} = 15.0 Hz) and 5.50 ppm, respectively.

In addition to the literature compounds employed, a number of new alkenyl complexes were prepared for use in the project. Reaction of HC≡CHCH₂OSiMe₂Bu^t with [RuHCl(CO)(PPh₃)₃] yielded a pale yellow product, formulated as the alkenyl complex [Ru(CH=CHCH₂OSiMe₂Bu^t)Cl(CO)(PPh₃)₂] (**7**). Singlet resonances in the ¹H NMR spectrum for the methyl and *tert*-butyl groups were observed at 0.15 and 0.78 ppm, respectively, along with a doublet for the methylene protons at 3.85 coupled to the H_β proton (*J*_{HH} = 6.9 Hz). A doublet of triplets of triplets was observed for H_β at 4.82 ppm due to coupling with H_β, the CH₂ protons, and the phosphine nuclei, while the resonance arising from H_α appeared at 7.74 as a doublet of triplets.

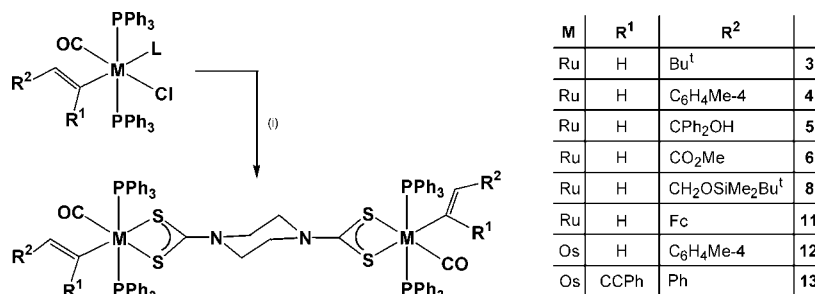
The silyl-substituted alkenyl complex **7** reacts with KS₂CNC₄H₈NCS₂K to give the off-white product [{Ru(CH=CHCH₂OSiMe₂Bu^t)(CO)(PPh₃)₂]₂(S₂CNC₄H₈NCS₂)] (**8**) in moderate yield (Scheme 4). The resonances for the alkenyl substituent proved particularly diagnostic, giving rise to singlets at -0.22 (SiCH₃) and 0.77 ppm (Bu^t) and a doublet at 3.44 ppm (CH₂, *J*_{HH} = 5.8 Hz).

In order to increase the number of metals incorporated into the system, ethynylferrocene was used to prepare the complexes

(21) Loumrhari, H.; Ros, J.; Yanez, R.; Torres, M. R. *J. Organomet. Chem.* **1991**, *408*, 233–239.

Scheme 3. Two Routes to a Homobimetallic Ruthenium Species^a

^a Legend: (i) S₂CNC₄H₈NH₂, NH₄BF₄; (ii) NEt₃, CS₂, [Ru(C(C≡CPh)=CHPh)Cl(CO)(BTD)(PPh₃)₂]; (iii) 0.5 equiv of KS₂CNC₄H₈NCS₂K.

Scheme 4. Direct Preparation of Homobimetallic Ruthenium and Osmium Species^a

^a Legend: (i) 0.5 equiv of KS₂CNC₄H₈NCS₂K; L = no ligand or BTDT (2,1,3-benzothiadiazole).

[Ru(CH=CHFc)Cl(CO)(PPh₃)₂] (**9**)²² and [Os(CH=CHFc)Cl(CO)(BTD)(PPh₃)₂] (**10**) in good yield from reaction with [RuHCl(CO)(PPh₃)₃] and [OsHCl(CO)(BTD)(PPh₃)₂]. The presence of the ferrocenyl unit (in **9**) was clearly indicated by resonances at 3.78 (C₅H₅), 3.88 (C₅H₄), and 3.96 ppm (C₅H₄) in the ¹H NMR spectrum, while H_α and H_β protons resonated as doublets (*J*_{HH} = 13.3 Hz) at 7.74 and 5.39 ppm.

Use of [Ru(CH=CHFc)Cl(CO)(PPh₃)₂] allows the introduction of a new carbon-bonded metal center into the system to create the tetrametallic product [{Ru(CH=CHFc)(CO)(PPh₃)₂]₂(S₂CNC₄H₈NCS₂)] (**11**) on reaction with KS₂CNC₄H₈NCS₂K (Scheme 4). Again, a multiplet was observed for the piperazine protons between 2.56 and 2.82 ppm in the ¹H NMR spectrum, while the ferrocenyl group gave rise to resonances slightly shifted with respect to those in the precursor. Resonances for H_α and H_β were observed at 7.70 and 5.84 ppm showing mutual coupling of 15.6 Hz. Somewhat surprisingly, a molecular ion was observed in the FAB mass spectrum at *m/z* 1967, albeit in low abundance.

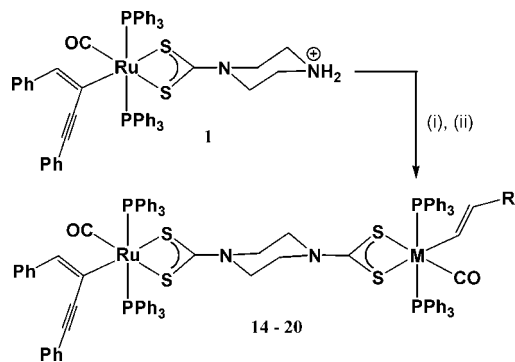
While a number of linked bimetallic complexes of ruthenium are known (Scheme 2), very few examples have been reported for osmium. These are limited to the recently reported complexes [OsCl(CO)(PPh₃)₂(PR₃)(CH=CHC₆H₃(C≡CH-3)CH=CH)-OsCl(CO)(PPh₃)₂(PR₃)] (R = Me, Ph) prepared by Jia and co-workers¹⁰ and [OsCl(CO)(PPr₃)₂(CH=CH(CH₂)₄CH=CH)OsCl(CO)(PPr₃)₂] by the group of Esteruelas.²³ Employing the versatile osmium starting materials [Os(alkenyl)Cl(CO)(BTD)-

(PPh₃)₂] (alkenyl = CH=CHC₆H₄Me-4, C(C≡CPh)=CHPh) in the reactions with KS₂CNC₄H₈NCS₂K leads to the formation of the yellow products [{Os(CH=CHC₆H₄Me-4)(CO)(PPh₃)₂]₂(S₂CNC₄H₈NCS₂)] (**12**) and [{Os(C(C≡CPh)=CHPh)(CO)(PPh₃)₂]₂(S₂CNC₄H₈NCS₂)] (**13**) in good to moderate yield (Scheme 4). Spectroscopic and analytical features were similar to those for the ruthenium analogues, with the exception of the resonances in the ³¹P NMR spectrum at 8.3 (**12**) and 6.6 ppm (**13**), which displayed a shift to higher field due to the greater shielding afforded by the osmium centers. A molecular ion was observed at *m/z* 1957 in the FAB mass spectrum of **12**, and an excellent agreement with calculated values was found for the microanalytical data.

With the routes to symmetrical species well established, our attention turned to exploring the wider potential of this methodology to prepare unsymmetrical bimetallic species. Using the complex [Ru(C(C≡CPh)=CHPh)(S₂CNC₄H₈NH₂)(CO)(PPh₃)₂]Cl (**1**) as the starting point due to the characteristic features in its IR and ¹H NMR spectra, the addition of different alkenyl species was investigated. Treatment of **1** with triethylamine and carbon disulfide followed by addition of [Ru(CH=CHBu^t)Cl(CO)(BTD)(PPh₃)₂] led to the formation of a yellow-brown product. Retention of the enynyl moiety was indicated by the ν_{C=C} absorption at 2152 cm⁻¹ in the solid-state infrared spectrum and a singlet resonance in the ¹H NMR spectrum at 6.21 ppm. Only one broadened ν_{CO} absorption was observed in the solution infrared spectrum (CH₂Cl₂) at 1912 cm⁻¹, but additional peaks in the ¹H NMR spectrum at 0.34 (s, Bu^t) and 4.54 ppm (d, CHBu^t, *J*_{HH} = 16.4 Hz) indicated the presence of the new metal unit. This was corroborated by two distinct phosphorus environments in the ³¹P NMR spectrum at 38.0 and

(22) Wilson, D. J. M.Sc. Thesis, Imperial College, 1996.

(23) Esteruelas, M. A.; Lahoz, F. J.; Onate, E.; Oro, L. A.; Valero, C.; Zeier, B. *J. Am. Chem. Soc.* **1995**, *117*, 7935–7942.

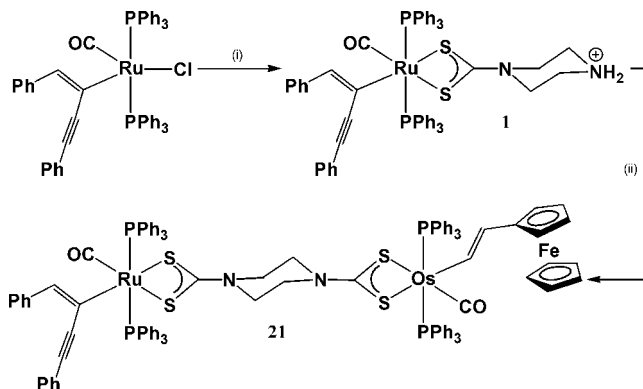
Scheme 5. Preparation of Unsymmetrical Bimetallic Ruthenium Species^a

^a Legend: (i) NEt₃, CS₂; (ii) [Ru(CH=CHR)Cl(CO)(BTD)(PPh₃)₂] (R = Bu^t (**14**), C₆H₄Me-4 (**15**), CPh₂OH (**16**)), [Ru(CH=CHR)Cl(CO)(PPh₃)₂] (R = CO₂Me (**17**), CH₂OSiMe₂Bu^t (**18**), C₅H₄FeC₅H₅ (**19**)), or [Os(CH=CHC₆H₄Me-4)Cl(CO)(BTD)(PPh₃)₂] (**20**).

40.6 ppm. By comparison with the chemical shift of the starting material, these were assigned to the Ru(PPh₃)₂ units bonded to the enynyl and tertiarybutyl alkenyl ligands, respectively. A fragment for loss of phosphine at *m/z* 1568 in the FAB mass spectrum and elemental analysis confirmed the overall formulation as [Ru(C≡CPh)=CHPh)(CO)(PPh₃)₂](S₂CNC₄H₈NCS₂){Ru(CH=CHR)(CO)(PPh₃)₂} (R = Bu^t, **14**).

In a similar manner (Scheme 5), further examples of unsymmetrical bimetallics with units bearing monosubstituted alkenyl ligands (R = C₆H₄Me-4 (**15**), CPh₂OH (**16**), CO₂Me (**17**), CH₂OSiMe₂Bu^t (**18**)) were prepared. These constitute the first examples of unsymmetrical organometallic complexes bridged by a dithiocarbamate linkage. Using [Ru(CH=CHFc)Cl(CO)(PPh₃)₂] (**9**), a trimetallic species, [Ru(C≡CPh)=CHPh)(CO)(PPh₃)₂](S₂CNC₄H₈NCS₂){Ru(CH=CHFc)(CO)(PPh₃)₂} (**19**), was prepared from **1** in the same manner. In addition to the peak at 37.8 ppm in the ³¹P NMR spectrum for the enynyl end of the molecule, a new resonance at 39.3 ppm was observed for the ferrocenyl alkenyl unit as well as typical resonances in the ¹H NMR spectrum, similar to those found in **9** and **11**. The success of these reactions led to an attempt to introduce a different metal center as the new end unit. The BTD and chloride ligands in the complex [Os(CH=CHC₆H₄Me-4)Cl(CO)(BTD)(PPh₃)₂] were readily displaced by the metalladithiocarbamate [Ru(C≡CPh)=CHPh)(S₂CNC₄H₈NCS₂)(CO)(PPh₃)₂][NHET₃], generated in situ, to yield the mixed-metal species [Ru(C≡CPh)=CHPh)(CO)(PPh₃)₂](S₂CNC₄H₈NCS₂){Os(CH=CHC₆H₄Me-4)(CO)(PPh₃)₂} (**20**) in moderate yield. This complex joins the species [RuCl(CO)(PPh₃)₂](CH=CH(CH₂)₄CH=CH)OsCl(CO)(PPh₃)₂] as one of very few known ruthenium–osmium bimetallic compounds bearing alkenyl ligands.²⁴ As expected, a substantial difference was observed in the chemical shift of the phosphorus nuclei attached to the ruthenium (38.0 ppm) and osmium (8.1 ppm) centers. Other spectroscopic features in the ¹H NMR spectrum were similar to those observed previously. A molecular ion was clearly identifiable in the FAB mass spectrum at *m/z* 1953 along with fragmentations due to loss of phosphine and a fragment attributed to [M – PPh₃ – alkenyl]⁺. Elemental analysis further supported the above formulation.

These results opened up the exciting possibility of a complex being accessible in which all three metals of the group 8 triad

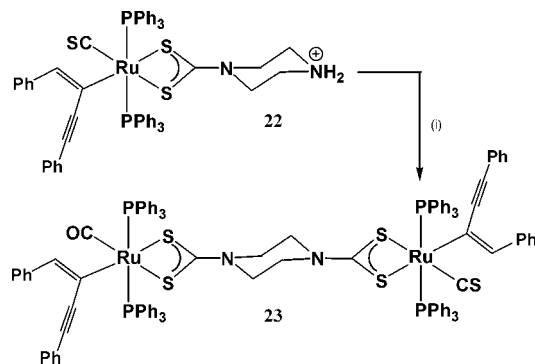
Scheme 6. Preparation of the Heterotrimetallic Group 8 Metal Complex **21**^a

^a Legend: (i) S₂CNC₄H₈NH₂, NH₄BF₄; (ii) NEt₃, CS₂, [Os(CH=CHFc)Cl(CO)(BTD)(PPh₃)₂].

are represented. This was indeed achieved with the synthesis of [Ru(C≡CPh)=CHPh)(CO)(PPh₃)₂](S₂CNC₄H₈NCS₂){Os(CH=CHFc)(CO)(PPh₃)₂} (**21**) by the same route (Scheme 6). Again, a broadened carbonyl absorption with a distinct shoulder to lower frequency was observed in the solution IR spectrum at 1927 cm⁻¹ (different from that found for the starting material) alongside a ν_{C=C} band at 2152 cm⁻¹ and a new resonance at 7.9 ppm in the ³¹P NMR spectrum pointed to the successful incorporation of the osmium unit. Typical resonances for the enynyl and ferrocenyl alkenyl ligands confirmed their presence. A peak assigned to loss of phosphine was identified at *m/z* 1784 in the FAB mass spectrum. Elemental analysis was found to agree well with calculated values. Although the compound was found to be reasonably microcrystalline, no crystals of sufficient quality for a structural determination could be grown. Apart from some cluster examples,^{25a} to the best of our knowledge, this FeRuOs species is only the second example of a complex containing all three metals of the triad after the complex *trans*-[(FcC≡C)C₆H₃{C≡CRuCl(dppm)}₂]{C≡COsCl(dppm)}₂ reported by Long and co-workers.^{25b} Very recently, Lang and co-workers have reported an elegant synthetic route to a heptametallic complex containing the group 8 triad along with Ti, Re, Pt, and Cu centers.^{25c}

Although the anionic metalladithiocarbamate [Ru(C≡CPh)=CHPh)(S₂CNC₄H₈NCS₂)(CO)(PPh₃)₂]⁻ was always generated in situ in the experiments outlined here, this species can be characterized as the [HNET₃]⁺ salt on addition of NEt₃ and CS₂ to a solution of compound **1** in dichloromethane followed by precipitation with diethyl ether. The anion gave rise to two piperazine environments in the ¹H NMR spectrum at 2.44 and 4.02 ppm along with a resonance for H_β at 6.29 ppm. The ³¹P NMR resonance at 37.8 ppm is little changed from that of the precursor **1**. On standing in solution for more than 1 h, formation of the symmetrical species **2** began to occur. This behavior has been noted for the zwitterion [Ru(S₂CNC₄H₈NCS₂)(dppm)]⁴.

A subtle variation on the unsymmetrical systems described above is the preparation of a bimetallic complex in which only one coligand differs at each end. The thiocarbonyl analogues of the alkenyl starting materials employed here are readily accessible from hydorruthenation of [RuHCl(CS)(BTD)(PPh₃)₂] or [RuHCl(CS)(PPh₃)₃].⁸ Accordingly, [Ru(C≡CPh)=CHPh)(S₂CNC₄H₈NH₂)(CS)(PPh₃)₂]Cl (**22**) was prepared from [Ru(C≡CPh)=CHPh)Cl(CS)(PPh₃)₂] by the same method as that used for **1**. Spectroscopic features were essentially identical to those for **1** other than the ν_{CS} absorption at 1246 cm⁻¹.

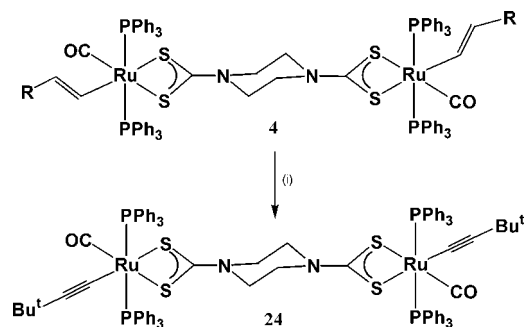
Scheme 7. Preparation of a Bimetallic Ruthenium Species (23) with both Carbonyl and Thiocarbonyl Ligands^a

^a Legend: (i) NEt₃, CS₂, [Ru(C(C≡CPh)=CHPh)Cl(CO)(PPh₃)₂].

Treatment of **22** with NEt₃ and CS₂ followed by addition of [Ru(C(C≡CPh)=CHPh)Cl(CO)(PPh₃)₂] resulted in the formation (Scheme 7) of [{Ru(C(C≡CPh)=CHPh)(CO)(PPh₃)₂}(S₂CNC₄H₈NCS₂){Ru(C(C≡CPh)=CHPh)(CS)(PPh₃)₂}] (**23**). As may be expected, multinuclear NMR spectroscopic features for both ends of the molecule, though clearly broadened, were so similar as to render them indistinguishable. However, a shift of the ν_{CS} absorption to 1259 cm⁻¹ and the presence of the ν_{CO} band at 1920 cm⁻¹ attested to the success of the reaction. A very broad ³¹P NMR resonance centered at 34.1 ppm was observed, while fragmentation for [M - PPh₃]⁺ at *m/z* 1702 and satisfactory elemental analysis supported the formulation as that above.

The examples above have illustrated the versatility of the piperazine dithiocarbamate linkage in the synthesis of diverse symmetrical and unsymmetrical organometallic compounds. The next challenge was to explore the ability of this ligand to support functional group transformations of the σ-bonded organic ligands. Treatment of the symmetrical tolyl-substituted alkenyl complex [{Ru(CH=CHC₆H₄Me-4)(CO)(PPh₃)₂}(S₂CNC₄H₈NCS₂)] (**4**) with an excess of HC≡CBu^t in refluxing toluene resulted in a tan product which displayed a ν_{CO} absorption in the solid-state infrared spectrum at 1947 cm⁻¹ along with a completely new band at 2102 cm⁻¹ in the region typical of alkynyl ν_{C≡C} bands. In the ¹H NMR spectrum, no AB system was observed for a tolyl group or H_α or H_β protons. Instead, a singlet integrating to 18 protons was observed at 0.94 ppm. The MALDI mass spectrum showed a peak at *m/z* 1706 corresponding to the molecular ion for the alkynyl complex [{Ru(C≡CBu^t)(CO)(PPh₃)₂}(S₂CNC₄H₈NCS₂)] (**24**) along with further fragmentations from loss of carbonyl and phosphine ligands (Scheme 8). Two closely separated peaks were observed in the room temperature ³¹P NMR spectrum at 38.9 and 39.3 ppm, indicating slightly different environments for the two metal units, which coalesced on warming.

An alternative route to trimetallic complexes was also explored using metal precursors of groups 10 and 12 (Scheme 9), which are well-known to form bis(dithiocarbamate) species. Sequential treatment of 2 equiv of [Ru(C(C≡CPh)=CHPh)(S₂CNC₄H₈NH₂)(CO)(PPh₃)₂]Cl (**1**) with excess triethylamine and carbon disulfide followed by 1 equiv of Ni(OAc)₂ led to a yellow product in low yield. As might be expected, the spectroscopic features for the desired complex [{Ru(C(C≡CPh)=CHPh)(S₂CNC₄H₈NCS₂)(CO)(PPh₃)₂}]₂Ni (**25**) were found to be very similar to those of **1**. In comparison to the same feature in **1**, a slight shift was observed for H_β in the ¹H NMR spectrum to 6.30 ppm and the piperazine protons were spread over a slightly greater range of chemical shifts.

Scheme 8. Preparation of a Bis(alkynyl)ruthenium Species (24)^a

^a Legend: (i) excess HC≡CBu^t, heat; R = C₆H₄Me-4.

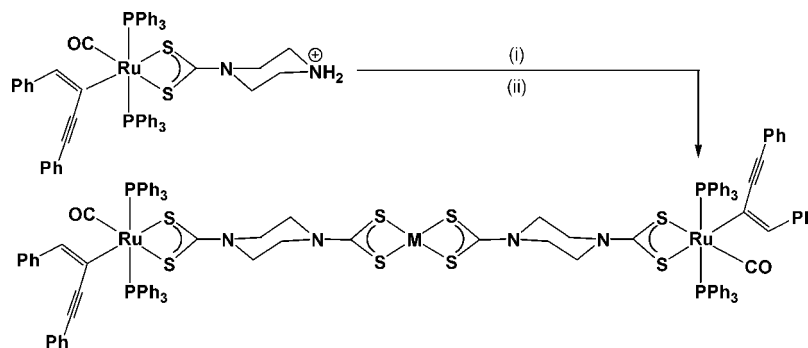
Attempts to record a potentially diagnostic ¹³C NMR spectrum were defeated by persistent precipitation of the complex from high concentration solutions over the period of data accumulation, leading to a poor signal-to-noise ratio. The mass spectrum failed to provide a molecular ion, only exhibiting a fragmentation attributed to *m/z* 1691 for loss of two phosphines and a carbonyl ligand. However, elemental analysis was found to be in excellent agreement with calculated values. Trimetallic compounds of the heavier congeners of group 10 were also prepared from PdCl₂(NCMe)₂ and PtCl₂(NCPh)₂ to yield [{Ru(C(C≡CPh)=CHPh)(S₂CNC₄H₈NCS₂)(CO)(PPh₃)₂}]₂M (M = Pd, **26**; M = Pt, **27**), respectively. Data for these complexes were found to be similar to those exhibited by **25**. The RuZnRu complex [{Ru(C(C≡CPh)=CHPh)(S₂CNC₄H₈NCS₂)(CO)(PPh₃)₂}]₂Zn (**28**) was synthesized in a similar manner from **1** with NEt₃, CS₂, and zinc acetate to provide a group 12 example. While a square-planar geometry around the d⁸ group 10 metals in **25–27** is assumed, the Zn(II) (d¹⁰) center in **28** is likely to adopt a tetrahedral arrangement.

Conclusion

The methodology described above illustrates how the piperazine dithiocarbamate system can be used to link a range of organometallic centers. The accessibility of unsymmetrical systems via this route is particularly significant, as this is often impossible to achieve using conventional bifunctional linkages. Furthermore, the robust nature of the bis(dithiocarbamate) linker has been illustrated by a successful functional group transformation performed on a bimetallic complex, converting a dialkenyl compound into one bearing alkynyl ligands. The tri- and tetrametallic species prepared further illustrate the flexibility of the approach, allowing metal units to function as the connecting moiety between ruthenium alkenyl complexes. The potential of this idea, illustrated here by four-coordinate group 10 and 12 metals, will now be explored using units based on d- and f-block metals capable of chelating a greater number of dithiocarbamate ligands in order to expand the geometrical possibilities of the linkage metal atom.

Experimental Section

General Comments. All experiments were carried out under aerobic conditions, and the majority of the complexes appear to be indefinitely stable toward the atmosphere in solution or in the solid state. Solvents were used as received from commercial sources. The following complexes have been described elsewhere: [RuHCl(CO)(P-

Scheme 9. Preparation of Ru₂M Heterotrimetallic Species^a

^a Legend: (i) NEt₃, CS₂; (ii) Ni(OAc)₂, PdCl₂(NCMe)₂, PtCl₂(NCPh)₂ or Zn(OAc)₂; M = Ni (**25**), Pd (**26**), Pt (**27**), Zn (**28**).

Ph₃)₃],²⁶ [RuHCl(CO)(BTD)(PPh₃)₂],²⁷ [OsHCl(CO)(BTD)(PPh₃)₂],^{18h} [RuHCl(CS)(PPh₃)₃],²⁸ [Ru(CR¹=CHR²)Cl(CO)(PPh₃)₂] (R¹ = H, R² = Bu^t,^{16h} CO₂Me¹⁶ⁱ and R¹ = C≡CPh, R² = Ph^{18a,b}), [Ru(CR¹=CHR²)Cl(CO)(BTD)(PPh₃)₂] (R¹ = H, R² = C₆H₄Me-4, CPh₂OH),^{18c} [Os(CR¹=CHR²)Cl(CO)(BTD)(PPh₃)₂] (R¹ = H, R² = C₆H₄Me-4; R¹ = C≡CPh, R² = Ph),^{18h} [PdCl₂(NCMe)₂],²⁹ [PtCl₂(NCPh)₂],³⁰ [S₂CNC₄H₈NH₂],^{4,31} and [KS₂CNC₄H₈NCS₂K].³² MALDI-MS and FAB-MS data were obtained using Micromass ToFSpec and Autospec Q instruments, respectively. The FAB mass spectrum for **15** was obtained at the EPSRC National Mass Spectrometry Service Center, University of Wales Swansea. Infrared data were obtained using a Perkin-Elmer Paragon 1000 FT-IR spectrometer. KBr plates were used for solid-state IR spectroscopy, and characteristic phosphine-associated infrared data are not reported. NMR spectroscopy was performed at 25 °C using Varian Mercury 300 or Varian Unity 500 (for complex **7**) spectrometers in CDCl₃ unless otherwise indicated. All couplings are in hertz, and ³¹P NMR spectra are proton-decoupled. Elemental analysis data were obtained from London Metropolitan University. The procedures given provide materials of sufficient purity for synthetic and spectroscopic purposes. Samples were recrystallized from a mixture of dichloromethane and ethanol for elemental analysis. Solvates were confirmed by integration of the ¹H NMR spectrum.

[Ru(C(C≡CPh)=CHPh)(CO)(PPh₃)₂(S₂CNC₄H₈NH₂)]Cl (**1**). The reagent [S₂CNC₄H₈NH₂] (220 mg, 1.356 mmol) was dissolved in methanol (20 cm³) and the complex [Ru(C(C≡CPh)=CHPh)Cl(CO)(PPh₃)₂] (1000 mg, 1.121 mmol) was added in dichloromethane (60 cm³). After the mixture was stirred at room temperature for 3 h, the volatiles were removed. The crude product was dissolved in a small amount of dichloromethane, and ethanol (20 cm³) was added. Slow concentration under reduced pressure gave a yellow product, which was filtered off, washed with hexane (10 cm³), and dried under vacuum. Yield: 820 mg (69%). The BTD analogue of the starting material can also be used to give a comparable yield of compound **1**. IR (CH₂Cl₂): 2153 (ν_{C≡C}), 1927 (ν_{CO}) cm⁻¹. IR (Nujol): 2148 (ν_{C≡C}), 1924 (ν_{CO}), 1592, 1311, 1267,

1245, 1203, 999 (ν_{C-S}) cm⁻¹. ¹H NMR: δ 2.59 (s, 4 H, NC₄H₈N), 3.49 (s, 4 H, NC₄H₈N), 6.29 (s, 1 H, H_β), 6.94–7.57 (m, 40 H, C₆H₅) ppm. ¹³C NMR (CD₂Cl₂): δ 41.4–42.1 (m, NC₄H₈N), 102.1, 98.4 (s × 2, C≡C), 124.5–140.77 (m, C₆H₅), 126.4 (s, =CH), 146.6 (s, RuC≡), 197.3 (t, CO, J_{PC} = 17.7 Hz), 207.7 (s, CS₂) ppm. ³¹P NMR: δ 38.0 (s, PPh₃) ppm. MS (FAB): *m/z* (%) 1018 (18) [M]⁺, 857 (10) [M - S₂CNC₄H₈NH₂]⁺, 815 (20) [M - alkenyl]⁺, 728 (56) [M - CO - PPh₃]⁺. Anal. Found: C, 66.0; H, 4.9; N, 2.6. Calcd for C₅₈H₅₁ClN₂O₂P₄RuS₂: C, 66.1; H, 4.9; N, 2.7.

[{Ru(C(C≡CPh)=CHPh)(CO)(PPh₃)₂}(S₂CNC₄H₈NCS₂)] (**2**).

(a) KS₂CNC₄H₈NCS₂K (35 mg, 0.111 mmol) was dissolved in MeOH (15 cm³) and water (2 cm³), and [Ru(C(C≡CPh)=CHPh)Cl(CO)(PPh₃)₂] (200 mg, 0.224 mmol) was added in dichloromethane (25 cm³). After the mixture was stirred at room temperature for 20 min, the solvent volume was reduced by rotary evaporation. The pale yellow product was filtered off, washed with water (5 cm³), ethanol (10 cm³), and hexane (10 cm³), and dried under vacuum. Yield: 170 mg (78%).

(b) [Ru(C(C≡CPh)=CHPh)(S₂CNC₄H₈NH₂)(CO)(PPh₃)₂]Cl (100 mg, 0.095 mmol) was dissolved in dichloromethane (15 cm³) and treated with NEt₃ (5 drops, excess) and CS₂ (5 drops, excess) followed by a dichloromethane solution (10 cm³) of [Ru(C(C≡CPh)=CHPh)Cl(CO)(PPh₃)₂] (85 mg, 0.095 mmol). After the mixture was stirred at room temperature for 20 min, the solvent volume was reduced by rotary evaporation. The pale yellow product was filtered off, washed with water (5 cm³), ethanol (10 cm³), and hexane (10 cm³), and dried under vacuum. Yield: 135 mg (73%). IR (CH₂Cl₂): 2144 (ν_{C≡C}), 1915 (ν_{CO}) cm⁻¹. IR (Nujol): 2153 (ν_{C≡C}), 1924 (ν_{CO}), 1591, 1277, 1212, 1161, 1000 (ν_{C-S}) cm⁻¹. ¹H NMR (C₆D₆): δ 2.21–2.27 (m, 8 H, NC₄H₈N), 6.32 (s, 2 H, H_β), 6.51–7.48 (m, 80 H, C₆H₅) ppm. ³¹P NMR: δ 38.3 (s, PPh₃) ppm. MS (FAB): *m/z* (%) 1952 (2) [M]⁺, 1689 (1) [M - PPh₃]⁺, 1485 (3) [M - PPh₃ - alkenyl]⁺. Anal. Found: C, 67.9; H, 4.6; N, 1.5. Calcd for C₁₁₂H₉₀N₂O₂P₄RuS₄·0.5CH₂Cl₂: C, 67.8; H, 4.6; N, 1.4.

[{Ru(CH=CHBu^t)(CO)(PPh₃)₂}(S₂CNC₄H₈NCS₂)] (**3**).

KS₂CNC₄H₈NCS₂K (20 mg, 0.064 mmol) was dissolved in MeOH (10 cm³), and the complex [Ru(CH=CHBu^t)Cl(CO)(PPh₃)₂] (100 mg, 0.129 mmol) was added in dichloromethane (15 cm³). After the mixture was stirred at room temperature for 20 min, all solvent was removed by rotary evaporation. The product was taken up in a small amount of dichloromethane and filtered through diatomaceous earth. Ethanol (15 cm³) was added, and a pale brown powder was obtained after concentration under reduced pressure. The product was filtered off, washed with ethanol (10 cm³) and hexane (10 cm³), and dried under vacuum. Yield: 64 mg (58%). IR (CH₂Cl₂): 1908 (ν_{CO}) cm⁻¹. IR (Nujol): 1911 (ν_{CO}), 1731, 1601, 1580, 1272, 1122, 1040, 999 (ν_{C-S}) cm⁻¹. ¹H NMR: δ 0.02 (s, 18 H, Bu^t), 1.99–2.60 (m, 8 H, NC₄H₈N), 5.95 (d, 2 H, H_β, ³J_{HH} = 17.3 Hz), 6.92–7.34 (m, 60 H + 2 H, C₆H₅ + H_α) ppm. ³¹P NMR: δ 40.4 (s, PPh₃) ppm. MS (FAB): *m/z* (%) 1631 (1) [M - alkenyl]⁺,

(25) (a) Hunstock, E.; Calhorda, M. J.; Hirva, P.; Pakkanen, T. A. *Organometallics* **2000**, *19*, 4624–4628. (b) Long, N. J.; Martin, A. J.; White, A. J. P.; Williams, D. J.; Fontani, M.; Laschi, F.; Zanello, P. *Dalton Trans.* **2000**, 3387–3392. (c) Packheiser, R.; Ecorchard, P.; Ruffer, T.; Lang, H. *Organometallics*, in press.

(26) Laing, K. R.; Roper, W. R. *J. Chem. Soc. A* **1970**, 2149, 2153.

(27) Procedure modified substituting BTD for BSD from: Alcock, N. W.; Hill, A. F.; Roe, M. S. *J. Chem. Soc., Dalton Trans.* **1990**, 1737–1740.

(28) Brothers, P. J.; Roper, W. R. *J. Organomet. Chem.* **1983**, *258*, 73–79.

(29) Andrews, M. A.; Chang, T. C.-T.; Cheng, C.-W. F.; Emge, T. J.; Kelly, K. P.; Koetzle, T. F. *J. Am. Chem. Soc.* **1984**, *106*, 5913–5920.

(30) Fraccarollo, D.; Bertani, R.; Mozzon, M.; Belluco, U.; Michelin, R. A. *Inorg. Chim. Acta* **1992**, *201*, 15–22.

(31) Dunderdale, J.; Watkins, T. A. *Chem. Ind. (London)* **1956**, 174, 175.

(32) Tombeux, J.; van Poucke, L. C.; Eeckhaut, Z. *Spectrochim. Acta* **1972**, *28A*, 1943–1947.

[Os(CH=CHFc)Cl(CO)(BTD)(PPh₃)₂] (**10**) (200 mg, 0.178 mmol), stirred for 2 h, to give a black product. Yield: 310 mg (84%). IR (CH₂Cl₂): 2152 ($\nu_{\text{C}=\text{C}}$), 2022, 1927 (ν_{CO}) cm⁻¹. IR (Nujol): 2149 ($\nu_{\text{C}=\text{C}}$), 1924 (ν_{CO}), 1591, 1216, 1188, 1279, 1000 ($\nu_{\text{C}-\text{S}}$) cm⁻¹. ¹H NMR (acetone-*d*₆): δ 3.43–4.00 (m, 8 H, NC₄H₈N), 4.21 (s, 5 H, C₅H₅), 4.57, 4.73 (s(br) \times 2, 4 H, C₅H₄), 6.35 (s, 1 H, =CHPh), 6.46 (d, 1 H, =CHFc, ³J_{HH} = 15.0 Hz), 6.90–7.70 (m, 70 H, C₆H₅), 8.04 (dt, 1 H, OsCH, ³J_{HH} = 15.0 Hz, J_{HP} unresolved) ppm. ³¹P NMR: δ 7.9 (s, OsPPh₃), 37.9 (s, RuPPh₃) ppm. MS (LSIMS): *m/z* (%) 1784 (1) [M – PPh₃]⁺, 1524 (4) [M – 2PPh₃]⁺. Anal. Found: C, 63.3; H, 4.4; N, 1.4. Calcd for C₁₀₈H₉₆FeN₂O₂OsP₄RuS₄: C, 63.4; H, 4.4; N, 1.4.

[Ru(C(C \equiv CPh)=CHPh)(CS)(PPh₃)₂(S₂CNC₄H₈NH₂)Cl] (**22**). The reagent S₂CNC₄H₈NH₂ (13 mg, 0.080 mmol) was dissolved in methanol (8 cm³), and the complex [Ru(C(C \equiv CPh)=CHPh)Cl(CS)(PPh₃)₂] (50 mg, 0.055 mmol) in dichloromethane (20 cm³) was added. After the mixture was stirred at room temperature for 1 h, during which a change from orange to yellow was observed, the volatiles were removed. The crude product was dissolved in a small amount of dichloromethane, and ethanol (10 cm³) was added. Slow concentration under reduced pressure gave a yellow product, which was filtered off, washed with hexane (10 cm³), and dried under vacuum. Yield: 40 mg (68%). IR (CH₂Cl₂): 2145 ($\nu_{\text{C}=\text{C}}$) cm⁻¹. IR (Nujol): 2150 ($\nu_{\text{C}=\text{C}}$), 1246 (ν_{CS}), 999 ($\nu_{\text{C}-\text{S}}$), 893, 846 cm⁻¹. NMR (*d*₆-acetone) ¹H: δ 3.10, 3.31 (s \times 2, 8 H, NC₄H₈N), 6.42 (s, 1 H, H β), 6.69–7.45 (m, 40 H, C₆H₅) ppm. ³¹P NMR: 37.0 (s, PPh₃) ppm. MS (FAB): *m/z* (%) 1035 (1) [M]⁺. Anal. Found: C, 64.9; H, 4.8; N, 2.7. Calcd for C₅₈H₅₁N₂P₂RuS₃: C, 65.1; H, 4.8; N, 2.6.

[[Ru(C(C \equiv CPh)=CHPh)(CO)(PPh₃)₂](S₂CNC₄H₈NCS₂){Ru-C(C(C \equiv CPh)=CHPh)(CS)(PPh₃)₂]} (**23**). This compound was prepared as for the synthesis of **14** using [Ru(C(C \equiv CPh)=CHPh)(S₂CNC₄H₈NH₂)(CS)(PPh₃)₂]Cl (**22**; 50 mg, 0.047 mmol), triethylamine (1 drop, excess), CS₂ (1 drop, excess), and [Ru(C(C \equiv CPh)=CHPh)Cl(CO)(PPh₃)₂] (42 mg, 0.047 mmol) to give a yellow-brown product. Yield: 67 mg (73%). IR (CH₂Cl₂): 2153 ($\nu_{\text{C}=\text{C}}$), 1923 (ν_{CO}), 1606 cm⁻¹. IR (Nujol): 2150 ($\nu_{\text{C}=\text{C}}$), 1921 (ν_{CO}), 1592, 1259 (ν_{CS}), 1260, 999 ($\nu_{\text{C}-\text{S}}$) cm⁻¹. ¹H NMR (C₆D₆): δ 2.08–3.25 (m, 8 H, NC₄H₈N), 6.35 (s(br), 2 H, H β), 6.92–7.99 (m, 80 H, C₆H₅) ppm. ³¹P NMR: δ 34.1 (s(br), PPh₃) ppm. MS (MALDI): *m/z* (%) 1702 (2) [M – PPh₃]⁺, 1557 (2) [M – 2(enynyl)]⁺. Anal. Found: C, 68.3; H, 4.4; N, 1.2. Calcd for C₁₁₂H₉₀N₂OP₄Ru₂S₅: C, 68.4; H, 4.6; N, 1.4.

[[Ru(C(C \equiv CPh)=CHPh)(CO)(PPh₃)₂](S₂CNC₄H₈NCS₂)] (**24**). [[Ru(CH=CHC₆H₄Me-4)(CO)(PPh₃)₂](S₂CNC₄H₈NCS₂)] (**4**; 80 mg, 0.045 mmol) and HC \equiv CBu^t (28 mg, 0.341 mmol) were heated under reflux in toluene for 3 h. All solvent was removed under reduced pressure, the product was taken up in a small amount of dichloromethane, and this mixture was filtered through diatomaceous earth. Ethanol (15 cm³) was added, and a tan powder was obtained by reducing the solvent volume. This was filtered off, washed with hexane (10 cm³), and dried under vacuum. Yield: 54 mg (70%). IR (CH₂Cl₂): 2103 ($\nu_{\text{C}=\text{C}}$), 1941 (ν_{CO}) cm⁻¹. IR (Nujol): 2102 ($\nu_{\text{C}=\text{C}}$), 1947 (ν_{CO}), 1279, 1215 cm⁻¹. ¹H NMR (C₆D₆): δ 0.94 (s, 18 H, Bu^t), 1.95–2.24 (m, 8 H, NC₄H₈N), 6.73–7.89 (m, 60 H, C₆H₅) ppm. ³¹P NMR: δ 38.9, 39.3 (s \times 2, PPh₃) ppm. MS (MALDI): *m/z* (%) 1706 (2) [M]⁺, 1444 (2) [M – PPh₃]⁺, 1418 (4) [M – CO – PPh₃]⁺, 1307 (4) [M – alkenyl – 2CO – PPh₃]⁺. Anal. Found: C, 61.8; H, 4.7; N, 1.9. Calcd for C₉₂H₈₆N₂O₂P₄Ru₂S₄·1.5CH₂Cl₂: C, 61.3; H, 4.9; N, 1.5.

[[Ru(C(C \equiv CPh)=CHPh)(CO)(PPh₃)₂(S₂CNC₄H₈NCS₂)₂)] (**25**). [Ru(C(C \equiv CPh)=CHPh)(S₂CNC₄H₈NH₂)(CO)(PPh₃)₂]Cl (**1**; 80 mg, 0.076 mmol) was dissolved in dichloromethane (15 cm³) and methanol (8 cm³). Triethylamine (4 drops, excess) and CS₂ (3 drops, excess) were added. After the mixture was stirred for 5 min, [Ni(O₂CMe)₂] (6.7 mg, 0.038 mmol) in dichloromethane (5 cm³) was added, the mixture was stirred for 2 h, and all solvent was

Table 1. Crystal Data and Structure Refinement Parameters for **1**·1.25EtOH

chem formula	C _{60.5} H _{58.5} ClN ₂ O _{2.25} P ₂ RuS ₂
fw	1112.17
cryst syst	monoclinic
cryst color	yellow
cryst size (mm)	0.22 \times 0.17 \times 0.02
space group	<i>P</i> 2 ₁ / <i>c</i>
<i>a</i> (Å)	21.2542(6)
<i>b</i> (Å)	16.2199(5)
<i>c</i> (Å)	18.9949(6)
α (deg)	90
β (deg)	105.006(2)
γ (deg)	90
<i>V</i> (Å ³)	6325.0(3)
<i>Z</i>	4
<i>D</i> _{calcd} (g/cm ³)	1.168
<i>T</i> (K)	150(2)
μ (Mo K α) (mm ⁻¹)	0.446
<i>F</i> (000)	2306
no. of rflns collected	40 498
no. of unique rflns/data (<i>R</i> _{int})	13 562/698 (0.0817)
<i>R</i> 1 (<i>I</i> > 2 σ (<i>I</i>))	0.0698
w <i>R</i> 2 (<i>I</i> > 2 σ (<i>I</i>))	0.1697
<i>R</i> 1 (all data)	0.1196
w <i>R</i> 2 (all data)	0.1974

then removed under reduced pressure. The yellow product was taken up in a small amount of dichloromethane and filtered through diatomaceous earth. Ethanol (10 cm³) was added, and the solvent volume was reduced by rotary evaporation. The product was filtered off, washed with hexane (15 cm³), and dried under vacuum. Yield: 47 mg (55%). IR (CH₂Cl₂): 2152 ($\nu_{\text{C}=\text{C}}$), 1926 (ν_{CO}) cm⁻¹. IR (Nujol): 2152 ($\nu_{\text{C}=\text{C}}$), 1925 (ν_{CO}), 1592, 1278, 1216, 1157, 999 ($\nu_{\text{C}-\text{S}}$), 908 cm⁻¹. ¹H NMR: δ 3.08–3.29 (m, 16 H, NC₄H₈N), 6.30 (s, 2 H, H β), 6.93–7.55 (m, 80 H, C₆H₅) ppm. ³¹P NMR: δ 38.0 (s, PPh₃) ppm. MS (FAB): *m/z* (%) 1691 (2) [M – 2PPh₃ – CO]⁺. Anal. Found: C, 63.0; H, 4.3; N, 2.5. Calcd for C₁₁₈H₉₈N₄O₂P₄Ru₂S₈Ni: C, 63.1; H, 4.4; N, 2.5.

[[Ru(C(C \equiv CPh)=CHPh)(CO)(PPh₃)₂(S₂CNC₄H₈NCS₂)₂]Pd] (**26**). This compound was prepared as for the synthesis of **25** using [Ru(C(C \equiv CPh)=CHPh)(S₂CNC₄H₈NH₂)(CO)(PPh₃)₂]Cl (**1**; 80 mg, 0.076 mmol), triethylamine (4 drops, excess), CS₂ (2 drops, excess), and [PdCl₂(NCMe)₂] (9.8 mg, 0.038 mmol) to provide a brown product. Yield: 49 mg (56%). IR (CH₂Cl₂): 2152 ($\nu_{\text{C}=\text{C}}$), 1927 (ν_{CO}) cm⁻¹. IR (Nujol): 2152 ($\nu_{\text{C}=\text{C}}$), 1921 (ν_{CO}), 1592, 1277, 1217, 1158, 999 ($\nu_{\text{C}-\text{S}}$) cm⁻¹. ¹H NMR: δ 2.82–3.40 (m, 16 H, NC₄H₈N), 6.28 (s, 2 H, H β), 6.92–7.67 (m, 80 H, C₆H₅) ppm. ³¹P NMR: δ 38.0 (s, PPh₃) ppm. MS (FAB): *m/z* (%) 1859 (1) [M – 2 alkenyl – CO]⁺, 1199 (1) [M – Ru(C(C \equiv CPh)=CHPh)(CO)(PPh₃)₂]⁺. Anal. Found: C, 61.8; H, 4.3; N, 2.5. Calcd for C₁₁₈H₉₈N₄O₂P₄Ru₂S₈Pd: C, 61.8; H, 4.3; N, 2.4.

[[Ru(C(C \equiv CPh)=CHPh)(CO)(PPh₃)₂(S₂CNC₄H₈NCS₂)₂]Pt] (**27**). This compound was prepared as for the synthesis of **25** using [Ru(C(C \equiv CPh)=CHPh)(S₂CNC₄H₈NH₂)(CO)(PPh₃)₂]Cl (**1**; 50 mg, 0.047 mmol), triethylamine (3 drops, excess), CS₂ (2 drops, excess), and [PtCl₂(NCPh)₂] (11.2 mg, 0.024 mmol) to yield a yellow product. Yield: 32 mg (56%). IR (CH₂Cl₂): 2153 ($\nu_{\text{C}=\text{C}}$), 1931 (ν_{CO}) cm⁻¹. IR (Nujol): 2152 ($\nu_{\text{C}=\text{C}}$), 1928 (ν_{CO}), 1278, 1217, 1158, 1000 ($\nu_{\text{C}-\text{S}}$) cm⁻¹. ¹H NMR: δ 2.78–3.30 (m, 16 H, NC₄H₈N), 6.30 (s, 2 H, H β), 6.85–7.72 (m, 80 H, C₆H₅) ppm. ³¹P NMR: δ 38.1 (s, PPh₃) ppm. MS (FAB): *m/z* (%) 2177 (2) [M – enynyl]⁺, 1981 (1) [M – 2 enynyl]⁺, 1687 (1) [M – 2 enynyl – PPh₃ – CO]⁺, 1550 (2) [M – Ru(enynyl)(PPh₃)₂]⁺. Anal. Found: C, 59.4; H, 4.3; N, 2.3. Calcd for C₁₁₈H₉₈N₄O₂P₄PtRu₂S₈: C, 59.5; H, 4.2; N, 2.4.

[[Ru(C(C \equiv CPh)=CHPh)(CO)(PPh₃)₂(S₂CNC₄H₈NCS₂)₂]Zn] (**28**). This compound was prepared as for the synthesis of **25** using [Ru(C(C \equiv CPh)=CHPh)(S₂CNC₄H₈NH₂)(CO)(PPh₃)₂]Cl (**1**; 50 mg, 0.047 mmol), triethylamine (3 drops, excess), CS₂ (2 drops, excess), and [Zn(O₂CMe)₂]·2H₂O (5.2 mg, 0.024 mmol) to yield a yellow product. Yield: 55 mg (52%). IR (CH₂Cl₂): 2152 ($\nu_{\text{C}=\text{C}}$), 1926 (ν_{CO})

cm⁻¹. IR (Nujol): 2152 ($\nu_{C\equiv C}$), 1923 (ν_{CO}), 1573, 1277, 1214, 1155, 999 (ν_{C-S}) cm⁻¹. ¹H NMR: δ 2.62–3.61 (m, 16 H, NC₄H₈N), 6.25 (s, 2 H, H β), 6.89–7.51 (m, 80 H, C₆H₅) ppm. ³¹P NMR: δ 38.0 (s, PPh₃) ppm. MS (FAB): *m/z* (%) 1397 (1) [M – Ru(enynyl)-(CO)(PPh₃)₂]⁺. Anal. Found: C, 59.5; H, 3.8; N, 2.4. Calcd for C₁₁₈H₉₈N₄O₂P₄Ru₂S₈Zn · 2CH₂Cl₂: C, 59.5; H, 4.2; N, 2.3.

Crystallographic Studies. Crystals of **1** were grown by slow diffusion of ethanol into a dichloromethane solution of the complex and subsequent slow evaporation. Single-crystal X-ray diffraction data were collected using graphite-monochromated Mo K α radiation ($\lambda = 0.71073$ Å) on an Enraf-Nonius KappaCCD diffractometer equipped with a Cryostream N₂ open-flow cooling device³³ at 150(2) K. Series of ω scans were performed in such a way as to cover a sphere of data to a maximum resolution of 0.77 Å.

Cell parameters and intensity data for **1** were processed using the DENZO-SMN package,³⁴ and the structure was solved by direct methods and refined by full-matrix least squares on F^2 using SHELXTL software.³⁵ Intensities were corrected for absorption effects by the multiscan method based on multiple scans of identical and Laue equivalent reflections (using the SORTAV software).³⁶

Where possible, non-hydrogen atoms were refined with anisotropic displacement parameters and the hydrogen atoms were

positioned geometrically and refined using a riding model. In addition to the [Ru(C(C \equiv CPh)=CHPh)(S₂CNC₄H₈NH₂)(CO)-(PPh₃)₂]⁺ (**1**) cation, there are also disordered solvent molecules and chloride counteranions which were located in the difference map. The chloride ion was refined using a model where it was split over three sites with occupancies of 0.65, 0.18, and 0.17 for Cl1, Cl1A, and Cl1B, respectively. Five partially occupied ethanol molecules were clearly visible in the difference map and refined with 25% occupancy each, using the same distance restraint to maintain plausible geometries. Crystal data and structure refinement parameters are included in Table 1.

Crystallographic data (excluding structure factors) for the structure of **1** have been deposited with the Cambridge Crystallographic Data Centre (CCDC 677008). Copies of the data can be obtained free of charge from The Cambridge Crystallographic Data Centre via www.ccdc.cam.ac.uk/data_request/cif.

Acknowledgment. J.D.E.T.W.-E. gratefully acknowledges Merton College for the provision of a Fellowship. We thank the OUP John Fell Fund for consumables and Johnson Matthey Ltd for a generous loan of ruthenium and osmium salts.

Supporting Information Available: A CIF file giving crystallographic data for the structure of **1**. This material is available free of charge via the Internet at <http://pubs.acs.org>.

OM800686F

(33) Cosier, J.; Glazer, A. M. *J. Appl. Crystallogr.* **1986**, *19*, 105.

(34) Otwinowski, Z.; Minor, W. In *Processing of X-ray Diffraction Data Collected in Oscillation Mode*; Carter, C. W., Sweet, R. M., Eds.; Academic Press: New York, 1997; Methods in Enzymology 276.

(35) SHELXTL, version 5.1; Bruker Analytical X-ray Instruments Inc., Madison, WI, 1999.

(36) Blessing, R. H. *Acta Crystallogr.* **1995**, *A51*, 33–38.

Electron-Deficient Iron Alkyl Complexes Supported by Diimine Ligand $(\text{Ph}_2\text{CN})_2\text{C}_2\text{H}_4$: Evidence for Reversible Ethylene Binding

Jeroen Volbeda, Auke Meetsma, and Marco W. Bouwkamp*

Molecular Inorganic Chemistry Department, Stratingh Institute for Chemistry, University of Groningen, Nijenborgh 4, 9747 AG Groningen, The Netherlands

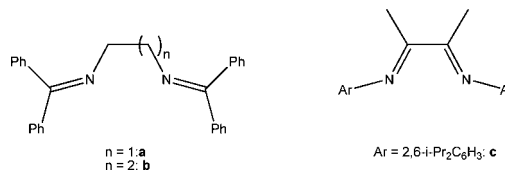
Received July 17, 2008

Reaction of diimine ligands $(\text{Ph}_2\text{CN})_2\text{C}_n\text{H}_{2n}$ ($n = 2$, **a**; $n = 3$, **b**) with FeCl_2 or FeBr_2 results in formation of the corresponding high-spin ferrous complexes $\{(\text{Ph}_2\text{CN})_2\text{C}_2\text{H}_4\}\text{FeX}_2$ (**1a**, $\text{X} = \text{Cl}$; **2a**, $\text{X} = \text{Br}$) and $\{(\text{Ph}_2\text{CN})_2\text{C}_3\text{H}_6\}\text{FeCl}_2$ (**1b**). Dialkyl $\{(\text{Ph}_2\text{CN})_2\text{C}_2\text{H}_4\}\text{Fe}(\text{CH}_2\text{SiMe}_3)_2$ (**3a**) was prepared by treatment of $(\text{py})_2\text{Fe}(\text{CH}_2\text{SiMe}_3)_2$ with diimine ligand **a**. Addition of $\text{B}(\text{C}_6\text{F}_5)_3$ to **3a** at -30°C resulted in Me_3SiCH_2 abstraction, affording $\{[(\text{Ph}_2\text{CN})_2\text{C}_2\text{H}_4]\text{Fe}(\text{CH}_2\text{SiMe}_3)[\text{Me}_3\text{SiCH}_2\text{B}(\text{C}_6\text{F}_5)_3]\}$ (**5a**). ^{19}F NMR spectroscopy revealed that this compound exists as a contact ion-pair in toluene solution. Compound **5a** decomposes at room temperature in bromobenzene- d_5 or toluene- d_8 , affording dication $\{[(\text{Ph}_2\text{CN})_2\text{C}_2\text{H}_4]_2\text{Fe}\}^{2+}$ (**6a**); at elevated temperatures in toluene- d_8 the formation of $\{[(\text{Ph}_2\text{CN})_2\text{C}_2\text{H}_4]\text{Fe}(\text{CH}_2\text{SiMe}_3)\text{C}_6\text{F}_5\}$ (**7a**) was observed as well. Neither ferrous chloride $\{(\text{Ph}_2\text{CN})_2\text{C}_2\text{H}_4\}\text{FeCl}_2$ activated with methylaluminoxane nor contact ion-pair **5a** is active in the polymerization of ethylene. Instead we were able, for the first time, to observe reversible ethylene binding to a cationic iron alkyl complex.

Introduction

Scheme 1

Ever since the initial publications by the groups of Brookhart¹ and Gibson,² in which they independently reported the use of pyridine-diimine complexes of iron as efficient catalysts for the polymerization of ethylene, many research groups have prepared related iron catalysts in order to tune catalyst performance, and with that the properties of the polymer obtained.³ Electron-deficient, cationic iron(II) alkyl complexes are often implied as the active species,⁴ although zerovalent⁵ and trivalent⁶ iron species have been proposed as well. It has been shown that the pyridine-diimine iron dialkyl complex $(\text{PDI})\text{Fe}(\text{CH}_2\text{SiMe}_3)_2$ ($\text{PDI} = 2,6\text{-}i\text{-Pr}_2\text{C}_6\text{H}_3\text{NC}(\text{Me})_2\text{C}_5\text{H}_3\text{N}$)⁷ can be converted into a monoalkyl cation by treatment with tris(pentafluorophenyl)borane and that the resulting well-defined iron alkyl cation



* Corresponding author. E-mail: M.W.Bouwkamp@rug.nl.

(1) Small, B. L.; Brookhart, M.; Bennett, A. M. *J. Am. Chem. Soc.* **1998**, *120*, 4049.

(2) Britovsek, G. J. P.; Gibson, V. C.; Kimberely, B. S.; Maddox, P. J.; McTavish, S. J.; Solan, G. A.; White, A. J. P.; Williams, D. J. *Chem. Commun.* **1998**, 849.

(3) For recent reviews on iron-catalyzed olefin polymerization catalysis, see: Bianchini, C.; Giambastiana, G.; Guerrero Rios, I.; Mantovani, G.; Meli, A.; Segarra, A. M. *Coord. Chem. Rev.* **2006**, *250*, 1391. Gibson, V. C.; Redshaw, C.; Solan, G. A. *Chem. Rev.* **2007**, *107*, 1745.

(4) (a) Deng, L.; Margl, P.; Ziegler, T. *J. Am. Chem. Soc.* **1999**, *121*, 6479. (b) Babik, S. T.; Fink, G. *J. Mol. Catal. A* **2002**, *188*, 245. (c) Britovsek, G. J. P.; Gibson, V. C.; Spitzmesser, S. K.; Tellman, K. P.; White, A. J. P.; Williams, D. J. *J. Chem. Soc., Dalton Trans.* **2002**, 1159. (d) Bryliakov, K. P.; Semikolenova, N. V.; Zudin, V. N.; Zakharov, V. A.; Talsi, E. P. *Catal. Commun.* **2004**, *5*, 45. (e) Castro, P. M.; Lahtinen, P.; Axenov, K.; Viidanoja, J.; Kotiaho, T.; Leskelä, M.; Repo, T. *Organometallics* **2005**, *24*, 3664.

(5) Scott, J.; Gambarotta, S.; Korobkov, I.; Budzelaar, P. H. M. *Organometallics* **2005**, *24*, 6298.

(6) (a) Britovsek, G. J. P.; Clentsmith, G. K. B.; Gibson, V. C.; Goodgame, D. M. L.; McTavish, S. J.; Pankhurst, Q. A. *Catal. Commun.* **2002**, *3*, 207. (b) Raucoules, R.; De Bruin, T.; Raybaud, P.; Adamo, C. *Organometallics* **2008**, *27*, 3368–3377.

(7) (a) Bouwkamp, M. W.; Bart, S. C.; Hawrelak, E. J.; Trovitch, R. J.; Lobkovsky, E.; Chirik, P. J. *Chem. Commun.* **2005**, 3406. (b) Scott, J.; Gambarotta, S.; Korobkov, I.; Budzelaar, P. H. M. *J. Am. Chem. Soc.* **2005**, *127*, 13019. (c) Cámpora, J.; Naz, A. M.; Palma, P.; Alvarez, E.; Reyes, M. L. *Organometallics* **2005**, *24*, 4878.

$\{(\text{PDI})\text{Fe}(\text{CH}_2\text{SiMe}_2\text{CH}_2\text{SiMe}_3)[\text{MeB}(\text{C}_6\text{F}_5)_3]\}$ is indeed active in the polymerization of ethylene.⁸ On the other hand, it is known that treatment of PDI iron complexes with alkyl aluminum species can result in ligand redistribution reactions,⁹ thus the exact nature of the active species in the MAO-activated system remains under debate.

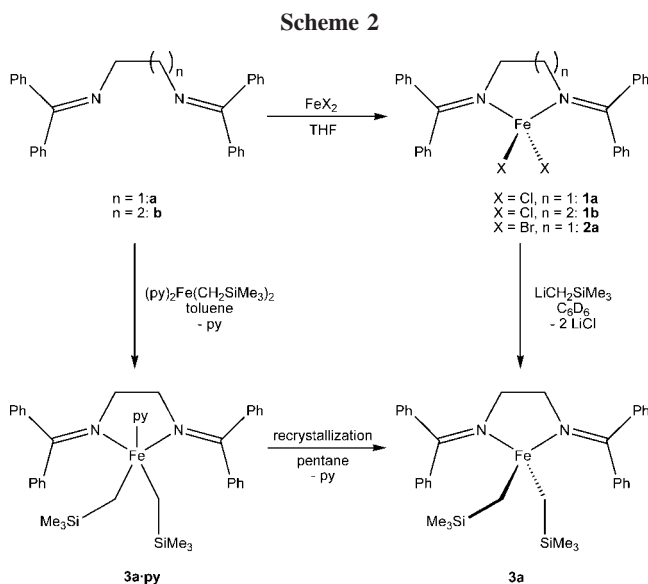
We are thus interested in the reactivity of cationic iron alkyl complexes supported by neutral imine derived ligands. Our initial focus has been on the synthesis and reactivity of iron complexes with nonconjugated diimine ligands $(\text{Ph}_2\text{CN})_2\text{C}_n\text{H}_{2n}$ ($n = 2$, **a**; $n = 3$, **b**; Scheme 1),¹⁰ and the results have been compared to those previously obtained with the well-known α -diimine ligand $(2,6\text{-}i\text{-Pr}_2\text{C}_6\text{H}_3\text{N})_2(\text{C}_2\text{Me}_2)$ (**c**, Scheme 1).¹¹ Included is the synthesis of neutral and cationic iron alkyl complexes with the C_2 -bridged diimine ligand **a**. The alkyl cation $\{[(\text{Ph}_2\text{CN})_2\text{C}_2\text{H}_4]\text{Fe}(\text{CH}_2\text{SiMe}_3)\}^+$ is inactive in the polymerization of olefins, but was found to reversibly bind ethylene.

(8) Bouwkamp, M. W.; Lobkovsky, E.; Chirik, P. J. *J. Am. Chem. Soc.* **2005**, *127*, 9660.

(9) Scott, J.; Gambarotta, S.; Korobkov, I.; Knijnenburg, Q.; De Bruin, B.; Budzelaar, P. H. M. *J. Am. Chem. Soc.* **2005**, *127*, 17204.

(10) (a) Tripathi, S. C.; Srivastava, S. C.; Shrimal, A. K.; Singh, O. P. *Inorg. Chim. Acta* **1985**, *98*, 19. (b) Paz-Sandoval, M. A.; Domínguez-Durán, M. E.; Pazos-Mayen, C.; Ariza-Castolo, A.; Rosales-Hoz, M. J.; Conretas, R. *J. Organomet. Chem.* **1995**, *492*, 1. (c) Petrovski, Z.; Pillinger, M.; Valente, A. A.; Gonçalves, I. S.; Hazell, A.; Romão, C. C. *J. Mol. Catal. A: Chem.* **2005**, *227*, 67. (d) Kia, R.; Mirkhani, V.; Kalman, A.; Deak, A. *Polyhedron* **2007**, *26*, 1711.

(11) Bart, S. C.; Hawrelak, E. J.; Schmisser, A. K.; Lobkovsky, E.; Chirik, P. J. *Organometallics* **2004**, *23*, 237.



Results and Discussion

Synthesis of Iron Halide Complexes. Ferrous dichlorides $\{(\text{Ph}_2\text{CN})_2\text{C}_2\text{H}_4\}\text{FeCl}_2$ (**1a**) and $\{(\text{Ph}_2\text{CN})_2\text{C}_3\text{H}_6\}\text{FeCl}_2$ (**1b**) and dibromide $\{(\text{Ph}_2\text{CN})_2\text{C}_2\text{H}_4\}\text{FeBr}_2$ (**2a**) were prepared by stirring THF suspensions of anhydrous FeCl_2 or FeBr_2 with the corresponding diimine ligands (Scheme 2). The compounds could be isolated in good yields (72–90%) by removal of the solvent and extraction with dichloromethane. After filtering the extracts over Celite compounds **1a,b** and **2a** were obtained as yellow (ligand **a**) or orange (ligand **b**) powders by evaporation of the solvent. The compounds have a high-spin ground state, similar to α -diimine complexes of this type.¹¹ Both compounds **1a** and **2a**¹² were studied by single-crystal X-ray diffraction (see Figure 1 for an ORTEP representation of **1a** and Table 1 for pertinent bond distances and angles of both structures; the structure of **2a** can be found in the Supporting Information). Both compounds crystallize in the $P2_1/c$ space group with two independent molecules in the asymmetric unit that have similar metrical parameters, and only one of each will be discussed here. The geometry around the iron center in complexes **1a** and **2a** can be best described as a distorted tetrahedron, with N(11)–Fe(1)–N(12) angles of 81.88(9) $^\circ$ and 81.7(3) $^\circ$ and X–Fe(1)–X angles of 126.09(3) $^\circ$ and 121.39(7) $^\circ$, respectively. Both compounds show a strong puckering in the Fe(1)–N(11)–C(114)–C(115)–N(12) ring, with one of the two carbon atoms of the C_2 -spacer deviating from the ligand plane. As a result, one of the imine moieties is pushed out of the Fe(1)–N(11)–N(12) plane (Figure 1). The $(\text{C}_{\text{ipso}})_2\text{CNCH}_2$ moieties are virtually planar, resulting in two sets of distinct phenyl groups: one that is directed toward the metal center and one that is pointing away. The metrical parameters of **1a** are similar to the corresponding ferrous chloride with an α -diimine ligand, $\{(2,6\text{-}i\text{-Pr}_2\text{C}_6\text{H}_3\text{N})_2\text{-}(\text{C}_2\text{Me}_2)\}\text{FeCl}_2$ (**1c**),¹³ with slightly larger Fe–N and Fe–Cl bond distances for the first (average Fe–N: 2.130(4) Å for **1a** and 2.1016(14) for **1c**; average Fe–Cl: 2.2588(13) Å for **1a** and 2.2222(10) Å for **1c**) and a larger bite angle (81.88(9) $^\circ$ for **1a** and 76.50(5) $^\circ$ for **1c**).

(12) A small amount of crystals of compound **2a** was obtained during the decomposition of compound **5a** in bromobenzene- d_5 . These crystals were used for a single-crystal X-ray analysis.

(13) Kervern, G.; Pintacuda, G.; Zhang, Y.; Oldfield, E.; Roukoss, C.; Kuntz, E.; Herdtweck, E.; Basset, J. M.; Cadars, S.; Lesage, A.; Copéret, C.; Emsley, L. *J. Am. Chem. Soc.* **2006**, 128, 13545.

As expected for high-spin ($S = 2$) iron complexes, the ^1H NMR spectra of the ferrous complexes prepared in this study reveal paramagnetically shifted resonances. Whereas most of these are found relatively close to the resonances observed for the free diimines, two resonances integrating to 4 protons each show more pronounced shifts. One of these is shifted to low field (δ 57.5–177.3 ppm) and one to high field (δ –26.9 to –53.3 ppm). These are tentatively assigned to the *o*-CH and *m*-CH of the phenyl group that is directed toward the iron center. See Figure 2 for a representative ^1H NMR spectrum.

Synthesis of Neutral Iron Alkyl Complexes. Treatment of **1a** or **2a** with 2 equiv of $\text{LiCH}_2\text{SiMe}_3$ in benzene- d_6 solution resulted in a color change from yellow to brownish-red. ^1H NMR spectroscopy of the reaction mixture revealed the number of signals expected for a C_{2v} symmetric dialkyl complex $\{(\text{Ph}_2\text{CN})_2\text{-C}_2\text{H}_4\}\text{Fe}(\text{CH}_2\text{SiMe}_3)_2$ (**3a**), taking into account that the protons for the methylene groups that are directly bound to the paramagnetic iron center are usually not observed.^{7,11} Performing these reactions on a preparative scale did not allow the clean formation of dialkyl complex **3a**. One explanation may be that alkylation reactions of iron halides with imine-based ligands can be susceptible to a number of side reactions, such as reduction of the iron center^{7a,14} and alkylation of the ligand.^{7b} Compound **3a**, however, could be obtained in good yield (70%) by treatment of the iron-dialkyl reagent $(\text{py})_2\text{Fe}(\text{CH}_2\text{SiMe}_3)_2$ ^{7c} with 1 equiv of the ligand. When the reaction was performed on an NMR tube scale and the volatiles of the reaction mixture were transferred into a tube with a known amount of ferrocene internal standard, it was found (by integration) that only 1 equiv of pyridine was released during the reaction, suggesting the formation of the monopyridine adduct $\{(\text{Ph}_2\text{CN})_2\text{C}_2\text{H}_4\}\text{-Fe}(\text{CH}_2\text{SiMe}_3)_2(\text{py})$ (**3a·py**). In the initial reaction mixture no free pyridine was observed, suggesting a fast (on the NMR time scale) exchange between free and bound pyridine. Recrystallization of **3a·py** from pentane at –30 $^\circ\text{C}$ afforded single crystals of the pyridine-free compound $\{(\text{Ph}_2\text{CN})_2\text{C}_2\text{H}_4\}\text{Fe}(\text{CH}_2\text{SiMe}_3)_2$ (**3a**). The geometry of **3a** (see Figure 1 for an ORTEP representation of **3a** and Table 1 for pertinent bond distances and angles) is very similar to that of complexes **1a** and **2a**, with slightly longer Fe–N bond distances. The Fe–N and Fe–C bond distances in **3a** are slightly elongated compared with those found in $\{(2,6\text{-}i\text{-Pr}_2\text{C}_6\text{H}_3\text{N})_2(\text{C}_2\text{Me}_2)\}\text{Fe}(\text{CH}_2\text{SiMe}_3)_2$ (**3c**).¹¹ As expected, iron dialkyl **3a** has a high-spin ground state ($\mu_{\text{eff}} = 4.9 \mu_{\text{B}}$).

Treatment of **1b** with $\text{LiCH}_2\text{SiMe}_3$ in benzene- d_6 in an NMR tube resulted in a reddish-brown, intractable mixture of products. Furthermore, dissolving $(\text{py})_2\text{Fe}(\text{CH}_2\text{SiMe}_3)_2$ and the C_3 -bridged diimine ligand (**b**) in benzene- d_6 did not result in formation of the corresponding dialkyl complex. Instead, a mixture of the starting materials was observed by ^1H NMR spectroscopy, even after shaking the NMR tube for 3 days at room temperature.

Synthesis of Cationic Iron Alkyl Complexes. THF-solvated cation $[\{(\text{Ph}_2\text{CN})_2\text{C}_2\text{H}_4\}\text{Fe}(\text{CH}_2\text{SiMe}_3)(\text{THF})][\text{BPh}_4]$ (**4a'**) was prepared in reasonable yield (53%) by reaction of a 1:1 mixture of dialkyl **3a** and Brønsted acid $[\text{PhNMe}_2\text{H}][\text{BPh}_4]$ in THF. The compound was isolated as yellow crystals by diffusion of pentane into a THF solution of the compound. X-ray analysis confirms its formulation, and an ORTEP representation is depicted in Figure 3 (see Table 1 for pertinent bond distances and angles). The geometry of the compound is similar to the other ferrous complexes described in this study, with slightly

(14) (a) Scott, J.; Gambarotta, S.; Korobkov, I.; Budzelaar, P. H. M. *Organometallics* **2005**, 24, 6298. (b) Fernández, I.; Trovitch, R. J.; Lobkovsky, E.; Chirik, P. J. *Organometallics* **2008**, 27, 109.

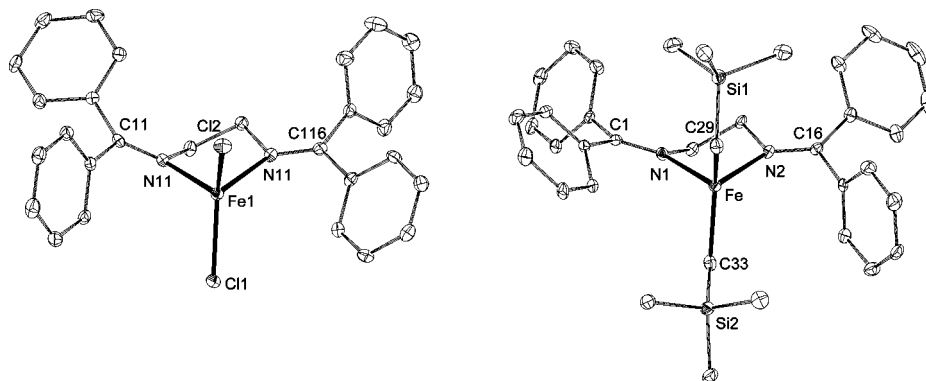


Figure 1. ORTEP representations at the 30% probability level of **1a** and **3a**. Hydrogen atoms are omitted for clarity.

Table 1. Pertinent Bond Distances and Angles for 1a, 2a, 3a, 4a', 6a, and 7a

	1a	2a	3a	4a'	6a	7a
Fe(1)–N(11) ^a	2.149(3)	2.114(8)	2.214(3)	2.120(3)	2.123(6)	2.186(5)
Fe(1)–N(12) ^b	2.112(2)	2.129(8)	2.176(3)	2.154(3)	2.095(6)	2.149(5)
Fe(1)–X ^c	2.2431(9)	2.443(2)	2.078(4)	2.055(2)	2.073(6)	2.132(7)
Fe(1)–Y ^d	2.2744(9)	2.374(2)	2.098(4)	2.024(4)	2.085(6)	2.077(6)
C(11)–N(11) ^{a,e}	1.296(3)	1.308(13)	1.287(5)	1.301(5)	1.306(9)	1.293(7)
C(116)–N(12) ^{b,f}	1.291(4)	1.295(12)	1.285(5)	1.292(5)	1.300(9)	1.292(7)
C(135)–N(13)					1.301(11)	
C(150)–N(14)					1.304(11)	
N(11)–Fe(1)–N(12) ^{a,b}	81.88(9)	81.7(3)	80.09(11)	81.52(11)	84.5(2)	80.34(17)
X–Fe(1)–Y ^{c,d}	126.09(3)	121.39(7)	131.66(16)	137.06(12)	83.5(2)	124.1(2)

^a Fe and N(1) for **3a** and **7a**. ^b Fe and N(2) for **3a** and **7a**. ^c X = Cl11 (**1a**); Br11 (**2a**); C(29) (**3a**); O(11) (**4a'**); N(13) (**6a**); C(29) (**7a**). ^d Y = Cl12 (**1a**); Br12 (**2a**); C(29) (**3a**); C(129) (**4a'**); N(14) (**6a**); C(35) (**7a**). ^e C(1) for **3a** and **7a**; C(17) for **6a**. ^f C(16) for **3a** and **7a**; C(122) for **6a**.

contracted metal–ligand bond distances, a result of the increased electron deficiency of the metal center.

A base-free iron alkyl complex (**5a**) was prepared by addition of a cold (–30 °C) toluene-*d*₈ solution of B(C₆F₅)₃ to a cooled solution of **3a** in toluene-*d*₈. This resulted in a color change from purple to yellow. After replacing the solvent with THF-*d*₆ a species was observed with a similar ¹H NMR spectrum to that of **4a'**, suggesting the initial formation of ion-pair [(Ph₂CN)₂C₂H₄]₂Fe(CH₂SiMe₃)[Me₃SiCH₂B(C₆F₅)₃] (**5a**, Scheme 3). The ESI-MS of a solution of **4a** in THF revealed a peak at *m/z* = 603.3 and 531.1 g/mol (calcd for the cation of **4a**, 603.3; for the cation of **5a**, 531.2) in the positive-ion spectrum and at *m/z* = 599.1 (calcd for [Me₃SiCH₂B(C₆F₅)₃], 599.1) in the negative-ion spectrum. Hence, similar to the α-diimine case, the coordination sphere of the iron center in **3a** is sufficiently open to allow abstraction of a Me₃SiCH₂ group,¹¹ and there is no indication for Me₃SiCH₂-methyl group abstraction.⁸ It should be noted that, in the case of the α-diimine complex, the iron alkyl cation [(2,6-*i*-Pr₂C₆H₃N)₂(C₂Me₂)Fe(CH₂SiMe₃)⁺ could not be observed. Instead, {(2,6-*i*-Pr₂C₆H₃N)₂(C₂Me₂)Fe(CH₂SiMe₃)C₆F₅ (**7c**) was obtained, the result of a fast C₆F₅ transfer in the initially generated ion-pair (*vide infra*).¹¹

The ¹⁹F NMR spectrum of **5a** in toluene-*d*₈ (at a concentration of 30.2 mM) revealed three resonances at δ –98.5 (*m*-F), –118.1 (*o*-F), and –152.3 (*p*-F) ppm for the pentafluorophenyl groups, indicative of a coordinated borate anion.^{15,16} Interestingly, the chemical shifts are sensitive to the concentration of the ion-pair, with the signals shifting to lower field upon dilution (Figure 4). In general a concentration dependency could suggest the presence of an equilibrium between a solvent-separated and a contact ion-pair, though in that case a shift in the opposite direction is expected. The concentration dependency observed here may be the result of the formation of higher aggregates at higher concentrations, which will in turn affect the strength of the ion-pairing.¹⁷ Addition of a drop of THF to a diluted toluene solution of **5a** (9.19 mM) results in a shift of the three fluorine resonances to δ –124.8 (*o*-F), 162.2 (*m*-F), and 162.5 (*p*-F) ppm. This suggests that there is still an interaction between the ions in THF adduct **4a** in toluene, although this interaction is much weaker compared to that in the contact ion-pair **5a**. When dissolving compound **5a** in THF-*d*₆, resonances are observed at δ –129.7 (*o*-F), –164.7 (*p*-F), and –166.8 (*m*-F) ppm, as expected for a noncoordinating anion.¹⁸

During the synthesis of the contact ion-pair (**5a**) at room temperature in toluene-*d*₈ or bromobenzene-*d*₅, a secondary iron species (**6a**) was observed as well. In bromobenzene-*d*₅ species **6a** was observed exclusively after standing for 24 h at room temperature. The compound was characterized as [(Ph₂CN)₂(C₂H₄)₂Fe][Me₃SiCH₂B(C₆F₅)₃]₂ (**6a**) by single-crystal X-ray analysis (see Figure 3 for an ORTEP representation and Table 1 for selected bond distances and angles).¹⁹ Iron dication **6a** can be prepared purposely by treating dialkyl complex **3a** with

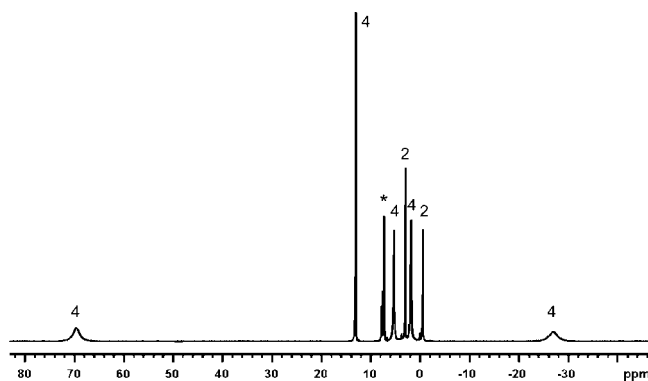


Figure 2. ¹H NMR spectrum of **1a**. The numbers represent the relative integrations; * marks the CDCl₃ solvent peak.

(15) (a) Sciarone, T. J. J.; Meetsma, A.; Hessen, B.; Teuben, J. H. *Chem. Commun.* **2002**, 1580. (b) Sciarone, T. J. J.; Meetsma, A.; Hessen, B. *Inorg. Chim. Acta* **2006**, 359, 1815. (c) Sciarone, T. J. J.; Nijhuis, C. A.; Meetsma, A.; Hessen, B. *Organometallics* **2008**, 27, 2058.

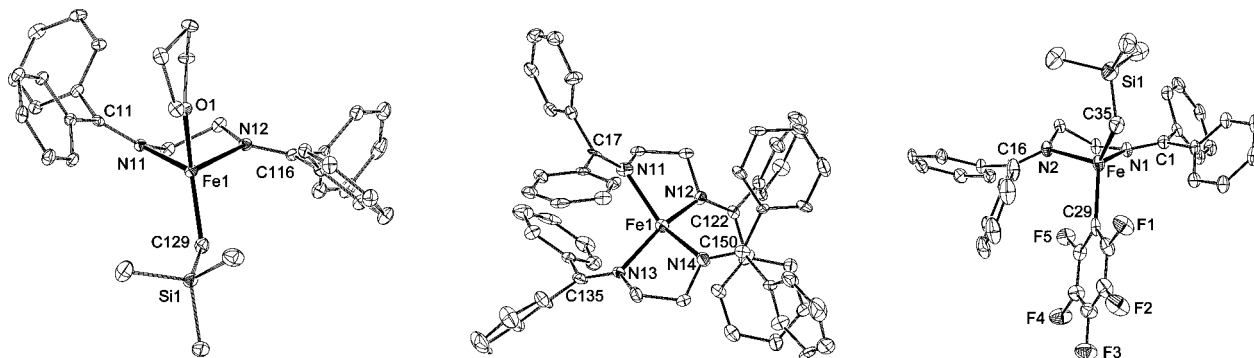
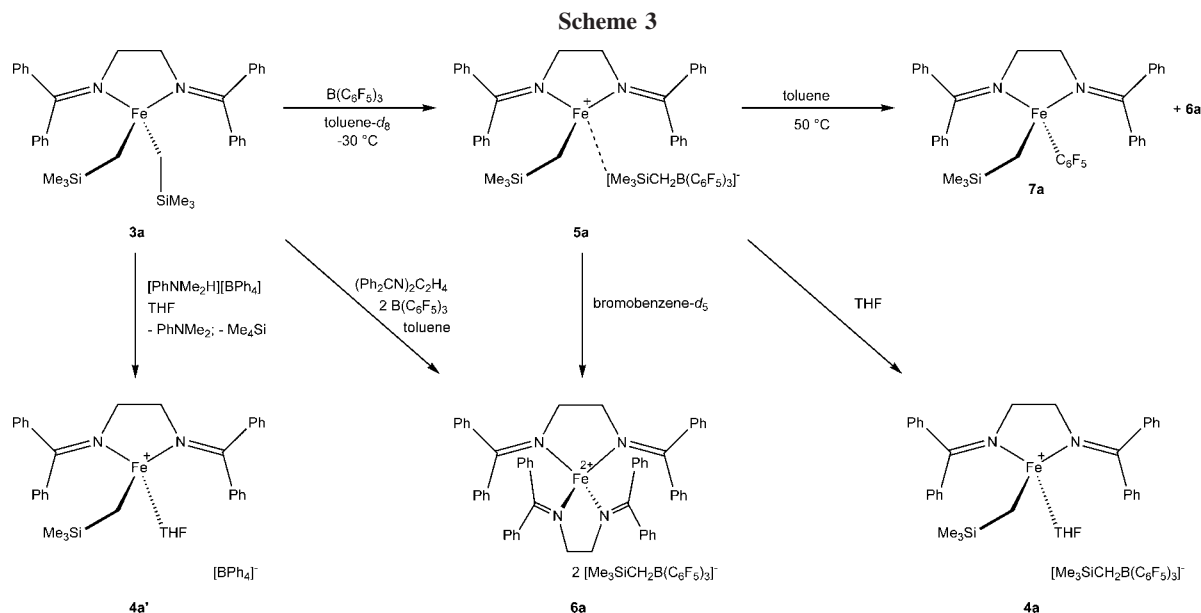


Figure 3. ORTEP representations at the 30% probability level of **4a'**, **6a**, and **7a**. Hydrogen atoms and counterions are omitted for clarity.



2 equiv of $\text{B}(\text{C}_6\text{F}_5)_3$ in the presence of an additional equivalent of the ligand in toluene solution (Scheme 3). A closer inspection of the structure of **6a** reveals that, in contrast to the other structures described in this paper, the iron center no longer adopts a distorted tetrahedral geometry. Instead its geometry is in between tetrahedral and square planar, with an angle between the $\text{N}(11)\text{--Fe}(1)\text{--N}(12)$ and $\text{N}(13)\text{--Fe}(1)\text{--N}(14)$ planes of $48.8(3)^\circ$. A similar ligand redistribution reaction was observed in the neutral ferrous amidinate complex $[\text{FeCl}_2\{\mu\text{-(2,6-}i\text{-Pr}_2\text{C}_6\text{H}_3\text{NC}\{\text{Ph}\}\text{NC}_2\text{H}_4\text{NMe}_2)\}]^{15c}$ and in the attempted synthesis of a cationic amidinate complexes of the type $[\{\text{PhC}(\text{N-2,6-}i\text{-Pr}_2\text{C}_6\text{H}_3)_2\text{Fe}(\text{CH}_2\text{SiMe}_3)\}]^+$.²⁰ The fate of the side product in the disproportionation reaction observed here is as yet unknown, though analysis of the reaction mixture by GC-MS reveals the

formation of $(\text{Me}_3\text{SiCH}_2)_2$, suggesting concomitant formation of $[\text{Fe}(\text{CH}_2\text{SiMe}_3)_2]$.

Thermolysis of **5a** in toluene (2 days, 50°C) resulted in formation of a mixture of compound **6a**, which precipitates as a yellow solid, and a new iron species, $\{\text{Ph}_2\text{CN}\}_2\text{C}_2\text{H}_4\text{Fe}(\text{CH}_2\text{SiMe}_3)\text{C}_6\text{F}_5$ (**7a**). Compound **7a** is highly soluble in aromatic and aliphatic solvents and could be isolated by

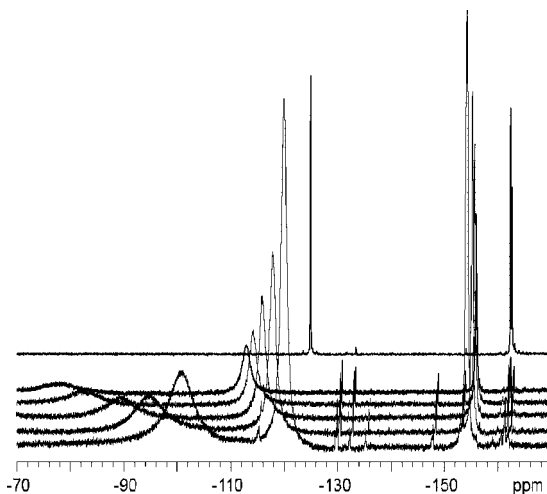


Figure 4. From bottom up: ^{19}F NMR spectra of the contact ion-pair **5a** in toluene- d_8 at 30.2, 19.4, 14.3, 11.4, and 9.19 mM, respectively, and of the THF adduct **4a** in toluene- d_8 .

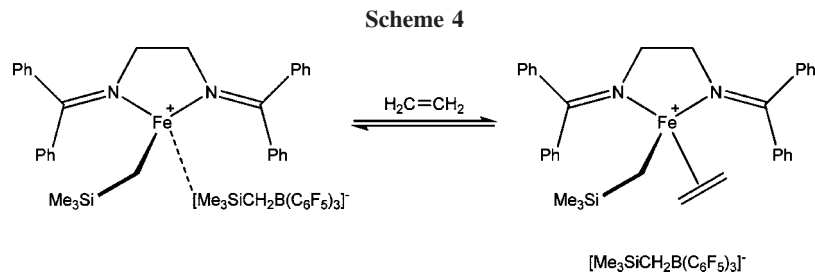
(16) Lee, H.; Hong, S.-D.; Park, Y.-W.; Jeong, B.-G.; Nam, D.-W.; Jung, H. Y.; Jung, M. W.; Song, K. H. *J. Organomet. Chem.* **2004**, *689*, 3402.

(17) (a) Beck, S.; Lieber, S.; Schaper, F.; Geyer, A.; Brintzinger, H.-H. *J. Am. Chem. Soc.* **2001**, *123*, 1483. (b) Stahl, N. G.; Zuccaccia, C.; Jensen, T. R.; Marks, T. J. *J. Am. Chem. Soc.* **2003**, *125*, 5256. (c) Zuccaccia, C.; Stahl, N. G.; Macchioni, A.; Chen, M.-C.; Roberts, J. A.; Marks, T. J. *J. Am. Chem. Soc.* **2004**, *126*, 1448.

(18) Horton, A. D.; De With, J.; Van der Linden, A. J.; Van de Weg, H. *Organometallics* **1996**, *15*, 2672.

(19) Single crystals were also obtained from a thermolysis experiment (50°C) of **5a** in toluene. This afforded a similar structure, but with cyclohexane rather than bromobenzene cocrystallized in the lattice. The cif file of the crystals structure determination can be found in the Supporting Information.

(20) Sciarone, T. J. J.; Nijhuis, C. A.; Meetsma, A.; Hessen, B. *Dalton Trans.* **2006**, 4896.



extraction with pentane. Cooling of the pentane solution to -30 °C afforded reddish-orange crystals suitable for X-ray analysis (see Figure 3 for an ORTEP representation of the molecule and Table 1 for pertinent bond distances and angles). Its structure is very similar to that of dialkyl **3a**, with shorter metal–nitrogen bond distances, a result of the increased electrophilicity of the metal center imparted by the electron-withdrawing pentafluorophenyl group. Again, a comparison of bond distances to the α -diimine analogue $\{(2,6\text{-}i\text{-Pr}_2\text{C}_6\text{H}_3\text{N})_2(\text{C}_2\text{Me}_2)\}\text{Fe}(\text{CH}_2\text{SiMe}_3)\text{-C}_6\text{F}_5$ (**7c**) shows longer iron–nitrogen bond distances in **7a**.¹¹ Performing the reaction in an NMR tube shows the expected formation of $\text{Me}_3\text{SiCH}_2\text{B}(\text{C}_6\text{F}_5)_2$, which could be identified using ^{19}F NMR spectroscopy. The ^{19}F NMR spectrum of **7a** revealed two resonances at 162 and -7.3 ppm for the pentafluorophenyl group attached to the iron center. One signal, presumably the *o*-F resonance, could not be observed.

Reactivity toward Ethylene. Well-defined iron alkyl cation **5a** was treated with ethylene, but no polymerization of the olefin was observed. Likewise, treatment of ferrous chloride **1a** with MAO (MAO = methylaluminoxane) in toluene in the presence of ethylene (5 bar, 30 min) did not result in ethylene uptake, and no formation of a substantial amount of polyethylene was observed. Following the reaction of **5a** with ethylene by NMR spectroscopy, however, revealed that compound **5a** is not unreactive toward the olefin (Scheme 4). After the addition of 1 equiv of ethylene to a 30.2 mM toluene- d_8 solution of **5a**, the ^1H NMR spectrum of the reaction mixture reveals a broad signal at 14.5 ppm ($\Delta\nu_{1/2} = 306$ Hz) for the olefin (Figure 5). This suggests formation of an ethylene adduct, in which the coordinated molecule of ethylene is in fast exchange, relative to the NMR time scale, with free ethylene in solution. As

expected, the signal shifts upfield upon increasing the ethylene concentration. The ^{19}F NMR spectrum of the reaction mixture corroborates such an equilibrium, as an increase of the ethylene pressure results in an upfield shift of the fluorine resonances toward the values expected for a ligand-separated ion-pair (Figure 5). Unfortunately, during the course of the reaction the formation of a yellowish-brown oil was observed, frustrating quantification of the equilibria involved. The yellowish oil was identified as $[\{(\text{Ph}_2\text{CN})_2(\text{C}_2\text{H}_4)_2\text{Fe}\}[\text{Me}_3\text{SiCH}_2\text{B}(\text{C}_6\text{F}_5)_3]_2$.

Conclusions

Diimines $(\text{Ph}_2\text{CN})_2\text{C}_n\text{H}_{2n}$ ($n = 2, 3$) are suitable ligands for the stabilization of electron-deficient iron complexes, and in case of the ligand with the C_2 bridge, both neutral and cationic iron alkyl complexes were prepared. Ligand binding is more labile compared to the α -diimine ligand framework, as the cationic iron alkyl complex $[\{(\text{Ph}_2\text{CN})_2\text{C}_2\text{H}_4\}\text{Fe}(\text{CH}_2\text{SiMe}_3)][\text{Me}_3\text{SiCH}_2\text{B}(\text{C}_6\text{F}_5)_3]$ rearranges to dication $[\{(\text{Ph}_2\text{CN})_2\text{C}_2\text{H}_4\}_2\text{Fe}]^{2+}$, the result of a ligand redistribution reaction. In toluene, at 50 °C a secondary thermolysis product was observed as well, which was identified as $\{(\text{Ph}_2\text{CN})_2\text{C}_2\text{H}_4\}\text{Fe}(\text{CH}_2\text{SiMe}_3)\text{C}_6\text{F}_5$. Whereas we were able, for the first time, to observe an ethylene adduct of an iron alkyl cation, the compound is not an active catalyst for the polymerization of olefins. This suggests that the barrier for ethylene insertion is the determining factor in this system. Unfortunately, a comparison with the α -diimine system is not possible, as in that case pentafluorophenyl abstraction from the borate anion is instantaneous and an iron alkyl cation cannot be observed.

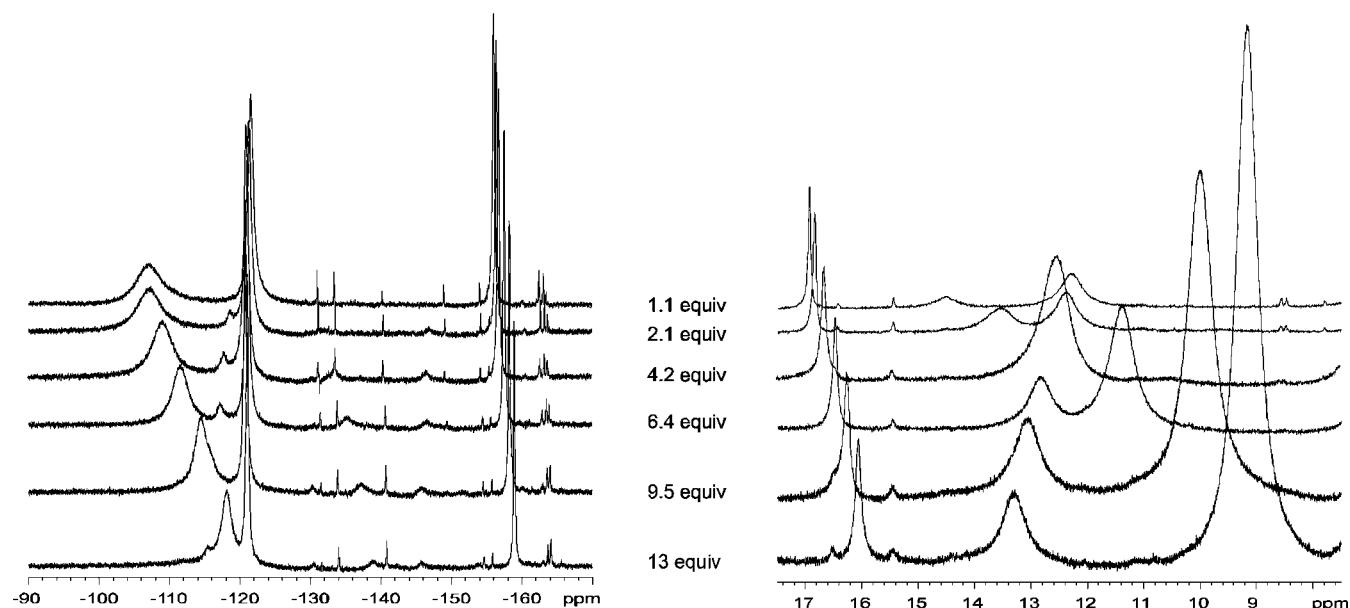


Figure 5. From top to bottom: ^{19}F NMR (left) and ^1H NMR (right) spectra of the reaction mixture containing compound **5a** and 1.1, 2.1, 4.2, 6.4, 9.5, and 13 equiv of ethylene in toluene- d_8 , respectively.

Experimental Section

General Considerations. All manipulations of air- and moisture-sensitive compounds were performed under a nitrogen atmosphere using standard Schlenk and vacuum line techniques or in an MBraun glovebox. Solvents (THF, pentane, toluene) were dried by percolation under a nitrogen atmosphere over columns of alumina, molecular sieves, and supported copper oxygen scavenger (BASF R3-11) or by distillation from Na/K alloy (cyclohexane, benzene-*d*₆, THF-*d*₈) or CaH₂ (chloroform-*d*, bromobenzene-*d*₅, dichloromethane). Reagents were purchased from commercial providers and used without purification unless stated otherwise. Anhydrous FeCl₂,²¹ (Ph₂CN)₂C₂H₄,²² (py)₂Fe(CH₂SiMe₃)₂,^{7c} LiCH₂SiMe₃,²³ [PhNMe₂H][BPh₄],²⁴ and B(C₆F₅)₃²⁵ were prepared following literature procedures. NMR spectra were recorded on Varian Inova 500, Varian Gemini VXR 400, Varian VXR 300, and Varian Gemini 200 instruments. ¹H chemical shifts are referenced to residual protons in deuterated solvents and are reported relative to tetramethylsilane; ¹⁹F chemical shifts are reported relative to α,α,α-trifluorotoluene (δ = −65 ppm), used as an external reference. For paramagnetic molecules, the chemical shifts are followed by the peak width at half-height in hertz, followed by integration value and, where possible, peak assignment. ¹H NMR spectra of paramagnetic complexes were recorded with a sweep width of 100 000 Hz, delay of 0 s, and acquisition time of 200 ms. Magnetic moments are determined by the Evans method.²⁶ Elemental analyses were performed by the Microanalytical Department at the University of Groningen. Reported values are the averages of two independent determinations. The electrospray ionization mass spectrometry (ESI-MS) experiments were conducted on an API III (PE SCIEX) triple quadrupole MS system with an IonSpray (pneumatically assisted electrospray) source equipped with a gas curtain, which is contained in a closed chamber that can be evacuated, flushed, and maintained under nitrogen. Typical sample analysis: in a glovebox, the sample was taken up into a 500 mL syringe (model 1750 RNR, Hamilton) and electrosprayed via a syringe pump operating at 10 mL/min. The capillary voltage was 3.5 kV. Mass spectra were recorded from *m/z* 50 to 900 (example) at 10 s per scan using a step size of 0.1 Da. The sampling orifice (nozzle) was at +35 V. The skimmer was located behind the sampling. Crystals suitable for a single-crystal X-ray analysis were grown as described in the text. A crystal was mounted on a glass fiber inside a drybox and transferred under an inert atmosphere to the cold nitrogen stream of a Bruker SMART APEX CCD diffractometer. Intensity data were corrected for Lorentz and polarization effects, scale variation, decay, and absorption: a multiscan absorption correction was applied, based on the intensities of symmetry-related reflections measured at different angular settings (SADABS),²⁷ and reduced to *F*_o². The structures were solved by Patterson methods, and extension of the model was accomplished by direct methods applied to difference structure factors using the program DIRDIF.²⁸ The positional and anisotropic displacement parameters for the non-hydrogen atoms were refined. Final refinement on *F*₂ was carried out by full-matrix least-squares techniques.

(21) Kovacic, P.; Brace, N. O. *Inorg. Synth.* **1960**, 6, 172.

(22) Ariza-Castolo, A.; Paz-Sandoval, M. A.; Contreras, R. *Magn. Reson. Chem.* **1992**, 30, 520.

(23) Lewis, H. L.; Brown, T. L. *J. Am. Chem. Soc.* **1970**, 92, 4664.

(24) Eshuis, J. J. W.; Tan, Y. Y.; Meetsma, A.; Teuben, J. H.; Renkema, J.; Evens, G. G. *Organometallics* **1992**, 11, 362.

(25) Pohlmann, J. L. W.; Brinckmann, F. E. *Z. Naturforsch. B* **1965**, 20, 5.

(26) Sur, S. K. *J. Magn. Reson.* **1989**, 82, 169.

(27) Sheldrick, G. M. *SADABS v2, Multi-Scan Absorption Correction Program*; University of Göttingen: Germany, 2001.

(28) Beurskens, P. T.; Beurskens, G.; De Gelder, R.; Garcí'a-Granda, S.; Gould, R. O.; Israël, R.; Smits, J. M. M. *The DIRDIF-99 Program System*; Crystallography Laboratory, University of Nijmegen: The Netherlands, 1999.

(Ph₂CN)₂C₂H₄ (**b**). A three-necked flask equipped with a reflux condenser was charged with benzophenone (4.07 g; 22.3 mmol), diaminopropane (0.92 mL; 11 mmol), a catalytic amount of *p*-toluenesulfonic acid, and xylenes (60 mL). The reaction mixture was warmed to reflux and stirred overnight, affording a yellow solution. Removal of the solvent by rotary evaporation afforded a yellow oil, which, upon addition of pentane and overnight cooling to −30 °C, turned solid. The pentane was decanted, and the off-white solid was dried *in vacuo*. Recrystallization from chloroform/pentane afforded 2.45 g (6.08 mmol; 56%) of the title compound. ¹H NMR (CDCl₃, RT): δ 7.12–7.53 (m, 20H, Ph), 3.45 (t, 4H, 6.85 Hz, CH₂), 2.04 (q, 2H, 6.89 Hz, CH₂). ¹³C NMR (CDCl₃, RT): δ 140.9, 138.0 (2 × Ph C_{ipso}), 130.7, 129.4, 129.3, 129.2, 128.9, 128.8 (6 × Ph CH), 52.8 (CH₂), 33.8 (CH₂). Anal. Calcd for C₂₉H₂₆N₂: C, 86.53; H, 6.51; N, 6.96. Found: C, 86.18; H, 6.48; N, 6.95.

{(Ph₂CN)₂C₂H₄}FeCl₂ (**1a**). THF (20 mL) was added to a mixture of **a** (1.55 g; 3.99 mmol) and FeCl₂ (0.514 g; 4.06 mmol). The resulting suspension was stirred overnight. The solvent was removed *in vacuo* and a yellow powder was obtained. The compound was extracted using dichloromethane. The extractions were filtered through a pad of Celite, affording a yellow solution. The solvent was removed *in vacuo*, affording 1.85 g (3.59 mmol, 90%) of the title compound as a yellow solid. Layering a dichloromethane solution of the solid with pentane resulted in crystals suitable for X-ray analysis. ¹H NMR (CDCl₃, RT): δ 69.6 (4H, 579 Hz), 13.1 (4H, 24 Hz), 5.3 (4H, 73 Hz), 2.9 (2H, 23 Hz), 1.8 (4H, 66 Hz), −0.5 (2H, 34 Hz), −26.9 (4H, 601 Hz). Anal. Calcd for C₂₈H₂₄Cl₂FeN₂: C, 65.27; H, 4.70; N, 5.44. Found: C, 64.64; H, 4.67; N, 5.25. μ_{eff} = 5.3 μ_B.

{(Ph₂CN)₂C₃H₆}FeCl₂ (**1b**). Compound **1b** was prepared analogous to **1a**, by treating **b** (1.47 g; 3.79 mmol) with FeCl₂ (0.480 g; 3.78 mmol) in THF (20 mL). This afforded 1.51 g (2.85 mmol; 75%) of **1b**. ¹H NMR (CDCl₃, RT): δ 126.0 (4H, 916 Hz), 35.6 (4H, 1009 Hz), 10.4 (4H, 35 Hz), 9.5 (2H, 51 Hz), 7.2 (4H, 44 Hz), 4.8 (2H, 32 Hz), 3.9 (2H, 411 Hz), −0.1 (4H, 98 Hz). A sample for analysis was recrystallized from CH₂Cl₂/cyclohexane. Anal. Calcd for C₂₉H₂₆Cl₂FeN₂·CH₂Cl₂: C, 58.66; H, 4.60; N, 4.56. Found: C, 58.42; H, 4.59; N, 4.42.

{(Ph₂CN)₂C₂H₄}FeBr₂ (**2a**). Compound **2a** was prepared analogous to **1a**, by treating FeBr₂ (0.179 g; 0.830 mmol) with **a** (0.324 g; 0.833 mmol) in THF (10 mL). This afforded 0.36 g (0.60 mmol; 72%) of **2a**. ¹H NMR (bromobenzene-*d*₅, RT): δ 70.1 (4H, 663 Hz), 14.1 (4H, 28 Hz), 5.8 (4H, 85 Hz), 2.6 (2H, 29 Hz), 1.7 (4H, 75 Hz), −2.4 (2H, 40 Hz), −36.1 (4H, 413 Hz). Anal. Calcd for C₂₈H₂₄Br₂FeN₂: C, 55.66; H, 4.00; N, 4.64. Found: C, 55.43; H, 3.96; N, 4.52.

Generation of {(Ph₂CN)₂C₂H₄}Fe(CH₂SiMe₃)₂ from 1a. Addition of a solution of LiCH₂SiMe₃ (9.5 mg; 0.10 mmol) in THF (0.5 mL) to **1a** (26.7 mg; 0.0518 mmol) resulted in a color change to purple. After 1 h the volatiles were pumped off. Pentane was added and removed *in vacuo* to remove residual THF. Analysis of the reaction mixture by ¹H NMR spectroscopy in benzene-*d*₆ revealed the formation of a mixture of products, one of which was identified as **3a** (see below).

Generation of {(Ph₂CN)₂C₂H₄}Fe(CH₂SiMe₃)₂ from 2a. LiCH₂SiMe₃ (6.6 mg; 0.070 mmol) in benzene-*d*₆ (0.4 mL) was added to an NMR tube with **2a** (21.4 mg; 0.0354 mmol). The resulting purple reaction mixture was analyzed by ¹H NMR spectroscopy and revealed the formation of **3a** (see below).

{(Ph₂CN)₂C₂H₄}Fe(CH₂SiMe₃)₂(py) (**3a**·py). In an NMR tube (py)₂Fe(CH₂SiMe₃)₂ (10.7 mg; 0.0275 mmol) and **a** (10.7 mg; 0.0275 mmol) were dissolved in benzene-*d*₆ (0.4 mL), resulting in a purple solution. ¹H NMR spectroscopy indicated the formation of **3a**·py. The volatiles were transferred to a second NMR tube charged with 4.9 mg (0.026 mmol) of ferrocene internal standard. ¹H NMR analysis thus revealed that during the reaction 1 equiv of free pyridine was generated. ¹H NMR of **3a**·py (C₆D₆, RT): δ 57.8

(4H, 13.6 Hz), 27.6 (2H, 804 Hz), 16.6 (1H, 242 Hz), 15.1 (2H, 217 Hz), 12.7 (22H, overlapping signals), 3.7–1.3 (6H, overlapping signals), –3.2 (2H, 51 Hz), –53.3 (4H, 1403 Hz). Two signals of 4H were not observed.

{(Ph₂CN)₂C₂H₄}Fe(CH₂SiMe₃)₂ (3a). Toluene (5 mL) was added to a mixture of (py)₂Fe(CH₂SiMe₃)₂ (75.5 mg; 0.193 mmol) and **a** (64.0 mg; 0.164 mmol), resulting in a purple solution. The reaction mixture was stirred for 2 h, after which the solvent was removed *in vacuo*. To the resulting purple oil was added toluene (5 mL), which was pumped off to remove residual pyridine. The solid was dissolved in pentane and filtered through a pad of Celite. Concentration of the solution and cooling at –30 °C resulted in 71.5 mg (0.116 mmol, 70%) of purple crystals of the title compound. ¹H NMR (C₆D₆, RT): δ 57.5 (4H, 601 Hz), 13 (22H, two overlapping signals), 2.9 (4H, 97 Hz), 2.0 (4H, 110 Hz), 0.9 (2H, 30 Hz), –3.2 (2H, 50 Hz), –53.3 (4H, 901 Hz). One signal of 4H was not observed. Anal. Calcd for C₃₆H₄₆FeN₂Si₂: C, 69.88; H, 7.49; N, 4.53. Found: C, 68.35; H, 7.44; N, 4.39. μ_{eff} = 4.9 μ_B.

[(Ph₂CN)₂C₂H₄}Fe(CH₂SiMe₃)THF][B(C₆H₅)₄] (4a′). THF (1 mL) was added to a mixture of **3a** (32.9 mg; 0.0532 mmol) and [PhNMe₂H][BPh₄] (23.6 mg; 0.0573 mmol). The resulting yellow-orange solution was cooled to –30 °C for 30 min and subsequently layered with pentane. After storing overnight at –30 °C orange crystals had formed. The supernatant was decanted, affording 26.1 mg (0.028 mmol; 53% yield) of orange crystals of **4a′**. ¹H NMR (THF-*d*₈; RT): δ 72.3 (4H, 833 Hz), 21.3 (9H, 170 Hz, SiMe₃), 13.2 (4H, 24 Hz), 10.0 (8H, 26 Hz, BPh₄), 8.2 (8H, 27 Hz, BPh₄), 7.6 (4H, 25 Hz, *p*-BPh₄), 3.8 (2H, 67 Hz), 1.68 (4H, overlaps with THF) –1.9 (2H, 33 Hz), –8.8 (4H, 61 Hz), –36.4 (4H, 726 Hz). One signal of 2H was not observed. Anal. Calcd for C₃₆H₄₆FeN₂Si₂: C, 78.08; H, 6.88; N, 3.04. Found: C, 77.40; H, 7.08; N, 2.69. μ_{eff} = 5.2 μ_B.

Generation of [(Ph₂CN)₂C₂H₄}Fe(CH₂SiMe₃)] [Me₃SiCH₂B(C₆H₅)₃] (5a). A solution of **3a** (5.9 mg; 0.0095 mmol) in toluene-*d*₈ and a solution of B(C₆F₅)₃ (4.9 mg; 0.0096 mmol) in toluene-*d*₈ were cooled to –30 °C. The B(C₆F₅)₃ solution was slowly added to the solution containing **3a**, affording an orange solution of **5a**. ¹H NMR (toluene-*d*₈, RT): δ 177.3 (4H, 857 Hz), 17.0 (4H, 56 Hz), 11.8 (9H, 228 Hz, SiMe₃), 4.6 (2H, 25 Hz), 2.3 (2H, 53 Hz), 1.1 (2H, 43 Hz), –1.68 (9H, 40 Hz), –26.3 (4H, 101 Hz), –45.2 (4H, 977 Hz). One signal of 2H was not observed. ¹⁹F NMR (30.2 mM in toluene-*d*₈, RT): –99.1 (6F, 2202 Hz, *m*-F), –118.7 (6F, 969 Hz, *o*-F), –152.0 (3F, 318 Hz, *p*-F).

Generation of [(Ph₂CN)₂C₂H₄}Fe(CH₂SiMe₃)(THF)] [Me₃SiCH₂B(C₆H₅)₃] (4a). A solution of **5a** was prepared as described above. The solvent was removed *in vacuo*, and the residue was dissolved in THF-*d*₈. The product was identified by ¹H NMR spectroscopy as the title compound. ¹H NMR (THF-*d*₈, RT): δ 72.9 (4H, 701 Hz), 21.8 (9H, 177 Hz, FeCH₂SiMe₃), 13.6 (4H, 46 Hz), 4.1 (2H, 90 Hz), 0.72 (2H, 16 Hz, B(CH₂SiMe₃)), –0.3 (9H, 9 Hz, B(CH₂SiMe₃)), –2.5 (2H, 54 Hz), –9.1 (4H, 76 Hz), –38.1 (4H, 593 Hz). Two signals could not be observed. ¹⁹F NMR (THF-*d*₆, RT): δ –129.7 (d, 22 Hz, 6F, *o*-F), –164.7 (ps.t., 20 Hz, 3F, *p*-F), –166.8 (ps.t., 21 Hz, 6F, *m*-F). ESI-MS (35 eV, THF): neg-ion mode, *m/z* 599.1 [Me₃SiCH₂B(C₆F₅)₃][–]; pos-ion mode, *m/z* 603.3 [(Ph₂CN)₂C₂H₄}Fe(CH₂SiMe₃)(THF)]⁺, 531.1 [(Ph₂CN)₂C₂H₄}Fe(CH₂SiMe₃)]⁺.

Decomposition of 5a in Toluene. A flask containing **3a** (0.106 g; 0.171 mmol), B(C₆F₅)₃ (0.087 g; 0.17 mmol), and toluene (5 mL) was stirred for 2 days at 50 °C, resulting in a brown solution and a yellow precipitate. The solution was filtered off and the solid was washed with toluene. The yellow solid was recrystallized from CH₂Cl₂/cyclohexane, affording 72.4 mg (0.0356 mmol; 21%) of yellow crystals of dication **6a**. ¹H NMR (CDCl₃; RT): δ 136.5 (4H, 587 Hz), 16.7 (4H, 20 Hz), 11.3 (4H, 60 Hz), 4.3 (2H, 20 Hz), 2.0 (2H, 19 Hz), 1.1 (2H, 25 Hz), 0.3 (9H, SiMe₃, 12 Hz), –1.6 (4H, 46 Hz), –31.6 (4H, 467 Hz). ¹⁹F NMR (CDCl₃; RT): δ –128.0 (2F, 47 Hz), –163.7 (1F,

44 Hz), 165.1 (2F, 55 Hz). Anal. Calcd for C₁₀₆H₈₂BF₁₅FeN₄Si₂: C, 60.18; H, 3.91; N, 2.65. Found: C, 59.57; H, 3.70; N, 2.52. μ_{eff} = 5.8 μ_B. The brown solution that was obtained from the reaction above was combined with the portions of toluene that were used to wash compound **6a**. The solvent was removed *in vacuo*, and the resulting black oil was extracted with pentane to yield a yellow solution. Cooling to –30 °C resulted in a small amount of orange crystals of **7a**. ¹H NMR (C₆D₆, RT): δ 111.2 (4H, 442 Hz), 15.3 (4H, 23 Hz), 7.1 (overlapping with solvent peak, 9H, SiMe₃), 6.7 (4H, 56 Hz), 3.2 (2H, 23 Hz), 1.6 (2H, 26 Hz), –3.3 (4H, 43 Hz), –32.0 (4H, 372 Hz). ¹⁹F NMR (C₆D₆, RT): δ 162.6 (1F, *p*-F, 144.7 Hz), –7.3 (2F, *m*-F, 59.1 Hz), one peak not found. When performing the thermolysis in toluene-*d*₈ and monitoring the reaction mixture by ¹⁹F NMR spectroscopy, the formation of Me₃SiCH₂B(C₆F₅)₂ was observed.

Decomposition of 5a in Bromobenzene-*d*₅. Compound **5a** was generated in an NMR tube as described above. After checking that compound **5a** had been generated cleanly, the toluene was pumped off and bromobenzene-*d*₅ was added to the reaction mixture. Within 10 min after the addition of bromobenzene-*d*₅ the formation of compound **6a** was observed. The reaction was found to be complete when the reaction mixture was left overnight at room temperature.

[(Ph₂CN)₂C₂H₄]Fe][Me₃SiCH₂B(C₆F₅)₃] (6a). Toluene (20 mL) was added to a mixture of **3a** (84.3 mg; 0.136 mol), **a** (53.0 mg; 0.136 mmol), and B(C₆F₅)₃ (140 mg; 0.273 mmol). The color changed to orange and a precipitate formed. The solid was washed with toluene and recrystallized from CH₂Cl₂/cyclohexane, affording 103 mg (0.0497 mmol; 37%) of **6a**.

Reaction of 5a with C₂H₄. Two toluene-*d*₈ solutions (total amount of solvent: 0.45 g), one with B(C₆F₅)₃ (5.3 mg; 0.010 mmol) and the other with **3a** (6.4 mg; 0.010 mmol), were cooled to –30 °C. The borane solution was added slowly to the solution of **3a** in toluene-*d*₈, resulting in a color change to yellowish-orange. The solution was degassed using three freeze–pump–thaw cycles, and ethylene was added using a calibrated gas bulb (9.4 mL, 98 mmHg; 0.049 mmol). ¹H and ¹⁹F NMR spectroscopy revealed spectra similar to that of **5a**, with the exception that a peak was observed at 12.5 (Δν_{1/2} = 178 Hz) in the ¹H NMR spectrum for a time-average signal for bound and free ethylene and an upfield shift of the resonances in the ¹⁹F NMR spectrum. In the course of the experiment a yellow precipitate starts forming, which was identified as dication **6a** by evaporating the volatiles and dissolution of the residue in THF-*d*₈.

Attempted Polymerization of Ethylene Using 1a/MAO. The polymerization experiment was performed in a temperature- and pressure-controlled stainless steel 1 L autoclave (Medimex). The autoclave was evacuated for 1 h at 125 °C prior to use. The reactor was cooled to 30 °C, filled with toluene (250 mL), and pressurized to 5 bar of ethylene. While stirring at 600 rpm, 1.33 mg of a 5 wt % solution of PMAO in toluene (5 mmol) and 2.6 mg (0.0050 mmol) of **1a** were injected. During the run the ethylene pressure was kept constant to within 0.2 bar of the initial pressure by replenishing flow. After 30 min reaction time the reactor was vented and the residual aluminum alkyls were destroyed by addition of 100 mL of ethanol. No substantial amount of polymer was observed.

Acknowledgment. This investigation was supported by The Netherlands Organization for Scientific Research (NWO). Prof. Dr. B. Hessen (University of Groningen) is gratefully acknowledged for the use of facilities and Dr. S. Bambirra (University of Groningen) for conducting the ESI-MS measurement.

Supporting Information Available: Crystallographic data for compounds **1a**, **2a**, **3a**, **4a′**, **6a**, and **7a**. This material is available free of charge via the Internet at <http://pubs.acs.org>.

Phosphine Addition to Pyruvoyl Ligands of Iron Complexes: Formation of Zwitterionic Metallalactones

J. Y. Salaün,^{*,†} R. Rumin,[†] F. Setifi,^{†,‡} S. Triki,[†] and P. A. Jaffrès[†]

Laboratoire de Chimie, Electrochimie Moléculaires et Chimie Analytique, UMR CNRS 6521, Université de Bretagne Occidentale, UFR Sciences et Techniques, 6 Avenue le Gorgeu, CS 93837, 29238 Brest Cédex, France, and Département de Chimie, Faculté des Sciences, Université Ferhat Abbas, de Sétif Algérie

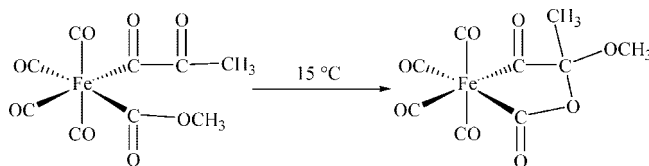
Received August 19, 2008

Tertiary phosphines react, at $-80\text{ }^{\circ}\text{C}$, with the pyruvoyl-substituted iron complex $(\text{CO})_4\text{Fe}[\text{C}(\text{O})\text{C}(\text{O})\text{CH}_3](\text{CO}_2\text{CH}_3)$ (**1**) to give rise to phosphonium-substituted metallalactones $(\text{CO})_3\text{Fe}[\text{C}(\text{O})\text{C}(\text{CH}_3)(\text{PR}_3)\text{OC}(\text{O})](\text{CO}_2\text{CH}_3)$ (**2**). These zwitterionic compounds are formed by an initial addition of the phosphine to the noncoordinated carbonyl of the pyruvoyl unit followed by the addition of the oxygen of this $\text{C}=\text{O}$ on a terminal carbonyl. They display an anionic metal center substituted by three organic ligands and a positive charge located on a phosphonium group. Attempts to extend the reaction to the related cationic pentacarbonyl pyruvoyl-substituted iron complex failed, as no reaction was observed with the same reagents. However, the expected products of these reactions, cationic phosphonium metallalactones $\{(\text{CO})_4\text{Fe}[\text{C}(\text{O})\text{C}(\text{CH}_3)(\text{PR}_3)\text{OC}(\text{O})]\}^+$, were obtained by acidic dissociation of the alkoxy carbonyl ligand of the relevant zwitterionic metallalactones.

Introduction

Catalytic carbonylation reactions are thought to take place from organometallic intermediates displaying carbonylated organic ligands. To appraise the involvement of such entities in the course of these reactions, the synthesis and the study of stable complexes of Pt, Mn, Co, or Fe bearing one or two carbonylated ligands have been performed.¹ Although sequential double migratory insertion of carbon monoxide into a $[\text{M}]-\text{R}$ bond affording a $[\text{M}]\text{C}(\text{O})\text{C}(\text{O})\text{R}$ linkage is only found to occur under very specific conditions,^{2–4} the possible intervention of α,β -dicarbonylated groups in multiple carbonylation processes has however been considered. It has been found that complexes containing a single $[\text{M}]\text{C}(\text{O})\text{C}(\text{O})\text{R}$ chain can be thermally decarbonylated, giving rise to the corresponding $[\text{M}]\text{C}(\text{O})\text{R}$ compound ($[\text{M}] = \text{Mn}(\text{CO})_5$ and $\text{R} = \text{CH}_3$, Ph ;⁵ $[\text{M}] = \text{trans-Pd}$ or $\text{Pt}(\text{PPh}_3)_2\text{Cl}$ and $\text{R} = \text{Ph}$;⁶ $[\text{M}] = \text{trans-Pt}(\text{PPh}_3)_2(\text{CO})^+$ and $\text{R} = \text{Ph}$ ⁷). Model compounds for dicarbonylation (those displaying an α,β -dicarbonylated ligand and an alkyl ligand) are also found to undergo thermal decarbonylation. Thus $\text{trans-}[\text{PhC}(\text{O})\text{C}(\text{O})]\text{Pt}(\text{PPh}_3)_2(\text{C}_2\text{H}_5)$ ⁸ and $\text{cis-}(\text{CO})_4\text{Fe}[\text{C}(\text{O})\text{CO}_2\text{C}_2\text{H}_5](\text{CH}_3)$ ⁹ give rise to $\text{trans-}[\text{PhC}(\text{O})]\text{Pt}(\text{PPh}_3)_2[\text{C}(\text{O})\text{C}_2\text{H}_5]$ and $\text{cis-}(\text{CO})_4\text{Fe}(\text{CO}_2\text{C}_2\text{H}_5)[\text{C}(\text{O})\text{CH}_3]$, respectively, which are formed by insertion of the carbon monoxide molecule, released by decarbonylation of the $\text{RC}(\text{O})\text{C}(\text{O})$ group, into the metal alkyl bond. A second reaction is also observed during decarbonylation of the iron complex at $6\text{ }^{\circ}\text{C}$: $\text{CH}_3\text{C}(\text{O})\text{CO}_2\text{C}_2\text{H}_5$ is formed by a $\text{Csp}_2-\text{Csp}_3$ carbon-carbon coupling between the two organic ligands. Complexes displaying the $\text{cis-}[\text{M}][\text{C}(\text{O})\text{C}(\text{O})\text{R}][\text{C}(\text{O})\text{R}']$ geometry, which might be expected to produce tricarbonylated organic compounds under thermal treatment, also display a decarbonylation reaction affording $\text{cis-}[\text{M}][\text{C}(\text{O})\text{R}][\text{C}(\text{O})\text{R}']$ complexes ($[\text{M}] = \text{Pt}(\text{PPh}_3)_2$, $\text{R} = \text{CH}_3$, C_2H_5 , Ph , OCH_3 , $\text{R}' = \text{C}_2\text{H}_5$, Ph ;¹⁰ $[\text{M}] = \text{Fe}(\text{CO})_4$, $\text{R} = \text{R}' = \text{OCH}_3$ or $\text{R} = \text{CH}_3$ and $\text{R}' = \text{OCH}_3$ ¹¹). However, the iron complexes again display a carbon-carbon coupling process upon decarbonylation, giving rise to dimethylxalate or methylpyruvate (dicarbonylation). The complex $\text{cis-}(\text{CO})_4\text{Fe}[\text{C}(\text{O})\text{C}(\text{O})\text{CH}_3](\text{CO}_2\text{CH}_3)$ (**1**), which is also a model compound for the study of the tricarbonylation process, has been unexpectedly found to generate upon heating at $15\text{ }^{\circ}\text{C}$ the metallalactonic complex $(\text{CO})_4\text{-Fe}[\text{C}(\text{O})\text{C}(\text{CH}_3)(\text{OCH}_3\text{OC}(\text{O}))]$ (Scheme 1), which is formally

Scheme 1



$(\text{CO})_4\text{Fe}[\text{C}(\text{O})\text{C}(\text{O})\text{CH}_3](\text{CO}_2\text{CH}_3)$ (**1**), which is also a model compound for the study of the tricarbonylation process, has been unexpectedly found to generate upon heating at $15\text{ }^{\circ}\text{C}$ the metallalactonic complex $(\text{CO})_4\text{-Fe}[\text{C}(\text{O})\text{C}(\text{CH}_3)(\text{OCH}_3\text{OC}(\text{O}))]$ (Scheme 1), which is formally

(9) Sabo-Etienne, S.; Larssonneur, A. M.; des Abbayes, H. *J. Chem. Soc., Chem. Commun.* **1989**, 1671.

(10) Chen, J. T.; Yeh, Y. S.; Yang, C. S.; Tsai, F. Y.; Huang, G. L.; Shu, B. C.; Huang, T. M.; Chen, Y. S.; Lee, G. H.; Cheng, M. C.; Wang, C. C.; Wang, Y. *Organometallics* **1994**, *13*, 4804.

(11) Laurent, P.; Salaün, J. Y.; Le Gall, G.; Sellin, M.; des Abbayes, H. *J. Organomet. Chem.* **1994**, *466*, 175.

* To whom correspondence should be addressed. E-mail Jean-Yves.Salaun@univ-brest.fr.

[†] Université de Bretagne Occidentale.

[‡] Université Ferhat Abbas.

(1) des Abbayes, H.; Salaün, J. Y. *Dalton Trans.* **2003**, 1041, and references therein.

(2) Geoffroy, G. L.; Sheridan, J. B.; Bassner, S. L.; Kelley, C. *Pure Appl. Chem.* **1989**, *61*, 1723.

(3) Cassar, L. *Ann. N.Y. Acad. Sci.* **1980**, *333*, 208.

(4) Gregg, B. T.; Cutler, A. R. *Organometallics* **1998**, *17*, 4169.

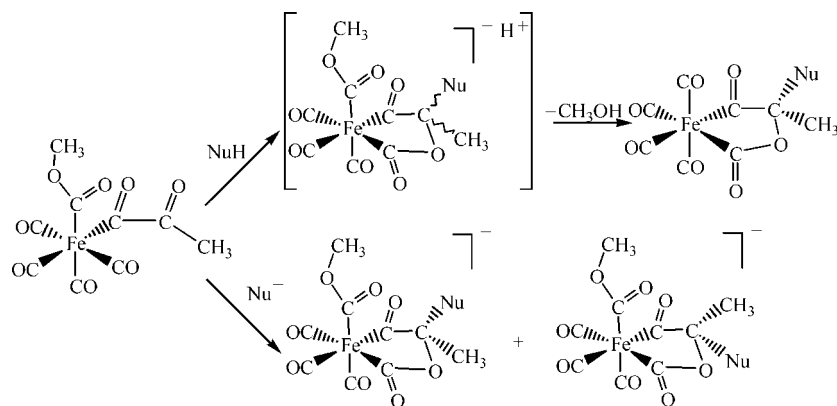
(5) Casey, C. P.; Bunnell, C. A.; Calabrese, J. C. *J. Am. Chem. Soc.* **1976**, *98*, 1166.

(6) Sen, A.; Chen, J. T.; Veller, W. M.; Whittle, J. *Am. Chem. Soc.* **1987**, *109*, 148.

(7) Huang, T. M.; You, Y. J.; Yang, C. S.; Tzeng, W. H.; Chen, J. T.; Cheng, M. C.; Wang, Y. *Organometallics* **1991**, *10*, 1020.

(8) Chen, J. T.; Huang, T. M.; Cheng, M. C.; Wang, Y. *Organometallics* **1991**, *10*, 2838.

Scheme 2



obtained by an addition of the oxygen of the β -carbonyl of the pyruvoyl ligand on the alkoxy carbonyl and by a migration of the OR group of this last ligand toward the carbon of the β -carbonyl.¹²

This reaction appears to be very similar to the ring-chain tautomerism observed in organic chemistry for γ -keto-esters,¹³ the organometallic complex being considered as a γ -keto-ester with a metal inserted into the link bridging the two organic functions. However, unlike the organic process, metallalactone formation is not reversible and does not require acid or base catalysis. Carrying out this reaction in the presence of different nucleophiles (NuH = ROH, RSH¹⁴ or Nu⁻ = RO⁻, RS⁻, and carbanions^{15,16}) has been found to induce the formation of Nu-substituted metallalactones $(\text{CO})_4\text{Fe}[\text{C}(\text{O})\text{C}(\text{CH}_3)(\text{Nu})\text{OC}(\text{O})]$ and *fac* $\{(\text{CO})_3\text{Fe}[\text{C}(\text{O})\text{C}(\text{CH}_3)(\text{Nu})\text{OC}(\text{O})](\text{CO}_2\text{CH}_3)\}$,²³ respectively (Scheme 2).

Mechanistically, the reaction proceeds (1) by specific addition of the nucleophiles on the β -carbonyl of the pyruvoyl ligand, which then appears as the most electrophilic site of the molecule (even more than the terminal carbonyls) and (2) by a ring formation resulting from an attack of the oxygen of this β -carbonyl on a terminal carbonyl and not, as previously supposed, on the alkoxy carbonyl ligand. An analogous observation has been made for a reaction between a hydride and a phenylglyoxyl manganese complex.¹⁷ Successful use of the same process in the reaction of the related acetyl complex *cis*- $(\text{CO})_4\text{Fe}[\text{C}(\text{O})\text{C}(\text{O})\text{CH}_3][\text{C}(\text{O})\text{CH}_3]$ with the same nucleophiles confirms that the presence of an alkoxy carbonyl ligand is not required for the formation of metallalactones.¹⁸ As mentioned above, nucleophiles displaying mobile protons, NuH, afford neutral bisubstituted metallalactones $(\text{CO})_4\text{Fe}[\text{C}(\text{O})\text{C}(\text{CH}_3)(\text{Nu})\text{OC}(\text{O})]$, while anionic nucleophiles, Nu⁻, give rise to trifunctionalized anionic metallalactones *fac*- $\{(\text{CO})_3\text{Fe}[\text{C}(\text{O})\text{C}(\text{CH}_3)(\text{Nu})\text{OC}(\text{O})](\text{CO}_2\text{CH}_3)\}^-$. The present article describes the results obtained when the reaction is

performed with tertiary phosphines (neutral nucleophiles with no mobile group). These nucleophiles may be expected either to attack the electrophilic β -carbonyl of the pyruvoyl ligand, thereby inducing formation of a phosphonium-substituted metallalactone, or, as usually observed, to substitute a terminal carbonyl of the metal center.

Results and Discussion

In organic chemistry, addition of primary or secondary phosphines to the carbonyl group of ketones or aldehydes affording α -hydroxyphosphines has been known for a long time.¹⁹ On the other hand, reactions performed with tertiary phosphines are more scarce and α -hydroxyphosphonium cations are obtained only in the presence of a strong acid.²⁰ In organometallic chemistry however, additions of nucleophiles including phosphines on unsaturated ligands (alkenes, alkynes, etc.) are numerous, while examples describing the counterpart of the organic reaction of addition of tertiary phosphines on carbonyls are scarce. They have always been performed on η^2 -acyl ligands and they give rise to η^2 -phosphonium C—O groups.²¹ The complexes formed are found to be stable for phosphines already linked to the metal via another coordinating group,^{21a-e} while adducts obtained by intermolecular attack of monophosphines (PR₃; R = CH₃; C₂H₅; etc.) seem more difficult to obtain.^{21f,g} An addition of a phosphine to a terminal carbonyl has also been reported; it is claimed that an intermediate displaying a [M]C(O)-phosphonium group is formed.²² The facile addition of nucleophiles to the β -carbon of the pyruvoyl ligand of **1** observed in our laboratory and giving rise to metallalactones prompted us to try to achieve similar reactions with tertiary phosphines with the aim of performing for the first

(19) (a) See for example: *Houben-Weil Methoden der Organischen Chemie*; Georg Thieme Verlag: Stuttgart, Germany, 1963; pp29 and 98. (b) Epstein, M.; Buckler, S. A. *Tetrahedron* **1962**, *18*, 1231. (c) Buckler, S. A.; Epstein, M. *Tetrahedron* **1962**, *18*, 1211.

(20) (a) Evangelidou-Tsolis, E.; Ramirez, F.; Pilot, J. F.; Smith, C. P. *Phosphorus Relat. Group V Elem.* **1974**, *4*, 109. (b) Lee, S. W.; Troglor, W. C. *J. Org. Chem.* **1990**, *55*, 2644.

(21) (a) Skagestad, V.; Tilst, M. *Organometallics* **1994**, *13*, 3134. (b) Tikkanen, W.; Ziller, J. W. *Organometallics* **1991**, *10*, 2266. (c) Grimmet, D. L.; Labinger, J. A.; Bonfiglio, J. N.; Masuo, S. T.; Shearin, E.; Miller, J. S. *Organometallics* **1983**, *2*, 1325. (d) Labinger, J. A.; Bonfiglio, J. N.; Grimmet, D. L.; Masuo, S. T.; Shearin, E.; Miller, J. S. *Organometallics* **1983**, *2*, 733. (e) Karsch, H. H.; Müller, G.; Krüger, C. *J. Organomet. Chem.* **1984**, *273*, 195. (f) Arnold, J.; Tilley, T. D.; Rheingold, A. L.; Geib, S. J.; Arif, A. M. *J. Am. Chem. Soc.* **1989**, *111*, 149. (g) Bonnesen, P. V.; Yau, P. K. L.; Hersh, W. H. *Organometallics* **1987**, *6*, 1587.

(22) Doherty, S.; Waugh, M.; Scanlan, T. H.; Elsegood, M. R. J.; Clegg, W. *Organometallics* **1999**, *18*, 679.

(23) Sellin, M.; Luart, D.; Salaün, J. Y.; Laurent, P.; Toupet, L.; des Abbayes, H. *Organometallics* **1996**, *15*, 521.

(12) Sellin, M.; Luart, D.; Salaün, J. Y.; Laurent, P.; Toupet, L.; des Abbayes, H. *J. Chem. Soc., Chem. Commun.* **1996**, 857.

(13) Valter, R. E.; Flitsh, R. E. *Ring-Chain Tautomerism*; Plenum: New York, 1985.

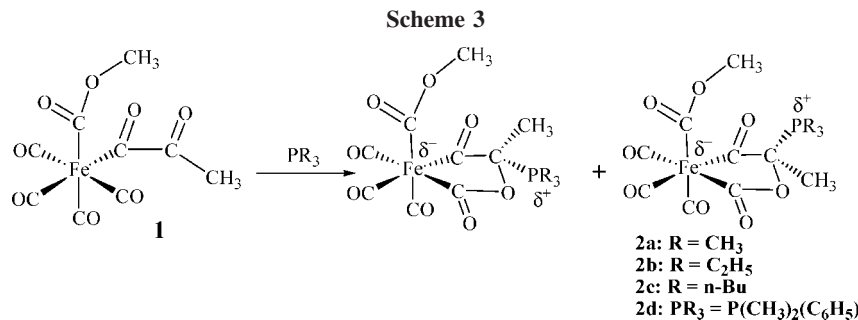
(14) Cabon, P.; Sellin, M.; Salaün, J. Y.; Patinec, V.; des Abbayes, H.; Kubicki, M. *Organometallics* **2002**, *21*, 2196.

(15) Cabon, P.; Rumin, R.; Salaün, J. Y.; Triki, S.; des Abbayes, H. *Organometallics* **2005**, *24*, 1709.

(16) Cabon, P.; Rumin, R.; Salaün, J. Y.; des Abbayes, H.; Triki, S. *Eur. J. Inorg. Chem.* **2006**, 1515.

(17) Selover, J. C.; Vaughn, G. D.; Strouse, C. E.; Gladysz, J. A. *J. Am. Chem. Soc.* **1986**, *108*, 1455.

(18) Salaün, J. Y.; Rumin, R.; des Abbayes, H.; Triki, S. *J. Organomet. Chem.* **2006**, *691*, 3667.



time an addition of these reagents on a non- η^2 -carbonyl and to obtain stable metallalactones substituted by phosphonium groups.

Reaction of $(\text{CO})_4\text{Fe}[\text{C}(\text{O})\text{C}(\text{O})\text{CH}_3](\text{CO}_2\text{CH}_3)$ (1**) with $\text{P}(\text{CH}_3)_3$, $\text{P}(\text{C}_2\text{H}_5)_3$, $\text{P}(n\text{-Bu})_3$, and $\text{P}(\text{CH}_3)_2(\text{C}_6\text{H}_5)$.** As shown by an IR monitoring of the reactions, **1** in solution in CH_2Cl_2 at -80°C reacts instantaneously with 1 equiv of these slightly hindered phosphines to afford a series of new complexes (**2**). The IR spectra of these compounds exhibit three strong $\nu_{\text{C}=\text{O}}$ bands between 2080 and 1990 cm^{-1} , very similar to those observed for the related anionic trifunctionalized metallalactones $\text{fac}-\{(\text{CO})_3\text{Fe}[\text{C}(\text{O})\text{C}(\text{CH}_3)(\text{Nu})\text{OC}(\text{O})](\text{CO}_2\text{CH}_3)]^-\}$ (Scheme 2), which are obtained by reaction of **1** with anionic nucleophiles (Nu^-) (three bands between 2084 and 1970 cm^{-1}).^{15,16} Since the noncyclic compound $\text{fac}-[(\text{CO})_3\text{Fe}(\text{CO}_2\text{CH}_3)_3]^-$ displays only two bands in this area, as required by C_{3v} symmetry (at 2080 and 2015 cm^{-1}),²³ the observation of the third IR-active $\nu_{\text{C}=\text{O}}$ is presumed to result from the presence of a metallacycle, the *fac*-trisubstitution, and the anionic character of the metal center of complexes **2** are confirmed by their ^{13}C NMR data (see Experimental Section). The fact that most of the resonances of these complexes are split into doublets suggests the formation of two isomers (Scheme 3) made possible by the presence of two different substituents on the quaternary carbon of the cycle in addition to the presence of three different organic substituents in *fac* positions on the metal center.

The signals of the three terminal carbonyls (six signals observed for the two isomers) are found between 205 and 207 ppm and fall within the range of the resonances observed for anionic homologues $\text{fac}-[(\text{CO})_3\text{Fe}(\text{CO}_2\text{CH}_3)_3]^-$ ²³ or $\text{fac}-\{(\text{CO})_3\text{Fe}[\text{C}(\text{O})\text{C}(\text{CH}_3)(\text{Nu})\text{OC}(\text{O})](\text{CO}_2\text{CH}_3)]^-\}$ (from 209 to 206 ppm)^{15,16} but differ from those of neutral metallalactones $(\text{CO})_4\text{Fe}[\text{C}(\text{O})\text{C}(\text{CH}_3)(\text{Nu})\text{OC}(\text{O})]$ (from 200 to 198 ppm).¹⁴ These data clearly show a trisubstitution and an increase of the electron density of the metal center of complexes **2**. The absence of coupling constants between the signals of the terminal carbonyls and the phosphorus suggests that the phosphine is not complexed to the metal. The presence of a metallacycle is shown by the resonances of the quaternary carbon of the ring between 83.8 and 86.2 ppm (two signals arising from the presence of the two isomers). The location of the phosphonium group on this sp^3 carbon leads to the large observed $^1\text{J}_{\text{C}-\text{P}}$ coupling constants (from 40 to 63 Hz). Smaller interactions are also observed between the phosphorus and the methyl group which also link to the sp^3 carbon, seen at 20–23 ppm ($^2\text{J}_{\text{C}-\text{P}} = 4.6\text{--}8.4$ Hz). It is worth noting that no coupling is measured between the phosphorus and the cyclic $\text{C}(\text{O})$ acyl bound to the metal at 269.2–273.3 ppm (^2J), whereas a small coupling, $^3\text{J}_{\text{C}-\text{P}} = 6\text{--}7.5$ Hz (through the oxygen), is observed for the cyclic $\text{C}(\text{O})\text{O}$ at 213.9–219.1 ppm. ^{31}P NMR spectra of **2** confirm the formation of two isomers for each product. Two resonances

are observed at 32.0 and 30.7 ppm for **2a** (60/40), 41.2 and 39.3 ppm for **2b** (66/33), 44.4 and 42.7 ppm for **2c** (55/45), and 28.8 and 24.4 ppm for **2d** (55/45). There is no clear relation between the ratio of the two isomers and the electronic or steric effects of the phosphines. An attempt to modify these ratios by increasing the bulkiness of the alkoxy carbonyl ligand, using the related complex $(\text{CO})_4\text{Fe}[\text{C}(\text{O})\text{C}(\text{O})\text{CH}_3][\text{CO}_2\text{C}(\text{CH}_3)_3]$ (**1a**), failed, as the ratios of the different metallalactonic isomers obtained with this complex are very similar to those observed with **1**. All data are in good agreement with a zwitterionic structure of **2** in which a negative charge is located on the trifunctionalized metal center, while the phosphonium group is associated with the positive charge. Conclusive evidence of the structure is provided by the X-ray diffraction study performed on isomer **2b(1)** of complex **2b**.

Structural Study of Complex **2b(1).** Single crystals of **2b(1)** were grown from a hexanes/dichloromethane mixture (90:10) at -30°C . An ORTEP diagram of the complex is displayed in Figure 1, crystallographic data are given in Table 1, and selected bond lengths and angles are gathered in Table 2.

Figure 1 shows only one isomer of the expected zwitterionic trifunctionalized metallalactone substituted by a phosphonium group. Many attempts to collect data for a crystal containing the second isomer (**2b(2)**) which was present in solution failed (proportions of the two isomers: 66/33). The same proportion between these two products was also observed in the remaining solution after crystallization or when crystals are dissolved at low temperature in CD_2Cl_2 . These results suggest that either **2b(2)** crystallizes together with **2b(1)** but not as single crystals or if **2b(1)** is the only isomer present in the solid state, a rapid isomerization could occur between these two compounds (during the crystallization and the dissolving of **2b(1)**). This isomerization could result, as reported for ruthenium alkoxy carbonyl

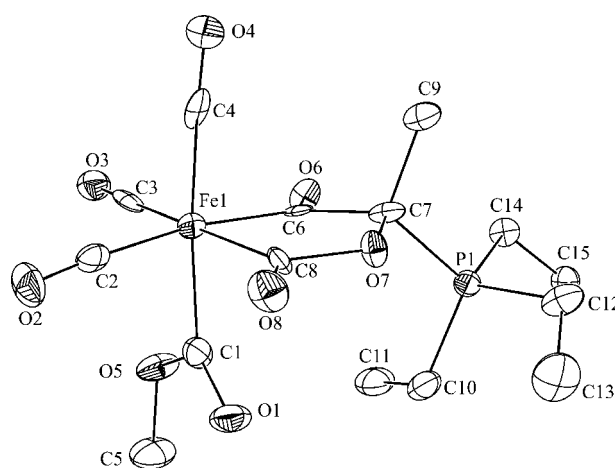


Figure 1. ORTEP view of **2b(1)** (50% probability ellipsoid) showing the asymmetric unit, the atom labeling scheme, and the molecular structure.

Table 1. Crystallographic Data for Compounds 2b(1) and 5b

	2b(1)	5b
formula	C ₁₅ H ₂₁ FeO ₈ P	C ₂₈ H ₃₆ B ₂ F ₈ Fe ₂ O ₁₄ P ₂
fw	416.14	943.83
cryst syst	orthorhombic	triclinic
space group	P2 ₁ 2 ₁ 2 ₁	P $\bar{1}$
a (Å)	9.409(2)	11.365(1)
b (Å)	10.736(2)	13.080(1)
c (Å)	17.932(3)	14.277(2)
α (deg)	90	111.19(1)
β (deg)	90	94.81(1)
γ (deg)	90	99.01(1)
V (Å ³)	1811.5(6)	1931.5(4)
Z	4	2
cryst size (mm)	0.26 × 0.06 × 0.05	0.16 × 0.14 × 0.11
D _{calcd} (g cm ⁻³)	1.526	1.623
F(000)	864	960
abs coeff, μ (mm ⁻¹)	0.960	0.934
T (K)	100(2)	170(2)
2θ limits (deg)	7.34–50.06	6.70–253.72
reflns collected	6751	15 304
reflns unique/R _{int}	2550/0.0851	5107/0.0383
reflns with I > 2σ(I)/N _v	1886/221	3738/505
R1 ^a	0.0709	0.0466
wR2 ^b	0.0991	0.0974
Goof ^c	1.026	1.017
Δρ _{max} /Δρ _{min} (e Å ⁻³)	0.513/−0.399	+0.611/−0.334
Flack param	0.10(4)	

$$^a \text{R1} = \sum |F_o - F_c| / F_o, \quad ^b \text{wR2} = \{\sum w(F_o^2 - F_c^2)^2 / \sum w(F_o^2)^2\}^{1/2},$$

$$^c \text{Goof} = \{\sum w(F_o^2 - F_c^2)^2 / (N_{\text{obs}} - N_{\text{var}})\}^{1/2}.$$

Table 2. Selected Bond Lengths (Å) and Bond Angles (deg) for 2b(1)

Fe(1)–C(1)	1.983(8)	O(7)–C(8)	1.407(9)
Fe(1)–C(2)	1.820(10)	O(7)–C(7)	1.429(8)
Fe(1)–C(3)	1.823(10)	O(6)–C(6)	1.224(9)
Fe(1)–C(4)	1.799(9)	O(8)–C(8)	1.218(9)
Fe(1)–C(8)	1.953(9)	C(9)–C(7)	1.531(10)
Fe(1)–C(6)	1.958(8)	C(7)–C(6)	1.562(11)
P(1)–C(7)	1.829(8)		
C(4)–Fe(1)–C(2)	94.6(4)	C(6)–Fe(1)–C(1)	87.2(3)
C(4)–Fe(1)–C(3)	95.2(3)	C(8)–O(7)–C(7)	116.2(6)
C(2)–Fe(1)–C(3)	96.4(3)	O(7)–C(7)–C(9)	109.6(6)
C(4)–Fe(1)–C(8)	88.0(3)	O(7)–C(7)–C(6)	109.3(6)
C(2)–Fe(1)–C(8)	90.1(4)	C(9)–C(7)–C(6)	107.9(6)
C(3)–Fe(1)–C(8)	172.4(4)	O(7)–C(7)–P(1)	105.2(5)
C(4)–Fe(1)–C(6)	90.8(3)	C(9)–C(7)–P(1)	110.6(5)
C(2)–Fe(1)–C(6)	170.9(3)	C(6)–C(7)–P(1)	114.3(5)
C(3)–Fe(1)–C(6)	90.3(4)	O(6)–C(6)–C(7)	115.5(7)
C(8)–Fe(1)–C(6)	82.7(4)	O(6)–C(6)–Fe(1)	130.9(6)
C(4)–Fe(1)–C(1)	172.8(4)	C(7)–C(6)–Fe(1)	113.4(5)
C(2)–Fe(1)–C(1)	86.5(4)	O(8)–C(8)–O(7)	112.8(7)
C(3)–Fe(1)–C(1)	91.8(3)	O(8)–C(8)–Fe(1)	130.5(7)
C(8)–Fe(1)–C(1)	84.8(3)	O(7)–C(8)–Fe(1)	116.7(6)

complexes, from a hopping of the alkoxy group of the alkoxy carbonyl ligand from one terminal carbonyl to another.²⁴ Unlike the related anionic complexes $\{(\text{CO})_3\text{Fe}[\text{C}(\text{O})\text{C}(\text{CH}_3)[\text{CH}(\text{CO}_2\text{C}_2\text{H}_5)_2]\text{OC}(\text{O})[(\text{CO}_2\text{R})]^{-}\}$ (R = OCH₃,¹⁶ CH₃¹⁸), respectively obtained as a single isomer, which display their diethylmalonyl groups and methoxycarbonyl or acetyl ligands in a *trans* position with respect to the medium plane of the metallacycle, the alkoxy carbonyl ligand and the phosphonium group of **2b(1)** are located in *cis* positions relative to the same plane.

To minimize steric interactions between these two groups, the bulky phosphonium adopts a pseudoequatorial position shown by a torsion angle of 131.7(4)° for P(1)–C(7)–C(6)–Fe(1) and by a distance between P(1) and the median plane of the

metallacycle of −1.206(8) Å. The methyl group (second substituent of the cyclic quaternary carbon) is then found in a pseudoaxial location (dihedral angle C(9)–C(7)–C(6)–Fe(1) = 104.9(6)°; distance to the median plane: 1.473(8) Å). The metallacycle is not rigorously planar, as C(7) and O(7) display deviations from the C(6)–Fe(1)–C(8) plane of 0.27(1) and 0.13(1) Å, respectively; O(7) and C(7) are located on the same side of this plane. The coordination around the metal center of **2b(1)** can be described as a distorted octahedron. As already observed for anionic metallacyclic iron complexes, the axial alkoxy carbonyl ligand is slightly bent toward the metallacycle: C(1)–Fe(1)–C(6) = 87.2(3)° and C(1)–Fe(1)–C(8) = 84.8(3)°. The presence of a five-membered metallacycle in the complex infers the observation of a small bite angle: C(6)–Fe(1)–C(8) = 82.7(4)°. This size falls within the range of the values measured for similar angles of homologous iron metallacycles,^{12,14–18,25} it is smaller than the angles measured between two nonchelating organic ligands (for example a value of 88.5(2)° is reported for *cis*-(CO)₄Fe(CO₂C₂H₅)₂²⁶). It is worth noting that C(2)–Fe(1)–C(3), the opposite angle on the metal center, displays a higher value than expected (96.4(3)°).

Reaction of (CO)₄Fe[C(O)C(O)CH₃](CO₂CH₃) (1) with Bulky Phosphines P(C₆H₅)₃ or P(C₆H₁₁)₃. Reaction of 1 with P(C₆H₅)₃. At −80 °C, no reaction is observed between P(C₆H₅)₃ and **1**; changes in the IR spectrum of the starting compound are detected only after 24 h at 10 °C. The ¹³C NMR spectrum of the crude product of this reaction shows a failure in the formation of the phosphonium-substituted metallalactone that might be expected (no signal with a large interaction with a phosphorus at ~80–90 ppm corresponding to a quaternary metallacyclic carbon substituted by a phosphonium). The products of the reaction appraised by ¹³C and ³¹P NMR are Fe(CO)₄[P(C₆H₅)₃] (33%; ³¹P NMR: 71.7 ppm; ¹³C NMR: 213.33 ppm, d, ²J_{C–P} = 18.7 Hz),²⁷ Fe(CO)₃[P(C₆H₅)₃]₂ (25%; ³¹P NMR: 82.3 ppm; ¹³C NMR: 214.15 ppm, t, ²J_{C–P} = 28.3 Hz),^{27,28} and the two *mer* isomers of (CO)₃Fe-[P(C₆H₅)₃](CO₂CH₃)[C(O)C(O)CH₃], **3a(1)** and **3a(2)** (Scheme 4), displaying, in the ³¹P NMR singlets at 42.85 ppm (20%) and 42.95 ppm (20%). Formation of **3a(1)** and **3a(2)** in the absence of their *fac* isomers is shown in the ¹³C NMR by the presence of two pairs of signals of 2:1 intensities corresponding to the terminal carbonyls. The specific formation of the *mer* isomers by substitution of a terminal carbonyl of **1** by a bulky phosphine is not surprising, as a similar result has already been observed for the related complex (CO)₄Fe(CO₂CH₃)₂.²⁹

The complexation of the phosphine to the metal center of **3a(1)** and **3a(2)** is shown by the couplings observed in the ¹³C NMR between the phosphorus and the different carbons linked to the iron: 254.57 ppm (d, ²J_{P–C} = 20.6 Hz) and 255.03 ppm (d, ²J_{P–C} = 19.2 Hz) for Fe–C(O)C(O); 206.50 ppm (d, ²J_{P–C} = 14.6 Hz) and 206.70 ppm (d, ²J_{P–C} = 13.5 Hz) for the two axial C≡O; 204.95 ppm (d, ²J_{P–C} = 7.5 Hz) and 204.90 ppm (d, ²J_{P–C} = 7.5 Hz) for the equatorial C≡O; 198.35 ppm (d,

(25) (a) Pettersen, R. C.; Cihonski, J. L.; Young, F. R.; Levenson, R. A. *J. Organomet. Chem. Commun.* **1975**, 370. (b) Hoffmann, K.; Weiss, E. *J. Organomet. Chem.* **1977**, 128, 389. (c) Aime, S.; Milone, L.; Sappa, E.; Tiripicchio, A.; Manotti Lanfredi, A. M. *J. Chem. Soc., Dalton Trans.* **1979**, 1664. (d) Karel, K. J.; Tulip, T. H.; Ittel, S. D. *Organometallics* **1990**, 9, 1276.

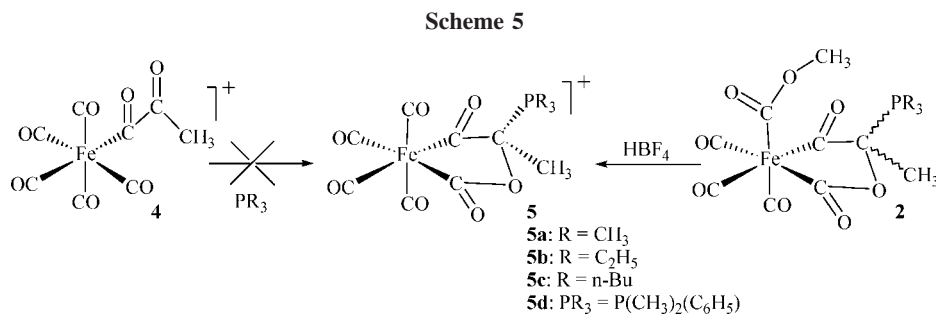
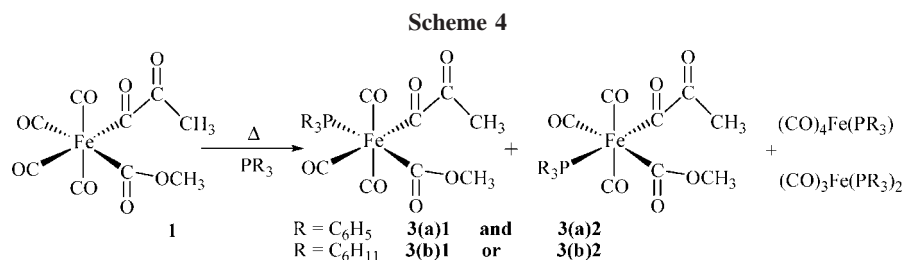
(26) Luat, D.; le Gall, N.; Salaün, J. Y.; Toupet, L.; des Abbayes, H. *Inorg. Chim. Acta* **1999**, 9, 166.

(27) Whitmore, K. H.; Lee, T. R. *J. Organomet. Chem.* **1985**, 282, 95.

(28) Inoue, H.; Takei, T.; Heckmann, G.; Fluck, E. *Z. Naturforsch.* **1991**, 46b, 682.

(29) Sellin, M.; Luat, D.; Salaün, J. Y.; Laurent, P.; des Abbayes, H. *J. Organomet. Chem.* **1998**, 562, 183.

(24) Gargulak, J. D.; Gladfelter, W. L. *Organometallics* **1994**, 13, 698.



$^2J_{\text{P-C}} = 14.0$ Hz) and 198.30 ppm (d, $^2J_{\text{P-C}} = 14.2$ Hz) for the C(O)OCH₃. A similar interaction is also displayed by the β -carbonyl of the pyruvate ligand at 201.58 ppm (d, $^3J_{\text{P-C}} = 16.2$ Hz) and at 201.20 ppm (d, $^3J_{\text{P-C}} = 16.0$ Hz). The coupling constants between the phosphorus of the phosphine and either the α -C(O) of the pyruvate or the carbonyl of the alkoxy carbonyl are equivalent, making any assignment of an exact geometry to **3a(1)** or **3a(2)** very difficult. Due to their low stability, several attempts at separation of these two complexes failed.

Reaction of 1 with P(C₆H₁₁)₃. As observed for P(C₆H₅)₃, a reaction between **1** and P(C₆H₁₁)₃ is obtained only at 15 °C (IR monitoring). As shown by its NMR data, the crude product of the reaction is composed of Fe(CO)₄[P(C₆H₁₁)₃] (55%), Fe(CO)₃[P(C₆H₁₁)₃]₂ (traces), (CO)₄Fe[C(O)C(CH₃)(OCH₃)OC(O)] (15%), and a single *mer* isomer of (CO)₃-Fe[P(C₆H₁₁)₃](CO₂CH₃)[C(O)C(O)CH₃] (**3b**) (25%) (data arising from these different complexes are detailed in the Experimental Section). The formation of the methoxy-substituted metallalactone very likely results from a direct thermolysis of **1**, which has been reported to occur at 15 °C.¹² Unexpectedly, only one *mer* isomer of **3b** is formed; the value observed for the coupling constant between the phosphorus and the α -carbonyl of the pyruvate (20.6 Hz) compared to that of 12.1 Hz measured for the alkoxy carbonyl ligand could suggest for this compound a structure with the phosphine in a *trans* position with respect to the pyruvate group. However, as this difference in the coupling constants was not observed for the related complexes **3(a)1** and **3(a)2**, this assignment remains tentative.

Attempts to Obtain Phosphonium-Substituted Cationic Metallalactones $\{(\text{CO})_4\text{Fe}[\text{C}(\text{O})\text{C}(\text{CH}_3)(\text{PR}_3)\text{OC}(\text{O})]\}^+$ (**5**): R = CH₃, **5a**; R = C₂H₅, **5b**; R = n-Bu, **5c**; PR₃ = P(CH₃)₂(C₆H₅), **5d**. By Reaction of PR₃ with $\{(\text{CO})_5\text{Fe}[\text{C}(\text{O})\text{C}(\text{O})\text{CH}_3]\}^+$ (**4**) we observed the selective formation of *cis*-(CO)₄Fe(CO₂C₂H₅)[C(O)C(O)CH₃] formed by addition of the nucleophile on one of the terminal carbonyls of the complex.¹⁴

As no trace of formation of the metallalactone, (CO)₄Fe[C(O)C(CH₃)(OC₂H₅)OC(O)], that might be expected was observed, the terminal carbonyls appear to be the most electrophilic sites of this cationic species. Tertiary phosphines, which are not supposed to react easily with terminal carbonyls, might, by an addition to the β -carbonyl of **4**, induce the formation of the cationic metallalactones $\{(\text{CO})_4\text{Fe}[\text{C}(\text{O})\text{C}(\text{CH}_3)(\text{PR}_3)\text{OC}(\text{O})]\}^+$ (**5**) (Scheme 5). Unfortunately, as shown by an IR monitoring, no reaction is observed at -40 °C between **4** and P(CH₃)₃ or [P(C₆H₅)₃]. Raising the temperature to 20 °C leads only to a decomposition of the starting complex (probably by decarbonylation of the pyruvate ligand). A possible decomposition of lactones **5** was also considered; however, their isolation as stable compounds by reaction of complexes **2** with HBF₄ (see below) proved this hypothesis to be wrong and confirms the low electrophilicity of the β -carbonyl of pyruvate ligands in cationic species.

By Dissociation of the Alkoxy carbonyl Ligand of 2. Dissociation of alkoxy carbonyl ligands in the presence of a strong acid is a well-known process.³⁰ This reaction has already been reported for alkoxy carbonyl iron complexes and yielded, after release of alcohol, several cationic iron carbonylated species.^{11,14,31} Reaction of complexes **2** with 1.1 equiv of HBF₄[O(CH₃)₂] in THF at -20 °C is found to afford very rapidly a series of new complexes **5**, whose low solubility in nonpolar solvents suggests a cationic nature. Their IR spectra (performed in THF) display a set of three broad $\nu_{\text{C=O}}$ bands between 2147 and 2056 cm⁻¹. The broadness of these signals can explain the presence of only three bands instead of the four signals required by a M(CO)₄ fragment with C_{2v} symmetry and generally observed for *cis*-disubstituted iron carbonyl complexes.^{11,12,14-16,23,31} The wave numbers measured for these $\nu_{\text{C=O}}$ bands fall within the range of those observed for neutral disubstituted iron complexes, 2138-2040 cm⁻¹. They are significantly different from their homologous monosubstituted cationic iron complexes (which exhibit three bands between 2195 and 2130 cm⁻¹) and from the $\nu_{\text{C=O}}$ bands observed for the starting zwitterionic complexes **2** (from 2080 to 1989 cm⁻¹),

(30) Fernandez, M. J.; Rodriguez, M. J.; Oro, L. A. *J. Organomet. Chem.* **1992**, *438*, 337.

(31) Salaün, J. Y.; le Gall, G.; Laurent, P.; des Abbayes, H. *J. Organomet. Chem.* **1992**, *441*, 99.

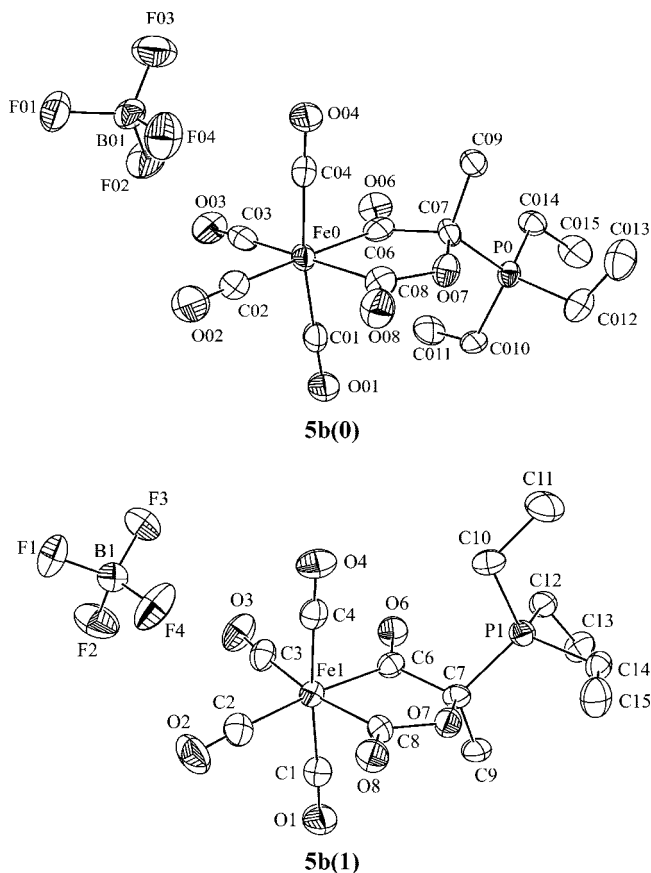


Figure 2. ORTEP view of **5b** (50% probability ellipsoids) showing the asymmetric unit, the atom-labeling scheme, and the molecular structure of the two molecular units, **5b(0)** and **5b(1)**.

whose metal center displays an anionic character. These data suggest for these cationic complexes the presence of a disubstituted neutral metal center and a positive charge located on a phosphonium group. The ^{13}C NMR spectra of cations **5** confirm the neutral nature of their metal center; the resonances of their terminal carbonyls (four signals between 199.6 and 194.35 ppm) are located between those of cationic monosubstituted iron compounds (196.1–190.4 ppm) and of anionic complexes (209.6 ppm for $(\text{CO})_3\text{Fe}(\text{CO}_2\text{CH}_3)_3^-$ or from 207.05 to 205.04 ppm for the zwitterionic metallalactones **2**). These chemical shifts are similar to those displayed by a neutral metallalactone (from 199.4 to 196.7 ppm). Due to the conversion of the alkoxycarbonyl ligand of each isomer of complexes **2** into a terminal carbonyl, each formed complex **5** is present as only a single isomer whose ^{13}C NMR spectra exhibit four resonances corresponding to the four terminal carbonyls. The nonequivalence of the two axial carbonyls is induced by the presence of two different substituents on the cyclic sp^3 carbon of the metallacycle. The resonances of these sp^3 metallacyclic carbons are observed at ~ 89.5 ppm, and the presence of the phosphonium substituent is shown by large $J_{\text{C}-\text{P}}$ coupling constants (between 52 and 63 Hz).

Structural Study of Complex 5b. An X-ray diffraction study performed on **5b** confirmed the structure proposed for the compounds of this series. Single crystals of **5b** were obtained from a CH_2Cl_2 solution at -30°C . The ORTEP diagram of the complex is displayed in Figure 2; crystallographic data are given in Table 1 (see Experimental Section), and selected bond lengths and angles are gathered in Table 3.

Complex **5b** is found in the crystal as two entities: **5b(0)** and **5b(1)** (Figure 2). These two forms can be described as

Table 3. Selected Bond Lengths (Å) and Bond Angles (deg) for **5b**

Fe(0)—C(01)	1.803(5)	O(07)—C(08)	1.362(5)
Fe(0)—C(02)	1.875(5)	O(07)—C(07)	1.450(5)
Fe(0)—C(03)	1.847(6)	O(06)—C(06)	1.221(5)
Fe(0)—C(04)	1.839(5)	O(08)—C(08)	1.200(5)
Fe(0)—C(08)	2.013(5)	C(09)—C(07)	1.529(6)
Fe(0)—C(06)	1.962(5)	C(07)—C(06)	1.555(6)
P(0)—C(07)	1.857(5)		
Fe(1)—C(1)	1.822(5)	O(7)—C(8)	1.400(5)
Fe(1)—C(2)	1.871(5)	O(7)—C(7)	1.433(5)
Fe(1)—C(3)	1.860(6)	O(6)—C(6)	1.204(5)
Fe(1)—C(4)	1.829(5)	O(8)—C(8)	1.194(5)
Fe(1)—C(8)	1.981(5)	C(9)—C(7)	1.531(6)
Fe(1)—C(6)	1.977(5)	C(7)—C(6)	1.564(6)
P(1)—C(7)	1.840(5)		
C(04)—Fe(0)—C(02)	93.3(2)	C(06)—Fe(0)—C(01)	88.7(2)
C(04)—Fe(0)—C(03)	92.2(2)	C(08)—O(07)—C(07)	117.5(3)
C(02)—Fe(0)—C(03)	94.5(2)	O(07)—C(07)—C(09)	110.4(4)
C(04)—Fe(0)—C(08)	90.2(2)	O(07)—C(07)—C(06)	108.9(4)
C(02)—Fe(0)—C(08)	90.3(2)	C(09)—C(07)—C(06)	108.4(4)
C(03)—Fe(0)—C(08)	174.4(2)	O(07)—C(07)—P(0)	105.9(3)
C(04)—Fe(0)—C(06)	84.1(2)	C(09)—C(07)—P(0)	110.7(3)
C(02)—Fe(0)—C(06)	172.3(2)	C(06)—C(07)—P(0)	112.5(3)
C(03)—Fe(0)—C(06)	92.8(2)	O(06)—C(06)—C(07)	118.0(4)
C(08)—Fe(0)—C(06)	82.5(2)	O(06)—C(06)—Fe(0)	127.9(4)
C(04)—Fe(0)—C(01)	171.8(2)	C(07)—C(06)—Fe(0)	113.9(3)
C(02)—Fe(0)—C(01)	93.3(2)	O(08)—C(08)—O(07)	116.3(4)
C(03)—Fe(0)—C(01)	92.0(2)	O(08)—C(08)—Fe(0)	128.4(4)
C(08)—Fe(0)—C(01)	85.0(2)	O(07)—C(08)—Fe(0)	115.3(3)
C(4)—Fe(1)—C(2)	92.9(2)	C(6)—Fe(1)—C(1)	88.7(2)
C(4)—Fe(1)—C(3)	91.1(2)	C(8)—O(7)—C(7)	118.1(4)
C(2)—Fe(1)—C(3)	97.4(2)	O(7)—C(7)—C(9)	110.7(4)
C(4)—Fe(1)—C(8)	85.9(2)	O(7)—C(7)—C(6)	108.5(4)
C(2)—Fe(1)—C(8)	91.5(2)	C(9)—C(7)—C(6)	110.2(4)
C(3)—Fe(1)—C(8)	170.8(2)	O(7)—C(7)—P(1)	105.4(3)
C(4)—Fe(1)—C(6)	88.9(2)	C(9)—C(7)—P(1)	111.3(3)
C(2)—Fe(1)—C(6)	173.9(2)	C(6)—C(7)—P(1)	110.7(3)
C(3)—Fe(1)—C(6)	88.4(2)	O(6)—C(6)—C(7)	118.5(4)
C(8)—Fe(1)—C(6)	82.8(2)	O(6)—C(6)—Fe(1)	128.5(4)
C(4)—Fe(1)—C(1)	174.2(2)	C(7)—C(6)—Fe(1)	112.9(3)
C(2)—Fe(1)—C(1)	88.9(2)	O(8)—C(8)—O(7)	116.0(4)
C(3)—Fe(1)—C(1)	94.1(2)	O(8)—C(8)—Fe(1)	129.0(4)
C(8)—Fe(1)—C(1)	88.5(2)	O(7)—C(8)—Fe(1)	115.0(3)

enantiomeric, as they display similar structures with an *S* C07 for **5b(0)** and an *R* C7 for **5b(1)** asymmetric carbons and as they can be related to each other by a virtual mirror plane located in a horizontal position orthogonally to the projection plane of Figure 2. **5b(0)** and **5b(1)** are however crystallographically independent molecules, and due to the presence of an inversion center required by the space group of crystallisation ($P\bar{1}$), their respective enantiomers are also present in the unit cell. The two enantiomers **5b(0)** and **5b(1)** display only slight differences in their bond lengths and angles. As observed for the zwitterionic compound **2b(1)**, the bulky $\text{P}(\text{C}_2\text{H}_5)_3$ phosphonium group adopts a pseudo-equatorial position with distances to the metallacyclic median plane of 1.216(5) Å for P(1) and 1.251(6) Å for P(0) (vs 1.206(8) Å for **2b(1)**). The methyl group, the other substituent of the C(7) (or C(07)) metallacyclic sp^3 carbons, is then located in pseudoaxial position with C(9) or C(09) median plane distances of $-1.496(6)$ and $-1.465(6)$ Å, respectively. The metallacycle of **5b(0)** is quasi-planar, with distances between C(07) and O(07) and the C(06)—Fe(0)—C(08) plane of $-0.146(8)$ and $0.056(7)$ Å, respectively. C(07) and O(07) are located from each side of this plane. On the other hand, C(7) and O(7), their homologues of the second form, **5b(1)**, are situated on the same side of this metallacyclic medium plane with distances between these two atoms and the C(6)—Fe(1)—C(8) plane of $-0.336(8)$ and $-0.141(7)$ Å, respectively. This molecule **5b(1)** then displays a less planar metallacycle than that of **5b(0)**. As observed for the zwitterionic complex **2b(1)**,

the coordination polyhedra around the metal centers of **5b(0)** and **5b(1)** are distorted octahedra built of four terminal carbonyls and the chelate. Again the bite angles of the metallacycles are small ($C(06)-Fe(0)-C(08) = 82.5(2)^\circ$; $C(6)-Fe(1)-C(8) = 82.8(2)^\circ$) and their opposite angles on the metal centers are found larger than 90° , with $C(03)-Fe(0)-C(02) = 94.5(2)^\circ$ and $C(3)-Fe(1)-C(2) = 97.4(2)^\circ$. The two axial terminal carbonyls are also bent toward the metallacycles. This is shown by an average value of 87.5° for the angles $C(1)-Fe(1)-C(6)$, $C(1)-Fe(1)-C(8)$, $C(4)-Fe(1)-C(6)$, and $C(4)-Fe(1)-C(8)$ and their homologues of the **5b(0)** molecular unit.

Conclusion

The reactions of an iron complex containing a pyruvoyl ligand, with tertiary phosphines, has allowed the high electrophilicity of the β -carbonyl of this polycarbonylated ligand of neutral complexes to be confirmed. For the first time, the addition of these phosphines has been performed on a non- η^2 -coordinated $C=O$. This reaction has been found to give rise to stable metallactones whose metallacycle formation results from an addition of the oxygen of the β -carbonyl of the pyruvoyl to a terminal carbonyl. These lactones display original zwitterionic geometries with an anionic charge located on the trisubstituted metal center and a cationic phosphonium group. However, the reaction seems limited to neutral compounds, as a similar cationic pyruvoyl iron complex was found to be unreactive toward the same phosphines. Cationic lactones, though not directly available from pyruvoyl cationic compounds, are obtained by dissociation in acidic medium of the alkoxy carbonyl ligand of the zwitterionic species **2**. These display a neutral metal center and a positive phosphonium group.

Experimental Section

All reactions were carried out using Schlenk techniques under a dry, oxygen-free argon atmosphere. All solvents were purified by preliminary distillation from an appropriate drying agent.³² CD_2Cl_2 and D_8 -THF were stored over molecular sieves under an inert atmosphere until needed. Infrared spectra were recorded in the range $2300-1600\text{ cm}^{-1}$ in solution in CH_2Cl_2 or THF using a FT-IR Nexus Nicolet spectrometer. 1H and ^{13}C NMR spectra were recorded at 0°C in CD_2Cl_2 or D_8 -THF on Bruker AMX-3 300, Bruker DRX 400, or Bruker DRX 500 spectrometers. Chemical shifts were measured relative to residual protonated solvents for 1H NMR spectra and to the solvent resonance for ^{13}C NMR spectra. ^{31}P spectra were externally referenced to H_3PO_4 (85%). Elemental analyses were performed by the "Service Central d'Analyses du CNRS". $Fe(CO)_5$, $MeONa$, $CH_3C(O)CO_2H$, and the different phosphines were purchased from commercial sources and used as received. Complex **1** was prepared as described elsewhere¹⁵ by reaction of $ClC(O)C(O)Me^{33}$ with $[(CO)_4Fe(CO_2Me)]^-$.³⁴

Reaction of 1 with $P(CH_3)_3$, $P(C_2H_5)_3$, $P(n-Bu)_3$, or $P(CH_3)_2(C_6H_5)$. General procedure: One equivalent of the appropriate phosphine (1.5 mmol) was added with stirring to a solution of **1** (450 mg, 1.5 mmol) in 30 mL of CH_2Cl_2 at -80°C . Monitoring of the reaction showed the instantaneous disappearance of the two $\nu_{C=O}$ bands of the starting complex, which were replaced by three new bands in the $\nu_{C=O}$ area. After 15 min at -80°C , the temperature of the solution was raised to -10°C and the solvent evaporated to dryness. The off-white residue was washed at -10°C with three portions of hexanes (20 mL) extracted with 3×20

mL of a hexanes/ CH_2Cl_2 (95:5) mixture to give after 12 h at -30°C white crystals of **2**.

Reaction of 1 with $P(CH_3)_3$. Preparation of 2a. The reaction, which was performed with a 1 M solution of $P(CH_3)_3$ in THF (1.5 mL), afforded after crystallization 310 mg of **2a** (55% yield). IR (CH_2Cl_2 , cm^{-1}): $\nu_{C=O}$ 2080 (s), 2015 (s), 1990 (s); $\nu_{C=O}$ 1695(w), 1655 (m), 1640 (w).

Major isomer (60%). 1H NMR (CD_2Cl_2 , 263 K, δ ppm): 3.39 (s, 3 H, OCH_3); 1.79 (d, $^2J_{P-H} = 14.5\text{ Hz}$, 9 H, PCH_3); 1.41 (d, $^3J_{P-H} = 16.3\text{ Hz}$, 3 H, CCH_3). $^{13}C\{^1H\}$ NMR (CD_2Cl_2 , 263 K, δ ppm): 270.61 (s, cyclic $C=O$); 214.25 (d, $^3J_{C-P} = 7.4\text{ Hz}$, cyclic $C(O)O$); 203.38 (s, $C(O)OCH_3$); 206.71 (s), 206.39 (s), 205.33 (s) (3 terminal CO); 83.80 (d, $^1J_{C-P} = 62.6\text{ Hz}$, cyclic quaternary carbon); 51.29 (s, OCH_3); 21.15 (d, $^2J_{C-P} = 8.2\text{ Hz}$, CCH_3); 7.70 (d, $^1J_{C-P} = 51.4\text{ Hz}$, PCH_3). $^{31}P\{^1H\}$ NMR (CD_2Cl_2 , 263 K, δ ppm): 32.0.

Minor isomer (40%). 1H NMR (CD_2Cl_2 , 263 K, δ ppm): 3.37 (s, 3 H, OCH_3); 1.80 (d, $^2J_{P-H} = 14.5\text{ Hz}$, 9 H, PCH_3); 1.40 (d, $^3J_{P-H} = 14.7\text{ Hz}$, 3 H, CCH_3). $^{13}C\{^1H\}$ NMR (CD_2Cl_2 , 263 K, δ ppm): 273.54 (s, cyclic $C=O$); 214.05 (d, $^3J_{C-P} = 7.5\text{ Hz}$, cyclic $C(O)O$); 200.75 (s, $C(O)OCH_3$); 207.05 (s), 205.93 (s), 205.25 (s) (3 terminal CO); 84.30 (d, $^1J_{C-P} = 61.5\text{ Hz}$, cyclic quaternary carbon); 50.95 (s, OCH_3); 20.20 (d, $^2J_{C-P} = 7.6\text{ Hz}$, CCH_3); 6.90 (d, $^1J_{C-P} = 51.4\text{ Hz}$, PCH_3). $^{31}P\{^1H\}$ NMR (CD_2Cl_2 , 263 K, δ ppm): 30.7. Anal. Calcd for $C_{12}FeH_{15}O_8P$: C, 38.53; Fe, 14.93; H, 4.04; P, 8.28. Found: C, 39.05; Fe, 14.61; H, 4.35; P, 8.15.

Reaction of 1 with $P(C_2H_5)_3$. Preparation of 2b. The reaction was performed with a 1 M solution of $P(C_2H_5)_3$ in THF (1.5 mL). It was found to afford after crystallization 312 mg of **2b** (50% yield). IR (CH_2Cl_2 , cm^{-1}): $\nu_{C=O}$ 2080 (s), 2005 (s), 1989 (s); $\nu_{C=O}$ 1680(w), 1640 (m), 1610 (sh).

Major isomer (66%). 1H NMR (CD_2Cl_2 , 263 K, δ ppm): 3.45 (s, 3 H, OCH_3); 1.92 (m, 6 H, PCH_2); 1.55 (d, $^3J_{P-H} = 12.0\text{ Hz}$, 3 H, CCH_3); 1.39 (m, 9 H, PCH_2CH_3). $^{13}C\{^1H\}$ NMR (CD_2Cl_2 , 263 K, δ ppm): 270.07 (s, cyclic $C=O$); 213.90 (d, $^3J_{C-P} = 7.0\text{ Hz}$, cyclic $C(O)O$); 202.91 (s, $C(O)OCH_3$); 206.35 (s), 206.11 (s), 205.04 (s) (3 terminal CO); 85.60 (d, $^1J_{C-P} = 52.0\text{ Hz}$, cyclic quaternary carbon); 50.91 (s, OCH_3); 22.60 (d, $^2J_{C-P} = 7.0\text{ Hz}$, CCH_3); 13.95 (d, $^2J_{C-P} = 12.7\text{ Hz}$, PCH_2CH_3); 11.09 (d, $^1J_{C-P} = 44.2\text{ Hz}$, PCH_2). $^{31}P\{^1H\}$ NMR (CD_2Cl_2 , 263 K, δ ppm): 41.2.

Minor isomer (33%). 1H NMR (CD_2Cl_2 , 263 K, δ ppm): 3.42 (s, 3 H, OCH_3); 1.85 (m, 6 H, PCH_2); 1.53 (d, $^3J_{P-H} = 10.0\text{ Hz}$, 3 H, CCH_3); 1.35 (m, 9 H, PCH_2CH_3). $^{13}C\{^1H\}$ NMR (CD_2Cl_2 , 263 K, δ ppm): 272.88 (s, cyclic $C=O$); 218.82 (s, cyclic $C(O)O$); 200.64 (s, $C(O)OCH_3$); 206.63 (s), 205.60 (s), 205.10 (s) (3 terminal CO); 86.21 (d, $^1J_{C-P} = 50.1\text{ Hz}$, cyclic quaternary carbon); 50.59 (s, OCH_3); 21.95 (d, $^2J_{C-P} = 5.0\text{ Hz}$, CCH_3); 14.25 (d, $^1J_{C-P} = 38\text{ Hz}$, PCH_2); 14.05 (d, $^3J_{C-P} = 10.0\text{ Hz}$, PCH_2CH_3). $^{31}P\{^1H\}$ NMR (CD_2Cl_2 , 263 K, δ ppm): 39.3. Anal. Calcd for $C_{15}FeH_{21}O_8P$: C, 43.29; Fe, 13.42; H, 5.09; P, 7.44. Found: C, 43.75; Fe, 13.32; H, 5.35; P, 7.15.

Reaction of 1 with $P(n-Bu)_3$. Preparation of 2c. The reaction, which was performed with 303 mg (375 μL) of $P(n-Bu)_3$, afforded after crystallization 340 mg of **2c** (45% yield). IR (CH_2Cl_2 , cm^{-1}): $\nu_{C=O}$ 2080 (s), 2018 (s), 1992 (s); $\nu_{C=O}$ 1675(w), 1630 (m), 1615 (sh).

Major isomer (55%). 1H NMR (CD_2Cl_2 , 263 K, δ ppm): 3.47 (s, 3 H, OCH_3); from 1.65 to 1.55 (m, 18 H, CH_2); 1.43 (d, $^3J_{P-H} = 11.0\text{ Hz}$, 3 H, CCH_3); 1.25 (t, $^3J_{H-H} = 7.0\text{ Hz}$, 9 H, $P(CH_2)_3CH_3$). $^{13}C\{^1H\}$ NMR (CD_2Cl_2 , 263 K, δ ppm): 269.68 (s, cyclic $C=O$); 214.04 (br s, cyclic $C(O)O$); 202.97 (s, $C(O)OCH_3$); 207.04 (s), 206.46 (s), 205.32 (s) (3 terminal CO); 85.48 (d, $^1J_{C-P} = 40.0\text{ Hz}$, cyclic quaternary carbon); 50.92 (s, OCH_3); 22.63 (d, $^2J_{C-P} = 4.6\text{ Hz}$, CCH_3); 24.8 (s), 24.45 (s), 24.30 (s) (3 CH_2); 13.89 (s, CH_3). $^{31}P\{^1H\}$ NMR (CD_2Cl_2 , 263 K, δ ppm): 44.4.

Minor isomer (45%). 1H NMR (CD_2Cl_2 , 263 K, δ ppm): 3.48 (s, 3 H, OCH_3); from 1.65 to 1.55 (m, 18 H, CH_2); 1.45 (d, $^3J_{P-H} = 12.0\text{ Hz}$, 3 H, CCH_3); 1.29 (t, $^3J_{H-H} = 7.0\text{ Hz}$, 9 H, $P(CH_2)_3CH_3$).

(32) Perrin, D. D.; Armarego, W. L. F.; Perrin, D. R. *Purification of Laboratory Chemicals*; Pergamon Press: New York, 1980.

(33) Ottenheijm, H. C. J.; Tijhuis, M. W. *Org. Synth.* **1983**, *61*, 1.

(34) McLean, J. L., Ph.D. Thesis, New York University, 1974.

$^{13}\text{C}\{^1\text{H}\}$ NMR (CD_2Cl_2 , 263 K, δ ppm): 272.90 (s, cyclic C=O); 214.04 (br s, cyclic C(O)O); 200.65 (s, C(O)OCH₃); 207.36 (s), 205.88 (s), 205.05 (s) (3 terminal CO); 86.17 (d, $^1J_{\text{C-P}} = 43.7$ Hz, cyclic quaternary carbon); 50.66 (s, OCH₃); 24.7 (s), 24.15 (s) (2 CH₂); 22.72 (d, $^2J_{\text{C-P}} = 5.0$ Hz, CCH₃); 18.15 (d, $^1J_{\text{C-P}} = 30$ Hz, PCH₂); 17.25 (s CH₂CH₃). $^{31}\text{P}\{^1\text{H}\}$ NMR (CD_2Cl_2 , 263 K, δ ppm): 42.7. Anal. Calcd for $\text{C}_{21}\text{FeH}_{33}\text{O}_8\text{P}$: C, 50.42; Fe, 11.16; H, 6.65; P, 6.19. Found: C, 50.77; Fe, 12.97; H, 5.48; P, 7.08.

Reaction of 1 with P(CH₃)₂(C₆H₅). Preparation of 2d. The process was performed with 210 mg (215 μL) of P(n-Bu)₃. We obtained after crystallization 392 mg of **2d** (60% yield). IR (CH_2Cl_2 , cm^{-1}): $\nu_{\text{C=O}}$ 2080 (s), 2008 (s), 1995 (s); $\nu_{\text{C-O}}$ 1700(br), 1635 (br), 1615 (sh).

Major isomer (55%). ^1H NMR (263 K, δ ppm): CD_2Cl_2 , from 7.35 to 6.95 (m, 5 H, aromatic); 3.25 (s, 3 H, OCH₃); 1.75 (d, $^2J_{\text{P-H}} = 46.5$ Hz, 6 H, PCH₃); 1.38 (d, $^3J_{\text{P-H}} = 6.7$ Hz, 3 H, CCH₃). $^{13}\text{C}\{^1\text{H}\}$ NMR (CD_2Cl_2 , 263 K, δ ppm): 272.81 (s, cyclic C=O); 217.07 (d, $^3J_{\text{C-P}} = 7.1$ Hz, cyclic C(O)O); 201.22 (s, C(O)OCH₃); 206.46 (s), 206.06 (s), 205.40 (s) (3 terminal CO); from 135 to 115 (6 aromatic carbons); 84.78 (d, $^1J_{\text{C-P}} = 57.4$ Hz, cyclic quaternary carbon); 51.20 (s, OCH₃); 22.07 (d, $^2J_{\text{C-P}} = 8.4$ Hz, CCH₃); 5.50 (d, $^1J_{\text{C-P}} = 38.78$ Hz, PCH₃). $^{31}\text{P}\{^1\text{H}\}$ NMR (CD_2Cl_2 , 263 K, δ ppm): 28.8.

Minor isomer (45%). ^1H NMR (CD_2Cl_2 , 263 K, δ ppm): from 7.35 to 6.95 (m, 5 H, aromatic); 3.27 (s, 3 H, OCH₃); 1.78 (d, $^2J_{\text{P-H}} = 48.7$ Hz, 6 H, PCH₃); 1.35 (d, $^3J_{\text{P-H}} = 6.5$ Hz, 3 H, CCH₃). $^{13}\text{C}\{^1\text{H}\}$ NMR (CD_2Cl_2 , 263 K, δ ppm): 269.26 (s, cyclic C=O); 219.07 (d, $^3J_{\text{C-P}} = 6.2$ Hz, cyclic C(O)O); 203.60 (s, C(O)OCH₃); 206.81 (s), 206.06 (s), 205.22 (s) (3 terminal CO); from 135 to 115 (6 aromatic carbons); 85.90 (d, $^1J_{\text{C-P}} = 57.56$ Hz, cyclic quaternary carbon); 50.64 (s, OCH₃); 20.68 (d, $^2J_{\text{C-P}} = 6.9$ Hz, CCH₃); 6.0 (d, $^1J_{\text{C-P}} = 39.1$ Hz, PCH₃). $^{31}\text{P}\{^1\text{H}\}$ NMR (CD_2Cl_2 , 263 K, δ ppm): 24.4. Anal. Calcd for $\text{C}_{17}\text{FeH}_{17}\text{O}_8\text{P}$: C, 46.82; Fe, 12.72; H, 3.93; P, 7.10. Found: C, 47.21; Fe, 12.65; H, 4.22; P, 7.05.

Crystallographic Analyses. Crystallographic data of compounds **2b(1)** and **5b** were collected at 100 and 170 K, respectively, on an Xcalibur 2 diffractometer (Oxford Diffraction) using graphite-monochromated Mo K α radiation ($\lambda = 0.71073$ Å). The two structures were solved by direct methods and successive Fourier difference syntheses and were refined on F^2 by weighted anisotropic full-matrix least-squares methods³⁵ except the C15 carbon atom of **2b(1)**, which was refined isotropically. All the non-hydrogen atoms were refined anisotropically. All the hydrogen atoms were calculated for both structures and therefore included as isotropic fixed contributors to F_c . The thermal ellipsoid drawings were made with the ORTEP program.³⁶ Data collection and data reduction were done with the CRYSLIS-CCD and CRYSLIS-RED programs.³⁷ All other calculations were performed with standard procedures (embedded with WinGX suite of programs).³⁸ Pertinent crystal data and structure refinement and selected bond distances and angles are listed in Tables 1–3, respectively. Complete crystallographic data, in CIF format, are included in the Supporting Information.

Reaction of 1 with Bulky Phosphines P(C₆H₅)₃ or P(C₆H₁₁)₃. Preparation of 3a and 3b. General procedure: To a solution of **1** (450 mg, 1.5 mmol) in 30 mL of CH_2Cl_2 at -20 °C was added under stirring 1.1 equiv of the phosphine (P(C₆H₅)₃, 430 mg; P(C₆H₁₁)₃, 460 mg). The temperature was raised to 10 °C, and the solution was stirred at this temperature for 24 h. After evaporation of the solvent the oily residue was extracted by two portions of 15 mL of a hexanes/dichloromethane (90/10%) mixture at 0 °C. The solvent was removed to yield a yellow oil.

Reaction of 1 with P(C₆H₅)₃. The yellow oil was obtained in 80% yield. IR (CH_2Cl_2 , cm^{-1}): $\nu_{\text{C=O}}$ 2105 (m), 2035 (s), 2010 (s); $\nu_{\text{C-O}}$, 1705(br), 1630 (br), 1600 (br,sh). ^1H NMR (CD_2Cl_2 , 263 K, δ ppm): from 7.90 to 7.15 (m, 46 H, aromatic); 3.68 (br s, 3 H, OCH₃); 2.26 (br s, 3 H, CCH₃). The $^{31}\text{P}\{^1\text{H}\}$ NMR (CD_2Cl_2 , 263 K, δ ppm) and the $^{13}\text{C}\{^1\text{H}\}$ NMR (CD_2Cl_2 , 263 K, δ ppm) spectra of the mixture allowed the identification of the following products. Fe(CO)₄[P(C₆H₅)₃] (33%): $^{31}\text{P}\{^1\text{H}\}$ NMR 71.7 ppm; ^{13}C NMR 213.33 ppm, (d, $^2J_{\text{C-P}} = 18.7$ Hz).²⁷ Fe(CO)₃[P(C₆H₅)₃]₂ (25%): $^{31}\text{P}\{^1\text{H}\}$ NMR 82.3 ppm; ^{13}C NMR 214.15 ppm, (t, $^2J_{\text{C-P}} = 28.3$ Hz).^{27,28} **3a(1)** and **3a(2)**: $^{31}\text{P}\{^1\text{H}\}$ NMR 42.85 (20%) and 42.95 ppm (20%); ^{13}C NMR 255.03 (d, $^2J_{\text{C-P}} = 19.2$ Hz), 254.57 (d, $^2J_{\text{C-P}} = 20.6$ Hz), Fe–C(O); 206.70 (d, $^2J_{\text{C-P}} = 13.6$ Hz), 206.50 (d, $^2J_{\text{C-P}} = 14.6$ Hz, 2 axial C=O); 204.95 (d, $^2J_{\text{C-P}} = 7.5$ Hz), 204.90 (d, $^2J_{\text{C-P}} = 7.5$ Hz, equatorial C=O); 201.58 (d, $^3J_{\text{P-C}} = 16.2$ Hz), 201.20 (d, $^3J_{\text{P-C}} = 16.0$ Hz), C(O)CH₃; 198.30 (d, $^2J_{\text{C-P}} = 14.2$ Hz), 198.35 (d, $^2J_{\text{C-P}} = 14.0$ Hz), C(O)OCH₃; 51.66 (s), 51.19 (s), OCH₃; 22.88 (s), 22.53 (s), C-CH₃. Numerous signals are observed between 133.0 and 127.5 (aromatic carbons).

Reaction of 1 with P(C₆H₁₁)₃. Preparation of 3b. The oil was obtained in 70% yield. ^1H NMR (CD_2Cl_2 , 263 K, δ ppm): 3.72 (s, 1.6H, OCH₃); 3.35 (s, 1H, OCH₃); from 2.70 to 1.50 (m, 60 H, cyclohexyl and CCH₃). According to its ^{31}P and its ^{13}C NMR spectra this oil was found to contain traces of Fe(CO)₃[P(C₆H₁₁)₃]₂: $^{31}\text{P}\{^1\text{H}\}$ NMR 89.1; $^{13}\text{C}\{^1\text{H}\}$ NMR 216.60 (t, $^2J_{\text{C-P}} = 26.9$ Hz); 55% of Fe(CO)₄[P(C₆H₁₁)₃]: $^{31}\text{P}\{^1\text{H}\}$ NMR 81.7; $^{13}\text{C}\{^1\text{H}\}$ NMR 214.20 (d, $^2J_{\text{C-P}} = 19.0$ Hz); 15% of (CO)₄Fe[C(O)C(CH₃)(OCH₃)OC⁴(O)-(Fe–C⁴)]^{12,14} (the proportion of this complex was evaluated by comparison of its OCH₃ signal at 3.35 ppm in the ^1H NMR with its homologue of **3b** at 3.72 ppm); and 25% of one isomer of the *mer*-P(C₆H₁₁)₃[(CO)₃Fe[C(O)C(O)CH₃](CO₂CH₃) complex (**3b**): $^{31}\text{P}\{^1\text{H}\}$ NMR 48.3; ^{13}C NMR 254.60 (d, $^2J_{\text{P-C}} = 20.6$ Hz, Fe–C(O)); 206.50 (d, $^2J_{\text{P-C}} = 14.6$ Hz, 2 axial C=O); 204.15 (d, $^2J_{\text{P-C}} = 9.4$ Hz, equatorial C=O); 200.20 (d, $^3J_{\text{P-C}} = 15.2$ Hz, C(O)CH₃); 196.10 (d, $^2J_{\text{P-C}} = 12.1$ Hz, C(O)OCH₃); 51.0 (s, OCH₃); 22.7 (s, CH₃). Numerous signals were observed between 37.5 and 26.8 ppm in the ^{13}C NMR; they correspond to the carbons of the different cyclohexyl groups.

Preparation of Cationic Metallalactones 5. General procedure: To 1 mmol of a lactone **2** in solution in 40 mL of THF at -20 °C was added under stirring 1.1 equiv of HBF₄·O(C₂H₅)₂ (150 μL). After 10 min the solvent was evaporated under vacuum to give a pale green, oily residue. This residue was washed with two portions of hexanes at 0 °C and extracted at this temperature by three portions (20 mL) of a CH_2Cl_2 /hexanes (90:10) mixture. The volume of the solution obtained was reduced under vacuum at -40 °C to give a white precipitate. After filtration **5** was obtained as a white powder, which was washed with two portions of hexanes at -10 °C.

Preparation of 5a. Following the general procedure, 375 mg of **2a** was found to afford 360 mg (85% yield) of **5a**, obtained as a white powder. IR (THF, cm^{-1}): $\nu_{\text{C=O}}$ 2145 (s), 2100 (s), 2070 (s); $\nu_{\text{C-O}}$ 1705(s), 1680 (s). ^1H NMR (CD_2Cl_2 , 263 K, δ ppm): 1.92 (d, $^2J_{\text{P-H}} = 23.8$ Hz, 9 H, PCH₃); 1.62 (d, $^3J_{\text{P-H}} = 25.2$ Hz, 3 H, CCH₃). $^{13}\text{C}\{^1\text{H}\}$ NMR (CD_2Cl_2 , 263 K, δ ppm): 254.8 (s, cyclic C=O); 198.0 (s, cyclic C(O)O); 199.5 (s), 199.4 (s), 197.7 (s), 196.2 (s) (4 terminal CO); 89.6 (d, $^1J_{\text{C-P}} = 63.0$ Hz, cyclic quaternary carbon); 20.5 (d, $^2J_{\text{C-P}} = 6.5$ Hz, CCH₃); 6.3 (d, $^1J_{\text{C-P}} = 55.5$ Hz, PCH₃). ^{31}P NMR(^1H) (CD_2Cl_2 , 263 K, δ ppm): 37.8. Anal. Calcd for BC₁₁F₄FeH₁₂O₇P: C, 30.74; Fe, 12.99; H, 2.81; P, 7.21. Found: C, 30.91; Fe, 12.48; H, 4.35; P, 6.85.

Preparation of 5b. The general procedure performed with **2b** (416 mg) was found to give rise to 330 mg (yield 70%) of **5b**. IR (THF, cm^{-1}): $\nu_{\text{C=O}}$ 2140 (s), 2085 (br, s), 2057 (s); $\nu_{\text{C-O}}$ 1723(s), 1692 (s). ^1H NMR (CD_2Cl_2 , 263 K, δ ppm): 2.37 (m, 6H, PCH₂); 1.62 (d, $^3J_{\text{P-H}} = 13.5$ Hz, 3 H, CCH₃); 1.35 (dt, $^3J_{\text{P-H}} = 18.5$ Hz, $^3J_{\text{H-H}} = 7$ Hz, 9 H, CH₂CH₃). $^{13}\text{C}\{^1\text{H}\}$ NMR (CD_2Cl_2 , 263 K, δ

(35) Sheldrick, M. *SHELX97. Programs for Crystal Structure Analysis*; University of Göttingen: Göttingen, Germany, 1997.

(36) Johnson, C. K. *ORTEP*, Rep. ONL-3794, Delft, The Netherlands, 1985.

(37) *CRYSLIS-CCD 170*; Oxford Diffraction, 2002.

(38) Farrugia, L. J. *J. Appl. Crystallogr.* **1999**, *32*, 837.

ppm): 252.65 (s, cyclic C=O); 195.33 (d, $^3J_{C-P} = 5$ Hz cyclic C(O)O); 199.08(s), 198.94 (s), 195.85 (s), 194.42 (s) (4 terminal CO); 89.8 (d, $^1J_{C-P} = 51.0$ Hz, cyclic quaternary carbon); 21.98 (d, $^2J_{C-P} = 6.0$ Hz, CCH₃); 11.72 (d, $^1J_{C-P} = 55.0$ Hz, PCH₂). 6.52(d, $^2J_{C-P} = 6.0$ Hz, CH₂CH₃). $^{31}P\{^1H\}$ NMR (CD₂Cl₂, 263 K, δ ppm): 45.3. Anal. Calcd for BC₁₄F₄FeH₁₈O₇P: C, 35.63; Fe, 11.83; H, 4.34; P, 6.56. Found: C, 36.02; Fe, 12.35; H, 4.49; P, 6.75.

Preparation of 5c. According to the general procedure the transformation of 500 mg of **2c** afforded 330 mg of **5c** (60% yield). IR (THF, cm⁻¹): $\nu_{C=O}$ 2139 (s), 2085 (br, s), 2056 (s); ν_{C-O} 1721(s), 1692 (s). 1H NMR (CD₂Cl₂, 263 K, δ ppm): 2.24 (m, 6H, PCH₂); 1.68 (d, $^3J_{P-H} = 13.9$ Hz, 3 H, CCH₃); 1.59 (m, 6 H, CH₂) 1.50 (m, 6 H, CH₂CH₃) 0.97 (m, 9 H, CH₂CH₃). $^{13}C\{^1H\}$ NMR (CD₂Cl₂, 263 K, δ ppm): 253.58 (s, cyclic C=O); 196.99 (s, cyclic C(O)O); 199.12(s), 198.75 (s), 195.74 (s), 194.35 (s) (4 terminal CO); 89.32 (d, $^1J_{C-P} = 52.0$ Hz, cyclic quaternary carbon); 21.49 (s, CCH₃); 17.72 (d, $^1J_{C-P} = 41.0$ Hz, PCH₂); 24.23, 24.01 (s, 2 CH₂); 13.22 (s, CH₂CH₃). $^{31}P\{^1H\}$ NMR (CD₂Cl₂, 263 K, δ ppm): 40.8. Anal. Calcd for BC₂₀F₄FeH₃₀O₇P: C, 43.20; Fe, 10.04; H, 5.44; P, 5.56. Found: C, 43.62; Fe, 9.75; H, 5.55; P, 5.75.

Preparation of 5d. The general procedure gave rise (starting from 440 mg of **2d**) to 320 mg (65% yield) of **5d**. IR (THF, cm⁻¹):

$\nu_{C=O}$ 2147 (m), 2087 (sh), 2059 (s); ν_{C-O} 1713(m), 1685 (m). 1H NMR (CD₂Cl₂, 263 K, δ ppm): from 7.81 to 7.45 (m, 5 H, aromatic); 2.32 (d, $^2J_{H-P} = 14.5$ Hz, 3H, PCH₃); 2.26 (d, $^2J_{H-P} = 14.0$ Hz, 3H, PCH₃); 1.65 (d, $^3J_{P-H} = 15.5$ Hz, 3 H, CCH₃). $^{13}C\{^1H\}$ NMR (CD₂Cl₂, 263 K, δ ppm): 254.87 (s, cyclic C=O); 197.87 (d, $^3J_{C-P} = 6.3$ Hz, cyclic C(O)O); 199.60(s), 197.57 (s), 197.49 (s), 195.95 (s) (4 terminal CO); 89.74 (d, $^1J_{C-P} = 61.5$ Hz, cyclic quaternary carbon); 20.66 (d, $^2J_{C-P} = 6.5$ Hz, CCH₃); 5.80 (d, $^1J_{C-P} = 70.0$ Hz, PCH₃); 5.42 (d, $^1J_{C-P} = 67.0$ Hz, PCH₃). $^{31}P\{^1H\}$ NMR (CD₂Cl₂, 263 K, δ ppm): 30.2. Anal. Calcd for BC₁₆F₄FeH₁₄O₇P: C, 39.07; Fe, 11.35; H, 2.87; P, 6.30. Found: C, 39.52; Fe, 11.65; H, 3.05; P, 6.15.

Acknowledgment. We thank the “Service de RMN, Faculté des Sciences et Technologie, Université de Bretagne Occidentale” for its assistance for data recording.

Supporting Information Available: X-ray structural information for complexes **2b(1)** and **5b**. This material is available free of charge via the Internet at <http://pubs.acs.org>.

OM800804B

10-Vertex Manganese–Dicarbollide Complexes from a Monocarbon Precursor. Synthesis and Cluster Vertex Functionalization of [1-OH-2,2,2-(CO)₃-closo-2,1,10-MnC₂B₇H₈][−]

Andreas Franken, Thomas D. McGrath,* and F. Gordon A. Stone

Department of Chemistry & Biochemistry, Baylor University, Waco, Texas 76798-7348

Received July 30, 2008

Reaction between [NBuⁿ]₄[closo-1-CB₇H₈] and [Mn₂(CO)₁₀] in THF (THF = tetrahydrofuran) at reflux temperatures, or at room temperature with ultraviolet irradiation, followed by addition of [N(PPh₃)₂]Cl, affords the manganese–dicarbollide salt [N(PPh₃)₂][1-OH-2,2,2-(CO)₃-closo-2,1,10-MnC₂B₇H₈] (**1**). Addition of NOBF₄ to **1** gives the neutral species [1-OH-2,2-(CO)₂-2-NO-closo-2,1,10-MnC₂B₇H₈] (**2**), which readily undergoes CO substitution with PEt₃ in the presence of Me₃NO to yield [1-OH-2-CO-2-NO-2-PEt₃-closo-2,1,10-MnC₂B₇H₈] (**3**). Protonation of **1** in the presence of dialkyl sulfides SR₂ affords the neutral complexes [1-SR₂-2,2,2-(CO)₃-closo-2,1,10-MnC₂B₇H₈] [R = Me (**4**); SR₂ = S(CH₂)₄ (**5**); R = {CH₂CH=CH₂} (**6**)]; the synthesis of **5** is accompanied by formation of a boron-substituted relative, [1-OH-6-{S(CH₂)₄}-2,2,2-(CO)₃-closo-2,1,10-MnC₂B₇H₇] (**7**). Addition of Me₃NO to **6** in CH₂Cl₂ produces the anions [1-(SCH₂CH=CH₂)-2,2,2-(CO)₃-closo-2,1,10-MnC₂B₇H₈][−] and [1,2-σ:η²-(SCH₂CH=CH₂)-2,2-(CO)₂-closo-2,1,10-MnC₂B₇H₈][−], isolated as the [N(PPh₃)₂]⁺ salts **10** and **11**, respectively. Iodinated derivatives of **1** are obtained by direct reaction with I₂: an equimolar reaction yields two species, [N(PPh₃)₂][1-I-2,2,2-(CO)₃-closo-2,1,10-MnC₂B₇H₈] (**12**) and [N(PPh₃)₂][1-OH-6-I-2,2,2-(CO)₃-closo-2,1,10-MnC₂B₇H₇] (**13**), whereas treatment with excess I₂ affords [N(PPh₃)₂][1,6,9-I₃-2,2,2-(CO)₃-closo-2,1,10-MnC₂B₇H₆] (**14**) as the only product. When **12** was heated with Cu powder in refluxing DMF (DMF = *N,N*-dimethylformamide) the “parent” unsubstituted compound [N(PPh₃)₂][2,2,2-(CO)₃-closo-2,1,10-MnC₂B₇H₉] (**15**) was the sole product. Further cluster functionalization was achieved by treating **14** with the Grignard reagent (*p*-tol)MgBr (*p*-tol = 4-Me-C₆H₄-), leading to [N(PPh₃)₂][6,9-(*p*-tol)₂-2,2,2-(CO)₃-closo-2,1,10-MnC₂B₇H₇] (**16**). The latter reacts with NOBF₄ in CH₂Cl₂ to form neutral [6,9-(*p*-tol)₂-2,2-(CO)₂-2-NO-closo-2,1,10-MnC₂B₇H₇] (**17**). X-ray diffraction studies have confirmed the structural details of compounds **1**, **2**, **7**, **8**, **11–13**, **15**, and **17**.

Introduction

As part of a program of study¹ that aims to expand our knowledge of the under-represented class of metallacarborane complexes containing monocarbon carbollide ligands,² we have recently focused on complexes that incorporate intermediate-sized carboranes as ligand substrates.^{3–9} In so doing, we have exploited the fact that the latter cages are now much more

readily available following the development of chemistry that stemmed from the “Brellocks reaction”.^{10–13}

In the course of this work, ironically, we have discovered a novel route to metal–dicarbollide complexes. These are formed by insertion of an {M(CO)₄} fragment into a monocarborene cage, affording products that contain the expected {M(CO)₃} cluster vertex plus an additional {COH} vertex, of which the latter cage carbon atom bearing a hydroxyl substituent evidently originates from a formerly metal-bound CO ligand.¹⁴ The presence of the –OH functionality at a cluster vertex opens up the possibility of further derivatization at this site, some of which we have recently reported for a system where the hydroxyl group is appended to a neutral {FeC₂B₇} cluster.¹⁵ The present work provides an interesting contrast to the latter series, as the {MnC₂B₇} cage here, although formally isoelectronic with its {FeC₂B₇} analogue, is anionic and thus behaves rather differently in its substitution chemistry, particularly in its reactions

* To whom correspondence should be addressed. E-mail: tom_mcgrath@baylor.edu.

(1) (a) McGrath, T. D.; Stone, F. G. A. *J. Organomet. Chem.* **2004**, *689*, 3891. (b) McGrath, T. D.; Stone, F. G. A. *Adv. Organomet. Chem.* **2005**, *53*, 1.

(2) (a) Grimes, R. N. In *Comprehensive Organometallic Chemistry*; Wilkinson, G., Abel, E. W., Stone, F. G. A., Eds.; Pergamon Press: Oxford, U.K., 1982; Vol. 1, Section 5.5. (b) Grimes, R. N. In *Comprehensive Organometallic Chemistry II*; Abel, E. W., Stone, F. G. A., Wilkinson, G., Eds.; Pergamon Press: Oxford, U.K., 1995; Vol. 1, Chapter 9. (c) Hosmane, N. S., Maguire, J. A. In *Comprehensive Organometallic Chemistry III*; Mingos, D. M. P., Crabtree, R. H., Eds.; Pergamon Press: Oxford, U.K., 2007; Vol. 3, Section 3.05. (d) Grimes, R. N. *Coord. Chem. Rev.* **2000**, *200–202*, 773.

(3) (a) Franken, A.; McGrath, T. D.; Stone, F. G. A. *Organometallics* **2005**, *24*, 5157. (b) Franken, A.; McGrath, T. D.; Stone, F. G. A. *J. Am. Chem. Soc.* **2006**, *128*, 16169. (c) Franken, A.; Hodson, B. E.; McGrath, T. D.; Stone, F. G. A. *Dalton Trans.* **2007**, 2254. (d) Franken, A.; McGrath, T. D.; Stone, F. G. A. *Organometallics* **2008**, *27*, 148.

(4) Franken, A.; McGrath, T. D.; Stone, F. G. A. *Inorg. Chem.* **2006**, *45*, 2669.

(5) Lu, X. L.; McGrath, T. D.; Stone, F. G. A. *Organometallics* **2006**, *25*, 2590.

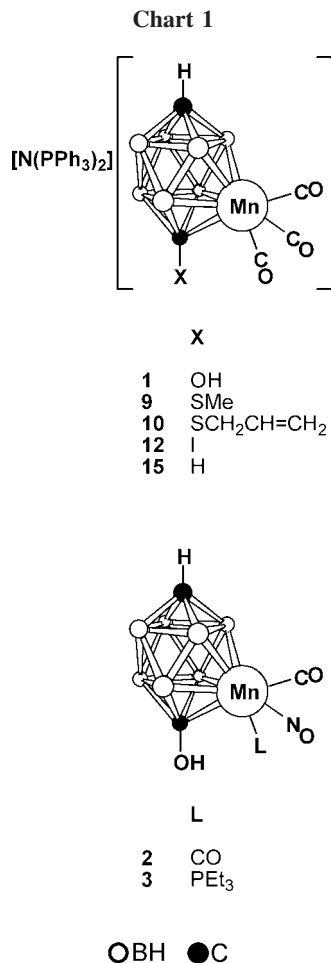
(6) Du, S.; Hodson, B. E.; Lei, P.; McGrath, T. D.; Stone, F. G. A. *Inorg. Chem.* **2007**, *46*, 6613.

(7) Carr, M.; McGrath, T. D.; Stone, F. G. A. *Inorg. Chem.* **2008**, *47*, 713.

(8) Carr, M.; McGrath, T. D.; Stone, F. G. A. *Organometallics* **2008**, *27*, 2099.

(9) Franken, A.; Hodson, B. E.; McGrath, T. D.; Stone, F. G. A. *Inorg. Chem.* **2008**, *47*, 8788.

(10) Brellocks, B. In *Contemporary Boron Chemistry*; Davidson, M. G., Hughes, A. K., Marder, T. B., Wade, K., Eds.; Royal Society of Chemistry: Cambridge, U.K., 2000; p 212.



with electrophiles, as we here discuss. Some aspects of this work have been communicated.¹⁴

Results and Discussion

Formation of the Parent Manganacarborane and Substitution at the Metal Center. We have recently reported a series of metal–dicarbollide species of general formulation [1-OH-2,2,2-(CO)₃-*closo*-2,1,10-MnC₂B₇H₈]ⁿ⁻ [*n* = 0, M = Fe or Ru; *n* = 1, M = Mn or Re]¹⁴ formed by treating [NBuⁿ₄][*closo*-1-CB₇H₈] with suitable metal–carbonyl reagents and have subsequently described selected reactivity studies on the *neutral* ferracarborane.¹⁵ In order to compare the latter with the closely related, but *anionic*, manganacarborane, we have separately examined its reactivity as the [N(PPH₃)₂]⁺ salt **1** (see Chart 1). Compound **1** is obtained by the thermal reaction of [Mn₂(CO)₁₀] with [NBuⁿ₄][*closo*-1-CB₇H₈] in refluxing THF. Spectroscopic monitoring of the reaction mixture (¹¹B NMR) reveals slow but selective formation of the 10-vertex {MnC₂B₇} metallacarborane product over a period of 48 h. The same reaction can be achieved in 2 h at room temperature under ultraviolet irradiation (Hg vapor arc lamp). In either case, addition of [N(PPH₃)₂]Cl and column chromatography then gave the desired product **1**.

Aside from the long-known {3,1,2-*closo*-MnC₂B₉} clusters,^{16–18} manganese–dicarbollide cage complexes are relatively rare.²

To our knowledge, the {2,1,10-*closo*-MnC₂B₇} framework in **1** (and in its derivatives discussed below) is the first example of a 10-vertex manganese–dicarbollide species, while analogous clusters are limited to a 9-vertex {MnC₂B₆} complex (ironically formed from a {C₂B₇} carborane substrate)¹⁹ and a 13-vertex {MnC₂B₁₀} system.²⁰ More elaborate, multiple-cluster {MnC₂B₄} complexes have also been reported.²¹ Compound **1** also constitutes a direct metallacarborane analogue of [Mn(CO)₃(η-C₅H₅)], one of the original “piano stool”-type compounds that now are so ubiquitous in organometallic chemistry.²²

The neutral ferracarborane analogue of **1** readily undergoes CO substitution by treatment with (for example) PEt₃ in the presence of Me₃NO (which removes one CO ligand as CO₂).^{14,15} In contrast, and as is to be expected, *anionic* **1** itself was resistant to CO replacement under similar conditions. Instead, treatment of **1** in CH₂Cl₂ with NOBF₄ forms a neutral, nitrosyl complex, [1-OH-2,2-(CO)₂-2-NO-*closo*-2,1,10-MnC₂B₇H₈] (**2**),^{18,20,23} which then is amenable to substitution to give [1-OH-2-CO-2-NO-2-PEt₃-*closo*-2,1,10-MnC₂B₇H₈] (**3**) by reaction with PEt₃ and Me₃NO. Spectroscopic data for compounds **1–3** are given in Tables 1 and 2, and the results of an X-ray diffraction structural study on **2** are presented in Figure 1. (A similar experiment on compound **1** was reported earlier.¹⁴)

All three of the complexes **1–3** display the expected spectroscopic properties: both **1** and **2** are mirror symmetric, and thus, consistent with this, their ¹¹B{¹H} NMR spectra contain four signals in the ratio 1:2:2:2, whereas the presence of three different Mn-bound ligands in **3** renders the molecule asymmetric and so the comparable spectrum contains seven resonances of unit integral (two coincide). In ¹³C{¹H} NMR spectra the two different types of cage carbon vertices resonate in distinct chemical shift ranges: the {CH} around δ 75–85 and the {COH} around δ 180–185, such significant deshielding being not unexpected given the presence of the terminal OH. The NMR spectra otherwise merit little comment. Likewise, the X-ray diffraction studies on **1**¹⁴ and **2** confirm the {2,1,10-MnC₂B₇} arrangement of vertices in the metallacarborane polyhedron, but otherwise reveal nothing unusual in the clusters’

(13) Brellochs, B.; Backovsky, J.; Střbr, B.; Jelínek, T.; Holub, J.; Bakardjiev, M.; Hnyk, D.; Hofmann, M.; Cisarová, I.; Wrackmeyer, B. *Eur. J. Inorg. Chem.* **2004**, 3605.

(14) Franken, A.; Lei, P.; McGrath, T. D.; Stone, F. G. A. *Chem. Commun.* **2006**, 3423.

(15) Franken, A.; McGrath, T. D.; Stone, F. G. A. *Organometallics* **2008**, *27*, 908.

(16) (a) Hawthorne, M. F.; Andrews, T. D. *J. Am. Chem. Soc.* **1965**, *87*, 2496. (b) Hawthorne, M. F.; Young, D. C.; Andrews, T. D.; Howe, D. V.; Pilling, R. L.; Pitts, D.; Reintjes, M.; Warren, L. F.; Wegner, P. A. *J. Am. Chem. Soc.* **1968**, *90*, 879.

(17) Valliant, J. F.; Morel, P.; Schaffer, P.; Kaldis, J. H. *Inorg. Chem.* **2002**, *41*, 628.

(18) Hata, M.; Kautz, J. A.; Lu, X. L.; McGrath, T. D.; Stone, F. G. A. *Organometallics* **2004**, *23*, 3590.

(19) Hawthorne, M. F.; Pitts, A. D. *J. Am. Chem. Soc.* **1968**, *89*, 7115.

(20) Hodson, B. E.; McGrath, T. D.; Stone, F. G. A. *Organometallics* **2005**, *24*, 3386.

(21) (a) Oki, A. R.; Zhang, H.; Hosmane, N. S. *Angew. Chem., Int. Ed. Engl.* **1992**, *31*, 432. (b) Hosmane, N. S.; Wang, Y.; Oki, A. R.; Zhang, H.; Maguire, J. A. *Organometallics* **1996**, *15*, 626.

(22) See, for example, together with references therein: (a) Treichel, P. M. In *Comprehensive Organometallic Chemistry*; Wilkinson, G.; Stone, F. G. A., Abel, E. W., Eds.; Pergamon Press: Oxford, U.K., 1982; Vol. 4, Chapter 29. (b) Treichel, P. M. In *Comprehensive Organometallic Chemistry II*; Abel, E. W., Stone, F. G. A., Wilkinson, G., Eds.; Pergamon Press: Oxford, U.K., 1995; Vol. 6, Chapter 5. (c) Sweigart, D. A.; Reingold, J. A., Son, S. U. In *Comprehensive Organometallic Chemistry III*; Mingos, D. M. P., Crabtree, R. H., Eds.; Pergamon Press: Oxford, U.K., 2007; Vol. 5, Section 5.10.

(23) Ellis, D. D.; Jelliss, P. A.; Stone, F. G. A. *Chem. Commun.* **1999**, 2385.

(11) (a) Střbr, B.; Tok, O. L.; Milius, W.; Bakardjiev, M.; Holub, J.; Hnyk, D.; Wrackmeyer, B. *Angew. Chem., Int. Ed.* **2002**, *41*, 2126. (b) Střbr, B. *Pure Appl. Chem.* **2003**, *75*, 1295.

(12) (a) Franken, A.; Kilner, C. A.; Thornton-Pett, M.; Kennedy, J. D. *Collect. Czech. Chem. Commun.* **2002**, *67*, 869. (b) Jelínek, T.; Thornton-Pett, M.; Kennedy, J. D. *Collect. Czech. Chem. Commun.* **2002**, *67*, 1035.

Table 1. Analytical and Physical Data^a

compound	ν_{\max} (CO) ^b /cm ⁻¹	analysis/% ^c		
		C	H	N
[N(PPh ₃) ₂][1-OH-2,2,2-(CO) ₃ -closo-2,1,10-MnC ₂ B ₇ H ₈] (1)	1991 s, 1903 s	61.2 ^d (61.4)	5.0 (4.9)	1.7 (1.8)
[1-OH-2,2,2-(CO) ₂ -2-NO-closo-2,1,10-MnC ₂ B ₇ H ₈] (2)	2089 s, 2049 s	18.3 (18.1)	3.5 (3.4)	5.2 (5.3)
[1-OH-2-CO-2-NO-2-PEt ₃ -closo-2,1,10-MnC ₂ B ₇ H ₈] (3)	2008 s	30.3 (30.4)	6.9 (6.8)	3.9 (3.9)
[1-SMe ₂ -2,2,2-(CO) ₃ -closo-2,1,10-MnC ₂ B ₇ H ₈] (4)	2012 s, 1934 s, 1925 s	27.1 (27.2)	4.5 (4.6)	
[1-{S(CH ₂) ₄ }-2,2,2-(CO) ₃ -closo-2,1,10-MnC ₂ B ₇ H ₈] (5)	2011 s, 1934 s, 1925 s	31.9 (32.3)	4.7 (4.8)	
[1-{S(CH ₂ CH=CH ₂) ₂ }-2,2,2-(CO) ₃ -closo-2,1,10-MnC ₂ B ₇ H ₈] (6)	2011 s, 1935 s, 1925 s	36.4 (36.6)	5.3 (5.0)	
[1-OH-6-{S(CH ₂) ₄ }-2,2,2-(CO) ₃ -closo-2,1,10-MnC ₂ B ₇ H ₇] (7)	2013 s, 1944 s, 1921 s	31.1 (30.8)	4.4 (4.6)	
[1,2-(SMe ₂) ₂ -2,2-(CO) ₂ -closo-2,1,10-MnC ₂ B ₇ H ₈] (8)	1926 s, 1862 s	27.3 (28.0)	5.7 (5.9)	
[N(PPh ₃) ₂][1-SMe-2,2,2-(CO) ₃ -closo-2,1,10-MnC ₂ B ₇ H ₈] (9)	1992 s, 1905 s	60.3 (60.6)	5.1 (5.0)	1.8 (1.7)
[N(PPh ₃) ₂][1-{SCH ₂ CH=CH ₂ }-2,2,2-(CO) ₃ -closo-2,1,10-MnC ₂ B ₇ H ₈] (10)	1992 s, 1907 s	61.7 (61.6)	5.2 (5.1)	1.8 (1.6)
[N(PPh ₃) ₂][1,2-σ-η ² -{SCH ₂ CH=CH ₂ }-2,2-(CO) ₂ -closo-2,1,10-MnC ₂ B ₇ H ₈] (11)	1934 s, 1872 s	62.0 (62.2)	5.4 (5.2)	1.8 (1.7)
[N(PPh ₃) ₂][1-1-2,2,2-(CO) ₃ -closo-2,1,10-MnC ₂ B ₇ H ₈] (12)	1996 s, 1913 s	53.7 (54.0)	4.1 (4.2)	1.5 (1.5)
[N(PPh ₃) ₂][1-OH-6-1-2,2,2-(CO) ₃ -closo-2,1,10-MnC ₂ B ₇ H ₇] (13)	2000 s, 1915 s	53.2 (53.0)	4.2 (4.1)	1.4 (1.5)
[N(PPh ₃) ₂][1,6,9-I ₃ -2,2,2-(CO) ₃ -closo-2,1,10-MnC ₂ B ₇ H ₆] (14)	2012 s, 1937 s	42.8 (42.3)	3.2 (3.1)	1.3 (1.2)
[N(PPh ₃) ₂][2,2,2-(CO) ₃ -closo-2,1,10-MnC ₂ B ₇ H ₉] (15)	1989 s, 1899 s	62.4 (62.6)	5.2 (5.0)	1.8 (1.8)
[N(PPh ₃) ₂][6,9-(<i>p</i> -tol) ₂ -2,2,2-(CO) ₃ -closo-2,1,10-MnC ₂ B ₇ H ₇] (16)	1988 s, 1899 s	68.3 (68.3)	5.3 (5.3)	1.6 (1.4)
[6,9-(<i>p</i> -tol) ₂ -2,2-(CO) ₂ -2-NO-closo-2,1,10-MnC ₂ B ₇ H ₇] (17)	2083 s, 2041 s	50.2 (50.3)	4.7 (4.9)	3.2 (3.3)

^a All compounds are yellow, except **2** and **8** (orange), and **3** (red). ^b Measured in CH₂Cl₂; a broad, medium-intensity band observed at ca. 2500–2550 cm⁻¹ in the spectra of all compounds is due to B–H absorptions. In addition, $\nu_{\max}(\text{NO})/\text{cm}^{-1}$: for **2**, 1812 s; for **3**, 1761 s; for **17**, 1814 s. ^c Calculated values are given in parentheses. ^d Crystallizes with 1 molar equiv of H₂O.

structures. It is to be expected that the C atoms occupy the antipodal, 4-connected 1- and 10-positions, while the metal center resides in its preferred 5-connectivity site (all eight such sites being otherwise equivalent in the 10-vertex polyhedron).²⁴ As the cage-containing portion of **1** is anionic, there is of course no hydrogen bonding involving the cluster-bound hydroxyl group, but neutral **2** does display this feature. However, the latter interaction is very weak.²⁵ donor⋯acceptor distances are more than 2.9 Å and the donor⋯H⋯acceptor angle is close to linear.

Synthesis and Reactivity of Cage-Substituted Zwitterionic Species. An alternative protocol for converting the anionic cluster in **1** to a neutral species that might be amenable to substitution of Mn-bound CO involves protonation in the presence of a suitable donor ligand. This procedure in related systems¹ typically results in boron-bound hydride abstraction (the hydride combines with a proton to eliminate H₂) and then attachment of the donor moiety to the denuded boron vertex. Thus, compound **1** was dissolved in SMe₂ and CF₃SO₃H was added, giving a neutral product that incorporates a SMe₂ molecule. Similar reactions with other dialkyl sulfides SR₂ gave apparently analogous products. In the present system, however, boron-substituted species generally were not obtained, and instead the compounds formed are [1-SR₂-2,2,2-(CO)₃-closo-2,1,10-MnC₂B₇H₈] [R = Me (**4**); SR₂ = S(CH₂)₄ (**5**); R = {CH₂CH=CH₂} (**6**)], in which the SR₂ unit has subrogated the C_{cage}-bound hydroxyl moiety (Chart 2). Only in the reaction using tetrahydrothiophene was B-substitution observed, giving [1-OH-6-{S(CH₂)₄}-2,2,2-(CO)₃-closo-2,1,10-MnC₂B₇H₇] (**7**; see Chart 2) as a second product.

The formation of compounds **4–6** is readily understood in terms of the mechanism represented in Scheme 1. Species **A** (corresponding to the anion of compound **1**) evidently preferentially undergoes protonation at the C_{cage}-bound hydroxyl group to give zwitterion **B**, which contains an OH₂ ligand bonded to the cluster carbon vertex. The water molecule is readily lost to give a vacancy at the C_{cage} atom (intermediate **C**), and this site

is then occupied by an incoming SR₂ molecule (**D**, corresponding to compounds **4–6**). It is not clear why the S(CH₂)₄ system is the only one to give a B-substituted product (**7**), although it may be speculated that such compounds are indeed also formed alongside **4** or **6** but in lesser quantities and hence are not detected. In this connection we note that in a related molybdenacarborane–thioether system some discrimination in reactivity and product ratios was also observed between different SR₂ substrates.²⁶

The spectroscopic properties of compounds **4–7** are straightforward. In their ¹H and ¹³C{¹H} NMR spectra, signals are seen in characteristic positions for the R groups of their SR₂ moieties, while the loss of the terminal hydroxyl group from the cage carbon vertex in **4–6** was immediately evident from the ¹³C chemical shift of that vertex, as the cage {CS} group resonates some 75 ppm to higher field. These three compounds also retain mirror symmetry, reflected in their ¹¹B{¹H} NMR spectra having only four peaks in the ratio 2:1:2:2. In contrast, compound **7** has molecular C₁ symmetry, as confirmed by seven separate signals in the corresponding spectrum. Of these, one at δ 1.0 remains a singlet upon retention of proton coupling and hence could be identified as a B–S(CH₂)₄-substituted vertex.

An X-ray diffraction study upon **7** revealed the molecular structure shown in Figure 2, definitively establishing that the tetrahydrothiophene ligand is clearly seen to be bonded to B(6), which lies in the upper {B₄} “belt” and is adjacent to the metal center. As B(6) resides off the notional mirror plane of the {MnC₂B₇} cluster, the whole molecule is rendered asymmetric, in agreement with the spectroscopic data.

Having obtained neutral products in the form of compounds **4–6**, the possibility of replacing one of the Mn-bound CO ligands was investigated by treatment of **4** with SMe₂ in the presence of Me₃NO, which successfully yielded the disubstituted species [1,2-(SMe₂)₂-2,2-(CO)₂-closo-2,1,10-MnC₂B₇H₈] (**8**; see Chart 2). An X-ray diffraction study (Figure 3) confirmed the sites of attachment of the two SMe₂ ligands as being the manganese center and the adjacent cluster carbon vertex. Perhaps more importantly, the presence of the latter C–SMe₂ functionality in **8** also serves to verify the presence of such a unit in the

(24) (a) Williams, R. E. *Adv. Inorg. Chem. Radiochem.* **1976**, *18*, 67. (b) Jemmis, E. D. *J. Am. Chem. Soc.* **1982**, *104*, 7017. (c) Ott, J. J.; Gimarc, B. M. *J. Am. Chem. Soc.* **1986**, *108*, 4303.

(25) Gilli, P.; Bertolasi, V.; Ferretti, V.; Gilli, G. *J. Am. Chem. Soc.* **1994**, *116*, 909.

(26) Du, S.; Kautz, J. A.; McGrath, T. D.; Stone, F. G. A. *J. Chem. Soc., Dalton Trans.* **2001**, 1846.

Table 2. ^1H , ^{13}C , ^{11}B , and ^{31}P NMR Data^a

compd	$^1\text{H}/\delta^b$	$^{13}\text{C}/\delta^c$	$^{11}\text{B}/\delta^d$
1	7.65–7.47 (m, 30H, Ph), 5.64 (br s, 1H, cage CH), 4.89 (s, 1H, cage COH)	226.0 (MnCO), 180.2 (br, cage CO), 133.9–126.5 (Ph), 75.0 (br, cage CH)	1.4, –4.8 (2B), –18.0 (2B), –23.8 (2B)
2	6.49 (br, 1H, cage CH), 5.92 (s, 1H, COH)	221.9 (CO), 182.3 (br, cage CO), 86.0 (br, cage CH)	12.0, 1.4 (2B), –11.6 (2B), –21.2 (2B)
3	6.35 (br, 1H, cage CH), 5.31 (s, 1H, COH), 1.97 (m, 6H, CH_2), 1.18 (m, 9H, CH_3)	228.1 (d, $J(\text{PC}) = 37$, CO), 185.7 (br, cage CO), 84.5 (br, cage CH), 18.7 (d, $J(\text{PC}) = 26$, PCH_2), 7.3 (CH_3)	6.5, 1.0, 0.1, –12.2, –13.5, –21.2 (2B)
4	7.26 (br s, 1H, cage CH), 3.33 (s, 6H, CH_3)	222.0 (CO), 108.2 (br, cage CS), 107.7 (br, cage CH), 32.0 (s, CH_3)	3.0 (2B), 1.0, –16.0 (2B), –20.9 (2B)
5	7.22 (br s, 1H, cage CH), 4.15, 3.94 (m \times 2, 2H \times 2, SCH_2), 2.54, 2.34 (m \times 2, 2H \times 2, CH_2)	221.9 (CO), 110.6 (br, cage CS), 106.7 (br, cage CH), 50.1 (SCH_2), 29.1 (CH_2)	3.0 (2B), 0.9, –15.3 (2B), –20.9 (2B)
6	6.88 (br s, 1H, cage CH), 5.66 (m, 2H, $=\text{CH}$), 5.31, 5.27 (m \times 2, 2 \times 2H, $=\text{CH}_2$), 4.00 (m, 4H, SCH_2)	221.7 (CO), 127.0 ($=\text{CH}_2$), 125.2 ($=\text{CH}$), 107.8 (br, cage CS), 106.3 (br, cage CH), 48.4 (SCH_2)	2.9 (2B), 0.8, –15.7 (2B), –20.7 (2B)
7	5.64 (br, 1H, cage CH), 4.28 (br, 1H, cage COH), 3.40 (br, 3 \times 1H, SCH_2), 3.06 (br, 1H, SCH_2), 2.12 (br, 4 \times 1H, CH_2)	223.1 (CO), 185.1 (br, cage CO), 68.1 (br, cage CH), 43.6, 41.2 ($\text{SCH}_2 \times 2$), 30.2, 30.1 ($\text{CH}_2 \times 2$)	4.7, 1.1 [B(6)], –0.5, –16.3, –18.5, –22.0, –24.1
8	7.04 (br s, 1H, cage CH), 3.32 (s, 6H, cage- SCH_3), 2.39 (s, 6H, Mn- SCH_3)	228.0 (CO), 108.3 (br, cage CS), 104.7 (br, cage CH), 31.6 (CH_3), 28.7 (CH_3)	4.0 (2B), –2.2, –17.6 (2B), –21.6 (2B)
9	7.65–7.46 (m, 30H, Ph), 6.25 (br s, 1H, cage CH), 2.68 (s, 3H, CH_3)	225.5 (CO), 133.8–126.5 (Ph), 109.4 (br, cage CS), 90.6 (br, cage CH), 23.5 (CH_3)	1.8, 0.0 (2B), –14.1 (2B), –21.5 (2B)
10	7.64–7.45 (m, 30H, Ph), 6.31 (br s, 1H, cage CH), 6.16 (m, 1H, $=\text{CH}$), 5.27 (m, 1H, $=\text{CH}_2$), 5.11 (m, 1H, $=\text{CH}_2$), 3.90 (m, SCH_2)	225.2 (CO), 135.5 ($=\text{CH}$), 133.8–126.5 (Ph), 115.8 ($=\text{CH}_2$), 113.4 (br, cage CS), 90.8 (br, cage C), 42.0 (SCH_2)	1.4, 0.1 (2B), –13.5 (2B), –21.4 (2B)
11	7.66–7.46 (m, 30H, Ph), 5.94 (br s, 1H, cage CH), 4.21 (m, 1H + 1H, $=\text{CH}$ and SCH_2), 4.00 (m, 1H, SCH_2), 2.86, 2.40 (m \times 2, 1H \times 2, $=\text{CH}_2$)	237.9 (CO), 231.3 (CO), 149.6 (br, cage CS), 133.8–126.5 (Ph), 84.7 (br, cage CH), 77.6 ($=\text{CH}$), 48.8 ($=\text{CH}_2$), 46.0 (SCH_2)	–2.0, –4.8, –6.9, –13.6, –14.9, –18.4, –20.2
12	7.65–7.46 (m, 30H, Ph), 6.77 (br, 1H, cage CH)	225.5 (CO), 133.8–126.5 (Ph), 95.3 (br, cage CH), 72.4 (br, cage CI)	7.4, 0.7 (2B), –13.7 (2B), –20.7 (2B)
13	7.63–7.46 (m, 30H, Ph), 5.66 (br s, 1H, cage COH), 4.82 (br s, 1H, cage CH)	225.0 (CO), 168.8 (br, cage COH), 133.8–126.5 (Ph), 78.2 (br, cage CH)	6.3, 0.7, –12.0 [B(6) + 1B], –16.5, –19.9, –21.4
14	7.66–7.24 (m, 30H, Ph), 6.67 (br, 1H, cage CH)	223.8 (CO), 133.8–126.5 (Ph), 99.0 (br, cage CH), 67.9 (br, cage CI)	13.5, –7.8 [2B, B(6,9)], –10.0 (2B), –17.8 (2B)
15	7.46–7.24 (m, 30H, Ph), 6.36 (br s, 1H, cage CH), 3.87 (br s, 1H, cage CH)	225.9 (CO), 134.3–125.9 (Ph), 106.3 (br, cage C), 93.5 (br, cage C)	0.0, –1.0 (2B), –19.6 (2B), –20.9 (2B)
16	7.62–6.98 (m, 38H, Ph and C_6H_4), 6.41, 4.00 (br s \times 2, 1H \times 2, cage CH \times 2), 2.25 (s, 6H, CH_3)	226.3 (CO), 135.3–126.4 (Ph and C_6H_4), 117.2 (br, B- C_6H_4), 108.4, 92.0 (br \times 2, cage CH \times 2), 20.9 (CH_3)	12.8 [2B, B(6,9)], 5.3, –17.0 (2B), –19.4 (2B)
17	7.67, 7.32 (br s \times 2, 1H \times 2, cage CH \times 2), 7.26–7.09 (m, 8H, C_6H_4), 2.30 (s, 6H, CH_3)	215.4 (CO), 138.6–127.6 (C_6H_4), 121.4 (br, cage C), 112.0 (br, B- C_6H_4), 100.5 (br, cage C), 21.8 (CH_3)	19.0 [2B, B(6,9)], 15.1, –12.0 (2B), –16.4 (2B)

^aChemical shifts (δ) in ppm, coupling constants (J) in hertz, measurements at ambient temperatures in CD_2Cl_2 . In addition: ^1H -decoupled ^{31}P chemical shifts (positive to high frequency of external 85% H_3PO_4): for **3**, δ 56.5; compounds **1**, **4**, **9–11**, and **12–16** show a singlet at δ 21.7 for the $[\text{N}(\text{PPh}_3)_2]^+$ cation. ^bResonances for terminal BH protons occur as broad unresolved signals in the range δ ca. –1 to +3. ^c ^1H -decoupled chemical shifts are positive to high frequency of SiMe_4 . ^d ^1H -decoupled chemical shifts are positive to high frequency of $\text{BF}_3 \cdot \text{Et}_2\text{O}$ (external); resonances are of unit integral except where indicated.

precursor **4** and—by implication—the presence of similar moieties in compounds **5** and **6**. Spectroscopic data for **8** similarly are consistent with the determined solid-state structure.

The reaction forming **8** apparently was accompanied by another pathway that formed small quantities of a different manganacarborane derivative whose presence was evident in ^{11}B NMR spectra. The same species was formed exclusively and in far superior yield by treatment of **4** with Me_3NO alone, a process that gives the anion $[\text{1-SMe-2,2,2-(CO)}_3\text{-closo-2,1,10-MnC}_2\text{B}_7\text{H}_8]^-$. The latter was isolated as its $[\text{N}(\text{PPh}_3)_2]^+$ salt (**9**; Chart 1) following addition of $[\text{N}(\text{PPh}_3)_2]\text{Cl}$ and chromatography. Formal loss of the S-bound $\{\text{Me}^+\}$ group from the zwitterionic precursor **4** is simply explained in terms of the reaction sequence proposed in Scheme 2.²⁷ (There is some precedent for Me_3NO attack upon the carbon atom adjacent to a formally positively charged heteroatom—in this case sulfur—

attached to a metallacarborane zwitterion.²⁸) In the present mechanism, it is suggested that one of the Me groups in **E** (corresponding to **4**) is abstracted by Me_3NO , giving **F** (the anion of compound **9**) plus “ $\{\text{MeO-NMe}_3\}^+$ ”: the latter fragment likely cleaves to release formaldehyde and the $[\text{NHMe}_3]^+$ cation.²⁸

A similar process to that which forms **9** from **4** occurred when compound **6** was treated with Me_3NO . This reaction was performed with the intention of removing an Mn-bound CO ligand to create a vacancy at the metal center that might become occupied by one of the pendant olefinic moieties of the sulfur-

(27) See also: McGrath, T. D.; Stone, F. G. A.; Sukcharoenphon, K. J. *Cluster Sci.* **2005**, *16*, 201.

(28) Du, S.; Franken, A.; Jelliss, P. A.; Kautz, J. A.; Stone, F. G. A.; Yu, P.-Y. *J. Chem. Soc., Dalton Trans.* **2001**, 2791.

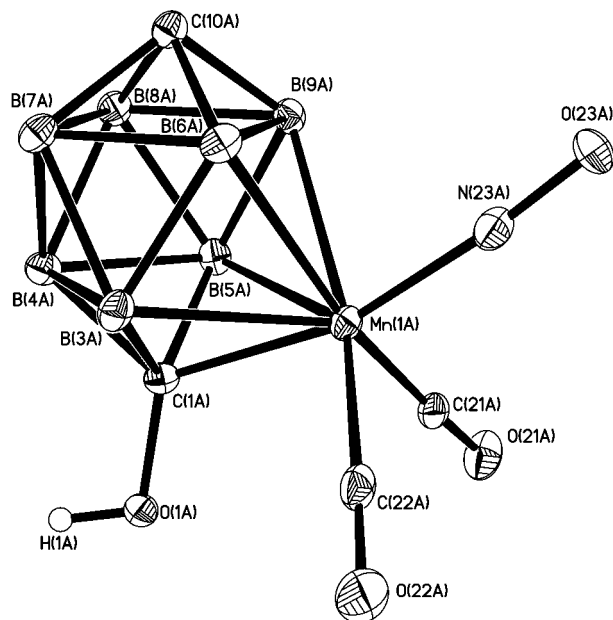


Figure 1. Structure of one of the crystallographically independent molecules of compound **2** showing the crystallographic labeling scheme. In this and subsequent figures, thermal ellipsoids are shown at 40% probability, and only hydroxyl H atoms are shown. Selected distances (Å) and angles (deg): Mn(1A)–C(21A) 1.847(3), Mn(1A)–C(22A) 1.866(3), Mn(1A)–N(23A) 1.696(3), Mn(1A)–C(1A) 1.998(3), O(1A)–C(1A) 1.401(3); N(23A)–Mn(1A)–C(1A) 164.82(12), O(1A)–C(1A)–Mn(1A) 120.08(19).

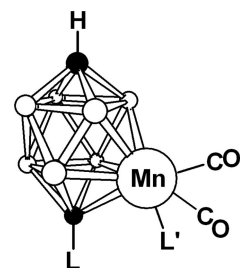
bound allyl groups. Instead, the reaction gave two anions: these are $[1-\{\text{SCH}_2\text{CH}=\text{CH}_2\}-2,2,2-(\text{CO})_3\text{-}closo\text{-}2,1,10\text{-MnC}_2\text{B}_7\text{H}_8]^-$, presumably formed by a process exactly analogous to that depicted in Scheme 2, and $[1,2-\sigma:\eta^2-\{\text{SCH}_2\text{CH}=\text{CH}_2\}-2,2-(\text{CO})_3\text{-}closo\text{-}2,1,10\text{-MnC}_2\text{B}_7\text{H}_8]^-$, assumed to result from first CO removal and olefin coordination and then Me_3NO attack upon the dangling (noncoordinated) propenyl unit (again, similar to the hydrocarbyl removal in Scheme 2). Both anions were isolated as their $[\text{N}(\text{PPh}_3)_2]^+$ salts **10** (see Chart 1) and **11** (Chart 2), respectively.

Both compounds **9** and **10** show the expected features in their IR and NMR spectroscopic data, and in particular integrated ^1H NMR spectra confirm the presence of an $[\text{N}(\text{PPh}_3)_2]^+$ cation and a cage–SR group in the ratio 1:1, indicating the loss of one R group from sulfur in each case and formation of a monoanionic cluster. Notably also, the CO stretching frequencies in **9** and **10** are similar to those in the parent compound **1**, again substantiating their anionic nature and, moreover, confirming that **6** (rather than **10**) is the precursor to compound **11**: it would be unlikely that $\text{CO} \rightarrow \{\text{olefin}\}$ substitution could occur in anionic **10** but rather must occur from neutral **6** prior to excision of the allyl unit.

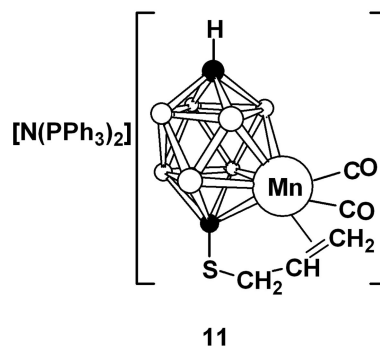
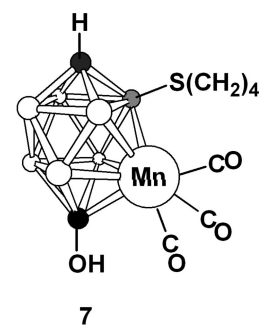
Initial structural characterization of **11** and confirmation that the S–allyl group was η^2 -bound to manganese was provided by an X-ray diffraction study, which afforded the structure shown in Figure 4. The $\eta^2\text{-}\{\text{C}(5)=\text{C}(6)\}$ unit ligating Mn is clearly seen [$\text{Mn}(2)\text{-C}(5) = 2.193(4)$, $\text{Mn}(2)\text{-C}(6) = 2.154(4)$, $\text{C}(5)\text{-C}(6) = 1.398(6)$ Å] and is typical in its geometry; we note that such complexes are relatively rare in Mn(I) chemistry,^{22a,c,29} and in this

(29) See, for example, together with references therein: McDaniel, K. F. In *Comprehensive Organometallic Chemistry II*; Abel, E. W., Stone, F. G. A., Wilkinson, G., Eds.; Pergamon Press: Oxford, U.K., 1995; Vol. 6, Chapter 4.

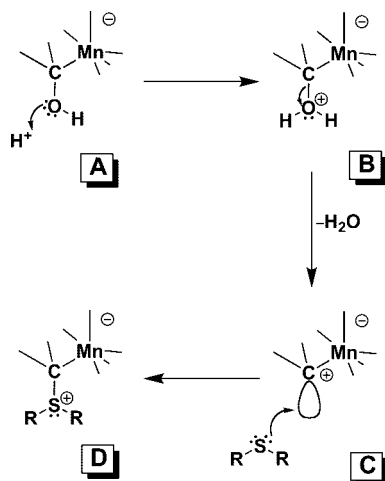
Chart 2



L	L'	
4	SMe_2	CO
5	$\text{S}(\text{CH}_2)_4$	CO
6	$\text{S}(\text{CH}_2\text{CH}=\text{CH}_2)_2$	CO
8	SMe_2	SMe_2



case moreover the π -bound alkene unit forms part of an intramolecular ring. The anion of **11** also constitutes an anionic relative of a similar, but neutral, $\text{Fe}-(\eta^2\text{-olefin})$ species derived from the iron analogue of **1**, but which instead contains an intramolecular ring derived from a pendant O–allyl moiety.¹⁵ Spectroscopic data for compound **11** are fully in agreement with the solid-state structure. Specifically, significant changes in the ^1H and ^{13}C chemical shifts of the olefinic unit are evident upon coordination to the metal center compared with the corresponding data for the noncoordinated moiety in the anion of **10**. In addition, attachment of this unit to manganese renders the whole anion asymmetric: consistent with this, the $^{11}\text{B}\{^1\text{H}\}$ NMR spectrum shows seven resonances of unit integral, rather than the 1:2:2:2 intensity pattern seen in the mirror-symmetric clusters in **6** and **10**.

Scheme 1. Proposed Mechanism for the Conversion of the Anion of 1 to Compounds 4–6


Initial attempts to treat the anions of compounds **9–11** with Me^+ (using $\text{CF}_3\text{SO}_3\text{Me}$), with the intention of methylating the sulfur center, met with very limited success. Compound **9** does afford **4**, albeit in only very modest yield, but (for example) the same reactions of **10** and **11** give mixtures that contain species with cage- $\{\text{S}(\text{Me})\text{CH}_2\text{CH}=\text{CH}_2\}$ groups, along with other unidentified products. It is evident that the Me^+ (and presumably other electrophiles) do not attack exclusively at the sulfur, as might be expected given that the negative charge is likely localized over the whole cluster. Formation of compound **7**, after all, results from electrophilic attack upon a cluster boron atom.

Synthesis and Reactivity of Cage-Iodo-Substituted Derivatives. In contrast to the set of reactions ultimately forming compounds **4–11**, where (initially) protonation in the presence of donor molecules leads to neutral B-(ligand)- or C-(ligand)-substituted species, which could undergo subsequent derivatization, an alternative means of introducing cluster functionality is through treatment of the manganacarborane anion of **1** with

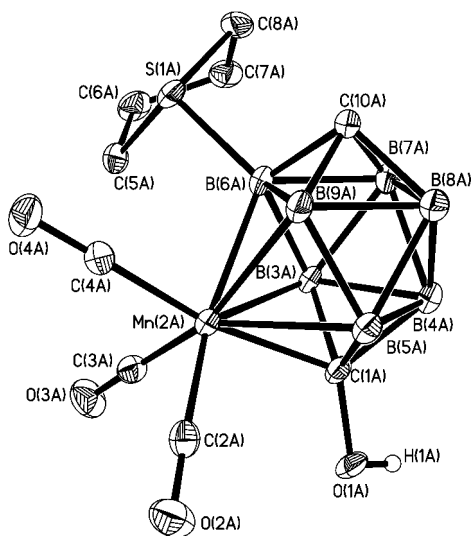


Figure 2. Structure of one of the crystallographically independent molecules of compound **7** showing the crystallographic labeling scheme. Selected distances (Å) and angles (deg): Mn(2A)–C(1A) 2.000(3), Mn(2A)–B(6A) 2.169(3), S(1A)–B(6A) 1.902(3), O(1A)–C(1A) 1.403(3); O(1A)–C(1A)–Mn(2A) 122.07(19), S(1A)–B(6A)–Mn(2A) 118.38(15).

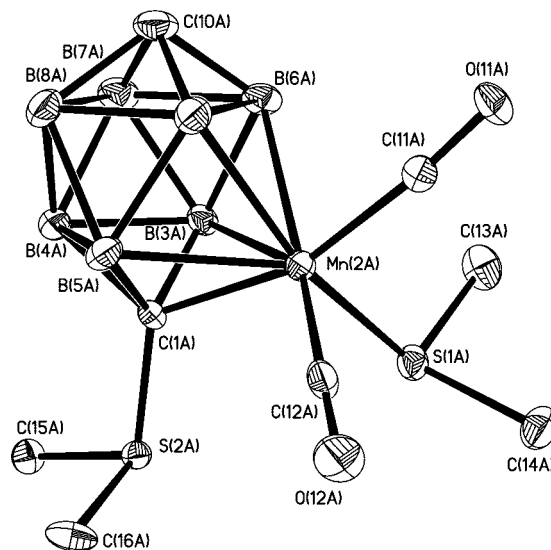
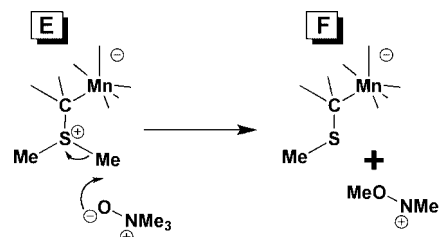


Figure 3. Structure of one of the crystallographically independent molecules of compound **8** showing the crystallographic labeling scheme. Selected distances (Å) and angles (deg): C(1A)–S(2A) 1.769(4), C(1A)–Mn(2A) 2.014(4), S(1A)–Mn(2A) 2.3069(13); S(2A)–C(1A)–Mn(2A) 119.4(2), C(1A)–Mn(2A)–S(1A) 95.81(11).

Scheme 2. Proposed Mechanism for the Conversion of 4 to the Anion of Compound 9


halogens. The latter methodology has been demonstrated¹⁸ to be useful in forming boron-substituted derivatives of the related, icosahedral manganacarborane anion $[\text{3,3,3-(CO)}_3\text{-}closo\text{-}3,1,2\text{-MnC}_2\text{B}_9\text{H}_{11}]^-$. (This relies on the relative immunity of the manganese(I) center in such species toward oxidation, an assumption that of course cannot always be made.³⁰) Typically such reactions with X_2 are envisaged to involve oxidative removal of a boron-bound hydride (formally giving $\text{HX} + \text{X}^-$), followed by immediate attachment to boron of the liberated X^- to give a B–X substituent.

Thus, treatment of compound **1** in CH_2Cl_2 with an equimolar amount of I_2 somewhat surprisingly gave a mixture of two different cage-iodo species. These are $[\text{N}(\text{PPh}_3)_2][1\text{-I-}2,2,2\text{-(CO)}_3\text{-}closo\text{-}2,1,10\text{-MnC}_2\text{B}_7\text{H}_8]$ (**12**; see Chart 1), where the iodine is bonded in place of the OH group at the cage carbon vertex, and $[\text{N}(\text{PPh}_3)_2][1\text{-OH-}6\text{-I-}2,2,2\text{-(CO)}_3\text{-}closo\text{-}2,1,10\text{-MnC}_2\text{B}_7\text{H}_7]$ (**13**; see Chart 3), where the iodine is bonded to a boron vertex. Whereas compound **13** can be described as the “expected” product [**B(6)** is intuitively the most likely site for boron substitution given the structure of compound **7**], formation of **12** may be understood in terms of a mechanism akin to that in Scheme 1 but with I^- (rather than SR_2) attacking intermediate **C** to give the anion of **12**. The acid that initially protonates the

(30) For example: Lu, X. L.; McGrath, T. D.; Stone, F. G. A. *Inorg. Chim. Acta* **2006**, *359*, 2665.

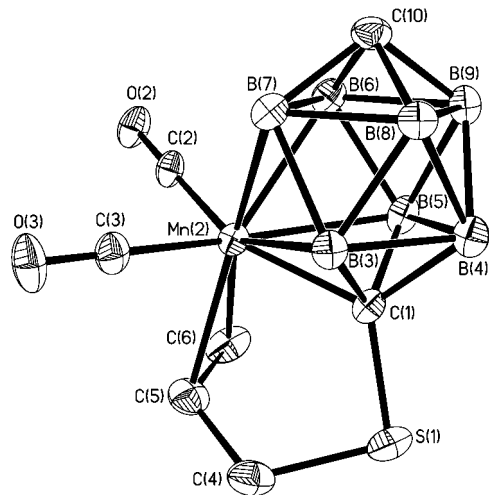


Figure 4. Structure of the anion of compound **11** showing the crystallographic labeling scheme. Selected distances (Å) and angles (deg): S(1)–C(1) 1.782(4), S(1)–C(4) 1.803(4), C(1)–Mn(2) 1.981(4), Mn(2)–C(5) 2.193(4), Mn(2)–C(6) 2.154(4), C(4)–C(5) 1.515(6), C(5)–C(6) 1.398(6); C(1)–S(1)–C(4) 94.94(19), S(1)–C(1)–Mn(2) 121.1(2), C(1)–Mn(2)–C(5) 83.92(16), C(1)–Mn(2)–C(6) 88.14(16), C(5)–C(4)–S(1) 111.8(3), C(6)–C(5)–C(4) 122.6(4), C(4)–C(5)–Mn(2) 109.6(3).

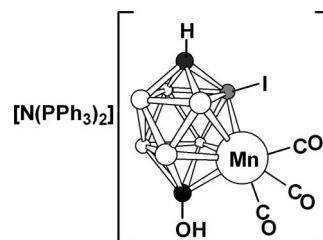
hydroxyl group presumably comes from the above-mentioned reaction of a cage B–H reacting with I₂ to give B–I plus HI.

Both compounds **12** and **13** were subjected to X-ray diffraction studies, which confirmed the site of iodine substitution in each case (see Figure 5). The spectroscopic data for the two species are fully in agreement with these determined structures, with—as would be expected—very simple spectra in each case. The presence of a cage-hydroxyl group in **13** but not in **12** is confirmed by a broad, low-field ¹³C resonance (δ 168.8) in the ¹³C{¹H} NMR spectrum of the former but not of the latter. The ¹¹B NMR spectra of the two are also informative: Whereas the ¹¹B{¹H} NMR spectrum of **12** reveals a 1:2:2:2 set of resonances, all of which become doublets upon retention of proton coupling, the corresponding spectrum for **13** contains seven separate signals (two coincide), of which one at δ –12.0 remains a singlet in the ¹¹B NMR spectrum. Thus the heteroborane cluster in **12** is symmetric and none of the boron vertices bears a substituent other than H, but the cage in **13** is asymmetric as a result of a B–iodo substituent at B(6), as seen in the molecular structures in Figure 5.

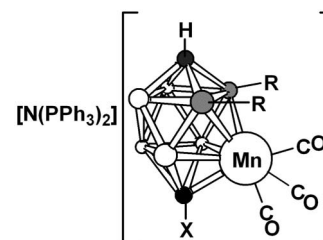
When the above reaction that formed **12** and **13** was carried out with an excess of I₂, a different product was obtained, namely, [N(PPh₃)₂][1,6,9-I₃-2,2,2-(CO)₃-*closo*-2,1,10-MnC₂B₇H₆] (**14**; Chart 3). Although crystals suitable for structural analysis could not be obtained, the composition of **14** was reasonably established by NMR spectroscopy. Specifically, ¹¹B NMR spectra indicated mirror symmetry but with double iodo substitution of the cluster, the substitution presumed to have taken place at B(6) and symmetry-equivalent B(9) given the site of the B–I unit in **13**. A third such substituent is located at C(1) (by analogy with **12**), as ¹H and ¹³C NMR data indicated a single {CH} vertex and that the second cage-carbon atom lacks a hydroxyl group and therefore must be {CI}. The structure of **16** (see below) also lends support to the formulation of **14**.

In seeking to demonstrate the utility of the cage–iodo functionalities of compounds **12**–**14** as a way of introducing other substituents to the manganacarborane cluster surface, a few selected reactions were carried out. In the present work, the substrates of choice were **12** and **14**, as they were formed

Chart 3

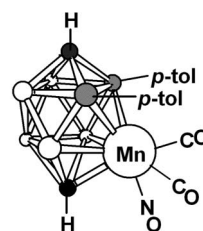


13



X R

14	I	I
16	H	<i>p</i> -tol



17

○ BH ● B ● C

in good yields. Several of the reactions attempted were unsuccessful or yielded mixtures, but two discussed below do demonstrate the problems and the potential of these systems. It was proposed that the C–I group in **12** might be susceptible to a coupling reaction of the Ullmann type³¹ upon treatment with Cu powder in DMF to afford a C(cage)–C(cage) dimeric species. However, evidently in this system the presence of trace amounts of H₂O was sufficient to interfere with the reaction and led to hydrolysis of the C(cage)–Cu intermediate,³¹ giving CuOH and the anion [2,2,2-(CO)₃-*closo*-2,1,10-MnC₂B₇H₆][–], isolated as the [N(PPh₃)₂]⁺ salt (**15**; Chart 1), as the only product. Spectroscopic characterization (Tables 1 and 2) and an X-ray diffraction study (Figure 6) all served to confirm the formulation of **15** as the unsubstituted cluster, which may be described as the hitherto unknown “parent” compound of all the species described herein.

As an alternative to the above, the B–I groups in compound **14** are also potentially susceptible to palladium-catalyzed “cross-

(31) (a) Ullmann, F.; Bielecki, J. *Chem. Ber.* **1901**, *34*, 2174. (b) Hassan, J.; Sevignon, M.; Gozzi, C.; Schulz, E.; Lemaire, M. *Chem. Rev.* **2002**, *102*, 1359.

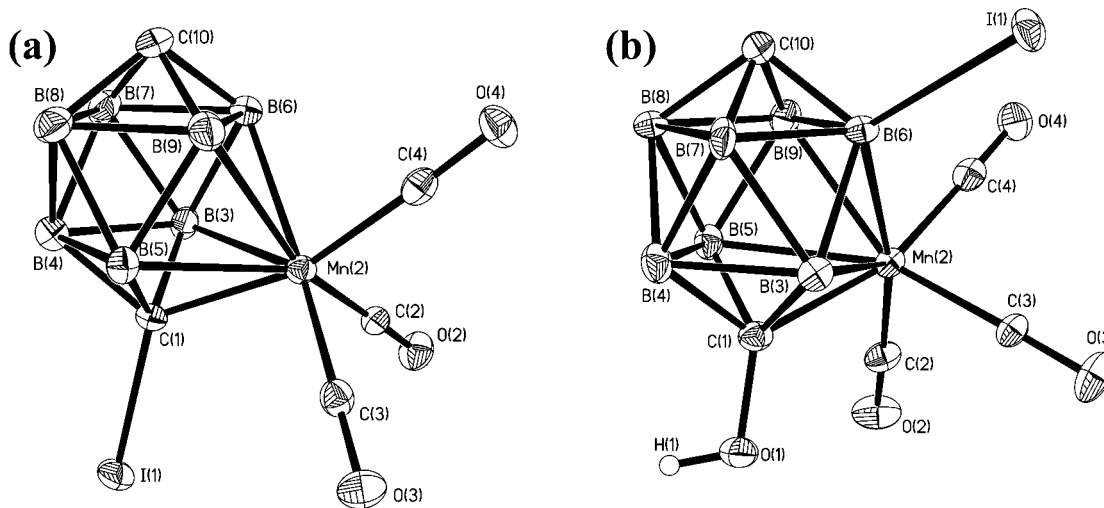


Figure 5. Structures of the anions of (a) compound **12** and (b) compound **13**, showing their crystallographic labeling schemes. Selected distances (Å) and angles (deg) are as follows. For **12**: I(1)–C(1) 2.124(3), Mn(2)–C(1) 1.998(3); Mn(2)–C(1)–I(1) 123.39(14). For **13**: B(6)–I(1) 2.270(6), C(1)–O(1) 1.402(6), Mn(2)–C(1) 1.998(5); O(1)–C(1)–Mn(2) 121.1(4), C(1)–Mn(2)–B(6) 83.0(2), Mn(2)–B(6)–I(1) 118.1(3).

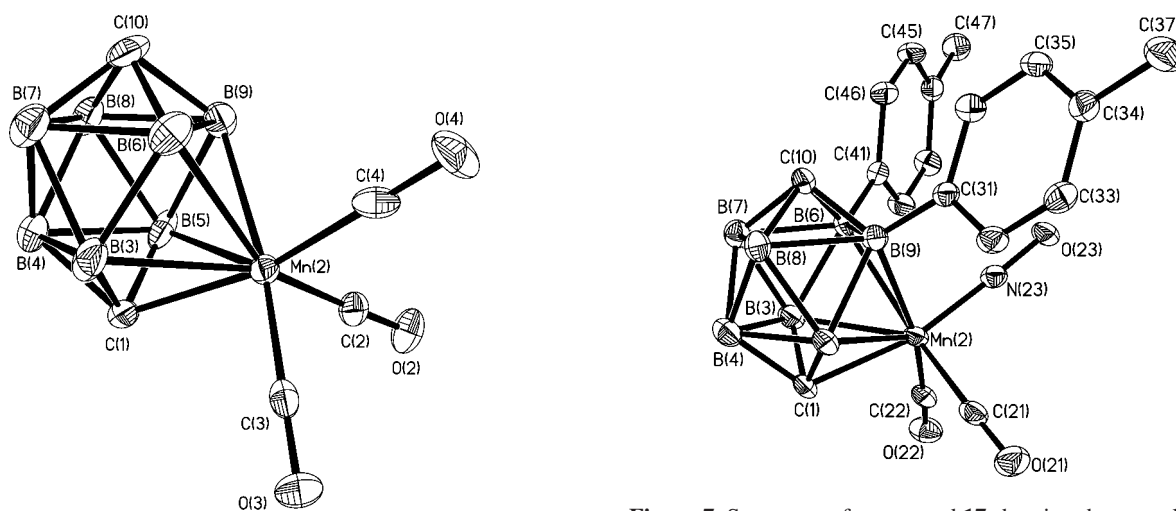


Figure 6. Structure of the anion of compound **15** showing the crystallographic labeling scheme. Selected distances (Å): Mn(2)–C(1) 2.002(5), Mn(2)–C(2) 1.796(5), Mn(2)–C(3) 1.796(5), Mn(2)–C(4) 1.777(5), Mn(2)–B(3) 2.241(6), Mn(2)–B(5) 2.228(6), Mn(2)–B(6) 2.205(6), Mn(2)–B(9) 2.195(6), B(6)⋯B(9) 1.920(9).

coupling” reactions with Grignard reagents, as has been used to form boron–carbon bonds in various cluster (hetero)boranes,³² including the 12-vertex analogues of **1** alluded to earlier.¹⁸ Thus, treatment of **14** in THF with a 10-fold excess of (*p*-tol)MgBr in the presence of [PdCl₂(PPh₃)₂] afforded [N(PPh₃)₂][6,9-(*p*-tol)₂-2,2,2-(CO)₃-*closo*-2,1,10-MnC₂B₇H₇] (**16**; see Chart 3), following standard acid workup and column chromatography. Similar to the formation of compound **15**, the loss of the cage {CI} group and its conversion to {CH} was again observed here, along with the two remaining {B–I} bonds being converted to {B–aryl} units. All these structural transformations were reasonably clear from spectroscopic data; crystals suitable for a definitive structural study could not be obtained until **16** was converted to the neutral nitrosyl derivative [6,9-(*p*-tol)₂-2,2-(CO)₂-2-NO-*closo*-2,1,10-MnC₂B₇H₇] (**17**; Chart 3) by a route parallel to that whereby **1** was converted to **2**.

Figure 7. Structures of compound **17** showing the crystallographic labeling scheme. Selected distances (Å) and angles (deg): Mn(2)–C(1) 2.014(3), Mn(2)–C(21) 1.851(4), Mn(2)–C(22) 1.847(4), Mn(2)–N(23) 1.677(3), Mn(2)–B(3) 2.255(5), Mn(2)–B(5) 2.250(4), Mn(2)–B(6) 2.277(4), Mn(2)–B(9) 2.273(4), B(6)–C(41) 1.568(5), B(9)–C(31) 1.557(5), B(6)⋯B(9) 2.047(6); N(23)–Mn(2)–C(1) 166.96(15), C(41)–B(6)–Mn(2) 117.4(3), C(31)–B(9)–Mn(2) 117.2(3).

The structure of **17** (Figure 7) confirms the B–I to B-(*p*-tol) conversion and loss of a substituent from C(1), while the siting of the aryl groups at both B(6) and B(9) maintains molecular symmetry within the cluster. Although the somewhat bulky tolyl moieties are bonded to adjacent boron atoms, and this interboron distance [B(6)⋯B(9) = 2.047(6) Å] is very long compared to other B⋯B separations in the molecule (ca. 1.77–1.86 Å), this elongation cannot be attributed to solely intramolecular crowding between the aryl substituents. The corresponding parameter in **2** is almost as large [1.994(5) Å], and indeed 10-vertex metalla(hetero)boranes with a metal center in the 2-position typically show such lengthening of this connectivity subtending the metal center. Spectroscopic data for **17** fully concur with the solid-state structure, while the data for **16** are similarly corroborative (and vice versa). The placing of the two boron

(32) For example: Barberà, G.; Vaca, A.; Teixidor, F.; Silanpää, R.; Kivekäs, R.; Viñas, C. *Inorg. Chem.* **2008**, *47*, 7309.

substituents in both **16** and **17** also substantiates the structure proposed for **14**.

Conclusions

The formation of the 10-vertex manganese–dicarbollide cluster in compound **1** from a monocarbon precursor, [*closo*-1-CB₇H₈][−], and [Mn₂(CO)₁₀] provides an *anionic* {MnC₂B₇} species that offers several similarities and contrasts when compared with the analogous, *neutral* {FeC₂B₇} compound obtained from the same carborane substrate and [Fe₂(CO)₉].^{14,15} Most importantly, the reactivity of the manganese species differs distinctly from the iron complex in several respects, some of which have been discussed here. Moreover, the demonstration that **1** itself can very straightforwardly and cleanly be synthesized by photochemical means rather than a thermal reaction augurs well for the applicability of this synthetic methodology to other metallacarborane systems, an area where this technique has traditionally been little used.⁷

In the present system, the pendant cage–OH group in the title compound again serves as a point where cluster functionalization can be achieved. Through protonation at this site, H₂O as a labile leaving group is generated and may be replaced by other donor species, demonstrated in this case for dialkylsulfide molecules and for the iodide anion. Conversely, iodination can also take place at cluster boron atoms by straightforward treatment with I₂. All of these compounds represent potential starting points for further derivatization, such as in the formation of **16** from **14** by reaction with a Grignard reagent. The new complexes presented herein are representatives of the relatively under-represented class of subicosahedral metallacarboranes; indeed, we believe these to be the first examples of 10-vertex manganese–dicarbollide species. We are actively pursuing in various directions the chemistry of these and related clusters.³³

Experimental Section

General Considerations. All reactions were carried out under an atmosphere of dry nitrogen using Schlenk line techniques, with photochemical syntheses carried out in a water-cooled photolysis cell, using a 350 W mercury vapor arc lamp for irradiation. Solvents were distilled from appropriate drying agents under nitrogen prior to use. Petroleum ether refers to that fraction of boiling point 40–60 °C. Chromatography columns (typically ca. 10–15 cm in length and ca. 2 cm in diameter) were packed with silica gel (Acros, 60–200 mesh). NMR spectra were recorded at the following frequencies (MHz): ¹H, 360.13; ¹³C, 90.56; ¹¹B, 115.5; and ³¹P 145.78. The compound [NBuⁿ][*closo*-1-CB₇H₈] was synthesized according to the literature method;¹³ all other materials were used as received.

Synthesis of [N(PPh₃)₂][1-OH-2,2,2-(CO)₃-*closo*-2,1,10-MnC₂B₇H₈] (1**).** The carborane salt [NBuⁿ][*closo*-1-CB₇H₈] (0.20 g, ca. 0.6 mmol) was dissolved in THF (20 mL), [Mn₂(CO)₁₀] (1.0 g, 2.6 mmol) was added, and the mixture was heated to reflux temperature for 48 h. After cooling to ambient temperature, solid [N(PPh₃)₂]Cl (0.50 g, 0.87 mmol) was added and solvent was removed under reduced pressure. The residue was dissolved in neat CH₂Cl₂ (5 mL) and applied to a chromatography column. Eluting with CH₂Cl₂–petroleum ether (4:1) gave first an orange band of unreacted [Mn₂(CO)₁₀] followed by a yellow fraction. Removal of solvents from the latter in vacuo yielded yellow microcrystals of **1** (0.42 g, 87%).

A similar reaction conducted for 2 h at room temperature under ultraviolet irradiation, rather than at reflux temperature, with identical workup, afforded **1** in comparable yields.

Synthesis of [1-OH-2,2-(CO)₂-2-NO-*closo*-2,1,10-MnC₂B₇H₈] (2**).** Compound **1** (ca. 0.4 g, 0.5 mmol) was dissolved in CH₂Cl₂ (20 mL), NOBF₄ (ca. 0.06 g, 0.52 mmol) was added, and the mixture was stirred at ambient temperature for 2 h. Solvent was removed in vacuo, and the residue was dissolved in CH₂Cl₂–petroleum ether (4:1) and transferred to the top of a chromatography column. Elution with the same mixture gave an orange fraction, from which removal of solvents in vacuo yielded orange microcrystals of **2** (0.06 g, 42%).

Synthesis of [1-OH-2-CO-2-NO-2-PEt₃-*closo*-2,1,10-MnC₂B₇H₈] (3**).** Compound **2** (ca. 0.07 g, 0.25 mmol) was dissolved in CH₂Cl₂ (10 mL), PEt₃ (0.25 mL, 1.7 mmol) and Me₃NO (ca. 0.025 g, 0.33 mmol) were added, and the resulting mixture was stirred at ambient temperature for 3 h. After removal of volatiles in vacuo, the residue was dissolved in CH₂Cl₂–petroleum ether (3:2, 2 mL) and transferred to the top of a chromatography column. Elution with the same solvent mixture yielded a red fraction. Removal of solvent from the latter gave red microcrystals of **3** (ca. 0.06 g, 67%).

Synthesis of C_{cage}-Dialkylsulfide-Substituted Compounds. (i) Compound **1** (ca. 0.4 g, 0.5 mmol) was suspended in SME₂ (20 mL), and CF₃SO₃H (ca. 0.14 mL, 2 mmol) was added. After stirring at ambient temperature for 2 h, volatiles were removed in vacuo, and the residue was dissolved in CH₂Cl₂–petroleum ether (4:1, 2 mL) and transferred to the top of a chromatography column. Elution with the same solvent mixture gave a yellow fraction, from which removal of solvent yielded yellow microcrystals of [1-SMe₂-2,2,2-(CO)₃-*closo*-2,1,10-MnC₂B₇H₈] (**4**; 0.12 g, 79%).

(ii) Compound **1** (ca. 0.4 g, 0.5 mmol) was dissolved in CH₂Cl₂ (20 mL), S(CH₂)₄ (1 mL, ca. 12 mmol) and CF₃SO₃H (ca. 0.14 mL, 2 mmol) were added, and the resultant mixture was stirred at ambient temperature for 2 h. Volatiles were removed in vacuo, and the residue was dissolved in CH₂Cl₂ (5 mL) and applied to a chromatography column. Elution with CH₂Cl₂ gave two yellow fractions, removal of solvent from which afforded yellow microcrystals of [1-{S(CH₂)₄}-2,2,2-(CO)₃-*closo*-2,1,10-MnC₂B₇H₈] (**5**; 0.12 g, 43%) and [1-OH-6-{S(CH₂)₄}-2,2,2-(CO)₃-*closo*-2,1,10-MnC₂B₇H₇] (**7**; 0.07 g, 32%), respectively.

(iii) Similarly, compound **1** (ca. 0.4 g, 0.5 mmol) in CH₂Cl₂ (20 mL) with S(CH₂CH=CH₂)₂ (0.64 mL, 5 mmol) and CF₃SO₃H (ca. 0.35 mL, 5 mmol), and using CH₂Cl₂–petroleum ether (4:1) as chromatographic eluent, yielded yellow microcrystals of [1-{S(CH₂CH=CH₂)₂}-2,2,2-(CO)₃-*closo*-2,1,10-MnC₂B₇H₈] (**6**; 0.13 g, 72%) as the sole product.

Reactions of Compound 4. (i) Compound **4** (ca. 0.15 g, 0.5 mmol) was dissolved in SME₂ (20 mL), Me₃NO (0.1 g, 1.3 mmol) was added, and the mixture was stirred at ambient temperature for 48 h. Excess SME₂ was removed in vacuo, and the residue was dissolved in CH₂Cl₂–petroleum ether (4:1; 2 mL) and transferred to the top of a chromatography column. Elution with the same solvent mixture yielded an orange fraction, from which removal of solvent yielded orange microcrystals of [1,2-(SME₂)₂-2,2-(CO)₂-*closo*-2,1,10-MnC₂B₇H₈] (**8**; 0.10 g, 63%).

(ii) Compound **4** (ca. 0.15 g, 0.5 mmol) was dissolved in CH₂Cl₂ (30 mL), and Me₃NO (0.1 g, 1.3 mmol) was added. After stirring at ambient temperature for 48 h, solid [N(PPh₃)₂]Cl (ca. 0.5 g, 0.87 mmol) was added, solvent was evaporated, and the residue was worked up as above to give yellow microcrystals of [N(PPh₃)₂][1-SMe₂-2,2,2-(CO)₃-*closo*-2,1,10-MnC₂B₇H₈] (**9**; 0.13 g, 32%).

Synthesis of [N(PPh₃)₂][1-{SCH₂CH=CH₂}-2,2,2-(CO)₃-*closo*-2,1,10-MnC₂B₇H₈] (10**) and [N(PPh₃)₂][1,2-σ-η²-{SCH₂CH=CH₂}-2,2-(CO)₂-*closo*-2,1,10-MnC₂B₇H₈] (**11**).** Compound **6** (ca. 0.18 g, 0.5 mmol) was dissolved in CH₂Cl₂ (20 mL), Me₃NO (0.2 g, 2.6 mmol) was added, and the mixture was stirred at ambient temperature for 48 h. After addition of [N(PPh₃)₂]Cl (ca. 0.5 g,

(33) Franken, A.; McGrath, T. D.; Stone, F. G. A. *Organometallics* (to be submitted).

Table 3. Crystallographic Data for Compounds **2**, **7**, **8**, **11–13**, **15**, and **17**

	2	7	8	11	12	13	15	17
formula	C ₄ H ₉ B ₇ MnNO ₄	C ₉ H ₁₆ B ₇ MnO ₄ S	C ₈ H ₂₀ B ₇ MnO ₂ S ₂	C ₄₃ H ₄₃ B ₇ MnNO ₂ P ₂ S	C ₄₁ H ₃₈ B ₇ MnNO ₃ P ₂	C ₄₁ H ₃₈ B ₇ MnNO ₄ P ₂	C ₄₁ H ₃₀ B ₇ MnNO ₃ P ₂	C ₁₈ H ₂₁ B ₇ MnNO ₃
fw	265.73	350.89	342.97	830.39	912.17	928.17	786.28	429.97
space group	P $\bar{1}$	P $\bar{1}$	P ₂ ,1,2,1	P ₂ /n	P ₂ /c	P ₂ /c	Pna2 ₁	C2/c
<i>a</i> , Å	7.4747(5)	9.0050(17)	9.055(3)	21.415(5)	13.3510(8)	17.504(3)	20.6834(18)	29.280(4)
<i>b</i> , Å	11.5795(8)	13.270(3)	10.809(4)	8.8603(19)	18.0201(10)	13.850(2)	17.0989(15)	7.7347(13)
<i>c</i> , Å	19.5413(15)	15.186(3)	33.451(10)	24.050(4)	17.4096(10)	17.354(3)	11.0349(9)	22.093(3)
α , deg	86.705(2)	64.723(7)	90	90	90	90	90	90
β , deg	82.216(2)	74.152(7)	90	109.469(10)	96.236(2)	95.498(4)	90	124.244(4)
γ , deg	89.562(2)	72.321(8)	90	90	90	90	90	90
<i>V</i> , Å ³	1673.0(2)	1541.6(5)	3274.0(19)	4302.4(15)	4163.7(4)	4187.7(11)	3902.6(6)	4136.1(10)
Z	6	4	8	4	4	4	4	8
ρ_{calcd} , g cm ⁻³	1.583	1.512	1.392	1.282	1.455	1.472	1.338	1.381
μ (Mo K α), mm ⁻¹	1.172	0.997	1.051	0.467	1.175	1.171	0.461	0.658
no. of rflns measd	29 718	23 999	27 205	39 135	49 862	44 368	35 961	14 998
no. of indep rflns	6069	8063	7069	8033	11 551	7593	7307	4227
<i>R</i> _{int}	0.0633	0.0493	0.0905	0.1199	0.0717	0.0690	0.0957	0.0847
<i>wR</i> ₂ , <i>R</i> ₁ ^a (all data)	0.0861, 0.0601	0.1118, 0.0917	0.0929, 0.0624	0.1267, 0.1129	0.0946, 0.0809	0.1245, 0.0726	0.1185, 0.0799	0.1133, 0.1175
<i>wR</i> ₂ , <i>R</i> ₁ (obsd ^b data)	0.0767, 0.0374	0.0960, 0.0511	0.0848, 0.0453	0.1101, 0.0599	0.0801, 0.0448	0.1133, 0.0502	0.1061, 0.0531	0.0938, 0.0554

^a $wR_2 = [\sum\{w(F_o^2 - F_c^2)^2\}/\sum\{w(F_o^2)^2\}]^{1/2}$; $R_1 = \sum|F_o| - |F_c|/\sum|F_o|$. ^b $F_o > 4\sigma(F_o)$. ^c Flack absolute structure parameter (*x*):³⁴ for **8**, -0.03(2); for **15**, 0.02(2).

0.87 mmol) and removal of solvent in vacuo, the residue was dissolved in CH₂Cl₂ and applied to a chromatography column. Elution with the same solvent successively gave two yellow fractions. Removal of solvent from each yielded yellow microcrystals of **10** (0.14 g, 32%) and **11** (0.18 g, 44%), respectively.

Reactions of 1 with Iodine. (i) Compound **1** (ca. 0.4 g, 0.5 mmol) was dissolved in CH₂Cl₂ (20 mL), and I₂ (ca. 0.13 g, 0.5 mmol) was added. After stirring at ambient temperature for 1 h, volatiles were removed in vacuo and the residue was dissolved in CH₂Cl₂ (5 mL) and transferred to the top of a chromatography column. Elution with CH₂Cl₂ gave two yellow fractions. Removal of solvent from these yielded [N(PPh₃)₂][1-I-2,2,2-(CO)₃-*closo*-2,1,10-MnC₂B₇H₈] (**12**; 0.25 g, 54%) and [N(PPh₃)₂][1-OH-6-I-2,2,2-(CO)₃-*closo*-2,1,10-MnC₂B₇H₇] (**13**; 0.13 g, 27%), respectively, as yellow microcrystals.

(ii) Compound **1** (ca. 0.4 g, 0.5 mmol) was dissolved in CH₂Cl₂ (20 mL), I₂ (ca. 1.0 g, 4 mmol) was added, and the mixture was stirred at ambient temperature for 1 h. Thereafter, H₂O (40 mL) and Na₂S₂O₃ (ca. 0.5 g, 4 mmol) were added to the reaction mixture, and the two-phase system was shaken vigorously to reduce the excess I₂. The organic layer was separated, the aqueous layer was extracted with CH₂Cl₂ (2 × 30 mL), and the combined yellow CH₂Cl₂ extracts were evaporated under reduced pressure. The resulting solid was dissolved in CH₂Cl₂ (5 mL) and transferred to the top of a chromatography column. Elution with CH₂Cl₂ gave a yellow fraction, removal of solvent from which yielded yellow microcrystals of [N(PPh₃)₂][1,6,9-I₃-2,2,2-(CO)₃-*closo*-2,1,10-MnC₂B₇H₆] (**14**; 0.48 g, 82%).

Reactions of the Iodinated Species. (i) To a solution of compound **12** (ca. 0.23 g, 0.25 mmol) in DMF (10 mL) was added Cu powder (0.2 g, 3.1 mmol), and the mixture was heated to reflux for 18 h. The suspension was cooled and filtered, and the filtrate was evaporated under reduced pressure to give a dark orange residue. The latter was dissolved in CH₂Cl₂-petroleum ether (4:1, 5 mL) and applied to a chromatography column. Elution with the same solvent mixture gave a yellow fraction, removal of solvent from which yielded yellow microcrystals of [N(PPh₃)₂][2,2,2-(CO)₃-*closo*-2,1,10-MnC₂B₇H₉] (**15**; 0.11 g, 54%).

(ii) Compound **14** (ca. 0.29 g, 0.25 mmol) was dissolved in THF (10 mL), (*p*-tol)MgBr (2.5 mL of a 1.0 M solution in Et₂O, 2.5 mmol) and [PdCl₂(PPh₃)₂] (20 mg, 0.03 mmol) were added, and the solution was stirred at room temperature for 18 h. The reaction mixture was cooled to 0 °C and quenched by dropwise addition of 5% HCl (40 mL), and the THF was removed under reduced pressure. The remaining aqueous solution was extracted with CH₂Cl₂ (3 × 10 mL), and the combined extracts were evaporated. The remaining residue was taken up in CH₂Cl₂-petroleum ether

(4:1, 5 mL) and transferred to the top of a chromatography column. Elution with the same solvent mixture gave a yellow fraction, from which were obtained, upon removal of solvent in vacuo, yellow microcrystals of [N(PPh₃)₂][6,9-(*p*-tol)₂-2,2,2-(CO)₃-*closo*-2,1,10-MnC₂B₇H₇] (**16**; 0.10 g, 42%).

Synthesis of [6,9-(*p*-tol)₂-2,2-(CO)₂-2-NO-*closo*-2,1,10-MnC₂B₇H₇] (17**).** Compound **16** (0.10 g, 0.1 mmol) was dissolved in CH₂Cl₂ (10 mL), NOBF₄ (ca. 0.02 g, 0.17 mmol) was added, and the mixture was stirred at ambient temperature for 30 min. After evaporation in vacuo, the residue was dissolved in CH₂Cl₂-petroleum ether (3:2, 5 mL) and transferred to the top of a chromatography column. Elution with the same solvent mixture gave a yellow fraction, from which removal of solvent in vacuo yielded yellow microcrystals of **17** (0.03 g, 65%).

X-ray Crystallographic Structure Determinations. Experimental data for compounds **2**, **7**, **8**, **11–13**, **15**, and **17** are presented in Table 3. All X-ray intensity data were collected at 110(2) K on a Bruker-Nonius X8 APEX CCD area-detector diffractometer using graphite-monochromated Mo K α X-radiation ($\lambda = 0.71073$ Å). Several sets of narrow data “frames” were collected at different values of θ , for various initial values of ϕ and ω , using 0.5° increments of ϕ or ω . The data frames were integrated using SAINT;³⁵ the substantial redundancy in data allowed an empirical absorption correction (SADABS)³⁵ to be applied, based on multiple measurements of equivalent reflections.

All structures were solved using conventional direct methods^{35,36} and refined by full-matrix least-squares on all *F*² data using SHELXTL version 6.12,³⁶ with anisotropic thermal parameters assigned to all non-H atoms. The locations of the cage-carbon atoms were verified by examination of the appropriate internuclear distances and the magnitudes of their isotropic thermal displacement parameters. All aromatic, methylene, and cluster hydrogen atoms were set riding in calculated positions, while methyl and hydroxyl hydrogens were refined using “rotating group” models;³⁶ all H atoms had fixed isotropic thermal parameters defined as $U_{\text{iso}}(\text{H}) = 1.2 \times U_{\text{iso}}(\text{parent})$, or $U_{\text{iso}}(\text{H}) = 1.5 \times U_{\text{iso}}(\text{parent})$ for methyl groups.

The asymmetric fraction of the unit cell in crystals of **2** contains three crystallographically independent molecules that interact with each other to form hydrogen-bonded helices that extend along the crystallographic *a* direction. As noted in the Discussion above, these interactions are relatively weak. In the asymmetric units of crystals of both **7** and **8**, there are two crystallographically independent

(34) Flack, H. D.; Bernardinelli, G. *J. Appl. Crystallogr.* **2000**, *33*, 1143.

(35) APEX 2, version 1.0; Bruker AXS: Madison, WI, 2003–2004.

(36) SHELXTL, version 6.12; Bruker AXS: Madison, WI, 2001.

molecules in the asymmetric unit. All of the other determinations reported herein had no unusual features, and all were refined without difficulty. The sole exception to this was that for compound **13**, for which the crystals obtained were only of modest quality, and thus the diffraction data obtained were relatively poor and required some constraining of temperature factors for one of the cluster boron atoms in order to facilitate stable refinement of the model.

Acknowledgment. We thank the Robert A. Welch Foundation and Baylor University for support. The Bruker-Nonius

X8 APEX diffractometer was purchased with funds received from the National Science Foundation Major Instrumentation Program (Grant CHE-0321214).

Supporting Information Available: Full details of the crystal structure analyses in CIF format; this material is available free of charge via the Internet at <http://pubs.acs.org>.

OM800730N

Reductive Reactivity of the Tetravalent Uranium Complex $[(\eta^5\text{-C}_5\text{Me}_5)(\eta^8\text{-C}_8\text{H}_8)\text{U}]_2(\mu\text{-}\eta^3\text{:}\eta^3\text{-C}_8\text{H}_8)$

William J. Evans,^{*,†} Michael K. Takase,[†] Joseph W. Ziller,[†] Antonio G. DiPasquale,[‡] and Arnold L. Rheingold[‡]

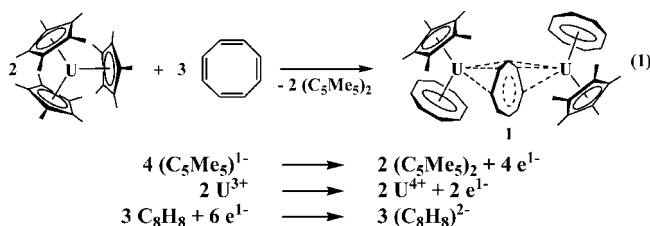
Department of Chemistry, University of California, Irvine, California 92697-2025, and Department of Chemistry and Biochemistry, University of California, San Diego, 9500 Gilman Drive, MC 0358, La Jolla, California 92093-0358

Received August 1, 2008

The reductive reactivity of the cyclooctatetraenide ligands in $[(\eta^5\text{-C}_5\text{Me}_5)(\eta^8\text{-C}_8\text{H}_8)\text{U}]_2(\mu\text{-}\eta^3\text{:}\eta^3\text{-C}_8\text{H}_8)$, **1**, was examined with polycyclic hydrocarbons, phenazine, and the diphenyldichalcogenide compounds PhEPh (E = S, Se, Te). Complex **1** does not reduce anthracene, acenaphthylene, or benzanthracene, but it acts as a two-electron reductant with phenazine to form 1 equiv of C_8H_8 and the bimetallic complex $[(\eta^5\text{-C}_5\text{Me}_5)(\eta^8\text{-C}_8\text{H}_8)\text{U}]_2(\mu\text{-}\eta^1\text{:}\eta^1\text{-C}_{12}\text{H}_8\text{N}_2)$, **2**. X-ray crystallography showed that the heteroleptic metallocene unit $[(\text{C}_5\text{Me}_5)(\text{C}_8\text{H}_8)\text{U}]^{1+}$ adopted an η^1 -coordination mode with the phenazine dianion rather than the η^3 -coordination previously found with the homoleptic f element metallocene cations $[(\text{C}_5\text{Me}_5)_2\text{M}]^{1+}$. Complex **1** also reacts as a two-electron reductant with PhEPh (E = S, Se, Te) to form C_8H_8 and the heteroleptic complexes $[(\eta^5\text{-C}_5\text{Me}_5)(\eta^8\text{-C}_8\text{H}_8)\text{U}]_2(\mu\text{-EPh})_2$ (E = S, **3**; Se, **4**; Te, **5**).

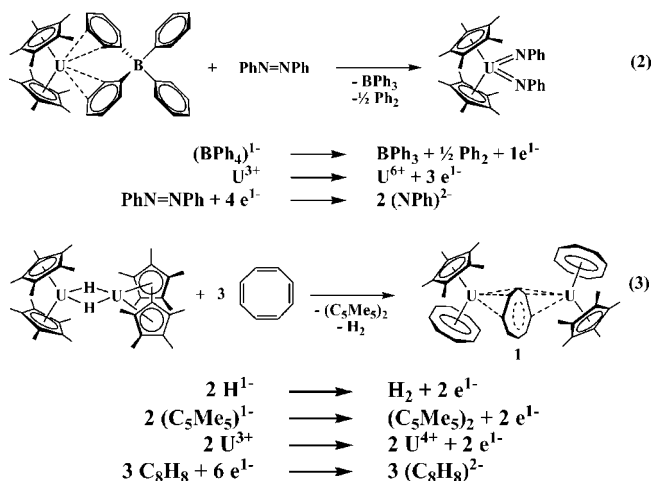
Introduction

Recent studies of the reductive chemistry of organoactinides have shown that traditional metal-based reduction reactions can be coupled with ligand-based reductions to accomplish multi-electron reductions.^{1–6} Equation 1 shows an example in which



a U^{3+} complex, $(\text{C}_5\text{Me}_5)_3\text{U}$, functions as a three-electron reductant to make a U^{4+} product by combining a one-electron $\text{U}^{3+}/\text{U}^{4+}$ redox couple with two $(\text{C}_5\text{Me}_5)^{1-}/(\text{C}_5\text{Me}_5)$ reductions.^{1–3} In efforts to better define this sterically induced reduction (SIR),^{1–3,7} control reactions with sterically “normal” complexes were examined and revealed that ligands such as $(\text{BPh}_4)^{1-}$ and

H^{1-} can also effect reduction along with metal-based processes.^{4,8–10} Equation 2 shows a four-electron reduction⁸ involving $(\text{BPh}_4)^{1-}$ and eq 3 shows a six-electron process¹⁰ involving both hydride



and $(\text{C}_5\text{Me}_5)^{1-}$ ligands. The reductive reactivity of ligands in sterically normal organoactinide complexes suggested that a wider variety of ligands should be studied.

The reductive chemistry of sterically normal $[(\eta^5\text{-C}_5\text{Me}_5)(\eta^8\text{-C}_8\text{H}_8)\text{U}]_2(\mu\text{-}\eta^3\text{:}\eta^3\text{-C}_8\text{H}_8)$, **1**,³ was of interest since this molecule contained three cyclooctatetraenide dianions. Each of these could potentially function as a two-electron reductant to provide ligand-based reduction chemistry according to eq 4. The combination of the three $(\text{C}_8\text{H}_8)^{2-}$ ligands could make bimetallic **1** a six-electron reductant that could deliver two $[(\text{C}_5\text{Me}_5)\text{U}]^{3+}$ units.

(9) Evans, W. J.; Nyce, G. W.; Forrestal, K. J.; Ziller, J. W. *Organometallics* **2002**, *21*, 1050–1055.

(10) Evans, W. J.; Miller, K. A.; Kozimor, S. A.; Ziller, J. W.; DiPasquale, A. G.; Rheingold, A. L. *Organometallics* **2007**, *26*, 3568–3576.

* Corresponding author. Fax: 949-824-2210. E-mail: wevans@uci.edu.

[†] University of California, Irvine.

[‡] University of California, San Diego.

(1) Evans, W. J.; Davis, B. L. *Chem. Rev.* **2002**, *102*, 2119–2136.

(2) Evans, W. J.; Nyce, G. W.; Johnston, M. A.; Ziller, J. W. *J. Am. Chem. Soc.* **2000**, *122*, 12019–12020.

(3) Evans, W. J.; Nyce, G. W.; Ziller, J. W. *Angew. Chem., Int. Ed.* **2000**, *39*, 240–242.

(4) Evans, W. J.; Kozimor, S. A.; Ziller, J. W. *Chem. Commun.* **2005**, 4681–4683.

(5) Evans, W. J.; Kozimor, S. A.; Ziller, J. W.; Kaltsoyannis, N. *J. Am. Chem. Soc.* **2004**, *126*, 14533–14547.

(6) Diaconescu, P. L.; Arnold, P. L.; Baker, T. A.; Mendiola, D. J.; Cummins, C. C. *J. Am. Chem. Soc.* **2000**, *122*, 6108–6109.

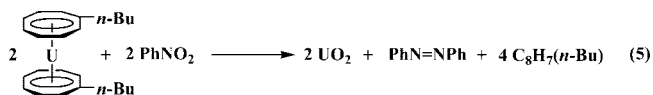
(7) Evans, W. J.; Kozimor, S. A.; Ziller, J. W. *Inorg. Chem.* **2005**, *44*, 7960–7969.

(8) Evans, W. J.; Miller, K. A.; Hillman, W. R.; Ziller, J. W. *J. Organomet. Chem.* **2007**, *692*, 3649–3654.



Complex **1** was also an interesting reagent since it contained two different types of cyclooctatetraenide ligands both in solution and in the solid state. As shown in Figure 1, the crystal structure contains two terminal $(\text{C}_8\text{H}_8)^{2-}$ ligands that are planar, as expected for an aromatic system, and bind as η^8 -ligands, as is typical in organo-f-element chemistry. However, the bridging $(\text{C}_8\text{H}_8)^{2-}$ ligand is nonplanar and coordinates to the two uranium centers in a bis η^3 -fashion. Reactivity studies could determine if this structural difference in the solid state would translate into reactivity differences for the ligands in solution, where a 2:1 ratio of $(\text{C}_8\text{H}_8)^{2-}$ resonances is observed. Complex **1** was also unusual in that the ^1H NMR resonances of the $(\text{C}_8\text{H}_8)^{2-}$ ligands, at -41.7 and -42.2 ppm, are at the far end of the range of values observed for U^{4+} complexes and are closer to values usually observed for $(\text{C}_8\text{H}_8)^{2-}$ ligands in U^{3+} complexes, Table 1.

The reductive chemistry of **1** is also of interest in comparison to uranocene, $(\text{C}_8\text{H}_8)_2\text{U}$, which contains only planar $(\eta^8\text{-C}_8\text{H}_8)^{2-}$ ligands.^{11–15} Uranocene has not been reported to have extensive reductive chemistry,^{16,17} but it is air sensitive, and reactions have been reported with iodine¹⁸ to form $(\text{C}_8\text{H}_8)\text{U}(\text{I}_2)(\text{THF})_2$ and with silanols.¹⁹ A mono-*n*-butyl-substituted derivative has been reported to react with nitrobenzene, forming $\text{PhN}=\text{NPh}$, UO_2 , and free *n*-butylcyclooctatetraene, eq 5.²⁰ To our knowledge, this is the only reductive reaction currently known for uranocenes in which the ligand is oxidized to form a free substituted cyclooctatetraene.



Although complex **1** was an attractive reagent for further studies of organoactinide reduction chemistry, its original synthesis according to eq 1 was challenging. The recent discovery of a synthetic pathway to **1** via eq 3¹⁰ made complex **1** readily accessible for reactivity studies. We report here that **1** has extensive reduction chemistry and functions primarily as a two-electron reductant with the substrates that have given characterizable products.

Experimental Section

The syntheses and manipulations described below were conducted under argon with rigorous exclusion of air and water using

(11) Streitwieser, A., Jr.; Mueller-Westerhoff, U. *J. Am. Chem. Soc.* **1968**, *90*, 7364.

(12) Streitwieser, A., Jr.; Muller-Westerhoff, U.; Sonnichsen, G.; Mares, F.; Morrell, D. G.; Hodgson, K. O.; Harmon, C. A. *J. Am. Chem. Soc.* **1973**, *95*, 8644.

(13) Zalkin, A.; Raymond, K. N. *J. Am. Chem. Soc.* **1969**, *91*, 5667–5668.

(14) Avdeef, A.; Raymond, K. N.; Hodgson, K. O.; Zalkin, A. *Inorg. Chem.* **1972**, *11*, 1083–1088.

(15) Seyferth, D. *Organometallics* **2004**, *23*, 3562–3583.

(16) Butcher, J. A., Jr.; Chambers, J. Q.; Pagni, R. M. *J. Am. Chem. Soc.* **1978**, *100*, 1012–1013.

(17) Butcher, J. A., Jr.; Pagni, R. M.; Chambers, J. Q. *J. Organomet. Chem.* **1980**, *199*, 223–227.

(18) Berthet, J. C.; Le Marechal, J. F.; Ephritikhine, M. *J. Organomet. Chem.* **1990**, *393*, C47–C48.

(19) Lorenz, V.; Fischer, A.; Bruser, W.; Edlmann, F. T.; Jacob, K.; Gelbrich, T.; Jones, P. G. *Chem. Commun.* **1998**, 2217–2218.

(20) Grant, C. B.; Streitwieser, A., Jr. *J. Am. Chem. Soc.* **1978**, *100*, 2433–2440.

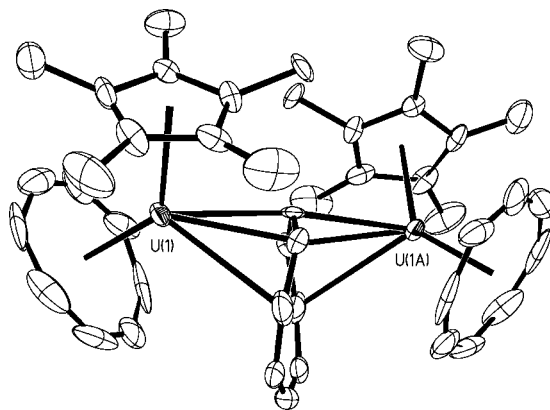


Figure 1. Molecular structure of $[(\text{C}_5\text{Me}_5)(\text{C}_8\text{H}_8)\text{U}]_2(\text{C}_8\text{H}_8)$, **1**,³ showing the $\eta^3:\eta^3$ binding and nonplanarity of the bridging $(\text{C}_8\text{H}_8)^{2-}$ ligand. Thermal ellipsoids are drawn at the 50% probability level and hydrogen atoms have been omitted for clarity.

glovebox, vacuum line, and Schlenk techniques. All glovebox manipulations were done in an argon-filled glovebox free of coordinating solvents. Solvents were dried over columns containing Q-5 and molecular sieves. NMR solvents were dried over sodium potassium alloy, degassed, and vacuum transferred prior to use. ^1H NMR spectra were recorded with a Bruker DRX 500 MHz spectrometer. $[(\text{C}_5\text{Me}_5)(\text{C}_8\text{H}_8)\text{U}]_2(\text{C}_8\text{H}_8)$, **1**, was prepared as previously described.¹⁰ 1,3,5,7- C_8H_8 was distilled over molecular sieves and degassed by three freeze–pump–thaw cycles before use. PhSSPh, PhSeSePh, PhTeTePh, and phenazine were purchased from Aldrich and sublimed before use. Elemental analyses were performed by Analytische Laboratorien (Lindlar, Germany) or on a Perkin-Elmer 2400 CHNS elemental analyzer.

$[(\text{C}_5\text{Me}_5)(\text{C}_8\text{H}_8)\text{U}]_2(\mu\text{-}\eta^1:\eta^1\text{-C}_{12}\text{H}_8\text{N}_2)$, **2**. A yellow solution of phenazine (43 mg, 0.24 mmol) in toluene (4 mL) was added to a dark brown solution of **1** (251 mg, 0.237 mmol) in toluene (6 mL) and stirred for 2 days. The solvent was evaporated under vacuum, leaving a tacky brown solid, which was washed with hexanes and dried under vacuum to yield **2** as a dark brown solid (215 mg, 80%). In an NMR scale experiment, free C_8H_8 was observed at 5.6 ppm in a 1:1 molar ratio with **2** by ^1H NMR spectroscopy. Crystals of **2** suitable for X-ray diffraction were grown at room temperature from a concentrated benzene solution. ^1H NMR (C_6D_6): δ 6.9 (s, C_5Me_5 , $\Delta\nu_{1/2} = 5$ Hz, 30H), -20.7 (s, $\text{C}_{12}\text{H}_8\text{N}_2$, $\Delta\nu_{1/2} = 10$ Hz, 4H), -33.3 (s, C_8H_8 , $\Delta\nu_{1/2} = 6$ Hz, 16H). ^{13}C NMR (C_6D_6): δ -26.2 (s, C_5Me_5), 227.7 (s, C_8H_8). All of the phenazine resonances could not be identified. IR: 3383m, 3261m, 3190m, 3047m, 2966s, 2899s, 2853s, 1591m, 1514s, 1501m, 1457s, 1376w, 1302s, 1279s, 1193w, 1124w, 889s, 726s cm^{-1} . Anal. Calcd for $\text{C}_{48}\text{H}_{54}\text{N}_2\text{U}_2$: C, 50.79; H, 4.80; N, 2.47. Found: C, 51.46; H, 4.48; N, 2.72.

$[(\text{C}_5\text{Me}_5)(\text{C}_8\text{H}_8)\text{U}]_2(\mu\text{-SPh})_2$, **3**. A colorless solution of PhSSPh (43 mg, 0.197 mmol) in toluene (4 mL) was added to a dark brown solution of **1** (208 mg, 0.197 mmol) in toluene (6 mL). After the solution was allowed to stir for 3 h, it was evaporated to dryness under vacuum. The resulting tacky brown solid was washed with hexanes and dried under vacuum to yield **3** as a light brown powder (189 mg, 82%). Free C_8H_8 was observed in a 1:1 molar ratio with **3** in a ^1H NMR experiment. ^1H NMR (C_6D_6): δ 7.7 (s, C_5Me_5 , $\Delta\nu_{1/2} = 17$ Hz, 30H), 5.2 (s, *SPh*, $\Delta\nu_{1/2} = 43$ Hz, 2H), 4.3 (s, *SPh*, $\Delta\nu_{1/2} = 60$ Hz, 4H), -20.6 (s, *SPh*, $\Delta\nu_{1/2} = 82$ Hz, 4H), -38.2 (s, C_8H_8 , $\Delta\nu_{1/2} = 34$ Hz, 16H). ^{13}C NMR (C_6D_6): δ -23.9 (s, C_5Me_5), 113 (s, *SPh*), 134 (s, *SPh*), 147 (s, *SPh*), 277 (s, C_8H_8). IR: 2907s, 2856s, 1774w, 1574m, 1471s, 1433m, 1373m, 1082m, 1021w, 921w, 902w, 725s, 691s cm^{-1} . Anal. Calcd for $\text{C}_{48}\text{H}_{56}\text{S}_2\text{U}_2$: C, 49.14; H, 4.81; S, 5.47; U, 40.58. Found: C, 48.85; H, 4.88; S, 5.32; U, 41.1.

$[(\text{C}_5\text{Me}_5)(\text{C}_8\text{H}_8)\text{U}]_2(\mu\text{-SePh})_2$, **4**. In a manner analogous to the preparation of **3**, **4** was isolated as a red powder (121 mg, 92%)

Table 1. ^1H NMR Shifts of the $(\text{C}_8\text{H}_8)^{2-}$ Ligands in Organouranium Complexes Arranged in Order of Increasing Oxidation State and Chemical Shift

complex	oxidation state	shift (ppm)	complex	oxidation state	shift (ppm)
$(\text{C}_5\text{Me}_5)(\text{C}_8\text{H}_8)\text{U}(\text{THF})^{57}$	3	-52.3 ^a	$(\text{C}_8\text{H}_8)\text{U}(\text{dmio})(\text{OPPh}_3)_2^{i,69}$	4	-31.46 ^d
$(\text{C}_5\text{Me}_5)(\text{C}_8\text{H}_8)\text{U}(\text{HMPA})^{b,58}$	3	-50.18 ^c	$(\text{C}_8\text{H}_8)\text{U}(\text{C}_5\text{H}_3(\text{SiMe}_3)_2)\text{I}(\text{HMPA})^{b,63}$	4	-31.45 ^c
$[(\text{C}_8\text{H}_8)\text{U}(\text{HMPA})_3][\text{BPh}_4]^{b,59}$	3	-47.4 ^d	$(\text{C}_8\text{H}_8)\text{U}(\text{acac})^{f,63}$	4	-31.37 ^d
$(\text{C}_8\text{H}_8)\text{U}(\text{tmp})(\text{HMPA})_2^{b,e,58}$	3	-43.16 ^c	$(\text{C}_5\text{H}_5)(\text{C}_8\text{H}_8)\text{U}(\text{HMPA})^{b,63}$	4	-31.36 ^a
$[\text{Zr}_2(\text{O}^i\text{Pr})_9][(\text{C}_8\text{H}_8)\text{U}]^{60}$	3	-39.8 ^a	$(\text{C}_8\text{H}_8)\text{U}(\text{dddt})(\text{py})^{f,k,68}$	4	-30.98 ^h
$\text{K}[(\text{C}_8\text{H}_8)\text{U}(\text{tmp})_2(\text{BH}_4)(\text{THF})]^{e,61}$	4	-53.27 ^d	$(\text{C}_8\text{H}_8)\text{U}(\text{dddt})(\text{py})^{f,k,69}$	4	-30.98 ^h
$(\text{C}_5\text{H}_5)(\text{C}_8\text{H}_8)\text{U}(\text{BH}_4)(\text{THF})^{62}$	4	-47.60 ^c	$(\text{C}_8\text{H}_8)\text{U}(\text{NEt}_2)(\text{BH}_4)(\text{THF})_4^{43}$	4	-30.6 ^d
$[(\text{C}_5\text{Me}_5)(\text{C}_8\text{H}_8)\text{U}]_2(\text{C}_8\text{H}_8)^3$	4	-42.2 ^a	$(\text{C}_8\text{H}_8)\text{U}(\text{dmio})(\text{HMPA})_2^{b,i,69}$	4	-30.44 ^d
		-41.7 ^a	$(\text{C}_8\text{H}_8)\text{U}(\text{BH}_4)(\text{OEt})^{33}$	4	-30.25 ^d
$(\mu-\eta^8,\eta^8-\text{C}_8\text{H}_8)[\text{U}(\text{NC}[^t\text{Bu}]\text{Mes})_3]_2^{44}$	4	-39.19 ^a	$[\text{Na}(\text{THF})][(\text{C}_8\text{H}_8)\text{U}(\text{S}^i\text{Bu})_3]^{71}$	4	-30.05 ^d
$(\text{C}_5\text{Me}_5)(\text{C}_8\text{H}_8)\text{U}^{18,63}$	4	-38.5 ^c	$(\text{C}_5\text{H}_5)(\text{C}_8\text{H}_8)\text{U}(\text{BH}_4)(\text{OPPh}_3)^{62}$	4	-29.99 ^d
		-34.02 ^d	$(\text{C}_8\text{H}_8)\text{U}(\text{acac})^{j,18,63,70}$	4	-29.6 ^c
		-37.5 ^d			-29.18 ^{a,c}
$(\text{C}_8\text{H}_8)\text{U}(\text{O}_3\text{SCF}_3)_2(\text{py})^{f,64}$	4	-37.18 ^a	$(\text{C}_8\text{H}_8)\text{U}(\text{mdt})(\text{OPPh}_3)_2^{i,69}$	4	-29.52 ^d
$(\text{C}_8\text{H}_8)\text{U}[\text{C}_5\text{H}_4(\text{SiMe}_3)_2]_2^{57}$	4	-36.20 ^a	$(\text{C}_5\text{Me}_5)(\text{C}_8\text{H}_8)\text{ClU}(\text{Cl})\text{U}(\text{C}_5\text{Me}_5)(\text{C}_8\text{H}_8)^{31}$	4	-29.3 ^a
$(\text{C}_5\text{H}_5)(\text{C}_8\text{H}_8)\text{U}(\text{NEt}_2)^{41}$	4	-35.88 ^c	$(\text{C}_8\text{H}_8)\text{U}(\text{NEt}_2)_2(\text{THF})^{65}$	4	-29.20 ^a
$(\text{C}_8\text{H}_8)\text{U}(\text{BH}_4)_2(\text{PPh}_3)^{62}$	4	-35.78 ^a	$[\text{Na}(18\text{-crown-6})]_2[(\text{C}_8\text{H}_8)\text{U}(\text{dddt})_2]^{k,72}$	4	-29.17 ^d
$(\text{C}_5\text{Me}_5)(\text{C}_8\text{H}_8)\text{U}(\text{NEt}_2)^{41}$	4	-35.5 ^a	$(\text{C}_8\text{H}_8)\text{U}(\text{O}^t\text{Bu})_2^{33}$	4	-28.86 ^d
$(\text{C}_5\text{Me}_5)(\text{C}_8\text{H}_8)\text{U}[\text{N}(\text{SiMe}_3)_2]^{31}$	4	-35.0 ^c	$(\text{C}_8\text{H}_8)\text{U}(\text{BH}_4)_2(\text{OPPh}_3)^{62}$	4	-28.82 ^d
		-35.43 ^d	$(\text{C}_8\text{H}_8)\text{U}(\text{mdt})(\text{HMPA})_2^{b,l,69}$	4	-28.78 ^d
$(\text{C}_8\text{H}_8)\text{U}_2(\text{THF})^{18,63}$	4	-35.18 ^c	$\text{Na}[(\text{C}_8\text{H}_8)\text{U}(\text{BH}_4)_2(\text{OEt})]^{33}$	4	-28.72 ^d
$(\text{C}_8\text{H}_8)\text{U}(\text{NEt}_2)^{65,66}$	4	-27.76 ^d	$[(\text{C}_8\text{H}_8)\text{U}(\text{NC}[\text{Me}]\text{NEt}_2)(\text{THF})_2][\text{BPh}_4]^{43}$	4	-28.3 ^h
		-35.07 ^a	$(\text{C}_8\text{H}_8)\text{U}(\text{CH}_2\text{Ph})_2(\text{HMPA})_2^{b,63}$	4	-27.95 ^c
$(\text{C}_5\text{Me}_5)(\text{C}_8\text{H}_8)\text{U}[\text{CH}_2(\text{SiMe}_3)]^{63}$	4	-35.0 ^a	$(\text{C}_8\text{H}_8)\text{U}(\text{OEt})_2^{33}$	4	-27.8 ^d
$(\text{C}_8\text{H}_8)\text{U}(\text{NEt}_2)[\text{CH}(\text{SiMe}_3)_2]^{43}$	4	-34.87 ^g			-24.02 ^h
$[(\text{C}_5\text{H}_5)(\text{C}_8\text{H}_8)\text{U}(\text{THF})_2][\text{BPh}_4]^{41}$	4	-34.3 ^a	$[(\text{C}_8\text{H}_8)\text{U}(\text{NEt}_2)(\text{THF})_2][\text{BPh}_4]^{41}$	4	-27.13 ^h
$(\text{C}_8\text{H}_8)\text{U}(\text{NEt}_2)[\text{N}(\text{SiMe}_3)_2]^{43}$	4	-34.23 ^c	$(\text{C}_8\text{H}_8)\text{U}(\text{CH}_2\text{SiMe}_3)_2(\text{HMPA})^{b,63}$	4	-26.57 ^c
$(\text{C}_5\text{H}_5)(\text{C}_8\text{H}_8)\text{U}[\text{N}(\text{SiMe}_3)_2]^{63}$	4	-34.0 ^d	$(\text{C}_8\text{H}_8)\text{U}(\text{dddt})(\text{HMPA})_2^{b,k,69}$	4	-26.13 ^d
$[(\text{C}_8\text{H}_8)\text{U}(\text{S}_2\text{CNEt}_2)(\text{THF})_2][\text{BPh}_4]^{43}$	4	-33.97 ^c	$(\text{C}_8\text{H}_8)\text{U}(\text{mdt})(\text{py})^{f,l,69}$	4	-24.82 ^h
$(\text{C}_5\text{H}_5)(\text{C}_8\text{H}_8)\text{U}^{63}$	4	-33.64 ^d	$[\text{K}(18\text{-crown-6})][(\text{C}_8\text{H}_8)\text{U}(\text{BH}_4)_3]^{33}$	4	-24.09 ^d
$[(\text{C}_8\text{H}_8)\text{U}(\text{BH}_4)(\text{THF})_2][\text{BPh}_4]^{67}$	4	-33.40 ^h	$(\text{C}_8\text{H}_8)\text{U}(\text{S}^i\text{Bu})_2^{71}$	4	-23.48 ^c
		-33.35 ^a			-23.36 ^{h,m}
$(\text{C}_8\text{H}_8)\text{U}(\text{BH}_4)_2(\text{THF})^{62}$	4	-33.27 ^d			-26.62 ^{h,n}
$(\text{C}_8\text{H}_8)\text{U}(\text{tmp})(\text{BH}_4)(\text{THF})^{e,61}$	4	-33.19 ^c	$(\text{C}_8\text{H}_8)\text{U}(\text{S}^i\text{Pr})_2^{71}$	4	-23.22 ^h
$(\text{C}_8\text{H}_8)\text{U}(\text{BH}_4)(\text{O}^i\text{Pr})^{33}$	4	-30.63 ^d			-23.20 ^c
		-33.14 ^d	$(\text{C}_8\text{H}_8)\text{U}(\text{s}^i\text{Bu})_2^{71}$	4	-22.96 ^c
$(\text{C}_8\text{H}_8)\text{U}(\text{tmp})(\text{OEt})^{e,61}$	4	-33.0 ^h			-22.88 ^{h,m}
$[(\text{C}_8\text{H}_8)\text{UCl}(\text{THF})_2][\text{BPh}_4]^{43}$	4	-32.88 ^h			-28.99 ^{h,n}
$[(\text{C}_5\text{Me}_5)(\text{C}_8\text{H}_8)\text{U}(\text{THF})_2][\text{BPh}_4]^{41}$	4	-32.77 ^d	$(\text{C}_8\text{H}_8)\text{U}(\text{O}_2\text{CNEt}_2)^{65}$	4	-21.06 ^d
$[(\text{C}_8\text{H}_8)\text{U}(\text{BH}_4)(\text{OPPh}_3)_3][\text{BPh}_4]^{67}$	4	-32.7 ^c	$[\text{Li}(\text{THF})_3][(\text{C}_8\text{H}_8)\text{U}(\text{CH}_2\text{SiMe}_3)_3]^{63}$	4	-19.96 ^a
$(\text{C}_5\text{Me}_5)(\text{C}_8\text{H}_8)\text{UCl}(\text{OCNH}(\text{CH}_2)_5)^{31}$	4	-30.64 ^d	$\text{Li}[(\text{C}_8\text{H}_8)\text{U}(\text{NEt}_2)_3]^{66}$	4	-15.84 ^d
$(\text{C}_8\text{H}_8)\text{U}(\text{BH}_4)(\text{O}^i\text{Bu})^{33}$	4	-32.60 ^d	$\text{K}[(\text{C}_8\text{H}_8)\text{U}(\text{NEt}_2)_3]^{65}$	4	-15.84 ^d
		-32.31 ^d	$[(\text{C}_8\text{H}_8)\text{U}(\text{HMPA})_3][\text{BPh}_4]^{b,67}$	5	-32.48 ^h
$[(\text{C}_8\text{H}_8)\text{U}(\text{tmp})(\text{HMPA})_2][\text{BPh}_4]^{b,e,61}$	4	-32.09 ^d	$[(\text{C}_8\text{H}_8)\text{U}(\text{NEt}_2)(\text{THF})_2][\text{BPh}_4]^{66}$	5	-29.71 ^d
$(\text{C}_8\text{H}_8)\text{U}_2(\text{HMPA})_2^{b,18,63}$	4	-32.07 ^h	$[\text{Na}(18\text{-crown-6})][(\text{C}_8\text{H}_8)\text{U}(\text{dddt})_2]^{k,72}$	5	-27.35 ^d
$[(\text{C}_8\text{H}_8)\text{U}(\text{BH}_4)(\text{HMPA})_3][\text{BPh}_4]^{b,67}$	4	-32.07 ^h	$[(\text{C}_8\text{H}_8)\text{U}(\text{NEt}_2)(\text{THF})][\text{BPh}_4]^{65,66}$	5	-15.3 ^d
$(\text{C}_8\text{H}_8)\text{U}(\text{dmio})(\text{py})^{f,i,68}$	4	-31.7 ^d	$(\text{C}_5\text{H}_5)(\text{C}_8\text{H}_8)\text{U}(\text{NEt}_2)_2^{65}$	5	-12.5 ^a
$(\text{C}_8\text{H}_8)\text{U}(\text{dmio})(\text{py})_2^{f,i,69}$	4	-31.6 ^d	$(\text{C}_8\text{H}_8)\text{U}(\text{NEt}_2)_3^{65,66}$	5	-9.5 ^{a,c}
$[(\text{C}_8\text{H}_8)\text{U}(\text{O}_2\text{CNEt}_2)(\text{THF})_2][\text{BPh}_4]^{43}$	4	-31.5 ^d	$(\text{C}_8\text{H}_8)\text{U}(\text{NMe}_2)_3^{65}$	5	-8.9 ^a
$(\text{C}_8\text{H}_8)\text{UCl}_2(\text{py})_2^{f,70}$	4	-31.50 ^d	$(\text{C}_8\text{H}_8)\text{U}(\text{O}^i\text{Pr})_3^{65}$	5	-6.6 ^a
$(\text{C}_8\text{H}_8)\text{UCl}_2(\text{THF})_2^{70}$	4	-24.04 ^h			
$(\text{C}_8\text{H}_8)\text{U}(\text{O}^i\text{Pr})_2^{33}$	4				

^a Solvent = benzene. ^b HMPA = hexamethyl phosphorus triamide. ^c Solvent = toluene. ^d Solvent = THF. ^e tmp = $\text{C}_4\text{Me}_4\text{P}$. ^f py = pyridine. ^g Solvent = acetonitrile. ^h Solvent = pyridine. ⁱ dmio = 1,3-dithiole-2-one-4,5-dithiolate. ^j acac = acetoacetate. ^k dddt = 5,6-dihydro-1,4-dithiine-2,3-dithiolate. ^l mdt = 1,3-dithiole-4,5-dithiolate. ^m Dimeric form. ⁿ Monomeric form.

from a yellow solution of PhSeSePh (33 mg, 0.104 mmol) in toluene (4 mL) and a dark brown solution of **1** (111 mg, 0.104 mmol) in toluene (6 mL). ^1H NMR (C_6D_6): δ 8.6 (s, C_5Me_5 , $\Delta\nu_{1/2}$ = 40 Hz, 30H), 6.7 (s, SePh , $\Delta\nu_{1/2}$ = 86 Hz, 2H), 5.9 (s, SePh , $\Delta\nu_{1/2}$ = 122 Hz, 4H), -16.7 (s, SePh , $\Delta\nu_{1/2}$ = 111 Hz, 4H), -37.8 (s, C_8H_8 , $\Delta\nu_{1/2}$ = 60 Hz, 16H). ^{13}C NMR (C_6D_6): δ -23.9 (s, C_5Me_5), 154 (s, SePh), 285 (s, C_8H_8). IR: 3048m, 2984m, 2901s, 2855m, 1576m, 1471s, 1449m, 1435m, 1379m, 1069m, 1021s, 999w, 736s, 693m, 667m cm^{-1} . Anal. Calcd for $\text{C}_{48}\text{H}_{56}\text{Se}_2\text{U}_2$: C, 45.50; H, 4.46; Se, 12.46; U, 37.58. Found: C, 44.93; H, 4.34; Se, 12.3; U, 38.4.

$[(\text{C}_5\text{Me}_5)(\text{C}_8\text{H}_8)\text{U}]_2(\mu\text{-TePh})_2$, **5**. In a manner analogous to the preparation of **3**, **5** was isolated as a light red powder (228 mg, 86%) from an orange solution of PhTeTePh (80 mg, 0.194 mmol) in toluene (4 mL) and a dark brown solution of **1** (206 mg, 0.194 mmol) in toluene (6 mL). ^1H NMR (C_6D_6): δ 9.7 (s, C_5Me_5 , $\Delta\nu_{1/2}$ = 18 Hz, 30H), 8.3 (s, TePh , $\Delta\nu_{1/2}$ = 33 Hz, 2H), 7.8 (s, TePh ,

$\Delta\nu_{1/2}$ = 34 Hz, 4H), -10.9 (s, TePh , $\Delta\nu_{1/2}$ = 38 Hz, 4H), -39.1 (s, C_8H_8 , $\Delta\nu_{1/2}$ = 29 Hz, 16H). ^{13}C NMR (C_6D_6): δ -24 (s, C_5Me_5), 119 (s, TePh), 135 (s, TePh), 165 (s, TePh), 297 (s, C_8H_8). IR: 3053m, 2898s, 2851m, 1570s, 1468s, 1430s, 1378m, 1016s, 900w, 722s, 695m, 650w cm^{-1} . Anal. Calcd for $\text{C}_{48}\text{H}_{56}\text{Te}_2\text{U}_2$: C, 42.26; H, 4.14; Te, 18.71; U, 34.90. Found: C, 42.52; H, 4.10; Te, 18.9; U, 34.0.

X-ray Data Collection, Structure Solution, and Refinement for 2. A brown crystal of approximate dimensions 0.10 × 0.10 × 0.20 mm was mounted on a glass fiber and transferred to a Bruker CCD platform diffractometer. The SMART²¹ program package was used to determine the unit-cell parameters and for data collection (30 s/frame scan time for a sphere of diffraction data). The raw

(21) SMART Software Users Guide, Version 5.1; Bruker Analytical X-Ray Systems, Inc.: Madison, WI, 1999.

Table 2. X-ray Data Collection Parameters for [(C₅Me₅)(C₈H₈)U]₂(C₁₂H₈N₂), 2, [(C₅Me₅)(C₈H₈)U]₂(SePh)₂, 4, and [(C₅Me₅)(C₈H₈)U]₂(TePh)₂, 5

	C ₄₈ H ₅₄ N ₂ U ₂ · (C ₆ H ₆) 2	C ₄₈ H ₅₆ Se ₂ U ₂ 4	C ₄₈ H ₅₆ Te ₂ U ₂ 5
fw	1213.10	1266.91	1364.19
temperature (K)	158(2)	208(2)	155(2)
cryst syst	monoclinic	orthorhombic	orthorhombic
space group	<i>P</i> 2 ₁ / <i>n</i>	<i>Pbca</i>	<i>Pbca</i>
<i>a</i> (Å)	18.183(3)	12.191(4)	19.204(6)
<i>b</i> (Å)	12.9333(19)	17.707(8)	9.975(3)
<i>c</i> (Å)	19.487(3)	19.051(5)	22.158(7)
α (deg)	90	90	90
β (deg)	105.644(2)	90	90
γ (deg)	90	90	90
volume (Å ³)	4412.9(11)	4113(3)	4245(2)
<i>Z</i>	4	4	4
ρ _{calcd} (Mg/m ³)	1.826	2.046	2.135
μ (mm ⁻¹)	7.369	9.669	9.000
R1 [<i>I</i> > 2.0σ(<i>I</i>)] ^a	0.0391	0.0424	0.0328
wR2 (all data) ^a	0.0861	0.01066	0.0665

^a Definitions: wR2 = [$\sum[w(F_o^2 - F_c^2)]^2 / \sum[w(F_o^2)]^2$]^{1/2}, R1 = $\sum|F_o| - |F_c| / \sum|F_o|$.

frame data were processed using SAINT²² and SADABS²³ to yield the reflection data file. Subsequent calculations were carried out using the SHELXTL²⁴ program. The diffraction symmetry was 2/*m*, and the systematic absences were consistent with the centrosymmetric monoclinic space group *P*2₁/*n*, which was later determined to be correct. The structure was solved by direct methods and refined on *F*² by full-matrix least-squares techniques. The analytical scattering factors²⁵ for neutral atoms were used throughout the analysis. Hydrogen atoms were included using a riding model. There was one molecule of benzene solvent present per formula unit. The solvent was refined as a regular hexagon with equal isotropic displacement parameters (EADP). Details are given in Table 2.

X-ray Data Collection, Structure Solution, and Refinement for 4. A black block 0.13 × 0.10 × 0.06 mm in size was mounted on a Cryoloop with Paratone oil. Data were collected in a nitrogen gas stream at 208(2) K using phi and omega scans. Crystal-to-detector distance was 60 mm and exposure time was 10 s per frame using a scan width of 0.3°. Data collection was 99.9% complete to 25.00° in θ . A total of 20739 reflections were collected covering the indices $-15 \leq h \leq 16$, $-22 \leq k \leq 20$, $-11 \leq l \leq 25$. 4958 reflections were found to be symmetry independent, with an R_{int} of 0.0585. Indexing and unit cell refinement indicated a primitive, orthorhombic lattice. The space group was found to be *Pbca* (No. 61). The data were integrated using the Bruker SAINT²² software program and scaled using the SADABS²³ software program. Solution by direct methods (SIR-2004) produced a complete heavy-atom phasing model consistent with the proposed structure. All non-hydrogen atoms were refined anisotropically by full-matrix least-squares (SHELXL-97). All hydrogen atoms were placed using a riding model. Their positions were constrained relative to their parent atom using the appropriate HFIX command in SHELXL-97.

X-ray Data Collection, Structure Solution, and Refinement for 5. A red crystal of approximate dimensions 0.12 × 0.21 × 0.25 mm was handled as described for 2. The diffraction symmetry was *mmm*, and the systematic absences were consistent with the orthorhombic space group *Pbca*, which was later determined to be correct. The molecule was located about an inversion center. The

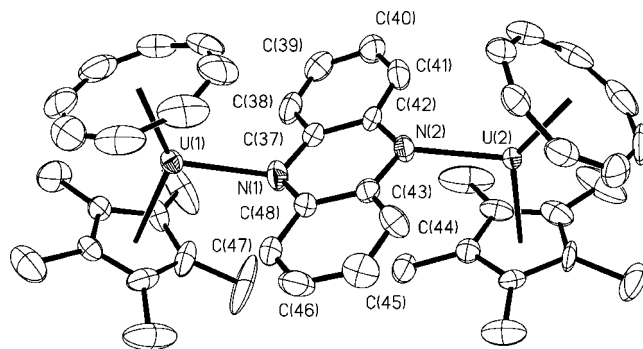


Figure 2. Molecular structure of [(C₅Me₅)(C₈H₈)U]₂(C₁₂H₈N₂), 2, with thermal ellipsoids drawn at the 50% probability level. Hydrogen atoms have been omitted for clarity.

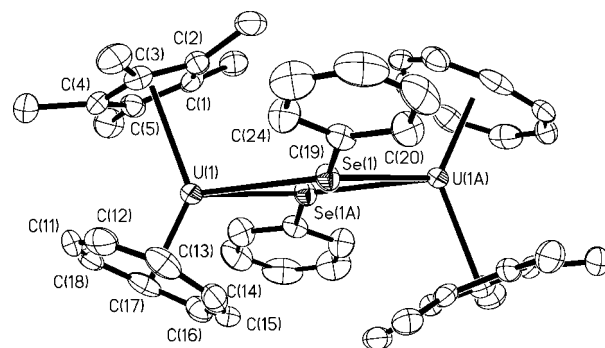
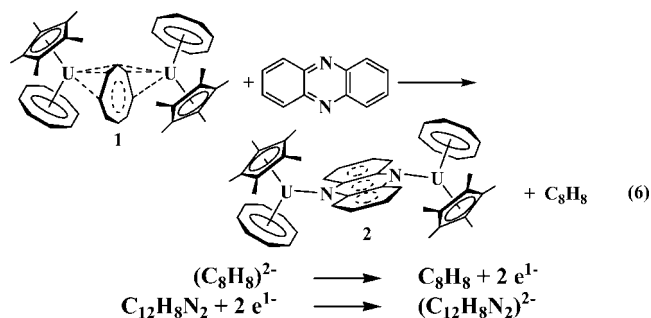


Figure 3. Molecular structure of [(C₅Me₅)(C₈H₈)U]₂(SePh)₂, 4, with thermal ellipsoids drawn at the 50% probability level. Hydrogen atoms have been omitted for clarity.

uranium atom was disordered and included using two components with site-occupancy factors of 0.955 and 0.045. The distance between the two components was 1.044 Å. The distances and angles reported refer only to those related to the major component U(1).

Results

Phenazine. C₁₂H₈N₂ was initially examined as a substrate since it is easily reducible (−0.364 V vs SCE)²⁶ and has been used successfully to test other f element reduction systems.^{27–29} Complex 1 reacts with phenazine in a 1:1 ratio to form the complex [(C₅Me₅)(C₈H₈)U]₂(μ-η¹:η¹-C₁₂H₈N₂), 2, which was characterized by ¹H and ¹³C NMR spectroscopy and identified by X-ray crystallography, eq 6, Figure 2. One equivalent of free C₈H₈ per equivalent of 2 was observed in an NMR scale reaction.



(22) SAINT Software Users Guide, Version 6.0; Bruker Analytical X-Ray Systems, Inc.: Madison, WI, 1999.

(23) Sheldrick, G. M. SADABS, Version 2.10; Bruker Analytical X-Ray Systems, Inc.: Madison, WI, 2002.

(24) Sheldrick, G. M. SHELXTL, Version 6.12; Bruker Analytical X-Ray Systems, Inc.: Madison, WI, 2001.

(25) International Tables for X-Ray Crystallography; Kluwer Academic Publishers: Dordrecht, 1992; Vol. C.

(26) Nechaeva, O. N.; Pushkareva, Z. V. Zh. Obshch. Khim. 1958, 28, 2693–2701.

(27) Evans, W. J.; Gonzales, S. L.; Ziller, J. W. J. Am. Chem. Soc. 1994, 116, 2600–2608.

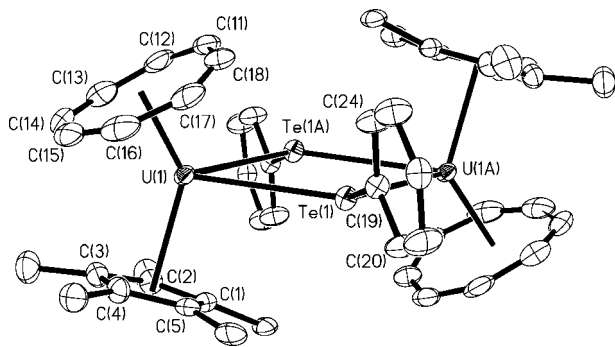


Figure 4. Molecular structure of $[(C_5Me_5)(C_8H_8)U]_2(TePh)_2$, **5**, with thermal ellipsoids drawn at the 50% probability level. Hydrogen atoms have been omitted for clarity.

In this two-electron reduction reaction, only one of the $(C_8H_8)^{2-}$ ligands in **1** was needed to reduce phenazine to the dianion $(C_{12}H_8N_2)^{2-}$. As a consequence, the net reaction generates two monocationic $[(C_5Me_5)(C_8H_8)U]^{1+}$ heteroleptic metallocene units along with the doubly reduced phenazine dianion. Isolation of **2** allows direct comparison of the mixed ligand $[(C_5Me_5)(C_8H_8)U]^{1+}$ metallocene with the more common homoleptic f element metallocene, $[(C_5Me_5)_2M]^{1+}$.

The solid-state structure of **2** revealed that the $[(C_5Me_5)(C_8H_8)U]^{1+}$ unit coordinates to the phenazine dianion in a bonding mode not previously seen in f element chemistry.^{27,28,30} Specifically, the $(C_{12}H_8N_2)^{2-}$ ligand bridges the uranium centers with an η^1 -bonding mode to each nitrogen. There are no other crystallographically characterized uranium $(C_{12}H_8N_2)^{2-}$ complexes in the literature, but the structure of **2** can be compared to the lanthanide complexes $[(C_5Me_5)_2Ln]_2(\mu-\eta^3:\eta^3-C_{12}H_8N_2)$ ($Ln = Sm$, **6**,²⁷ La , **7**,^{28,30}). In the lanthanide complexes, the phenazine dianion bridges the metals using three adjacent atoms in an aza-allyl mode on each side, Scheme 1.

The X-ray diffraction study also revealed that in the solid state the heteroleptic metallocene units are arranged so that the two $(C_5Me_5)^{1-}$ ligands are in a *cis* rather than *trans* orientation with respect to each other, and concomitantly the same is true for the $(C_8H_8)^{2-}$ ligands. Heteroleptic bimetallic f element complexes more often have a *trans* arrangement of ligands: $(C_5Me_5)(C_8H_8)ClU(\mu-Cl)U(C_8H_8)(C_5Me_5)$ ³¹ and $\{(C_5Me_5)[C_8H_6(Si^iPr_3)_2]U\}_2(\mu-\eta^1:\eta^2-C_3O_3)$ ³² are two examples. However, both *cis* and *trans* structures are found for $[(C_8H_8)UX]_2(\mu-OR)_2$ ($X = BH_4$, $R = Et$; $X = O^iPr$, $R = ^iPr$).³³ It is possible that isomers exist in this case also since two pairs of $(C_5Me_5)^{1-}$ and $(C_8H_8)^{2-}$ resonances are observed in the crude reaction mixture before recrystallization.

Table 3 shows a comparison of selected bond distances and angles for **2** versus the $[(C_5Me_5)_2Ln]_2(C_{12}H_8N_2)$ complexes in order to evaluate how the heteroleptic $[(C_5Me_5)(C_8H_8)U]^{1+}$ metallocene cation compares with the homoleptic metallocene

cations $[(C_5Me_5)_2Ln]^{1+}$. The similarities in effective size of $(C_5Me_5)^{1-}$ and $(C_8H_8)^{2-}$ ligands have been described previously.^{34,35}

The 139.1° $(C_5Me_5$ ring centroid) $-U-(C_8H_8$ ring centroid) angle in **2** is similar to the 135.9° analogue in **6** and 136.4° and 136.3° analogues in **7**. The $U-N$ distances are more difficult to compare using Shannon ionic radii³⁶ since the coordination numbers differ in these complexes. Seven-coordinate U^{4+} is 0.07 Å smaller than seven-coordinate Sm^{3+} and 0.182 Å smaller than nine-coordinate Sm^{3+} . By either metric, the $2.323(5)$ and $2.333(6)$ Å $U-N$ bonds in **2** seem to be longer than expected in comparison to the $2.360(2)$ Å distance in the samarium complex **6**. The $U-N$ bonds in **2** also seem long in comparison to other $U^{4+}-N$ distances in the literature, e.g., $(C_5Me_5)(C_8H_8)U[N(SiMe_3)_2]$ [$2.284(4)$ Å],³¹ $(C_5Me_5)_2U[NH(C_6H_3Me_2-2,6)]_2$ [$2.267(6)$ Å],³⁷ $(C_5Me_5)_2U(NEt_2)_2$ [$2.167(9)$ and $2.162(9)$ Å],³⁸ and $[(C_5Me_5)_2U(NMe_2)(CN^iBu)_2][BPh_4]$ [$2.22(1)$ Å].^{39,40} However, the $U-N$ distances in **2** are similar to the $2.318(4)$ Å $U-N$ distance in tetravalent $[(Me_5SiC_5H_4)_3U]_2(\mu\text{-pyrazine})$.⁴⁵ The $U-N$ distances in tetravalent **2** are more similar to those in the trivalent uranium complexes $(C_5Me_5)_2U[N(SiMe_3)_2]$ [$2.352(2)$ Å],⁹ $(C_5Me_5)U[N(SiMe_3)_2]_2$ [$2.358(19)$ and $2.23(3)$ Å],⁴⁶ $U[N(SiMe_3)_2]_3$ [$2.330(4)$ Å],⁴⁷ and $\{[(Me_3Si)_2N](C_5Me_5)U\}_2(C_6H_6)$ [$2.306(2)$ Å],⁵ all of which contain anionic N-donor ligands. In comparison, the trivalent complexes of neutral N-donor ligands such as $(Me_5SiC_5H_4)_3U(\text{lutidine})$ ⁴⁸ and $(Me_5SiC_5H_4)_3U(\text{pyrimidine})$ ⁴⁸ have $U-N$ distances of $2.646(4)$ and $2.688(7)$ Å. This argues against the possibility that **2** contains U^{3+} and neutral phenazine.

The atoms comprising the phenazine dianion in **2** are coplanar to within 0.09 Å. In a comparison, the dianions in **6** and **7** are planar to within 0.06 Å.

Anthracene and Related Polycyclic Aromatic Hydrocarbons.

The reactivity of anthracene with **1** was also examined, since it too has proven to be a viable substrate with f element reductants.^{27,29} When it was determined that **1** does not reduce anthracene (-1.98 and -2.44 V vs SCE),⁴⁹ reactions with acenaphthylene (-1.65 and -1.89 V vs SCE)⁴⁹ and benzan-

(34) Evans, W. J.; Clark, R. D.; Ansari, M. A.; Ziller, J. W. *J. Am. Chem. Soc.* **1998**, *120*, 9555–9563.

(35) Evans, W. J.; Johnston, M. A.; Greci, M. A.; Ziller, J. W. *Organometallics* **1999**, *18*, 1460–1464.

(36) Shannon, R. D. *Acta Crystallogr., Sect. A* **1976**, *A32*, 751–767.

(37) Straub, T.; Frank, W.; Reiss, G. J.; Eisen, M. S. *J. Chem. Soc., Dalton Trans.* **1996**, 2541–2546.

(38) Boisson, C.; Berthet, J.-C.; Lance, M.; Nierlich, M.; Vigner, J.; Ephritikhine, M. *J. Chem. Soc., Chem. Commun.* **1995**, 543–544.

(39) Boisson, C.; Berthet, J. C.; Lance, M.; Nierlich, M.; Ephritikhine, M. *J. Organomet. Chem.* **1997**, *548*, 9–16.

(40) Other examples include $[(C_5Me_5)U(NEt_2)_2(THF)_2][BPh_4]$ [$2.17(1)$ and $2.18(1)$ Å],⁴¹ $(C_5Me_5)U[N(CH_2CH_2NSiMe_3)_3]$ [$2.264(15)$, $2.28(2)$, $2.25(2)$, and $2.61(2)$ Å],⁴² $(C_5Me_5)U(NMe_2)_3(THF)$ [$2.25(2)$, $2.31(3)$, and $2.35(5)$ Å],³⁸ $[(C_8H_8)U(NEt_2)(THF)_3][BPh_4]$ [$2.18(2)$ Å],⁴³ $Na(C_8H_8)U-[NC^iBu](Mes)_3]$ [$2.225(5)$, $2.295(4)$, and $2.286(5)$ Å],⁴⁴ $(C_8H_8)_2U_2[NC^iBu](Mes)_6]$ [$2.161(3)$, $2.174(4)$, and $2.186(3)$ Å].⁴⁴

(41) Berthet, J.-C.; Boisson, C.; Lance, M.; Vigner, J.; Nierlich, M.; Ephritikhine, M. *J. Chem. Soc., Dalton Trans.* **1995**, 3027–3033.

(42) Scott, P.; Hitchcock, P. B. *J. Chem. Soc., Dalton Trans.* **1995**, 603–609.

(43) Boisson, C.; Berthet, J. C.; Ephritikhine, M.; Lance, M.; Nierlich, M. *J. Organomet. Chem.* **1996**, *522*, 249–257.

(44) Diaconescu, P. L.; Cummins, C. C. *J. Am. Chem. Soc.* **2002**, *124*, 7660–7661.

(45) Mehdoui, T.; Berthet, J.-C.; Thuery, P.; Ephritikhine, M. *Eur. J. Inorg. Chem.* **2004**, *199*, 6–2000.

(46) Avens, L. R.; Burns, C. J.; Butcher, R. J.; Clark, D. L.; Gordon, J. C.; Schake, A. R.; Scott, B. L.; Watkin, J. G.; Zwick, B. D. *Organometallics* **2000**, *19*, 451–457.

(47) Stewart, J. L.; Andersen, R. A. *Polyhedron* **1998**, *17*, 953–958.

(48) Mehdoui, T.; Berthet, J.-C.; Thuery, P.; Ephritikhine, M. *Dalton Trans.* **2004**, 579–590.

(49) De Boer, E. *Adv. Organomet. Chem.* **1964**, *2*, 115–155.

(28) Evans, W. J.; Perotti, J. M.; Kozimor, S. A.; Champagne, T. M.; Davis, B. L.; Nyce, G. W.; Fujimoto, C. H.; Clark, R. D.; Johnston, M. A.; Ziller, J. W. *Organometallics* **2005**, *24*, 3916–3931.

(29) Evans, W. J.; Lee, D. S.; Ziller, J. W.; Kaltsayannis, N. *J. Am. Chem. Soc.* **2006**, *128*, 14176–14184.

(30) Scholz, J.; Scholz, A.; Weimann, R.; Janiak, C.; Schumann, H. *Angew. Chem., Int. Ed. Engl.* **1994**, *1233*, 1171–1174.

(31) Evans, W. J.; Kozimor, S. A.; Ziller, J. W. *Polyhedron* **2006**, *25*, 484–492.

(32) Summerscales, O. T.; Cloke, F. G. N.; Hitchcock Peter, B.; Green Jennifer, C.; Hazari, N. *Science* **2006**, *311*, 829–831.

(33) Arliguie, T.; Baudry, D.; Ephritikhine, M.; Nierlich, M.; Lance, M.; Vigner, J. *J. Chem. Soc., Dalton Trans.* **1992**, 1019–1024.

Table 3. Selected Bond Distances (Å) and Angles (deg) for [(C₅Me₅)(C₈H₈)U]₂(C₁₂H₈N₂), **2**, [(C₅Me₅)₂Sm]₂(C₁₂H₈N₂), **6**,²⁷ and [(C₅Me₅)₂La]₂(C₁₂H₈N₂), **7**,^{28,30}

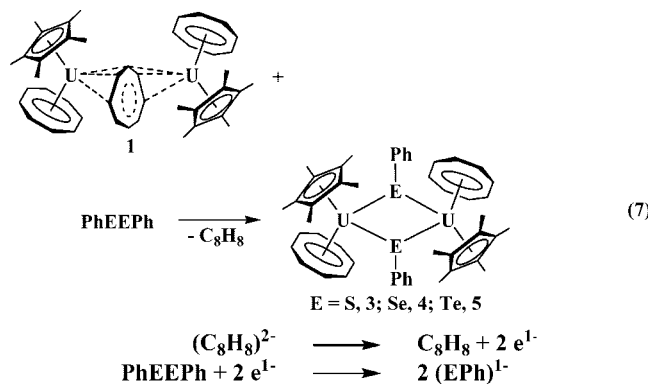
	2		6	7
U(1)–Cnt1(C ₅ Me ₅) ^a	2.478	M(1)–Cnt1(C ₅ Me ₅) ^b	2.436	2.525(1) 2.529
U(1)–Cnt2(C ₈ H ₈) ^a	1.936	M(1)–Cnt2(C ₅ Me ₅) ^b	2.421	2.541(1) 2.536
U(2)–Cnt3(C ₅ Me ₅) ^a	2.472			
U(2)–Cnt4(C ₈ H ₈) ^a	1.971			
U(1)–N(1)	2.333(6)	M(1)–N(1)	2.360(2)	2.452(2) 2.447(2)
U(2)–N(2)	2.323(5)	M(1)–C(21)		2.920(2) 2.910(2)
U(1)–C(C ₅ Me ₅) range	2.716(7)–2.769(6)	M(1)–C(22)		2.931(2) 2.929(3)
U(2)–C(C ₅ Me ₅) range	2.718(7)–2.767(7)	M(1)–C(25A)	2.866(3)	
U(1)–C(C ₈ H ₈) range	2.627(8)–2.670(8)	M(1)–C(26A)	2.877(2)	
U(2)–C(C ₈ H ₈) range	2.648(8)–2.732(7)			
U(1)–C(C ₅ Me ₅) av	2.751			
U(2)–C(C ₅ Me ₅) av	2.688			
U(1)–C(C ₈ H ₈) av	2.654			
U(2)–C(C ₈ H ₈) av	2.7466			
U–C(C ₅ Me ₅) av	2.7489			
U–C(C ₈ H ₈) av	2.671			
Cnt1–U(1)–N(1) ^a	102.1			
Cnt2–U(1)–N(1) ^a	118.5			
Cnt1–U(1)–Cnt2 ^a	139.1	Cnt1–M(1)–Cnt2 ^b	136.4	135.9(1) 136.3
Cnt3–U(2)–N(2) ^a	100.6			
Cnt4–U(2)–N(2) ^a	120.7			
Cnt3–U(2)–Cnt4 ^a	138.6			

^a Cnt1 is C(1)–C(5); Cnt2 is C(21)–C(28); Cnt3 is C(11)–C(15); Cnt4 is C(29)–C(36). ^b Cnt1 is C(1)–C(5); Cnt2 is C(11)–C(15).

thracene (–1.58 and –1.93 V vs SCE)⁴⁹ were examined. Neither of these substrates are reduced.

Diphenyldichalcogenides. Another class of substrates that has proven useful in characterizing f element reduction chemistry are the PhEPh compounds (E = S, Se, Te), which have reduction potentials of –1.75,⁵⁰ –1.20,⁵⁰ and –1.06 V⁵¹ vs SCE, respectively. Although PhSSPh has a more negative reduction potential than the first reduction potential of benzanthracene, it is reduced by **1**, as are PhSeSePh and PhTeTePh. Hence, kinetic factors including precoordination may be important in determining which substrates can be reduced by **1**.

The reaction of **1** with the PhEPh substrates in a 1:1 ratio produced crystalline solids of the formula [(C₅Me₅)(C₈H₈)U]₂(μ-EPh)₂ in each case (E = S, **3**; Se, **4**; Te, **5**), eq 7, Figures 3 and 4. One equivalent of free C₈H₈ per equivalent of **3**, **4**, and **5** was observed in each reaction mixture by ¹H NMR spectroscopy.



copy. In these reactions, as in eq 6 above, **1** functions as a two-electron reductant to convert 1 equiv of PhEPh to two (EPh)¹⁻ ligands.

(50) Bradbury, J. R.; Masters, A. F.; McDonnell, A. C.; Brunette, A. A.; Bond, A. M.; Wedd, A. C. *J. Am. Chem. Soc.* **1981**, *103*, 1959–1964.

(51) Liftman, Y.; Albeck, M. *Electrochim. Acta* **1984**, *29*, 95–98.

Table 4. ¹H NMR Spectral Data of [(C₅Me₅)(C₈H₈)U]₂(SPh)₂, **3**,⁵² [(C₅Me₅)(C₈H₈)U]₂(SePh)₂, **4**,¹⁰ and [(C₅Me₅)(C₈H₈)U]₂(TePh)₂, **5**,⁵³

complex	(C ₅ Me ₅) ¹⁻ shift	complex	(C ₅ Me ₅) ¹⁻ shift
[(C ₅ Me ₅)(C ₈ H ₈)U] ₂ (SPh) ₂ , 3	7.7	(C ₅ Me ₅) ₂ U(SPh) ₂	13.3
[(C ₅ Me ₅)(C ₈ H ₈)U] ₂ (SePh) ₂ , 4	8.6	(C ₅ Me ₅) ₂ U(SePh) ₂	14.0
[(C ₅ Me ₅)(C ₈ H ₈)U] ₂ (TePh) ₂ , 5	9.7	(C ₅ Me ₅) ₂ U(TePh) ₂	15.1
(C ₅ Me ₅) ₂ U(SPh)Me	9.4		
(C ₅ Me ₅) ₂ U(SePh)Me	9.7		
(C ₅ Me ₅) ₂ U(TePh)Me	9.8		

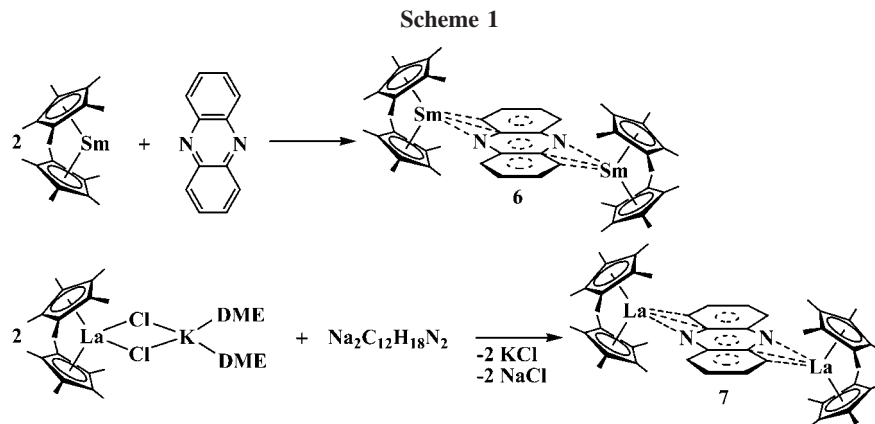
Complexes **3**–**5** were characterized by ¹H and ¹³C NMR spectroscopy, and **4** and **5** were definitively characterized by X-ray crystallography, Figures 3 and 4. The ¹H NMR spectra of **3**, **4**, and **5** show a progressive downfield shift for each of the (C₅Me₅)¹⁻, (C₈H₈)²⁻, and (EPh)¹⁻ resonances as the chalcogen is changed from S to Se to Te, Table 4. Such a trend is also observed for (C₅Me₅)₂U(EPh)₂ (E = S,⁵² Se,¹⁰ and Te⁵³) and (C₅Me₅)₂U(EPh)Me (E = S, Se, Te).⁵³

In both **4** and **5**, two [(C₅Me₅)(C₈H₈)U]¹⁺ moieties are connected by two bridging (EPh)¹⁻ ligands. In contrast to **2**, the (C₅Me₅)¹⁻ and (C₈H₈)²⁻ ligands are in a *trans* orientation around the bridging groups. Selected bond distances and angles are given in Table 5. The 3.058(1) and 3.070(1) Å U–(μ-Se) distances in **4** are similar to those in [(C₅Me₅)₂Sm(μ-SePh)₂] [3.0478(4) and 3.0558(4) Å].⁵⁴ The similarity of the M–Se distances in these complexes is consistent with the similarity of the eight-coordinate Shannon radius of Sm³⁺, 1.079 Å,³⁶ and the extrapolated value for 10-coordinate U⁴⁺, ca. 1.09 Å. The U–(μ-Se) distances in **4** are longer than the 2.7997(7), 2.8011(7), and 2.8432(7) Å U–(terminal Se) distances in

(52) Lescop, C.; Arliguie, T.; Lance, M.; Nierlich, M.; Ephritikhine, M. *J. Organomet. Chem.* **1999**, *580*, 137–144.

(53) Evans, W. J.; Miller, K. A.; Ziller, J. W.; DiPasquale, A. G.; Heroux, K. J.; Rheingold, A. L. *Organometallics* **2007**, *26*, 4287–4293.

(54) Evans, W. J.; Miller, K. A.; Lee, D. S.; Ziller, J. W. *Inorg. Chem.* **2005**, *44*, 4326–4332.



$(C_5Me_5)_2U(SePh)_2$ ¹⁰ and $(C_5Me_5)_2U(SePh)Me$,⁵³ respectively, as expected for bridging versus terminal ligands.

The structure of **5** is only the third crystallographically characterized example of a molecular complex containing a U–Te bond.^{53,55} The U–(μ -Te) distances in **5** are about 0.30 Å longer than those in **4**, a difference that is larger than the 0.23 Å difference in Shannon radii of Te²⁻ and Se²⁻. In comparison, the U–E distances in $(C_5Me_5)_2U(SePh)_2$ and $(C_5Me_5)_2U(TePh)_2$ differed by 0.24 Å,⁵⁴ and the Sm–E distances in $[(C_5Me_5)_2Sm(\mu-SePh)]_2$ and $[(C_5Me_5)_2Sm(\mu-TePh)]_2$ differed by 0.17–0.20 Å.

Although **4** and **5** have nearly identical (C_5Me_5) ring centroid–U–(C_8H_8 ring centroid) and U–E–U' angles, these complexes differ in the orientation of the phenyl rings, as shown in Figures 3 and 4. In **4**, the plane of the phenyl rings displays a 21.3° angle with respect to the U_2Se_2 plane. This puts the phenyl rings in the middle of the (C_5Me_5) –U–(C_8H_8) wedge and keeps the phenyl substituents away from the $(C_5Me_5)^{1-}$ and $(C_8H_8)^{2-}$ rings. The longer U–Te distances in **5** may allow the phenyl rings to adopt the 77.7° average angle between the planes of the phenyl rings and the U_2Te_2 plane.

Nitrobenzene. The reaction of **1** with nitrobenzene (–1.15 V vs SCE)⁵⁶ was examined for comparison with the (ⁿBu-

Table 5. Selected Bond Distances (Å) and Angles (deg) for $[(C_5Me_5)(C_8H_8)U]_2(SePh)_2$, **4**, and $[(C_5Me_5)(C_8H_8)U]_2(TePh)_2$, **5**

	4	5
U(1)–Cnt1(C_5Me_5) ^a	2.482	2.472
U(1)–Cnt2(C_8H_8) ^a	1.968	1.969
U(1)–E(1)	3.0575(11)	3.3589(7)
U(1)–E(1A)	3.0704(9)	3.3725(10)
U(1)–C(C_5Me_5) range	2.744(7)–2.774(7)	2.728(6)–2.773(6)
U(1)–C(C_8H_8) range	2.641(8)–2.714(7)	2.653(7)–2.718(6)
U(1)–C(C_5Me_5) av	2.7576	2.752
U(1)–C(C_8H_8) av	2.676	2.6861
Cnt1–U(1)–E(1) ^a	105.8	98.0
Cnt1–U(1)–E(1) ^a	113.1	107.0
Cnt2–U(1)–E(1A) ^a	100.6	119.1
Cnt2–U(1)–E(1A) ^a	117.5	112.1
Cnt1–U(1)–Cnt2 ^a	135.3	135.8
U(1A)–E(1)–U(1) ^a	120.74(3)	120.810(18)

^a Cnt1 is C(1)–C(5); Cnt2 is C(11)–C(18).

C_8H_8)U reaction, eq 5. Reduction occurs and free C_8H_8 is observed, but the other reaction products were not readily identifiable.

Discussion

$[(C_5Me_5)(C_8H_8)U]_2(C_8H_8)$, **1**, has been shown to act as a two-electron reductant with substrates such as phenazine and the PhEPh compounds (E = S, Se, Te). In these reductions, one of the $(C_8H_8)^{2-}$ ligands per molecule is oxidized to free C_8H_8 and two $(C_8H_8)^{2-}$ ligands are retained in the bimetallic product. Since the 1:2 ratio of bridging to terminal $(C_8H_8)^{2-}$ ligands in **1** is the same as the 1:2 ratio of reactive $(C_8H_8)^{2-}$ and unreactive $(C_8H_8)^{2-}$ species in the reductions, it is attractive to assign the reductive reactivity to the bridging $(C_8H_8)^{2-}$ species. Moreover, since the bridging $(C_8H_8)^{2-}$ ligand is unusual in its nonplanar solid-state structure, it could have enhanced reactivity. However, there is no hard evidence to support these correlations. In solution, the full asymmetry of the bridging ligand of **1** is not observed by ¹H NMR spectroscopy, although two $(C_8H_8)^{2-}$ resonances are observable in a 2:1 ratio.

Complex **1** provides a facile synthetic route to the heteroleptic metallocene moiety $[(C_5Me_5)(C_8H_8)U]^{1+}$ through reactions like eq 6 and 7. This provides an opportunity to compare a mixed ligand monocationic metallocene to the more common $[(C_5Me_5)_2M]^{1+}$ monocationic moiety. If the central $(C_8H_8)^{2-}$ functions as a two-electron reductant, this allows **1** to react equivalently to two trivalent $(C_5Me_5)(C_8H_8)U$ moieties.

(71) Leverd, P. C.; Arliguie, T.; Lance, M.; Nierlich, M.; Vigner, J.; Ephritikhine, M. *J. Chem. Soc., Dalton Trans.* **1994**, 501–504.

(72) Arliguie, T.; Fourmigue, M.; Ephritikhine, M. *Organometallics* **2000**, *19*, 109–111.

(55) Gaunt, A. J.; Scott, B. L.; Neu, M. P. *Angew. Chem., Int. Ed.* **2006**, *45*, 1638–1641.

(56) Maki, A. K.; Geske, D. H. *J. Am. Chem. Soc.* **1961**, *83*, 1852–1860.

(57) Schake, A. R.; Avens, L. R.; Burns, C. J.; Clark, D. L.; Sattelberger, A. P.; Smith, W. H. *Organometallics* **1993**, *12*, 1497–1498.

(58) Cendrowski-Guillaume, S. M.; Le Gland, G.; Nierlich, M.; Ephritikhine, M. *Eur. J. Inorg. Chem.* **2003**, 1388–1393.

(59) Cendrowski-Guillaume, S. M.; Nierlich, M.; Ephritikhine, M. *Eur. J. Inorg. Chem.* **2001**, 1495–1498.

(60) Evans, W. J.; Nycy, G. W.; Greci, M. A.; Ziller, J. W. *Inorg. Chem.* **2001**, *40*, 6725–6730.

(61) Cendrowski-Guillaume, S. M.; Nierlich, M.; Ephritikhine, M. *J. Organomet. Chem.* **2002**, *643–644*, 209–213.

(62) Baudry, D.; Bulot, E.; Ephritikhine, M.; Nierlich, M.; Lance, M.; Vigner, J. *J. Organomet. Chem.* **1990**, *388*, 279–287.

(63) Berthet, J.-C.; Le Marechal, J.-F.; Ephritikhine, M. *J. Organomet. Chem.* **1994**, *480*, 155–161.

(64) Berthet, J. C.; Nierlich, M.; Ephritikhine, M. *Eur. J. Inorg. Chem.* **2002**, 850–858.

(65) Boisson, C.; Berthet, J.-C.; Lance, M.; Vigner, J.; Nierlich, M.; Ephritikhine, M. *J. Chem. Soc., Dalton Trans.* **1996**, 947–953.

(66) Berthet, J. C.; Ephritikhine, M. *J. Chem. Soc., Chem. Commun.* **1993**, 1566–1567.

(67) Cendrowski-Guillaume, S. M.; Lance, M.; Nierlich, M.; Ephritikhine, M. *Organometallics* **2000**, *19*, 3257–3259.

(68) Arliguie, T.; Thuery, P.; Fourmigue, M.; Ephritikhine, M. *Organometallics* **2003**, *22*, 3000–3003.

(69) Arliguie, T.; Thuery, P.; Fourmigue, M.; Ephritikhine, M. *Eur. J. Inorg. Chem.* **2004**, 4502–4509.

(70) Boussie, T. R.; Moore, R. M., Jr.; Streitwieser, A.; Zalkin, A.; Brennan, J.; Smith, K. A. *Organometallics* **1990**, *9*, 2010–2016.

The chemistry of $(C_5Me_5)(C_8H_8)U$ has previously been explored only through its solvated derivative $(C_5Me_5)(C_8H_8)U(THF)$.⁵⁷ $(C_5Me_5)(C_8H_8)U(THF)$ and **1** differ in that the former complex would derive its reductive reactivity from U^{3+} , whereas the latter formally uses the reductive capacity of $(C_8H_8)^{2-}$.

Conclusion

Tetravalent $[(C_5Me_5)(C_8H_8)U]_2(C_8H_8)$, **1**, functions as a two-electron reductant with phenazine and PhEPh substrates to make bimetallic heteroleptic tetravalent complexes containing one $(C_5Me_5)^{1-}$ ligand and one $(C_8H_8)^{2-}$ ligand per uranium. The mixed ligand metallocene unit, $[(C_5Me_5)(C_8H_8)U]^{1+}$, offers an alternative to the common $[(C_5Me_5)_2U]^{2+}$ moiety and is ef-

fectively the actinide equivalent of $[(C_5Me_5)_2Ln]^{1+}$. Reductive chemistry with solvent-free $[(C_5Me_5)(C_8H_8)U]^{1+}$ is readily accessible synthetically through **1**.

Acknowledgment. We thank the National Science Foundation for support of this research.

Supporting Information Available: X-ray data collection, structure solution, and refinement (PDF) and X-ray diffraction details of compounds **2**, **3**, and **5** (CIF, CCDC No. 697218–697200). This material is available free of charge via the Internet at <http://pubs.acs.org>.

OM800747S

Oligomerization of α -Olefins via Chromium Metallacycles

David S. McGuinness*

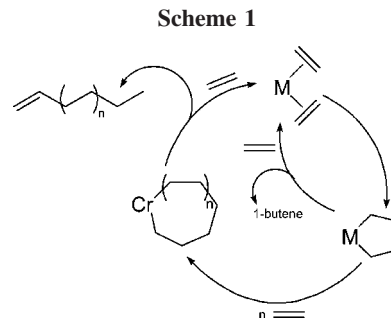
School of Chemistry, University of Tasmania, Private Bag 75, Hobart, Tasmania 7000, Australia

Received August 27, 2008

Chromium complexes that oligomerize and polymerize olefins via a metallacycle mechanism represent possible models for the commercially important Phillips catalyst, which is still poorly understood mechanistically. Comparisons between the two might provide insight into the process, and as such the oligomerization of α -olefins (propene to 1-octene) with chromium(III)–bis(carbene)pyridine complexes in combination with MAO has been studied. Linear α -olefins are homo-oligomerized, as well as co-oligomerized with ethylene, via a mechanism most likely involving metallacycles. Homo-oligomerization of α -olefins leads predominantly to head-to-tail dimers with vinylidene unsaturation, while a less favorable coupling leads to linear internal olefin dimers. With shorter chain monomers, trimerization and tetramerization become more significant, albeit still minor processes. The kinetics of 1-octene dimerization were studied and are found to be first-order in chromium but zero-order in 1-octene concentration. The results are interpreted in terms of the likely rate-determining step of the reaction, and comparisons are drawn between the behavior of this system and the heterogeneous Phillips catalyst.

1. Introduction

The oligomerization and polymerization of ethylene via the metallacyclic mechanism (Scheme 1) has received much attention lately, primarily due to its implication in the selective trimerization and tetramerization of ethylene to 1-hexene and 1-octene, respectively.^{1–3} The key to the selectivity of these systems seems to lie in the energetically preferred tendency of M–C₆ and M–C₈ metallacycles to undergo product releasing β -hydrogen shift rather than further ethylene insertion. At the same time, a constrained geometry of the metallacycle prevents the β -hydrogen shift reaction at the M–C₄ stage, and, as such, very low amounts of 1-butene are produced. While most of the recent interest in this mechanism stems from this selectivity effect, such a mechanism has long been proposed as one possibility for the polymerization of ethylene with the industrial chromium on silica Phillips catalyst, one of the most important yet mechanistically controversial catalyst systems known.^{4,5} It is certainly the case that chromium catalysts seem to have a certain predisposition to the metallacycle mechanism, as most trimerization and tetramerization catalysts are based upon this metal. Additionally, the possibility of an extended metallacycle mechanism, leading to higher oligomers and polymer, has recently been confirmed in a number of studies with homogeneous chromium catalysts.^{6–8} This work supports the possibility



of metallacycles being responsible for polyethylene production on heterogeneous chromium catalysts, although the mechanism still remains highly uncertain.

In contrast to ethylene, very few studies have investigated the effect of higher α -olefins on the metallacycle mechanism. The formation and growth of metallacycles from α -olefins is expected to be slower than is the case for ethylene, while the rate of decomposition might be less affected. This should manifest in a different oligomer distribution (carbon number selectivity). The secondary incorporation of one molecule of α -olefin (1-hexene/1-octene) is well-known for trimerization and tetramerization catalysts; however, incorporation of more than one α -olefin unit is not observed with these systems.^{3,9,10} In addition, the codimerization of ethylene and 1-butene with titanium complexes is thought to occur via a metallacycle mechanism.¹¹ To our knowledge, the only known system capable of homo-oligomerizing higher α -olefins via a metallacycle mechanism is the chromium–triazacyclohexane system of Köhn and Wasserscheid.^{12,13} This catalyst selectively converts α -olefins to isomeric trimers, which are of interest as synthetic

* To whom correspondence should be addressed. E-mail: david.mcguinness@utas.edu.au.

(1) Dixon, J. T.; Green, M. J.; Hess, F. M.; Morgan, D. H. *J. Organomet. Chem.* **2004**, 689, 3641.

(2) Wass, D. F. *Dalton Trans.* **2007**, 816.

(3) Overett, M. J.; Blann, K.; Bollmann, A.; Dixon, J. T.; Haasbroek, D.; Killian, E.; Maumela, H.; McGuinness, D. S.; Morgan, D. H. *J. Am. Chem. Soc.* **2005**, 127, 10723.

(4) Groppo, E.; Lamberti, C.; Bordiga, S.; Spoto, G.; Zecchina, A. *Chem. Rev.* **2005**, 105, 115.

(5) Theopold, K. H. *CHEMTECH* **1997**, 27, 26.

(6) Tomov, A. K.; Chirinos, J. J.; Jones, D. J.; Long, R. J.; Gibson, V. C. *J. Am. Chem. Soc.* **2005**, 127, 10166.

(7) Tomov, A. K.; Chirinos, J. J.; Long, R. J.; Gibson, V. C.; Elsegood, M. R. *J. Am. Chem. Soc.* **2006**, 128, 7704.

(8) McGuinness, D. S.; Suttill, J. A.; Gardiner, M. G.; Davies, N. W. *Organometallics* **2008**, 27, 4238.

(9) Deckers, P. J. W.; Hessen, B.; Teuben, J. H. *Organometallics* **2002**, 21, 5122.

(10) Bowen, L. E.; Wass, D. F. *Organometallics* **2006**, 25, 555.

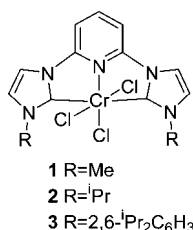
(11) You, Y.; Girolami, G. S. *Organometallics* **2008**, 27, 3172.

(12) Köhn, R. D.; Haufe, M.; Kociok-Köhn, G.; Grimm, S.; Wasserscheid, P.; Keim, W. *Angew. Chem., Int. Ed.* **2000**, 39, 4337.

(13) Wasserscheid, P.; Grimm, S.; Köhn, R. D.; Haufe, M. *Adv. Synth. Catal.* **2001**, 343, 814.

lubricants. The same catalyst converts ethylene to polyethylene (with some 1-hexene also formed), presumably also via a metallacycle mechanism. Such incorporation of α -olefins into metallacycles is relevant to ongoing debate around the mechanism of the Phillips catalyst, which is also known to incorporate α -olefins into the polymeric chain. Comparison of the products formed in each case might provide further insight into the mechanism of the Phillips catalyst.

We recently reported⁸ that bis(carbene)pyridine complexes of chromium (1–3), previously¹⁴ established as highly active ethylene oligomerization catalysts (in combination with MAO), do so via an extended metallacycle mechanism. These systems were also found to incorporate the α -olefins formed in the process into higher oligomers, again via a metallacycle route. Herein, we report investigations into the oligomerization of α -olefins with these catalysts. Product selectivities and reaction kinetics have been studied to gain further insight into metallacycle formation, growth, and decomposition.



2. Results and Discussion

2.1. Ethylene/1-Octene Co-oligomerization. Previously it was shown that α -olefins, formed as the primary products during ethylene oligomerization with 1–3, become incorporated into the reaction, leading to small amounts of vinylidenes and linear internal olefins.⁸ In an extension to this work, the oligomerization reaction with 2/MAO was carried out in 1-octene as the solvent [$p(\text{ethylene}) = 1$ bar gauge]. Along with a distribution of linear α -olefins resulting from ethylene homo-oligomerization, a second major distribution of vinylidene olefins was also formed (Figure 1). The major product formed is 2-ethyl-1-octene, which results from coupling of ethylene and 1-octene via metallacycle **I**, Scheme 2. Support for a metallacycle mechanism for α -olefin incorporation comes from co-oligomerization of CH₂CH₂, CD₂CD₂, and 1-octene, which produced only D₀ and D₄ isotopomers of 2-ethyl-1-octene, therefore ruling out a Cossee–Arlman linear growth mechanism.^{15,16}

Progressively lower amounts of C₁₂ and C₁₄ vinylidenes result from further ethylene insertion into metallacycle **I**; however, it was noted that the amount of C₁₆ vinylidene is well above that expected from a statistical distribution (Figure 1, inset). The major C₁₆ product (90%) is 2-hexyl-1-decene. While this compound would be produced by three ethylene insertions into metallacycle **I**, the greatly increased amount suggests that it is also being produced by a second process. This second process is the oxidative coupling of two 1-octene units to afford metallacycle **II** (Scheme 2), representing metallacyclic dimerization of α -olefins (confirmed below). Although not clearly apparent in Figure 1, the amount of C₁₈ formed is also elevated above that expected from a statistical distribution arising from

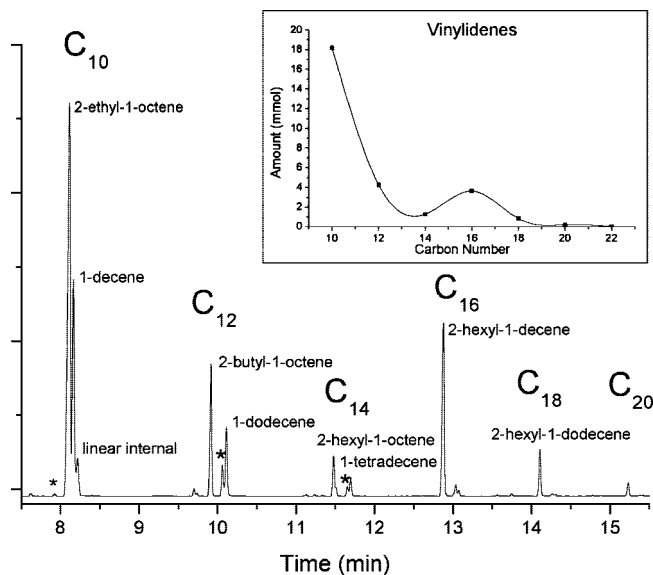
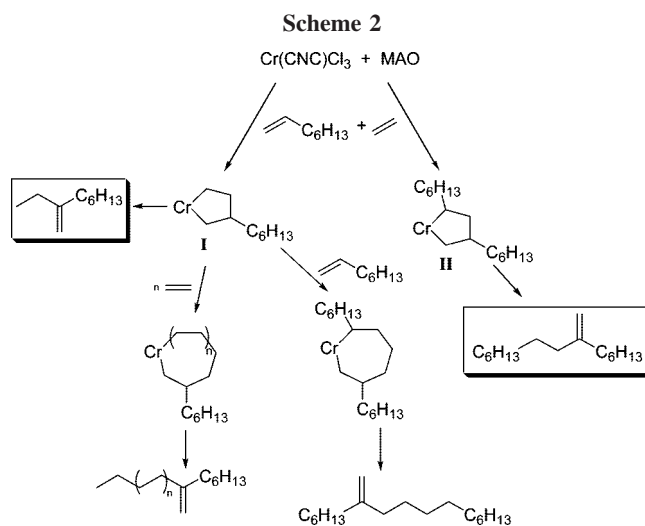


Figure 1. GC-FID trace of the C₁₀₊ olefins formed in the co-oligomerization of ethylene/1-octene with 2/MAO (inset: plot of amount of vinylidene olefins (mmol) versus carbon number). *Vinylidene products resulting from the incorporation of α -olefins generated by ethylene homo-oligomerization.



ethylene insertions into metallacycle **I**. Initially it was thought that this must arise from ethylene insertion into metallacycle **II**; however, such a route cannot generate the structure of the main C₁₈ oligomer (2-hexyl-1-dodecene). Instead, 1-octene insertion into metallacycle **I** must be responsible, as shown in Scheme 2.¹⁷ This product therefore represents cotrimerization with incorporation of two α -olefins and demonstrates that higher α -olefins are capable of inserting into the Cr–C₄ metallacycle of the active species formed from catalyst 2. As a result of these observations, it was decided to investigate the homo-oligomerization of α -olefins with catalysts 1–3.

2.2. α -Olefin Oligomerization. The results of oligomerization of α -olefins catalyzed by 1–3/MAO are shown in Table 1. The combination of complex 2 and 1-octene was trialed first (entry 1), which led to a turnover number in 1-octene of 1120 after 3 h. There is no real increase in productivity after 24 h, indicating that the catalyst has deactivated after 3 h. The major

(14) McGuinness, D. S.; Gibson, V. C.; Wass, D. F.; Steed, J. W. *J. Am. Chem. Soc.* **2003**, *125*, 12716.

(15) Agapie, T.; Schofer, S. J.; Labinger, J. A.; Bercaw, J. E. *J. Am. Chem. Soc.* **2004**, *126*, 1304.

(16) Agapie, T.; Labinger, J. A.; Bercaw, J. E. *J. Am. Chem. Soc.* **2007**, *129*, 14281.

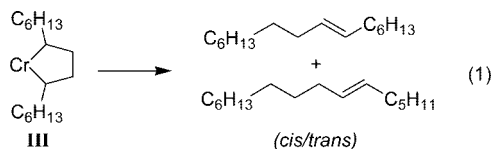
(17) Co-oligomerization of C₂H₄, C₂D₄, and 1-octene yielded only D₀ and D₄ isotopomers of the main C₁₈ product (2-hexyl-1-dodecene), again indicating a metallacycle mechanism for its formation.

Table 1. α -Olefin Oligomerization with Complexes 1–3/MAO^a

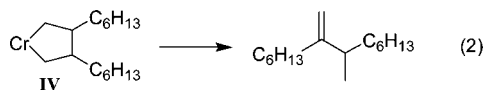
entry	α -olefin	catalyst ([Cr] mM)	TON 3 h	TON 24 h	linear		
					vinylidene dimer (wt %)	internal dimer (wt %)	trimer (wt %)
1	1-octene	2(0.33)	1120	1170	91	9	trace
2	1-octene	1(0.33)	190	412	86	12	2
3	1-octene	3(0.33)	2420	3480	75	16	7
4	1-octene	3(0.067)		8600	74	15	9
5	1-pentene	3(0.33)	4920	6370	62	22	11 ^b
6	1-butene	3(0.33)	3085		68	16	12 ^c
7	propene	3(0.33)	1800		50 ^d	7	20 ^e

^a Conditions: toluene (20 mL), α -olefin (10 mL), 500 equiv of MAO, 20 °C. ^b 1 wt % tetramer also formed. ^c 2 wt % tetramer also formed. ^d 4-Methyl-2-pentene and 4-methyl-1-pentene amounting to 19 wt % also formed; see text. ^e 4 wt % tetramer also formed.

product formed is the head-to-tail vinylidene dimer 2-hexyl-1-decene (91%), followed by linear internal olefin dimers (9%). The linear dimers (at least three double bond isomers were partially resolvable by GC–MS) would result from decomposition of metallacycle **III** (reaction 1) with the position of the double bond being dependent upon the site of β -hydrogen transfer (endocyclic or exocyclic). Given that three isomers are detected, cis/trans isomers must be also be present, although the exact identity of these linear internal olefins was not investigated further. Trace products of formula C₂₄H₄₈ were also detected, corresponding to 1-octene trimers. This again indicates that α -olefins are capable of inserting into the Cr–C₄ metallacycles formed from **2**, albeit unfavorable as compared to metallacycle decomposition.

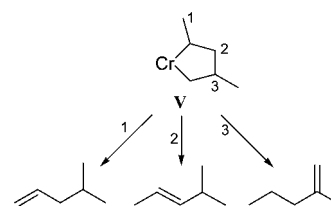


Catalyst **1** led to much lower conversion of 1-octene (entry 2), although the product distribution was similar to that obtained with **2**. In contrast, **3** was the most active catalyst for 1-octene conversion (entry 3), as it was for ethylene oligomerization.¹⁴ In this case, increased amounts of linear internal olefin dimers resulted, and the amount of trimers increased to 7%.¹⁸ Additionally, at least three other minor dimers resulted (2 wt % in total). Not all of these minor dimers were identified; however, hydrogenation of the sample produced 7,8-dimethyltetradecane, indicating one of these compounds is the vinylidene resulting from decomposition of metallacycle **IV** (reaction 2).



The remaining experiments were conducted using complex **3**. Entry 4 reveals that relatively high turnover numbers can be achieved with a prolonged run time (24 h) and low catalyst loading, although the system was not optimized further as we

(18) As pointed out by a referee, the increase in the amount of trimers formed with complex **3** (the most sterically encumbered complex) is somewhat counterintuitive. Complex **3** is inherently more active than **1** and **2**, both in ethylene and in α -olefin oligomerization. We are unsure of the reason for this, but it may be related more to electronic factors than to sterics (as increased bulk might be expected to slow catalysis, if anything). The greater incidence of trimerization might simply result from the higher rate of alkene insertion with **3**. At the same time, however, the sterics of the α -olefin do seem to play a role, as shorter chain monomers do lead to increases in the trimer and tetramer fractions (Table 1).

Scheme 3

were primarily interested in product selectivities. Oligomerization of 1-pentene (entry 5) proceeds at approximately twice the rate of 1-octene oligomerization (as judged by the turnover number), and the product selectivity is shifted somewhat. In particular, 1% tetramer was formed in this run. With 1-butene (entry 6),¹⁹ the dimer selectivity shifts again, but there is no clear trend in selectivity within the dimer fraction for different monomers. In this run, 2% tetramer was formed, and there does seem to be a gradual increase in trimers and tetramers with shorter chain monomers. A significant decrease in the selectivity toward the main vinylidene dimer (2-methyl-1-pentene) was found when propene was tested (entry 7). This is partly due to increased trimer and tetramer formation (20% and 4%, respectively). However, a significant change in selectivity within the dimer fraction is also observed, which is now made up of 25% 4-methyl-2-pentene and 4-methyl-1-pentene. These represent double bond isomers of the main dimer, 2-methyl-1-pentene (66% of the C₆ fraction), and would originate from β -hydrogen transfer from three different sites of metallacycle **V** (Scheme 3). The corresponding isomers are not observed in runs with longer chain monomers (although may be accounted for by minor unidentified products), and the reason for this selectivity change is unclear.

2.3. Kinetics of 1-Octene Dimerization. Theoretical studies of ethylene trimerization catalysts generally suggest that metallacyclopentane formation is fast, while metallacycle growth is the rate-determining step.^{20–22} Therefore, the kinetics of product formation are controlled by insertion of ethylene into the M–C₄ metallacycle. With the present system in combination with α -olefins, insertion into the metallacyclopentane is not favored, providing an opportunity to investigate the kinetics of metallacycle formation and decomposition. As such, the rates of formation of the major 1-octene dimerization products (2-hexyl-1-decene and internal hexadecenes) have been measured for complex **3**/MAO. Rate plots for these dimers at two chromium concentrations are shown in Figure 2. These measurements were limited to around 1 h such that catalyst degradation did not affect the results. This corresponds to approximately one-half-life, and as such a halving of the 1-octene concentration over the run. At a given chromium concentration, the rates of formation of both vinylidene and internal olefin dimers are constant, showing that the reaction is zero-order in 1-octene. This is somewhat surprising given that two molecules of 1-octene are involved in the reaction. In contrast, dimerization is first-order in chromium, and the rate equation can be expressed as $r = k[\text{Cr}]$, where the rate constant

(19) The productivities reported for the gaseous monomers (1-butene, propene) are not comparable to those for the liquid monomers (1-octene, 1-pentene), due to differences in purity. The liquid monomers were distilled from sodium-benzophenone and can be considered rigorously anhydrous and oxygen free. 1-Butene and propene, on the other hand, were used as received (Aldrich 99%).

(20) Tobisch, S.; Ziegler, T. *Organometallics* **2003**, *22*, 5392.

(21) Blok, A. N. J.; Budzelaar, P. H. M.; Gal, A. W. *Organometallics* **2003**, *22*, 2564.

(22) Janse van Rensburg, W.; Grove, C.; Steynberg, J. P.; Stark, K. B.; Huyser, J. J.; Steynberg, P. J. *Organometallics* **2004**, *23*, 1207.

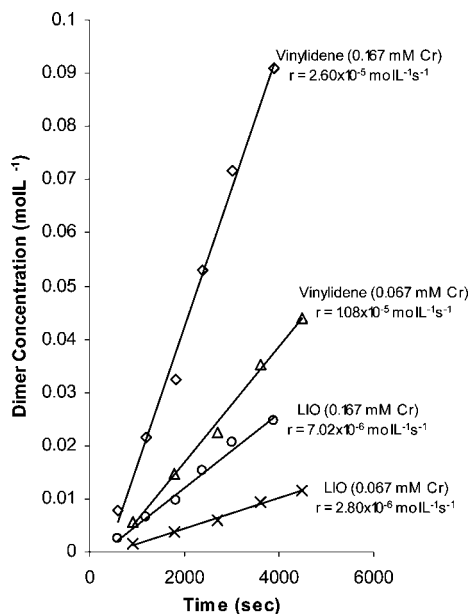
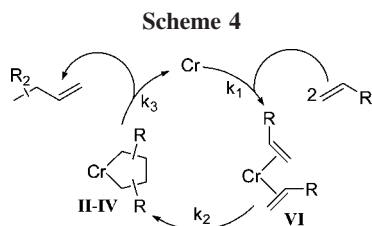


Figure 2. Kinetic plot for the formation of 2-hexyl-1-decene (vinylidene) and linear internal olefins (LIO) in 1-octene dimerization with **3**/MAO. Conditions: toluene (20 mL), 1-octene (10 mL), 500 equiv of MAO, 20 °C.



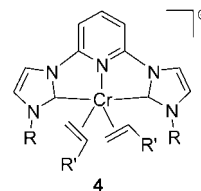
k for vinylidene formation is 0.16 s^{-1} and that for internal olefins is 0.042 s^{-1} .²³

There are two possible mechanistic explanations for such a rate equation (Scheme 4). The first is that formation of a bis-olefin complex **VI** is fast, followed by a rate-determining oxidative coupling to form the metallacycle (as such, **VI** would represent the catalyst resting state, $k_2 < k_1, k_3$). Applying the steady state approximation to **VI**, the rate equation would be $r = k_2[\text{VI}]$. The second possibility is that metallacycle formation is fast, followed by a rate-determining β -hydrogen shift and product release, in which case the catalyst resting state would be the metallacycles **II–IV** ($k_3 < k_1, k_2$). In this case, the steady state approximation would yield the rate equation $r = k_3[\text{II–IV}]$. It is difficult to differentiate between these two possibilities. On the one hand, β -hydride transfer in metallacyclopentanes is predicted to be slow^{20,21,24} (and is so for selective trimerization catalysts), suggesting this may be the rate-determining step. On the other hand, 1-butene formation is very rapid when **1–3** are employed in ethylene oligomerization, showing that, with the present systems at least, metallacyclopentane decomposition is facile. To investigate this further, quick-kill experiments were conducted in which attempts were made to hydrolyze any metallacycles present. At very high catalyst loadings ($[\text{Cr}] \approx$

9.5 mM), 1-octene dimerization was quenched with dilute hydrochloric acid 30 s into a run. Hydrolysis of chromium metallacycles would be expected to generate the corresponding paraffins, while hydrolysis of a bis-olefin complex would simply release the olefins. Despite the presence of the expected 1-octene dimers, there were no traces of paraffin, suggesting that there is no appreciable concentration of metallacycles present. While negative evidence such as this is by no means conclusive, it does lean toward a rate-determining oxidative coupling and a bis-olefin catalyst resting state.

3. Summary and Conclusions

This work has shown that chromium complexes of bis(carbene)pyridine ligands catalyze the oligomerization of α -olefins when activated with MAO, leading predominantly to head-to-tail dimers with vinylidene unsaturation. The results strongly indicate a metallacycle mechanism is operative, in common with ethylene oligomerization. Although not investigated in this work, it is possible to speculate as to what form the active species might take. The fact that MAO is the activator of choice suggests that a formally cationic complex is responsible.²⁵ This is supported by the fact that activation with $\text{AlR}_3/\text{Ph}_3\text{C–B}(\text{C}_6\text{F}_5)_4$ is also effective, albeit less so than that with MAO.¹⁴ A $\text{Cr}^{\text{I}} \rightarrow \text{Cr}^{\text{III}}$ cycle is one possibility, starting at complex **4**. Such a redox couple has been suggested for chromium trimerization and tetramerization catalysts that incorporate neutral ancillary ligands.^{15,26,27}



While the reaction of **1–3**/MAO with ethylene produces longer chain oligomers and some polymer, the change to α -olefins leads to a dramatic shift in selectivity to dimers. Selectivity is controlled by the rates of chain propagation (insertion) versus chain termination (metallacycle decomposition) and reveals that the relative rate of chain termination is increased when α -olefins are present. This is most likely because further insertion into a disubstituted metallacyclopentane is more difficult on steric grounds. However, termination is also accelerated in the co-oligomerization of ethylene and α -olefins, showing that incorporation of even one α -olefin into the metallacycle favors decomposition. Several parallels can be drawn between this system and the heterogeneous Phillips catalyst. First, it has likewise been reported that the presence of α -olefin promotes chain termination in ethylene polymerization with the Phillips catalyst.²⁸ Second, α -olefin incorporation in this case leads predominantly to terminal vinylidene unsaturation in the polymer (with rare internal unsaturation). Thus, the preference for termination via vinylidene formation matches that found in this work. Additionally, the Phillips catalyst will catalyze the homopolymerization of α -olefins, and as in this

(23) As different internal olefin isomers are not fully resolvable by GC, the rate constant measured represents the sum of the rate constants for each individual isomer. As each originates from a common metallacycle (**III**), the measured rate constant reflects the rate of decomposition of this metallacycle.

(24) de Bruin, T. J. M.; Magna, L.; Raybaud, P.; Toulhoat, H. *Organometallics* **2003**, *22*, 3404.

(25) Chen, E. Y.-X.; Marks, T. J. *Chem. Rev.* **2000**, *100*, 1391.

(26) Köhn, R. D.; Smith, D.; Mahon, M. F.; Prinz, M.; Mihan, S.; Kociok-Köhn, G. *J. Organomet. Chem.* **2003**, *683*, 200.

(27) Rucklidge, A. J.; McGuinness, D. S.; Tooze, R. P.; Slawin, A. M. Z.; Pelletier, J. D. A.; Hanton, M. J.; Webb, P. B. *Organometallics* **2007**, *26*, 2782.

(28) McDaniel, M. P. *Adv. Catal.* **1985**, *33*, 47.

work the reaction is zero-order in olefin.²⁹ All of these observations can also be explained on the basis of a Cossee–Arlman linear chain growth mechanism, but they do at least show that the behavior of the Phillips catalyst closely matches that of a catalyst with an established metallocycle mechanism.

4. Experimental Section

4.1. General Comments. All manipulations were carried out using standard Schlenk techniques or in a nitrogen glovebox, using solvents purified by passage through an Innovative Technologies solvent purification system (purification over activated alumina, copper catalyst, and/or molecular sieves). Ethylene was purified by passage through activated 3 Å molecular sieves followed by alumina. 1-Octene and 1-pentene were distilled from sodium/benzophenone, while 1-butene and propene were purchased from Aldrich and used as received. Methylaluminoxane (MAO) in toluene was supplied by Albemarle. ¹H NMR spectra were recorded on a Varian Mercury Plus NMR spectrometer operating at 300 MHz, with spectra referenced against residual solvent peaks.

4.2. 1-Octene/Ethylene Co-oligomerization. Catalyst **2** (10 μmol) was suspended in 37 mL of 1-octene and treated with 1000 equiv of MAO. Ethylene was immediately added to a pressure of 1 bar gauge. The solution was held at 25 °C with vigorous stirring for 30 min, after which it was quenched with 10% HCl and an internal standard (nonane, 1.00 mL) was added. The organic fraction was analyzed by GC-FID, while no solid polymer was formed. ¹H NMR analysis of the reaction solution showed a composition of 6 mol % internal olefins (5.30–5.40 ppm), 77 mol % α-olefins (4.84–5.00 ppm), and 17 mol % vinylidene olefins (4.68–4.78 ppm). After removal of the volatiles under vacuum (leaving the C₁₀₊ oligomers), the composition was 4 mol % internal, 12 mol % α, and 84 mol % vinylidene. A total of 8.4 g of oligomers was formed in the run, with the following carbon-number weight percentages: C₄ (12.2%); C₆ (13.2%); C₁₀ (44.4%); C₁₂ (12.2%); C₁₄ (4.0%); C₁₆ (10.4%); C₁₈ (2.5%); C₂₀ (0.8%); C₂₂ (0.3%).

4.3. 1-Octene/C₂H₄/C₂D₄ Co-oligomerization. The co-oligomerization reaction was repeated with a mixture of 1:1 C₂H₄:C₂D₄.

GC–MS analysis revealed only D₀ and D₄ isotopomers of 2-ethyl-1-octene and 2-hexyl-1-dodecene.

4.4. α-Olefin Oligomerization. The general procedure is illustrated here by the dimerization of 1-octene with catalyst **2** (Table 1, entry 1). Ten micromoles of **2** was suspended in 10 mL of 1-octene, 0.250 g of *n*-tridecane (internal standard), and toluene such that the final volume was 30 mL (in cases where gaseous olefins (1-butene, propene) were used, the toluene suspension was saturated with the olefin by continued bubbling). MAO solution (500 equiv) was added, and the temperature was held at 20 °C through the use of a water bath. Aliquots were taken at desired intervals, quenched with 10% HCl, and analyzed by GC-FID. Removal of volatiles under vacuum left only 2-hexyl-1-decene and linear internal hexadecenes. ¹H NMR (toluene-*d*₈): 0.88 (t, 6H, CH₃); 1.25 (m, br, 16H, CH₂); 1.43 (q, br, 4H, CH₂CH₃); 2.01 (2t, 4H, CH₂C(R)=CH₂); 4.81 (s, 2H, C=CH₂, 83 mol %); 5.42 (m, br, 2H, HC(R)=C(R)H, 17 mol %).

4.5. Oligomer Analysis. Oligomers were identified by GC–MS analysis of both olefinic and hydrogenated samples. Hydrogenation was carried out over PtO₂ at 80 °C under 12 bar of hydrogen (generally overnight). A combination of characteristic electron ionization spectra together with Kovats' retention indices was used, together with NMR analysis where required. Further details of oligomer identification are given in the Supporting Information of ref 8.

Acknowledgment. We thank Albemarle Asia Pacific for donating MAO solution and Tony Caselli of Plastral Pty Ltd. for facilitating this. Noel Davies is thanked for acquisition of GC–MS data and analysis. The Australian Research Council is thanked for financial support and a QEII Fellowship to D.S.M.

Supporting Information Available: Details of ethylene/1-octene co-oligomer distribution analysis and procedure for 1-octene dimerization kinetic experiments. This material is available free of charge via the Internet at <http://pubs.acs.org>.

(29) Weiss, K.; Krauss, H.-L. *J. Catal.* **1984**, *88*, 424.

Isobutene Polymerization Using Chelating Diboranes: Polymerization in Aqueous Suspension and Hydrocarbon Solution

Stewart P. Lewis, Jianfang Chai, and Scott Collins*

Department of Polymer Science, The University of Akron, Akron, Ohio 44325-3909

Timo J. J. Sciarone, Lee D. Henderson, Cheng Fan, Masood Parvez, and Warren E. Piers*

Department of Chemistry, The University of Calgary, Calgary, Alberta, Canada

Received August 7, 2008

The use of the chelating diboranes $o\text{-C}_6\text{F}_4[\text{B}(\text{C}_6\text{F}_5)_2]_2$ (**1**) and $o\text{-C}_6\text{F}_4(9\text{-BC}_{12}\text{F}_8)_2$ (**2**: 9-BC₁₂F₈ = 1,2,3,4,5,6,7,8-octafluoro-9-boraffluorene) for the polymerization of isobutene (IB) in aqueous suspension or in hydrocarbon solution was studied. Polymerizations in aqueous suspension provided polymer of moderate MW and at variable conversion and were dependent on temperature, mode of diborane addition, the presence of surfactant, and the acidity of and nature of the anion present in the aqueous phase. The T dependence of MW over the T range -80 to -20 °C was studied in aqueous suspension, and higher MW polymer was formed at lower T . The hydrolysis and methanolysis of diboranes **1** and **2** was studied by NMR spectroscopy. Reactions of diborane **1** with excess MeOH or water afford solutions containing oxonium acids $[o\text{-C}_6\text{F}_4\{\text{B}(\text{C}_6\text{F}_5)_2\}_2(\mu\text{-OR})][(\text{ROH})_n\text{H}]$ (**7**: R = H, $n > 2$; **3**: R = Me, $n = 3$). When diborane **1** is present in excess over water or MeOH, degradation of the diborane is observed. In this case the products are $o\text{-C}_6\text{F}_4\{\text{B}(\text{C}_6\text{F}_5)_2\}\text{H}$ (**5**) and $(\text{C}_6\text{F}_5)_2\text{BOH}$ **7** or $(\text{C}_6\text{F}_5)_2\text{BOME}$ **4**, respectively. In the case of diborane **2**, $o\text{-C}_6\text{F}_4(9\text{-BC}_{12}\text{F}_8)\text{B}(2\text{-C}_{12}\text{F}_8\text{-}2''\text{-H})(\mu\text{-OH}) \cdot 7\text{H}_2\text{O}$ (**17**) and $o\text{-C}_6\text{F}_4(9\text{-BC}_{12}\text{F}_8)\text{B}(2\text{-C}_{12}\text{F}_8\text{-}2''\text{-H})(\mu\text{-OME})$ (**11**) were isolated from reactions of **2** with water and MeOH, respectively, and were characterized by X-ray crystallography. None of these degradation products effect IB polymerization in aqueous suspension. As a model for initiation of polymerization, the reaction of diborane **2** with 1,1-diphenylethylene (DPE) was studied. Addition of MeOH at low T results in efficient formation of the ion-pair $[\text{Ph}_2\text{CMe}][o\text{-C}_6\text{F}_4(9\text{-BC}_{12}\text{F}_8)_2(\mu\text{-OME})]$ via protonation of DPE. Polymerizations in hydrocarbon media were exothermic and rapid and gave quantitative yields of polymer even at very low concentrations of diborane **1**. The T dependence of MW was studied in hydrocarbon solution and showed non-Arrhenius behavior. This was explained by competitive chain transfer to monomer at elevated T and chain transfer to molecular water at lower T .

Introduction

Protic or electrophilic initiators that give rise to weakly coordinating anions (WCA),¹ partnered with propagating carbocations in isobutene polymerization,² are a topic of significant interest in the context of butyl rubber manufacturing at elevated temperature.³ A variety of initiator systems are effective in neat monomer, hydrocarbon, or more polar media,⁴ and generally a rather weak temperature dependence is observed for the MW of poly(isobutene) or butyl rubber formed. These polymerizations are uncontrolled and with MW values in several cases

comparable to those that can be achieved using γ -ray initiation involving “free” carbocations.⁵

Several years ago we communicated that chelating diborane **1**⁶ (Chart 1), in combination with cumyl chloride (CumCl), was

* Corresponding author. E-mail: collins@uakron.edu.

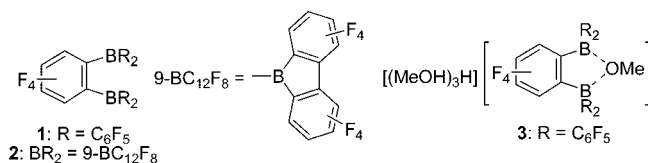
(1) (a) Reed, C. A. *Chem. Commun.* **2005**, 1669–1677. (b) Reed, C. A. *Acc. Chem. Res.* **1998**, *31*, 133–139. (c) Lupinetti, A. J.; Strauss, S. H. *Chemtracts* **1998**, *11*, 565–595. (d) Strauss, S. H. *Chem. Rev.* **1993**, *93*, 927–42.

(2) (a) *Cationic Polymerization: Fundamentals and Applications*; Faust, R., Shaffer, T. D., Eds.; ACS Symp. Ser. 665, 1997. (b) *Cationic Polymerizations: Mechanisms, Synthesis, and Applications*; Matyjaszewski, K., Ed.; Dekker: New York, 1996. (c) Anionic Polymerization to Cationic Polymerization. In *Encyclopedia of Polymer Science and Engineering*, Vol. 2, 2nd ed.; Mark, H. F., Ed.; John Wiley and Sons Inc.: New York, 1985. (d) Kennedy, J. P.; Marechal, E., *Carbocationic Polymerization*; John Wiley and Sons: New York, 1982.

(3) Kresge, E. N.; Schatz, R. H.; Wang, H.-C. Isobutylene Polymers. In *Encyclopedia of Polymer Science and Engineering*, 2nd ed.; Vol. 8, Mark, H. F., Bikales, N. M., Overberger, C. G., Menges, G., Eds.; Wiley-Interscience: New York, 1987; pp 423–448.

(4) (a) Tse, C. K. W.; Penciu, A.; McInenly, P. J.; Kumar, K. R.; Drewitt, M. J.; Baird, M. C. *Eur. Polym. J.* **2004**, *40*, 2653–2657. (b) Tse, C. K. W.; Kumar, K. R.; Drewitt, M. J.; Baird, M. C. *Macromol. Chem. Phys.* **2004**, *205*, 1439–1444. (c) Cordoneanu, A.; Baird, M. C. *Macromolecules* **2004**, *37*, 6744–6747. (d) McInenly, P. J.; Drewitt, M. J.; Baird, M. C. *Macromol. Chem. Phys.* **2004**, *205*, 1707–1712. (e) Kumar, K. R.; Penciu, A.; Drewitt, M. J.; Baird, M. C. *J. Organomet. Chem.* **2004**, *689*, 2900–2904. (f) Garratt, S.; Carr, A. G.; Langstein, G.; Bochmann, M. *Macromolecules* **2003**, *36*, 4276–4287. (g) Kumar, K. R.; Hall, C.; Penciu, A.; Drewitt, M. J.; McInenly, P. J.; Baird, M. C. *J. Polym. Sci., Part A: Polym. Chem.* **2002**, *40*, 3302–3311. (h) Baird, M. C. *Chem. Rev.* **2000**, *100*, 1471–1478. (i) Jacob, S.; Pi, Z.; Kennedy, J. P. In *Ionic Polymerizations and Related Processes*; Puskas, J. E., Ed.; Nato Sci. Ser., Ser. E; Kluwer: Dordrecht, The Netherlands, 1999; Vol. 359, pp 1–12. (j) Jacob, S.; Pi, Z.; Kennedy, J. P. *Polym. Mater. Sci. Eng.* **1999**, *80*, 495. (k) Jacob, S.; Pi, Z.; Kennedy, J. P. *Polym. Bull.* **1998**, *41*, 503–510. (l) Carr, A. G.; Dawson, D. M.; Bochmann, M. *Macromolecules* **1998**, *31*, 2035–2040. (m) Carr, A. G.; Dawson, D. M.; Bochmann, M. *Macromol. Rapid Commun.* **1998**, *19*, 205–207. (n) Barsan, F.; Karan, A. R.; Parent, M. A.; Baird, M. C. *Macromolecules* **1998**, *31*, 8439–8447. (o) Shaffer, T. D. *ACS Symp. Ser.* **1997**, *665*, 96–105. (p) Shaffer, T. D. *ACS Symp. Ser.* **1997**, *665*, 1–11. (q) Shaffer, T. D.; Ashbaugh, J. R. *J. Polym. Sci., Part A: Polym. Chem.* **1997**, *35*, 329–344. (r) Shaffer, T. D.; Ashbaugh, J. R. *Polym. Prepr.* **1996**, *37*, 339–40. (s) Bochmann, M.; Dawson, D. M. *Angew. Chem., Int. Ed. Engl.* **1996**, *35*, 2226–2228.

Chart 1



effective for isobutene polymerization in the presence of the sterically hindered pyridine 2,6-di-*tert*-butyl-4-methylpyridine (DtBMP).⁷ More recently, we have studied the polymerization and allied chemistry of diborane **1** and diborole **2**⁸ in combination with cumyl ether and cumyl azide initiators,⁹ as well as the roles of DtBMP in polymerizations initiated by diborane **1** and CumCl.¹⁰

A picture that emerges from these studies is that although these diboranes are effective for ionization of cumyl halide and related initiators, giving rise to weakly coordinating, chelated anions partnered with the cumyl cation,¹¹ isobutene polymerizations in hydrocarbon media using these initiators and the diboranes are complicated by facile chain transfer. Also, DtBMP is not an entirely innocent additive in polymerizations featuring weakly coordinating anions. The highly Brønsted acidic chain ends are susceptible to termination in the presence of sufficiently high concentrations of this hindered pyridine. (The study of chain transfer processes under these conditions is complicated by the presence of *excess* DtBMP. We have recently discovered a Lewis acidic additive that is an effective scavenger of water in hydrocarbon media, compared to diborane **1**. Future work will focus on the study of chain transfer featuring controlled initiation under these conditions.)

Another picture that emerges from these studies is that both of these diboranes are rather resistant to hydrolysis and the hydrolysis products are not strong Brønsted acids (*vide infra*). Thus, unlike conventional Lewis acids, these polymerizations readily proceed in the presence of variable quantities of dissolved water (*vide infra*), and an excess of DtBMP over Lewis acid (and water) is required to efficiently sequester the Brønsted acid formed from these diboranes and water.

In 2005 we reported that the use of diborane **1** in aqueous isobutene suspension afforded moderate conversions to polymer of moderate MW.¹² Although styrene and related monomers

had been earlier polymerized in aqueous suspension¹³ and most recently in a controlled fashion using either BF₃·OEt₂¹⁴ or B(C₆F₅)₃,¹⁵ this was the first report of significant polymer formation from isobutene in the presence of a large excess of water.

At the time, our understanding of this novel process was largely incomplete: the nature of the initiator was not known nor was it obvious that diborane **1** versus a degradation product was involved in initiation. The only mechanistic information we had was that the novel, stable oxonium acid **3** formed from diborane **1** and excess MeOH (Chart 1)¹² was ineffective as an initiator, as were compounds of comparable Brønsted acidity to **3** (e.g., [(Et₂O)₂H][B(C₆F₅)₄]¹⁶) or Lewis acidity to diborane **1** [B(C₆F₅)₃ or 9,10-bis(perfluorophenyl)-9,10-dibora-perfluoroanthracene¹⁷].

In this paper we report more detailed polymerization studies in both aqueous suspension and hydrocarbon solution using both diborane **1**¹⁸ and diborole **2** that shed considerable insight into the nature of the processes limiting both MW and conversion under these conditions. We also studied and report in detail the reactions of these two compounds with water and MeOH, including the characterization of the degradation products formed and their efficacy as initiators of polymerization. We have also studied the reaction of diborole **2** with 1,1-diphenylethylene (DPE) in the presence of MeOH as a model for protic initiation involving these compounds.

Results and Discussion

Polymerization of Isobutene in Aqueous Suspension.

Polymerization of isobutene in aqueous suspension was studied in three aqueous media featuring strong electrolytes, aqueous LiCl (mp -65 °C),¹⁹ 38 wt % sulfuric acid, and 48 wt % fluoroboric acid. The latter two media were initially selected on the basis of low freezing point (ca. -70 and -90 °C, respectively) and commercial availability. In all cases, there was no noticeable reaction between isobutene and any of these media, prior to the introduction of diborane or diborole. Polymerizations were quenched by the addition of an excess of 2-propanol at low *T*; the use of a hydrocarbon-soluble base such as NEt₃ in lieu of 2-propanol did not affect the outcome of these experiments.

It should be noted that these suspensions are unstabilized, and so rapid, mechanical stirring (>500 rpm) was employed to

(5) (a) Williams, F. *Macromolecules* **2005**, *38*, 206–209, and references therein. (b) Williams, F.; Shinkawa, A.; Kennedy, J. P. *J. Polym. Sci.* **1976**, *56*, 421–430. (c) Kennedy, J. P.; Shinkawa, A.; Williams, F. *J. Polym. Sci.* **1971**, *9* (A-1), 1551–1561. (d) Kennedy, J. P.; Milliman, G. E. *Adv. Chem. Ser.* **1969**, *91*, 287–305. (e) Kennedy, J. P.; Thomas, R. M. *Adv. Chem. Ser.* **1962**, *34*, 111–119. (f) Kennedy, J. P.; Thomas, R. M. *J. Polym. Sci.* **1961**, *49*, 189–202. (g) Thomas, R. M.; Sparks, W. J.; Frolich, P. K.; Otto, M.; Mueller-Cunradi, M. *J. Am. Chem. Soc.* **1940**, *62*, 276–280.

(6) (a) Henderson, L. D.; Piers, W. E.; Irvine, G. J.; McDonald, R. *Organometallics* **2002**, *21*, 340–345. (b) Williams, V. C.; Irvine, G. J.; Piers, W. E.; Li, Z.; Collins, S.; Clegg, W.; Elsegood, M. R. J.; Marder, T. B. *Organometallics* **2000**, *19*, 1619–1621. (c) Williams, V. C.; Piers, W. E.; Clegg, W.; Elsegood, M. R. J.; Collins, S.; Marder, T. B. *J. Am. Chem. Soc.* **1999**, *121*, 3244–3245.

(7) Lewis, S. P.; Taylor, N. J.; Piers, W. E.; Collins, S. *J. Am. Chem. Soc.* **2003**, *125*, 14686–87.

(8) Chase, P. A.; Henderson, L. D.; Piers, W. E.; Parvez, M.; Clegg, W.; Elsegood, M. R. *J. Organometallics* **2006**, *25*, 349–357.

(9) Chai, J.; Lewis, S. P.; Collins, S.; Sciarone, T. J. J.; Henderson, L. D.; Chase, P. A.; Irvine, G. J.; Piers, W. E.; Elsegood, M. R. J.; Clegg, W. *Organometallics* **2007**, *26*, 5667–5679.

(10) Chai, J.; Lewis, S. P.; Kennedy, J. P.; Collins, S. *Macromolecules* **2007**, *40*, 7421–7424.

(11) (a) Matyjaszewski, K.; Sigwalt, P. *Macromolecules* **1987**, *20*, 2679–2689. (b) Laube, T.; Olah, G. A.; Bau, R. *J. Am. Chem. Soc.* **1997**, *119*, 3087–3092.

(12) Lewis, S. P.; Henderson, L. D.; Chandler, B. D.; Parvez, M.; Piers, W. E.; Collins, S. *J. Am. Chem. Soc.* **2005**, *127*, 46–47.

(13) (a) Cauvin, S.; Ganachaud, F. *Macromol. Symp.* **2004**, *215*, 179–190. (b) Cauvin, S.; Ganachaud, F.; Touchard, V.; Hemery, P.; Leising, F. *Macromolecules* **2004**, *37*, 3214–3221. (c) Cauvin, S.; Sadoun, A.; Dos Santos, R.; Belleneq, J.; Ganachaud, F.; Hemery, P. *Macromolecules* **2002**, *35*, 7919–7927. (d) Satoh, K.; Kamigaito, M.; Sawamoto, M. *J. Polym. Sci., Part A: Polym. Chem.* **2000**, *38*, 2728–2733. (e) Satoh, K.; Kamigaito, M.; Sawamoto, M. *Macromolecules* **2000**, *33*, 5836–5840. (f) Satoh, K.; Kamigaito, M.; Sawamoto, M. *Macromolecules* **2000**, *33*, 4660–4666. (g) Satoh, K.; Kamigaito, M.; Sawamoto, M. *Macromolecules* **1999**, *32*, 3827–3832.

(14) (a) Radchenko, A. V.; Kostjuk, S. V.; Vasilenko, I. V.; Ganachaud, F.; Kaputsky, F. N. *Eur. Polym. J.* **2007**, *43*, 2576–2583. (b) Satoh, K.; Nakashima, J.; Kamigaito, M.; Sawamoto, M. *Macromolecules* **2001**, *34*, 396–401. (c) Satoh, K.; Kamigaito, M.; Sawamoto, M. *Macromolecules* **2000**, *33*, 5405–5410.

(15) (a) Kostjuk, S. V.; Radchenko, A. V.; Ganachaud, F. *Macromolecules* **2007**, *40*, 482–490. (b) Kostjuk, S. V.; Ganachaud, F. *Macromolecules* **2006**, *39*, 3110–3113.

(16) Jutzi, P.; Müller, C.; Stämmler, A.; Stämmler, H.-G. *Organometallics* **2000**, *19*, 1442–1444.

(17) Metz, M. V.; Schwartz, D. J.; Stern, C. L.; Marks, T. J.; Nickias, P. N. *Organometallics* **2002**, *21*, 4159–4168.

(18) Lewis, S. P. Univ. of Akron, Akron, OH, 2004, Diss. Abstr. Int. 2004, *65*, 770; *Chem. Abstr.* 143:173195.

(19) Akopov, E. *Zh. Prikl. Kim.* **1963**, *36*, 1916–19.

Table 1. Isobutene Polymerization in Aqueous LiCl Suspension^a

entry	initiator (mM) ^b	surfactant ^c	M_w (kg mol ⁻¹)	PDI	yield (%)
1	1 (0.322)		22.8	2.30	44
2	1 (0.322)		29.4	2.38	39
3	1 (0.322)	DTMB	61.0	2.74	5
4	1 (0.322)	DTMB	47.4	2.68	4
5	1 (0.322)	SDS	31.8	2.37	32
6	1 (0.322)	SDS	34.9	2.47	30
7	2 (0.627)		91.9	2.27	40
8	2 (0.627)	SDS	39.5	1.74	25
9	2 (0.627)	SDS	75.4	2.47	26

^a The diborane initiator dissolved in 1 mL in toluene was added rapidly to a stirred (500 rpm) mixture of 18.0 mL of isobutene and 18.0 mL of aqueous LiCl [LiCl (23 wt %) NaCl (1.2 wt %) H₂O (75.8 wt %)] at -60 °C unless otherwise noted. ^b The concentration of diborane used is reported with respect to the total volume of the organic phase. ^c Where used, 0.100 g of dodecyltrimethylammonium bromide (DTMB) or sodium dodecylsulfate (SDS) was added to the aqueous phase.

Table 2. Isobutene Polymerization in Aqueous Sulfuric Acid Suspension^a

entry	initiator	surfactant ^b	M_w (kg mol ⁻¹)	PDI	yield (%)
1	1		28.3	2.05	29
2	1		25.3	2.21	27
3	1 ^c		22.0	3.86	46
4	1 ^c		27.6	3.38	30
5	1 ^d		17.4	2.63	24
6	2 ^d		18.7	3.11	26
7	1	SDS	33.8	2.24	17
8	1	SDS	37.2	2.69	18
9	1	DTMB	83.4	3.16	2
10	1	DTMB	69.8	2.86	3
11	1	DTMOTf	41.3	2.32	18
12	1	DTMOTf	35.8	2.82	14

^a The diborane initiator dissolved in 1.0 mL of toluene was added rapidly to a stirred (500 rpm) mixture of 18.0 mL of isobutene and 18.0 mL of aqueous H₂SO₄ [H₂SO₄ = 38 wt %] at -60 °C unless otherwise noted. The final concentration of diborane was 0.625 mM. ^b Where used, 0.100 g of DTMB, SDS, or dodecyltrimethylammonium triflate (DTMOTf) was added to the aqueous phase. ^c A stock solution of diborane or diborole in toluene (1.0 mL) was added over 5 min to a suspension of 15.0 mL of isobutene and 15.0 mL of 5.0 M aqueous LiHSO₄ at -45 °C. ^d A stock solution of diborane or diborole in toluene (1.0 mL) was added over 10 min to a suspension of 15.0 mL of isobutene and 15.0 mL of 5.0 M aqueous LiHSO₄ at -45 °C.

create a dispersion. On addition of a toluene stock solution of diborane or diborole, an exothermic reaction was noted, depending on the rate of addition, this being particularly pronounced in the case of diborane, while these mixtures took on a milky appearance as reaction progressed. On the other hand, phase separation was observed to occur when stirring was stopped, at least in those suspensions featuring monomer diluted with hexane.

The results of these experiments are summarized in Tables 1–3. Table 1 summarizes the results obtained in aqueous LiCl suspension at -60 °C. Table 2 summarizes the results obtained in 38 wt % sulfuric acid at the same *T* along with a few experiments in aqueous LiHSO₄ at somewhat higher *T*, while Table 3 reports results obtained in aqueous fluoroboric acid at -80 °C. These *T* were dictated by the freezing points of the aqueous phase and increased viscosity of the aqueous medium as one approaches the freezing point; in essence, effective dispersal of the monomer was possible only at the *T* indicated.

Polymer yields are higher in aqueous fluoroboric acid, while those in sulfuric acid are lower compared with aqueous LiCl. The first effect is likely related to the significantly lower *T* employed, as experiments in aqueous HBF₄ indicated significant decreases in both MW and conversion at higher *T* (*vide infra*). We speculate that as the *T* is increased, the solubility of water

Table 3. Isobutene Polymerization in Aqueous Fluoroboric Acid Suspension^a

entry	initiator (mM)	surfactant ^b	<i>T</i> (°C)	M_w (kg mol ⁻¹)	PDI	yield (%)
1	1 (0.322)		-80	41.4	2.37	58
2	1 (0.322)		-80	37.2	2.43	54
3	2 (0.625)		-80	49.4	2.15	58
4	2 (0.625)		-80	42.4	2.22	64
5	1 (0.625) ^c		-80	29.3	2.05	61
6	2 (0.625) ^c		-80	39.5	2.04	29
7	1 (0.322)	SDS	-80	27.2	2.08	47
8	1 (0.322)	SDS	-80	36.2	2.34	42
9	1 (0.322)	DTMBF ₄	-80	33.4	2.22	47
10	1 (0.322)	DTMBF ₄	-80	31.8	2.13	52
11	1 (0.625) ^d		-80	41.0	1.73	85
12	1 (0.625) ^d		-80	41.3	1.82	80
13	1 (0.625) ^d		-73	31.7	2.06	87
14	1 (0.625) ^d		-73	32.1	2.10	92
15	1 (0.625) ^d		-60	31.0	2.28	95
16	1 (0.625) ^d		-60	38.1	2.37	78
17	1 (0.625) ^d		-40	13.0	2.36	76
18	1 (0.625) ^d		-22	4.60	2.28	30
19	1 (0.625) ^d		-22	6.10	2.17	19

^a The diborane initiator dissolved in 1.0 mL of toluene was added rapidly to a stirred (500 rpm) mixture of 18.0 mL of isobutene and 18.0 mL of aqueous HBF₄ [HBF₄ = 7.0 M] at -80 °C unless otherwise noted. ^b Where used, 0.100 g of SDS or dodecyltrimethylammonium tetrafluoroborate (DTMBF₄), was added to the aqueous phase. ^c A stock solution of diborane or diborole in toluene (1.0 mL) was added over 10 min to a suspension of 15.0 mL of isobutene and 15.0 mL of aqueous HBF₄. ^d A stock solution of diborane in toluene (1.0 mL) was added over 1.0 min to a suspension of 10.0 mL of isobutene, 5.0 mL of hexane, and 15.0 mL of aqueous HBF₄.

in the organic phase increases to the point where formation of higher order, less acidic, oxonium acids (analogous to **3**) interferes with either initiation or propagation within the droplet.

The lower yields encountered in aqueous sulfuric acid versus aqueous LiCl at the same *T* may be related to the acidity of the aqueous phase. That the acidic nature of these aqueous phases is deleterious is revealed by the experiments with aqueous LiHSO₄, where even at higher *T* (-45 °C), conversions are higher while MW is at least comparable to experiments in aqueous H₂SO₄ conducted at lower *T* (Table 2, entries 3/4 vs 1/2). Since the ionic strength of these media are comparable (both are about 5 M in HSO₄), these differences are due to the higher acidity of the latter medium.

Unfortunately, there are no commonly available fluoroborate salts whose aqueous solutions possess low melting temperatures comparable to that of fluoroboric acid. On the other hand, particularly using diborane **1**, conversions of monomer can approach 100% in that medium at low *T* if diluted with hexane (*vide infra*).

As far as polymer MW is concerned, no clear pattern emerges from these data other than that of temperature. Thus, at -80 °C, \bar{M}_w varies between 30 and 40 kg mol⁻¹ in aqueous HBF₄, while at -60 °C, \bar{M}_w varies between 20 and 30 kg mol⁻¹ in aqueous LiCl or H₂SO₄. Surprisingly, in aqueous LiHSO₄ at -45 °C, \bar{M}_w varied between 17 and 28 kg mol⁻¹ and was found to be sensitive to the rate of addition of initiator (entries 3–5, Table 2).

Also, rather contradictory results were obtained using diborane **1** versus diborole **2** in the different media. In aqueous LiCl, 3–4 times higher MW polymer was formed at similar levels of conversion using the diborole (Table 1, entry 7 vs 1 and 2). This feature was not observed in aqueous HBF₄ (Table 3, entries 1/2 vs 3/4), although conversion and MW appeared sensitive to the rate of initiator addition (entry 5 vs 6). Almost identical outcomes were observed in aqueous LiHSO₄ at -45 °C with either initiator (entry 5 vs 6, Table 2) using a controlled addition rate.

As can be seen from the results in Tables 1–3, the MWD are broad with PDI between 2 and 3, as would be expected for a polymerization process dominated by chain transfer. In the cases reported in Tables 1–3, the polymer featured a unimodal MWD with a low MW tail. The skew or asymmetry of the MWD was sensitive to whether the suspension was quenched at, for example, low T versus warming to room temperature prior to quenching. The latter conditions led to increased formation of low MW oligomers and as a result were generally avoided.

During this work, it became apparent that the rate of addition of initiator to these suspensions was a very significant variable influencing the results. The diborole is bright yellow in solution; formation of donor adducts⁸ and/or hydrolysis (*vide infra*) leads to formation of colorless products. When this compound is added rapidly to these suspensions, the yellow color of the diborole persists for some time after the addition is complete, while at sufficiently slow addition rates (5–10 min, depending on T , amount of initiator and medium used), the suspensions remain colorless. Under the former conditions, polymer yields and MW are generally significantly higher than under the latter conditions.

For example, in aqueous HBF_4 suspension with 10.0 mL of monomer diluted by 5.0 mL of hexane, addition of 0.25 mL of 0.01 M diborole within 5 s resulted in the formation of poly(isobutene) (PIB) with $\bar{M}_w = 62.5 \text{ kg mol}^{-1}$ at 36% conversion, while addition of 1.0 mL of 0.01 M diborole over a 5 min period afforded PIB with $\bar{M}_w = 27.7 \text{ kg mol}^{-1}$ at 27% conversion.

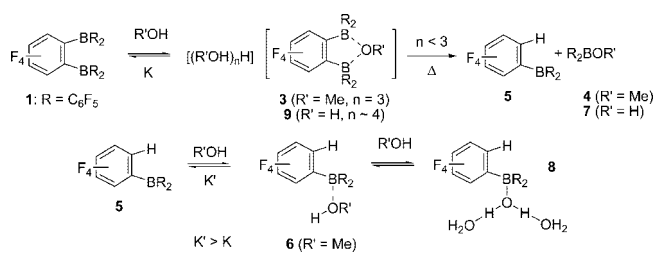
This behavior was also evident using the diborane initiator. Rapid addition of this compound to monomer is highly exothermic and can result in reflux of the monomer. One would normally expect a negative impact on both conversion and MW. However, in those experiments where a slower, controlled addition of this compound was conducted, lower MW polymer was formed at similar conversion (e.g., Table 3, entries 1 and 2 vs 5). If this compound was added sufficiently slowly, only trace amounts of PIB were formed.¹⁸

Finally, the use of ionic surfactants to stabilize these suspensions was studied. Although the high ionic strength of these aqueous phases mitigates against formation of micelles, it was anticipated that the particle size of the droplets would be more uniform under these conditions, possibly allowing for a more controlled initiation.

In all cases, the use of a surfactant led to a decrease in conversion, and this effect was particularly pronounced in the case of dodecyltrimethylammonium bromide (DTMB) in aqueous LiCl or H_2SO_4 (Table 1, entries 3 and 4 or Table 2, entries 9 and 10). In contrast, when using dodecyltrimethylammonium triflate (DTMOTf) in aqueous H_2SO_4 or dodecyltrimethylammonium tetrafluoroborate (DTMBF_4) in aqueous HBF_4 , comparable results were obtained to those observed using sodium dodecylsulfate (SDS) in either medium (Table 2, entries 11/12 vs 7/8 and Table 3, entries 9/10 vs 7/8). In either case, one suffers about a 10% drop in conversion under otherwise similar conditions.

The use of SDS or DTMBF_4 surfactant led to a statistically insignificant change in \bar{M}_w in aqueous HBF_4 (i.e., 39.3 ± 3.0 vs $32.2 \pm 3.8 \text{ kg mol}^{-1}$), while surprisingly a significant increase in \bar{M}_w was observed in aqueous H_2SO_4 using either SDS or DTMOTf (25.8 ± 2.8 vs $37.0 \pm 3.2 \text{ kg mol}^{-1}$) and to a lesser extent in aqueous LiCl using SDS (26.1 ± 4.7 vs $33.4 \pm 2.2 \text{ kg mol}^{-1}$).

Scheme 1



Part of this is almost certainly related to the lower conversions encountered: experiments using DTMB that featured dramatically lower conversions also provided the highest MW polymer (Table 1, entries 3 and 4 and Table 2, entries 9 and 10).

It is now reasonably well understood that anions tend to preferentially aggregate at the interface in dispersed media of this sort, where they can disrupt local water structure at the interface.²⁰ Ordering of water structure near an interface results in a local decrease in density, thus facilitating diffusion through the interface. In particular, the Hofmeister series can be used to predict the efficacy of anions for this process, and in the present case, diffusion of water through the interface is expected to increase in the order $\text{BF}_4^{20c} \ll \text{ROSO}_3 \sim \text{HSO}_4^{20c} \sim \text{CF}_3\text{SO}_3 < \text{Br} \ll \text{Cl}$.

One possible interpretation of the results obtained to date is that lower conversions encountered in stabilized suspension are a reflection of increased diffusion of water into the droplet during chain growth at constant T .

Since \bar{M}_w does not show a consistent trend, it is less clear whether a similar explanation applies. In particular, since all of the experiments using a surfactant featured an uncontrolled addition rate, and this is known to be an important variable influencing polymer MW, it could be that variations in addition, etc., account for any difference in the results observed. We do note that the poor reproducibility in \bar{M}_w between the two experiments conducted with the diborole in the presence of SDS (Table 1, entries 8 and 9) is likely a reflection of this.

Finally, the T dependence of MW and conversion was studied in the case of isobutene polymerization in aqueous HBF_4 suspension. In these experiments, the isobutene was diluted with hexane ($[\text{IB}] = 8.36 \text{ M}$) since this results in better T control and higher conversion in suspension, as well as in solution polymerizations (*vide infra*). Over the T range -80 to -40 °C, conversions varied between 75% and 95% with no discernible trend, but they do decrease to 20–30% at -22 °C (see Table 3, entries 11–19). Evidently, at sufficiently low T , the MW of the polymer formed is largely independent of T (entries 11–16) but decreases rapidly above -60 °C. We will defer discussion of these results until those obtained in the virtual absence of water are presented (*vide infra*).

Hydrolysis and Alcoholysis of Diborane 1. As mentioned in the Introduction, the reaction of diborane **1** with MeOH has been previously studied, and in the presence of excess MeOH, the novel and stable oxonium acid **3** is formed (Scheme 1).¹² In that study various amounts of MeOH were added to diborane **1**, initially at low T , with the outcome of this reaction being highly solvent and T dependent for amounts of MeOH ≤ 1.0 equiv (Table 4, entries 1–7).

In polar media such as CD_2Cl_2 , oxonium acid **3** is present at low T , while in toluene- d_8 at low T , or on warming a CD_2Cl_2

(20) (a) Pegramnt, L. M.; Record, M. T., Jr. *J. Phys. Chem. B* **2007**, *111*, 5411–5417. (b) Wick, C. D.; Dang, L. X. *J. Phys. Chem. B* **2005**, *109*, 15574–15579. (c) Taylor, R. P.; Kuntz, I. D., Jr. *J. Am. Chem. Soc.* **1972**, *94*, 7963–65.

Table 4. Product Distribution from the Reaction of Diborane **1** with MeOH

entry	MeOH (equiv)	<i>T</i> (K)	solvent	1	3	4	5	6
1	0.5	298	toluene- <i>d</i> ₈	50	0	25	25	0
2	0.5	193	CD ₂ Cl ₂	88	12	0	0	0
3	0.5	298	CD ₂ Cl ₂	50	0	25	25	0
4	1.0	213	toluene- <i>d</i> ₈	30	17	26	26	0
5	1.0	298	toluene- <i>d</i> ₈	0	0	50	50	0
6	1.0	213	CD ₂ Cl ₂	31	39	15	15	0
7	1.0	298	CD ₂ Cl ₂	0	0	50	50	0
8	2.0	298	toluene- <i>d</i> ₈	0	0	50	0	50
9	3.0	298	toluene- <i>d</i> ₈	0	33	33	0	33
10	4.0	298	CD ₂ Cl ₂	0	100	0	0	0

solution above $-60\text{ }^\circ\text{C}$, any oxonium acid present decomposes to form $(\text{C}_6\text{F}_5)_2\text{BOMe}$ **4**^{12,21} and $(o\text{-C}_6\text{F}_4\text{H})\text{B}(\text{C}_6\text{F}_5)_2$ **5**. The identity of these compounds was verified by independent synthesis (see Supporting Information), while the ¹H, ¹⁹F, and ¹¹B chemical shifts and assignments for all of these compounds are reported in Table 5.

Evidently, compounds **4** and **5** arise from chemoselective cleavage of the *o*-phenylene B–C bonds of diborane **1** (Scheme 1). We strongly suspect that this cleavage results from reversible protonation of the anion in **3**, either at O to form an unobserved $\mu\text{-MeOH}$ adduct or possibly in an irreversible and direct manner involving *ipso* electrophilic aromatic substitution at one of the B–C bonds. In particular, the acidity of the oxonium acid **3** will be sensitive to the number of MeOH molecules that solvate the proton,²² and a minimum of three are needed to stabilize this compound at room temperature. Presumably, the higher stability of **3** in polar media at low *T* reflects its ionic constitution, such that protonation to form the neutral degradation products is less facile.

Borane **5** is sufficiently Lewis acidic (and less sterically hindered) that it competes effectively with diborane **1** for MeOH, forming monoadduct **6**. Thus, when ≥ 1.0 equiv of MeOH is present, a quasi-equilibrium is established between **1**, **3**, **4**, and **6** at low *T* in toluene-*d*₈, with ion-pair **3** favored in CD₂Cl₂ at low *T* (Table 4, entry 4 vs 6). At sufficiently high *T*, all of diborane **1** is converted into **4** and **5** (or **6**) depending on the amount of MeOH initially present.

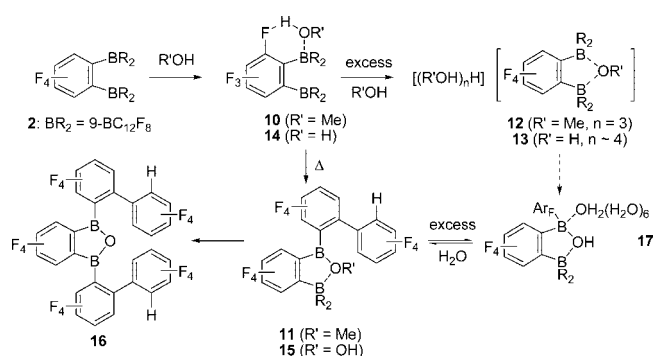
If excess MeOH is present (i.e., ≥ 4 equiv) ion-pair **3** is the exclusive product formed at low *T* and is stable in solution at room temperature. Additional MeOH, over and above that needed to form **3**, exchanges with the MeOH molecules that solvate the proton; this exchange process is rapid at all temperatures in CD₂Cl₂.

The formation of ion-pair **3** from **1** and MeOH is reversible in the sense that ion-pair **3** can serve as a source of MeOH in the presence of excess **1**. This was shown by an experiment where **3** was generated from **1** and excess MeOH (8.0 equiv). Addition of 3.0 equiv of diborane **1** to a solution of **3** (1.0 equiv + 4.0 equiv of MeOH) at room temperature led to formation of **4** (and **6**).

Similar chemistry is also observed on addition of various amounts of water to diborane **1** in toluene-*d*₈ solution at low *T* (Scheme 1). Predictably, the stoichiometry of these reactions was rather difficult to control, given the low solubility of water in this solvent as well as it is ultimate physical state at low *T*.

(21) This compound has been structurally characterized: Donghi, D.; Maggioni, D.; Beringhelli, T.; D'Alfonso, G.; Mercandelli, P.; Sironi, A. *Eur. J. Inorg. Chem.* **2008**, *10*, 1645–1653.

(22) (a) Stoyanov, E. S.; Kim, K.-C.; Reed, C. A. *J. Am. Chem. Soc.* **2006**, *128*, 1948–1958. (b) Färcașiu, D.; Hâncu, D. *J. Chem. Soc., Faraday Trans.* **1997**, *93*, 2161–2165. (c) Arnett, E. M.; Quirk, R. P.; Burke, J. J. *J. Am. Chem. Soc.* **1970**, *92*, 1260–1266.

Scheme 2

However, when ca. 1–2 equiv of water was added, the cleavage products **5** and the known borinic acid **7**²³ were formed at the expense of **1**. When larger amounts of water were added, an aquo complex **8** was formed from **5** in much the same manner as observed in the case of MeOH. Compound **8** has been structurally characterized (see Supporting Information) and is analogous in structure to the known compound $(\text{C}_6\text{F}_5)_3\text{B} \cdot (\text{H}_2\text{O})_3$.²⁴ An oxonium acid **9** analogous to **3** was formed in the presence of excess water, but it was exclusively generated only by adding D₂O to solid diborane **1** at room temperature. This compound was characterized spectroscopically but has not been obtained in pure form.

Hydrolysis and Alcoholysis of Diborole 2. Similar chemistry was investigated with diborole **2**; in the case of MeOH, addition of 1 equiv to diborole **2** in either toluene-*d*₈ or CD₂Cl₂ at low *T* results in the formation of *exo*-MeOH adduct **10** (Scheme 2). The formation of **10** had been noted earlier in reactions involving ionization of cumyl methyl ether by diborole **2**.⁹ In this case, adduct **10** can be generated at $-80\text{ }^\circ\text{C}$ in sufficient amounts (19%) to allow for its spectroscopic characterization, though its formation was accompanied by some thermal degradation to borinic ester **11** (*vide infra*, $\sim 13\%$). In particular, the *exo* adduct formulation was confirmed by a cross-peak in the two-dimensional ¹⁹F–¹H correlation spectrum between the methanol proton (dq at δ 6.58) and a ¹⁹F resonance at δ -133.5 . The same correlation was established by a 1D selective decoupling experiment. Irradiation of this ¹⁹F signal reduces the doublet of quartets structure for the methanol proton to a quartet due to H–H coupling only. In toluene-*d*₈, *exo*-MeOH adduct **10** was also formed, but no ¹⁹F coupling to the methanol proton was apparent from the spectra in this more basic solvent.

Coordination of MeOH to the *exo* side is not unexpected for diborole **2**; even unhindered donors such as acetonitrile have a strong preference for *exo* coordination to this compound.⁸ In contrast, unhindered donors such as acetonitrile exhibit *endo*-coordination to diborane **1**.

On warming adduct **10**, reaction to form borinic ester **11** is observed; compound **11** was reported earlier,⁹ but has now been structurally characterized and the molecular structure appears in Figure 1, while crystallographic and metrical data are reported as Supporting Information. The characteristic structural feature of ester **11** is that the OMe group bridges to both B atoms in

(23) (a) X-ray structure: Beringhelli, T.; D'Alfonso, G.; Donghi, D.; Maggioni, D.; Mercandelli, P.; Sironi, A. *Organometallics* **2003**, *22*, 1588–1590. (b) See also: Metcalfe, R. A.; Kreller, D. I.; Tian, J.; Kim, H.; Taylor, N. J.; Corrigan, J. F.; Collins, S. *Organometallics* **2002**, *21*, 1719–1726. (c) Preparation/characterization: Chambers, R. D.; Chivers, T. *J. Chem. Soc.* **1965**, 393, 3–9.

(24) Danopoulos, A. A.; Galsworthy, J. R.; Green, M. L. H.; Doerrer, L. H.; Cafferkey, S.; Hursthouse, M. B. *Chem. Commun.* **1998**, *22*, 2529–2530.

Table 5. ^1H , ^{19}F , and ^{11}B NMR Chemical Shifts and Assignments for Hydrolysis and Methanolysis Products of Diborane 1

compound (solvent)	δ F1	δ F2	δ F3	δ F4	δ $-\text{B}(\text{C}_6\text{F}_5)_2$ (F_o, F_p, F_m)	δ ^1H	δ ^{11}B
1 [X = B(C ₆ F ₅) ₂] (C ₆ D ₆)	-127.6	-141.6			-128.5, -141.6, -161.5		
3 [(MeOH) _n H][<i>o</i> -C ₆ F ₄ [B(C ₆ F ₅) ₂] ₂ (μ -OMe)] (<i>n</i> = 3, CD ₂ Cl ₂)	-137.4	-163.8			-132.4, -160.2, -166.1	(MeOH) 6.19, (-OMe) 3.65, (MeOH) 3.53	3.8
(C ₆ F ₅) ₂ BOMe 4 (C ₆ D ₆)					-132.7, -148.8, -160.9	(-OMe) 3.24	40.3
5 [X = H] (C ₆ D ₆)	-137.7	-141.0	-153.6	-125.4	-129.0, -143.7, -160.0	(aryl- <i>H</i>) 6.66	40.3
6 [X = H] (C ₆ D ₆)	-139.5	-155.2	-156.9	-133.6	-133.8, -153.9, -161.9	(aryl- <i>H</i>) 6.49, (MeOH) 4.70, (MeOH) 2.25	4.6
1 (CD ₂ Cl ₂) -62 °C	-125.1	-147.2			-125.9, -140.3, -159.9		
5 (<i>d</i> ₈ -toluene) -60 °C	-137.7	-139.7	-154.0	-125.4	-128.4, -141.4 -159.1	(aryl- <i>H</i>) 6.66	
(C ₆ F ₅) ₂ BOH 7 (<i>d</i> ₈ -toluene)					-132.8, -147.8, -160.9	(-OH) 6.32	42.2
8 [X = H] (<i>d</i> ₈ -toluene) -60 °C	-139.0	-154.3	-156.2	-133.4	-134.0, -152.7, -161.2	(aryl- <i>H</i>) 6.52, (-OH) 6.28, (H ₂ O) 4.52	
[(H ₂ O) _n H][<i>o</i> -C ₆ F ₄ [B(C ₆ F ₅) ₂] ₂ (μ -OH)] (9 , <i>n</i> ~ 4, CD ₂ Cl ₂)	-138.9	-163.4			-135.0, -160.3, -166.4		-0.4

the solid state and in solution. However, the bridging is asymmetrical as one would expect with bond lengths of O(1)–B(2) = 1.397(3) Å and O(1)–B(1) = 1.640(3) Å, respectively differing by about 17% with the former being typical of a B–O single bond involving trigonal boron. The five-membered, chelate ring is essentially planar with the sum of the dihedral angles $\angle\text{B}(1)–\text{C}(2)–\text{C}(7)–\text{B}(2) = -5.4(2)^\circ + \angle\text{C}(2)–\text{C}(7)–\text{B}(2)–\text{O}(1) = 2.7(2)^\circ + \angle\text{C}(7)–\text{B}(2)–\text{O}(1)–\text{B}(1) = 1.0(2)^\circ + \angle\text{B}(2)–\text{O}(1)–\text{B}(1)–\text{C}(2) = -3.7(2)^\circ + \angle\text{C}(7)–\text{C}(2)–\text{B}(1)–\text{O}(1) = 5.4(2)^\circ = 0.0(2)^\circ$. Both B(2) and O(1) have sp² hybridization with the sum of the bond angles about each atom being 359.9(2)° and 360.0(2)°, respectively. Though B(1) is approximately tetrahedral, there is significant angle strain in both the borole, as well as five-membered chelate, rings as is evident from C(8)–B(1)–C(19) and C(2)–B(1)–O(1) angles of 99.5(2)° and 96.8(2)°, respectively. Surprisingly, this chelate structure is preserved in the presence of strong monodentate donors such as pyridine, which coordinate to B(2) rather than the more Lewis acidic borole moiety.²⁵

An oxonium acid **12**, analogous to **3**, is formed from diborole **2** if at least four equivalents of MeOH are initially present. As suggested in Scheme 2, formation of **12** may involve adduct **10** as an intermediate, where the latter is sufficiently acidic to protonate free MeOH. The monodentate anion that would result could rearrange to the chelated form, provided excess MeOH is present to stabilize the oxonium acid formed.

In the case of hydrolysis, the chemistry is similar. Controlled addition of stoichiometric water at low *T* leads initially to *exo* adduct **14** which degrades in a similar manner at higher *T* to form borinic acid **15**. On prolonged standing at room temperature in toluene-*d*₈ solution, this compound degrades to the symmetrical anhydride **16** through cleavage of the remaining borole ring; compound **16** has been structurally characterized as its mono-THF adduct (see Supporting Information). In the presence of excess water, oxonium acid **13** is produced and is stable in solution at room temperature. However, when water was removed rapidly *in vacuo* from these solutions, anhydride **16** was isolated (as a bis hydrate). Slow evaporation of water resulted in the crystallization of borinic acid **15**, isolated as heptahydrate **17**.

Compound **17** has been characterized by X-ray crystallography, and its molecular structure is depicted in Figure 2. It has the same basic chelate structure as observed for **11**, though a water molecule is coordinated to B(2), rendering it tetrahedral. In addition, six additional water molecules are present in the lattice (not shown) involved in a network of hydrogen bonds to each other, O(2), O(1), and several F atoms. Since both B atoms are tetrahedral, the bonds to O(1) are significantly longer at O(1)–B(2) and O(1)–B(1) = 1.520(3) and 1.540(3) Å. In fact both B–O bonds are equivalent in length to that of the

dative interaction of O(2)–B(2) at 1.527(3) Å. The five-membered, chelate ring is planar, with the sum of the dihedral angles about all five atoms being $-0.1(2)^\circ$, while O(1) is approximately sp² hybridized at least on comparing the B–O–B angle in this structure [$116.7(2)^\circ$] to that of ester **11** [$113.5(2)^\circ$]. (The H atom bonded to O(1) was not located and constrained to a calculated position.)

Since oxonium acid **13** is formed and is stable in the presence of excess H₂O, the eventual isolation of **16**·(H₂O)₂ or **17** implies that as water is removed through evaporation, the formation of adduct **14** from **13** must be reversible or that cleavage of **13** to form **15** occurs directly as the degree of solvation of the proton in the oxonium acid is diminished.

Relation of Hydrolysis Chemistry to Isobutene Polymerization. Given the complexity of these reactions as well as the nature of the products formed, it is quite conceivable that any of the Lewis or Brønsted acidic byproduct resulting from hydrolysis of diborane **1** or diborole **2** could be involved in initiation of polymerization in aqueous suspension (or hydrocarbon solution, *vide infra*).

While not all of the stable byproducts described previously have been individually tested, several control experiments suggest that they are probably not involved. As already mentioned, stable oxonium acid **3** does not initiate polymerization of isobutene in aqueous suspension, nor does a mixture of this compound, borane **5**, and borinic ester **4** when previously generated by addition of 2–3 equiv of MeOH to diborane **1**. Also, the combination of borinic acid **7** and excess B(C₆F₅)₃ is also ineffective for polymerization in aqueous suspension, while the latter compound is also inactive by itself. Finally, though the presence of excess water no doubt moderates the Brønsted acidity of chelated borinic acid **17**, this compound was also ineffective as an initiator of isobutene polymerization in aqueous suspension.

A related question is to what extent do these decomposition reactions intrude during polymerization in aqueous suspension or hydrocarbon solution. This is rather difficult to answer using isobutene itself, but we did investigate the reaction of 1,1-diphenylethylene (DPE) with MeOH in the presence of diborole **2** as a model for protic initiation.^{4f,26}

In fact, using conventionally dried CD₂Cl₂, there was sufficient moisture present that DPE (20 μmol) was converted to a 1:1 mixture of DPE (67% conversion) and indan **18**²⁷ in the

(25) Sciarone, T. J. J. Parvez, M., unpublished structural results.

(26) (a) Sauvet, G.; Vairon, J. P.; Sigwalt, P. *J. Polym. Sci., Polym. Symp.* **1975**, *52*, 173–87. (b) Ioone, T. W.; Lee-Ruff, E.; Khazanie, P. G.; Hopkinson, A. C. *J. Chem. Soc., Perkin Trans. 2* **1975**, *6*, 607–609. (c) Olah, G. A.; Halpern, Y. *J. Org. Chem.* **1971**, *36*, 2354–2356.(27) Bergmann, E.; Weiss, H. *Just. Lieb. Ann. Chem.* **1930**, *480*, 49–59.

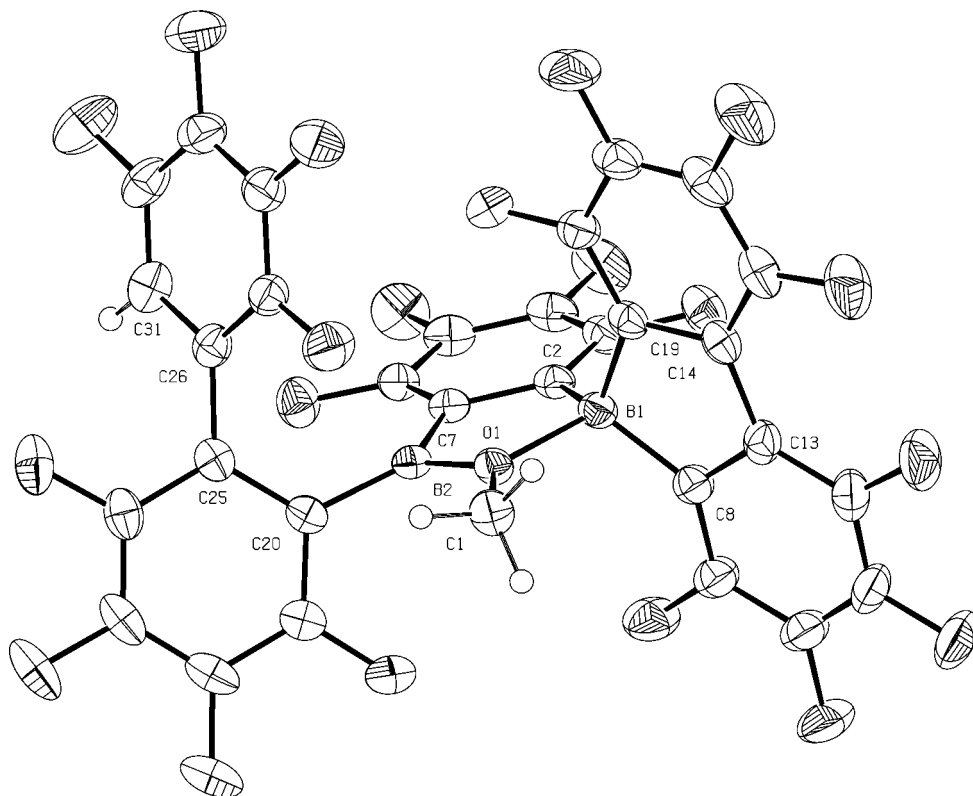
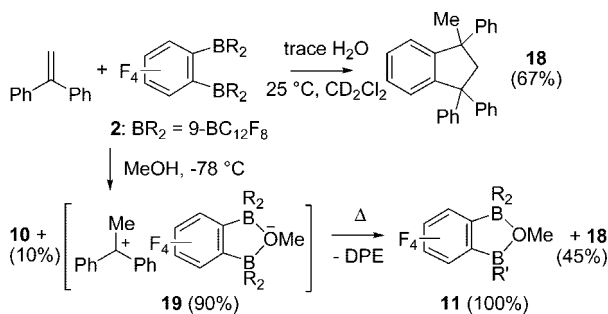


Figure 1. Molecular structure of borinic ester **11** with 50% thermal ellipsoids depicted.

Scheme 3

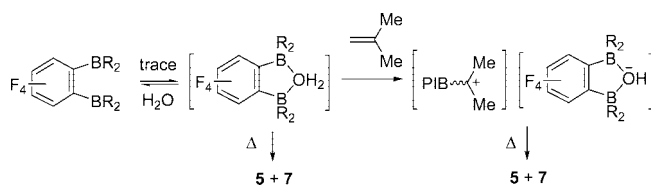


presence of 1 equiv of diborole **2** at room temperature (Scheme 3). Conversion of DPE to **18** may be minimized to ca. 20–30% at room temperature by using CD_2Cl_2 that has been more thoroughly dried and DPE that has been freshly distilled from CaH_2 .

Subsequent addition of MeOH (~1.0 equiv with respect to diborole **2**) at -80°C to this solution led to complete conversion of the remaining DPE to stable ion-pair **19**²⁸ (ca. 90% conversion of diborole **2**) as well as *exo*-MeOH adduct **10** (ca. 10%). As the temperature was increased, first *exo* adduct **10** (at ca. -40°C) and then ion-pair **19** (above -20°C) degraded to form ester **11** and in the latter case indan **18**.

Thus, at low T in polar media, protic initiation is reasonably efficient in the case of this model reaction. In particular, competing dimerization of DPE to form the $\text{MeCPh}_2\text{CH}_2\text{CPh}_2$ cation, which is seen in analogous reactions involving $\text{CF}_3\text{SO}_3\text{H}$ or TiCl_4 ,^{26a} was not observed. Although DPE is much more basic than isobutene, we are confident that protic initiation in aqueous suspension involves analogous chemistry with diborole **2** or diborane **1** and dissolved water.

This raises the interesting question as to what species is responsible for protonation of isobutene versus degradation via B–C bond cleavage. In our view, monodentate aquo complexes formed from either diborole or certainly diborane are insufficiently acidic for this purpose. For example, $\text{B}(\text{C}_6\text{F}_5)_3$ and compound **5** are both kinetically stronger Lewis acids than diborane **1**, yet neither is effective for protic initiation in aqueous suspension (or hydrocarbon solution). Instead, we believe a μ -aquo complex that is transiently formed from water and diborane **1** is sufficiently acidic to irreversibly protonate isobutene (eq 1). In the absence of a suitable base, degradation to form borane **5** and borinic acid **7** intervenes.



That this structural motif is possible is revealed by the molecular structure for compound **20**, crystals of which were isolated from an attempt to crystallize oxonium acid **12**, evidently from wet MeOH (Figure 3). Compound **20** is a mono-aquo adduct of borinic ester **11**, which features the μ -OH₂ interaction invoked above; this compound has defied rational attempts to synthesize it and has only been structurally characterized.

The dative coordination of water to the two B atoms is almost symmetrical with rather long B1–O1 and B2–O1 distances of 1.541(5) and 1.568(5) Å, respectively. Both B atoms are tetrahedral in this structure so that the B1–O2 distance for the MeO moiety is now elongated to 1.523(5) Å compared to that seen in the parent borinic ester **11**. Strain is present within the chelate and borole rings as evident from the B2–O1–B1,

(28) (a) Olah, G. A. *J. Am. Chem. Soc.* **1964**, *86*, 932–4. (b) Farnum, D. G. *J. Am. Chem. Soc.* **1964**, *86*, 934–5.

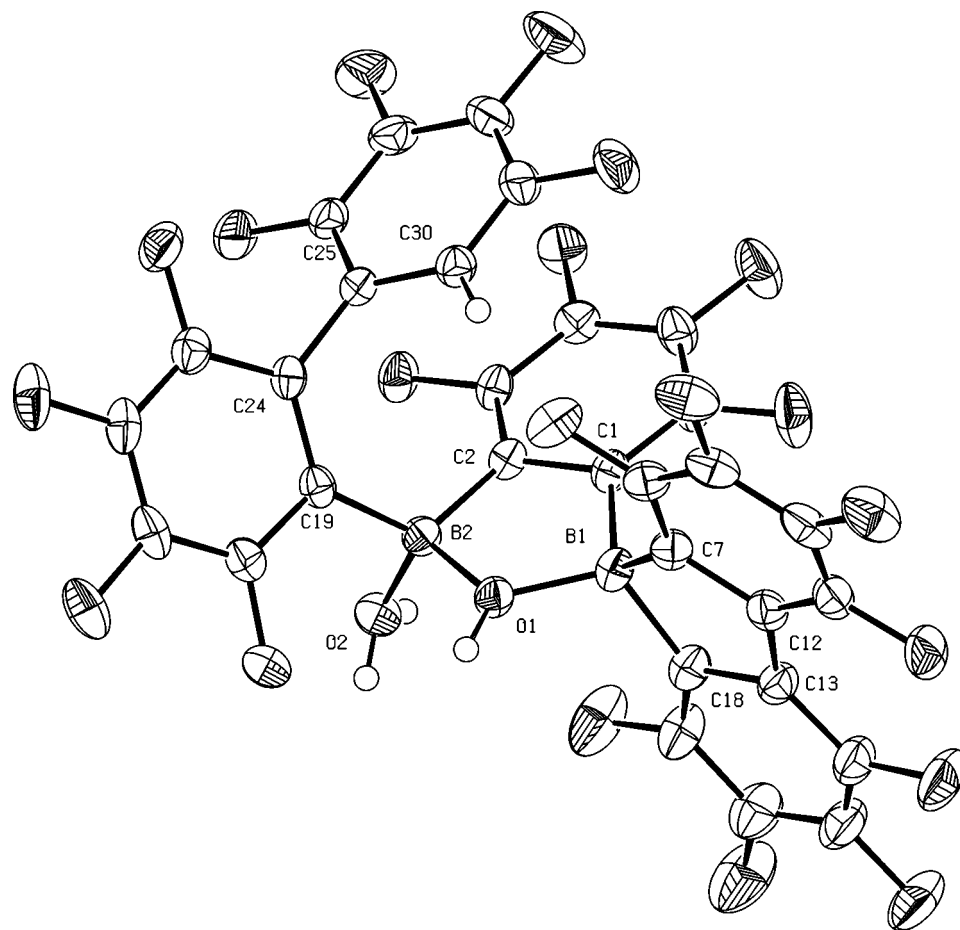


Figure 2. Molecular structure of borinic acid **17** with 50% thermal ellipsoids depicted. Six additional water molecules present in the unit cell are not depicted.

O1–B1–C2, C7–B2–O1, and C20–B2–C31 angles of 116.2(3)°, 98.2(3)°, 97.1(3)°, and 98.5(3)°, respectively. The five-membered chelate ring is puckered, with the sum of the dihedral angles involving B1, O1, B2, C7, and C2 = $-5.0(5)^\circ$; in essence O1 lies outside the plane defined by the other four atoms by 0.278(2) Å, with the mean deviation from this plane being 0.029(4) Å for B1, B2, C2, and C7.

Polymerization of Isobutene in Hydrocarbon Solution. The aqueous suspension process can be viewed as a series of bulk or solution polymerizations carried out in a dispersed medium, featuring better *T* control and potentially higher conversions due to lower process viscosity. It was therefore of interest to compare our results to polymerizations carried out in solution in the virtual absence of H₂O.

Polymerizations of isobutene undiluted or in hexane solution were conducted on a vacuum line, where both monomer and solvent had been stirred with and then vacuum transferred from tri-*n*-octylaluminum. The total impurity content under these conditions is $<2.5 \times 10^{-5}$ M, as measured by titration using a stock solution of benzophenone ketyl.¹⁸ More recent work has shown that solutions of monomer in CH₂Cl₂ purified in this same manner have residual H₂O contents $\leq 7 \times 10^{-6}$ M, as verified by titration with a solution of [Ph₃C][B(C₆F₅)₄], which serves as a *selective* indicator for H₂O.²⁹ Undoubtedly, the residual H₂O content in hydrocarbon media is lower than this.

In these polymerizations, toluene solutions of diborane or diborole were added by syringe; these polymerizations were characterized by rapid increases in viscosity, and in the case of neat monomer, it was impossible to avoid “solidification” of

the swollen mass. Quantitative conversions of monomer were obtained in hydrocarbon solution except where very low levels of initiator (2 μM) were used. The results obtained are summarized in Table 6.

Essentially, polymerization ceases below ca. 2 μM of compound **1** (entry 7). This is probably an indication that background H₂O levels are between 2 and 20 μM under these conditions. On the other hand, with [1] = 2.0 mM, stopping experiments revealed that *at least* 15 mM DtBMP was needed to prevent protic initiation under these conditions (see Experimental Section). Since DtBMP does not react directly with dissolved water, it is clear that the Brønsted acid formed from water and diborane **1** must be *kinetically* competent to protonate isobutene (2.76 M) even when [DtBMP] = 2.0 mM! We are unaware of any precedent for this behavior using classical Lewis acids: we suspect it arises due to the hindered nature of the (strong) Brønsted acid formed in this case.

The first seven entries of Table 6 demonstrate the use of progressively lower amounts of diborane initiator. Entries 3–7 were conducted at the same time using the same stock solution. It can be seen that MW increases significantly as the amount of diborane added is reduced. We suspect this feature arises from better *T* control on dilution of this compound. Entries 8–11 demonstrate that much lower MW polymer is formed in undiluted monomer, a feature that we attribute, in part, to poor *T* and mass transfer control. The conversions in entries 10 and

(29) Słomkowski, S.; Penczek, S. *J. Chem. Soc., Perkin Trans. 2* **1974**, 1718–1722, and references therein.

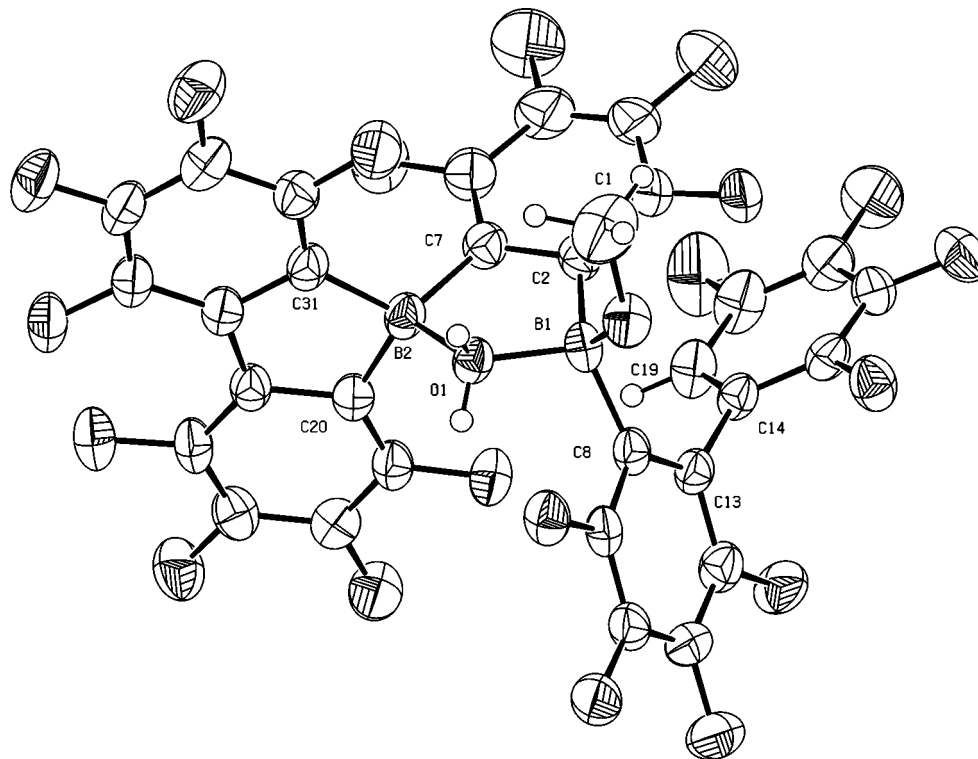


Figure 3. Molecular structure of compound **20** with 50% thermal ellipsoids depicted. Disordered MeOH and CH₂Cl₂ molecules present in the unit cell are not depicted.

11 are not quantitative, suggesting moisture levels may well have been higher in these two experiments.

The final two entries in this table reveal that significantly lower MW polymer is produced using the diborole initiator (compare entries 19/20 vs 3/4). In addition, the MWD of the derived polymers were considerably narrower than those formed using the diborane. Since polymerizations conducted using this initiator were significantly less exothermic than those using the diborane, we have to attribute these differences as being characteristic of this diborole. Similar behavior has also been noted in polymerizations featuring cationogenic initiation.⁹

Note that the behavior of the diborole initiator in hydrocarbon solution is opposite that observed in aqueous suspension; we suggest this is because physical factors (rate of addition, degree of dispersion, nature of the aqueous medium, etc.) limit MW in aqueous suspension rather than, for example, intrinsic factors such as the nature of the counteranion, etc.

The *T* dependence of MW in hydrocarbon solution was studied over the range -90 to -20 °C. These data appear in Table 6 and are plotted in Figure 4 along with the data obtained in aqueous suspension (Table 3) in the form of Arrhenius plots. Surprisingly, almost identical behavior is seen here as in aqueous suspension!

In hydrocarbon solution, polymer MW is virtually independent of *T* between -60 and -90 °C, suffering a pronounced decrease at higher *T*. The limiting slope of this curve at higher *T* corresponds to an activation energy for MW (ΔE_{MW}) of -5.2 kcal mol⁻¹. This corresponds to a ΔE_{MW} value often attributed to chain transfer to monomer, although it must be admitted that the literature value $\Delta E_{MW} = -5.9$ kcal mol⁻¹ relates to experiments conducted in more polar media.^{41-k}

Although the high MW of the PIB samples formed under anhydrous conditions precluded convenient spectroscopic determination of end-groups, the lower MW materials formed in aqueous suspension could be analyzed by ¹H NMR spectroscopy. Although not all samples were analyzed in this fashion,

those that were exhibited both *exo*- and *endo*-terminal unsaturation (ca. 60:40 ratio) consistent with chain transfer to monomer. However, these samples were formed at temperatures well below (i.e., -60 to -80 °C) where one would expect this chain transfer process to dominate based on the Arrhenius plots depicted in Figure 4.

The shallow *T* dependence of MW observed at even lower *T* has been observed before using conventional Lewis acids in polar media and has been interpreted as arising from a change in MW controlling events.³⁰ The nature of the process responsible for this “cross-over” behavior is not well understood and has been attributed to, for example, termination to counteranion and polymer precipitation. However, this cannot be the case here; all of these polymerizations are quantitative and characterized by highly efficient chain transfer based on dissolved [H₂O] or even diborane ($I_{eff} > 1000\%$).

Another explanation, again in polar media ($\epsilon \gg 4$), is that primarily unpaired cations propagate at low *T*, while ion-pairs dominate the kinetics at higher *T* so that the *T* dependence of MW should show a “kink” because of the *T* dependence of the equilibrium constant governing the concentration of these two species. This theory predicts that polymerizations in apolar media such as hexane ($\epsilon = 2.2$) should not show this phenomenon as the kinetics are dominated by ion-pairs at all accessible temperatures.³¹

Recent work from the group of Bochmann has highlighted the role of dissolved or molecular H₂O in isobutene homo/copolymerizations featuring weakly coordinating (and hydrolytically resistant) counteranions.^{4f} Although they did not analyze their MW data in this fashion, a Mayo plot of X_n^{-1} vs [H₂O]/[IB] is linear with a slope corresponding to the transfer (or termination) constant for H₂O, $C_{H_2O} = 126.2$ at -35 °C (see Supporting Information).

In other words, transfer to dissolved H₂O would be 100 times faster than propagation at equivalent concentrations of H₂O and monomer at this *T*. It should be noted that this result could have

Table 6. Isobutene Polymerization in Hydrocarbon Solution^a

entry	initiator (mM)	<i>T</i> (°C)	<i>M_w</i> (kg mol ⁻¹)	PDI	yield (%)
1	1 (2.0)	-80	340	2.38	100
2	1 (2.0)	-80	227	3.18	100
3	1 (0.2)	-80	159	5.68	100
4	1 (0.2)	-80	170	3.82	100
5	1 (0.02)	-80	316	1.99	97
6	1 (0.02)	-80	294	2.03	100
7	1 (0.002)	-80	518	1.90	3
8	1 (0.2) ^b	-80	69.0	3.16	100
9	1 (0.2) ^b	-80	41.3	2.49	100
10	1 (0.02) ^b	-80	98.6	4.34	31
11	1 (0.02) ^b	-80	59.4	3.47	39
12	1 (2.0)	-90	185	2.45	100
13	1 (2.0)	-90	269	3.24	100
14	1 (2.0)	-64	194	2.87	100
15	1 (2.0)	-40	94.8	2.25	100
16	1 (2.0)	-40	86.4	3.75	100
17	1 (2.0)	-20	37.0	2.27	100
18	1 (2.0)	-20	32.3	2.39	100
19	2 (0.2)	-80	88.6	2.09	100
20	2 (0.2)	-80	139	2.14	100

^a The diborane initiator dissolved in 1.0 mL in toluene was added to a magnetically stirred solution of isobutene (2.76 M in hexane) unless otherwise noted. ^b A stock solution of diborane in toluene (1.0 mL) was added to 12.0 mL of isobutene at -80 °C.

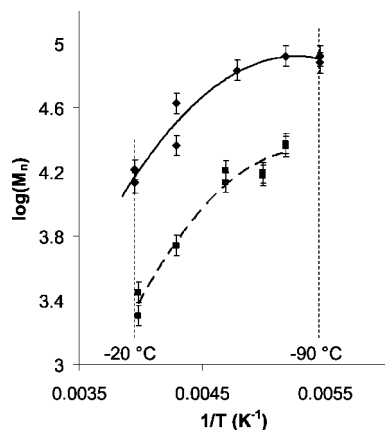


Figure 4. Temperature dependence of MW in hydrocarbon solution (solid curve) and aqueous HBF₄ suspension (dashed curve) initiated by diborane 1.

been anticipated from the early work of Williams and other workers who studied γ -ray-initiated polymerizations of isobutene;³² scrupulous purification of monomer and (hydrocarbon) solvent are required where the rate constant for “termination to polar impurities” exceeds that of propagation by a similar magnitude.^{5a}

Recent kinetic work has indicated that propagation in isobutene polymerization occurs via ion-pairs with a specific rate constant of ca. $10^8 \text{ M}^{-1} \text{ s}^{-1}$, which is largely independent of T .³³ With this

(30) (a) Dimitrov, I.; Faust, R. *Macromolecules* **2004**, *37*, 9753–9760. (b) Kennedy, J. P.; Trivedi, P. *Adv. Polym. Sci.* **1978**, *28*, 113–151. (c) Kennedy, J. P.; Rengachary, S. *Adv. Polym. Sci.* **1974**, *14*, 1–48. (d) Kennedy, J. P.; Squires, R. G. *Polymer* **1965**, *6*, 579–87.

(31) Plesch, P. H.; Austin, J. C. *J. Polym. Sci Part A: Polym. Chem.* **2008**, *46*, 4265–4284, and references therein.

(32) (a) Bates, T. H.; Best, J. V. F.; Williams, F. *Nature (London)* **1960**, *188*, 469–70. (b) Bates, T. H.; Williams, F. *Nature (London)* **1960**, *187*, 665–9. (c) Brownstein, S.; Bywater, S.; Worsfold, D. J. *Makromol. Chem.* **1961**, *48*, 127–34. (d) Best, J. V. F.; Bates, T. H.; Williams, F. *Trans. Faraday Soc.* **1962**, *58*, 192–205. (e) Ueno, K.; Hayashi, K.; Okamura, S. *Polymer* **1966**, *7*, 431–439. (f) Huang, R. Y. M.; Westlake, J. F. *J. Polym. Sci., Part A1* **1970**, *8*, 49–61. (g) Huang, R. Y. M.; Westlake, J. F. *J. Polym. Sci., Polym. Lett. Ed.* **1969**, *7*, 713–17. (h) Taylor, R. B.; Williams, F. *J. Am. Chem. Soc.* **1969**, *91*, 3728–3732.

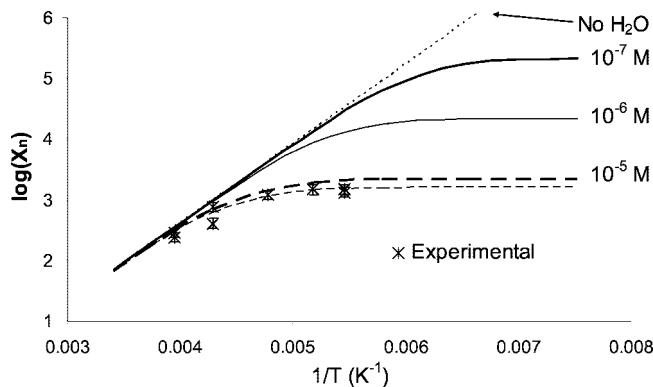


Figure 5. Simulated temperature dependence of MW in hydrocarbon solution initiated by diborane 1 assuming various dissolved [H₂O]. See Supporting Information for assumptions and data.

information, and under the assumption that $C_{\text{H}_2\text{O}}$ is also independent of T (i.e., both processes are characterized by a nonzero activation entropy and a very low activation enthalpy), it is possible to simulate the effect of dissolved [H₂O] on MW as a function of T if this process and chain transfer to monomer are the only ones involved (see Supporting Information).

This analysis is shown in Figure 5, where it is clear that the observed data can be accommodated by a background [H₂O] of about 10^{-5} M . The agreement with the value estimated by titration with benzophenone ketyl is fortuitous since the T dependence of some of these processes is unknown. However, these diboranes do not react as readily with H₂O (in comparison to conventional Lewis acids), so one can envisage that H₂O will act as a potent chain transfer agent.

If so, it is clear that the lower molecular weights seen in aqueous suspension are almost entirely due to the higher levels of dissolved H₂O that are inevitably present. [Some experiments that involved addition of diborane solution (changes from yellow to colorless when “wet”) to an aqueous suspension of hexane (5.0 mL) and toluene (10.0 mL) at various rates revealed that the (mutual) rate of diffusion of H₂O into the droplet at -78 °C in fluoroboric acid was $<10^{-4} \text{ mmol s}^{-1}$, while background levels of H₂O in the droplet were between 10^{-4} and 10^{-5} M .] Evidently, at least under some conditions at low enough T , there is not enough H₂O present to prematurely terminate chains given the high conversions seen, but many of the other effects can be interpreted in terms of differential lowering of H₂O content as a function of diborane structure (i.e., susceptibility to degradation by water) and/or mode and rate of addition.

Conclusions

The work summarized here provides considerable insight into the nature of the initiation, propagation, and chain transfer processes involving aqueous suspension polymerization of isobutene using chelating diboranes 1 and 2. In addition, experiments in hydrocarbon solution, which serve as a model for the suspension process, highlight the probable role of dissolved water as a potent chain transfer agent in polymerizations involving hydrolytically resistant Lewis acids that give rise to weakly coordinating counteranions. It is evident that chain transfer to water will limit MW in aqueous suspension and to the point where it will prove very challenging to develop an aqueous suspension process for the synthesis of high MW PIB

(33) De, P.; Faust, R. *Macromolecules* **2005**, *38*, 9897–9900, and references therein.

or copolymers thereof. In particular, on the basis of the behavior of these diboranes in nearly anhydrous hexane solution, it is clear that the required levels of background moisture in the monomer droplets would have to be in the ppm range.

Experimental Section

Part I. All of the synthetic or NMR scale reactions involving diborane **1** or diborole **2** and various reactants (i.e., MeOH, H₂O, or DPE) were performed at the University of Calgary. Details of these experiments are provided as Part II of the Experimental Section.

All polymerization experiments were conducted at the University of Akron, as were control polymerization experiments involving the hydrolysis products of diborane **1** or diborole **2**. The syntheses of diborane **1** and diborole **2** for use in all polymerization experiments were conducted at the University of Akron according to literature procedures^{6c,8} or modifications thereof.¹⁸ Borinic acid **7** was prepared by controlled hydrolysis of B(C₆F₅)₃ as described in the literature.³⁴

All solvents and reagents were purchased from commercial sources and purified as required. Hexane and toluene used in polymerization experiments were predried by passage through columns of A2 alumina and Q5 deoxo catalyst under N₂³⁵ or distilled from Na metal and benzophenone under N₂. Dichloromethane was dried and distilled from P₂O₅ under N₂. Further purification of dichloromethane or hexane was achieved by stirring with tri-*n*-octylaluminum under N₂ followed by vacuum transfer just prior to polymerization as explained below. Stock solutions of diborane **1** and diborole **2** were prepared in anhydrous toluene or hexane and stored in an Innovative Technologies glovebox at -30 °C prior to use.

Isobutene was grade 2.0 (99.0%) provided by Praxair and was purified by passage through a column of BASF R3-11 deoxo catalyst and activated molecular sieves 4 Å; initial exposure of the latter to isobutene must be accomplished slowly, and with cooling of the column if needed, to avoid significant exotherm and resulting cracking of isobutene. Isobutene was further purified by vacuum transfer from tri-*n*-octylaluminum just prior to polymerization as explained below.

Routine NMR spectra were recorded on Varian Mercury 300 and Inova 400 MHz instruments. ¹H and ¹⁹F NMR spectra are referenced to residual protonated solvent and 2,3,5,6-tetrafluoroxylene (δ -145.7 vs CFCl₃), respectively. GPC analyses were performed by a technician affiliated with the Institute of Polymer Science and using a Waters GPC system equipped with a set of five, linear Styragel columns, eluting with THF at 1.002 mL/min at 35 °C. Polymer was detected using a Waters differential refractive index, Viscotek 110 differential viscometer, and Wyatt Technology Dawn EOS, 18-angle light scattering detectors. Data were analyzed using the Astra 4.0 software provided by Wyatt Technology using a dn/dc value for poly(isobutene) of 0.108 mL g⁻¹³⁶ and assuming 100% mass recovery. This procedure was found to be reliable, and the results were periodically checked through blind analyses of poly(isobutene) standards provided by American Polymer Standards Corp.

Polymerization of Isobutene in Aqueous Suspension. Two different procedures were employed, each involving the addition of a toluene stock solution of diborane **1** and diborole **2** to isobutene monomer, either neat or diluted with hexane:

(34) Schottek, J.; Becker, P.; Kullmer, I. (Targor GMBH) *PCT Int. Appl. WO 2000037476*, 2000.

(35) Pangborn, A. B.; Giardello, M. A.; Grubbs, R. H.; Rosen, R. K.; Timmers, F. J. *Organometallics* **1996**, *15*, 1518–20.

(36) Puskas, J. E.; Chen, Y.; Kulbaba, K.; Kaszas, G. *J. Polym. Sci. Part A: Polym. Chem.* **2006**, *44*, 1777–83.

Procedure A: Uncontrolled Addition of Diborane.¹⁸ A three-neck, 100 mL round-bottom flask, with a central 24/40 and two 14/20 side necks, was charged with 20 mL of LiCl/NaCl/H₂O stock and 0.100 g of surfactant if used. The flask was then fitted with a 14/20 septum, 14/20 gas-inlet adapter, and 24/40 outer/inner air-free adapter with in-line PTFE stopcock, after which it was affixed to a vacuum line. The contents of the flask were then subjected to a single freeze–pump–thaw cycle, and then 18.0 mL of isobutene was vacuum transferred into the flask. The flask was then warmed to -60 °C (through use of a CHCl₃/dry ice bath) and sealed under N₂. The flask was then connected to a double manifold and placed back under N₂, after which the 24/40 outer/inner air-free adapter was replaced with a stir bearing/shaft/blade assembly. The flask contents were then stirred under N₂ at -60 °C at about 500 rpm. Next, 1.0 mL of diborane or diborole stock (1.19 × 10⁻⁵ mol) was then added rapidly by syringe (**Caution:** can be violently exothermic), after which the reactor contents turned milky white in color. Polymerization was allowed to continue for a full hour before warming the reactor contents to room temperature by diluting the flask with additional water and CH₂Cl₂. During this period very little gas evolution occurred. The organic phase was then extracted with CH₂Cl₂ and dried over MgSO₄ before isolating polymer by removal of volatiles under reduced pressure. Yield: 6.10 g (48% conversion).

Procedure B: Controlled Addition of Diborane. A three-neck, 100 mL round-bottom flask, calibrated with a mark corresponding to 10.0 mL and equipped with a central 24/40 and two 14/20 side necks, was fitted with a 14/20 stopper, a 14/20 gas-inlet adapter, and a 24/40 outer/inner air-free adapter with in-line PTFE stopcock, after which it was connected to a vacuum line. Then, 10.0 mL of isobutene was condensed into the flask, and the flask and adapter were removed from the vacuum line. The flask was then connected to a double manifold, after which the 24/40 outer/inner air-free adapter was replaced with a stir bearing/shaft/blade assembly and the remaining 14/20 neck fitted with a septum under a flow of N₂. The flask was then maintained at -78 °C (through use of a acetone/dry ice bath) and kept under slight positive N₂ pressure. The flask contents were then stirred under N₂ at -78 °C at 500 ± 10 rpm, while 5.0 mL of hexane and 15.0 mL of aqueous HBF₄ were added sequentially via syringe. Next, 1.0 mL of diborane or diborole stock (1.19 × 10⁻⁵ mol) was then added over periods varying between 30 s and 10 min using a syringe pump at a controlled rate. Polymerization was allowed to continue for a full hour before quenching with 2-propanol and warming the contents to room temperature. The organic phase was diluted with hexane and transferred to a separatory funnel. The aqueous phase was withdrawn, and the organic phase washed with water and then dried over MgSO₄. The mixture was filtered, washing with additional hexane before isolating polymer by removal of volatiles *in vacuo* using a rotary evaporator until constant weight was obtained. Samples were transferred to vials and dried overnight in a vacuum oven at 90 °C and 30 in. Hg prior to GPC analysis.

Procedure C: Polymerization of Isobutene in Hexane Solution. A dry 250 mL round-bottom 24/40 single-neck flask was charged with 11.9 g (18 mL) of hexane, 0.82 g (1 mL) of tri-*n*-octylaluminum, and a magnetic stir bar inside a glovebox. This was then sealed with an air-free style adapter equipped with an in-line PTFE vacuum stopcock and the apparatus connected to a vacuum line. The mixture of solvent and drying agent was then degassed by application of three sequential freeze–pump–thaw cycles and subsequently charged with 5.50 mL of isobutene via vacuum transfer. Next, a dry 100 mL, two-neck, round-bottom flask previously silanized with Me₂SiCl₂ and containing a magnetic stir bar and glass stopper was connected to the vacuum line, and the entire assembly was flame-dried under vacuum, refilled with N₂, and then fitted with a septum. The solvent/monomer/drying agent mixture was then stirred at -78 °C for 30 min before vacuum

Table 7

entry	DtBMP (mM)	M_w (10^3 kg mol $^{-1}$)	PDI	yield (%)
1	20			0
2	20			0
3	15	605	2.3	0.5 ₀
4	15	753	4.9	0.4 ₇
5	5	552	3.6	1.4 ₄
6	5	370	4.2	0.9 ₈
7	2	287	2.2	6.8 ₂
8	2	293	2.1	6.0 ₂
9	2	302	2.5	5.7 ₆
10		195	3.2	100
11		285	2.4	100

transferring volatile material to the 100 mL flask. The contents of the 100 mL flask were then warmed to -78 °C and stirred for 15 min under a blanket of N_2 prior to injection of 750, 75, or 7.5 μ L of a 0.065 M solution of diborane **1** in toluene.

A rapid increase in viscosity occurred immediately upon addition, particularly at higher concentrations of diborane (**Caution**: strongly exothermic), and stirring often ceased entirely while the reaction was allowed to proceed for 1 h at -78 °C under a blanket of nitrogen. The viscous solution was diluted with hexane and washed with a mixture of water and MeOH. The resultant polymer solutions were dried over Na_2SO_4 , filtered, and concentrated to dryness *in vacuo*. Polymer samples were dried in a vacuum oven at 30 in. Hg at 90 °C for 24 h prior to analysis.

Stopping Experiments with 2,6-Di-*tert*-butyl-4-methylpyridine (DtBMP). Stopping experiments using DtBMP were conducted in the same fashion as in Procedure C but involved the addition of 1.00, 0.75, 0.50, 0.25, or 0.10 mL of a stock solution of DtBMP (0.5 M in hexane) prior to the addition of diborane **1** (0.065 M in toluene, final concentration = 2.0 mM). Polymerization was allowed to proceed for 1 h at -78 °C before quenching with 1 mL of methanol. All volatiles were removed and the residue washed with methanol prior to being taken up in hexanes. The resultant polymer solutions were filtered, concentrated *in vacuo*, and dried in a vacuum oven at 30 in. Hg at 90 °C for 24 h prior to analysis by GPC. The results are summarized in Table 7.

Impurity Levels in Hydrocarbon Solution. A stock solution of sodium benzophenone ketyl in xylenes/tetraglyme was prepared as follows: A mixture of xylenes (100 mL) and tetraglyme (20 mL) was stirred over molten Na metal under N_2 in a glovebox for several hours. The mixture was cooled, filtered, and stirred over fresh Na metal, and this process was repeated, until the molten Na was shiny and no further decomposition of tetraglyme (which produces a dark brown residue) was noted. Benzophenone was then gradually added to the cooled suspension until the deep blue purple color of the ketyl persisted, and the entire mixture, containing excess Na metal, was stored in a Schlenk storage flask with integral stopcock in a glovebox. Aliquots were removed by syringe and added, outside the glovebox, to an known excess of degassed, standardized aqueous HCl. The excess acid was titrated to a phenolphthalein end-point using a standard aqueous NaOH solution. Stock solutions prepared in this manner maintain their titer for many months provided excess Na is present; a typical concentration is 0.02 M.

A solution of IB and hexane, prepared and purified as described in Procedure C, was warmed to room temperature under N_2 until most of the IB had evaporated. The remaining solution was titrated to a persistent, pale blue end-point using the stock ketyl solution. A typical result was $2.5 \pm 0.3 \times 10^{-5}$ M based on a stoichiometry of 2 mol of ketyl consuming 1 mol of water and the original volume of the hexane/IB solution.

Control Experiments in Aqueous Suspension or Hydrocarbon Solution.

Attempted Polymerization Using Borinic Acid **7 and $B(C_6F_5)_3$.** Procedure B was followed using 15.0 mL of undiluted isobutene and 15.0 mL of aqueous HBf_4 at -78 °C. One milliliter

of a toluene stock solution containing borinic acid **7** (0.01 M) and $B(C_6F_5)_3$ (0.01 M) was added over 1 min at -78 °C. No exotherm or change in appearance of the mixture was noted. After 1 h the mixture was quenched with 2-propanol and warmed to room temperature; vigorous gas evolution was observed to occur during this process. Extraction of the aqueous phase with hexane did not provide any polymeric material.

Attempted Polymerization Using $B(C_6F_5)_3$. Procedure C was followed using 5.50 mL of isobutene and 18.0 mL of hexane at -78 °C. One milliliter of a toluene stock solution of $B(C_6F_5)_3$ (0.02 M) was added rapidly at -78 °C. No exotherm or change in appearance of the mixture was noted. After 1 h the mixture was quenched with 2-propanol and warmed to room temperature; vigorous gas evolution was observed to occur during this process. Evaporation of the hexane did not provide any polymeric material.

Attempted Polymerization Using Borinic Acid **17.** Procedure B was followed using 10.0 mL of isobutene, diluted with 5.0 mL of hexane and 15.0 mL of aqueous HBf_4 at -78 °C. One milliliter of a dichloromethane stock solution containing borinic acid **17** (0.01 M) was added over 1 min at -78 °C. No exotherm or change in appearance of the mixture was noted. After 1 h the mixture was quenched with 2-propanol and warmed to room temperature; vigorous gas evolution was observed to occur during this process. Extraction of the aqueous phase with hexane did not provide any polymeric material.

Attempted Polymerization Using a Mixture Borinic Ester **5 and Borane **4**.** Procedure C was followed using 5.50 mL of isobutene diluted with 18.0 mL of hexane. A solution of diborane **1** (84 mg) in toluene (10 mL) was treated with ~ 2.0 equiv of MeOH (1.0 μ L) at -78 °C. The solution was warmed to room temperature; a ^{19}F NMR spectrum of this mixture revealed complete conversion of diborane **1** to a mixture of borinic ester **5**, borane **4**, and its MeOH adduct **6**. To the mixture of isobutene and hexane at -78 °C was added 2.0 mL of this solution via syringe so as to give a final concentration of about 2 mM expressed as diborane **1**. No exotherm or change in appearance of the mixture was noted. After 1 h the mixture was quenched with 2-propanol and warmed to room temperature; vigorous gas evolution was observed to occur during this process. Evaporation of the hexane did not provide any polymeric material.

Part II. An Innovative Technologies or Vacuum Atmospheres argon-filled glovebox was used for the storage and manipulation of oxygen- and moisture-sensitive compounds. Thermally unstable compounds were stored in a -35 °C freezer installed on the respective glovebox. All reactions were performed on a double manifold, high-vacuum line using modified Schlenk techniques.³⁷ Residual oxygen and moisture were removed from Ar by passage through an Oxisorb-W scrubber from Matheson Gas Products. Commonly utilized specialty glassware included a swivel frit assembly, thick-walled (5 mm) Carius tubes, and round-bottom flasks with in-line adaptors all equipped with Teflon stopcocks. All glassware was stored in a 110 °C oven for a minimum of 12 h before immediate transfer into the glovebox antechamber or assembled on the vacuum line and evacuated while hot. Unless otherwise noted, the introduction of solvent in all manipulations was via vacuum transfer with condensation at -78 °C. Liquid nitrogen (-196 °C), dry ice/acetone (-78 °C), dry ice/acetonitrile (-45 °C), and water/ice (0 °C) baths were used for cooling receiving flasks and to maintain low-temperature conditions.

Solvents were purchased from Aldrich or Cambridge Isotopes and dried and deoxygenated before use by the following procedures. Toluene, hexanes, and tetrahydrofuran (THF) solvents were dried and purified using the Grubbs/Dow purification system³⁵ and stored

(37) Burger, B. J.; Bercaw, J. E. *Experimental Organometallic Chemistry*; American Chemical Society: Washington, D.C., 1987.

in evacuated 500 mL thick-walled flasks over titanocene³⁸ (toluene and hexanes) or sodium/benzophenone ketyl (THF). Benzene, *d*₆-benzene, and *d*₈-toluene, were dried and stored over sodium/benzophenone ketyl in thick-walled Schlenk tubes under vacuum. Diethyl ether and methylene chloride were predried over LiAlH₄ and CaH₂, respectively, and subsequently stored over sodium/benzophenone ketyl and CaH₂, respectively. Methylene chloride-*d*₂ was predried over 4 Å molecular sieves and stored over CaH₂. All of these solvents and reagents were distilled directly into reaction vessels or separate predried Schlenk storage vessels prior to use. Chloroform, chloroform-*d*, and D₂O were used as received.

Routine NMR spectra were recorded on a Bruker AC-200 MHz, AMX-300 MHz (¹⁹F –282.4 MHz), Bruker AC-300 MHz, or Avance DRX-400 [equipped with a gradient ¹H/¹³C probe] spectrometer. All 2D NMR experiments [¹⁹F, ¹⁹F-COSY, ¹⁹F, ¹⁹F-NOESY, ¹H, ¹³C-HMQC, ¹H, ¹H-NOESY, ¹H, ¹⁹F-COSY, or NOESY] were performed using a Bruker Avance AMX-300 MHz or DRX-400 MHz spectrometer. All ¹H NMR spectra were referenced to SiMe₄ through the residual ¹H resonance(s) of the solvent: C₆D₆ ($\delta = 7.15$ ppm), *d*₈-toluene ($\delta = 2.09, 6.98, 7.02, \text{ and } 7.09$ ppm), *d*₈-THF ($\delta = 1.73$ and 3.58 ppm), or CD₂Cl₂ ($\delta = 5.32$ ppm). ¹³C{¹H} NMR spectra are also referenced relative to SiMe₄ through the resonance(s) of the deuterated solvent: C₆D₆ ($\delta = 128.0$ ppm), *d*₈-toluene ($\delta = 20.4, 125.2, 128.0, 128.9, \text{ and } 137.5$ ppm), *d*₈-THF ($\delta = 25.4$ and 67.6 ppm), or CD₂Cl₂ ($\delta = 54.0$ ppm). ¹⁹F NMR spectra were referenced externally to C₆F₆: $\delta = -163.0$. Temperature calibration for NMR experiments was achieved by monitoring the ¹H NMR spectrum of pure methanol.³⁹ For all air- and/or moisture-sensitive compounds and reactions, NMR samples were prepared in the glovebox and the NMR tubes were capped with rubber septa. Unless otherwise stated, all spectroscopic data are reported at room temperature (298 K).

Elemental analyses were performed on a Control Equipment Corporation 440 elemental analyzer by Mrs. Dorothy Fox, Mrs. Roxanna Smith, or Mrs. Olivera Blagojevic at the University of Calgary.

Spectroscopic Studies of the Addition of MeOH to C₆F₄-1,2-[B(C₆F₅)₂]₂. In a glovebox, C₆F₄-1,2-[B(C₆F₅)₂]₂, **1** (10 mg, 0.012 mmol), was loaded into a 5 mm NMR tube and dissolved in *d*₈-toluene (0.4 mL) or CD₂Cl₂ (0.4 mL). The sample was capped with a rubber septum, removed from the glovebox, and cooled to –78 °C in a dry ice/acetone bath. Varying equivalents (0.5–10.0 equiv) of dry and degassed methanol (0.72 M in *d*₈-toluene or CD₂Cl₂) were injected into the NMR tube via gastight syringe at low temperature. The NMR tube was placed in a spectrometer, cooled to –60 °C, and the reaction was monitored up to room temperature. A complete listing of spectral data at various *T* and stoichiometries is provided as Supporting Information.

(C₆F₄-1,2-[B(C₆F₅)₂]₂ + 8.0 MeOH) + 3 C₆F₄-1,2-[B(C₆F₅)₂]₂. A solution of **3** was prepared by the addition of MeOH (35 μ L, 1.36 mM in *d*₈-toluene) via gastight syringe to a capped 5 mm NMR tube charged with C₆F₄-1,2-[B(C₆F₅)₂]₂, **1** (5 mg, 0.006 mmol), dissolved in *d*₈-toluene (0.2 mL) at room temperature. To this solution was added an additional 3 equiv of C₆F₄-1,2-[B(C₆F₅)₂]₂, **1** (15 mg, 0.018 mmol), dissolved in *d*₈-toluene (0.3 mL). ¹H NMR (*d*₈-toluene, 298 K): δ 6.58 (m, 1H, –C₆F₄H), 3.65 (s, ~0.3H, μ -OMe), 3.37 (br s, 2H, (C₆F₅)₂BOMe), 2.55 (br s, 4H, MeOH). ¹⁹F NMR (*d*₈-toluene, 298 K): 6% **3**, δ –131.7 (8F, *o*-B(C₆F₅)₂), –136.5 (2F, –C₆F₄), –158.4 (4F, *p*-B(C₆F₅)₂), –164.2 (2F, –C₆F₄), –164.8 (8F, *m*-B(C₆F₅)₂); 47% **6**, δ –133.4 (4F, *o*-B(C₆F₅)₂(MeOH)), –133.5 (1F, –C₆F₄(MeOH)), –139.6 (1F, –C₆F₄(MeOH)), –154.5 (2F, *p*-B(C₆F₅)₂(MeOH)), –155.6 (1F, –C₆F₄(MeOH)), –156.8 (2F, –C₆F₄(MeOH)), –161.9 (4F, *m*-B(C₆F₅)₂

(MeOH)); 47% **4**, δ –132.3 (4F, *o*-B(C₆F₅)₂), 148.5 (2F, *p*-B(C₆F₅)₂), 160.6 (4F, *m*-B(C₆F₅)₂).

Spectroscopic Studies of the Addition of H₂O to C₆F₄-1,2-[B(C₆F₅)₂]₂. In a glovebox solid C₆F₄-1,2-[B(C₆F₅)₂]₂, **1** was loaded into a 5 mm NMR tube and dissolved in *d*₈-toluene (0.4 mL). The sample was capped with a rubber septum, removed from the glovebox and cooled to –78 °C in a dry ice/acetone bath. Varying equivalents of degassed water (0.5 – 8.0 equiv. or a large excess) were injected into the NMR tube via gastight syringe at low temperature. The NMR tube was placed in a spectrometer, cooled to –60 °C and the reaction was monitored up to room temperature. A complete listing of spectral data is provided as Supporting Information.

Spectroscopic Studies of the Addition of MeOH to C₆F₄-1,2-[B(C₁₂F₈)₂]₂. In a glovebox solid C₆F₄-1,2-[B(C₁₂F₈)₂]₂, **2**, was loaded into a 5 mm NMR tube and dissolved in *d*₈-toluene (0.4 mL). The sample was capped with a rubber septum, removed from the glovebox, and cooled to –78 °C in a dry ice/acetone bath. Varying equivalents of dry and degassed methanol (0.713 M in *d*₈-toluene) were injected into the NMR tube via gastight syringe at low temperature. The NMR tube was placed in a spectrometer cooled to –60 °C, and the reaction was monitored up to room temperature. A complete listing of spectral data is provided as Supporting Information.

Spectroscopic Studies of the Addition of H₂O to C₆F₄-1,2-[B(C₁₂F₈)₂]₂. In a glovebox solid C₆F₄-1,2-[B(C₁₂F₈)₂]₂, **2**, was loaded into a 5 mm NMR tube and dissolved in *d*₈-toluene (0.4 mL). The sample was capped with a rubber septum, removed from the glovebox, and cooled to –78 °C in a dry ice/acetone bath. Varying equivalents of water were injected into the NMR tube via gastight syringe at low temperature. The NMR tube was placed in a spectrometer cooled to –60 °C, and the reaction was monitored up to room temperature. A complete listing of spectral data is provided as Supporting Information.

Generation of MeOH Adduct 10. Diborole **2** (15 mg, 20 μ mol) was dissolved in CD₂Cl₂ (0.5 mL). The solution was placed in an NMR tube, which was sealed with a rubber septum, and the tube was cooled to –78 °C. A stock solution of MeOH (0.394 M in CD₂Cl₂, 50 μ L, 20 μ mol) was injected through the septum. The tube was briefly shaken and subsequently introduced in the precooled (–80 °C) NMR probe. Spectra (¹H, ¹⁹F) were recorded from –80 to 0 °C with 10 deg intervals

NMR spectroscopic data for **10**: ¹H NMR (300 MHz, CD₂Cl₂, 193 K): δ 6.58 (dq, *J* = 19 Hz, 4.0 Hz, 3.58, 1H, MeOH), (d, *J* = 3.5 Hz, 3H, MeOH). ¹⁹F NMR (282 MHz, CD₂Cl₂, 193 K): δ –124.6 (m, 2F, BC₁₂F₈), –130.2 (dd, *J* = 24 Hz, 12 Hz, 1F, C₆F₄), –130.6 (m, 2F, BC₁₂F₈), –131.0 (s, br, 2F, BC₁₂F₈), –132.6 (s, br, 2F, BC₁₂F₈), –133.5 (m, br, 3F, BC₁₂F₈+, C₆F₄), –140.8 (m, 2F, BC₁₂F₈), –152.4 (t, *J* = 20 Hz, 2F, BC₁₂F₈), –153.4 (t, *J* = 22 Hz, 2F, BC₁₂F₈), –153.6 (t, *J* = 22 Hz, 1F, C₆F₄), –155.7 (t, *J* = 22 Hz, 1F, C₆F₄). 2D ¹H/¹⁹F correlation: 6.58, –133.5. Selective decoupling of ¹⁹F at δ 133.5 gave δ 6.58 (q, *J* = 4.0 Hz).

¹H NMR (300 MHz, PhMe-*d*₈, 213 K): δ 4.04 (br s, 1H, MeOH), 2.01 (s, 3H, MeOH). ¹⁹F NMR (282 MHz, PhMe-*d*₈, 213 K): δ –124.6 (2F, BC₁₂F₈), –129.2 (2F, BC₁₂F₈), –129.2 (2F, BC₁₂F₈), –130.6 (1F, C₆F₄), –130.8 (2F, BC₁₂F₈), –132.0 (1F, C₆F₄), –140.1 (2F, BC₁₂F₈), –150.2 (2F, BC₁₂F₈), –151.7 (2F, BC₁₂F₈), –152.2 (1F, C₆F₄), –153.1 (2F, BC₁₂F₈), –154.4 (1F, C₆F₄).

X-ray Crystallographic Characterization of Borinic Ester 11.⁹ An orange block crystal of dimensions 0.20 × 0.16 × 0.12 mm was coated with Paratone 8277 oil (Exxon) and mounted on a glass fiber. All measurements were made on a Nonius KappaCCD diffractometer with graphite-monochromated Mo K α radiation. Details of crystal data and structure refinement are provided as Supporting Information. The data were collected using ω and φ

(38) Marvich, R. H.; Brintzinger, H.-H. *J. Am. Chem. Soc.* **1971**, *93*, 2046.

(39) Ammann, C.; Meier, P.; Merbach, A. E. *J. Magn. Reson.* **1982**, *46*.

scans.⁴⁰ The data were corrected for Lorentz and polarization effects and for absorption using a multiscan method.⁴¹ Since the crystal did not show any sign of decay during data collection, a decay correction was deemed unnecessary.

The structure was solved by the direct methods⁴² and expanded using Fourier techniques.⁴³ The non-hydrogen atoms were refined anisotropically. Hydrogen atoms were included at geometrically idealized positions and were not refined. The final cycle of full-matrix least-squares refinement using SHELXL97⁴⁴ converged with unweighted and weighted agreement factors, $R = 0.0457$ and $wR = 0.1199$ (all data), respectively, and goodness of fit, $S = 1.033$. The weighting scheme was based on counting statistics, and the final difference Fourier map was essentially featureless. Figure 1 was plotted with the aid of PLATON.⁴⁵

X-ray Crystallographic Characterization of Compound 20.

A colorless needle of dimensions $0.70 \times 0.20 \times 0.04$ mm was coated with Paratone 8277 oil (Exxon) and mounted on a glass fiber. All measurements were made on a Nonius KappaCCD diffractometer with graphite-monochromated Mo $K\alpha$ radiation. Details of crystal data and structure refinement are provided as Supporting Information. The data were collected using ω and φ scans.⁴⁰ The data were corrected for Lorentz and polarization effects and for absorption using a multiscan method.⁴¹ Since the crystal did not show any sign of decay during data collection, a decay correction was deemed unnecessary.

The structure was solved by the direct methods⁴² and expanded using Fourier techniques.⁴³ The non-hydrogen atoms were refined anisotropically. The structure contains disordered dichloromethane and methanol molecules of solvation with unequal site occupancy factors of 0.870(5) and 0.716(6), respectively, for the major components. The EADP command was used to refine the U_{ij} 's as constrained parameters of the disordered atoms. The C–O distance was fixed using the command DFIX in the methanol molecule. Hydrogen atoms were included at geometrically idealized positions and were not refined. The final cycle of full-matrix least-squares refinement using SHELXL97⁴⁴ converged with unweighted and weighted agreement factors, $R = 0.0559$ and $wR = 0.1345$ ($I \geq 2\sigma(I)$), respectively, and goodness of fit, $S = 1.057$. The weighting scheme was based on counting statistics, and the final difference Fourier map was essentially featureless. Figure 3 was plotted with the aid of PLATON.⁴⁵

Synthesis of 1,2-C₆F₄(9-BC₁₂F₈)(B(H₂O)(C₁₂HF₈)(μ -OH)·6H₂O (17). Diborole **2** (130 mg, 0.17 mmol) was dissolved in water (2 mL). An aliquot of the solution was dissolved in D₂O for NMR analysis. ¹⁹F NMR data for **13** (282 MHz, D₂O, 298 K): δ -134.4 (4F, BC₁₂F₈), -136.3 (4F, BC₁₂F₈), -139.8 (2F, C₆F₄), -157.4 (4F, BC₁₂F₈), -158.2 (4F, BC₁₂F₈), -161.4 (2F, C₆F₄). After evaporation of ca. 25% of the water in air, colorless single crystals of compound **17** were deposited. Yield: 69 mg (51%). Anal. Calcd for C₃₀H₄B₂F₂₀O₂·6H₂O: C 39.77, H 1.78. Found: C 40.60, H 1.55.

X-ray Crystallographic Characterization of Borinic Acid 17. A colorless prismatic crystal of dimensions $0.20 \times 0.18 \times 0.12$ mm was coated with Paratone 8277 oil (Exxon) and mounted on a glass fiber. All measurements were made on a Nonius KappaCCD diffractometer with graphite-monochromated Mo $K\alpha$ radiation. Details of crystal data and structure refinement are provided as

Supporting Information. The data were collected using ω and φ scans.⁴⁰ The data were corrected for Lorentz and polarization effects and for absorption using a multiscan method.⁴¹

The structure was solved by the direct methods⁴² and expanded using Fourier techniques.⁴³ The non-hydrogen atoms were refined anisotropically. Of the six molecules of water of hydration, three were disordered over two sites each with site occupancy factors for O6, O7, and O8 of 0.789(3), 0.848(3), and 0.813(3), respectively, while the smaller fractions O6', O7', and O8' had occupancy factors of 0.211(3), 0.152(3), and 0.187(3), respectively. The same U_{ij} values were assigned to the disordered O atoms (using EADP within SHELXL), and H atoms for all water molecules were constrained at geometrically idealized position with O---H distances = 0.82 Å. Other hydrogen atoms were included at geometrically idealized positions and were not refined. The final cycle of full-matrix least-squares refinement using SHELXL97⁴⁴ converged with unweighted and weighted agreement factors, $R = 0.0462$ and $wR = 0.1303$ (all data), respectively, and goodness of fit, $S = 1.024$. The weighting scheme was based on counting statistics, and the final difference Fourier map was essentially featureless. Figure 2 was plotted with the aid of PLATON.⁴⁵

Reaction of 2 with Excess Water. Diborole **2** (0.25 g, 0.33 mmol) was dissolved in water (2 mL), and the water was subsequently pumped off. Residual water was removed by redissolution in CH₂Cl₂ and evaporation of the volatiles *in vacuo* to afford an off-white powder. Recrystallization from CH₂Cl₂ gave white crystals (135 mg, 50%). ¹H NMR (300 MHz, toluene-*d*₈, 353 K): δ 6.35 (m, 2H, Ar^F-H), 3.46 (s, br, 4H, H₂O) indicated the presence of a dihydrate of **16**. ¹⁹F NMR (282 MHz, toluene-*d*₈, 353 K): δ -129.3 (2F), -131.3(2F), -137.3(m, 2F), -138.2, -139.4 (2F), -151.0(2F), -152.4(2F), -154.1(2F), -154.3(2F), -155.6. Spectroscopic data for anhydrous **16**: ¹H NMR (*d*₈-toluene, 298 K): δ 6.54 (m, 2H, C₆F₄HC₆F₄B). ¹⁹F NMR (*d*₈-toluene, 298 K): δ -122.9 (2F, -C₆F₄), -129.2 (2F, C₆F₄HC₆F₄B), -137.4 (2F, C₆F₄HC₆F₄B), -137.7 (2F, C₆F₄HC₆F₄B), -139.4 (2F, C₆F₄HC₆F₄B), -141.8 (2F, -C₆F₄), -146.8 (2F, C₆F₄HC₆F₄B), -151.6 (2F, C₆F₄HC₆F₄B), -151.9 (2F, C₆F₄HC₆F₄B), -153.6 (2F, C₆F₄HC₆F₄B). ¹¹B{¹H} NMR (*d*₈-toluene, 298 K): δ 42.1.

Crystals of a THF adduct of compound **16** were isolated on attempted recrystallization of borinic acid **15** from a mixture of THF and hexane over several days. Crystallographic data for **16**·THF are provided as Supporting Information.

Generation of Ion Pair 19 from 2 and MeOH in the Presence of DPE. Diborole (**2**) (15 mg, 20 μ mol) was dissolved in dry CD₂Cl₂ (0.4 mL) and placed in an NMR tube covered with a rubber septum. Dry 1,1-diphenylethene (DPE, freshly distilled from CaH₂) (50 μ L, 0.397 M in CD₂Cl₂) was injected through the septum. Upon addition, the solution turned red locally, but after mixing, the solution was yellow again. ¹H NMR spectroscopy indicated a 20–30:70–80 mixture of 1,3,3-triphenyl-3-methylindan (**18**) and DPE. The ¹⁹F NMR spectrum showed only **2** with <1% degradation. ¹H NMR spectroscopic data for indan **18**: ¹H NMR (300 MHz, CD₂Cl₂, 298 K): δ 7.33–7.00 (m, 19H, Ph overlap with Ph of Ph₂C=CH₂), 3.39 (d, $J = 14$ Hz, 1H), 3.12 (d, $J = 14$ Hz, 1H), 1.27 (s, 3H, Me), for Ph₂C=CH₂: δ 7.33–7.00 (10H, Ph, overlap with indan Ph), 5.47 (s, 2H, CH₂).

To generate **19**, the NMR tube described above was immediately cooled to -78 °C and MeOH (50 μ L, 0.397 M in CD₂Cl₂) was added. The sample was introduced into a precooled (-80 °C) NMR probe. Spectra (¹H and ¹⁹F) were recorded at -80, -60, -40, -20, and 0 °C and room temperature.

At -80 °C ion pair [Ph₂CMe][2-*u*-OMe] (**19**) and methanol adduct **10** were observed in ~90:10 ratio (by ¹H NMR integration). NMR spectroscopic data for **19**: ¹H NMR (300 MHz, CD₂Cl₂, 213 K): δ 8.31 (t, $J = 7.3$ Hz, 2H, *p*-H), 7.98 (d, $J = 7.5$ Hz, 4H, *o*-H), 7.87 (t, $J = 7.8$ Hz, 4H, *m*-H), 3.67 (s, 3H, Me), 2.68 (s, 3H, *u*-OMe). ¹⁹F NMR (282 MHz, CD₂Cl₂, 213 K): δ -132.0 (4F,

(40) Hooft, R. *COLLECT*; Nonius BV, Delft, The Netherlands, 1998.

(41) Otwinowski, Z.; Minor, W. *Methods Enzymol.* **1997**, 276, 307.

(42) SIR92: Altomare, A.; Casciaro, M.; Giacovazzo, C.; Guagliardi, A. *J. Appl. Crystallogr.* **1993**, 26, 343.

(43) Beurskens, P. T.; Admiraal, G.; Beurskens, G.; Bosman, W. P.; de Gelder, R.; Israel, R.; Smits, J. M. M., *The DIRDIF-94 program system*, Technical Report of the Crystallography Laboratory; University of Nijmegen: The Netherlands, 1994.

(44) Sheldrick, G. M., *SHELXL97*; University of Göttingen: Germany, 1997.

(45) (a) Spek, A. L. *PLATON*; Utrecht University, Padualaan 8, 3584 CH Utrecht, The Netherlands, 1980–2008. (b) Spek, A. L. *J. Appl. Crystallogr.* **2003**, 36, 7–13.

$C_{12}F_8$), -136.0 (4F, $C_{12}F_8$), -138.8 (2F, C_6F_4), -156.8 (4F, $C_{12}F_8$), -157.8 (4F, $C_{12}F_8$), -161.3 (2F, C_6F_4). Formation of 1,3,3-triphenyl-3-methylindan (**18**) was confirmed after the experiment by GC-MS ($m/z = 360$). Warming the sample to -40 °C and above resulted in conversion of **19** (and **10**) to **11**, which was the major boron-containing product at the end of the experiment.

Acknowledgment. S.P.L., J.C., and S.C. acknowledge The University of Akron and Goodyear Tire and Rubber Co. for financial support of this work. We also wish to acknowledge Prof. Joseph P. Kennedy, who suggested that aqueous suspension polymerization of isobutene would be a feasible and useful process. T.J.J.S., L.D.H., M.E.P., and W.E.P. wish to acknowledge the Natural Sciences and Engineering

Research Council of Canada for generous financial support of this project.

Supporting Information Available: Experimental procedures for the synthesis of borinic ester **4** and borane **5**, NMR spectroscopic data for compounds **6–16** formed *in situ* from diboranes **1** or **2** and water or MeOH, Mayo plot of MW^{-1} vs $[H_2O]:[IB]$ using data from ref 4f, equation and data used to estimate the T dependence of PIB MW at various $[H_2O]$ as depicted in Figure 5, and crystallographic information files for compounds **8**, **11**, **17**, **20**, and **16**·THF. This material is available free of charge via the Internet at <http://pubs.acs.org>.

OM8007629

Synthesis and Characterization of Single Thiolato-Bridged Heterodinuclear Complexes: Irreversible Isomerization of $\text{Cp}(\text{CO})_2\text{W}(\mu\text{-SPh})(\mu\text{-Cl})\text{Ru}(\text{CO})(\text{Cl})(\text{PPh}_3)$ to $\text{Cp}(\text{CO})(\text{Cl})\text{W}(\mu\text{-SPh})(\mu\text{-Cl})\text{Ru}(\text{CO})_2(\text{PPh}_3)$ via Chloride and Carbonyl Ligand Migration

Md. Munkir Hossain,[†] Hsiu-Mei Lin,[§] Chih-Min Wang,^{†,‡} and Shin-Guang Shyu^{*,†,‡}

Institute of Chemistry, Academia Sinica, Taipei, Taiwan, Republic of China, Department of Chemistry, National Central University, Chungli, Taiwan, Republic of China, and Institute of Bioscience and Biotechnology, National Taiwan Ocean University, Keelung, Taiwan, Republic of China

Received August 15, 2008

Reaction between $\text{CpW}(\text{CO})_3\text{SPh}$ and $\text{RuCl}_2(\text{PPh}_3)_x$ ($x = 3$ and 4) in dichloromethane at room temperature afforded a single thiolato-bridged heterodinuclear complex, $\text{Cp}(\text{CO})_2\text{W}(\mu\text{-SPh})(\mu\text{-Cl})\text{Ru}(\text{CO})(\text{Cl})(\text{PPh}_3)$ (**1**) in high yield. Irreversible isomerization of **1** to $\text{Cp}(\text{CO})(\text{Cl})\text{W}(\mu\text{-SPh})(\mu\text{-Cl})\text{Ru}(\text{CO})_2(\text{PPh}_3)$ (**2**), which exists as a mixture of stereoisomers **2a** and **2b**, occurs via chloride and carbonyl ligand migration during thermolysis of **1** in toluene at 80°C . Compounds **1**, **2a**, and **2b** were characterized by single-crystal X-ray diffraction analysis. Migration of π -acceptor carbonyl ligands from W atom to Ru atom during the conversion of $\text{CpW}(\text{CO})_3\text{SPh} + \text{RuCl}_2(\text{PPh}_3)_3 \rightarrow \mathbf{1} \rightarrow \mathbf{2}$ with concomitant migration of σ -donor chloride ligand from Ru to W atom in **1** is reported.

Introduction

The dynamic behavior of ligands in fluxional molecules has been well documented in the last three decades¹ and has been observed for organic, inorganic, and organometallic compounds. Among them, ligand migration in organometallic complexes containing metal–metal bonds is of special interest because such occurrence and rationalization are appropriate models for a better understanding of ligand migration in clusters and surface mobility of chemisorbed species.² Ligand migration occurs in different ways, and metal to ligand and metal to metal migrations are more common. Ligands such as acyl,³ alkoxycarbonyl,^{3e} formyl,^{3b,3c} silyl,⁴ germyl,⁵ stannyl,⁵ plumblyl,⁵ hydride,⁶ phosphinate,⁷ and phosphorane⁸ were demonstrated to migrate from a transition metal to the ligand η^5 -cyclopentadienyl ring. In metal

carbonyl compounds, carbonyl migration between metals is very common.¹ However, significantly fewer studies on carbonyl migration on heterometallic clusters than those on homometallic clusters were reported.¹ Furthermore, although the reversible carbonyl ligand migration is usual in metal carbonyl clusters, the irreversible migration of CO ligand from one metal to another metal is less common.⁹

Chloride migration is a unique way to synthesize organic molecules¹⁰ including biological conversion of trichloroethylene to chloral by cytochrome P-450.¹¹ Chloride ion can form a bridging bond in clusters, but its migration on clusters and dinuclear complexes is rare.^{12,13}

Sulfides and phosphines are usual bridging ligands for binding different metals. Thiolato-bridged complexes become more significant over the phosphido-bridged ones when catalytic and

* Corresponding author. E-mail: sgshyu@chem.sinica.edu.tw.

[†] Institute of Chemistry, Academia Sinica.

[‡] Department of Chemistry, National Central University.

[§] Institute of Bioscience and Biotechnology, National Taiwan Ocean University.

(1) (a) Band, E.; Muetterties, E. L. *Chem. Rev.* **1978**, *78*, 639. (b) Shriver, D. F.; Kaesz, H. D.; Adams, R. D. *The Chemistry of Metal Clusters Complexes*; VCH: New York, 1990. (c) Farrugia, L. J. *J. Chem. Soc., Dalton Trans.* **1997**, 1783. (d) Waterman, S. M.; Humphrey, M. G. *Organometallics* **1999**, *18*, 3116. (e) Siegel, J. S.; Baldrige, K. K.; Linden, A.; Dorta, R. *J. Am. Chem. Soc.* **2005**, *127*, 10644. (f) Cadenbach, T.; Gemel, C.; Schmid, R.; Fischer, R. A. *J. Am. Chem. Soc.* **2005**, *127*, 17068. (g) Zenkina, O. V.; Konstantinovskii, L.; Freeman, D.; Shimon, L. J. W.; Vander Boom, M. E. *Inorg. Chem.* **2008**, *47*, 3815.

(2) (a) Muetterties, E. L. *Science* **1977**, *196*, 839. (b) Muetterties, E. L.; Rhodin, T. N.; Band, E.; Brucker, C. F.; Pretzer, W. R. *Chem. Rev.* **1979**, *79*, 91.

(3) (a) Heah, P. C.; Gladysz, J. A. *J. Am. Chem. Soc.* **1984**, *106*, 7636. (b) Heah, P. C.; Patton, A. T.; Gladysz, J. A. *J. Am. Chem. Soc.* **1986**, *108*, 1185. (c) Milletti, M. C.; Fenske, R. F. *Organometallics* **1989**, *8*, 420. (d) Liebeskind, L. S.; Welker, M. E. *Organometallics* **1983**, *2*, 194. (e) Abbott, S.; Baird, G. J.; Davies, S. G.; Dordor-Hedgecock, I. M.; Marberly, T. R.; Walker, J. C.; Warner, P. J. *Organomet. Chem.* **1985**, *289*, C13.

(4) (a) Pannell, K. H.; Rozell, J. M.; Lii, J.; Tien-Mayr, S.-Y. *Organometallics* **1988**, *7*, 2524. (b) Berryhill, S. R.; Sharenow, B. *J. Organomet. Chem.* **1981**, *221*, 143. (c) Pannell, K. H.; Cervantes, J.; Parkanyi, L.; Cervantes-Lee, F. *Organometallics* **1990**, *9*, 859. (d) Thum, G.; Ries, W.; Greissinger, D.; Malisch, W. *J. Organomet. Chem.* **1983**, *252*, C67. (e) Pannell, K. H.; Cervantes, J.; Hernandez, C.; Casslas, J.; Vincenti, S. *Organometallics* **1986**, *5*, 1056. (f) Sharma, S.; Cervantes, J.; Mata-Mata, J. L.; Brun, M.-C.; Cervantes-Lee, F.; Pannell, K. H. *Organometallics* **1995**, *14*, 4269.

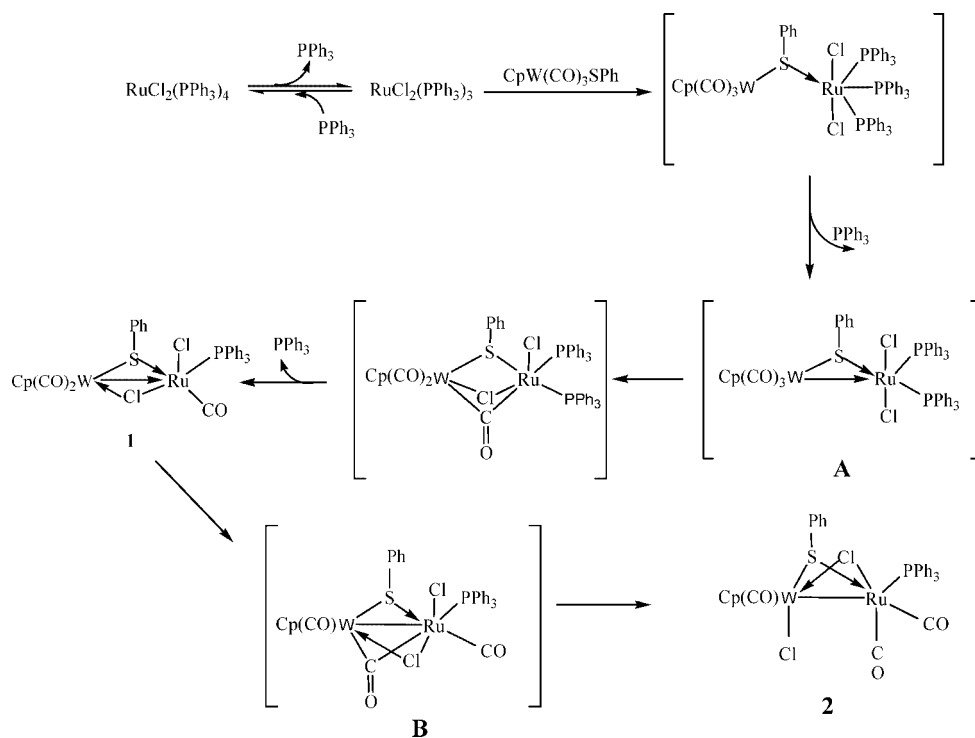
(5) Cervantes, J.; Vincenti, S. P.; Kappor, R. N.; Pannell, K. H. *Organometallics* **1989**, *8*, 744.

(6) (a) Crocco, G. L.; Gladysz, J. A. *J. Am. Chem. Soc.* **1988**, *110*, 6110. (b) Crocco, G. L.; Gladysz, J. A. *J. Chem. Soc., Chem. Commun.* **1985**, 283.

(7) Nakazawa, H.; Sone, M.; Miyoshi, K. *Organometallics* **1989**, *8*, 1564. (8) Kubo, K.; Nakazawa, H.; Kawamura, K.; Mizuta, T.; Miyoshi, K. *J. Am. Chem. Soc.* **1998**, *120*, 6715.

(9) (a) Man, M. L.; Zhou, Z.; Ng, S. M.; Lau, C. P. *J. Chem. Soc., Dalton Trans.* **2003**, 3727. (b) *Metal Clusters in Chemistry*; Braunstein, P., Oro, L. A., Raithby, P. R., Eds.; Wiley, VCH, 1999. (c) Hidai, M.; Orsaku, M.; Ue, M.; Koyasu, Y.; Kodama, T.; Uchida, Y. *Organometallics* **1983**, *2*, 292.

Scheme 1



biological activities are concerned.¹⁴ Many of them are bimetallic complexes.^{14a14c} The common source of the thiolate ligands in the synthesis of thiolato complexes with M–SR bonding is organic sulfides such as RSH and RSSR.¹⁵ In addition, metallothiolate can transfer thiolate ligand to another metal center and is also used as a thiolate ligand source in the synthesis of thiolato complexes.¹⁶ A vast number of bimetallic compounds containing (μ -SR)₂ bridges were reported.¹⁷ Because only a

small number of heterobimetallic compounds with a single (μ -SR) bridge have been synthesized, the synthesis of such complexes becomes more challenging in chemistry.¹⁸

In continuation of our studies in heterobimetallic complexes,^{16,19} this article reports the synthesis and characterization of two less common single-thiolato-bridged heterobimetallic complexes, Cp(CO)₂W(μ -SPh)(μ -Cl)Ru(CO)(Cl)(PPh₃) (**1**) and Cp(CO)W(μ -SPh)(μ -Cl)Ru(CO)₂(PPh₃) (**2**), and a novel intramolecular exchange of carbonyl and chloride ligands between different metal centers (W and Ru) in the conversion of **1** to **2**.

Results and Discussion

Synthesis and Characterization of 1. When a dichloromethane solution of CpW(CO)₃SPh and RuCl₂(PPh₃)₃ was stirred at room temperature for 12 h, the heterodinuclear compound Cp(CO)₂W(μ -SPh)(μ -Cl)Ru(CO)(Cl)(PPh₃) (**1**) was formed in high yield (Scheme 1).

Compound **1** is a 34e heterodinuclear metal–metal bonded compound with a thiolato and a chloride bridge (Figure 1) and is stable both as a solid and in solution. Its structure was characterized by single-crystal X-ray diffraction analysis.

Absorption peaks at 2010 and 1954 cm⁻¹ in the IR spectrum of **1** are assigned to the $\nu(\text{C}\equiv\text{O})$ bands of the two terminal carbonyls on W based on the comparison with that of W–CO (2031, 1938 cm⁻¹) of CpW(CO)₃SPh.²⁰ The Ru–CO absorption

(18) Guerchais, J. E.; LeQuere, J. L.; Petillon, F. Y.; Muir, L. J. M.; Muir, K. W.; Sharp, D. W. A. *J. Chem. Soc., Dalton Trans.* **1982**, 283. (b) Ehrl, W.; Vahrenkamp, H. *Chem. Ber.* **1972**, 105, 1471. (c) Uson, R.; Uson, M. A.; Herrero, S.; Rello, L. *Inorg. Chem.* **1998**, 37, 4473.

(19) (a) Hossain, Md. M.; Lin, H.-M.; Zhu, J.; Lin, Z.; Shyu, S.-G. *Organometallics* **2006**, 25, 440. (b) Hossain, Md. M.; Lin, H.-M.; Shyu, S.-G. *Organometallics* **2004**, 23, 3941. (d) Hossain, Md. M.; Lin, H.-M.; Shyu, S.-G. *Eur. J. Inorg. Chem.* **2001**, 2655. (e) Shyu, S.-G.; Hsu, J.-Y.; Lin, P.-J.; Wu, W.-J.; Peng, S.-M.; Lee, G.-H.; Wen, Y.-S. *Organometallics* **1994**, 13, 1699.

(20) Weinmann, D. J.; Abrahamson, H. B. *Inorg. Chem.* **1987**, 26, 2133.

(10) (a) Bunnet, J. F. *Acc. Chem. Res.* **1972**, 5, 139. (b) Sauter, F.; Frohlich, H.; Kalt, W. *Synthesis* **1989**, 771. (c) Frohlich, H.; Kalt, W. *J. Org. Chem.* **1990**, 55, 2993. (d) Nelson, D. J.; Sager, S. H. *Heteroat. Chem.* **1998**, 9, 623. (e) Piers, E.; Brown, R. K. *Can. J. Chem.* **1963**, 41, 329. (f) Eaborn, C.; Lickiss, P. D.; Najim, S. T. *J. Chem. Soc., Perkin Trans.* **1993**, 391. (g) Pietri, N.; Monnier, M.; Aycard, J.-P. *J. Org. Chem.* **1998**, 63, 2462. (h) Koch, R.; Wang, M. W.; Wentrup, C. *J. Org. Chem.* **1996**, 51, 6809. (i) Popkova, V. Y.; Anisimov, V. M.; Dolenko, G. N.; Semenenko, M. N.; Fedoseev, V. M. *J. Chem. Soc., Perkin Trans.* **1995**, 1375.

(11) Miller, R. E.; Guengerich, F. P. *Biochemistry* **1982**, 21, 1090.

(12) (a) Balch, A. L.; Fossett, L. A.; Olmstead, M. M., Jr. *Organometallics* **1986**, 5, 1929. (b) Balch, A. L.; Fossett, L. A.; Olmstead, M. M., Jr. *Organometallics* **1988**, 7, 430. (c) Balch, A. L.; Fossett, L. A.; Guimerans, R. R.; Olmstead, M. M.; Reedy Jr, P. E.; Wood, F. E. *Inorg. Chem.* **1986**, 25, 1248. (d) Balch, A. L.; Fossett, L. A.; Guimerans, R. R.; Olmstead, M. M., Jr. *Inorg. Chem.* **1986**, 25, 1397.

(13) Esswein, A. J.; Veige, A. S.; Nocera, D. G. *J. Am. Chem. Soc.* **2005**, 127, 16641.

(14) (a) Sokpa, E. I. K.; Calfee, D. T.; Allred, B. R. T.; Davis, J. L.; Haub, E. K.; Rich, A. K.; Porter, A.; Mashuta, M. S.; Richardson, J. F.; Noble, M. E. *Inorg. Chem.* **1999**, 38, 802. (b) DuBois, M. R. *Chem. Rev.* **1989**, 89, 1. (c) Garcia, J. J.; Mann, B. E.; Adams, N. A.; Bailey, N. A.; Maitlis, P. J. *Am. Chem. Soc.* **1995**, 117, 2179. (d) Nishibayash, Y.; Wakiji, I.; Hidia, M. *J. Am. Chem. Soc.* **2000**, 122, 11019. (e) Qu, J.-P.; Masui, D.; Ishii, Y.; Hidia, M. *Chem. Lett.* **1998**, 1003. (f) Nishibayash, Y.; Yamanashi, M.; Wakiji, I.; Hidia, M. *Angew. Chem., Int. Ed.* **2000**, 39, 2909. (g) Takagi, Y.; Matsuzaka, H.; Ishii, Y.; Hidia, M. *Organometallics* **1997**, 16, 4445.

(15) (a) Ahmed, M.; Bruce, R.; Knox, G. R. *J. Organomet. Chem.* **1966**, 6, 1. (b) Brandenburg, K. L.; Heeg, M. J.; Abrahamson, H. B. *Inorg. Chem.* **1987**, 26, 1064. (c) Lang, R. F.; Ju, T. D.; Kiss, G.; Hoff, C. D.; Bryan, J. C.; Kubas, G. J. *J. Am. Chem. Soc.* **1994**, 116, 7917. (d) Abrahamson, H. B.; Marxen, H. *Organometallics* **1993**, 12, 2835.

(16) Hossain, Md. M.; Lin, H.-M.; Shyu, S.-G. *Organometallics* **2003**, 22, 3262, and reference therein.

(17) (a) Stephan, D. W.; Nadaski, T. T. *Coord. Chem. Rev.* **1996**, 147, 147. (b) Blower, P. J.; Dilwarth, J. R. *Coord. Chem. Rev.* **1987**, 121, 121.

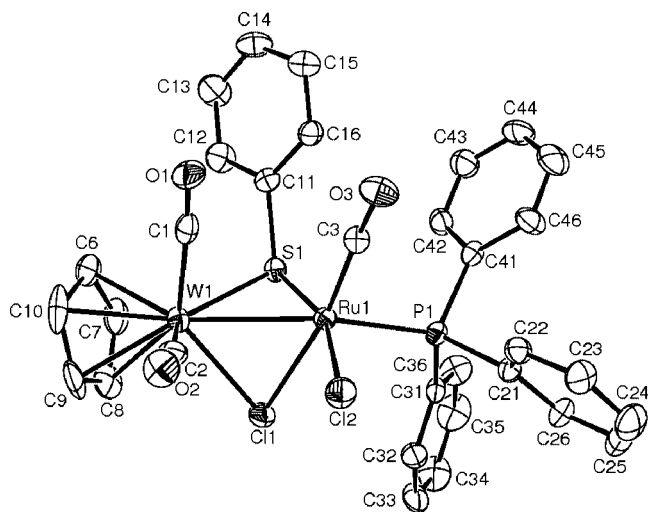


Figure 1. ORTEP drawing of **1**, with 30% thermal ellipsoids. Hydrogen atoms are omitted.

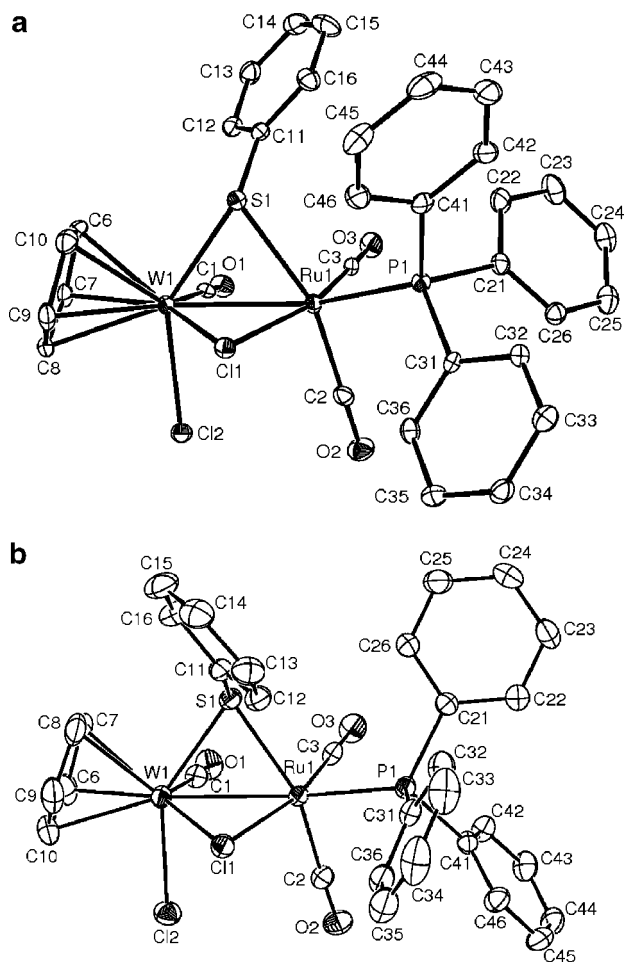


Figure 2. (a) ORTEP drawing of **2a**, with 30% thermal ellipsoids. Hydrogen atoms are omitted. (b) ORTEP drawing of **2b**, with 30% thermal ellipsoids. Hydrogen atoms are omitted.

should be around 1950 cm^{-1} based on the comparison with the $\nu(\text{C}\equiv\text{O})$ bands of $\text{Ru}-\text{CO}$ ($1948, 1955\text{ cm}^{-1}$) of $(\text{CO})(\text{PPh}_3)_2\text{Ru}(\mu\text{-Cl})(\mu\text{-SPh})_2\text{Ru}(\text{CO})(\text{PPh}_3)_2$,²¹ and the broad peak at 1954

cm^{-1} in the IR spectrum of **1** could be the superposition of one of the $\text{W}-\text{CO}$ adsorption peaks and the $\text{Ru}-\text{CO}$ adsorption peak.

During the formation of **1**, one of the carbonyl ligands on the W site in $\text{CpW}(\text{CO})_3\text{SPh}$ migrates onto the Ru site. It may not be a scrambling reaction because **1** is formed in high yield (93%). Although formal oxidation states of W and Ru in $\text{CpW}(\text{CO})_3\text{SPh}$, $\text{RuCl}_2(\text{PPh}_3)_3$, and **1** are both +2, the migration of the carbonyl ligand is possibly electronic in nature. A possible pathway for the formation of **1** is shown in Scheme 1.

$\text{RuCl}_2(\text{PPh}_3)_3$ is a 16e complex and therefore is a coordinatively unsaturated species. The metathiolate $\text{CpW}(\text{CO})_3\text{SPh}$ can coordinate to the Ru in $\text{RuCl}_2(\text{PPh}_3)_3$ through a lone pair of electrons on the sulfur atom to form a non-metal–metal-bonded 36e dimer, $\text{CpW}(\text{CO})_3(\mu\text{-SPh})\text{RuCl}_2(\text{PPh}_3)_3$, with a $\mu\text{-SPh}$ bridge. A dative metal–metal bond from W to Ru may replace a bulky PPh_3 ligand on Ru, forming the 34e complex

$\text{CpW}(\text{CO})_3(\mu\text{-SPh})\text{RuCl}_2(\text{PPh}_3)_2$ (denoted as **A**) to release the steric hindrance and brings the two metals closer. Through the formation of the dative metal–metal bonding, the Ru in **A** becomes electron rich, and the electron density on W is reduced. This difference in electron density drives the migration of the π -acceptor carbonyl ligand from the electron-deficient W atom²² to the electron-rich Ru atom^{22,23b} to substitute a weak π -acceptor triphenylphosphine ligand through the formation of the bridging chloride to redistribute the electron density of the metals to form **1**.

The reaction of $\text{CpW}(\text{CO})_3\text{SPh}$ and $\text{RuCl}_2(\text{PPh}_3)_4$ under identical conditions also afforded **1** in high yield because triphenylphosphine ligands in both $\text{RuCl}_2(\text{PPh}_3)_4$ and $\text{RuCl}_2(\text{PPh}_3)_3$ are labile. Production of the similar intermediate $\text{RuCl}_2(\text{PPh}_3)_2(\text{solvent})_2$ ²⁴ for both complexes in solvents with weak coordination abilities has been reported.

Thermolysis of 1. After heating at $80\text{ }^\circ\text{C}$, the color of the toluene solution of **1** changed from violet to yellow. Compound **2**, an orange solid, was obtained after chromatography.

The elemental analysis of **2** is similar to that of **1**. This implies that compound **2** has the same empirical formula of **1**. The room-temperature $^{31}\text{P}\{^1\text{H}\}$ and ^1H NMR spectra of **2** show two peaks for the triphenylphosphine and the cyclopentadiene ring, respectively, and do not contain signals corresponding to **1**. No $J_{\text{P-W}}$ satellites are observed in the $^{31}\text{P}\{^1\text{H}\}$ NMR spectrum, showing that the triphenylphosphine ligand is coordinated to Ru. IR of **2** shows three terminal CO absorption peaks, indicating no bridging CO is present, and the pattern of the spectra (both the number of peaks and their positions) is different from that of **1**. All this implies that two isomers (denoted **2a** and **2b**) are present in **2**, and compounds **1** and **2** are constitutional isomers.

The variable-temperature $^{31}\text{P}\{^1\text{H}\}$ and ^1H NMR spectra of the compounds indicate that the isomers do not convert to each other in the variable-temperature range of the experiment (65 to $-68\text{ }^\circ\text{C}$) because the ratios of the intensities of triphenylphosphine and cyclopentadiene signals are similar as a function of temperature.²⁵

(22) (a) Shima, T.; Ito, J.-I.; Suzuki, H. *Organometallics* **2001**, *20*, 10. (b) Ohki, Y.; Matsuura, N.; Marumoto, T.; Kawaguchi, H.; Tatsumi, K. *J. Am. Chem. Soc.* **2003**, *125*, 7978.

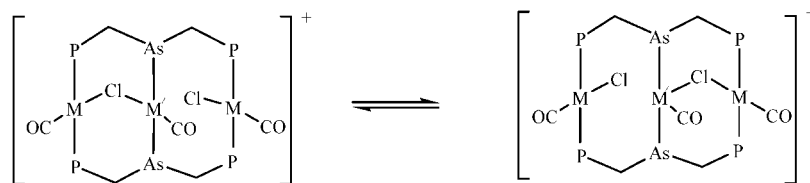
(23) (a) Meiere, S. H.; Keane, J. M.; Gunnoe, T. B.; Sabat, M.; Harman, W. D. *J. Am. Chem. Soc.* **2003**, *125*, 2024. (b) Matsuo, Y.; Kuninobu, Y.; Ito, S.; Nakamura, E. *Chem. Lett.* **2004**, *33*, 68.

(24) Stephenson, T. A.; Wilkinson, G. J. *Inorg. Nucl. Chem.* **1966**, *28*, 945.

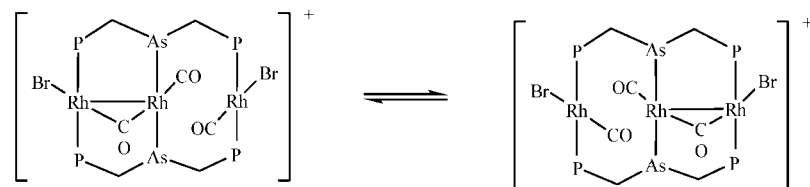
(25) Cholli, A. L.; Lau, M. L. *Appl. Spectrosc.* **1993**, *47*, 357.

(21) Kuznik, N.; Krompice, S.; Bieg, T.; Baj, S.; Skutil, K.; Chrobok, A. *J. Organomet. Chem.* **2003**, *665*, 167.

Chart 1



Bridge/Terminal Halogen Exchange



Bridge/Terminal Carbonyl Exchange

Separation of **2a** and **2b** failed. However, two different types of single crystals of **2** for single-crystal X-ray diffraction analysis were obtained from the same batch of compound **2** by ether diffusion into a dichloromethane solution of **2** at different temperatures. Violet single crystals of **2a** and **2b** were obtained at -4 and -15 °C, respectively, from two sets of crystal growth experiments from the same batch of **2**. The molecular structures of **2a** and **2b** are shown in Figure 2a and b, respectively. Two independent molecules of **2a** were crystallized in the asymmetric unit cell.

Both **2a** and **2b** are 34e heterodinuclear metal–metal bonded compounds with a thiolato and a chloride bridge (Figure 2a and b). The only difference in their structures is the orientation of the lone pair of electrons and the phenyl group on the sulfur atom of the thiolato bridge with respect to the folded RuSCIW core. In **2a**, the phenyl group on sulfur points away from the bridging Cl of the folded RuSCIW core. In **2b**, the orientations of the phenyl group and the lone pair of electrons on sulfur are opposite that of **2a**, with the phenyl group pointing toward and the lone pair of electrons pointing away from the bridging Cl. Thus **2a** and **2b** are stereoisomers.

Two absorption peaks at 2033 and 1971 cm^{-1} in the IR spectrum of **2** are assigned to the $\nu(\text{C}\equiv\text{O})$ bands of the two terminal carbonyls on Ru based on the comparison with that of the Ru–CO (2016, 2079, and 1951 cm^{-1}) in $[\text{Ru}(\text{CO})_2(\text{PPh}_3)(\mu\text{-SPh})_2]_2$.²⁶ The third absorption peak at 1887 cm^{-1} is assigned to the $\nu(\text{C}\equiv\text{O})$ band of the carbonyl on W based on the comparison with that of the W–CO (1881 cm^{-1}) in $\text{Cp}(\text{CO})\text{-}(\text{Cl})\text{W}(\mu\text{-CMe})(\mu\text{-Cl})\text{Ru}(\text{CO})(\text{PPh}_3)_2$.²⁷ Broad peaks at 1972 and 1887 cm^{-1} may be due to the superposition of the signals of the two isomers in the sample.

In the thermolysis of **1**, one CO on W and the terminal Cl on Ru in **1** are replaced by a terminal Cl and a terminal CO,

respectively, to form **2**, and the environments of the other ligands are kept identical with that of **1** (Figure 2a and b). Ligand migrations in organometallic complexes are common and occur in both intermolecular and intramolecular pathways.^{3–8,28} Isomerization of **1** to **2** is irreversible and is proposed to be intramolecular in nature because the conversion of **1** to **2** is almost quantitative without any byproducts. In addition, thermolysis of **1** under ^{13}C O resulted in the decomposition of **1** before isomerization and no compound **2** was obtained. Complex $\text{CpW}(\text{CO})_3\text{Cl}$ is observed in the decomposition product. This observation further indirectly excludes the intermolecular isomerization process through external CO from W–CO bond breaking to form the Ru–CO bond in **2**. The external CO-induced transfer reaction of a silyl group in the phosphido-bridged bimetallic Fe–Pt system has been observed.²⁸ In addition, bridge/terminal halide exchange and bridge/terminal carbonyl exchange in trinuclear complexes were reported (Chart 1).¹² However, to the best of our knowledge, the internal mutual carbonyl–chloride migration between heteroatoms (W and Ru) in **1** to form **2** has not been observed previously.

In **1**, both chloride and carbonyl ligands have bridging ability. Considering the flexibility of carbonyl and chloride ligands toward terminal/bridging mode, we suggest that the 34e dimer **B** (Scheme 1) is the intermediate during the isomerization of **1** to **2**.

The Ru atom in **1** is electron rich because of the dative W–Ru bonding and the electron-donating phosphine ligand. Donation of an electron from the Ru metal to the π^* of CO on W to form the bridging carbonyl to form the 34e dimer **B** can reduce the electron density on Ru (Scheme 1). The terminal chloride ligand on Ru in **B** can coordinate to the adjacent W to form a bridging chloride and pushes the bridging carbonyl to Ru to accomplish the CO migration. The original bridging chloride ligand completes the chloride migration by converting itself to a W terminal Cl to form **2**. Although we are not able to isolate any intermediate, similar bonding modes of CO and Cl in the proposed intermediate **B** (Scheme 1) were structurally established in $[\text{Rh}_2(\text{Ph}_2\text{PCH}_2\text{PPh}_2)_2(\mu\text{-Cl})(\mu\text{-CO})(\text{CO})_2]^+$,^{29a} $[\text{Re}_2(\text{Ph}_2\text{PCH}_2\text{PPh}_2)_2(\mu\text{-Cl})(\mu\text{-CO})(\text{CO})\text{Cl}_2(\text{EtCN})]^+$,^{29b} and $(\text{CO})_3\text{Mo}(\mu\text{-Cl})(\mu\text{-CO})(\text{Ph}_2\text{PCH}_2\text{PPh}_2)\text{Rh}(\text{NBD})$.^{29c}

The redistribution of electron density in the isomerization of **1** to **2** is revealed by the frequency change of CO absorption peaks in their IR spectra. The lower stretching frequency (1887

(26) Shiu, K.-B.; Wang, S.-L.; Liao, F.-L.; Chiang, M. Y.; Peng, S.-M.; Lee, G.-H.; Wang, J.-C.; Liou, L.-S. *Organometallics* **1998**, *17*, 1790.

(27) Howard, J. A. K.; Laurie, J. C. V.; Stone, F. G. A. *J. Chem. Soc., Dalton. Trans.* **1985**, 2017.

(28) (a) Braunstein, P.; Knorr, M.; Hirle, B.; Reinhard, G.; Schubert, U. *Angew. Chem., Int. Ed. Engl.* **1992**, *31*, 1583. (b) Braunstein, P.; Faure, T.; Knorr, M. *Organometallics* **1999**, *18*, 1791.

(29) (a) Cowie, M. *Inorg. Chem.* **1979**, *18*, 286. (b) Cotton, F. A.; Dunbar, K. R.; Falvello, L. R.; Walton, R. A. *Inorg. Chem.* **1985**, *24*, 4180. (c) Cano, M.; Heras, J. V.; Ovejero, P.; Pinilla, E.; Monge, A. *J. Organomet. Chem.* **1991**, *410*, 101.

Table 1. Selected Bond Lengths (Å) and Bond Angles (deg) for 1, 2a, and 2b

bonds	1	2a	2b
W1–S1	2.488(2)	2.4720(14)	2.4846(7)
W1–C1	1.993(10)	1.979(7)	1.950(3)
W1–C2	1.999(9)		
W1–C11	2.481(2)	2.4862(15)	2.4734(7)
W1–C12		2.4905(15)	2.4857(8)
W1–C6	2.268(9)	2.253(6)	2.276(3)
W1–C7	2.338(10)	2.291(6)	2.238(3)
W1–C8	2.380(9)	2.381(6)	2.289(3)
W1–C9	2.289(9)	2.363(6)	2.387(4)
W1–C10	2.270(9)	2.285(6)	2.368(3)
Ru1–S1	2.366(2)	2.3921(16)	2.4038(8)
Ru1–C11	2.466(2)	2.4316(15)	2.4514(7)
Ru1–C12	2.401(2)		
Ru1–P1	2.314(2)	2.3847(16)	2.3981(7)
Ru1–C2		1.896(7)	1.905(3)
Ru1–C3	1.818(8)	1.855(7)	1.843(3)
C11–S1	1.793(8)	1.800(6)	1.800(3)
angles			
W1–S1–Ru1	71.54(6)	68.89(4)	68.89(2)
W1–C11–Ru1	70.06(6)	68.05(4)	68.328(19)
S1–W1–C11	73.38(7)	72.65(5)	79.09(2)
S1–W1–C1	82.3(2)	91.24(16)	83.19(2)
S1–W1–C2	130.1(3)		
S1–W1–Ru1	52.22(5)	54.18(4)	54.176(17)
S1–W1–C12		140.39(5)	143.55(3)
C1–W1–C2	76.8(3)		
C1–W1–C11	131.9(2)	131.21(18)	128.25(9)
C1–W1–Ru1	77.5(2)	77.93(17)	74.77(9)
C1–W1–C12		83.77(17)	87.37(9)
C2–W1–C11	88.0(3)		
C2–W1–Ru1	79.0(3)		
C11–W1–Ru1	54.73(5)	55.03(3)	55.460(17)
C11–W1–C12		81.38(5)	79.49(3)
C12–W1–Ru1		86.47(4)	89.38(2)
S1–Ru1–P1	97.86(7)	103.05(5)	109.77(3)
S1–Ru1–C11	75.79(8)	75.02(5)	81.10(3)
S1–Ru1–C12	160.96(8)		
S1–Ru1–C2		161.45(19)	158.26(9)
S1–Ru1–C3	103.0(2)	95.07(18)	89.16(9)
S1–Ru1–W1	56.24(5)	56.93(4)	56.936(18)
P1–Ru1–C11	101.89(8)	98.96(5)	101.60(3)
P1–Ru1–C12	97.17(8)		
P1–Ru1–C2		94.29(19)	91.97(9)

cm^{-1}) of carbonyl on W in **2** than that in **1** (2010 and 1954 cm^{-1}) indicates a stronger back-donation from W to carbonyl in **2**. Consistently, the stretching frequencies of Ru carbonyl ligands in **2** (2033 and 1972 cm^{-1}) are higher than that in **1** (1954 cm^{-1}), indicating a weaker back-donation from Ru to its carbonyl ligands in **2**. This is because the number of π -acceptor carbonyl ligands on the Ru center and W center has been changed from one in **1** to two in **2** and from two in **1** to one in **2**, respectively.

Scrambling of Cl and CO between different metals was reported in the synthesis of $\text{Cp}(\text{CO})(\text{Cl})\text{W}(\mu\text{-CMe})(\mu\text{-Cl})\text{Ru}(\text{CO})(\text{PPh}_3)_2$ by the reaction between $\text{CpW}(\text{CO})_2\text{CMe}$ and $\text{RuCl}_2(\text{PPh}_3)_3$. Chloride and carbonyl migrations between W and Ru were proposed in the reaction; however no intermediate was observed.²⁷ The synthesis of **1** and the conversion of **1** to **2** in this report provide a stepwise and almost quantitative reaction path of the migration of carbonyl ligands from the W to Ru site and chloride ligand from the Ru to W site in the formation of **2** from $\text{CpW}(\text{CO})_3\text{SPh}$ and $\text{RuCl}_2(\text{PPh}_3)_x$ ($x = 3$ and 4).

X-ray Structures of 1, 2a, and 2b. The structures of compounds **1**, **2a**, and **2b** were determined by X-ray diffraction analysis. The ORTEP drawings of **1**, **2a**, and **2b** are shown in Figures 1b, 2a, and 2b, respectively. Selected bond distances and bond angles are listed in Table 1.

These complexes have a similar core structure: one chloride bridge, one thiolato bridge, and a metal–metal bond between the metals. The W1–Ru1 bond distances in **1**, **2a**, and **2b** are 2.8394(9), 2.7481(av), and 2.7657(3) Å, respectively, and are well in accord with the literature values.³⁰ These bond distances are varied according to the variation of their respective acute angles W–S–Ru (71.54(6)°, 68.64 (av)°, and 68.89(2)°) and W–Cl–Ru (70.06(6)°, 68.06(av)°, and 68.328 (19)°). The W1–Ru1 distance (2.8394(9) Å) is comparatively long and is consistent with the dative bonding character. The W1–Ru1 bond distances in **2a** and **2b** are 0.1 Å shorter than that in **1**, implying that metal–metal bonds in **2a** and **2b** are comparatively covalent.

The Cl(1)–W(1)–Ru(1)–S(1) dihedral angles are 96.03(9)°, 93.21(6)°, and 102.33(3)° in **1**, **2a**, and **2b**, respectively. A bigger dihedral angle in **2b** than in **2a** reflects a larger steric hindrance between the phenyl group on the bridging sulfur atom and the bridging chloride. In **2b**, the phenyl group points to the center of the SWRuCl core. In **2a**, the phenyl group points in the opposition direction and has a smaller interaction with the bridging chloride. The SWRuCl core structures of **1** and **2a** are similar, with the phenyl group on the sulfur pointing away from the center of the core.

The average bond distances of Ru1–P1 (2.3914 Å) and Ru–C (1.8747 Å) in **2** are longer than that of Ru1–P1 (2.314(2) Å) and Ru1–C3 (1.818(8) Å) in **1**. This implies that back-donation of electrons from Ru to these ligands is reduced in **2**. This is consistent with the IR data observed.

Conclusions

This paper describes the synthesis of single thiolato-bridged heterodinuclear W–Ru complexes **1** and **2** in high yield. During thermolysis of **1** in toluene, isomerization of **1** to **2** occurred via chloride and carbonyl ligand migration. The migration of the carbonyl and chloride ligands in the conversion of $\text{CpW}(\text{CO})_3\text{SPh} + \text{RuCl}_2(\text{PPh}_3)_x$ ($x = 3$ and 4) \rightarrow **1** \rightarrow **2** is stepwise. Heterobimetallic complexes with early and late transition metals are effective as Lewis acid and Lewis base pairs in catalytic reactions.³¹ Isomerization of **1** to **2** indicates a possibility that the Lewis acidity and Lewis basicity of the metals can be altered by the mutual redistribution of the π -acceptor and σ -donor ligands among the metals during their reactions.

Experimental Section

General Procedures. All reactions and other manipulations were performed under an atmosphere of nitrogen using standard Schlenk

- (30) (a) Mashima, K.; Mikami, A.; Nakamura, A. *Chem. Lett.* **1992**, 1795. (b) Shiu, K.-B.; Wang, S.-L.; Liao, F.-L.; Chiang, M. Y.; Peng, S.-M.; Lee, G.-H.; Wang, J.-C.; Liou, L.-S. *Organometallics* **1998**, *17*, 1790. (c) Nishibayashi, Y.; Imajima, H.; Onodera, G.; Inada, Y.; Hidia, M.; Uemura, S. *Organometallics* **2004**, *23*, 5100. (d) Shacht, H.; Haltiwanger, R. C.; DuBois, M. R. *Inorg. Chem.* **1992**, *31*, 1728. (e) Dev, S.; Imagawa, K.; Mizobe, Y.; Cheng, G.; Wakatsuki, Y.; Yamazaki, H.; Hidia, M. *Organometallics* **1989**, *8*, 1232. (f) Kondo, T.; Uenoyama, S.-Y.; Fujita, K.-I.; Mitsudo, T.-A. *J. Am. Chem. Soc.* **1999**, *121*, 482. (g) Hankin, D. M.; Danopoulos, A. A.; Wilkinson, G.; Sweet, T. K. N.; Hurshouse, M. B. *J. Chem. Soc., Dalton. Trans.* **1996**, 4063. (h) Lukas, C. R.; Newlands, M. J.; Gabe, E. J.; Lee, F. L. *Can. J. Chem.* **1987**, *65*, 898. (i) Zhuang, B.; Sun, H.; Pan, G.; He, L.; Wei, Q.; Zhou, Z.; Peng, S.; Wu, K. *J. Organomet. Chem.* **2001**, *640*, 127. (j) Canich, J. A. M.; Cotton, F. A.; Dunbar, K. R.; Falvello, L. R. *Inorg. Chem.* **1988**, *27*, 804. (k) Darenbourg, D.; Sanchez, K. M.; Reibenspies, J. *Inorg. Chem.* **1988**, *27*, 3636. (l) Bitterwolf, T. E.; Saygh, A. A.; Shade, J. E.; Rheingold, A. L.; Yap, G. P. A.; Lable-Sands, L. M. *Inorg. Chim. Acta* **2000**, *800*, 300–302.

- (31) Wheatly, N.; Kalk, P. *Chem. Rev.* **1999**, *99*, 3379.

Table 2. Summary of Crystal Data for **1**, **2a**, and **2b**

	1	2a	2b
formula	C ₃₂ H ₂₅ O ₃ Cl ₂ PSWRu	C ₁₂₉ H ₁₀₀ O ₁₂ Cl ₁₀ P ₄ S ₄ W ₄ Ru ₄	C ₃₂ H ₂₅ O ₃ Cl ₂ PSWRu
fw	876.37	3588.39	876.37
space group	P21/c	P21/c	P $\bar{1}$
a [Å]	10.634(18)	23.134(7)	10.3393(4)
b [Å]	19.703(4)	14.8948(4)	10.4859(4)
c [Å]	14.856(3)	18.7904(5)	16.1041(9)
α [deg]			93.722(2)
β [deg]	103.46(3)	103.8290(10)	101.160(2)
γ [deg]			115.6210(10)
V [Å ³]	3027.2(10)	6287.1(3)	1522.56(12)
ρ (calcd) [Mg m ⁻³]	1.923	1.896	1.912
Z	4	2	2
cryst dimens [mm]	0.31 × 0.16 × 0.13	0.16 × 0.14 × 0.14	0.15 × 0.1 × 0.07
temp [K]	293(2)	293(2)	296(2)
λ (Mo K α) [Å]	0.71073	0.71073	0.71073
2 θ range [deg]	50.0	50.0	50.0
scan type	ω	ω	ω
no. of reflns	5618	41 281	22 333
no. of obsd reflns	5314 (>2.0 σ (I))	11 098 (>2.5 σ (I))	6918 (>2.5 σ (I))
no. of params refined	365	757	370
R	0.0369	0.0362	0.0232
R _w	0.0884	0.0747	0.0513
GoF	0.981	1.062	0.986
D _{map} min., max. [e/Å ³]	-1.631, 1.326	-1.340, 1.340	-0.376, 1.045

techniques. Commercially available chemicals were purchased and used without further purification. All solvents were dried with Na and benzophenone under N₂ and distilled immediately prior to use. Compounds CpW(CO)₃SPh and RuCl₂(PPh₃)_x (x = 3 and 4) were prepared following reported procedures.³² The ¹H and ³¹P{¹H} NMR spectra were recorded using a Bruker Ac-300 spectrometer. Variable-temperature ¹H and ³¹P{¹H} NMR spectra were recorded using a Bruker DRX500/AV400 spectrometer. The ³¹P{¹H} shifts are referenced to 85% H₃PO₄. Microanalyses were performed by use of a Perkin-Elmer 2400 CHN analyzer.

Synthesis of 1. Dichloromethane (50 mL) was added to a solid mixture of CpW(CO)₃SPh (100 mg, 0.226 mmol) and RuCl₂(PPh₃)₃ (216 mg, 0.226 mmol), and the solution was stirred for 12 h at room temperature. The solution was concentrated, and a brown precipitate was obtained by adding hexane. After separation by filtration, the residue was dissolved in dichloromethane (5 mL) and was chromatographed on silica gel using dichloromethane as an eluent. Compound **1** was obtained as a violet solid from the violet band after removing the solvent. Yield: 184 mg, 93%. Anal. Calcd for C₃₂H₂₅O₃PSCl₂WRu: C, 43.82; H, 2.85. Found: C, 43.52, H, 3.11. IR (CH₂Cl₂): ν (CO) 2009 (s), 1954 (vs, br) cm⁻¹. ¹H NMR (CDCl₃): δ 7.73–6.78 (m, 20H, C₆H₅), 5.69 (s, 5H, C₅H₅). ³¹P{¹H} NMR (CH₂Cl₂): δ 57.87 (s). Reaction between CpW(CO)₃SPh (50 mg, 0.113 mmol) and RuCl₂(PPh₃)₄ (138 mg, 0.113 mmol) in dichloromethane (30 mL) under similar reaction conditions afforded **1** in 91% yield (89 mg).

Thermolysis of 1. A toluene solution (30 mL) of **1** (100 mg, 0.114 mmol) was heated at 80 °C for 3 h. The color of the solution changed from violet to yellow. The solvent was removed, and the residue was dissolved in dichloromethane (5 mL). After chromatography on silica gel using dichloromethane/hexane (4:1) as the eluent, compound **2** was obtained with 96% yields (96 mg). Anal. Calcd for C₃₂H₂₅O₃PSCl₂WRu: C, 43.82; H, 2.85. Found: C, 43.49, H, 3.25. IR (CH₂Cl₂): ν (CO) 2033 (vs), 1972 (vs, br), 1887 (m, br) cm⁻¹. ¹H NMR (CDCl₃): δ 7.47–6.78 (m, 20H, C₆H₅), 5.49 (s, 5H, C₅H₅), 5.44 (s, 5H, C₅H₅). ³¹P{¹H} NMR (CH₂Cl₂): δ 46.45 (s), 44.55 (s).

Thermolysis of 1 in the Presence of ¹³CO. A toluene solution (10 mL) of **1** (50 mg, 0.057 mmol) was degassed by freeze–thaw method and was heated at 80 °C for 3 h under ¹³CO. The reaction

mixture was monitored by ³¹P{¹H} and ¹H NMR. Compound **1** was decomposed to CpW(CO)₃Cl³³ with trace amounts of other compounds. No isomerization of **1** to **2** was observed.

Crystal Structure Determination of 1, 2a, and 2b. Single crystals of **1** for X-ray diffraction analysis were grown by slow evaporation of dichloromethane solution layered by hexane at -4 °C. Single crystals of **2a** and **2b** were grown from two sets of crystal growth experiments by ether diffusion into a dichloromethane solution of **2** at -4 and -15 °C, respectively, from the same batch of **2**. The crystals of **1**, **2a**, and **2b** were mounted on a glass fiber for data collection, and the data of **1**, **2a**, and **2b** were collected by using Mo K α radiation at CCD. Detailed data collection parameters are given in Table 2. Data collections were carried out by Mo K α radiation (λ = 0.71073 Å) on a Bruker X8 Apex CCD at room temperature. The unit-cell parameters were obtained by least-squares fit to the automatically centered settings for reflections on a Bruker X8 Apex CCD diffractometer. Intensity data were collected by using the $\omega/2\theta$ scan mode. The structures were solved by direct methods (SHELX-97). All non-hydrogen atoms were located from the difference Fourier maps and were refined by full-matrix least-squares procedures. Hydrogen atoms were included in idealized positions but not refined. Calculations and full-matrix least-squares refinements were performed utilizing the WINGX program package.

Acknowledgment. We acknowledge the National Science Council, ROC, Department of Industrial Technology, Ministry of Economic Affairs, ROC (grant no. 97-EC-17-A-08-R7-0706), and Academia Sinica for financial support of this work.

Supporting Information Available: Tables of atomic coordinates, isotropic and anisotropic displacement parameters, and all bond distances and angles; experimental details of the X-ray studies for **1**, **2a**, and **2b**; variable-temperature spectra of ³¹P{¹H} and ¹H NMR. This material is available free of charge via the Internet at <http://pubs.acs.org>.

OM800789M

(32) (a) Watkins, D. D.; George, T. A. *J. Organomet. Chem.* **1975**, *102*, 71. (b) Havlin, R.; Knox, G. R. *Z. Naturforsch., B* **1966**, *21*, 1108. (c) Stephenson, T. A.; Wilkinson, G. *J. Inorg. Nucl. Chem.* **1966**, *28*, 945.

(33) (a) Xia, W.; Goetting, L. B.; Debad, J. D.; Palmer, B. J.; Hill, R. H. *J. Photochem. Photobiol., A* **1993**, *71*, 221. (b) Striejewske, W. S.; Atwood, J. D. *J. Coord. Chem.* **1996**, *38*, 145. (c) Piskounov, A. V.; Maslennikov, S. V.; Spirina, I. V.; Maslennikov, V. P. *Appl. Organomet. Chem.* **2000**, *14*, 590.

The First Phenanthrene-Fused Imidazol-2-ylidene and Its Transition-Metal Complexes

Daniela Tapu,^{*,†} Clayton Owens,[†] Donald VanDerveer,[‡] and Kevin Gwaltney[†]

Department of Chemistry and Biochemistry, Kennesaw State University, 1000 Chastain Road, Kennesaw, Georgia 30144, and X-ray Crystallography Laboratory, Department of Chemistry, Clemson University, Clemson, South Carolina 29634

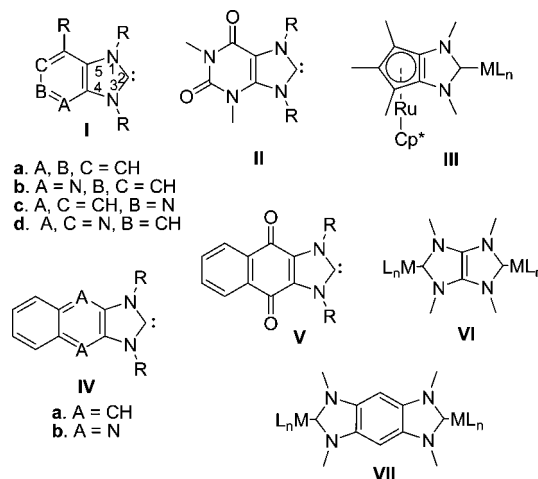
Received August 22, 2008

A new phenanthrene-fused N-heterocyclic carbene was generated and characterized in solution. The synthesis of air-stable Rh, Ir, and Ag complexes, supported by the new phenanthrene-fused imidazol-2-ylidene ligand, is described. Deprotonation of phenanthrene-fused imidazolium salt **4** in the presence of $[M(\text{COD})\text{Cl}]_2$ ($M = \text{Rh}, \text{Ir}$) afforded complexes **6** and **7** in excellent yields. The silver complex was obtained by reaction of **4** with Ag_2O . The solid state molecular structures of these complexes have been determined by X-ray diffraction studies. The fluorescence emission spectra of **4**, **6**, and **7** are compared to that of phenanthrene.

Introduction

Since the first stable crystalline carbene was reported in 1991, “Arduengo”-type carbenes have emerged as a powerful class of carbon-based ligands.¹ Owing to their unique electronic and steric properties, they have been incorporated in a large variety of catalytically active metal complexes.² The demand for carbenes with different 3D shapes and/or substitution patterns has rapidly increased. Therefore, it has become increasingly important to determine what effect the modification of the carbene’s architecture has on its electronic properties, which largely determine the ligand behavior.³ One of the strategies that have been used to modify the ligand properties of imidazol-2-ylidenes is annulation with different carbo- and heterocyclic groups. Annulation is possible in the 4–5, 1–5, and 3–4 positions of the imidazole ring. The first stable 4,5-annulated imidazol-2-carbene reported was benzimidazol-2-ylidene, **Ia**.⁴ This carbene exhibits the topology of an unsaturated N-heterocyclic carbene, but shows spectroscopic and structural properties, as well as the reactivity, of saturated imidazolidin-2-ylidenes. A few other examples of 4,5-fused unsaturated “Arduengo-type” carbenes and/or their corresponding metal complexes were reported recently (Chart 1).⁵ These studies have

Chart 1. Examples of 4–5 Annulated Imidazol-2-ylidenes



shown that annulation significantly influences the stability and the σ -donor/ π -acceptor properties of the carbene species, and this may be used as a versatile tool for the fine-tuning of their electronic properties.

Interest in the development of new polycyclic aromatic annulated imidazol-2-ylidenes and their corresponding transition-metal complexes has arisen due to their potential application in catalysis and in fluorescent devices. Phenanthrene and its derivatives are a class of aromatic compounds whose photo-physical properties have been widely studied.⁶ A phenanthrene-fused imidazol-2-ylidene provides a promising framework in which the carbene center is a component of an electron-rich, extended aromatic system. This feature not only tunes the donor properties of the carbene center but also imposes geometric constraints on the N-substituents, influencing their steric impact. Herein, the synthesis and structural characterization of four metal complexes derived from 1,3-dibutylphenanthro[9,10-*d*]imidazol-2-ylidene are reported, as well as the *in situ* characterization of

* To whom correspondence should be addressed. Tel: 1-678-797-2259. Fax: 1-770-423-6744. E-mail: dtapu@kennesaw.edu.

[†] Kennesaw State University.

[‡] Clemson University.

(1) Arduengo, A. J., III; Harlow, R. L.; Kline, M. J. *Am. Chem. Soc.* **1991**, *113*, 361.

(2) Herrmann, W. A.; Weskamp, T.; Bohm, V. P. W. *Adv. Organomet. Chem.* **2001**, *48*, 1.

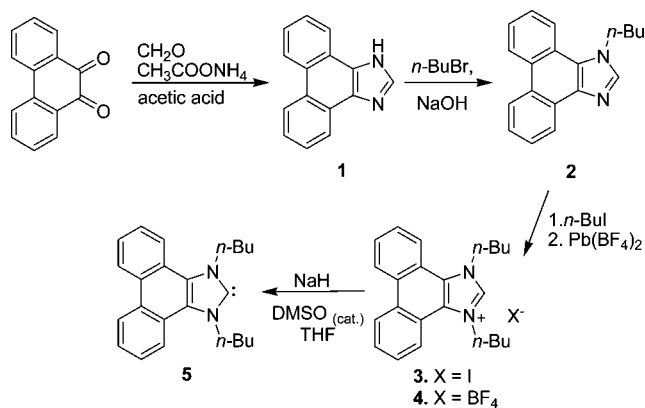
(3) Diez-González, S.; Nolan, S. P. *Coord. Chem. Rev.* **2007**, *251*, 874.

(4) Hahn, F. E.; Wittenbecher, L.; Boese, R.; Bläser, D. *Chem.—Eur. J.* **1999**, *5*, 1931.

(5) (a) Saravanakumar, S.; Kindermann, M. K.; Heinicke, J.; Köckerling, M. *Chem. Commun.* **2006**, 640. (b) Saravanakumar, S.; Oprea, A. I.; Kindermann, M. K.; Jones, P. G.; Heinicke, J. *Chem.—Eur. J.* **2006**, *12*, 3143. (c) Sanderson, M. D.; Kamplajn, J. W.; Bielawski, C. W. *J. Am. Chem. Soc.* **2006**, *128*, 16514. (d) Ullah, F.; Bajor, G.; Veszprémi, T.; Jones, P. G.; Heinicke, J. W. *Angew. Chem., Int. Ed.* **2007**, *46*, 2697. (e) Arduengo, A. J., III; Tapu, D.; Marshall, W. J. *Angew. Chem., Int. Ed.* **2005**, *44*, 7240. (f) Arduengo, A. J., III; Tapu, D.; Marshall, W. J. *J. Am. Chem. Soc.* **2005**, *127*, 16400. (g) Khramov, D. M.; Boydston, A. J.; Bielawski, C. W. *Angew. Chem., Int. Ed.* **2006**, *45*, 6186. (h) Li, W. Ph.D. Thesis, University of Alabama, Tuscaloosa, 2004.

(6) (a) Birks, J. B. *Photophysics of Aromatic Molecules*; Wiley-Interscience: London, 1970. (b) Zhang, P.; Winnik, A.; Wang, Z. Y. *J. Photochem. Photobiol., A* **1995**, *89*, 13.

Scheme 1. Synthesis of Imidazolium Salt 4 and Carbene 5



the free carbene. Some preliminary studies of their photophysical properties are also reported.

Results and Discussion

Synthesis of the Carbene Precursor. A general method for accessing N-heterocyclic carbenes is the deprotonation of the appropriate imidazolium salt precursors. Four steps were necessary to access imidazolium salt **4** (Scheme 1).⁷ Initially, 1*H*-phenanthro[9,10-*d*]imidazole (**1**) was prepared by a multicomponent condensation starting from the commercially available 9,10-phenanthrenequinone, formaldehyde, and ammonium acetate in acetic acid. Although a photochemical synthesis of **1** was reported previously,⁸ an improved general synthesis would facilitate studies and applications of these materials. Our method yields **1** almost quantitatively. Subsequent alkylation of **1** with *n*-butyl bromide in the presence of sodium hydroxide yields 1-butylphenanthro[9,10-*d*]imidazole (**2**). A second alkylation of **2** with butyl iodide at 100 °C provided imidazolium iodide **3**. The tetrafluoroborate **4** was prepared to circumvent potential halide exchange and any subsequent separation problems in reactions involving metal chlorides.

The ¹³C and ¹H NMR spectra of **3** and **4** are virtually identical and consistent with the proposed structures. In the ¹H NMR spectrum, the imidazolium proton appears at δ 9.82 ppm in *d*₆-DMSO (δ 9.73 ppm in *d*₈-THF), while the ¹³C NMR shift of C2 appears at δ 141.6 ppm (*d*₆-DMSO). A characteristic feature in the NMR spectra of **3** and **4** is the strong downfield shift of an NCH₂ proton signal (δ 4.92 ppm), which can be attributed to the diamagnetic ring current of the fused phenanthrene.

Generation of the Free Carbene. Our attempt to generate the free carbene through deprotonation of **4** with potassium *tert*-butoxide in THF resulted in rapid decomposition. However, in an NMR experiment treatment of **4** with NaH/DMSO_(cat) in dry THF proceeded cleanly to afford free carbene **5**. The free carbene was sufficiently stable to be analyzed by NMR spectroscopy. The ¹³C NMR spectrum of **5** revealed a signal at δ 225.10 ppm. This chemical shift is higher than that of nonannulated imidazol-2-ylidene (δ ¹³C = 217 ppm)^{5a} but lower than that of benzo- and naphtha-annulated imidazol-2-ylidenes (δ ¹³C = 231.8^{4,9} and 239.9 ppm).^{5b} These values

suggest a decreased π -charge density at C2 of **5** in comparison to the nonannulated counterpart and an increased π -charge density at the carbene center compared with benzo- and naphtha-annulated imidazol-2-ylidenes.¹⁰ Unfortunately, **5** was found to decompose upon concentration, which precluded its isolation. However, **5** was found to persist in solution for days at room temperature.¹¹

Synthesis of Metal Complexes. Having demonstrated that free carbene **5** can be generated *in situ*, subsequent efforts were focused on the coordination of this carbene to various transition metals. Access to metal complexes of imidazol-2-ylidenes is mainly based on three different synthetic routes: (a) the complexation of the free, preisolated carbene, (b) the *in situ* deprotonation of carbene precursors (carbenium ions), and (c) the use of a metal–carbene complex as a transfer agent. Rhodium(I) and iridium(I) complexes **6** and **7** were prepared by *in situ* deprotonation of **4** with potassium *tert*-butoxide in the presence of [M(COD)Cl]₂. The reactions were conducted at room temperature. Both complexes are quite stable. They can be handled in air and purified by column chromatography on silica gel. They are soluble in THF and halogenated solvents (dichloromethane, chloroform). Both **6** and **7** are stable indefinitely in solution (dichloromethane) at room temperature, but decompose in air at higher temperatures. The identity of the compounds was confirmed by ¹H and ¹³C NMR spectroscopy as well as elemental analysis. These metal complexes exhibit ¹³C chemical shifts and coupling constants that are comparable to those of other reported rhodium–carbene complexes.¹² The chemical shift for C2 in **6** is 190.9 ppm with a characteristic coupling constant ¹J_{Rh–C} of 51.6 Hz. The carbons in the two COD double bonds are coupled with the rhodium atom differently (¹J_{Rh–C} = 6.8, 14.5 Hz), which is consistent with their placement *trans* to different groups. The downfield shift of the NCH₂ protons in complexes **6** and **7** is even stronger than in the annulated imidazolium salts **3** and **4**. The anisotropy of the 1,5-COD ligand in **6** and **7** shifts the second NCH₂ signal further downfield.

When carbon monoxide was bubbled through a solution of **6** in dichloromethane, the complex **8** was obtained in excellent yield. The carbonyl stretching frequencies for **8** were found to be ν_{CO} = 2074 (sym.) and 1994 (asym.) cm⁻¹. These results indicate that carbene **5** is among the strongest σ -donors in the unsaturated series of Arduengo-type carbenes, but still weaker than the best known C-ligands.¹³ Its σ -donating power is similar to that of the recently reported *N,N*-disubstituted diaminocarbene containing a 1,1'-disubstituted ferrocene moiety in its back-

(10) Arduengo, A. J., III; Dixon, D. A.; Kumashiro, K. K.; Lee, C.; Power, W. P.; Zilm, K. W. *J. Am. Chem. Soc.* **1994**, *116*, 6361.

(11) To avoid concentration, we attempted to crystallize carbene **5** by slow diffusion of hexane into a saturated THF solution of **5**. No crystals were obtained. After 6 days the obtained brown solution was treated with sulfur. The resulting thione was recovered in 76% yield. Further details on the synthesis of this thione and its coordination properties will be reported elsewhere.

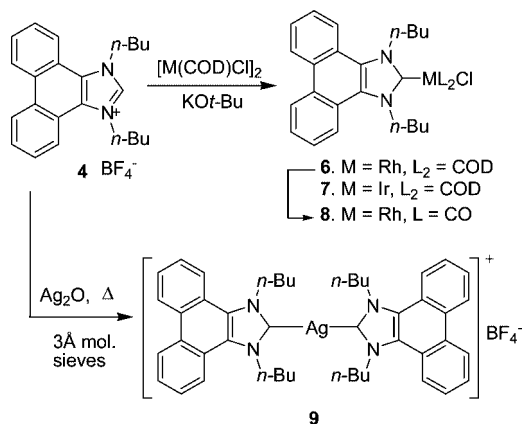
(12) (a) Çetinkaya, B.; Hitchcock, P. B.; Lampert, M. F.; Shaw, D. B.; Spyropoulos, K.; Warhurst, N. J. W. *J. Organomet. Chem.* **1993**, *459*, 311. (b) Vázquez-Serrano, L. D.; Owens, B. T.; Buriak, J. M. *Chem. Commun.* **2002**, 2518. (c) Hillier, A. C.; Lee, H. M.; Stevens, E. D.; Nolan, S. P. *Organometallics* **2001**, *20*, 4246. (d) Chianese, A. R.; Li, X.; Janzen, M. C.; Faller, J. W.; Crabtree, R. H. *Organometallics* **2003**, *22*, 1663. (e) Türkmen, H.; Pape, T.; Hahn, F. E.; Çetinkaya, B. *Organometallics* **2008**, *27*, 571.

(13) (a) Hermann, W. A.; Schütz, J.; Frey, G. D.; Herdtweck, E. *Organometallics* **2006**, *25*, 2437. (b) Mayr, M.; Wurst, K.; Ongania, K.; Buchmeister, M. R. *Chem.–Eur. J.* **2004**, *10*, 1256. (c) Lavallo, V.; Mafhouz, J.; Canac, Y.; Dannadieu, B.; Schoeller, W.; Bertrand, G. *J. Am. Chem. Soc.* **2004**, *126*, 8670. (d) Bazinet, P.; Yap, G. P. A.; Richeson, D. S. *J. Am. Chem. Soc.* **2003**, *125*, 13314.

(7) A similar carbene precursor, 1,3-dimethylphenanthro[9,10-*c*]imidazolium iodide, has been reported (without characterization) as a catalyst for benzoin condensation: Miyashita, A.; Suzuki, Y.; Kobayashi, M.; Kuriyama, N.; Higashino, T. *Heterocycles* **1996**, *43*, 509.

(8) Purushothaman, E.; Rajasekharan-Pillai, V. N. *Indian J. Chem.* **1989**, *28*, 290.

(9) (a) Boesveld, W. M.; Gehrhus, B.; Hitchcock, P. B.; Lappert, M. F.; Schleyer, P. V. R. *Chem. Commun.* **1999**, 755. (b) Gehrhus, B.; Hitchcock, P. B.; Lappert, M. F. *J. Chem. Soc., Dalton Trans.* **2000**, 3094.

Scheme 2. Synthesis of Rhodium, Iridium, and Silver Complexes 6, 7, 8, and 9


bone.¹⁴ The synthesis and characterization of rhodium and iridium complexes **6** and **7** establishes the fundamental properties and applicability of the carbene **5** as a ligand in organometallic chemistry.

The generation of metal complexes from **4** is also possible with basic metal precursors. An example is the reaction of **4** with silver oxide, which gives the cationic bis(1,3-dibutylphenanthro[9,10-*d*]imidazol-2-ylidene) silver complex **9** in good yields. However, this reaction takes place above 80 °C and only in the presence of 3 Å molecular sieves. Since imidazol-2-ylidene silver complexes are capable of transmetalation,¹⁵ this points the way to other transition-metal complexes of **5**. The silver complex **9** is insoluble in all common organic solvents except DMSO, in which it is sparingly soluble and slowly decomposes. A spectroscopically pure sample of **9** in DMSO shows decomposition to imidazolium salt **4** within days at room temperature. The carbene carbon signal for **9** was not found, which is not unusual.¹⁶ The dynamic behavior as well as the poor relaxation of the quaternary carbenic carbon could be factors contributing to the absence of the C2 resonance.

Structural Studies. A single crystal of **6** suitable for X-ray crystallographic measurements was grown by slow diffusion of hexane into a saturated chloroform solution of **6**. Crystal data and details of the crystal structure determination are presented in Table 1. Selected bond lengths and angles are given in Table 2.

Rhodium complex **6** crystallizes in the monoclinic space group *P2*(1)/*n*. Rhodium is coordinated in a square-planar fashion by the carbene, the centers of the two C=C bonds of COD ligand, and the chloride (Figure 1). The plane of the carbene is oriented almost perpendicular (interplanar angle 87.8°) to the rhodium coordination plane. The C2–Rh bond distance of 2.031(3) Å is typical for this type of carbene coordination.¹⁷

The average distance between rhodium and olefinic carbons *trans* to the carbene [$r_{av}(\text{Rh}-\text{C}28(29)) = 2.213(3)$ Å] is slightly larger than the average distance between rhodium and double-

bond carbons *trans* to the chlorine atom [$r_{av}(\text{Rh}-\text{C}24(25)) = 2.111(3)$ Å]. This indicates a stronger *trans*-influence (effect) of the carbene moiety and a weaker rhodium–(C=C) bond for the carbons *trans* to C2 than *trans* to chloride.

Slow diffusion of hexane into a saturated dichloromethane solution of **7** allowed crystals suitable for X-ray structure determination to be grown. Complex **7** crystallizes in the monoclinic space group *P2*(1)/*n*, and it is nearly isostructural with rhodium complex **6**. Selected bonds and angles for **7** are given in Table 2. The asymmetric unit contains two unique molecules.

As shown in the ORTEP plot (Figure 2), complex **7** adopts square-planar coordination geometry around the iridium center. The C2–Ir bond distance is 2.022(6) and 2.034(6) Å, respectively. The same *trans* influence is observed for the carbene center. The C=C bond of COD *trans* to C2 is shorter and displays longer Ir–C distances.

The solid state structure of **9** was identified by X-ray crystallography. X-ray quality crystals were obtained by recrystallization in DMSO. The silver complex **9** displays crystallographic 2-fold symmetry. As depicted in Figure 3, the coordination geometry of the silver atom is essentially linear, with a C2–Ag–C2' bond angle of 178.45(17)° (Table 2). The C–Ag bond distance of 2.100(3) Å and the internal ring angle (N1–C2–N3) at the carbene center of 106.6(3)° are within the range of other known NHC silver complexes.¹⁸

Spectral Studies. Absorption maxima in dichloromethane are 256, 263, and 254 nm for **4**, **6**, and **7**, respectively. In dichloromethane, **4**, **6**, and **7** exhibit fluorescence emission in the region 330–430 nm, similar to phenanthrene. The fluorescence emission spectra of **4**, **6**, **7**, and phenanthrene are shown in Figure 4. With excitation at 256 nm, imidazolium salt **4** exhibits over 3 times stronger emission than phenanthrene, while the emission intensities for **6** and **7** are 0.7% and 9% compared to phenanthrene.

The quantum yields of **4**, **6**, and **7** are 0.18, 2.0×10^{-3} , and 0.012, respectively, as determined by integration of their emission spectra and comparison to the emission spectrum of phenanthrene.¹⁹ As observed in other covalent complexes, fluorescence quenching is likely caused by the heavy atom effect, where singlet excited state population decreases due to intersystem crossing.²⁰ Additionally, it is evident that the electronic structure is affected by both substitution of the phenanthryl moiety and metal complexation since emission peaks for **4**, **6**, and **7** are blue-shifted relative to phenanthrene and since the relative intensities of the bands are different (Table 3). Further studies on these new fluorescent materials are currently under investigation in our laboratory.

In conclusion, a novel phenanthrene-fused imidazol-2-ylidene was prepared and characterized. This carbene was characterized in solution, and it has a decreased π -charge density at C2 in comparison to the nonannulated counterpart and an increased π -charge density at the carbene center compared with other polyaromatic fused carbenes. As determined by IR spectroscopy, **5** is among the strongest σ -donors in the unsaturated series of Arduengo-type carbenes. Furthermore, details on the chemistry of this fused carbene with respect to its ability to support catalytically relevant metal complexes were provided. Four metal complexes that incorporate this ligand have been syn-

(14) Khramov, D. M.; Rosen, E. L.; Lynch, V. M.; Bielawski, C. W. *Angew. Chem., Int. Ed.* **2008**, *47*, 1.

(15) (a) Herrmann, W. A.; Köcher, C.; Grossen, L. *J. Chem.–Eur. J.* **1996**, *2*, 1627. (b) Seo, H.; Kim, B. Y.; Lee, J. H.; Park, H.-J.; Son, S. U.; Chung, Y. K. *Organometallics* **2003**, *22*, 4783.

(16) Alcarazo, M.; Roseblade, S. J.; Cowley, A. R.; Fernández, R.; Brown, J. M.; Lassaletta, J. M. *J. Am. Chem. Soc.* **2005**, *127*, 3290.

(17) (a) Herrmann, W. A.; Baskakov, D.; Herdtweck, E.; Hofmann, S. D.; Bunlaksananusorn, T.; Rampf, F.; Rodefeld, L. *Organometallics* **2006**, *25*, 2449. (b) Cavell, K. J.; Elliott, M. C.; Nielsen, D. J.; Paine, J. S. *Dalton Trans.* **2006**, 4922.

(18) For a review on silver complexes see: Garrison, J. C.; Youngs, W. J. *Chem. Rev.* **2005**, *105*, 3978.

(19) Dawson, W. R.; Windsor, M. W. *J. Phys. Chem.* **1968**, *72*, 3251.

(20) Ballardini, R.; Varani, G.; Indelli, M. T.; Scandola, F. *Inorg. Chem.* **1986**, *25*, 3858.

Table 1. Selected X-ray Crystallographic Data for Complexes 6, 7, and 9

	6	7	9
empirical formula	C ₃₁ H ₃₈ ClN ₂ Rh	C ₃₁ H ₃₈ ClN ₂ Ir	C ₄₆ H ₅₂ N ₄ AgBF ₄
fw	577.02	666.28	844.60
cryst size (mm)	0.43 × 0.22 × 0.17	0.48 × 0.29 × 0.24	0.34 × 0.17 × 0.17
temp (K)	153(2)	153(2)	153(2)
cryst syst	monoclinic	monoclinic	monoclinic
space group	<i>P</i> 2(1)/ <i>n</i>	<i>P</i> 2(1)/ <i>n</i>	<i>C</i> 2/ <i>c</i>
<i>a</i> (Å)	9.1656(18)	25.476(5)	19.426(4)
<i>b</i> (Å)	18.482(4)	9.0377(18)	15.038(3)
<i>c</i> (Å)	18.705(4)	25.771(5)	15.379
α (deg)	90	90	90
β (deg)	101.36(3)	113.07(3)	94.84(3)
γ (deg)	90	90	90
<i>V</i> (Å ³)	3106.5(11)	5459.2(19)	4476.9(16)
<i>Z</i>	4	8	4
<i>D_c</i> (g cm ⁻³)	1.489	1.621	1.269
diffractometer/scan	Rigaku AFC8S/CCD/ω	Rigaku AFC8S/CCD/ω	Rigaku AFC8S/CCD/ω
radiation/wavelength (Å)	0.71073	0.71073	0.71073
θ max (deg)	25.15	25.04	25.03
index range (<i>hkl</i>)	-10 ≤ <i>h</i> ≤ 10 -14 ≤ <i>k</i> ≤ 22 -22 ≤ <i>l</i> ≤ 22	-30 ≤ <i>h</i> ≤ 30 -7 ≤ <i>k</i> ≤ 10 -26 ≤ <i>l</i> ≤ 30	-23 ≤ <i>h</i> ≤ 21 -17 ≤ <i>k</i> ≤ 17 -18 ≤ <i>l</i> ≤ 18
reflections measd	20 913	30 382	16 258
independent reflns (<i>R_{int}</i>)	5538 (0.0259)	9619 (0.0489)	3959 (0.0396)
data/restraints/params	5538/7/388	9619/0/635	3959/0/255
max., min. transmn	0.8595, 0.6935	0.3793, 0.1971	0.9196, 0.8480
final <i>R</i> indices (<i>I</i> > 2σ(<i>I</i>))	<i>R</i> 1 = 0.0354, w <i>R</i> 2 = 0.0803	<i>R</i> 1 = 0.0432, w <i>R</i> 2 = 0.1026	<i>R</i> 1 = 0.0491, w <i>R</i> 2 = 0.1274
<i>R</i> indices (all data)	<i>R</i> 1 = 0.0414, w <i>R</i> 2 = 0.0852	<i>R</i> 1 = 0.0570, w <i>R</i> 2 = 0.1133	<i>R</i> 1 = 0.0548, w <i>R</i> 2 = 0.1337
goodness-of-fit on <i>F</i> ²	1.121	1.074	1.078
peak/hole (e Å ⁻³)	1.102/-0.632	2.278/-1.825	0.683/-0.681

Table 2. Selected Bond Lengths (Å) and Angles (deg) for 6, 7, and 9

	6	7 ^a	9
M-C2	2.031(3)	2.022(6)/2.034(6)	2.100(3)
M-X	2.3676(11)	2.3684(17)/2.3703(16)	
M-C24	2.104(3)	2.101(7)/2.130(7)	
M-C25	2.118(3)	2.119(7)/2.105(7)	
M-C28	2.202(3)	2.180(7)/2.202(7)	
M-C29	2.224(3)	2.205(7)/2.192(7)	
C2-N1	1.358(4)	1.359(8)/1.359(8)	1.345(4)
C2-N3	1.355(4)	1.370(8)/1.364(8)	1.350(4)
C3A-C15A	1.382(4)	1.381(8)/1.393(9)	1.380(5)
C15A-N1	1.396(4)	1.391(8)/1.387(8)	1.401(4)
C3A-N3	1.399(4)	1.401(8)/1.399(8)	1.403(4)
M-C2-N1	127.7(2)	124.8(4)/106.3(5)	126.4(2)
M-C2-N3	126.0(2)	129.4(4)/128.3(5)	126.9(2)
N1-C2-N3	106.3(2)	105.7(5)/106.3(5)	106.6(3)
C11-M-C2	90.02(8)	88.97(17)/88.43(17)	
C11-M-C24	156.12(8)	158.3(2)/163.4(2)	
C11-M-C25	163.97(8)	162.5(2)/157.4(3)	
C11-M-C28	89.92(8)	91.71(19)/91.3(2)	
C11-M-C29	92.28(8)	93.34(18)/89.6(2)	
C2-M-C2'			178.45(17)

^a The two sets correspond to two unique molecules in the unit cell.

thesized and fully characterized. The solid state molecular structures of these complexes have been confirmed by X-ray diffraction studies. The fluorescence emission spectra of **4**, **6**, and **7** were determined and compared to those of phenanthrene. Further studies on these new fluorescent compounds and their analogues are underway and will be reported in the future.

Experimental Section

All reactions were carried out without any special need for inert conditions, except where indicated. Reagents were purchased from commercial sources and used as supplied. [Rh(COD)Cl]₂ and [Ir(COD)Cl]₂ were purchased from Strem. NMR spectra were recorded on a Bruker DPX 300 (¹H, 300 MHz; ¹³C, 75.5 MHz) or a Bruker AMX 500 (¹H, 500 MHz; ¹³C, 125.7 MHz). Chemical shifts are described in parts per million downfield shifted from SiMe₄.

Synthesis of 1*H*-Phenanthro[9,10-*d*]imidazole (1). A mixture of 9,10-phenanthrenequinone (30 g, 0.144 mol), formaldehyde (23.1 mL, 37 wt %), glacial acetic acid (560 mL), and ammonium acetate (230.7 g, 2.99 mol) was refluxed for 4 h. After cooling, the reaction mixture was diluted with water (600 mL) and neutralized with concentrated aqueous ammonia (28–30% wt) to pH 7. A light cream precipitate formed. It was filtered, washed with water, acetone, dichloromethane, and ethyl ether, and then dried to give 31.3 g of product (99% yield). The spectral data were in accordance with those described in the literature.²¹

Synthesis of 1-Butylphenanthro[9,10-*d*]imidazole (2). To a mixture of **1** (20 g, 0.092 mol) and sodium hydroxide (4 g, 0.1 mol) was added DMSO (200 mL). The reaction mixture was stirred at room temperature for 2 h. After addition of butyl bromide (10 mL, 0.092 mol), the reaction was stirred at room temperature for

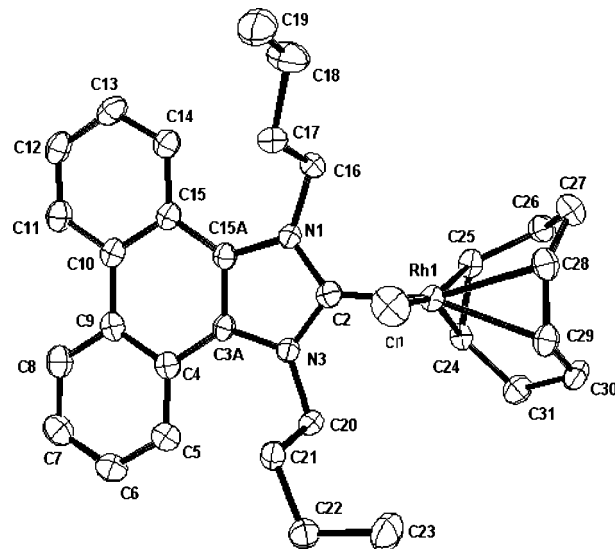


Figure 1. Molecular structure of complex **6** showing 50% probability ellipsoids. Hydrogen atoms have been omitted for clarity.

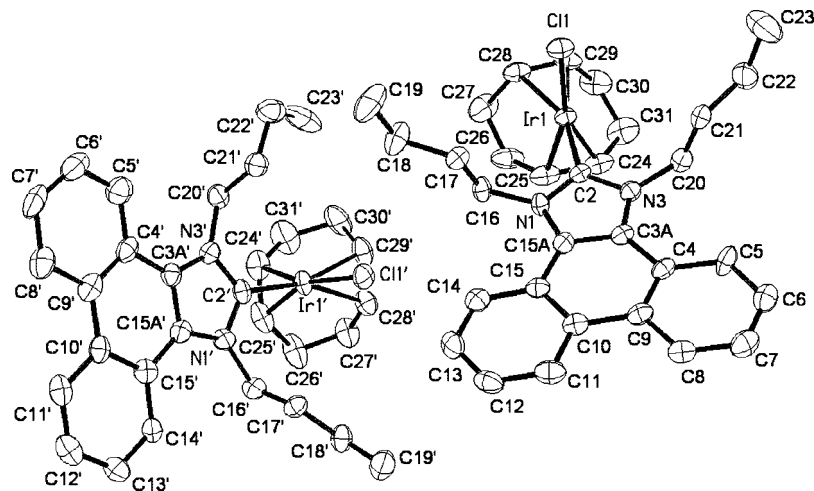


Figure 2. Molecular structure of complex **7** showing 50% probability ellipsoids. Hydrogen atoms have been omitted for clarity. There are two crystallographically independent complexes.

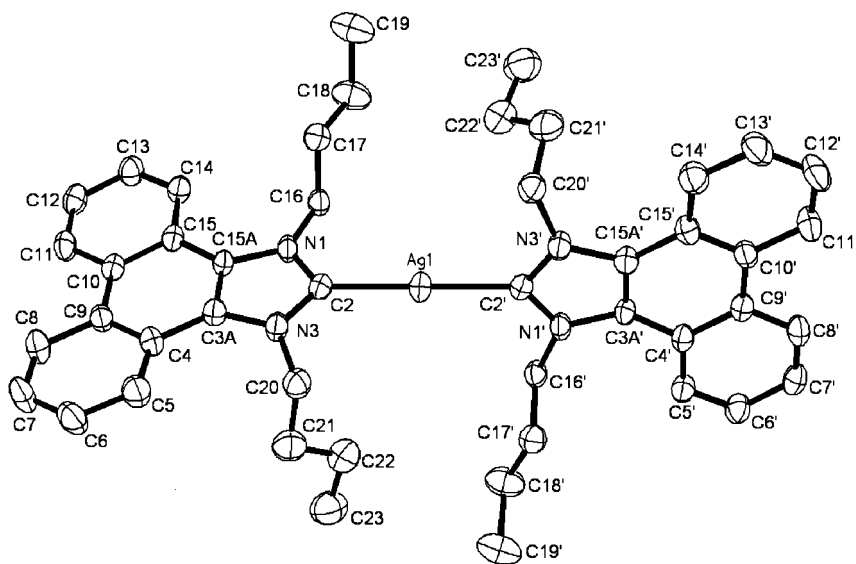


Figure 3. Molecular structure of complex **9** showing 50% probability ellipsoids. Hydrogen atoms have been omitted for clarity.

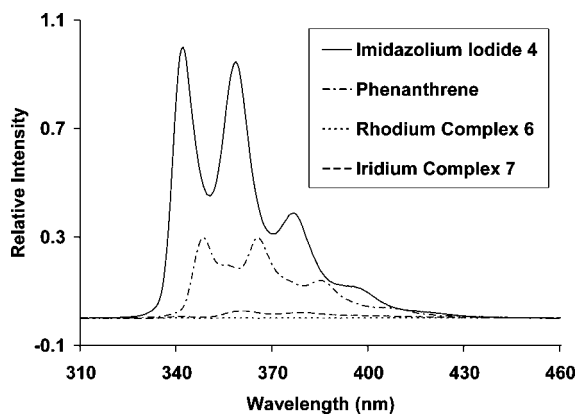


Figure 4. Emission spectra of **4**, **6**, **7**, and phenanthrene (standard) at 256 nm in CH_2Cl_2 (1.0×10^{-5} mol L^{-1}).

another 25 min. The temperature was increased to 37 °C, and the reaction mixture was stirred at this temperature overnight. The solvent was removed; the residue was taken up in acetonitrile and filtered. The volatiles were removed from the filtrate, and the solid residue was further purified by trituration with ethyl ether to give 23.84 g of solid. (94.8% yield).

Table 3. Emission Peak Positions for **4**, **6**, **7**, and Phenanthrene (Ph) in Dichloromethane

compound	maximum emission (nm) [relative intensity] ^a			
4	342 [1.00]	358.5 [0.946]	376.5 [0.387]	395 sh [0.117]
7	342 [0.00732]	361 [0.0270]	378 [0.0211]	
6	341 [0.00204]	359 [0.00204]	378 [0.00145]	
Ph	348 [0.297]	365.5 [0.298]	385.5 [0.139]	407 sh [0.0384]

^a Excitation at 256 nm, 0.5 s integration time, 300 points, 1.24 mm slit width; sh = shoulder; emission maximum indicated in **bold**.

¹H NMR (*d*₆-DMSO, 300 MHz): δ 8.89 (d, 1H, $^3J = 8.1$ Hz, ArH), 8.79 (d, 1H, $^3J = 8.2$ Hz, ArH), 8.57 (d, 1H, $^3J = 7.9$ Hz, ArH), 8.31 (d, 1H, $^3J = 8.1$ Hz, ArH), 8.25 (s, 1H, C2-H), 7.71 (q, 2H, $^3J = 7.9$ Hz, ArH), 7.60 (q, 2H, $^3J = 7.9$ Hz, ArH), 4.65 (t, 2H, $^3J = 7.0$ Hz, NCH₂), 1.83 (pentet, 2H, $^3J = 7.3$ Hz, NCH₂CH₂), 1.30 (sextet, 2H, $^3J = 7.4$ Hz, CH₂CH₃), 0.85 (t, 3H, $^3J = 7.4$ Hz (CH₃)). ¹³C NMR (*d*₆-DMSO, 75.5 MHz): δ 143.72 (NCN), 138.46 (ArC), 128.48 (ArC), 127.83 (ArC), 127.68 (ArC), 125.76 (ArC), 125.47 (ArC), 124.92 (ArC), 124.83 (ArC), 123.98 (ArC), 123.30 (ArC), 122.24 (ArC), 121.65 (ArC), 47.18 (NCH₂), 32.32 (NCH₂CH₂), 19.51 (CH₂CH₃), 13.91 (CH₃). Anal. Calcd for C₁₉H₁₈N₂ (274.37): C, 83.17; H, 6.61; N, 10.21. Found: C, 83.06; H, 6.63; N, 10.22.

Synthesis of 1,3-Dibutylphenanthro[9,10-*d*]imidazolium Iodide (3). Compound **2** (17.57 g, 64 mmol) and 75 mL of *n*-butyl iodide were added into a pressure flask. The flask was sealed, and the reaction mixture was stirred at 100 °C for 38 h. The volatiles were removed under vacuum, and the residue was triturated with ethyl acetate to leave, after evaporation, 27.5 g of pure product (yield 93%). ¹H NMR (*d*₆-DMSO, 300 MHz): δ 9.82 (s, 1H, C2H), 9.11 (d, 2H, ³J = 8.4 Hz, ArH), 8.55 (d, 2H, ³J = 8.3 Hz, ArH), 7.91 (m, 4H, ArH), 4.93 (t, 4H, ³J = 7.1 Hz, NCH₂), 2.01 (p, 4H, ³J = 7.4 Hz, NCH₂CH₂), 1.48 (sextet, 4H, ³J = 7.4 Hz, CH₂CH₃), 0.976 (t, 6H, ³J = 7.4 Hz, CH₃). ¹³C NMR (*d*₆-DMSO, 75.5 MHz): δ 141.57 (NCN), 129.81 (ArC), 129.24 (ArCH), 128.62 (ArC), 126.31(ArC), 125.25 (ArC), 122.89 (ArC), 120.92 (ArC), 50.47 (NCH₂), 30.99 (NCH₂CH₂), 19.37 (CH₂CH₃), 13.97 (CH₃). Anal. Calcd for C₂₃H₂₇N₂I (458.38): C, 60.26; H, 5.93; N, 6.11. Found: C, 60.42; H, 5.94; N, 6.15.

Synthesis of 1,3-Dibutylphenanthro[9,10-*d*]imidazolium Tetrafluoroborate (4). Imidazolium salt **3** (2.5 g, 5.45 mmol) was dissolved in about 300 mL of acetone. An aqueous solution of Pb(BF₄)₂ (1.22 mL, 50% wt) was added to immediately form a yellow precipitate. The mixture was stirred at room temperature for 2 h and filtered. The filtrate was evaporated to give 2.096 g of pure product (yield 92%). The spectral data were identical to those for imidazolium salt **3**. Anal. Calcd for C₂₃H₂₇N₂BF₄ (418.29): C, 66.04; H, 6.50; N, 6.69. Found: C, 66.03; H, 6.49; N, 6.67.

NMR Tube Reaction for the Generation of 1,3-Dibutylphenanthro[9,10-*d*]imidazol-2-ylidene (5). Imidazolium salt **4** and sodium hydride (1:4 mol ratio) were suspended in *d*₈-THF under nitrogen. A catalytic amount of *d*₆-DMSO was added and the NMR tube was sealed. The resulting solution was subjected to ¹H NMR and ¹³C NMR measurements, which indicated the formation of the carbene **5** within 20 min. This solution did not show major decomposition overnight, as indicated by ¹H NMR. ¹H NMR (*d*₈-THF, 300 MHz): δ 8.74 (d, 2H, ³J = 8.1 Hz, ArH), 8.34 (d, 2H, ³J = 8.1 Hz, ArH), 7.56 (t, 2H, ³J = 7.0 Hz, ArH), 7.46 (t, 2H, ³J = 7.0 Hz, ArH), 4.70 (t, 4H, ³J = 7.1 Hz, NCH₂) 1.84 (p, 4H, ³J = 7.1 Hz, NCH₂CH₂), 1.39 (sextet, 4H, ³J = 7.3 Hz, CH₂CH₃), 0.86 (t, 6H, ³J = 7.3 Hz, CH₃). ¹³C NMR (*d*₈-THF, 300 MHz): δ 225.10 (NCN), 129.50 (ArC), 128.61(ArC), 128.01 (ArC), 125.69 (ArC), 125.09 (ArC), 124.05 (ArC), 122.71 (ArC), 52.16 (NCH₂), 33.95 (NCH₂CH₂), 20.73 (CH₂CH₃), 14.37 (CH₃).

Synthesis of (1,3-Dibutylphenanthro[9,10-*d*]imidazol-2-ylidene)rhodium(1,5-cyclooctadiene) Chloride (6). To a mixture of imidazolium salt **4** (0.50 g, 1.2 mmol), [Rh(COD)Cl]₂ (0.295 g, 0.6 mmol), and KO^t-Bu (0.134 g, 1.2 mmol) was added dry THF (50 mL) under inert conditions. The reaction mixture was stirred at room temperature for 12 h. The solvent was removed *in vacuo*, and the residue was purified by flash chromatography (silica, eluted with dichloromethane) to give **6** as a yellow solid. Yield: 0.65 g, 94%. ¹H NMR (CDCl₃, 300 MHz): δ 8.80 (d, 2H, ³J = 8.1 Hz, ArH), 8.34 (d, 2H, ³J = 8.1 Hz, ArH), 7.73 (t, 2H, ³J = 7.0 Hz, ArH), 7.66 (t, 2H, ³J = 7.0 Hz, ArH), 5.80 (dd, 1H, ²J = 12.3 Hz, ³J = 5.3 Hz, NCH₂), 5.76 (dd, 1H, ²J = 12.3 Hz, ³J = 5.3 Hz, NCH₂) 5.27 (dd, 1H, ²J = 12.2 Hz, ³J = 4.2 Hz, NCH₂) 5.22 (dd, 1H, ²J = 12.2 Hz, ³J = 4.2 Hz, NCH₂) 5.20 (bs, 2H, CH₂CO_D), 3.46 (bs, 2H, CH₂CO_D), 2.52 (m, 4H, (CH₂)₂CO_D), 2.33 (m, 2H, NCH₂CH₂), 2.04 (m, 2H, (CH₂)₂CO_D), 1.98 (m, 2H, NCH₂CH₂), 1.76 (sextet, 4H, ³J = 7.3 Hz, CH₂CH₃), 1.18 (t, 6H, ³J = 7.3 Hz, CH₃). ¹³C NMR (CDCl₃, 75.5 MHz): δ 190.9 (d, ¹J_{Rh-C} = 51.56 Hz, NCN), 128.30 (ArC), 128.03 (ArC), 127.40 (ArC), 125.56 (ArC), 124.05 (ArC), 121.60 (ArC), 121.41 (ArC), 98.85 (d, ¹J_{RhC} = 6.84 Hz, CH₂CO_D), 68.8 (d, ¹J_{RhC} = 14.76 Hz), 51.76 (NCH₂), 32.99 (NCH₂CH₂), 31.72 ((CH₂)₂CO_D), 28.99 ((CH₂)₂CO_D), 20.41 (CH₂CH₃), 13.85 (CH₃). Anal. Calcd for C₃₁H₃₈N₂RhCl (577.02): C, 64.52; H, 6.63; N, 4.85. Found: C, 64.58; H, 6.69; N, 4.83.

Synthesis of (1,3-Dibutylphenanthro[9,10-*d*]imidazol-2-ylidene)iridium(1,5-cyclooctadiene) Chloride (7). To a mixture of imidazolium salt **4** (0.41 g, 0.98 mmol), [Ir(COD)Cl]₂ (0.33 g, 0.49 mmol), and KO^t-Bu (0.135 g, 1.2 mmol) was added dry THF (50 mL) under inert conditions. The reaction mixture was stirred at room temperature for 12 h. The solvent was removed under vacuum, and the residue was purified by flash chromatography (silica, eluted with dichloromethane) to give **7** as a yellow solid. Yield: 0.48 g, 73%. ¹H NMR (CDCl₃, 300 MHz): δ 8.81 (d, 2H, ³J = 8.4 Hz, ArH), 8.34 (d, 2H, ³J = 8.1 Hz, ArH), 7.73 (t, 2H, ³J = 7.0 Hz, ArH), 7.67 (t, 2H, ³J = 7.0 Hz, ArH), 5.61 (dd, 1H, ²J = 12.4 Hz, ³J = 5.4 Hz, NCH₂), 5.56 (dd, 1H, ²J = 12.4 Hz, ³J = 5.3 Hz, NCH₂) 5.12 (dd, 1H, ²J = 12.1 Hz, ³J = 4.1 Hz, NCH₂) 5.07 (dd, 1H, ²J = 12.1 Hz, ³J = 4.2 Hz, NCH₂) 4.77 (m, 2H, CH₂CO_D), 3.05 (m, 2H, CH₂CO_D), 2.32 (m, 4H, (CH₂)₂CO_D), 2.21 (m, 2H, NCH₂CH₂), 1.99 (m, 2H, NCH₂CH₂), 1.85 (m, 2H, (CH₂)₂CO_D), 1.75 (m, 2H, (CH₂)₂CO_D), 1.69 (sextet, 4H, ³J = 7.3 Hz, CH₂CH₃), 1.14 (t, 6H, ³J = 7.3 Hz, CH₃). ¹³C NMR (CDCl₃, 90.5 MHz): δ 187.32 (NCN), 128.48 (ArC), 127.94 (ArC), 127.47 (ArC), 125.63 (ArC), 124.12 (ArC), 121.79 (ArC), 121.47 (ArC), 84.99 (CH₂CO_D), 52.53(CH₂CO_D), 51.41 (N CH₂), 33.67 (NCH₂ CH₂), 31.71 ((CH₂)₂CO_D), 29.64 ((CH₂)₂CO_D), 20.31 (CH₂CH₃), 13.79 (CH₃). Anal. Calcd for C₃₁H₃₈N₂IrCl (666.33): C, 55.87; H, 5.74; N, 4.20. Found: C, 56.00; H, 5.79; N, 4.16.

Synthesis of (1,3-Dibutylphenanthro[9,10-*d*]imidazol-2-ylidene)rhodium(CO)₂ Chloride (8). Complex **6** (100 mg, 0.17 mmol) was dissolved in dichloromethane (20 mL) and placed under an atmosphere of CO(g) for 2 h. The remaining solvent was then removed, and the resulting solid was triturated with pentane to remove residual COD. The remaining solid was dried *in vacuo* to yield 0.09 mg (99% yield) of **8** as a light yellow powder. ¹H NMR (CDCl₃, 300 MHz): δ 8.78 (d, 2H, ³J = 7.7 Hz, ArH), 8.29 (d, 2H, ³J = 7.7 Hz, ArH), 7.71 (m, 4H), 5.29 (dd, 1H, ²J = 11.2 Hz, ³J = 5.5 Hz, NCH₂), 5.25 (dd, 1H, ²J = 11.2 Hz, ³J = 5.5 Hz, NCH₂) 5.08 (dd, 1H, ²J = 11.2 Hz, ³J = 4.9 Hz, NCH₂) 5.03 (dd, 1H, ²J = 11.2 Hz, ³J = 4.9 Hz, NCH₂) 2.18 (m, 2H, NCH₂CH₂), 1.99 (m, 2H, NCH₂CH₂), 1.68 (m, 4H, NCH₂CH₃), 1.10 (t, 6H, ³J = 7.35 Hz, CH₃). ¹³C NMR (CDCl₃, 75.5 MHz): δ 185.4 (d, ¹J_{Rh-C} = 53.97 Hz), 182.77 (d, ¹J_{Rh-C} = 74.43 Hz), 181.13 (d, ¹J_{Rh-C} = 43.94 Hz), 128.89 (ArC), 128.03 (ArC), 127.75 (ArC), 126.27 (ArC), 124.25 (ArC), 121.53 (ArC), 121.42 (ArC), 52.07 (NCH₂), 31.59 (NCH₂CH₂), 20.12 (CH₂CH₃), 13.85 (CH₃). IR ν_{CO} (cm⁻¹): 2074, 1994. Anal. Calcd for C₂₅H₂₆N₂O₂RhCl (524.84): C, 57.21; H, 4.99; N, 5.34. Found: C, 57.05; H, 4.97; N, 5.28.

Synthesis of Bis(1,3-dibutylphenanthro[9,10-*d*]imidazol-2-ylidene)silver Tetrafluoroborate (9). A pressure vessel was charged with **4** (0.56 g, 1.34 mmol), Ag₂O (0.31 g, 1.34 mmol), 3 Å molecular sieves (0.8 g), and 15 mL of dry dichloromethane. The flask was sealed and the reaction mixture was stirred at 80 °C for 24 h. The volatiles were removed, and the solid residue was extracted with DMSO and filtered. The filtrate was evaporated and triturated with ethyl acetate to give 0.462 g of **7** (80% yield).

¹H NMR (*d*₆-DMSO, 300 MHz): δ 9.08 (d, 4H, ³J = 8.2 Hz, ArH), 8.56 (d, 4H, ³J = 8.1 Hz, ArH), 7.90 (t, 4H, ³J = 7.5, ArH), 7.82 (t, 8H, ³J = 7.5, ArH), 5.12 (t, 4H, ³J = 6.8 Hz, NCH₂), 2.00 (p, 8H, ³J = 7.2 Hz, NCH₂CH₂), 1.55 (sextet, 8H, ³J = 7.4 Hz, CH₂CH₃), 0.97 (t, 12H, ³J = 7.3 Hz, CH₃). ¹³C NMR (*d*₆-DMSO, 75.5 MHz): δ C2 not detected, 129.23 (ArC), 128.84 (ArC), 127.44 (ArC), 127.40 (ArC), 125.11 (ArC), 122.52 (ArC), 121.48 (ArC), 52.87 (NCH₂), 32.67 (NCH₂CH₂), 20.07 (CH₂CH₃), 14.24 (CH₃). Further purification was not possible due to decomposition. Anal. Calcd for C₄₆H₅₂N₄AgBF₄ (855.62): C, 64.57; H, 6.12; N, 6.54. Found: C, 62.57; H, 6.24; N, 6.32.

Acknowledgment. A collaboration with Professor A. J. Arduengo III and his group is gratefully acknowledged. This work has been supported by internal grants from Kennesaw

State University (Mentor Protégé grant no. DT01FY2008-01 and a 2008-2009 CETL Incentive Grant) and the National Science Foundation (CHE-0413521, CHE-0115760, and CHE-0342921).

Supporting Information Available: A complete description of the X-ray crystallographic determination on **6**, **7**, and **9** including

tables of fractional coordinates, isotopic and anisotropic thermal parameters, and bond distances and angles, as well as fluorescence emission spectra of **4**, **6**, **7**, and phenanthrene. This material is available free of charge via the Internet at <http://pubs.acs.org>.

OM800822M

(21) Krebs, F. C.; Spanggaard, H. *J. Org. Chem.* **2002**, *67*, 7185–7192.

Reductive Elimination and Dissociative β -Hydride Abstraction from Pt(IV) Hydroxide and Methoxide Complexes

Nicole A. Smythe,[†] Kyle A. Grice,[†] B. Scott Williams,^{*‡} and Karen I. Goldberg^{*‡}

Department of Chemistry, Box 351700, University of Washington, Seattle, Washington 98195-1700, and The Joint Science Department of The Claremont Colleges, W. M. Keck Science Center, 925 North Mills Avenue, Claremont, California 91711

Received September 17, 2008

The platinum(IV) hydroxide and methoxide complexes *fac*-(dppbz)PtMe₃(OR) (dppbz = *o*-bis(diphenylphosphino)benzene; R = H (**1**), CH₃ (**2**)) have been prepared and characterized. Thermolysis of hydroxide **1** produces (dppbz)PtMe₂ (**3**) and methanol in a rare example of directly observed sp³ carbon–oxygen reductive elimination from a metal center to form an alcohol. Competitive carbon–carbon reductive elimination to form (dppbz)PtMe(OH) (**5**) and ethane also occurs. In contrast, the major reaction observed upon thermolysis of the methoxide analog **2** is neither carbon–oxygen nor carbon–carbon reductive elimination. Instead, products expected from formal β -hydride elimination followed by carbon–hydrogen reductive elimination are detected. Mechanistic studies suggest the operation of an alternative mechanism to that most commonly accepted for this fundamental reaction; a dissociative β -hydride abstraction pathway is proposed.

Introduction

Reductive elimination and β -hydride elimination are two fundamental transformations that are ubiquitous in metal-mediated processes. Consequently, significant effort has been directed toward understanding their mechanisms.¹ However, studies of these elimination reactions have largely focused on systems involving metal–carbon bonds; comparatively little is known about the related reactions with metal–heteroatom linkages. The fact that there are fewer studies of the mechanisms of fundamental reactions of late metal hydroxides and alkoxides relative to those of late metal alkyls may be attributable to there being fewer monomeric hydroxide and alkoxide complexes available for study.² Since theoretical and experimental studies have shown that late metal M–O bonds are at least as strong as their alkyl analogs,³ it has been proposed that the relative scarcity of such species may in fact stem from their access to low energy decomposition pathways,^{2a,c} including reductive elimination and β -hydride elimination. Thus, the elucidation of the mechanisms of these fundamental reactions for metal–heteroatom species is important. Recent contributions appear to indicate that the more polar nature of metal–heteroatom bonds and the presence of heteroatom electron lone pairs can result in significant differences in reaction mechanisms from

those of their metal–carbon analogs. This contribution focuses on these differences in reductive elimination and β -hydride elimination pathways when hydroxide and alkoxide groups are involved.

In contrast to the large number of examples and mechanistic studies of C–C reductive elimination reactions,⁴ there are relatively few reported direct observations of C–O reductive

(4) Reference 1b, pp 170–175.

(5) (a) Mann, G.; Hartwig, J. F. *J. Am. Chem. Soc.* **1996**, *118*, 13109. (b) Hartwig, J. F. *Angew. Chem., Int. Ed. Engl.* **1998**, *37*, 2046, and references therein. (c) Hartwig, J. F. *Acc. Chem. Res.* **1998**, *31*, 852. (d) Mann, G.; Incarvito, C.; Rheingold, A. L.; Hartwig, J. F. *J. Am. Chem. Soc.* **1999**, *121*, 3224. (e) Shelby, Q.; Kataoka, N.; Mann, G.; Hartwig, J. *J. Am. Chem. Soc.* **2000**, *122*, 10718. (f) Mann, G.; Shelby, Q.; Roy, A. H.; Hartwig, J. F. *Organometallics* **2003**, *22*, 2775.

(6) (a) Widenhoefer, R. A.; Zhong, H. A.; Buchwald, S. L. *J. Am. Chem. Soc.* **1997**, *119*, 6787. (b) Widenhoefer, R. A.; Buchwald, S. L. *J. Am. Chem. Soc.* **1998**, *120*, 6504, and references therein.

(7) Komiyama, S.; Akai, Y.; Tanaka, K.; Yamamoto, T.; Yamamoto, A. *Organometallics* **1985**, *4*, 1130.

(8) (a) Matsunaga, P. T.; Mavropoulos, J. C.; Hillhouse, G. L. *Polyhedron* **1995**, *14*, 175. Note that the reductive elimination from Ni(II) is promoted by oxidants, and thus Ni(III) is likely involved in the reactions. (b) Han, R.; Hillhouse, G. L. *J. Am. Chem. Soc.* **1997**, *119*, 8135. (c) Koo, K.; Hillhouse, G. L. *Organometallics* **1998**, *17*, 2924.

(9) Haarman, H. F.; Kaagman, J.-W. F.; Smeets, W. J. J.; Spek, A. L.; Vrieze, K. *Inorg. Chim. Acta* **1998**, *270*, 34.

(10) Dick, A. R.; Kampf, J. W.; Sanford, M. S. *J. Am. Chem. Soc.* **2005**, *127*, 12790.

(11) (a) Canty, A. J.; Jin, H. *J. Organomet. Chem.* **1998**, *565*, 135. (b) Canty, A. J.; Jin, H.; Skelton, B. W.; White, A. H. *Inorg. Chem.* **1998**, *37*, 3975. (c) Canty, A. J.; Denney, M. C.; van Koten, G.; Skelton, B. W.; White, A. H. *Organometallics* **2004**, *23*, 5432.

(12) Thompson, J. S.; Randall, S. L.; Atwood, J. D. *Organometallics* **1991**, *10*, 3906. See ref 5a for more information on this reaction.

(13) Sanford, M. S.; Groves, J. T. *Angew. Chem., Int. Ed.* **2004**, *43*, 588.

(14) (a) Vedernikov, A. N.; Binfield, S. A.; Zavalij, P. Y.; Khusnutdinova, J. R. *J. Am. Chem. Soc.* **2006**, *128*, 82. (b) Khusnutdinova, J. R.; Zavalij, P. Y.; Vedernikov, A. N. *Organometallics* **2007**, *26*, 3466. (c) Khusnutdinova, J. R.; Newman, L. L.; Zavalij, P. Y.; Lam, Y.-F.; Vedernikov, A. N. *J. Am. Chem. Soc.* **2008**, *130*, 2174.

(15) Williams, B. S.; Goldberg, K. I. *J. Am. Chem. Soc.* **2001**, *123*, 2576, and references therein.

(16) Luinstra, G. A.; Wang, L.; Stahl, S. S.; Labinger, J. A.; Bercaw, J. E. *J. Organomet. Chem.* **1995**, *504*, 75.

* Corresponding authors. E-mail: goldberg@chem.washington.edu; williams@jsd.claremont.edu.

[†] University of Washington.

[‡] Joint Science Department of the Claremont Colleges.

(1) (a) Collman, J. P.; Hegedus, L. S.; Norton, J. R.; Finke, R. G. *Principles and Applications of Organotransition Metal Chemistry*; University Science Books: Sausalito, CA, 1987; pp 322–353; 386–389. (b) Crabtree, R. H. *The Organometallic Chemistry of the Transition Metals*, 4th ed.; John Wiley & Sons: Hoboken, NJ, 2005; pp 55–60.

(2) (a) Bryndza, H. E.; Tam, W. *Chem. Rev.* **1988**, *88*, 1163. (b) Fulton, J. R.; Holland, A. W.; Fox, D. J.; Bergman, R. G. *Acc. Chem. Res.* **2002**, *35*, 44. (c) Roesky, H. W.; Singh, S.; Yusuff, K. K. M.; Maguire, J. A.; Hosmane, N. S. *Chem. Rev.* **2006**, *106*, 3813.

(3) (a) Bryndza, H. E.; Fong, L. K.; Paciello, R. A.; Tam, W.; Bercaw, J. E. *J. Am. Chem. Soc.* **1987**, *109*, 1444. (b) Holland, P. L.; Andersen, R. A.; Bergman, R. G.; Huang, J.; Nolan, S. P. *J. Am. Chem. Soc.* **1997**, *119*, 12800.

elimination.^{5–16} Those cases involving alkyl and hydroxide groups to produce alcohols, a potentially highly valuable product release step in catalysis, are exceptionally rare.^{14,16} Notably, several examples of C(sp³)–O reductive elimination reactions to form methyl aryl ethers and methyl carboxylates have recently been reported.¹⁵ In these reactions, which occur at Pt(IV) centers, a common two-step pathway involving dissociation of the anionic oxygen group followed by nucleophilic attack of the oxyanion on the cationic Pt(IV) alkyl intermediate has been proposed. A similar nucleophilic coupling has also been proposed as the product-forming step in platinum-catalyzed alkane oxidation reactions.^{16,17} In contrast to these C–O reductive elimination reactions, C–C bond formation typically occurs via a concerted three-centered transition state.⁴ Thus, the mechanisms of reductive elimination involving metal–oxygen bonds can be quite different than those involving metal–carbon bonds.

Whereas alkyl C–O reductive elimination is a relatively rare reaction, β -hydride elimination is accepted as a common and predictable decomposition pathway for transition metal alkoxides. Notably, the reaction of alcohols and bases with transition metal halides is a traditional method of preparing metal hydride complexes.¹⁸ Such reactions are thought to proceed via metathesis of the halide for an alkoxide group followed by β -hydride elimination from the intermediate metal-alkoxide species. It has been generally assumed that the latter step proceeds by the same mechanism that has been established for metal alkyl complexes.¹⁹ As described in organometallic textbooks, for metal alkyl complexes, the hydride moves from the β -carbon of the alkyl through a four-coordinate planar transition state to an open site on the metal that is *cis* to the alkyl ligand. This *cis* open site is a requirement for this mechanism, and the stability of many metal alkyls with β -hydrogens has been attributed to the lack of labile ancillary ligands or other access to a *cis* open site on the metal.¹ However, a few examples of β -hydride elimination from metal alkoxide complexes have been recently reported wherein a *cis* open site does not appear to be available,^{20–23} suggesting that an alternative mechanism is needed in at least some cases to account for this fundamental reaction when metal–heteroatom bonds are involved.

In this contribution, we report the synthesis, characterization, and thermal reactivity of the monomeric platinum(IV) hydroxide and alkoxide complexes *fac*-(dppbz)PtMe₃(OR) (dppbz = *o*-bis-(diphenylphosphino)benzene; R = H (**1**), CH₃ (**2**)). C–O reductive elimination was observed upon thermolysis of the platinum(IV)-hydroxide complex **1** in C₆D₆. This is the first direct observation of carbon–oxygen reductive elimination involving an alkyl and hydroxide group to form alcohol in a nonaqueous solvent system. Studies of this reaction indicate that the mechanism is different than that of C–C reductive elimination. Despite hydroxide being a relatively poor leaving group and the reaction taking place in a nonpolar solvent, dissociation of the heteroatom group followed by nucleophilic C–O coupling, similar to the mechanism proposed for other C(sp³)–O

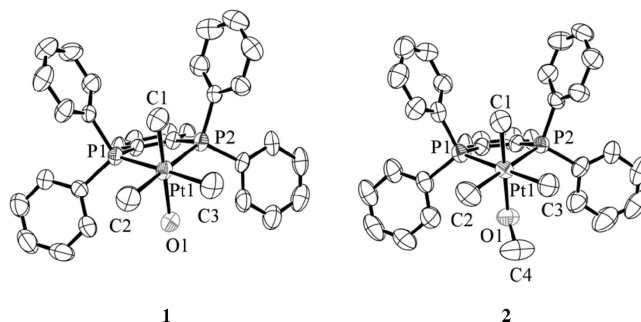


Figure 1. ORTEP drawing of complexes **1** and **2**, with thermal ellipsoids at the 50% probability level. Hydrogen atoms are omitted for clarity.

couplings from Pt(IV),¹⁵ is indicated. Given the rarity of the formation of an alcohol by C(sp³)–O reductive elimination from a metal center^{14a,b} and the promise of this coupling as a product-forming step in catalysis, this mechanistic insight is relevant to rational catalyst design efforts.

In contrast to the C–O reductive elimination reaction observed from the hydroxide complex **1**, thermolysis of the methoxide analog **2** leads primarily to products expected from formal β -hydride elimination followed by C–H reductive elimination. Notably, this *formal* β -hydride elimination occurs from a coordinatively saturated alkoxide complex without an easily accessible *cis* open site. Evidence of alkoxide dissociation is presented and a *dissociative* β -hydride abstraction mechanism, distinct from the traditional β -hydride elimination mechanism of metal alkyls, is proposed for this reaction. This dissociative β -hydride abstraction may be a general and unappreciated decomposition pathway for metal alkoxides and amide species. It is significant that both alkyl C–O reductive elimination and formal β -hydride elimination from the Pt(IV) complexes reported herein involve initial heterolytic cleavage of the Pt–O bond. A similar reaction step for a metal alkyl species (heterolytic M–C bond cleavage) would be unreasonable. Thus, entirely different mechanisms for these fundamental reactions of reductive elimination and β -hydride elimination, distinct from those of metal alkyls, are possible for metal alkoxides.

Results

Synthesis and Characterization of Platinum Complexes 1 and 2. The monomeric Pt(IV) hydroxide and methoxide complexes, *fac*-(dppbz)PtMe₃(OR) (R = H (**1**) and CH₃ (**2**)), were prepared via metathesis reactions of the appropriate potassium salts with the Pt(IV) trifluoroacetate and acetate complexes, respectively. Reaction of *fac*-(dppbz)PtMe₃(O₂CCF₃) with excess KOH proceeds in toluene at 35 °C to form the Pt(IV) hydroxide complex **1**, which was isolated in 95% yield. The analogous Pt(IV) methoxide complex **2** was prepared by reaction of *fac*-(dppbz)PtMe₃(O₂CCH₃) with excess KOMe in toluene at ambient temperature and was isolated in 75% yield. Both **1** and **2** have been characterized by X-ray crystallography, and the ORTEP diagrams appear in Figure 1. Selected bond lengths and angles are presented in Table 1. Complete details of the structures are given in Supporting Information.

Both species **1** and **2** exhibit the characteristic ¹H NMR signals for *fac*-L₂PtMe₃(X) species. In the ¹H NMR spectrum of each species, there are signals for two equivalent equatorial and one axial Pt(IV) methyl groups, with both signals exhibiting coupling to ¹⁹⁵Pt and ³¹P. The ¹H NMR spectrum for **1** in C₆D₆ shows a Pt(IV) hydroxide signal at –2.39 ppm, which exhibits coupling to ¹⁹⁵Pt (²J_{Pt–H} = 13 Hz) as well as to two equivalent

(17) (a) Periana, R. A.; Taube, D. J.; Gamble, S.; Taube, H.; Satoh, T.; Fujii, H. *Science* **1998**, *280*, 560. (b) Stahl, S. S.; Labinger, J. A.; Bercaw, J. E. *Angew. Chem., Int. Ed.* **1998**, *37*, 10235.

(18) Reference 1a, p 90.

(19) Reference 1a, p 95.

(20) Blum, O.; Milstein, D. *J. Am. Chem. Soc.* **1995**, *117*, 4582.

(21) Blum, O.; Milstein, D. *J. Organomet. Chem.* **2000**, *479*, 593–594.

(22) Ritter, J. C. M.; Bergman, R. G. *J. Am. Chem. Soc.* **1998**, *120*, 6826.

(23) Fafard, C. M.; Ozerov, O. V. *Inorg. Chim. Acta* **2007**, *360*, 286.

Table 1. Selected Bond Lengths (Å) and Angles (deg) in Structures of **1** and **2**

1		2	
Pt–C1	2.061(10)	Pt–C1	2.080(6)
Pt–C2	2.087(10)	Pt–C2	2.072(7)
Pt–C3	2.090(9)	Pt–C3	2.095(7)
Pt–P1	2.352(2)	Pt–P1	2.3559(17)
Pt–P2	2.356(2)	Pt–P2	2.3650(17)
Pt–O1	2.116(7)	Pt–O1	2.138(4)
		O1–C4	1.410(10)
		C4–O1–Pt	120.2(5)
P1–Pt–P2	83.98(8)	P1–Pt–P2	83.89(6)
C2–Pt–C3	86.4(4)	C2–Pt–C3	88.1(3)
O1–Pt–P1	88.77(19)	O1–Pt–P1	86.58(14)
O1–Pt–P2	90.0(2)	O1–Pt–P2	87.43(14)
O1–Pt–C2	88.3(4)	O1–Pt–C2	91.1(3)
O1–Pt–C3	88.5(4)	O1–Pt–C3	92.1(2)
O1–Pt–C1	175.7(4)	O1–Pt–C1	177.7(2)

^{31}P nuclei ($^3J_{\text{P-H}} = 2.7$ Hz). In the ^1H NMR spectrum of **2** in C_6D_6 , a methoxide signal is observed at 4.04 ppm with Pt satellites ($^3J_{\text{Pt-H}} = 24.4$ Hz). Finally, in the $^{31}\text{P}\{^1\text{H}\}$ NMR spectra, both **1** and **2** display singlets with ^{195}Pt satellites at 15.3 and 18.2 ppm, with $^1J_{\text{Pt-P}} = 1161$ and 1159 Hz, respectively.

The X-ray structures of **1** and **2** both show a distorted octahedral geometry around the Pt(IV) center with the two structures exhibiting similar angles and bond distances between the phosphorus and platinum atoms. Notably, the axial and equatorial platinum–methyl bond lengths are very similar in **1** (2.06 Å (ax) vs. 2.09 Å (eq)), and the same is observed for **2** (2.08 Å (ax) vs 2.07 and 2.10 Å (eq)), suggesting that the *trans* influence of hydroxide and methoxide are both reasonably similar to that of a triaryl substituted phosphine at a Pt(IV) center.

The Pt–O bond lengths of previously reported Pt(IV) hydroxide complexes range from 1.94 to 2.08 Å,²⁴ yet none of these contain a platinum(IV) hydroxide species wherein the hydroxo-group is *trans* to a methyl group. Similarly, in related structurally characterized platinum(IV) methoxide complexes in which the methoxide ligands are *trans* to hydroxide, hydroperoxide-, methoxide-, acetate-, or pyridine-derived ligands, the Pt(IV)–O bonds range in length from 1.88 to 2.05 Å.^{14b,25} A Pt–O bond length of 2.116(7) Å is observed in the crystal structure of **1**, and the Pt–O bond length of **2** is 2.138(4) Å. These values are significantly longer than previously reported Pt–O bond lengths in Pt(IV) hydroxide and methoxide complexes, presumably due to the stronger *trans* influence of the axial methyl group relative to those of OH, OCH₃, Cl, or NR₃.

Equilibrium between 1 and 2. It has been shown that a hydroxide ligand can exchange with an alcohol at a transition metal center to generate a metal alkoxide species and water in a reversible reaction.^{2a,3a} Similar reactivity was found for the hydroxide and methoxide complexes **1** and **2** which were observed to equilibrate with one another in the presence of methanol or water, respectively (Scheme 1). The equilibrium constant for this reaction was estimated by monitoring a solution prepared by the addition of water (ca. 2 equiv) to **2** in C_6D_6 (6.3 mM) over 3 days at ambient temperature. Examination of the solution by ^1H and $^{31}\text{P}\{^1\text{H}\}$ NMR spectroscopy revealed

(24) Based on a search of Pt(IV) hydroxide crystal structures in the Cambridge Structural Database using Conquest 1.8. Copyright CCDC 2006. Bruno, I. J.; Cole, J. C.; Edgington, P. R.; Kessler, M.; Macrae, C. F.; McCabe, P.; Pearson, J.; Taylor, R. *Acta Crystallogr.* **2002**, *B58*, 389.

(25) (a) Lee, Y.-A.; Jung, O.-S. *Angew. Chem., Int. Ed.* **2001**, *40*, 3868. (b) Rostovtsev, V. V.; Henling, L. M.; Labinger, J. A.; Bercaw, J. E. *Inorg. Chem.* **2002**, *41*, 3608. (c) Dick, A. R.; Kampf, J. W.; Sanford, M. S. *Organometallics* **2005**, *24*, 482.

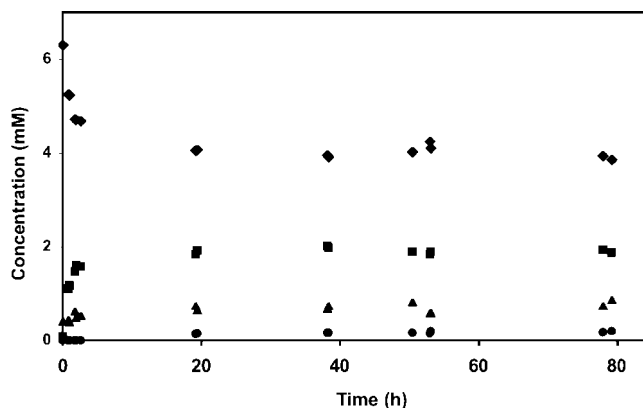


Figure 2. Reactant and product concentrations at 23 °C in C_6D_6 for reaction between **2** ($[\text{2}]_0 = 6.3$ mM) and water ($[\text{water}]_0 = 13$ mM) to form **1** and methanol. Small amounts of **3** ($[\text{3}]_0 = 0.4$ mM) and *fac*-(dppbz)PtMe₃(OCH₂OCH₃) (**4**) also formed. (**1** = ■, **2** = ◆, **3** = ▲, **4** = ●).

the formation of **1** and methanol as the concentration of **2** decreased. Equilibrium was reached after ca. 19 h at ambient temperature (Scheme 1, Figure 2).

The equilibrium constant ($K_{\text{eq}} = \text{ca. } 0.3$) for this reaction was calculated from eq 1 using the equilibrium concentrations measured by ^1H NMR spectroscopy for **1**, **2**, and methanol and calculated for water.²⁶

$$K_{\text{eq}} = \frac{([\text{1}][\text{CH}_3\text{OH}])}{([\text{2}][\text{H}_2\text{O}])} \quad (1)$$

The Pt(II) species (dppbz)PtMe₂, **3**,²⁷ was detected as early as 10 h into the reaction and accounted for 5–10% of the total Pt species in solution at equilibrium. In addition, a small amount (ca. 2–3%) of *fac*-(dppbz)PtMe₃(OCH₂OCH₃) (**4**, *vide infra*) was also observed. The presence of these other products limited the accuracy to which K_{eq} could be determined.²⁸

In a separate experiment, the reverse reaction, that between methanol and **1**, was also demonstrated. A solution of methanol (700 mM) and **1** (14 mM) in THF-*d*₈ at ambient temperature was prepared, and formation of the methoxide complex **2** (ca. 50%) was observed by $^{31}\text{P}\{^1\text{H}\}$ NMR spectroscopy within 10 min. As with the reaction of **2** and water, formation of a small amount of the Pt(II) complex (dppbz)PtMe₂ (**3**) (<10%) was noted.

Thermolysis of 1. Thermolysis of **1** (4.8–9.5 mM) at 120 °C in C_6D_6 yielded the C–O reductive elimination products (dppbz)PtMe₂ (**3**) (74–93%) and methanol (34–68%), as the major organometallic and organic products, respectively (Scheme 2, Table 2). The C–C reductive elimination products (dppbz)-PtMe(OH) (**5**) (7–26%) and ethane (8–25%)²⁹ were also observed in these reactions. Thus, the thermolysis of **1** is similar to that of the related *fac*-L₂PtMe₃(OR) complexes (L₂ = dppe

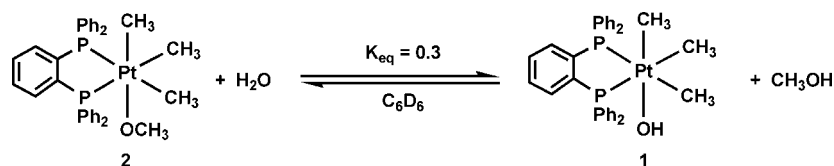
(26) The concentrations of complexes **1–3** and methanol were determined by integration of their respective ^1H NMR signals against an internal standard (toluene). The ^1H NMR signal for water was broad and overlapped with the axial methyl signals of **1** and **3** and therefore was not integrated. The concentration of water used in the calculation of the equilibrium constant was taken to be the initial concentration of water ($[\text{H}_2\text{O}]_0$) with the concentration of methanol formed ($[\text{CH}_3\text{OH}]_t$) deducted from it.

(27) (a) Crumpton, D. M.; Goldberg, K. I. *J. Am. Chem. Soc.* **2000**, *122*, 962. (b) Crumpton-Bregel, D. M.; Goldberg, K. I. *J. Am. Chem. Soc.* **2003**, *125*, 9442.

(28) Complex **3** is a product of decomposition reactions from both **1** and **2**. Methanol can also be generated in these reactions.

(29) As a result of the volatility of several of the organic species (methane, ethane, etc.), it is expected that some portion of these products is present in the headspace of the NMR tube, and therefore integrated yields are low estimates of the actual yields.

Scheme 1



Scheme 2

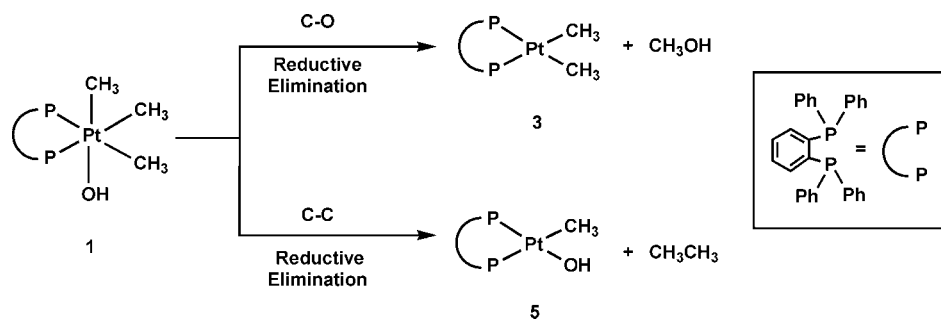


Table 2. Yields of Products from Thermolyses of **1** (4.8–9.5 mM) in C_6D_6 at 120 °C with and without Additives of H_2O (53 mM) and $CsOH \cdot H_2O$ (500 mM)

product	% yield	% yield (with H_2O)	% yield (with $CsOH \cdot H_2O$)
(dppbz)PtMe ₂ (3)	74–93	87–90	93–97
CH_3OH	34–68	51–72	72–76
(dppbz)PtMe(OH) (5)	7–26	10–13	3–7
C_2H_6 ²⁹	8–25	10–13	3–7

or dppbz, OR = carboxylate or aryloxide; dppe = 1,2-bis(diphenylphosphino)ethane in which C–O and C–C reductive elimination reactions occurred competitively.¹⁵ Notably, while the thermolyses of the related *fac*-(dppe)PtMe₃(OAc) and *fac*-(dppbz)PtMe₃(OAr) complexes exhibited reproducible first-order kinetics for the disappearance of the Pt(IV) complexes, the time required for complete conversion of different samples of **1** was observed to range from 5 h to more than 300 h at 120 °C.

In the thermolyses of **1**, although the Pt product of C–O coupling, **3**, was formed in high yield, the organic product, methanol, was observed in significantly lower yield. In addition, the ¹H NMR spectra of the samples upon completion of thermolysis showed the presence of other organic products: methyl formate (0–3%), methane (1–7%), and minor amounts of three unidentified organic products.³⁰ It is also of interest that other Pt(IV) species, *fac*-(dppbz)PtMe₃(OMe) (**2**), *fac*-(dppbz)PtMe₃(OCH₂OCH₃) (**4**), and an unidentified *fac*-(dppbz)PtMe₃(X) species (**6**),³¹ were observed transiently during thermolysis of **1**. The maximum yields of **2**, **4**, and **6** detected at any point in the thermolysis were 12%, 5%, and 2%, respectively. No signals for these species remained visible in either the ¹H or ³¹P NMR spectra at the conclusion of the

(30) The presence of three minor unidentified products was indicated by the observation of three small singlets at 3.49 ppm (ca. 1%), 4.68 ppm (0–5%), and 5.25 ppm (0–3%). Estimated yields of these unknown organic products (calculated on the assumption that the integral of each singlet represents three hydrogens) indicate that the contribution of these species to the overall product distribution is small.

(31) The coupling patterns observed in the ¹H NMR spectrum of complex **6** are similar to those observed for other *fac*-(dppbz)PtMe₃X complexes. The coupling constant (¹J_{PP} = 1114 Hz) associated with the phosphorus signal of this complex in the ³¹P{¹H} NMR spectrum of this complex is comparable to those of other Pt(IV) (1080–1200 Hz), rather than Pt(II) (1700–1800 Hz), dppbz complexes, in which the phosphines are *trans* to methyl groups. No hydroxide signal was observed for **6**; see Experimental Section for NMR characterization of **6**.

Table 3. Yields of Products in Thermolyses of **2** (6–7 mM) in C_6D_6 at 100 °C^{32,33}

platinum product	% yield	organic product	% yield
(dppbz)PtMe ₂ (3)	94–100	(CH ₃) ₂ O	ca. 1
(dppbz)PtMe(OMe) (7)	0–6	C_2H_6 ²⁹	3–7
		CH_2O	ca. 1
		CH_3OCHO	32–44
		(CH ₃ O) ₂ CO	21–33
		CH_4 ²⁹	12–20
		CH_3OH	19–21

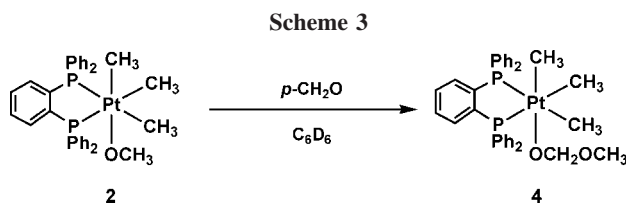
thermolysis of **1**. Mass balance of the Pt was confirmed in the reaction as **3** and **5** were the only Pt-containing species in solution upon reaction completion and the sum of the concentrations of these complexes matched the starting concentration of **1**.

Thermolysis of 2. It was anticipated that if carbon–oxygen reductive elimination were to occur from **2**, (dppbz)PtMe₂ (**3**) and dimethyl ether would be formed. Similarly, C–C reductive elimination from **2** would generate (dppbz)PtMe(OMe) (**7**) and ethane. Thermolysis reactions of **2** at 100 °C in C_6D_6 proceeded to completion over 33–35 days and produced **3** as the major organometallic product (94–100%) (Table 3). However, less than 1% of the corresponding organic product from the C–O coupling reaction, dimethyl ether, was detected. Instead, a variety of other organic products, including methyl formate and dimethyl carbonate, were observed (Table 3).³² The C–C reductive elimination products, (dppbz)PtMe(OMe) (**7**) (0–6%) and ethane (3–7%), were observed as very minor products in this thermolysis reaction.

As was the case in the thermolysis of **1**, transient organometallic species were observed during the reaction. Small amounts of *fac*-(dppbz)PtMe₃(OCH₂OCH₃) (**4**) (maximum of 7%) and *fac*-(dppbz)PtMe₃(OH) (**1**) (maximum of 5%) were detected at intermediate reaction times.

(32) In addition to the species listed in Table 3, two minor unidentified species showing singlets at 3.47 (0–3%) and 3.27 (ca. 1%) ppm in the ¹H NMR spectrum were also evident. Estimated yields of these unknown organic products (calculated on the assumption that the integral of each singlet represents three hydrogens) indicate that the contribution of these species to the overall product distribution is small.

(33) Note that the total yield of organic products, including the estimates for the two unidentified species at 3.47 and 3.27, is 92 ± 9% (see refs 29 and 32). Methane is not included, as it is a byproduct of the formation of formaldehyde, methyl formate, and dimethyl carbonate (vide infra). The total Pt product yield is 100 ± 4%.



Reaction of 2 with Formaldehyde. The formation of species **4** in the thermolysis of **2** suggests a possible insertion reaction of CH_2O into a Pt(IV)–OCH₃ bond. To investigate this proposal, 10 equiv of paraformaldehyde (*p*-CH₂O) was added to **2** in C₆D₆ (7 mM). After only 15 min at ambient temperature, the platinum species identifiable by NMR spectroscopy were **2** and **4** in roughly equal amounts, and a trace amount of **3** (Scheme 3). The addition of an even greater excess of *p*-CH₂O (>33 equiv, not all of which initially dissolved) to **2** in C₆D₆ at ambient temperature resulted in the complete conversion of **2** to *fac*-(dppbz)PtMe₃(OCH₂OCH₃) (**4**) and several unidentified *fac*-(dppbz)PtMe₃(X)³⁴ species within 15 min. The unidentified complexes are most likely the products of multiple insertions of CH₂O into a Pt–O bond based on the similarity of their ¹H and ³¹P{¹H} NMR spectral data to those of **4**.

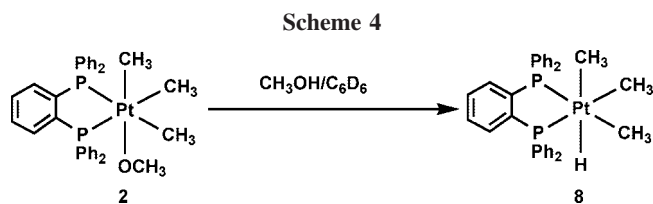
Species **4** was characterized by ¹H and ³¹P{¹H} NMR spectroscopy but could not be successfully isolated from the other insertion products. In a similar fashion, the addition of excess *p*-CH₂O to **1** in C₆D₆ produced several new Pt species, which were assigned by NMR as *fac*-(dppbz)PtMe₃(OCH₂)_xOH complexes. The insertion of formaldehyde into a Pt–O bond is an interesting reaction with very little precedent in the literature.³⁵

Thermolysis of 1 in the Presence of H₂O. Thermolyses of **1** in C₆D₆ in the presence of 10 equiv of water (53 mM) at 120 °C in C₆D₆ produced consistently higher yields of C–O reductive elimination products, **3** (87–90%), and methanol (51–72%) than did thermolyses of **1** without added water (Table 2). The products of C–C reductive elimination, **5** and ethane, were observed as minor products (10–13%). These thermolyses of **1** demonstrated not only increased yields of methanol but also increased consistency in the yields of the different products. For example, the yield of **3** produced in the thermolyses samples of **1** to which no water was added ranged from 74–93%. With the addition of water, this range was narrowed to 87–90%. It should also be noted that in “anhydrous” samples, the heating time required for complete conversion of **1** (5.1–9.5 mM) varied from 5 to 300 h at 120 °C, while the reaction time for **1** at 120 °C in the presence of 10 equiv of water was consistently less than 18 h. Thus, variable amounts of adventitious water in the “anhydrous” samples may have contributed to the lack of uniformity in reaction time and product yields.

A maximum of 7% yield of the methoxide complex **2** was detected at intermediate reaction times during the thermolyses of **1** with added water, less than was observed in the anhydrous thermolyses (12%). Methane was still detected (3–6%), but methyl formate and the three other signals ascribed to minor

(34) The coupling patterns of the ¹H NMR spectra of these complexes are similar to those observed for other *fac*-(dppbz)PtMe₃X complexes. The coupling constants (¹J_{PtP} = 1140–1160 Hz) associated with the phosphorus signals of these complexes in the ³¹P{¹H} NMR spectra of these complexes are comparable to other Pt(IV) (1080–1200 Hz), rather than Pt(II) (1700–1800 Hz), dppbz complexes, in which the phosphines are *trans* to methyl groups.

(35) (a) Litz, K. E.; Banaszak Holl, M. M.; Kampf, J. W.; Carpenter, G. B. *Inorg. Chem.* **1998**, *37*, 6461. (b) For a similar reaction at Ni(II) see ref 8b.



organic products in the ¹H NMR spectrum (vide supra) were not observed.³⁶

Thermolysis of 1 in the Presence of CsOH and H₂O. Thermolysis of **1** in the presence of an excess of CsOH·H₂O (ca. 10 equiv, 50 mM) at 120 °C in C₆D₆ produced much higher and more consistent yields of both **3** (93–97%) and methanol (72–76%) than were seen in the absence of added hydroxide (Table 2). These reactions were complete in ca. 60–70 h. C–C reductive elimination products, **5** and ethane, were evident in low yields (3–7%). No methyl formate was detected but very small amounts of methane (2–3%) were observed in the ¹H NMR spectra.³⁷

Reaction of 2 with Methanol. Upon dissolution of **2** in a 50:50 mixture of CH₃OH/C₆D₆ at ambient temperature, *fac*-(dppbz)PtMe₃H (**8**) was formed within a few minutes, as observed by ¹H NMR spectroscopy (Scheme 4).

Species **2** was completely consumed in under 20 min, but the product **8** was unstable in solution, slowly decomposing to form (dppbz)PtMe₂ (**3**) and methane as previously reported.²⁷ This reaction of **2** was significantly faster than the reaction of **2** in pure C₆D₆, in which complete consumption of the same concentration of **2** typically required over 33 days at 100 °C. Dissolution of **2** in a 50:50 mixture of CD₃OD/C₆D₆ formed *fac*-(dppbz)PtMe₃D (**8-d₁**) within a few minutes by ¹H NMR spectroscopy. Compound **8-d₁** then reacted to form CH₃D and **3** over time.

Thermolysis of fac-(dppbz)PtMe₃(OCD₃) (2-d₃). In order to demonstrate that the source of hydride in **8** was the methoxide ligand in **2**, the partially deuterated complex *fac*-(dppbz)PtMe₃(OCD₃) (**2-d₃**) was prepared from *fac*-(dppbz)PtMe₃(O₂CCH₃) and KOCD₃. Upon thermolysis of **2-d₃**, CH₃D and ethane were observed. No other organic products were observed in significant yield by ¹H NMR spectroscopy. The observation of CH₃D is consistent with the formation of *fac*-(dppbz)PtMe₃D (**8-d₁**), followed by C–D reductive elimination.

Reaction of 2 with [18-crown-6-K][OCD₃]. When an excess of [18-crown-6-K][OCD₃] was added to a thermolysis reaction of **2** in C₆D₆, slow exchange of OCD₃ into the methoxide position of **2** was observed via ¹H NMR spectroscopy in competition with formation of the Pt(II) product (dppbz)PtMe₂ (**3**). After 2 h at 100 °C, ca. 10% of the methoxide complex **2** had been converted to **2-d₃**, while approximately 10% of the initial quantity of **2** had been converted to (dppbz)PtMe₂ (**3**).

(36) The presence of excess water in the thermolyses of **1** also slightly increased the maximum observed yield of the unidentified transient Pt(IV) species (**6**) from 2% to 5%. Notably, it was shown in independent experiments that the addition of water to the Pt(IV) hydroxide complex **1** (5.7 mM in C₆D₆) also resulted in the generation of species **6** at ambient temperature (80% conversion over 4 weeks).³¹ However, pure samples of **6** could not be isolated, which inhibited further characterization. The very slow formation of **6** (weeks at ambient temperature) argues against characterization of **6** as a simple hydrogen-bonded species **1**·H₂O. A sample of **6** in THF was analyzed by ESI-MS and shows a signal at *m/z* = 1478 with an isotopic pattern indicative of two platinum atoms. The molar mass of a dimeric complex with the form of [(dppbz)PtMe₃(OH)·H₂O]₂ would be 1443 g/mol.

(37) In addition, two other trace organic products (4.68 ppm, 0–1%; 5.25 ppm, 3–4%)³⁰ were observed.

Discussion

Reductive Elimination from Pt(IV). A variety of Pt(IV) model complexes have been observed to exhibit sp^3 C–Y (Y = hydrogen, carbon, pnictogen, chalcogen, halogen) reductive elimination.^{15,38–54} Many of these reactions have been studied in detail and their mechanisms elucidated. Reductive eliminations from Pt(IV) complexes can be categorized into two basic mechanisms: one involving concerted bond formation and one proceeding via nucleophilic attack. These two mechanism types generally, but not exclusively, correspond to C–C/C–H and C–heteroatom reductive elimination, respectively.

The concerted reductive elimination of a hydrocarbon from isolated octahedral Pt(IV) complexes via C–H or C–C reductive elimination has been shown to generally require preliminary ligand loss to form a five-coordinate intermediate.²⁷ Reductive elimination of the hydrocarbon then takes place in a concerted fashion through a three-centered (C–M–H or C–M–C) transition state.^{54,55} Initial ligand loss from the six-coordinate compound can occur via ancillary neutral ligand dissociation,^{51,54} dechelation of one “arm” of a polydentate ligand,^{27,39} or dissociation of an anionic X^- ligand to form a cationic five-coordinate species.^{15,38,41} Recently, neutral five-coordinate Pt(IV) alkyl species have been isolated.⁴⁰ These five-coordinate complexes undergo thermally promoted C–C reductive elimination without preliminary ancillary ligand dissociation,⁴⁰ consistent with the idea that the formation of a five-coordinate species allows for direct C–C coupling.

There is one study in the literature that reports evidence for a direct C–H reductive elimination from an octahedral Pt(IV)

complex.²⁷ In that investigation, *fac*-(dppbz)PtMe₃H, **8**, and the related complex *fac*-(dppe)PtMe₃H were proposed to directly eliminate methane from the six-coordinate geometry because of the very similar rates and activation parameters displayed by the two reactions, in spite of the difference in rigidity between the dppe and dppbz ligands.⁵⁶

Bercaw and co-workers have demonstrated that in their Pt(IV) system sp^3 C–O bond formation proceeds via an S_N2 reaction, in which inversion of stereochemistry at carbon was observed.^{17b} Similarly, Groves and Sanford have reported a Rh(III) system that undergoes sp^3 C–O reductive elimination reactions in which both S_N2 hallmarks of inversion of stereochemistry and higher reaction rates for primary than for secondary alkyl groups were observed.¹³ Vedernikov et al. have also reported reductive elimination reactions to form sp^3 C–O bonds in aqueous solution which seem to proceed via nucleophilic attack.^{14a,b} That the nucleophilic attack mechanism has been documented with a variety of metals and heteroatom groups speaks to its generality. However, a couple of recent examples indicate that C–heteroatom coupling from high valent d^6 late metals does not occur exclusively by this nucleophilic attack mechanism. Concerted reductive elimination of methyl iodide from a Rh(III) complex has recently been proposed by Milstein.⁵⁷ Notably, this elimination occurs from a five- rather than a six-coordinate species, perhaps indicating that the intimate mechanism of coupling bears some resemblance to that of C–C reductive elimination reactions from high valent d^6 metal centers. Furthermore, Vedernikov has recently reported a concerted C(sp^3)–O reductive elimination from Pt(IV) to form epoxides.^{14c} Thus, evidently both concerted and nucleophilic attack mechanisms are possible for C(sp^3)–heteroatom bond formation from high valent d^6 metals. Overall, there are relatively few examples of C(sp^3)–heteroatom coupling reactions from d^6 metal centers and the nucleophilic attack pathway appears to be the more common mechanism of reaction.

Thermal reactions of a variety of *fac*-(L₂)PtMe₃X complexes with different X groups (L₂ = dppe, dppbz; X = I, O₂CR, OAr, N(R)SO₂Ar) have been found to yield alkyl C–heteroatom reductive elimination products.^{15,38,41} Evidence has been presented indicating that all of these C–heteroatom couplings occur by a common mechanism as shown in Scheme 5. Following dissociation of X^- and formation of a five-coordinate Pt(IV) cation, nucleophilic attack of the X^- group on the axial methyl group of the Pt(IV) cation forms MeX and (L₂)PtMe₂. Notably, as a five-coordinate Pt(IV) intermediate bearing multiple methyl groups is formed in these systems, C–C reductive elimination to form ethane is also viable and observed.

Mechanism of Reductive Elimination from *fac*-(dppbz)-PtMe₃(OH) (1). The Pt(IV) hydroxide complex **1** undergoes C–O reductive elimination in competition with C–C reductive elimination, behavior that is remarkably similar to that observed for the aryloxy and carboxylate analogues *fac*-(dppbz)PtMe₃(OR) (OR = *p*-XC₆H₄O, OAc, O₂CCF₃).¹⁵ However, the organic products observed upon thermolysis of **1** are more varied than those observed in the thermolysis reactions of the related carboxylate and aryloxy compounds, wherein the products were limited to those resulting directly from competitive C–O and C–C reductive elimination reactions.¹⁵

(38) Goldberg, K. I.; Yan, J.; Breitung, E. M. *J. Am. Chem. Soc.* **1995**, *117*, 6889.

(39) Arthur, K. L.; Wang, Q. L.; Bregel, D. M.; Smythe, N. A.; O'Neill, B. A.; Goldberg, K. I.; Moloy, K. G. *Organometallics* **2005**, *24*, 4624.

(40) (a) Fekl, U.; Goldberg, K. I. *J. Am. Chem. Soc.* **2002**, *124*, 6804. (b) Fekl, U.; Kaminsky, W.; Goldberg, K. I. *J. Am. Chem. Soc.* **2003**, *125*, 15286. (c) Kloek, S. M.; Goldberg, K. I. *J. Am. Chem. Soc.* **2007**, *129*, 3460. (d) Luedtke, A. T.; Goldberg, K. I. *Inorg. Chem.* **2007**, *46*, 8496.

(41) Pawlikowski, A. V.; Getty, A. D.; Goldberg, K. I. *J. Am. Chem. Soc.* **2007**, *129*, 10382.

(42) Madison, B. L.; Thyme, S. B.; Keene, S.; Williams, B. S. *J. Am. Chem. Soc.* **2007**, *129*, 9538.

(43) Cauty, A. J.; Rodemann, T.; Skelton, B. W.; White, A. H. *Organometallics* **2006**, *25*, 3996.

(44) Wik, B. J.; Ivanovic-Burmazovic, I.; Tilset, M.; Van Eldik, R. *Inorg. Chem.* **2006**, *459*, 3613.

(45) Procelewska, J.; Zahl, A.; Liehr, G.; Van Eldik, R.; Smythe, N. A.; Williams, B. S.; Goldberg, K. I. *Inorg. Chem.* **2005**, *44*, 7732.

(46) Jenkins, H. A.; Klempner, M. J.; Prokopchuk, E. M.; Puddephatt, R. J. *Inorg. Chim. Acta* **2003**, *352*, 72.

(47) Jensen, M. P.; Wick, D. D.; Reinartz, S.; White, P. S.; Templeton, J. L.; Goldberg, K. I. *J. Am. Chem. Soc.* **2003**, *125*, 8614.

(48) Vedernikov, A. N.; Caulton, K. G. *Angew. Chem., Int. Ed.* **2002**, *41*, 4102.

(49) Reinartz, S.; White, P. S.; Brookhart, M.; Templeton, J. L. *Organometallics* **2000**, *19*, 3854.

(50) Fekl, U.; Zahl, A.; van Eldik, R. *Organometallics* **1999**, *18*, 4256.

(51) (a) Brown, M. P.; Puddephatt, R. J.; Upton, C. E. E. *J. Chem. Soc., Dalton Trans.* **1974**, 2457. (b) Roy, S.; Puddephatt, R. J.; Scott, J. D. *J. Chem. Soc., Dalton Trans.* **1989**, 2121. (c) Hill, G. S.; Redina, L. M.; Puddephatt, R. J. *Organometallics* **1995**, *14*, 4966. (d) Jenkins, H. A.; Yap, G. P. A.; Puddephatt, R. J. *Organometallics* **1997**, *16*, 1946. (e) Hill, G. S.; Puddephatt, R. J. *Organometallics* **1997**, *16*, 4522. (f) Hill, G. S.; Yap, G. P. A.; Puddephatt, R. J. *Organometallics* **1999**, *18*, 1408.

(52) Stahl, S. S.; Labinger, J. A.; Bercaw, J. E. *J. Am. Chem. Soc.* **1995**, *117*, 9371.

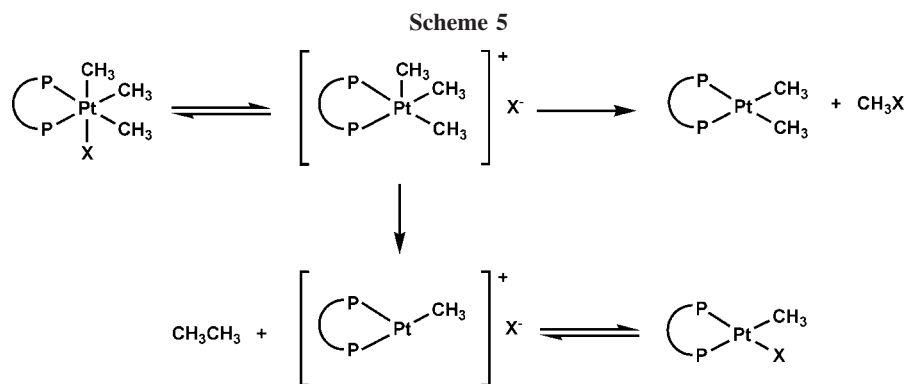
(53) Appleton, T. G.; Clark, H. C.; Manzer, L. E. *J. Organomet. Chem.* **1974**, *65*, 275.

(54) Puddephatt, R. J. *Coord. Chem. Rev.* **2001**, *219*, 157, and references therein.

(55) (a) Hill, G. S.; Puddephatt, R. J. *Organometallics* **1998**, *17*, 1478. (b) Bartlett, K. L.; Goldberg, K. I.; Borden, W. T. *J. Am. Chem. Soc.* **2000**, *122*, 1456.

(56) A computational study of models of **8** and the related dppe system with different substituents on the phosphorus atoms proposed that phosphine dissociation may occur concurrently with C–H reductive elimination. Michel, C.; Laio, A.; Mohamed, F.; Krack, M.; Parrinello, M.; Milet, A. *Organometallics* **2007**, *26*, 1241.

(57) Frech, C. M.; Milstein, D. *J. Am. Chem. Soc.* **2006**, *128*, 12434.



The presence of additional products indicates that other reactions occur concurrently with and/or subsequently to C–O and C–C reductive elimination. Notably, other Pt(IV) species were observed at intermediate times during the reaction. However, the only Pt products observed at the end of the reaction were (dppbz)PtMe₂ (**3**) and (dppbz)PtMe(OH) (**5**).

The reaction of methanol with **1** to produce **2** (Scheme 1) explains the observation of **2** (up to 12%) at intermediate times in the thermolysis of **1** in C₆D₆. On the basis of the equilibrium reaction shown in Scheme 1, it was anticipated that the formation of **2** could be suppressed by the addition of water to the thermolyses of **1**. Indeed, thermolysis of **1** in the presence of a large amount of water (ca. 10 equiv) led to a smaller amount of **2** (7%) observed during the reaction and higher yields of C–O reductive elimination products (dppbz)PtMe₂ (**3**) (from 74–93% to 87–90%) and methanol (from 34–68% to 51–72%).

If the C–O and C–C reductive eliminations from complex **1** proceed through a mechanism of initial dissociation of the hydroxide to form a five-coordinate ionic intermediate analogously to the aryloxide and carboxylate complexes *fac*-(dppbz)PtMe₃(OR) (Scheme 5, X = OR), then the addition of hydroxide would be expected to inhibit C–C coupling. Indeed, thermolysis of **1** in the presence of CsOH·H₂O shows a reduction in the yield of the C–C coupled products, **5** (3–7%) and ethane (3–7%) and produces a larger yield of C–O coupling products, **3** (93–97%) and methanol (72–76%), relative to thermolyses of **1** in the absence of hydroxide. Similar results were found when the thermolyses of *fac*-(dppbz)PtMe₃(OAc) and *fac*-(dppbz)PtMe₃(OAr) were carried out in the presence of added acetate and added aryloxides, respectively; C–C reductive elimination was inhibited and high yields of C–O coupled products were observed.¹⁵

The mechanism shown in Scheme 5 with X = OH is consistent with other observations as well. In the presence of water, the conjugate acid of hydroxide, both the C–O and C–C coupling reactions from **1** clearly proceeded faster, being complete in less than 18 h, compared to up to 300 h without added water. Similar behavior was observed in thermolysis of the analogous Pt(IV) carboxylate, aryloxide, and sulfonamide complexes, *fac*-(dppbz)PtMe₃X (X = O₂CR, OAr, NHSO₂Ar), with addition of the conjugate acids of the X[−] group, HO₂CR, HOAr and NH₂SO₂Ar, respectively.^{15,41,58} Addition of the acid accelerates the formation of the five-coordinate intermediate cation by assisting initial X[−] dissociation through hydrogen bonding. Note that acceleration could be observed regardless of which mechanistic step in the two-step mechanism is rate-

determining. If the first step were rate-limiting, hydrogen bonding would directly increase the rate of the reaction by increasing the rate of this dissociation step. The hydrogen bonding interaction would also be expected to decrease the nucleophilicity of the resulting anion and thus inhibit the second step of the reaction (C–X bond formation). However, an overall acceleration in the C–X reductive elimination could be explained on the basis of a larger influence of the hydrogen bonding on the dissociation step as was observed in the C–O reductive elimination reactions of the aryloxide analogs of **1** and **2**.¹⁵

Although this C(sp³)–OH coupling from **1** may at first seem to be a logical extension of the mechanisms observed in these previous cases of C–O reductive elimination from Pt(IV),¹⁵ it should be noted that dissociation of hydroxide in a nonpolar organic solvent such as benzene is expected to be significantly more unfavorable than dissociation of acetate or aryloxide. Notably, the only other example of directly observed C–O reductive elimination to produce an alcohol is a reaction in aqueous solution wherein hydrogen bonding to the water molecules would be expected to stabilize the hydroxide anion.^{14,59}

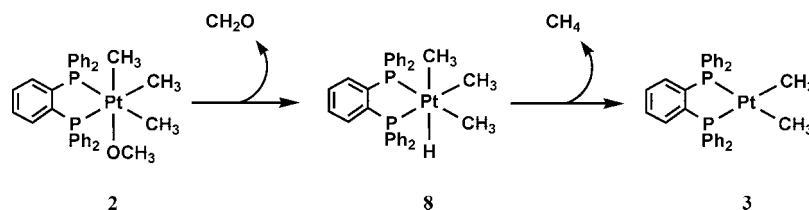
While there seems to be a common mechanism for the reductive elimination reactions of **1** and those of the related carboxylate and aryloxide species, the C–O coupling reaction from **1** adds a new level of complexity, as the product, methanol, is not innocent in the reaction. Like water, methanol accelerates reductive elimination from **1** by assisting the dissociation of hydroxide through hydrogen bonding. As a consequence, the formation of the five-coordinate cationic intermediate is facilitated and both C–O and C–C coupling pathways accelerate as the reaction progresses.¹⁵ This autoaccelerative effect was also observed in the thermolysis of *fac*-(dppbz)PtMe₃(NHSO₂Ar) species in which the product MeNHSO₂Ar can hydrogen bond and assist dissociation of the NHSO₂Ar[−] anion from the starting material.⁴¹ The fact that the methanol product reacts with the platinum hydroxide **1** to generate water and the platinum methoxide complex **2** adds further complications, as the reaction pathways and products resulting from thermolysis of **2** become available (vide infra).

Reductive Elimination in the Thermolysis of *fac*-(dppbz)-PtMe₃(OMe) (2**).** Contrary to our initial expectations based on the observed reactivity of **1**, the organic products of C–O (dimethyl ether) and C–C (ethane) reductive elimination accounted for only a small portion of the products of thermolysis of **2** (1% and 3–7%, respectively, Table 3, vide supra). While

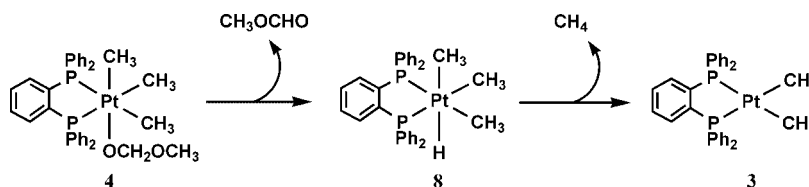
(58) Acceleration of an O–H reductive elimination from a Pd(II)(O₂CR)(H) complex by protic additives was recently reported by Stahl and co-workers. Konnick, M. M.; Stahl, S. S. *J. Am. Chem. Soc.* **2008**, *130*, 5753.

(59) Note that other examples (see ref 17b) are known in which water acts as the nucleophile. There is one other claim in the literature of direct C–O reductive elimination involving hydroxide,¹² but later experiments by Hartwig and Mann on a related system⁵⁴ have suggested that the reaction proceeds via nucleophilic attack of the iridium hydroxide group on methyl iodide and not a reductive elimination step.

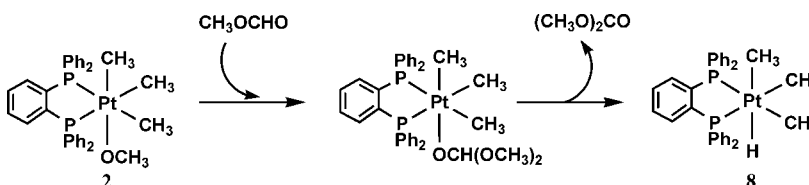
Scheme 6



Scheme 7



Scheme 8



the small contribution from these processes prevented detailed mechanistic study of the reaction, these products are presumably generated by a mechanism similar to the one discussed for reductive elimination from **1**, with the substitution of methoxide for hydroxide as the nucleophile (Scheme 5, X = OMe).

Were C–O reductive elimination to occur from *fac*-(dppbz)PtMe₃(OCH₂OCH₃) (**4**, observed as an intermediate at concentrations of up to 7% of total Pt), it would yield (dppbz)PtMe₂ (**3**) and dimethoxymethane, the latter of which was observed by ¹H NMR spectroscopy (ca. 1%).⁶⁰ The lack of significant quantities of products resulting from C–O reductive elimination (dimethyl ether and dimethoxymethane) in the thermolysis of **2** points toward the existence of one or more lower energy pathways that lead to the other products observed in the reaction.

Formal β -Hydride Elimination from **2.** In the thermolysis of **2**, products expected from formal β -hydride reactions, i.e., formaldehyde (and its further reaction products), methyl formate, dimethyl carbonate, and methane, were far more plentiful than those generated by C–C or C–O reductive elimination from **2**. The initial products expected for β -hydride elimination from **2** would be formaldehyde and *fac*-(dppbz)PtMe₃H (**8**) (Scheme 6).

Thermal studies of **8** have been reported in which **8** was observed to undergo direct C–H reductive elimination to form methane and (dppbz)PtMe₂ (**3**) at 25 °C.²⁷ Therefore, species **8** would not be stable at the 100 °C temperature of the thermolyses. Consistent with this analysis, along with a high yield of **3**, a significant amount of methane (12–20% in solution) was observed by ¹H NMR spectroscopy after the thermolysis of **2** in C₆D₆. When the thermolysis of **2**-d₃ was carried out under identical conditions, CH₃D was the only isotopomer of methane observed, indicating that the source of the hydride in **8** (and subsequently in methane) was the methoxy group of **2**. The actual amount of methane produced probably exceeded that measured by integration of the ¹H NMR signal (12–20%), as some of the methane would enter the headspace of the NMR tube.

Formaldehyde was detected only in trace amounts in the thermolyses of **2**.⁶¹ However, *fac*-(dppbz)PtMe₃(OCH₂OCH₃), **4** was observed at intermediate reaction times during the thermolysis of **2** (maximum concentration of 7% of total Pt). It was shown in an independent experiment that *p*-formaldehyde reacts with **2** at room temperature to form **4**, suggesting that formaldehyde formed in the thermolysis of **2** could insert into the Pt–O bond of **2**, thereby reducing the concentration of formaldehyde. This product of formaldehyde trapping, **4**, can also undergo formal β -hydride elimination to generate *fac*-(dppbz)PtMe₃H (**8**) and methyl formate (Scheme 7). In contrast to formaldehyde, methyl formate does not autopolymerize and was quantified by ¹H NMR (32–44% yield).

A third organic product observed in the thermolysis of **2** is dimethyl carbonate (21–33% yield). In a process similar to the formation of methyl formate, the formation of dimethyl carbonate could involve the insertion of methyl formate into the Pt–O bond of **2** to form a new Pt(IV) species with a dimethoxymethoxide ligand. Subsequent β -hydride elimination would lead to **8** and dimethyl carbonate as illustrated in Scheme 8.

The Pt(IV) dimethoxymethoxide intermediate in Scheme 8 was not detected in the thermolysis of **2**. However, it should be noted that attempts to synthesize Pt(IV) species analogous to **2** with larger alkoxide ligands (e.g., ethoxide, isopropoxide) were unsuccessful, and only **3** and the organic products from formal β -hydride elimination were observed.⁶²

Finally, methanol was detected in 19–21% yield in the thermolysis of **2**. It is possible that methanol was formed by the dehydrogenation of formaldehyde by the methoxide complex (**2**) to form CO, methanol and the hydride complex (**8**). The

(60) Accurate integration of the signals for dimethoxymethane (δ 3.12 (s, 6H), δ 4.38 (s, 2H)) was not possible due to the very close proximity of other peaks.

(61) In organic solvents, formaldehyde autopolymerizes, and so large amounts would not be expected to be observable by ¹H NMR spectroscopy. Walker, J. F. *Formaldehyde*; Chapman & Hall: New York, 1964.

(62) Smythe, N. A. Reactivity Studies of Platinum(IV) Hydroxide and Methoxide Complexes and the Study of Pincer Palladium(II) Complexes as Potential Catalysts for Olefin Epoxidation. Ph.D. Thesis, University of Washington, Seattle, WA, 2004.

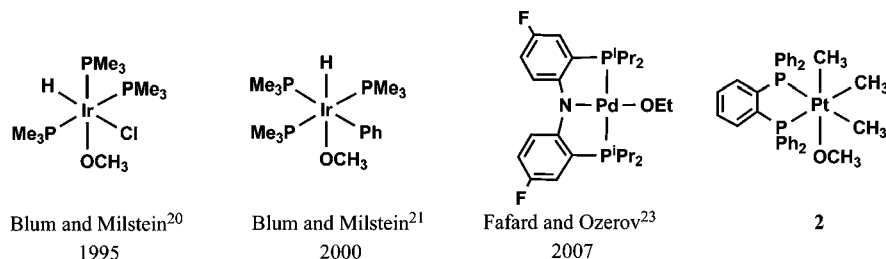
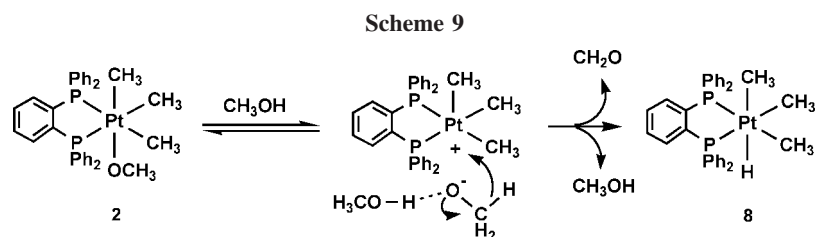


Figure 3. Complexes undergoing alcohol-promoted formal β -hydride elimination.



Pt(IV) hydride **8** would then undergo C–H reductive elimination to form **3** and methane. Such reactivity has previously been reported from Pt(II) methoxide complexes.⁶³ Methanol could also be generated from reaction of **2** and adventitious water as shown in Scheme 1 (vide supra).

An Alcohol-Promoted Dissociative β -Hydride Abstraction Mechanism. The prevalence of products expected from a formal β -hydride elimination in the thermolysis of **2** is surprising for a coordinatively saturated, 18-electron complex. The accepted mechanism of β -hydride elimination, well-established for alkyl groups¹ and generally thought to be operative in similar reactions of alkoxides and amides,⁶⁴ requires an open site on the metal center *cis* to the β -hydrogen-bearing ligand. Complex **2** has no ligand that would easily dissociate to generate an open site *cis* to the methoxide. While dissociation of one arm of the bisphosphine chelate could generate such an open site, earlier studies of reductive elimination from a related complex, (dppbz)PtMe₄ suggest that phosphine dissociation is not kinetically accessible at 100 °C.²⁷ The fact that addition of methanol to a C₆D₆ solution of **2** rapidly generates the hydride complex **8** at room temperature, while the thermal reaction of **2** in C₆D₆ occurs over the course of hours to days at 100 °C, indicates that methanol dramatically accelerates this formal β -hydride elimination process. While this acceleration of β -hydride elimination in the presence of alcohol may seem unusual, we suspect that it is more widespread than is currently appreciated. Two similar examples of acceleration of formal β -hydride elimination of an alkoxide in the presence of alcohol at iridium have been reported,^{20,21} as well as one at palladium.²³ A common feature of **2** and both iridium complexes is that the alkoxides from which the formal β -hydride elimination occurs are saturated, 18-electron d⁶ metal compounds (Figure 3).

For the iridium chloro complex (Figure 3, far left), the reaction to form the analogous hydride complex was substantially accelerated by the presence of methanol. The authors also reported that added P(CD₃)₃ did not incorporate into the complex on the time scale of the reaction. Presumably to accommodate the traditional mechanism of β -hydride elimination previously established in alkyl systems, the authors proposed that the role of methanol was to assist in the dissociation of the chloride to generate an open site *cis* to the methoxide ligand.²⁰ For the phenyl complex (Figure 3, center left), the lack of dissociable ligands and the lack of P(CD₃)₃ incorporation caused Blum and Milstein to argue that methanol was assisting the dissociation of the methoxide ligand itself.²¹ More recently, Fafard and

Ozerov observed that β -hydride elimination from a Pd(II) ethoxide species was dramatically accelerated in the presence of ethanol and similarly proposed alcohol-assisted dissociation of the alkoxide.²³

In light of these examples, we propose that a *dissociative β -hydride abstraction* mechanism may be an important and general pathway in formal β -hydride elimination reactions from late metal alkoxides. In such a process, initial dissociation, often promoted by hydrogen bonding from a Brønsted acid, precedes the abstraction by the metal of a β -hydride, which then resides in the coordination site vacated by the alkoxide. This second step of the proposed mechanism is very similar to the Cannizzaro reaction in organic chemistry.⁶⁵ Scheme 9 depicts this mechanism for the conversion of methoxide **2** to hydride **8** and formaldehyde. While the previous examples from Ir and Pd involve alkoxide dissociation assisted by the alcohol, it is also possible that dissociative reactions could proceed without assistance, albeit under more forcing conditions, as was observed for the thermolysis of **2** in C₆D₆. In addition, this pathway should also be available for other anionic ligands that both are capable of dissociation and bear β -hydrogens. Indeed, this was proposed as a significant decomposition route of *fac*-(dppbz)PtMe₃(N(Me)SO₂Ar), in which products consistent with β -hydride elimination were observed.⁴¹

Thus, the dissociative β -hydride abstraction mechanism either with methanol assistance as shown in Scheme 9 or without methanol assistance under alcohol-free conditions is proposed as a primary reaction pathway for **2**. The results of our previous studies of the effect of conjugate acids, HX, on reaction pathways that proceed via preliminary dissociation of X[−] (reductive elimination from *fac*-L₂PtMe₃X complexes (L₂ = dppe, dppbz, X = OH, O₂CR, OAr, N(H)SO₂Ar))^{15,41} support the role of methanol in assisting methoxide dissociation from **2**. Notably, all of those reactions also proceed, albeit more slowly, in the absence of HX by a similar dissociative pathway. This is also expected to be in the case for dissociative β -hydride abstraction from **2**, which requires forcing thermal conditions in the absence of methanol. That the thermolysis of **2** at 100 °C in the presence of [18-crown-6-K][OCD₃] results in forma-

(63) Bryndza, H. E.; Calabrese, J. C.; Marsi, M.; Roe, D. C.; Tam, W.; Bercaw, J. E. *J. Am. Chem. Soc.* **1986**, *108*, 4805.

(64) Zhao, J.; Hesslink, H.; Hartwig, J. F. *J. Am. Chem. Soc.* **2001**, *123*, 7220.

(65) March, J. *Advanced Organic Chemistry*, 4th ed., John Wiley & Sons: New York, 1992; pp 1233–1235.

tion of **2-d₃** on the same time scale as the β -hydrogen abstraction reaction to form **3** is consistent with the dissociation of methoxide being kinetically competent as a preliminary reaction step.

One other possible mechanism of formal β -hydride elimination from **2** involves dissociation of methoxide from **2** to form a cationic intermediate, which then can abstract a β -hydride from a second molecule of **2**, thereby generating **8**, formaldehyde, and the cation again. Ritter and Bergman have proposed a similar type of behavior in β -hydride elimination from Cp*(PMe₃)Ir(OCH₂R)Ph, in which the presence of iridium cations was observed to catalyze the formation of the corresponding iridium hydrides and aldehydes.²² It is difficult to fully investigate a similar situation in this Pt(IV) system as the five-coordinate Pt(IV) cation is not stable. In addition, the rate of β -hydride elimination from **2** is irreproducible, likely due to adventitious water or a variable amount of another acid. Finally, it would be difficult to measure the rate dependence on the concentration of **2** since it is only sparingly soluble under the reaction conditions. Thus, a bimolecular β -hydride elimination mechanism cannot be ruled out for **2**, although it seems unlikely given the steric bulk of **2**.

Critical in the above discussion is that the Pt(IV) example described herein and the reported Ir(III) and Pd(II) examples all seem to involve an abstraction of an alkoxide β -hydride rather than a traditional β -hydride elimination to a *cis* open site. Since the mechanism involves preliminary dissociation of the alkoxide, the presence of alcohol accelerates the dissociation and therefore the overall reaction. Ozerov's results with a 16-electron Pd(II) ethoxide complex indicate that this alcohol-assisted pathway can even operate under conditions when an open *cis* site is nominally available.²³ Notably, a classical method for preparing metal-hydrides is the addition of base and excess alcohol to a metal halide complex. The presence of alcohol may be key to accelerating a similar dissociative β -hydride abstraction in these cases. In addition, the observation of an analogous type of dissociative β -hydride abstraction in the thermal reactions of sulfonamide complexes *fac*-(dppbz)PtMe₃(N(Me)SO₂Ar)⁴¹ suggests that this reaction pathway is important for other heteroatomic groups as well. Indeed, it is likely that the mechanism depicted in Scheme 9 for **2** is representative of an underappreciated mechanism of formal β -hydride elimination available to both coordinatively saturated and unsaturated late metal complexes with β -hydrogen laden heteroatom ligands. Thus, unlike their metal alkyl counterparts, for metal alkoxides and metal amides, there are at least two viable modes for β -hydride elimination. In addition to the traditional route of transfer of the β -hydride to a *cis* open site, the β -hydride can be abstracted by an open site generated via dissociation of the heteroatom group itself.

Summary and Conclusions

Two fundamental organometallic reactions, reductive elimination and dissociative β -hydride abstraction, were observed as the primary reactions resulting from thermolysis of *fac*-(dppbz)PtMe₃(OH) (**1**) and *fac*-(dppbz)PtMe₃(OMe) (**2**), respectively. Thermolysis of **1** produces (dppbz)PtMe₂ (**3**) and methanol in good yield. The C–O reductive elimination reaction can be optimized by adding water and hydroxide to the thermolysis, resulting in high yields (72–76%) of methanol. This is a rare example of a directly observed alkyl C–O reductive elimination to yield an alcohol. Despite the expected poor leaving group ability of hydroxide in a nonpolar solvent, the mechanistic evidence implicates a C–O reductive elimina-

tion mechanism proceeding via hydroxide dissociation followed by nucleophilic attack on the Pt(IV) methyl group. Thus, the mechanism for C–O coupling is essentially identical to that demonstrated in other C–X couplings from similar *fac*-L₂Pt(IV)Me₃X (X = I, O₂CR, OAr, N(R)SO₂Ar) complexes in which the X anions are significantly better leaving group candidates.^{15,38,41}

Formation of methanol as a product of the thermolysis of **1** has two important effects on the reaction. First, the hydrogen-bonding ability of methanol assists in dissociation of the hydroxide ligand, increasing the rate of both C–O and C–C elimination. Second, methanol can exchange with **1** to form the analogous methoxide, *fac*-(dppbz)PtMe₃(OMe) (**2**). This situation is similar to the behavior noted in reductive elimination to form sulfonamides from *fac*-(dppbz)PtMe₃(NHSO₂Ar),⁴¹ in which the hydrogen-bonding capability of HN(Me)SO₂Ar resulted in both sulfonamide anion exchange and acceleration of elimination.

In contrast to the reactivity observed for **1**, C–O reductive elimination is a very minor reaction in the thermolysis of the Pt(IV) methoxide complex **2**. Instead, products resulting from formal β -hydride elimination are observed. Again, this behavior is similar to that observed for the sulfonamide complexes, in which products of formal β -hydrogen elimination resulted from the decomposition of *fac*-(dppbz)PtMe₃(N(Me)SO₂Ar) species.⁴¹ Both of these systems lack ancillary ligands capable of facile dissociation. Thus, the standard textbook mechanism established for β -hydride elimination involving a concerted four-centered transition state seems implausible. Instead, we propose a dissociative β -hydride abstraction mechanism, in which dissociation of the methoxide or sulfonamide group is followed by hydride abstraction by the metal from the dissociated anion. The lack of appreciable amounts of C–O reductive elimination products in the thermolysis of **2** indicates that β -hydride abstraction from the dissociated methoxide is a lower energy pathway than nucleophilic attack by the methoxide on the methyl group. Thus, β -hydride abstraction may be a complication in reactions for which C–X reductive elimination reactions are desired if the X group bears β -hydrogens. As similar observations of alcohol-promoted formal β -hydride elimination of alkoxides with no accessible open *cis* coordination site have been reported in the past several years, it seems that this alternative mechanism of dissociative β -hydride abstraction may be quite general. Thus, just as multiple mechanisms are possible for reductive elimination reactions (e.g., “concerted” and two-step “dissociation and nucleophilic attack”), depending on the nature of the metal-bound atoms that are forming the bond, more than one common mechanism also appears viable for β -hydride elimination reactions. Depending on the type of metal-bound atom and the availability of a *cis* open site, the reaction can proceed via a traditional β -hydride elimination involving transfer of a hydride to a *cis* open site on the metal, as is seen with metal alkyls, or via a “dissociative β -hydride abstraction” wherein heterolytic metal–ligand cleavage is followed by abstraction of hydride from the dissociated ligand. Thus, our current long-held mechanistic understanding of this fundamental reaction, originally proposed and well-established for metal alkyl complexes, requires amendment when alkoxide or amide ligands are involved in which case a dissociative β -hydride abstraction pathway should also be considered.

Experimental Section

General Considerations. Unless otherwise noted, all transformations were carried out under a N₂ atmosphere in a drybox (O₂

< 1 ppm, H₂O < 0.5 ppm) or using standard Schlenk techniques. THF, benzene, and toluene were distilled under vacuum from sodium/benzophenone ketyl. Pentane was distilled from CaH₂. Methanol was triply distilled from sodium under vacuum. Deuterated solvents were dried by analogous methods and transferred under vacuum. KH was purchased as a suspension in mineral oil, isolated on a fritted glass funnel, washed multiple times with hexanes and pentane, dried under vacuum, and kept in the drybox. *o*-Bis(diphenylphosphino)benzene (dppbz) was purchased from Strem, treated with KH in THF, and recrystallized from THF/pentane. Other reagents, unless specified, were used as received from commercial suppliers. The complexes *fac*-(dppbz)PtMe₃(O₂CCH₃) and *fac*-(dppbz)PtMe₃(O₂CCF₃) were prepared by established literature procedures.¹⁵ [18-crown-6-K][OCD₃] was synthesized according to an established literature procedure for the protio analog.⁶⁶ KOH was produced by the reaction of potassium metal with water (2 equiv) in toluene and left under vacuum for 3 days after removal of the toluene. Celite was dried for >48 h at >150 °C under vacuum. Thermolysis samples were heated in a Neslab Ex-250HT elevated temperature bath. NMR spectra were recorded on Bruker DPX200, AF300, or DRX499 spectrometers. All coupling constants are reported in Hz. ¹H NMR spectra were referenced by using residual solvent peaks and are reported in ppm downfield of tetramethylsilane. ³¹P{¹H} NMR spectra were referenced to external H₃PO₄ (0 ppm). GC/MS data was collected on a Hewlett-Packard 5971 GC-mass spectrometer. Electrospray MS data was collected on a Bruker Esquire ion trap LC-mass spectrometer.

Preparation of *fac*-(dppbz)PtMe₃(OH) (1). A Teflon-stoppered glass vessel was charged with *fac*-(dppbz)PtMe₃(O₂CCF₃) (267 mg, 0.33 mmol), toluene (100 mL), and KOH (387 mg, 6.9 mmol). The reaction mixture was heated to 35 °C for 2 days. The solution was cooled, and excess KH was added to the reaction mixture, which was left to stir for 1 h at ambient temperature. This solution was filtered through a Teflon syringe filter, and the filtrate was reduced in volume to 30 mL in vacuo and left to crystallize. White crystals were harvested, and solvent was reduced under vacuum to 5 mL to yield a second crop of crystals. Combined yield from two crystallizations = 223 mg, 95%. ³¹P{¹H} NMR (C₆D₆): δ 15.3 (s w/Pt satellites, ¹J_{PPt} = 1161). ¹H NMR (C₆D₆): δ -2.39 (t w/Pt satellites, 1H, ³J_{PH} = 2.7, ²J_{PHH} = 13.0, Pt-OH), 0.02 (t w/Pt satellites, 3H, ³J_{PH} = 6.6, ²J_{PHH} = 63.8, Pt-CH₃ *trans* to hydroxide), 1.68 (t w/Pt satellites, 6H, ³J_{PH} = 7.4, ²J_{PHH} = 60.0, Pt-CH₃ *cis* to hydroxide), 6.7–7.4 (m, 20H, aryl protons on dppbz ligand), 8.67 (m, 4H, aryl protons on dppbz ligand). Anal. for C₃₃H₃₄O₂Pt: Calcd C, 56.33; H, 4.87; Found C, 56.38; H, 4.90.

Preparation of *fac*-(dppbz)PtMe₃(OCH₃) (2). Small pieces of potassium metal (880 mg, 22.5 mmol) and methanol (500 μ L, 12.3 mmol) were added to toluene and left to stir for 1 day. The potassium metal was then removed and *fac*-(dppbz)PtMe₃(O₂CCH₃) (130 mg, 0.160 mmol) was added. The solution was stirred for five days and then filtered through a medium porosity fritted glass funnel or a syringe equipped with a Teflon filter. The solvent was removed under vacuum and the product was recrystallized from toluene layered with pentane. Yield = 86.2 mg, 75%. ³¹P{¹H} NMR (C₆D₆): δ 18.2 (s w/Pt satellites, ¹J_{PPt} = 1159). ¹H NMR (C₆D₆): δ 0.01 (t w/Pt satellites, 3H, ³J_{PH} = 6.6, ²J_{PHH} = 64.0, Pt-CH₃ *trans* to methoxide), 1.76 (t w/Pt satellites, 6H, ³J_{PH} = 7.7, ²J_{PHH} = 60.0, Pt-CH₃ *cis* to methoxide), 4.04 (s w/Pt satellites, 3H, ³J_{PH} = 24.4, Pt-OCH₃), 6.7–7.4 (m, 20H, aryl protons on dppbz ligand), 8.44 (m, 4H aryl protons on dppbz ligand). Anal. for C₃₄H₃₆O₂Pt: Calcd.: C, 56.90; H, 5.06; Found: C, 57.11; H, 5.09. *fac*-(dppbz)PtMe₃(OCD₃) was prepared similarly, except for the substitution of methanol-*d*₄ for methanol.

Treatment of Thermolysis Samples. In a typical set of experiments for thermolysis of **1** without additives, complex **1** (20.0

mg, 0.028 mmol) was added in a drybox to a Teflon-stoppered glass vessel and subsequently brought out of the drybox. C₆D₆ (10 mL) was added by vacuum transfer, and then 4.4 mL of this solution was removed in vacuo to concentrate the solution of **1**. In the drybox, toluene was added to the solution as an NMR standard. For each sample, 0.6 mL (0.003 mmol, 5 mM) of this solution was loaded into a medium-walled NMR tube (Wilmad 504-PP), which was subsequently sealed on a vacuum line. In the reactions involving additional H₂O, this reagent (0.035 mmol; 50 μ L of 0.069 M H₂O in C₆D₆ solution) was also added to the NMR tube prior to sealing. For the thermolysis of **1** in the presence of cesium hydroxide, **1** (1.7 mg, 0.0024 mmol), CsOH·H₂O (4.2 mg, 0.025 mmol), toluene as a NMR standard, and C₆D₆ (0.5 mL) were loaded into a medium-walled NMR tube (Wilmad 504-PP) which was subsequently sealed on a vacuum line. For thermolysis of **2** or **2-d**₃, 0.5 mL of a solution of **2** or **2-d**₃ (0.003 mM) and toluene as a NMR standard in C₆D₆ were loaded into a medium-walled NMR tube (Wilmad 504-PP) that had been fitted with a 14/20 ground glass joint.

In all thermolyses, after loading the NMR tube, the sample was affixed to a stopcock adaptor, cooled in a liquid N₂ bath, and evacuated under high vacuum. The tube was then flame-sealed under active vacuum. The sealed NMR tubes were heated, and the reactions were quenched at various time intervals by rapidly cooling the tubes in ice water. Thermolysis tubes were stored in a laboratory freezer (-20 °C) or in liquid N₂ when not being heated or monitored by NMR spectroscopy. All ¹H and ³¹P{¹H} NMR spectra were collected on a Bruker DRX499 spectrometer, averaging the integrals for three acquisitions at a given reaction time. For each acquisition, eight scans were collected with a 60 s recycle delay. Signals for all species were integrated relative to the internal standard (toluene, T₁ = 11 s). Mass balance of Pt complexes (>95%) was confirmed by integration of Pt-CH₃ signals (*trans* to P) against the internal standard at the end of the reaction.

Reaction of **1 with CH₃OH.** In a drybox, **1** (5.0 mg, 0.0071 mmol) and an internal NMR standard (toluene, 1 μ L, 0.01 mmol) were loaded into a medium-walled J. Young NMR tube (Wilmad 504-PP). THF-*d*₈ (0.5 mL) was vacuum transferred into the sample. After initial ¹H and ³¹P{¹H} NMR spectra were collected, this sample was brought back into the drybox, and methanol (0.014 mL, 0.35 mmol, ca. 48 equiv) was added. ¹H and ³¹P{¹H} NMR spectra were collected within 10 min of adding methanol. The reaction was left to react at ambient temperature and was monitored for 3 days by ¹H and ³¹P{¹H} NMR spectroscopy.

Reaction of **2 with H₂O.** In a drybox, **2** (2.4 mg, 0.0033 mmol) and an internal NMR standard (toluene, 0.5 μ L, 0.005 mmol) were loaded into a medium-walled J. Young NMR tube (Wilmad 504-PP). C₆D₆ (0.5 mL) was vacuum-transferred into the sample. After initial ¹H and ³¹P{¹H} NMR spectra were collected, this sample was brought back into the drybox, and water (0.035 mL of a 0.185 M solution in C₆D₆, 0.007 mmol) was added. ¹H and ³¹P{¹H} NMR spectra were collected at least twice per hour for the first 6 h and then at least every 15 h for the next 75 h at ambient temperature. ¹H NMR spectra were integrated against the internal standard.

Reaction of **1 with H₂O.** In a drybox, **1** (10.0 mg, 0.014 mmol) and an internal NMR standard (toluene, 3 μ L, 0.03 mmol) were loaded into a 2 mL volumetric flask. The solution was diluted to 2 mL with C₆D₆; 0.4 mL of this solution was added to a medium-walled NMR tubes. Water (3.0 μ L) was added to the sample, and the tube was frozen and flame-sealed under active vacuum. The sample was thawed and left at ambient temperature. The progress of the reactions was monitored by ¹H and ³¹P{¹H} NMR spectroscopy at various time intervals for at least 4 weeks. ¹H NMR spectra were integrated against the internal standard. Complex **6** was observed to form over time, with a maximum of 80% yield after 4 weeks. NMR characterization of **6**: ³¹P{¹H} NMR (C₆D₆): δ 15.0 (s w/Pt satellites, ¹J_{PPt} = 1114). ¹H NMR: (C₆D₆): δ 0.14 (t w/Pt

(66) Kurcok, P.; Jedlinski, Z.; Kowalczyk, M. *J. Org. Chem.* **1993**, *58*, 4219.

satellites, 3H, $^3J_{\text{PH}} = 7.7$, $^2J_{\text{PH}} = 73.9$, Pt-CH₃ *trans* to O), 1.75 (t w/ Pt satellites, 6H, $^3J_{\text{PH}} = 6.9$, $^2J_{\text{PH}} = 56.3$, Pt-CH₃ *trans* to P), 6.7–8.8 (m, 24H, aryl protons on dppbz ligand).

Reaction of 2 with *p*-CH₂O. In a drybox, **2** (2.5 mg, 0.0035 mmol), *p*-CH₂O (1.0 mg, 0.033 mmol) and benzyl ether (ca. 0.01 mmol, internal standard) were loaded into a medium-walled NMR tube (Wilmad 504-PP). C₆D₆ (0.5 mL) was vacuum-transferred into the tube. The sample was kept frozen while the tube was flame-sealed under active vacuum. The sample was thawed and ¹H and ³¹P{¹H} NMR spectra were acquired within 15 min at ambient temperature. NMR characterization of *fac*-(dppbz)PtMe₃(OCH₂OCH₃) (**4**): ³¹P{¹H} NMR (C₆D₆): δ 20.1 (s w/ Pt satellites, $^1J_{\text{PtP}} = 1139$). ¹H NMR: δ 0.01 (3H, t w/ Pt satellites, $^3J_{\text{PH}} = 6.6$, $^2J_{\text{PH}} = 68.4$, Pt-CH₃ *trans* to O); 1.73 (6H, t w/ Pt satellites, $^3J_{\text{PH}} = 7.5$, $^2J_{\text{PH}} = 58.0$, Pt-CH₃ *trans* to P); 3.53 (s, Pt-OCH₂OCH₃); 5.56 (s w/ Pt satellites, $^3J_{\text{PH}} = 18.7$, Pt-OCH₂OCH₃); 6.7–8.46 (m, 24H, aryl protons on dppbz ligand).

This procedure was also carried out with a larger excess of *p*-CH₂O (6.3 mg, 0.21 mmol) relative to **2** (4.5 mg, 0.0063 mmol) in C₆D₆ (0.8 mL). ¹H and ³¹P{¹H} NMR spectra taken within 15 min at ambient temperature showed complete consumption of **2**. The ¹H NMR spectrum was complex and several singlets, including some with Pt satellites, were observed between 3–5 ppm. These signals are assumed to correspond to OCH₂ units produced by the iterative insertion of formaldehyde into the Pt–O bond of **4** and those of subsequent insertion products. The ³¹P{¹H} NMR spectrum displayed signals assigned to **4** (δ 20.13 ppm, $^1J_{\text{PtP}} = 1138$ Hz) and two other species: δ 20.44 ppm, $^1J_{\text{PtP}} = 1140$ Hz and δ 20.56 ppm, $^1J_{\text{PtP}} = 1134$ Hz. The approximate percentages of total Pt of these species were 30%, 48%, and 22%, respectively, as estimated by ³¹P{¹H} NMR peak heights.

Reaction of 2 with CH₃OH. In a drybox, **2** (2.5 mg, 0.0035 mmol), C₆D₆ (0.3 mL), methanol (0.3 mL), and an internal NMR standard (toluene, 1 μL, 0.01 mmol) were loaded into a medium-walled J. Young NMR tube (Wilmad 504-PP). The reaction was

monitored by ¹H and ³¹P{¹H} NMR spectroscopy. Signals for **2** disappeared within 20 min at ambient temperature and were replaced by those of **8**. Slow decomposition of **8** was observed with signals for **3** and methane appearing over time. The analogous experiment was also conducted with CD₃OD, in which **8-*d*₁** was observed and CH₃D and **3** were observed to form over time.

Reaction of 2 with [18-crown-6-K][OCD₃]. In a drybox, **2** (2.8 mg, 0.0039 mmol), [18-crown-6-K][OCD₃] (32.9 mg, 0.097 mmol), and an internal NMR standard (hexamethylbenzene, 2.1 mg, 0.013 mmol) were loaded into a medium-walled J. Young NMR tube (Wilmad 504-PP). The tube was evacuated under high vacuum, and C₆D₆ (0.42 mL) was vacuum-transferred into the sample. Despite the use of the crown ether, [18-crown-6-K][OCD₃] did not completely dissolve and solid [18-crown-6-K][OCD₃] was observable in the reaction mixture. The reaction was monitored by ¹H NMR spectroscopy. The NMR tube was heated at 100 °C for varying amounts of time, and then the reaction was quenched by rapidly cooling the tube in ice water (0 °C). A direct comparison of the integrals for Pt-CH₃ signals (*trans* to O) and Pt-OCH₃ for **2** in the ¹H NMR spectra was used to determine how much of the methoxide ligand had exchanged with OCD₃. As the reaction progressed, signals for CH₄, CH₃D, and [18-crown-6-K][OCH₃] (OCH₃ δ = 4.12 in C₆D₆) were observed in the ¹H NMR spectra.

Acknowledgment. The authors thank the National Science Foundation (CHE-0137394 and CHE-0719372) for support and Dr. W. Kaminsky for X-ray structural determinations.

Supporting Information Available: CIF files for *fac*-(dppbz)PtMe₃(OH) (**1**) and *fac*-(dppbz)PtMe₃(OMe) (**2**). This material is available free of charge via the Internet at <http://pubs.acs.org>.

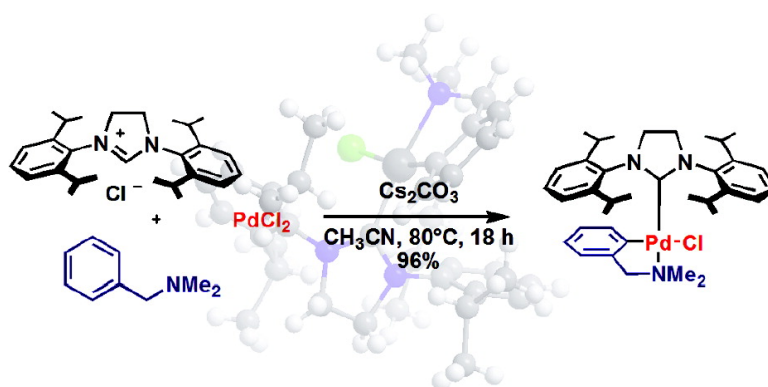
OM800905Q

Practical One-Pot, Three-Component Synthesis of N-Heterocyclic Carbene (NHC) Ligated Palladacycles Derived from *N,N*-Dimethylbenzylamine

Eric Assen B. Kantchev, and Jackie Y. Ying

Organometallics, 2009, 28 (1), 289-299 • DOI: 10.1021/om8008475 • Publication Date (Web): 16 December 2008

Downloaded from <http://pubs.acs.org> on April 22, 2009



More About This Article

Additional resources and features associated with this article are available within the HTML version:

- Supporting Information
- Access to high resolution figures
- Links to articles and content related to this article
- Copyright permission to reproduce figures and/or text from this article

[View the Full Text HTML](#)

Practical One-Pot, Three-Component Synthesis of N-Heterocyclic Carbene (NHC) Ligated Palladacycles Derived from *N,N*-Dimethylbenzylamine

Eric Assen B. Kantchev and Jackie Y. Ying*

Institute of Bioengineering and Nanotechnology, 31 Biopolis Way, The Nanos, Singapore 138669

Received September 2, 2008

Further explorations of the catalytic potential of N-heterocyclic carbene (NHC) ligated palladacycles as catalysts for Pd-mediated transformations have been hampered by the lack of general and practical methods for their synthesis. In this work, we describe a novel, practical approach to NHC-ligated palladacycles by a three-component, one-pot reaction of imidazolium salts, PdCl₂, and *N,N*-dimethylbenzylamine in the presence of excess K₂CO₃ under reflux in reagent-grade acetonitrile in air. 1,3-Diarylimidazolium salts afford the corresponding NHC–Pd(dmba)Cl (dmba = *N,N*-dimethylbenzylamine-κ²N,C) complexes in >80% yield. The conversion of 1,3-diaryl-4,5-dihydroimidazolium and 1,3-dialkylimidazolium or benzimidazolium salts requires the use of stronger base (Cs₂CO₃) and/or higher temperature (100 °C). The Pd-bound chloride anion can be exchanged with silver salts or sodium salts. The NHC–palladacycle adducts have been characterized by single-crystal X-ray crystallography.

Introduction

N-heterocyclic carbenes (NHCs)^{1–3} have recently emerged as high-performance ligands or organocatalysts in a variety of organic reactions,⁴ including Pd-mediated cross-couplings.⁵ In particular, monoligated Pd complexes of bulky *N,N*-diaryl-substituted carbenes⁶ (1–4, Figure 1) have shown high levels of activity and wide applicability. Usually, NHCs 1–4 are prepared by deprotonation of imidazolium or 4,5-dihydroimidazolium salts with strong bases^{1,3} and then captured by suitable Pd precursors. As many Pd-catalyzed cross-coupling reactions involve either basic organometallic reagent or external base, active catalysts can be prepared directly in the reaction mixture starting from common Pd precursors and imidazolium salts, usually in a 1:1 or 1:2 molar ratio.^{7,8} However, since these conditions are not optimized for the complexation of NHC to Pd, often the yield of the active catalyst is low and its chemical composition is hard to control.^{8,9} Therefore, the preparation of well-defined NHC–Pd precatalysts that can be easily activated when introduced into the reaction in high yields under optimized conditions represents a significant improvement over the in situ

catalyst generation. Such precatalysts usually require additional, sacrificial ligands for the stabilization of the active species, a monoligated NHC–Pd complex. In the past few years, IPr–Pd(0) or IPr–Pd(II) derivatives with *p*-quinone,¹⁰ π-allyl,¹¹ carboxylate,¹² 3-chloropyridine,^{9,13} and acetylacetonate (acac)¹⁴ stabilizing ligands have been shown to exhibit high activity in a number

* To whom correspondence should be addressed. E-mail: jyying@ibn.a-star.edu.sg.

(1) General reviews on NHC's and their coordination to metals: (a) Hahn, F. E.; Jahnke, M. C. *Angew. Chem., Int. Ed.* **2008**, *47*, 3122–3172. (b) Herrmann, W. A. *Angew. Chem., Int. Ed.* **2002**, *41*, 1290–1309.

(2) Reviews on NHCs and other stable carbenes: (a) Hahn, F. E. *Angew. Chem., Int. Ed.* **2006**, *45*, 1348–1352. (b) Bourissou, D.; Guerret, O.; Gabbai, F. P.; Bertrand, G. *Chem. Rev.* **2000**, *100*, 39–91. (c) Herrmann, W. A.; Köcher, C. *Angew. Chem., Int. Ed.* **1997**, *36*, 2162–2187.

(3) Arduengo, A. J., III; Harlow, R. L.; Kline, M. J. *Am. Chem. Soc.* **1991**, *113*, 361–363.

(4) For comprehensive treatment of the application of NHC-based catalysts for organic reactions, see: (a) *N-Heterocyclic Carbenes in Transition Metal Catalysis*; Glorius, F., Ed.; Springer-Verlag: Berlin, Heidelberg, 2007; Topics in Organometallic Chemistry Vol. 28. (b) *N-Heterocyclic Carbenes in Synthesis*; Nolan, S. P., Ed.; Wiley-VCH: Weinheim, Germany, 2006.

(5) Review: Kantchev, E. A. B.; O'Brien, C. J.; Organ, M. G. *Angew. Chem., Int. Ed.* **2007**, *46*, 2768–2813.

(6) Arduengo, A. J., III; Krcfczyk, R.; Schmutzler, R. *Tetrahedron* **1999**, *55*, 14523–14534.

(7) (a) Burstein, C.; Lehmann, C. W.; Glorius, F. *Tetrahedron* **2005**, *61*, 6207–6217. (b) Lerma, I. S.; Cawley, M. J.; Cloke, F. G. N.; Arentsen, K.; Scott, J. S.; Pearson, S. E.; Hayler, J.; Caddick, S. J. *Organomet. Chem.* **2005**, *690*, 5841–5848. (c) Hadei, N.; Kantchev, E. A. B.; O'Brien, C. J.; Organ, M. G. *Org. Lett.* **2005**, *7*, 3805–3807. (d) Song, C.; Ma, Y.; Chai, Q.; Ma, C.; Jiang, W.; Andrus, M. B. *Tetrahedron* **2005**, *61*, 7438–7446. (e) Arentsen, K.; Caddick, S.; Cloke, F. G. N.; Herring, A. P.; Hitchcock, P. B. *Tetrahedron Lett.* **2004**, *45*, 3511–3515. (f) Fairlamb, I. J. S.; Kapdi, A. R.; Lee, A. F. *Org. Lett.* **2004**, *6*, 4435–4438. (g) Frisch, A. C.; Zapf, A.; Briel, O.; Kayser, B.; Shaikh, N.; Beller, M. J. *Mol. Catal.* **2004**, *214*, 231–239. (h) Altenhoff, G.; Goddard, R.; Lehmann, C.; Glorius, F. *J. Am. Chem. Soc.* **2004**, *126*, 15195–15201. (i) Altenhoff, G.; Goddard, R.; Lehmann, C. W.; Glorius, F. *Angew. Chem., Int. Ed.* **2003**, *42*, 3690–3693. (j) Gao, C.; Tao, X.; Qian, Y.; Huang, J. *Chem. Commun.* **2003**, 1444–1445. (k) Sato, Y.; Yoshino, T.; Mori, M. *Org. Lett.* **2003**, *5*, 31–33. (l) Yang, C.; Nolan, S. P. *Organometallics* **2002**, *21*, 1020–1022. (m) Yang, C.; Nolan, S. P. *J. Org. Chem.* **2002**, *67*, 597–593. (n) Grasa, G. A.; Viciu, M. S.; Huang, J.; Zhang, C.; Trudell, M. L.; Nolan, S. P. *Organometallics* **2002**, *21*, 2866–2873. (o) Yang, C.; Nolan, S. P. *Synlett* **2001**, 1539–1542. (p) Grasa, G. A.; Viciu, M. S.; Huang, J.; Nolan, S. P. *J. Org. Chem.* **2001**, *66*, 7729–7737. (q) Lee, S.; Hartwig, J. F. *J. Org. Chem.* **2001**, *66*, 3402–3415. (r) Shauffer, S. R.; Lee, S.-W.; Stambuli, J. P.; Hauck, S. I.; Hartwig, J. F. *Org. Lett.* **2000**, *2*, 1423–1426. (s) Cheng, J.; Trudell, M. L. *Org. Lett.* **2001**, *3*, 1371–1374. (t) Zhang, C.; Trudell, M. L. *Tetrahedron Lett.* **2000**, *41*, 595–598. (u) Huang, J.; Grasa, G.; Nolan, S. P. *Org. Lett.* **1999**, *1*, 1307–1309. (v) Huang, J.; Nolan, S. P. *J. Am. Chem. Soc.* **1999**, *121*, 9889–9890.

(8) Hadei, N.; Kantchev, E. A. B.; O'Brien, C. J.; Organ, M. G. *J. Org. Chem.* **2005**, *70*, 8503–8507.

(9) Organ, M. G.; Avola, S.; Dubovyk, I.; Hadei, N.; Kantchev, E. A. B.; O'Brien, C. J.; Valente, C. *Chem. Eur. J.* **2006**, *12*, 4749–4755.

(10) Selvakumar, K.; Zapf, A.; Spannenberg, A.; Beller, M. *Chem. Eur. J.* **2002**, *8*, 3901–3906.

(11) (a) Marion, N.; Navarro, O.; Mei, J.; Stevens, E. D.; Scott, N. M.; Nolan, S. P. *J. Am. Chem. Soc.* **2006**, *128*, 4101–4111. (b) Viciu, M. S.; Navarro, O.; Germaneau, R. F.; Kelly, R. A., III; Sommer, W.; Marion, N.; Stevens, E. D.; Luigi, C.; Nolan, S. P. *Organometallics* **2004**, *23*, 1629–1635. (c) Viciu, M. S.; Germaneau, R. F.; Nolan, S. P. *Org. Lett.* **2002**, *4*, 4053–4056. (d) Viciu, M. S.; Germaneau, R. F.; Navarro-Fernandez, O.; Stevens, E. D.; Nolan, S. P. *Organometallics* **2002**, *21*, 5470–5472.

of Pd-mediated processes. Some of these complexes are now commercially available. Palladacycles¹⁵ are also suitable for the stabilizing ligand role. Under the reaction conditions, palladacycles behave as well-defined precatalysts¹⁶ that release catalytically active, ligandless Pd species in a controlled manner, depending on the temperature, solvent, coreactants, and nature of the cyclopalladated ligand.¹⁷ Ligation of dimeric palladacycles with a single spectator ligand (e.g., a bulky phosphane) enhances the usefulness of the corresponding precatalysts because a more active monoligated phosphane–Pd complex¹⁸ is formed when the precatalyst is activated. For instance, the palladacycle derived from *N,N*-dimethylbenzylamine (**5**; dmbsa)^{19–22}—a commercially available, inexpensive palladacycle precursor—and its phosphane adducts^{19,23} have been shown to be highly active precatalysts for Suzuki–Miyaura, Buchwald–Hartwig, and Heck–Mizoroki reactions, even with such challenging substrates as nonactivated aryl chlorides. NHC-ligated palladacycles have been somewhat less explored. Nolan et al. showed that N,C-palladacycles derived from *N,N*-dimethyl-2-aminobiphenyl ligated with IPr or IMes efficiently mediated Suzuki–Miyaura, Buchwald–Hartwig, enolate arylation, and haloarene dehalogenation reactions even at room temperature.²⁴ The precatalysts were prepared by simple substitution of a bridging chloride in the palladacyclic dimer with the isolated carbenes **1** and **2**. In a similar fashion, a catalyst was prepared very recently by the reaction of the free

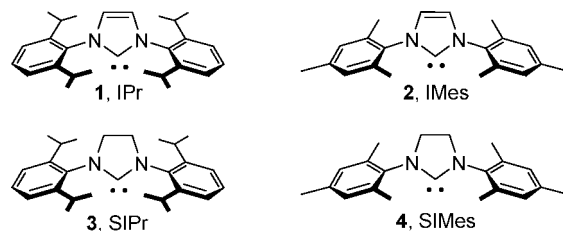


Figure 1. Highly active, versatile NHC ligand for catalytic applications.

IPr carbene and cyclopalladated ferrocenylimine²⁵ donor ligands. The resulting NHC–palladacycles were excellent catalysts for Buchwald–Hartwig amination and Suzuki–Miyaura coupling. Iyer et al. explored N,C-palladacycles derived from *N,N*-dimethylbenzylamine, acetophenone, and benzophenone oximes with simple 1,3-diphenyl-4,5-dihydroimidazolyl-2-ylidene as catalysts for Heck–Mizoroki and Suzuki–Miyaura couplings of activated substrates at low catalyst loadings.²⁶ Remarkably, these complexes were first prepared by Hiraki et al. as early as 1978 via thermal decomposition of the corresponding saturated carbene dimer in situ.²⁷ As that was almost two decades before the potential of NHCs as spectator ligands in Pd-catalyzed organic transformations was recognized in the seminal paper by Herrmann et al.,²⁸ no catalytic studies were reported at that time. Herrmann et al. have prepared a number of NHC-ligated N,C- and P,C-palladacycles in a similar manner.²⁹ Among them, excellent precatalysts for Heck–Mizoroki reaction were found. Very recently, the same group disclosed a more practical procedure for NHC–palladacycle preparation relying on the in situ generation of the carbene in the presence of purified, preformed palladacycles.³⁰ Whereas NaOAc was a suitable base for the unsaturated NHCs, cyclic diaminocarbene precursors still demanded the use of *t*BuOK. Bedford et al. prepared phosphite-derived P,C-palladacycles ligated with SIPr (**3**) and SIMes (**4**) via μ -chloride displacement with the saturated carbene prepared in situ from the corresponding chloroform adduct.³¹ These precatalysts showed moderate activity in the Suzuki couplings of aryl bromides. However, aryl chlorides and alkyl bromides³² failed to couple. With the above in mind, we reasoned that hitherto unknown complexes of [Pd(dmbsa)Cl]₂ (**6**) with carbenes **1–4** have the potential to be highly active and versatile cross-coupling catalysts. However, all the methods discussed above suffer from practical drawbacks, such as handling of isolated moisture- and air-sensitive carbenes and the strong bases required for NHC preparation (for instance, in a glovebox), narrow scope, and/or medium-to-low yields. Thus, the first step

(12) (a) Singh, R.; Viciu, M. S.; Kramareva, N.; Navarro, O.; Nolan, S. P. *Org. Lett.* **2005**, *7*, 1829–1832. (b) Singh, R.; Nolan, S. P. *J. Organomet. Chem.* **2005**, *690*, 5832–5840. (c) Viciu, M. S.; Stevens, E. D.; Petersen, J. L.; Nolan, S. P. *Organometallics* **2004**, *23*, 3752–3755. (d) Jensen, D. R.; Schultz, M. J.; Mueller, J. A.; Sigman, M. S. *Angew. Chem., Int. Ed.* **2003**, *42*, 3810–3813.

(13) O'Brien, C. J.; Kantchev, E. A. B.; Valente, C.; Hadei, N.; Chass, G. A.; Lough, A.; Hopkinson, A. C.; Organ, M. G. *Chem. Eur. J.* **2006**, *12*, 4743–4748.

(14) (a) Marion, N.; de Frémont, P.; Pujik, I. M.; Ecarnot, E. C.; Amoroso, D.; Bell, A.; Nolan, S. P. *Adv. Synth. Catal.* **2007**, *349*, 2380–2384. (b) Marion, N.; Ecarnot, E. C.; Navarro, O.; Amoroso, D.; Bell, A.; Nolan, S. P. *J. Org. Chem.* **2006**, *71*, 3816–3821. (c) Navarro, O.; Marion, N.; Scott, N. M.; Gonzalez, J.; Amoroso, D.; Bell, A.; Nolan, S. P. *Tetrahedron* **2005**, *61*, 9716–9722.

(15) General overview on palladacycles: Dupont, J.; Consorti, C. S.; Spencer, J. *Chem. Rev.* **2005**, *105*, 2527–2571.

(16) Reviews on catalytic applications of palladacycles: (a) Beletskaya, I. P.; Cheprakov, A. V. *J. Organomet. Chem.* **2004**, *689*, 4055–4082. (b) Bedford, R. B. *Chem. Commun.* **2003**, 1787–1796. (c) Dupont, J.; Pfeffer, M.; Spencer, J. *Eur. J. Inorg. Chem.* **2001**, 1917–1927.

(17) (a) Corma, A.; García, H.; Leyva, A. *Tetrahedron* **2005**, *61*, 9848–9854. (b) Beletskaya, I. P.; Kashin, A. N.; Karlstedt, N. B.; Mitin, A. V.; Cheprakov, A. V.; Kazankov, G. M. *J. Organomet. Chem.* **2001**, *622*, 89–96.

(18) Review: Christmann, U.; Vilar, R. *Angew. Chem., Int. Ed.* **2005**, *44*, 366–374.

(19) Bedford, R. B.; Cazin, C. S. J.; Coles, S. J.; Gelbrich, T.; Horton, P. N.; Hursthouse, M. B.; Light, M. E. *Organometallics* **2003**, *22*, 987–999.

(20) Pfeffer, M. *Inorg. Synth.* **1989**, *26*, 211–214.

(21) (a) Janecki, T.; Jeffreys, J. A. D.; Pauson, P. L.; Pietrzykowski, A.; McCullough, K. J. *Organometallics* **1987**, *6*, 1553–1560. (b) Cockburn, B. N.; Howe, D. V.; Keating, T.; Johnson, B. F. G.; Lewis, J. *Dalton Trans.* **1973**, 404–410. (c) Kasahara, A.; Izumi, T. *Bull. Chem. Soc. Jpn.* **1969**, *42*, 1765–1766. (d) Cope, A. C.; Friedrich, E. C. *J. Am. Chem. Soc.* **1968**, *90*, 909–913. (e) Bedford, R. B.; Cazin, C. S. J.; Coles, S. J.; Gelbrich, T.; Hursthouse, M. B.; Scordia, V. J. M. *Dalton Trans.* **2003**, 3350–3356.

(22) Thompson, J. M.; Heck, R. F. *J. Org. Chem.* **1975**, *40*, 2667–2674.

(23) (a) Bedford, R. B.; Hazelwood, S. L.; Limmert, M. E.; Brown, J. D.; Ramdeehul, A. R.; Cowley, A. R.; Coles, S. J.; Hursthouse, M. B. *Organometallics* **2003**, *22*, 1364–1371. (b) Schnyder, A.; Ingolise, A. F.; Studer, M.; Blaser, H.-U. *Angew. Chem., Int. Ed.* **2002**, *41*, 3668–3871.

(24) (a) Navarro, O.; Marion, N.; Onishi, Y.; Kelly, R. A., III; Nolan, S. P. *J. Org. Chem.* **2006**, *71*, 685–692. (b) Navarro, O.; Kelly, R. A., III; Nolan, S. P. *J. Am. Chem. Soc.* **2003**, *125*, 16194–16195. (c) Viciu, M. S.; Kelly, R. A.; Stevens, E. D.; Naud, F.; Studer, M.; Nolan, S. P. *Org. Lett.* **2003**, *5*, 1479–1482.

(25) (a) Li, J.; Cui, M.; Yu, A.; Wu, Y. *J. Organomet. Chem.* **2007**, *692*, 3732–3742. (b) Li, J.-Y.; Yu, A.-J.; Wu, Y.-J.; Yu, Z.; Du, C.-X.; Yang, H.-W. *Polyhedron* **2007**, *26*, 2629–2637.

(26) Iyer, S.; Jayanthi, A. *Synlett* **2003**, 1125–1128.

(27) Hiraki, K.; Onishi, M.; Sewaki, K.; Sugino, K. *Bull. Chem. Soc. Jpn.* **1978**, *51*, 2548–2550.

(28) Herrmann, W. A.; Elison, M.; Fischer, J.; Köchter, C.; Arthus, G. R. *J. Angew. Chem., Int. Ed.* **1995**, *34*, 2371–2373.

(29) (a) Frey, G. D.; Schütz, J.; Herdtweck, E.; Herrmann, W. A. *Organometallics* **2005**, *24*, 4416–4426. (b) Tanase, A. D.; Frey, G. D.; Herdtweck, E.; Hoffmann, S. D.; Herrmann, W. A. *J. Organomet. Chem.* **2007**, *692*, 3316–3327.

(30) Frey, G. D.; Schütz, J.; Herrmann, W. A. *J. Organomet. Chem.* **2006**, *691*, 2403–2408.

(31) Bedford, R. B.; Betham, M.; Blake, M. E.; Frost, R. M.; Horton, P. N.; Hursthouse, M. B.; López-Nicolás, R.-M. *Dalton Trans.* **2005**, 2774–2779.

(32) Bedford, R. B.; Betham, M.; Coles, S. J.; Frost, R. M.; Hursthouse, M. B. *Tetrahedron* **2005**, *61*, 9663–9669.

Scheme 1. One-Pot, Three-Component Synthesis of NHC–Pd(dmab)Cl from Imidazolium Salts

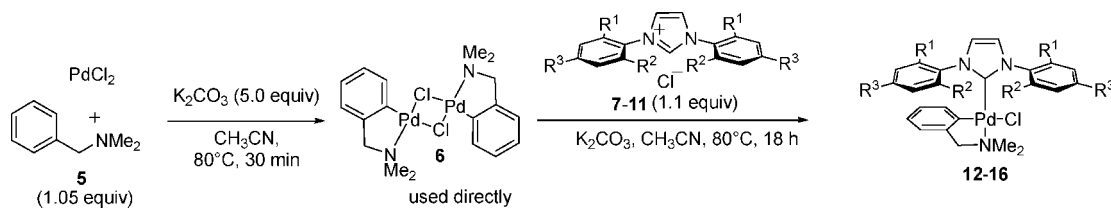


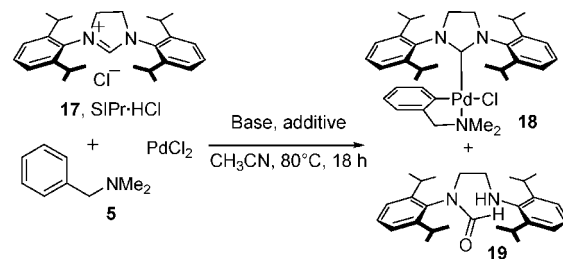
Table 1. Yields of NHC-Ligated Palladacycles from Scheme 1

entry	NHC·HCl	R ¹	R ²	R ³	yield, %
1	none				98 (6)
2	IPr·HCl (7)	<i>i</i> Pr	<i>i</i> Pr	H	82 (12)
3	IEt·HCl (8)	Et	Et	H	81 (13)
4	IMes·HCl (9)	Me	Me	Me	96 (14)
5	ITbp·HCl (10)	<i>t</i> Bu	H	H	81 (15)
6	IPr ^p ·HCl (11)	<i>i</i> Pr	H	H	86 (16)

toward successful catalysts³³ would be to develop a practical and general synthetic method for preparing a range of NHC–palladacycle adducts.

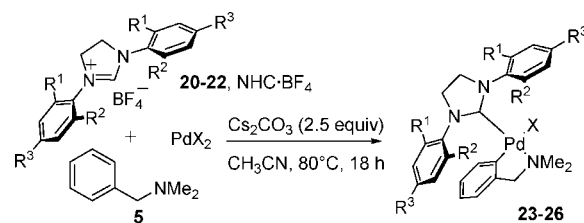
Results and Discussion

Synthesis of NHC–Palladacycles from 1,3-Diarylimidazolium Salts and Their 4,5-Dihydro Analogues. We reasoned that the addition of an equimolar amount of *N,N*-dimethylbenzylamine (**5**) to PdCl₂ would lead to formation of a 1:1 adduct, which could be converted to the corresponding dimeric palladacycle **6** upon addition of a weak base. Moreover, if the same base could also be used to generate NHC in situ from imidazolium salts, then the desired NHC-ligated palladacycles would be formed directly, without any intermediate isolation. Our initial attempts to carry out the palladacycle formation using PdCl₂/K₂CO₃ or Pd(OAc)₂ in a number of solvents (e.g., CH₂Cl₂, toluene, THF, dioxane, and neat **5**) resulted in rapid decomposition of the reactants and formation of Pd black. However, heating of PdCl₂ and the amine **5** (1.00 and 1.05 equiv, respectively) in CH₃CN led to the formation of a dark orange, clear solution, which turned canary yellow within 5 min upon the addition of 5 equiv of K₂CO₃ at that temperature (Scheme 1). The known palladacyclic dimer **6**²⁰ was isolated in 98% yield (Table 1, entry 1). Encouraged by these results, we added the commercially available IPr·HCl (**7**; 1.10 equiv) to the crude palladacyclic solution at 80 °C. After the mixture was stirred for 18 h, complex **12** was isolated in 82% yield (Table 1). The reaction also proceeded well with other imidazolium salts. The known IEt·HCl (**8**)^{8,34} and the commercially available IMes·HCl (**9**) led to the corresponding NHC-ligated palladacycles **13** and **14** (81% and 96% isolated yields, respectively). Hitherto unknown, less sterically hindered ligands carrying only one ortho substituent on the N-bound aryl group, *t*Bu (ITbp·HCl, **10**) or *i*Pr (IPr^p·HCl, **11**), also gave the corresponding complexes in

Table 2. Optimization of the Conditions for Synthesis of the SIPr–Pd(dmab)Cl Complex (**18**)

entry	base (amt, equiv)	additive	yield, %	
			18	19
1	K ₂ CO ₃ (5.0)	none	34	26
2	K ₂ CO ₃ (5.0)	4 Å MS	74	7
3	Cs ₂ CO ₃ (2.5)	4 Å MS	96	<2

Table 3. Synthesis of NHC–Pd(dmab)X (X = Cl, Br) Complexes from 1,3-Diaryl-4,5-dihydroimidazolium Salts



entry	PdX ₂	NHC·HBF ₄	R ¹	R ²	R ³	yield, % ^a
1	PdCl ₂	SIMes·HBF ₄ (20)	Me	Me	Me	98 (23)
2	PdBr ₂	SIMes·HBF ₄ (20)	Me	Me	Me	67 (24)
3	PdCl ₂	SITbp·HBF ₄ (21)	<i>t</i> Bu	H	H	90 (25)
4	PdCl ₂	SIPr ^p ·HBF ₄ (22)	<i>i</i> Pr	H	H	80 (26)

^a The reactions were conducted in the presence of 4 Å molecular sieves.

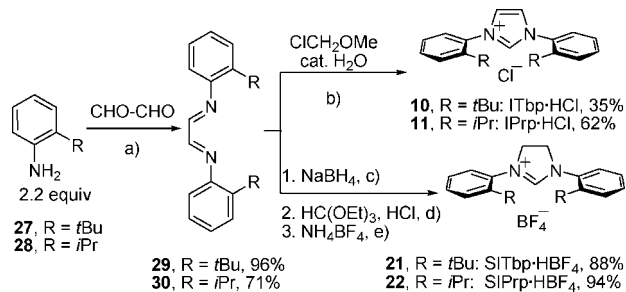
similarly high yields (81% for **15** and 86% for **16**). We further extended the scope of the reaction to the analogous saturated carbenes. When the commercially available SIPr·HCl (**17**) was used under the standard conditions, the corresponding SIPr–Pd(dmab)Cl complex (**18**) was obtained in moderate yield, which was contaminated with significant amounts of unreacted carbene precursor and *N,N'*-bis(2,6-diisopropylphenyl)-*N*-formylethylenediamine (**19**), a product of base-promoted hydrolytic ring opening of the carbene precursor (Table 2). This result can be explained by taking the lower acidity of the 4,5-dihydroimidazolium salts (compared to that of the unsaturated analogues) and their susceptibility to hydrolysis into account. The addition of powdered 4 Å molecular sieves at the beginning of the reaction suppressed the undesirable 4,5-dihydroimidazolium salt hydrolysis without introducing major operational hurdles into the process. The use of a stronger base (Cs₂CO₃) yielded the targeted product **18** in almost quantitative yield (96%). Under these conditions, the commercially available 1,3-bis(2,4,6-trimethylphenyl)-4,5-dihydroimidazolium tetrafluoroborate (**20**; SIMes·HBF₄) produced the corresponding NHC-ligated palladacycle **23** in similarly high yield (Table 3, entry 1) without

(33) Kantchev, E. A. B.; Peh, G.-R.; Zhang, C.; Ying, J. Y. *Org. Lett.* **2008**, *10*, 3949–3952.

(34) Sprengers, J. W.; Wassenaar, J.; Clement, N. D.; Cavell, K. J.; Elsevier, C. J. *Angew. Chem., Int. Ed.* **2005**, *44*, 2026–2029.

(35) While this work was in progress, precursors to ligands **21**^{35a} and **22**^{35b,c} and/or metal complexes thereof were prepared independently: (a) Kuhn, K. M.; Grubbs, R. H. *Org. Lett.* **2008**, *10*, 2075–2077. (b) Stylianides, N.; Danopoulos, A. A.; Pugh, D.; Hancock, F.; Zanotti-Gerosa, A. *Organometallics* **2007**, *26*, 5627–5635. (c) Stewart, I. C.; Ung, T.; Pletnev, A. A.; Berlin, J. M.; Grubbs, R. H.; Schrodi, Y. *Org. Lett.* **2007**, *9*, 1589–1592.

(36) For a recent report of similar atropisomers caused by bulky *N*-aryl substituents in 4,5-dihydroimidazol-2-ylidenes, see: Luan, X.-J.; Mariz, R.; Gatti, M.; Costabile, C.; Poater, A.; Cavallo, L.; Dorta, R. *J. Am. Chem. Soc.* **2008**, *130*, 6848–6858.

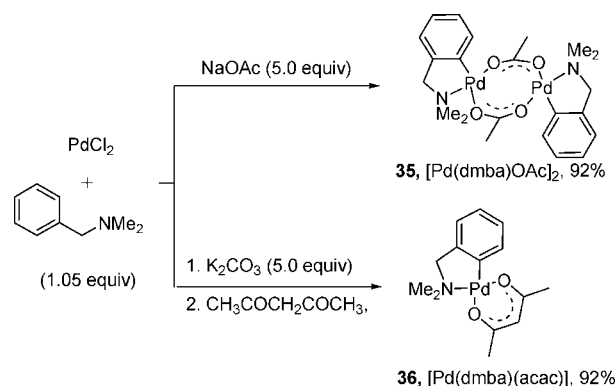
Scheme 2. Synthesis of Novel 1,3-Bis(*o*-alkylaryl)-Substituted NHC Ligand Precursors^a


^a Conditions: (a) MeOH–H₂O (10:1), room temperature, 1.5–18 h; (b) THF, 40 °C, 18 h; (c) MeOH–THF (1:1), reflux, 30 min; (d) concentrated HCl (1.2 equiv), 120 °C, 1 h; (e) H₂O, room temperature, 15 min.

any formation of the corresponding hydrolysis product. The use of PdBr₂ instead of PdCl₂ resulted in the preparation of an analogous complex containing bromide as the counterion at a somewhat lower yield (**24**, 67%) (Table 3, entry 2). Less sterically hindered analogues (**21**, **22**)³⁵ also formed palladacyclic complexes in excellent yields (90% for **25** and 80% for **26**) (Table 3, entries 3 and 4) under these conditions. Surprisingly, compound **25** was obtained as a mixture of two inseparable isomers in a molar ratio of 2.6:1 (¹H NMR spectroscopy). The X-ray single-crystal structure of complex **25** (Figure 2e) showed the expected trans configuration between the carbene carbon and the dimethylamino ligand. Most likely, the two isomers are atropisomers that only exist in solution and arise from restricted rotation around one or more bonds in the saturated NHC ligand carrying *N*-2-*tert*-butylphenyl substituents.³⁶

The novel carbene precursors used in this work were prepared from the corresponding *N,N*-diarylazabutadienes (**29** and **30**) (Scheme 2) by either treatment with chloromethyl ethyl ether to yield the unsaturated imidazolium salts ITbp·HCl (**10**, 35%) and IPrp·HCl (**11**, 62%) or reduction with NaBH₄ followed by cyclization with triethyl orthoformate/HCl to form the corresponding 4,5-dihydro analogues.^{6,8} For easier purification, the saturated carbene precursors were isolated as tetrafluoroborates (SITbp·HBF₄, **21**, 88%; SIPrp·HBF₄, **22**, 94%) after simple precipitation with NH₄BF₄ from aqueous solution.

Anion Exchange Reactions of NHC–Palladacycle Chlorides. The nature of the Pd-bound anion could potentially affect the ease of activation of the palladacyclic precatalysts. Therefore, we endeavored to develop methods for preparing NHC–palladacycles carrying anions other than chloride or bromide. Anion exchange between **12** and various Ag salts resulted in the formation of the corresponding carboxylate, sulfonate, or hexafluorophosphate analogues **31–34** (Table 4) in high yields. As hexafluorophosphate is a noncoordinating anion, the product was isolated as the acetonitrile adduct (1:1). This anion-exchange reaction is driven by the formation of insoluble AgCl. Hence, we reasoned that the limited solubility of NaCl or KCl in acetonitrile could allow similar reactions to take place with the less expensive Na or K salts, allowing for the palladacycle formation, NHC ligation, and anion exchange to be combined in a single synthetic operation without isolation of any intermediates. Treatment of amine **5** with PdCl₂ in refluxing acetonitrile using NaOAc instead of K₂CO₃ resulted in a clean formation (92% isolated yield) (Scheme 3) of the known²² acetate-bridged dimeric palladacycle **35**. Similarly, the addition of acetylacetonone (acac-H) to the crude palladacycle

Scheme 3. Anion-Exchange Reactions of in Situ Prepared Palladacycles^a


^a Conditions: CH₃CN, 80 °C, 30–45 min.

Table 4. Anion Exchange of IPr–Pd(dmmba)Cl (12**) with Silver Salts**

entry	AgX	solvent	yield, %
1	AgOAc	CH ₂ Cl ₂ –acetone (4:1)	96 (31)
2	AgTFA ^a	CH ₂ Cl ₂ –acetone (4:1)	99 (32)
3	AgOTf ^b	CH ₂ Cl ₂ –acetone (4:1)	96 (33)
4	AgPF ₆	CH ₂ Cl ₂ –CH ₃ CN (5:1)	97 (34) ^c

^a TFA = trifluoroacetate. ^b Tf = trifluoromethylsulfonyl. ^c The compound was obtained as the Pd-bound acetonitrile adduct (Figure 2).

Table 5. One-Pot, Four-Component, Sequential NHC–Palladacycle Synthesis and Anion Exchange

entry	X	R ¹	R ²	yield, %
1	I	<i>t</i> Bu	H	96 (37 , X = I)
2	OAc	<i>i</i> Pr	<i>i</i> Pr	61 (12 , X = Cl) + 13 (31 , X = OAc)
3	TFA	<i>i</i> Pr	<i>i</i> Pr	46 (12 , X = Cl) + 43 (32 , X = TFA)
4	OTf	<i>i</i> Pr	<i>i</i> Pr	94 (33 , X = OTf)

chloride **6** (using 5 equiv of K₂CO₃ as the base) led to the formation of the known³⁷ complex [Pd(dmmba)(acac)] (**36**) in 92% isolated yield. Next, we integrated the in situ NHC–palladacycle preparation protocol and anion exchange by simply adding the corresponding Na salt (3 equiv) and heating for an additional 30 min before workup (Table 5). Whereas the use of NaI gave complete conversion to the corresponding NHC-ligated Pd–I palladacycle **37**, the use of sodium carboxylates resulted in incomplete anion exchange. Sodium acetate yielded 61% of the chloride-ligated complex **12** and its acetate analogue **31** (13%) and sodium trifluoroacetate yielded 46% of **12** and 43% of the trifluoroacetate analogue **32**. In contrast, complete ion exchange was observed with sodium trifluoromethanesulfonate, and complex **33** was obtained in 94% yield.

(37) Reichert, B. E.; West, B. O. *J. Organomet. Chem.* **1974**, *71*, 291–297.

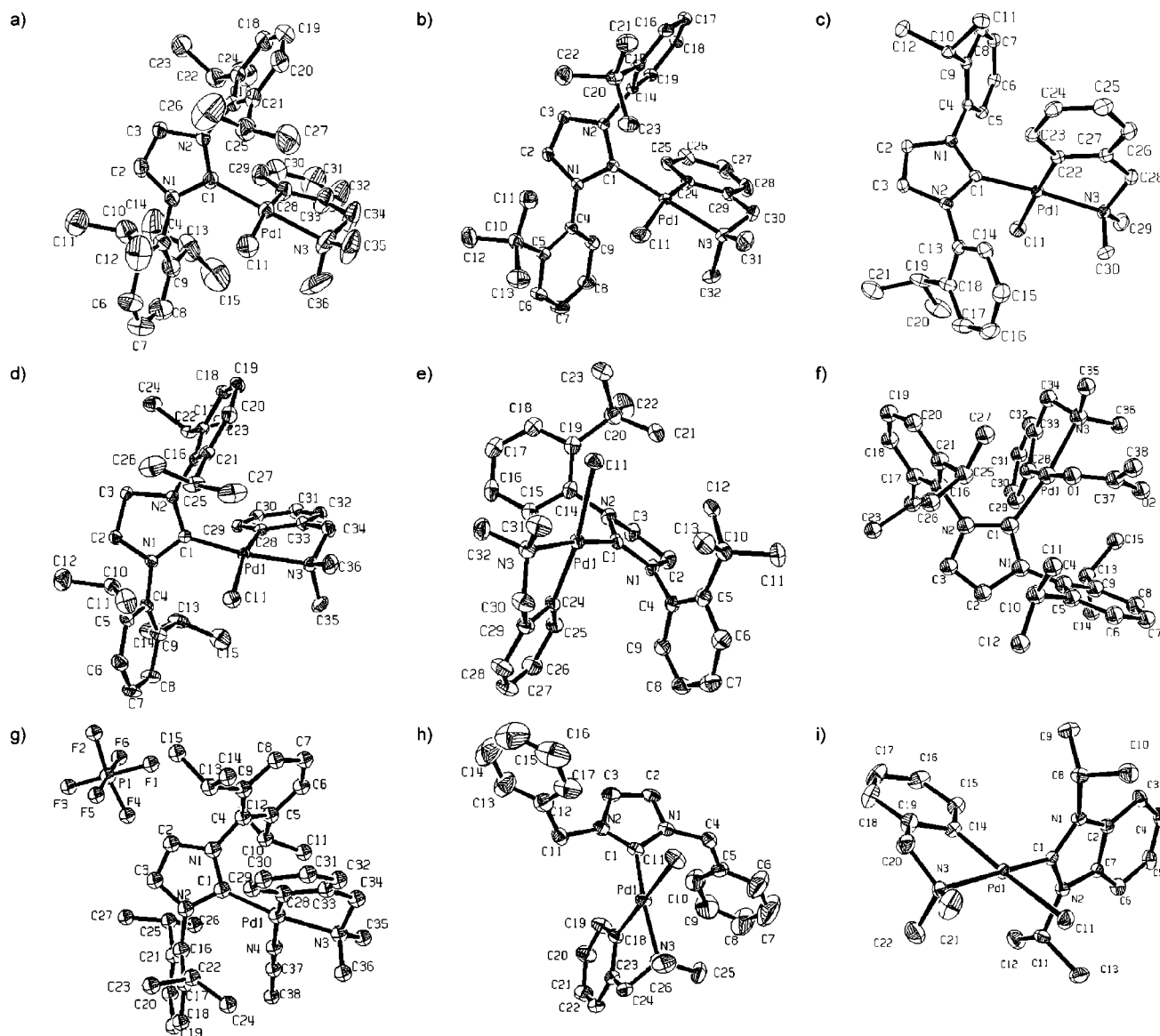


Figure 2. ORTEP representations of the X-ray single-crystal structures of NHC–palladacycles: (a) **12**; (b) **15**; (c) **16**; (d) **18**; (e) **25**; (f) **31** (the unit cell contains two molecules of **31** and one molecule of CH_2Cl_2 ; only one molecule of **31** is shown for clarity); (g) **33**; (h) **42**; (i) **45**. The thermal ellipsoids were drawn at the 30% probability level, and the hydrogen atoms were omitted for clarity.

Synthesis of NHC–Palladacycles from 1,3-Dialkylimidazolium and 1,3-Dialkylbenzimidazolium Salts. Our initial experiments with 1,3-dibenzylimidazolium hexafluorophosphate³⁸ (**38**) under the conditions of Scheme 1 resulted in only 4% of the expected product **42** (Table 6). The use of Cs_2CO_3 at 80 and 100 °C resulted in 22% and 31% of **42**, respectively. The reaction mixture at the end point appeared dark, with a significant amount of Pd black present. Shortening the reaction time to 30 min led to an improvement in product yield to 78%. In an analogous fashion, commercially available 1,3-dimethylimidazolium chloride (**39**) yielded 67% and 45% of the corresponding complex **43** at 30 min and 18 h, respectively. However, the commercially available isopropyl analogue **40** yielded about the same amount of product **44** irrespective of the time (65% after 18 h; 62% after 30 min). Presumably, the bulkier carbene results in a more stable palladacycle complex.

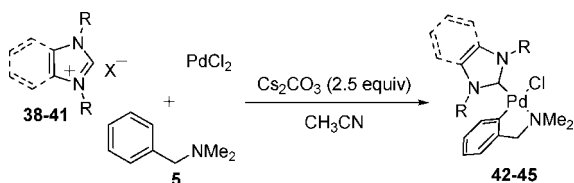
(38) Prepared by anion exchange with NH_4PF_6 from the known chloride: Harlow, K. J.; Hill, A. F.; Welton, T. *Synthesis* **1996**, 697–698.

1,3-Diisopropylbenzimidazolium hexafluorophosphate³⁹ (**41**) also reacted in good yield, providing the first example of a benzimidazol-2-ylidene-ligated palladacycle (**45**).

The actual mechanism of the ligation of palladacycles with in situ generated NHCs is not clear at this point. Since N substituents have little effect on the electronic nature and stability of the unsaturated imidazol-2-ylidenes,¹ the relative difficulty with which alkyl-substituted carbenes react with in situ formed $[\text{Pd}(\text{dmba})\text{Cl}]_2$ most likely rules out the involvement of the free carbene, despite recent reports of NHC generation under similar conditions.⁴⁰ The tolerance of the protocol presented herein to air and moisture also corroborates such a conclusion. It is plausible that the palladacycle forms a transient π complex with the imidazolium salts, causing the acidity of the latter to increase and facilitating the complex formation.

(39) Prepared by anion exchange with NH_4PF_6 from the known bromide: Huynh, H. V.; Han, Y.; Ho, J. H. H.; Tan, G. K. *Organometallics* **2006**, 25, 3267–3274.

(40) Bostai, B.; Novák, Z.; Bényei, A. C.; Kotschy, A. *Org. Lett.* **2007**, 9, 3437–3439.

Table 6. Synthesis of NHC–Pd(dmba)Cl Complexes from 1,3-Dialkylimidazolium and 1,3-Dialkylbenzimidazolium Salts

entry	conditions ^a	NHC ^b	R	X	yield, %
1	K ₂ CO ₃ , 80 °C, 18 h ^c	Im	Bn (38)	PF ₆	4 (42)
2	80 °C, 18 h	Im	Bn (38)	PF ₆	22 (42)
3	100 °C, 18 h	Im	Bn (38)	PF ₆	31 (42)
4	100 °C, 30 min	Im	Bn (38)	PF ₆	78 (42)
5	100 °C, 18 h	Im	Me (39)	Cl	45 (43)
6	100 °C, 30 min	Im	Me (39)	Cl	67 (43)
7	100 °C, 18 h	Im	<i>i</i> Pr (40)	Cl	65 (44)
8	100 °C, 30 min	Im	<i>i</i> Pr (40)	Cl	62 (44)
9	80 °C, 18 h	BzIm	<i>i</i> Pr (41)	PF ₆	68 (45) ^d
10	100 °C, 30 min	BzIm	<i>i</i> Pr (41)	PF ₆	83 (45) ^d

^a The palladacycle was always prepared at 80 °C. ^b Im = imidazolyl-2-ylidene; BzIm = benzimidazolyl-2-ylidene. ^c 5 equiv of K₂CO₃ was used. ^d The reactions were conducted in the presence of 4 Å molecular sieves.

Perhaps this complexation is more pronounced for 1,3-diarylimidazolium salts: hence, the relative ease of complexation when such carbene precursors are employed. Alternative mechanistic explanations also cannot be discounted at this point.

Molecular Structure of NHC–Palladacycles. The NHC–Pd(dmba)Cl complexes were characterized by X-ray crystallography (Figure 2). Selected bond lengths and angles and dihedral angles are given in Table 7, and the single-crystal data and X-ray collection parameters are given in Table 8. In the crystalline state, the complexes all show the characteristic slightly distorted square-planar Pd(II) center with the NHC and dimethylamino ligands mutually trans. The carbene ligand's five-membered-ring topology varies slightly for different carbenes. The NHC ligand retains the bond angles characteristic for a singlet carbene (~104° for the imidazol-2-ylidenes and ~107° for benzimidazol-2-ylidene and 4,5-dihydroimidazol-2-ylidene). The C1–N1 bond is 1.346–1.362 Å, regardless of the carbene type, whereas the N1–C4 bond is 1.384–1.394 Å for imidazol-2-ylidene and benzimidazol-2-ylidene and 1.485–1.490 Å for the backbone saturated analogues. Likewise, the C4–C5 bond length lies in the range of 1.327–1.336 Å for imidazol-2-ylidene, 1.394 Å for benzimidazol-2-ylidene, and 1.502–1.524 Å for the saturated carbenes, in accordance with changing bond types from double to single. This is accompanied by puckering of the carbene ring—the N1–C4–C5–N2 dihedral angle is close to 0 (–1.09 to +1.20°) for the unsaturated carbenes (sp²) and +16.71 to +19.05° for the saturated analogues (sp³). The two N-aryl rings are in all cases rotated out of conjugation, and the dihedral angles C1–N1/2–C2/6–C3/7 show large variation from carbene to carbene (58.83–128.66°). There is no apparent correlation between compound structure and dihedral angle value and sign for these low-barrier torsions. In all complexes, the Pd–C1 (1.966–1.996 Å) and Pd–C8 bonds (1.985–2.004 Å) are within the expected range for a single Pd–C bond. The Pd–N3 and Pd–Cl bond lengths are within the ranges of 2.128–2.142 and 2.379–2.424 Å, respectively. The substitution of the chloride for acetate or acetonitrile leads to shorter C–O and C–N bonds (2.112 and 2.118 Å, respectively), without significantly affecting the rest of the structure. The Pd center exhibits a slight distortion from the perfect square-planar configuration as a result from its being a part of the five-membered palladacycle ring. The ranges for the C1–Pd–X

angle (X = Cl, O, N), C1–Pd–C8 angle, and N3–Pd–X angle (X = Cl, O, N) are 89.37–95.56, 90.86–94.61, and 90.13–95.37°, respectively. The imidazole and palladacycle rings are closer to perpendicular than to coplanar: the absolute values for the N1–C1–Pd–C8 dihedral angle vary between 60.46 and 117.65°. The five-membered palladacycle moiety is puckered (with the C8–C9–C10–N3 dihedral angle in the range of 25.67–36.20°) due to the presence of sp³ carbon and nitrogen atoms (the N3–C10–C9 angle ranges from 107.89 to 109.53°, typical for tetrahedral carbons).

Conclusions

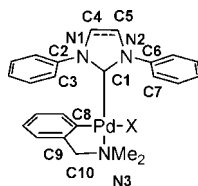
We have developed a novel, practical synthesis of NHC-ligated palladacycles by one-pot, three-component, sequential reaction of *N,N*-dimethylbenzylamine, PdCl₂ or PdBr₂, and a wide range of imidazolium salts and their 4,5-dihydro- or benzo-fused counterparts in refluxing acetonitrile in the presence of mild bases (K₂CO₃ and Cs₂CO₃, respectively) in air. Whereas the complexation of the in situ prepared 1,3-diarylimidazol-2-ylidenes is facile, the saturated analogues require a stronger base and the addition of 4 Å molecular sieves to suppress the competing carbene precursor hydrolysis. 1,3-Dialkylimidazolium and 1,3-dialkylbenzimidazolium salts generally require more forcing conditions and strict control of the reaction time for satisfactory complexation. All complexes show a characteristic distorted-square-planar Pd(II) center with the carbene and dimethylamino ligands mutually trans and the planes of the imidazole ring and the heterocycle close to perpendicular. The extension of this methodology to other classes of cyclometalated ligands and the use of the resulting complexes in catalysis are underway.

Experimental Section

General Considerations. All reagents and solvents were purchased from commercial sources and were used without further purification, unless otherwise indicated. Deuterated solvents were purchased from Sigma-Aldrich. TLC plates were purchased from VWR. ¹H and ¹³C NMR data were acquired at 25 °C with a Bruker AV 400 spectrometer. Flash chromatography was performed in a CombiFlash Sq16 on normal phase silica gel cartridges with hexane–ethyl acetate gradients.

General Procedure for the Synthesis of NHC–Pd(dmba)Cl Complexes from 1,3-Diarylimidazolium Salts (Table 1). A pressure tube was charged with PdCl₂ (177 mg, 1.00 mmol) and a stir bar, and then acetonitrile (5 mL, HPLC grade) and *N,N*-dimethylbenzylamine (160 μL, 178 mg, 1.05 mmol) were added. The mixture was stirred at 80 °C until PdCl₂ dissolved completely, forming a dark orange, clear solution (in ~20–25 min). Finely powdered K₂CO₃ (691 mg, 5.00 mmol) was added, and the mixture was heated at 80 °C until the palladacycle formation was complete, as indicated by the change in the color of the mixture to canary yellow (in ~5 min). Immediately, NHC·HCl (1.10 mmol) was added, and the mixture was heated at 80 °C with vigorous stirring over 18 h. The mixture was filtered on a pad of Celite (CH₂Cl₂), the volatiles were removed, and the residue was purified by flash chromatography (ethyl acetate gradient in CH₂Cl₂: 0% over 5 min, 0–30% over 15 min).

IPr–Pd(dmba)Cl (12). From IPr·HCl (**7**; 467 mg), **12** (543 mg, 82%) was obtained as an off-white solid. ¹H NMR (CDCl₃, 400 MHz): δ 7.40 (t, *J* = 7.6 Hz, 2H), 7.30 (d, *J* = 7.6 Hz, 2H), 7.21 (s, 2H), 6.82–6.70 (m, 3H), 6.53 (d, *J* = 7.6 Hz, 1H), 3.46 (s, 2H), 3.37 (m, 2H), 3.15 (m, 2H), 2.39 (s, 6H), 1.49 (d, *J* = 6.8 Hz, 6H), 1.18 (d, *J* = 6.8 Hz, 6H), 1.02 (d, *J* = 6.8 Hz, 6H), 0.81 (d, *J* = 6.4 Hz, 6H). ¹³C NMR (CDCl₃, 100 MHz): δ 177.5, 150.5,

Table 7. Selected Bond Lengths, Bond Angles, and Dihedral Angles for NHC–Pd(dmmba)X Complexes: X = Cl for **12**, **15**, **16**, **18**, **25**, **42**, and **45**; X = O for **31**, and X = N for **33**

param	12	15	16	18	25	31	33	42	45
Bond Lengths, Å									
C1–N1	1.360	1.362	1.362	1.353	1.345	1.361	1.349	1.346	1.350
N1–C4	1.395	1.394	1.402	1.485	1.490	1.387	1.384	1.384	1.394
C4–C5	1.330	1.335	1.336	1.502	1.524	1.327	1.327	1.332	1.392
C1–Pd	1.996	1.988	1.966	1.976	1.972	1.974	1.992	1.978	1.973
C8–Pd	2.004	1.989	1.997	1.999	1.994	1.985	1.985	2.006	1.991
Pd–X	2.379	2.408	2.415	2.402	2.424	2.112	2.118	2.406	2.393
Pd–N3	2.133	2.133	2.128	2.142	2.140	2.139	2.131	2.138	2.137
Bond Angles, deg									
N1–C1–N2	104.94	103.99	104.34	107.76	107.71	103.88	104.57	104.59	107.16
C1–Pd–X	91.56	95.88	90.48	97.46	95.53	93.01	95.96	89.37	89.75
C1–Pd–C8	94.61	91.13	92.15	91.64	90.86	91.47	90.93	94.16	92.74
N3–Pd–X	91.40	95.36	95.36	90.13	91.83	93.77	92.05	94.73	95.57
N3–C10–C9	108.61	109.53	109.53	108.24	109.39	108.31	107.89	109.04	108.79
Dihedral Angles, deg									
N1–C4–C5–N2	1.05	0.09	0.32	19.05	16.71	–0.81	–1.09	–0.58	1.20
C1–N1–C2–C3	120.67	90.51	72.74	128.66	104.89	62.30	58.83		106.71
C1–N2–C6–C7	–78.34	–73.84	–117.70	–88.42	–59.44	86.15	–100.19		–113.93
N1–C1–Pd–C8	–69.37	–74.95	–96.36	117.65	–68.29	64.63	60.46	70.62	78.46
C8–C9–C10–N3	33.65	28.55	25.67	36.20	31.44	–34.59	–36.51	–29.81	–29.60

147.8, 147.8, 144.7, 136.2, 136.1, 129.7, 125.4, 124.6, 124.0, 123.8, 122.6, 121.5, 72.6, 49.8, 29.0, 28.3, 26.4, 26.2, 23.2, 23.2. Anal. Calcd for C₃₆H₄₈ClN₃Pd (664.66): C, 65.05; H, 7.28; N, 6.32. Found: C, 65.14; H, 7.41; N, 6.53.

IEt–Pd(dmmba)Cl (13). From IEt·HCl (**8**; 406 mg), **13** (492 mg, 81%) was obtained as a white solid. ¹H NMR (CDCl₃, 400 MHz): δ 7.30 (t, *J* = 7.6 Hz, 2H), 7.24 (dd, *J* = 7.6, 1.2 Hz, 2H), 7.16 (s, 2H), 7.04 (dd, *J* = 7.6, 1.2 Hz, 2H), 6.78 (td, *J* = 7.6, 1.2 Hz, 1H), 6.71 (d, *J* = 7.2, 1.0 Hz, 1H), 6.68 (td, *J* = 7.6, 1.2 Hz, 1H), 6.58 (d, *J* = 7.2, 1.0 Hz, 1H), 3.44 (s, 2H), 2.94 (m, 2H), 2.87 (m, 2H), 2.70 (m, 2H), 2.61 (m, 2H), 2.40 (s, 6H), 1.19 (t, *J* = 7.2 Hz, 6H), 1.18 (d, *J* = 7.6 Hz, 6H). ¹³C NMR (CDCl₃, 100 MHz): δ 175.6, 150.0, 147.2, 143.1, 140.0, 137.3, 137.1, 129.1, 126.3, 126.0, 124.1, 123.4, 122.7, 121.1, 72.3, 50.0, 25.9, 25.2, 15.3, 14.7. Anal. Calcd for C₃₂H₄₀ClN₃Pd (608.55): C, 63.16; H, 6.63; N, 6.90. Found: C, 63.16; H, 6.69; N, 6.65.

IMes–Pd(dmmba)Cl (14). From IMes·HCl (**9**; 375 mg), **14** (555 mg, 96%) was obtained as a white solid. ¹H NMR (CDCl₃, 400 MHz): δ 7.10 (s, 2H), 6.99 (s, 2H), 6.83–6.76 (m, 4H), 6.70 (td, *J* = 7.6, 1.2 Hz, 1H), 6.58 (d, *J* = 7.2, 1.2 Hz, 1H), 3.53 (s, 2H), 2.45 (s, 6H), 2.44 (s, 6H), 2.29 (s, 6H), 2.23 (s, 6H). ¹³C NMR (CDCl₃, 100 MHz): δ 175.6, 149.3, 147.6, 138.3, 138.3, 137.4, 136.2, 133.9, 129.4, 128.7, 123.9, 123.2, 123.0, 121.2, 72.2, 50.0, 21.1, 20.2, 19.8. Anal. Calcd for C₃₀H₃₆ClN₃Pd (580.50): C, 62.07; H, 6.25; N, 7.24. Found: C, 62.02; H, 6.37; N, 7.40.

ITbp–Pd(dmmba)Cl (15). From ITbp·HCl (**10**; 406 mg), **15** (492 mg, 81%) was obtained as an off-white solid. ¹H NMR (CDCl₃, 400 MHz): δ 7.62 (dd, *J* = 8.4, 1.6 Hz, 2H), 7.42 (dd, *J* = 8.0, 1.2 Hz, 2H), 7.30–7.22 (m, 2H), 7.29 (s, 2H), 6.93–6.81 (m, 5H), 6.39 (d, *J* = 7.2 Hz), 3.51 (s, 2H), 2.42 (s, 6H), 1.51 (s, 18H). ¹³C NMR (CDCl₃, 100 MHz): δ 176.7, 151.8, 148.0, 146.7, 137.6, 137.5, 131.8, 129.8, 128.7, 125.1, 125.1, 124.7, 123.0, 121.6, 72.4, 49.6, 36.7, 32.8. Anal. Calcd for C₃₂H₄₀ClN₃Pd (608.55): C, 63.16; H, 6.63; N, 6.90. Found: C, 63.13; H, 6.44; N, 6.56.

IPrp–Pd(dmmba)Cl (16). From IPrp·HCl (**11**; 375 mg), **16** (500 mg, 86%) was obtained as an off-white solid. ¹H NMR (CDCl₃, 400 MHz): δ 8.62 (broad s, 2H), 7.38 (broad m, 6H), 7.23 (s, 2H), 6.92–6.15 (broad m, 4H), 3.51 (broad s, 2H), 2.97 (broad s, 2H), 2.50 (broad s, 6H), 1.58–1.18 (broad s, 6H), 1.18–0.76 (broad s,

6H). ¹³C NMR (CDCl₃, 100 MHz): δ 176.7, 147.9, 146.1–144.4 (broad), 137.5 (broad), 135.7 (broad), 130.7 (broad), 129.2, 126.5 (broad), 125.4 (broad), 125.4, 123.1, 123.0, 121.6, 71.8, 50.1, 27.7, 25.6 (broad), 24.2 (broad). Anal. Calcd for C₃₂H₄₀ClN₃Pd (580.50): C, 62.07; H, 6.25; N, 7.24. Found: C, 61.93; H, 6.45; N, 6.71.

Reaction of SIPr·HCl (17) and Palladacycle 6 under the Conditions of Table 2, Entry 1. SIPr·HCl (460 mg, 1.05 mmol) was used. The crude mixture was purified using flash chromatography (solvent A was 9:1 hexane–CH₂Cl₂, solvent B was ethyl acetate; gradient of 0–15% B over 30 min). The amide **19** eluted first (at 8% solvent B), followed by complex **18** (at 12% solvent B). Compound **19** (113 mg, 26%) was obtained as a white solid. ¹H NMR (CDCl₃, 400 MHz): δ 8.11 (s, 1H), 7.27–7.22 (m, 2H), 7.09–7.02 (m, 3H), 3.89 (t, *J* = 7.1 Hz, 2H), 3.31 (broad s, 1H), 3.21 (heptet, *J* = 6.8 Hz, 2H), 3.14 (t, *J* = 7.1 Hz, 2H), 3.04 (heptet, *J* = 6.8 Hz, 2H), 1.26 (d, *J* = 6.8 Hz, 6H), 1.23–1.13 (m, 18H). ¹³C NMR (CDCl₃, 100 MHz): δ 163.9, 147.6, 142.9, 142.2, 135.4, 129.5, 124.5, 123.8, 123.5, 48.8, 48.7, 28.3, 27.7, 25.4, 24.2, 24.1, 23.5. A small amount (7%) of another carbonyl bond rotamer was also observed. Selected resonances: ¹H NMR (CDCl₃, 400 MHz) δ 8.56 (s, 1H), 3.77 (t, *J* = 7.1 Hz, 2H); ¹³C NMR (CDCl₃, 100 MHz) δ 163.0, 52.0, 50.0. Anal. Calcd for C₂₇H₄₀N₂O (408.62): C, 79.36; H, 9.87; N, 6.86. Found: C, 79.04; H, 9.76; N, 6.72.

General Procedure for the Synthesis of NHC–Pd(dmmba)Cl Complexes from 1,3-Diaryl-4,5-dihydroimidazolium Salts (Table 3). A pressure tube was charged with PdCl₂ (177 mg, 1.00 mmol), finely powdered 4 Å molecular sieves (1 g), and a stir bar, and then acetonitrile (5 mL, HPLC grade kept over 4 Å molecular sieves) and *N,N*-dimethylbenzylamine (160 μL, 177 mg, 1.05 mmol) were added. The mixture was stirred at 80 °C until PdCl₂ dissolved completely, forming a dark orange, clear solution (in ~20–25 min). Finely powdered Cs₂CO₃ (815 mg, 2.50 mmol) was added, and the mixture was heated at 80 °C until the palladacycle formation was complete, as indicated by the change in the color of the mixture to canary yellow (in ~5 min). Immediately, the required 4,5-dihydroimidazolium salt (1.05 mmol) was added, and the mixture was heated at 80 °C with vigorous stirring over 18 h. The mixture was filtered over a pad of Celite (CH₂Cl₂), the volatiles were removed, and the residue was purified by flash chromatography

Table 8. Selected Crystallographic Data and X-ray Collection Parameters for NHC–Pd(dmiba)Cl Complexes 12, 15, 16, 18, 25, 31, 33, and 45

param	12	15	16	18	25	31–0.5CH ₂ Cl ₂	33	42	45
formula	C ₃₆ H ₄₈ ClN ₃ Pd	C ₃₂ H ₄₀ ClN ₃ Pd	C ₃₀ H ₃₆ ClN ₃ Pd	C ₃₆ H ₅₀ ClN ₃ Pd	C ₃₂ H ₄₀ ClN ₃ Pd	C ₃₈ H ₅₂ ClN ₃ O ₂ Pd	C ₃₃ H ₅₁ F ₆ N ₄ PPd	C ₂₆ H ₂₈ ClN ₃ Pd	C ₂₃ H ₃₀ ClN ₃ Pd
mol wt	664.62	608.52	580.47	666.64	610.54	730.68	815.20	524.36	478.34
temp, K	243(2)	223(2)	223(2)	223(2)	223(2)	223(2)	223(2)	223(2)	223(2)
cryst. syst.	orthorhombic	monoclinic	monoclinic	monoclinic	monoclinic	orthorhombic	monoclinic	monoclinic	monoclinic
space group	<i>Pbca</i>	<i>P2₁/n</i>	<i>P2₁/c</i>	<i>P2₁/c</i>	<i>C2/c</i>	<i>Pbca</i>	<i>P2₁/n</i>	<i>P2₁/c</i>	<i>P2₁/c</i>
cryst size, mm ³	0.36 × 0.36 × 0.16	0.56 × 0.46 × 0.26	0.30 × 0.18 × 0.06	0.50 × 0.40 × 0.32	0.40 × 0.06 × 0.06	0.60 × 0.50 × 0.36	0.58 × 0.16 × 0.04	0.60 × 0.20 × 0.08	0.30 × 0.20 × 0.10
<i>a</i> , Å	14.5682(5)	13.5849(6)	13.1003(7)	15.2685(7)	27.2962(11)	22.1198(7)	10.3961(18)	13.6799(10)	13.201(2)
<i>b</i> , Å	18.4516(7)	16.2049(7)	15.2782(8)	13.3002(6)	16.6141(7)	18.1254(6)	20.434(3)	12.6283(10)	9.5609(16)
<i>c</i> , Å	26.1633(10)	14.0474(6)	15.1532(8)	17.3267(8)	16.1329(6)	37.6542(13)	19.073(3)	15.7681(11)	17.634(3)
α , deg	90	90	90	90	90	90	90	90	90
β , deg	90	106.5850(10)	115.0280(10)	102.8110(10)	104.4150(10)	90	103.673(3)	114.944(2)	93.208(4)
γ , deg	90	90	90	90	90	90	90	90	90
<i>V</i> , Å ³	7032.9(4)	2963.8(2)	2748.1(3)	3431.0(3)	7086.0(5)	15096.7(9)	3937.0(12)	2469.9(3)	2222.2(6)
<i>Z</i>	8	4	4	4	8	16	4	4	4
<i>D</i> _{calc} , Mg m ⁻³	1.255	1.364	1.403	1.291	1.145	1.286	1.375	1.410	1.430
μ , mm ⁻¹	0.630	0.741	0.795	0.646	0.620	0.597	0.572	0.877	0.966
θ range, deg	1.56–25.00	1.84–27.50	1.72–27.49	1.95–27.50	1.45–27.50	1.42–27.50	1.48–27.50	1.64–27.50	1.55–27.50
no. of rflns collected	39 455	20 537	19 174	24 147	27 724	116 608	26 984	17 005	16 920
no. of indep rflns	6181	6796	6273	7892	8130	17 343	9055	5682	5097
<i>R</i> _{int}	0.0713	0.0257	0.0459	0.0296	0.0572	0.0500	0.0804	0.0451	0.0661
max/min transmission	0.9059/0.8049	0.8307/0.6817	0.9538/0.7963	0.8199/0.7383	0.9638/0.7896	0.8137/0.7157	0.9775/0.7328	0.9332/0.6213	0.9096/0.7603
final <i>R</i> indices (<i>I</i> > 2 σ (<i>I</i>))	0.0671	0.0307	0.0422	0.0360	0.0680	0.0460	0.0695	0.0563	0.0479
wR2	0.1374	0.0773	0.0910	0.0857	0.1854	0.1048	0.1540	0.1205	0.1101
<i>R</i> indices (all data)	0.0956	0.0361	0.0588	0.0431	0.0886	0.0614	0.0998	0.0758	0.0696
wR2	0.1495	0.0801	0.0947	0.0893	0.1998	0.1100	0.1672	0.1280	0.1213
goodness of fit on <i>F</i> ²	1.142	1.026	1.023	1.055	1.106	1.047	1.014	1.108	1.022
peak/hole, e Å ⁻³	0.864/–0.539	0.768/–0.304	0.828/–0.326	0.846/–0.246	1.692/0.562	1.224/–0.950	1.503/–1.452	1.015/–0.817	1.152/–0.576

(solvent A was 9:1 hexane-CH₂Cl₂, solvent B was ethyl acetate; gradient of 0–40% B over 20 min).

SIPr-Pd(dmba)Cl (18). From SIPr·HCl (**17**; 460 mg), **18** (640 mg, 96%) was obtained as a white solid. ¹H NMR (CDCl₃, 400 MHz): δ 7.36–7.28 (m, 4H), 7.22 (m, 1H), 7.10 (dd, *J* = 7.2, 1.6 Hz, 2H), 6.85 (m, 3H), 6.78 (m, 1H), 4.16 (m, 2H), 4.10 (m, 2H), 3.59 (m, 4H), 3.40 (s, 2H), 2.32 (s, 6H), 1.60 (d, *J* = 6.8 Hz, 6H), 1.26 (d, *J* = 6.8 Hz, 6H), 1.21 (d, *J* = 6.8 Hz, 6H), 0.74 (d, *J* = 6.8 Hz, 6H). ¹³C NMR (CDCl₃, 100 MHz): δ 205.4, 150.7, 148.0, 147.9, 146.3, 136.9, 136.0, 128.8, 125.3, 124.4, 124.0, 122.8, 121.7, 72.6, 54.2, 49.5, 29.0, 28.4, 27.0, 26.3, 24.3, 23.6. Anal. Calcd for C₃₆H₅₀ClN₃Pd (666.68): C, 64.86; H, 7.56; N, 6.30. Found: C, 65.19; H, 7.76; N, 6.39.

SIMes-Pd(dmba)Cl (23). From SIMes·HBF₄ (**20**; 414 mg), **23** (570 mg, 98%) was obtained as a white solid. ¹H NMR (CDCl₃, 400 MHz): δ 7.17 (dd, *J* = 7.2, 1.3 Hz, 1H), 6.96 (broad s, 2H), 6.89–6.83 (m, 2H), 6.79 (td, *J* = 6.9, 1.9 Hz, 1H), 6.75 (broad s, 2H), 4.12–4.03 (m, 2H), 4.01–3.94 (m, 2H), 3.46 (s, 6H), 2.67 (s, 6H), 2.36 (s, 6H), 2.29 (s, 6H). ¹³C NMR (CDCl₃, 100 MHz): δ 204.1, 149.0, 147.6, 138.8, 137.8, 137.5, 136.4, 135.3, 129.6, 128.8, 123.9, 123.0, 121.3, 72.1, 51.8, 49.8, 21.0, 20.4, 20.0. Anal. Calcd for C₃₀H₃₈ClN₃Pd (582.52): C, 61.86; H, 6.58; N, 6.93. Found: C, 61.40; H, 6.68; N, 6.93.

SIMes-Pd(dmba)Br (24). From SIMes·HBF₄ (**20**; 414 mg) and PdBr₂ (266 mg, 1.00 mmol), **24** (417 mg, 67%) was obtained as a white solid. ¹H NMR (CDCl₃, 400 MHz): δ 7.18 (dd, *J* = 7.2, 1.6 Hz, 1H), 6.96 (broad s, 2H), 6.89–6.85 (m, 2H), 6.79 (m, 1H), 6.74 (broad s, 2H), 4.12–4.05 (m, 2H), 4.01–3.96 (m, 2H), 3.45 (s, 2H), 2.67 (s, 6H), 2.44 (s, 6H), 2.28 (s, 6H), 2.26 (s, 2H). ¹³C NMR (CDCl₃, 100 MHz): δ 203.8, 150.8, 147.5, 138.6, 137.6, 137.5, 136.5, 135.3, 129.7, 129.6, 128.9, 123.9, 123.1, 121.4, 72.1, 51.9, 50.0, 21.0, 20.9, 20.2. Anal. Calcd for C₃₀H₃₈BrN₃Pd (625.13): C, 57.47; H, 6.11; N, 6.70. Found: C, 57.04; H, 5.81; N, 6.44.

SITBp-Pd(dmba)Cl (25). From SITBp·HBF₄ (**21**; 441 mg), **25** (552 mg, 90%) was obtained as a white solid. The compound was obtained as a mixture of two inseparable atropisomers: ¹H NMR (CDCl₃, 400 MHz): δ 8.68–6.80 (12H), 4.42–3.80 (4H), 3.57–3.27 (4H), 2.40–2.28 (6H), 1.70–1.63 (12H), 1.40–1.38 (6H). ¹³C NMR (CDCl₃, 100 MHz): δ 208.1, 204.3, 151.8–121.7 (36 aromatic carbons), 72.3, 72.0, 57.7, 57.0, 56.3, 50.2, 49.4, 49.1, 36.9, 36.5, 33.0, 32.6, 32.3. Anal. Calcd for C₃₂H₄₂ClN₃Pd (610.57): C, 62.95; H, 6.93; N, 6.88. Found: C, 62.90; H, 7.01; N, 6.79.

SIPrp-Pd(dmba)Cl (26). From SIPrp·HBF₄ (**22**; 414 mg), **26** (469 mg, 80%) was obtained as a white solid. ¹H NMR (CDCl₃, 400 MHz): δ 9.0–7.6 (broad s, 2H), 7.39–7.24 (broad m, 6H), 7.05 (broad m, 1H), 6.87–6.79 (broad m, 3H), 4.22 (broad s, 2H), 4.12 (broad s, 2H), 3.45 (s, 2H), 3.16 (broad s, 2H), 2.39 (broad s, 6H), 1.50–1.24 (broad s, 6H), 1.10–0.82 (broad s, 6H). ¹³C NMR (CDCl₃, 100 MHz): δ 205.7, 147.8, 146.0–144.7 (broad), 138.7, 135.7, 131.7–130.3 (broad), 128.4, 126.5 (broad), 126.2 (broad), 125.2, 123.1, 121.6, 71.6, 54.2, 49.8, 28.2, 25.0 (broad), 23.9 (broad). Anal. Calcd for C₃₀H₃₈ClN₃Pd (582.52): C, 61.86; H, 6.58; N, 6.93. Found: C, 61.64; H, 6.28; N, 7.06.

***N,N*-(2-*tert*-Butylphenyl)-1,4-diazabuta-1,4-diene (29).** To a solution of 2-*tert*-butylaniline (**27**; 20.4 mL, 19.6 g, 131 mmol) in a mixture of methanol (50 mL) and water (5 mL) was added glyoxal solution (40% in water; 7.5 mL, 9.43 g, 65 mmol), and the resulting mixture was stirred over 1.5 h. The yellow crystalline mass was filtered off, dried with a stream of air, and vacuum-dried over P₂O₅. Diimine **29** was obtained as a yellow solid (19.91 g, 96%) and used directly for the next step. A small portion was crystallized (methanol) to provide an analytically pure sample. ¹H NMR (CDCl₃, 400 MHz): δ 8.28 (s, 2H), 7.44 (m, 2H), 7.27 (m, 4H), 6.94 (m, 2H), 1.47 (s, 18H). ¹³C NMR (CDCl₃, 100 MHz): δ 158.6, 150.2, 143.7, 127.2, 127.1, 126.4, 118.9, 35.8, 30.5. Anal. Calcd for C₂₂H₂₈N₂ (320.47): C, 82.45; H, 8.81; N, 8.74. Found: C, 82.88; H, 8.65; N, 8.79.

ITbp·HCl (10). To a solution of the diimine **29** (6.41 g, 10 mmol) in THF (20 mL) were added chloromethyl ethyl ether (1.0 mL, 1.04 g, 11 mmol) and water (0.2 mL) in succession, and the mixture was stirred at 40 °C over 18 h. The solvent was removed to dryness, and the residue was partitioned between ethyl acetate (50 mL) and water (50 mL). The organic layer was further extracted with water (25 mL × 2). The combined aqueous layers were then extracted with CH₂Cl₂ (25 mL × 4). The combined CH₂Cl₂ layers were dried (MgSO₄), the solvent was removed under reduced pressure, and the residue was triturated with CH₂Cl₂/ethyl acetate (1:5). ITbp·HCl (**10**; 1.28 g, 35%) was obtained as an off-white solid. ¹H NMR (CD₂Cl₂, 400 MHz): δ 11.7–9.7 (broad s, 1H), 8.4–6.7 (broad s, 2H), 7.74 (m, 2H), 7.62 (td, *J* = 8.8, 1.6 Hz, 2H), 7.45 (td, *J* = 7.6, 1.2 Hz, 2H), 1.36 (s, 18H). ¹³C NMR (CD₂Cl₂, 100 MHz): δ 145.9 (broad), 140.9 (broad), 131.7, 129.1 (broad), 127.6, 125.6 (broad), 36.0, 31.8. Anal. Calcd for C₂₃H₂₉ClN₂ (368.94): C, 74.88; H, 7.92; N, 7.59. Found: C, 75.05; H, 7.89; N, 7.72.

SITbp·HBF₄ (21). In a two-necked 250 mL round-bottomed flask equipped with a reflux condenser and a stopper, a solution of diimine **29** (3.20 g, 10 mmol) in THF (50 mL) and methanol (50 mL) was brought to reflux. NaBH₄ (3.78 g, 100 mmol) was added portionwise over 30 min. After the mixture was cooled, the colorless solution obtained was quenched with water (200 mL), most of the organic solvent was removed under reduced pressure, and the residue was extracted with CH₂Cl₂ (50 mL × 3). The combined organic layers were dried (MgSO₄), and the solvent was removed under reduced pressure. The residue was dissolved in HC(OEt)₃ (25 mL), and concentrated HCl (12.0 M, 1.00 mL, 12 mmol) was added dropwise. The mixture was heated at 120 °C over 1 h and cooled. The volatiles were removed under high vacuum to dryness, the crude chloride salt was dissolved in water (10 mL), and a solution of NH₄BF₄ (5.24 g, 50 mmol) in water (20 mL) was added. The solid was filtered off, rinsed with a minimal amount of water followed by diethyl ether, and redissolved in CH₂Cl₂ (50 mL). The solution was dried (MgSO₄) and evaporated. SITbp·HBF₄ (**21**; 3.68 g, 88%) was obtained as an off-white solid after drying under high vacuum. ¹H NMR (CDCl₃, 400 MHz): δ 7.88 (broad m, 1H), 7.82–7.72 (broad m, 2H), 7.54 (dd, *J* = 8.0, 0.8 Hz, 2H), 7.54 (m, 2H), 7.35 (broad m, 2H), 4.68 (broad s, 4H), 1.48 (s, 18H). ¹³C NMR (CDCl₃, 100 MHz): δ 159.0, 146.6, 133.6, 131.0, 130.8, 128.7, 128.6, 55.8, 35.9, 32.2. Anal. Calcd for C₂₃H₃₁BF₄N₂ (422.31): C, 65.41; H, 7.40; N, 6.63. Found: C, 65.40, H, 7.47, N, 6.53.

***N,N*-(2-Isopropylphenyl)-1,4-diazabuta-1,4-diene (30).** Freshly distilled 2-isopropylaniline (**28**; 5.7 mL, 5.41 g, 40 mmol) and glyoxal solution (40% in water; 2.3 mL, 2.93 g, 20 mmol) were added to a degassed (Ar stream over 20 min) mixture of methanol (20 mL) and water (2 mL), and this mixture was stirred over 18 h. The dark-colored reaction mixture was diluted with water (50 mL), and methanol was removed under reduced pressure. The crude product was extracted in diethyl ether (50 mL × 3), the combined organic layers were dried (MgSO₄), and the volatiles were evaporated under reduced pressure. Diimine **30** was obtained as a yellow oil (4.84 g, 71%) after flash chromatography (80 g Combiflash cartridge, ethyl acetate gradient in hexane: 0% over 10 min, followed by 0–3% over 15 min, and 3% over 10 min). ¹H NMR (CD₂Cl₂, 400 MHz): δ 8.35 (s, 2H), 7.38 (dd, *J* = 7.6, 1.6 Hz, 2H), 7.30 (td, *J* = 7.6, 1.6 Hz, 2H), 7.24 (td, *J* = 7.6, 1.2 Hz, 2H), 7.00 (dd, *J* = 7.6, 1.2 Hz, 2H), 3.59 (heptet, *J* = 6.8 Hz, 2H), 1.28 (d, *J* = 6.8 Hz, 12H). ¹³C NMR (CDCl₃, 100 MHz): δ 159.7, 148.4, 143.2, 127.7, 126.8, 125.8, 117.4, 27.9, 23.3. Anal. Calcd for C₂₀H₂₄N₂ (292.42): C, 82.15; H, 8.81; N, 8.74. Found: C, 81.86; H, 9.17; N, 9.00.

IPrp·HCl (11). The procedure for compound **10** was followed, using diimine **30** (2.92 g, 10 mmol), chloromethyl ethyl ether (1.0 mL, 1.04 g, 12 mmol), and water (0.1 mL) in THF (10 mL).

IPr \cdot HCl (**11**; 2.11 g, 62%) was obtained as an off-white solid. ^1H NMR (CDCl_3 , 400 MHz): δ 11.7–9.7 (broad s, 1H), 8.4–6.7 (broad s, 2H), 7.74 (m, 2H), 7.62 (td, $J = 8.8, 1.6$ Hz, 2H), 7.45 (td, $J = 7.6, 1.2$ Hz, 2H), 1.36 (s, 9H). ^{13}C NMR (CDCl_3 , 100 MHz): δ 143.7, 138.2, 132.3, 131.8, 127.8, 127.7, 127.0, 124.7, 28.3, 23.9. Anal. Calcd for $\text{C}_{21}\text{H}_{25}\text{ClN}_2$ (340.89): C, 73.99; H, 7.39; N, 8.22. Found: C, 74.07; H, 7.24; N, 8.02.

SIPr \cdot HBF $_4$ (22). The procedure for compound **21** was followed, starting with **30** (2.92 g, 10 mmol). SIPr \cdot HBF $_4$ (**22**; 3.94 g, 94%) was obtained as an off-white solid after drying under high vacuum. ^1H NMR (CD_2Cl_2 , 400 MHz): δ 7.74–7.70 (m, 3H), 7.48–7.40 (m, 4H), 7.32–7.27 (m, 2H), 4.61 (s, 4H), 3.08 (heptet, $J = 6.8$ Hz), 1.36 (d, $J = 6.8$ Hz, 12H). ^{13}C NMR (CDCl_3 , 100 MHz): δ 156.9, 144.7, 132.5, 131.0, 128.1, 127.7, 127.0, 54.0, 28.4, 24.2. Anal. Calcd for $\text{C}_{21}\text{H}_{27}\text{BF}_4\text{N}_2$ (394.26): C, 63.97; H, 6.90; N, 7.11. Found: C, 63.57, H, 6.46; N, 6.83.

General Procedure for the Ion Exchange of IPr–Pd(dmba)Cl Complexes with Ag Salts (Table 4). To a solution of the silver salt (1 mmol) in acetone (2 mL), a solution of complex **12** (665 mg, 1 mmol) in CH_2Cl_2 (8 mL) was added. The mixture was stirred over 1 h, filtered, and evaporated to dryness.

IPr–Pd(dmba)OAc (31). From AgOAc (167 mg), **31** (663 mg, 96%) was obtained as a white solid after chromatography with CH_2Cl_2 –ethyl acetate/methanol (volume ratio 5:1) gradient, 0–100% over 20 min. ^1H NMR (CDCl_3 , 400 MHz): δ 7.32 (t, $J = 7.6$ Hz, 2H), 7.22 (broad d, $J = 7.6$ Hz, 2H), 7.12 (s, 2H), 7.10 (broad d, $J = 7.6$ Hz, 2H), 6.68 (t, $J = 7.2$ Hz, 2H), 6.61 (m, 3H), 6.38 (d, $J = 7.6$ Hz, 1H), 3.24 (s, 2H), 3.20 (m, 2H), 2.81 (m, 2H), 2.18 (s, 6H), 1.40 (s, 3H), 1.33 (d, $J = 6.4$ Hz, 6H), 1.10 (d, $J = 6.4$ Hz, 6H), 0.93 (d, $J = 6.8$ Hz, 6H), 0.79 (d, $J = 6.4$ Hz, 6H). ^{13}C NMR (CDCl_3 , 100 MHz): δ 178.3, 176.0, 148.2, 148.0, 147.0, 145.1, 136.0, 135.8, 129.6, 125.4, 124.2, 124.1, 123.8, 122.4, 121.7, 72.3, 49.2, 28.7, 28.5, 26.3, 25.3, 23.0, 22.8. Anal. Calcd for $\text{C}_{38}\text{H}_{51}\text{N}_3\text{O}_2\text{Pd}$ (688.25): C, 66.31; H, 7.47; N, 6.11. Found: C, 66.70; H, 7.63; N, 6.31.

IPr–Pd(dmba)TFA (32). From AgTFA (221 mg), **32** (733 mg, 99%) was obtained as a white solid after chromatography with CH_2Cl_2 –ethyl acetate gradient, 0–100% over 20 min. ^1H NMR (CDCl_3 , 400 MHz): δ 7.42 (t, $J = 7.6$ Hz, 2H), 7.30 (d, $J = 7.6$ Hz, 2H), 7.25 (s, 2H), 7.21 (d, $J = 7.6$ Hz, 2H), 6.80 (td, $J = 6.8, 1.2$ Hz, 2H), 6.70 (m, 2H), 6.70 (d, $J = 7.6$ Hz, 1H), 3.34 (s, 2H), 3.29 (m, 2H), 2.84 (m, 2H), 2.24 (s, 6H), 1.36 (d, $J = 6.8$ Hz, 6H), 1.19 (d, $J = 6.8$ Hz, 6H), 1.03 (d, $J = 6.8$ Hz, 6H), 0.88 (d, $J = 6.8$ Hz, 6H). ^{13}C NMR (CDCl_3 , 100 MHz): δ 177.3, 160.8 (q, $^2J_{\text{C-F}} = 35$ Hz), 147.6, 146.7, 145.9, 145.0, 136.0, 135.8, 135.4, 129.7, 125.7, 124.5, 124.3, 123.9, 122.7, 121.0, 116.6 (q, $^1J_{\text{C-F}} = 292$ Hz), 72.0, 49.1, 28.6, 28.5, 26.3, 26.3, 23.0, 22.4. Anal. Calcd for $\text{C}_{38}\text{H}_{49}\text{F}_3\text{N}_3\text{O}_2\text{Pd}$ (742.22): C, 61.49; H, 6.52; N, 5.66. Found: C, 62.06; H, 6.67; N, 5.77.

IPr–Pd(dmba)OTf (33). From AgOTf (257 mg), **33** (745 mg, 96%) was obtained as a white solid after chromatography with CH_2Cl_2 –ethyl acetate gradient, 0–100% over 20 min. ^1H NMR (CDCl_3 , 400 MHz): δ 7.45 (t, $J = 4.0$ Hz, 2H), 7.31 (d, $J = 4.0$ Hz, 4H), 7.30 (s, 2H), 7.21 (td, $J = 7.6, 1.2$ Hz, 1H), 6.76–6.71 (m, 2H), 6.36 (dd, $J = 4.2, 0.8$ Hz, 1H), 3.45 (s, 2H), 3.03 (broad s, 4H), 2.38 (s, 6H), 1.35–0.95 (broad, 24H). ^{13}C NMR (CDCl_3 , 100 MHz): δ 175.5, 160.8, 147.3, 145.7, 141.1, 135.5, 134.6, 130.7, 126.3, 125.1, 124.9, 124.6, 122.6, 121.8, 121.0, 120.3 (q, $^1J_{\text{C-F}} = 317$ Hz), 71.0, 49.5, 29.0, 26.3, 22.8. Anal. Calcd for $\text{C}_{37}\text{H}_{48}\text{F}_3\text{N}_3\text{O}_3\text{PdS}$ (778.28): C, 57.10; H, 6.22; N, 5.40. Found: 57.07; H, 6.08; N, 4.94.

IPr–Pd(dmba)PF $_6$ ·CH $_3$ CN (34). From AgPF $_6$ (257 mg) in CH_2Cl_2 (10 mL) and CH_3CN (2 mL), **34** (745 mg, 96%) was obtained as a white solid after chromatography with CH_2Cl_2 –acetonitrile, 0–20% over 20 min. ^1H NMR (CDCl_3 , 400 MHz): δ 7.45 (t, $J = 8.0$ Hz, 2H), 7.38 (m, 2H), 7.39–7.17 (broad m, 4H), 6.88 (t, $J = 6.8$ Hz, 2H), 6.79–6.74 (m, 2H), 6.30 (d, $J =$

7.2 Hz, 1H), 3.44 (s, 2H), 3.21 (broad s, 2H), 2.60 (broad s, 2H), 2.36 (s, 6H), 2.05 (s, 3H), 1.59–1.26 (broad s, 6H), 1.26–1.00 (broad m, 12H), 0.92–0.52 (broad s, 6H). ^{13}C NMR (CDCl_3 , 100 MHz): δ 174.7, 147.7, 145.9 (broad), 145.2 (broad), 135.3, 134.8, 130.5, 126.3, 125.3, 124.9 (broad), 124.5 (broad), 123.9, 122.7, 120.7, 71.8, 50.0, 28.9 (broad), 28.6 (broad), 26.3, 26.3, 22.9 (broad), 22.7 (broad), 21.1. Anal. Calcd for $\text{C}_{38}\text{H}_{51}\text{F}_3\text{N}_4\text{PPd}$ (815.22): C, 55.99; H, 6.31; N, 6.87. Found: C, 55.78; H, 6.65; N, 6.89.

[Pd(dmba)OAc] $_2$ (35). A 100 mL round-bottomed flask was charged with PdCl $_2$ (885 mg, 5.00 mmol) and a stir bar. Next, acetonitrile (20 mL, HPLC grade) and *N,N*-dimethylbenzylamine (790 μL , 878 mg, 5.25 mmol) were added. The mixture was stirred at 80 °C until PdCl $_2$ dissolved completely, forming a dark orange, clear solution (in ~20–25 min). Finely powdered NaOAc (2.05 g, 25.0 mmol) was added, and the mixture was heated at 80 °C over 20 min. The mixture was filtered over a pad of Celite (CH_2Cl_2), the volatiles were removed, and the residue was dissolved in CH_2Cl_2 (30 mL), washed with water (50 mL \times 3), dried (MgSO $_4$), and evaporated. The dimeric acetate-bridged palladacycle **35** (1.38 g, 92%) was obtained as a yellow solid after trituration with hexanes. The ^1H and ^{13}C NMR spectra were in accordance with the literature.

[Pd(dmba)(acac)] $_2$ (36). A 100 mL round-bottomed flask was charged with PdCl $_2$ (885 mg, 5.00 mmol) and a stir bar. Next, acetonitrile (20 mL, HPLC grade) and *N,N*-dimethylbenzylamine (790 μL , 878 mg, 5.25 mmol) were added. The mixture was stirred at 80 °C until PdCl $_2$ dissolved completely, forming a dark orange, clear solution (in ~20–25 min). Finely powdered K $_2\text{CO}_3$ (3.46 g, 25.0 mmol) was added, and the mixture was heated at 80 °C over 10 min. Acetylacetone (540 μL , 527 mg, 5.25 mmol) was added, and the mixture was stirred for another 15 min. The mixture was worked up as specified for compound **35**. Complex **36** (1.56 g, 92%) was obtained as a yellow solid after trituration with hexanes. The ^1H and ^{13}C NMR spectra were in accordance with the literature.

ITbp–Pd(dmba)I (37, Table 5). A pressure tube was charged with PdCl $_2$ (177 mg, 1.00 mmol) and a stir bar. Next, acetonitrile (5 mL, HPLC grade) and *N,N*-dimethylbenzylamine (160 μL , 178 mg, 1.05 mmol) were added. The mixture was stirred at 80 °C until PdCl $_2$ dissolved completely, forming a dark orange, clear solution (in ~20–25 min). Finely powdered K $_2\text{CO}_3$ (691 mg, 5.00 mmol) was added, and the mixture was heated at 80 °C until the palladacycle formation was complete, as indicated by the change in the color of the mixture to canary yellow (in ~5 min). Immediately, ITbp·HCl (**10**; 385 mg, 1.05 mmol) was added, and the mixture was heated at 80 °C with vigorous stirring over 18 h. Next, NaI (450 mg, 3.00 mmol) was added, and the mixture was heated at 80 °C for another 30 min. The mixture was filtered over a pad of Celite (CH_2Cl_2), the volatiles were removed, and the residue was purified by flash chromatography (hexane–ethyl acetate: 0–100% over 20 min). Complex **33** (672 mg, 96%) was isolated as a pale orange solid. ^1H NMR (CDCl_3 , 400 MHz): δ 7.62 (dd, $J = 8.4, 1.6$ Hz, 2H), 7.50 (dd, $J = 8.4, 1.6$ Hz, 2H), 7.32 (s, 2H), 7.32–7.28 (m, 2H), 6.99 (td, $J = 3.2, 1.6$ Hz, 1H), 6.92–6.86 (m, 4H), 6.23 (dd, $J = 4.00, 1.6$ Hz, 2H), 3.56 (s, 2H), 2.60 (s, 6H), 1.50 (s, 18H). ^{13}C NMR (CDCl_3 , 100 MHz): δ 176.1, 156.2, 148.2, 146.3, 137.6, 136.7, 131.7, 130.0, 128.7, 125.6, 125.1, 125.0, 123.5, 122.0, 72.2, 51.7, 36.8, 33.3. Anal. Calcd for $\text{C}_{32}\text{H}_{40}\text{IN}_3\text{Pd}$ (700.00): C, 54.91; H, 5.76; N, 6.00. Found: C, 54.68; H, 6.19; N, 6.02.

General Procedure for the Synthesis of NHC–Pd(dmba)Cl Complexes from 1,3-Dialkylimidazolium and 1,3-Dialkylbenzimidazolium Salts (Table 1). A pressure tube was charged with PdCl $_2$ (177 mg, 1.00 mmol) and a stir bar. Next, acetonitrile (5 mL, HPLC grade) and *N,N*-dimethylbenzylamine (160 μL , 178 mg, 1.05 mmol) were added. The mixture was stirred at 80 °C until PdCl $_2$ dissolved completely, forming a dark orange, clear solution (in ~20–25 min). Finely powdered Cs $_2\text{CO}_3$ (814 mg, 2.50 mmol) was added, and the mixture was heated at 80 °C until the palladacycle formation

was complete, as indicated by the change in the color of the mixture to canary yellow (in ~5 min). Immediately, the required imidazolium or benzimidazolium salt (1.10 mmol) was added, the temperature was increased to 100 °C, and the heating was continued for 30 min at that temperature with vigorous stirring. The mixture was filtered over a pad of Celite (CH₂Cl₂), the volatiles were removed, and the residue was purified by flash chromatography (solvent A, CH₂Cl₂; solvent B, ethyl acetate–methanol (volume ratio 4:1) gradient, 0–30% B in A over 15 min).

Bn₂Im–Pd(dmba)Cl (42). From Bn₂Im·HPF₆ (**38**; 356 mg), **42** (411 mg, 78%) was obtained as an off-white solid. ¹H NMR (CDCl₃, 400 MHz): δ 7.49–7.42 (m, 4H), 7.35–7.29 (m, 6H), 7.02 (dd, *J* = 7.6, 1.2 Hz, 1H), 6.98 (td, *J* = 7.6, 1.2 Hz, 1H), 6.79 (td, *J* = 7.2, 2.4 Hz, 1H), 6.77 (s, 2H), 6.15 (dd, *J* = 7.6, 1.2 Hz, 1H), 5.69 (d, *J* = 14.8 Hz, 2H), 5.60 (d, *J* = 14.8 Hz, 2H), 3.94 (m, 2H), 2.85 (s, 6H). ¹³C NMR (CDCl₃, 100 MHz): δ 173.5, 149.2, 148.5, 136.1, 135.9, 129.0, 128.8, 128.3, 125.6, 123.8, 122.3, 120.9, 72.2, 55.5, 50.3. Anal. Calcd for C₂₆H₂₈ClN₃Pd (524.39): C, 59.55; H, 5.38; N, 8.01. Found: C, 59.52; H, 5.41; N, 7.90.

Me₂Im–Pd(dmba)Cl (43). From Me₂Im·HCl (**39**; 146 mg), **43** (248 mg, 67%) was obtained as an off-white solid. ¹H NMR (CDCl₃, 400 MHz): δ 7.02 (dd, *J* = 1.6, 0.4 Hz, 1H), 6.95 (td, *J* = 7.6, 1.2 Hz, 1H), 6.95 (s, 2H), 6.75 (ddd, *J* = 7.6, 1.6, 0.4 Hz, 1H), 5.95 (dd, *J* = 7.6, 1.2 Hz, 1H), 3.97 (s, 6H), 3.92 (s, 2H), 2.83 (s, 6H). ¹³C NMR (CDCl₃, 100 MHz): δ 173.3, 149.9, 135.3, 124.9, 124.1, 123.4, 123.0, 72.2, 50.1, 38.6. Anal. Calcd for C₁₄H₂₀ClN₃Pd (372.20): C, 45.18; H, 5.42; N, 11.29. Found: C, 45.32; H, 5.47; N, 11.21.

***i*Pr₂Im–Pd(dmba)Cl (44).** From *i*Pr₂Im·HCl (**40**; 259 mg), **44** (256 mg, 62%) was obtained as an off-white solid. ¹H NMR (CDCl₃, 400 MHz): δ 7.03 (s, 2H), 7.00 (dd, *J* = 7.2, 0.8 Hz, 1H), 6.94 (td, *J* = 7.6, 1.2 Hz, 1H), 6.72 (td, *J* = 7.6, 1.6 Hz, 1H), 5.97 (dd, *J* = 7.2, 0.8 Hz, 1H), 5.53–5.43 (m, 2H), 3.91 (s, 2H), 2.83 (s, 6H), 1.54 (d, *J* = 2.4 Hz, 6H), 1.36 (d, *J* = 2.8 Hz, 6H). ¹³C NMR (CDCl₃, 100 MHz): δ 176.7, 148.5, 147.8, 136.3, 125.2, 123.6, 122.2, 116.9, 116.5, 72.1, 53.1, 50.2, 23.7, 22.8. Anal. Calcd for C₁₈H₂₈ClN₃Pd (428.31): C, 50.48; H, 6.59; N, 9.81. Found: C, 50.12; H, 6.23; N, 9.80.

***i*Pr₂BzIm–Pd(dmba)Cl (45).** From *i*Pr₂BzIm·HPF₆ (**41**; 383 mg), **45** (399 mg, 83%) was obtained as an off-white solid. At the beginning of the reaction, finely powdered 4 Å molecular sieves (1 g) were added. ¹H NMR (CDCl₃, 400 MHz): δ 7.63 (m, 2H), 7.28–7.24 (m, 3H); 7.21 (s, 2H), 7.03 (dd, *J* = 7.6, 1.2 Hz), 6.94 (td, *J* = 7.6, 1.2 Hz), 6.67 (td, *J* = 7.6, 1.4 Hz, 1H), 6.17–6.06 (m,

2H), 3.96 (s, 2H), 2.88 (s, 6H), 1.76 (d, *J* = 7.2 Hz, 6H), 1.62 (d, *J* = 7.2 Hz, 6H). ¹³C NMR (CDCl₃, 100 MHz): δ 183.8, 148.3, 136.7, 125.2, 123.8, 122.4, 122.1, 122.1, 112.6, 112.6, 72.2, 54.6, 50.4, 21.1, 20.8. Anal. Calcd for C₂₂H₃₀ClN₃Pd (478.32): C, 55.24; H, 6.32; N, 7.41. Found: C, 55.26; H, 6.38; N, 7.44.

Single-Crystal X-ray Structural Determination. Single crystals for all complexes were grown by a slow infusion of *n*-pentane into concentrated solutions of the NHC–palladacycles in CH₂Cl₂. Suitable crystals were mounted on quartz fibers, and X-ray data were collected on a Bruker AXS APEX diffractometer, equipped with a CCD detector, using graphite-monochromated Mo K α radiation (λ = 0.710 73 Å). The collecting frames of data, indexing reflection, and determination of lattice parameters and polarization effects were performed with the SMART suite of programs.⁴¹ The integration of intensity of reflections and scaling was performed by SAINT.⁴¹ The empirical absorption correction was performed by SADABS.⁴² The space group determination, structure solution, and least-squares refinements on $|F|^2$ were carried out with SHELXTL.⁴³ The structures were solved by direct methods to locate the heavy atoms, followed by difference maps for the light non-hydrogen atoms. Anisotropic thermal parameters were refined for the rest of the non-hydrogen atoms. The hydrogen atoms were placed in their ideal positions.

Acknowledgment. This work was funded by the Institute of Bioengineering and Nanotechnology (Biomedical Research Council, Agency for Science, Technology and Research, Singapore). We thank Geok Kheng Tan (X-Ray Crystallography Centre, National University of Singapore) for the single-crystal X-ray structure determination experiments.

Supporting Information Available: Crystallographic information files (CIF) for compounds **12**, **15**, **16**, **18**, **25**, **31**, **33**, **42**, and **45**. This material is available free of charge via the Internet at <http://pubs.acs.org>.

OM8008475

(41) SMART (Version 5.631) and SAINT (Version 6.63) Software Reference Manuals; Bruker AXS: Karlsruhe, Germany, 2000.

(42) Sheldrick, G. M. SADABS: Software for Empirical Absorption Correction; University of Göttingen, Göttingen, Germany, 2001.

(43) SHELXTL Reference Manual (Version 6.10); Bruker AXS: Karlsruhe, Germany, 2000.

Synthesis and Reactivity of a Tetragallium Macrocycle

Stefan M. Kilyanek, Xiangdong Fang, and Richard F. Jordan*

Department of Chemistry, The University of Chicago, 5735 S. Ellis Avenue, Chicago, Illinois 60637

Received September 16, 2008

The reaction of GaCl₃ with 1,8-bis(trimethylstannyl)biphenylene produces the tetragallium macrocycle (C₁₂H₆)₄Ga₄Cl₄ (**1**) in high yield. Compound **1** contains a cyclic array of four Ga(biphenylene) units that form a 20-membered ring. The Ga atoms are bridged by μ₂-Cl atoms so that the Ga atoms are four-coordinate. The structure adopts a saddle-shaped conformation with approximate D_{2d} symmetry. **1** reacts with Lewis bases (CH₃CN and THF) and halide ions (Cl⁻ and Br⁻) to form (C₁₂H₆)₂Ga₂Cl₂L and (C₁₂H₆)₂Ga₂Cl₂X⁻ species.

Introduction

The binding of cations by crown ethers, cryptands, and other multidentate Lewis bases has been studied extensively.¹ In contrast, the coordination of anions by multidentate Lewis acids is less well developed, possibly because of the challenges associated with incorporating several Lewis acid units in the same molecule.^{2,3} Most previous studies have focused on bidentate Lewis acids, including systems based on 1,8-difunctionalized naphthalenes,^{4–6} and macrocyclic species that incorporate Hg or Sn as Lewis acid sites.^{7–9} Multidentate Lewis acids based on group 13 elements may exhibit enhanced reactivity and could have applications in anion recognition and sequestering^{2a–d} and as activators for olefin polymerization catalysts.^{2e} Schnöckel reported that the reaction of AlCl₃ with 2,3-Me₂-butadiene produces a cyclic hexa-aluminum species, cyclo-μ-(CH₂CMe=CMeCH₂)₆(μ-Cl)₆Al₆.¹⁰ Uhl showed that R₂GaH hydrides react with terminal alkynes to form (GaR)₆(CR')₄ heteroadamantane cages that contain three-coordinate Ga cen-

ters.¹¹ Gabbai reported that the reaction of GaCl₃ with 1,8-bis(trimethylstannyl)naphthalene yields several products including the trigallacycle species (C₁₀H₆)₃Ga₃(μ₃-O)(μ-Cl).¹² A variety of cyclic and polycyclic species in which Al or Ga centers are linked by group 15 element units have also been

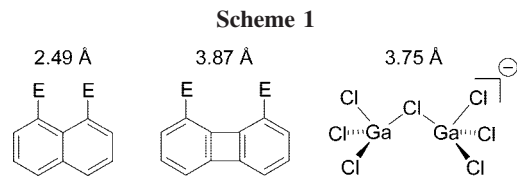
(6) For other bidentate Lewis acids see: (a) Schulte, M.; Gabbai, F. P. *Chem.—Eur. J.* **2002**, *8*, 3802. (b) Gabbai, F. P. *Angew. Chem., Int. Ed.* **2003**, *42*, 2218. (c) Dorsey, C. L.; Jewula, P.; Hudnall, T. W.; Hoefelmeyer, J. D.; Taylor, T. J.; Honesty, N. R.; Chiu, C. W.; Schulte, M.; Gabbai, F. P. *Dalton Trans.* **2008**, *33*, 4442. (d) Hudnall, T. W.; Kim, Y. M.; Bebbington, M. W. P.; Bourissou, D.; Gabbai, F. P. *J. Am. Chem. Soc.* **2008**, *130*, 10890. (e) Beckwith, J. D.; Tschinkl, M.; Picott, A.; Tsunoda, M.; Backman, R.; Gabbai, F. P. *Organometallics* **2001**, *20*, 3169. (f) Tschinkl, M.; Bachman, R. E.; Gabbai, F. P. *Organometallics* **2000**, *19*, 2633. (g) Tschinkl, M.; Hoefelmeyer, J. D.; Cocker, T. M.; Bachman, R. E.; Gabbai, F. P. *Organometallics* **2000**, *19*, 1826. (h) Gabbai, F. P.; Schier, A.; Riede, J.; Hynes, M. J. *Chem. Commun.* **1998**, 897. (i) Tschinkl, M.; Backman, R. E.; Gabbai, F. P. *Chem. Commun.* **1999**, 1367. (j) Tschinkl, M.; Schier, A.; Riede, J.; Gabbai, F. P. *Organometallics* **1999**, *18*, 1747. (k) Tschinkl, M.; Schier, A.; Riede, J.; Mehlretter, G.; Gabbai, F. P. *Organometallics* **1998**, *17*, 2921. (l) Tschinkl, M.; Schier, A.; Riede, J.; Schmidt, E.; Gabbai, F. P. *Organometallics* **1997**, *16*, 4759. (m) Kawachi, A.; Tani, A.; Shimada, J.; Yamamoto, Y. *J. Am. Chem. Soc.* **2008**, *130*, 4222. (n) Boshra, R.; Venkatasubbaiah, K.; Doshi, A.; Lalancette, R. A.; Kakalis, L.; Jäkle, F. *Inorg. Chem.* **2007**, *46*, 10174. (o) Tamao, K.; Hayashi, T.; Ito, Y.; Shiro, M. *Organometallics* **1992**, *11*, 2099. (p) Ebata, K.; Inada, T.; Kabuto, C.; Sakurai, H. *J. Am. Chem. Soc.* **1994**, *116*, 3595. (q) Asao, N.; Shibato, A.; Itagaki, Y.; Jourdan, F.; Maruoka, K. *Tetrahedron Lett.* **1998**, *39*, 3177. (r) Kira, M.; Kwon, E.; Kabuto, C.; Sakamoto, K. *Chem. Lett.* **1999**, *28*, 1183. (s) Panisch, R.; Bolte, M.; Muller, T. *J. Am. Chem. Soc.* **2006**, *128*, 9676. (t) Khalimon, A. Y.; Lin, Z. H.; Simionescu, R.; Vyboishchikov, S. F.; Nikonov, G. I. *Angew. Chem., Int. Ed.* **2007**, *46*, 4531. (u) Wrackmeyer, B.; Milius, W.; Tok, O. L. *Chem.—Eur. J.* **2003**, *9*, 4732.

* Corresponding author. E-mail: rfjordan@uchicago.edu.

(1) Lehn, J. M. *Supramolecular Chemistry*; VCH Press: Weinheim, 1995.
 (2) Reviews: (a) Beer, P. D.; Gale, P. A. *Angew. Chem., Int. Ed.* **2001**, *40*, 486. (b) Wuest, J. D. *Acc. Chem. Res.* **1999**, *32*, 81. (c) Vaugois, J.; Simard, M.; Wuest, J. D. *Coord. Chem. Rev.* **1995**, *145*, 55. (d) Hawthorne, M. F.; Zheng, Z. *Acc. Chem. Res.* **1997**, *30*, 267. (e) Chen, E. Y.-X.; Marks, T. J. *Chem. Rev.* **2000**, *100*, 1391. (f) Melaimi, M.; Gabbai, F. P. *Adv. Organomet. Chem.* **2005**, *53*, 61. (g) Wilson, P. A.; Hannant, M. H.; Wright, J. A.; Cannon, R. D.; Bochmann, M. *Macromol. Symp.* **2006**, *236*, 100. (h) Piers, W. E. *Adv. Organomet. Chem.* **2005**, *52*, 1. (i) Schmidtchen, F. P.; Berger, M. *Chem. Rev.* **1997**, *97*, 1609.
 (3) Computational studies: (a) Jacobson, S.; Pizer, R. *J. Am. Chem. Soc.* **1993**, *115*, 11216. (b) Williams, S. D.; Harper, W.; Mamantov, G.; Tortorelli, L. J.; Shankle, G. J. *Comput. Chem.* **1996**, *17*, 1696.
 (4) For a review see: (a) Piers, W.; Irvine, G. J.; Williams, V. C. *Eur. J. Inorg. Chem.* **2000**, 2131.
 (5) Bidentate boron Lewis acids: (a) Hoefelmeyer, J. D.; Schulte, M.; Tschinkl, M.; Gabbai, F. P. *Coord. Chem. Rev.* **2002**, *235*, 93. (b) Schulte, M.; Gabbai, F. P. *Can. J. Chem.* **2002**, *80*, 1308. (c) Katz, H. E. *J. Am. Chem. Soc.* **1985**, *107*, 1420. (d) Katz, H. E. *Organometallics* **1987**, *6*, 1134. (e) Katz, H. E. *J. Org. Chem.* **1989**, *54*, 2179. (f) Jia, L.; Yang, X.; Stern, C.; Marks, T. J. *Organometallics* **1994**, *13*, 3755. (g) Shriver, D. F.; Biallas, M. J. *J. Am. Chem. Soc.* **1967**, *89*, 1078. (h) Williams, V. C.; Piers, W. E.; Clegg, W.; Elsegood, M. R.; Collins, S.; Marder, T. B. *J. Am. Chem. Soc.* **1999**, *121*, 3244. (i) Aldridge, S.; Bresner, C.; Fallis, I. A.; Coles, S. J.; Hurshouse, M. B. *Chem. Commun.* **2002**, 740. (j) Williams, V. C.; Irvine, G. J.; Piers, W. E.; Li, Z.; Collins, S.; Clegg, W.; Elsegood, M. R. J.; Marder, T. B. *Organometallics* **2000**, *19*, 1619. (k) Gabbai, F. P.; Schier, A.; Riede, J. *Angew. Chem., Int. Ed.* **1998**, *37*, 622. (l) Metz, M. V.; Schwartz, D. J.; Stern, C. L.; Nickias, P. N.; Marks, T. J. *Angew. Chem., Int. Ed.* **2000**, *39*, 1312. (m) Schilling, B.; Kaiser, V.; Kaufmann, D. *Chem. Ber.* **1997**, *130*, 923.

(7) Multidentate Lewis acid coordination of organic carbonyls: Vaugois, J.; Simard, M.; Wuest, J. D. *Coord. Chem. Rev.* **1995**, *145*, 55.

(8) Multidentate Lewis acids based on Hg: (a) Lee, H.; Knobler, C. B.; Hawthorne, M. F. *J. Am. Chem. Soc.* **2001**, *123*, 8543. (b) Lee, H.; Diaz, M.; Knobler, C. B.; Hawthorne, M. F. *Angew. Chem., Int. Ed.* **2000**, *39*, 776. (c) Yang, X.; Knobler, C. B.; Hawthorne, M. F. *Angew. Chem., Int. Ed.* **1991**, *30*, 1507. (d) Yang, X.; Knobler, C. B.; Hawthorne, M. F. *J. Am. Chem. Soc.* **1992**, *114*, 380. (e) Yang, X.; Knobler, C. B.; Zheng, Z.; Hawthorne, M. F. *J. Am. Chem. Soc.* **1994**, *116*, 7142. (f) Hawthorne, M. F.; Yang, X.; Zheng, Z. *Pure Appl. Chem.* **1994**, *66*, 245. (g) Hawthorne, M. F.; Zheng, Z. *Acc. Chem. Res.* **1997**, *30*, 267. (h) Bayer, M. J.; Jalisatgi, S. S.; Smart, B.; Herzog, A.; Knobler, C. B.; Hawthorne, M. F. *Angew. Chem., Int. Ed.* **2004**, *43*, 1854. (i) Wedge, T. J.; Hawthorne, M. F. *Coord. Chem. Rev.* **2003**, *240*, 111. (j) Wuest, J. D. *Acc. Chem. Res.* **1999**, *32*, 81. (k) Tikhonova, I. A.; Dolgushin, F. M.; Tugashov, K. I.; Ellert, O. G.; Novotortsev, V. M.; Furin, G. G.; Antipin, M. Yu.; Shur, V. B. *J. Organomet. Chem.* **2004**, *689*, 82. (l) Tikhonova, I. A.; Dolgushin, F. M.; Yakovenko, A. A.; Tugashov, K. I.; Petrovskii, P. V.; Furin, G. G.; Shur, V. B. *Organometallics* **2005**, *24*, 3395. (m) Nadeau, F.; Simard, M.; Wuest, J. D. *Organometallics* **1990**, *9*, 1311. (n) Wuest, J. D.; Zacharie, B. *J. Am. Chem. Soc.* **1987**, *109*, 4714.



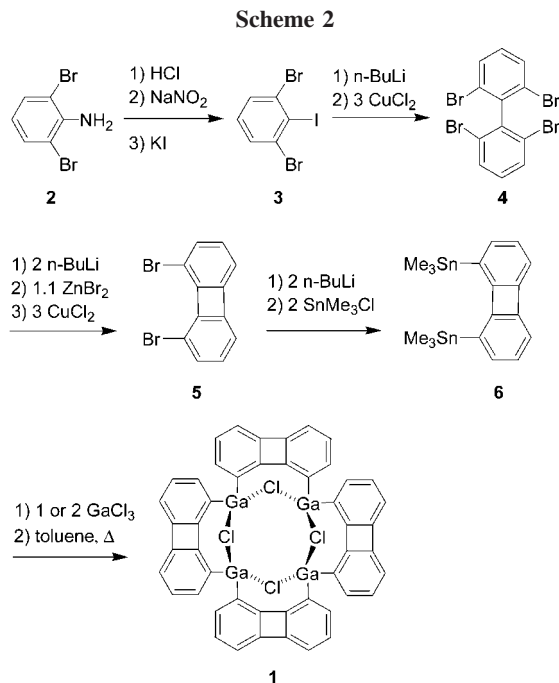
studied.¹³ Here we describe the synthesis, structure, and reactivity of a tetragallium macrocycle in which the Ga centers are linked by 1,8-biphenylene units.

Results and Discussion

Target Design. The objective of the present work was to prepare multigallium species in which the Ga centers are linked by 1,8-biphenylene units (Scheme 1). Gallium substituents at the C1 and C8 positions of an undistorted biphenylene unit (E in Scheme 1) would be separated by ca. 3.87 Å,¹⁴ which should favor binding of chloride and other anions to the two Ga centers. For comparison, the Ga---Ga distance in Ga₂Cl₇⁻ is 3.75 Å.¹⁵ In contrast, the C1 and C8 positions of the 1,8-naphthalene unit are separated by only ca. 2.49 Å.¹⁴

Synthesis and Structure of (C₁₂H₆)₄Ga₄Cl₄ (1). The key starting material for this work, 1,8-dibromobiphenylene (5), was prepared by Scheme 2 using modified literature procedures.^{16–18}

Lithium halogen exchange of 5 with ⁿBuLi, followed by reaction with Me₃SnCl, afforded 1,8-bis(trimethylstannyl)biphenylene (6, 69%). Compound 6 is stable to air and water but undergoes partial destannylation on silica gel to form 1-(trimethylstannyl)biphenylene.¹⁹ The reaction of 6 with 2 equiv of GaCl₃ in refluxing toluene followed by cooling to room temperature affords (C₁₂H₆)₄Ga₄Cl₄ (1), which crystallizes from solution and



was isolated in 53% yield. The reaction of 6 with 1 equiv of GaCl₃ affords 1 in 68% isolated yield.

The molecular structure of 1 was established by X-ray crystallography and is shown in Figure 1. Compound 1 contains a cyclic array of four Ga-biphenylene units, which form a 20-membered ring. Each pair of adjacent Ga atoms is bridged by a μ₂-Cl atom, so that the Ga centers have distorted tetrahedral geometry. The structure adopts a saddle-shaped conformation with approximate D_{2d} symmetry. The Ga atoms form a square-planar array, and the pairs of adjacent Cl atoms lie on opposite sides of the Ga₄ plane. The biphenylene rings are tilted 135° (C(1)–C(24A)) and –130° (C(7)–C(18)) out of the Ga₄ plane. The Ga---Ga distances (Ga(1)–Ga(2) 4.095 Å, Ga(3)–Ga(2) 4.094 Å) are slightly larger than the expected value of 3.87 Å (Scheme 1).

The ¹H NMR spectra of 1 in toluene-*d*₈, benzene-*d*₆, C₆D₅Cl, or CD₂Cl₂ solution contain either a single set of doublet (1H), triplet (1H), and doublet (1H) resonances, or a second-order multiplet, for the biphenylene groups, consistent with a highly symmetric structure. Additionally, the atmospheric pressure photoionization mass spectrum (APPI-MS) of a CD₂Cl₂ solution of 1 contains a prominent molecular ion peak. These results imply that the tetranuclear structure of 1 is retained in solution in noncoordinating solvents. The positive ion MALDI mass spectrum (DHB matrix, from toluene solution) of 1 contains a prominent signal for 1•H⁺.

Reaction of 1 with CH₃CN. While 1 might be expected to bind Lewis bases and anions with concomitant cleavage of Ga–Cl–Ga bridges, in fact more complex chemistry leading to digallium products is observed. Dissolution of 1 in refluxing CH₃CN followed by cooling to room temperature results in crystallization of the yellow binuclear complex (C₁₂H₆)₂Ga₂Cl₂(NCCH₃) (7, Scheme 3), which was isolated in 45% yield. The molecular structure of 7 was established by X-ray crystallography and is shown in Figure 2. Compound 7 contains a cyclic array of two Ga-biphenyl units that form a 10-membered ring. The Ga atoms are bridged by a μ₂-Cl atom. One Ga contains a terminal chloride and the other contains a CH₃CN ligand. The structure adopts a sawhorse conformation with approximate C_s symmetry.

(9) Multidentate Lewis acids based on Sn: (a) Blanda, M. T.; Horner, J. H.; Newcomb, M. *J. Org. Chem.* **1989**, *54*, 4626. (b) Newcomb, M.; Madonik, A. M.; Blanda, M. T.; Judice, J. K. *Organometallics* **1987**, *6*, 145. (c) Newcomb, M.; Horner, J. H.; Blanda, M. T. *J. Am. Chem. Soc.* **1987**, *109*, 7878. (d) Blanda, M. T.; Newcomb, M. *Tetrahedron Lett.* **1989**, *30*, 3501. (e) Newcomb, M.; Horner, J. H.; Blanda, M. T.; Squatrito, P. J. *J. Am. Chem. Soc.* **1989**, *111*, 6294. (f) Horner, J. H.; Squatrito, P. J.; McGuire, N.; Riebenspies, J. P.; Newcomb, M. *Organometallics* **1991**, *10*, 1741. (g) Zobel, B.; Duthie, A.; Dakternieks, D.; Tiekink, E. R. T. *Organometallics* **2001**, *20*, 2820. (h) Zobel, B.; Duthie, A.; Dakternieks, D.; Tiekink, E. R. T. *Organometallics* **2001**, *20*, 3347. (i) Jurkschat, K.; Kuivila, H. G.; Liu, S.; Zubietta, J. A. *Organometallics* **1989**, *8*, 2755. (j) Schulte, M.; Gabriele, G.; Schurmann, M.; Jurkschat, K. *Organometallics* **2003**, *22*, 328.

(10) Dohmeier, C.; Mattes, R.; Schnöckel, H. *J. Chem. Soc., Chem. Commun.* **1990**, 358.

(11) Uhl, W.; Cuypers, L.; Neumuller, B.; Weller, F. *Organometallics* **2002**, *21*, 2365.

(12) Hoefelmeyer, J. D.; Brode, D. L.; Gabbaï, F. P. *Organometallics* **2001**, *20*, 5653.

(13) (a) von Hanisch, C.; Stahl, S. *Angew. Chem., Int. Ed.* **2006**, *45*, 302. (b) Hoskin, A. J.; Stephan, D. W. *Angew. Chem., Int. Ed.* **2001**, *40*, 1865. (c) Janik, J. F.; Wells, R. L.; Young, V. G.; Rheingold, A. L.; Guzey, I. A. *J. Am. Chem. Soc.* **1998**, *120*, 532.

(14) Distances are from DFT structures optimized at the B3LYP/6-311++G** level. See Supporting Information for details. For structural and computational studies of biphenylene see: (a) Waser, J.; Lu, C. S. *J. Am. Chem. Soc.* **1944**, *66*, 2035. (b) Yokozeki, A., Jr.; Bauer, S. *J. Am. Chem. Soc.* **1974**, *96*, 1026. (c) Maksiaë, Z. B.; Kovaaek, D.; Eckert-Maksiaë, M.; Böckmann, M.; Klessinger, M. *J. Phys. Chem.* **1995**, *99*, 6410. (d) Zimmermann, R. *J. Mol. Struct.* **1996**, *377*, 35. (e) Verdal, N.; Hudson, B. S. *Chem. Phys. Lett.* **2007**, *434*, 241.

(15) *Chemistry of Aluminum Gallium Indium and Thallium*; Downs, A. J., Ed.; Blackie Academic & Professional: Glasgow, 1993; p 135.

(16) Du, C.-J. F.; Hart, H.; Ng, K.-K. D. *J. Org. Chem.* **1986**, *51*, 3162.

(17) Rajca, A.; Sazonov, A.; Rajca, S.; Ross, C. R., II.; Stezowski, J. J. *J. Am. Chem. Soc.* **1996**, *118*, 7272.

(18) Kabir, S. M. H.; Iyoda, M. *Synthesis* **2000**, *13*, 1839.

(19) Destannylation of 1 to 1-(trimethylstannyl)biphenylene on silica gel was confirmed by 2D-TLC and GC-MS.

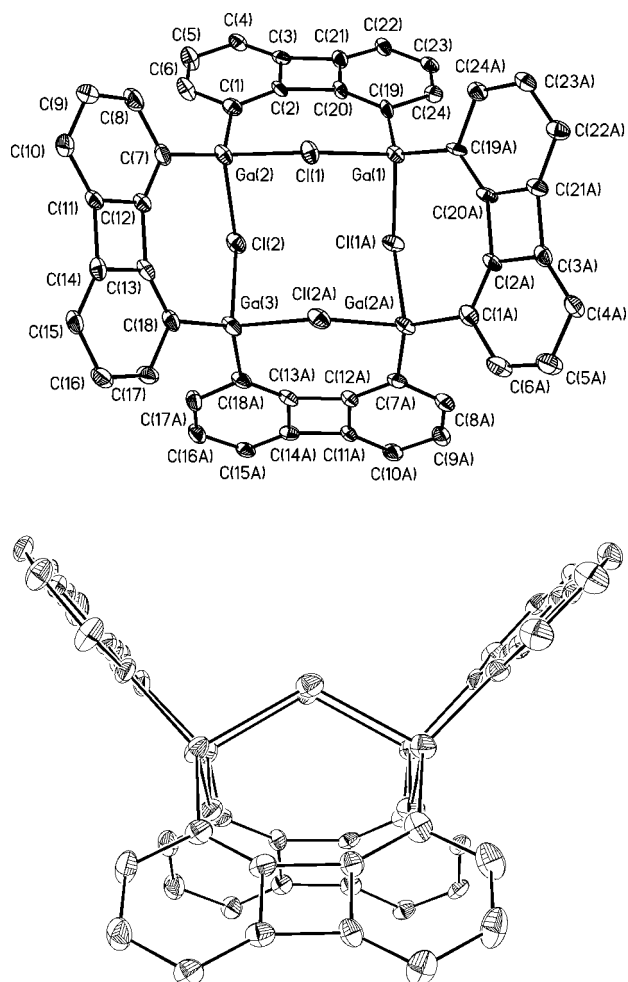
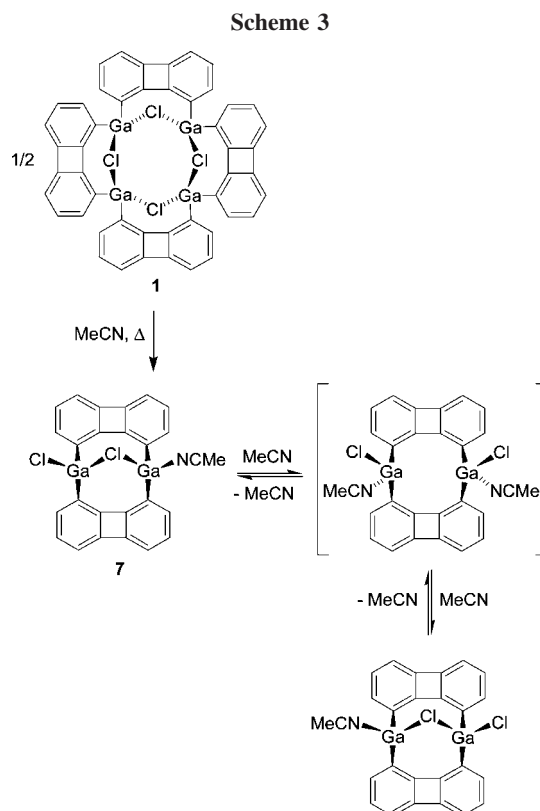


Figure 1. Two views of the molecular structure of **1** (50% probability ellipsoids). H atoms are omitted. Key bond distances (Å) and angles (deg): Ga(1)–C(19) 1.936(4), Ga(1)–Cl(1A) 2.3465(10), Ga(2)–C(1) 1.947(4), Ga(2)–C(7) 1.935(4), Ga(2)–Cl(1) 2.3613(10), Ga(2)–Cl(2) 2.3401(10), Ga(3)–C(18) 1.950(4), Ga(3)–Cl(2) 2.3610(10), Ga(1)–Cl(1)–Ga(2) 120.88(4), Ga(2)–Cl(2)–Ga(3) 121.14(4), Cl(1)–Ga(1)–Cl(1A) 101.47(5), Cl(2)–Ga(2)–Cl(1) 96.30(4), Cl(2A)–Ga(3)–Cl(2) 99.68(5), C(19A)–Ga(1)–C(19) 127.1(2), C(19A)–Ga(1)–Cl(1) 108.93(11), C(19)–Ga(1)–Cl(1) 103.84(10), C(7)–Ga(2)–C(1) 128.94(15), C(7)–Ga(2)–Cl(2) 110.11(12), C(1)–Ga(2)–Cl(2) 105.29(11), C(1)–Ga(2)–Cl(1) 108.50(11), C(18)–Ga(3)–C(18A) 130.1(2), C(18)–Ga(3)–Cl(2A) 102.29(11), C(18A)–Ga(3)–Cl(2A) 109.36(11), C(18)–Ga(3)–Cl(2) 109.36(11), C(18A)–Ga(3)–Cl(2) 102.29(11), C(20)–C(19)–Ga(1) 127.6(3), C(24)–C(19)–Ga(1) 118.6(3), C(2)–C(1)–Ga(2) 126.8(3), C(6)–C(1)–Ga(2) 119.5(3), C(12)–C(7)–Ga(2) 126.7(3), C(8)–C(7)–Ga(2) 119.7(3), C(13)–C(18)–Ga(3) 127.6(3), C(17)–C(18)–Ga(3) 118.0(3).

The ^1H NMR spectrum of **7** in CD_2Cl_2 solution contains two doublets (δ 6.98 and 6.83, 2H each) for the H2 hydrogens, a triplet (4H) and a doublet (4H) for the H3 and H4 hydrogens, and a resonance for one bound acetonitrile ligand (δ 2.63, 3H) that is shifted downfield from the free acetonitrile position (δ 1.95). These results are consistent with the C_s -symmetric structure of **7** observed in the solid state.

As illustrated in Figures 3 and 4, addition of excess free acetonitrile to a CD_2Cl_2 solution of **7** causes significant changes in the ^1H NMR spectrum. In the presence of 0.01 M free CH_3CN , the two H2 resonances are coalesced to one broad resonance at the average chemical shift, and the resonances for free and bound acetonitrile are broadened. As the concentration



of free CH_3CN is increased, the H2 resonance sharpens, and the resonances for free and bound acetonitrile coalesce. These results show that **7** undergoes associative exchange with free CH_3CN and that this process results in exchange of the two ends of the biphenylene units. The mechanism in Scheme 3 is consistent with these observations.

Reaction of 1 with THF. Addition of excess THF to a CH_2Cl_2 solution of **1** followed by removal of the volatiles and drying under vacuum yields a yellow solid that is formulated as the THF adduct $(\text{C}_{12}\text{H}_6)_2\text{Ga}_2\text{Cl}_2(\text{THF})$ (**8**, Scheme 4). The ^1H NMR spectrum of **8** in CD_2Cl_2 solution is very similar to

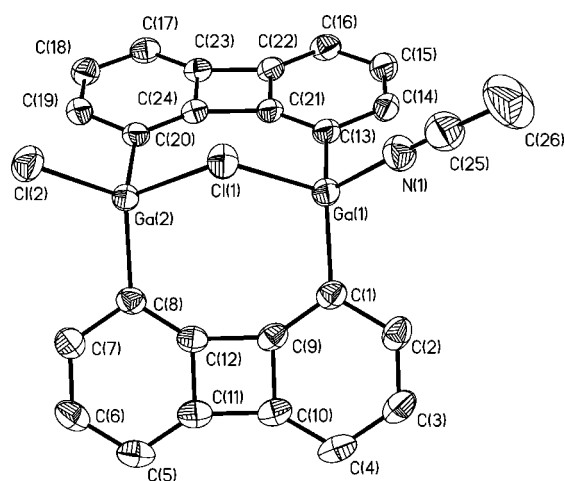


Figure 2. Molecular structure of **7** (50% probability ellipsoids). H atoms are omitted. Key bond distances (Å) and angles (deg): C(1)–Ga(1) 1.943(2), C(8)–Ga(2) 1.961(2), C(13)–Ga(1) 1.948(2), C(20)–Ga(2) 1.956(2), Ga(1)–Cl(1) 2.3220(7), Ga(2)–Cl(1) 2.3905(7), Ga(2)–Cl(2) 2.2158(7), Ga(1)–N(1) 2.002(2), N(1)–C(25) 1.112(4), N(1)–Ga(1)–Cl(1) 94.86(7), C(13)–Ga(1)–C(1) 131.08(10), C(20)–Ga(2)–C(8) 130.69(10), Cl(1)–Ga(2)–Cl(2) 100.22(3), Ga(1)–Cl(1)–Ga(2) 107.23(3).

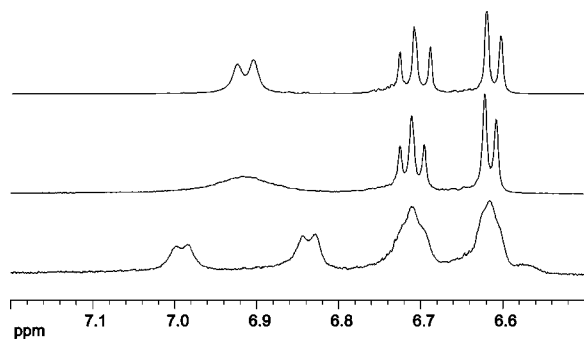


Figure 3. Aryl region of the ^1H NMR spectrum of **7** (CD_2Cl_2 , 23°C) in the presence of excess free CH_3CN . From bottom to top: $[\text{CH}_3\text{CN}]_{\text{free}} = 0.002, 0.01, \text{ and } 0.04 \text{ M}$.

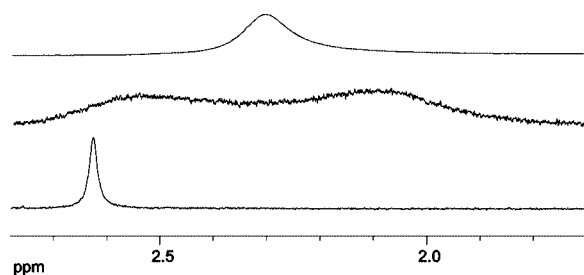
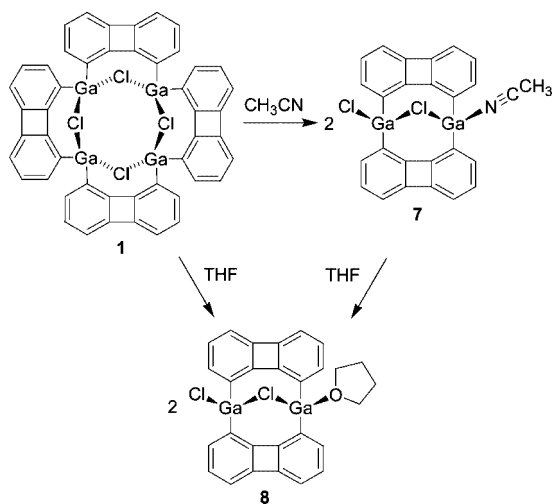


Figure 4. CH_3CN region of the ^1H NMR spectra of **7** (CD_2Cl_2 , 23°C) in the presence of excess free CH_3CN . From bottom to top: $[\text{CH}_3\text{CN}]_{\text{free}} = 0.002, 0.01, \text{ and } 0.04 \text{ M}$.

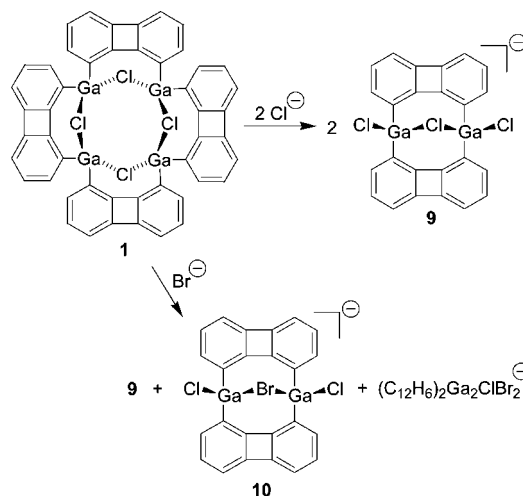
Scheme 4



that of **7** and contains two low-field doublets (2H each) for the H2 hydrogens and resonances for one bound THF ligand per $(\text{C}_{12}\text{H}_6)_2\text{Ga}_2$ unit, which are shifted downfield by ca. 0.6 ppm from the free THF positions. When increasing amounts of free THF are added, the H2 resonances broaden and coalesce to a sharp doublet, and the free and bound THF resonances coalesce to one set of resonances at the weighted average of the free and bound THF chemical shifts. This behavior is consistent with an associative THF exchange process analogous to the CH_3CN exchange process in Scheme 3. **8** is also formed by dissolution of **7** in THF.

Reaction of 1 with Chloride Ion. The reaction of **1** with 2 equiv of $[\text{NBu}_4]\text{Cl}$ in CD_2Cl_2 solution at 23°C results in the quantitative formation of the dinuclear chloride adduct $[\text{NBu}_4][(\text{C}_{12}\text{H}_6)_2\text{Ga}_2\text{Cl}_3]$ (**9**, Scheme 5), which was isolated as a white solid by removal of the volatiles from the CH_2Cl_2

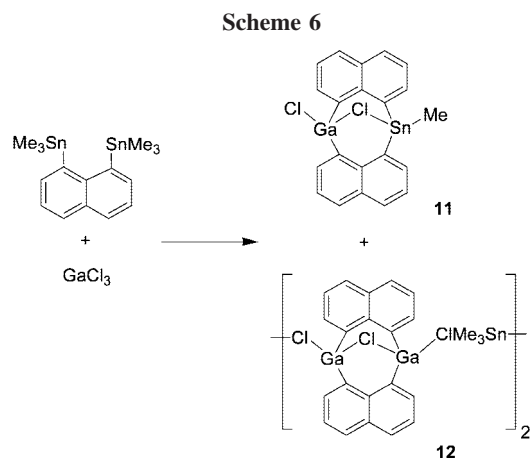
Scheme 5



solution. The solubility of **1** in CD_2Cl_2 is significantly enhanced by the presence of $[\text{NBu}_4]\text{Cl}$ due to the formation of **9**. The negative ion ESI mass spectrum of **9** in CH_2Cl_2 solution contains a prominent molecular ion peak for $(\text{C}_{12}\text{H}_6)_2\text{Ga}_2\text{Cl}_3^-$. The ^1H NMR spectrum of **9** is consistent with a C_{2v} -symmetric structure and the presence of two biphenylene units per NBu_4^+ cation. The negative ion MALDI mass spectrum of **9** contains a strong signal for the $(\text{C}_{12}\text{H}_6)_2\text{Ga}_2\text{Cl}_3^-$ anion. When stoichiometric amounts of $[\text{NBu}_4]\text{Cl}$ are added to **1**, **9** is formed cleanly and unreacted **1** is observed in solution by NMR.

Reaction of 1 with Bromide Ion. The reaction of **1** with 2 equiv of $[\text{NBu}_4]\text{Br}$ in CD_2Cl_2 yields a mixture of $(\text{C}_{12}\text{H}_6)_2\text{Ga}_2\text{Cl}_{3-x}\text{Br}_x^-$ ($x = 0-2$) anions. The negative ion ESI mass spectrum of the resulting solution contains prominent signals for $(\text{C}_{12}\text{H}_6)_2\text{Ga}_2\text{Cl}_3^-$ (**9**) and $(\text{C}_{12}\text{H}_6)_2\text{Ga}_2\text{Cl}_2\text{Br}^-$ (**10**) and a smaller signal for $(\text{C}_{12}\text{H}_6)_2\text{Ga}_2\text{ClBr}_2^-$. The ^1H NMR spectrum contains signals for **9** and a second set of resonances for symmetric biphenylene units that overlap with the resonances for **9** and shows that a total of two biphenylene units are present per NBu_4^+ cation. The second set of biphenylene resonances is assigned to **10**; resonances for $(\text{C}_{12}\text{H}_6)_2\text{Ga}_2\text{ClBr}_2^-$ (which was detected in the ESI mass spectrum) could not be distinguished. The formation of **9** suggests that $(\text{C}_{12}\text{H}_6)_2\text{Ga}_2\text{X}_3^-$ species can exchange halides in solution. When substoichiometric amounts of $[\text{NBu}_4]\text{Br}$ are added to **1**, a mixture of **9** and **10** is formed and unreacted **1** is observed in solution by NMR.

Comparison of 1,8-Biphenylene and 1,8-Naphthalene Systems. The clean formation of **1** in Scheme 2 and the reaction of **1** with Lewis bases and chloride to form $(\text{C}_{12}\text{H}_6)_2\text{Ga}_2\text{Cl}_2\text{L}$ and $(\text{C}_{12}\text{H}_6)_2\text{Ga}_2\text{Cl}_3^-$ species (Schemes 4 and 5) contrast with the chemistry observed for the 1,8-naphthalene system.^{6g,12} Gabbaï reported that 1,8-bis(trimethylstannyl)naphthalene reacts with 1 equiv of GaCl_3 at -25°C to form a mixture of stannagallacycle **11** (21%) and digallacycle **12** (which crystallizes as a dimeric SnMe_3Cl adduct, 10%), as shown in Scheme 6.¹² At 65°C , this reaction produces **11** in 65% yield. Chloride-bridged polygallium species analogous to **1** were not observed, although in the presence of water $(\text{C}_{10}\text{H}_6)_4\text{Ga}_3(\mu_3\text{-O})(\mu\text{-Cl})$ (**13**) is formed. These results show that exchange of both SnMe_3 units by Ga units is possible in the 1,8-naphthalene system and suggest that the mixed Sn/Ga compound **11** is thermodynamically favored over the Ga_2 species **12**. The difference in reactivity between the 1,8-naphthalene and 1,8-biphenylene systems likely arises from the difference in the structures of the backbone units. The short Ga---Ga distance in the 1,8- Ga_2 -naphthalene framework (Scheme 1) requires an acute Ga-($\mu\text{-Cl}$)-Ga angle (**12**,



76.9°; **13**, 73.7°) to accommodate a μ -Cl bridge with reasonable Ga—Cl distances. In contrast, the Ga---Ga distance in the 1,8-Ga₂-biphenylene framework is nearly optimum for the formation of μ -Cl bridges. The Ga—(μ -Cl)—Ga angles in **1** (120.9°, 121.1°) and **7** (107.2°) are in the same range as that for the unconstrained species Ga₂Cl₇[−] (109°).²⁰

Conclusion

The reaction of GaCl₃ with 1,8-bis(trimethylstannyl)biphenylene (**6**) produces the tetragallium macrocycle (C₁₂H₆)₄Ga₄Cl₄ (**1**) in high yield. **1** reacts with Lewis bases (CH₃CN, THF) to form (C₁₂H₆)₂Ga₂Cl₂L species, which undergo associative exchange with free L. **1** reacts with halide ions (Cl[−] and Br[−]) to form (C₁₂H₆)₂Ga₂Cl₂X[−] species, which can exchange halides in solution. The Ga---Ga distance in the 1,8-Ga₂-biphenylene framework is nearly optimum for the formation of unstrained μ -Cl bridges.

Experimental Section

General Procedures. All reactions were performed under a nitrogen atmosphere unless otherwise specified. Nitrogen was purified by passage through activated molecular sieves and Q-5 oxygen scavenger. Diethyl ether, tetrahydrofuran, toluene, benzene-*d*₆, toluene-*d*₈, and THF-*d*₈ were distilled from sodium/benzophenone ketyl. CH₃CN was dried over P₂O₅ and stored over 3 Å molecular sieves. CD₃CN was degassed by three freeze-pump-thaw cycles and dried over 3 Å molecular sieves for 24 h. This process was repeated three times. 2,6-Dibromo-1-iodobenzene (**3**),¹⁶ 2,2',6,6'-tetrabromobiphenyl (**4**),¹⁷ and 1,8-dibromobiphenylene (**5**)¹⁸ were prepared by modified literature procedures (see Supporting Information).

NMR spectra were recorded on Bruker AVANCE DRX-400 or DMX-500 spectrometers in flame-sealed or Teflon-valved NMR tubes at ambient probe temperature unless otherwise specified. ¹H and ¹³C chemical shifts are reported versus SiMe₄ and were determined by reference to the residual solvent resonances. ²⁹Sn chemical shifts are referenced to SnMe₄. Coupling constants are reported in Hz. MALDI mass spectra were obtained with a PerSeptive Biosystems Voyager DE-PRO instrument. ESI mass spectra were recorded on an Agilent 1100 LC-MSD. A 5 μ L sample was injected by flow injection using an autosampler. Purified nitrogen was used as the nebulizing and drying gas. APPI mass spectra were obtained on the Agilent 1100 LC-MSD instrument

using a Kr lamp that emits photons at 10.0–10.6 eV as the photoionization source. In all cases where assignments are given, the observed isotope patterns closely matched the calculated patterns. The listed *m/z* value corresponds to the most intense peak in the isotope pattern. Elemental analyses were performed by Midwest Microlab, LCC (Indianapolis, IN).

1,8-Bis(trimethylstannyl)biphenylene (6). A solution of ⁿBuLi (2.5 M in hexane, 5.5 mL, 14 mmol) was added dropwise to a solution of 1,8-dibromobiphenylene (**5**, 1.83 g, 5.90 mmol) in Et₂O (20 mL) at 20 °C. The mixture was stirred for 30 min. A solution of Me₃SnCl (3.56 g, 17.8 mmol) in Et₂O (50 mL) was added dropwise at 20 °C. The solution was stirred for 12 h. The solution was washed with saturated aqueous [NH₄]Cl solution (100 mL). The organic layer was separated and the aqueous layer was extracted with Et₂O (3 \times 100 mL). The combined organic fractions were dried over MgSO₄ and the solvent was removed under vacuum. The resulting yellow solid was recrystallized from boiling pentane to afford 1,8-bis(trimethylstannyl)biphenylene as colorless needles in two crops (total yield 1.94 g, 69%). Mp: 117.5–118.5 °C. ¹H NMR (C₆D₆): δ 6.83 (dd, *J* = 8.0 and 1.0, satellites: *J*(¹¹⁹Sn—H) = 42, 2H, H2 and H7), 6.55 (dd, *J* = 8.0 and 6.8, 2H, H3 and H6), 6.45 (dd, *J* = 6.8 and 1.0, 2H, H4 and H5), 0.23 (s, 18H, satellites: *J*(¹¹⁹Sn—H) = 58, SnMe₃). ¹³C{¹H} NMR (CD₂Cl₂): δ 163.1, 152.1, 136.8, 132.2, 127.7, 116.6, −6.9 (SnMe₃). ¹¹⁹Sn{¹H} NMR (benzene-*d*₆): δ −37.3. GC-MS: *m/z* 478 (M⁺). Anal. Calcd for C₁₈H₂₄Sn₂: C, 45.25; H, 5.06. Found: C, 45.50; H, 5.06.

(C₁₂H₆)₄Ga₄Cl₄ (1). A suspension of 1,8-bis(trimethylstannyl)biphenylene (**6**, 0.182 g, 0.380 mmol) and GaCl₃ (0.0662 g, 0.376 mmol) in toluene (12 mL) was refluxed for 12 h and then cooled at 20 °C. Yellow crystals formed. The crystals were separated, washed with pentane (2 \times 4 mL), and dried under vacuum to afford a yellow powder (0.0672 g, 69%). **1:2 ratio:** A suspension of **6** (1.23 g, 2.57 mmol) and GaCl₃ (0.911 g, 5.17 mmol) in toluene (10 mL) was refluxed for 12 h. The mixture was cooled at 20 °C to afford yellow crystals, which were isolated, washed with toluene (3 \times 10 mL), and dried under vacuum to afford a fine yellow powder (0.348 g, 52%). **1** is sparingly soluble in benzene, toluene, and CH₂Cl₂ and chlorobenzene at 20 °C. ¹H NMR (CD₂Cl₂): δ 6.85 (dd, *J*_{H2–H3} = 8.1, *J*_{H2–H4} = 1.0, 4H, H2), 6.75 (2nd order multiplet, *J*_{H3–H2} = 8.1, *J*_{H3–H4} = 6.9, 4H, H3), 6.73 (2nd order multiplet, *J*_{H4–H3} = 6.9, *J*_{H4–H2} = 1.0, 4H, H4); *J* values were determined by simulation. ¹³C{¹H} NMR (CD₂Cl₂): δ 161.2, 152.6, 134.1, 130.4, 128.5, 119.2. Anal. Calcd for C₄₈H₂₄Cl₄Ga₄: C, 56.44; H, 2.37. Found: C, 56.70; H, 2.71. MALDI-MS (DHB matrix, toluene): *m/z* calcd for C₄₈H₂₄Cl₄Ga₄H⁺ 1023.8, found 1023.2. APPI-MS (CD₂Cl₂): *m/z* calcd for C₄₈H₂₄Cl₄Ga₄⁺ 1022.77, found 1022.8.

(C₁₂H₆)₂Ga₂Cl₂(CH₃CN) (7). A mixture of **1** (35 mg, 0.035 mmol) and CD₃CN (5 mL) was refluxed until all of the yellow solid disappeared. The solution was cooled to 20 °C, and yellow crystals formed. The crystals were isolated by removing the mother liquor by syringe (17 mg, 45%). X-ray crystallography showed that this material is 7 \cdot CH₃CN. Alternatively, a mixture of **1** and CD₃CN (1.5 mL) was refluxed until all of the yellow solid disappeared and then evaporated to dryness under vacuum. The pale yellow solid was dried under vacuum at room temperature to yield **7**, which contained some free CH₃CN. Vacuum drying of this solid at 75 °C yielded material that contained only a trace amount of free CH₃CN. Data for **7**: ¹H NMR (CD₂Cl₂): δ 6.98 (d, *J* = 6.0, 2H, H2), 6.83 (d, *J* = 6.8, 2H, H2), 6.71 (m, 4H, H3), 6.61 (m, 4H, H4), 2.63 (s, 3H, NCC₃H₃). ¹³C{¹H} NMR (CD₂Cl₂): δ 135.2, 132.5, 128.3, 118.5, 3.9; C9–C12 were not observed. Multiple elemental analyses of spectroscopically pure samples gave inconsistent results.

Generation of (C₁₂H₆)₂Ga₂Cl₂(THF) (8). An NMR tube was charged with **1** (1.9 mg), CD₂Cl₂ (0.6 mL), and THF (0.4 mL) and agitated for 5 min at 23 °C. NMR analysis at 23 °C revealed that **1** was completely converted to **8**. The volatiles were removed from

(20) (a) A larger Ga—(μ -Cl)—Ga angle (138°) was observed in (C₆F₅)₂Ga₂(μ -Cl)[−] King, W.; Scott, B.; Eckert, J.; Kubas, G. *Inorg. Chem.* **1999**, *38*, 1069. (b) Smaller Ga—(μ -Cl)—Ga angles (ca. 90°) are observed in double-bridged Ga—(μ -Cl)₂—Ga species. Lustig, C.; Mitzel, N. W. *Z. Naturforsch.* **2004**, *59b*, 140.

the solution of **8**, CD_2Cl_2 , and THF under vacuum, and the resulting pale yellow solid was dried under vacuum for 20 min. CD_2Cl_2 (0.6 mL) was added, resulting in a pale yellow solution. NMR analysis showed that **8** and 6.9 equiv of free THF were present. Data for **8**: ^1H NMR (CD_2Cl_2 , in the presence of 6.9 equiv of free THF): δ 7.00 (d, $J = 7.9$, 2H, H2), 6.82 (d, $J = 8.0$, 2H, H2), 6.72 (m, 4H, H3), 6.61 (t, $J = 6.4$, 4H, H4), 4.32 (m, 4H, THF), 2.18 (m, 4H, THF); free THF resonances at δ 3.73 and 1.84 were also present. $^{13}\text{C}\{^1\text{H}\}$ NMR (CD_2Cl_2 , in the presence of 6.9 equiv of free THF): δ 152.6, 135.1, 132.4, 128.3, 128.1, 118.5, 118.2, 74.6 (THF), 30.1 (THF); free THF resonances at δ 68.7 and 25.9 were also present; C1, C8, C9, C11 were not observed.

[NBu₄][(C₁₂H₆)₂Ga₂Cl₃] (9). An NMR tube was charged with **1** (11.9 mg, 0.0116 mmol) and $[\text{NBu}_4]\text{Cl}$ (6.1 mg, 0.022 mmol), and CD_2Cl_2 (0.6 mL) was added by vacuum transfer at -196 °C. The tube was warmed to room temperature and a yellow solution formed. The tube was monitored periodically by NMR. Resonances for several new unsymmetrical species grew in and disappeared. The formation of **9** was complete after 10 h. **9** was isolated by slow evaporation of the solvent in a glovebox. ^1H NMR (CD_2Cl_2): δ 6.95 (dd, $J = 7.9$ and 0.8, 4H), 6.63 (t, $J = 7$, 4H), 6.53 (dd, $J = 6.8$ and 0.8, 4H), 2.94 (m, 8H, NCH₂), 1.46 (m, 8H, CH₂), 1.31 (m, 8H, CH₂), 0.94 (t, $J = 7.3$, 12H, CH₃). $^{13}\text{C}\{^1\text{H}\}$ NMR (CD_2Cl_2): δ 160.4, 151.4, 135.8, 134.68, 127.34, 117.34, 58.9, 24.1, 20.0, 13.8. Negative ion ESI-MS (CD_2Cl_2): m/z calcd for $\text{C}_{24}\text{H}_{12}\text{Cl}_3\text{Ga}_2^-$, 544.8, found 544.8. Negative ion MALDI-MS (α -cyano-4-hydroxycinnamic acid external calibration matrix, CD_2Cl_2): m/z calcd for $\text{C}_{24}\text{H}_{12}\text{Cl}_3\text{Ga}_2^-$, 544.8, found 544.8. Anal. Calcd for $\text{C}_{40}\text{H}_{48}\text{Cl}_3\text{Ga}_2\text{N}$: C, 60.92; H, 6.13; N, 1.77. Found: C, 60.29; H, 6.08; N, 2.03.

Reaction of 1 with [NBu₄]Br. An NMR tube was charged with **1** (2.1 mg, 2.0 μmol) and $[\text{NBu}_4]\text{Br}$ (1.3 mg, 4.0 μmol), and CD_2Cl_2 was added by vacuum transfer at -196 °C. The tube was warmed to room temperature and a pale yellow solution formed. ^1H NMR and ESI-MS analyses showed that the major species present were **9** and $[\text{NBu}_4][(\text{C}_{12}\text{H}_6)_2\text{Ga}_2\text{Cl}_2\text{Br}]$ (**10**). Data for **10**: ^1H NMR (CD_2Cl_2): δ 6.94 (d, $J = 7.9$), 6.65 (t, $J = 7.0$), 6.52 (d, $J = 6.8$). Negative ion ESI-MS (CD_2Cl_2): m/z calcd for $\text{C}_{24}\text{H}_{12}\text{Cl}_2\text{BrGa}_2^-$, 590.8, found 590.8. ESI-MS also showed that $(\text{C}_{12}\text{H}_6)\text{Ga}_2\text{ClBr}_2^-$ was present as a minor species (m/z calcd for $\text{C}_{24}\text{H}_{12}\text{ClBr}_2\text{Ga}_2^-$, 634.7, found 634.8).

X-ray Crystallography. Crystallographic data are summarized in Table 1. Details are provided in the Supporting Information. Data were collected on a Bruker SMART (7) or Bruker SMART APEX (1) diffractometer using Mo K α radiation (0.71073 Å). Non-hydrogen atoms were refined with anisotropic displacement coefficients. Hydrogen atoms were included in the structure factor calculation at idealized positions and were allowed to ride on the neighboring atoms with relative isotropic displacement coefficients.

Table 1. Summary of X-ray Diffraction Data

	1	7 · 2CH ₃ CN
formula	C ₄₈ H ₂₄ Cl ₄ Ga ₄	C ₃₀ H ₂₁ Cl ₂ Ga ₂ N ₃
fw	1021.35	633.84
cryst syst	monoclinic	trigonal
space group	C2/c	R $\bar{3}$
<i>a</i> (Å)	15.793(3)	40.653(3)
<i>b</i> (Å)	22.495(5)	40.653(3)
<i>c</i> (Å)	16.567(4)	9.8092(10)
α (deg)	90	90
β (deg)	107.125(4)	90
γ (deg)	90	120
<i>V</i> (Å ³)	5625(2)	14040(2)
<i>Z</i>	4	18
temp (K)	100(2)	173(2)
cryst, color, habit	pale yellow, rod	yellow, block
GOF on <i>F</i> ²	1.061	1.070
final <i>R</i> indices	<i>R</i> 1 = 0.0436	<i>R</i> 1 = 0.0305
(<i>I</i> > 2 σ (<i>I</i>)) ^a	w <i>R</i> 2 = 0.1212	w <i>R</i> 2 = 0.0841
<i>R</i> indices	<i>R</i> 1 = 0.0504	<i>R</i> 1 = 0.0380
(all data)	w <i>R</i> 2 = 0.1237	w <i>R</i> 2 = 0.0881

^a *R*1 = $\sum||F_o| - |F_c||/\sum|F_o|$; w*R*2 = $[\sum[w(F_o^2 - F_c^2)^2]/\sum[w(F_o^2)^2]]^{1/2}$, where $w = q[\sigma^2(F_o^2) + (aP)^2 + bP]^{-1}$.

Specific comments for each structure are as follows. Single crystals of **1** were grown from chlorobenzene at 23 °C. These crystals contained 1.7 equiv of C₆H₅Cl per molecule of **1**, which were disordered; the C₆H₅Cl molecules were excluded using the PLATON SQUEEZE software package. Single crystals of **7** were grown from CD₃CN. These crystals contain two acetonitrile molecules per molecule of **7**, which were modeled as disordered groups, each 0.50 occupied. Each has two separate positions, which are necessarily correlated. These acetonitrile molecules were restrained (24 restraints) to be linear with normal bond distances and were refined with anisotropic displacement parameters.

Acknowledgment. This work was supported by the National Science Foundation (CHE-0516950). Dr. Ian Steele (University of Chicago) and Dr. Victor G. Young, Jr. (X-Ray Crystallographic Laboratory, 160 Kolthoff Hall, Department of Chemistry, University of Minnesota) are thanked for their assistance with X-ray crystallography.

Supporting Information Available: Synthetic procedures and NMR data for **3**, **4**, and **5**, additional NMR data for **1**, X-ray crystallographic data for **1** and **7** (cif files), and computational details. This material is available free of charge via the Internet at <http://pubs.acs.org>.

OM800902D

Chiral Aminotroponimate Zinc Complexes

Nils Meyer[†] and Peter W. Roesky^{*‡}

Institut für Chemie and Biochemie, Freie Universität Berlin, Fabeckstrasse 34-36, 14195 Berlin, Germany, and Institut für Anorganische Chemie, Universität Karlsruhe, Engesserstrasse 15, 76128 Karlsruhe, Germany

Received September 4, 2008

The enantiomerically pure bridged aminotroponimines (*S,S*)- and (*R,R*)-H₂{(*i*PrATI)₂diph}, in which two amino-isopropyl-troponimine moieties are linked by 1,2-(*S,S*)- or 1,2-(*R,R*)-diamino-1,2-diphenylethane, have been used as ligands in zinc chemistry. The bimetallic zincmethyl-, -ethyl, and phenyl complexes containing the enantiomerically pure bridged aminotroponimines (*S,S*)- or (*R,R*)-{(iPrATI)₂diph}²⁻ were prepared by the reaction of ZnR₂ (R = Me, Et, Ph) with the neutral ligands. As a result the compounds [(*S,S*)-{(iPrATI)₂diph}(ZnR)₂] (R = Me (**1**), Et (**2**)) and [(*R,R*)-{(iPrATI)₂diph}(ZnPh)₂] (**3**) were obtained. Moreover, the new ligands (*S,S*)-H₂{((*R*)-PhCHCH₃ATI)₂diph} and (*R,R*)-H₂{((*R*)-PhCHCH₃ATI)₂diph}, which are diastereomers, were prepared by using (*R*)-1-amino-1-phenylethane instead of isopropylamine in the ligand synthesis. Reacting these ligands with ZnMe₂ resulted in the enantiomerically pure compounds [(*S,S*)-{(R)-PhCHCH₃ATI)₂diph}(ZnMe)₂] (**4**) and [(*R,R*)-{(R)-PhCHCH₃ATI)₂diph}(ZnMe)₂] (**5**). Compounds **1–5** were investigated by single-crystal X-ray diffraction, showing a distorted trigonal-planar coordination of the zinc atoms.

Introduction

Aminotroponimines (ATIHS) are a well-known class of ligands that were discovered in the 1960s.¹ It was shown that aminotroponimines could act as ligands for a wide range of main group, transition, and f-block elements.² Usually ATI ligands behave as anionic bidentate nitrogen donor ligands and form very stable chelate complexes with a delocalization of the negative charge through the seven-membered ring, obtaining a 10π-electron backbone (Scheme 1).

The aminotroponimate ligand was also introduced into the coordination sphere of zinc.³ The first structurally characterized ATI zinc complexes were reported by our group.⁴ Recently Blechert et al. and our group have also shown that zinc compounds of the type [(iPr)₂ATI}ZnMe] are highly active precatalysts for the hydroamination^{5,6} of alkenes and alkynes.⁷ We have also described the preparation of zinc complexes with sterically and electronically modified ATI ligands and the influence of the modifications on their catalytic activity.⁸ The new zinc precatalysts show, besides their good catalytic activity and selectivity, high tolerance toward polar and functional groups and high stability toward air and moisture. Moreover zinc is nontoxic and one of the least expensive metals. These advantages makes zinc superior to the previous used catalysts for this reaction mainly based on lithium,⁹ group 4 metals,¹⁰

the lanthanides,^{11–13} the platinum metals,¹⁴ calcium,¹⁵ copper,¹⁶ silver,¹⁷ and gold.¹⁸

Motivated by these studies, we were interested in the preparation of zinc compounds with chiral ATI ligands. In the present contribution we describe the synthesis and characterization of new enantiomerically pure chiral-bridged aminotropon-

(6) Recent reviews: (a) Roundhill, D. M. *Chem. Rev.* **1992**, *92*, 1–27. (b) Müller, T. E.; Beller, M. *Chem. Rev.* **1998**, *98*, 675–703. (c) Johannsen, M.; Jørgensen, K. A. *Chem. Rev.* **1998**, *98*, 1689–1708. (d) Nobis, M.; Driessen-Hölscher, B. *Angew. Chem.* **2001**, *113*, 4105–4108; *Angew. Chem., Int. Ed.* **2001**, *40*, 3983–3985. (e) Brunet, J.-J.; Neibecker, D. In *Catalytic Heterofunctionalization*, Togni, A.; Grützmacher, H., Eds.; VCH: Weinheim, 2001; pp 91–141. (f) Seayad, J.; Tillack, A.; Hartung, C. G.; Beller, M. *Adv. Synth. Catal.* **2002**, *344*, 795–813. (g) Pohlki, F.; Doye, S. *Chem. Soc. Rev.* **2003**, *32*, 104–114. (h) Bytschkov, I.; Doye, S. *Eur. J. Org. Chem.* **2003**, 935–946. (i) Roesky, P. W.; Müller, T. E. *Angew. Chem.* **2003**, *115*, 2812–2814; *Angew. Chem., Int. Ed.* **2003**, *42*, 2708–2710. (j) Hartwig, J. F. *Pure Appl. Chem.* **2004**, *76*, 507–516. (k) Hong, S.; Marks, T. J. *Acc. Chem. Res.* **2004**, *37*, 673–686. (l) Hultsch, K. C. *Adv. Synth. Catal.* **2005**, *347*, 367–391.

(7) Zulus, A.; Dochnahl, M.; Hollmann, D.; Löhnwitz, K.; Herrmann, J.-S.; Roesky, P. W.; Blechert, S. *Angew. Chem.* **2005**, *117*, 7972–7976; *Angew. Chem., Int. Ed.* **2005**, *44*, 7794–7798.

(8) (a) Meyer, N.; Löhnwitz, K.; Zulus, A.; Roesky, P. W.; Dochnahl, M.; Blechert, S. *Organometallics* **2006**, *25*, 3730–3734. (b) Dochnahl, M.; Löhnwitz, K.; Pissarek, J. W.; Biyikal, M.; Schulz, S. R.; Schön, S.; Meyer, N.; Roesky, P. W.; Blechert, S. *Chem.–Eur. J.* **2007**, *13*, 6654–6666. (c) Dochnahl, M.; Pissarek, J. W.; Blechert, S.; Löhnwitz, K.; Roesky, P. W. *Chem. Commun.* **2006**, 3405–3407. (d) Dochnahl, M.; Löhnwitz, K.; Pissarek, J. W.; Roesky, P. W.; Blechert, S. *Dalton Trans.* **2008**, 2844–2848.

(9) Horrillo Martinez, P.; Hultsch, K. C.; Hampel, F. *Chem. Commun.* **2006**, 2221–2223.

(10) (a) Wood, M. C.; Leitch, D. C.; Yeung, C. S.; Kozak, J. A.; Schafer, L. L. *Angew. Chem.* **2007**, *119*, 358–362; *Angew. Chem., Int. Ed.* **2007**, *46*, 354–358. (b) Kaspar, L. T.; Fingerhut, B.; Ackermann, L. *Angew. Chem.* **2005**, *117*, 6126–6128; *Angew. Chem., Int. Ed.* **2005**, *44*, 5972–5974. (c) Heutling, A.; Pohlki, F.; Bytschkov, I.; Doye, S. *Angew. Chem.* **2005**, *117*, 3011–3013; *Angew. Chem., Int. Ed.* **2005**, *44*, 2951–2954.

(11) Conticello, V. P.; Brard, L.; Giardello, M. A.; Tsuji, Y.; Sabat, M.; Stern, C. L.; Marks, T. J. *J. Am. Chem. Soc.* **1992**, *114*, 2761–2762. (b) Stern, D.; Sabat, M.; Marks, T. J. *J. Am. Chem. Soc.* **1992**, *114*, 9558–9575. (c) Haar, C. M.; Stern, C. L.; Marks, T. J. *Organometallics* **1996**, *15*, 1765–1784. (d) Roesky, P. W.; Deninger, U.; Stern, C. L.; Marks, T. J. *Organometallics* **1997**, *16*, 4486–4492.

* Corresponding author. E-mail: roesky@chemie.uni-karlsruhe.de.

[†] Freie Universität Berlin.

[‡] Universität Karlsruhe.

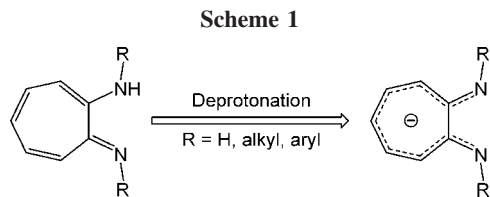
(1) (a) Brasen, W. R.; Holmquist, H. E.; Brenson, R. E. *J. Am. Chem. Soc.* **1960**, *82*, 995–996. (b) Brasen, W. R.; Holmquist, H. E.; Brenson, R. E. *J. Am. Chem. Soc.* **1961**, *83*, 3125–3135.

(2) Review: (a) Roesky, P. W. *Chem. Soc. Rev.* **2000**, *29*, 333–345.

(3) (a) Forbes, C. E.; Holm, R. H. *J. Am. Chem. Soc.* **1970**, *92*, 2297–2303. (b) Franz, K. J.; Singh, N.; Spingler, B.; Lippard, S. J. *Inorg. Chem.* **2000**, *39*, 4081–4092.

(4) (a) Gamer, M. T.; Roesky, P. W. *Eur. J. Inorg. Chem.* **2003**, 2145–2148. (b) Herrmann, J. S.; Luinstra, G. A.; Roesky, P. W. *J. Organomet. Chem.* **2004**, *689*, 2720–2725.

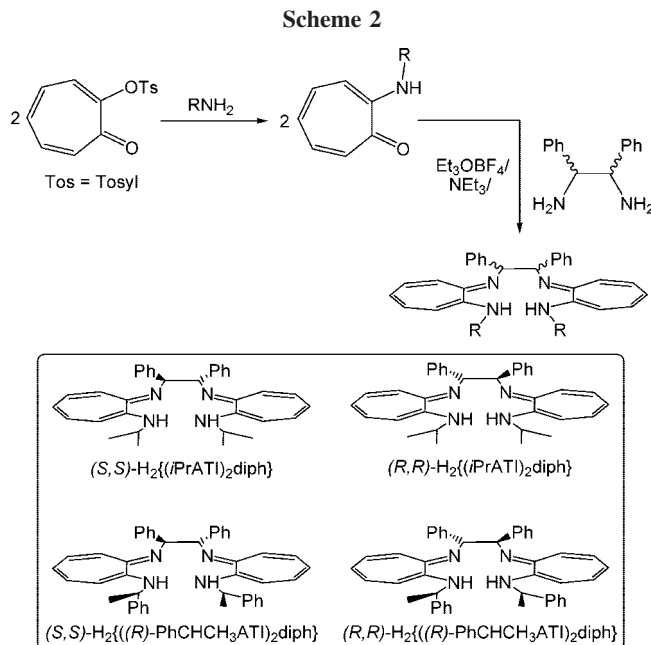
(5) Müller, T. E. In *Encyclopedia of Catalysis*; Horváth, J. T., Ed.; Wiley: New York, 2002.



imine ligands (*S,S*)-H₂{(*R,R*)-PhCHCH₃ATI₂diph} and (*R,R*)-H₂{(*R,R*)-PhCHCH₃ATI₂diph} (Scheme 2). These ligands and the previously described (*S,S*)- or (*R,R*)-H₂{(*i*PrATI₂)₂diph}¹⁹ were used for the preparation of dimetallic zinc alkyl and aryl complexes.

Experimental Section

General Procedures. All manipulations of air-sensitive materials were performed with the rigorous exclusion of oxygen and moisture in flame-dried Schlenk-type glassware either on a dual-manifold Schlenk line, interfaced to a high-vacuum (10⁻⁴ Torr) line, or in an argon-filled M. Braun glovebox. Ether solvents (tetrahydrofuran and ethyl ether) were predried over Na wire and distilled under nitrogen from K (THF) or Na wire (ethyl ether) benzophenone ketyl prior to use. Hydrocarbon solvents (toluene and *n*-pentane) were distilled under nitrogen from LiAlH₄. Deuterated solvents were obtained from Chemotrade Chemiehandelsgesellschaft mbH (all ≥99 atom % D) and were degassed, dried, and stored *in vacuo* over Na/K alloy in resealable flasks. CDCl₃ was used as purchased. NMR spectra were recorded on a JNM-LA 400 FT-NMR spectrometer. Chemical shifts are referenced to internal solvent resonances and are reported relative to tetramethylsilane. Elemental



analyses were carried out with an Elementar Vario EL III. (*R,R*)-H₂{(*i*PrATI₂)₂diph},¹⁹ (*S,S*)-H₂{(*i*PrATI₂)₂diph},¹⁹ (*R*)-{(PhCHCH₃)ATI}H, and ZnPh₂²⁰ were prepared according to literature procedures. ZnMe₂ and ZnEt₂ were purchased from Aldrich Inc.

(*S,S*)-H₂{(*R*)-PhCHCH₃ATI₂diph} and (*R,R*)-H₂{(*R*)-PhCHCH₃ATI₂diph}. 2-(*N*-(*R*)-(1-phenylethylamino)tropone²¹ (5.9 mmol, 1.33 g) in 10 mL of methylene chloride was slowly added to a solution of Et₃OBF₄ (5.9 mmol, 1.12 g) in 10 mL of methylene chloride under an argon atmosphere. After stirring at room temperature for 3 h 5 mL of Et₃N was added to the orange solution. The mixture was stirred for another 15 min, and then 1,2-(*S,S*)- or 1,2-(*R,R*)-diphenylethylenediamine (1.00 g, 4.7 mmol) in 10 mL of methylene chloride was added to the mixture and the solution turned yellow immediately. After stirring for 18 h the volatiles were removed *in vacuo* and the residue was extracted twice with toluene. The solution was concentrated to 2 mL and layered with pentane to obtain the product as a yellow powder.

(*S,S*)-H₂{(*R*)-PhCHCH₃ATI₂diph}. Yield: 2.14 g (4.3 mmol, 80%). ¹H NMR (CDCl₃, 400 MHz, 25 °C): δ 1.62 (d, 6 H, CH₃, *J*_{H,H} = 6.6 Hz), 4.73 (q, 2 H, CH, *J*_{H,H} = 6.6 Hz), 5.07 (s, 2 H, CH), 5.99 (t, 2 H, CH_{ring}, *J*_{H,H} = 9.4 Hz), 6.07 (d, 2 H, CH_{ring}, *J*_{H,H} = 10.5 Hz), 6.20 (d, 2 H, CH_{ring}, *J*_{H,H} = 11.2 Hz), 6.49–6.59 (m, 4 H, CH_{ring}), 7.14–7.33 (m, 16 H, Ph), 7.62–7.65 (m, 4 H, Ph), 8.72 (br s, 2 H, NH). ¹³C{¹H} NMR (CDCl₃, 100.4 MHz, 25 °C): δ 24.9, 54.3, 67.0, 109.9, 113.9, 118.1, 126.1, 126.6, 126.9, 127.7, 128.0, 128.2, 128.5, 129.9, 141.3, 144.9, 151.5, 153.6. MS (EI, 70 eV, 175 °C): *m/z* (%) 626 [M⁺] (2), 105 (100).

(*R,R*)-H₂{(*R*)-PhCHCH₃ATI₂diph}. Yield: 1.63 g (3.2 mmol, 68%). ¹H NMR (CDCl₃, 400 MHz, 25 °C): δ 1.53 (d, 6 H, CH₃, *J*_{H,H} = 6.6 Hz), 4.63 (q, 2 H, CH, *J*_{H,H} = 6.6 Hz), 4.98 (s, 2 H, CH), 5.90 (t, 2 H, CH_{ring}, *J*_{H,H} = 8.5 Hz), 5.98 (d, 2 H, CH_{ring}, *J*_{H,H} = 10.3 Hz), 6.12 (d, 2 H, CH_{ring}, *J*_{H,H} = 12.1 Hz), 6.40–6.49 (m, 4 H, CH_{ring}), 7.07–7.23 (m, 16 H, Ph), 7.53–7.56 (m, 4 H, Ph), 8.59 (br s, 2 H, NH). ¹³C{¹H} NMR (CDCl₃, 100.4 MHz, 25 °C): δ 25.3, 54.3, 67.3, 109.9, 113.9, 118.1, 126.1, 126.6, 126.8, 127.8, 128.0, 128.2, 128.5, 128.6, 129.9, 141.3, 148.4, 151.6. TOF MS: 627 [M + H]⁺ (100).

[(*S,S*)-{(iPrATI)₂diph}(ZnR)₂] (R = Me (1), Et (2)). A solution of ZnR₂ was slowly added to (*S,S*)-H₂{(*i*PrATI)₂diph} in 20 mL of toluene at -78 °C. The resulting yellow reaction mixture was

(12) (a) Gagne, M. R.; Marks, T. J. *J. Am. Chem. Soc.* **1989**, *111*, 4108–4109. (b) Gagne, M. R.; Stern, C. L.; Marks, T. J. *J. Am. Chem. Soc.* **1992**, *114*, 275–294. (c) Li, Y.; Marks, T. J. *J. Am. Chem. Soc.* **1996**, *118*, 9295–9306. (d) Roesky, P. W.; Stern, C. L.; Marks, T. J. *J. Am. Chem. Soc.* **1997**, *119*, 4705–4711. (e) Li, Y.; Marks, T. J. *J. Am. Chem. Soc.* **1998**, *120*, 1757–1771. (f) Arredondo, V. M.; McDonald, F. E.; Marks, T. J. *J. Am. Chem. Soc.* **1998**, *120*, 4871–4872. (g) Arredondo, V. M.; McDonald, F. E.; Marks, T. J. *J. Am. Chem. Soc.* **1999**, *121*, 3633–3639. (h) Hong, S.; Marks, T. J. *J. Am. Chem. Soc.* **2002**, *124*, 7886–7887. (i) Ryu, J. S.; Li, G. Y.; Marks, T. J. *J. Am. Chem. Soc.* **2003**, *125*, 12584–12605. (j) Hong, S.; Tian, S.; Metz, M. V.; Marks, T. J. *J. Am. Chem. Soc.* **2003**, *125*, 14768–14783.

(13) (a) Kim, Y. K.; Livinghouse, T.; Bercaw, J. E. *Tetrahedron Lett.* **2001**, *42*, 2933–2935. (b) Kim, Y. K.; Livinghouse, T. *Angew. Chem.* **2002**, *114*, 3797–3799; *Angew. Chem., Int. Ed.* **2002**, *41*, 3645–3647. (c) Kim, Y. K.; Livinghouse, T.; Horino, Y. *J. Am. Chem. Soc.* **2003**, *125*, 9560–9561. (d) O'Shaughnessy, P. N.; Knight, P. D.; Morton, C.; Gillespie, K. M.; Scott, P. *Chem. Commun.* **2003**, 1770–1771. (e) Gribkov, D. V.; Hultzsck, K. C.; Hampel, F. *Chem.—Eur. J.* **2003**, *9*, 4796–4810. (f) Hultzsck, K. C.; Gribkov, D. V. *Chem. Commun.* **2004**, 730–731. (g) Hultzsck, K. C.; Hampel, F.; Wagner, T. *Organometallics* **2004**, *23*, 2601–2612. (h) Gribkov, D. V.; Hultzsck, K. C.; Hampel, F. *J. Am. Chem. Soc.* **2006**, *128*, 3748–3759. (i) Riegert, D.; Collin, J.; Medour, A.; Schulz, E.; Trifonov, A. *J. Org. Chem.* **2006**, *71*, 2514–2517.

(14) Rh:(a) Utsunomiya, M.; Kuwano, R.; Kawatsura, M.; Hartwig, J. F. *J. Am. Chem. Soc.* **2003**, *125*, 5608–5609. (b) Takemiya, A.; Hartwig, J. F. *J. Am. Chem. Soc.* **2006**, *128*, 6042–6043. (c) Dorta, R.; Egli, P.; Zürichner, F.; Togni, A. *J. Am. Chem. Soc.* **1997**, *119*, 10857–10858. Pd: (d) Utsunomiya, M.; Hartwig, J. F. *J. Am. Chem. Soc.* **2003**, *125*, 14286–14287. Pt: (f) Bender, C. F.; Widenhoefer, R. A. *J. Am. Chem. Soc.* **2005**, *127*, 1070–1071.

(15) Crimmin, M. R.; Caseley, I. J.; Hill, M. S. *J. Am. Chem. Soc.* **2005**, *127*, 2042–2043.

(16) Taylor, J. G.; Whittall, N.; Hii, K. K. *Org. Lett.* **2006**, *8*, 3561–3564.

(17) Sun, J.; Kozmin, S. A. *Angew. Chem.* **2006**, *118*, 5113–5115; *Angew. Chem., Int. Ed.* **2006**, *45*, 4991–4993.

(18) (a) Brouwer, C.; He, C. *Angew. Chem.* **2006**, *118*, 1776–1779; *Angew. Chem., Int. Ed.* **2006**, *45*, 1744–1747. (b) Han, X.; Widenhoefer, R. A. *Angew. Chem.* **2006**, *118*, 1779–1781; *Angew. Chem., Int. Ed.* **2006**, *45*, 1747–1749. (c) Zhang, Z.; Liu, C.; Kinder, R. E.; Han, X.; Qian, H.; Widenhoefer, R. A. *J. Am. Chem. Soc.* **2006**, *128*, 9066–9073. (d) Kang, J. E.; Kim, H. B.; Lee, J. W.; Shin, S. *Org. Lett.* **2006**, *8*, 3537–3540.

(19) Meyer, N.; Zulys, A.; Roesky, P. W. *Organometallics* **2006**, *25*, 4179–4182.

(20) Kojima, K.; Kimura, M.; Ueda, S.; Tamara, Y. *Tetrahedron* **2006**, *26*, 7512–7520.

(21) Roesky, P. W. *J. Organomet. Chem.* **2001**, *621*, 277–283.

allowed to warm to ambient temperature and stirred for 16 h. The solution was concentrated until a yellow residue appeared. The residue was dissolved by heating, and the resulting orange solution was allowed to stand at room temperature. The product was obtained as yellow crystals after 8 h. X-ray quality crystals were selected directly from this crop.

[(*S,S*)-{(iPrATI)₂diph}(ZnMe)₂], **1**. (*S,S*)-H₂{(iPrATI)₂diph}: 0.75 g; 1.5 mmol; ZnMe₂: 2 M (toluene), 1.5 mL, 3.0 mmol. Yield: 0.62 g (0.9 mmol, 60%). ¹H NMR (C₆D₆, 400 MHz, 25 °C): δ -0.12 (s, 3 H, ZnCH₃), 1.27 (d, 6 H, CH(CH₃)₂, *J*_{H,H} = 6.2 Hz), 1.42 (d, 6 H, CH(CH₃)₂, *J*_{H,H} = 6.2 Hz), 3.98 (sept, 2 H, CH(CH₃)₂, *J*_{H,H} = 6.2 Hz), 5.45 (s, 2 H, CH), 6.46 (t, 2 H, CH_{ring}, *J*_{H,H} = 9.0 Hz), 6.82 (d, 2 H, CH_{ring}, *J*_{H,H} = 11.6 Hz), 6.98–7.17 (m, 12 H, CH_{ring} + Ph), 7.30–7.36 (m, 4 H, Ph). ¹³C{¹H} NMR (C₆D₆, 100.4 MHz, 25 °C): δ -12.0 (ZnCH₃), 25.7 (CH(CH₃)₂), 25.4 (CH(CH₃)₂), 48.3 (CH(CH₃)₂), 71.2 (CH), 113.4, 114.8, 119.4, 127.3, 128.4, 128.7, 135.0, 135.1, 142.1, 160.8, 161.2. MS (EI): *m/z* (%) 643 ([M - CH₃]⁺ 2), 564 ([M - CH₃ - ZnCH₃]⁺ 95), 521 ([M - CH₃ - ZnCH₃ - CH(CH₃)₂]⁺ 100). C₃₆H₄₂N₄Zn₂ (661.53): C, 65.36; H, 6.40; N, 8.47. Found: C, 65.35; H, 6.81; N, 8.33.

[(*S,S*)-{(iPrATI)₂diph}(ZnEt)₂], **2**: (*S,S*)-H₂{(iPrATI)₂diph}: 1.00 g, 2 mmol; ZnEt₂: 1 M (hexane), 4.2 mL, 4.2 mmol. Yield: 0.60 g (0.9 mmol, 45%). ¹H NMR (C₆D₆, 400 MHz, 25 °C): δ 0.49 (dq, 2 H, CH₂CH₃, *J*_{H,H} = 5.1 Hz, *J*_{H,H} = 8.2 Hz), 0.55 (dq, 2 H, CH₂CH₃, *J*_{H,H} = 5.1 Hz, *J*_{H,H} = 8.2 Hz), 1.06 (d, 6 H, CH(CH₃)₂, *J*_{H,H} = 6.1 Hz), 1.20 (d, 6 H, CH(CH₃)₂, *J*_{H,H} = 6.1 Hz), 1.44 (t, 6 H, CH₂CH₃, *J*_{H,H} = 8.2 Hz), 3.73 (sept., 2 H, CH(CH₃)₂, *J*_{H,H} = 6.2 Hz), 5.27 (s, 2 H, CH), 6.24 (t, 2 H, CH_{ring}, *J*_{H,H} = 9.2 Hz), 6.57 (d, 2 H, CH_{ring}, *J*_{H,H} = 11.4 Hz), 6.75–6.98 (m, 12 H, CH_{ring} + Ph), 7.13–7.15 (m, 4 H, Ph). ¹³C{¹H} NMR (C₆D₆, 100.4 MHz, 25 °C): δ 1.2 (CH₂CH₃), 12.9 (CH₂CH₃), 23.3 (CH(CH₃)₂), 25.5 (CH(CH₃)₂), 48.1 (CH(CH₃)₂), 71.3 (CH), 113.4, 114.6, 119.3, 127.4, 128.4, 128.6, 135.0, 135.1, 142.0, 160.8, 161.0. MS (EI): *m/z* (%) 659 ([M - CH₂CH₃]⁺ 12), 564 ([M - CH₂CH₃ - ZnCH₂CH₃]⁺ 90), 521 ([M - CH₂CH₃ - ZnCH₂CH₃ - CH(CH₃)₂]⁺ 48), 343 ([1/2 M]⁺ 24), 315 ([1/2 M - CH₂CH₃]⁺ 23), 173 (100). C₃₈H₄₆N₄Zn₂ (689.58): C, 66.19; H, 6.72; N, 8.12. Found: C, 66.10; H, 6.36; N, 8.06.

[(*R,R*)-{(iPrATI)₂diph}(ZnPh)₂], **3**. Toluene (5 mL) was added to a mixture of ZnPh₂ (0.33 g, 1.5 mmol) and (*R,R*)-H₂{(iPrATI)₂diph} (0.37 g, 0.8 mmol) and the resulting yellow solution was stirred for 2 h at ambient temperature. The solution was concentrated until a yellow residue appeared. The residue was dissolved by heating, and the resulting orange solution was allowed to stand at room temperature. The product was obtained as yellow crystals after 24 h. X-ray quality crystals were selected directly from this crop. Yield: 0.43 g (0.5 mmol, 67%). ¹H NMR (C₆D₆, 400 MHz, 25 °C): δ 0.79 (d, 6 H, CH(CH₃)₂, *J*_{H,H} = 6.1 Hz), 1.08 (d, 6 H, CH(CH₃)₂, *J*_{H,H} = 6.1 Hz), 3.53 (sept, 2 H, CH(CH₃)₂, *J*_{H,H} = 6.1 Hz), 4.96 (s, 2 H, CH), 5.85 (t, 2 H, CH_{ring}, *J*_{H,H} = 8.7 Hz), 6.02–6.10 (m, 4 H, CH_{ring}), 6.37 (d, 2 H, CH_{ring}, *J*_{H,H} = 11.0 Hz), 6.53 (t, 2 H, CH_{ring}, *J*_{H,H} = 9.9 Hz), 6.60–6.62 (m, 6 H, Ph), 6.75–6.78 (m, 4 H, Ph), 6.84–6.85 (m, 6 H, Ph), 7.15–7.16 (m, 4 H, Ph). ¹³C{¹H} NMR (C₆D₆, 100.4 MHz, 25 °C): δ 23.9 (CH(CH₃)₂), 26.0 (CH(CH₃)₂), 48.5 (CH(CH₃)₂), 70.6 (CH), 113.9, 116.2, 120.2, 126.3, 127.3, 127.7, 127.8, 128.0, 134.9, 135.2, 128.7, 141.8, 150.6, 160.6, 160.9. MS (EI): *m/z* (%) = 564 ([M - Ph, -Ph]⁺ 100), 521 ([M - Ph, -Ph, -CH(CH₃)₂]⁺ 48). Raman (solid, *ν*/cm⁻¹): 3053(m), 3043(w), 3033(w), 3000(w), 2970(w), 2929(w), 2861(w), 1593(s), 1576(m), 1506(m), 1468(s), 1429(s), 1419(s), 1395(m), 1269(w), 1226(w), 1022(m), 999(vs). C₄₆H₄₆N₄Zn₂ (785.66): C, 70.32; H, 5.90; N, 7.13. Found: C, 69.76; H, 5.97; N, 7.09.

[(*S,S*)-{((*R*)-PhCHCH₃ATI)₂diph}(ZnMe)₂] (**4**) and [(*R,R*)-{((*R*)-PhCHCH₃ATI)₂diph}(ZnMe)₂] (**5**). ZnMe₂ in toluene (1.2 M, 1.1 mmol, 0.9 mL) was slowly added to (*S,S*)-H₂{((*R*)-PhCHCH₃ATI)₂diph} or (*R,R*)-H₂{((*R*)-PhCHCH₃ATI)₂diph} (0.31

g, 0.5 mmol) in 20 mL of toluene. The resulting orange solution was stirred for 16 h at ambient temperature, filtered off, concentrated, and layered with pentane. The product was obtained as a yellow, crystalline solid. X-ray quality crystals were selected directly from this crop.

[(*S,S*)-{((*R*)-PhCHCH₃ATI)₂diph}(ZnMe)₂], **4**. Yield: 0.16 g (0.2 mmol, 40%). ¹H NMR (C₆D₆, 400 MHz, 25 °C): δ -0.20 (s, 6 H, ZnCH₃), 1.63 (d, 6 H, PhCHCH₃, *J*_{H,H} = 6.6 Hz), 4.71 (q, 2 H, PhCHCH₃, *J*_{H,H} = 6.6 Hz), 5.34 (s, 2 H, CH), 6.11–6.16 (m, 2 H, CH_{ring}), 6.64–6.66 (m, 4 H, CH_{ring}), 6.76–7.11 (m, 20 H, CH_{ring} + Ph), 7.22–7.24 (m, 4 H, Ph). ¹³C{¹H} NMR (C₆D₆, 100.4 MHz, 25 °C): δ -10.6 (ZnCH₃), 27.6 (PhCHCH₃), 57.89 (PhCHCH₃), 70.9 (CH), 114.2, 115.9, 120.1, 126.2, 126.8, 127.3, 128.4, 128.7, 128.9, 134.9, 135.0, 141.9, 145.0, 161.3, 161.5. C₄₆H₄₆N₄Zn₂ (785.66): C, 70.32; H, 5.90; N, 7.13. Found: C, 70.17; H, 6.23; N, 7.10.

[(*R,R*)-{((*R*)-PhCHCH₃ATI)₂diph}(ZnMe)₂], **5**. Yield: 0.24 g (0.3 mmol, 60%). ¹H NMR (C₆D₆, 400 MHz, 25 °C): δ -0.17 (s, 6 H, ZnCH₃), 1.96 (d, 6 H, PhCHCH₃, *J*_{H,H} = 6.6 Hz), 5.06 (q, 2 H, PhCHCH₃, *J*_{H,H} = 6.6 Hz), 5.49 (s, 2 H, CH), 6.31 (t, 2 H, CH_{ring}, *J*_{H,H} = 9.2 Hz), 6.85–6.95 (m, 6 H, CH_{ring}), 7.17–7.25 (m, 10 H, CH_{ring} + Ph), 7.33–7.40 (m, 12 H, Ph). ¹³C{¹H} NMR (C₆D₆, 100.4 MHz, 25 °C): δ -12.4 (ZnCH₃), 28.3 (PhCHCH₃), 58.0 (PhCHCH₃), 71.3 (CH), 115.6, 116.2, 120.3, 126.3, 127.0, 127.4, 128.6, 128.7, 129.1, 135.4, 135.5, 142.0, 145.5, 161.3, 161.7. C₄₆H₄₆N₄Zn₂ (785.66): C, 70.32; H, 5.90; N, 7.13. Found: C, 70.23; H, 5.76; N, 7.24.

X-ray Crystallographic Studies of 1, 2, 3, 4, and 5. Crystals of **1**, **2** and **3** were grown from saturated toluene solutions. Crystals of **4** and **5** were grown by slow diffusion of pentane into a toluene solution. Suitable crystals were covered in mineral oil (Aldrich) and mounted onto a glass fiber. The crystals were transferred directly to the -70 °C cold N₂ stream of a Stoe IPDS 2T diffractometer. Subsequent computations were carried out on an Intel Pentium IV PC.

All structures were solved by the Patterson method (SHELXS-97²²). The remaining non-hydrogen atoms were located from successive difference Fourier map calculations. The refinements were carried out by using full-matrix least-squares techniques on *F*, minimizing the function (F_o - F_c)², where the weight is defined as 4F_o²/2(F_o²) and F_o and F_c are the observed and calculated structure factor amplitudes using the program SHELXL-97.²³ In the final cycles of each refinement, all non-hydrogen atoms were assigned anisotropic temperature factors. Carbon-bound hydrogen atom positions were calculated. The hydrogen atom contributions were calculated, but not refined. The final values of refinement parameters are given in Table 1. The locations of the largest peaks in the final difference Fourier map calculation as well as the magnitude of the residual electron densities in each case were of no chemical significance. Positional parameters, hydrogen atom parameters, thermal parameters, and bond distances and angles have been deposited as Supporting Information. Crystallographic data (excluding structure factors) for the structures reported in this paper have been deposited with the Cambridge Crystallographic Data Centre as supplementary publication nos. 705512–705516. Copies of the data can be obtained free of charge on application to CCDC, 12 Union Road, Cambridge CB21EZ, UK (fax: (+44)1223-336-033; e-mail: deposit@ccdc.cam.ac.uk).

Results and Discussion

Ligand Synthesis. The synthesis of the enantiomerically pure chiral-bridged aminotroponimine ligands (*S,S*)-H₂{(iPr-

(22) Sheldrick, G. M. *SHELXS-97, Program of Crystal Structure Solution*; University of Göttingen: Germany, 1997.

(23) Sheldrick, G. M. *SHELXL-97, Program of Crystal Structure Refinement*; University of Göttingen: Germany, 1997.

Table 1. Crystallographic Details of 1, 2, 3, 4, and 5^a

	1	2	3	4	5
formula	C ₃₆ H ₄₂ N ₄ Zn ₂	C ₃₈ H ₄₆ N ₄ Zn ₂	C ₄₆ H ₄₆ N ₄ Zn ₂	C ₄₆ H ₄₆ N ₄ Zn ₂	C ₄₆ H ₄₆ N ₄ Zn ₂
fw	661.48	689.53	785.61	785.61	785.61
space group	<i>P</i> 2 ₁ (No. 2)	<i>C</i> 222 ₁ (No. 20)	<i>C</i> 222 ₁ (No. 20)	<i>P</i> 1 (No. 1)	<i>P</i> 2 ₁ 2 ₁ (No. 19)
<i>a</i> , Å	10.3934(10)	14.4675(7)	16.5128(7)	10.3246(5)	9.4194(5)
<i>b</i> , Å	9.9696(6)	18.2870(14)	17.8044(13)	11.0133(5)	15.4966(7)
<i>c</i> , Å	15.9184	26.9299(18)	27.1153(14)	17.4536(9)	27.0132(11)
α, deg	90.00	90.00	90.00	84.878(4)	90.00
β, deg	94.368(8)	90.00	90.00	81.151(4)	90.00
γ, deg	90.00	90.00	90.00	89.787(4)	90.00
<i>V</i> , Å ³	1644.6(2)	7128.7(8)	7971.9(8)	1953.06(16)	3943.1(3)
<i>Z</i>	2	8	8	2	4
density (g/cm ³)	1.336	1.285	1.309	1.336	1.323
radiation	Mo Kα (λ = 0.71073 Å)	Mo Kα (λ = 0.71073 Å)	Mo Kα (λ = 0.71073 Å)	Mo Kα (λ = 0.71073 Å)	Mo Kα (λ = 0.71073 Å)
μ, mm ⁻¹	1.488	1.376	1.240	1.265	1.253
absorp corr	Integration (X-Shape)	Integration (X-Shape)	Integration (X-Shape)	Integration (X-Shape)	Integration (X-Shape)
refl. collected	11 772	15 040	20 005	24 913	35 290
unique refls	8788 [<i>R</i> _{int} = 0.0444]	9353 [<i>R</i> _{int} = 0.0284]	10 714 [<i>R</i> _{int} = 0.0443]	13 074 [<i>R</i> _{int} = 0.0342]	6960 [<i>R</i> _{int} = 0.0983]
obsd refls	6992	7991	7980	12 242	5500
data; params	8788/385	9353/403	10 714/469	13 074/937	6960/469
<i>R</i> ¹ ; <i>wR</i> ² ^c	0.0401; 0.1117	0.0411; 0.0987	0.0321; 0.0738	0.0264; 0.0630	0.0455; 0.0760

^a All data collected at 203 K. ^b $R1 = \sum ||F_o| - |F_c|| / \sum |F_o|$. ^c $wR2 = \{ \sum [w(F_o^2 - F_c^2)^2] / \sum [w(F_o^2)^2] \}^{1/2}$.

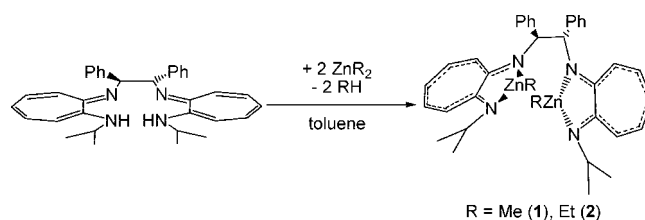
ATI)₂diph} and (*R,R*)-H₂{(*i*PrATI)₂diph}, in which two isopropylaminotroponimine units are linked by enantiomerically pure 1,2-diamino-1,2-diphenylethane, has been described previously by our group, and the ligand was introduced into lanthanide chemistry (Scheme 2).¹⁹ They can be obtained in a straightforward synthesis, by reaction of isopropylamine with 2-(tosyloxy)troponone first to form 2-(*N*-isopropylamino)troponone in almost quantitative yield. Further treatment of 2-(*N*-isopropylamino)troponone with Me₃O·BF₄, triethylamine, and 1,2-(*S,S*)-diamino-1,2-diphenylethane (1,2-(*R,R*)-diamino-1,2-diphenylethane) led to the desired product as a yellow solids.

In an attempt to create a sterical, more demanding ligand, we replaced the isopropyl group with enantiopure (*R*)-1-amino-1-phenylethane (Scheme 2). The new ligands (*S,S*)-H₂{((*R*)-PhCHCH₃ATI)₂diph} and (*R,R*)-H₂{((*R*)-PhCHCH₃ATI)₂diph}, which are diastereomers, were prepared in a similar fashion to (*S,S*)-H₂{(*i*PrATI)₂diph}, using (*R*)-1-amino-1-phenylethane instead of isopropylamine in the first reaction step. The thus obtained 2-(*N*-(*R*)-(1-phenylethylamino)troponone²¹ was then treated with Me₃O·BF₄, triethylamine, and 1,2-(*S,S*)- or 1,2-(*R,R*)-diamino-1,2-diphenylethane to give the new chiral enantiopure ligands in good yields (Scheme 2). Both new compounds were characterized by ¹H and ¹³C{¹H} NMR and mass spectroscopy. The signals are consistent with the structures given in Scheme 2. It should be mentioned that the chiral nonbridged ligand *N*-(*S*)-1-phenylethyl-2-(*S*)-1-phenylethylamino)troponimine was prepared by H. Brunner et al. in a different approach.²⁴

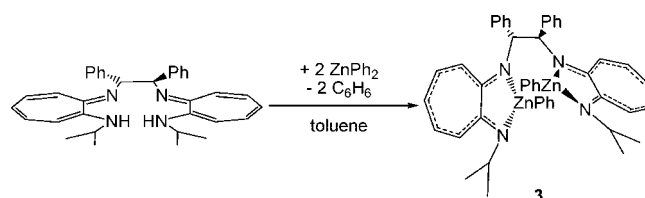
Metal Complexes. The dimetallic zinc complexes [(*S,S*)-{(iPrATI)₂diph}(ZnR)₂] (R = Me (**1**), Et (**2**)) were synthesized by reaction of the neutral ligand (*S,S*)-H₂{(*i*PrATI)₂diph} with 2 equiv of the corresponding zinc organyls ZnR₂ (R = Me, Et) in toluene at low temperatures (Scheme 3). [(*R,R*)-{(iPrATI)₂diph}(ZnPh)₂] (**3**) was obtained in a similar fashion by reaction of (*R,R*)-H₂{(*i*PrATI)₂diph} with ZnPh₂ (Scheme 4). Compounds **1–3** could be obtained as orange, analytically pure solids by crystallization directly from the reaction mixtures. The new complexes have been characterized by standard analytical/spectroscopic techniques.

Complexes **1** and **2** show the characteristic signals for the methyl and ethyl ligands in the ¹H and ¹³C{¹H} NMR spectra (**1**: Zn(CH₃), δ(C₆D₆): ¹H, -0.12 ppm, δ(C₆D₆) ¹³C{¹H}, -12.0

Scheme 3



Scheme 4



ppm); **2**: Zn(CH₂CH₃), δ(C₆D₆) ¹H, 0.49, 0.55 ppm; δ(C₆D₆) ¹³C{¹H}, 1.2 ppm; starting materials ZnMe₂, δ ¹H, 0.51 ppm, δ ¹³C{¹H}, -4.2 ppm²⁵ and ZnEt₂, δ ¹H, 0.08 ppm; δ ¹³C{¹H}, 6.82 ppm).²⁶ While for the ZnCH₃ protons for **1** a singlet is observed, the ZnCH₂CH₃ protons for **2** are split into two doublets of quartets because of geminal coupling, which is a result of diastereotopic splitting and concomitant coupling with the CH₃ protons. The diastereotopic splitting is not observed in chiral zincethyl compounds with less sterically demanding ligands.²⁷ Compound **3** also shows the expected set of signals in the ¹H and ¹³C{¹H} NMR spectra. The signals of the phenyl ligand can be observed in the aromatic region, but the overlapping with the signals of the ATI and the aromatic protons from the chiral bridge made it difficult to assign them precisely. The EI mass spectra show the [M - R]⁺ and [M - 2R]⁺ (R = Me, Et, Ph) fragments for compounds **1**, **2**, and **3**. The peaks of the molecular ion [M]⁺ fragments could not be observed. Furthermore, the structures of **1**, **2**, and **3** were confirmed by single-crystal X-ray diffraction in the solid state (Figures 1–3). Data collection parameters and selected bond lengths and angles are

(25) Gayler, L. A.; Wilkinson, G. *Inorg. Synth.* **1979**, *19*, 253–257.

(26) Abram, M. H.; Rolfe, P. H. *J. Organomet. Chem.* **1967**, *7*, 35–43.

(b) Müller, H.; Rösch, L.; Erb, W.; Zeisberg, R. *J. Organomet. Chem.* **1977**, *140*, C17–C20.

(27) Chakraborty, D.; Chen, E. Y. X. *Organometallics* **2003**, *22*, 769–774.

(24) Brunner, H.; Knott, A. J. *Organomet. Chem.* **1985**, *195*, 211–221.

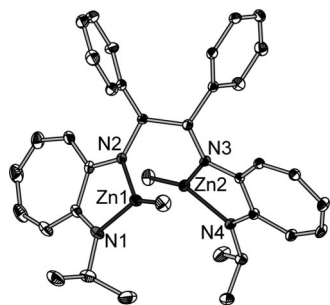


Figure 1. Perspective ORTEP view of the molecular structure of **1**. Thermal ellipsoids are drawn to encompass 30% probability. Hydrogen atoms are omitted for clarity.

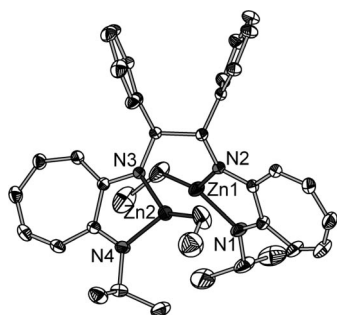


Figure 2. Perspective ORTEP view of the molecular structure of **2**. Thermal ellipsoids are drawn to encompass 30% probability. Hydrogen atoms are omitted for clarity.

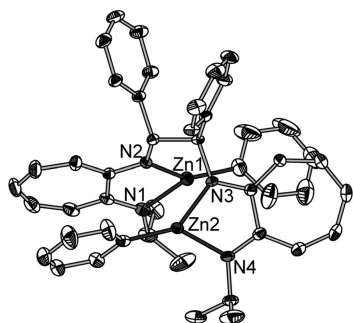


Figure 3. Perspective ORTEP view of the molecular structure of **3**. Thermal ellipsoids are drawn to encompass 30% probability. Hydrogen atoms are omitted for clarity.

given in Tables 1 and 2. Compound **1** crystallizes in the chiral monoclinic space group $P2_1$ with two molecules in the unit cell, while **2** and **3** crystallize in the orthorhombic chiral space group $C222_1$, with eight molecules in the unit cell. As observed for other aminotroponimate zinc compounds, the metal atoms of all three complexes are coordinated in a trigonal-planar fashion.^{4,7,8} Despite the different organic ligands all compounds show a similar geometry. The Zn–N distances are between 1.965(2) and 1.983(3) Å, comparable to the previously published nonchiral ATI zinc compounds.^{4,7,8} The Zn–C distances are in the range 1.943(4)–1.949(4) Å for **1** and 1.955(4)–1.970(4) Å for **2**. These distances are typical for zinc methyl and ethyl bonds.^{7,8,28} For **3** the Zn–C distances are 1.934(4) and 1.940(3) Å, which is again in the expected range.²⁹ The torsion angles N2–C–C–N3 along the C–C bond of the chiral bridges are 49.4(4)° (**1**), 53.8(3)° (**2**), and 55.03° (**3**).

(28) Dove, A. P.; Gibson, V. C.; Marshall, E. L.; White, A. J. P.; Williams, D. J. *Dalton Trans.* **2004**, 570–578.

(29) Prust, J.; Stasch, A.; Zheng, W.; Roesky, H. W.; Alexopoulos, E.; Uson, I.; Böhrler, D.; Schuchardt, T. *Organometallics* **2001**, *20*, 3825–3828.

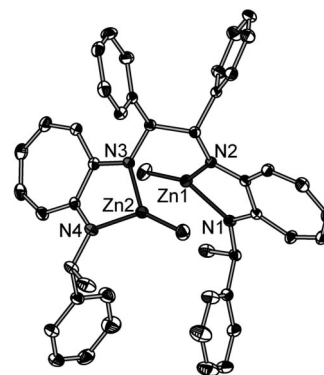
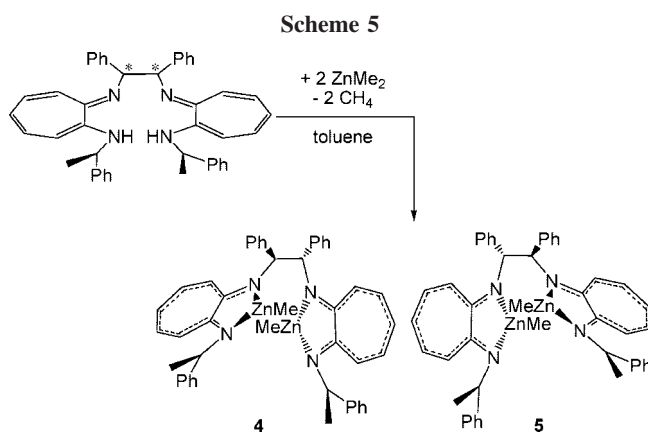


Figure 4. Perspective ORTEP view of the molecular structure of **4**. Thermal ellipsoids are drawn to encompass 30% probability. Hydrogen atoms are omitted for clarity. Only one of the independent molecules is shown.

Table 2. Crystallographic Details of [(*i*PrAT)ZnMe]₂ (**2a**) and [(*i*PrAT)ZnEt]₂ (**2b**)

	1	2	3	4	5
Bond Lengths (Å)					
Zn1–N1	1.965(4)	1.975(3)	1.972(3)	1.987(2)	1.978(3)
Zn1–N2	1.968(3)	1.974(2)	1.945(2)	1.972(2)	1.985(3)
Zn1–C	1.943(4)	1.955(4)	1.934(4)	1.951(3)	1.928(5)
Zn2–N3	1.983(3)	1.970(2)	1.965(2)	1.981(2)	1.959(3)
Zn2–N4	1.982(2)	1.971(3)	1.968(2)	1.973(2)	1.980(3)
Zn2–C	1.949(4)	1.970(4)	1.940(3)	1.950(3)	1.940(5)
Zn1–Zn2	3.669(1)	3.867(1)	3.493(1)	3.662(6)	3.761(1)
Bond Angles (deg)					
N1–Zn1–N2	81.47(14)	81.55(10)	81.79(11)	82.06(9)	81.38(14)
N1–Zn1–C	139.0(2)	138.99(10)	130.29(13)	132.18(11)	141.95(2)
N2–Zn1–C	137.90(2)	138.46(10)	146.22(13)	145.73(12)	136.66(2)
N3–Zn2–N4	81.56(13)	81.37(10)	81.75(9)	81.78(9)	82.16(13)
N3–Zn2–C	144.63(17)	141.26(2)	139.72(11)	138.83(13)	142.98(2)
N4–Zn2–C	132.72(2)	134.96(2)	137.78(11)	139.34(13)	133.10(2)



It should also be mentioned that attempts to synthesize a monometallic complex of the type [(*S,S*)-{(*i*PrATI)₂diph}Zn] were not successful. Reaction of 1 equiv of dimethyl- or diethylzinc with the neutral ligand, also at elevated temperatures, always gave the dimetallic species **1** or **2** exclusively.

Reaction of the sterical more demanding ligands (*S,S*)-H₂{((*R*)-PhCHCH₃ATI)₂diph} and (*R,R*)-H₂{((*R*)-PhCHCH₃-ATI)₂diph}, which have four stereocenters, with 2 equiv of ZnMe₂ in toluene gave the enantiopure complexes [(*S,S*)-{((*R*)-PhCHCH₃ATI)₂diph}(ZnMe)₂] (**4**) and [(*R,R*)-{((*R*)-PhCHCH₃ATI)₂diph}(ZnMe)₂] (**5**) (Scheme 5). Complexes **4** and **5** were obtained as yellow crystalline, analytically pure solids when the concentrated reaction mixtures were layered with pentane. Complexes **4** and **5** were characterized by ¹H and ¹³C NMR spectroscopy and elemental analysis.

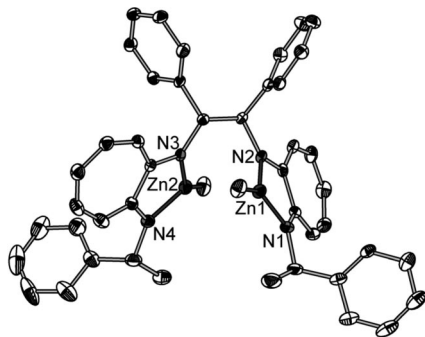


Figure 5. Perspective ORTEP view of the molecular structure of **5**. Thermal ellipsoids are drawn to encompass 30% probability. Hydrogen atoms are omitted for clarity.

^1H NMR as well as $^{13}\text{C}\{^1\text{H}\}$ NMR spectra are consistent with the solid state structures (see below). The signals of the $\text{Zn}(\text{CH}_3)$ group again are observed at a high field (**4**: $\delta(\text{C}_6\text{D}_6)$ ^1H , -0.19 ppm, $\delta(\text{C}_6\text{D}_6)$ $^{13}\text{C}\{^1\text{H}\}$, -10.6 ppm; **5**: $\delta(\text{C}_6\text{D}_6)$ ^1H , -0.17 ppm, $\delta(\text{C}_6\text{D}_6)$ $^{13}\text{C}\{^1\text{H}\}$, -12.4 ppm). The molecular structures of **4** and **5** were also confirmed by single-crystal X-ray diffraction in the solid state (Figures 4 and 5). Data collection parameters and selected bond lengths and angles are given in Tables 1 and 2. Compound **4** crystallizes in the chiral triclinic space group P_1 with two molecules in the asymmetric unit and in the unit cell; **5**, in the chiral monoclinic space group $P2_12_12_1$ with four molecules in the unit cell. The Zn–N distances are between 1.972(2) and 1.987(2) Å, almost the same as in the previously described structures of **1**, **2**, and **3** and comparable zinc methyl compounds.^{7,8} The Zn–C distances are also in the expected range (1.950(3), 1.951(3) Å (**4**); 1.928(5), 1.940(5) Å (**5**)).^{7,8,25} The torsion angles N2–C–C–N3 along the C–C bond of the chiral bridges are 49.5(3)° (**4**) and 47.8(4)° (**5**).

Compounds **1** and **2** were used as catalysts in the intramolecular hydroamination/cyclization reaction of nonactivated terminal aminoolefins. It turned out that the substrates are converted to the cyclic product at elevated temperature in high yields, but almost no enantioselectivities (less than 10%) were obtained. Details of the reactions are found in the Supporting Information.

Summary

We have prepared dimetallic zincmethyl, -ethyl, and phenyl complexes having the enantiomerically pure bridged aminotropoiminato ligands (S,S)- $\{(i\text{PrATI})_2\text{diph}\}^{2-}$, (R,R)- $\{(i\text{PrATI})_2\text{diph}\}^{2-}$, (S,S)- $\{((R)\text{-PhCHCH}_3\text{ATI})_2\text{diph}\}^{2-}$, and (R,R)- $\{((R)\text{-PhCHCH}_3\text{ATI})_2\text{diph}\}^{2-}$ in the coordination sphere. The zinc complexes were obtained by reaction of ZnR_2 ($R = \text{Me}$, Et, Ph) with the corresponding neutral ligands. As a result, the compounds $[(S,S)\text{-}\{(i\text{PrATI})_2\text{diph}\}(\text{ZnR})_2]$ ($R = \text{Me}$ (**1**), Et (**2**)), $[(R,R)\text{-}\{(i\text{PrATI})_2\text{diph}\}(\text{ZnPh})_2]$ (**3**), $[(S,S)\text{-}\{((R)\text{-PhCHCH}_3\text{ATI})_2\text{diph}\}(\text{ZnMe})_2]$ (**4**), and $[(R,R)\text{-}\{((R)\text{-PhCHCH}_3\text{ATI})_2\text{diph}\}(\text{ZnMe})_2]$ (**5**) were synthesized. The molecular structures of all new complexes were confirmed by single-crystal X-ray diffraction in the solid state.

Acknowledgment. This work was supported by the Deutsche Forschungsgemeinschaft and the Fonds der Chemischen Industrie. Additionally, generous support from J. Jenter and A. Zulys is gratefully acknowledged.

Supporting Information Available: Experimental details of the hydroamination experiments and X-ray crystallographic files in CIF format for the structure determinations of **1–5** are available free of charge via the Internet at <http://pubs.acs.org>.

OM800858T

Facile Single or Double C–H Bond Activation on a Cp* Ligand Promoted by the Presence of Alkynylphosphine Ligands

María Bernechea, Jesús R. Berenguer,* Elena Lalinde,* and Javier Torroba

Departamento de Química-Grupo de Síntesis Química de La Rioja, UA-CSIC, Universidad de La Rioja, 26006 Logroño, Spain

Received September 5, 2008

The behavior of the cationic alkynylphosphine complex $[\text{Rh}(\eta^5\text{-Cp}^*)\text{Cl}(\text{PPh}_2\text{C}\equiv\text{CPh})_2](\text{CF}_3\text{SO}_3)$ (**1**) under thermal or basic conditions is described. Complex **1** rearranges thermally (toluene, reflux) to generate a solution from which a mixture formed by **1**, the monohydroalkylated derivative $[\text{Rh}\{\kappa^2\text{P}:\eta^5\text{-C}_5\text{Me}_4\text{-(CH}_2\text{CPh=CHPPH}_2)\}\text{Cl}(\text{PPh}_2\text{C}\equiv\text{CPh})](\text{CF}_3\text{SO}_3)$ (**2**), and the symmetrical 1,2-dihydroalkylated derivative $[\text{Rh}\{\kappa^2\text{PP}':\eta^5\text{-C}_5\text{Me}_3\text{-1,2-(CH}_2\text{CPh=CHPPH}_2)_2\}\text{Cl}](\text{CF}_3\text{SO}_3)$ (**3'**) (~30:60:10, respectively) can be isolated. From this mixture, compounds **1** and **2** cocrystallize together, giving rise to a solid solution, as has been confirmed by X-ray crystallography. In contrast, treatment of $[\text{Rh}(\eta^5\text{-Cp}^*)\text{Cl}(\text{PPh}_2\text{C}\equiv\text{CPh})_2](\text{CF}_3\text{SO}_3)$ (**1**) with Na_2CO_3 evolves with the formation of the new asymmetrical 1,2- and 1,3-dihydroactivated isomers $[\text{Rh}\{\kappa^2\text{PP}':\eta^5\text{-1,2-(PPh}_2\text{CH}_2\text{CPh=CH)C}_5\text{Me}_3(\text{CH}_2\text{CPh=CHPPH}_2)\}\text{Cl}](\text{CF}_3\text{SO}_3)$ (**3**, X-ray) and $[\text{Rh}\{\kappa^2\text{PP}':\eta^5\text{-1,3-(PPh}_2\text{CH}_2\text{CPh=CH)C}_5\text{Me}_3(\text{CH}_2\text{CPh=CHPPH}_2)\}\text{Cl}](\text{CF}_3\text{SO}_3)$ (**4**), generated by the occurrence of a simultaneous 1,2- or 1,3-double C–H bond addition to the triple bonds, together with an additional isomerization process. A detailed study of this reaction (reflux or room temperature) provides evidence that these asymmetrical deactivated complexes (**3**, **4**) are generated by initial formation of the corresponding symmetrical 1,2- and 1,3-dihydroalkylated species **3'** and **4'**, respectively.

Introduction

In recent years considerable attention has been focused on the synthesis of functionalized cyclopentadienyl ligands $\text{C}_5\text{Me}_4\text{X}$,^{1–14} where X is a pendant arm bearing a functionality which can hold or orient potential reactants or can chelate to the metal center. In this area, particular interest has been devoted to hemilabile bidentate tetramethyl^{12,15–23} (or the less abundant

tridentate trimethyl^{24–28}) cyclopentadienylphosphine ligands, mainly due to their implication in homogeneous catalytic processes.^{1,12,15,16,18,19,21,28} Two different synthetic approaches have been used for the preparation of complexes containing these ligands: (i) prior synthesis of the hybrid ligand followed by coordination to the metal,^{16,17,19,28} and (ii) intramolecular coupling of both the previously coordinated phosphine and cyclopentadienyl groups.^{15,18,20–23} The first strategy normally leads to poor overall yields, as it involves multiple steps based on classical organic methods, while the second approach provides a method of overcoming this problem.

On the other hand, alkynylphosphines have been shown to be a very useful type of ligand with excellent promise in coordination chemistry,²⁹ mainly due to their ability to coordinate via the phosphorus atom and/or the $\text{C}\equiv\text{C}$ moiety, thus favoring the formation of a rich variety of homo- and het-

* To whom correspondence should be addressed. E-mail: elena.lalinde@unirioja.es (E.L.); jesus.berenguer@unirioja.es (J.R.B.).

- (1) Butenschön, H. *Chem. Rev.* **2000**, *100*, 1527.
- (2) Siemelling, U. *Chem. Rev.* **2000**, *100*, 495.
- (3) Liu, S.; Wang, H.; Zhang, P. C.; Weng, L. H.; Hou, X. F. *Organometallics* **2008**, *27*, 713.
- (4) da Costa, A. P.; Viciano, M.; Sanaú, M.; Merino, S.; Tejada, J.; Peris, E.; Royo, B. *Organometallics* **2008**, *27*, 1305.
- (5) Caldwell, H.; Pregosin, P. S. *Organometallics* **2008**, *27*, 1591.
- (6) Fairchild, R. M.; Holman, K. T. *Organometallics* **2008**, *27*, 1823.
- (7) Beweries, T.; Burlakov, V. V.; Peitz, S.; Bach, M. A.; Arndt, P.; Baumann, W.; Spannenberg, A.; Rosenthal, U. *Organometallics* **2007**, *26*, 6827.
- (8) Krut'ko, D. P.; Kirsanov, R. S.; Belov, S. A.; Borzov, M. V.; Churakov, A. V. *J. Organomet. Chem.* **2007**, *692*, 1465.
- (9) Burlakov, V. V.; Arndt, P.; Baumann, W.; Spannenberg, A.; Rosenthal, U. *Organometallics* **2006**, *25*, 1317.
- (10) Hanasaka, F.; Fujita, K.; Yamaguchi, R. *Organometallics* **2006**, *25*, 4643.
- (11) Mach, K.; Gyepes, R.; Kubista, J.; Horacek, M. *Inorg. Chem. Commun.* **2006**, *9*, 156.
- (12) Chin, C. S.; Kim, Y.; Lee, H. *Inorg. Chim. Acta* **2004**, *357*, 3064.
- (13) Godoy, F.; Klahn, A. H.; Lahoz, F. J.; Balana, A. I.; Oelckers, B.; Oro, L. A. *Organometallics* **2003**, *22*, 4861.
- (14) Rüba, E.; Mereiter, K.; Schmid, R.; Kirchner, K.; Bustelo, E.; Puerta, M. C.; Valera, P. *Organometallics* **2002**, *21*, 2912.
- (15) Marr, A. C.; Nieuwenhuyzen, M.; Pollock, C. L.; Saunders, G. C. *Organometallics* **2007**, *26*, 2659.
- (16) McConnell, A. C.; Pogrozelec, P. J.; Slawin, A. M. Z.; Williams, G. L.; Elliott, P. I. P.; Haynes, A.; Marr, A. C.; Cole-Hamilton, D. J. *Dalton Trans.* **2006**, 91.
- (17) Krut'ko, D. P.; Borzov, M. V.; Veksler, E. N.; Churakov, A. V.; Kuz'mina, L. G. *J. Organomet. Chem.* **2005**, *690*, 4036.

- (18) Bellabarba, R. M.; Saunders, G. C. *Polyhedron* **2004**, *23*, 2659.
- (19) Döhring, A.; Jensen, V. R.; Jolly, P. W.; Thiel, W.; Weber, J. C. *Organometallics* **2001**, *20*, 2234.
- (20) Schmitt, G.; Ulrich, D.; Wolmerhäuser, G.; Regitz, M.; Scherer, O. J. *Z. Anorg. Allg. Chem.* **1999**, *625*, 702.
- (21) Weber, L.; Quasdorff, B.; Stammeler, H.-G.; Newmann, B. *Chem. Eur. J.* **1998**, *4*, 469.
- (22) Weber, L.; Kaminski, O.; Quasdorff, B.; Rühlcke, A.; Stammeler, H.-G.; Newmann, B. *Organometallics* **1996**, *15*, 123.
- (23) Baker, R. T.; Calabrese, J. C.; Harlow, R. L.; Williams, I. D. *Organometallics* **1993**, *12*, 830.
- (24) Barthel-Rosa, L. P.; Catalano, V. J.; Maitra, K.; Nelson, J. H. *Organometallics* **1996**, *15*, 3924.
- (25) Atherton, M. J.; Fawcett, J.; Holloway, J. H.; Hope, E. G.; Russell, D. R.; Saunders, G. C. *J. Organomet. Chem.* **1999**, *582*, 163.
- (26) Fawcett, J.; Friedrichs, S.; Holloway, J. H.; Hope, E. G.; McKee, V.; Nieuwenhuyzen, M.; Russell, D. R.; Saunders, G. C. *J. Chem. Soc., Dalton Trans.* **1998**, 1477.
- (27) Atherton, M. J.; Fawcett, J.; Holloway, J. H.; Hope, E. G.; Karacar, A.; Russell, D.; Saunders, G. C. *J. Chem. Soc., Chem. Commun.* **1995**, 191.
- (28) Fryznk, M. D.; Mao, S. S. H.; Zaworotko, M. J.; MacGillivray, L. R. *J. Am. Chem. Soc.* **1993**, *115*, 5336.
- (29) Low, J. P. *J. Cluster Sci.* **2008**, *19*, 5.

eropolynuclear species.^{29–47} Furthermore, they present a varied and rich chemistry related to several processes, among which are (i) the phosphorus–carbon bond cleavage to generate phosphido and alkynyl fragments via interaction with metal carbonyl clusters,^{29,48–50} (ii) their possible engagement in characteristic insertion reactions of the triple bonds^{35,51–55} or their activation with electrophilic or nucleophilic substrates,^{56–58} and also (iii) intermolecular coupling of the alkynyl moieties leading to the association of two coordinated alkynylphosphines.^{31,52,59–66} The last reactions are of particular interest, owing to the fact that they are employed in the synthesis of

macrocyclic systems from bis(diphenylphosphino) complexes with high atom efficiency^{61,62} and in the study of Bergman-cyclization processes of bis(phosphino)enediynes upon complexation to metal ions.^{63,64,66} Our research group has obtained very interesting results in the study of these coupling reactions on platinum and palladium precursors containing at least two alkynylphosphines, having reported the formation of novel coordinated diphosphinonaphthalene or 1,2-diarylalkenyl-1,2-diphosphine ligands, activated by complexation of a “cis-Pt(C₆F₅)₂” fragment,^{35,52} under thermal or photochemical conditions.³¹

Following from this work, and with the aim of studying the influence of the geometry and the metal center in these types of processes, we have tried to induce thermally similar coupling reactions in the cationic rhodium(III) complex [Rh(η^5 -Cp*)Cl(PPh₂C≡CPh)₂](TfO). Nevertheless, instead of a coupling process, the reaction progresses through the unexpected activation of one or two C–H bonds on the Cp* ligand and their formal addition to the triple bond of the phosphine ligands, giving rise to the formation of novel cyclopentadienyl–ene–phosphine ligands, which has no precedent in the literature. The C–H bond activation of η^5 -coordinated Cp* ligands constitutes an important reaction, which affords tetramethylfulvene compounds^{14,67–73} or species with functionalized cyclopentadienyl ligands.^{5,7,9,11,12,15,18,21,22,24,67,71,73,74} As this process is commonly activated by heat^{7,9,15,67,69,70} or by treatment with base,^{3,5,24,68,73,74} we have also examined the behavior of [Rh(η^5 -Cp*)Cl(PPh₂C≡CPh)₂](CF₃SO₃) (**1**) in tetrahydrofuran in the presence of a weak base such as Na₂CO₃.

Results and Discussion

Synthetic Studies. The results of the behavior of the complex [Rh(η^5 -Cp*)Cl(PPh₂C≡CPh)₂](CF₃SO₃) (**1**) under thermal or basic conditions are summarized in Scheme 1. As it is shown, the treatment of [Rh(η^5 -Cp*)Cl(PPh₂C≡CPh)₂](CF₃SO₃) (**1**) with a weak base such as Na₂CO₃ (Scheme 1, step i) in tetrahydrofuran under reflux conditions (16 h) evolves with the formation of the new asymmetrical 1,2-dihydroactivated complex [Rh(κ^2 PP': η^5 -1,2-(PPh₂CH₂CPh=CH)C₅Me₃(CH₂CPh=CH)PPh₂)Cl](CF₃SO₃) (**3**). The complex is obtained impure with a minute amount of the corresponding symmetrical 1,2-isomer [Rh(κ^2 PP': η^5 -C₅Me₃-1,2-(CH₂CPh=CH)PPh₂)₂Cl](CF₃SO₃) (**3'**), which can be eliminated by crystallization from acetone/hexane to give pure **3** as an orange solid (see the Experimental Section). The formation of the asymmetrical 1,2-diaactivated complex **3** involves a double-hydroalkylation reaction (formation of **3'**), together with an additional isomerization process, leading to the unsaturated tridentate ligand {1,2-(PPh₂CH₂CPh=CH)C₅Me₃(CH₂CPh=CH)PPh₂}, which acts as a κ^2 PP': η^5 10-electron

(30) García, A.; Lalinde, E.; Moreno, M. T. *Eur. J. Inorg. Chem.* **2007**, 3553.

(31) García, A.; Gómez, J.; Lalinde, E.; Moreno, M. T. *Organometallics* **2006**, *25*, 3926.

(32) Bernechea, M.; Luga, N.; Gil, B.; Lalinde, E.; Lavigne, G. *Organometallics* **2006**, *25*, 684.

(33) Díez, A.; Forniés, J.; García, A.; Lalinde, E.; Moreno, M. T. *Inorg. Chem.* **2005**, *44*, 2443.

(34) Forniés, J.; García, A.; Gil, B.; Lalinde, E.; Moreno, M. T. *Dalton Trans.* **2004**, 3854.

(35) Berenguer, J. R.; Bernechea, M.; Forniés, J.; García, A.; Lalinde, E.; Moreno, M. T. *Inorg. Chem.* **2004**, *43*, 8185.

(36) Berenguer, J. R.; Bernechea, M.; Forniés, J.; García, A.; Lalinde, E. *Organometallics* **2004**, *23*, 4288.

(37) Harding, D. A. J.; Hope, E. G.; Fawcett, J.; Solans, G. A. J. *Organomet. Chem.* **2007**, *692*, 5474.

(38) Wei, C. H.; Wu, C. E.; Huang, Y. L.; Kulysev, R. G.; Hong, F. E. *Chem. Eur. J.* **2007**, *13*, 1583.

(39) Ochida, A.; Sawamura, M. *Chem. Asian J.* **2007**, *2*, 609.

(40) Vian, L.; Willis, A. C.; Humphrey, M. G. *J. Organomet. Chem.* **2007**, *692*, 2086.

(41) Praingam, N.; Anderson, G. K.; Rath, N. P. *Inorg. Chim. Acta* **2007**, *360*, 1767.

(42) Liu, Y. C.; Li, C. I.; Yeh, W. Y.; Lee, G. H.; Peng, S. M. *Inorg. Chim. Acta* **2006**, *359*, 2361.

(43) Díez, J.; Gamasa, M. P.; J., G.; Lastra, E.; Villar, A. *Eur. J. Inorg. Chem.* **2006**, 78.

(44) Baumgartner, T.; Fiege, M.; Pontzen, F.; Arteaga-Müller, R. *Organometallics* **2006**, *25*, 5657.

(45) Bardají, M.; de la Cruz, M. T.; Jones, P. G.; Laguna, A.; Martínez, J.; Villacampa, M. D. *Inorg. Chim. Acta* **2005**, *358*, 1365.

(46) Louattani, E.; Suades, J. J. *Organomet. Chem.* **2000**, *604*, 234.

(47) Went, M. J. *Polyhedron* **1995**, *14*, 465, and references therein.

(48) Colquhoun, V. P.; Goeta, A. E.; Low, J. P. *J. Cluster Sci.* **2007**, *18*, 564.

(49) Albinati, A.; Filipi, V.; Leoni, P.; Marchetti, L.; Pasquali, M.; Passarelli, V. *Chem. Commun.* **2005**, 2155.

(50) Davies, J. E.; Mays, M. J.; Raithby, P. R.; Sarveswaran, K.; Solan, G. A. *Dalton Trans.* **2001**, 1269.

(51) Araujo, M. H.; Pereira, R. M. S.; Vargas, M. D.; Braga, D.; Grepioni, F. J. *Organomet. Chem.* **2005**, *690*, 4611.

(52) Charmant, J. P. H.; Forniés, J.; Gómez, J.; Lalinde, E.; Moreno, M. T.; Orpen, A. G.; Solano, S. *Angew. Chem., Int. Ed.* **1999**, *38*, 3058.

(53) El Harouch, Y.; Cadierno, V.; Igau, A.; Donnadiou, B.; Majoral, J. P. *Organomet. Chem.* **2004**, *689*, 953, and references therein.

(54) Bennett, M. A.; Castro, J.; Edwards, A. J.; Kopp, M. R.; Wenger, E.; Willis, A. C. *Organometallics* **2001**, *20*, 980, and references therein.

(55) Rosa, P.; Le Floch, P.; Richard, L.; Mathey, F. *J. Am. Chem. Soc.* **1997**, *119*, 9417.

(56) Huang, Y. L.; Chang, C. P.; Hong, F. E. *Dalton Trans.* **2006**, 5454.

(57) Liu, X.; Ong, T. K. H.; Selvaratnam, S.; Vittal, J. J.; White, A. J. P.; Williams, D. J.; Leung, P. W. *J. Organomet. Chem.*, **2002**, *643–644*, 4.

(58) Bennett, M. A.; Kwan, L.; Rae, A. D.; Wenger, E.; Willis, A. C. *Dalton Trans.* **2002**, 226.

(59) Shine, T. W.; Yeh, W. Y.; Lee, G. H.; Peng, S. M. *J. Organomet. Chem.* **2007**, *692*, 3619.

(60) Chang, C. P.; Kulysev, R. G.; Hong, F. E. *J. Organomet. Chem.* **2006**, *691*, 5831.

(61) Martin-Redondo, M. P.; Scoles, L.; Sterenberg, B. T.; Udachin, K. A.; Carty, A. J. *J. Am. Chem. Soc.* **2005**, *127*, 5038.

(62) Baumgartner, T.; Huynh, K.; Schleidt, S.; Lough, A. J.; Manners, I. *Chem. Eur. J.* **2002**, *8*, 4622.

(63) Schmitt, E. W.; Huffman, J. C.; Zaleski, J. M. *Chem. Commun.* **2001**, 167.

(64) Coalter, N. L.; Concolino, T. E.; Streib, W. E.; Hughes, C. G.; Rheingold, A. L.; Zaleski, J. M. *J. Am. Chem. Soc.* **2000**, *122*, 3112.

(65) Mahieu, A.; Miquel, Y.; Igau, A.; Donnadiou, B.; Majoral, J.-P. *Organometallics* **1997**, *16*, 3086.

(66) Warner, B. P.; Millar, S. P.; Broene, R. D.; Buchwald, S. L. *Science* **1995**, *269*, 814.

(67) Kraft, B. M.; Lachicotte, R. J.; Jones, W. D. *Organometallics* **2002**, *21*, 727.

(68) Riley, P. N.; Parker, J. R.; Fanwick, P. E.; Rothwell, I. P. *Organometallics* **1999**, *18*, 3579.

(69) Varga, V.; Mach, K.; Polasek, M.; Sedmera, P.; Hiller, J.; Thewalt, U.; Troyanov, S. I. *J. Organomet. Chem.* **1996**, *506*, 241.

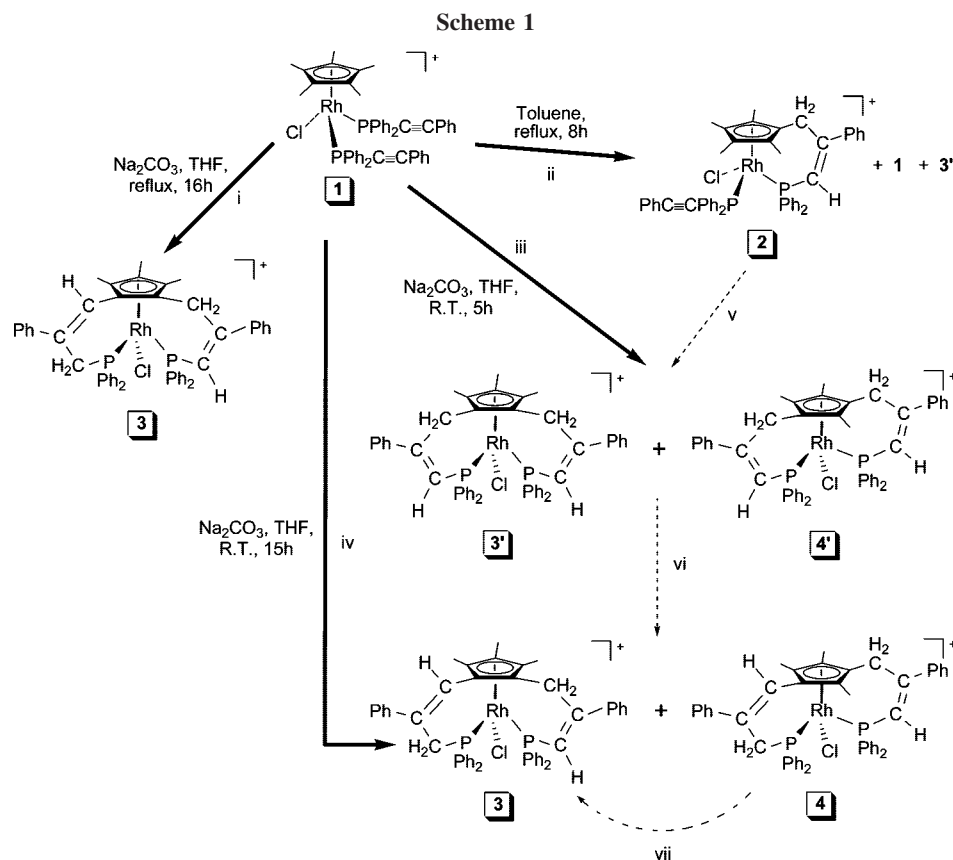
(70) Luinstra, G. A.; Teuben, J. H. *J. Am. Chem. Soc.* **1992**, *114*, 3361.

(71) Klahn, A. H.; Oelckers, B.; Godoy, F.; Garland, M. T.; Vega, A.; Perutz, R. N.; Higgit, C. L. *J. Chem. Soc., Dalton Trans.* **1998**, 3079.

(72) Fan, L.; Wei, C.; Aighirhio, F. I.; Turner, M. L.; Gusev, O. V.; Morozova, L. N.; Knowles, D. R. T.; Maitlis, P. M. *Organometallics* **1996**, *15*, 98.

(73) Gusev, O. V.; Sergeev, S.; Saez, I. M.; Maitlis, P. M. *Organometallics* **1994**, *13*, 2059.

(74) Fujita, K.; Nakamura, M.; Yamaguchi, R. *Organometallics* **2001**, *20*, 100.



donor, as has been confirmed by an X-ray crystallographic study (see below). As far as we know, only two other examples have been reported where the C–H bond activation on a Cp* ligand gives rise to a chelating $\kappa\text{P}:\eta^5$ ligand presenting a vinylic chain between the phosphorus atom and the cyclopentadienyl group.^{75,76}

In contrast, when complex **1** is refluxed in toluene in the absence of base (8 h, Scheme 1, step ii), the resulting solution is found to be a mixture of the precursor **1** with the monohydroalkylated derivative $[\text{Rh}\{\kappa\text{P}:\eta^5\text{-C}_5\text{Me}_4(\text{CH}_2\text{CPh}=\text{CHPPH}_2)\text{-Cl}(\text{PPh}_2\text{C}\equiv\text{CPh})\}(\text{CF}_3\text{SO}_3)]$ (**2**) and the *symmetrical* 1,2- and 1,3-dihydroalkylated complexes **3'** and $[\text{Rh}\{\kappa^2\text{PP}':\eta^5\text{-C}_5\text{Me}_3\text{-1,3-(CH}_2\text{CPh}=\text{CHPPH}_2)_2\}\text{Cl}](\text{CF}_3\text{SO}_3)$ (**4'**) ($^{31}\text{P}\{^1\text{H}\}$ NMR, approximate molar ratio 25:57:12:6 for **1**:**2**:**3'**:**4'**). The usual workup of the solution afforded a solid mixture of **1** and **2**, together with a small quantity of **3'** (Scheme 1, step ii, approximate molar ratio 30:60:10 for **1**:**2**:**3'**). Unfortunately, chromatographic methods failed to produce any pure product from the mixture, and all attempts at recrystallization in different solvents did not change the relative amounts of these three complexes. Slow diffusion of hexane into a solution of the mixture of **1**, **2**, and **3'** in acetone afforded orange monocystals suitable for X-ray diffraction. In spite of the fact that all the crystals had the same appearance under the microscope, the spectroscopic data of their solutions still revealed the presence of the three complexes in the previously mentioned relative molar ratio (**1**:**2**:**3'** \approx 30:60:10). Thus, several of these crystals were chosen, and in all cases, X-ray diffraction studies showed that the monohydroalkylated complex **2** cocrystallizes together with the starting product **1** to form a solid solution (Figure 1a), which was modeled in a 60:40 molar ratio (**2**:**1**), allowing us to fully determine the structure of

complex **2** (Figure 1b). It should be noted that the presence of a solid solution in molecular solids is not a common feature but is a phenomenon well documented in the literature.^{77–85} Unfortunately, we failed in choosing a crystal with the symmetrical 1,2-dihydroalkylated compound **3'** as a component. The formation of complexes **2** and **3'** or **4'** under thermal conditions implies only the formal activation of one or two C–H bonds of the Cp* ligand by interaction with the alkynyl fragments, giving rise to the final formation of new C–H and C–C bonds and, thereby, to the novel unsaturated bi- and tridentate ligands $\kappa\text{P}:\eta^5\text{-C}_5\text{Me}_4\text{CH}_2\text{CPh}=\text{CHPPH}_2$ and $\kappa^2\text{PP}':\eta^5\text{-C}_5\text{Me}_3(\text{CH}_2\text{CPh}=\text{CHPPH}_2)_2$.

In an attempt to optimize the synthesis of the monohydroalkylated complex **2** and, probably, also to improve the formation of the symmetrical 1,2-isomer **3'**, which were thought to be intermediates in the formation of the final asymmetrical 1,2-derivative **3**, we decided to examine the reaction of the complex $[\text{Rh}(\eta^5\text{-Cp}^*)\text{Cl}(\text{PPh}_2\text{C}\equiv\text{CPh})_2](\text{CF}_3\text{SO}_3)$ (**1**) with Na_2CO_3 in THF at room temperature. Under these conditions,

(77) Hill, A. F.; Rae, A. D.; Schultz, M.; Willis, A. C. *Organometallics* **2007**, *26*, 1325.

(78) Huang, J.; Chen, S.; Guzei, I. A.; Yu, L. *J. Am. Chem. Soc.* **2006**, *128*, 11985.

(79) Freedman, D. A.; Janzen, D. E.; Vreeland, J. L.; Tully, H. M.; Mann, K. R. *Inorg. Chem.* **2002**, *41*, 3820.

(80) Pidcock, E.; DeBeer, S.; Obias, H. V.; Hedman, B.; Hodgson, K. O.; Karlin, K. D.; Solomon, E. I. *J. Am. Chem. Soc.* **1999**, *121*, 1870.

(81) Capdevila, M.; Carrasco, Y.; Clegg, W.; Coxal, R. A.; González-Duarte, P.; Lledós, A.; Ramírez, J. A. *J. Chem. Soc., Dalton Trans.* **1999**, 3101.

(82) Wang, L.-S.; Fettingner, J. C.; Poli, R. *J. Am. Chem. Soc.* **1997**, *119*, 4453.

(83) Härkönen, A. U.; Ahlgren, M.; Pakkanen, T. A.; Pursiainen, J. *Organometallics* **1997**, *16*, 689.

(84) Argazz, R.; Bergamin, P.; Costa, E.; Gee, V.; Hogg, J. K.; Martín, A.; Orpen, A. G.; Pringle, P. G. *Organometallics* **1996**, *15*, 5591.

(85) Radu, N. S.; Hollander, F. J.; Tilley, T. D.; Rheingold, A. L. *J. Chem. Soc., Chem. Commun.* **1996**, 2459.

(75) Weber, L.; Kaminski, O.; Quasdorff, B.; Stämmler, H.-G.; Neumann, B. *J. Organomet. Chem.* **1997**, *529*, 329.

(76) Weber, L.; Kaminski, O.; Boese, R.; Bläser, D. *Organometallics* **1995**, *14*, 820.

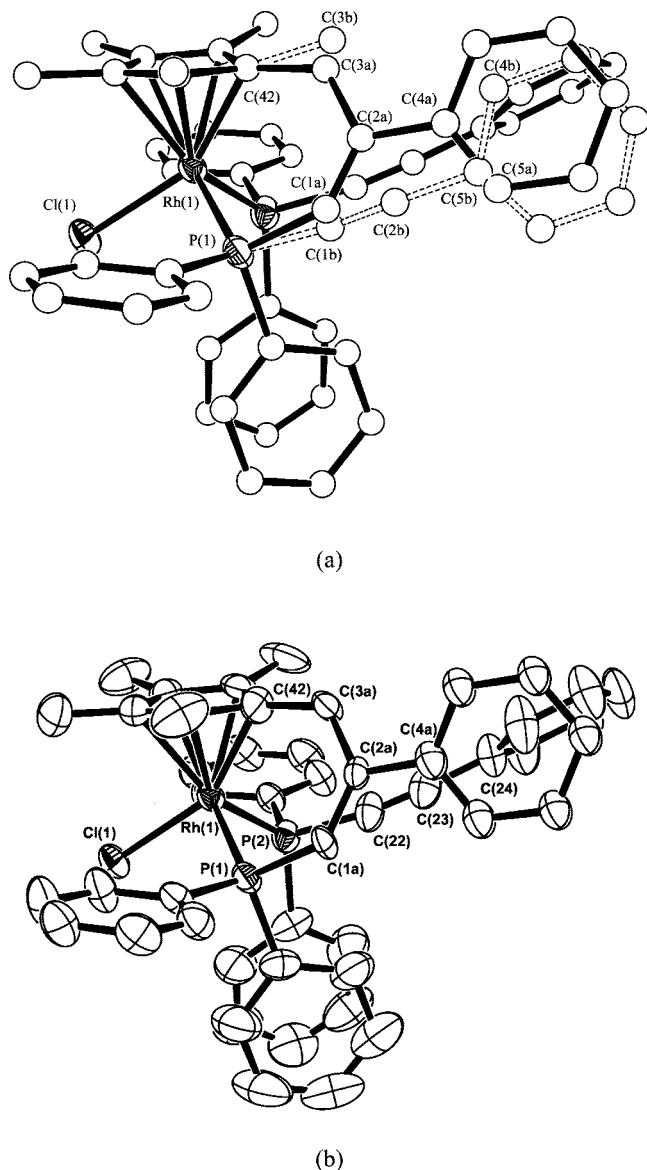


Figure 1. (a) ORTEP view of the solid solution of the cations in **1** and **2** modeled in a 40:60 molar ratio, respectively. All atoms are superimposed except C(1)–C(9). (b) ORTEP view of the cation $[\text{Rh}(\kappa\text{P}:\eta^5\text{-C}_5\text{Me}_4\text{CH}_2\text{CPh}=\text{CHPPH}_2)\text{Cl}(\text{PPH}_2\text{C}\equiv\text{CPh})]^+$ in complex **2**. Ellipsoids are drawn at the 50% probability level. Hydrogen atoms and solvent have been omitted for clarity.

after 5 h of reaction a mixture of the symmetrical diactivated 1,2- (**3'**) and 1,3-derivatives (**4'**) (60:40 **3':4'**) can be obtained (Scheme 1, step iii). However, after 15 h the reaction evolves to a mixture of **3** with the new isomeric, and also asymmetrical, 1,3-dihydroactivated derivative $[\text{Rh}\{\kappa^2\text{PP}'\text{:}\eta^5\text{-1,3-(PPH}_2\text{-CH}_2\text{CPh}=\text{CH})\text{C}_5\text{Me}_3(\text{CH}_2\text{CPh}=\text{CHPPH}_2)\}\text{Cl}](\text{CF}_3\text{SO}_3)$ (**4**) in a ca. 1:1 molar ratio (Scheme 1, step iv). Unfortunately, all efforts to isolate any pure compounds from both of these mixtures by chromatography or recrystallization have been fruitless.

The monitoring by multinuclear NMR spectroscopy of the reaction under basic conditions, either at room temperature (Figure 2 for time-dependent $^{31}\text{P}\{^1\text{H}\}$ NMR spectra) or under reflux conditions, has allowed us to complete the picture (formation of **3** from **1**), which is also shown in Scheme 1 (see the Experimental Section for details). As expected, the first product observed after 20 min was the monohydroalkylation complex **2**. This complex evolves in the presence of Na_2CO_3 (excess) through a second hydroalkylation reaction to the

formation of the 1,2- and 1,3-symmetrical intermediate derivatives **3'** and **4'** (Scheme 1, step v), which subsequently slowly isomerize (15 h) to the corresponding asymmetrical compounds **3** and **4**, presumably by sequential deprotonation and protonation processes (1,3-hydrogen shift, Scheme 1, step vi). Interestingly, under these conditions complex **4** is not stable, and the reaction mixture evolves (3 days) toward complex **3** as the most abundant product (approximate molar ratio 75:15:5:5 for **3:4:3':4'**). This fact indicates that the asymmetrical 1,3-diaactivated complex **4** isomerizes to the asymmetrical 1,2-derivative **3** (Scheme 1, step vii), a process which implies the breaking and forming of C–C bonds, probably because **3** is the most thermodynamically stable compound. However, it is worth pointing out that the solid mixtures of both **3'/4'** and **3/4** remain essentially unaltered in solution (CDCl_3 or HDA) at room temperature for long periods of time in the absence of base, thus indicating that the isomerization processes (**3', 4' → 3, 4**; **4 → 3**) require the presence of the base.

The initial C–H activation (formation of **2**) could be rationalized according to two different formal mechanisms (Scheme 2). The first is a simple intramolecular transprotonation (Scheme 2, route i), in which the migration of a proton from the Cp* ring to the acetylenic C_α atom could be followed by a $\text{CH}_2\text{-C}_\beta$ coupling process. This route could be favored under thermal conditions due to the well-known polarization of the triple bond in P-coordinated alkynephosphines. Alternatively, the deprotonation of a methyl group could give a η^4 -fulvene- or η^6 -fulvene–Rh(I) intermediate (Scheme 2, route ii). The subsequent oxidative $\text{CH}_2\text{-C}_\beta$ coupling, followed by a final protonation of the C_α carbon, to compensate the negative charge on this atom, would also generate the monohydroalkylated product **2**. Although this last route could seem less probable in the absence of base, due to the wide experimental evidence related with the electrophilic character of the *exo*-methylene groups ($=\text{CH}_2$) on fulvene ligands,^{6,13,71,74,86,87} nucleophilic behavior has been also found in some η^4 -fulvene–rhodium complexes.^{73,88} Although it has also been observed under thermal conditions, the additional C–H activation on **2**, giving rise to **3'** and **4'**, seems to be more favored in the presence of base.

Spectroscopic and Crystallographic Characterization. In spite of the fact that **3** is the only pure complex obtained, the isomeric nature of all the derivatives described has been established by elemental analyses and mass spectrometry. Thus, the mass spectra (MALDI(+)) of **3** (Figure S1b in the Supporting Information) and of different mixtures (see the Experimental Section and Figures S1a and S1c in the Supporting Information) show the peaks corresponding to m/z 845 ($[\text{M}]^+$ 23–73%) and 810 ($[\text{M} - \text{Cl}]^+$ 100%) ($\text{M} = \text{C}_{50}\text{ClH}_{45}\text{PRh}$). All complexes (**2**, **3'**, **4'**, **3**, and **4**) have been also fully characterized by NMR spectroscopy (including $^1\text{H}\{^{31}\text{P}\}$ and two-dimensional $^1\text{H}\text{-}^1\text{H}$ -COSY, $^1\text{H}\text{-}^{13}\text{C}$ HSQC, and HMBC and $^1\text{H}\text{-}^{31}\text{P}$ -HMBC NMR experiments, see Figure S2 in the Supporting Information for **3**) carried out from several mixtures of the complexes. In addition, the molecular structures of a solid mixture of **1** and **2** (Figure 1, Table 1) and of **3** (Figure 3, Table 2) have been characterized by X-ray diffraction analyses.

As noted above, in spite of forming a solid solution with the starting product **1** (Figure 1a), complex **2** has been fully

(86) Castro, A.; Turner, M. L.; Maitlis, P. M. *J. Organomet. Chem.* **2003**, *674*, 45.

(87) Fan, L.; Turner, M. L.; Adams, H.; Bailey, N. A.; Maitlis, P. M. *Organometallics* **1995**, *14*, 676.

(88) Bellabarba, R. M.; Nieuwenhuyzen, M.; Saunders, G. C. *Organometallics* **2002**, *21*, 5726.

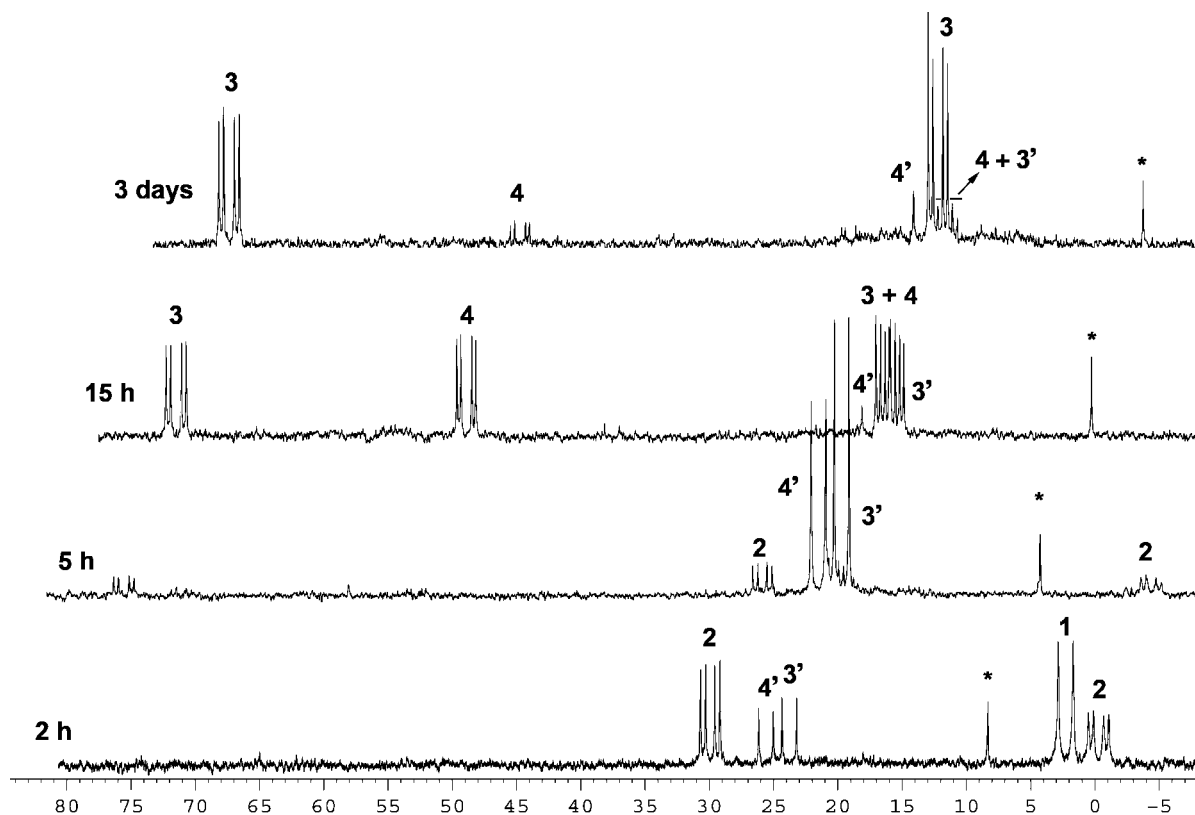


Figure 2. $^{31}\text{P}\{^1\text{H}\}$ NMR spectra showing the evolution of the reaction of the complex $[\text{Rh}(\eta^5\text{-Cp}^*)\text{Cl}(\text{PPh}_2\text{C}\equiv\text{CPh})_2](\text{CF}_3\text{SO}_3)$ (**1**) with Na_2CO_3 at room temperature (asterisks indicate peaks due to $\text{O}=\text{PP}_2\text{C}\equiv\text{CPh}$).

Scheme 2

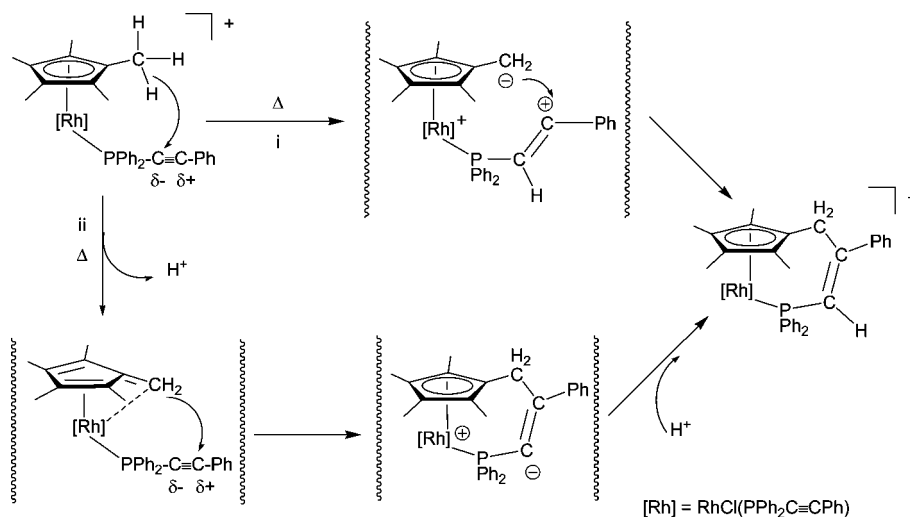


Table 1. Selected Bond Distances (Å) and Angles (deg) for $[\text{Rh}(\kappa\text{P}:\eta^5\text{-(CH}_2\text{CPh=CHPPh}_2\text{C}_5\text{Me}_4)]\text{Cl}(\text{PPh}_2\text{C}\equiv\text{CPh})(\text{CF}_3\text{SO}_3)$ (**2**)

Rh(1)–C(Cp*)	2.238(7)–2.264(7)	Rh(1)–C(42)	2.143(7)	Rh(1)–Cl(1)	2.4148(16)
Rh(1)–P(1)	2.3019(17)	Rh(1)–P(2)	2.3140(18)	P(2)–C(22)	1.750(7)
C(22)–C(23)	1.168(10)	P(1)–C(1a)	1.830(14)	C(1a)–C(2a)	1.335(18)
C(2a)–C(4a)	1.480(14)	C(2a)–C(3a)	1.527(16)	C(3a)–C(42)	1.516(14)
P(1)–Rh(1)–Cl(1)	98.31(6)	P(2)–Rh(1)–Cl(1)	94.07(6)		
P(1)–Rh(1)–P(2)	95.22(6)	C(42)–Rh(1)–Cl(1)	152.2(2)		
C(42)–Rh(1)–P(1)	95.2(2)	C(42)–Rh(1)–P(2)	108.7(2)		
C(22)–P(2)–Rh(1)	110.9(3)	P(2)–C(22)–C(23)	172.4(8)		
C(22)–C(23)–C(24)	175.7(9)	C(1a)–P(1)–Rh(1)	109.6(4)		
P(1)–C(1a)–C(2a)	131.9(10)	C(1a)–C(2a)–C(4a)	120.0(11)		
C(1a)–C(2a)–C(3a)	126.1(10)	C(42)–C(3a)–C(2a)	125.7(10)		

structurally characterized (Figure 1b), confirming the presence of a functionalized η^5 -cyclopentadienyl ring. The angles and distances observed in this study for molecule **1** are similar to

those found in the structure reported earlier.⁸⁹ In the proposed modelization, complex **2** shares with molecule **1** the chlorine atom, the $\text{P}(2)\text{Ph}_2\text{C}\equiv\text{CPh}$ phosphine, and the $\eta^5\text{-C}_5\text{Me}_4$ fragment

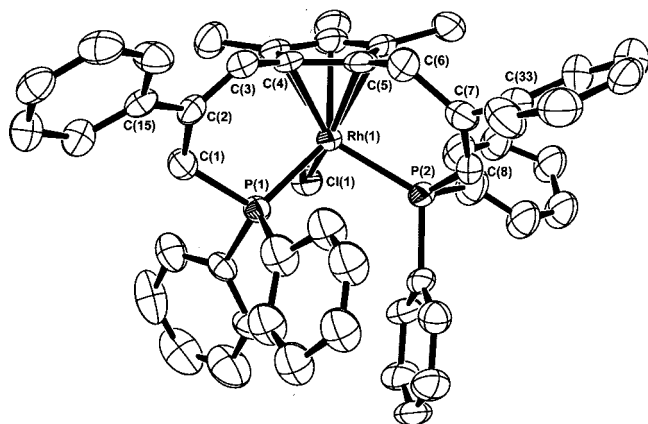


Figure 3. ORTEP view of the cation $[\text{Rh}\{\kappa^2\text{PP}':\eta^5\text{-1,2-(PPh}_2\text{CH}_2\text{CPh=CH)C}_5\text{Me}_3(\text{CH}_2\text{CPh=CHPPh}_2)\}\text{Cl}]^+$ in complex **3**. Ellipsoids are drawn at the 50% probability level. Hydrogen atoms and solvent have been omitted for clarity.

of the new chelating $\kappa\text{P}:\eta^5$ ligand. Thus, the Rh–Cl distance (2.4148(16) Å) and the structural details of the terminal phosphine P(2)Ph₂C≡CPh (P–C_α = 1.750(7) Å; C_α–C_β = 1.168(10) Å; P–C_α–C_β = 172.4(8)°; C_α–C_β–C_γ = 175.7(9)°) remain practically unchanged in relation to those found in the starting product (Rh–Cl = 2.4048(11) Å; P–C_α = 1.742(5), 1.759(5) Å; C_α–C_β = 1.201(6), 1.191(6) Å; P–C_α–C_β = 178.1(4), 177.9(5)°; C_α–C_β–C_γ = 177.3(5), 178.1(5)°).⁸⁹ With regard to the new $\kappa\text{P}:\eta^5$ -vinylphosphine ligand, the P–C_α (P(1)–C(1a)) distance increases slightly from 1.742(5) Å (in $[\text{RhCp}^*\text{Cl}(\text{PPh}_2\text{C}\equiv\text{CPh})_2]^+$ (**1**)⁸⁹) to 1.830(14) Å. Nevertheless, both the P–C_α (P(1)–C(1a)) and the vinylic C_α=C_β (C(1a)–C(2a) = 1.335(18) Å) distances are comparable to those found in other κP -vinylphosphine complexes, such as $[\eta^5\text{-Cp}^*]\text{RhCl}(\text{PPh}_2\text{CH=CH}_2)_2]\text{PF}_6$ (P–C_α = 1.803(8), 1.812(8) Å; C_α=C_β = 1.304(10), 1.306(10) Å).²⁴ The angles around the C_α (P(1)–C(1a)–C(2a) = 131.9(10)°) and C_β atoms (120.0(11), 126.1(10)°) are typical of sp² carbon atoms, although the angle at the C_α atom is slightly distorted, probably due to steric strain of the new chelate ligand. In relation to the $\eta^5\text{-C}_5\text{Me}_4\text{CH}_2$ ring, it should be noted that the distance Rh(1)–C(42) (2.143(7) Å) is clearly shorter than the distances between the rhodium and the rest of the cyclopentadienyl ring carbon atoms (2.238(7)–2.264(7) Å), in agreement with the low trans influence of the chlorine ligand, pointing to some degree of $\eta^1:\eta^4$ distortion of the ring. Finally, unlike the case for the precursor **1**, the presence of two different types of phosphine ligands in **2** generates a chiral center. Notwithstanding, the mixture of **1** and **2** crystallizes in a centrosymmetric space group (P2₁/n) with both of the enantiomers for **2** (*R* and *S,R* in Figure 1) present in the unit cell.

Complex **2** has been spectroscopically characterized from the mixture of **1**, **2**, and **3'** (~30:60:10). Thus, the ³¹P{¹H} NMR spectra of the microcrystalline samples always show, together with the doublet corresponding to the starting product (δ 2.3, ¹J_{P–Rh} = 140.8 Hz, **1**), the two expected resonances due to complex **2** (δ 30.0, dd, ¹J_{P–Rh} = 135.5 Hz; –0.30, dd, ¹J_{P–Rh} = 144.8; ²J_{P–P} = 49 Hz) and an additional small doublet (δ 23.8, ¹J_{P–Rh} = 138.5) corresponding to the presence of the symmetrical 1,2-dihydroalkylated complex **3'**. In **2**, the high-frequency resonance (δ_P 30), which is strongly deshielded in relation to the resonance for the precursor **1**, is attributed to the vinylphosphine phosphorus atom, whereas the low-frequency signal is assigned to the terminal alkynylphosphine. In the context of this work, it should be pointed out that these

assignments are comparable to those reported by Nelson and co-workers²⁴ for the monohydroalkylated derivative $[\text{Rh}\{\eta^5\text{-C}_5\text{Me}_4(\text{CH}_2\text{CH}_2\text{CH}_2\text{PPh}_2)\}\text{Cl}(\text{PPh}_2\text{CH=CH}_2)]^+$ (δ 31.8, –6.7), detected only as an intermediate species, and the final 1,2- and 1,3-dihydroalkylated complexes $[\text{Rh}\{\eta^5\text{-C}_5\text{Me}_3\text{-1,2-(CH}_2\text{CH}_2\text{CH}_2\text{-PPh}_2)_2\}\text{Cl}]^+$ (δ 19.1) and $[\text{Rh}\{\eta^5\text{-C}_5\text{Me}_3\text{-1,3-(CH}_2\text{CH}_2\text{CH}_2\text{PPh}_2)_2\}\text{Cl}]^+$ (δ 22.8), which were obtained by starting from the cationic complex $[\text{Rh}(\eta^5\text{-Cp}^*)\text{Cl}(\text{PPh}_2\text{CH=CH}_2)_2]\text{PF}_6$ under basic conditions. The ¹H NMR spectrum exhibits for complex **2** the vinylic proton at δ 6.61 (d, ²J_{H–P} = 8.3 Hz), which is in good agreement with resonances observed in similar complexes (~7 ppm),^{24,90–92} and in the 3–4 ppm region the expected ABMP pattern (M, P = ³¹P) (δ(H) 3.71, ddd; 3.13, d) for the two diastereotopic methylenic protons corresponding to the C₅Me₄CH₂ group of the new $\kappa\text{P}:\eta^5$ -tetramethylcyclopentadienylvinylphosphine ligand (see Figure S3 in the Supporting Information). The high-field signal (δ 3.13) appears as a doublet (²J_{H–H} = 17.6 Hz), while the proton at 3.71 ppm presents additional couplings with the two phosphorus atoms (⁴J_{H–P} = 11.6, 4.7 Hz). The highest value is assigned to the coupling with the PPh₂C≡CPh phosphorus atom, according to the behavior observed in the selective phosphorus-decoupling experiments (Supporting Information, Figure S3c).⁹³ The spectrum of the mixture also shows an additional AB system centered at 3.36 ppm (*J*_{H–H} = 17.1 Hz), which remains unchanged during recording of the ¹H{³¹P} NMR experiments, due to the methylenic protons of the C₅Me₃(CH₂)₂ group of the symmetrical 1,2-dihydroalkylation derivative **3'**. In the ¹³C{¹H} NMR spectrum, the signals due to the four methyl (δ 9.5, 9.1, 8.5, 8.2), the methylenic (δ 24.9), and the five quaternary (δ 111.3–94.1) carbon atoms of the C₅Me₄CH₂ group of complex **2** are clearly resolved, subtracting the corresponding resonances of the precursor **1**. The vinylic and acetylenic fragments of **2** appear at 159.2 (=CPh), 119.4 (PC=), 112.3 (≡CPh), and 78.8 (PC≡) ppm. The spectrum also shows signals due to **3'**, but they cannot be assigned unequivocally from this mixture (see below for its assignment using a 60:40 mixture of **3'** and **4'**).

For complex **3**, a view of the structure of the cation, which confirms the C–H bond activation of two methyl groups in the 1,2 positions of the Cp* ring, is given in Figure 3 (Table 2). A detailed observation of the distances between the carbon atoms of the P(2)–C(8)–C(7)–C(6) and P(1)–C(1)–C(2)–C(3) chains indicates that the double bonds are located between the C_α and C_β carbon atoms in the first chain (C(7)–C(8) = 1.351(10) vs C(6)–C(7) = 1.551(10) Å) and between the C_β and C_γ carbon atoms (C(2)–C(3) = 1.375(10) vs C(1)–C(2) = 1.491(9) Å) in the second chain. The presence of the double bonds is also corroborated by the angles around the alkenylic (sp²) carbons, which are close to the expected value of 120° (C(2)–C(3)–C(4) = 127.7(7)°, C(3)–C(2)–C(1) = 120.9(6)°, C(15)–C(2)–C(1) = 118.7(6)°, C(3)–C(2)–C(15) = 120.3(6)°; C(7)–C(8)–P(2) = 130.5(6)°, C(8)–C(7)–C(6) = 128.5(7)°, C(8)–C(7)–C(33) = 118.2(7)°, C(33)–C(7)–C(6) = 113.2(6)°).

(89) Berenguer, J. R.; Bernechea, M.; Forniés, J.; Gómez, J.; Lalinde, E. *Organometallics* **2002**, *21*, 2314.

(90) Redwine, K. D.; Hansen, H. D.; Bowley, S.; Isbell, J.; Sánchez, M.; Vodak, D.; Nelson, J. H. *Synth. React. Inorg. Met.-Org. Chem.* **2000**, *30*, 379.

(91) Redwine, K. D.; Hansen, H. D.; Bowley, S.; Isbell, J.; Vodak, D.; Nelson, J. H. *Synth. React. Inorg. Met.-Org. Chem.* **2000**, *30*, 409.

(92) Hansen, H. D.; Nelson, J. H. *Organometallics* **2000**, *19*, 4740.

(93) However, as can be observed in Figure S3b in the Supporting Information, decoupling at the δ(P)–0.3 signal has not been completely achieved and this has precluded the calculation of the corresponding coupling constant. Nevertheless, the simulation and iteration of the spectrum with the program g-NMR (version 3.6 for Macintosh, Figure S4 in the Supporting Information) has afforded similar values for the coupling constants (²J_{H–H} = 17.2 Hz; ⁴J_{H–P} = 11.7, 4.8 Hz).

Table 2. Selected Bond Distances (Å) and Angles (deg) for [Rh(κ^2PP' : η^5 -1,2-(PPh₂CH₂CPh=CH)C₅Me₃(CH₂CPh=CHPPh₂)]Cl(CF₃SO₃) (3)

Rh(1)–C(Cp*)	2.214(6)–2.289(7)	Rh(1)–C(4)	2.172(6)	Rh(1)–C(5)	2.137(7)
Rh(1)–Cl(1)	2.3795(18)	Rh(1)–P(1)	2.3108(17)	Rh(1)–P(2)	2.2870(18)
P(1)–C(1)	1.853(7)	C(1)–C(2)	1.491(9)	C(2)–C(3)	1.375(10)
C(2)–C(15)	1.484(9)	C(3)–C(4)	1.440(10)	P(2)–C(8)	1.807(8)
C(5)–C(6)	1.472(11)	C(6)–C(7)	1.551(10)	C(7)–C(8)	1.351(10)
C(7)–C(33)	1.506(11)				
<hr/>					
P(1)–Rh(1)–Cl(1)	90.28(6)	P(2)–Rh(1)–Cl(1)	94.80(7)		
P(2)–Rh(1)–P(1)	100.73(6)	C(4)–Rh(1)–Cl(1)	134.88(19)		
C(4)–Rh(1)–P(1)	88.04(18)	C(4)–Rh(1)–P(2)	129.76(19)		
C(5)–Rh(1)–Cl(1)	152.9(2)	C(5)–Rh(1)–P(1)	113.8(2)		
C(5)–Rh(1)–P(2)	92.9(2)	C(1)–P(1)–Rh(1)	109.7(2)		
C(2)–C(1)–P(1)	115.8(5)	C(3)–C(2)–C(1)	120.9(6)		
C(15)–C(2)–C(1)	118.7(6)	C(3)–C(2)–C(15)	120.3(6)		
C(2)–C(3)–C(4)	127.7(7)	C(8)–P(2)–Rh(1)	111.1(2)		
C(7)–C(8)–P(2)	130.5(6)	C(8)–C(7)–C(6)	128.5(7)		
C(5)–C(6)–C(7)	119.1(7)	C(8)–C(7)–C(33)	118.2(7)		
C(33)–C(7)–C(6)	113.2(6)				

The coordination of the η^5 -CH₂C₅Me₃CH= ring is asymmetric, with the Rh–C(4,5) distances (2.172(6), 2.137(7) Å) being shorter than the rest of the Rh–C(Cp*) distances (2.214(6)–2.289(7) Å), a feature which is consistent with the lower trans influence of the chlorine atom, in relation to the phosphorus atoms. The metal coordination is completed with the phosphorus atoms of the vinyl (PPh₂CPh=CH₂) and allyl (PPh₂CH₂CPh=CH) phosphine fragments, thus generating chirality on the rhodium atom (Figure 3 shows the enantiomer *S*), but as the complex crystallizes in the centrosymmetric space group *P*2₁/*c*, both enantiomeric cations, *R* and *S*, are present in the unit cell.

The difference between the chains in **3**, as well as in **4**, is also evidenced in the ³¹P{¹H} NMR spectra, which show the expected two resonances (doublet of doublets) for each complex. Due to their similarity with the resonances observed in complex **2**, the signals at highest field (δ 24.3, ¹J_{Rh–P} = 139, ²J_{P–P} = 44.5 Hz for **3**; δ 23.6, ¹J_{P–Rh} = 139, ²J_{P–P} = 38.5 Hz for **4**) are tentatively assigned to the corresponding phosphorus atom of the vinyl phosphine (*PCH*=) arms, while the lowest field resonances (δ 79.0, ¹J_{P–Rh} = 147 Hz for **3**; δ 56.8, ¹J_{P–Rh} = 141 Hz for **4**) are, therefore, ascribed to the phosphorus atoms of the remaining arms (*PCH*₂). In contrast, the intermediate 1,2- (**3'**) and 1,3- (**4'**) symmetrical diactivated isomers only show the expected doublet resonances at δ 23.8 (**3'**) and 25.7 (**4'**) (see Figure 2, ¹J_{P–Rh} = 138.5 Hz in both complexes). The ¹³C{¹H} NMR spectra also agree with the proposed formulations. Thus, the 1,2- (**3**) and 1,3- (**4**) asymmetrical diactivated derivatives show three methyl, one methylenic, and five quaternary signals due to the carbon atoms of their corresponding CH₂C₅Me₃CH= groups, as well as four resonances due to the two different vinylic fragments. As expected, the symmetrical 1,2- (**3'**) and 1,3- (**4'**) dihydroalkylated intermediates present simpler patterns, showing only two methyl, one methylenic, and three quaternary carbon signals for the C₅Me₃(CH₂)₂ unit and two signals for the equivalent vinylic fragments (see the Experimental Section). In support of the structural proposal suggested for the intermediate complex **3'**, we note that the quaternary cyclopentadienyl resonances of **3'** (δ 121.6, 103.7, and 99.5) resemble those of [η^5 -C₅Me₃-1,2-(CH₂CH₂-CH₂PPh₂)₂]RhCl]⁺ (δ 121.45, 103.6, and 94.1) described by Nelson and co-workers.²⁴ This feature, together with the fact that **3'** is the only species that remains in small amounts with complex **3** in the final crude product of the reaction carried out with base under reflux conditions (see the Experimental Section), led us to propose this intermediate as the corresponding symmetrical 1,2-diactivated derivative. Notwithstanding, we are aware that this assignment is only a suitable spectroscopic proposal, since we have not been able to isolate this complex as a pure compound or carry out a solid-state X-ray structural study.

The ¹H NMR spectrum of complex **3** presents four signals associated by pairs in the 3.4–4.0 ppm region due to both CH₂ groups. The inner pair of signals, which are assigned to the two methylenic protons (CH₂) of the PCH₂ fragment by a ¹H–³¹P-HMBC NMR experiment (Figure S2a in the Supporting Information), appears as an AB system at δ 3.6 and 3.5 (*J*_{H–H} = 16.5 Hz) in the ¹H{³¹P} NMR spectrum, while in the ¹H NMR spectrum they show additional couplings with the phosphorus atoms, the values of which (⁴*J*_{H–P} ≈ 5 and <10 Hz) have been calculated by selective decoupling ¹H{³¹P} experiments. The outer doublets (δ 3.95 and 3.34, *J*_{H–H} = 20.5 Hz) are thus attributed to the two methylenic protons (CH₂) of the η^5 -C₅Me₃CH₂ fragment. In this region, complex **4** shows three signals (3.96 (1H), 3.6 (1H) (*P*-CH₂); 3.5 (C₅Me₃CH₂, 2H)), whose multiplicity cannot be unambiguously assigned due to extensive overlap with the signals of **3**. Both **3** and **4** show two different signals corresponding to the vinylic protons (δ 6.8–6.26, see the Experimental Section), which have been assigned by ¹H–¹³C-HSQC experiments. With regard to the corresponding symmetrical 1,2- (**3'**) and 1,3- (**4'**) diactivation intermediates, the ¹H NMR spectra show the AB system centered at 3.36 Hz, which has also been observed in the mixture of **1**, **2**, and **3'** previously described (Figure S3 in the Supporting Information), assigned to the diastereotopic CH₂ protons of **3'**, and a broad singlet at δ 3.44 corresponding to **4'**, in which the 1,3-disposition would give rise to a more similar environment for the diastereotopic methylenic protons. As expected, both of them show only one resonance corresponding to the vinylic protons at δ 6.75 (**3'**) and 6.80 (**4'**), which have been again located by ¹H–¹³C-HSQC experiments.

Conclusion

In summary, we have shown that easy C–H bond activations can be promoted in the complex [(η^5 -Cp*)RhCl(PPh₂C≡CPh)₂](CF₃SO₃) (**1**) by either thermal or basic treatment, generating functionalized chelating mono- κ - η^5 - and di- κ - η^5 -cyclopentadienylphosphine ligands by subsequent reaction with the triple bonds of the PPh₂C≡CPh ligands. As far as we know, this is the first occasion in which alkynylphosphine ligands have been involved in hydroalkylation processes. The thermal treatment produces mainly the activation of one Cp* C–H bond to give the new κ - η^5 -C₅Me₃CH₂CPh=CHPPh₂ ligand. In contrast, the presence of a weak base, such as Na₂CO₃, favors the double C–H bond activation to afford initially two symmetrical 1,2- (**3'**) and 1,3- (**4'**) diactivation derivatives, which subsequently isomerize easily by a 1,3-hydrogen shift to give the asymmetrical 1,2- (**3**) and 1,3- (**4**) [Rh{ κ^2PP' : η^5 -(PPh₂CH₂CPh=CH)C₅Me₃(CH₂CPh=CHPPh₂)]Cl]⁺ derivatives. In the reaction mixture complex **4** is

also unstable, evolving to complex **3**, which is the thermodynamically most stable. Finally, it should be remarked that all the complexes described in this paper (**1**, **2**, **3**, **4**, **3'**, and **4'**) are isomers.

Experimental Section

All reactions were carried out under an atmosphere of dry argon, using standard Schlenk techniques. Solvents were dried by standard procedures and distilled under dry Ar before use. Elemental analyses and IR, mass, and NMR spectroscopic measurements were performed as described elsewhere.⁹⁴ Two-dimensional NMR experiments have been carried out on a Bruker ARX 400 spectrometer.

Thermal Activation of [Rh(η^5 -Cp*)Cl(PPh₂C≡CPh)₂](CF₃SO₃) (1**). Characterization of [Rh(κ^2 PP': η^5 -C₅Me₃-1,2-(CH₂CPh=CHPPh₂)₂)Cl](CF₃SO₃) (**3'**), and [Rh(κ^2 PP': η^5 -C₅Me₃-1,3-(CH₂CPh=CHPPh₂)₂)Cl](CF₃SO₃) (**4'**) in the approximate molar ratio 25:57:12:6, respectively (³¹P{¹H} NMR). Evaporation of the solvent and treatment of the residue with diethyl ether afforded a mixture of complexes **1**, **2**, and **3'** (~30:60:10, respectively) as a yellow solid (0.13 g), which could not be separated by chromatography or repeated crystallizations in different solvents. The spectroscopic data of **2** have been obtained from this mixture (Anal. Found: C, 61.64; H, 4.49; S, 3.25. Calcd for C₅₁ClF₃H₄₅O₃P₂RhS: C, 61.55; H, 4.56; S, 3.22). Mass spectrum (MALDI(+)) of the reaction mixture of **1**, **2**, **3'**, and **4'**: *m/z* 845 ([M]⁺ 23%), 810 ([M - Cl]⁺ 100%) (M = C₅₀ClH₄₅PRh).**

This reaction has been optimized to obtain the maximum relative amount of complex **2**. Longer reaction times lead to mixtures having higher proportions of complexes **3'** and **4'**.

Data for **2** are as follows. IR (cm⁻¹): ν (C≡C) 2172 (m); ν (C=C) 1590 (w); ν (TfO) 1272 (s), 1224 (m), 1150 (m), 1031 (m). ¹H NMR (CDCl₃, δ): 8.2–6.7 (m, Ph); 6.61 (d, ²J_{H-P} = 8.3, 1H, PCH=C); 3.71 (ABMP system, J_{H-H} = 17.6, ⁴J_{H-P} = 11.6, ⁴J_{H-P} = 4.7, 1H, CH₂); 3.13 (AB system, J_{H-H} = 17.6, 1H, CH₂); 1.59 (d, ⁴J_{H-P} = 5.4, 3H, CH₃, C₅Me₄); 1.56 (d, ⁴J_{H-P} = 6.7, 3H, CH₃, C₅Me₄); 1.42 (d, ⁴J_{H-P} ≈ 5, CH₃, C₅Me₄; the signal overlaps with the triplet corresponding to the CH₃ (Cp*) of **1**); 1.34 (s broad, CH₃, C₅Me₄). ¹³C NMR (CDCl₃, δ): 159.2 (d, ²J_{P-C} = 14.0, PCH=CPh); 140.6 (d, ³J_{P-C} = 15.6, *ipso*-C, PCH=CPh); 135–125 (m, Ph); 122.4 (s, Ph); 119.4 (d, ¹J_{P-C} = 52.3, PCH=); 119.5 (d, J_{P-H} = 3.0, Ph); 119.2 (s, Ph); 112.3 (d, ²J_{P-C} = 11.9, C β); 111.3 (dd, ¹J_{Rh-C} = 5.2, ²J_{P-C} ≈ 3, C₅Me₄); 108.6 (dd, ¹J_{Rh-C} = 16.3, ²J_{P-C} = 2.8, CCH₂, C₅Me₄); 108.3 (d, ¹J_{Rh-C} = 15.7, C₅Me₄); 106.9 (d, ²J_{P-C} = 3.1, C₅Me₄); 94.1 (d, ¹J_{Rh-C} = 6.4, C₅Me₄); 78.8 (d, ¹J_{P-C} = 104.1, C α); 24.9 (d, ³J_{P-C} = 5.5, C₅Me₄CH₂); 9.5 (d, ³J_{P-C} = 2.5, C₅Me₄); 9.1 (d, ³J_{P-C} = 2.7, C₅Me₄); 8.5 (d, ³J_{P-C} = 2.1, C₅Me₄); 8.2 (s, C₅Me₄). ¹⁹F NMR (CDCl₃, δ): -78.42 (s, 3F, CF₃). ³¹P{¹H} NMR (CDCl₃, δ): 30.0 (dd, ¹J_{P-Rh} = 135.5, η^5 -P); -0.3 (dd, ¹J_{P-Rh} = 144.8, PPh₂C≡CPh) (²J_{P-P} = 53.0).

Thermal Activation of **1 in the Presence of Base. Synthesis of [Rh(κ^2 PP': η^5 -1,2-(PPh₂CH₂CPh=CH)C₅Me₃(CH₂CPh=CHPPh₂)₂)Cl](CF₃SO₃) (**3**). A 0.12 g (1.14 mmol) portion of Na₂CO₃ was added to a solution of compound **1** (0.15 g, 0.15 mmol) in THF, and the mixture was heated to reflux. A study of the reaction (³¹P{¹H} NMR) shows the presence of complexes **2**, **3'**, and **4'**, together with starting product **1** (41:22:12:25 relative molar ratio, respectively), after 20 min of reaction. With the passing of the reaction time, the relative amount of complexes **3'** and **4'** increased and, after 6 h, complexes **3** and [Rh(κ^2 PP': η^5 -1,3-(PPh₂CH₂CPh=CH)C₅Me₃(CH₂CPh=CHPPh₂)₂)Cl](CF₃SO₃) (**4**) were already observed (**3**:**4**:**3'**:**4'** relative molar ratio 19:3:51:27). After 10 h, the main product detected was complex **3** with a small amount of intermediates **3'** and **4'** (78:18:4 relative molar**

ratio, respectively). Finally, after 16 h of reaction, only complex **3** was detected, together with a small amount of compound **3'** (93:7 relative molar ratio, respectively). Then, the solvent was removed and the solid residue (**3** + **3'**) extracted with CH₂Cl₂ to give an orange solid (0.13 g). Recrystallization from acetone/hexane yielded compound **3** as a crystalline orange solid (0.04 g, yield 36%). Anal. Calcd for C₅₁ClF₃H₄₅O₃P₂RhS: C, 61.55; H, 4.56; S, 3.22. Found: C, 61.37; H, 4.32; S, 3.08. MS MALDI(+): *m/z* 845 [M]⁺ 73%; 810 [M - Cl]⁺ 100% (M = C₅₀ClH₄₅PRh). IR (cm⁻¹): ν (C=C) 1600 (w), 1574 (w); ν (TfO) 1273 (s), 1224 (m), 1148 (m), 1032 (m). ¹H NMR (CDCl₃, δ): 7.96 (m), 7.66 (m), 7.52 (m), 7.40 (m), 7.14 (m), 7.0 (m), 6.8 (m), 6.71 (m), 6.4 (m) (30 H, Ph); 6.75 (PCH=C, 1H, overlapped with the aromatic signals); 6.58 (C₅Me₃CH=, 1H, overlapped with the aromatic signals); 3.95 (d, J_{H-H} = 20.5, 1H, C₅Me₃CH₂); 3.6, 3.5 (ABXY system, J_{H-H} = 16.5, 2H, PCH₂); 3.34 (d, J_{H-H} = 20.5, 1H, C₅Me₃CH₂); 1.96 (d, ⁴J_{H-P} = 8.1, 3H, CH₃, C₅Me₃); 1.89 (d, ⁴J_{H-P} = 4.5, 3H, CH₃, C₅Me₃); 1.28 ("t", ⁴J_{H-P} = 6.5, 3H, CH₃, C₅Me₃). ¹³C NMR (CDCl₃, δ): 161.5 (d, ²J_{P-C} = 14.7, PCH=CPh); 144.8 (d, ²J_{P-C} = 3.3, PCH₂CPh=); 142.1 (d, ³J_{P-C} = 15.9, *ipso*-C, PCH=CPh); 141.1 (d, ³J_{P-C} = 4.7, *ipso*-C, PCH₂CPh=); 135–125 (m, Ph); 127.9 (dm, ¹J_{Rh-C} ≈ 10, CCH=, C₅Me₃); 123.5 (dd, ¹J_{Rh-C} = 6.5, ²J_{P-C} = 3.4, C₅Me₃); 122.5, 119.3 (s, Ph); 115.7 (d, ³J_{P-C} = 5.5, C₅Me₃CH=); 114.8 (d, ¹J_{P-C} = 52.6, PCH=); 109.5 (ddd, ¹J_{Rh-C} = 9.6, ²J_{P-C} = 3.2, 1.7, C₅Me₃); 101.9 (d, J_{P-H} = 5.8, Ph); 101.8 (dd, ¹J_{Rh-C} = 14.5, ²J_{P-C} = 3.7, C₅Me₃); 83.2 (doublet of pseudotriplets, ¹J_{Rh-C} = 7.3, ²J_{P-C} ≈ 2.5, CCH₂, C₅Me₃); 35.9 (d, ¹J_{P-C} = 23.3, PCH₂); 26.3 (d, ³J_{P-C} = 3.0, C₅Me₃CH₂); 10.4 (d, ³J_{P-C} = 2.1, C₅Me₃); 10.0 (d, ³J_{P-C} = 2.4, C₅Me₃); 9.9 (d, ³J_{P-C} = 3.7, C₅Me₃). ¹⁹F NMR (CDCl₃, δ): -78.35 (s, 3F, CF₃). ³¹P NMR (CDCl₃, δ): 79.0 (dd, ¹J_{P-Rh} = 147, PCH₂); 24.3 (dd, ¹J_{P-Rh} = 139, PCH=) (²J_{P-P} = 44.5).

Activation of **1 at Room Temperature. Synthesis of Mixtures of **3** and **4** (50:50) and **3'** and **4'** (60:40).** A solution of **1** (0.15 g, 0.15 mmol) in THF was treated with Na₂CO₃ (0.16 g, 1.5 mmol), and the mixture was stirred at room temperature, while the reaction was monitored by ³¹P{¹H} NMR spectroscopy (see Figure 2). After 15 h, the most abundant species were compounds **3** and **4** (~50:50). Then, the solvent was removed and the crude mixture extracted with CH₂Cl₂ and filtered. The filtrate was evaporated to dryness and treated with Et₂O, yielding a mixture of complexes **3** and **4** (~50:50 molar ratio) as an orange solid (0.135 g, yield 90%). By a similar treatment, but with the reaction being stopped after 5 h, we obtained a mixture of complexes **3'** and **4'** (~60:40) as an orange solid (0.12 g, yield 83%). All attempts to isolate any of these complexes by chromatography or recrystallization from these mixtures have been also fruitless. Mass spectra (MALDI(+)) of these mixtures show peaks corresponding to *m/z* 845 ([M]⁺ 37%) and 810 ([M - Cl]⁺ 100%) (M = C₅₀ClH₄₅PRh).

When the initial mixture is allowed to react for 3 days, complex **3** was the most abundant species (approximate molar ratio **3**:**4**:**3'**:**4'** 75:15:5:5).

Data for **4 (Obtained from the Mixture of **3** and **4** (50:50)).** Anal. Calcd for C₅₁ClF₃H₄₅O₃P₂RhS: C, 61.55; H, 4.56; S, 3.22. Found: C, 61.63; H, 4.45; S, 3.11. ¹H NMR (CDCl₃, δ): 7.96 (m), 7.65 (m), 7.53 (m), 7.41 (m), 7.15 (m), 7.02 (m), 6.82 (m), 6.71 (m), 6.3 (br s) (Ph corresponding to **3** and **4**); 6.8 (PCH=C, 1H, overlapped with the aromatic signal); 6.26 (m, C₅Me₃CH=, 1H); 3.96 (1H), 3.6 (1H) (PCH₂); 3.5 (C₅Me₃CH₂, 2H) (the multiplicity of both of the methylenic signals has not been clearly elucidated owing to extensive overlap with the signals corresponding to complex **3**); 1.81 (d, ⁴J_{H-P} = 6.6, 3H, CH₃, C₅Me₃); 1.76 (d, ⁴J_{H-P} = 7.4, 3H, CH₃, C₅Me₃); 1.30 (m, 3H, CH₃, C₅Me₃; this signal overlaps with one corresponding to complex **3**). ¹³C NMR (CDCl₃, δ): 160.0 (d, ²J_{P-C} = 13.5, PCH=CPh); 142.0 (d, ²J_{P-C} ≈ 5, PCH₂CPh=); 141.3 (d, ³J_{P-C} ≈ 5, *ipso*-C, PCH₂CPh=); 140.7 (d, ³J_{P-C} = 15.1, *ipso*-C, PCH=CPh); 135–125 (m, Ph); 118.8 (d,

(94) Berenguer, J. R.; Lalinde, E.; Torroba, J. *Inorg. Chem.* **2007**, *46*, 9919.

Table 3. Crystallographic Data for 2 and 3

	2	3
empirical formula	C ₅₁ H ₄₅ ClF ₃ O ₃ P ₂ RhS	C ₅₁ H ₄₅ ClF ₃ O ₃ P ₂ RhS
formula wt	995.23	995.23
temp (K)	123(1)	100(1)
cryst syst	monoclinic	monoclinic
space group	<i>P2₁/n</i>	<i>P2₁/c</i>
<i>a</i> (Å)	15.4650(3)	16.0340(6)
<i>b</i> (Å)	15.0860(3)	15.2010(6)
<i>c</i> (Å)	19.0140(4)	19.6740(4)
α (deg)	90	90
β (deg)	90.5170(10)	113.367(2)
γ (deg)	90	90
<i>V</i> (Å ³)	4435.88(15)	4401.9(3)
<i>Z</i>	4	4
<i>D</i> _{calcd} (Mg/m ³)	1.490	1.502
abs coeff (mm ⁻¹)	0.621	0.626
<i>F</i> (000)	2040	2040
cryst size (mm)	0.4 × 0.4 × 0.2	0.15 × 0.15 × 0.10
θ range for data collecn (deg)	3.41–26.37	3.63–25.35
no. of data/restraints/params	9033/25/556	8048/28/589
goodness of fit on <i>F</i> ²	1.039	1.076
final <i>R</i> indices (<i>I</i> > 2σ(<i>I</i>))	<i>R</i> 1 = 0.0861, <i>wR</i> 2 = 0.2357	<i>R</i> 1 = 0.0786, <i>wR</i> 2 = 0.1750
<i>R</i> indices (all data)	<i>R</i> 1 = 0.1131, <i>wR</i> 2 = 0.2644	<i>R</i> 1 = 0.0988, <i>wR</i> 2 = 0.1861
largest diff peak, hole (e Å ⁻³)	1.565, -2.070	2.467, -1.109

¹*J*_{P-C} = 51.6, PCH=); 116.6 (dd, ¹*J*_{Rh-C} = 4.9, ²*J*_{P-C} = 2.9, C₅Me₃); 115.2 (d, ³*J*_{P-C} = 5.0, C₅Me₃CH=); 109.7 (dbr, ¹*J*_{Rh-C} ≈ 10, C₅Me₃); 108.6 (d, ¹*J*_{Rh-C} = 10.5, C₅Me₃); 102.2 (pseudotriplet, ²*J*_{P-C} ≈ 4, CCH=C, C₅Me₃); 98.2 (d, ¹*J*_{Rh-C} ≈ 7.7, C₅Me₃); 31.4 (d, ¹*J*_{P-C} = 26.7, PCH₂); 29.7 (s, C₅Me₃); 25.3 (d, ³*J*_{P-C} ≈ 5, C₅Me₃CH₂); 9.8 (d, ³*J*_{P-C} = 3.2, C₅Me₃); 9.2 (d, ³*J*_{P-C} = 3.4, C₅Me₃). ¹⁹F NMR (CDCl₃, δ): -78.35 (s, 3F, CF₃). ³¹P NMR (CDCl₃, δ): 56.8 (dd, ¹*J*_{P-Rh} = 141); 23.6 (dd, ¹*J*_{P-Rh} = 139) (²*J*_{P-P} = 38.5).

Data for 3'. Anal. Calcd for C₅₁H₄₅ClF₃O₃P₂RhS: C, 61.55; H, 4.56; S, 3.22. Found (from a mixture of 3' and 4' 60:40): C, 61.41; H, 4.39; S, 3.29. ¹H NMR (CDCl₃, δ): 8–6.4 (m, Ph); 6.75 (PCH=C, 2H, overlapped with the aromatic signal); 3.36 (AB system, δ_A 3.30, δ_B 3.42, *J*_{H-H} = 17.1, 4H, C₅Me₃CH₂); 1.77 (d, ⁴*J*_{H-P} = 2.8, 3H, CH₃, C₅Me₃); 1.22 ("t", ⁴*J*_{H-P} ≈ 5, 6H, CH₃, C₅Me₃). ¹³C NMR (CDCl₃, δ): 159.5 (d, ²*J*_{P-C} = 8, PCH=CPh); 140.5 (d, ³*J*_{P-C} ≈ 9, *ipso*-C, PCH=CPh); 135–125 (m, Ph); 121.6 (d, ²*J*_{P-C} = 3.1, C₅Me₃); 116.4 (d, ¹*J*_{P-C} = 57.1, PCH=); 103.7 (dd, ¹*J*_{Rh-C} = 12, ²*J*_{P-C} = 5, C₅Me₃); 99.5 (d, ¹*J*_{Rh-C} = 7.7, C₅Me₃); 24.6 (sbr, C₅Me₃CH₂); 9.3 (sbr, 1CH₃, C₅Me₃); 8.8 (sbr, 2CH₃, C₅Me₃). ³¹P NMR (CDCl₃, δ): 23.8 (d, ¹*J*_{P-Rh} = 138.5).

Data for 4'. ¹H NMR (CDCl₃, δ): 8–6.4 (m, Ph); 6.80 (PCH=C, 2H, overlapped with the aromatic signal); 3.44 (sbr, 4H, C₅Me₃CH₂); 1.61 ("t", ⁴*J*_{H-P} ≈ 3, 6H, CH₃, C₅Me₃); 0.88 (sbr, 3H, CH₃, C₅Me₃). ¹³C NMR (CDCl₃, δ) 159.6 (d, ²*J*_{P-C} = 8, PCH=CPh); 140.6 (d, ³*J*_{P-C} ≈ 9, *ipso*-C, PCH=CPh); 135–125 (m, Ph); 117.2 (d, ¹*J*_{P-C} = 52.0, PCH=); 109.9 (dd, ¹*J*_{Rh-C} = 5.6, ²*J*_{P-C} ≈ 3, C₅Me₃); 107.1 (dm, ¹*J*_{Rh-C} ≈ 5, C₅Me₃); 92.4 (d, ¹*J*_{Rh-C} = 7.4, C₅Me₃); 25.0 (sbr, C₅Me₃CH₂); 9.4 (sbr, 1CH₃, C₅Me₃); 9.0 (sbr, 2CH₃, C₅Me₃). ³¹P NMR (CDCl₃, δ): 25.7 (d, ¹*J*_{P-Rh} = 138.5).

X-ray Crystallography. Table 3 reports details of the structural analyses for all of the complexes studied. Orange crystals of complex 3 and of a solid solution of complexes 1 and 2 were obtained by slow diffusion of *n*-hexane into acetone solutions of complex 3 or a mixture of complexes 1, 2, and 3' (30:60:10, respectively) at room temperature. X-ray intensity data were collected with a NONIUS κCCD area-detector diffractometer, using graphite-monochromated Mo Kα radiation. Images were processed using the DENZO and SCALEPACK suite of programs.⁹⁵ The structures were solved by Patterson and Fourier methods using the DIRDIF92 program,⁹⁶ and the absorption correction was performed using SORTAV.⁹⁷ All structures were refined by full-matrix least squares on *F*² with SHELXL-97,⁹⁸ and all non-hydrogen atoms

were assigned anisotropic displacement parameters. For the solid solution of complexes 1 and 2, we present the best of the analyses performed on three different crystals chosen from the same crude mixture. In the three cases the analyses were modeled in a 40:60 molar ratio (1:2). Both isomers share most of the structure, except the carbon atoms C1–C9 (**a** for the vinylphosphine ligand in 2 and **b** for the alkynylphosphine in 1). No restraints on bond distances or angles were made in refining the positions of C1a/b, C2a/b, and C3a/b. For complex 3, two phenyl rings (C27–C32 and C39–C44) present positional disorder, which could be refined over two positions with partial occupancy factors of 0.5/0.5 and 0.6/0.4, respectively. In both structural determinations the triflate cation was also disordered and modeled adequately. Complexes 2 and 3 have a chiral center at the Rh atom with both of the enantiomers, *R* and *S*, present in the unit cell (Figure 1 shows the enantiomer *R* and Figure 3 the enantiomer *S*). Finally, in both structural determinations some residual peaks greater than 1 e Å⁻³ were observed in the vicinity of the heavy atoms or the disordered triflates, but these had no chemical significance.

Acknowledgment. We wish to thank the Ministerio de Ciencia y Tecnología of Spain and the European Regional Development Fund (Project CTQ2005-08606-C02-02/BQU) for financial support. M.B. and J.T. thank the CAR for a grant. We thank Professor J. Forniés for helpful discussions and encouragement.

Supporting Information Available: Figures giving mass spectra (MALDI(+)) of a mixture of complexes 1, 2, 3', and 4', of pure complex 3, and a mixture of complexes 3 and 4, ¹H–³¹P-HMBC and ¹H–¹³C HSQC and HMBC NMR spectra of 3, ¹H, selective ¹H{³¹P}, and ¹H{³¹P} NMR spectra of the mixture of complexes 1, 2, and 3', and simulation of the ¹H NMR spectra of complex 2 and CIF files giving further crystallographic data of the structure determinations of 3 and the solid mixture of 1 and 2. This material is available free of charge via the Internet at <http://pubs.acs.org>.

OM800867H

(96) Beurskens, P. T.; Beurskens, G.; Bosman, W. P.; de Gelder, R.; García-Granda, S.; Gould, R. O.; Smith, J. M. M.; Smykalla, C. The DIRDIF92 Program System, Technical Report of the Crystallography Laboratory; University of Nijmegen, Nijmegen, The Netherlands, 1992.

(97) Blessing, R. H. *Acta Crystallogr.* **1995**, A51, 33.

(98) Sheldrick, G. M. SHELX-97, Program for the Refinement of Crystal Structures; University of Göttingen, Göttingen, Germany, 1997.

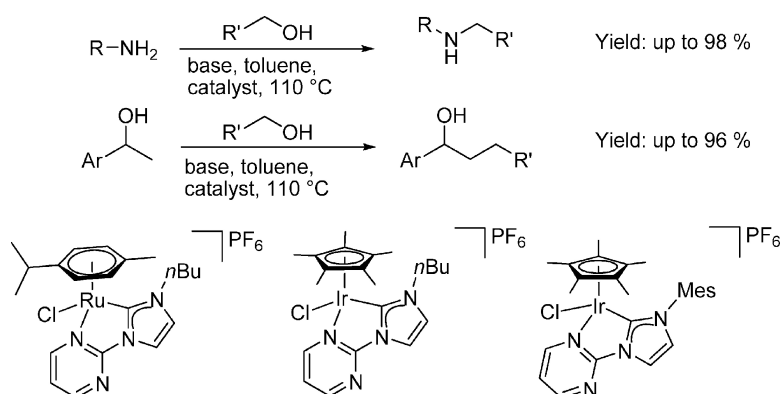
(95) Otwinowski, Z.; Minor, W. In *Methods in Enzymology*; Carter, C. V., Jr., Sweet, R. M., Eds.; Academic Press: New York, 1997; Vol. 276A, p 307.

Iridium and Ruthenium Complexes with Chelating N-Heterocyclic Carbenes: Efficient Catalysts for Transfer Hydrogenation, β -Alkylation of Alcohols, and N-Alkylation of Amines

Dinakar Gnanamgari, Effiette L. O. Sauer, Nathan D. Schley, Chase Butler, Christopher D. Incarvito, and Robert H. Crabtree

Organometallics, 2009, 28 (1), 321-325 • DOI: 10.1021/om800821q • Publication Date (Web): 26 November 2008

Downloaded from <http://pubs.acs.org> on April 14, 2009



More About This Article

Additional resources and features associated with this article are available within the HTML version:

- Supporting Information
- Access to high resolution figures
- Links to articles and content related to this article
- Copyright permission to reproduce figures and/or text from this article

[View the Full Text HTML](#)

Iridium and Ruthenium Complexes with Chelating N-Heterocyclic Carbenes: Efficient Catalysts for Transfer Hydrogenation, β -Alkylation of Alcohols, and N-Alkylation of Amines

Dinakar Gnanamgari, Effiette L. O. Sauer, Nathan D. Schley, Chase Butler, Christopher D. Incarvito, and Robert H. Crabtree*

Department of Chemistry, Yale University, 225 Prospect Street, P.O. Box 208107, New Haven, Connecticut 06520-8107

Received August 22, 2008

Air-stable Ir and Ru complexes of a chelating pyrimidine-functionalized N-heterocyclic carbene were synthesized. The complexes were characterized by NMR spectroscopy and single-crystal X-ray diffraction and were found to be catalytically active for transfer hydrogenation, β -alkylation of secondary alcohols with primary alcohols, and N-alkylation of amines with primary alcohols. Notably, the Ir complexes were found to catalyze the N-alkylation of amines using the mild base NaHCO_3 .

Introduction

N-Heterocyclic carbenes (NHCs) have attracted much attention as stable ligands for homogeneous catalysis.¹ They constitute a sterically and electronically tunable ligand set that supports catalysis. However, the principles regarding their structure–property relationships are underdeveloped. NHCs are more electron donating and tend to be sterically more demanding than phosphine ligands with the same substituents.² NHCs have been used as ligands for a multitude of reactions including transfer hydrogenation,³ C–C coupling,⁴ olefin metathesis,^{1f} and hydrosilylation.⁵

Functionalized NHCs⁶ having an additional donor group are an important class of ligands in organometallic catalysis. Many reports have appeared on NHCs functionalized with phosphine,⁷

pyridine,⁸ oxazoline,⁹ amido,¹⁰ and ether¹¹ donor functions. These ligands allow for potential hemilability, and several such cases have been reported.¹²

Transfer hydrogenation of C=O and C=N groups is a reaction for which NHC metal complexes³ have demonstrated particularly good activity. The C=O case has been most extensively studied, leading to important applications such as racemization¹³ of chiral alcohols and asymmetric reductions.¹⁴ In recent years, an alcohol activation strategy for C–C and C–N coupling reactions has received increased attention, in part because it replaces toxic halides as alkylating agents with relatively benign alcohols.¹⁵ In addition, reactions such as β -alkylation of secondary alcohols with primary alcohols¹⁶ and N-alkylation of amines with alcohols^{16b,17} produce water as the sole byproduct and are thus atom economical.

We now report novel chelating NHC pyrimidine Ir and Ru complexes that can be synthesized in good yields even in the presence of air. They are catalytically active for three useful

* Corresponding author. E-mail: robert.crabtree@yale.edu.

(1) (a) Arduengo, A. J.; Dias, H. V. R.; Harlow, R. L.; Kline, M. *J. Am. Chem. Soc.* **1992**, *114*, 5530–5534. (b) Herrmann, W. A.; Kocher, C. *Angew. Chem., Int. Ed. Engl.* **1997**, *36*, 2163–2187. (c) Herrmann, W. A. *Angew. Chem., Int. Ed.* **2002**, *41*, 1290–1309. (d) Lappert, M. F. *J. Organomet. Chem.* **1988**, *358*, 185–214. (e) Bourissou, D.; Guerret, O.; Gabbai, F. P.; Bertrand, G. *Chem. Rev.* **2000**, *100*, 39–91. (f) Sanford, M. S.; Love, J. A.; Grubbs, R. H. *Organometallics* **2001**, *20*, 5314–5318. (g) Scott, N. M.; Nolan, S. P. *Eur. J. Org. Chem.* **2005**, 1815–1828.

(2) (a) Crabtree, R. H. *J. Organomet. Chem.* **2005**, *690*, 5451–5457. (b) Diez-Gonzalez, S.; Nolan, S. P. *Coord. Chem. Rev.* **2007**, *251*, 874–883.

(3) (a) Corberan, R.; Peris, E. *Organometallics* **2008**, *27*, 1954–1958. (b) Voutchkova, A. M.; Gnanamgari, D.; Jakobsche, C. E.; Butler, C.; Miller, S. J.; Parr, J.; Crabtree, R. H. *J. Organomet. Chem.* **2008**, *693*, 1815–1821. (c) Poyatos, M.; McNamara, W.; Incarvito, C.; Peris, E.; Crabtree, R. H. *Chem. Commun.* **2007**, 2267–2269. (d) Gnanamgari, D.; Moores, A.; Rajaseelan, E.; Crabtree, R. H. *Organometallics* **2007**, *26*, 1226–1230.

(4) (a) Dragutan, V.; Dragutan, I.; Delaude, L.; Demonceau, A. *Coord. Chem. Rev.* **2007**, *251*, 765–794. (b) Liu, Z.; Zhang, T.; Shi, M. *Organometallics* **2008**, *27*, 2668–2671. (c) Xi, Z.; Liu, B.; Chen, W. *J. Org. Chem.* **2008**, *73*, 3954–3957.

(5) (a) Jimenez, M. V.; Perez-Torrente, J. J.; Bartolome, M. I.; Gierz, V.; Lahoz, F. J.; Oro, L. A. *Organometallics* **2008**, *27*, 224–234. (b) Poyatos, M.; Maisse-Francois, A.; Bellemin-Laponnaz, S.; Gade, L. H. *Organometallics* **2006**, *25*, 2634–2641.

(6) (a) Kuhl, O. *Chem. Soc. Rev.* **2007**, *36*, 592–607. (b) Pugh, D.; Danopoulos, A. A. *Coord. Chem. Rev.* **2007**, *251*, 610–641. (c) Ray, L.; Shaikh, M. M.; Ghosh, P. *Organometallics* **2007**, *26*, 958–964.

(7) (a) Lee, C. C.; Ke, W. C.; Chan, K. T.; Lai, C. L.; Hu, C. H.; Lee, H. M. *Chem.–Eur. J.* **2007**, *13*, 582–591. (b) Hahn, F. E.; Jahnke, M. C.; Pape, T. *Organometallics* **2006**, *25*, 5927–5936. (c) Yang, C. L.; Lee, H. M.; Nolan, S. P. *Org. Lett.* **2001**, *3*, 1511–1514.

(8) (a) Danopoulos, A. A.; Tsoureas, N.; Macgregor, S. A.; Smith, C. *Organometallics* **2007**, *26*, 253–263. (b) Mas-Marza, E.; Sanau, M.; Peris, E. *J. Organomet. Chem.* **2005**, *690*, 5576–5580. (c) Mas-Marza, E.; Sanau, M.; Peris, E. *Inorg. Chem.* **2005**, *44*, 9961–9967.

(9) Gade, L. H.; Bellemin-Laponnaz, S. *Coord. Chem. Rev.* **2007**, *251*, 718–725.

(10) (a) Liao, C. Y.; Chan, K. T.; Zeng, J. Y.; Hu, C. H.; Tu, C. Y.; Lee, H. M. *Organometallics* **2007**, *26*, 1692–1702. (b) Spencer, L. P.; Winston, S.; Fryzuk, M. D. *Organometallics* **2004**, *23*, 3372–3374. (c) Arnold, P. L.; Liddle, S. T. *Chem. Commun.* **2006**, 3959–3971.

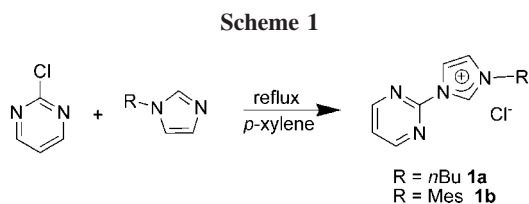
(11) Herrmann, W. A.; Goossen, L. J.; Spiegler, M. *J. Organomet. Chem.* **1997**, *547*, 357–366.

(12) (a) Corberan, R.; Sanau, M.; Peris, E. *Organometallics* **2007**, *26*, 3492–3498. (b) Wang, R. H.; Zeng, Z.; Twamley, B.; Piekarski, M. M.; Shreeve, J. M. *Eur. J. Org. Chem.* **2007**, 655–661. (c) Huynh, H. V.; Yeo, C. H.; Tan, G. K. *Chem. Commun.* **2006**, 3833–3835. (d) Arnold, P. L.; Blake, A. L.; Wilson, C. *Chem.–Eur. J.* **2005**, *11*, 6095–6099. (e) Hahn, F. E.; Holtgrewe, C.; Pape, T.; Martin, M.; Sola, E.; Oro, L. A. *Organometallics* **2005**, *24*, 2203–2209. (f) Chen, J. C. C.; Lin, I. J. B. *Organometallics* **2000**, *19*, 5113–5121.

(13) Yamaguchi, K.; Koike, T.; Kotani, M.; Matsushita, M.; Shinachi, S.; Mizuno, N. *Chem.–Eur. J.* **2005**, *11*, 6574–6582.

(14) Gladiali, S.; Alberico, E. *Chem. Soc. Rev.* **2006**, *35*, 226–236.

(15) (a) Skucas, E.; Ngai, M. Y.; Komanduri, V.; Krische, M. J. *Acc. Chem. Res.* **2007**, *40*, 1394–1401. (b) Hamid, M.; Slatford, P. A.; Williams, J. M. J. *Adv. Synth. Catal.* **2007**, *349*, 1555–1575. (c) Guillena, G.; Ramon, D. J.; Yus, M. *Angew. Chem., Int. Ed.* **2007**, *46*, 2358–2364. (d) Fujita, K.; Yamaguchi, R. *Synlett* **2005**, 560–571.



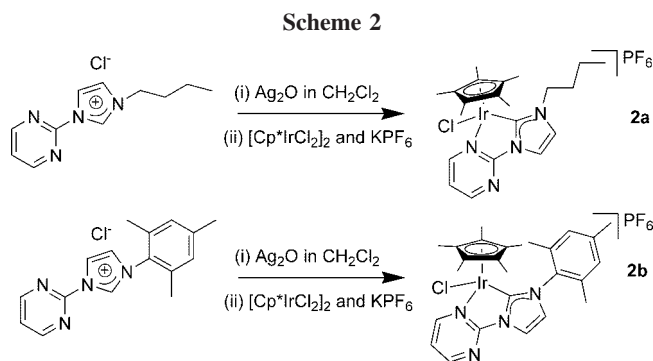
reactions dependent on transfer hydrogenation: the reduction of ketones and imines, β -alkylation of secondary alcohols with primary alcohols, and N-alkylation of amines with alcohols using the mild base NaHCO_3 .

Results and Discussion

The present ligand design was adopted in the hope that the potentially labile pyrimidine would provide hemilability so that the free pyrimidyl group might then act as an internal base, perhaps obviating the need for added base in catalysis. As discussed below, we found no evidence of hemilability, but we were able to substitute the much weaker NaHCO_3 for the usual strong base, KOH, in the catalytic N-alkylation of amines. Rather than this being a result of the anticipated internal base effect, however, this may instead be the result of the monocationic character of the catalyst induced by the bis-neutral donor structure of the present chelating NHC ligand compared with the monodentate NHCs more commonly encountered.^{16b} The resulting monopositive ionic charge might be expected to facilitate deprotonation of the coordinated alcohol. The present catalysts have at least as good or better activity than previously reported systems.^{16b}

Synthesis of Precursors for Chelating NHC Pyrimidine Ligands. The imidazolium salts used as precursors for the chelating NHC pyrimidine ligands were synthesized by direct alkylation of 1-substituted imidazoles. The reaction of 2-chloropyrimidine with stoichiometric amounts of 1-*n*-butylimidazole or 1-mesitylimidazole in refluxing *p*-xylene gave the corresponding pyrimidine imidazolium salts (Scheme 1). The salts were isolated in moderate yields and were characterized by elemental analysis and ^1H and $^{13}\text{C}\{^1\text{H}\}$ NMR spectroscopy. The ^1H NMR spectra of **1a** and **1b** in CDCl_3 showed a very low field resonance in the range δ 10.3–11.3 ppm characteristic of the NCHN imidazolium proton.

Synthesis of NHC Pyrimidine Ir(III) Salts. The Ir(III) salts **2a** and **2b** were prepared by in situ transmetalation from the silver carbene¹⁸ complexes of compounds **1a** and **1b** (Scheme 2). Treatment with Ag_2O under light-free conditions in CH_2Cl_2



at room temperature formed the presumed silver carbene, which was filtered and directly added to $[\text{Cp}^*\text{IrCl}_2]_2$ and KPF_6 . The mixture was stirred for 2 h, then filtered through Celite and concentrated to yield yellowish-orange solids **2a** and **2b** in good yields. After recrystallization from CH_2Cl_2 /pentane, compounds **2a** and **2b** were characterized by ^1H and $^{13}\text{C}\{^1\text{H}\}$ NMR, elemental analysis, and X-ray diffraction.

Both **2a** and **2b** lack the NCHN proton resonance of the precursor imidazolium ion but show the resonances for the backbone protons of the imidazolium fragment in the range δ 8.8–8.9 ppm. The chelate formation was initially suggested by the appearance of three distinct peaks in the ^1H NMR for the pyrimidine ring that are absent in the free imidazolium salt, showing that the symmetry of the pyrimidine is lost on binding. The molecular structures of **2a** (Figure 1) and **2b** (Figure 2), determined by single-crystal X-ray diffraction, confirm the formation of a chelate. The Ir–C_{carbene} distances of **2a** and **2b** are 2.146 and 2.044 Å, respectively, lying in the expected range.¹⁹

To explore potential hemilability in **2a**, we undertook a variable-temperature NMR experiment. No broadening of the three pyrimidine ^1H resonances was observed, even at 110 °C. This result suggests that the chelate is stable and that no hemilability occurs under these conditions.

Synthesis of NHC Pyrimidine Ru(II) Salt. The Ru(II) salt **3a** was made in an analogous manner to the syntheses described above. Treatment of **1a** with Ag_2O and transmetalation of the resulting silver carbene to $[\text{Ru}(p\text{-cymene})_2\text{Cl}_2]_2$ in the presence of KPF_6 gave a yellow solid **3a** (Scheme 3) in good yield. As expected, the compound **3a** lacked the NCHN proton and

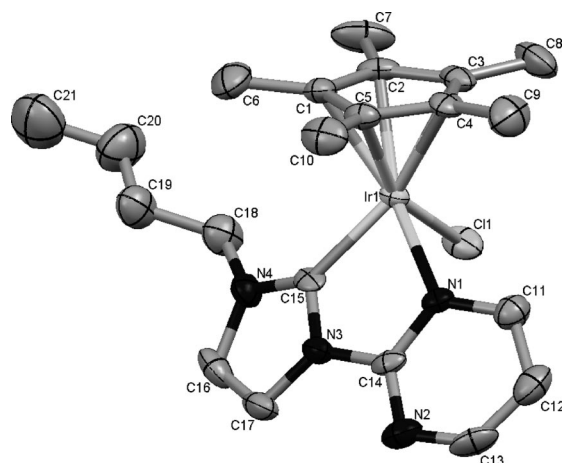


Figure 1. Molecular structure of **2a**. Selected bond lengths (Å) and angles (deg): Ir(1)–cent 1.821(6), Ir(1)–C(15) 2.146(5), Ir(1)–Cl(1) 2.4028(15), Ir(1)–N(1) 2.103(5), C(15)–Ir(1)–Cl(1) 86.78(16), C(15)–Ir(1)–N(1) 75.7(2).

(16) (a) Cho, C. S.; Kim, B. T.; Kim, H. S.; Kim, T. J.; Shim, S. C. *Organometallics* **2003**, *22*, 3608–3610. (b) da Costa, A. P.; Viciano, M.; Sanau, M.; Merino, S.; Tejada, J.; Peris, E.; Royo, B. *Organometallics* **2008**, *27*, 1305–1309. (c) Fujita, K.; Asai, C.; Yamaguchi, T.; Hanasaka, F.; Yamaguchi, R. *Org. Lett.* **2005**, *7*, 4017–4019. (d) Martinez, R.; Ramon, D. J.; Yus, M. *Tetrahedron* **2006**, *62*, 8982–8987. (e) Viciano, M.; Sanau, M.; Peris, E. *Organometallics* **2007**, *26*, 6050–6054. (f) Gnanamgari, D.; Leung, C. H.; Schley, N. D.; Hilton, S. T.; Crabtree, R. H. *Org. Biomol. Chem.* **2008**, *6*, 4442–4445.

(17) (a) Fujita, K.; Li, Z. Z.; Ozeki, N.; Yamaguchi, R. *Tetrahedron Lett.* **2003**, *44*, 2687–2690. (b) Fujita, K. I.; Fujii, T.; Yamaguchi, R. *Org. Lett.* **2004**, *6*, 3525–3528. (c) Tillack, A.; Hollmann, D.; Michalik, D.; Beller, M. *Tetrahedron Lett.* **2006**, *47*, 8881–8885. (d) Hamid, M.; Williams, J. M. J. *Chem. Commun.* **2007**, 725, 727.

(18) (a) Chianese, A. R.; Li, X. W.; Janzen, M. C.; Faller, J. W.; Crabtree, R. H. *Organometallics* **2003**, *22*, 1663–1667. (b) Lin, I. J. B.; Vasam, C. S. *Comments Inorg. Chem.* **2004**, *25*, 75–129.

(19) (a) Tanabe, Y.; Hanasaka, F.; Fujita, K.; Yamaguchi, R. *Organometallics* **2007**, *26*, 4618–4626. (b) Corberan, R.; Sanau, M.; Peris, E. *J. Am. Chem. Soc.* **2006**, *128*, 3974–3979. (c) Hanasaka, F.; Fujita, K.; Yamaguchi, R. *Organometallics* **2005**, *24*, 3422–3433. (d) Hanasaka, F.; Fujita, K. I.; Yamaguchi, R. *Organometallics* **2004**, *23*, 1490–1492.

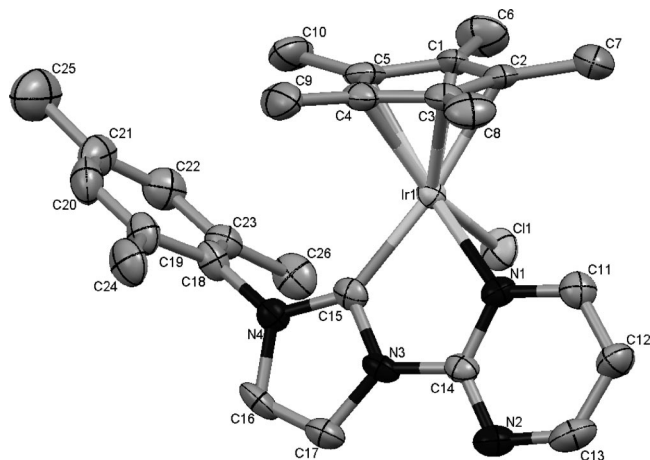


Figure 2. Molecular structure of **2b**. Selected bond lengths (Å) and angles (deg): Ir(1)–cent 1.830(6), Ir(1)–C(15) 2.044(7) Ir(1)–Cl(1) 2.3927(19), Ir(1)–N(1) 2.109(6), C(15)–Ir(1)–Cl(1) 86.98(19), C(15)–Ir(1)–N(1) 76.7(3).

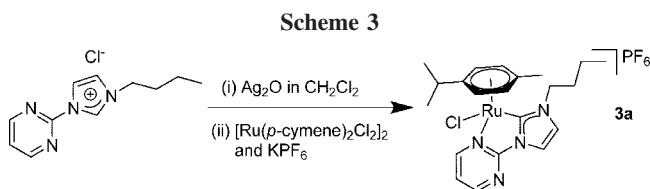


Table 1. Catalytic Transfer Hydrogenation^a

entry	catalyst	substrate	<i>t</i> (h)	TON ^b	% yield
1	2a	acetophenone	3	98	98
2	2b	acetophenone	3	86	86
3	3a	acetophenone	3	98	98
4	2a	cyclohexanone	6	90	90
5	2b	cyclohexanone	6	94	94
6	3a	cyclohexanone	5	99	99
7	2a	<i>N</i> -benzylideneaniline	6	58	58
8	2b	<i>N</i> -benzylideneaniline	6	37	37
9	3a	<i>N</i> -benzylideneaniline	5	80	80

^a 2.00 mmol of ketone or imine, KOH (10 mol %), 1 mol % catalyst in 3.0 mL of *i*PrOH at 82 °C. % yields were determined by ¹H NMR using 1,3,5-trimethoxybenzene as an internal standard. ^b TON = (mmol of product)/(mmol of catalyst) after time *t*.

showed the characteristic set of three distinct ¹H NMR peaks for the pyrimidine ring, confirming the loss of symmetry and formation of a chelate. Compound **3a** was characterized by ¹H and ¹³C{¹H} NMR and elemental analysis.

Catalytic Activity. Catalysts **2a**, **2b**, and **3a** were tested for activity in a variety of reactions. The compounds proved to be versatile and were successful in catalyzing transfer hydrogenation and the alkylation of both secondary alcohols and amines. Compounds **2a**, **2b**, and **3a** all catalyzed the transfer hydrogenation of C=O and C=N bonds in *i*PrOH/KOH at 82 °C (Table 1), but compound **3a** showed the best activity. The results obtained were comparable to previously published work from our laboratory using a bistriazole Rh(III) catalyst.^{3c}

β -Alkylation of secondary alcohols with primary alcohols (Table 2) is an important multistep reaction that combines dehydrogenation to the aldehyde or ketone, aldol coupling, loss of water, and hydrogenation of the resulting enone to the coupled alcohol into a tandem procedure. Several complexes¹⁶ have been reported that catalyze this reaction, including the extremely

Table 2. β -Alkylation of Secondary Alcohols with Primary Alcohols^a

entry	catalyst	Ar	R	<i>t</i> (h)	% conv	% alc	% ket
1	2a	Ph	Ph	3	93	100	0
2	2b	Ph	Ph	3	86	100	0
3	3a	Ph	Ph	3	10	100	0
4	2a ^b	Ph	Ph	3	64	100	0
5	2a	Ph	4-Cl(C ₆ H ₄)	3	96	100	0
6	2a	Ph	4-Cl(C ₆ H ₄)	6	100	80	20
7	2a	Ph	4-Me(C ₆ H ₄)	3	90	100	0
8	2a	Ph	<i>n</i> -Pr	5	82	60	22

^a 2.00 mmol of secondary alcohol and primary alcohol, 2.0 mmol of KOH (100 mol %), 1 mol % catalyst, 0.5 mL of toluene at 110 °C. Conversions determined by ¹H NMR using 1,3,5-trimethoxybenzene as an internal standard. ^b 0.5 mol % of catalyst.

Table 3. N-Alkylation of Amines with Alcohols^a

entry	catalyst	R	R'	% amine	% imine
1	2a	Ph	PhCH ₂	86	2
2	2b	Ph	PhCH ₂	62	23
3	3a	Ph	PhCH ₂	53	2
4	2a	Ph	Ph	98	<1
5	2a	Ph	PhCH ₂ CH ₂	55	4
6	2a	<i>n</i> -Pr	Ph	43	<1
7	2a	<i>n</i> -Pr	PhCH ₂	56	<1
8	2a	> <i>n</i> -Pr	PhCH ₂ CH ₂	25	<1

^a 1.00 mmol of alcohol and amine, 1 mol % catalyst, 0.5 mmol NaHCO₃ (50 mol %), and 4 Å molecular sieves (MS) in 0.2 mL of toluene at 110 °C. % yields were determined by ¹H NMR using 1,3,5-trimethoxybenzene as an internal standard.

active terpyridine Ru and Ir complexes we recently reported,^{16f} which form the coupled alcohols even in air. Here, we report our finding that NHC pyrimidine complexes **2a**, **2b**, and **3a** are also active for the β -alkylation of secondary alcohols with primary alcohols.

Complexes **2a** and **2b** were more active than **3a**, and conversion to the desired products could be achieved with catalyst loadings as low as 0.5 mol % (Table 2, entry 4) and with relatively short reaction times of 3 to 6 h. Compound **2a**, in particular, is more active than the best previously reported catalysts.^{16b} The selectivity pattern observed is dependent on reaction times. Longer reaction times favor the dehydrogenation of the coupled alcohol to give the ketone as observed in entry 6. This pattern has been reported^{16b,20} before. Presumably, H₂ is liberated in this step.

N-Alkylation of amines¹⁷ with alcohols is of interest for its relevance to the atom-economical synthesis of pharmaceutically significant molecules.²¹ We found that complexes **2a**, **2b**, and **3a** are all catalytically active for this reaction (Table 3). In contrast to the normal requirement for strong bases like KOH, we found that NaHCO₃, a weak base, is adequate. Only one other such system is known.²² These results are comparable to or better than any previously reported systems.^{16b,17a,17b}

Conclusion

We have reported novel chelating NHC pyrimidine complexes of Ir and Ru that are catalytically active for a variety of significant reactions: transfer hydrogenation and alkylation of

(20) Fujita, K.; Tanino, N.; Yamaguchi, R. *Org. Lett.* **2007**, *9*, 109–111.

(21) Kobayashi, S.; Ishitani, H. *Chem. Rev.* **1999**, *99*, 1069–1094.

secondary alcohols and of amines. These catalysts have the potential to be active in other interesting and important reactions. Further studies are underway to study the mechanism of the present system and its applicability to other reactions.

Experimental Section

[Cp*IrCl₂]₂²³ and [Ru(*p*-cymene)₂Cl₂]₂²⁴ were prepared according to known procedures. The syntheses of the ligand precursors and the metal complexes were conducted under air using reagent grade solvents with no special precautions. All of the compounds used in the syntheses were obtained from Aldrich and Strem and used as received unless otherwise indicated. All of the catalytic runs were conducted under an atmosphere of nitrogen using standard Schlenk techniques. NMR spectra were recorded at room temperature in CDCl₃ or CD₂Cl₂ on a 400 or 500 MHz Bruker spectrometer and referenced to the residual solvent peak (δ in ppm and J in Hz). Elemental analyses were performed by Atlantic Microlabs Inc.

Synthesis of 1-Pyrimidyl-3-butylimidazolium Chloride (1a).

1-*n*-Butylimidazole (0.653 mL, 5 mmol) was combined with 2-chloropyrimidine (572 mg, 5 mmol) in a flask with 5 mL of *p*-xylene. The mixture was refluxed for 3 days. The solvent was then decanted off, and the resulting hygroscopic brown solid was washed with ether and dried overnight. The salt was recrystallized from CH₂Cl₂/pentane: Yield: 1.19 g, 96%. ¹H NMR (CDCl₃): δ 11.15 (s, 1H, N-CH-N), 8.87 (d, J = 4.8, 2H, H_{pyrimidine}), 8.19 (s, 1H, imidazole_{backbone}), 7.86 (s, 1H, imidazole_{backbone}), 7.52 (t, J = 4.8, 1H, H_{pyrimidine}), 4.80 (t, J = 7.2, 2H, NCH₂ of *n*-Bu), 2.04–1.90 (m, 2H, CH₂ of *n*-Bu), 1.42 (m, 2H, CH₂ of *n*-Bu), 0.93 (t, J = 7.4, 3H, CH₃ of *n*-Bu). ¹³C NMR (126 MHz, CDCl₃): δ 159.97, 152.53, 136.99, 123.91, 122.37, 118.80, 50.99, 32.50, 19.68, 13.72. Anal. Calcd for C₁₁H₁₅N₄Cl: C, 55.34; H, 6.33; N, 23.47. Found: C, 55.10; H, 6.60; N, 23.20.

Synthesis of 1-Pyrimidyl-3-mesitylimidazolium Chloride (1b).

1-Mesitylimidazole^{25,26} (736 mg, 4 mmol) was combined with 2-chloropyrimidine (498 mg, 4.4 mmol) in a flask with 10 mL of *p*-xylene and refluxed for 24 h under inert atmosphere. The solvent was removed under reduced pressure with mild heating, and the resulting solid was washed with 25 mL of diethyl ether, extracted with dichloromethane, and filtered through Celite to afford a hygroscopic pale brown solid. Yield: 0.548 g, 46%. ¹H NMR (CDCl₃): δ 10.38 (s, 1H, N-CH-N), 8.92 (d, J = 4.9, 2H, H_{pyrimidine}), 8.65 (t, J = 1.8, 1H), 8.00 (t, J = 1.9, 1H), 7.68 (t, J = 4.9, 1H, H_{pyrimidine}), 6.98 (s, 2H), 2.29 (s, 3H), 2.13 (s, 6H). ¹³C NMR (CDCl₃): δ 160.04, 152.14, 141.65, 136.04, 134.08, 130.64, 130.01, 126.35, 122.99, 120.46, 21.19, 17.86. Anal. Calcd for C₁₆H₁₇N₄Cl. C, 63.89; H, 5.70; N, 18.63. Found: C, 63.50; H, 5.75; N, 18.39.

Representative Procedure for Synthesis of Metal Complexes.

A suspension of the appropriate imidazolium chloride (**1a** or **1b**) and silver oxide (0.5 equiv) in CH₂Cl₂ was stirred at room temperature in the dark for 1.5 h. The mixture was then filtered through a pad of Celite into the appropriate metal precursor and KPF₆ (2.1 equiv) and stirred at room temperature for 2 h. The suspension was filtered through Celite to remove silver salts, and the solvent was removed under reduced pressure. The resulting solid was washed with ether, dried under vacuum, and recrystallized from CH₂Cl₂/pentane.

Table 4. X-ray Experimental Data of Compounds **2a** and **2b**

	2a	2b
formula	C ₂₁ H ₂₉ ClF ₆ IrN ₄ P	C ₂₆ H ₃₁ ClF ₆ IrN ₄ P
MW	710.10	772.17
temp (K)	232(2)	223(2)
crystal system	orthorhombic	monoclinic
<i>a</i> (Å)	7.5743(4)	16.0826(18)
<i>b</i> (Å)	15.7519(8)	9.9821(11)
<i>c</i> (Å)	21.3385(11)	17.7748(19)
α (deg)	90	90
β (deg)	90	93.406(3)
γ (deg)	90	90
volume (Å ³)	2545.9(2)	2848.5(5)
<i>Z</i>	4	4
absorp coeff (cm ⁻¹)	54.73	49.00
no. of reflns collected	17 746	10 060
no. of ind. reflns	5800 [R(int) = 0.0459]	5821 [R(int) = 0.0440]
<i>T</i> _{max} , <i>T</i> _{min}	0.3928 and 0.2733	0.5863 and 0.4203
goodness of fit (GOF)	1.115	1.091
final <i>R</i> indices [<i>I</i> > 2 σ (<i>I</i>)]	R1 = 0.0359, wR2 = 0.0727	R1 = 0.0503, wR2 = 0.0929
<i>R</i> indices (all data)	R1 = 0.0406, wR2 = 0.0740	R1 = 0.0735, wR2 = 0.1018
largest diff peak and hole (e Å ⁻³)	1.424 and -0.758	2.325 and -1.145

Chloro(pentamethylcyclopentadienyl)(1-(2-pyrimidyl)-3-*n*-butyl)imidazol-2-ylidene)iridium(III) Hexafluorophosphate (2a). Transmetalation was carried out in CH₂Cl₂ (25 mL) with **1a** (290 mg, 1.22 mmol), Ag₂O (141 mg, 0.61 mmol), [Cp*IrCl₂]₂ (485 mg, 0.61 mmol), and KPF₆ (471 mg, 2.56 mmol). The product was a yellowish-orange hygroscopic solid. Yield: 693 mg, 80%. ¹H NMR (CDCl₃): δ 8.87–8.82 (m, 2H, imidazole_{backbone}), 7.88 (d, J = 2.3, 1H, H_{pyrimidine}), 7.59 (t, J = 5.3, 1H, H_{pyrimidine}), 7.28–7.24 (m, 1H, H_{pyrimidine}), 4.32–4.24 (m, 2H, NCH₂ of *n*-Bu), 1.87 (m, 2H, CH₂ of *n*-Bu), 1.81 (s, 15H, Cp*), 1.45–1.35 (m, 2H, CH₂ of *n*-Bu), 0.97 (t, J = 7.4, 3H, CH₃ of *n*-Bu). ¹³C NMR (126 MHz, CDCl₃): δ 165.34, 161.22, 159.48, 157.68, 124.19, 121.30, 118.16, 93.00, 50.93, 32.99, 20.02, 13.97, 9.55. Anal. Calcd for C₂₁H₂₉N₄ClF₆PIr: C, 35.52; H, 4.12; N, 7.89. Found: C, 35.82; H, 4.25; N, 7.54.

Chloro(pentamethylcyclopentadienyl)(1-(2-pyrimidyl)-3-mesityl)imidazol-2-ylidene)iridium(III) Hexafluorophosphate (3a). Transmetalation was carried out in CH₂Cl₂ (25 mL) with **1b** (163 mg, 0.541 mmol), Ag₂O (70 mg, 0.30 mmol), [Cp*IrCl₂]₂ (215 mg, 0.270 mmol), and KPF₆ (151 mg, 0.820 mmol). The product was a yellow solid. Yield: 306 mg, 73%. ¹H NMR (CDCl₃): δ 9.07 (d, J = 4.0, 1H), 8.94 (d, J = 3.0, 1H), 8.15 (d, J = 2.1, 1H), 7.88 (t, J = 5.0, 1H), 7.11 (s, 1H), 7.07 (s, 1H), 7.03 (d, J = 2.1, 1H), 2.40 (s, 3H), 2.24 (s, 3H), 2.21 (s, 3H), 1.55 (s, 15H). ¹³C NMR (CD₂Cl₂): δ 165.11, 161.73, 159.89, 158.00, 141.72, 137.25, 136.04, 134.33, 130.72, 130.11, 127.43, 122.23, 118.64, 93.74, 21.39, 19.14, 18.67, 9.36. Anal. Calcd for C₂₆H₃₁N₄ClF₆PIr: C, 40.44; H, 4.05; N, 7.26. Found: C, 40.17; H, 4.01; N, 7.12.

Chloro(*p*-cymene)(1-(2-pyrimidyl)-3-*n*-butyl)imidazol-2-ylidene)ruthenium(II) Hexafluorophosphate (3a). Transmetalation was carried out in CH₂Cl₂ (25 mL) with **1a** (135 mg, 0.566 mmol), Ag₂O (66 mg, 0.284 mmol), [Ru(*p*-cymene)₂Cl₂]₂ (173 mg, 0.282 mmol), and KPF₆ (218 mg, 1.18 mmol). The product was a dark yellow hygroscopic solid. Yield: 275 mg, 78%. ¹H NMR (CDCl₃): δ 9.56 (d, J = 4.2, 1H, imid_{backbone}), 8.74 (d, J = 3.5, 1H, imid_{backbone}), 7.81 (d, J = 2.1, 1H, H_{pyrimidine}), 7.52 (t, J = 5.1, 1H, H_{pyrimidine}), 7.26 (d, J = 2.2, 1H, H_{pyrimidine}), 6.19 (d, J = 6.1, 1H, CH_{arom}), 6.11 (d, J = 6.0, 1H, CH_{arom}), 5.99 (d, J = 6.1, 1H, CH_{arom}), 5.48 (d, J = 5.9, 1H, CH_{arom}), 4.43 (m, 2H, NCH₂ of *n*-Bu), 2.49 (m, 1H, CH_{arom}), 2.18 (s, 3H, CH_{3arom}), 2.02–1.90 (m, 2H, CH₂ of *n*-Bu), 1.50–1.39 (m, 2H, CH₂ of *n*-Bu), 1.04–0.94 (m, 9H). ¹³C NMR (CDCl₃): δ 183.41, 165.36, 160.09, 156.51, 124.52, 120.65, 117.42, 91.10, 89.63, 87.31, 83.09, 51.69, 32.58, 31.44, 22.82, 22.24, 20.11, 19.32, 13.90. Anal. Calcd for C₂₁H₂₈N₄ClF₆PRu: C, 40.82; H, 4.57; N, 9.07. Found: C, 40.81; H, 4.66; N, 8.84.

(22) Fujita, K. I.; Enoki, Y.; Yamaguchi, R. *Tetrahedron* **2008**, *64*, 1943–1954.

(23) Ball, R. G.; Graham, W. A. G.; Heinekey, D. M.; Hoyano, J. K.; McMaster, A. D.; Mattson, B. M.; Michel, S. T. *Inorg. Chem.* **1990**, *29*, 2023–5.

(24) Hodson, E.; Simpson, S. J. *Polyhedron* **2004**, *23*, 2695–2707.

(25) Occhipinti, G.; Bjorsvik, H. R.; Tornroos, K. W.; Furstner, A.; Jensen, V. R. *Organometallics* **2007**, *26*, 4383–4385.

(26) Gardiner, M. G.; Herrmann, W. A.; Reisinger, C. P.; Schwarz, J.; Spiegler, M. *J. Organomet. Chem.* **1999**, *572*, 239–247.

Representative Procedure for Transfer Hydrogenation of Unsaturated Substrates. Ketone (2.00 mmol) or imine (2.00 mmol), KOH (0.2 mmol), catalyst (0.020 mmol), and 1,3,5-trimethoxybenzene (used as an internal standard) were weighed into an oven-dried Schlenk flask. Dry *i*PrOH (3.0 mL) was added to the flask, and the mixture was refluxed for the time specified under nitrogen. The reaction was cooled, and an aliquot was filtered through a pad of Celite and analyzed by ¹H NMR.

Representative Procedure for β -Alkylation of Secondary Alcohols with Primary Alcohols. Secondary alcohol (2.00 mmol), primary alcohol (2.00 mmol), KOH (2.00 mmol), catalyst (0.020 mmol), and 1,3,5-trimethoxybenzene (used as an internal standard) were combined in an oven-dried Schlenk flask. Dry toluene (0.5 mL) was added to the flask, and the mixture was refluxed under nitrogen for the specified amount of time. The reaction was cooled and diluted with 1.0 mL of CH₂Cl₂, and the reaction mixture was filtered through a pad of Celite. The filtrate was concentrated under reduced pressure, and the resulting residue was analyzed by ¹H NMR.

Representative Procedure for N-Alkylation of Amines with Alcohols. Alcohol (1.00 mmol), amine (1.00 mmol), and 1,3,5-trimethoxybenzene (0.111 mmol, used as an internal standard) were weighed into an oven-dried Schlenk flask containing 4 Å molecular sieves (60 mg). Sodium bicarbonate (0.500 mmol) was added, followed by dry toluene (0.20 mL). The mixture was put under an atmosphere of nitrogen, and catalyst (0.010 mmol) was added before stoppering the flask and immersing it in a preheated oil bath (110 °C) for 45 h. The reaction was cooled and diluted with 0.5 mL of toluene (to rinse the sides of the flask), and the reaction mixture was filtered over a pad of Celite. The filtrate was concentrated under reduced pressure, and the resulting residue was analyzed by ¹H and ¹³C NMR and GC-MS.

X-ray Diffraction Studies of Compounds 2a and 2b. Crystal samples were mounted with epoxy cement on the tip of a fine glass fiber. All measurements were made on a Rigaku SCXMini diffractometer with graphite-monochromated Mo K α radiation. Two omega scans consisting of 180 data frames each were collected with a frame width of 1.0°. The data frames were processed and scaled using the Rigaku CrystalClear.²⁷ The data were corrected for Lorentz and polarization effects. The structure was solved by direct methods and expanded using Fourier techniques.²⁸ The non-hydrogen atoms were refined anisotropically, and hydrogen atoms were treated as idealized contributions. The final cycle of full-matrix least-squares refinement²⁹ on *F* was applied until convergence of unweighted and weighted factors of $R = \sum |F_o| - |F_c| / \sum |F_o|$; $R_w = \{\sum [w(F_o^2 - F_c^2)^2] / \sum [w(F_o^2)]\}^{1/2}$. Crystal data and experimental details for the crystals of **2a** and **2b** are given in Table 4.

Acknowledgment. We thank the Sanofi-Aventis Corp. and the U.S. Department of Energy for generous financial support. ELOS thanks NSERC Canada for postdoctoral funding.

Supporting Information Available: Tables of crystallographic data, atomic coordinates, bond lengths, and bond angles for complexes **2a** and **2b**. Table of optimization for the N-alkylation of aniline with benzyl alcohol. This material is available free of charge via the Internet at <http://pubs.acs.org>.

OM800821Q

(27) *CrystalClear* and *CrystalStructure*; Rigaku/MS: The Woodlands, TX, 2005.

(28) Sheldrick, G. M. *SHELXS* (direct methods); 1990. Sheldrick, G. M.; Schneider, T. R. *SHELXL* (refinement); 1997.

(29) Least-squares function minimized: $\sum w(F_o^2 - F_c^2)^2$.

First Cyclic Carbodiphosphoranes of Copper(I) and Gold(I) and Their Application in the Catalytic Cleavage of X–H Bonds (X = N and O)

Rosa Corberán,[†] Sebastien Marrot,[‡] Nicolas Dellus,[‡] Nathalie Merceron-Saffon,[§]
Tsuyoshi Kato,^{*,‡} Eduardo Peris,^{*,†} and Antoine Baceiredo^{*,‡}

Departament de Química Inorgànica i Orgànica, Universitat Jaume I, Avenida Vicente Sos Baynat s/n, 12080 Castellón, Spain, Laboratoire Hétérochimie Fondamentale et Appliquée, UMR 5069, Université Paul Sabatier, 118 Route de Narbonne, 31062 Toulouse Cedex 09, France, and Structure Fédérative Toulousaine en Chimie Moléculaire, FR 2599, Université Paul Sabatier, 118 Route de Narbonne, 31062 Toulouse Cedex 09, France

Received September 15, 2008

Three new carbodiphosphorane complexes, (PHCP)M(*t*BuO) (PHCP = carbodiphosphorane; M = Cu, Au) and (PHCP)CuCl, were readily prepared by reaction of the carbodiphosphorane **2** with CuCl or AuCl(Me₂S). The three complexes have been fully characterized, and their crystal structures have been determined. The two *tert*-butoxide complexes were tested in the catalytic anti-Markovnikov hydroamination and hydroalkoxylation of acrylonitrile, involving the first catalytic application of a carbodiphosphorane complex reported to date.

Introduction

The research interest in the application of group 11 metals in catalytic organic synthesis is growing rapidly in parallel to the development of new ligands.¹ Among these new ligands, N-heterocyclic carbenes (NHCs) have provided complexes with improved catalytic activity and higher thermal stability.² Considered as more electron-donating than phosphines, NHCs lack a clear pattern for the modulation of their basicity,³ although now it is accepted that this property ranges from the less basic triazolediylidenes⁴ to the more basic “abnormal” carbenes.⁵ Also, the fan-shaped topology of NHCs prevents an easy steric tuning of this type of ligands, which is often restricted to the modulation of the size of the N-substituents on the azole ring.

Recent examples of NHC complexes of Cu(I)^{6–8} and Au(I)^{9,10} (**I**, Scheme 1) have shown improved or modified catalytic properties, probably due to a dual effect of the ligand, increasing the electron-richness of the metal and stabilizing the metal center. The main limitation of these complexes is that their linear geometry reduces the steric control of the catalytic center, thus limiting the stereoselective outcome of the processes.

* Corresponding author. E-mail: eperis@qio.uji.es; antoine.baceiredo@chimie.ups-tlse.fr.

[†] Universitat Jaume I.

[‡] Laboratoire Hétérochimie Fondamentale et Appliquée, Université Paul Sabatier.

[§] Structure Fédérative Toulousaine en Chimie Moléculaire, Université Paul Sabatier.

(1) Lipshutz, B. H.; Yamamoto, Y. *Chem. Rev.* **2008**, *108*, 2793.

(2) (a) Herrmann, W. A.; Elison, M.; Fischer, J.; Kocher, C.; Artus, G. R. *J. Angew. Chem., Int. Ed. Engl.* **1995**, *34*, 2371. (b) Herrmann, W. A.; Kocher, C. *Angew. Chem., Int. Ed. Engl.* **1997**, *36*, 2163. (c) Peris, E.; Crabtree, R. H. *Coord. Chem. Rev.* **2004**, *248*, 2239. (d) Crudden, C. M.; Allen, D. P. *Coord. Chem. Rev.* **2004**, *248*, 2247. (e) Cesar, V.; Bellemin-Lapponnaz, S.; Gade, L. H. *Chem. Soc. Rev.* **2004**, *33*, 619. (f) Bourissou, D.; Guerret, O.; Gabbai, F. P.; Bertrand, G. *Chem. Rev.* **2000**, *100*, 39. (g) Cavell, K. J.; McGuinness, D. S. *Coord. Chem. Rev.* **2004**, *248*, 671. (h) Herrmann, W. A. *Angew. Chem., Int. Ed.* **2002**, *41*, 1291. (i) Peris, E.; Crabtree, R. H. *C. R. Chimie* **2003**, *6*, 33. (j) Mata, J. A.; Poyatos, M.; Peris, E. *Coord. Chem. Rev.* **2007**, *251*, 841.

(3) Diez-Gonzalez, S.; Nolan, S. P. *Coord. Chem. Rev.* **2007**, *251*, 874.

(4) Mas-Marza, E.; Mata, J. A.; Peris, E. *Angew. Chem., Int. Ed.* **2007**, *46*, 3729.

(5) (a) Grundemann, S.; Kovacevic, A.; Albrecht, M.; Faller, J. W.; Crabtree, R. H. *Chem. Commun.* **2001**, 2274. (b) Chianese, A. R.; Kovacevic, A.; Zeglis, B. M.; Faller, J. W.; Crabtree, R. H. *Organometallics* **2004**, *23*, 2461. (c) Appelhans, L. N.; Zuccaccia, D.; Kovacevic, A.; Chianese, A. R.; Miecznikowski, J. R.; Macchioni, A.; Clot, E.; Eisenstein, O.; Crabtree, R. H. *J. Am. Chem. Soc.* **2005**, *127*, 16299.

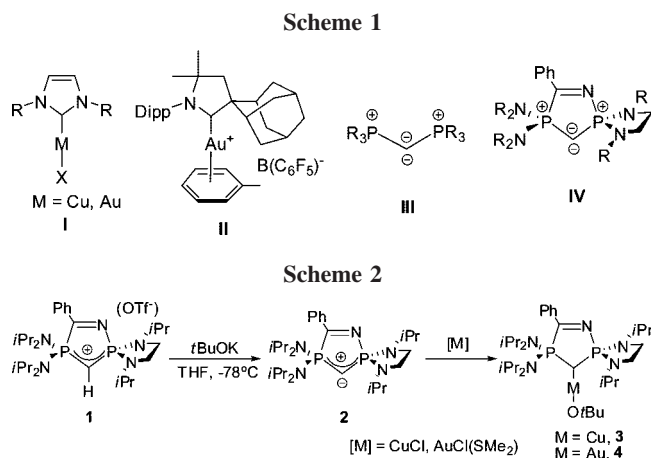
(6) (a) Diaz-Requejo, M. M.; Perez, P. J. *J. Organomet. Chem.* **2005**, *690*, 5441. (b) Fructos, M. R.; de Fremont, P.; Nolan, S. P.; Diaz-Requejo, M. M.; Perez, P. J. *Organometallics* **2006**, *25*, 2237. (c) Lebel, H.; Davi, M.; Diez-Gonzalez, S.; Nolan, S. P. *J. Org. Chem.* **2007**, *72*, 144. (d) Alexakis, A.; Winn, C. L.; Guillen, F.; Pytkowicz, J.; Roland, S.; Mangeney, P. *Adv. Synth. Catal.* **2003**, *345*, 345. (e) Larsen, A. O.; Leu, W.; Oberhuber, C. N.; Campbell, J. E.; Hoveyda, A. H. *J. Am. Chem. Soc.* **2004**, *126*, 11130. (f) Kaur, H.; Zinn, F. K.; Stevens, E. D.; Nolan, S. P. *Organometallics* **2004**, *23*, 1157. (g) Diez-Gonzalez, S.; Scott, N. M.; Nolan, S. P. *Organometallics* **2006**, *25*, 2355. (h) Diez-Gonzalez, S.; Correa, A.; Cavallo, L.; Nolan, S. P. *Chem.—Eur. J.* **2006**, *12*, 7558. (i) Guillen, F.; Winn, C. L.; Alexakis, A. *Tetrahedron: Asymmetry* **2001**, *12*, 2083. (j) Arnold, P. L.; Rodden, M.; Davis, K. M.; Scarisbrick, A. C.; Blake, A. J.; Wilson, C. *Chem. Commun.* **2004**, 1612. (k) Gawley, R. E.; Narayan, S. *Chem. Commun.* **2005**, 5109. (l) Fructos, M. R.; Belderrain, T. R.; Nicasio, M. C.; Nolan, S. P.; Kaur, H.; Diaz-Requejo, M. M.; Perez, P. J. *J. Am. Chem. Soc.* **2004**, *126*, 10846. Munro-Leighton, C.; Delp, S. A.; Blue, E. D.; Gunnoe, T. B. *Organometallics* **2007**, *26*, 1483. (n) Munro-Leighton, C.; Delp, S. A.; Alsop, N. M.; Blue, E. D.; Gunnoe, T. B. *Chem. Commun.* **2008**, 111. (o) Dubinina, G. G.; Furutachi, H.; Vivic, D. A. *J. Am. Chem. Soc.* **2008**, *130*, 8600.

(7) Laitar, D. S.; Muller, P.; Sadighi, J. P. *J. Am. Chem. Soc.* **2005**, *127*, 17196.

(8) Munro-Leighton, C.; Blue, E. D.; Gunnoe, T. B. *J. Am. Chem. Soc.* **2006**, *128*, 1446.

(9) (a) Schneider, S. K.; Herrmann, W. A.; Herdtweck, E. Z. *Anorg. Allg. Chem.* **2003**, *629*, 2363. (b) Fructos, M. R.; Belderrain, T. R.; de Fremont, P.; Scott, N. M.; Nolan, S. P.; Diaz-Requejo, M. M.; Perez, P. J. *Angew. Chem., Int. Ed.* **2005**, *44*, 5284. (c) Corberan, R.; Ramirez, J.; Poyatos, M.; Peris, E.; Fernandez, E. *Tetrahedron: Asymmetry* **2006**, *17*, 1759. (d) Bonati, F.; Burini, A.; Pietroni, B. R.; Bovio, B. *J. Organomet. Chem.* **1991**, *408*, 271. (e) Bohler, C.; Stein, D.; Donati, N.; Grutzmacher, H. *New J. Chem.* **2002**, *26*, 1291. (f) Marion, N.; Diez-Gonzalez, S.; de Fremont, P.; Noble, A. R.; Nolan, S. P. *Angew. Chem., Int. Ed.* **2006**, *45*, 3647. (g) Akana, J. A.; Bhattacharyya, K. X.; Muller, P.; Sadighi, J. P. *J. Am. Chem. Soc.* **2007**, *129*, 7736. (h) Catalano, V. J.; Malwitz, M. A.; Etogo, A. O. *Inorg. Chem.* **2004**, *43*, 5714.

(10) Lin, I. J. B.; Vasam, C. S. *Can. J. Chem.—Rev. Can. Chim.* **2005**, *83*, 812.



Very recently, Bertrand et al. reported a series of remarkably robust cationic gold complexes (**II**, Scheme 1) with cyclic (alkyl)(amino)carbene (CAAC) ligands. These complexes exhibit unique catalytic activities in reactions such as cross-coupling for allene synthesis¹¹ and hydroaminations using ammonia.¹²

Carbodiphosphoranes (**III**, Scheme 1) formally display a central carbon atom with two negative charges.¹³ The potential abilities of these compounds to behave as ligands have been extensively reported,¹⁴ including examples of Cu(I)¹⁵ and Au(I)^{16,17} complexes. We recently described the preparation and coordinating abilities of cyclic carbodiphosphoranes (PHCPs, **IV**) with very bulky substituents and showed that their electron-donating character is superior to that of NHCs.¹⁸ In addition, with the two bulky amino groups attached to each phosphorus atom oriented in a quasi-perpendicular disposition to the heterocyclic ring, PHCPs offer a clear increase of the steric hindrance compared to classical NHCs. Despite the obvious attractive features of PHCPs, their use in catalysis has not been reported yet.

As a way of extending the use of PHCPs to other potential catalytically active metal fragments, we now describe the coordination of our previously reported carbodiphosphorane **2**¹⁸ (Scheme 2) to Cu(I) and Au(I) and the catalytic activity of the resulting complexes toward the NH and OH additions to electron-deficient olefins.

(11) Lavallo, V.; Frey, G. D.; Kousar, S.; Donnadiu, B.; Bertrand, G. *Proc. Natl. Acad. Sci. U.S.A.* **2007**, *104*, 13569.

(12) Lavallo, V.; Frey, G. D.; Donnadiu, B.; Soleilhavoup, M.; Bertrand, G. *Angew. Chem., Int. Ed.* **2008**, *47*, 5224.

(13) (a) Kolodiazny, O. I. *Phosphorous Ylides: Chemistry and Application in Organic Synthesis*; Wiley-VCH: New York, 1999. (b) Kolodiazny, O. I. *Tetrahedron* **1996**, *52*, 1855.

(14) (a) Tonner, R.; Oexler, F.; Neumuller, B.; Petz, W.; Frenking, G. *Angew. Chem., Int. Ed.* **2006**, *45*, 8038. (b) Petz, W.; Kutschera, C.; Neumuller, B. *Organometallics* **2005**, *24*, 5038. (c) Petz, W.; Kutschera, C.; Heitbaum, M.; Frenking, G.; Tonner, R.; Neumuller, B. *Inorg. Chem.* **2005**, *44*, 1263. (d) Petz, W.; Weller, F.; Uddin, J.; Frenking, G. *Organometallics* **1999**, *18*, 619. (e) Sundermeyer, J.; Weber, K.; Peters, K.; Vonschering, H. G. *Organometallics* **1994**, *13*, 2560. (f) Bruce, A. E.; Gamble, A. S.; Tonker, T. L.; Templeton, J. L. *Organometallics* **1987**, *6*, 1350. (g) Baldwin, J. C.; Kaska, W. C. *Inorg. Chem.* **1979**, *18*, 686. (h) Bestmann, H. J. *Angew. Chem., Int. Ed. Engl.* **1977**, *16*, 349. (i) Kubo, K.; Jones, N. D.; Ferguson, M. J.; McDonald, R.; Cavell, R. G. *J. Am. Chem. Soc.* **2005**, *127*, 5314.

(15) Zybilla, C.; Muller, G. *Organometallics* **1987**, *6*, 2489.

(16) Vicente, J.; Singhal, A. R.; Jones, P. G. *Organometallics* **2002**, *21*, 5887.

(17) Schmidbauer, H.; Zybilla, C. E.; Muller, G.; Kruger, C. *Angew. Chem., Int. Ed. Engl.* **1983**, *22*, 729.

(18) Marrot, S.; Kato, T.; Gornitzka, H.; Bacciredo, A. *Angew. Chem., Int. Ed.* **2006**, *45*, 2598.

Results and Discussion

The deprotonation of the salt **1** with *t*BuOK at -78 °C cleanly leads to the carbodiphosphorane **2**. Addition of CuCl or AuCl(Me₂S) yields the corresponding (PHCP)M(OR) (M = Cu, **3**; M = Au, **4**) complexes in moderate yields.

The corresponding (PHCP)CuCl complex **5** can be obtained in high yield by the addition of CH₂Cl₂ or CHCl₃ (Scheme 3) to the alkoxide complex **3**.

The Cu(I) complex, **3**, is an air- and moisture-sensitive species, while the Au(I) compound, **4**, is stable in the solid state in the presence of air for several days. Both compounds were characterized by means of ordinary spectroscopic techniques and X-ray diffraction, although they proved too unstable to obtain satisfactory elemental analysis. The more relevant features of the NMR spectra are the two doublets due to the phosphorus atoms in the ³¹P NMR (δ 69.8 and 62.8 ppm, **3**; δ 64.1 and 60.4 ppm, **4**) and the signal due to the metalated carbon in the ¹³C NMR spectra (δ 7.3 ppm, **3**; δ 3.5 ppm, **4**). Compound **5** shows similar ³¹P NMR resonances at 70.6 and 63.2 ppm (J_{PP} = 186 Hz), although we were unable to observe the signal due to the metalated carbene carbon by ¹³C NMR spectroscopy. The molecular structure of **5** was unambiguously determined by means of X-ray diffraction.

Figures 1 and 2 show the molecular structures of **3** and **4**, respectively. Both molecules show a linear disposition of the ligands about the metal, with C–Cu–O and C–Au–O angles of 175.8° and 175.9°, respectively. The Cu–C (1.892 Å) and Au–C (2.039 Å) distances lie in the expected range for

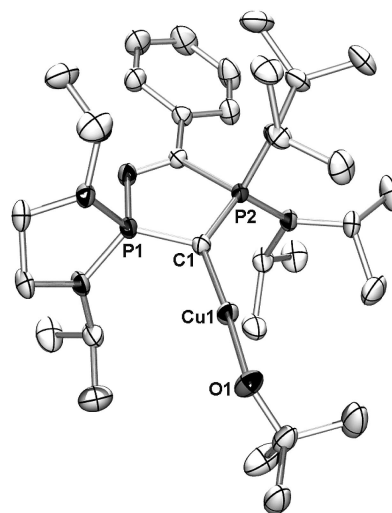


Figure 1. Molecular diagram of compound **3**. Selected bond distances (Å) and angles (deg): P(1)–C(1) 1.6887(15), P(2)–C(1) 1.6763(15), Cu(1)–C(1) 1.8923(15), Cu(1)–O(1) 1.8431(11), O(1)–Cu(1)–C(1) 175.81(6), P(1)–C(1)–P(2) 106.90(8). Ellipsoids are at 50% probability. *tert*-Butanol and toluene molecules are omitted for reasons of clarity.

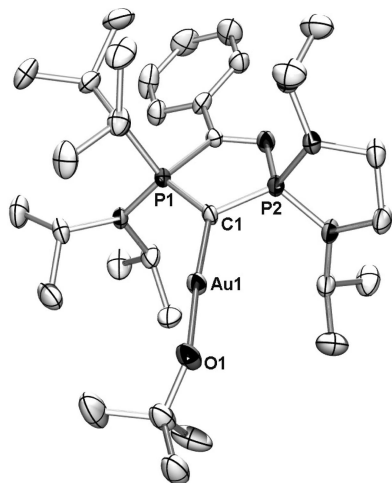


Figure 2. Molecular diagram of compound **4**. Selected bond distances (Å) and angles (deg): P(1)–C(1) 1.687(7), P(2)–C(1) 1.674(7), Au(1)–C(1) 2.018(6), Au(1)–O(1) 2.039(5), O(1)–Au(1)–C(1) 175.9(2), P(1)–C(1)–P(2) 108.5(4). Ellipsoids are at 50% probability. *tert*-Butanol and toluene molecules are omitted for reasons of clarity.

C_{sp^2} –Cu^{19,20} and –Au.^{10,21} The Cu–C distance is very similar to that reported for a previous Cu-hexaphenylcarbodiphosphorane complex.¹⁷ The Cu–O bond (1.843 Å) is slightly longer than that of reported copper alkoxide complexes with NHC ligands (1.79–1.81 Å),²⁰ which might indicate the increased polarization of the Cu–O bond due to the second lone pair on the carbon atom of the carbodiphosphorane. It is interesting to point out that the *i*Pr groups of the amino substituents are oriented toward the metal, thus providing an effective steric hindrance around the Cu–C axis. All other distances and angles are unexceptional.

Figure 3 shows the molecular diagram of complex **5**. It is essentially similar to **3**, with the only difference that the *tert*-butoxide ligand has been replaced by a Cl ligand. This replacement has little influence on the Cu–C bond distance (1.891 Å), which is virtually identical to that shown in **3**.

The catalytic properties of compounds **3** and **4** were tested in the anti-Markovnikov hydroamination and hydroalkoxylation of acrylonitrile, a reaction for which Cu(I) and Au(I) catalysts have been used,²² including two recent examples with Cu–NHC complexes.¹⁰ The results are shown in Table 1.

Both catalysts were active in the addition of amines and alcohols to acrylonitrile and were selective toward the formation of the anti-Markovnikov products. As a general trend, the Cu(I) complex **3** provided higher conversions than its Au(I) analogue **4**. To evaluate the stability of complex **3**, we performed the catalytic addition of aniline to acrylonitrile under argon, nitrogen, or air. The conversion was higher when the reaction was carried out under argon (entry 1), but, remarkably, the catalyst remained active under nitrogen (entry 2) or air (entry 3).

Hydroalkoxylation was slower than hydroamination. When phenol was used as substrate, we achieved a conversion of 72%

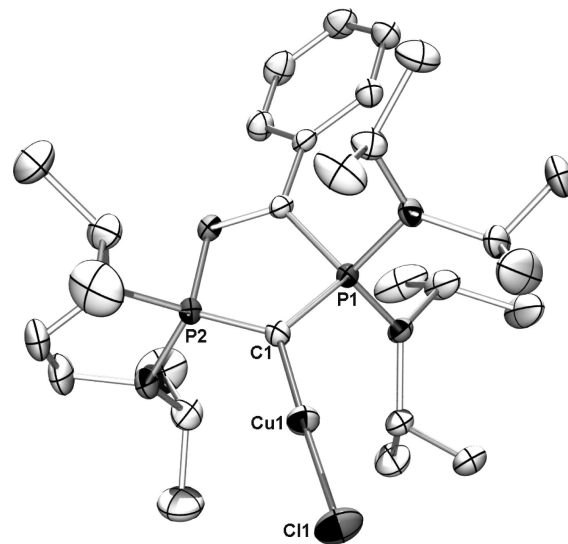


Figure 3. Molecular diagram of compound **5**. Selected bond distances (Å) and angles (deg): P(1)–C(1) 1.6869(19), P(2)–C(1) 1.6700(19), Cu(1)–C(1) 1.8914(19), Cu(1)–Cl(1) 2.1174(6), C(1)–Cu(1)–Cl(1) 177.96(6), P(1)–C(1)–P(2) 107.20(11). Ellipsoids are at 50% probability. Dichloromethane molecule is omitted for reasons of clarity.

Table 1. Anti-Markovnikov Hydroamination and Hydroalkoxylation of Acrylonitrile^a

$R'X-H + NC-CH=CH_2 \xrightarrow[C_6D_6, R.T.]{cat. (5.5 mol\%)} NC-CH_2-CH_2-XR'$				
X = NH, O				
entry	R'X-H	cat.	time (h)	conv (%)
1	PhNH ₂	3	1.5	83
2 ^b		3	2	70
3 ^c		3	2	52
4		4	1	10
5	PhOH	3	40	72
6 ^d		3	12	48
7		4	40	60
8 ^d		4	12	32
9	MeOH	4	23	10
10 ^d		4	12	76

^a Reaction conditions: 0.366 mmol of R'X-H, 0.367 mmol of acrylonitrile, 0.0202 mmol of catalyst, 0.5 mL of C₆D₆, RT. Conversions determined by ¹H NMR spectroscopy using 1,3,5-trimethoxybenzene (0.03 mmol) as internal standard. ^b Under nitrogen. ^c Under air. ^d T: 80 °C.

after 40 h (entry 5). This result clearly improves the catalytic performance shown by previously reported Cu^I-NHC complexes in the same catalytic reaction, in which a maximum conversion of 64% was reached after 40 h at 80 °C.⁸ Under the same reaction conditions, catalyst **4** provided a lower conversion (60%, entry 7).

When hydroalkoxylation was carried out at 80 °C (entries 6, 8, and 10), conversions did not increase beyond 12 h, probably due to catalyst decomposition.

In general, catalysts **3** and **4** showed higher reaction rates than previously reported Cu(I) and Au(I) catalysts. However, we believe that their lower stability is responsible for the lower conversions achieved since, apparently, catalyst decomposition occurs after a few hours. Efforts to improve catalyst stability are currently underway.

Conclusions

We have described the synthesis and full characterization of new Cu(I) and Au(I) complexes with a bulky cyclic carbo-

(19) (a) Goj, L. A.; Blue, E. D.; Munro-Leighton, C.; Gunnoe, T. B.; Petersen, J. L. *Inorg. Chem.* **2005**, *44*, 8647. (b) Goj, L. A.; Blue, E. D.; Delp, S. A.; Gunnoe, T. B.; Cundari, T. R.; Pierpont, A. W.; Petersen, J. L.; Boyle, P. D. *Inorg. Chem.* **2006**, *45*, 9032.

(20) Mankad, N. P.; Laitar, D. S.; Sadighi, J. P. *Organometallics* **2004**, *23*, 3369.

(21) (a) de Fremont, P.; Scott, N. M.; Stevens, E. D.; Nolan, S. P. *Organometallics* **2005**, *24*, 2411. (b) Laitar, D. S.; Muller, P.; Gray, T. G.; Sadighi, J. P. *Organometallics* **2005**, *24*, 4503.

(22) (a) Yang, C. G.; He, C. *J. Am. Chem. Soc.* **2005**, *127*, 6966. (b) Zhang, J. L.; Yang, C. G.; He, C. *J. Am. Chem. Soc.* **2006**, *128*, 1798.

Table 2. Crystallographic Data

	3	4	5
empirical formula	C ₄₃ H ₇₈ CuN ₅ O ₂ P ₂	C ₄₃ H ₇₈ AuN ₅ O ₂ P ₂	C ₂₉ H ₅₃ Cl ₃ CuN ₅ P ₂
mol wt	822.58	956.01	703.59
T (K)	173	173	173
radiation	Mo K α (monochr): 0.71073 λ (Å)		
cryst syst	monoclinic	monoclinic	monoclinic
space group	P2(1)/c	P2(1)/c	P2(1)/n
a (Å)	10.28410(10)	10.28720(10)	9.7630(3)
b (Å)	24.0545(3)	24.1891(3)	20.1285(7)
c (Å)	19.4759(3)	19.4552(2)	18.3889(6)
α (deg)	90	90	90
β (deg)	103.4260(10)	104.1410(10)	95.413(2)
γ (deg)	90	90	90
V (Å ³)	4686.25(10)	4694.49(9)	3597.6(2)
Z	4	4	4
D _{calcd} (Mg/m ³)	1.166	1.353	1.299
μ (Mo K α) (mm ⁻¹)	0.572	3.240	0.945
total, unique no. of reflns	68 080, 11 113	49 244, 7915	65 965, 8869
R _{int}	0.0507	0.0355	0.0581
no. of params, restrictions	498, 0	495, 0	373, 0
R, R _w [$I > 2\sigma(I)$]	0.0354, 0.0837	0.0580, 0.1409	0.0388, 0.0931
GOF	1.021	1.026	1.026
min., max. resid dens (e Å ⁻³)	-0.255, 0.380	-1.094, 9.929	-0.470, 0.609

diphosphorane ligand. The new compounds have been tested in the catalytic hydroamination and hydroalkoxylation of acrylonitrile. Despite the moderate conversions achieved, the reaction rate was clearly accelerated compared with that using NHC-copper catalysts, and we believe that these preliminary results are encouraging. To our knowledge, this is the first catalytic application involving carbodiphosphorane ligands. Due to their strong electron-donor character, the use of this type of ligands in homogeneous catalysis may lead to a new generation of catalysts with improved performances, especially when catalytic reactions require electron-rich metallic centers. A typical process where electron-rich metallic centers are needed is the activation of CO₂, a process for which (NHC)-Cu complexes have already shown good efficiency.⁷ In an extension of the application of our complexes, we are currently exploring their activity in reactions implying the reduction of CO₂.

Experimental Section

General Procedures. All manipulations were performed under an inert atmosphere of argon by using standard Schlenk techniques. Dry, oxygen-free solvents were employed. ¹H, ¹³C, and ³¹P NMR spectra were recorded on Bruker Avance 300 spectrometers. ¹H NMR and ¹³C NMR chemical shifts are reported in ppm relative to Me₄Si as external standard. ³¹P NMR downfield chemical are expressed in ppm relative to 85% H₃PO₄. Compound **1** was prepared according to the previously reported method.^{2,3}

Synthesis of 3. THF (5 mL) was added to a mixture of *t*BuOK (369 mg, 3.28 mmol), CuCl (108 mg, 1.10 mmol), and **1** (736 mg, 1.10 mmol) at -78 °C. The cold bath was removed, and the mixture was stirred at room temperature for 30 min. The formation of compound **3** was verified by ³¹P NMR. The solvent was evaporated and the crude solid was extracted with a mixture of toluene/pentane (80:20, 10 mL). After keeping the solution in the freezer overnight, the pure compound **3** was obtained as deep red crystals. Yield: 380 mg (52%). ³¹P{¹H} NMR (C₆D₆, 25 °C, 121 MHz): δ 69.8, 62.8 ppm (²J_{PP} = 195 Hz). ¹H NMR (C₆D₆, 25 °C, 300 MHz): δ 0.86 (d, ³J_{HH} = 6.9 Hz, 6H, CH₃), 1.12 (d, ³J_{HH} = 6.9 Hz, 12H, CH₃), 1.15 (d, ³J_{HH} = 7.2 Hz, 12H, CH₃), 1.21 (d, ³J_{HH} = 6.6 Hz, 6H, CH₃), 1.77 (br s, 9H, OC(CH₃)₃), 2.83 (d, ³J_{HH} = 8.7 Hz, 4H, CH₂), 3.5 (m, 2H, NCH), 4.11 (m, 4H, NCH), 6.93 (m, 3H, CH_{arom}),

8.28 (d, ³J_{HH} = 9.0 Hz, 2H, CH_{arom}). ¹³C{¹H} NMR (C₆D₆, 25 °C, 75 MHz): δ 7.3 (t, ¹J_{CP} = 84 Hz, PCP), 21.1 (d, ³J_{CP} = 4.8 Hz, CH₃), 21.4 (d, ³J_{CP} = 2.5 Hz, CH₃), 24.0 (d, ³J_{CP} = 5.5 Hz, CH₃), 26.0 (d, ³J_{CP} = 2.0 Hz, CH₃), 37.4 (d, ²J_{CP} = 8.7 Hz, CH₂), 37.8 (s, OC(CH₃)₃), 42.9 (d, ²J_{CP} = 8.0 Hz, NCH), 48.2 (d, ²J_{CP} = 5.5 Hz, NCH), 70.7 (s, OC(CH₃)₃), 128.2 (s, CH_{arom}), 129.1 (s, CH_{arom}), 131.8 (s, CH_{arom}), 137.1 (dd, J = 26.2 and 32.2 Hz, C_{arom} ipso), 184.3 (dd, ²J_{CP} = 6.75 Hz and ¹J_{CP} = 52.5 Hz, C=N). The compound proved too unstable to obtain satisfactory elemental analysis.

Synthesis of 4. THF (10 mL) was added to a mixture of *t*BuOK (501 mg, 4.47 mmol), [AuCl(SMe₂)] (440 mg, 1.49 mmol), and **1** (1.0 g, 1.10 mmol) at -78 °C. The cold bath was removed, and the mixture was stirred at room temperature for 30 min. The formation of compound **4** was verified by ³¹P NMR. The solvent was evaporated and the crude solid was extracted with a mixture of toluene/pentane (80:20, 10 mL). After keeping the solution in the freezer overnight, the pure compound **4** was obtained as reddish-purple crystals. Yield: 427 mg (34%). ³¹P{¹H} NMR (C₆D₆, 25 °C, 121 MHz): δ 64.1, 60.4 ppm (²J_{PP} = 225 Hz). ¹H NMR (C₆D₆, 25 °C, 300 MHz): δ 0.93 (d, ³J_{HH} = 6.9 Hz, 6H, CH₃), 1.21 (d, ³J_{HH} = 6.9 Hz, 12H, CH₃), 1.26 (d, ³J_{HH} = 6.6 Hz, 12H, CH₃), 1.32 (d, ³J_{HH} = 6.9 Hz, 6H, CH₃), 1.87 (s, 9H, CH₃ *t*BuO), 2.87 (m, 4H, CH₂), 3.52 (m, 2H, NCH), 4.23 (m, 4H, NCH), 7.02 (m, 3H, CH_{arom}), 8.26 (d, ³J_{HH} = 6.6 Hz, 2H, CH_{arom}). ¹³C{¹H} NMR (C₆D₆, 25 °C, 75 MHz): δ 3.5 (dd, ¹J_{CP} = 112.0 Hz and ¹J_{CP} = 111.96 Hz, PCP), 21.0 (d, ³J_{CP} = 4.2 Hz, CH₃), 21.5 (d, ³J_{CP} = 2.6 Hz, CH₃), 23.1 (d, ³J_{CP} = 5.4 Hz, CH₃), 26.0 (d, ³J_{CP} = 2.0 Hz, CH₃), 36.5 (s, OC(CH₃)₃), 37.5 (dd, ²J_{CP} = 9.0 Hz and ⁴J_{CP} = 2.1 Hz, CH₂), 42.9 (d, ²J_{CP} = 7.5 Hz, NCH), 48.3 (d, ²J_{CP} = 5.4 Hz, NCH), 71.0 (s, OC(CH₃)₃), 128.4 (s, CH_{arom}), 129.1 (s, CH_{arom}), 132.1 (s, CH_{arom}), 137.2 (dd, J = 25.6 and 30.2 Hz, C_{arom} ipso), 184.8 (dd, ²J_{CP} = 8.0 Hz and ¹J_{CP} = 56.7 Hz, C=N). The compound proved too unstable to obtain satisfactory elemental analysis.

Synthesis of 5. CDCl₃ (0.5 mL) was added to **3** (300 mg, 0.36 mmol) at room temperature. The conversion was monitored by ³¹P NMR. After 1 h, all the volatiles were eliminated under vacuum. The pure product was obtained by crystallization in CH₂Cl₂/pentane at -25 °C. Yield: 131 mg (59%). ³¹P{¹H} NMR (CDCl₃, 25 °C, 121 MHz): δ 63.2, 70.6 ppm (²J_{PP} = 186 Hz). ¹H NMR (CDCl₃, 25 °C, 300 MHz): δ 0.98 ppm (d, ³J_{HH} = 6.7 Hz, 6H, CH₃), 1.17 (d, ³J_{HH} = 6.7 Hz, 6H, CH₃), 1.21 (d, ³J_{HH} = 6.9 Hz, 12H, CH₃), 1.35 (d, ³J_{HH} = 7.0 Hz, 12H, CH₃), 3.25 (d, ³J_{HP} = 8.9 Hz, 4H, CH₂), 3.34 (sept-d, ³J_{HH} = 6.7 Hz and ²J_{HP} = 9.9 Hz, 2H, NCH), 4.10 (sept-d, ³J_{HH} = 7.0 Hz and ²J_{HP} = 11.3 Hz, 4H, NCH), 7.36 (t, ³J_{HH} = 7.5 Hz, 2H, CH_{arom}), 7.45 (m, 1H, CH_{arom}), 8.14 (d, ³J_{HH}

(23) Kato, T.; Gornitzka, H.; Baccaredo, A.; Schoeller, W. W.; Bertrand, G. *J. Am. Chem. Soc.* **2002**, *124*, 2506.

= 7.2 Hz, 2H, CH_{arom}). ¹³C{¹H} NMR (CDCl₃, 25 °C, 75 MHz): δ 21.1 ppm (d, ³J_{CP} = 4.9 Hz, CH₃), 21.5 (d, ³J_{CP} = 2.6 Hz, CH₃), 24.0 (d, ³J_{CP} = 5.7 Hz, CH₃), 26.0 (d, ³J_{CP} = 2.2 Hz, CH₃), 37.4 (dd, ²J_{CP} = 9.2 Hz and ⁴J_{CP} = 1.4 Hz, CH₂), 42.9 (d, ²J_{CP} = 7.8 Hz, NCH), 48.2 (d, ²J_{CP} = 5.6 Hz, NCH), 128.4 (s, CH_{arom}), 128.9 (s, CH_{arom}), 132.1 (s, CH_{arom}), 136.4 (dd, *J* = 26.1 and 31.9 Hz, C_{ipso}), 184.0 (dd, ²J_{CP} = 6.1 Hz and ¹J_{CP} = 53.9 Hz, CN). The compound proved too unstable to obtain satisfactory elemental analysis.

X-ray Diffraction Studies. Single crystals of **3**, **4**, and **5** were mounted on a glass fiber in a random orientation. Data collection was performed at low temperature using an oil-coated shock-cooled crystal on a Bruker AXS APEX II diffractometer, with Mo K α radiation (λ = 0.71073 Å) and a nominal crystal to detector distance of 4.9 cm. Space group assignment was based on systematic absences, E statistics, and successful refinement of the structures. All the structures were solved by direct methods using SHELXS-97 and were refined by full-matrix least-squares procedures on *F*² using SHELXL-97.²⁴ All non-hydrogen atoms were refined anisotropically. Hydrogen atoms were assigned to ideal positions and refined using a riding model. Details of the data collection, cell dimensions, and structure refinement are given in Table 2. The diffraction frames were integrated using the SAINT package.²⁵

(24) Sheldrick, G. M. *Acta Crystallogr., Sect. A* **2008**, *64*, 112.

For compound **4**, we observed an important residual density located around the Au atom due, probably, to the quality of the crystal.

Catalytic Hydroamination and Hydroalkoxylation of Acrylonitrile. Acrylonitrile (0.367 mmol), amine or alcohol (0.366 mmol), catalyst (0.0202 mmol), and 0.5 mL of C₆D₆ were introduced in a J. Young-style NMR tube under argon. The resulting mixture was stirred at room temperature. Conversions were determined by ¹H NMR spectroscopy using 1,3,5-trimethoxybenzene as internal standard (0.03 mmol).

Acknowledgment. We gratefully acknowledge financial support from the Ministerio de Ciencia e Innovación of Spain (CTQ2005-05187 and CTQ2007-31175-E/BQU) and from the CNRS (ERA-Chemistry program). We would also like to thank the Spanish MEC for a fellowship (R.C.).

Supporting Information Available: CIF providing crystallographic data for **3–5**. This material is available free of charge via the Internet at <http://pubs.acs.org>.

OM8008958

(25) SAINT, Bruker Analytical X-ray System, version 5.0. ed.; Bruker: Madison, WI, 1998.

Dehydrofluorination of Hydrofluorocarbons by Titanium Alkylidyne via Sequential C–H/C–F Bond Activation Reactions. A Synthetic, Structural, and Mechanistic Study of 1,2-CH Bond Addition and β -Fluoride Elimination

Alison R. Fout, Jennifer Scott, Deanna L. Miller, Brad C. Bailey,[†] Maren Pink, and Daniel J. Mindiola*

Department of Chemistry and the Molecular Structure Center, Indiana University, Bloomington, Indiana 47405

Received September 18, 2008

The neopentylidene-neopentyl complex (PNP)Ti=CH^tBu(CH₂^tBu) (**1**; (PNP[−] = N[2-P(CHMe₂)₂-4-methylphenyl]₂) extrudes neopentane in neat fluorobenzene under mild conditions (25 °C) to generate the transient titanium alkylidyne (PNP)Ti≡C^tBu (**A**), which subsequently undergoes regioselective 1,2-CH bond addition of a fluorobenzene across the Ti≡C linkage to generate (PNP)Ti=CH^tBu(*o*-FC₆H₄) (**2**). Kinetic and mechanistic studies suggest that the C–H activation process is pseudo-first-order in titanium, with the α -hydrogen abstraction being the rate-determining step and the post-rate-determining step being the C–H bond activation of fluorobenzene. At 100 °C complex **2** does not equilibrate back to **A** and the preference for C–H activation in benzene versus fluorobenzene is 2:3, respectively. Compound **1** also reacts readily, and in most cases cleanly, with a series of hydrofluoroarenes (HAr_F), to form a family of alkylidene-arylfuoride derivatives of the type (PNP)Ti=CH^tBu(Ar_F). Thermolysis of the latter compounds generates the titanium alkylidene-fluoride (PNP)Ti=CH^tBu(F) (**14**) by a β -fluoride elimination, concurrent with formation of *o*-benzynes. β -Fluoride elimination to yield **14** occurs from **2** under elevated temperatures with $k_{\text{average}} = 4.96(16) \times 10^{-5} \text{ s}^{-1}$ and with activation parameters $\Delta H^\ddagger = 29(1) \text{ kcal/mol}$ and $\Delta S^\ddagger = -3(4) \text{ cal/mol} \cdot \text{K}$. It was found that β -fluoride elimination is accelerated when electron-rich groups are adjacent to the fluoride group, thus implying that a positive charge buildup at the arylfluoride ring occurs in the activated complex of **2**. The alkylidene derivative (PNP)Ti=CHSiMe₃(CH₂SiMe₃) (**15**) also undergoes α -hydrogen abstraction to form the putative (PNP)Ti≡CSiMe₃ (**B**) at higher temperatures (>70 °C) and dehydrofluorinates the same series of HAr_F when the reaction mixture is thermolyzed at >100 °C over 72 h to produce *o*-benzynes and the fluoride analogue (PNP)Ti=CHSiMe₃(F) (**26**). Only in the case of the substrate 1,2-F₂C₆H₄ can the kinetic C–H activation product (PNP)Ti=CHSiMe₃(*o,m*-F₂C₆H₃) be isolated and crystallographically characterized. 1-Fluorohexane and fluorocyclohexane can also be dehydrofluorinated by intermediates **A** and **B**. No intermediates are observed, but in the case of 1-fluorohexane, the terminal olefin is spectroscopically identified. The dehydrofluorination of HAr_F and hydrofluoroalkanes (HAl_F) can be made cyclic via the quantitative conversion of the alkylidene-fluorides to **1** and **15**, by means of transmetalation with LiCH₂XMe₃ (X = C and Si), and the reactivity of **1** with halobenzenes is also presented and discussed.

1. Introduction

Activation of the carbon–fluoride σ bond found in hydrofluorocarbons (HFCs) represents a major challenge for organometallic chemists due to its resistance to oxidative degradation and overall chemical inertness of the C–F bond.¹ Consequently, once released into the environment, these intrinsic features increase the atmospheric lifetimes of such potentially potent greenhouse gases (300–2000 years).² As a result, the removal

of these fluoride-containing moieties from our environment and their conversion into more useful commodity byproducts remains an essential topic among chemists. Fluoride removal can be achieved by defluorination, dehydrofluorination, or hydrodefluorination reactions that often rely on the use of reactive transition-metal complexes.³ Indeed, catalytic C–F bond activation has been reported in a number of cases; however, only a few of these involve the use of homogeneous systems.⁴ Of paramount importance in this research is therefore an in-depth understanding of the possible mechanisms involved in the cleavage of C–F bonds as well as the isolation of intermediates along the dehydrofluorination pathway. This is especially true if such a process can be achieved under mild conditions.

Although the C–F aryl σ bond is one of the strongest bonds, the binding affinities of hydrofluoroarenes (HAr_F) toward

* Corresponding author. E-mail: mindiola@indiana.edu.

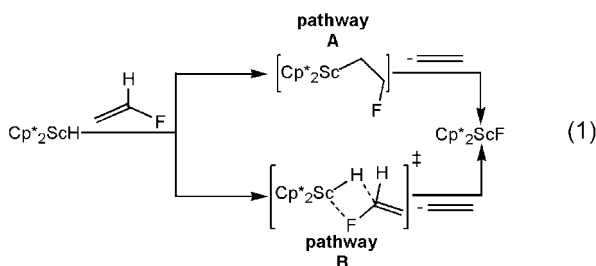
[†] Present address: Department of Chemistry, Massachusetts Institute of Technology, Cambridge, MA 02139.

(1) Smart, B. E. In *The Chemistry of Functional Groups, Supplement D*; Patai S., Rappoport, Z., Eds.; John Wiley & Sons: New York, 1983; Chapter 14.

(2) (a) Kiplinger, J. L.; Richmond, T. G.; Osterberg, C. E. *Chem. Rev.* **1994**, *94*, 373. (b) Burdeniuc, J.; Crabtree, R. H. *Chem. Ber./Recl.* **1997**, *130*, 145. (c) Jones, W. D. *Dalton Trans.* **2003**, 3991. (d) Richmond, T. G. In *Topics in Organometallic Chemistry*; Murai, S., Ed.; Springer: New York, 1999; Vol. 3, p 243.

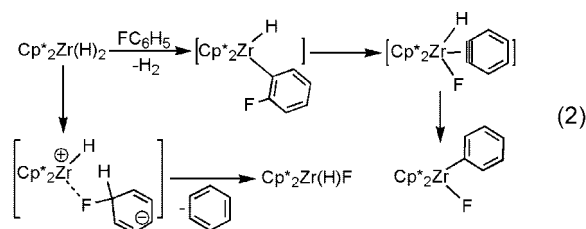
(3) (a) Aizenberg, M.; Milstein, D. *Science* **1994**, 265–359. (b) Aizenberg, M.; Milstein, D. *J. Am. Chem. Soc.* **1995**, *117*, 8674.

organometallic reagents are such that the arene itself becomes more susceptible to nucleophilic attack, rendering the fluoride a better leaving group than one would expect.¹ As such, C–F bond activation has been shown to occur using a number of electron-deficient metal complexes,² as well as in an unsaturated Ti(III) center.⁵ Although a well-defined mechanism for how these transformations take place is currently uncertain, a variety of mechanisms have been postulated, including electron transfer, homolytic cleavage, oxidative addition, β -fluoride elimination, and nucleophilic, electrophilic, or radical pathways.^{1,5,6} Unfortunately, given the drastic conditions required to achieve C–F activation, intermediates leading to the breaking of this tough bond have been for the most part only proposed, but not isolated. Indeed, the lack of kinetically stable intermediates in the C–F bond cleavage of vinyl fluoride by Cp^*_2ScH to form Cp^*_2ScF has led to the proposal of two separate pathways (eq 1).⁷ These pathways could proceed via migratory insertion followed by β -fluoride elimination (pathway A) or by a concerted nucleophilic attack of a hydride on the substrate by means of a σ -bond metathesis (pathway B).⁷



Also of notable mention, the C–F activation of hydrofluoroalkanes (HAl_F), which are more harmful to the environment, versus HAr_F are usually proposed to involve different mechanisms. For example, Jones et al. have suggested a free radical chain mechanism for the C–F bond rupture of HAl_F using $\text{Cp}^*_2\text{Zr}(\text{H})_2$, resulting in the formation of $\text{Cp}^*_2\text{Zr}(\text{H})\text{F}$ and the corresponding alkane (eq 2).⁸ Complex $\text{Cp}^*_2\text{Zr}(\text{H})_2$ is also capable of defluorinating fluorobenzene, but this process appears to proceed via two different but competitive pathways. The first entails direct nucleophilic attack of the hydride on the fluorobenzene ring to make a zwitterion and subsequent fluoride abstraction by zirconium to generate the hydrogenated arene. The second pathway involves *ortho* C–H activation of the fluorobenzene followed by β -fluoride elimination, and finally insertion of the benzyne into the metal hydride to form

$\text{Cp}^*_2\text{Zr}(\text{C}_6\text{H}_5)\text{F}$ (eq 2).⁸ Andersen and co-workers reported hydrogen for fluoride exchange for a series of HAr_F and HAl_F reactions using $\text{Cp}'_2\text{CeH}$ ($\text{Cp}' = 1,2,4\text{-}(\text{Me}_3\text{C})_3\text{C}_3\text{H}_2$) or its corresponding metallacycle.⁹ In some instances the kinetic product resulting from C–H activation could be isolated.^{9a,9c} Despite the variety of proposed mechanisms for defluorination of HFCs, a well-defined early transition metal system that can activate both saturated and unsaturated HFCs, by virtue of a similar dehydrofluorination pathway, to our knowledge has not been discovered.



We recently reported that the transient titanium alkylidyne $(\text{PNP})\text{Ti}\equiv\text{C}^i\text{Bu}$ ($\text{PNP}^- = \text{N}[2\text{-P}(\text{CHMe}_2)_2\text{-4-methylphenyl}]_2$) activated strong C–F bonds of HAr_F under mild conditions, presumably by means of 1,2-CF bond addition across the $\text{Ti}\equiv\text{C}$ multiple bond.^{10,11} Hence, the reaction of C_6F_6 with the alkylidyne synthon $(\text{PNP})\text{Ti}\equiv\text{CH}^i\text{Bu}(\text{CH}_2^i\text{Bu})$ (**1**) ($\text{PNP}^- = \text{N}[2\text{-P}(\text{CHMe}_2)_2\text{-4-methylphenyl}]_2$) represented the first example of intermolecular aryl C–F bond activation promoted by a metal carbon multiple bond.¹² Parallel to this result, we have also shown that the transient titanium alkylidyne can readily activate C–H bonds of HAr_F ¹³ to afford C–H bond activation products with the fluoride group being *ortho* with respect to the Ti–C bond.¹³ Herein, we report that the transient titanium alkylidynes $(\text{PNP})\text{Ti}\equiv\text{CR}$ ($\text{R} = ^i\text{Bu}$, **A**; SiMe_3 , **B**) engage not only in regioselective C–H activation of an extensive list of HAr_F but also in intramolecular C–F activation pathways, ultimately dehydrofluorinating the formal HAr_F concurrent with the discharge of an organic byproduct (*o*-benzyne formation). Aliphatic HFCs can also be dehydrofluorinated under mild conditions, and the nature of the organic product suggests a similar mechanism being operative with respect to HAr_F dehydrofluorination. The type of HAr_F has allowed us to isolate both kinetic and thermodynamic products, as well as investigate the mechanism behind the sequential C–H/C–F bond activations. A mechanistic study surrounding the dehydrofluorination of saturated and unsaturated HFCs will be presented and discussed in this work.

2. Results and Discussion

2a. Intermolecular C–H Activation of HAr_F by a Transient Titanium Neopentylidyne. Previous work in our laboratory had established that complex **1** readily extruded neopentane

(4) For some heterogeneous catalytic C–F activations: (a) Burdeniuc, J.; Crabtree, R. H. *Organometallics* **1998**, *17*, 1582. (b) Stanger, K. J.; Angelici, R. J. *J. Mol. Catal. A: Chem.* **2004**, *207*, 59. (c) Kiplinger, J. L.; Richmond, T. G. *J. Am. Chem. Soc.* **1996**, *118*, 1805. (d) Yang, H.; Gao, H.; Angelici, R. J. *Organometallics* **1999**, *18*, 2285. (e) Young, R. J.; Grushin, V. V. *Organometallics* **1999**, *18*, 284. Silyl cations mediating catalytic C–F activation: (f) Scott, V. J.; Çelenligil-Çetin, R.; Ozerov, O. V. *J. Am. Chem. Soc.* **2005**, *127*, 2852. (g) Widdowson, D. A.; Wilhelm, R. *Chem. Commun.* **1999**, 2211. (h) Bohm, V. P. W.; Gstottmayr, C. W. K.; Weskamp, T.; Herrmann, W. A. *Angew. Chem., Int. Ed.* **2001**, *40*, 3387. Homogeneous catalytic C–F activation: (i) Ishii, Y.; Chatani, N.; Yorimitsu, S.; Murai, S. *Chem. Lett.* **1998**, 157. (k) Braun, T.; Perutz, R. N.; Sladek, M. I. *Chem. Commun.* **2001**, 2254. (l) Kuhl, S.; Schneider, R.; Fort, Y. *Adv. Synth. Catal.* **2003**, *345*, 341. (m) Vela, J.; Smith, J. M.; Yu, Y.; Ketterer, N. A.; Flaschenriem, C. J.; Lachicotte, R. J.; Holland, P. L. *J. Am. Chem. Soc.* **2005**, *127*, 7857. (n) Douvris, C.; Ozerov, O. V. *Science* **2008**, *321*, 1188.

(5) Jones, W. D. *Dalton Trans.* **2003**, 3991.

(6) Burk, M. J.; Staley, D. L.; Tumas, W. *J. Chem. Soc., Chem. Commun.* **1990**, 809.

(7) Burger, B. J. Ph.D. Thesis, California Institute of Technology, 1987.

(8) Kraft, B. M.; Lachicotte, R. J.; Jones, W. D. *J. Am. Chem. Soc.* **2001**, *123*, 10973.

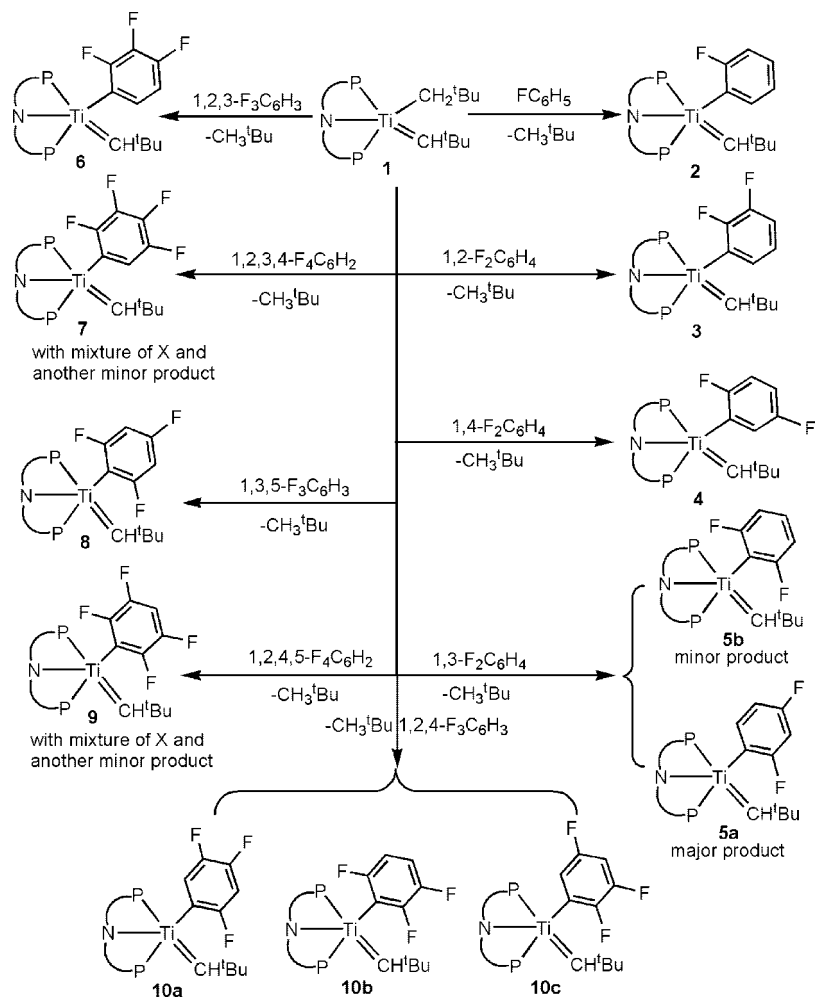
(9) (a) Werkema, E. L.; Andersen, R. A. *J. Am. Chem. Soc.* **2008**, *130*, 7153. (b) Werkema, E. L.; Messines, E.; Perrin, L.; Maron, L.; Eisenstein, O.; Andersen, R. A. *J. Am. Chem. Soc.* **2005**, *127*, 7781. (c) Maron, L.; Werkema, E. L.; Perrin, L.; Eisenstein, O.; Andersen, R. A. *J. Am. Chem. Soc.* **2005**, *127*, 279.

(10) Bailey, B. C.; Fan, H.; Huffman, J. C.; Baik, M.-H.; Mindiola, D. J. *J. Am. Chem. Soc.* **2007**, *129*, 8781.

(11) Bailey, B. C.; Fan, H.; Baum, E. W.; Huffman, J. C.; Baik, M.-H.; Mindiola, D. J. *J. Am. Chem. Soc.* **2005**, *127*, 16016.

(12) The activation of a C–F bond in perfluoropyridine by a transient zirconium imido has been reported: Hoyt, H. M.; Michael, F. E.; Bergman, R. G. *J. Am. Chem. Soc.* **2004**, *126*, 1018.

(13) Bailey, B. C.; Huffman, J. C.; Mindiola, D. J. *J. Am. Chem. Soc.* **2007**, *129*, 5302.

Scheme 1. Intermolecular C–H Activation Reactions from a Series of HAr_F with **1** to Produce Compounds **2**–**10**

to generate a transient titanium neopentylidyne **A**, which then activated the C–H bonds in solvent media to form an alkylidene-alkyl derivative.^{10,11} When the alkylidyne precursor **1** was dissolved in fluorobenzene, C–H activation would take place adjacent to the C–F group.¹³ Regioselective C–H activation of HAr_F has previously been explored. For example, Perutz and co-workers conducted systematic DFT studies on the regioselective C–F over C–H activation of pentafluorobenzene with a Pt(H₂PCH₂CH₂PH₂) complex.¹⁴ Likewise, the regioselective activation of the haloaryl C–H bond has been recently described by the groups of Legzdins and Piers.¹⁵ In our case, it was found that FC₆H₅, 1,2-F₂C₆H₄, and 1,4-F₂C₆H₄ all yielded the alkylidene-fluorophenyl complexes (PNP)Ti=CH^tBu(*o*-FC₆H₄) (**2**), (PNP)Ti=CH^tBu(*o,m*-F₂C₆H₃) (**3**), and (PNP)Ti=CH^tBu(*o,m'*-F₂C₆H₃) (**4**), respectively, when the HAr_F was treated with **1** (Scheme 1).¹³ The connectivity in **2**–**4** was clearly evident from multinuclear NMR spectroscopic data in addition to X-ray structural studies.¹³ Exploration of the asymmetrical HAr_F, 1,3-F₂C₆H₄, suggested that only two C–H activation products were generated when the mixture was assayed by ¹⁹F NMR spectroscopy. These products were the result

of *ortho* C–H activation with respect to the fluoride groups, namely, the compounds (PNP)Ti=CH^tBu(*o,p*-F₂C₆H₃) (**5a**) and (PNP)Ti=CH^tBu(*o,o'*-F₂C₆H₃) (**5b**), shown in Scheme 1. On the basis of multinuclear NMR spectroscopy, isomer **5a** was judged to be the major product. The mixture of **5** could be cocrystallized and exposed C–H activation to be occurring at the least hindered position relative to one of the fluorides, as well as *ortho* to both fluoride groups (Figure 1, *vide infra*). Similarly, Legzdins reported that the reaction of Cp*W(NO)(CH₂CMe₃) with 1,3-F₂C₆H₄ resulted in *ortho* C–H activation and formation of two isomers. The major product, Cp*W(NO)(CH₂CMe₃)(*o,p*-F₂C₆H₃) (84%), was the result of activation of the less hindered site compared to the more sterically hindered minor product, Cp*W(NO)(CH₂CMe₃)(*o,o'*-F₂C₆H₃) (16% yield).^{15a} In our case as well as Legzdins', activation of the C–H group *meta* to F was not observed. For the case of the HAr_F 1,2,3-F₃C₆H₃ and 1,2,3,4-F₄C₆H₂, C–H activation also yielded a product with the fluoride in the *ortho* position to form (PNP)Ti=CH^tBu(*o,m,p*-F₃C₆H₂) (**6**) and (PNP)Ti=CH^tBu(*o,m,m',p*-F₄C₆H) (**7**), respectively (Scheme 1). In the formation of complex **7**, examination of the reaction mixture revealed another product labeled “X” in minor amounts along with traces of an impurity (*vide infra*). Intuitively, C–H activation of 1,3,5-F₃C₆H₃ yielded the product (PNP)Ti=CH^tBu(*o,o',p*-F₃C₆H₂) (**8**) when treated with **1** (Scheme 1). Unfortunately, treatment of **1** with 1,2,4,5-F₄C₆H₂ resulted in the formation of (PNP)Ti=CH^tBu(*o,o',m,m'*-F₄C₆H₂) (**9**) and two minor products, one of which was also “X” (Scheme 2). When

(14) (a) Bosque, R.; Clot, E.; Fantacci, S.; Maseras, F.; Eisenstein, O.; Perutz, R. N.; Renkema, K. B.; Caulton, K. G. *J. Am. Chem. Soc.* **1998**, *120*, 12634. (b) Reinhold, M.; McGrady, J. E.; Perutz, R. N. *J. Am. Chem. Soc.* **2004**, *126*, 5268. (c) Clot, E.; Oelckers, B.; Klahn, A. H.; Eisenstein, O.; Perutz, R. N. *Dalton Trans.* **2003**, 4065.

(15) (a) Tsang, J. Y. K.; Buschhaus, M. S. A.; Legzdins, P.; Patrick, B. O. *Organometallics* **2006**, *25*, 4215. (b) Ma, K.; Piers, W. E.; Parvez, M. J. *Am. Chem. Soc.* **2006**, *128*, 3303.

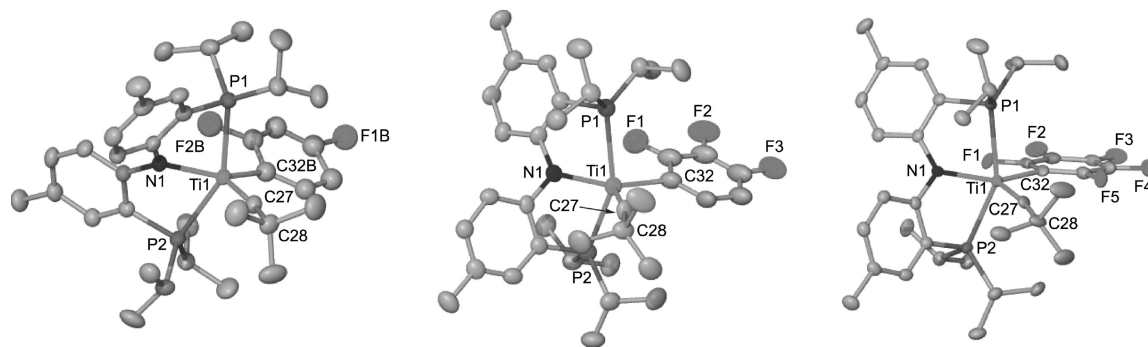
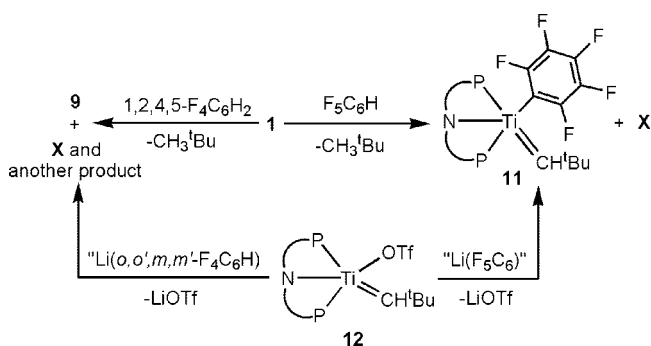


Figure 1. Solid state structures of compounds **5** (only the **5a** isomer is shown, left), **6** (middle), and **11** (right) depicting thermal ellipsoids at the 50% probability level. H atoms and solvent molecules have been omitted for the purpose of clarity. Selected bond lengths (Å) and angles (°deg): For **5**, Ti1–C27 = 1.870(5), Ti1–P1 = 2.5675(14), Ti1–P2 = 2.6200(14), Ti1–N1 = 2.045(4), Ti1–C32B = 2.147(5), Ti1–C27–C28 = 167.4(4), P1–Ti1–P2 = 150.45(5), N1–Ti1–C32 = 138.22(15). For **6**, Ti1–C27 = 1.870(9), Ti1–P1 = 2.635(4), Ti1–P2 = 2.576(3), Ti1–N1 = 2.041(8), Ti1–C32 = 2.139(6), Ti1–C27–C28 = 166.6(9), P1–Ti1–P2 = 150.73(12), N1–Ti1–C32 = 140.6(3). For **11**, Ti1–C27 = 1.869(6), Ti1–P1 = 2.6318(7), Ti1–P2 = 2.5683(7), Ti1–N1 = 2.0355(16), Ti1–C32 = 2.1647(14), Ti1–C27–C28 = 169.7(6), P1–Ti1–P2 = 151.26(2), N1–Ti1–C32 = 139.10(7).

Scheme 2. Treatment of 1 with F₅C₆H to Produce 10 along with Another Product Denoted “X”^a



^a Complex **11** can be prepared cleanly and independently from **12** and “Li(F₅C₆)” (thawing from –190 °C). Complex **9** can also be prepared from **12** and thawing Li(*o,o',m,m'*-F₄C₆H), but as a mixture of **X** and an unidentified byproduct.

1,2,4-F₃C₆H₃ reacted with **1**, three alkylidene-aryluoride isomers were clearly visible from the ¹³C and ¹⁹F NMR spectrum. We propose these isomers to be the compounds (PNP)Ti=CH^tBu(*o,p,m'*-F₃C₆H₂) (**10a**), (PNP)Ti=CH^tBu(*o,o',m'*-F₃C₆H₂) (**10b**), and (PNP)Ti=CH^tBu(*o,m,m'*-F₃C₆H₂) (**10c**), all of which are depicted in Scheme 1. In the reaction of pentafluorobenzene with **1**, a mixture of two products is observed. One of the products is proposed to be the pentafluorophenyl complex (PNP)Ti=CH^tBu(F₅C₆) (**11**). This mixture slowly decayed over 1 week to yield one compound we denote temporarily as **X** (*vide infra*) and which is not the C–H activated material **11** (Scheme 2). This byproduct formed from **1** and F₅C₆H has the same spectroscopic features as one of the two minor products observed from treating **1** with 1,2,3,4-F₄C₆H₂ and 1,2,4,5-F₄C₆H₂ (*vide supra*). Therefore, the activation of the C–H group to yield putative compounds **9** and **11**, however, by an independent approach by treatment of the corresponding HAR_F with ^tBuLi thawing from –190 °C, thus forming “Li(F₅C₆)” or “Li(F₄C₆H)” *in situ*, followed by addition of (PNP)Ti=CH^tBu(OTf) (**12**).¹⁶ Although the reaction of Li(F₅C₆) with **12** is clean, treating **12** with “Li(*o,o',m,m'*-F₄C₆H)” resulted in formation of **9** along with another product,

which was identified to be the third unidentified minor impurity from the reaction of **1** and 1,2,3,4-F₄C₆H₂ (Scheme 2). We have been unable thus far to identify this minor product. Table 1 compiles spectroscopic data for the alkylidene-aryluoride derivatives **2–11**.

In all cases, and based on our previous mechanistic studies for the C–H activation of benzene, we propose that α-hydrogen abstraction toward the formation of **A** takes place prior to C–H activation of the HAR_F (*vide infra*).^{10,11} Coordination of the HAR_F to the alkylidene precursor, **1**, is not likely taking place in these sets of reactions since (PNP)Ti=CH^tBu(C₆H₅) (**13**), a reagent that equilibrates to **A** at higher temperatures (>90 °C),^{10,11} fails to react with the same list of HAR_F at room temperature. Therefore, binding of the HAR_F is not facilitating α-hydrogen abstraction in **1**.

Complexes **2–11** all display diagnostic alkylidene resonances in the ¹³C (281–275 ppm) and ¹H NMR (9.2–6.8 ppm) spectra, and the ³¹P NMR spectroscopic data (two doublets with J_{P–P} = 43–28 Hz) are clearly consistent with pseudo-C_s symmetric systems arising from skewing of the aryl backbone in the PNP ancillary. The solid state structures of compounds **5** (isomers **5a** and **5b**),¹⁷ **6**,¹⁸ and **11** have been determined as well (Figure 1), and all systems are comparable to the molecular structures of **2–4**. In each case, the Ti=C distances (1.870(5) Å, **5**; 1.8659(17) Å, **6**) are consistent with these compounds bearing a terminal alkylidene ligand (Figure 1), while the Ti···F distances (2.99(4) Å, **5**; 3.03(2) Å, **6**) are too long to imply that a rigid coordination or pseudo-cyclometalation is taking place in the solid state. In fact, these distances are much longer when compared to the few structural examples of Ti(IV)-fluoroarene adducts (2.113(7)–2.151(2) Å) such as the cationic titanium imide salt [(nacnac)Ti=NAr(FC₆H₅)]⁺[B(C₆F₅)₄][–] (nacnac[–] = [ArNCⁱBu]₂CH, Ar = 2,6-ⁱPr₂C₆H₃)¹⁹ and the titanocene(III) cation [Cp*₂Ti(FC₆H₅)]⁺[BPh₄][–].²⁰ The crystal structure of **11** differs

(17) The X-ray structure of **5** contains co-crystals of the isomers **5a** and **5b** as well as disorder about the Ti1–C32 bond, resulting in an additional isomer of **5a**. The Ar^F moiety is isotropically refined due to this combination of disorder.

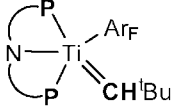
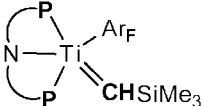
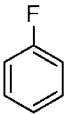
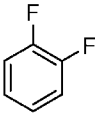
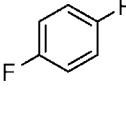
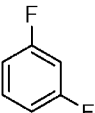
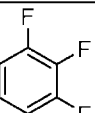
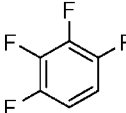
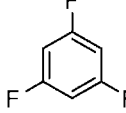
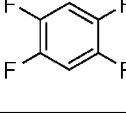
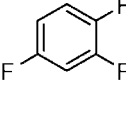
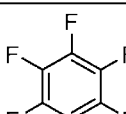
(18) The X-ray structure of **6** contains a disorder in the Ar^F moiety. The site occupancy ratio was 68:32 and modeled using the appropriate set of restraints and constraints.

(19) Basuli, F.; Aneetha, H.; Huffman, J. C.; Mindiola, D. J. *J. Am. Chem. Soc.* **2005**, *127*, 17992.

(20) Bouwkamp, M. W.; Budzelaar, P. H. M.; Gercama, J.; Del Hierro Morales, I.; de Wolf, J.; Meetsma, A.; Troyanov, S. I.; Teuben, J. H.; Hessen, B. *J. Am. Chem. Soc.* **2005**, *127*, 14310.

(16) Bailey, B. C.; Huffman, J. C.; Mindiola, D. J.; Weng, W.; Ozerov, O. V. *Organometallics* **2005**, *24*, 1390.

Table 1. List of Salient NMR Spectroscopic Features (bolded in complex) for Compounds 2–11 and 16–25

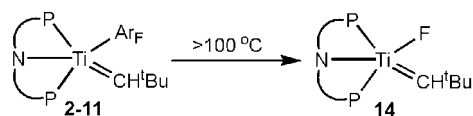
		
	For 2: ¹ H: 8.05 ppm ¹³ C: 275.4 ppm ³¹ P: 30.9 (d), 23.1 (d) ppm, ² J _{P-P} (32 Hz) ¹⁹ F: -91.1 ppm	For 16: ¹ H: 12.79 ppm ¹³ C: 309.8 ppm ³¹ P: 32.0 (d), 23.8 (d) ppm, ² J _{P-P} (44 Hz) ¹⁹ F: -113.0 ppm
	For 3: ¹ H: 7.64 ppm ¹³ C: 277.5 ppm ³¹ P: 31.1 (d), 23.1 (d) ppm, ² J _{P-P} (31 Hz) ¹⁹ F: -116.0, -140.4 ppm	For 17: ¹ H: 12.39 ppm ¹³ C: 314.5 ppm ³¹ P: 32.2 (d), 24.9 (d) ppm, ² J _{P-P} (43 Hz) ¹⁹ F: -111.5, -109.9 ppm
	For 4: ¹ H: 7.91 ppm ¹³ C: 277.5 ppm ³¹ P: 31.1 (d), 23.1 (d) ppm, ² J _{P-P} (32 Hz) ¹⁹ F: -99.0, -123.8 ppm	For 18: ¹ H: 12.69 ppm ¹³ C: 312.0 ppm ³¹ P: 32.2 (d), 23.6 (d) ppm, ² J _{P-P} (34 Hz) ¹⁹ F: -122.8, -97.9 ppm
	For 5a and 5b: ¹ H: 7.11 ppm ¹³ C: 276.8, 276.3 ppm ³¹ P: 30.9 (d), 30.8 (d), 23.2 (d), 23.1 (d) ppm, ² J _{P-P} (31 Hz) ¹⁹ F: -112.3, -94.2, -79.3 ppm	For 19: ¹ H: 12.69 ppm ¹³ C: 310.8 ppm ³¹ P: 31.8 (d), 23.6 (d) ppm, ² J _{P-P} (34 Hz) ¹⁹ F: -111.8 ppm
	For 6: ¹ H: 7.19 ppm ¹³ C: 278.0 ppm ³¹ P: 31.1 (d), 23.2 (d) ppm, ² J _{P-P} (32 Hz) ¹⁹ F: -165.4, -138.8, -135.2 ppm	For 20: ¹ H: 12.66 ppm ¹³ C: 312.9 ppm ³¹ P: 32.3 (d), 23.7 (d) ppm, ² J _{P-P} (33 Hz) ¹⁹ F: -165.4, -138.2, -135.4 ppm
	For 7: ¹ H: 7.19 ppm ¹³ C: 280.3 ppm ³¹ P: 31.3 (d), 23.2 (d) ppm, ² J _{P-P} (31 Hz) ¹⁹ F: -159.3, -156.4, -151.8, -141.2 ppm	For 21: ¹ H: 12.76 ppm ¹³ C: 314.7 ppm ³¹ P: 33.0 (d), 24.0 (d) ppm, ² J _{P-P} (42 Hz) ¹⁹ F: -156.5, -151.1, -139.9, -112.6 ppm
	For 8: ¹ H: 6.95 ppm ¹³ C: 278.0 ppm ³¹ P: 31.2 (d), 23.3 (d) ppm, ² J _{P-P} (43 Hz) ¹⁹ F: -111.4, -90.9, -76.5 ppm	For 22: ¹ H: 12.39 ppm ¹³ C: 314.5 ppm ³¹ P: 32.2 (d), 24.9 (d) ppm, ² J _{P-P} (33 Hz) ¹⁹ F: -111.5, -109.9 ppm
	For 9: ¹ H: 7.20 ppm ¹³ C: 280.5 ppm ³¹ P: 31.4 (d), 23.3 (d) ppm, ² J _{P-P} (30 Hz) ¹⁹ F: -141.5, -138.6, -122.2, -109.3 ppm	For 23: ¹ H: 12.32 ppm ¹³ C: 314.3 ppm ³¹ P: 33.5 (d), 24.9 (d) ppm, ² J _{P-P} (31 Hz) ¹⁹ F: -142.1, -136.5, -124.2, -112.6 ppm
	For 10a, 10b, 10c: ¹ H: 9.20 ppm ¹³ C: 279.5, 279.2, 278.3 ppm ³¹ P: 31.3 (d), 31.2 (d), 23.3 (d), 23.2 (d) ppm, ² J _{P-P} (33 Hz) ¹⁹ F: -153.9, -134.2, -118.7, -117.0, -104.5, -100.2, -85.5 ppm	For 24: ¹ H: 12.8, 12.6, 12.4 ppm ¹³ C: 314.1 ppm ³¹ P: 32.9 (d), 24.0 (d), 32.6 (d), 23.9 (d) ppm, ² J _{P-P} (42 Hz) ¹⁹ F: -150.1, -146.5, -143.5, -136.3, -135.2, -133.5, -123.6, -117.8, -115.7 ppm
	For 11: ¹ H: 6.77 ppm ¹³ C: 281.3 ppm ³¹ P: 31.4 (d), 23.3 (d) ppm, ² J _{P-P} (30 Hz) ¹⁹ F: -163.0, -160.7, -156.4, -119.8, -106.9 ppm	For 25: ¹ H: 12.23 ppm ¹³ C: 312.6 ppm ³¹ P: 33.2 (d), 24.5 (d) ppm, ² J _{P-P} (41 Hz) ¹⁹ F: -162.6, -154.4, -139.3 ppm

slightly from 2–6 since it shows a contact between the alkylidene α -H and the *o*-F of the aryl ring (~ 2.45 Å).²² The Ti=C distance (1.858(5) Å) in **11** is similar to that of **5** and **6** and does not display a titanium fluoride interaction.

2b. C–F Activation Reactions in Titanium Alkylidene-Fluorophenyl Derivatives. Complexes 2–11 are all shown to be kinetic products under an atmosphere of nitrogen since thermolysis at 100 °C over 48 h resulted in the quantitative

formation of the neopentylidene-fluoride complex (PNP)Ti=CHtBu(F) (**14**) (Scheme 3). Production of the latter complex is evident from the ¹⁹F NMR spectrum (Ti–F, 166.2 ppm), which is comparable to other alkylidene-fluoride compounds reported by our group.¹¹ Likewise, the ³¹P NMR spectrum

(21) The C–F distance is 3.341(9) and 3.678(2) Å for the donor acceptor in the hydrogen bond.

Scheme 3. C–F Activation in Compounds 2–11 to Produce 14

Ar_F = *o*-FC₆H₄, *o,m*-F₂C₆H₃, *o,m'*-F₂C₆H₃, *o,o'*-F₂C₆H₃, and isomer *o,p*-F₂C₆H₃, *o,m,p*-F₃C₆H₂, *o,m,p,m'*-F₄C₆H, *o,p,o'*-F₃C₆H₂, *o,o',m,m'*-F₄C₆H, isomers *o,p,m'*-F₃C₆H₂, *o,o',m*-F₃C₆H₂, *o,m,m'*-F₃C₆H₂, and F₅C₆

of **14** reveals $^2J_{P-F}$ (17 Hz) and $^2J_{P-P}$ (55 Hz) values resulting in two doublets of doublets (Table 2). We could not, however, resolve $^2J_{C-F}$ coupling for the alkylidene resonance in the ^{13}C NMR spectrum (314 ppm, $J_{C-H} = 103$ Hz). The 1H NMR spectrum displayed a downfield singlet at 11.79 ppm for the alkylidene hydrogen. In fact, comparison of the crude 1H and ^{31}P NMR spectra from the reaction of 1,2,3,4-F₄C₆H₂ and pentafluorobenzene with **1** at room temperature reveals complex **14** to be the other product “X” generated in these reactions (*vide supra*, Schemes 1 and 2).

Given the rarity of terminal alkylidene-fluorides^{11,22} we proceeded to collect solid state structural data for **14**. Interestingly, the solid state structure of **14** differed from that of **12** since the α -hydrogen was pointed away from the fluoride ligand (Figure 2). This orientation seemed counterintuitive given the potential formation of a strong hydrogen bond to form a locked alkylidene rotamer. Low-temperature NMR spectral data of **14**, collected at -55 °C, did not resolve the alkylidene α -hydrogen to the corresponding rotamers.

2c. *o*-Benzyne Trapping and Isotopic Labeling Experiments. Formation of **14** from the neopentylidene-aryl fluorides **2–11** implied that β -fluoride elimination was taking place. To exclude a radical pathway, which has been proposed for d⁰ zirconocene dihydrides,⁸ the organic byproducts generated from the C–F activation were analyzed using a combination of isotopic labeling as well as organic traps. Vacuum transfer of the volatiles from the thermolysis of **2** in C₇D₈ revealed several organic products generated from C–F bond cleavage. Examination of this solution by GC-MS suggested one product originating from the Diels–Alders addition of *o*-benzyne to C₇D₈ (MW = 176 g/mol inferred by GC-MS), as well as the presence of biphenylene (MW = 152 g/mol). Likewise, a significant amount of C₆H₄D₂ (MW = 80 g/mol) was observed, presumably due to benzylic C–D abstraction from the solvent media. Attempts to thermolyze **2** with other traps, such as furan, resulted in complicated mixtures, possibly due to the reactive nature of the alkylidene ligand present in **2**. In fact, no 1,4-epoxy-1,4-dihydronaphthalene was observed for the latter reaction when judged by 1H NMR spectra and GC-MS.²³ The use of durene as a trap in the thermolysis of **2** yielded only a small fraction of the cycloaddition product, as indicated by GC-MS (MW = 210 g/mol). Given the ability of *o*-benzyne to undergo free radical chemistry, potentially resulting in unwanted pathways including the formation of biphenylene or triphenylene side products,^{24–26} we resorted to generating *o*-tetrafluorobenzyne. This reagent is inclined to show more controllable dienophile chemistry as opposed to secondary radical pathways.²⁷ Accordingly, thermolysis of **11** in durene at 100 °C over 7 days resulted in the clean formation of **14** concurrent with production of the

[6+2]-cycloaddition product 5,6,7,8-tetrafluoro-1,4-dihydro-2,3,9,10-tetramethyl-1,4-ethenonaphthalene depicted in Scheme 4.

Formation of the latter organic product was confirmed via a combination of GC-MS and 1H and ^{19}F NMR spectroscopy.^{9,26,27} Therefore, this work unambiguously confirms that C–F activation in precursors **2–11** must be transpiring through a β -fluoride elimination pathway concomitant with *o*-benzyne extrusion.

2d. Dehydrofluorination of HFCs by C–H and C–F Activation Reactions Involving a Transient Titanium Trimethylsilylmethylidyne. Complex **1** undergoes α -hydrogen abstraction much more readily than the trimethylsilylmethylidene-trimethylsilylmethyl derivative (PNP)Ti=CHSiMe₃-(CH₂SiMe₃) (**15**), but the latter complex is also a synthon to the alkylidyne analogue intermediate **B**, albeit at higher temperatures.^{10,11} Consequently, treatment of **15** with all of the HAR_F substrates (discussed previously with **1**) at room temperature resulted in no reaction. Only upon heating (>60 °C) was there a noticeable transformation, toward a mixture of the corresponding fluoroaryl-alkylidene derivatives (PNP)Ti=CHSiMe₃(Ar_F) (Ar_F = *o*-FC₆H₄ (**16**), *o,m*-F₂C₆H₃ (**17**), *o,p*-F₂C₆H₃ (**18**), *o,o'*-F₂C₆H₃ (**19**), *o,m,p*-F₃C₆H₂ (**20**), *o,m,m'*-F₄C₆H (**21**), *o,o',p*-F₃C₆H₂ (**22**), *o,o',m,m'*-F₄C₆H (**23**), *o,p,m'*-F₃C₆H₂ (**24a**) and isomers *o,o',m*-F₃C₆H₂ (**24b**) and *o,m,m'*-F₃C₆H₂ (**24c**), and F₅C₆ (**25**)), and the fluoride (PNP)Ti=CHSiMe₃(F) (**26**). In some instances, starting material was also present in the reaction mixture (Scheme 5). Table 1 compiles salient spectroscopic features for the trimethylsilylmethylidene-Ar_F derivatives, while Table 2 provides some spectroscopic signatures for **26**. Analogous to **14**, complex **26** displayed a diagnostic ^{19}F NMR spectroscopic resonance at 165.2 ppm, while the ^{31}P NMR spectrum evinced two doublets of doublets arising from $^2J_{P-F}$ coupling with the inequivalent phosphine arms of the bound PNP ligand (Table 2). As observed for **1**, formation of **26** from **15** and the HAR_F likely proceeds via an intermolecular C–H activation step followed by β -fluoride elimination, concurrent with formation of *o*-benzyne or fluoro-*o*-benzyne derivatives.

In general, the reactions are slow, and complete decay of **15** is observed only after extensive periods of time at 60 °C (~3 weeks). Unfortunately, the extended periods of time resulted in partial decomposition to a mixture of products, which included (PNP)H as well as other metal-based materials when judged by ^{31}P NMR spectroscopy. This feature is not surprising given that **15** itself has a limited half-life in C₆H₆ (~3 h at >60 °C).^{10,11} Therefore, formation of **26** from **15** and the corresponding HAR_F can be expedited to ~72 h by thermolysis of **15** at >100 °C. Under these conditions, no kinetic products are observed in the reaction mixture. Only in one case were we fortunate enough to crystallize the kinetic product, (PNP)Ti=CHSiMe₃(*o,m*-F₂C₆H₃) (**17**), from the reaction of **15** with 1,2-F₂C₆H₄ at 60 °C over 3 weeks. Upon isolation, complex **17** does indeed transform to **26** under thermolytic conditions at 100 °C over 48 h, further endorsing the hypothesis that C–H activation of the HAR_F is the first step along the dehydrofluorination sequence. In the formation of complexes **21**, **23**, and **25**, the reactions are not clean, and the ^{31}P NMR spectra displayed three

(24) Dyke, A. M.; Hester, A. J.; Lloyd-Jones, G. C. *Synthesis* **2006**, 24, 4093.

(25) (a) Roberts, J. D.; Semenow, D. A.; Simmons, H. E.; Carlsmith, L. A. *J. Am. Chem. Soc.* **1956**, 78, 601. (b) Pellissier, H.; Santelli, M. *Tetrahedron* **2003**, 59, 701.

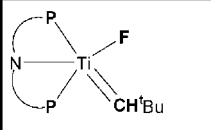
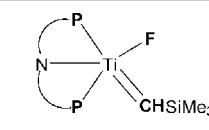
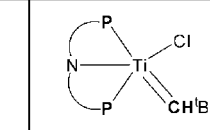
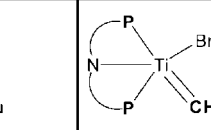
(26) Callander, D. D.; Coe, P. L.; Tatlow, J. C. *Chem. Commun.* **1966**, 143.

(27) Jones, W. D. *Acc. Chem. Res.* **2003**, 36, 140.

(22) (a) Huang, D.; Koren, P. R.; Folting, K.; Davidson, E. R.; Caulton, K. G. *J. Am. Chem. Soc.* **2000**, 122, 8916. (b) Schrock, R. R. *Chem. Rev.* **2002**, 102, 145.

(23) (a) Sander, W. *Acc. Chem. Res.* **1999**, 32, 669. (b) Heaney, H. *Chem. Rev.* **1962**, 62, 81.

Table 2. List of Salient NMR Spectroscopic Features (bolded in complex) for Compounds **14**, **26**, **32**, and **33**

			
For 14 : ¹ H: 11.79 ppm ¹³ C: 314.0 ppm ³¹ P: 33.6 (dd), 23.6 (dd) ppm ² J _{P-P} (55 Hz), ² J _{P-F} (17 Hz), ¹⁹ F: 166.2 ppm	For 26 : ¹ H: 15.01 ppm ¹³ C: 320.6 ppm ³¹ P: 35.4 (dd), 22.8 (dd) ppm ² J _{P-P} (58 Hz), ² J _{P-F} (18 Hz), ¹⁹ F: 165.2 ppm	For 32 : ¹ H: 9.24 ppm ¹³ C: 306.8 ppm ³¹ P: 36.0 (d), 24.3 (d) ppm, ² J _{P-P} (42 Hz)	For 33 : ¹ H: 8.36 ppm ¹³ C: 299.9 ppm ³¹ P: 37.3 (d), 25.6 (d) ppm, ² J _{P-P} (53 Hz)

products, those of C–H and C–F activation as well as another unknown impurity that we have been unable to identify thus far.

To unambiguously confirm the connectivity in **17**, single-crystal X-ray diffraction data was collected. As depicted in

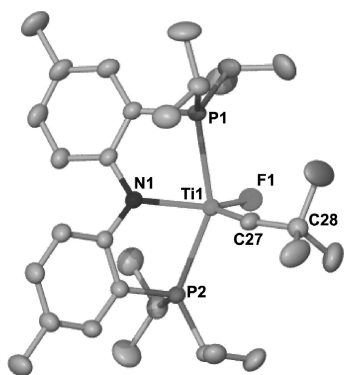
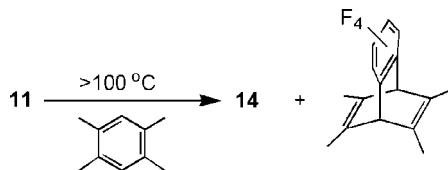


Figure 2. Solid state structure of compound **14** depicting thermal ellipsoids at the 50% probability level. H atoms and solvent molecules have been omitted for the purpose of clarity. Selected bond lengths (Å) and angles (°deg): Ti1–C27 = 1.878(2), Ti1–P1 = 2.5946(7), Ti1–P2 = 2.5815(7), Ti1–N1 = 2.1027(17), Ti1–F1 = 1.812(14), Ti1–C27–C28 = 156.2(3), P1–Ti1–P2 = 150.32(2).

Scheme 4. Formation of **14** and *o*-Benzyne Trapping by Thermolysis of **11** in Neat Durene



Scheme 5. Reactivity of **15** with Fluoroarenes at >100 °C to Form **26** and Organic Byproducts (benzyne byproducts not shown) or at 60 °C to Form (PNP)Ti=CHSiMe₃(Ar_F) and **26** as a Mixture

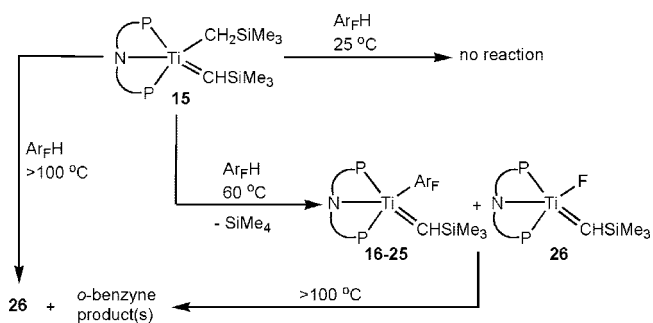


Figure 3, the solid state structure of **17** portrays a rare example of a distorted and terminal trimethylsilylmethylidene complex (Ti=C, 1.859(3) Å, Ti=C–Si 157.7(2)°)^{10,11,16,28} in addition to a difluorophenyl ligand. Analogous to **3**, the fluoride groups on the ring are *ortho* and *meta* with respect to the C–H activation site, and the phenyl ring is oriented in the C=Ti–C_{aryl} plane. As noted in the mono-, di-, and trifluorophenyl derivatives **2**, **5**, and **6**, the Ti···F distance (3.268(2) Å) is too long to suggest the presence of a strong interaction in the solid state. Similar to the solid state structure of **3**, complex **17** has the alkylidene trimethylsilyl methylidene hydrogen oriented away from the Ar_F groups (Figure 3).

2e. Dehydrofluorination of Fluoroalkanes by Complexes **1 and **15**.** HAr_F are not the only substrates amenable to dehydrofluorination since complex **1** also gradually transforms to **14** quantitatively in the presence of 1-fluorohexane (FC₆H₁₃) at 25 °C over 12 h (Scheme 6). Examination of the volatiles by GC-MS and ¹H NMR spectroscopy reveals formation of the olefin 1-hexene. This result further supports the notion that C–H activation and β-fluoride elimination are taking place along the dehydrofluorination pathway of the fluoroalkane. The GC-MS also yielded traces of other organic products that we are currently attempting to identify. The formation of the terminal olefin in the reaction of **1** with 1-fluorohexane implies that C–H activation at the 2-position of the fluoroalkane is likely occurring to form a transient titanium alkylidene-fluoroalkyl, which then undergoes β-fluoride elimination to form **14** (Scheme 6). We cannot refute, however, the possibility of C–H activation taking place away from the fluoride group and the system undergoing “chain walking” to ultimately produce the titanium-fluoride product.²⁹ Jordan and co-workers have reported similar halide elimination reactions when attempting to polymerize and copolymerize polar monomers such as vinyl ethers and halides.³⁰

(28) Bridging trimethylsilylmethylidenes have been reported: (a) Riley, P. N.; Fanwick, P. E.; Rothwell, I. P. *Chem. Commun.* **1997**, 1109. (b) Riley, P. N.; Fanwick, P. E.; Rothwell, I. P. *Dalton Trans.* **2001**, 181.

(29) (a) Ittel, S. D.; Johnson, L. K.; Brookhart, M. *Chem. Rev.* **2000**, *100*, 1169. (b) Guan, Z. *Chem.–Eur. J.* **2002**, *8*, 3086. (c) Guan, Z. *J. Polym. Sci. Part A: Polym. Chem.* **2003**, *41*, 3680.

(30) (a) Strazisar, S. A.; Wolczanski, P. T. *J. Am. Chem. Soc.* **2001**, *123*, 4728. (b) Boone, H. W.; Athey, P. S.; Mullins, M. J.; Philipp, D.; Muller, R.; Goddard, W. A. *J. Am. Chem. Soc.* **2002**, *124*, 8790. (c) Kang, M.; Sen, A.; Zakharov, L.; Rheingold, A. L. *J. Am. Chem. Soc.* **2002**, *124*, 12080. (d) Shen, H.; Jordan, R. F. *Organometallics* **2003**, *22*, 2080. (e) Gaynor, S. G. *Macromolecules* **2003**, *36*, 4692. (f) Stockland, R. A., Jr.; Foley, S. R.; Jordan, R. F. *J. Am. Chem. Soc.* **2003**, *125*, 796. (g) Foley, S. R.; Stockland, R. A., Jr.; Shen, H.; Jordan, R. F. *J. Am. Chem. Soc.* **2003**, *125*, 4350. (h) Foley, S. R.; Shen, H.; Qadeer, U. A.; Jordan, R. F. *Organometallics* **2004**, *23*, 600. (i) Luo, S.; Jordan, R. F. *J. Am. Chem. Soc.* **2006**, *128*, 12072. (j) Stockland, R. A., Jr.; Jordan, R. F. *J. Am. Chem. Soc.* **2000**, *122*, 6315. (k) van Rooyen, P. H.; Schindhutte, M.; Lotz, S. *Organometallics* **1992**, *11*, 1104. (l) Wu, F.; Dash, A.; Jordan, R. F. *J. Am. Chem. Soc.* **2004**, *126*, 15360.

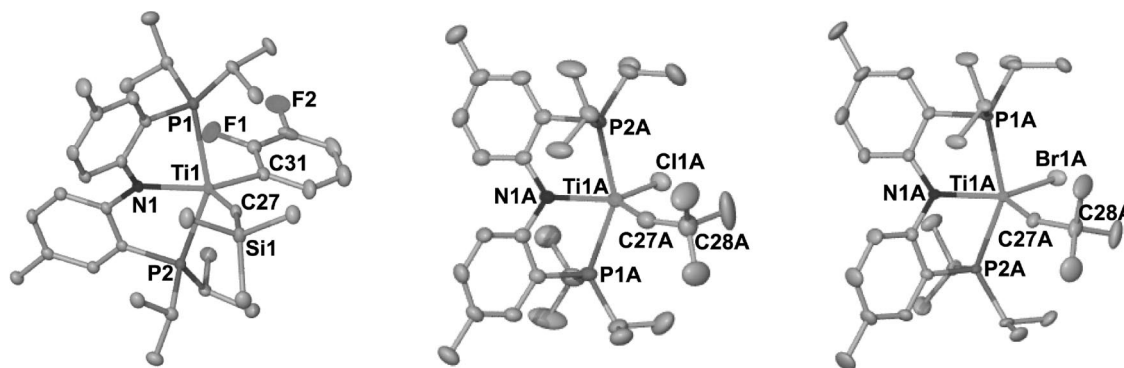
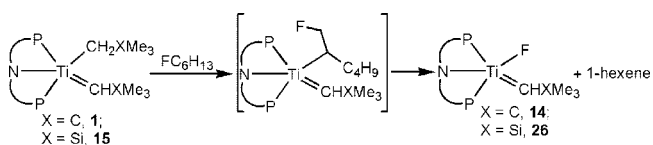


Figure 3. Solid state structures of compounds **17** (left), **32** (middle), and **33** (right) depicting thermal ellipsoids drawn at the 50% probability level. H atoms and solvent molecules have been omitted for the purpose of clarity. Selected bond lengths (Å) and angles (deg): For **17**, Ti1–C27 = 1.859(3), Ti1–P1 = 2.5678(11), Ti1–P2 = 2.5764(11), Ti1–N1 = 2.049(2), Ti1–C31 = 2.2400(19), Ti1–C27–Si1 = 157.7(2), P1–Ti1–P2 = 149.24(3), N1–Ti1–C31 = 138.84(9). For **32**, Ti1–C27A = 1.871(4), Ti1A–P1A = 2.5887(11), Ti1A–P2A = 2.6036(11), Ti1A–N1A = 2.080(3), Ti1A–C11A = 2.2903(11), Ti1–C27A–C28A = 153.4(3), P1A–Ti1A–P2A = 149.83(4), N1A–Ti1A–C11A = 131.45(8). For **33**, Ti1–C27A = 1.874(4), Ti1A–P1A = 2.5992(11), Ti1A–P2A = 2.5595(11), Ti1A–N1A = 2.076(3), Ti1A–Br1A = 2.4343(7), Ti1–C27A–C28A = 152.6(3), P1A–Ti1A–P2A = 149.67(4), N1A–Ti1A–Br1A = 137.85(9).

Scheme 6. Dehydrofluorination of 1-Fluorohexane Using Precursors **1 and **15****



Isotopic labeling studies using (PNP)Ti=CD^tBu(CD²tBu) (**1**)-*d*₃ and 1-fluorohexane reveal that the alkyldiene intermediate **A** is generated in this reaction, since the α-hydrogen in **14** is not isotopically enriched (based on the ¹H and ²H NMR spectra). Interestingly, a competition experiment between **1** and a 1:1 mixture of fluorohexane and fluorobenzene revealed a slight preference for C–H/C–F activation of fluorohexane over fluorobenzene (58% to 42%, respectively).

Jones and co-workers have proposed divergent pathways taking place for the hydrodefluorination of HAR_F versus that for HAL_F. For example, the possibility of β-fluoride elimination, by virtue of a benzyne intermediate Cp*₂Zr(H)(F)(η²-C₆H₄), has been invoked as a likely pathway for the isomerization of Cp*₂Zr(H)(*o*-FC₆H₄) to the fluoride complex Cp*₂Zr(F)(C₆H₅), while a radical chain mechanism involving a putative Zr(III) species Cp*₂Zr(H) has been suggested in the hydrodefluorination of HAL_F (eq 2).⁸ In our case, the dehydrofluorination mechanism appears to be common for both HAR_F and HAL_F, presumably due to the propensity of intermediate **A** to first activate the C–H bond of the substrate.

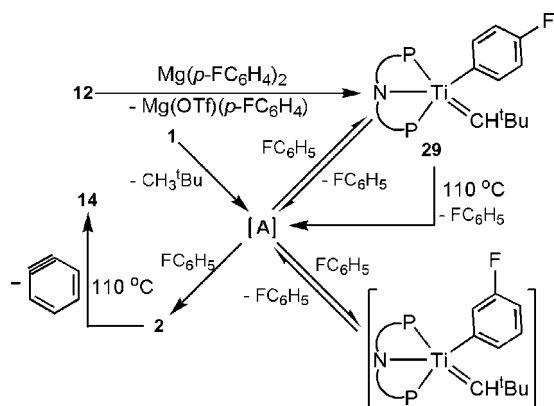
Likewise, complex **15** also promotes the dehydrofluorination of 1-fluorohexane at >60 °C to yield **26** and 1-hexene. As with **1**, traces of some unidentified organic species are observed in the reaction of **15** with the terminal HAL_F when the volatiles are analyzed by GC-MS (Scheme 6). The reaction of **1** or **15** with fluorocyclohexane also resulted in some formation of **14** and **26**, respectively. However, other titanium-based products were observed via ³¹P NMR spectroscopy, and the organic byproduct could not be conclusively scrutinized.

2f. Mechanistic Studies of the Regioselective C–H Activation of HAR_F by **1.** The ability to isolate both kinetic and thermodynamic products from the dehydrofluorination reaction of HAR_F using **1** as our reagent allowed both the C–H and C–F activation steps to be investigated independently. Accordingly, kinetic parameters for the conversion of **1** → **2** were assessed experimentally by monitoring the decay of **1** using

³¹P NMR spectroscopy in FC₆H₅ and revealed a $k_{\text{average}} = 5.896(5) \times 10^{-5} \text{ s}^{-1}$ at 25 °C. As anticipated for a C–H activation reaction by a transient Ti≡C^tBu linkage in **A**,^{10,11} the conversion was found to obey pseudo-first-order kinetics with respect to titanium, which is in excellent agreement with the reaction energy profile suggested by our earlier experiments and DFT calculations reported for the C–H activation of benzene.^{10,11} Not surprisingly, under a depleted amount of fluorobenzene, formation of **2** is not clean, given the ability of intermediate **A** to react with both the arene and other media, such as benzene, cyclohexane, hexane, 1-fluorohexane, fluorocyclohexane, and pentane. In fact, competition experiments of **1** with FC₆H₅ and C₆H₆ (1:1) consistently produced a 60:40 mixture of **2** and **13**, respectively. This result implies that the preference of one product over the other may be slightly influenced by a binding event of the fluoro group inasmuch as a positive polarization at the *ortho* hydrogen by an inductive effect. In fact, we speculate that the regioselective activation of the C–H bond in the HAR_F is dominated by a combination of sterics, the binding affinity of the fluoro group to the Ti, and incipient positive charge at the *o*-carbon promoted by the fluoro group (*vide infra*).

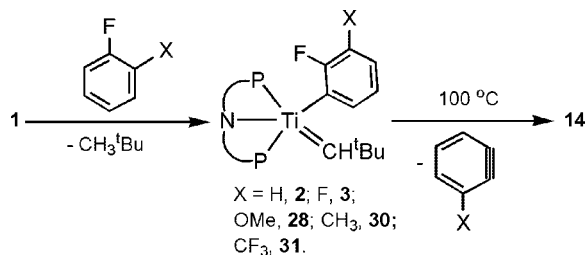
Competition experiments between FC₆H₅ and 1,3,5-F₃C₆H₃ (55% to 45%) as well as 1,3,5-F₃C₆H₃ and C₆H₆ (51% to 49%) do not show any preference for C–H activation of one substrate over the other, hence suggesting that there is a fine line between electronic and thermodynamic preference. Clearly, a binding event is not accelerating C–H activation of the HAR_F. This feature is further corroborated by the fact that treatment of **1** with anisole results solely in *ortho* C–H activation with respect to the OCH₃ group to form (PNP)Ti=CH^tBu(*o*-CH₃OC₆H₄) (**27**)¹¹ after 1 day at 25 °C. The rate for the conversion of **1** to **27** ($4.26 \times 10^{-5} \text{ s}^{-1}$) is similar to that of the conversion of **1** → **2** and is in agreement with the rate-determining step likely being formation of **A**. This result also implies that binding of the fluoride group, if any, does not have a significant effect on the rate. If **1** is treated with 2-fluoroanisole, we observe exclusive activation of the C–H bond *ortho* to the fluoro group to form the compound (PNP)Ti=CH^tBu(*o*-F,*m*-CH₃OC₆H₃) (**28**) ($k_{\text{average}} = 1.71(7) \times 10^{-4} \text{ s}^{-1}$), depicted in Scheme 8.¹³ The latter result also suggests that the fluoro group must enhance positive polarization on the *ortho*-hydrogen as opposed to the ether site being a better donor. Preference for C–H activation adjacent to the fluoro substituent is also observed when **1** is dissolved in

Scheme 7. Proposed Ring-Walking Stemming from the Reaction of **1 with FC₆H₅, and via the Formation of **A**, to Eventually Produce Complex **2**^a**



^a The independent preparation of compound **29** is also illustrated as well as its conversion at 110 °C to **2**, and ultimately **14** via intermediate **A**.

Scheme 8. Synthesis of Compounds **2, **3**, **28**, **30**, and **31** from Regioselective C–H Activation Using **1** and Subsequent Thermolysis at 100 °C to Afford **14** and Substituted *o*-Benzyne**



4-fluoroanisole to yield a 3:1 mixture of regioisomers (PNP)Ti=CH^tBu(*o*-F,*m'*-CH₃OC₆H₃) and (PNP)Ti=CH^tBu(*o*-CH₃O,*m'*-FC₆H₃), respectively.¹³ On the basis of all of our comparative studies, we cannot disregard the possibility of **A** activating a distant C–H bond in a substrate such as FC₆H₅ and then undergoing ring-walking,^{9a} via α -hydrogen abstraction steps,^{15a} to ultimately afford the final product **2** (Scheme 8). This is not unreasonable to propose since Legzdins reported the *meta* and *para* intermediates to be kinetic products preceding the *ortho* C–H bond activation of chlorobenzene.^{15a} To further elucidate whether or not ring-walking could be taking place in the C–H activation pathway leading to *ortho*-selectivity, complex (PNP)Ti=CH^tBu(*p*-FC₆H₄) (**29**) was synthesized independently, in 90% yield, from **12** and 1 equiv of Mg(*p*-FC₆H₄)₂ (Scheme 7). Upon heating **29** for 18 h at 110 °C in C₆D₆, the formation of complex **14** was evident in the ³¹P NMR spectrum. However, only at high temperature does complex **29** form **14**, therefore implying that fluorobenzene must be first eliminated to form transient **A**, followed by ring-walking to ultimately produce **14** (Scheme 7). Since the thermolysis is conducted in benzene, we cannot argue against C–H activation of the media (i.e., C₆D₆) occurring under these conditions. Monitoring the thermolysis of **29** in C₆D₆ does not reveal formation of **13**. In fact, low-temperature ³¹P and ¹⁹F NMR spectroscopic data (10 °C) collected on a sample of **1**, after immediately dissolving in FC₆H₅, do not reveal other product(s), apart from **2** being generated in the reaction mixture. However, one would argue against the proposal of ring-walking since the barrier to equilibration to **A** should be comparable to, if not higher than,

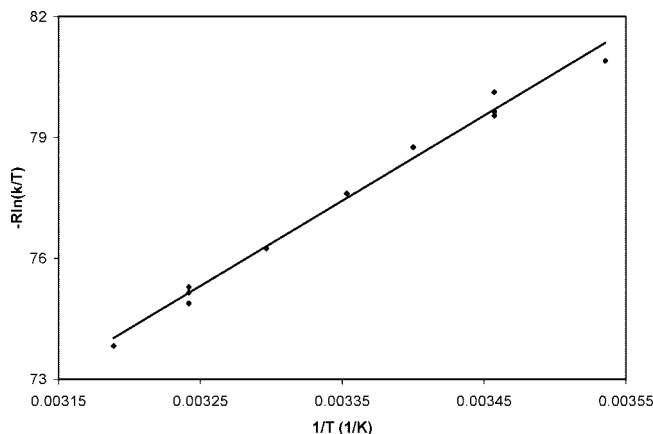


Figure 4. Eyring plot for the **1** → **2** transformation in FC₆H₅.

the barrier predicted and experimentally assessed for the **13** ↔ **A** equilibration (~30.1 kcal/mol at 298.15 K).¹³

Temperature dependence studies of the **1** → **2** transformation between 10 and 40 °C allowed for extraction of the activation parameters from the Eyring plot: $\Delta H^\ddagger = 21(1)$ kcal/mol and $\Delta S^\ddagger = -7(3)$ cal/molK⁻¹, yielding a $\sim\Delta G^\ddagger = 23$ kcal/mol at 298.15 K (Figure 4). Not surprisingly, our activation parameters are similar to previously reported experimental values obtained for the C–H activation of benzene ($\Delta H^\ddagger = 24(7)$, $\Delta S^\ddagger = -2(3)$ cal/mol K⁻¹, $\sim\Delta G^\ddagger = 24.7$ kcal/mol), which suggested that a similar reaction coordinate is operative here.¹¹ These parameters are also in reasonable agreement with the DFT prediction of 27.8 kcal/mol for the rate-determining step along the C–H activation of benzene.^{10,11} The intermolecular *k_H/k_D* ratio is remarkably close to unity (1.01(17) at 25 °C) when substituting FC₆D₅ for FC₆H₅, suggesting that the overall rate of the reaction has minor contributions from the C–H bond activation of the HAR_F.²⁷ As anticipated for an α -hydrogen abstraction being the rate-determining step to yield intermediate **A**, the rates for the decay of **1** and **1-d₃** are substantially different, thus yielding a *k_H/k_D* ratio of 4.04(7) at 25 °C. This result also discards an associative mechanism, whereby **1** binds the fluorobenzene substrate, given the similarities of the KIEs between benzene and fluorobenzene. Our smaller difference in KIE versus Wolczanski's systems (KIE = 5–14)³¹ might be rationalized on the basis of a more asymmetric H⁺ transfer from the C_{alkylidene} to the C_{alkyl} group in **1**, consistent with our proposed and more acute four-centered transition state leading to **A**. This feature is analogous to the transition state computed along the activation of a benzene C–H bond.¹¹ The meridional constraint imposed by the PNP ancillary could be enforcing a more distorted H⁺ migration to the departing neopentyl group. The data therefore provide strong credence to the rate-determining step being the α -hydrogen abstraction to generate a transient titanium alkylidyne intermediate **A**. On this basis, one would expect the C–H activation step not to contribute significantly to the KIE values obtained at 25 °C.

2g. Mechanistic Studies of the C–F Bond Activation of Fluorobenzene via the Kinetic Product **2.** As noted earlier, our ability to cleanly isolate most of the C–H activation kinetic products derived from **1** and the corresponding HAR_F (*vide supra*) allowed for mechanistic studies on the C–F activation step leading to formation of **14**. Concentration dependence

(31) (a) Bennett, J. L.; Wolczanski, P. T. J. *Am. Chem. Soc.* **1994**, *116*, 2179. (b) Bennett, J. L.; Wolczanski, P. T. J. *Am. Chem. Soc.* **1997**, *119*, 10696.

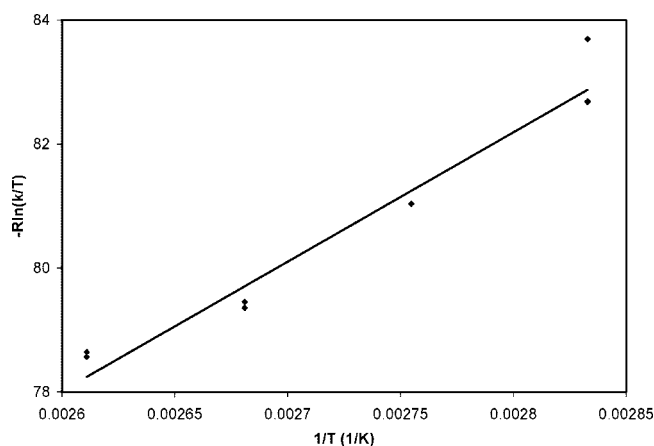


Figure 5. Eyring plot for the **2** → **14** transformation in toluene.

studies on the thermolysis of **2** (0.078, 0.156, and 0.234 mM solutions in toluene) suggests an intramolecular C–F activation pathway since the rate ($k_{\text{average}} = 4.9(3) \times 10^{-5} \text{ s}^{-1}$) does not change significantly at 100 °C. As a result, the C–F activation reaction derived from **2**, and leading to **14**, was found to obey first-order kinetics with respect to titanium. The conversion of **2** → **14** was assessed experimentally by monitoring the decay of **2** using ^{31}P NMR spectroscopy in a C_7H_8 solution to reveal a $k_{\text{average}} = 4.96(16) \times 10^{-5} \text{ s}^{-1}$ at 100 °C. Likewise, the rate of the reaction does not deviate when thermolysis of **2** is conducted in other nonpolar aprotic solvents such as benzene or methylcyclohexane. Unfortunately, monitoring the reaction in a polar aprotic solvent such as THF, pyridine, or 2,6-lutidine resulted in a myriad of products.

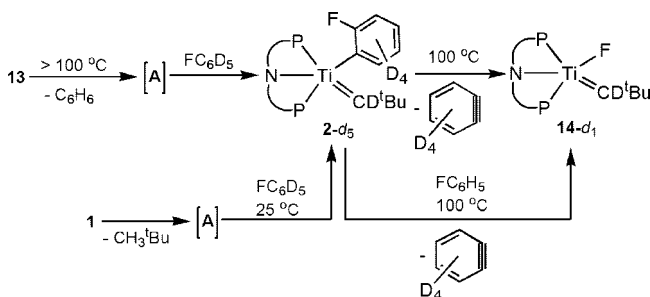
Extraction of the activation parameters from the Eyring plot (85–115 °C) revealed $\Delta H^\ddagger = 29(1) \text{ kcal/mol}$ and $\Delta S^\ddagger = -3(4) \text{ cal/mol K}^{-1}$, yielding a $\sim \Delta G^\ddagger = 30 \text{ kcal/mol}$ at 298.15 K (Figure 5). From our entropy value there is no clear evidence for less or more ordering in the transition state. This result can, however, be rationalized in terms of an “early” transition state being formed with respect to formation of **14** where there is some $\text{Ti} \cdots \text{F}$ interaction concomitant with weakening of the $\text{Ti}-\text{C}_{\text{aryl}}\text{F}$ bond. Unfortunately, the high barrier $\sim \Delta G^\ddagger$ of 30 kcal/mol for this reaction argues against this hypothesis and favors a “late” transition state given the energy penalty in generating a reactive species such as *o*-benzyne. In other words, the C–F bond should be nearly broken and the leaving *o*-benzyne nearly formed in the activated complex. For the activated complex of **2**, the constrained geometry is most likely due to the $\text{Ti} \cdots \text{F}$ interaction. The plausibility of intermolecular interactions (such as $\text{H} \cdots \text{F}$) seems dubious to propose given the steric constraint offered by the aryl, alkylidene, and PNP ancillaries. The solid state structure of **14** also argues against this possibility given that there is not even a weak intermolecular $\text{H} \cdots \text{F}$ interaction. Likewise, our concentration dependence studies veto this possibility, because the rate did not fluctuate significantly under those conditions (*vide supra*). Therefore, we speculate that the activated complex must have significant $\text{Ti} \cdots \text{F}$ bond formation concurrent with $\text{Ti}-\text{C}_{\text{aryl}}\text{F}$ weakening en route to extrusion of the *o*-benzyne.

Fortunately, our ability to selectively activate the C–H group *ortho* to the fluoride in substrates such as 1,2- $\text{F}_2\text{C}_6\text{H}_4$ and 2-F-anisole, to form **3** and **28**, respectively, provided the premise to vary the H in complex **2** to other substituents. Accordingly, treating **1** with other *ortho*-substituted HAr_F , such as 2-fluorotoluene and fluorobenzotrifluoride, resulted in selective C–H activation *ortho* with respect to the fluoride, to furnish the aryl

Table 3. Rates for the Conversion of **2**, **3**, **28**, **30**, and **31** to Complex **14** Performed at 100 °C

reaction	rate constants at 100 °C
2 → 14	$4.96(16) \times 10^{-5} \text{ s}^{-1}$
3 → 14	$1.1(5) \times 10^{-5} \text{ s}^{-1}$
28 → 14	$1.71(7) \times 10^{-4} \text{ s}^{-1}$
30 → 14	$3.54(18) \times 10^{-4} \text{ s}^{-1}$
31 → 14	$7.5(9) \times 10^{-5} \text{ s}^{-1}$

Scheme 9. Synthesis of **14-d₁** from Two Independent Routes and Attempted Exchange of **2-d₅** with FC_6H_5

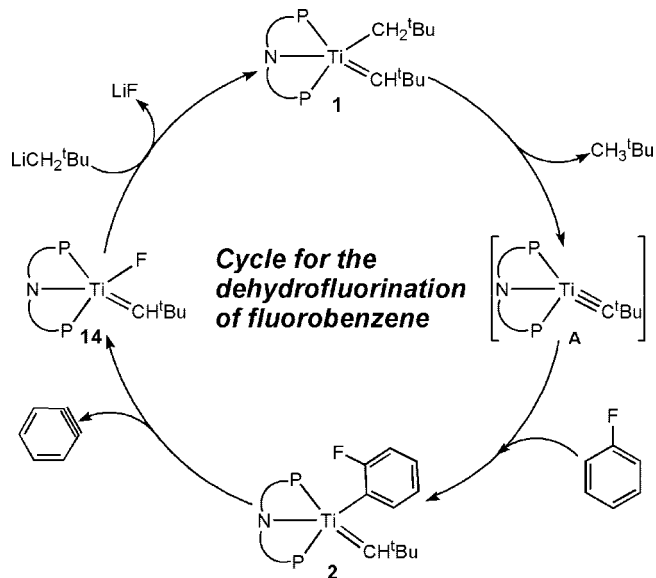
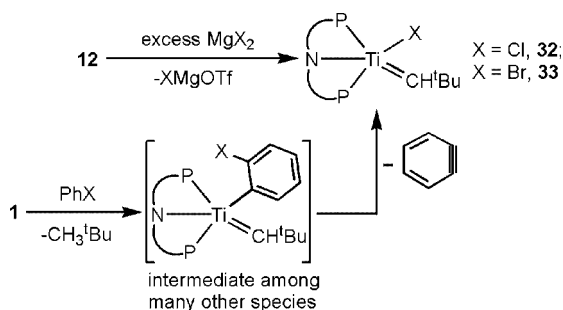


derivatives $(\text{PNP})\text{Ti}=\text{CH}^t\text{Bu}(o\text{-F},m\text{-CH}_3\text{C}_6\text{H}_3)$ (**30**) and $(\text{PNP})\text{Ti}=\text{CH}^t\text{Bu}(o\text{-F},m\text{-CF}_3\text{C}_6\text{H}_3)$ (**31**), respectively (Scheme 8). An attempt to selectively activate the C–H bond in substrates such as 1-fluoro-2-nitrobenzene or 1-chloro-2-fluorobenzene was unsuccessful.

Table 3 summarizes the rate constants measured at 100 °C for the transformation of **2**, **3**, **28**, **30**, and **31** to product **14** and the corresponding organic byproduct most likely generated from *o*-benzyne degradation (Scheme 8). Unfortunately, we were unable to obtain a linear, free-energy relationship observed from the Hammett correlation using the substituent constants σ_m (*meta*-substituent constants, see Supporting Information).³² For clarity, our *meta*-substituent constant corresponds to the X substituent with respect to the $\text{Ti}-\text{C}_{\text{aryl}}$ bond. From our rate constants, however, it can be inferred that the more electron-donating substituent (i.e., CH_3) resulted in a faster C–F cleavage rate, while the more electron-withdrawing (i.e., OCH_3 , F, CF_3) slowed the rate of β -fluoride elimination. The sterics (provided by X) do not appear to be playing a significantly large role in this type of transformation since the rate for C–F activation of **4** to **14** ($k_{\text{average}} = 1.38(13) \times 10^{-5} \text{ s}^{-1}$) is not significantly different from the conversion of **3** to **14** ($k_{\text{average}} = 1.1(5) \times 10^{-5} \text{ s}^{-1}$). The slowing of the rate inflicted by the electron withdrawing substituent X implies a positive charge buildup at the arylfluoride moiety for the activated complex **2-TS**.

Previous work had demonstrated that complex **13** can slowly equilibrate back to intermediate **A** with a $k_{\text{average}} = 1.2(2) \times 10^{-5} \text{ s}^{-1}$ at 95 °C, and activation parameters $\Delta H^\ddagger = 31(16) \text{ kcal/mol}$ and $\Delta S^\ddagger = 3(9) \text{ cal/molK}^{-1}$ (ΔG^\ddagger value of $\sim 30.1 \text{ kcal/mol}$ at 298.15 K).¹¹ Since C–F activation in intermediates such as **2–11** generally occurs at temperatures above 90 °C, we inquired whether a pre-equilibrium step, to form an intermediate such as **A**, preceded β -fluoride elimination. In accordance with Scheme 10, thermolysis of **13** in FC_6D_5 at 100 °C does yield $(\text{PNP})\text{Ti}=\text{CD}^t\text{Bu}(\text{F})$ (**14-d₁**), thus consistent with sequential C–H and C–F bond activation reactions involving intermediates **A** and **2-d₅**, respectively. This also supports the notion that the barrier leading to **A** should at least approach or exceed the barrier to formation of **14** from **2** ($\geq 30.1 \text{ kcal/mol}$ at 298.15 K, *vide supra*). By increasing the α -hydrogen abstraction barrier,

(32) Issaacs, N. S. *Physical Organic Chemistry*; ELBS, Longman: Avon, U.K., 1987.

Scheme 10. Cyclic Dehydrofluorination of Fluorobenzene Applying Precursor 1 and FC₆H₅ as the Model Reagent**Scheme 11. Salt Metathesis to Prepare the Halide Derivatives 32 and 33 Using Precursor 12^a**

β -fluoride elimination is then overcome in the case of the alkylidene synthon, **13**, thus preventing the isolation of an intermediate such as **2**. To address if **2** converts back to **A** by an α -hydrogen abstraction and under the conditions leading to C–F activation, complex **2-d₅** was independently prepared from **1** and FC₆D₅ and subsequently thermolyzed in FC₆H₅ at 100 °C over 7 days. No proton incorporation into the α -alkylidene carbon of the product **14-d₁** (formed quantitatively) was observed when judged by ¹H NMR spectroscopy, hence implying that **2** does not pre-equilibrate to **A** under those conditions (Scheme 9). Therefore, the barrier for β -fluoride elimination must be lower than the α -hydrogen abstraction barrier in the reverse direction, **2** \rightarrow **A**. Despite us not knowing a relative ground state energy for **2** (with respect to **1**), our experimental data suggest that the reverse barrier, **2** \rightarrow **A**, must be well above \sim 30 kcal/mol.

To further elucidate the role of the fluoride in the bond-breaking event, the thermolysis of **27** was explored with the idea of promoting a β -methoxide elimination.^{33,34} Complex **27** is conveniently prepared via treatment of **1** with neat anisole (*vide supra*),¹³ but heating solutions of **27** at 90 °C over 48 h in toluene resulted in a myriad of unidentifiable products. Therefore, the fluoride group is essential in promoting the β -elimination step in these types of systems.

2h. Cyclic Dehydrofluorination of Fluorobenzene. Complex **14** or **26** can be readily converted back to **1** and **15** in 88% or

70% isolated yield, respectively, by transmetalation with LiCH₂tBu³⁵ or LiCH₂SiMe₃, to formally close the cycle for the dehydrofluorination of HAR_F and HAL_F. Given that formation of **14** and **26** is virtually quantitative for HAR_F and HAL_F, the overall yield for the recycling of titanium essentially depends on the last step of the cycle. Since the latter reaction is also quantitative by ¹H and ³¹P NMR spectroscopy, the cycle for dehydrofluorination is quantitative overall. Scheme 10 displays the cycle for dehydrofluorination of HFCs using precursor **1** and fluorobenzene as our model substrate. As established from this work, the formation of intermediate **A** from **1** is rate-determining along the C–H activation of fluorobenzene to form the kinetic product **2**. Thermolysis of **2** resulted in Ti–F bond formation concomitant with formation of benzyne and **14**. The use of durene as a trap along the formation of **14** from **2** is not imperative, given the ability of benzyne to undergo other decomposition pathways that do not appear to involve the degradation of **2** or **14**.^{24–26}

The propensity of complex **1** to dehydrofluorinate substrates such as HAR_F and HAL_F in a stepwise fashion, and under relatively mild conditions, led us to examine the possibility of carrying out catalytic reactions using an excess of an alkylating reagent in the presence of **1** and fluorobenzene at 100 °C. Unfortunately, the tendency of nucleophiles such as Zn(CH₂tBu)₂,³⁵ Mg(CH₂tBu)₂,³⁵ ClMg(CH₂tBu), and LiCH₂tBu³⁵ to react preferentially with fluorobenzene over **14** (or not react with **14** at all) under these conditions has prevented the use of **1** as a dehydrofluorination catalyst. In fact, an attempt to replace the fluoride in **14** with a hydride, by using neat Et₃SiH, did not result in a reaction, even under forcing conditions (>75 °C over 72 h). Likewise, the catalytic dehydrofluorination of HAL_F is also unlikely since independent treatment of compound **1** with terminal olefins (a byproduct from the dehydrofluorination of HAL_F) resulted in a mixture of products, which we have been unable to characterize.

2i. Reactivity of Complex 1 with Haloarene Derivatives.

Treatment of **1** or **15** with other haloarenes, such as PhX (X = Cl and Br), resulted in complicated mixtures when assayed by ³¹P NMR spectroscopy. To assess whether putative products such as (PNP)Ti=CHtBu(Cl) (**32**) or (PNP)Ti=CHtBu(Br) (**33**) were formed in these mixtures, they were prepared independently using salt metathesis of **12** with excess MgX₂ (X = Cl and Br) in THF. Accordingly, treatment of **12** with MgX₂ cleanly produced the halide derivatives **32** and **33** in 68% and 88% yield, respectively (Scheme 11). Table 2 displays salient spectroscopic features for these two complexes. Unlike the alkylidene precursor reported by Legzdins and co-workers, Cp*W(NO)(CH₂tBu)₂,^{15a} we were unable to isolate any aryl C–H activated products from the reaction of PhX (X = Cl and Br) with **1**. Although a myriad of products are observed, formation of **32** and **33** is evident, albeit in low concentrations, when judged by ³¹P NMR spectroscopy and in comparison with independently prepared samples (*vide supra*). This result suggests some formation of an alkylidene-arylhalide such as (PNP)Ti=CHtBu(*o*-XC₆H₄), although other explanations are possible (Scheme 11). Our capacity to generate and crystallize the alkylidene-halide derivatives **32** and **33** allowed us to closely study the orientation of the neopentylidene α -hydrogen. As depicted in Figure 3, the alkylidene hydrogen is pointing away from the Cl or Br ligand. Analogously to **14**, no H-bonding or striking differences are observed in **32** and **33**.

2j. Proposed Overall Reaction Coordinate for Sequential C–H and C–F Activation. Theoretical studies reported earlier for the C–H activation of arenes by a transient titanium

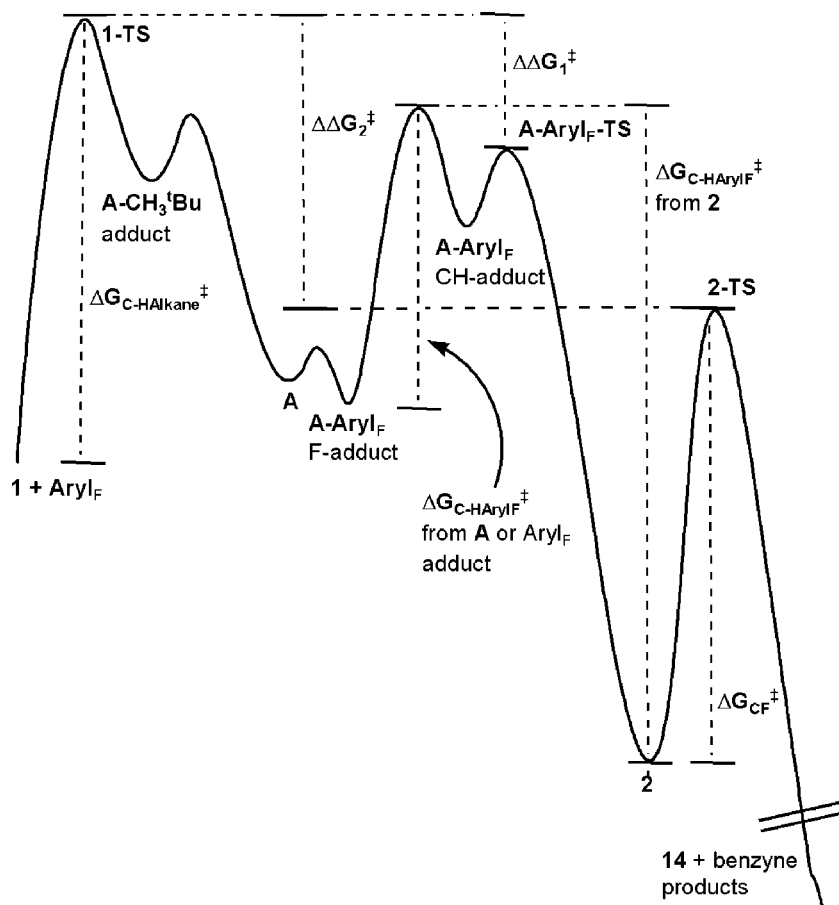


Figure 6. Proposed reaction coordinate for the C–H and C–F activation steps along the $1 \rightarrow 14$ conversion.

alkylidyne,^{10,11} as well as kinetic analysis described in this work, clearly support the idea of compound **1** undergoing an initial α -hydrogen abstraction, with this step being overall rate-determining ($\Delta G_{\text{C-HAlkane}}^{\ddagger}$) in the C–H activation sequence to produce **2**. Such an event likely occurs by the alkane adduct (PNP)Ti \equiv C^tBu(CH₃^tBu) (**A-CH₃^tBu**), eventually undergoing entropy-assisted loss of CH₃^tBu to yield the transient and reactive alkylidyne **A** (Figure 6). As observed in the benzene C–H activation reaction coordinate, theoretical studies suggest that **1-TS** should be representative of a “late” transition state (CH₃^tBu nearly formed at **1-TS**) with respect to formation of **A**.¹¹ Our kinetic studies involving the C–H activation of fluorobenzene suggest a similar pathway along formation of **A**. In the case presented here, the fluorinated substrate (i.e., FC₆H₅) would bind to the four-coordinate Lewis acidic titanium center to generate the F-coordinated fluorobenzene adduct (PNP)Ti \equiv C^tBu(FC₆H₅) (**A-Aryl_F**, F-bound).¹³ Binding of the HAR_F should not stabilize the (PNP)Ti \equiv C^tBu scaffold significantly, since coordination of a much stronger Lewis base such as pyridine has been computed to be virtually barrierless and not exceedingly exergonic with respect to **A**.³⁶ Therefore, **A** and **A-Aryl_F** (F-bound) should be virtually isothermal. Our

speculation is further corroborated by the minor selectivity of **A** toward the C–H bond of FC₆H₅ versus C₆H₆, to form **2** versus **13** in a 3:2 ratio, respectively (*vide supra*). Likewise, we do not observe any significant preference in the dehydrofluorination competition reaction of **1** with 1-fluorohexane versus FC₆H₅. Putative **A-Aryl_F** (F-bound), however, does not necessarily have to lie along the reaction coordinate to **2**. In addition, a similar C–H bond rupture selectivity is observed in anisole, thus supporting the idea of formation of an adduct along the C–H activation sequence. Whether intermediate **A-Aryl_F** (F-bound) undergoes rearrangement to a C–H bound σ -adduct or a π -complex is uncertain at this point. Regardless, rearrangement of **A-Aryl_F** (F-bound) to the Aryl_F, **A-Aryl_F** (CH-adduct), has an energy penalty $\Delta G_{\text{C-HAryl}_F}^{\ddagger}$ that most likely arises from an entropic component as well as a steric constraint in the F-bound versus the more sterically crowded CH-bound hydrofluoroarene adduct (Figure 6). As noted in the C–H activation of benzene, intermediate **A-Aryl_F** (CH-adduct) should possess an “early” transition state (with the hydrofluoroaryl C–H bond essentially not broken, **A-Aryl_F-TS**) with respect to formation of **2**. However, in Figure 6 we are speculating that $\Delta G_{\text{C-HAryl}_F}^{\ddagger}$ (FC₆H₅ binding to **A**) is rate-determining along the C–H bond breaking

(33) For some examples on CH-activation/ β -alkoxide elimination: (a) Bradley, C. A.; Veiros, L. F.; Pun, D.; Lobkovsky, E.; Keresztes, I.; Chirik, P. J. *J. Am. Chem. Soc.* **2006**, *128*, 16600. (b) Buchwald, S. L.; Nielsen, R. B.; Dewan, J. C. *Organometallics* **1988**, *7*, 2324. (c) Karlsson, S.; Halberg, A.; Gronowitz, S. *J. Organomet. Chem.* **1991**, *403*, 133. (d) Rousset, C. J.; Swanson, D. R.; Lamaty, F.; Negishi, E. *Tetrahedron Lett.* **1989**, *30*, 5105. (e) Ito, H.; Taguchi, T.; Hanzawa, Y. *Tetrahedron Lett.* **1992**, *33*, 1295. (f) Ito, H.; Taguchi, T.; Hanzawa, Y. *Tetrahedron Lett.* **1992**, *33*, 7873. (g) Morken, J. P.; Didiuk, M. T.; Hoveyda, A. H. *J. Am. Chem. Soc.* **1993**, *115*, 6997.

(34) For some examples of β -alkoxide elimination in early-transition-metal chemistry: (a) Takahashi, T.; Suzuki, N.; Kageyama, M.; Kondakov, D. Y.; Hara, R. *Tetrahedron Lett.* **1993**, *34*, 4811. (b) Suzuki, N.; Kondakov, D. Y.; Kageyama, M.; Kotora, M.; Hara, R.; Takahashi, T. *Tetrahedron* **1995**, *51*, 4519. (c) Hara, R.; Ura, Y.; Huo, S.; Kasai, K.; Suzuki, N.; Takahashi, T. *Inorg. Chim. Acta* **2000**, *300*, 741. (d) Ito, H.; Nakamura, T.; Taguchi, T.; Hanzawa, Y. *Tetrahedron* **1995**, *51*, 4507.

(35) Schrock, R. R.; Fellmann, J. D. *J. Am. Chem. Soc.* **1978**, *100*, 3359.

(36) Bailey, B. C.; Fan, H.; Huffman, J. C.; Baik, M.-H.; Mindiola, D. J. *J. Am. Chem. Soc.* **2006**, *128*, 6798.

step. Synthesis of *o*-*d*₁-fluorobenzene and intramolecular KIE measurements could give us some insight into this mechanistic feature; however, we have been unable to obtain interpretable data from these experiments.³⁷ The preference for the activation of the HAr_F versus the aliphatic C–H bond (from CH₃^tBu) is clearly reflected by the asymmetry in the reaction profile, $\Delta\Delta G_1^\ddagger$. The reverse reaction, formation of HAr_F and **A** or **A-Aryl_F** from precursor **2**, is thermodynamically inaccessible due to the high barrier $\Delta G_{C-HAr_{Y}F}$ associated with this process. Intuitively, the barrier $\Delta G_{C-HAr_{Y}F}$ from **2** must be greater than ΔG_{C-F}^\ddagger since **2** does not equilibrate with **A** or adduct **A-Aryl_F** under forcing conditions. Therefore, aryl fluoride ring-walking via intermediate **A** (or adduct) is unlikely given the high barrier, $\Delta G_{C-HAr_{Y}F}$, that complex **2** needs to overcome. Although we have experimentally demonstrated that ring-walking is feasible at temperatures > 100 °C, this pathway seems irrelevant to the mild conditions applied for the **1** → **2** transformation. Therefore, complex **2** must be the only regioisomer produced, and intramolecular C–F activation results in formation of **14** and *o*-benzynes. Traversing the high barrier ΔG_{C-F}^\ddagger to produce **14** and *o*-benzyne is compensated by formation of the strong Ti–F bond, thus placing compound **14** exceedingly lower in energy than **2** and even further below precursor **1**. As indicated in Figure 6, complex **2** β-fluoride eliminates, mostly likely concertedly via **2-TS**. Our experimental data suggest the presence of a significant Ti–F interaction and positive charge buildup at the Ar_F ring of **2-TS**, thus consistent with a late-activated complex with respect to formation of **14** (refer to Table 1 and Scheme 8). The idea of a benzyne intermediate, (PNP)Ti=CH^tBu(F)(η²-C₆H₄), being generated along formation of **14** is unlikely for two reasons. First, one would expect reactivity of this dienophile with the adjacent alkylidene motif. Second, the coordinatively saturated environment about the Ti(IV) center is unlikely, especially with the sterically imposing PNP and neopentylidene ancillaries.

Replacing ^tBu with SiMe₃ in precursor **1**, namely, complex **15**, brings about significant consequences to the reaction profile displayed in Figure 6. One clear illustration to this effect is that $\Delta\Delta G_2^\ddagger$ must be greater for the dehydrofluorination reaction of HAr_F by **15**. In fact, this barrier is much greater than in **1** to the extent that $\Delta\Delta G_2^\ddagger$ overcomes $\Delta G_{C-HAr_{Y}F}^\ddagger$ with respect to **A** or its F-bound hydrofluoroarene adduct. Such a contrast is primarily due to the greater $\Delta G_{C-Halkane}^\ddagger$ needed when traversing from **15** to transient alkylidyne **B**, hence preventing kinetic products such as **16**–**25** from being cleanly isolated under milder conditions (i.e., 60 °C).

3. Conclusions

Although dehydrofluorination has occurred via a number of metal complexes, a well-defined early transition metal system that could activate both HAr_F and HAl_F by a similar mechanism was previously not known. We were able to discern the mechanistic pathway, since the isolable intermediates can be characterized and studied for the subsequent step: β-fluoride elimination. Under this premise, we have illustrated that the transient titanium alkylidynes **A** and **B** participate in stepwise C–H/C–F bond activation to form the titanium fluoride complexes **14** and **26** under relatively mild conditions. Compound **1** selectively activates the *ortho* C–H bond to the fluorine moiety in an array of HAr_F to produce a series of alkylidene-fluoroaryl complexes

2–**11**. Compounds **2**–**11** are all kinetic products in the overall dehydrofluorination pathway since their thermolysis results in the formation of the alkylidene-fluoride **14** via β-fluoride elimination and formation of benzyne. Trapping of the organic byproduct, benzyne, was achieved by heating **11** in neat durene at 100 °C to form the [6+2]-cycloaddition product 5,6,7,8-tetrafluoro-1,4-dihydro-2,3,9,10-tetramethyl-1,4-ethenonaphthalene. Another titanium alkylidene derivative, **15**, dehydrofluorinated the same series of HAr_F at higher temperatures to produce the alkylidene-fluoride complex **26**, also via C–H bond activation and intramolecular C–F bond cleavage. Of great importance was the dehydrofluorination of 1-fluorohexane by complexes **1** and **15** to produce 1-hexene and **14** and **26**, respectively. Isolation of the organic byproduct, 1-hexene, allowed us to propose the same dehydrofluorination pathway for both the HAr_F and HAl_F: 1,2-CH bond addition followed by β-fluoride elimination.

4. Experimental Section

General Procedures. Unless otherwise stated, all operations were performed in a M. Braun Laboratory Master double-drybox under an atmosphere of purified nitrogen or using high-vacuum standard Schlenk techniques under an argon atmosphere. Anhydrous *n*-hexane, pentane, toluene, and benzene were purchased from Aldrich in Sure-Seal reservoirs (18 L) and dried by passage through two columns of activated alumina and a Q-5 column. Diethyl ether was dried by passage through a column of activated alumina. THF was distilled, under nitrogen, from purple sodium benzophenone ketyl and stored under sodium metal. Distilled THF was transferred under vacuum into bombs before being pumped into a drybox. HAr_F and HAl_F were dried via addition of CaH₂ and stirring for 3 days; more CaH₂ was added and stirred for one more day. The HAr_F and HAl_F were vacuum transferred under inert atmosphere. The solvent was then passed through a column of alumina to obtain dry HAr_F and HAl_F. C₆D₆ was purchased from Cambridge Isotope Laboratory (CIL), degassed, and transferred to 4 Å molecular sieves. Celite, alumina, and 4 Å molecular sieves were activated under vacuum overnight at 200 °C. Li(PNP) (PNP = N[2-P(CHMe₂)₂-4-methylphenyl]₂)[−],¹⁶ LiCH₂^tBu,³⁵ LiCD₂^tBu,³⁵ Mg(*p*-FC₆H₄)₂,³⁸ (PNP)Ti=CH^tBu(CH₂^tBu)(**1**),¹⁰ (PNP)Ti=CH^tBu(*o*-FC₆H₄)(**2**),¹³ (PNP)Ti=CH^tBu(*o,m*-F₂C₆H₃)(**3**),¹³ (PNP)Ti=CH^tBu(*o,m'*-F₂C₆H₃)(**4**),¹³ (PNP)Ti=CH^tBu(OTf)(**12**),^{10,11} (PNP)Ti=CH^tBu(C₆H₅)(**13**),^{10,11} (PNP)Ti=CH^t(SiMe₃)(CH₂SiMe₃)(**15**)^{10,11} and (PNP)Ti=CH^tBu(*o*-CH₂OC₆H₄)(**27**)¹³ were prepared according to literature procedures. All other chemical were used as received. CHN analyses were performed by Midwest Microlabs, Indianapolis, IN. ¹H, ¹³C, and ³¹P NMR spectra were recorded on Varian 400 or 300 MHz NMR spectrometers. ¹H and ¹³C NMR are reported with reference to solvent resonances (residual C₆D₅H in C₆D₆, 7.16 and 128.0 ppm). ¹⁹F NMR chemical shifts are reported with respect to external HOCOFC₃ (−78.5 ppm). ³¹P NMR chemical shifts are reported with respect to external H₃PO₄ (aqueous solution, 0.0 ppm). X-ray diffraction data were collected on an APEX II Kappa Duo (Bruker) system under a stream of N₂(g) at low temperatures.

General Preparation of Complexes 2–11 from 1. In a vial compound **1** [100 mg, 0.162 mmol] was dissolved in neat HAr_F (1 mL) and stirred at 25 °C for 20 h. The green solution changed to red and was dried *in vacuo*. Pentane (10 mL) was added and the compound was filtered. After filtration the filtrate was dried *in vacuo* to remove any excess and remaining HAr_F. Pentane (6 mL) was used to extract the product, the solution filtered, and the filtrate reduced in volume (~1 mL) *in vacuo* and cooled to −35 °C to afford **2**–**11** as red solids. For spectroscopic details please refer to the Supporting Information.

General Preparation of Complexes 9 and 11 from 12. Diethyl ether (2 mL) was added to the HAr_F (48 μL) and cooled (N₂(l)) in

(37) We have been unable to obtain pure and anhydrous *o*-*d*₁-fluorobenzene in order to obtain reliable KIE data. Bak, B. *J. Org. Chem.* **1956**, *21*, 797.

a cold well for 30 min. Diethyl ether (2 mL) was also added to *n*-butyllithium (0.27 mL, 1.6 M in hexanes) and cooled (N_2 (l)) in a cold well for 30 min. Prior to addition, the *n*-butyllithium was allowed to warm slightly and then added dropwise to a cold solution of the HA_rF in the cold well. After 30 min in the cold well the solution was used. **12** [300 mg, 0.431 mmol] was dissolved in pentane and cooled N_2 (l) in a cold well for 30 min and added dropwise to the cold stirring solution of $Li(F_3C_6)$ or $Li(o,o',m,m'-F_4C_6H)$. The red suspension warmed slowly over a period of 2 h and then was left to stir overnight (12 h). The red suspension was then dried *in vacuo*. Pentane (10 mL) was used to extract the complex, and the solution was filtered. The filtrate was reduced in volume *in vacuo* (2 mL) and cooled to $-35^\circ C$ to afford **9** or **11**. For complete experimental and spectroscopic details please refer to the Supporting Information.

General Preparation for Complex 14 from Thermolysis of 2–11. In a J. Young tube was dissolved **2–11** [100 mg] in benzene at room temperature. The solution was heated to $100^\circ C$ for 72 h. The solution gradually changed color from red to red-brown, upon which volatiles were removed *in vacuo*. The residue was extracted with pentane (10 mL) and filtered. The filtrate was reduced in volume under reduced pressure (2 mL) and then cooled to $-35^\circ C$ to give red-brown crystals of **14** in quantitative yields by ^{31}P NMR spectroscopy. Refer to Supporting Information for experimental and spectroscopic details.

Benzynes Trapping Reaction. In a J. Young tube complex **11** [100 mg, 0.280 mmol] was added, and to this solid was introduced durene [100 mg, 0.746 mmol]. The solids were placed in a $100^\circ C$ oil bath for one week. The J. Young tube was brought into the glovebox, and to this was added C_6D_6 (0.7 mL). The volatiles were then vacuum transferred and inspected by multinuclear NMR spectroscopy and GC-MS. For the Diels–Alder product 5,6,7,8-tetrafluoro-1,4-dihydro-2,3,9,10-tetramethyl-1,4-ethenonaphthalene: 1H NMR ($23^\circ C$, 399.8 MHz, C_6D_6): 4.38 (br s, 2 H), 1.58 (s, 12H). ^{19}F NMR ($23^\circ C$, C_6D_6): δ -165.2 (s, 2H), -152.9 (s, 2H). GC-MS (*m/z*): 282.

General C–H/C–F Activation Reactions to Form Complexes 16–25. In a J. Young tube compound **15** [100 mg, 0.154 mmol] was dissolved in neat HA_rF (1 mL). The reaction was heated at $90^\circ C$ for 1–48 h, causing a color change from dark green to a deep reddish-brown. The product was extracted with pentane (10 mL), dried *in vacuo*, and redissolved in pentane. The solution was filtered, and the filtrate was reduced in volume (2 mL) *in vacuo* and cooled to $-35^\circ C$ to afford complexes **16–25**. Formation of **26** was evident in some cases. See Supporting Information for more reaction and spectroscopic details.

General C–H/C–F Activation Reactions to Form Complex 26. In a J. Young tube compound **15** [100 mg, 0.154 mmol] was dissolved in neat HA_rF (1 mL). The reaction was heated at $100^\circ C$ for 48–96 h, causing a color change from dark green to a deep reddish-brown. The product was extracted with pentane (10 mL), dried *in vacuo*, and redissolved in pentane. The solution was filtered, and the filtrate was reduced in volume (2 mL) *in vacuo* and cooled to $-35^\circ C$ to afford **26**. See Supporting Information for more reaction and spectroscopic details.

Preparation of (PNP)Ti=CH'Bu(*p*-FC₆H₄) (29). In a vial complex **12** [115 mg, 0.165 mmol] was dissolved in toluene and cooled to $-35^\circ C$. In a vial $Mg(p-FC_6H_4)_2$ [35 mg, 0.165 mmol] was dissolved in toluene and cooled to $-35^\circ C$ and added to a stirring solution of **12**. After 24 h the red suspension was concentrated *in vacuo*, pentane was added (10 mL), and the solution was filtered through a bed of Celite to remove $Mg(p-FC_6H_4)(OTf)$. The red filtrate was then concentrated (2 mL) and cooled to $-35^\circ C$ to obtain red crystals of **29** [96 mg, 0.149 mmol, 90% yield]. 1H NMR ($23^\circ C$, 399.8 MHz, C_6D_6): δ 8.02 (s, 1H, *p*-FC₆H₄), 7.39 (d, 1H, (PNP)Ti=CH'Bu), 7.24 (m, 1H, *p*-FC₆H₄), 7.19 (d, 1H, *p*-FC₆H₄), 7.04–6.97 (m, 4H, C_6H_3), 6.87(m, 1H, C_6H_3), 6.84

(m, 1H, C_6H_3), 6.77 (m, 1H, *p*-FC₆H₄), 2.54 (septet, 1H, CHMe₂), 2.44 (septet, 1H, CHMe₂), 2.21 (septet, 1H, CHMe₂), 2.19 (s, 3H, C_6H_3 -Me), 2.12 (s, 3H, C_6H_3 -Me), 2.07 (septet, 1H, CHMe₂), 1.55–1.36 (m, 6H, CHMe₂), 1.30–1.10 (m, 12H, CHMe₂), 1.03 (s, 9H, (PNP)Ti=CH'Bu), 1.00 (m, 3H, CHMe₂), 0.68–0.60 (m, 3H, CHMe₂). ^{13}C NMR ($23^\circ C$, 100.6 MHz, C_6D_6): δ 275.3 (s, 1C, (PNP)Ti=CH'Bu(*p*-FC₆H₄)), 173.2 (s, 1C, *p*-FC₆H₄), 172.6 (s, 1C, *p*-FC₆H₄), 167.3 (s, 1C, *p*-FC₆H₄), 165.1 (s, 1C, *p*-FC₆H₄), 158.7 (d, 1C, C_6H_3), 153.2(d, 1C, C_6H_3), 139.2 (s, 1C, *p*-FC₆H₄), 133.2 (s, 1C, C_6H_3), 132.6 (s, 1C, C_6H_3), 131.6 (s, 1C, C_6H_3), 130.1 (s, 1C, C_6H_3), 129.0 (d, 1C, C_6H_3), 127.1 (d, 1C, C_6H_3), 123.1 (s, 1C, C_6H_3), 121.4 (d, 1C, C_6H_3), 119.0 (d, 1C, C_6H_3), 116.0 (d, 1C, C_6H_3), 49.0 (s, 1C, (PNP)Ti=CH'Bu), 32.6 (s, 1C, (PNP)Ti=CH'Bu), 25.2 (d, 1C, CHMe₂), 24.9 (d, 1C, CHMe₂), 23.6 (d, 1C, CHMe₂), 23.0 (d, 1C, CHMe₂), 21.0 (s, 1C, C_6H_3 -Me), 20.8 (s, 1C, CHMe₂), 20.6 (s, 1C, C_6H_3 -Me), 20.0 (s, 1C, CHMe₂), 19.6 (d, 1C, CHMe₂), 18.9 (d, 1C, CHMe₂), 18.3 (s, 1C, CHMe₂), 18.2 (d, 1C, CHMe₂), 17.8 (d, 1C, CHMe₂), 16.4 (d, 1C, CHMe₂). ^{31}P NMR ($23^\circ C$, 121.5 MHz, C_6D_6): δ 23.2 (d, $^2J_{P-P}$ = 42 Hz), 31.0 (d, $^2J_{P-P}$ = 42 Hz). ^{19}F NMR ($23^\circ C$, C_6D_6): -91.5 (br s, 1F, *p*-FC₆H₄).

Preparation of (PNP)Ti=CH'Bu(*o*-F,*m*-CH₃C₆H₃) (30). In a vial **1** [100 mg, 0.162 mmol] was dissolved in neat 2-fluorotoluene (~0.5 mL) and stirred for 12 h at room temperature. The green solution changed to red. The red solution was extracted with pentane (10 mL) and dried *in vacuo*. Pentane (10 mL) was added and the solution was filtered. The filtrate was again dried *in vacuo* to remove any excess 2-fluorotoluene. Pentane (6 mL) was added, and the solution was reduced in volume (2 mL) *in vacuo* and cooled to $-35^\circ C$ to afford **30** [84 mg, 0.236 mmol, 79% yield] as a red powder (5% impurity present in sample by ^{31}P NMR). 1H NMR ($23^\circ C$, 399.8 MHz, C_6D_6): δ 7.39 (s, 1H, (PNP)Ti=CH'Bu(*o*-F,*m*-CH₃C₆H₃)), 7.26–7.20 (m, 2H, C_6H_3), 7.03 (dd, 1H, C_6H_3), 7.00–6.89 (m, 3H, C_6H_3 and (*o*-F,*m*-CH₃C₆H₃)), 6.83 (dd, 2H, C_6H_3), 6.76 (s, 1H, *o*-F,*m*-CH₃C₆H₃), 2.54 (septet, 2H, CHMe₂), 2.54 (septet, 1H, CHMe₂), 2.46 (septet, 1H, CHMe₂), 2.25 (septet, 1H, CHMe₂), 2.20 (*o*-F,*m*-CH₃C₆H₃), 2.12 (s, 3H, C_6H_3 -Me), 2.04 (s, 3H, C_6H_3 -Me), 2.05 (m, 2H, CHMe₂), 1.98 (septet, 1H, CHMe₂), 1.53 (dd, 3H, CHMe₂), 1.40 (dd, 3H, CHMe₂), 1.28–1.15 (m, 6H, CHMe₂), 1.13–1.00 (m, 6H, CHMe₂), 1.04 (s, 9H, (PNP)Ti=CH'Bu(*o*-F,*m*-CH₃C₆H₃)), 0.97–0.86 (m, 6H, CH Me₂), 0.65 (dd, 3H, CH Me₂). ^{13}C NMR ($23^\circ C$, 100.6 MHz, C_6D_6): δ 274.4 (s, 1C, (PNP)Ti=CH'Bu(*o*-F,*m*-CH₃C₆H₃)), 173.2 (*o*-F,*m*-CH₃C₆H₃), 163.0 (*o*-F,*m*-CH₃C₆H₃), 160.6 (*o*-F,*m*-CH₃C₆H₃), 158.7 (C_6H_3), 153.3 (C_6H_3), 133.2 (C_6H_3), 132.7 (*o*-F, *m*-CH₃C₆H₃), 131.6 (C_6H_3), 131.5 (*o*-F,*m*-CH₃C₆H₃), 130.4 (*o*-F,*m*-CH₃C₆H₃), 130.0 (C_6H_3), 127.1 (C_6H_3), 124.8 (C_6H_3), 123.9 (C_6H_3), 123.2 (C_6H_3), 118.9 (C_6H_3), 116.1 (C_6H_3), 115.1 (C_6H_3), 48.9 ((PNP)Ti=CH'Bu(*o*-F,*m*-CH₃-C₆H₃)), 32.6 ((PNP)Ti=CH'Bu(*o*-F,*m*-CH₃C₆H₃)), 25.3 (C_6H_3 -Me), 25.1 (C_6H_3 -Me), 23.7 (CHMe₂), 23.3 (CHMe₂), 21.0 (CHMe₂), 20.7 (CHMe₂), 20.6 (CHMe₂), 20.0 (CHMe₂), 19.5 (d, CHMe₂), 19.0 (d, CHMe₂), 18.3 (CHMe₂), 18.1 (CHMe₂), 17.6 (d, CHMe₂), 16.4 (d, CHMe₂). ^{31}P NMR ($23^\circ C$, 121.5 MHz, C_6D_6): δ 30.6 (dd, $^2J_{P-P}$ = 32 Hz), 22.8 (dd, $^2J_{P-P}$ = 32 Hz). ^{19}F NMR ($23^\circ C$, C_6D_6): δ -117.9 (s, 1F, (PNP)Ti=CH'Bu(*o*-F,*m*-CH₃C₆H₃)). The 5% impurity remains after the conversion of **30** to **14**.

Preparation of (PNP)Ti=CH'Bu(*o*-F,*m*-CF₃C₆H₃) (31). In a vial (PNP)Ti=CH'Bu(CH₂Bu) (**1**) [200 mg, 0.323 mmol] was dissolved in neat 2-fluorobenzotrifluoride (~0.5 mL) and stirred for 12 h at room temperature. The green solution changed to red. The red solution was extracted with pentane (10 mL) and dried *in vacuo*. Pentane (10 mL) was added and the compound was filtered. The filtrate was again dried *in vacuo* to remove any excess 2-fluorobenzotrifluoride. Pentane (6 mL) was added, and the solution was reduced in volume (2 mL) *in vacuo* and cooled to $-35^\circ C$ to afford **31** [209 mg, 0.294 mmol, 90% yield] as a red

powder (8% impurity present in sample by ^{31}P NMR). ^1H NMR (23 °C, 399.8 MHz, C_6D_6): δ 7.39 (s, 1H, (PNP)Ti=CH'Bu(*o*-F,*m*-CF₃C₆H₃)), 7.24 (m, 1H, (*o*-F,*m*-CF₃C₆H₃)) 7.22 (d, 1H, C₆H₃), 7.04 (m, 1H, (*o*-F,*m*-CF₃C₆H₃)), 6.97 (d, 2H, C₆H₃), 6.90 (d, 2H, C₆H₃), 6.84 (m, 2H, C₆H₃ and (*o*-F,*m*-CF₃C₆H₃)), 2.56–2.42 (m, 2H, CHMe₂), 2.25 (m, 2H, C HMe₂), 2.20 (s, 3H, C₆H₃-Me), 2.11 (s, 3H, C₆H₃-Me), 1.98 (septet, 1H, CHMe₂), 1.52 (dd, 3H, CHMe₂), 1.40 (dd, 3H, CHMe₂), 1.26–1.10 (m, 9H, CHMe₂), 1.04 (s, 9H, (PNP)Ti=CH'Bu(*o*-F,*m*-CF₃C₆H₃)), 1.01–0.88 (m, 6H, CHMe₂), 0.65 (dd, 3H, CHMe₂). ^{13}C NMR (23 °C, 100.6 MHz, C_6D_6): δ 278.2 (s, 1C, (PNP)Ti=CH'Bu(*o*-F,*m*-CF₃C₆H₃)), 172.0 (*o*-F,*m*-CF₃C₆H₃)164.2 (*o*-F,*m*-CF₃C₆H₃), 161.8 (*o*-F,*m*-CF₃C₆H₃), 161.1 (*o*-F,*m*-CF₃C₆H₃), 158.7 (*o*-F,*m*-CF₃C₆H₃), 158.2 (C₆H₃), 152.2 (C₆H₃), 144.6 (*o*-F,*m*-CF₃C₆H₃), 133.9 (C₆H₃), 133.2 (C₆H₃), 132.4 (C₆H₃), 131.5 (C₆H₃), 127.1 (C₆H₃), 125.5 (C₆H₃), 123.2 (C₆H₃), 120.4 (C₆H₃), 119.4 (C₆H₃), 115.9 (C₆H₃), 49.3 ((PNP)Ti=CH'Bu(*o*-F,*m*-CF₃C₆H₃)), 32.4 ((PNP)Ti=CH'Bu(*o*-F,*m*-CF₃C₆H₃)), 25.3 (C₆H₃-Me), 25.0 (C₆H₃-Me), 24.2 (CHMe₂), 24.0 (CHMe₂), 23.5 (CHMe₂), 23.2 (CHMe₂), 20.9 (CHMe₂), 20.6 (CHMe₂), 19.9 (d, CHMe₂), 19.3 (d, CHMe₂), 18.8 (CHMe₂), 18.2 (CHMe₂), 17.7 (d, CHMe₂), 16.4 (d, CHMe₂). ^{31}P NMR (23 °C, 121.5 MHz, C_6D_6): δ 31.1 (d, $^2J_{\text{P-P}} = 32$ Hz), 23.2 (d, $^2J_{\text{P-P}} = 32$ Hz). ^{19}F NMR (23 °C, C_6D_6): δ -61.8 (s, 3F, (PNP)Ti=CH'Bu(*o*-F,*m*-C F₃C₆H₃)), -114.6 (s, 1F, (PNP)Ti=CH'Bu(*o*-F,*m*-CF₃C₆H₃)). The 8% impurity remains after the conversion of **31** to **14**.

General Preparation of Complexes 32 and 33. In a vial, **12** [122 mg, 0.175 mmol] was dissolved in THF and cooled to -35 °C. MgX₂ [0.175 mmol] (as a solid) was added to the stirring solution of **12**, and the mixture was stirred overnight. The THF was removed *in vacuo*, the resulting powder was dissolved in pentane (10 mL), and the solution was filtered through a bed of Celite. The red filtrate was reduced in volume (~2 mL) *in vacuo* and cooled to -35 °C to afford **32** and **33** as red-brown plates (conversion to **32** and **33** was quantitative by ^{31}P NMR spectroscopy). Refer to Supporting Information for complete spectroscopic details.

General Preparation for the C–H Activation Competition Reactions. In a vial **1** [100 mg, 0.162 mmol] was dissolved in a preprepared mixture of 1:1 solution (total 0.5 mL) and stirred for 12 h at room temperature. The green solution changed to red. The red solution was extracted with pentane (6 mL) and dried *in vacuo*. Pentane (10 mL) was added and the compound was filtered. The filtrate was again dried *in vacuo*. Pentane (6 mL) was added, and the solution was dried *in vacuo* and redissolved in C_6D_6 . The ^{31}P and ^1H NMR spectra illustrated the preference of one solvent over the other.

Fluorobenzene versus benzene: **2** (63%) to **13** (37%).

Fluorobenzene versus fluorohexane: **2** (42%) to **14** (58%).

Fluorobenzene versus 1,3,5-trifluorobenzene: **2** (45%) to **8** (55%).

Preparation of (PNP)Ti=CH'Bu(F) (14) from 1-Fluorohexane and 1. In a J. Young tube was dissolved **1** [100 mg, 0.162 mmol] in neat 1-fluorohexane (~0.5 mL, excess) at room temperature. The solution was heated to 50 °C for 5 h (reaction is also complete at room temperature over a period of 48 h). The solution changed from green to red, and the solution was dried under vacuum. The residue was extracted with pentane (10 mL) and filtered. The filtrate was reduced in volume (2 mL) under reduced pressure and cooled to -35 °C to give a red solid [68 mg, 0.120 mmol, 75% yield]. The multinuclear NMR spectra gave the corresponding resonances to **14**.

Isotopic Labeling Studies for 1-Fluorohexane Dehydrofluorination. In a vial was dissolved 1-*d*₃ [75 mg, 0.128 mmol] in neat 1-fluorohexane (~0.5 mL, excess) at room temperature. The solution was heated to 50 °C for 5 h. The solution changed from green to red, and the solution was dried under vacuum. The residue was extracted with pentane and filtered. The filtrate was reduced in volume under reduced pressure to give a red solid, and the multinuclear NMR spectra gave the corresponding resonances to **14**.

Isolation of 1-Hexene. In a J. Young tube was dissolved **1** [200 mg, 0.324 mmol] in deuterated cyclohexane (~0.5 mL) at room temperature, and to this was added three drops of 1-fluorohexane. The solution was heated to 50 °C for 5 h. The solution changed from green to red, and the solution was then vacuum transferred. Analysis of the ^1H NMR spectrum and GC-MS verified the formation of 1-hexene. ^1H NMR (23 °C, 399.8 MHz, C_6D_{12}): 5.75 (m, 1H, CH₂=CHCH₂CH₂CH₂CH₃), 4.97 (m, 2H, CH₂=CHCH₂CH₂-CH₂CH₃), 1.96 (m, 2H, CH₂=CHCH₂CH₂CH₂CH₃), 1.44 (m, 4H, CH₂=CHCH₂CH₂C H₂CH₃), 0.98 (t, 1H, CH₂=CHCH₂CH₂-CH₂CH₃). MS-GC: theoretical, 84; found, 84.

Preparation of (PNP)Ti=CHSiMe₃(F) (16) from 1-Fluorohexane and 15. In a J. Young tube was dissolved **15** [200 mg, 0.307 mmol] in neat 1-fluorohexane (~0.5 mL, excess) at room temperature. The solution was heated at 100 °C for 5 h, changing from green to red. The solution was extracted with pentane (10 mL) and dried *in vacuo*. The residue was dissolved in pentane and filtered through a bed of Celite. The red filtrate was reduced in volume (2 mL) under reduced pressure to give a red solid [146 mg, 0.251 mmol, 78% yield]. The multinuclear NMR spectra gave the corresponding resonances to **16**.

Isolation of 1-Hexene. In a J. Young tube was dissolved **15** [200 mg, 0.307 mmol] in deuterated cyclohexane (~0.5 mL) at room temperature, and to this was added three drops of 1-fluorohexane. The solution was heated to 100 °C for 5 h. The solution changed from green to red, and the volatiles were vacuum transferred. Analysis of the ^1H NMR spectrum and GC-MS verified the formation of 1-hexene.

Recycling of 14 to 1. In a vial **14** [100 mg, 0.177 mmol] was dissolved in pentane (5 mL) and cooled to -35 °C. To this was added an analogous cold solution containing LiCH₂Bu [14 mg, 0.179 mmol] in pentane (5 mL). After 30 min the green suspension was filtered, then concentrated *in vacuo* (~1 mL) and placed in the freezer to obtain pure **1** as green crystals [91 mg, 0.147 mmol, 83%]. The reaction is quantitative by ^{31}P NMR spectroscopy and matches the spectroscopic details for the previously published **1**.

Recycling of 26 to 15. In a vial **26** [100 mg, 0.172 mmol] was dissolved in pentane (5 mL) and cooled to -35 °C. To this was added a cold solution of an analogous cold solution containing LiCH₂SiMe₃ [16 mg, 0.172 mmol] in pentane (5 mL). After 30 min the green suspension was filtered, then concentrated *in vacuo* (~1 mL) and placed in the freezer to obtain pure **15** as green crystals [79 mg, 0.121 mmol, 70%]. The reaction is quantitative by ^{31}P NMR spectroscopy and matches the spectroscopic details for the previously published **15**.

Kinetic Studies. The kinetic experiments were conducted as described below for the reaction of **1** to **2** and **2** to **14**. Standard deviations for the entropy (ΔS^\ddagger) and enthalpy (ΔH^\ddagger) were calculated on the basis of the two equations described by Girolami et al. (shown).³⁸ The NMR temperature probe was calibrated using an ethylene glycol standard and σT was determined by calculating the standard deviation in temperature measurement fluctuations and averaged over several temperatures. The standard deviations for the rates at three temperatures, collected in triplicates, were averaged to obtain σk .

$$(\sigma\Delta H^\ddagger)^2 = \frac{R^2 T_{\text{max}}^2 T_{\text{min}}^2}{\Delta T^2} \left\{ \left(\frac{\sigma T}{T} \right)^2 \left[\left(1 + T_{\text{min}} \frac{\Delta E}{\Delta T} \right)^2 + \left(1 + T_{\text{max}} \frac{\Delta E}{\Delta T} \right)^2 \right] + 2 \left(\frac{\sigma k}{k} \right)^2 \right\}$$

$$(\sigma\Delta S^\ddagger)^2 = \frac{R^2}{\Delta T^2} \left\{ \left(\frac{\sigma T}{T} \right)^2 \left[T_{\text{max}}^2 \left(1 + T_{\text{min}} \frac{\Delta E}{\Delta T} \right)^2 + T_{\text{min}}^2 \left(1 + T_{\text{max}} \frac{\Delta E}{\Delta T} \right)^2 \right] + \left(\frac{\sigma k}{k} \right)^2 \left(T_{\text{max}}^2 + T_{\text{min}}^2 \right) \right\}$$

$$\Delta E = [\ln(k_{\text{max}}/T_{\text{max}}) - \ln(k_{\text{min}}/T_{\text{min}})] \text{ and } \Delta T = (T_{\text{max}} - T_{\text{min}})$$

For the Conversion of 1 → 2. In each experiment, 50 mg of **1** [0.086 mmol] was dissolved in 0.4 mL of FC₆H₅ and placed

Table 4

	5	6	11	14	17	32	33
molecular formula	C ₃₇ H ₅₃ F ₂ NP ₂ Ti	C ₃₇ H ₅₂ F ₃ NP ₂ Ti	C ₃₇ H ₅₀ F ₅ NP ₂ Ti	C _{33.5} H ₅₆ FNP ₂ Ti	C ₃₆ H ₅₃ F ₂ NP ₂ SiTi	C _{32.25} H ₅₃ ClNP ₂ Ti	C ₆₇ H ₁₁₂ Br ₂ N ₂ P ₄ Ti ₂
fw	659.64	677.64	713.62	601.63	675.72	600.05	1325.09
temp, K	150(2)	150(2)	15(2)	150(2)	150(2)	150(2)	100(2)
wavelength, Å	0.71073	0.71073	0.44280	0.71073	0.71073	0.71073	0.49595
cryst shape/color	red plate	red plate	red plate	yellow plate	orange plate	red plate	red plate
cryst system,	monoclinic,	monoclinic,	monoclinic,	triclinic,	triclinic,	monoclinic,	monoclinic,
space group	<i>P</i> ₂ / <i>c</i>	<i>P</i> ₂ / <i>c</i>	<i>P</i> ₂ / <i>c</i>	<i>P</i> 1	<i>P</i> 1	<i>P</i> ₂ / <i>c</i>	<i>P</i> ₂ / <i>c</i>
<i>a</i> , Å	18.3014(13)	18.321(4)	18.7157(16)	10.8159(11)	10.027(2)	11.7571(12)	11.7142(7)
<i>b</i> , Å	10.6649(7)	10.832(2)	10.5268(9)	11.8622(15)	11.267(3)	41.721(4)	41.7972(16)
<i>c</i> , Å	20.9379(14)	21.141(4)	20.9994(18)	15.0323(19)	16.941(4)	14.7551(14)	14.6885(7)
α, deg	90	90	90	76.574(3)	99.512(4)	90	90
β, deg	115.1570(10)	115.027(3)	115.152(2)	83.775(4)	91.907(4)	90.052(2)	90.487(2)
γ, deg	90	90	90	75.316(4)	99.270(4)	90	90
volume, Å ³	3699.1(4)	3801.6(13)	3744.9(6)	1812.1(4)	1859.5(8)	7237.7(12)	7191.5(6)
<i>Z</i>	4	4	4	2	2	8	4
<i>d</i> _{calcd} , g cm ⁻³	1.184	1.184	1.266	1.114	1.207	1.101	1.224
absorp coeff, mm ⁻¹	0.353	0.348	0.194	0.350	0.383	0.418	0.779
reflns collected	27 475	18 262	50 522	46 981	11 743	46 196	78 118
reflns obsd (<i>I</i> > 2σ(<i>I</i>))	5804	2533	6634	8351	4313	8333	14 652
data/restraints/params	8522/238/424	6552/194/406	8743/154/426	8351/7/532	6594/12/390	13 635/48/749	17 753/354/719
R1 (<i>I</i> > 2σ(<i>I</i>))/R1	0.0899/0.1272	0.1096/0.2357	0.0448/0.0661	0.0455/0.07511	0.0465/0.0930	0.0545/0.1090	0.0659/0.0819
(all data)							
wR2 (<i>I</i> > 2σ(<i>I</i>))/wR2	0.2431/0.2748	0.2767/0.3595	0.1110/0.1226	0.1336/0.1163	0.1011/0.1189	0.1259/0.1480	0.1785/0.1972
(all data)							
GoF ^a	1.055	0.968	1.014	1.013	1.031	1.019	1.075

^a Goodness-of-fit = $[\sum[w(F_o^2 - F_c^2)^2]/N_{\text{observns}} - N_{\text{params}}]^{1/2}$, all data; R1 = $\sum(F_o - F_c)/\sum F_o$; wR2 = $[\sum[w(F_o^2 - F_c^2)^2]/\sum[w(F_o^2)^2]]^{1/2}$.

inside an oven-dried J. Young NMR tube with a HPCy₃ capillary as an internal standard. The NMR tube was then placed in a temperature-controlled and calibrated NMR probe (10.0–40.0 °C) and monitored at set time intervals until ~90% conversion to **2**. No side products were evident by ³¹P NMR spectroscopy. The HPCy₃ internal standard was referenced to –112 ppm and integrated to 1000. The decay of one doublet of the phosphine resonances of the starting material was recorded with time, and the resulting data were fit to a first-order kinetics plot. The rate constant at 25 °C ($5.896(5) \times 10^{-5} \text{ s}^{-1}$) is an average of three trials. The experiment was repeated at various temperatures (triplicate runs at 15 and 35 °C and single runs at 10, 20, 30, and 40 °C) to obtain activation parameters of $\Delta H^\ddagger = 21(1) \text{ kcal/mol}$ and $\Delta S^\ddagger = -7(3) \text{ eu}$. Inter- and intramolecular kinetic isotope effects (KIE) were determined in a similar manner to that described above. To obtain the intramolecular KIE, (PNP)Ti=CD³Bu(CD₂Bu) (**2-d**₃) was prepared using LiCD₂Bu³⁵ in place of LiCH₂Bu.³⁵ An average of three trials at 25 °C produced a KIE of 4.04(7). To obtain the intermolecular KIE, the reaction was performed using **1** in FC₆D₅ as a solvent versus FC₆H₅. Triplicate runs were monitored at 25 °C to obtain a KIE of 1.01(17).

For the Conversion of 2 → 14. Complex **2** [50 mg, 0.078 mmol] was dissolved in 0.5 mL of toluene and placed inside an oven-dried J. Young NMR tube with a HPCy₃ capillary as an internal standard. The NMR tube was then placed in a temperature-controlled and calibrated NMR probe (85.0–115.0 °C) and monitored at set time intervals until ~90% conversion to **14**. No side products were evident by ³¹P NMR spectroscopy. The HPCy₃ internal standard was referenced to –112 ppm and integrated to 1000. The decay of one doublet of the phosphine resonances of the starting material was recorded with time, and the resulting data were fit to a first-order kinetics plot. The rate constant at 100 °C ($4.96(16) \times 10^{-5} \text{ s}^{-1}$) is an average of three trials. The experiment was repeated at various temperatures (triplicate runs at 90 and 110 °C and single runs at 85, 95, 105, and 115 °C) to obtain activation parameters of $\Delta H^\ddagger = 29(1) \text{ kcal/mol}$ and $\Delta S^\ddagger = -3(4) \text{ eu}$. The intramolecular kinetic isotope effect was determined in a similar manner to that described above, monitoring the conversion of **2-d** to **14-d** at 100 °C. An average of three trials produced a KIE of 1.0(3).

For the Conversion of 3, 4, 28, 30, and 31 → 14. Complexes **3**, **4**, **28**, **30**, and **31** [50 mg] were dissolved in 0.5 mL of toluene and placed inside an oven-dried J. Young NMR tube with a HPCy₃ capillary as an internal standard. The NMR tube was then placed in a temperature-controlled and calibrated NMR probe (85 °C) and monitored at set time intervals until ~90% conversion to **14**. No side products were evident by ³¹P NMR spectroscopy. The HPCy₃ internal standard was referenced to –112 ppm and integrated to 1000. The decay of one doublet of the phosphine resonances of the starting material was recorded with time, and the resulting data were fit to a first-order kinetics plot. The rates for the conversions of **3**, **4**, **28**, **30**, and **31** → **14** are listed in Table 3.

Concentration Dependence Studies. Following the protocol described above concentration-dependent studies at 85 °C were carried out at varying concentrations (0.078, 0.156, 0.234 M) in titanium for the conversion of **2** → **14**.

X-ray Crystallography. Crystals of suitable size were mounted on glass fibers and measured at low temperatures (nitrogen and helium). The data collection for compounds **5**, **6**, **14**, **17**, and **32** was carried out using Mo Kα radiation (graphite monochromator) with a frame time of 10–90 s and a detector distance of 6.0 cm. Three major sections of frames were collected with 0.30° steps in ω at different ϕ settings and a detector position of –43° in 2θ . Data to a resolution of 0.77 Å were considered in the reduction. Final cell constants were calculated from the *xyz* centroids of the strong reflections from the actual data collection after integration.³⁹ The intensity data were corrected for absorption.⁴⁰ For compounds **11** and **32**, the data collection was carried out using synchrotron radiation ($\lambda = 0.44280$ and 0.49595 , diamond 111 monochromator, two mirrors to exclude higher harmonics) with a frame time of 1 s and a detector distance of 6.0 cm. A randomly oriented region of reciprocal space was surveyed to the extent of a hemisphere. Two major sections of frames were collected with 0.50ϕ and a detector position of –30° and 0° in 2θ . Data to a resolution of 0.80 Å were considered in the reduction. Final cell constants were calculated from the *xyz* centroids of the strong reflections from the actual data collection after integration.³⁹ The intensity data were corrected for absorption.⁴⁰ Table 4 depicts all pertinent crystal and refinement data.

Acknowledgment. We thank Indiana University–Bloomington, the Dreyfus Foundation, the Sloan Foundation, and the NSF (CHE-0348941) for financial support of this research. We would also like to thank the SCrAPS program and ChemMatCARS for structure data (compounds **11** and **33**). ChemMatCARS Sector 15 is principally supported by the National Science Foundation/Department of Energy under grant number CHE-0535644. Use of the Advanced Photon Source was supported by the U.S. Department of Energy, Office of Science, Office of Basic Energy Sciences, under Contract No. DE-AC02-06CH11357. J.S. acknowledges NSERC for a postdoctoral fellowship, and D.L.M thanks the STARS program at Indiana University for some financial

(39) Cheon, J.; Rogers, D. M.; Girolami, G. S. *J. Am. Chem. Soc.* **1997**, *119*, 6804.

assistance. We would also like to thank Dr. John C. Huffman, Dr. Hongjun Fan, Prof. K. G. Caulton, and Prof. L. K. Montgomery for insightful discussions.

Supporting Information Available: Complete kinetic data (**1** → **2**, and **2** → **14**), crystallographic data (**5**, **6**, **11**, **14**, **17**, **32**, and **33**), and synthetic and spectroscopic details (including multinuclear NMR spectra) for all compounds and mixtures are available free of charge via the Internet at <http://pubs.acs.org>.

OM800910Q

(40) *SAINT*; Bruker Analytical X-Ray Systems: Madison, WI, current version.

(41) An empirical correction for absorption anisotropy: Blessing, R. *Acta Crystallogr.* **1995**, *A51*, 33.

Synthesis of the First Stable Palladium Allenylidene Complexes

Florian Kessler, Normen Szesni, Kaija Pöhako, Bernhard Weibert, and Helmut Fischer*

Fachbereich Chemie, Universität Konstanz, Fach 727, 78457 Konstanz, Germany

Received September 1, 2008

Oxidative addition of $\text{BrC}\equiv\text{CC}(=\text{O})\text{NR}_2$ to $[\text{Pd}(\text{PPh}_3)_4]$ affords the *trans*-alkynylbromopalladium complexes *trans*- $[\text{Br}(\text{PPh}_3)_2\text{Pd}-\text{C}\equiv\text{CC}(=\text{O})\text{NR}_2]$ ($\text{NR}_2 = \text{NMe}_2$ (**2a**), $\text{N}(\text{CH}_2)_4$ (**2b**)). Subsequent reaction of **2a,b** with P^iPr_3 in excess gives *trans*- $[\text{Br}(\text{P}^i\text{Pr}_3)_2\text{Pd}-\text{C}\equiv\text{CC}(=\text{O})\text{NR}_2]$ (**5a,b**). The analogous reaction of **2b** with $\text{P}(\text{C}_6\text{H}_4\text{OMe-4})_3$ gives *trans*- $[\text{Br}(\text{P}(\text{C}_6\text{H}_4\text{OMe-4})_3)_2\text{Pd}-\text{C}\equiv\text{CC}(=\text{O})\text{NR}_2]$ (**7b**), and that of **2a** with trifluoroacetate gives *trans*- $[(\text{F}_3\text{CCOO})(\text{PPh}_3)_2\text{Pd}-\text{C}\equiv\text{CC}(=\text{O})\text{NMe}_2]$ (**9a**). Methylation of **2a,b**, **7b**, and **9a** with either MeOTf or $[\text{Me}_3\text{O}]\text{BF}_4$ and ethylation of **2a,b** with $[\text{Et}_3\text{O}]\text{BF}_4$ yield the first cationic allenylidene complexes of palladium, *trans*- $[\text{R}^*(\text{PR}'_3)_2\text{Pd}-\text{C}\equiv\text{CC}(\text{OMe})\text{NR}_2]^+\text{X}^-$ ($\text{R}^* = \text{Br}, \text{CF}_3\text{COO}$; $\text{R}' = \text{Ph}, \text{C}_6\text{H}_4\text{OMe-4}, ^i\text{Pr}$; $\text{X} = \text{OTf}, \text{BF}_4$).

Introduction

The synthesis of the first allenylidene complexes, $\text{L}_n\text{M}=\text{C}=\text{C}=\text{C}(\text{R}^1)\text{R}^2$, was reported in 1976 simultaneously by Fischer et al. ($\text{M} = \text{Cr}, \text{W}$)¹ and Berke ($\text{M} = \text{Mn}$).² Fischer's synthesis involved Lewis acid induced ethanol abstraction from ethoxycarbene complexes $[(\text{CO})_5\text{M}=\text{C}(\text{OEt})(\text{CH}=\text{C}(\text{NMe}_2)\text{Ph})]$. Berke obtained the manganese allenylidene complex $[\text{Cp}(\text{CO})_2\text{Mn}=\text{C}=\text{C}=\text{C}(\text{tBu})_2]$ on treatment of the methyl propiolate complex $[\text{Cp}(\text{CO})_2\text{Mn}(\text{HC}\equiv\text{CCOOMe})]$ with an excess of tBuLi , presumably via an alkynyl complex as an intermediate. Since then a large number of allenylidene complexes of many transition metals have been prepared, including complexes of titanium, chromium, tungsten, manganese, rhenium, iron, ruthenium, osmium, rhodium, and iridium.³ Most syntheses now use propargylic alcohols, $\text{HC}\equiv\text{CC}(\text{R})(\text{R}')\text{OH}$, as sources of the allenylidene C_3 fragment. Coordination of the propargylic alcohol to the transition metal is followed by its rearrangement into a hydroxyvinylidene ligand. On subsequent elimination of water, allenylidene ligands are formed. This strategy was originally introduced by Selegue.⁴ Some of these complexes have been used as catalyst precursors:⁵ for instance,

in ring-closing metathesis,⁶ in ring-opening metathesis,⁷ in the dehydrogenative dimerization of tin hydrides,⁸ and in selective transesterification of substituted vinyl ethers.⁹

Allenylidene complexes of palladium have been unknown until now, and consequently their catalytic activity has not been studied. This is surprising, especially when considering the broad range of applications of palladium complexes in organic synthesis and catalysis.¹⁰ Many commonly used catalysts for CC coupling reactions such as, for example, the Mizoroki–Heck reaction or the Suzuki coupling reaction are based on palladium complexes.

We now report on the synthesis and the spectroscopic properties of the first palladium allenylidene complexes from readily available *N,N*-dimethylpropiolamides as the C_3 source.

Results and Discussion

Initially, we envisioned the transmetalation of allenylidene ligands from chromium to palladium, since *N*-heterocyclic carbene ligands such as pyrazolin-3-ylidene and pyrazolidin-

* To whom correspondence should be addressed. E-mail: helmut.fischer@uni-konstanz.de. Fax: +7531-883136.

(1) Fischer, E. O.; Kalder, H. J.; Frank, A.; Köhler, F. H.; Huttner, G. *Angew. Chem.* **1976**, *88*, 683; *Angew. Chem., Int. Ed. Engl.* **1976**, *15*, 623.

(2) Berke, H. *Angew. Chem.* **1976**, *88*, 684; *Angew. Chem., Int. Ed. Engl.* **1976**, *15*, 624.

(3) For reviews see: (a) Bruce, M. I.; Swincer, A. G. *Adv. Organomet. Chem.* **1983**, *22*, 59. (b) Bruce, M. I. *Chem. Rev.* **1991**, *91*, 197. (c) Doherty, S.; Corrigan, J. F.; Carty, A. J.; Sappa, E. *Adv. Organomet. Chem.* **1995**, *37*, 39. (d) Werner, H. J. *Chem. Soc., Chem. Commun.* **1997**, 903. (e) Bruce, M. I. *Chem. Rev.* **1998**, *98*, 2797. (f) Touchard, D.; Dixneuf, P. H. *Coord. Chem. Rev.* **1998**, *178–180*, 409. (g) Cadierno, V.; Gamasa, M. P.; Gimeno, J. *Eur. J. Inorg. Chem.* **2001**, 571. (h) Winter, R. F.; Zális, S. *Coord. Chem. Rev.* **2004**, *248*, 1565. (i) Rigaut, S.; Touchard, D.; Dixneuf, P. H. *Coord. Chem. Rev.* **2004**, *248*, 1585. (j) Cadierno, V.; Gamasa, M. P.; Gimeno, J. *Coord. Chem. Rev.* **2004**, *248*, 1627. (k) Cadierno, V.; Crochet, P.; Gimeno, J. In *Metal Vinylidenes and Allenylidenes in Catalysis*; Bruneau, C., Dixneuf, P. H., Eds.; Wiley-VCH: Weinheim, Germany, 2008; p 61 ff.

(4) Selegue, J. P. *Organometallics* **1982**, *1*, 217.

(5) For recent reviews see: (a) Castarlenas, R.; Fischmeister, C.; Bruneau, C.; Dixneuf, P. H. *J. Mol. Catal. A* **2004**, *213*, 31. (b) Bruneau, C.; Dixneuf, P. H. *Angew. Chem.* **2006**, *118*, 2232; *Angew. Chem., Int. Ed.* **2006**, *45*, 2176.

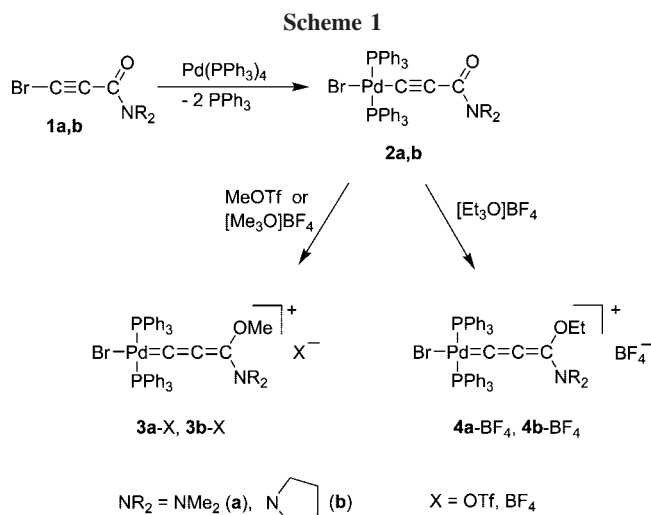
(6) (a) Fürstner, A.; Picquet, M.; Bruneau, C.; Dixneuf, P. H. *Chem. Commun.* **1998**, 1315. (b) Picquet, M.; Touchard, D.; Bruneau, C.; Dixneuf, P. H. *New J. Chem.* **1999**, *23*, 141. (c) Osipov, S. N.; Artushin, O. I.; Kolomiets, A. F.; Bruneau, C.; Picquet, M.; Dixneuf, P. H. *Eur. J. Org. Chem.* **2001**, 3891. (d) Picquet, M.; Bruneau, C.; Dixneuf, P. H. *Chem. Commun.* **1998**, 2249. (e) Sémeril, D.; Le Nôtre, J.; Bruneau, C.; Dixneuf, P. H.; Kolomiets, A. F.; Osipov, S. N. *New J. Chem.* **2001**, *25*, 16. (f) Schanz, H.-J.; Jafarpour, L.; Stevens, E. D.; Nolan, S. P. *Organometallics* **1999**, *18*, 5187. (g) Jafarpour, L.; Huang, J.; Stevens, E. D.; Nolan, S. P. *Organometallics* **1999**, *18*, 3760. (h) Le Gendre, P.; Picquet, M.; Richard, P.; Moise, C. *J. Organomet. Chem.* **2002**, *643–644*, 231. (i) Fürstner, A.; Müller, T. *J. Am. Chem. Soc.* **1999**, *121*, 7814. (j) Fürstner, A.; Thiel, O. R. *J. Org. Chem.* **2000**, *65*, 1738. (k) Özdemiir, I.; Cetinkaya, E.; Cetinkaya, B.; Cicek, M.; Sémeril, D.; Bruneau, C.; Dixneuf, P. H. *Eur. J. Inorg. Chem.* **2004**, 418. (l) Akiyama, R.; Kobayashi, S. *Angew. Chem.* **2002**, *114*, 2714; *Angew. Chem., Int. Ed.* **2002**, *41*, 2602.

(7) (a) Saoud, M.; Romerosa, A.; Peruzzini, M. *Organometallics* **2000**, *19*, 4005. (b) Castarlenas, R.; Sémeril, D.; Noels, A. F.; Demonceau, A.; Dixneuf, P. H. *J. Organomet. Chem.* **2002**, *663*, 235. (c) Alaoui Abdallaoui, I.; Sémeril, D.; Dixneuf, P. H. *J. Mol. Catal. A* **2002**, *182–183*, 577.

(8) Maddock, S. M.; Finn, M. G. *Angew. Chem.* **2001**, *113*, 2196; *Angew. Chem., Int. Ed.* **2001**, *40*, 2138.

(9) Saoud, M.; Romerosa, A.; Manas Carpio, S.; Gonsalvi, L.; Peruzzini, M. *Eur. J. Inorg. Chem.* **2003**, 1614.

(10) See e.g.: (a) Heck, R. F. *Palladium Reagents in Organic Synthesis*; Academic Press: London, 1985. (b) de Meijere, A.; Diederich, F. Eds. *Metal-Catalyzed Cross-Coupling Reactions*; Wiley-VCH: Weinheim, Germany, 2004. (c) Tsuji, J. *Palladium Reagents and Catalysis*; Wiley: Chichester, U.K., 2004.



3-ylidene proved readily transferable from pentacarbonylchromium complexes to gold, palladium, and platinum in high yield.¹¹ The analogous transmetalation of several allenylidene ligands from chromium to tungsten likewise proceeded quickly in yields ranging from 83 to 97%.¹² However, all attempts to transfer allenylidene ligands from chromium to palladium met with failure. Therefore, the strategy had to be changed and an approach starting from alkynyl complexes was investigated.

Recently, we developed an easy to perform one-pot synthesis for π -donor-substituted allenylidene pentacarbonyl complexes of chromium and tungsten. Sequential reaction of the solvent complexes $[(\text{CO})_5\text{M}(\text{THF})]$ ($\text{M} = \text{Cr, W}$) with appropriate deprotonated alkynes as the C_3 source and $[\text{R}_3\text{O}]\text{BF}_4$ as the alkylating agent afforded the corresponding amino- and alkoxy-allenylidene complexes in very good yields.¹³ Modification of this route turned out to also be applicable to the preparation of palladium allenylidene complexes.

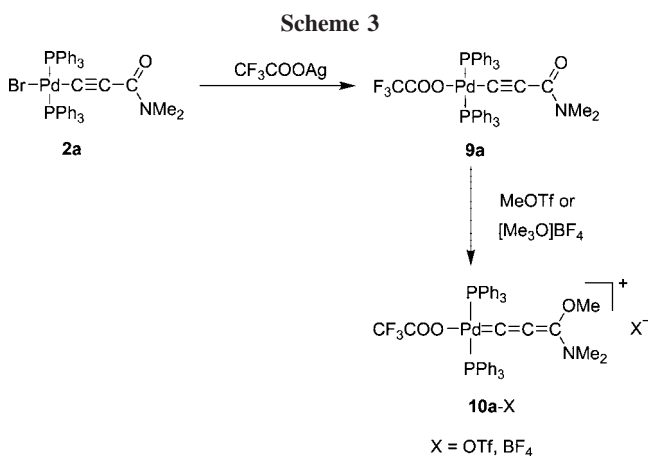
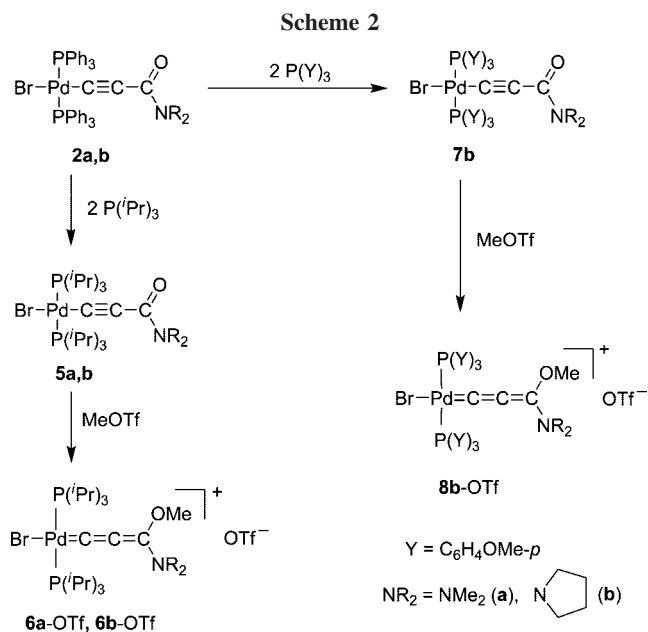
Terminal halogenoalkynes are known to react with zerovalent palladium complexes by oxidative addition, affording stable palladium(II) alkynyl complexes.¹⁴ Thus, treatment of a suspension of $[\text{Pd}(\text{PPh}_3)_4]$ in CH_2Cl_2 at ambient temperature with $\text{BrC}\equiv\text{CC(=O)NMe}_2$ (**1a**) afforded the neutral alkynyl complex **2a** (Scheme 1). Bromoalkyne **1a** was obtained by reaction of propynoic acid dimethylamide with *N*-bromosuccinimide (NBS). Pure alkynyl complex **2a** was isolated, after repeated crystallization from mixtures of CH_2Cl_2 and Et_2O , as a colorless solid in 85% yield. The subsequent alkylation of **2a** at -50°C with a slight excess of MeOTf proceeded smoothly and afforded the cationic palladium allenylidene complex **3a-OTf** as a light yellow solid in 91% yield after crystallization from pentane- CH_2Cl_2 mixtures (Scheme 1). The corresponding BF_4 salt, **3a-BF₄**, was obtained when $[\text{Me}_3\text{O}]\text{BF}_4$ instead of MeOTf was used as the alkylation agent. The complexes **2b**, **3b-OTf**, **3b-BF₄**, **4a-BF₄**, and **4b-BF₄** were synthesized accordingly.

(11) Kessler, F.; Szesni, N.; Maass, C.; Hohberger, C.; Weibert, B.; Fischer, H. *J. Organomet. Chem.* **2007**, *692*, 3005.

(12) Szesni, N.; Drexler, M.; Fischer, H. *Organometallics* **2006**, *25*, 3989.

(13) (a) Fischer, H.; Szesni, N.; Roth, G.; Burzlaff, N.; Weibert, B. *J. Organomet. Chem.* **2003**, *683*, 301. (b) Fischer, H.; Szesni, N. *Coord. Chem. Rev.* **2004**, *248*, 1659.

(14) (a) Burgess, J.; Howden, M. E.; Kemmitt, R. D. W.; Sridhara, N. S. *J. Chem. Soc., Dalton Trans.* **1978**, 1577. (b) Klein, H. F.; Zettel, B. D. *Chem. Ber.* **1995**, *128*, 343. (c) Mann, G.; Baranano, D.; Hartwig, J. F.; Rheingold, A. L.; Guzai, I. A. *J. Am. Chem. Soc.* **1998**, *120*, 9205. (d) Weigelt, M.; Becher, D.; Poetsch, E.; Bruhn, C.; Steinborn, D. Z. *Anorg. Allg. Chem.* **1999**, *625*, 1542. (e) Osakada, K.; Hamada, M.; Yamamoto, T. *Organometallics* **2000**, *19*, 458.

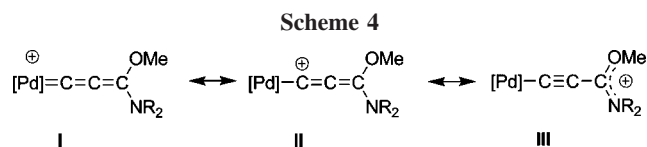


Modification of the properties of the allenylidene complex can be achieved by variation of the terminal substituents of the allenylidene ligand and the coligands at palladium. The variation of the terminal substituents was achieved by starting from alkyne **1b** instead of **1a** and employing $[\text{Et}_3\text{O}]\text{BF}_4$ as the alkylation agent; otherwise the same reaction sequence was followed (Scheme 1).

The metal-bound C_α atom and the terminal C_γ atom in allenylidene complexes are electrophilic centers (see resonance forms II and III in Scheme 4).³ Therefore, nucleophilic additions to these centers might compete with substitution of halides for the bromide ligand or of phosphines for the PPh_3 ligands. To avoid such side reactions at the allenylidene ligand, the alkynyl complexes **2a,b** were chosen as the starting compounds for the modification of the coligand set in allenylidene complexes.

Treatment of a solution of **2a,b** in CH_2Cl_2 with 2.2 equiv of the more nucleophilic phosphines P^iPr_3 and $\text{P}(\text{C}_6\text{H}_4\text{OMe-}4)_3$ led to quantitative exchange of both PPh_3 ligands. Complexes **5a,b** and **7b** were obtained as colorless or pale yellow solids after several recrystallization cycles from Et_2O in 70–74% yield. These alkynyl complexes were subsequently converted into cationic allenylidene complexes by alkylation with MeOTf. The resulting allenylidene complexes were then isolated in 98% (**6a-OTf**), 97% (**6b-OTf**), and 91% yield (**8b-OTf**) (Scheme 2).

When $\text{Ag}^+[\text{CF}_3\text{COO}]^-$ was added to a solution of **2a** in CH_2Cl_2 , AgBr instantaneously precipitated and the trifluoroac-



etato complex **9a** was isolated as a colorless solid in 96% yield. Alkylation of **9a** with MeOTf or $[\text{Me}_3\text{O}]\text{BF}_4$ finally afforded the allenylidene complexes **10a-OTf** and **10a-BF₄** in 90% and 86% yields, respectively (Scheme 3).

All new alkynyl and allenylidene complexes were characterized by spectroscopic means and by elemental analysis. The structures of **5b** and **10a-BF₄** were additionally established by X-ray diffraction studies.

From the observation of only one singlet in the ^{31}P NMR spectra it followed that the two phosphine ligands are mutually trans. There was no indication of the presence of a cis isomer. Two singlets for the two N-bound methyl groups in the NMR spectra of all alkynyl complexes indicated a rather high barrier to rotation around the $\text{C}(\text{sp}^2)\text{-N}$ bond. From the coalescence of the two signals of complex **2a** in $\text{C}_2\text{D}_2\text{Cl}_4$ at 115 °C an energy barrier of $\Delta G^\ddagger = 76.1 \pm 0.4$ kJ/mol was calculated. The barrier is slightly lower than that in free propiolamides ($\text{RC}\equiv\text{CC}(\text{=O})\text{NMe}_2$, R = H, Me, Ph: 79.6–82.1 kcal/mol),¹⁵ indicating minor back-donation from palladium to the alkynyl ligand and almost negligible interaction of the metal with the $\text{C}(\text{=O})\text{NMe}_2$ fragment. The resonances of the alkynyl ligand in the ^{13}C NMR spectra compared well with those of known palladium alkynyl complexes.^{14d} As expected, increasing the electron density at palladium in the series **9a**, **2a**, **7b** led to a shift of the ^{13}C resonance of the metal-bound alkynyl C_α atom to lower field. The resonances of C_β and C_γ were unaffected by varying the substitution pattern of the metal center.

The formation of the cationic allenylidene complexes by alkylation of the alkynyl complexes was accompanied by a pronounced shift of the C_α resonance to lower field by about 45 ppm, a shift of the C_β resonance to higher field ($\Delta\delta \approx 11$ ppm) and a shift of the $\nu(\text{CC})$ vibration to lower energy by 10–15 cm^{-1} . The resonances of the C_γ atom and the N–CH₃ groups were again almost unaffected by the alkylation. Similar trends have been observed on alkylation of alkynylpentacarbonylchromate complexes to give neutral allenylidene complexes.¹² The extent of these shifts and the observation of two resonances for the dimethylamino substituent in the ^1H and ^{13}C NMR spectra demonstrate the importance of the zwitterionic resonance forms II and III for the overall bond description of these cationic allenylidene complexes (Scheme 4).¹² As in **2a**, **5a**, **7b**, and **9a**, both phosphine ligands are mutually trans, as indicated by the presence of only one signal for both phosphorus nuclei in the ^{31}P NMR spectra.

A comparison of the spectroscopic data of these cationic palladium allenylidene complexes with those of the related neutral complexes $[(\text{CO})_5\text{M}=\text{C}=\text{C}=\text{C}(\text{NMe}_2)\text{OMe}]$ (M = Cr, W) reveals that in cationic palladium allenylidene complexes the alkynyl character (see III in Scheme 4) is significantly more pronounced than in the corresponding group 6 complexes, as evidenced by the $\nu(\text{CC})$ vibration at higher energy by about 70–90 cm^{-1} .

The solid-state structures of the alkynyl complex **5b** (Figure 1) and of the cationic allenylidene complex **10a-BF₄** (Figure 2)

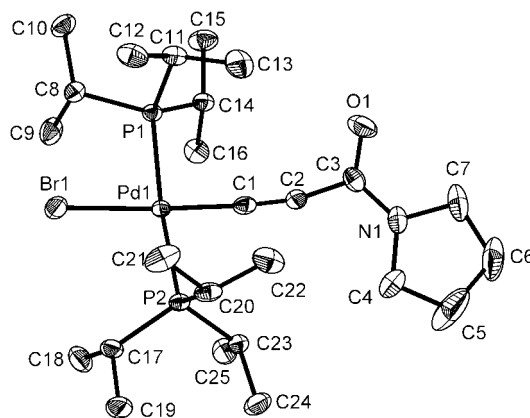


Figure 1. Structure of the alkynyl complex **5b** in the crystal (ellipsoids drawn at the 50% probability level; hydrogen atoms omitted for clarity). Important distances (Å) and angles (deg): Pd(1)–C(1) = 1.947(3), Pd(1)–Br(1) = 2.4629(8), Pd(1)–P(1) = 2.3581(9), Pd(1)–P(2) = 2.3500(9), C(1)–C(2) = 1.209(5), C(2)–C(3) = 1.454(4), C(3)–O(1) = 1.244(4), C(3)–N(1) = 1.331(4), N(1)–C(4) = 1.466(5); C(1)–Pd(1)–Br(1) = 176.41(9), Pd(1)–C(1)–C(2) = 175.6(3), C(1)–C(2)–C(3) = 168.1(3), C(2)–C(3)–O(1) = 120.5(3), C(2)–C(3)–N(1) = 117.5(3).

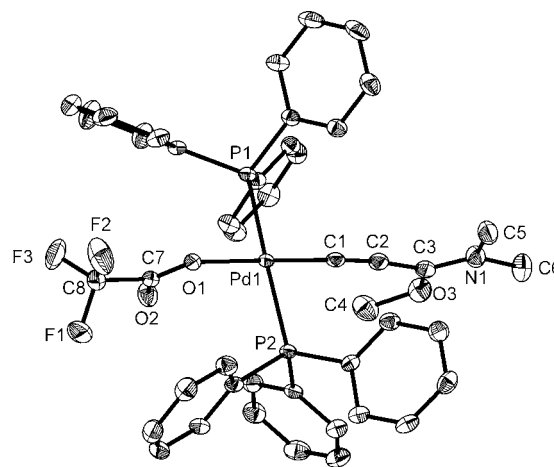


Figure 2. Structure of the cation of complex **10a-BF₄** in the crystal (ellipsoids drawn at the 50% probability level; hydrogen atoms, two molecules of methylene chloride, and the anion BF_4^- omitted for clarity). Important distances (Å) and angles (deg): Pd(1)–C(1) = 1.925(3), Pd(1)–O(1) = 2.067(2), Pd(1)–P(1) = 2.3338(9), Pd(1)–P(2) = 2.3303(9), C(1)–C(2) = 1.217(4), C(2)–C(3) = 1.420(4), C(3)–N(1) = 1.296(4), C(3)–O(3) = 1.330(4), O(3)–C(4) = 1.446(4), O(1)–C(7) = 1.267(3), O(2)–C(7) = 1.223(4); C(1)–Pd(1)–O(1) = 178.69(9), Pd(1)–C(1)–C(2) = 176.7(2), C(1)–C(2)–C(3) = 172.6(3), C(2)–C(3)–N(1) = 123.0(3), C(2)–C(3)–O(3) = 120.8(3), N(1)–C(3)–O(3) = 116.2(3).

were determined by X-ray diffraction studies. The complex **10a-BF₄** crystallizes from dichloromethane with two molecules of CH_2Cl_2 ; the BF_4^- anion is slightly disordered. In both complexes the palladium atom engages in square-planar coordination. In **5b** the plane formed by the atoms C(3), O(1), and N(1) and the coordination plane of palladium are almost coplanar (torsion angle O(1)–C(3)–Pd(1)–P(1) = 12.0°). In contrast, the allenylidene plane (formed by the atoms C(3), N(1), and O(3)) and the trifluoroacetate plane in **10a-BF₄** are perpendicular (89.6 and 87.9°, respectively) to the coordination plane of palladium. In both complexes the Pd–C₃ chain is slightly bent: Pd–C(1)–C(2) = 175.6(3)° (**5b**) and 176.7(2)° (**10a-BF₄**), C(1)–C(2)–C(3) = 168.1(3)° (**5b**) and 172.6(3)° (**10a-BF₄**). However, a modest

(15) (a) Oki, M. *Applications of Dynamic NMR Spectroscopy to Organic Chemistry*; VCH: Deerfield Beach, FL, 1985. (b) Jackman, L. M.; Cotton, F. A., Eds. *Dynamic Nuclear Magnetic Resonance Spectroscopy*; Academic Press: New York, 1975.

deviation from linearity of the MC₃ fragment in allenylidene complexes is often observed.³

The Pd–C bond (1.925(3) Å) in the allenylidene complex **10a**-BF₄ is close to the shorter limit of observed Pd–C bond lengths and is shorter than the Pd–C bond in the related cationic N-heterocyclic carbene (NHC) complexes *trans*-[L(PR₃)₂Pd(NHC)]⁺ (1.97–2.01 Å)¹⁶ or in the neutral alkynyl complexes *trans*-[L(PR₃)₂Pd–C≡CR] (1.947(3) Å in **5b**; range usually observed 1.95–2.07 Å^{14d,17}). Similarly to other neutral π-donor-substituted allenylidene complexes of chromium and tungsten^{11–13,18} the C(1)–C(2) bond is very short (1.217(4) Å) and only slightly longer than in the alkynyl complex **5b** (1.209(5) Å). Conversely, the C(2)–C(3) bond in **10a**-BF₄ (1.420(4) Å) is rather long and is even longer than that in [(CO)₅Cr=C=C(O-adamantyl)NMe₂] (1.366(7) Å)¹⁸ but, as expected, is shorter than in **5b** (1.454(4) Å). The terminal bonds of the chain, C(3)–O(3) and C(3)–N(3), however, compare well with those in related complexes.

In summary, the first isolable palladium allenylidene complexes are accessible by a straightforward two-step synthesis from readily available bromoalkynes. The new complexes are remarkably stable. For instance, after heating for 14 h at 160 °C the intensity of the ν(CC) vibration in the IR spectra of **3a**-OTf only decreased to a minor degree, thus confirming the stability of the new allenylidene complexes. They exhibit all characteristic features of π-donor-substituted allenylidene complexes.

Experimental Section

All reactions were performed under a nitrogen atmosphere by using standard Schlenk techniques. Solvents were dried by distillation from CaH₂ (CH₂Cl₂), LiAlH₄ (pentane), and sodium (Et₂O). The yields refer to analytically pure compounds and are not optimized. ¹H, ¹³C, ¹⁹F, and ³¹P NMR spectra were recorded on a Jeol JNX 400, a Varian Inova 400, or a Bruker Avance 400 spectrometer at ambient temperature. Chemical shifts are reported relative to the residual solvent peaks or tetramethylsilane (¹H, ¹³C) and 100% H₃PO₄ (³¹P). Other instrumentation: IR, Biorad FTS 60; MS, Finnigan MAT 312; elemental analysis, Heraeus Elementar Vario EL. *N,N*-Dimethylpropiolamide¹⁹ and [Pd(PPh₃)₄]²⁰ were synthesized according to literature procedures. All other reagents were used as obtained from commercial suppliers.

1-Bromo-*N,N*-dimethylpropiolamide (1a). A solution of 0.97 g (10 mmol) of *N,N*-dimethylpropiolamide in 40 mL of acetone was treated at ambient temperature with 2.16 g (12 mmol) of NBS and 150 mg (0.9 mmol) of AgNO₃. After 60 min the reaction mixture was poured onto 200 mL of ice water. The aqueous phase was extracted three times with 30 mL portions of ethyl acetate. The combined organic extracts were dried over MgSO₄. The solid was then filtered off and the solvent removed in vacuo. The crude product was filtered over a short plug of silica using CH₂Cl₂/acetone

(5:1) as the eluant. Removal of the solvent gave 1.36 g (7.9 mmol; 79%) of **1** as a colorless solid. ¹H NMR (400 MHz, CDCl₃): δ 2.88 (s, 3H, NCH₃), 3.12 (s, 3H, NCH₃). ¹³C NMR (100 MHz, CD₂Cl₂): δ 34.0 (NCH₃), 38.0 (NCH₃), 55.2 (C≡CBr), 73.4 (C≡CBr), 153.0 (C(O)NMe₂). IR (CH₂Cl₂): ν(C≡C) 2198 cm⁻¹. EI-MS (70 eV): *m/z* (%) 176 (48) [M⁺], 161 (100) [(M – CH₃)⁺]. Anal. Calcd for C₅H₆BrNO (176.01): C, 34.12; H, 3.44; N, 7.96. Found: C, 34.09; H, 3.51; N, 8.05.

1-Bromo-*N,N*-tetramethylenepropiolamide (1b). The synthesis of **1b** was carried out analogously to **1a**. The crude product was purified by column chromatography using CH₂Cl₂ as solvent. Yield: 1.72 g (8.51 mmol; 85%) of **1b** as a white powder. ¹H NMR (400 MHz, CDCl₃): δ 1.90 (m, 4H, CH₂CH₂), 3.44 (t, *J* = 7.0 Hz, 2H, NCH₂), 3.61 (t, *J* = 7.0 Hz, 2H, NCH₂). ¹³C NMR (100 MHz, CDCl₃): δ 24.6 (CH₂), 25.3 (CH₂), 45.4 (NCH₂), 48.0 (NCH₂), 53.8 (C≡CBr), 74.6 (C≡CBr), 177.4 (C(O)NC₄H₈). IR (CH₂Cl₂): ν(CCC) 2196 cm⁻¹. EI-MS (70 eV): *m/z* (%) 202 (79) [M⁺], 146 (22) [(M – C₄H₈)⁺], 132 (100) [(M – NC₄H₈)⁺], 122 (29) [(M – Br)⁺], 99 (100) [(M – Br – C≡C)⁺]. Anal. Calcd for C₇H₈BrNO (202.05): C, 41.61; H, 3.99; N, 6.93. Found: C, 42.46; H, 4.37; N, 8.21.

***trans*-Bromobis(triphenylphosphine)(3-dimethylamino-3-oxy-1-propynyl)palladium(II) (2a)**. A suspension of 1.16 g (1 mmol) of [Pd(PPh₃)₄] in 30 mL of CH₂Cl₂ was treated with 0.26 g (1.5 mmol) of **1a** at ambient temperature. The mixture was stirred for 30 min, upon which it becomes a clear yellow solution. Then, 100 mL of dry Et₂O was added. The light yellow precipitate was filtered off and washed repeatedly with Et₂O (3 × 30 mL) and pentane (2 × 50 mL). Repeated crystallization of the crude product from CH₂Cl₂/Et₂O gave 0.69 g (0.85 mmol; 85%) of pure **2a** as an off-white powder. ¹H NMR (400 MHz, CD₂Cl₂): δ 2.19 (s, 3H, NCH₃), 2.49 (s, 3H, NCH₃), 7.38–7.47 (m, 18H, ArH), 7.68–7.73 (m, 12H, ArH). ¹³C NMR (100 MHz, CD₂Cl₂): δ 33.2 (NCH₃), 37.6 (NCH₃), 104.1 (t, ²*J*_{PC} = 10.8 Hz, Pd–C≡C), 107.7 (Pd–C≡C), 128.4 (t, ³*J*_{PC} = 4.8 Hz, *m*-C), 130.9 (*p*-C), 131.4 (t, ¹*J*_{PC} = 25.0 Hz, *i*-C), 135.3 (t, ²*J*_{PC} = 6.7 Hz, *o*-C), 154.4 (C(O)NMe₂). ³¹P NMR (162 MHz, CD₂Cl₂): δ 24.7. IR (CH₂Cl₂): ν(C≡C) 2109 cm⁻¹; ν(CO) 1609 cm⁻¹. UV–vis (CH₂Cl₂): λ_{max} (nm) (log ε) 240 (4.489), 305 (4.314). FAB-MS: *m/z* (%) 725 (28) [(M – Br)⁺]. Anal. Calcd for C₄₁H₃₆BrNOP₂Pd·CH₂Cl₂ (807.01): C, 56.56; H, 4.29; N, 1.57. Found: C, 57.09; H, 4.60; N, 1.55.

***trans*-Bromobis(triphenylphosphine)(3-*N,N*-tetramethyleamino-3-oxy-1-propynyl)palladium(II) (2b)**. A suspension of 1.16 g (1 mmol) of [Pd(PPh₃)₄] in 30 mL of dry CH₂Cl₂ was treated with 0.30 g (1.5 mmol) of **1b** at ambient temperature. The mixture was stirred for a further 30 min, upon which it became a clear yellow solution. The solvent was removed in vacuo, and the crude product was purified by column chromatography using petroleum ether/CH₂Cl₂/acetone mixtures. Yield: 0.71 g (0.85 mmol; 85%) of **2b** as a pale yellow powder. ¹H NMR (400 MHz, CDCl₃): δ 1.37 (m, 2H, CH₂), 1.56 (m, 2H, CH₂), 2.26 (t, *J* = 7.0 Hz, 2H, NCH₂), 3.03 (t, *J* = 7.0 Hz, 2H, NCH₂), 7.34–7.40 (m, 18 H, ArH), 7.67–7.72 (m, 12 H, ArH). ¹³C NMR (100 MHz, CDCl₃): δ 24.6 (CH₂) 25.0 (CH₂), 44.2 (NCH₂), 46.9 (NCH₂), 105.0 (t, ³*J*_{PC} = 5.8 Hz, Pd–C≡C), 107.1 (t, ²*J*_{PC} = 13.4 Hz, Pd–C≡C), 128.0 (t, ³*J*_{PC} = 4.8 Hz, *m*-C), 130.4 (*p*-C), 130.9 (t, ¹*J*_{PC} = 24.9 Hz, *i*-C), 135.0 (t, ²*J*_{PC} = 6.7 Hz, *o*-C), 152.9 (C(O)NC₄H₈). ³¹P NMR (162 MHz, CDCl₃): δ 21.7. IR (CH₂Cl₂): ν(CCC) 2115 cm⁻¹. UV–vis (CH₂Cl₂): λ_{max} (nm) (log ε) 302 (4.373). FAB-MS: *m/z* (%) 834 (7) [M⁺], 751 (8) [(M – Br – 2H)⁺], 489 (16) [(M – Br – 2H – PPh₃)⁺], 367 (41) [(M – Br – 2H – PPh₃ – C₇H₈NO)⁺]. Anal. Calcd for C₄₃H₃₈BrNOP₂Pd (833.04): C, 62.00; H, 4.60; N, 1.68. Found: C, 61.86; H, 4.63; N, 1.57.

***trans*-Bromobis(triphenylphosphine)(3-dimethylamino-3-methoxy-1,2-propadienyldiene)palladium(II) Trifluoromethanesulfonate (3a-OTf)**. A solution of 0.5 g (0.62 mmol) of **2a** in 30 mL of CH₂Cl₂ was treated dropwise with 0.07 mL (0.62 mmol) of MeOTf at –50

(16) See e.g.: (a) Fürstner, A.; Seidel, G.; Kremzow, D.; Lehmann, C. W. *Organometallics* **2003**, *22*, 907. (b) Schneider, S. K.; Roembke, P.; Julius, G. R.; Raubenheimer, H. G.; Herrmann, W. A. *Adv. Synth. Catal.* **2006**, *348*, 1862. (c) Schuster, O.; Raubenheimer, H. G. *Inorg. Chem.* **2006**, *45*, 7997.

(17) (a) Behrens, U.; Hoffmann, K. J. *Organomet. Chem.* **1977**, *129*, 273. (b) van der Voort, E.; Spek, A. L.; de Graaf, W. *Acta Crystallogr., Sect. C: Cryst. Struct. Commun.* **1987**, *43*, 2311. (c) Osakada, K.; Sakata, R.; Yamamoto, T. *Organometallics* **1997**, *16*, 5354. (d) Kim, Y.-J.; Lee, S.-H.; Lee, S.-H.; Jeon, S.-I.; Lim, M. S.; Lee, S. W. *Inorg. Chim. Acta* **2005**, *358*, 650.

(18) Szesni, N.; Weibert, B.; Fischer, H. *Inorg. Chim. Acta* **2006**, *359*, 617.

(19) Crow, W. D.; Leonard, N. J. *J. Org. Chem.* **1965**, *30*, 2660.

(20) Tellier, F.; Sauvetre, R.; Normant, J. F. *J. Organomet. Chem.* **1985**, *292*, 19.

°C. After 10 min at -50 °C, the solution was warmed to ambient temperature. The progress of the reaction was followed by IR spectroscopy. When all of the starting material was consumed, the solvent was removed in vacuo. The remaining residue was washed twice with 30 mL of Et₂O and recrystallized from mixtures of CH₂Cl₂ and pentane. Pure **3a**-OTf (0.55 g, 0.56 mmol; 91%) was obtained as a light yellow powder. ¹H NMR (400 MHz, CD₂Cl₂): δ 3.23 (s, 3H, NCH₃), 3.40 (s, 3H, NCH₃), 3.74 (s, 3H, OCH₃), 7.03–7.11 (m, 18H, ArH), 7.21–7.25 (m, 12H, ArH). ¹³C NMR (100 MHz, CD₂Cl₂): δ 35.1 (NCH₃), 40.3 (NCH₃), 61.7 (OCH₃), 96.1 (C_β), 120.9 (q, ¹J_{CF} = 316.4 Hz, CF₃), 128.9 (t, ³J_{PC} = 5.8 Hz, *m*-C), 129.9 (t, ¹J_{PC} = 25.3 Hz, *i*-C), 132.2 (*p*-C), 135.4 (t, ²J_{PC} = 6.0 Hz, *o*-C), 150.9 (t, ³J_{PC} = 5.5 Hz, C_α), 154.1 (C_γ). ³¹P NMR (162 MHz, CD₂Cl₂): δ 24.5. IR (THF): ν(CCC) 2099 cm⁻¹. UV–vis (CH₂Cl₂): λ_{max} (nm) (log ε) 236 (4.563), 298 (4.361). FAB-MS: *m/z* (%) 821 (56) [(M – CF₃SO₃)⁺], 560 (48) [(M – CF₃SO₃ – PPh₃)⁺]. Anal. Calcd for C₄₃H₃₉BrF₃NO₄P₂PdS (971.11): C, 53.18; H, 4.05; N, 1.44. Found: C, 53.49; H, 4.46; N, 1.34.

trans-Bromobis(triphenylphosphine)(3-dimethylamino-3-methoxy-1,2-propadienyldiene)palladium(II) Tetrafluoroborate (3a-BF₄). The synthesis of **3a**-BF₄ from 1.0 g (1.24 mmol) of **2a** and 0.25 g (1.70 mmol, 1.4 equiv) of [Me₃O]BF₄ in 60 mL of CH₂Cl₂ was carried out analogously to **3a**-OTf. Yield: 0.70 g (0.77 mmol; 62%) of **3a**-BF₄ as a yellow powder. ¹H NMR (400 MHz, CD₂Cl₂): δ 2.69 (s, 3 H, NCH₃), 2.91 (s, 3 H, NCH₃), 3.31 (s, 3 H, OCH₃), 7.45–7.56 (m, 18 H, ArH), 7.66–7.71 (m, 12 H, ArH). ¹³C NMR (100 MHz, CD₂Cl₂): δ 37.7 (NCH₃), 41.7 (NCH₃), 61.3 (OCH₃), 128.8 (t, ³J_{PC} = 5.6 Hz, *m*-C), 130.2 (t, ¹J_{PC} = 25.7 Hz, *i*-C), 131.8 (*p*-C), 135.1 (t, ²J_{PC} = 6.4 Hz, *o*-C), C_α, C_β, C_γ, not observed. ³¹P NMR (162 MHz, CD₂Cl₂): δ 24.7. IR (CH₂Cl₂): ν(CCC) 2098 cm⁻¹. UV–vis (CH₂Cl₂): λ_{max} (nm) (log ε) 298 (4.368). FAB-MS: *m/z* (%) 822 (72) [(M – BF₄)⁺], 560 (37) [(M – BF₄ – PPh₃)⁺]. Anal. Calcd for C₄₂H₃₉BBBrF₄NOP₂Pd • 0.5CH₂Cl₂ (908.85): C, 53.66; H, 4.24; N, 1.47. Found: C, 53.83; H, 4.51; N, 1.49.

trans-Bromobis(triphenylphosphine)(3-*N,N*-tetramethyleneamino-3-methoxy-1,2-propadienyldiene)palladium(II) Trifluoromethanesulfonate (3b-OTf). The synthesis of **3b**-OTf from 0.32 g (0.38 mmol) of **2b** and 0.04 mL (0.38 mmol) of MeOTf in 20 mL of CH₂Cl₂ was carried out analogously to **3a**-OTf. Yield: 0.82 g (0.82 mmol; 97%) of **3b**-OTf as a yellow powder. ¹H NMR (400 MHz, CD₂Cl₂): δ 1.70 (m, 2 H, CH₂), 1.87 (m, 2 H, CH₂), 2.68 (t, *J* = 7.0 Hz, 2 H, NCH₂), 3.27 (s, 3 H, OCH₃), 3.34 (t, *J* = 7.0 Hz, 2 H, NCH₂), 7.42–7.50 (m, 18 H, ArH), 7.63–7.67 (m, 12 H, ArH). ¹³C NMR (100 MHz, CD₂Cl₂): δ 24.2 (CH₂), 24.4 (CH₂), 48.9 (NCH₂), 51.4 (NCH₂), 60.4 (OCH₃), 93.8 (C_β), 128.5 (t, ³J_{PC} = 5.6 Hz, *m*-C), 129.8 (t, ¹J_{PC} = 25.9 Hz, *i*-C), 131.4 (*p*-C), 134.7 (t, ²J_{PC} = 6.2 Hz, *o*-C), 147.8 (C_α), 150.9 (C_γ). ³¹P NMR (162 MHz, CDCl₃): δ 24.9. IR (CH₂Cl₂): ν(CCC) 2100 cm⁻¹; ν(CO) 1612 cm⁻¹. UV–vis (CH₂Cl₂): λ_{max} (nm) (log ε) 296 (4.437). FAB-MS: *m/z* (%) 847 (32) [(M – OTf)⁺], 586 (20) [(M – OTf – PPh₃)⁺], 505 (11) [(M – OTf – PPh₃ – Br)⁺], 323 (59) [(M – OTf – 2 PPh₃)⁺]. Anal. Calcd for C₄₅H₄₁BrF₃NO₄P₂PdS (997.15): C, 54.20; H, 4.14; N, 1.40. Found: C, 54.16; H, 4.19; N, 1.36.

trans-Bromobis(triphenylphosphine)(3-*N,N*-tetramethyleneamino-3-methoxy-1,2-propadienyldiene)palladium(II) Tetrafluoroborate (3b-BF₄). The synthesis of **3b**-BF₄ from 0.48 g (0.58 mmol) of **2b** and 0.10 g (0.69 mmol, 1.2 equiv) of [Me₃O]BF₄ in 30 mL of CH₂Cl₂ was carried out analogously to **3a**-OTf. Yield: 0.52 g (0.56 mmol; 97%) of **3b**-BF₄ as a yellow powder. ¹H NMR (400 MHz, CDCl₃): δ 1.69 (m, 2 H, CH₂), 1.86 (m, 2 H, CH₂), 2.67 (t, *J* = 7.0 Hz, 2 H, NCH₂), 3.24 (s, 3 H, OCH₃), 3.34 (t, *J* = 7.0 Hz, 2 H, NCH₂), 7.37–7.51 (m, 18 H, ArH), 7.63–7.70 (m, 12 H, ArH). ¹³C NMR (100 MHz, CDCl₃): δ 24.5 (CH₂), 24.7 (CH₂), 49.2 (NCH₂), 51.7 (NCH₂), 60.7 (OCH₃), 94.3 (C_β), 128.8 (t, ³J_{PC} = 5.3 Hz, *m*-C), 130.1 (t, ¹J_{PC} = 26.0 Hz, *i*-C), 131.7 (*p*-C), 135.1 (t, ²J_{PC} = 6.2 Hz, *o*-C), 151.2 (C_α), 154.1 (C_γ). ³¹P NMR (162 MHz, CD₂Cl₂): δ 25.0. IR (CH₂Cl₂): ν(CCC) 2101 cm⁻¹; ν(CO) 1609

cm⁻¹. UV–vis (CH₂Cl₂): λ_{max} (nm) (log ε) 300 (4.376). FAB-MS: *m/z* (%) 847 (19) [(M – BF₄)⁺], 586 (16) [(M – BF₄ – PPh₃)⁺], 505 (9) [(M – BF₄ – PPh₃ – Br)⁺], 324 (40) [(M – BF₄ – 2 PPh₃)⁺]. Anal. Calcd for C₄₄H₄₁BBBrF₄NOP₂Pd • 0.5CH₂Cl₂ (934.89): C, 54.69; H, 4.33; N, 1.43. Found: C, 54.52; H, 4.51; N, 1.35.

trans-Bromobis(triphenylphosphine)(3-dimethylamino-3-ethoxy-1,2-propadienyldiene)palladium(II) Tetrafluoroborate (4a-BF₄). The synthesis of **4a**-BF₄ from 91 mg (0.11 mmol) of **2a** and 21 mg (0.11 mmol) of [Et₃O]BF₄ in 5 mL of CH₂Cl₂ was carried out analogously to **3a**-OTf. Yield: 77 mg (0.08 mmol; 76%) of **4a**-BF₄ as a yellow powder. ¹H NMR (400 MHz, CD₂Cl₂): δ 1.01 (t, *J* = 7.0 Hz, 2 H, CH₃), 2.69 (s, 3 H, NCH₃), 2.90 (s, 3 H, NCH₃), 3.54 (q, *J* = 7.0 Hz, 2 H, CH₂), 7.45–7.56 (m, 18 H, ArH), 7.67–7.72 (m, 12 H, ArH). ¹³C NMR (100 MHz, CD₂Cl₂): δ 14.3 (OCH₂CH₃), 37.5 (NCH₃), 41.4 (NCH₃), 71.9 (OCH₂CH₃), 93.1 (t, ³J_{PC} = 4.8 Hz, C_β), 128.8 (t, ³J_{PC} = 5.8 Hz, *m*-C), 130.1 (t, ¹J_{PC} = 25.9 Hz, *i*-C), 131.7 (*p*-C), 135.0 (t, ²J_{PC} = 5.8 Hz, *o*-C), 149.3 (t, ²J_{PC} = 12.5 Hz, C_α), 152.9 (C_γ). ³¹P NMR (162 MHz, CD₂Cl₂): δ 24.8. IR (CH₂Cl₂): ν(CCC) 2099 cm⁻¹. UV–vis (CH₂Cl₂): λ_{max} (nm) (log ε) 300 (4.335). FAB-MS: *m/z* (%) 834 (44) [(M – BF₄)⁺], 573 (18) [(M – BF₄ – PPh₃)⁺]. Anal. Calcd for C₄₃H₄₁BBBrF₄NOP₂Pd (922.88): C, 55.96; H, 4.48; N, 1.52. Found: C, 56.02; H, 4.50; N, 1.44.

trans-Bromobis(triphenylphosphine)(3-*N,N*-tetramethyleneamino-3-ethoxy-1,2-propadienyldiene)palladium(II) Tetrafluoroborate (4b-BF₄). The synthesis of **4b**-BF₄ from 0.81 g (0.97 mmol) of **2b** and 0.18 g (0.97 mmol) of [Et₃O]BF₄ in 30 mL of CH₂Cl₂ was carried out analogously to **3a**-OTf. Yield: 0.92 g (0.96 mmol; 99%) of **4b**-BF₄ as a yellow powder. ¹H NMR (400 MHz, CD₂Cl₂): δ 0.95 (t, *J* = 7.0 Hz, 3 H, OCH₂CH₃), 1.86 (m, 2 H, CH₂), 2.67 (t, *J* = 7.0 Hz, 2 H, NCH₂), 3.31 (t, *J* = 7.0 Hz, 2 H, NCH₂), 3.48 (q, *J* = 7.0 Hz, 2 H, OCH₂CH₃), 7.42–7.50 (m, 18 H, ArH), 7.62–7.67 (m, 12 H, ArH). ¹³C NMR (100 MHz, CD₂Cl₂): δ 14.2 (OCH₂CH₃), 24.1 (CH₂), 24.3 (CH₂), 48.8 (NCH₂), 51.3 (NCH₂), 70.7 (OCH₂CH₃), 94.1 (C_β), 128.4 (t, ³J_{PC} = 5.7 Hz, *m*-C), 129.8 (t, ¹J_{PC} = 26.0 Hz, *i*-C), 131.4 (*p*-C), 134.7 (t, ²J_{PC} = 5.7 Hz, *o*-C), 145.8 (C_α), 150.1 (C_γ). ³¹P NMR (162 MHz, CD₂Cl₂): δ 21.8. IR (CH₂Cl₂): ν(CCC) 2101 cm⁻¹; ν(CO) 1604 cm⁻¹. UV–vis (CH₂Cl₂): λ_{max} (nm) (log ε) 297 (4.462). FAB-MS: *m/z* (%) 861 (50) [(M – BF₄)⁺], 600 (37) [(M – BF₄ – PPh₃)⁺]. Anal. Calcd for C₄₅H₄₃BBBrF₄NOP₂Pd (948.92): C, 56.96; H, 4.57; N, 1.48. Found: C, 56.83; H, 4.53; N, 1.55.

trans-Bromobis(triisopropylphosphine)(3-dimethylamino-3-oxy-1-propynyl)palladium(II) (5a). At ambient temperature, a solution of 0.55 g (0.68 mmol) of **2a** in 30 mL of CH₂Cl₂ was treated with 0.29 mL (1.50 mmol, 2.2 equiv) of P^rPr₃. The progress of the reaction was monitored by IR spectroscopy. When all of the starting material was consumed (60 min), the solvent was removed in vacuo and the crude product purified by column chromatography using a petroleum ether/Et₂O mixture as the eluant. Removal of the solvent gave 0.29 g (0.47 mmol, 70%) of pure **5a** as a white powder. ¹H NMR (400 MHz, CD₂Cl₂): δ 1.35 (q, *J* = 7.04 Hz, 36H, CH(CH₃)₂), 2.82 (s, 3H, NCH₃), 2.89 (m, 6H, CH(CH₃)₂), 3.10 (s, 3H, NCH₃). ¹³C NMR (100 MHz, CD₂Cl₂): δ 20.1 (CH(CH₃)₂), 24.7 (t, ²J_{PC} = 11.5 Hz, CH(CH₃)₂), 33.7 (NCH₃), 38.0 (NCH₃), 103.7 (t, ³J_{PC} = 4.8 Hz, Pd–C≡C), 107.7 (t, ²J_{PC} = 12.6 Hz, Pd–C≡C), 155.3 (C(O)NMe₂). ³¹P NMR (162 MHz, CD₂Cl₂): δ 42.1. IR (THF): ν(C≡C) 2098 cm⁻¹; ν(CO) 1605 cm⁻¹. UV–vis (CH₂Cl₂): λ_{max} (nm) (log ε) 251 (4.134), 288 (4.167). MS (FAB): *m/z* (%) 604 (19) [M⁺], 523 (24) [(M – Br)⁺], 362 (11) [(M – Br – P^r(Pr)₃)⁺]. Anal. Calcd for C₂₃H₄₈BrNOP₂Pd (602.91): C, 45.82; H, 8.02; N, 2.32. Found: C, 46.03; H, 7.97; N, 2.39.

trans-Bromobis(triisopropylphosphine)(3-*N,N*-tetramethyleneamino-3-oxy-1-propynyl)palladium(II) (5b). The synthesis of **5b** from 1.23 g (1.48 mmol) of **2b** and 0.62 mL (3.25 mmol, 2.2 equiv) of P^rPr₃ in 30 mL of CH₂Cl₂ was carried out analogously to **5a**. The crude product was purified by column chromatography using

an ether/CH₂Cl₂/acetone mixture. Yield: 0.65 g (1.03 mmol; 70%) of **5b** as a white powder. ¹H NMR (400 MHz, CDCl₃): δ 1.38 (m, 36 H, CH(CH₃)₂), 1.87 (br, 4H, CH₂CH₂), 2.94 (m, 6 H, CH(CH₃)₂), 3.40 (t, *J* = 6.6 Hz, 2H, NCH₂), 3.53 (t, *J* = 6.6 Hz, 2H, NCH₂). ¹³C NMR (100 MHz, CDCl₃): δ 19.6 (CH(CH₃)₂), 24.0 (t, ²*J*_{PC} = 11.6 Hz, CH(CH₃)₂), 24.3 (CH₂), 25.2 (CH₂), 44.3 (NCH₂), 47.0 (NCH₂), 103.9 (t, ³*J*_{PC} = 4.8 Hz, Pd–C≡C), 106.0 (t, ²*J*_{PC} = 12.4 Hz, Pd–C≡C), 153.1 (C(O)NC₄H₈). ³¹P NMR (162 MHz, CDCl₃): δ 41.7. IR (CH₂Cl₂): ν(CCC) 2106 cm⁻¹. UV–vis (CH₂Cl₂): λ_{max} (nm) (log ε) 287 (4.224). FAB-MS: *m/z* (%) 629 (39) [M⁺], 549 (18) [(M – Br)⁺], 470 (6) [(M – P(Pr)₃)⁺], 389 (9) [(M – Br – P(Pr)₃)⁺], 347 (6) [(M – P(Pr)₃)⁺ – C₇H₈NO], 267 (38) [(M – Br – P(Pr)₃ – C₇H₈NO)⁺]. Anal. Calcd for C₂₅H₅₀BrNOP₂Pd (628.95): C, 47.74; H, 8.01; N, 2.23. Found: C, 47.68; H, 7.74; N, 2.57.

trans-Bromobis(triisopropylphosphine)(3-dimethylamino-3-methoxy-1,2-propadienyldiene)palladium(II) Trifluoromethanesulfonate (6a-OTf). The synthesis of **6a-OTf** from 0.3 g (0.50 mmol) of **5a** and 0.06 mL (0.50 mmol) of MeOTf in 30 mL of CH₂Cl₂ was carried out analogously to **3a-OTf**. Complex **6a-OTf** was recrystallized from Et₂O. Yield: 0.37 g (0.49 mmol; 98%) of **6a-OTf** as a colorless powder. ¹H NMR (400 MHz, CD₂Cl₂): δ 1.35 (q, *J* = 7.04 Hz, 36H, CH(CH₃)₂), 2.85 (m, 6H, CH(CH₃)₂), 3.25 (s, 3H, NCH₃), 3.45 (s, 3H, NCH₃), 4.20 (s, 3H, OCH₃). ¹³C NMR (100 MHz, CD₂Cl₂): δ 20.0 (CH(CH₃)₂), 25.0 (t, ²*J*_{PC} = 11.8 Hz, CH(CH₃)₂), 38.3 (NCH₃), 42.1 (NCH₃), 61.7 (OCH₃), 94.6 (t, ³*J*_{PC} = 3.8 Hz, C_β), 121.4 (q, ¹*J*_{CF} = 320.0 Hz, CF₃), 150.3 (t, ²*J*_{PC} = 10.6 Hz, C_ω), 153.7 (C_γ). ³¹P NMR (162 MHz, CD₂Cl₂): δ 45.3. IR (THF): ν(CCC) 2083 cm⁻¹. UV–vis (CH₂Cl₂): λ_{max} (nm) (log ε) 247 (4.103), 279 (4.371). FAB-MS: *m/z* (%) 618 (75) [(M – OTf)⁺], 458 (48) [(M – OTf – P(Pr)₃)⁺]. Anal. Calcd for C₂₅H₅₁BrF₃NO₄P₂PdS (767.01): C, 40.80; H, 6.98; N, 1.90. Found: C, 39.38; H, 6.33; N, 1.54.

trans-Bromobis(triisopropylphosphine)(3-*N,N*-tetramethyleneamino-3-methoxy-1,2-propadienyldiene)palladium(II) Trifluoromethanesulfonate (6b-OTf). The synthesis of **6b-OTf** from 0.18 g (0.27 mmol) of **5b** and 0.03 mL (0.27 mmol) of MeOTf in 10 mL of CH₂Cl₂ was carried out analogously to **3a-OTf**. Yield: 0.21 g (0.26 mmol; 97%) of **6b-OTf** as a white powder. ¹H NMR (400 MHz, CDCl₃): δ 1.33 (m, 36 H, CH(CH₃)₂), 2.02 (br, 4H, CH₂CH₂), 2.84 (m, 6 H, CH(CH₃)₂), 3.76 (t, *J* = 7.0 Hz, 4 H, NCH₂), 4.15 (s, 3 H, OCH₃). ¹³C NMR (100 MHz, CDCl₃): δ 19.9 (CH(CH₃)₂), 24.7 (t, ¹*J*_{PC} = 11.1 Hz, CH(CH₃)₂), 24.3 (CH₂), 24.5 (CH₂), 49.3 (NCH₂), 51.8 (NCH₂), 60.7 (OCH₃), 95.3 (t, ³*J*_{PC} = 3.8 Hz, C_β), 120.8 (q, ¹*J*_{CF} = 320.0 Hz, CF₃), 147.1 (t, ²*J*_{PC} = 11.6 Hz, C_ω), 151.1 (C_γ). ³¹P NMR (162 MHz, CDCl₃): δ 45.1. IR (CH₂Cl₂): ν(CCC) 2086 cm⁻¹; ν(CO) 1612 cm⁻¹. UV–vis (CH₂Cl₂): λ_{max} (nm) (log ε) 280 (4.365). FAB-MS: *m/z* (%) 644 (70) [(M – OTf)⁺], 483 (65) [(M – OTf – PPh₃)⁺], 403 (13) [(M – OTf – PPh₃ – Br)⁺]. Anal. Calcd for C₂₇H₅₃BrF₃NO₄P₂PdS (793.05): C, 40.89; H, 6.74; N, 1.77. Found: C, 40.85; H, 7.19; N, 1.54.

trans-Bromobis[tris(4-methoxyphenyl)phosphine](3-*N,N*-tetramethyleneamino-3-oxy-1-propynyl)palladium(II) (7b). The synthesis of **7b** from 0.42 g (0.50 mmol) of **2b** and 0.39 g (1.10 mmol, 2.2 equiv) of P(C₆H₄OMe-4)₃ in 30 mL of CH₂Cl₂ was carried out analogously to **5a**. The crude product was purified by column chromatography using a petroleum ether/CH₂Cl₂/acetone mixture. Yield: 0.37 g (0.37 mmol; 74%) of **7b** as a pale yellow powder. ¹H NMR (400 MHz, CDCl₃): δ 1.40 (m, 2H, CH₂), 1.58 (m, 2H, CH₂), 2.32 (t, *J* = 6.8 Hz, 2H, NCH₂), 3.06 (t, *J* = 6.6 Hz, 2H, NCH₂), 3.78 (s, 18H, OCH₃), 6.85–6.87 (m, 12 H, ArH), 7.57–7.61 (m, 12 H, ArH). ¹³C NMR (100 MHz, CDCl₃): δ 24.5 (CH₂), 24.9 (CH₂), 44.1 (NCH₂), 47.0 (NCH₂), 55.1 (OCH₃), 104.5 (t, ³*J*_{PC} = 3.5 Hz, Pd–C≡C), 109.2 (t, ³*J*_{PC} = 9.0 Hz, Pd–C≡C), 113.5 (ArC), 122.7 (t, ²*J*_{PC} = 27.8 Hz, ArC), 136.3 (ArC), 153.1 (C(O)NC₄H₈), 161.1 (ArC). ³¹P NMR (162 MHz, CDCl₃): δ 20.2. IR (CH₂Cl₂): ν(CCC) 2114 cm⁻¹. UV–vis (CH₂Cl₂): λ_{max} (nm) (log ε)

317 (4.420). FAB-MS: *m/z* (%) 1013 (20) [M⁺], 933 (85) [(M – Br)⁺], 580 (27) [(M – Br – P(C₆H₄OMe-*p*)₃)⁺]. Anal. Calcd for C₄₉H₅₀BrNO₇P₂Pd × 0.5 CH₂Cl₂ (1013.21): C, 56.32; H, 4.87; N, 1.33. Found: C, 55.69; H, 4.86; N, 1.02.

trans-Bromobis[tris(4-methoxyphenyl)phosphine](3-*N,N*-tetramethyleneamino-3-methoxy-1,2-propadienyldiene)palladium(II) Trifluoromethanesulfonate (8b-OTf). The synthesis of **8b-OTf** from 0.58 g (0.57 mmol) of **7b** and 0.07 mL (0.57 mmol) of MeOTf in 20 mL of CH₂Cl₂ was carried out analogously to **3a-OTf**. Yield: 0.62 g (0.52 mmol; 91%) of **8b-OTf** as a yellow powder. ¹H NMR (400 MHz, CDCl₃): δ 1.68 (m, 2H, CH₂), 1.85 (m, 2H, CH₂), 2.72 (m, 2H, NCH₂), 3.35 (m, 2H, NCH₂), 3.78 (s, 3H, OCH₃), 3.81 (s, 18 H, OCH₃), 6.92–6.95 (m, 12 H, ArH), 7.52–7.57 (m, 12 H, ArH). ¹³C NMR (100 MHz, CDCl₃): δ 24.1 (CH₂), 24.4 (CH₂), 48.7 (NCH₂), 51.3 (NCH₂), 55.4 (OCH₃), 60.5 (OCH₃), 93.9 (C_β), 114.0 (ArC), 121.6 (t, ¹*J*_{PC} = 28.7 Hz, ArC), 136.3 (t, ²*J*_{PC} = 7.1 Hz, ArC), 151.1 (C_γ), 161.8 (ArC), 177.0 (C_ω). ³¹P NMR (162 MHz, CDCl₃): δ 20.4. ¹⁹F NMR (376 MHz, CDCl₃): δ –78.2. IR (CH₂Cl₂): ν(CCC) 2098 cm⁻¹. UV–vis (CH₂Cl₂): λ_{max} (nm) (log ε) 328 (4.352). FAB-MS: *m/z* (%) 1028 (8) [(M – OTf)⁺], 948 (8) [(M – OTf – Br)⁺], 595 (23) [(M – OTf – Br – P(C₆H₄OMe-*p*)₃)⁺]. Anal. Calcd for C₅₁H₅₃BrF₃NO₁₀P₂PdS (1177.32): C, 52.03; H, 4.54; N, 1.19. Found: C, 52.10; H, 4.72; N, 1.26.

trans-(Trifluoroacetato)bis(triphenylphosphine)(3-dimethylamino-3-oxy-1-propynyl)palladium(II) (9a). A suspension of 0.55 g (0.68 mmol) of **2a** and 0.15 g (0.68 mmol) of CF₃COOAg in 30 mL of dry CH₂Cl₂ was stirred for 30 min. The precipitate (AgBr) that formed was filtered off. The solvent of the crude reaction mixture was removed in vacuo. Crystallization of the crude product from CH₂Cl₂/Et₂O gave 0.54 g (0.65 mmol; 96%) of **9a** as a colorless powder. ¹H NMR (400 MHz, CD₂Cl₂): δ 1.93 (s, 3H, NCH₃), 2.47 (s, 3H, NCH₃), 7.41–7.51 (m, 18H, ArH), 7.71–7.79 (m, 12H, ArH). ¹³C NMR (100 MHz, CD₂Cl₂): δ 33.2 (NCH₃), 37.2 (NCH₃), 93.8 (t, ²*J*_{PC} = 10.7 Hz, Pd–C≡C), 107.4 (Pd–C≡C), 107.4 (CF₃COO), 128.4 (t, ³*J*_{PC} = 5.7 Hz, *m*-C), 129.6 (t, ¹*J*_{PC} = 25.0 Hz, *i*-C), 131.2 (*p*-C), 134.1 (t, ²*J*_{PC} = 5.3 Hz, *o*-C), 154.3 (C(O)NMe₂), 174.3 (CF₃COO). ³¹P NMR (162 MHz, CD₂Cl₂): δ 23.9. IR (THF): ν(C≡C) 2114 cm⁻¹; ν(CO) 1680, 1609 cm⁻¹. UV–vis (CH₂Cl₂): λ_{max} (nm) (log ε) 239 (4.513), 297 (4.449). FAB-MS: *m/z* (%) 727 (11) [(M – CF₃COO)⁺], 631 (62) [(M – CF₃COO – C₅H₆NO)⁺], 369 (62) [(M – CF₃COO – C₅H₆NO – PPh₃)⁺]. Anal. Calcd for C₄₃H₃₆F₃NO₃P₂Pd · CH₂Cl₂ (840.13): C, 57.13; H, 4.14; N, 1.51. Found: C, 57.52; H, 4.30; N, 1.81.

trans-(Trifluoroacetato)bis(triphenylphosphine)(3-dimethylamino-3-methoxy-1,2-propadienyldiene)palladium(II) Trifluoromethanesulfonate (10a-OTf). The synthesis of **10a-OTf** from 0.49 g (0.58 mmol) of **9a** and 0.07 mL (0.62 mmol) of MeOTf in 30 mL of CH₂Cl₂ was carried out analogously to **3a-OTf**. Recrystallization from mixtures of CH₂Cl₂ and pentane afforded 0.52 g (0.52 mmol, 90%) of pure **10a-OTf** as a colorless powder. ¹H NMR (400 MHz, CD₂Cl₂): δ 2.46 (s, 3H, NCH₃), 2.80 (s, 3H, NCH₃), 3.03 (s, 3H, OCH₃), 7.38–7.47 (m, 18H, ArH), 7.58–7.65 (m, 12H, ArH). ¹³C NMR (100 MHz, CD₂Cl₂): δ 38.0 (NCH₃), 41.5 (NCH₃), 61.2 (OCH₃), 95.6 (C_β), 110.9 (CF₃COO), 120.0 (SO₃CF₃), 128.3 (t, ¹*J*_{PC} = 25.8 Hz, *i*-C), 129.3 (t, ³*J*_{PC} = 5.8 Hz, *m*-C), 132.1 (*p*-C), 134.7 (t, ²*J*_{PC} = 6.7 Hz, *o*-C), 137.9 (t, ³*J*_{PC} = 5.7 Hz, C_ω), 153.7 (C_γ), 172.8 (CF₃COO). ³¹P NMR (162 MHz, CD₂Cl₂): δ 25.9. IR (THF): ν(CCC) 2102 cm⁻¹; ν(CO) 1678 cm⁻¹. UV–vis (CH₂Cl₂): λ_{max} (nm) (log ε) 251 (4.359), 307 (4.528). FAB-MS: *m/z* (%) 855 (13) [(M – OTf)⁺], 592 (80) [(M – OTf – PPh₃)⁺], 478 (39) [(M – OTf – PPh₃ – CF₃COO)⁺]. Anal. Calcd for C₄₅H₃₉F₆NO₆P₂ · PdS · 0.5CH₂Cl₂ (1004.23): C, 52.21; H, 3.85; N, 1.34. Found: C, 51.94; H, 4.07; N, 1.44.

trans-(Trifluoroacetato)bis(triphenylphosphine)(3-dimethylamino-3-methoxy-1,2-propadienyldiene)palladium(II) Tetrafluoroborate (10a-BF₄). The synthesis of **10a-BF₄** from 0.47 g (0.56 mmol) of **9a** and 99 mg (0.67 mmol, 1.2 equiv) of [Me₃O]BF₄ in 30 mL of

CH_2Cl_2 was carried out analogously to **3a**-OTf. Yield: 0.45 g (0.48 mmol; 86%) of **10a**- BF_4 as an off-white powder. ^1H NMR (400 MHz, CDCl_3): δ 2.55 (s, 3 H, NCH_3), 2.89 (s, 3 H, NCH_3), 3.10 (s, 3 H, OCH_3), 7.49–7.57 (m, 18 H, ArH), 7.68–7.72 (m, 12 H, ArH). ^{13}C NMR (100 MHz, CD_2Cl_2): δ 38.0 (NCH_3), 41.7 (NCH_3), 61.3 (OCH_3), 128.4 (t, $^1J_{\text{PC}} = 25.9$ Hz, *i*-C), 129.4 (t, $^3J_{\text{PC}} = 5.7$ Hz, *m*-C), 132.2 (*p*-C), 134.9 (t, $^2J_{\text{PC}} = 6.4$ Hz, *o*-C), 153.8 (C $_{\gamma}$); C $_{\alpha}$, C $_{\beta}$, CF_3COO not observed. ^{31}P NMR (162 MHz, CD_2Cl_2): δ 26.2. IR (THF): $\nu(\text{CCC})$ 2103 cm^{-1} ; $\nu(\text{CO})$ 1678 cm^{-1} . UV–vis (CH_2Cl_2): λ_{max} (nm) (log ϵ) 307 (4.450). FAB-MS: *m/z* (%) 854 (33) [(M – BF_4) $^+$], 663 (100) [(M – BF_4 – CF_3COO – Ph) $^+$], 631 (49) [(M – BF_4 – CF_3COO – $\text{CCC}(\text{OMe})\text{NMe}_2$) $^+$], 592 (68) [(M – BF_4 – PPh_3) $^+$], 479 (37) [(M – BF_4 – PPh_3 – CF_3COO) $^+$], 369 (82) [(M – BF_4 – PPh_3 – CF_3COO – $\text{CCC}(\text{OMe})\text{NMe}_2$) $^+$]. Anal. Calcd for $\text{C}_{44}\text{H}_{39}\text{BF}_7\text{NO}_3\text{P}_2\text{Pd}$ (941.96): C, 56.10; H, 4.17; N, 1.49. Found: 56.03; H, 4.22; N, 1.42.

X-ray Structural Analysis of **5b** and **10a**- BF_4 . Data for **5b**:

$\text{C}_{25}\text{H}_{50}\text{BrNOP}_2\text{Pd} \cdot \text{CDCl}_3$, $M_r = 748.28$, monoclinic, space group $P2_1/c$, $a = 8.9048(18)$ Å, $b = 11.445(2)$ Å, $c = 32.830(7)$ Å, $\beta = 91.24(3)^\circ$, $V = 3345.1(12)$ Å 3 , $Z = 4$, $d_{\text{calcd}} = 1.486$ g cm^{-3} , $F(000) = 1536$, $\mu = 2.104$ mm^{-1} , $2\theta_{\text{max}} = 51.3^\circ$, index ranges $-10 \leq h \leq 10$, $-13 \leq k \leq 13$, $-39 \leq l \leq 39$, 36 114 data (6273 unique), $R(\text{int}) = 0.0931$, 319 parameters, $R1$ ($I > 2\sigma(I)$) = 0.0343, $wR2 = 0.0776$, goodness of fit on F^2 1.042, $\Delta\rho_{\text{max}}$ ($\Delta\rho_{\text{min}}$) = 0.649 (–0.855) e Å $^{-3}$.

Data for **10a- BF_4** : $\text{C}_{46}\text{H}_{43}\text{BCl}_4\text{F}_7\text{NO}_3\text{P}_2\text{Pd}$, $M_r = 1111.76$, monoclinic, space group $P2_1/n$, $a = 11.612(2)$ Å, $b = 23.143(5)$ Å, $c = 18.136(4)$ Å, $\beta = 90.71(3)^\circ$, $V = 4873.5(17)$ Å 3 , $Z = 4$, $d_{\text{calcd}} =$

1.515 g cm^{-3} , $F(000) = 2248$, $\mu = 0.733$ mm^{-1} , $2\theta_{\text{max}} = 53.7^\circ$, index ranges $-14 \leq h \leq 14$, $-29 \leq k \leq 29$, $-23 \leq l \leq 22$, 70 118 data: (10 300 unique), $R(\text{int}) = 0.0879$, 586 parameters, $R1$ ($I > 2\sigma(I)$) = 0.0406, $wR2 = 0.0959$, goodness of fit on F^2 1.023, $\Delta\rho_{\text{max}}$ ($\Delta\rho_{\text{min}}$) = 1.132 (–0.975) e Å $^{-3}$.

Single crystals suitable for an X-ray structural analysis of **5b** were grown from CDCl_3 and those of **10a**- BF_4 by slow diffusion of hexane into a concentrated solution of **10a**- BF_4 in CH_2Cl_2 at 4 °C. The measurements were performed at 100(2) K with a crystal mounted on a glass fiber on a Stoe IPDS II diffractometer (graphite monochromator, Mo K α radiation, $\lambda = 0.71073$ Å). The structures were solved by direct methods using the SHELX-97 program package.²¹ The positions of the hydrogen atoms were calculated by assuming ideal geometry, and their coordinates were refined together with those of the attached carbon atoms as the riding model. All other atoms were refined anisotropically.

Acknowledgment. Support of this work by the Wacker-Chemie GmbH (gift of chemicals) is gratefully acknowledged.

Supporting Information Available: CIF files of the complexes **5b** and **10a**- BF_4 and tables giving the bond distances, bond angles, and torsion angles of **5b** and **10a**- BF_4 . This material is available free of charge via the Internet at <http://pubs.acs.org>.

OM800843E

(21) Sheldrick, G. M. SHELXTL-97, Programs for Crystal Structure Analysis; University of Göttingen, Göttingen, Germany, 1997.

Evaluation of Molybdenum and Tungsten Metathesis Catalysts for Homogeneous Tandem Alkane Metathesis

Brad C. Bailey,[†] Richard R. Schrock,^{*,†} Sabuj Kundu,[‡] Alan S. Goldman,[‡] Zheng Huang,[§] and Maurice Brookhart[§]

Department of Chemistry 6-331, Massachusetts Institute of Technology, Cambridge, Massachusetts 02139, Department of Chemistry and Chemical Biology, Rutgers, The State University of New Jersey, Piscataway, New Jersey 08854, and Department of Chemistry, University of North Carolina, Chapel Hill, North Carolina 27599

Received September 9, 2008

Over 40 molybdenum and tungsten imido alkylidene mono(alkoxide) mono(pyrrolide) (MAP) or bis(alkoxide) olefin metathesis catalysts were examined in combination with Ir-based pincer-type catalysts for the metathesis of *n*-octane. The imido group, alkoxide, and metal in the metathesis catalysts were all found to be important variables. The best catalyst was W(NAr)(CHR)(OSiPh₃)₂ (Ar = 2,6-diisopropylphenyl), which performed about twice as well as the only previously employed catalyst, Mo(NAr)(CHR)[OCMe(CF₃)₂]₂. Product yields decreased at temperatures greater than 125 °C, most likely because of the instability of the metathesis catalysts at such temperatures. POCOP Ir catalysts gave higher yields than PCP Ir catalysts, although the latter exhibited some selectivity for formation of tetradecane. Eight catalysts were synthesized in situ through addition of alcohols to bis(2,5-dimethylpyrrolide) complexes; in situ catalysts were shown to perform approximately as well as the isolated complexes, which suggests that 2,5-dimethylpyrrole is not detrimental to the alkane metathesis process and that potential catalysts can be screened more conveniently in this way.

Introduction

As petroleum supplies dwindle, interest in new methods for the manipulation of current feedstocks will increase.¹ The ability to convert low-molecular-weight (MW) to high-MW alkanes is a challenging goal in this context. In particular, when Fischer–Tropsch chemistry and subsequent hydrocracking are employed to convert biomass, gas, or coal to liquids, it would be highly desirable to upgrade the resulting low-MW *n*-alkanes to high-grade (high cetane number) diesel fuel, particularly *n*-alkanes in the C9–C19 range. Such transformations potentially can be achieved via “alkane metathesis” (AM).

Alkane metathesis was first reported in 1973 by Burnett and Hughes,² who showed that when butane was passed over a mixture of a heterogeneous platinum on alumina (a dehydrogenation catalyst) and tungsten oxide on silica (an olefin metathesis catalyst) at ~400 °C, alkanes of lower and higher MW were formed, predominantly propane and pentane (25% and 16%, respectively). Heterogeneous “single component” Ta or W catalysts that function as alkane metathesis catalysts at much lower temperatures have been reported by the Basset

group.³ For example, propane can be converted in low yields to a mixture of C1 to C6 alkanes using silica-supported or alumina-supported Ta hydride catalysts. These catalysts are believed to operate through reactions that involve formation of alkylidene complexes and olefins from alkanes. Both branched and linear products are formed, as well as methane.

We have reported homogeneous AM systems that are comprised of two homogeneous catalysts (“tandem catalysts”) operating independently in the same solution (“tandem systems”); Scheme 1.⁴ One is an Ir-based pincer dehydrogenation/hydrogenation catalyst,⁵ while the second is Mo(NAr)-(CHCMe₂Ph)(OR_{F6})₂ (Ar = 2,6-*i*-Pr₂C₆H₃; OR_{F6} = OCMe(CF₃)₂), an olefin metathesis catalyst.⁶ A second system has been investigated using the Ir pincer complex in combination with the heterogeneous olefin metathesis catalyst Re₂O₇ on

(3) (a) Basset, J. M.; Copéret, C.; Lefort, L.; Maunders, B. M.; Maury, O.; Le Roux, E.; Saggio, G.; Soignier, S.; Soulivong, D.; Sunley, G. J.; Taoufik, M.; Thivolle-Cazat, J. *J. Am. Chem. Soc.* **2005**, *127*, 8604. (b) Le Roux, E.; Taoufik, M.; Copéret, C.; de Mallmann, A.; Thivolle-Cazat, J.; Basset, J.-M.; Maunders, B. M.; Sunley, G. *J. Angew. Chem., Int. Ed.* **2005**, *44*, 6755. (c) Vidal, V.; Theolier, A.; Thivolle-Cazat, J.; Basset, J.-M. *Science* **1997**, *276*, 99. (d) Thieuleux, C.; Copéret, C.; Dufaud, V.; Marangelli, C.; Kuntz, E.; Basset, J.-M. *J. Mol. Catal. A* **2004**, *213*, 47.

(4) (a) Goldman, A. S.; Roy, A. H.; Huang, Z.; Ahuja, R.; Schinski, W.; Brookhart, M. *Science* **2006**, *312*, 257. (b) Ahuja, R.; Kundu, S.; Goldman, A. S.; Brookhart, M.; Vincente, B. C.; Scott, S. L. *Chem. Commun.* **2008**, 253.

(5) (a) Götter-Schnetmann, I.; White, P.; Brookhart, M. *J. Am. Chem. Soc.* **2004**, *126*, 1804. (b) Götter-Schnetmann, I.; Brookhart, M. *J. Am. Chem. Soc.* **2004**, *126*, 9330. (c) Liu, F.; Pak, E. B.; Singh, B.; Jensen, C. M.; Goldman, A. S. *J. Am. Chem. Soc.* **1999**, *121*, 4086. (d) Xu, W.; Rosini, G. P.; Krogh-Jespersen, K.; Goldman, A. S.; Gupta, M.; Jensen, C. M.; Kaska, W. C. *Chem. Commun.* **1997**, 2273. (e) Zhu, K.; Achord, P. D.; Zhang, X.; Krogh-Jespersen, K.; Goldman, A. S. *J. Am. Chem. Soc.* **2004**, *126*, 13044.

(6) Schrock, R. R.; Murdzek, J. S.; Bazan, G. C.; Robbins, J.; DiMare, M.; O'Regan, M. *J. Am. Chem. Soc.* **1990**, *112*, 3875.

* To whom correspondence should be addressed. E-mail: rrs@mit.edu.

[†] Massachusetts Institute of Technology.

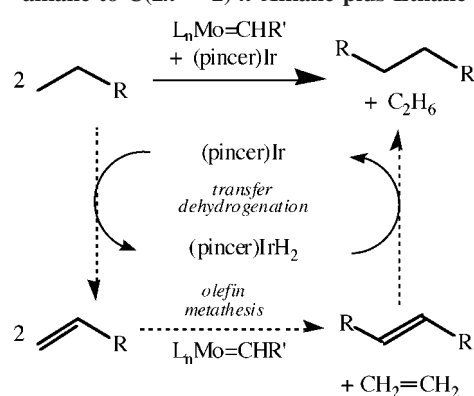
[‡] Rutgers, The State University of New Jersey.

[§] University of North Carolina.

(1) (a) Arndtsen, B. A.; Bergman, R. G.; Mobley, T. A.; Peterson, T. H. *Acc. Chem. Res.* **1995**, *28*, 154. (b) Shilov, A. E.; Shul'pin, G. B. *Chem. Rev.* **1997**, *97*, 2879. (c) Sen, A. *Acc. Chem. Res.* **1998**, *31*, 550. (d) Jones, W. D. *Science* **2000**, *287*, 1942. (e) Crabtree, R. H. *Dalton Trans.* **2001**, *17*, 2437. (f) Labinger, J. A.; Bercaw, J. E. *Nature* **2002**, *417*, 507. (g) Goldman, A. S.; Goldberg, K. I. In *Activation and Functionalization of C-H Bonds*; Goldberg, K. I., Goldman, A. S., Eds.; American Chemical Society: Washington, DC, 2004; ACS Symposium Series 885, pp 1–43.

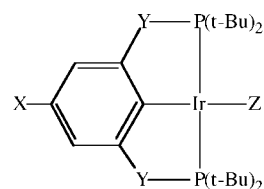
(2) Burnett, R. L.; Hughes, T. R. *J. Catal.* **1973**, *31*, 55.

Scheme 1. Alkane Metathesis by a (pincer)Ir Transfer-Dehydrogenation Catalyst and a Mo-Based Olefin Metathesis Catalyst Illustrated with Conversion of 2 mol of C(*n*) *n*-alkane to C(2*n* - 2) *n*-Alkane plus Ethane



alumina.⁷ The reactions are run in neat alkane (e.g., *n*-octane or *n*-decane); in some cases, after several days at 125 °C, an equilibrium distribution of linear alkanes is approached with production of chains longer and shorter than that of the initial alkane. No branched product or methane is observed. The homogeneous systems appear to be limited primarily by decomposition of the Mo-based metathesis catalyst. The Ir catalysts are relatively stable under the reaction conditions. The two documented modes of decomposition of Mo-based metathesis catalysts are bimolecular coupling of alkylidenes and rearrangement of metallacyclobutanes; both produce olefins and various reduced metal species.⁸ The low concentration of ethylene, which may promote rearrangement of metallacyclobutane intermediates,⁹ as well as the low rate of bimolecular coupling of alkylidenes at low catalyst concentrations, are believed to contribute to sustained metathesis activity for extended periods at 125 °C. While there is some possibility that alkylidenes actually are being re-formed from olefins and reduced metal species at high temperatures,¹⁰ no evidence for that process has been obtained in AM systems.

The only homogeneous olefin metathesis catalyst that has been reported for use in AM has been Mo(NAr)-(CHCMe₂Ph)(OR)₂. Since Mo and W catalysts of this type are modular,⁸ and since new catalysts have been discovered through addition of alcohols to bis(pyrrolide) precursors,^{11,12} hundreds of catalysts are now readily available. In this contribution we survey a number of known and new Mo and W alkylidene catalysts for activity in alkane metathesis of *n*-octane utilizing the five different iridium catalysts shown below.



- 1: X = H; Y = O; Z = C₂H₄
- 2: X = H; Y = O; Z = H₂
- 3: X = OMe; Y = O; Z = C₂H₄
- 4: X = OMe; Y = CH₂; Z = H₂
- 5: X = H; Y = CH₂; Z = H₂

Results and Discussion

New Mo and W catalysts were prepared in one of two ways. Mono(alkoxide) mono(pyrrolide) (MAP) complexes were prepared through alcoholysis of the bis(2,5-dimethylpyrrolide) precursor M(NR)(CHCMe₂Ph)(Me₂Pyr)₂ (Me₂Pyr = 2,5-dimethylpyrrolide) with 1 equiv of the respective alcohol.^{11,12} Bis(alkoxide) complexes of the type M(NR)(CHCMe₂Ph)(OR)₂ were prepared from M(NR)(CHCMe₂Ph)(OTf)₂(DME) precursors through salt metathesis reactions with various lithium alkoxides (see the Experimental Section and the Supporting Information). All new catalysts are soluble in common organic solvents and exhibit ¹H and ¹³C NMR spectra that are similar to those of previously characterized species. Spectroscopic details of the synthesis and characterization of new compounds (**8**, **9**, **15**, **16**, **23**, **24**, **29**, **30**, **33–35**, **39**, and **42–44**; Table 1) are available as Supporting Information.

Catalytic runs utilizing iridium catalyst **1** with **6–44** afforded product concentrations that varied from 15 to 3380 mM (Table 1). The one catalyst that has been employed in the literature so far (**31**) yielded total product concentrations of 1430 and 1640 mM in two different runs. Each catalytic run was performed with a 10 mM stock solution of **1** and the desired Mo or W catalyst (16 mM) in octane with mesitylene (28 mM) as the internal standard. Catalyst mixtures were placed in a glass ampule, which was then flame-sealed and heated to 125 °C. After 4 days at 125 °C, the tube was opened and the contents were analyzed by standard gas chromatography.

A few trends can be extracted from Table 1. First, different imido groups often give rise to dramatically different behavior. For example, complex **31** (1430, 1640 mM) is superior to either **10** (41 mM) or **20** (334, 358 mM); **10** and **20** contain (2-(trifluoromethyl)phenyl)imido and adamantylimido ligands, respectively, instead of a (2,6-diisopropylphenyl)imido ligand. The tungsten complex **38** (2030 mM) performed much better than the (2,6-dichlorophenyl)imido complex (**22**; 419 mM) but about the same as the (2,6-dimethylphenyl)imido complex (**40**; 2230 mM).

The electrophilicity of the metal center also plays a pivotal role. For example, as the electron-withdrawing ability of the alkoxide bound to tungsten increases (from trifluoro- to hexafluoro- to nonafluoro-*tert*-butoxide), the product concentration increases from 1200 mM (**30**) to 2030 mM (**38**) to 2760 mM (**43**). Interestingly, the same trend does not hold throughout for molybdenum. Although the hexafluoro-*tert*-butoxide molybdenum complex (**31**; 1430 mM) is superior to the trifluoro-*tert*-butoxide (**27**; 808 mM), the nonafluoro-*tert*-butoxide catalyst (**19**) gives an unexpectedly low yield of the product (242 mM). The greatest product concentration (3380 mM) was obtained using catalyst **44**, which contains tungsten and two triphenylsiloxy ligands. Triphenylsiloxy and variations have been largely overlooked as auxiliary ligands in high-oxidation-state metathesis chemistry.⁸ The success of triphenylsiloxy is somewhat surprising in view of the possibility of aryl CH activation and formation of an alkyl from an alkylidene, an

(7) Ivin, K. J.; Mol, J. C. *Olefin Metathesis and Metathesis Polymerization*; Academic Press: San Diego, CA, 1997.

(8) (a) Schrock, R. R.; Czekelius, C. C. *Adv. Synth. Catal.* **2007**, *349*, 55. (b) Schrock, R. R. *Adv. Synth. Catal.* **2007**, *349*, 41. (c) Schrock, R. R. *Chem. Rev.* **2002**, *102*, 145.

(9) (a) Tsang, W. C. P.; Hultzsck, K. C.; Alexander, J. B.; Bonitatebus, P. J., Jr.; Schrock, R. R.; Hoveyda, A. H. *J. Am. Chem. Soc.* **2003**, *125*, 2652. (b) Tsang, W. C. P.; Schrock, R. R.; Hoveyda, A. H. *Organometallics* **2001**, *20*, 5658. (c) Leduc, A.-M.; Salameh, A.; Soulivong, D.; Chabanas, M.; Basset, J.-M.; Coperet, C.; Solans-Monfort, X.; Clot, E.; Eisenstein, O.; Boehm, V. P. W.; Roeper, M. J. *Am. Chem. Soc.* **2008**, *130*, 6288.

(10) (a) Freundlich, J. S.; Schrock, R. R.; Davis, W. M. *J. Am. Chem. Soc.* **1996**, *118*, 3643. (b) Hirsekorn, K. F.; Veige, A. S.; Marshak, M. P.; Koldobskaya, Y.; Wolczanski, P. T.; Cundari, T. R.; Lobkovsky, E. B. *J. Am. Chem. Soc.* **2005**, *127*, 4809. (c) Schrock, R. R.; Duval-Lungulescu, M.; Tsang, W. C. P.; Hoveyda, A. H. *J. Am. Chem. Soc.* **2004**, *126*, 1948.

(11) Singh, R.; Schrock, R. R.; Mueller, P.; Hoveyda, A. H. *J. Am. Chem. Soc.* **2007**, *129*, 12654.

(12) Hock, A.; Schrock, R. R.; Hoveyda, A. H. *J. Am. Chem. Soc.* **2006**, *128*, 16373.

Table 1. Total Product Concentration from Reaction of 1 (10 mM) and Various Mo and W Alkylidene Complexes (16 mM) at 125 °C in *n*-Octane after 4 Days^a

compd	catalyst	total product (mM)	compd	catalyst	total product(mM)
6	Mo(NAr)(CHR)(pyr) ₂	15	26	Mo(NAr)(CHR)(OAr) ₂	759
7	Mo(NAd)(CHR)(pyr) ₂	25	27	Mo(NAr)(CHR)(OCMe ₂ CF ₃) ₂	808
8	W(NAr)(CHR)[OCMe(C ₆ F ₅) ₂] ₂	25	28	Mo(NAr)(CHR)(OAr)(pyr)	936, 1220
9	Mo(NAr)(CHR)[OCMe(C ₆ F ₅) ₂] ₂	33	29	W(NAr)(CHR)(OAr)(pyr)	1040
10	Mo(NAr ^{CF₃})(CHR)[OCMe(CF ₃) ₂] ₂	41	30	W(NAr)(CHR)(OCMe ₂ CF ₃) ₂	1200
11	W(NAr)(CHR)(pyr) ₂	81	31	Mo(NAr)(CHR)[OCMe(CF ₃) ₂] ₂	1430,1640
12	Mo(NAr)(CHR)(CH ₂ - <i>t</i> -Bu) ₂	89	32	W(NAr)(CHR)[OC(CF ₃) ₃](pyr)	1550
13	W(NAr)(CHR)(CH ₂ - <i>t</i> -Bu) ₂	122	33	W(NAr)(CHR)(BINAP-TBS) ₂	1580
14	Mo(NAr ^{CF₃})(CHR)(pyr) ₂	130	34	W(NAr)(CHR)[OCMe(CF ₃) ₂](pyr)	1670
15	W(NAr)(CHR)(OAr) ₂	141	35	Mo(NAr)(CHR)(OSiPh ₃)(pyr)	1800
16	Mo(NAr)(CHR)(O-1-PhCy)(pyr)	152,162	36	W(NAr)(CHR)[OC(CF ₃) ₃] ₂ ^b	1890
17	Mo(NAr)(CHR)(OTBS) ₂	159	37	Mo(NAr)(CHR)(OSiPh ₃) ₂	1970
18	Mo(NAr)(CHR)(BIPHEN)	184	38	W(NAr)(CHR)[OCMe(CF ₃) ₂] ₂	2030
19	Mo(NAr)(CHR)[OC(CF ₃) ₃] ₂	242	39	W(NAr)(C ₃ H ₆)[OC(CF ₃) ₃] ₂	2210
20	Mo(NAd)(CHR)[OCMe(CF ₃) ₂] ₂	334,358	40	W(NAr')(CHR)[OCMe(CF ₃) ₂] ₂	2230
21	Mo(NAr)(CHR)(BINAP _{m-CF₃})	359	41	W(NAr)(CHR)[OC(CF ₃) ₃] ₂ ^c	2310
22	W(NAr'')(CHR)[OCMe(CF ₃) ₂] ₂	419	42	W(NAr)(CHR)(OSiPh ₃)(pyr)	2380
23	Mo(NAr)(CHR)[OSi(O- <i>t</i> -Bu) ₃](pyr)	480	43	W(NAr)(CHR)[OC(CF ₃) ₃] ₂	2760
24	Mo(NAr)(CHR)(BINAP-TBS) ₂	486,593	44	W(NAr)(CHR)(OSiPh ₃) ₂	3380
25	Mo(NAr)(CHR)[OCMe(CF ₃) ₂](pyr)	746,794	45	W(NAr)(CHR)[OC(CF ₃) ₃] ₂ ^d	3015

^a Legend: CHR = CHCMe₂Ph; Ar = 2,6-diisopropylphenyl; Ar' = 2,6-dimethylphenyl; Ar'' = 2,6-dichlorophenyl; Ar^{CF₃} = 2-(trifluoromethyl)phenyl; Ad = 1-adamantyl; pyr = 2,5-dimethylpyrrolide; BIPHEN = 3,3'-di-*tert*-butyl-5,5',6,6'-tetramethyl-1,1'-biphenyl-2,2'-diolate; BINAP_{m-CF₃} = 3,3'-bis(3,5-bis(trifluoromethyl)phenyl)-BINOL; BINAP-TBS = 2'-((*tert*-butyldimethylsilyloxy)-1,1'-binaphthyl-2-olate. Repeated run values are given in some instances. ^b Reaction at 175 °C. ^c Reaction at 150 °C. ^d Reaction at 100 °C, maximizing after 14 days.

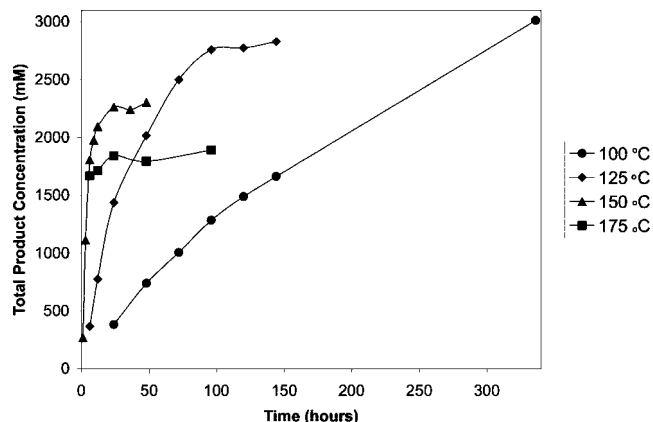
Table 2. Comparison of Mo and W M(NAr)(CHCMe₂Ph)(ligand)₂ Catalysts^a

ligands	Mo	W	W/Mo
(OAr) ₂	759	141	0.19
(CH ₂ - <i>t</i> -Bu) ₂	89	122	1.4
(OAr)(pyr)	936, 1220	1043	0.9–1/1
(OCMe ₂ CF ₃) ₂	808	1196	1.5
(OSiPh ₃)(pyr)	1800	2376	1.3
[OCMe(CF ₃) ₂] ₂	1430, 1640	2030	1.2–1.4
[OCMe(CF ₃) ₂](pyr)	746, 794	1670	2.1–2.2
(BINAP-TBS) ₂	486, 593	1580	2.7–3.3
(OSiPh ₃) ₂	1970	3380	1.7
[OC(CF ₃) ₃] ₂	242	2760	11.4

^a All values are given in mM of total product formed.

example of which is known for complexes of this type.¹³ Silicon is likely to reduce the amount of donation of π electron density to the metal and make the metal much more electron deficient than in a typical alkoxide, apparently even nonafluoro-*tert*-butoxide.

Perhaps the most significant trend seen in Table 1 is the superior performance of tungsten catalysts. Of the top 16 catalysts, 13 are W-based. The Mo analogue of the best catalyst in Table 1 (W-based **44**) is **37**, which, interestingly, gives the best performance (1970 mM product) of all the Mo-based catalysts investigated. Several Mo and W (2,6-diisopropylphenyl)imido catalysts are given in Table 2. With the exception of the catalysts that contain two 2,6-diisopropylphenoxide ligands (**15** and **26**), the W catalysts performed marginally to much better than Mo catalysts. The large ratio of product obtained with **43** vs **19** (11.4:1) is noteworthy. The disparity between W and Mo catalysts might be ascribed to a greater stability of W toward reduction, either by rearrangement of metallacyclobutane intermediates or through bimolecular decomposition of alkylidenes. There are numerous examples of stable, isolable

**Figure 1.** Plots of total product employing **43** and **1** in *n*-octane at 100, 125, 150, and 175 °C.

tungstacyclobutane complexes,^{9a,14} but molybdacyclobutanes have only been observed spectroscopically.^{15,6} Interestingly, the isolated tungstacyclobutane complex (**39**) performed nearly as well (2210 mM; Table 1) as the neophylidene species (**43**; 2760 mM). The lower value for **39** might be ascribed to the presence of one ethylene per W in the initial species, which is likely to retard the performance of the Ir catalyst and perhaps also the W catalyst.

In a reaction in which **43** and **1** were employed as catalysts in *n*-octane the reactions were also run at 100 °C (**45**), 150 °C (**41**), and 175 °C (**36**) and the formation of product was monitored over time (Figure 1). At 175 °C, ~1700 mM product is observed after 6 h, with little increase thereafter. At 150 °C, ~24 h is required to approach completion (ca. 2300 mM). At 125 °C, the reaction takes much longer (96 h), but the total product yield (2830 mM) is greater than at either 150 or 175

(13) Schrock, R. R.; DePue, R. T.; Feldman, J.; Yap, K. B.; Yang, D. C.; Davis, W. M.; Park, L.; DiMare, M.; Schofield, M.; Anhaus, J.; Walborsky, E.; Evitt, E.; Krüger, C.; Betz, P. *Organometallics* **1990**, *9*, 2262.

(14) (a) Schrock, R. R.; DePue, R. T.; Feldman, J.; Schaverien, C. J.; Dewan, J. C.; Liu, A. H. *J. Am. Chem. Soc.* **1988**, *110*, 1423. (b) Feldman, J.; Davis, W. M.; Schrock, R. R. *Organometallics* **1989**, *8*, 2266. (c) Feldman, J.; Davis, W. M.; Thomas, J. K.; Schrock, R. R. *Organometallics* **1990**, *9*, 2535.

(15) Feldman, J.; Murdzek, J. S.; Davis, W. M.; Schrock, R. R. *Organometallics* **1989**, *8*, 2260.

Table 3. Concentration Dependence of **1 and **43** on Product Formation^a**

concn of 43 (mM)	concn of 1 (mM)	total product concn (mM)
8	10	2540
16	10	2760
32	10	2370
16	5	1630
16	80	4250
128	10	236
16	20	3180

^a All catalytic runs are at 125 °C in *n*-octane after 4 days.

Table 4. In Situ Generated Catalysts from **6 or **11** and the Corresponding Alcohol^a**

catalyst	isolated catalyst (mM)	in situ catalyst (mM)
25	746, 794	654
26	759	830
28	936, 1220	933
31	1430, 1640	1530
34	1670	1660
38	2030	2530
43	2760	1640
44	3380	2040

^a Reactions were run in *n*-octane with **1** and analyzed after 4 days. For MAP complexes, only 1 equiv of the alcohol was used.

°C. At 100 °C the reaction is impractically slow (maximizing only after 14 days), but in the end a slightly higher yield is obtained than at 125 °C. The distribution of alkanes is virtually independent of either time or temperature and appears as approximately a Gaussian distribution centered at octane (see the Supporting Information).

Studies aimed at elucidating the effect of varying the concentrations of olefin metathesis catalyst and dehydrogenation catalyst were conducted (Table 3). Increasing the concentration of **1** from 5 to 20 mM (with **43** at 16 mM) nearly doubles the amount of product that is formed (from 1600 to 3180 mM). Varying the concentration of the metathesis catalyst **43** from 8 to 32 mM has only a small influence on the product yield, but the yield drops sharply (to 236 mM) with a large W loading (128 mM). Increasing the metathesis catalyst concentration is likely to lead to more bimolecular decomposition, but the amount of catalyst should reach a level where bimolecular decomposition is slow regardless of the loading and AM should continue. Therefore, either W interferes with the Ir catalyst directly at such a high loading or some W catalyst decomposition product interferes with the Ir and/or W catalyst at such a high loading.

Preparing, isolating, and storing each catalyst in Table 1 is relatively time-consuming. Therefore, it would be desirable to employ a universal precursor that would yield catalysts upon addition of the respective alcohols and would enable rapid screening of potential catalysts. Bis(pyrrolide) complexes **6** and **11** readily undergo protonolysis reactions with a variety of alcohols to give MAP or bis(alkoxide) complexes (e.g., **25**, **26**, **28**, **31**, **34**, **38**, **43**, and **44**). Accordingly, stock solutions of **1**, *n*-octane, and either **6** or **11** were treated with 1 or 2 equiv of various alcohols and the activity of the resulting catalyst or catalysts was measured after 4 days at 125 °C (Table 4). In six of the eight cases the in situ generated catalysts performed approximately as well as the isolated complexes. Therefore, free 2,5-dimethylpyrrole that is generated upon alcoholysis of **6** or **11** does not appear to interfere strongly with the dehydrogenation/hydrogenation process. (It is already known that free 2,5-dimethylpyrrole does not interfere with metathesis reactions that

Table 5. Comparison of Iridium Catalysts **1–5 with W/Mo Complexes **28**, **29**, **31**, **43**, and **44****

Mo/W catalyst	1	2	3	4	5
28	936, 1220	1040	400	491	836
29	1040	823	396	823	977
31	1430, 1640	1500	300	391	677
43	2760	2560	846	378	521
44	3380	3160	190	1270	1280

involve biphenolate or binaphtholate catalysts.¹⁶) In situ generated **43** and **44** do not appear to be as effective as the isolated catalysts. Nonafluoro-*tert*-butyl alcohol and triphenylsilanol are relatively acidic and therefore may be involved in side reactions that produce inactive byproducts. Notably, both **6** and **11** are virtually inactive for alkane metathesis in the absence of added alcohol (15 and 81 mM product yields respectively; Table 1).

Variations that involve four Mo/W catalysts (**28**, **29**, **31**, **43**, and **44**) and five iridium catalysts (**1–5**) were also explored (Table 5). Catalyst (or catalyst precursors) **1** and **2** give greater yields of product than **3–5**. Whether an ethylene or a dihydride iridium complex is employed (**1** or **2**, respectively) has only a small effect on product yield.

AM reactions using POCOP-based dehydrogenation catalysts **1–3** afford *n*-alkane products with a distribution of MW's approximating a Gaussian curve centered at *n*-octane. In contrast, reactions employing PCP-based catalysts **4** and **5** afford varying degrees of selectivity for tetradecane (Figures 2 and 3); this selectivity has no precedent in previously reported AM systems. Tetradecane is the product expected from the terminal dehydrogenation of *n*-octane to 1-octene, followed by cross-metathesis to yield 7-tetradecene and ethylene, and finally olefin rehydrogenation. Rapid isomerization of the dehydrogenation product 1-octene, in competition with cross-metathesis, can account for the formation of alkanes other than tetradecane and ethane. The origin of the differences in selectivity, between POCOP-based and PCP-based dehydrogenation catalysts, as well as differences between various olefin metathesis catalysts, is currently under investigation.

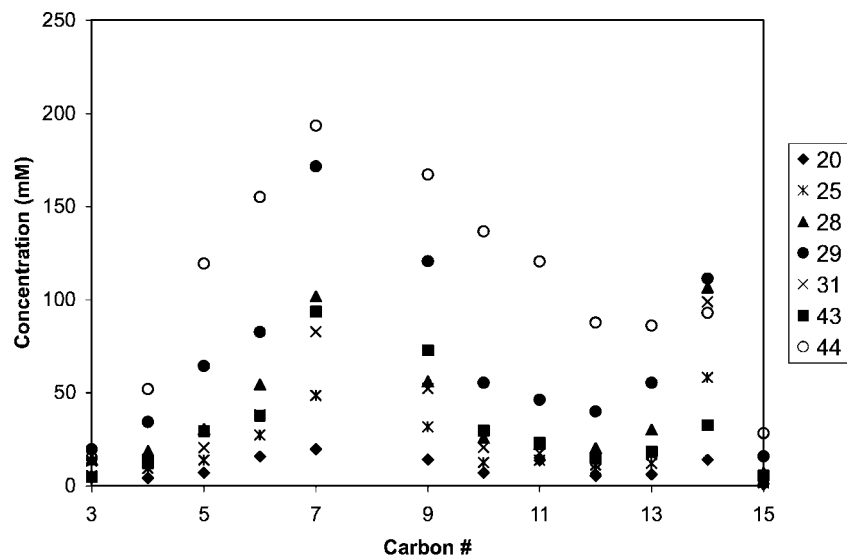
Conclusions

A variety of molybdenum and tungsten MAP or bis(alkoxide) olefin metathesis catalysts were examined for alkane metathesis of *n*-octane. The nature of the imido group, alkoxide, and metal were all found to be important variables, with tungsten catalysts generally performing best: in particular, a (diisopropylphenyl)imido bis(triphenylsiloxide) complex. Product yields were diminished at temperatures greater than 125 °C, most likely because of the instability of the olefin metathesis catalysts at such temperatures. The POCOP-based catalysts **1** and **2** gave higher yields than *p*-methoxy-substituted catalysts **3** and **4**, while the PCP-based catalysts **4** and **5** exhibited some selectivity for tetradecane at levels that were dependent upon which olefin metathesis catalyst was used.

Experimental Section

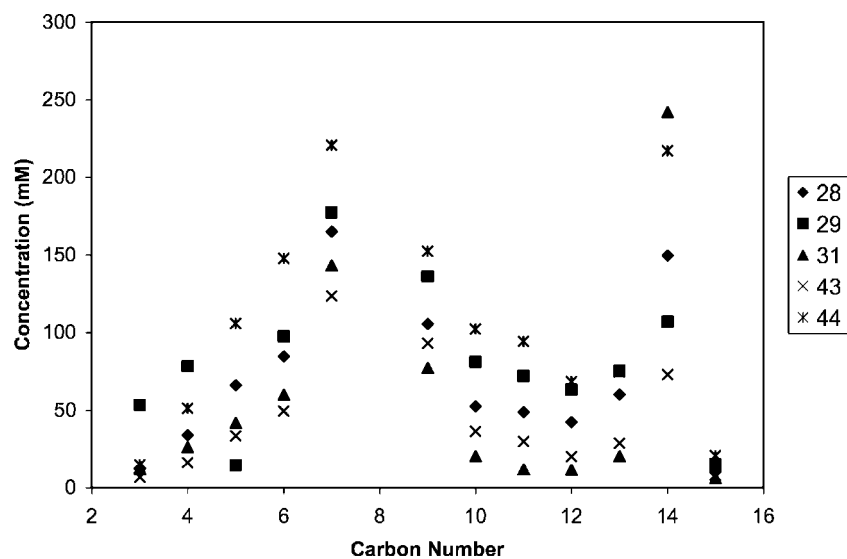
General Comments. All manipulations were conducted under an argon atmosphere in a Vacuum Atmospheres drybox or using Schlenk techniques. All glassware was oven-dried prior to use. Ether, pentane, toluene, dichloromethane, toluene, and benzene were degassed and passed through activated alumina columns. Dimethoxyethane was distilled in vacuo from a dark purple solution of sodium

(16) Pilyugina, T. Ph.D. Thesis, Massachusetts Institute of Technology, 2007.



Entry	C 2/3	C 4	C 5	C 6	C 7	C 9	C 10	C 11	C 12	C 13	C 14	C 15
20	4	4	7	16	20	14	7	14	5	6	14	1
25	6	9	14	27	49	32	13	14	9	12	58	2
28	14	19	31	55	102	56	26	23	21	30	107	7
29	20	34	64	83	172	121	56	46	40	55	111	16
31	13	14	21	38	83	52	21	18	11	17	99	4
43	5	12	30	38	94	73	30	23	15	19	33	6
44	15	52	119	155	193	167	137	121	88	86	93	28

Figure 2. Product distribution from reaction involving **4** and Mo/W olefin metathesis catalysts **20**, **25**, **28**, **29**, **31**, **43**, and **44** after 4 days at 125 °C.



Entry	C 2/3	C 4	C 5	C 6	C 7	C 9	C 10	C 11	C 12	C 13	C 14	C 15
28	13	34	66	85	165	106	53	49	42	60	150	10
29	53	78	15	98	177	136	81	72	63	75	107	15
31	12	26	42	60	143	77	21	12	12	21	242	6
43	7	16	33	49	123	93	36	30	20	29	73	8
44	15	51	106	148	221	152	102	94	68	75	217	21

Figure 3. Product distribution from reaction involving **5** and Mo/W olefin metathesis catalysts **28**, **29**, **31**, **43**, and **44** after 4 days at 125 °C.

benzophenone ketyl and degassed three times through freeze–pump–thaw techniques. All dried and deoxygenated solvents were stored over molecular sieves in an argon-filled glovebox. C_6D_6 was dried over 4 Å Linde-type molecular sieves. NMR spectra were recorded on a Varian 300 or 500 MHz spectrometer at room temperature. Chemical shifts for 1H and ^{13}C spectra were referenced to the residual $^1H/^{13}C$ resonances of the deuterated solvent (1H , δ 7.16 C_6D_6 ; ^{13}C , δ 128.0 C_6D_6) and are reported as parts per million

relative to tetramethylsilane. The following abbreviations refer to the multiplicity: s, singlet; d, doublet; t, triplet; m, multiplet; br, broad signal. Complexes **1**,⁷ **2**,¹⁷ **3**,¹⁷ **4**,¹⁸ **5**, **4**, **6**,¹⁹ **7**,¹⁹ **10**,²⁰ **11**,²¹ **12**,²² **13**,¹³ **14**,¹⁹ **17**,²³ **18**,²⁴ **19**,²⁵ **20**,²⁵ **21**,¹⁹ **22**,²⁶ **25**,¹¹ **26**,⁶ **27**,²⁷ **28**,¹¹ **31**,²⁸ **37**,²³ **38**,²⁹ and **40**³⁰ were prepared according to literature

(17) Goettker-Schnetmann, I.; White, P. S.; Brookhart, M. *Organometallics* **2004**, *23*, 1766.

procedures. Synthesis and characterization data for the new complexes (**8**, **9**, **15**, **16**, **23**, **24**, **29**, **30**, **33–35**, **39**, and **42–44**) can be found in the Supporting Information.

Procedure for Alkane Metathesis Catalytic Runs. A stock solution of the iridium catalyst (10 mM), *n*-octane, and mesitylene (28.8 mM, as the internal standard) was prepared inside of an argon-filled glovebox. To a vial charged with the respective Mo or W olefin metathesis catalyst (8 mmol) was added 500 μ L of the previously described stock solution. The solution was stirred until

(18) Krogh-Jespersen, K.; Czerw, M.; Zhu, K.; Singh, B.; Kanzelberger, M.; Darji, N.; Achord, P. D.; Renkema, K. B.; Goldman, A. S. *J. Am. Chem. Soc.* **2002**, *124*, 10797.

(19) Singh, R.; Czekelius, C.; Schrock, R. R.; Mueller, P.; Hoveyda, A. H. *Organometallics* **2007**, *26*, 2528.

(20) Oskam, J. H.; Fox, H. H.; Yap, K. B.; McConville, D. H.; O'Dell, R.; Lichtenstein, B. J.; Schrock, R. R. *J. Organomet. Chem.* **1993**, *459*, 185.

(21) Kreickmann, T.; Arndt, S.; Schrock, R. R.; Mueller, P. *Organometallics* **2007**, *26*, 5702.

(22) Sinha, A.; Schrock, R. R. *Organometallics* **2004**, *23*, 1643.

(23) Wampler, K. M.; Schrock, R. R.; Hock, A. S. *Organometallics* **2007**, *26*, 6674.

(24) Alexander, J. B.; La, D. S.; Cefalo, D. R.; Hoveyda, A. H.; Schrock, R. R. *J. Am. Chem. Soc.* **1998**, *120*, 4041.

(25) Oskam, J. H.; Schrock, R. R. *J. Am. Chem. Soc.* **1993**, *115*, 11831.

(26) Arndt, S.; Schrock, R. R.; Mueller, P. *Organometallics* **2007**, *26*, 1279.

(27) Bazan, G. C.; Oskam, J. H.; Cho, H. N.; Park, L. Y.; Schrock, R. R. *J. Am. Chem. Soc.* **1991**, *113*, 6899.

(28) Murdzek, J. S.; Schrock, R. R. *Organometallics* **1987**, *6*, 1373.

(29) Bauch, C. G.; Wagener, K. B.; Boncella, J. M. *Makromol. Chem.* **1991**, *12*, 413.

(30) Thorn-Csanyi, E.; Dehmel, J.; Luginsland, H.; Zilles, J. U. *J. Mol. Catal. A* **1997**, *115*, 29.

homogeneity was obtained and then syringed into a glass ampule with a ground-glass joint. A vacuum adapter was fixed onto the ampule, which was taken outside of the box. The solution was then frozen in a dry ice/acetone bath and the headspace was evacuated. Samples were flame-sealed and placed into a temperature-calibrated oven. Each sample was removed from the oven at the completion of the catalytic run, and the contents were passed through a short plug of alumina to remove most of the color. The resulting solution was subjected to GC analysis, and the peaks were integrated with respect to mesitylene. GC response factors were calculated with C7–C15 standards and fit to a straight line. Integrations were totaled for all alkanes and normalized to 6154 mM (corresponds to 500 μ L of *n*-octane). For concentration-dependent catalytic runs, the previously stated procedure was used with a slight modification. Solid iridium and olefin metathesis catalysts were carefully measured directly in the ampule so that addition of a stock solution of 500 μ L of octane with mesitylene (28 mM) afforded the desired concentration of the respective olefin metathesis catalyst and iridium catalyst.

Acknowledgment. This work was supported by the NSF (Grant No. CHE-0650456) as part of the Center for Enabling New Technologies through Catalysis (CENTC). B.C.B. thanks Keith Wampler for the generous donation of complex **17**.

Supporting Information Available: Text giving experimental details for the syntheses of all new compounds. This material is available free of charge via the Internet at <http://pubs.acs.org>.

OM800877Q

Multicomponent Cascade Reactions Triggered by Cycloaddition of Fischer Alkoxy Alkynyl Carbene Complexes with Strained Bicyclic Olefins[§]

Manuel A. Fernández-Rodríguez, Facundo Andina,[†] Patricia García-García,
Christian Rocaboy,[‡] and Enrique Aguilar*

Instituto Universitario de Química Organometálica “Enrique Moles”, Unidad Asociada al CSIC,
Universidad de Oviedo, Julián Clavería 8, 33006, Oviedo, Spain

Received October 6, 2008

A broad range of substituted 2-cyclopentenone derivatives are prepared by a multicomponent sequential reaction of chromium alkoxy alkynyl carbene complexes with strained bicyclic olefins. An unprecedented behavior of the carbene complexes, which react through the carbene carbon and both acetylenic carbons, in a [2+2+1]/[2+1] cascade sequence, allows the synthesis of multicomponent products, which (a) incorporate two units of the same strained bicyclic olefin, (b) incorporate two different olefins, and/or (c) involve intramolecular [2+1] reactions. Evidence of the formation of 2-cyclopentenone-derived Fischer carbene complexes as reaction intermediates is provided, as they are trapped with different types of olefins or undergo alkyne insertion.

Introduction

Multicomponent reactions (MCRs) have recently emerged as extremely powerful synthetic organic methods in terms of operational simplicity or atom economy and represent an important approach to diversity-oriented organic synthesis.¹ In this regard, the extraordinary ability of group VI metal-derived Fischer carbene complexes (FCCs)² to participate in such reactions has been extensively developed in the last decades and has allowed the selective construction of a wide range of highly functionalized structures through several selective processes, which include either hetero- or carbocyclizations.³

On the other hand, since the discovery of the carbene complexes by Fischer and Maasböl in 1964,⁴ their behavior toward alkenes was one of the first and longest studied processes. In general, the reaction proceeds under thermal conditions by a formal [2+1] cycloaddition of the olefin to furnish a cyclopropane as the main product,⁵ although alkene metathesis and carbene ligand insertion into a olefinic β -C–H bond⁶ have also been observed as principal pathways in a few examples. The cyclopropanation reaction of FCCs with alkenes was first reported⁷ and developed for electron-deficient olefins⁸ and subsequently extended to electron-rich alkenes,⁹ 1,3-dienes,¹⁰ and more recently simple olefins.¹¹ Besides the metal moiety and the electronic nature of the alkene, the process is

[§] Dedicated to Prof. J. Barluenga on the occasion of his 69th birthday.

* Corresponding author. E-mail: eah@uniovi.es.

[†] Current address: Ragactives, Parque Tecnológico de Boecillo, Parcelas 2 y 3, 47151 Boecillo, Valladolid, Spain.

[‡] Current address: Villapharma Research, Parque Tecnológico de Fuente Álamo, Ctra. del Estrecho-Lobosillo, 30320 Fuente Álamo, Murcia, Spain.

(1) For reviews about MCRs see: (a) *Multicomponent Reactions*; Zhu, J., Bienaymé, H., Eds.; Wiley-VCH: New York, 2005. (b) Ramón, D.; Yus, M. *Angew. Chem., Int. Ed.* **2005**, *44*, 1602–1634. (c) Zhu, J. *Eur. J. Org. Chem.* **2003**, 1133–1144. (d) Hulme, C.; Core, V. *Curr. Med. Chem.* **2003**, *10*, 51–80. (e) Ugi, I. *Pure Appl. Chem.* **2001**, *73*, 187–191. (f) Tietze, L. F.; Modi, A. *Med. Res. Rev.* **2000**, *20*, 304–322. (g) Dömling, A.; Ugi, I. *Angew. Chem., Int. Ed.* **2000**, *39*, 3168–3210. (h) Bienaymé, H.; Hulme, C.; Odon, G.; Schmitt, P. *Chem.–Eur. J.* **2000**, *6*, 3321–3329. (i) Dax, S. L.; McNally, J. J.; Youngman, M. A. *Curr. Med. Chem.* **1999**, *6*, 255–270. (j) Weber, L.; Illgen, K.; Almstetter, M. *Synlett* **1999**, 366–374. (k) Armstrong, R. W.; Combs, A. P.; Tempest, P. A.; Brown, S. D.; Keting, T. A. *Acc. Chem. Res.* **1996**, *29*, 123–131. (l) Posner, G. H. *Chem. Rev.* **1986**, *86*, 831–844.

(2) Selected reviews: (a) Herndon, J. W. *Coord. Chem. Rev.* **2007**, *251*, 1158–1258. (b) Gómez-Gallego, M.; Mancheño, M. J.; Sierra, M. A. *Acc. Chem. Res.* **2005**, *38*, 44–53. (c) Barluenga, J.; Santamaría, J.; Tomás, M. *Chem. Rev.* **2004**, *104*, 2259–2283. (d) Herndon, J. W. *Coord. Chem. Rev.* **2004**, *248*, 3–79. (e) Barluenga, J.; Flórez, J.; Fañanás, F. J. *J. Organomet. Chem.* **2001**, *624*, 5–17. (f) Dötz, K. H.; Jäkel, C.; Haase, W.-C. *J. Organomet. Chem.* **2001**, *617–618*, 119–132. (g) Sierra, M. A. *Chem. Rev.* **2000**, *100*, 3591–3638. (h) De Meijere, A.; Schirmer, H.; Duestsch, M. *Angew. Chem., Int. Ed.* **2000**, *39*, 3964–4002. Recent books: (i) *Metal Carbenes in Organic Synthesis*; Dötz, K. H., Ed.; John Wiley & Sons: New York, 2004; *Topics in Organometallic Chemistry* Vol. 13. (j) *Carbene Chemistry: from Fleeting Intermediates to Powerful Reagents*; Bertrand, G., Ed.; Marcel Dekker, 2002. (k) Zaragoza Dörwald, F. In *Metal Carbenes in Organic Synthesis*; Wiley-VCH: New York, 1999.

(3) For a review of FCCs in MCRs see: Barluenga, J.; Fernández-Rodríguez, M. A.; Aguilar, E. *J. Organomet. Chem.* **2005**, *690*, 539–587.

(4) Fischer, E. O.; Maasböl, A. *Angew. Chem., Int. Ed. Engl.* **1964**, *3*, 580.

(5) Reviews: (a) Harvey, D. F.; Sigano, D. M. *Chem. Rev.* **1996**, *96*, 271–288. (b) Doyle, M. In *Comprehensive Organometallic Chemistry II*; Abel, E. W., Stone, F. G. A., Wilkinson, G., Eds.; Pergamon: Oxford, 1995; Vol. 12, pp 387–420. (c) Reissig, H.-U. In *Organometallics in Organic Synthesis*; Werner, H., Erker, G., Eds.; Springer: Berlin, 1989; Vol. 2, pp 311–322. (d) Brookhart, M.; Studabaker, W. B. *Chem. Rev.* **1987**, *87*, 411–432.

(6) (a) Harvey, D. F.; Brown, M. F. *Tetrahedron Lett.* **1990**, *31*, 2529–2532. (b) Wienand, A.; Reissig, H.-U. *Angew. Chem., Int. Ed. Engl.* **1990**, *29*, 1129–1131. (c) For an example with an iron carbene complex: Semmelhack, M.; Tamura, R. *J. Am. Chem. Soc.* **1983**, *105*, 6570–6572.

(7) (a) Cooke, M. D.; Fischer, E. O. *J. Organomet. Chem.* **1973**, *56*, 279–284. (b) Dötz, K. H.; Fischer, E. O. *Chem. Ber.* **1972**, *105*, 1356–1367. (c) Fischer, E. O.; Dötz, K. H. *Chem. Ber.* **1970**, *103*, 1273–1278.

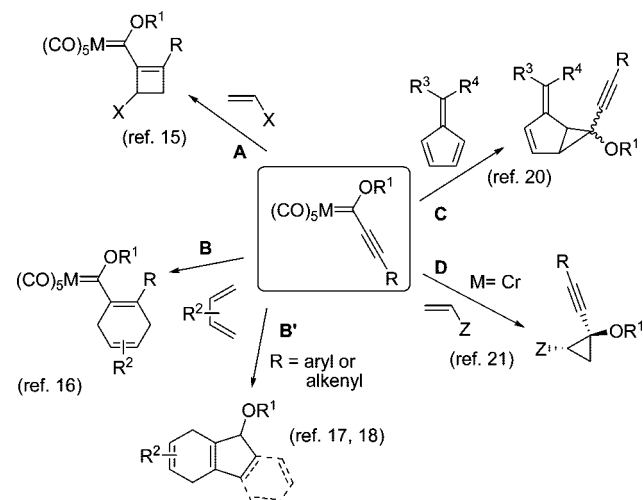
(8) (a) Barluenga, J.; Suárez-Sobrino, A. L.; Tomás, M.; García-Granda, S.; Santiago-García, R. *J. Am. Chem. Soc.* **2001**, *123*, 10494–10501. (b) Barluenga, J.; Suárez-Sobrino, A. L.; Tomás, M. *Synthesis* **2000**, 935–940. (c) Hoffmann, M.; Reissig, H.-U. *Synlett* **1995**, 625–627. (d) Wienand, A.; Reissig, H.-U. *Chem. Ber.* **1991**, *124*, 957–965. (e) Herdon, J. W.; Tumer, S. U. *J. Org. Chem.* **1991**, *56*, 286–294. (f) Wienand, A.; Reissig, H.-U. *Organometallics* **1990**, *9*, 3133–3142. (g) Herdon, J. W.; Tumer, S. U. *Tetrahedron Lett.* **1989**, *30*, 4771–4774. (h) Wienand, A.; Reissig, H.-U. *Tetrahedron Lett.* **1988**, *29*, 2315–2318.

(9) (a) Casey, C. P.; Cesa, M. C. *Organometallics* **1982**, *1*, 87–94. (b) Dorrer, B.; Fischer, E. O.; Kalbfus, W. *J. Organomet. Chem.* **1974**, *81*, C20–C22. (c) Fischer, E. O.; Dötz, K. H. *Chem. Ber.* **1972**, *105*, 3966–3973.

highly dependent on the substitution of the carbene complex. Thus, alkyl and aryl FCCs are suitable reagents for the cyclopropanation of activated alkenes and 1,3-dienes, while simple olefins are cyclopropanated only with alkenyl- and heteroaryl-substituted complexes.¹¹ Moreover, when electron-deficient olefins are used, the double bond of the alkenyl FCCs can also partake in the process, leading to a mixture of the expected cyclopropanes and cyclopentene derivatives as a result of a formal [3+2] cycloaddition, whose distribution can be controlled by the selection of the appropriate conditions.^{10b–10d} In a particular case, conjugated enals or enones react with aryl or alkenyl FCCs to produce dihydrofurans, due to the spontaneous evolution, under the reaction conditions, of the initially formed cyclopropanes to the final formal [4+1] adducts.¹² Cyclopentene derivatives are selectively obtained when neutral or silyloxy-substituted 1,3-dienes are employed.¹³ Furthermore, it has been established that, under suitable reaction conditions, alkenyl FCCs participate as dienophiles in Diels–Alder cycloadditions with 1,3-dienes and heterodienes.^{6a,14}

In a similar manner, alkynyl FCCs display several patterns of reactivity depending on the nature of the alkene they are reacted with. In this way, they are known to react through the triple bond of the carbene ligand with electron-rich olefins to afford cyclobutene carbene complexes by a [2+2] cycloaddition¹⁵ (A, Scheme 1). When confronted with neutral and electron-rich 1,3-dienes and heterodienes, [4+2] cycloadditions result to afford cyclohexenyl carbene complexes (B, Scheme 1);¹⁶ in the latter case, when the acetylenic carbene ligand bears an aryl or an alkenyl substituent (R = Ar or C=C), products can evolve, spontaneously or by warming, to form cyclopentadienes by the known cyclopentannulation process (B', Scheme 1).^{17,18} Interestingly, by appropriate election of both the vinyl-

Scheme 1. Reaction of Alkynyl FCCs toward Activated Olefins and 1,3-Dienes



substituted alkynyl FCC and the diene, the initially formed cycloadducts are able to undergo a double or triple cascade [4+2] cycloaddition/cyclopentannulation process, furnishing highly functionalized polycyclic compounds.¹⁸ On the other hand, the cyclopropanation of alkynyl FCCs with olefins has remained unknown until recently. Aumann was the first one to propose the formation of an alkynyl cyclopropane from a FCC as an intermediate in a cascade reaction;¹⁹ the cyclopropane adducts were shortly isolated for the first time, using specially reactive olefins such as fulvenes (C, Scheme 1).²⁰ More recently, we have also disclosed a general procedure for the diastereoselective cyclopropanation of electron-deficient olefins with chromium alkynyl FCCs (D, Scheme 1).²¹

Having in mind the high dependence of the process on the alkene employed, we decided to explore the behavior of highly reactive strained olefins. In a previous communication, we described the initial results of MCRs of alkynyl FCCs with strained and hindered bicyclic olefins such as norbornene derivatives.²² The major products, obtained in a single operation, incorporate up to four different components, generating a cyclopentenone and cyclopropane rings through the formation of five new σ C–C bonds in a formal [2+2+1]/[2+1] cycloaddition. Herein, we report a thorough study of the scope and limitations of both inter- and intramolecular multicomponent processes. In addition, we report a formal [2+2+1]/[3+2] cycloaddition by using an internal alkyne as the fourth component.

Results and Discussion

1. Reaction with Norbornene: Preliminary Results and Process Optimization. The initial studies were carried out with methoxy phenylethynyl chromium carbene complex **1a** and norbornene **2a** (Scheme 2).

(10) Electron-deficient 1,3-dienes: (a) Barluenga, J.; Tomás, M.; López-Peñalga, J. A.; Rubio, E. *J. Chem. Soc., Chem. Commun.* **1995**, 665–666. (b) Buchert, M.; Hoffmann, M.; Reissig, H.-U. *Chem. Ber.* **1995**, *128*, 605–614. (c) Buchert, M.; Reissig, H.-U. *Chem. Ber.* **1992**, *125*, 2723–2729. (d) Buchert, M.; Reissig, H.-U. *Tetrahedron Lett.* **1988**, *29*, 2319–2320. Electron-rich 1,3-dienes: (e) Takeda, K.; Sakurama, K.; Yoshii, E. *Tetrahedron Lett.* **1997**, *38*, 3257–3260. (f) Wulff, W. D.; Yang, D. C.; Murray, C. K. *J. Am. Chem. Soc.* **1988**, *110*, 2653–2655. Nonactivated 1,3-dienes: (g) Harvey, D. F.; Lund, K. P. *J. Am. Chem. Soc.* **1991**, *113*, 8916–8921. (h) See also refs 8e and 8i.

(11) (a) Barluenga, J.; López, S.; Flórez, J. *Chem.–Eur. J.* **2001**, *7*, 4723–4729. (b) Barluenga, J.; López, S.; Trabanco, A. A.; Fernández-Acebes, A.; Flórez, J. *J. Am. Chem. Soc.* **2000**, *122*, 8145–8154. (c) Barluenga, J.; Fernández-Acebes, A.; Trabanco, A. A.; Flórez, J. *J. Am. Chem. Soc.* **1997**, *119*, 7591–7592.

(12) Barluenga, J.; Fanlo, H.; López, S.; Flórez, J. *Angew. Chem., Int. Ed.* **2007**, *46*, 4136–4140.

(13) Neutral 1,3-dienes: (a) Barluenga, J.; López, S.; Trabanco, A. A.; Flórez, J. *Angew. Chem., Int. Ed.* **2003**, *42*, 231–233. (b) Zaragoza Dörwald, F. *Angew. Chem., Int. Ed.* **2003**, *42*, 1332–1334. Silyloxy-substituted 1,3-dienes: (c) Hoffmann, M.; Buchert, M.; Reissig, H.-U. *Chem.–Eur. J.* **1999**, *5*, 876–882. (d) Hoffmann, M.; Buchert, M.; Reissig, H.-U. *Angew. Chem., Int. Ed. Engl.* **1997**, *36*, 283–285.

(14) Wulff, W. D. *Organometallics* **1998**, *17*, 3116–3134, and references therein.

(15) (a) Barluenga, J.; Aznar, F.; Palomero, M. A.; Barluenga, S. *Org. Lett.* **1999**, *1*, 541–543. (b) Wulff, W. D.; Faron, K. L.; Su, J.; Springer, J. P.; Rheingold, A. L. *J. Chem. Soc., Perkin Trans. 1* **1999**, 197–219, and references therein. (c) Faron, K. L.; Wulff, W. D. *J. Am. Chem. Soc.* **1988**, *110*, 8727–8729. (d) When the reaction of 2,3-dihydrofuran and alkynyl FCCs is carried out at temperatures over 90 °C, a [2+2]/[2+1] tandem reaction sequence takes place: Pérez-Anes, A.; García-García, P.; Suárez-Sobriño, A. L.; Aguilar, E. *Eur. J. Org. Chem.* **2007**, 3480–3487.

(16) (a) Barluenga, J.; Tomás, M.; López-Peñalga, J. A.; Rubio, E. *Tetrahedron Lett.* **1997**, *38*, 3981–3984, and references therein. (b) Wulff, W. D.; Tang, P.-C.; Chan, K.-S.; McCallum, J. S.; Yang, D. C.; Gilbertson, S. R. *Tetrahedron* **1985**, *41*, 5813–5832. (c) Wulff, W. D.; Yang, D. C. *J. Am. Chem. Soc.* **1984**, *106*, 7565–7567.

(17) Barluenga, J.; Fernández-Rodríguez, M. A.; Aguilar, E. *Org. Lett.* **2002**, *21*, 3659–3662, and references therein.

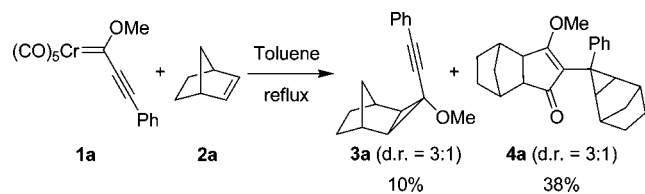
(18) (a) Barluenga, J.; Aznar, F.; Barluenga, S.; Fernández, M.; Martín, A.; García-Granda, S.; Piñera-Nicolás, A. *Chem.–Eur. J.* **1998**, *4*, 2280–2298. (b) Barluenga, J.; Aznar, F.; Barluenga, S.; Martín, A.; García-Granda, S.; Martín, E. *Synlett* **1998**, 473–474.

(19) Wu, H.-P.; Aumann, R.; Fröhlich, R.; Saarenko, P. *Chem.–Eur. J.* **2001**, *7*, 700–710.

(20) Barluenga, J.; Martínez, S.; Suárez-Sobriño, A. L.; Tomás, M. *J. Am. Chem. Soc.* **2002**, *124*, 5948–5949.

(21) Barluenga, J.; Fernández-Rodríguez, M. A.; García-García, P.; Aguilar, E.; Merino, I. *Chem.–Eur. J.* **2006**, *12*, 303–313.

(22) Barluenga, J.; Fernández-Rodríguez, M. A.; Andina, F.; Aguilar, E. *J. Am. Chem. Soc.* **2002**, *124*, 10978–10979.

Scheme 2. Reaction of Methoxy Phenylethynyl Chromium Carbene Complex **1a with Norbornene **2a****


First, we performed the reaction using an excess of olefin (5 equiv) in refluxing toluene for 30 min, which resulted in the isolation of compound **4a** in 38% yield as a 3:1 mixture of diastereomers, which could be separated by semipreparative HPLC using hexane/2-propanol as eluent. The structure of **4a** was tentatively proposed based on NMR studies (COSY, HMQC, HMBC, NOESY) and confirmed by X-ray diffraction of the major diastereomer (**4a maj**),²³ which was crystallized from hexane/dichloromethane (90/10) (Figure 1). In addition, cyclopropyl derivative **3a** was isolated as a minor product (10% yield) in a 3:1 diastereomeric ratio. The diastereomers could be separated by semipreparative HPLC using hexane as eluent; their relative stereochemistry was determined by a NOESY experiment.

A close examination of both the global reaction to furnish compound **4a** and the proper structure of **4a** displays several interesting features: (a) it has incorporated two units of norbornene, one unit of carbene ligand, and a CO moiety as a result of a formal tandem [2+2+1]/[2+1] cycloaddition process; (b) the alkynyl carbene complex reacts in an unprecedented manner through the carbene carbon and both acetylenic carbons and allows the incorporation of a carbonyl ligand into a cyclopentenone ring; (c) five σ C–C new bonds have been formed and two rings have been created; and (d) it represents a highly functionalized compound that should be amenable to further transformations.

With the structure of both cycloadducts identified, we proceeded to optimize the reaction conditions with a double objective: to improve the global yield and to direct the process toward the cascade [2+2+1]/[2+1] adduct **4a**. Temperature, number of equivalents of olefin, solvent, and nature of the metal of the carbene complex were the variables considered. In all cases, the consumption of the starting material and, therefore, the completion of the reaction were indicated by a color change and monitored by TLC. It was observed that the reaction required temperatures higher than 70 °C to proceed; however, experiments conducted in the range of 70 to 160 °C mainly differed in the reaction time (Table 1, entry 1), with 110 °C

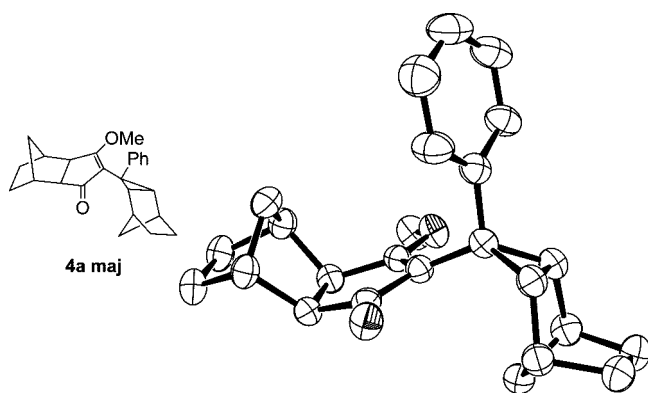


Figure 1. ORTEP drawing of **4a maj**. Ellipsoids are shown at the 50% level.

Table 1. Optimization of the Tandem [2+2+1]/[2+1] Cycloaddition

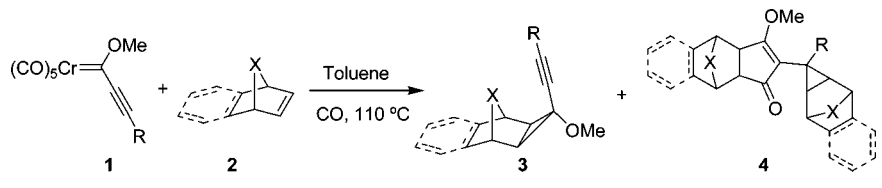
entry	N equiv	solvent	T (°C) ^a	reaction time (t)	3a (%) ^b	4a (%) ^b
1	5	toluene	70–160	10 min–7 h	~10	~40
2	5	toluene	110	30 min	10	38
3	5	DME	90	12 h	12	24
4	5	hexane	80	1 h	5	30
5 ^c	5	CH ₂ Cl ₂	90	5 h	11	35
6	10	toluene	110	30 min	12	43
7 ^d	10	toluene	80–110	30 min–24 h		~50
8 ^e	10	toluene	110	55 min	12	60
9 ^{e,f}	10	toluene	110	55 min	18	61
10 ^{e,g}	10	toluene	110	55 min	7	70
11 ^{e,g}	10	toluene	110	45 min	4 ^h	75

^a Bath temperature. ^b Isolated yield based on the starting carbene complex **1a**. ^c Reaction conducted in a sealed tube. ^d Reaction performed under CO pressure in a sealed tube (initially 1 atm, reaction pressure not quantified). ^e Slow addition of the carbene complex **1a** to the reaction mixture (addition time: entries 8–10, 45 min; entry 11, 35 min). ^f Conducted with continuous N₂ bubbling. ^g Performed under 1 atm of CO. ^h dr = 4:1.

being the temperature of choice (entry 2). The polarity of the solvent played a decisive role in the reaction: solvents such as DMF or THF (not listed in Table 1) resulted in only carbene decomposition, whereas reactions conducted in DME (1,2-dimethoxyethane), hexane, or dichloromethane either provided lower yields, required longer reaction times, or both (entries 3–5 vs 2). Toluene was then considered the solvent of choice for the reaction. The process was also sensitive to the nature of the metal, as the analogous tungsten carbene complex decomposed instead of adding to olefin **2a**. Regarding the number of equivalents of norbornene, better results were achieved when 10 equiv were employed instead of the initial 5 equiv (entries 2 vs 6); a greater excess of the alkene (20 equiv) did not increase the yield. Interestingly, cycloadduct **4a** was selectively obtained when the reaction was performed under a moderate pressure of CO (entry 7); however, the tandem cycloaddition was also inhibited under high CO pressures. After such initial screening only a slight enhancement in the yield was achieved (entry 7 vs 1). Considering that it was probably due to thermal decomposition of the starting carbene complex **1a**, the reaction was performed by slow addition of the carbene complex to the reaction mixture, leading to an improved combined 72% yield (entry 8). Moreover, while the proportion of the cyclopropane **3a** was increased by bubbling N₂ through the reaction mixture (entry 9), it was diminished to 4–7% when the reaction was performed under CO atmosphere (entries 10, 11). Therefore, the highest yield of the desired [2+2+1]/[2+1] cycloadduct **4a** (75%) was reached when the reaction was performed under CO atmosphere and the carbene addition time was kept at 35 min (entry 11).

2. Scope of the Reaction. Reactions of a series of strained and sterically hindered bicyclic olefins **2a–g**, structurally related to norbornene, and methoxy alkynyl FCCs **1a–f** were evaluated under the optimized reaction conditions; the results are summarized in Table 2.

Moderate to good yields of tandem adducts **4** were selectively or exclusively obtained with all the alkenes employed, **2a–f**, with the exception of *endo-2g*, which led to decomposition of

Table 2. Scope of Tandem [2+2+1]/[2+1] Cycloaddition of FCCs **1** with Bicyclic Olefins **2**


Entry ^a	1	R	Alkene 2	3	Yield (%) ^b	d.r. ^c	4	Yield (%) ^b	d.r. ^c
1	1a	Ph	2a	3a	4	4:1	4a	75	3:1
2 ^d	1a	Ph	2b		-		4b	65	3:1
3	1a	Ph	2c	3b	<2	-	4c	65	- ^e
4	1a	Ph	2d		-		4d	43	- ^f
5	1a	Ph	2e		-		4e	66	- ^g
6	1a	Ph	2f		-		4f	59	3:1
7	1a	Ph	2g		-			-	
8	1b		2a	3c	16	2:1	4g	58	3:1
9	1c	Bu	2a	3d	10	3:1	4h	59	3:1
10	1d	<i>t</i> -Bu	2a	3e	26	4:1	4i	53	1:1
11	1e	TMS	2e	3f	32	>95:<5	4j	16	1.6:1
12	1f		2a	3g	45	2:1		-	

^a All the experiments were conducted by slow addition of carbene complex **1** (1 equiv) to olefin **2** (10 equiv) in refluxing toluene under CO atmosphere unless otherwise stated. ^b Isolated yield based on the starting carbene complex **1**. ^c Diastereomeric ratio determined by ¹H NMR (300 MHz) of the isolated products. ^d Performed by slow addition of **1a** (1 equiv) to **2b** (10 equiv) and BHT (4%) in refluxing toluene with N₂ bubbling; polymerized norbornadiene of undetermined molecular weight was also isolated. ^e Mixture of eight isomers. ^f Obtained as a mixture of isomers in a 3:1 ratio. ^g Obtained as a mixture of three diastereomers in a 56:20:24 ratio.

the starting carbene complex (entries 1–7). The reaction with norbornadiene **2b** had to be conducted in the presence of 2,6-di-*tert*-butyl-4-methylphenol (BHT, 4%) and with nitrogen bubbling to minimize undesired polymerization of the olefin (entry 2). While double-bond chemoselectivity was observed for bis-cyclopentadiene **2c**, the reaction led to a mixture of eight isomers (entry 3). The [2+2+1]/[2+1] sequence tolerated the presence of heteroatoms (olefins **2d–f**, entries 4–6), as well as amide or carbamate groups in the olefin (i.e., **2d**, **2f**, entries 4, 6) but not an anhydride moiety (**2g**, entry 7).

Noteworthy, the influence of the substitution in the alkynyl carbene complex is significant, and as a result, variable mixtures of cycloadducts **3** and **4** were obtained. Thus, reactions of aryl- (entries 1–7), alkenyl- (entry 8), or alkyl- (entry 9) substituted

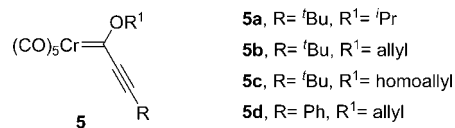
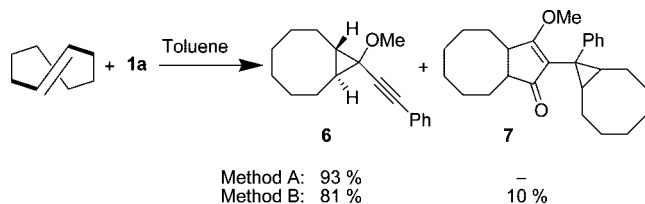


Figure 2. Other alkoxy alkynyl FCCs tested.

alkynyl FCCs selectively formed the multicomponent adducts **4**; however, bulky alkyl- or silyl-substituted alkynyl carbene complexes increased the amount of cyclopropane adducts **3** (entries 10, 11). In this regard, reaction of FCC **1f**, which bears an extraordinarily bulky substituent that totally blocks the triple bond,¹⁷ resulted in the complete inhibition of the multicomponent process (entry 12). The MCR was also suppressed when a sterically more demanding group is placed in the alkoxy moiety

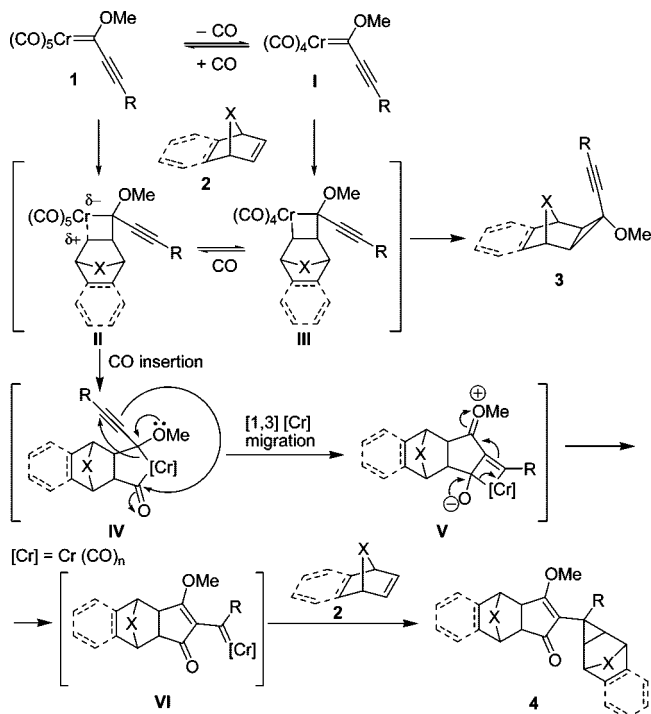
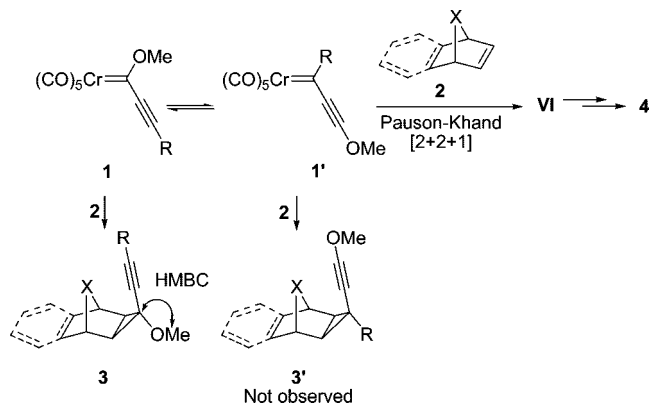
Scheme 3. Reaction of Methoxy Phenylethynyl Chromium Carbene Complex **1a with (*E*)-Cyclooctene**


of the alkynyl FCC (i.e., FCC **5a**, Figure 2); carbene decomposition was observed instead.

Considering that the large strain energy exhibited by bicyclic olefins **2** was highly responsible for this new reactivity pattern of FCCs, we explored the behavior of other strained olefins such as (*E*)-cyclooctene. However, the reaction of **1a** with (*E*)-cyclooctene following method A conditions [**1a**: (*E*)-cyclooctene 1:10, toluene, reflux] resulted in the direct cyclopropanation of the double bond, while 10% of four-component cycloadduct **7** was obtained under method B reaction conditions [slow addition of **1a** (1 equiv) to (*E*)-cyclooctene (10 equiv) in refluxing toluene under a CO atmosphere], as an almost equimolar 1:1:1 mixture of three diastereomers (Scheme 3). Once more, the yield of the [2+2+1]/[2+1] MCR sequence adduct increases when the process is performed under a CO atmosphere, as it has been previously observed for olefins **2**.

Other tested olefins, structurally related to norbornene, include cyclopentene or bicycle[2.2.2]oct-2-ene; however, under the reaction conditions only carbene decomposition was observed. These results pointed out that, in addition to the ring strain, which seems to be necessary to initiate the reaction, steric hindrance appears to play an important role to direct the reaction toward the four-component adducts in acceptable yields. With all these considerations, we thought that 3,4-disubstituted cyclobutenes would display the necessary requirements for the reaction; however, a wide range of experiments performed with FCC **1a** and several rather accessible cyclobutenes²⁴ [such as *trans*-3,4-dichloro-1-cyclobutene, *cis*-3,4-dichloro-1-cyclobutene, bicyclo[5.2.0]non-8-ene, or bicyclo[4.2.0]oct-7-ene] were unsuccessful; only intractable mixtures of carbene and cyclobutene decomposition compounds were detected.

3. Mechanism of the [2+2+1]/[2+1] Tandem Cycloaddition. With all these results in hand, we propose the mechanism depicted in Scheme 4. An initial CO ligand decooordination from carbene complexes **1** could occur, thus generating a tetracarbonyl species **I**; bicyclic olefins **2** will probably add to **1** or **I** in a 1,2-fashion or by a [2+2] cycloaddition, leading to the dipolar addition product **II** or metallacyclobutane **III**, respectively, which may be in equilibrium. Intermediate **III** may evolve to the formation of cyclopropanes **3**, this pathway being enhanced in the absence of CO; however, when the reaction is carried out in the presence of CO, the alternative route shown could be highly preferred. Then, a CO insertion should take place to generate **IV**, followed by a 1,3-metal migration,²⁵ which could be promoted by the electron pair of the methoxy group of **IV**. The resulting metallacyclobutane **V** would evolve to form a vinylogous methoxy-stabilized

Scheme 4. Proposed Mechanism for the [2+2+1]/[2+1] Tandem Cycloaddition

Scheme 5. Alternative Mechanism for the Formation of Carbene Complex **VI via FCC Isomerization Followed by a Pauson–Khand Reaction**


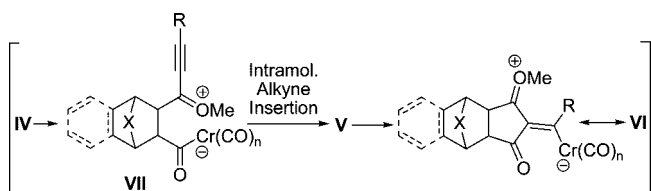
carbene species **VI**,²⁶ which will account for the formation of compounds **4** in the final steps.

An alternative mechanism that involves an initial rearrangement of FCCs **1** followed by a Pauson–Khand-type [2+2+1] cyclization reaction (PKR)²⁷ would also explain the formation of intermediate **VI**. However, this possibility was completely ruled out due to the following facts: (a) such rearrangement is not thermodynamically favored for heteroatom-stabilized chro-

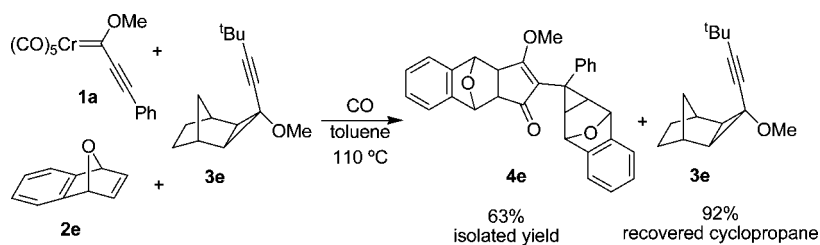
(24) (a) Hoberg, H.; Frölich, C. *Synthesis* **1981**, 830–831. (b) Leigh, W. J.; Zheng, K.; Clark, K. B. *J. Org. Chem.* **1991**, *56*, 1574–1580. (c) Liu, R. S. *J. Am. Chem. Soc.* **1967**, *89*, 112–114.

(25) 1,3-Metal group migrations have previously been observed in FCC chemistry: Barluenga, J.; Trabanco, A. A.; Flórez, J.; García-Granda, S.; Llorca, M. A. *J. Am. Chem. Soc.* **1998**, *120*, 12129–12130.

(26) The transformation of **IV** into **VI** could follow a mechanism involving even more steps (“less concerted”) via the methoxy-induced ring-opening of the metallacyclopentanone moiety on **IV** to form **VII** and the subsequent intramolecular alkyne insertion via metallacycle **V**:



Scheme 6. Cross-Reaction Attempted between FCC 1a, Olefin 2e, and Cyclopropane 3e



No cross-type products detected!

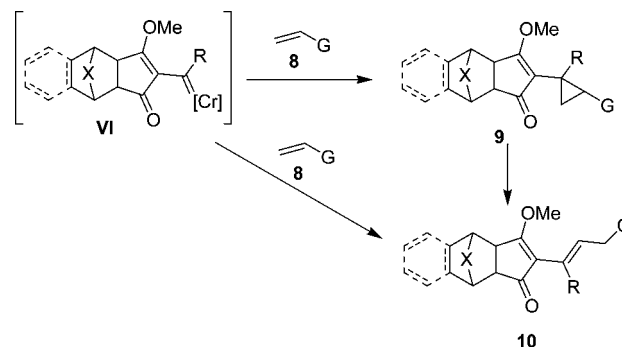
mium FCCs,^{28,29} and (b) neither the participation of the rearranged carbene **1'** in the reaction nor the formation of cyclopropanes **3'** has been detected (Scheme 5). On the contrary, a very clear signal in the HMBC spectra between the methoxy group and the quaternary carbon of the cyclopropanes corroborates the proposed structure for cyclopropanes **3**.

The option that **3** could be an intermediate for the formation of **4** was discarded by performing a cross-reaction. Considering that the corresponding cyclopropane **3** was not observed in the coupling of **2e** and **1a** (Table 1, entry 5), a cross-reaction was attempted by slow addition of **1a** (0.2 mmol, 1 equiv) to a solution of **2e** (3 equiv) and **3e** (1 equiv) in refluxing toluene under CO atmosphere (Scheme 6). The carbene **1a** disappeared in 30 min (TLC), and no cross-type products were detected either in the NMR spectrum of the crude residue or after column chromatography (in fact, unreacted cyclopropane **3e** was almost completely recovered). Such result, therefore, evidenced that, once it was formed, cyclopropane **3e** did not evolve under the reaction conditions.

4. [2+2+1]/[2+1] Coupling Reaction Sequence Involving Two Different Olefins. The [2+2+1]/[2+1] tandem cycloaddition process presented above allows a rapid access to highly functionalized polycyclic compounds that incorporate up to four components, among which two are the same bicyclic olefin. Obviously, 1 equiv of the strained bicyclic olefin **2** is required to initiate the reaction sequence; however, we questioned if a second and different olefin may be used to provide the fourth and final component, therefore introducing an extra element of diversity³⁰ into the reaction products.

Ethyl vinyl ether **8a** was initially chosen as fourth component for the [2+2+1]/[2+1] reaction sequence. After optimization of the stoichiometric ratio of the reactants, polycyclic compounds **9a** and **10a** were isolated in 7% and 25% yields (together with some amount of **3a** and **4a**) in a reaction carried out with FCC **1a**, norbornene **2a**, and ethyl vinyl ether **8a** in a 1:5:15

Scheme 7. Proposed Mechanism for the Formation of Compounds 9 and 10



ratio in toluene at 110 °C (Table 3, entry 1). Cyclopropane **9a** is the expected product, and it may be explained as the result of the cyclopropanation of the double bond of **8a** by carbene intermediate **VI**; on the other hand, compound **10a** is an acyclic adduct that also incorporates electron-rich olefin **8a** as the fourth component. Two plausible routes may explain its formation: (1) a rearrangement of **9a**, similar to the one previously proposed for other cyclopropanations involving chromium carbene complexes with electron-deficient olefins,^{8f} or (2) an alternative mechanism that does not imply the formation of the cyclopropane (Scheme 7).^{6b} Gratifyingly, the formation of such reaction products supports the role of carbene complex **VI** as an intermediate of the proposed reaction mechanism. The stereochemistry of adduct **10a** was determined by a NOESY experiment.

The reaction was also tested at 80 °C, and although much longer reaction times were required (5 h vs 30 min), it provided a notable increase in the combined amount of compounds **9a** and **10a** (entry 2). Interestingly, the reaction with benzooxanorbornadiene **2e** resulted in a considerable (80%) combined yield of adducts **9b** and **10b** (entry 3). Other significant results obtained are listed in Table 3.

The reactions were carried out with FCC **1a** and bicyclic olefins **2a** and **2e**, in toluene, at the two temperatures indicated in Table 3. In general, the reactions at 110 °C were completed in 30 min, while at 80 °C they required 3–6 h, although higher selectivity and combined yields were achieved. Other non-bicyclic olefins tested were 1-hexene **8b** (entries 4–6) and styrene **8c** (entries 7–10) as simple monosubstituted olefins and methyl acrylate **8d**, an electron-deficient olefin, which underwent incorporation into the four-component adducts **9g** and **10g** at 80 °C (entry 11); remarkably, **8d** undergoes direct cyclopropanation²¹ by FCC **1a** at 110 °C, even in the presence of norbornene **2a**. Terminal monosubstituted dienes were also employed, such as *trans*-1,3-pentadiene **8e** and isoprene **8f**, to find that the incorporation into the four-component adducts took place through the less hindered double bond (entries 12, 13); in these reactions cyclohexenes, which came from a [4+2]

(27) Selected recent reviews on the Pauson–Khand reaction: (a) Pérez-Castells, J. *Top. Organomet. Chem.* **2006**, *19*, 207–257. (b) Gibson, S. E.; Mainolfi, N. *Angew. Chem., Int. Ed.* **2005**, *44*, 3022–3037. (c) Blanco-Urgoiti, J.; Añorbe, L.; Pérez-Serrano, L.; Domínguez, G.; Pérez-Castells, J. *Chem. Soc. Rev.* **2004**, *33*, 32–42. (d) Boñaga, L. V. R.; Krafft, M. E. *Tetrahedron* **2004**, *60*, 9795–9833. (e) Alcaide, B.; Almendros, P. *Eur. J. Org. Chem.* **2004**, 3377–3383. (f) Gibson, S. E.; Stevanazzi, A. *Angew. Chem., Int. Ed.* **2003**, *42*, 1800–1810.

(28) Metallotropic [1,3]-carbene shifts have been reported for alkynyl-carbene complexes of several metals: (a) Lee, D.; Kim, M. *Org. Biomol. Chem.* **2007**, *5*, 3418–3427. Also, for a chromium-manganese exchange: (b) Ortin, Y.; Coppel, Y.; Lujan, N.; Mathieu, R.; McGlinchey, M. *Chem. Commun.* **2001**, 1690–1691.

(29) For chromium (and also for molybdenum and tungsten) alkynyl-carbene complexes the metallotropic [1,3]-shift equilibrium is displaced toward the formation of the corresponding heteroatom-stabilized FCC: (a) Barluenga, J.; García-García, P.; de Sáa, D.; Fernández-Rodríguez, M. A.; Bernardo de la Rúa, R.; Ballesteros, A.; Aguilar, E.; Tomás, M. *Angew. Chem., Int. Ed.* **2007**, *46*, 2610–2612. (b) Barluenga, J.; Bernardo de la Rúa, R.; de Sáa, D.; Ballesteros, A.; Tomás, M. *Angew. Chem., Int. Ed.* **2005**, *44*, 4981–4983.

(30) Schreiber, S. L. *Science* **2000**, *287*, 1964–1969.

Table 3. Scope of [2+2+1]/[2+1] Cycloaddition Reactions Involving Four Different Components

Entry ^a	2	8	T (°C) ^b	4	Yield (%) ^c	9	Yield (%) ^{c,d}	10	Yield (%) ^c
1 ^e	2a		110	4a	13	9a	7	10a	25
2	2a	8a	80	4a	13	9a	13	10a	28
3	2e	8a	80	-	-	9b	12	10b	68
4 ^e	2a		80	-	-	9c	17 ^f	10c	39 ^f
5	2e	8b	110	4e	26	9d	11	10d	41
6	2e	8b	80	4e	26	9d	22	10d	40
7 ^e	2a		110	4a	11	9e	20	10e	39
8	2a	8c	80	4a	11	9e	12	10e	25
9	2e	8c	110	4e	11	9f	10	10f	37
10	2e	8c	80	4e	10	9f	24	10f	38
11	2e		80	-	-	9g	15 ^g	10g	41 ^g
12 ^h	2e		80	4e	12	9h	22	10h	26
13 ^h	2e		80	4e	19	9i	7 ⁱ	10i	19
14	2e		110	4e	40	9j	37	-	-
15	2e	8g	80	4e	27	9j	52	-	-

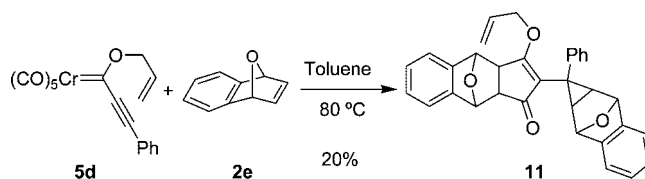
^a Reactions were conducted in a sealed tube using a 1:5:15 ratio of carbene complex **1a** and olefins **2** and **8**, heated at the given temperature for 30 min to 6 h before completion. ^b Bath temperature. ^c Isolated yield based on the starting carbene complex **1a**. ^d Obtained as mixtures of diastereoisomers; for the diastereomeric ratio [estimated by ¹H NMR (300 MHz) of the isolated products], see the Supporting Information. ^e Cyclopropane **3a** was also isolated (entry 1, 6%; entry 4, 4%; entry 7, 5%). ^f Compounds **9c** and **10c** could not be separated; the yield was estimated by NMR from a 56% combined isolated yield. ^g Obtained as an undetermined mixture of isomers. ^h The corresponding [4+2] Diels–Alder cyclohexenes, formed by reaction between olefin **2e** and dienes **8e,f**, were also isolated (entry 12, 13%; entry 13, 19%; yields based on olefin **2e**). ⁱ Not isolated; estimated yield, from a mixture with **10i**.

Diels–Alder reaction between **2e** and the dienes, were also isolated as byproducts.

Nonactivated disubstituted olefins were also checked. No coupling was observed for (*Z*)-cyclooctene or 2-ethyl-1-butene, but it occurred with a more reactive olefin such as cyclopentene **8g**. Again, the reaction outcome was highly dependent on the temperature: four-different-component cyclopropane **9j** was the major product at 80 °C (52%, dr = 1.5:1, entry 15), while **4e** was the main product at 110 °C (40%, entry 14).

Finally, other unsaturated systems such as imines, enamines, or aldehydes were also tested; however, they were not compatible with the reaction sequence, as they readily reacted with alkynyl FCCs **1**, inhibiting the tandem cycloaddition sequence. Complex reaction mixtures were formed in all these reactions.

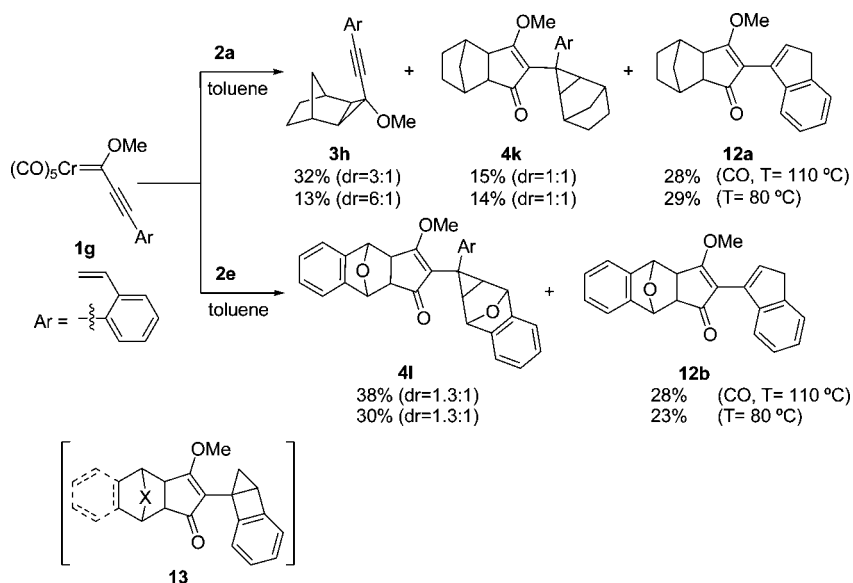
5. [2+2+1]/Intramolecular [2+1] Reaction Sequence. Considering the lack of selectivity of the four different component coupling reaction, which led to mixtures of three or four products, we turned to study the intramolecular cyclopropanation version of this reaction. However, no evidence of coupling was detected in the complex mixtures formed by reaction between bicyclic olefins **2a,e** and FCCs **5b,c** (Figure 2), which present a double bond in the alkoxy moiety but a bulky substituent in

Scheme 8. Intermolecular [2+2+1]/[2+1] Sequence with Allyloxy FCC **5d**

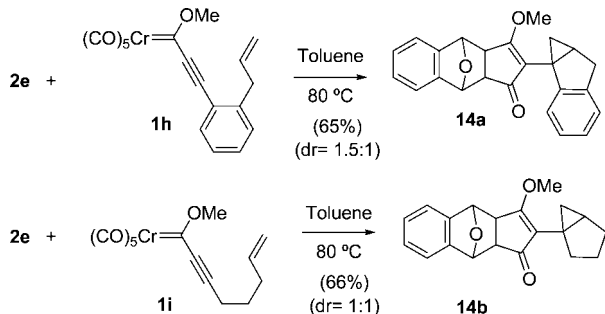
the triple bond. Only FCC **5d**, with a less bulky substituent in the triple bond, was able to undergo an [2+2+1]/[2+1] intermolecular coupling with two molecules of **2e** to render a low yield (20%) of product **11** (which, in fact, is a compound of type **4**) in Scheme 8; therefore, the expected final intramolecular cyclopropanation step did not take place for the reaction of FCC **5d** and alkene **2e**.

Then, we decided to place the double bond in the carbon skeleton linked to the triple bond. Thus, FCC **1g** (Scheme 9), which presents an *ortho*-vinyl group, was prepared²³ and reacted with **2a** in toluene at 110 °C under CO atmosphere, to give a mixture of cyclopropanation product **3h**, the intermolecular four-component adduct **4k**, and cycloadduct **12a**, which proceeds

Scheme 9. Inter- and Intramolecular [2+2+1]/[2+1] Sequences with FCC 1g



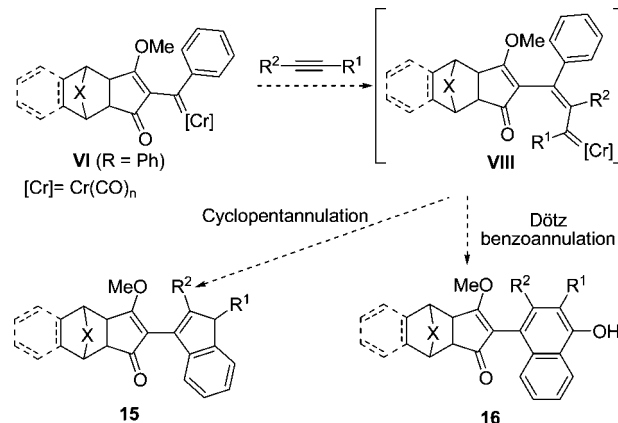
Scheme 10. [2+2+1]/Intramolecular [2+1] Sequences with Olefin 2e and FCCs 1h,i



from the intramolecular cyclopropanation of the vinyl group, in a 75% combined yield. Lowering the temperature to 80 °C and performing the reaction in the absence of CO resulted basically in a decrease of the yield of cyclopropane **3h**. However, the direct cyclopropanation was suppressed when olefin **2e** was employed; only the sequentially formed adducts **4l** and indene **12b** were isolated in moderate combined yields. Again, slightly lower yields were reached in the absence of CO at 80 °C.

The [2+2+1] reaction followed by an intramolecular cyclopropanation, starting from FCC **1g**, would lead to a nondetected highly strained structure **13** (Scheme 9), which should be relatively unstable and would evolve toward the formation of indenyl adducts **12**. On the other hand, the formation of strained [2.1.0] structure **13** would be relatively disfavored, which may explain the production of mixtures of both inter- and intramolecular [2+2+1]/[2+1] adducts.³¹ Therefore, if the FCC incorporates a 1,6-enyne unit, the final intramolecular cycloaddition should be the major reaction pathway because the [3.1.0] bicyclic system would certainly be less strained than the [2.1.0] system. To prove this hypothesis, FCCs **1h** and **1i** were reacted with bicyclic olefin **2e** in toluene at 80 °C in the absence of CO (Scheme 10). Under these conditions, cycloadducts **14a** and **14b**, which were formed exclusively by a [2+2+1]/intramolecular cyclopropanation sequence, were isolated

Scheme 11. Alkyne Insertion in VI (R = Ph) and Possible Evolution Patterns



in good yields as mixtures of diastereomers. As expected and contrary to what occurs for adducts **13**, [3.1.0] bicyclic compounds **14** formed via intramolecular cyclopropanation do not undergo ring expansion.

6. Internal Alkynes as Fourth Partner in the Four-Component Coupling. Taking into account the previously proposed mechanism (Scheme 4), we next hypothesized that the intermediate vinylogous methoxy-stabilized carbene complex **VI** (R = Ph) should be able to insert an alkyne unit to form **VIII**, which may evolve either by a cyclopentannulation or by a Dötz benzoannulation processes³² to generate new and highly functionalized indenenes **15** or naphthols **16** (Scheme 11).

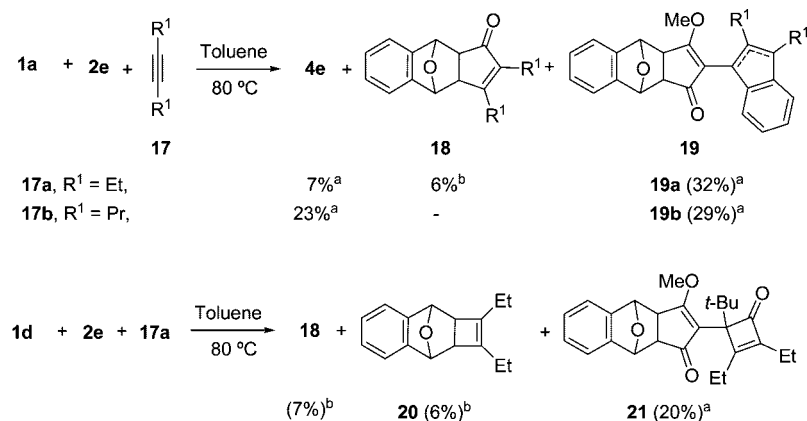
However, the presence of terminal alkynes inhibits the cascade reaction by promoting a Pauson–Khand reaction leading to cyclopentenones. This result has allowed the development of a substoichiometric tungsten-catalyzed intermolecular PKR, although of limited scope.³³ On the other hand, the insertion of an alkyne as the fourth component could be achieved indeed using an internal alkyne, such as 3-hexyne **17a**, which reacted with FCC **1a** and bicyclic olefin **2e** in toluene (Scheme

(31) A nucleophilic mechanism has been proposed for the indene formation from structurally similar intermediates, based on the correlation between the efficiency of the process and the nucleophilicity of the olefin: Zhang, L.; Herndon, J. W. *Organometallics* **2004**, *23*, 1231–1235.

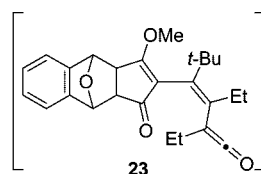
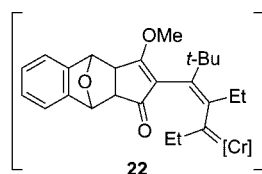
(32) (a) Dötz, K. H.; Tomuschat, P. *Chem. Soc. Rev.* **1999**, *28*, 187. (b) Minatti, A.; Dötz, K. H. *Top. Organomet. Chem.* **2004**, *13*, 123–156, and references therein.

(33) García-García, P.; Fernández-Rodríguez, M. A.; Rocaboy, C.; Andina, F.; Aguilar, E. *J. Organomet. Chem.* **2008**, *693*, 3092–3096.

Scheme 12. Internal Alkynes as Fourth Component in the Tandem Reaction



^a Isolated yields based on starting FCC. ^b Isolated yields based on **2e**.



12). Indene **19a** was obtained as major product, although minor quantities of both **4e** and Pauson–Khand adduct **18** were also isolated. Other internal alkynes, such as 4-octyne **17b**, were also incorporated as fourth partner, although to a slightly lesser extent since a 29% yield of indene **19b** was produced.

Alkyne insertion was also observed when the more stable FCC **1d** was employed. Note that **1d** bears a *t*-Bu group, and therefore, it cannot undergo annulation reaction; instead, the intermediate carbene complex **22** evolved to cyclobutenone **21**, through the insertion of a second carbonyl unit to form **23** and after a final electrocyclization step. Compound **21** is a five-component adduct, which presents a quaternary carbon and was isolated as a 1:1 diastereomer mixture. A 7% yield of **18** and a 6% yield of [2+2] adduct **20** were isolated as byproducts. Finally, the results displayed in Scheme 12 also support the role of carbene complex **VI** as an intermediate in the proposed reaction mechanism of Scheme 4.

Conclusions

In summary, alkoxy alkynyl Fischer carbene complexes react in an unprecedented manner through a [2+2+1]/[2+1] sequence with strained and hindered olefins (i.e., bicyclo[2.2.1]heptene derivatives), yielding highly functionalized polycycles that incorporate up to four different components (two of them may be identical). This cascade sequence is initiated by an interaction between the bicyclic olefin and the FCC, which takes part through its three reactive positions: the carbene and both acetylenic carbons. Two new rings and five σ C–C bonds are created in the process. Either electron-rich, neutral, or electron-

deficient olefins may act as the fourth component in the reaction sequence, which would lead to the final products by being trapped by intermediate carbene complex **VI**. The presence of an extra double bond in the appropriate position of the FCC considerably increases the selectivity of the reaction and allows the formation of the [2+2+1]/intramolecular [2+1] adducts as the sole reaction products. Terminal alkynes inhibit the cascade reaction, while internal alkynes are also suitable reagents to act as the fourth component in the reaction sequence: when the FCC bears an aromatic group, indenenes are obtained in a [2+2+1]/[3+2] cascade; otherwise cyclobutenones, which result from the further insertion of a carbonyl group, are formed.

Acknowledgment. We are very grateful to Prof. Barluenga for helpful discussions and, especially, for encouraging us to pursue this research. We thank the Ministerio de Ciencia y Tecnología (Spain) (grant CTQ2004-08077-C02-01, predoctoral fellowships to P.G.-G. and F.A., postdoctoral fellowship to C.R.), Principado de Asturias (project IB05-136), and the Fundación Ramón Areces for the financial support received. F.A. thanks the Universidad de Oviedo and CSIC for undergraduate fellowships.

Supporting Information Available: Complete Experimental Section including detailed experimental procedures, spectroscopic data for all new compounds, and crystallographic information files (CIF). This material is available free of charge via the Internet at <http://pubs.acs.org>.

OM800958D

Notes

Concise Synthesis of Enantiopure (S)-(+)-2,2'-Bis(tert-butyldimethylsilyl)-1,1'-diphosphaferrocene: Anion-Dependence of Its Coordination to Palladium(II) Centers

Yves Cabon, Duncan Carmichael,* and Xavier-Frédéric Le Goff

Laboratoire "Hétéroéléments et Coordination" Ecole Polytechnique, CNRS,
91128 Palaiseau Cedex, France

Received January 4, 2008

Summary: A convenient synthesis of enantiopure (S)-(+)-2,2'-bis(tert-butyldimethylsilyl)-3,3',4,4'-tetramethyl-1,1'-diphosphaferrocene is described. The compound shows unusual coordination properties with respect to Otsuka's Pd(II) dimer di-(S)-chloro-[1-[1-(dimethylamino)ethyl]-2-naphthyl-C,N]palladium(II).

Introduction

The now-extensive chemistry of enantiopure C_2 -symmetrical phosphines can be traced to Kagan and Dang's seminal studies of the tartrate-derived DiOP.¹ The ubiquitousness of backbone-chiral ligands of this sort reflects their well-documented synthetic and conformational² simplicity as well as the very easy access to a wide range of many enantiopure C_2 -symmetric precursors that is provided by the chiral pool.^{3–6} Other classes of enantiopure C_2 -symmetric ligands (e.g., P^{7–9} or axially^{10,11} chiral) frequently deliver equivalent or superior enantioselectivity; their lesser prevalence can be explained, at least in part, by the effort required to develop simple and efficient routes to the requisite enantiopure building blocks.

Metalloocene-based phosphines^{12–15} offer exceptional potential because of their easily varied ligand bite angles¹⁶ and high modularity¹⁷ but, because convenient large-scale routes to simple enantiopure planar-chiral C_2 -symmetrical derivatives are scarce,^{18–23} enantiopure phosphorus-containing metallocenes generally show C_1 ^{24,25} or C_2 -symmetry combining planar and central chiralities.^{26–29} In principle, since the influence of the planar chirality should be expressed particularly favorably if the donor atom is embedded within the metallocene skeleton, we were interested to devise a semimacroscopic route to enantiopure C_2 -symmetrical planar-chiral phosphoferrocenes; this discrete class was hitherto represented only by **1**, which was obtained on a small

* Corresponding author. E-mail: duncan.carmichael@polytechnique.edu.
Fax: intl + 33 1 69334440. Tel: intl + 33 1 69334415.

- (1) Kagan, H. B.; Dang, T. P. *J. Am. Chem. Soc.* **1972**, *94*, 6429.
- (2) Inasmuch as, for example, a square-planar complex containing a C_2 -symmetric ligand and a prochiral substrate will have only two isomers, while a C_1 -symmetric phosphine will generate four. See for example: Ramsden, J. A.; Claridge, T. D. W.; Brown, J. M. *J. Chem. Soc., Chem. Commun.* **1995**, 2469.
- (3) Dieguez, M.; Claver, C.; Pamies, O. *Eur. J. Org. Chem.* **2007**, 462, 1–4634.
- (4) Dieguez, M.; Pamies, O. P.; Claver, C. *Chem. Rev.* **2004**, *104*, 3189–3215.
- (5) Dieguez, M.; Pamies, O.; Ruiz, A.; Diaz, Y.; Castillon, S.; Claver, C. *Coord. Chem. Rev.* **2004**, *248*, 2165–2192.
- (6) Blaser, H. U. *Chem. Rev.* **1992**, *92*, 935–952.
- (7) Crepy, K. V. L.; Imamoto, T. *Adv. Synth. Catal.* **2003**, *345*, 79–101.
- (8) Johansson, M. J.; Kann, N. C. *Mini-Rev. Org. Chem.* **2004**, *1*, 233–247.
- (9) Grabulosa, A.; Granell, J.; Muller, G. *Coord. Chem. Rev.* **2007**, *251*, 25–90.
- (10) Berthod, M.; Mignani, G.; Woodward, G.; Lemaire, M. *Chem. Rev.* **2005**, *105*, 1801–1836.
- (11) Shimizu, H.; Nagasaki, I.; Saito, T. *Tetrahedron* **2005**, *61*, 5405–5432.

- (12) Arrayas, R. G.; Adrio, J.; Carretero, J. C. *Angew. Chem., Int. Ed.* **2006**, *45*, 7674–7715.
- (13) Barbaro, P.; Bianchini, C.; Giambastiani, G.; Parisel, S. L. *Coord. Chem. Rev.* **2004**, *248*, 2131–2150.
- (14) Atkinson, R. C. J.; Gibson, V. C.; Long, N. J. *Chem. Soc. Rev.* **2004**, *33*, 313–328.
- (15) Colacot, T. J. *Chem. Rev.* **2003**, *103*, 3101–3118.
- (16) Brown, J. M.; Guiry, P. J. *Inorg. Chim. Acta* **1994**, *220*, 249–259.
- (17) Blaser, H. U.; Brieden, W.; Pugin, B.; Spindler, F.; Studer, M.; Togni, A. *Top. Catal.* **2002**, *19*, 3–16.
- (18) Zhang, W. B.; Kida, T.; Nakatsuji, Y.; Ikeda, I. *Tetrahedron Lett.* **1996**, *37*, 7995–7998.
- (19) Reetz, M. T.; Beuttenmuller, E. W.; Goddard, R.; Pasto, M. *Tetrahedron Lett.* **1999**, *40*, 4977–4980.
- (20) Zhang, W. B.; Shimanuki, T.; Kida, T.; Nakatsuji, Y.; Ikeda, I. *J. Org. Chem.* **1999**, *64*, 6247–6251.
- (21) Laufer, R.; Veith, U.; Taylor, N. J.; Snieckus, V. *Can. J. Chem.* **2006**, *84*, 356–369.
- (22) Wang, Y. P.; Weissensteiner, W.; Spindler, F.; Arion, V. B.; Mereiter, K. *Organometallics* **2007**, *26*, 3530–3540.
- (23) Zhang, H. L.; Hou, X. L.; Dai, L. X.; Luo, Z. B. *Tetrahedron: Asymmetry* **2007**, *18*, 224–228. For further selected examples see also: Voituriez, A.; Panossian, A.; Fleury-Bregeot, N.; Retailleau, P.; Marinetti, A. *J. Am. Chem. Soc.* **2008**, *130*, 14030–14031. Pickett, T. E.; Francesc, X.; Roca, F. X.; Richards, C. J. *J. Org. Chem.* **2003**, *68*, 2592–2599.
- (24) Stepnika, P., Ed. *Ferrocenes: Ligands, Materials and Biomolecules*; John Wiley: Chichester, 2008.
- (25) Ferber, B.; Kagan, H. B. *Adv. Synth. Catal.* **2007**, *349*, 493–507.
- (26) Many of these are derived from the Ugi amine: Marquarding, D.; Klusacek, H.; Gokel, G.; Hoffmann, P.; Ugi, I. *J. Am. Chem. Soc.* **1970**, *92*, 5389–5393. See for example: Josiphos: Blaser, H. U.; Brieden, W.; Pugin, B.; Spindler, F.; Studer, M.; Togni, A. *Top. Catal.* **2002**, *19*, 3–16. Walphos: Sturm, T.; Xiao, L.; Weissensteiner, W. *Chimia* **2001**, *55*, 688–693.
- (27) Liu, D.; Li, W.; Zhang, X. M. *Org. Lett.* **2002**, *4*, 4471–4474.
- (28) Berens, U.; Burk, M. J.; Gerlach, A.; Hems, W. *Angew. Chem., Int. Ed.* **2000**, *39*, 1981–1984. Marinetti, A.; Labrue, F.; Genet, J. P. *Synlett* **1999**, 1975–1977.
- (29) Hayashi, T.; Yamamoto, A.; Hojo, M.; Kishi, K.; Ito, Y.; Nishioka, E.; Miura, H.; Yanagi, K. *J. Organomet. Chem.* **1989**, *370*, 129–139.

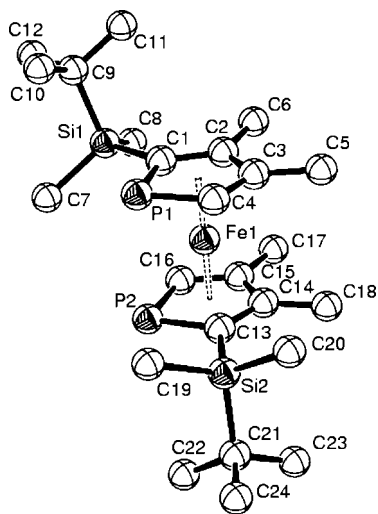


Figure 1. Molecular structure (50% probability ellipsoids) of *rac*-1,1'-diphosphaferrocene **6**. Selected bond lengths (Å) and angles (deg): P1–C1 1.792(3), C1–C2 1.429(4), C2–C3 1.430(5), C3–C4 1.398(5), P1–Fe 2.273(1), C1–Fe 2.079(3), C2–Fe 2.075(3), C3–Fe 2.091(3), C4–Fe 2.092(3); C4–P1–C1 89.83(2), P1–C1–C2 111.2(2), C1–C2–C3 112.90, C2–C3–C4 111.9(3), C3–C4–P1 114.1(2), P1–Centroid–Centroid–P2 8.3.

scale by chiral HPLC.³⁰ These compounds present the unusual electronic characteristics of the sp^2 -hybridized phosphorus atom³¹ and the possibility of very facile installation and variation of substituents in the 2-position through well-established [1,5] sigmatropic shift chemistry.^{32–34}

The silyl-substituted phospholide required for the study was prepared in a one-pot synthesis from 1-phenyl-3,4-dimethylphosphole **2**³⁵ through an amended version of our previously described methodology³² which furnishes **4** conveniently in 82% yield on ca. 20 g scales. The colorless, air-sensitive phospholide reacts cleanly with anhydrous $FeCl_2$ to provide mixed (ca. 1:1) diastereomers of the requisite phosphoferrocenes, which were separated from refluxing ether; the desired *rac*-complex **6** crystallized preferentially upon cooling in a nonoptimized yield of 17% (Figure 1).³⁶ The bright red phosphoferrocene products proved air-stable as solids and were found to be quite convenient to handle.

Resolving phosphines that contain no organic functional groups is often tedious and, on the laboratory scale, palladium-based reagents are frequently employed.^{9,37,38} Obvious constraints mean that such protocols are rarely employed on larger batches but the well-documented^{39–45} poor compatibility of relatively “hard” palladium(II) centers with “soft” 1,1'-diphosphaferrocene donors of the type implicated here allows a straightforward and economical resolution.⁴⁶ Otsuka's naphthyl-1-ethylamine-derived complex **10**^{37,38,47} is unreactive toward phosphoferrocenes **6** in donor solvents; however, it shows weak coordination in dichloromethane that can be driven to completion by the addition of silver tetrafluoroborate.⁴⁸ The product diastereomers, which show an Fe:Pd stoichiometry of 1:2, are quite easily separated by washing with ethylacetate and the less

soluble complex **8** was obtained in monocrystalline form, suitable for a diffraction study, through vapor diffusion of pentane into its dichloromethane solution (Figure 2).

The unusual⁴⁹ monocationic dimer contains an (*S*)-configured phosphametalocene and a chloride anion bridging the two (*S*)-configured Pd components. The requirement for the silver salt implies a fragility of complex **8** in the presence of halide and, consistently, addition of iodide in polar solvents releases the phosphametalocene and regenerates palladium dimer.⁵⁰ The two components can be separated by rinsing with pentane, thus allowing the (rather costly) enantiopure palladium fragment to be recovered conveniently and recycled.

The approach presented here opens up a straightforward and concise route, which does not require the intervention of preparative chiral HPLC, to the hitherto relatively inaccessible enantiopure planar-chiral C_2 -symmetrical phosphametalocene structure. The product, **9**, can be made to associate or dissociate from enantiopure Pd(II) centers through variation of halide concentration and this provides an unusual and very simple means of recycling the resolving agent. The generality of these procedures and the potential of ligands such as **9** to provoke further unusual coordination chemistry are under investigation.

We thank CNRS, Ecole Polytechnique, and the Fondation de l'Ecole Polytechnique (“Gaspard Monge” grant to Y.C.) for support and Dr. J. M. Brown, FRS (Oxford), for access to the MicroTOF spectrometer.

Experimental Section

All operations were performed either using cannula techniques on Schlenk lines under an atmosphere of dry nitrogen or in a Braun Labmaster 130 drybox under dry purified argon. 1-Phenyl-3,4-dimethylphosphole **2**³⁵ and Otsuka's complex **10**³⁸ were obtained as described previously. Solvents were distilled under dry nitrogen, THF and ether from sodium-benzophenone ketyl, pentane from sodium-benzophenone ketyl-tetraglyme, methanol from sodium methoxide, and dichloromethane from P_4O_{10} . Deuterobenzene was used as received from Aldrich, while deuteriochloroform was deacidified through neutral alumina prior to use. Other solvents were also used as received. NMR measurements were made on a Bruker Avance 300 spectrometer and are referenced to internal C_6D_5H or $CHCl_3$ and external H_3PO_4 as appropriate. Mass spectra were obtained from dichloromethane solutions on a Bruker electrospray MicroTOF spectrometer. Melting points were measured between glass slides in air.

Compound 4. 1-Phenyl-3,4-dimethylphosphole, **2** (14.6 g, 78 mmol) and freshly beaten lithium strips (2.4 g, 1% sodium, 344 mmol) were stirred in THF for 2.5 h. The excess lithium was removed and, after addition of *t*-BuCl (15 mL, 137 mmol), the mixture was stirred overnight. The pale solution was evaporated to dryness, treated with toluene, again evaporated to dryness, and extracted with pentane (50 mL). The pentane extracts were separated and discarded; the residue was then resuspended in THF, treated with a single portion of freshly sublimed TBSCl (10.2 g, 68.0 mmol) at ice-bath temperature, evaporated to dryness *in vacuo* at $\leq 20^\circ C$, extracted with pentane (2×75 mL), filtered through Celite, and pumped down ($\leq 20^\circ C$) to give a pale oil. Resuspension in ice-cold THF (200 mL), addition of KO^tBu (7.6 g, 68.0 mmol), and stirring for 20 min was followed by concentration of the solution under reduced pressure to give a pale red oil. Addition of pentane, followed by vigorous stirring, gave a white precipitate of the solvent-free potassium 2-*tert*-butyldimethylsilyl-3,4-dimethylphospholide, **4**, which was collected, washed with pentane (2×20 mL), and dried (14.7 g, 56 mmol, 72%).

(30) Qiao, S.; Hoic, D. A.; Fu, G. C. *Organometallics* **1998**, *17*, 773–774.

(31) Le Floch, P. *Coord. Chem. Rev.* **2006**, *250*, 627–681.

(32) Carmichael, D.; Mathey, F.; Ricard, L.; Seeboth, N. *Chem. Commun.* **2002**, 2976–2977.

(33) Mathey, F. *Acc. Chem. Res.* **2004**, *37*, 954–960.

(34) Holand, S.; Jeanjean, M.; Mathey, F. *Angew. Chem., Int. Ed.* **1997**, *36*, 98–100.

(35) Holand, S.; Jeanjean, M.; Mathey, F. *Angew. Chem., Int. Ed.* **1997**, *36*, 98–100.

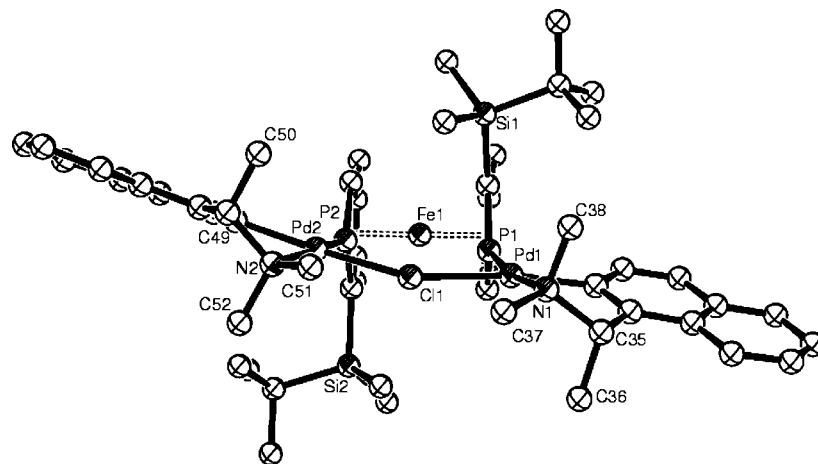


Figure 2. Molecular structure (50% probability ellipsoids) of **8** (dichloromethane of solvation and BF_4^- counterion removed for clarity). Selected bond lengths (Å) and angles (deg): Pd(1)–C(25) 2.007(4); Pd(1)–P(1) 2.227(1); Pd(1)–N(1) 2.121(3); Pd(1)–Cl(1) 2.415(1); Pd(2)–C(39) 2.024(4); Pd(2)–N(2) 2.127(3); Pd(2)–P(2) 2.224(1); Pd(2)–Cl(1) 2.400(1); Pd(2)–Cl(1)–Pd(1) 137.8(1).

^{31}P (THF- d_8): δ 110.5. ^1H (THF- d_8): δ 6.91 (d, 1H, P-CH, $^2J_{\text{H-P}}$ = 39 Hz), 2.35 (s, 3H, CH_3), 2.28 (s, 3H, CH_3), 1.02 (s, 9H,

$\text{C}(\text{CH}_3)_3$), -0.54 (s, 6H, $\text{Si}(\text{CH}_3)_2$). ^{13}C (THF- d_8): δ 134.1 (d, P-CH, $^1J_{\text{C-P}}$ = 45 Hz), 131.6 (s, P-CH-CMe), 129.6 (d, P-C(TBS)-CMe, $^1J_{\text{C-P}}$ = 62 Hz), 129.3 (s, P-C(TBS)CMe), 26.5 (d, $\text{C}(\text{CH}_3)_3$, $^4J_{\text{C-P}}$ = 2 Hz), 16.7 (s, CH_3), 15.8 (s, CH_3), 7.3 (s, $-\text{C}(\text{CH}_3)_3$), -3.1 (d, $-\text{Si}(\text{CH}_3)_2\text{tBu}$, $^3J_{\text{C-P}}$ = 10 Hz) ppm.

(36) The preparation and separation of *meso*- and *rac*-diastereomers of 2,2'-bis(trimethylsilyl)-3,3',4,4'-tetramethyl-1,1'-diphosphaferrocene, through a much longer synthetic route, has been reported previously by Deschamps and Mathey. No attempt to separate enantiomers was described. See: Deschamps, B.; Mathey, F. *Bull. Soc. Chim. Fr.* **1996**, *133*, 541–545.

(37) Wild, S. B. *Coord. Chem. Rev.* **1997**, *166*, 291–311.

(38) Tani, K.; Brown, L. D.; Ahmed, J.; Ibers, J. A.; Yokota, M.; Nakamura, A.; Otsuka, S. *J. Am. Chem. Soc.* **1977**, *99*, 7876–7886.

(39) Sava, X.; Ricard, L.; Mathey, F.; Le Floch, P. *Organometallics* **2000**, *19*, 4899–4903.

(40) Ogasawara, M.; Yoshida, K.; Hayashi, T. *Organometallics* **2001**, *20*, 3913–3917.

(41) Ganter, C.; Kaulen, C.; Englert, U. *Organometallics* **1999**, *18*, 5444–5446.

(42) Hayashi, Ogasawara, et al have prepared enantiopure 1,1'-phosphametallocenes (M = Fe, Ru) without recourse to resolution by using phospholyl ligands that are 2,5-disubstituted with C-chiral (either biaryl or menthyl) groups. These provide good precedence for enantioselection. See: Ogasawara, M.; Ito, A.; Yoshida, K.; Hayashi, T. *Organometallics* **2006**, *25*, 2715–2718. Ogasawara, M.; Yoshida, K.; Hayashi, T. *Organometallics* **2001**, *20*, 3913.

(43) Melaimi, M.; Ricard, L.; Mathey, F.; Le Floch, P. *J. Organomet. Chem.* **2003**, *684*, 189–193.

(44) Melaimi, M.; Mathey, F.; Le Floch, P. *J. Organomet. Chem.* **2001**, *640*, 197–199.

(45) Sava, X.; Ricard, L.; Mathey, F.; Le Floch, P. *Chem.–Eur. J.* **2001**, *7*, 3159–3166.

(46) Dunina, V. V.; Razmyslova, E. D.; Gorunova, O. N.; Livantsov, M. V.; Grishin, Y. K. *Tetrahedron: Asymmetry* **2005**, *16*, 817–826.

(47) Alcock, N. W.; Hulmes, D. I.; Brown, J. M. *J. Chem. Soc., Chem. Commun.* **1995**, 395–397.

(48) The corresponding phenylethylamine derivative reacts with the phosphaferrrocene complexes in the absence of Ag^+ , but separation of the product diastereomers is difficult.

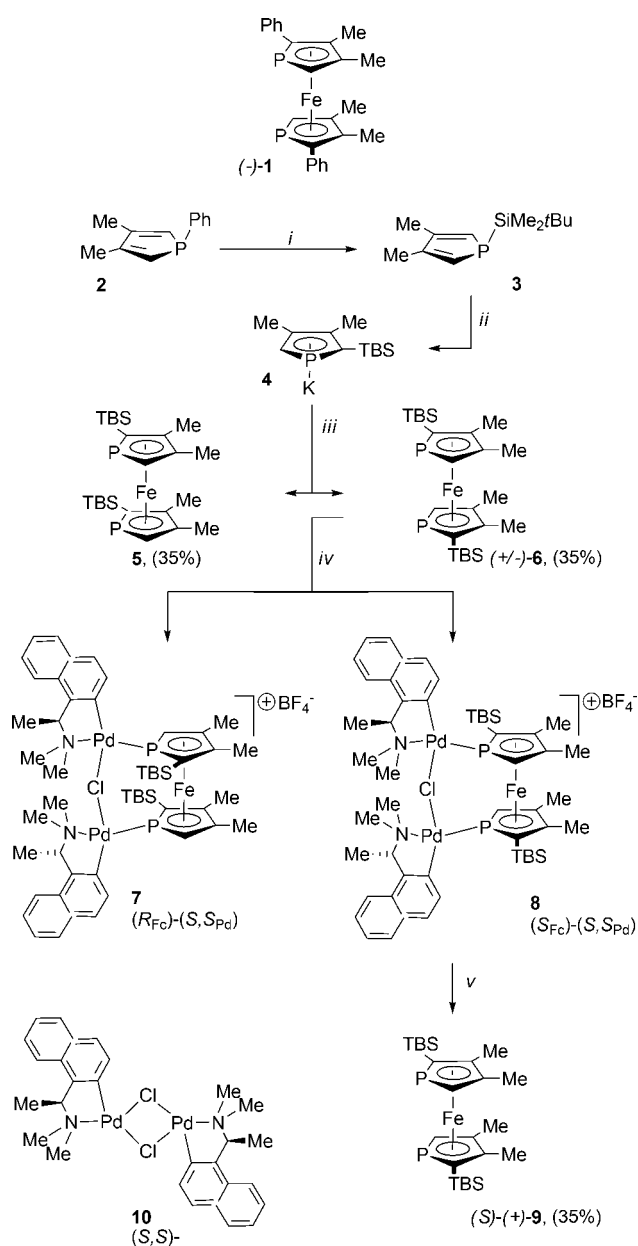
(49) A analogue, containing a bridging biquinoline ligand, has been characterized crystallographically. See: Dai, L. X.; Zhou, Z. H.; Zhang, Y. Z.; Ni, C. Z.; Zhang, Z. M.; Zhou, Y. F. *J. Chem. Soc., Chem. Commun.* **1987**, 1760–1762.

(50) As noted by a referee, the parallel ring orientation observed in the phosphaferrrocene inhibits a chelating coordination mode at the palladium(II) center, which might otherwise be observed with compounds such as 1,1'-diphosphazirconocene dichlorides: Nief, F.; Mathey, F.; Ricard, L. *J. Organomet. Chem.* **1990**, *384*, 271–278. The latter compounds are face-inverting, so different methods of resolution are likely to be preferable in these cases. For an elegant approach, see: Hollis, T. K.; Wang, L. S.; Tham, F. *J. Am. Chem. Soc.* **2000**, *122*, 11737–11738. Freeman, W. P.; Ahn, Y. J.; Hollis, T. K.; Whitaker, J. A.; Vargas, V. C.; Rubio, R. J.; Alingog, K. D.; Bauer, E. B.; Tham, F. S. *J. Organomet. Chem.* **2008**, *693*, 2415–2423.

(51) The palladium reagent is recovered as the corresponding iodo-bridged dimer (identified by comparison of the ^1H NMR spectrum with an authentic sample). Stirring in acetone with a silver salt and subsequent addition of chloride allows the dichloro-bridged complex **10** to be recovered conveniently.

Compound 6. FeCl_2 (240 mg, 1.89 mmol) was added in one portion to a THF (20 mL) solution of potassium 2-TBS-3,4-dimethylphospholide, **4** (1.00 g, 3.78 mmol). The red solution was stirred for 2 h and the solvent was then removed under reduced pressure. The resulting solids were extracted into pentane (20 mL), which was filtered through Celite and removed under reduced pressure. The crude red ca. 1:1 mixture of *rac*- and *meso*-diastereoisomers **5** and **6** (899 mg, 1.78 mmol, 94%) was taken up in ether (5 mL) and crystallized at -40°C . The mother liquor was removed while still cold, giving a solid showing a de of ca. 65%. Two further analogous recrystallizations from ether at -40°C gave the orange-red diastereopure *rac*-complex **6** (163 mg, 0.32 mmol, 17%). Material suitable for the X-ray diffraction study was obtained by slow cooling of a saturated refluxing methanol solution. ^{31}P NMR (C_6D_6): δ -44.2 (AA'XX', $^2J_{\text{P-H}}=35.1$ Hz, $J_{\text{P-P}}=10.5$ Hz, $J_{\text{P-H}}=0.6$ Hz). ^1H NMR (C_6D_6): δ 3.43 (AA'XX, 2H, CH-, $^2J_{\text{H-P}}=35.1$ Hz, $J_{\text{H-P}}=0.6$ Hz, $J_{\text{H-H}}=0$ Hz), 1.81 (s, 6H, CH-C(CH_3)-), 1.77 (s, 6H, C(TBS)-C(CH_3)), 0.94 (s, 18H, C(CH_3) $_3$), 0.68 (s, 6H, SiMeBu(CH_3)), 0.20 (s, 6H, SiMeBu(CH_3)). ^{13}C NMR (C_6D_6): δ 104.0 (s, CH-CMe-), 98.9 (s, C(TBS)-CMe-), 87.0 (d, CH, $^1J_{\text{C-P}}=69.3$ Hz), 83.8 (d, P-C(TBS)-), $^1J_{\text{C-P}}=79.7$ Hz), 27.34 (s, C(CH_3) $_3$), 18.5 (s, CMe $_3$), 17.7 (s, C(TBS)-C(CH_3)-), 16.0 (s, CH-C(CH_3)), 0.0 (s, SiMeBu(CH_3)), -1.0 (s, SiMeBu(CH_3)) ppm. HRMS: found 506.1804, requires 506.1806. Anal. Calcd for $\text{C}_{24}\text{H}_{44}\text{FeP}_2\text{Si}_2$: C, 56.90; H, 8.76. Found: C, 56.93; H, 8.71. Mp = 172 – 172.5°C .

Compound 8. A dichloromethane solution (5 mL) of *rac*-2,2'-bis(TBS)-3,3',4,4'-tetramethyl-1,1'-diphosphaferrocene, **6** (100 mg, 0.20 mmol), was treated with equimolar palladium dimer **10** (134.3 mg, 0.20 mmol) and silver tetrafluoroborate (38.9 mg, 0.20 mmol). After stirring for 10 min, the deep yellow solution was filtered through Celite and the solvent was removed under reduced pressure. The yellow mixture of diastereomers was triturated in ethylacetate (5 mL) and centrifuged, and the mother liquor was removed. The process was repeated three times. The residue was recovered and dried under reduced pressure, yielding the diastereopure yellow powder **8**. Single crystals suitable for the diffraction study were obtained by vapor diffusion of pentane into a solution of the compound in dichloromethane (104 mg, 0.08 mmol, 42%). ^{31}P NMR ($\text{DCM}-d_2$): δ 61.4 (d, $^2J_{\text{P-H}}=32$ Hz). ^1H NMR ($\text{DCM}-d_2$): δ 7.80 (d, 2H, H_4 and H_7 , $^3J_{\text{H-H}}=9.1$ Hz), 7.51 (m, 2H, H_5 and H_6), 7.36

Scheme 1^a

^a Reaction scheme: (i) Li (excess), THF, 0 °C, 3 h; then *t*BuCl (excess), THF, 20 °C, 12 h; then TBSCl (1 equiv), THF, 0 °C, 10 min. (ii) KOTfBu, (1 equiv), 0 °C, 2 h; *i*+*ii*: 72%. (iii) FeCl₂, (1 equiv), 20 °C, 2 h; then crystallisation from Et₂O; for **6**: 17%. (iv) **10** (1 equiv), AgBF₄ (1 equiv), CH₂Cl₂, 20 °C, 30 min; then trituration with EtOAc; for **8**: 42%. (v) NaI (2 equiv), THF, 20 °C, 1 h, 90%.

(d, *H*₉, *J* = 9.3 Hz), 7.08 (dd, *H*₂, *J* = 9.1 and 6.0 Hz), 4.59 (qq, 1H, N-CH, ³*J*_{H-H} = 7.1 Hz, ⁴*J*_{H-H} = 5.4 Hz), 3.55 (d, P-CH, ²*J*_{H-P} = 32 Hz), 3.12 (3H, NMe(CH₃), ⁴*J*_{H-H} = 5.4 Hz), 3.02 (s, 3H, N(CH₃)Me), 2.29 (s, 3H, P-CH-C(CH₃)), 2.12 (s, 3H, P-C(TBS)-C(CH₃)), 1.92 (s, 3H, NMe₂-CH(CH₃)), 0.97 (s, 9H, C(CH₃)₃), 0.60 (s, 3H, Si(CH₃)Me(*t*Bu)), 0.11 (s, 3H, SiMe(CH₃)(*t*Bu)). ¹³C NMR (DCM-*d*₂): δ 149.2 (s, C₁), 146.0 (s, C₁₀), 137.6 (d, C₂, *J* = 21.4 Hz), 131.2 (s, C₃), 128.8 (s, C₄), 128.3 (s, C₈), 126.3 (s, C₅), 125.8 (d, C₉, *J* = 7.1 Hz), 125.1 (s, C₆), 123.4 (s, C₇), 103.3 (d, -P-CH-CMe, ²*J*_{C-P} = 6.4 Hz), 100.6 (s, P-C(TBS)-CMe), 73.3 (s, NMe₂-CHMe), 69.5 (d, P-C(TBS), ¹*J*_{C-P} = 61.0 Hz), 66.7 (d, P-CH, ¹*J*_{C-P} = 40.8 Hz), 53.2 (s, NMe(CH₃)), 49.7 (s, N(CH₃)Me), 26.4 (s, C(CH₃)₃), 23.6 (s, NMe₂-CH(CH₃)), 18.3 (s, CMe₃), 13.9 (d, P-CH-C(CH₃), ³*J*_{C-P} = 6 Hz), 13.4 (d, P-C(TBS)-C(CH₃), ³*J*_{C-P} = 7 Hz), 0.0 (s, -Si(CH₃)Me(*t*Bu)), -2.9 (s, -SiMe(CH₃)(*t*Bu)). Anal. Calcd for C₁₀₅H₁₅₄B₂Cl₄F₈Fe₂N₄P₄Pd₄Si₄ (8 • 1/2CH₂Cl₂): C, 49.24; H, 6.06. Found: C, 49.14; H, 6.14. Mp = 224–225 °C (dec). The mother liquors were combined and shown to have a de of ca. 80% in favor of **7**.

Compound 9. A THF (3 mL) solution of the diastereopure palladium complex **8** (100 mg, 0.08 mmol) was treated with sodium iodide (24.0 mg, 0.16 mmol). The solution was stirred for 30 min, and the THF was removed under reduced pressure. The solids were extracted with pentane (10 mL), and the extract was filtered through Celite. Removal of solvent under reduced pressure gave deep red, air-stable crystals of **9** (36.9 mg, 0.07 mmol, 90%). [α]_D²⁵ +55 (c 0.5, CH₂Cl₂). Anal. Calcd for C₂₄H₄₄FeP₂Si₂: C, 56.90; H, 8.76. Found: C, 56.77; H, 8.71. Mp: 165–167 °C. Other data as for **6**.

Crystallographic data: **6**: C₂₄H₄₄FeP₂Si₂, *M* = 506.56, monoclinic, space group *P*2₁/*c*, *a* = 7.462(1) Å, *b* = 23.903(1) Å, *c* = 16.032(1) Å, β = 108.35(1)°, *V* = 2714.1(4) Å³, *Z* = 4, *D*_c = 1.240 g cm⁻³, *F*(000) = 1088. Graphite-monochromated Mo Kα radiation, λ = 0.71069 Å, μ = 0.77 cm⁻¹, *T* = 150(1) K. Of 6216 independent reflections collected on a Kappa CCD diffractometer from a red needle of dimensions 0.20 × 0.20 × 0.04 mm over *h* = -9 to 6, *k* = -31 to 28, *l* = -17 to 20, 4911 having *I* > 2σ(*I*) were refined on *F*² using direct methods in SHELXL. *w**R*₂ = 0.146, *R*₁ = 0.055, GoF = 1.062. For **8** • 1/2CH₂Cl₂: C₁₀₅H₁₅₄B₂Cl₄F₈Fe₂N₄P₄Pd₄Si₄, *M* = 2561.4, tetragonal, space group *P*41212, *a* = 21.022(1) Å, *b* = 21.022(1) Å, *c* = 30.883(1) Å, *V* = 13648.0(1) Å³, *Z* = 4, *D*_c = 1.288 g cm⁻³, *F*(000) = 5424. Graphite-monochromated Mo Kα radiation, λ = 0.71069 Å, μ = 0.973 cm⁻¹, *T* = 150.0(10) K. Of 15 613 independent reflections from an orange needle of 0.40 × 0.16 × 0.12 mm collected as above over *h* = -27 to 26; *k* = -22 to 25; *l* = -28 to 40, 14 179 having *I* > 2σ(*I*) were refined on *F*² using direct methods in SHELXL. *w**R*₂ = 0.128, *R*₁ = 0.045, GoF = 1.072, Flack's parameter = -0.015(17). Full data are provided as Supporting Information.

Supporting Information Available: CIF files and full crystallographic tables for complexes **6** and **8**. This material is available free of charge via the Internet at <http://pubs.acs.org>.

OM800009E

Chlorination of Boron on a Ruthenium-Coordinated Hydridotris(pyrazolyl)borate (Tp) Ligand: A Caveat for the Use of $\text{TpRu}(\text{PPh}_3)_2\text{Cl}$

Nicholas A. Foley,[†] Robyn J. Abernethy,[#] T. Brent Gunnoe,^{*,†} Anthony F. Hill,[#] Paul D. Boyle,[§] and Michal Sabat[†]

Department of Chemistry, University of Virginia, Charlottesville, Virginia 22904-4319, Research School of Chemistry, Australian National University, Canberra, A.C.T. 0200, Australia, and Department of Chemistry, North Carolina State University, Raleigh, North Carolina 27695-8024

Received August 19, 2008

Summary: A side-product that accompanies the synthesis of the widely utilized starting material $\text{TpRu}(\text{PPh}_3)_2\text{Cl}$ (Tp = hydridotris(pyrazolyl)borate) has been identified as the complex ${}^{\text{Cl}}\text{TpRu}(\text{PPh}_3)_2\text{H}$ (${}^{\text{Cl}}\text{Tp}$ = chlorotris(pyrazolyl)borate), which provides a rare example of a boron-halogenated pyrazolylborate ligand. The reaction of ${}^{\text{Cl}}\text{TpRu}(\text{PPh}_3)_2\text{H}$ with dichloromethane or chloroform quantitatively produce ${}^{\text{Cl}}\text{TpRu}(\text{PPh}_3)_2\text{Cl}$.

Introduction

Since the first report of the Tp (Tp = hydridotris(pyrazolyl)borate) ligand in 1967 by Trofimenko,¹ poly(pyrazolyl)borates have been widely incorporated into inorganic and organometallic complexes.^{2–6} The early perception that the Tp ligand was simply a cyclopentadienyl mimic was soon replaced by the realization that the Tp scaffold offers substantial flexibility, and a wide array of Tp derivatives have been produced with significant attention focused on the introduction of functional groups on the pyrazolyl moieties. Modification of the substituents on boron has received comparatively little attention, in part due to its remote location from the usual point of interest, the metal center.

The complex $\text{TpRu}(\text{PPh}_3)_2\text{Cl}$ has proven to be a valuable starting material and entry point to ruthenium tris(pyrazolyl)borate chemistry.^{5,7–11} Although the published synthesis of this

key intermediate is generally reliable,¹² herein we report that it is typically attended by the formation of a minor and readily separable side-product, ${}^{\text{Cl}}\text{TpRu}(\text{PPh}_3)_2\text{H}$ (**1**) (${}^{\text{Cl}}\text{Tp}$ = chlorotris(pyrazolyl)borate). Although boron-chlorination has been observed within poly(methimazolyl)borate chemistry,^{13–15} to our knowledge, complex **1** is only the second example of a cleanly isolated and fully characterized pyrazolyl-borate complex with a Cl–B bond. The previous example of such a system was only recently reported by Slugovc et al.¹⁶ In addition, on the basis of an X-ray diffraction study and elemental analysis, Harman et al. have reported the generation of an approximate 1:1 mixture of TpMo and ${}^{\text{Cl}}\text{TpMo}$ complexes from the reaction of MoCl_5 , KTp, and nitric oxide.¹⁷ Given (i) the persistent concern that trace impurities can obscure the true nature of catalytic processes, thereby complicating their informed development, (ii) the generally reactive nature of metal hydride complexes, and (iii) the widespread use and synthetic versatility and utility of $\text{TpRu}(\text{PPh}_3)_2\text{Cl}$, disclosure of the formation and characterization of this impurity seemed important as a caveat for the use of $\text{TpRu}(\text{PPh}_3)_2\text{Cl}$ as a synthon.

Results and Discussion

The complex $\text{TpRu}(\text{PPh}_3)_2\text{Cl}$ is synthesized at room temperature upon reaction of KTp with $\text{RuCl}_2(\text{PPh}_3)_3$ in dichloromethane.¹² Upon standard precipitation of $\text{TpRu}(\text{PPh}_3)_2\text{Cl}$ with ethanol, the filtrate is typically discarded. However, solvent removal and recrystallization of the filtrate residue from dichloromethane and hexanes provides ${}^{\text{Cl}}\text{TpRu}(\text{PPh}_3)_2\text{H}$ (**1**) in 4% isolated yield. An X-ray diffraction study of **1** afforded the molecular structure (Table 1 and Figure 1). The hydride atom position was obtained from a difference map and was allowed to refine isotropically, giving a Ru–H distance of 1.52(2) Å, an unremarkable metric for a neutral octahedral ruthenium(II) hydride complex.¹⁸ The Ru–P1 and Ru–P2 distances of

* Corresponding author. E-mail: tbg7h@virginia.edu.

[†] University of Virginia.

[#] Australian National University.

[§] North Carolina State University.

(1) Trofimenko, S. *J. Am. Chem. Soc.* **1967**, *89*, 3170–3177.

(2) Trofimenko, S. *Scorpionates: The Coordination Chemistry of Poly(pyrazolyl)borate Ligands*; Imperial College Press: London, 1999.

(3) Lail, M.; Pittard, K. A.; Gunnoe, T. B. *Adv. Organomet. Chem.* **2008**, *56*, 95–153.

(4) Caldwell, L. M. Alkylidyne Complexes Ligated by Poly(pyrazolyl)borates. In *Advances in Organometallic Chemistry*; Academic Press: New York, 2008; Vol. 56, pp 1–94.

(5) Becker, E.; Pavlik, S.; Kirchner, K. *Adv. Organomet. Chem.* **2008**, *56*, 155–197.

(6) Crossley, I. R. *Adv. Organomet. Chem.* **2008**, *56*, 199–321.

(7) Pavlik, S.; Puchberger, M.; Mereiter, K.; Kirchner, K. *Eur. J. Inorg. Chem.* **2006**, *413*, 7–4142.

(8) Buriez, B.; Burns, I. D.; Hill, A. F.; White, A. J. P.; Williams, D. J.; Wilton-Ely, J. D. E. *Organometallics* **1999**, *18*, 1504–1516.

(9) Lo, Y.-H.; Lin, Y.-C.; Lee, G.-H.; Wang, Y. *Organometallics* **1999**, *18*, 982–988.

(10) Mizobe, Y.; Hosomizu, M.; Hidai, M. *Inorg. Chim. Acta* **1998**, *273*, 238–243.

(11) Slugovc, C.; Sapunov, V. N.; Wiede, P.; Mereiter, K.; Schmid, R.; Kirchner, K. *J. Chem. Soc., Dalton Trans.* **1997**, *22*, 4209–4216.

(12) Alcock, N. W.; Burns, I. D.; Claire, K. S.; Hill, A. F. *Inorg. Chem.* **1992**, *31*, 2906–2908.

(13) Hill, A. F.; Smith, M. K. *Chem. Commun.* **2005**, 1920–1922.

(14) Melnick, J. G.; Parkin, G. *Dalton Trans.* **2006**, 4207–4210.

(15) Pang, K. L.; Tanski, J. M.; Parkin, G. *Chem. Commun.* **2008**, 1008–1010.

(16) Burtscher, D.; Perner, B.; Mereiter, K.; Slugovc, C. *J. Organomet. Chem.* **2006**, *691*, 5423–5430.

(17) Mocella, C. J.; Delafuente, D. A.; Keane, J. A.; Warner, G. R.; Friedman, L. A.; Sabat, M.; Harman, W. D. *Organometallics* **2004**, *23*, 3772–3779.

(18) Bruno, I. J.; Cole, J. C.; Edgington, P. R.; Kessler, M.; Macrae, C. F.; McCabe, P.; Pearson, J.; Taylor, R. *Acta Crystallogr.* **2002**, *B58*, 389–397.

Table 1. Selected Crystallographic Data for $^{101}\text{Ru}(\text{PPh}_3)_2\text{H}$ (**1**) and $^{101}\text{Ru}(\text{PPh}_3)_2\text{Cl}$ (**2**)

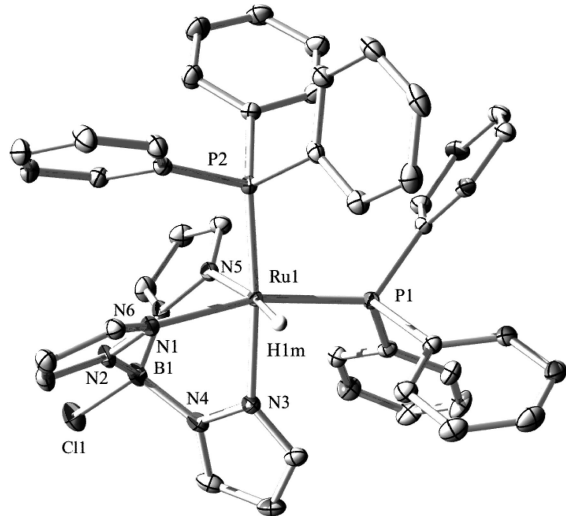
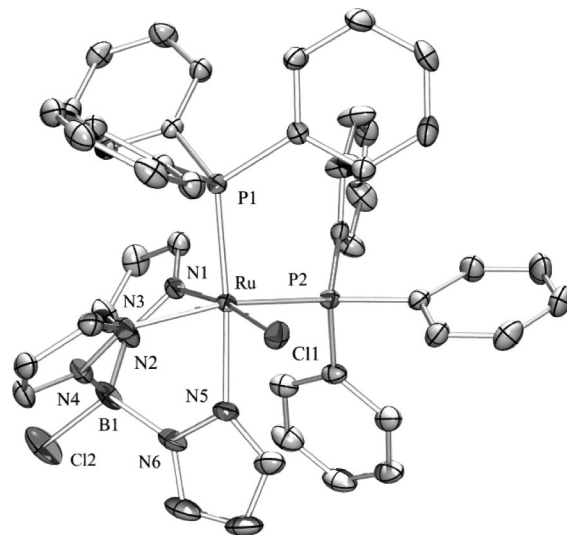
	complex 1	complex 2
empirical formula	$\text{C}_{45}\text{H}_{40}\text{BClN}_6\text{P}_2\text{Ru}$	$\text{C}_{45}\text{H}_{39}\text{BCl}_2\text{N}_6\text{P}_2\text{Ru}$
fw	874.12	908.54
cryst syst	monoclinic	monoclinic
space group	$P2_1/c$	$P2_1/n$
<i>a</i> , Å	17.6883(4)	10.2969(1)
<i>b</i> , Å	12.2903(3)	23.6386(2)
<i>c</i> , Å	18.8918(4)	16.8964(1)
β , deg	107.9956(8)	90.705(1)
<i>V</i> , Å ³	3906.1(1)	4112.35(6)
<i>Z</i>	4	4
<i>D</i> _{calcd} , g/cm ³	1.486	1.467
cryst size (mm)	0.30 × 0.22 × 0.16	0.35 × 0.27 × 0.12
R1, wR2 (<i>I</i> > 2(<i>I</i>))	0.038, 0.048	0.030, 0.068
GOF	1.37	1.05

Table 2. ¹¹B Chemical Shifts

complex	¹¹ B (δ)
$^{101}\text{Ru}(\text{PPh}_3)_2\text{H}$ (1)	1.31
$^{101}\text{Ru}(\text{PPh}_3)_2\text{Cl}$ (2)	1.13
$\text{TpRu}(\text{PPh}_3)_2\text{Cl}^{12}$	-3.67

2.2909(4) and 2.289(1) Å, respectively, are slightly shorter than those reported for the complex $\text{TpRu}(\text{PPh}_3)_2\text{Cl}$ (2.332(3) and 2.349(3) Å).¹² Notably, and perhaps counterintuitively, the BN₃ pyramid of **1** is marginally flattened (N–B–N angle sum = 328.1°) relative to the Tp ligand in $\text{TpRu}(\text{PPh}_3)_2\text{Cl}$ (N–B–N angle sum = 322.9°) despite the inclusion of the larger chloride substituent on boron. ³¹P{¹H} NMR spectroscopy reveals a significant downfield shift for the phosphorus resonance from 42.9 ppm to 67.1 ppm, which, when coupled with shorter Ru–P distances, is suggestive of increased P→Ru σ -donation. Consistent with the presence of a hydride ligand, the ¹H NMR spectrum of **1** clearly shows a triplet at -13.75 ppm with ²*J*_{PH} = 27 Hz, which is typical of a *fac*-RuHP₂ arrangement. ¹¹B NMR spectroscopy of complex **1** revealed a downfield chemical shift to 1.31 ppm relative to the reported resonance at -3.67 ppm for $\text{TpRu}(\text{PPh}_3)_2\text{Cl}$ (Table 2).¹²

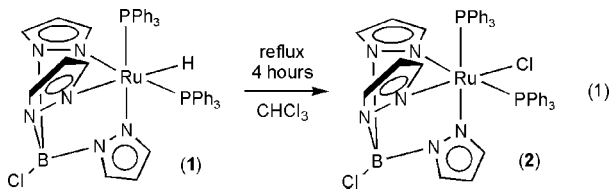
In refluxing chloroform, complex **1** converts to $^{101}\text{Ru}(\text{PPh}_3)_2\text{Cl}$ (**2**) over 4 h (eq 1), which can be isolated by

**Figure 1.** ORTEP of $^{101}\text{Ru}(\text{PPh}_3)_2\text{H}$ (**1**) (50% displacement ellipsoids, carbon-bound hydrogen atoms omitted). Selected bond lengths (Å): Ru1–H1m, 1.52(2); Ru1–P1, 2.2909(4); Ru1–P2, 2.289(1); Ru1–N1, 2.130(1); Ru1–N3, 2.171(1); Ru1–N5, 2.203(1); N2–B1, 1.543(2); N4–B1, 1.533(2); N6–B1, 1.534(2); B1–C11, 1.838(2). Selected bond angles (deg): N7–Ru1–C10, 87.1(1); N7–Ru1–P1, 94.38(7); C10–Ru1–P1, 93.40(8); P1–Ru1–P2, 98.32(1).**Figure 2.** ORTEP of $^{101}\text{Ru}(\text{PPh}_3)_2\text{Cl}$ (**2**) (50% displacement ellipsoids, carbon-bound hydrogen atoms omitted). Selected bond lengths (Å): Ru–Cl, 2.4115(5); Ru–P1, 2.3632(5); Ru–P2, 2.3721(5); Ru–N1, 2.100(2); Ru–N3, 2.143(2); Ru–N5, 2.112(2); N2–B1, 1.534(3); N4–B1, 1.533(3); N6–B1, 1.531(3); B1–C11, 1.841(3). Selected bond angles (deg): P2–Ru–C11, 98.78(2); N3–Ru–C11, 86.59(5); N5–Ru–C11, 85.20(5); P1–Ru–P2, 101.75(2); N6–B1–C12, 109.9(2).

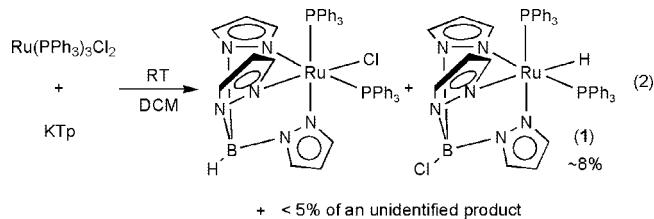
crystallization via slow evaporation. A solid-state X-ray diffraction study of a single crystal of complex **2** has confirmed its molecular structure (Table 1 and Figure 2). Interestingly, upon replacement of the hydride of **1** with Cl, the Ru–P bond distances lengthened to 2.3632(5) and 2.3721(5) Å, returning to bond distances similar to those of $\text{TpRu}(\text{PPh}_3)_2\text{Cl}$ (2.332(3) and 2.349(3) Å).¹² However, relative to $\text{TpRu}(\text{PPh}_3)_2\text{Cl}$, the BN₃ pyramid of **2** maintains a similar degree of flatness (N–B–N angle sum = 327.1°) also observed in complex **1**. ¹¹B NMR spectroscopy gave a singlet at 1.13 ppm for **2**, a minor change from the ¹¹B chemical shift of **1** (1.31 ppm). The ³¹P{¹H} NMR spectrum of **2** shows a singlet and a return of the phosphorus resonance from the more downfield position of **1** (67.1 ppm) to 41.7 ppm, a shift consistent with that of $\text{TpRu}(\text{PPh}_3)_2\text{Cl}$ (42.9 ppm), suggesting that the presence of the ¹⁰¹Tp ligand has little effect on the metal center's electronics relative to the parent Tp ligand. Rather, as would be expected, the spectroscopic and crystallographic data are more responsive to variations in the direct metal coordination sphere including replacement of Ru–H with Ru–Cl.

Heating complex **1** in CDCl₃ at 60 °C results in the quantitative formation of $^{101}\text{Ru}(\text{PPh}_3)_2\text{Cl}$ (**2**) along with the observation of CDHCl₂ (1:1:1 triplet at 5.29 ppm, ²*J*_{DH} = 1 Hz) and a small amount of CH₂Cl₂ (molar ratio of CDHCl₂ to CH₂Cl₂ is approximately 7.6:1). Efforts to independently synthesize **2** from $\text{TpRu}(\text{PPh}_3)_2\text{Cl}$ and *N*-chlorosuccinimide (NCS) failed, resulting in only an uncharacterized green material devoid of ³¹P NMR signals other than free PPh₃. Complex **2** can also be synthesized from **1** and dichloromethane, but this route requires extended heating (18 h) at 100 °C in a sealed pressure tube.

Complex **1** is isolated in low yield (always <5% isolated yield) from the reaction of RuCl₂(PPh₃)₃ and KTp. In order to determine the amount of **1** produced during the synthesis of $\text{TpRu}(\text{PPh}_3)_2\text{Cl}$, we monitored the conversion of KTp and RuCl₂(PPh₃)₃ by ¹H NMR spectroscopy over a 24 h period. The NMR spectrum of the product mixture reveals predominate



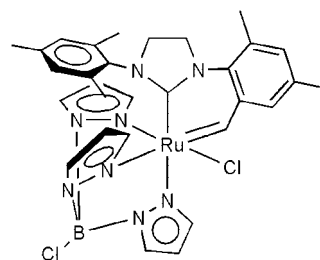
formation of $\text{TpRu}(\text{PPh}_3)_2\text{Cl}$, the formation of $\text{TpRu}(\text{PPh}_3)_2\text{H}$ (**1**) in approximately 8% yield (eq 2), and another unidentified complex in low yield ($\sim 5\%$). The latter complex is not $\text{TpRu}(\text{PPh}_3)_2\text{Cl}$ (**2**).



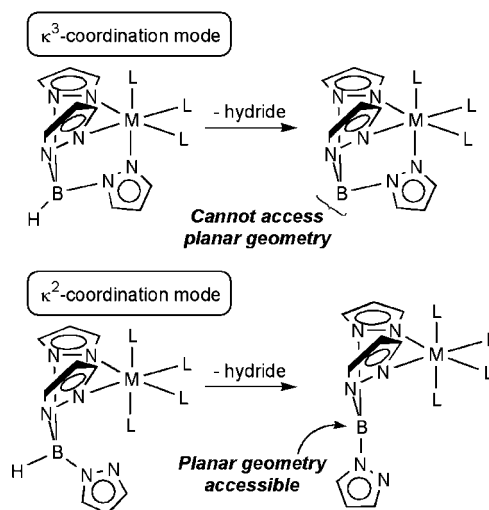
We performed experiments in an effort to determine whether complex **1** forms from $\text{TpRu}(\text{PPh}_3)_2\text{Cl}$ or from a competitive side reaction en route to formation of $\text{TpRu}(\text{PPh}_3)_2\text{Cl}$. Stirring spectroscopically pure $\text{TpRu}(\text{PPh}_3)_2\text{Cl}$ in dichloromethane and one additional equivalent of KTp for 24 h at room temperature (the conditions for the synthesis of complex **1**) does not result in the production of detectable quantities (^1H , ^{31}P NMR) of either complex **1** or **2**. However, after 24 h disappearance of several new pyrazolyl resonances are observed by ^1H NMR spectroscopy, none of which correspond to the known complex Tp_2Ru .¹⁹ Heating $\text{TpRu}(\text{PPh}_3)_2\text{Cl}$ in dichloromethane at 80°C for 24 h results in no observable change by ^1H NMR spectroscopy. We may therefore exclude the possibility that $\text{TpRu}(\text{PPh}_3)_2\text{Cl}$ is a spontaneous precursor to **1**. To explore the possibility of an acid-mediated reaction (e.g., residual HCl from the preparation of $\text{RuCl}_2(\text{PPh}_3)_3$), $\text{TpRu}(\text{PPh}_3)_2\text{Cl}$ was heated in CDCl_3 at 60°C for 30 h in the presence of 1 equiv of HCl , which did not yield detectable quantities of either **1** or **2**. Thus, consistent with the proposal from the Slugovc group that the formation of chloro(κ^3 - (N,N,N) -chlorotris(pyrazolyl)borate)(κ^2 - (C,C) -1-(2,4,6-trimethylphenyl)-3-(4,6-dimethylphenyl-2-methylidene)-4,5-dihydroimidazol-2-ylidene)ruthenium (**3**) likely proceeds via a $\text{Ru}-\text{Cl}/\text{B}-\text{H}$ metathesis prior to κ^3 -coordination of Tp (see below),¹⁶ it seems most likely that the formation of **1** is the result of a side reaction during the formation of $\text{TpRu}(\text{PPh}_3)_2\text{Cl}$ before the TpRu cage becomes fully closed and chemically robust.

To our knowledge, complex **3** is the only other pyrazolylborate complex bearing a $\text{Cl}-\text{B}$ bond that has been fully characterized (Chart 1).¹⁶ Complex **3** was isolated in 13% yield as a byproduct from the reaction of a $\text{Ru}(\text{II})$ dichloride precursor with KTp , which resulted in a mixture of compounds by ^1H NMR spectroscopy. A comparison of the structures of **1** and **3** reveals, within precision limits, identical $\text{B}-\text{Cl}$ bond lengths {1.839(2) Å for **3** and 1.838(2) Å for **1**} and similar $\text{Tp Ru}-\text{N}$ bond distances {average $\text{Ru}-\text{N}$ bond distance is 2.176(2) Å for **3** and 2.168(1) Å for **1**}. In addition to structural similarities, the formation of **1** may occur by a pathway similar to **3**. The formation of **3** has been proposed to occur by $\text{B}-\text{H}/\text{Cl}$ bond metathesis via κ^2 - $\text{N},\text{B}-\text{H}$ coordination, followed by hydride

Chart 1. Chloro(κ^3 - (N,N,N) -chlorotris(pyrazolyl)borate)(κ^2 - (C,C) -1-(2,4,6-trimethylphenyl)-3-(4,6-dimethylphenyl-2-methylidene)-4,5-dihydroimidazol-2-ylidene)ruthenium (**3**)



Scheme 1. κ^3 -Coordination of Tp Ligand Inhibits Hydride Transfer Relative to κ^2 - or κ^1 -Coordinated Variants



transfer to Ru and subsequent $\text{B}-\text{Cl}$ bond formation. In a κ^1 - or κ^2 -coordination mode, the Tp ligand is more likely to transfer a hydride equivalent since the resulting trisubstituted boron can access a planar geometry, which is inaccessible for κ^3 -coordinated Tp ligands (Scheme 1). For the formation of **3**, ruthenium-hydride intermediates are suggested to form but were not observed. In the geometrically more agile poly(methimazolyl)borate class of chelates, such $\text{B}-\text{H}$ activation processes are implicit in the formation of metallaboratranes including cases where migration of the hydrogen between boron and the metal center has been shown to be reversible (Scheme 2).^{20–23} Furthermore, the reaction of $[\text{Fe}(\text{CO})_2\{\text{B}(\text{mt}^{\text{Bu}})_3\}]$ ($\text{mt}^{\text{Bu}} = N$ -tert-butylmercaptoimidazolyl) with chlorinated solvents has been shown to provide the B -chlorotris(mercaptoimidazolyl)borate complex $[\text{FeCl}\{\text{CIB}(\text{mt}^{\text{Bu}})_3\}]$ with attendant rupture of the $\text{Fe}\rightarrow\text{B}$ dative bond.²⁴ To invoke such processes within poly(pyrazolyl)borate systems would clearly involve greater, but perhaps not insurmountable, geometric strain.

Conclusions

The complex $\text{TpRu}(\text{PPh}_3)_2\text{Cl}$ is a catalyst for the transformation of terminal alkynes to nitriles²⁵ and is a well-known and

(20) Hill, A. F.; Owen, G. R.; White, A. J. P.; Williams, D. J. *Angew. Chem., Int. Ed.* **1999**, *38*, 2759–2761.

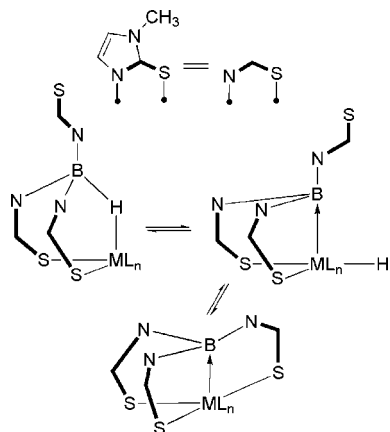
(21) Crossley, I. R.; Hill, A. F. *Dalton Trans.* **2008**, 201–203.

(22) Hill, A. F. *Organometallics* **2006**, *25*, 4741–4743.

(23) Foreman, M. R. S. J.; Hill, A. F.; Owen, G. R.; White, A. J. P.; Williams, D. J. *Organometallics* **2003**, *22*, 4446–4450.

(24) Figueroa, J. S.; Melnick, J. G.; Parkin, G. *Inorg. Chem.* **2006**, *45*, 7056–7058.

(19) Jalon, F. A.; Otero, A.; Rodriguez, A. J. *Chem. Soc., Dalton Trans.* **1995**, 1629–1633.

Scheme 2. Metallaboratrane Formation via B–H Activation^{20–23}


frequently used precursor to a variety of other complexes.^{5,7–11} Using published procedures, the complex ^{Cl}TpRu(PPh₃)₂H (**1**) is reproducibly formed in low yield during the synthesis of TpRu(PPh₃)₂Cl. The mechanism by which **1** forms is currently unknown; however, experimental data suggest it occurs as a side reaction from an intermediate during the formation of TpRu(PPh₃)₂Cl likely prior to κ³-Tp cage closure. Considering the known reactivity of metal hydrides, the possible presence of **1** in samples of TpRu(PPh₃)₂Cl should be borne in mind given its wide use. For example, the purification of TpRu(PPh₃)₂Cl via precipitation using ethanol is vital, and since **1** is more soluble than TpRu(PPh₃)₂Cl and typically remains in the filtrate after isolation of TpRu(PPh₃)₂Cl, it would be imprudent to overharvest the liquor during precipitation/crystallization sequences. It should perhaps be noted that, when characterizing Tp complexes, it is rare for ¹¹B NMR spectra to be measured,²⁶ and the typical broadness of the ¹H resonance for the BH group often results in it not being identified or reported. It is therefore possible that unrecognized ^{Cl}Tp complexes might be more widespread than previously considered, especially when reacting KTp {and related tris(pyrazolyl)borates} with metal halides and the products are only characterized by ¹H NMR spectroscopy and/or mass spectrometry. For example, note that the elemental analysis and mass spectrometry data for **1** would not differentiate it from TpRu(PPh₃)₂Cl. Thus, the routine use of X-ray crystallography for reactions between pyrazolyl-borate salts and substrates with metal–halide bonds may be prudent.

Experimental Section

General Methods. Unless otherwise noted, all synthetic procedures were performed under anaerobic conditions in a nitrogen-filled glovebox or by using standard Schlenk techniques. Glovebox purity was maintained by periodic nitrogen purges and was monitored by an oxygen analyzer (O₂(g) < 15 ppm for all reactions). Tetrahydrofuran (stored over 4 Å molecular sieves) was dried by distillation from sodium/benzophenone. Hexanes (stored over 4 Å molecular sieves) and methylene chloride were purified by passage through a column of activated alumina and degassed prior to use. Chloroform-*d*₁ and benzene-*d*₆ were degassed with three freeze–pump–thaw cycles and stored under a N₂ atmosphere over 4 Å molecular sieves.

(25) Fukumoto, Y.; Dohi, T.; Masaoka, H.; Chatani, N.; Murai, S. *Organometallics* **2002**, *21*, 3845–3847.

(26) Northcutt, T. O.; Lachicotte, R. J.; Jones, W. D. *Organometallics* **1998**, *17*, 5148–5152.

¹H NMR spectra were recorded on a Varian Mercury 300 or 400 MHz spectrometer and ¹³C NMR (operating frequency 75 MHz) spectra on a Varian Mercury 300 MHz spectrometer. All ¹H and ¹³C(¹H) NMR spectra are referenced against residual proton signals (¹H NMR) or the ¹³C resonances of the deuterated solvent (¹³C NMR). ³¹P and ¹¹B NMR spectra were obtained on a Varian 400 MHz spectrometer and referenced against an external standard of H₃PO₄ (δ = 0) and BF₃·Et₂O (δ = 0), respectively. Resonances due to the Tp ligand in ¹H NMR spectra are listed by chemical shift and multiplicity only (all coupling constants for the Tp ligand are ~2 Hz). IR spectra were acquired using a Mattson Genesis II FT-IR as thin films on NaCl. The preparation, isolation, and characterization of RuCl₂(PPh₃)₃¹ and TpRu(PPh₃)₂Cl¹² have been previously reported. All other reagents were used as purchased from commercial sources. Elemental analyses were performed by Atlantic Microlabs, Inc.

^{Cl}TpRu(PPh₃)₂H (1). The previously reported synthetic procedure for TpRu(PPh₃)₂Cl (12.6 g, 0.013 mol) was followed.¹² Following the collection of TpRu(PPh₃)₂Cl via vacuum filtration, slow evaporation from the dichloromethane/hexanes filtrate (under an atmosphere of dinitrogen) results in the formation of dark yellow crystals. The solid crystalline material was collected after 3 days and dried in vacuo (0.377 g, 4.2%). The filtrate was evaporated to dryness, and analysis by ¹H NMR spectroscopy revealed only residual amounts of complex **1**. IR (NaCl): ν_{Ru–H} = 1959 cm⁻¹. ¹H NMR (CDCl₃, δ): 8.19, 7.85, 6.85, 6.48 (6H total, 1:2:2:1 integration, each a d, Tp 3 or 5 positions), 7.16, 7.00 (30H total, each a broad multiplet, 2 PPh₃), 5.83, 5.20 (3H total, 1:2 integration, each a t, Tp 4 position), -13.75 (1H, t, ²J_{PH} = 27 Hz). ¹³C(¹H) NMR (CDCl₃, δ): 147.7, 146.1 (Tp 3 and 5 positions), 138.6 (vt, J_{CP} = 12.8 Hz, ipso PPh₃), 134.0 (t, J_{CP} = 4.7 Hz, PPh₃), 128.4 (s, PPh₃), 127.5 (t, J_{CP} = 4.7 Hz, PPh₃), 104.6, 104.4 (Tp 4 positions) (NOTE: one set of Tp 3 or 5 position carbons could not be located in the ¹³C NMR potentially due to coincidental overlap). ³¹P(¹H) NMR (CDCl₃, δ): 67.1 (PPh₃). ¹¹B NMR (CDCl₃, δ): 1.31 {ClB(C₃N₂H₃)₃}. Anal. Calcd for C₄₅H₄₀BN₆P₂ClRu: C, 61.83; H, 4.61; N, 9.61. Found: C, 61.54; H, 4.68; N, 9.58.

^{Cl}TpRu(PPh₃)₂Cl (2). ^{Cl}TpRu(PPh₃)₂H (**1**) (0.064 g, 0.073 mmol) was heated to reflux in CHCl₃ (~8 mL). After 4 h the solution volume was reduced to approximately 1 mL and passed through a 1 in. plug of silica with a 1:1 mixture of THF/hexanes. The resultant yellow band was collected and dried to a solid in vacuo (0.040 g, 60%). Alternatively, this reaction can be performed by heating **1** in dichloromethane in a sealed pressure tube at 100 °C for 18 h with approximately the same isolated yield. ¹H NMR (CDCl₃, δ): 8.04, 7.92, 7.34, 6.95 (6H total, 1:2:1:2 integration, each d, Tp 3 or 5 position), 7.18, 7.04 (30H total, each a broad multiplet, 2 PPh₃), 5.69 (2H, m, Tp 4 position), 5.19 (1H, t, Tp 4 position). ¹³C(¹H) NMR (CDCl₃, δ): 150.1, 146.7 (Tp 3 and 5 positions), 135.2 (vt, J_{CP} = 17.6 Hz, ipso PPh₃), 134.9, 134.8 (Tp 3 and 5 positions), 134.0 (t, J_{CP} = 4.5 Hz, PPh₃), 129.0 (s, PPh₃), 127.5 (t, J_{CP} = 4.4 Hz, PPh₃), 105.2, 104.9 (Tp 4 positions). ³¹P(¹H) NMR (CDCl₃, δ): 41.7 (PPh₃). ¹¹B NMR (CDCl₃, δ): 1.13 {ClB(C₃N₂H₃)₃}. Anal. Calcd for C₄₅H₃₉BN₆P₂Cl₂Ru: C, 59.49; H, 4.33; N, 9.25. Found: C, 59.55; H, 4.47; N, 9.14.

Supporting Information Available: Complete tables of crystal data, collection and refinement data, atomic coordinates, bond distances and angles, anisotropic displacement coefficients for X-ray structures of complexes **1** and **2**, and ¹H NMR spectra of **1** and **2**. This material is available free of charge via the Internet at <http://pubs.acs.org>.

Synthesis and Reactivity of Three New N-Heterocyclic Silylenes

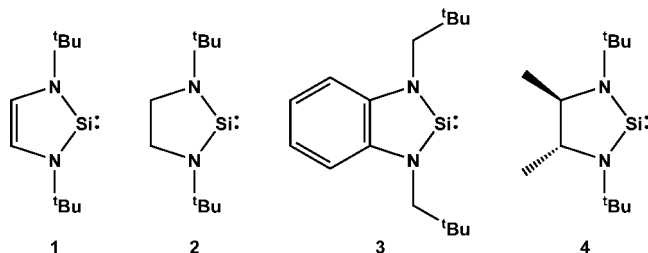
Adam C. Tomasik, Amitabha Mitra, and Robert West*

Organosilicon Research Center, Department of Chemistry, University of Wisconsin–Madison,
1101 University Avenue, Madison, Wisconsin 53706

Received June 30, 2008

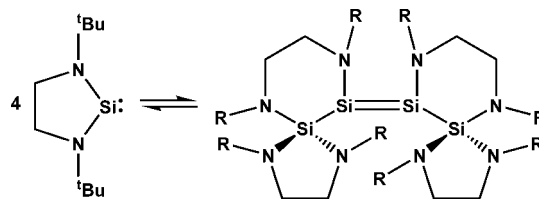
Summary: Three new stable silylenes, *rac*-1,3,4-tri-*tert*-butyl-1,3-diaza-2-silacyclopentane-2-ylide (**5**), 1,3-di-*tert*-butyl-4,4-dimethyl-1,3-diaza-2-silacyclopentane-2-ylide (**6**), and *rac*-1,3-di-*tert*-butyl-4-methyl-1,3-diaza-2-silacyclopentane-2-ylide (**7**), have been synthesized by the reaction of their corresponding dibromides with KC_8 . Unlike the analogous silylene **2**, which lacks any backbone substitution and tetramerizes in concentrated solution or as a solid, silylenes **5**, **6**, and **7** show no tendency to oligomerize. The reactions of **5** with *tert*-butanol and chloroalkanes give only 1:1 O–H or C–Cl insertion products; with adamantyl azide **5** yields the spiro-silatetrazoline **8**, while with mesityl azide it gives the azadisilacyclopropane **9**.

Silylenes, divalent, dicoordinate silicon species, have long been known to be key intermediates in numerous thermal and photochemical reactions.¹ Until relatively recently, however, silylenes have been observable only at low temperatures. The N-heterocyclic silylenes **1–3**, silicon analogues of the Arduengo N-heterocyclic carbenes,^{2–5} were first reported during the mid-1990s along with a few other examples.^{6,7} These molecules are stable at room temperature under anaerobic conditions and benefit from both electronic stabilization by the amino groups and steric protection by the bulky alkyl groups. Silylene **2**, however, is stable only in dilute solution.



In the pure solid state or in a concentrated solution, **2** reversibly tetramerizes into a diaminodisilyldisilene (a dark red solid) (Chart 1).^{4,5} Recently, silylene **4** was added to the group

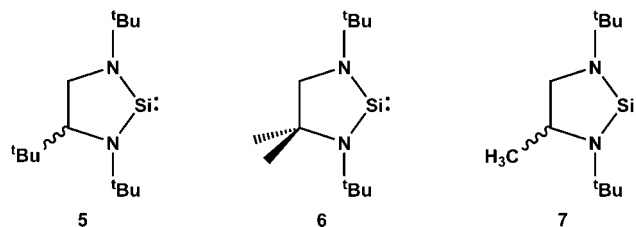
Chart 1. Tetramerization of **2** (R = *t*Bu)



of known thermally stable silylenes; it shows no tendency to undergo oligomerization.⁸

Several studies have examined the behavior of silylenes **1** and **2** toward a wide range of organic, inorganic, and organometallic substrates.^{1,9} Among these, reactions with organic azides, alcohols, and alkyl halides have been reported. The reactions of **2** with PhN_3 , *p*- $tolN_3$, Ph_3CN_3 , and Ph_3SiN_3 all yield the silatetrazolines **A–D** (Figure 1).¹⁰ The reaction of **1** with adamantyl azide (AdN_3) gives a similar product, **E**, while the reaction of silylene **3** with AdN_3 produces the azadisilacyclopropane **F**, although the latter species was not crystallographically authenticated.¹¹ Typically, silylenes will react with alcohols and alkyl halides via oxidative addition. For silylenes **1** and **2** most alcohols give a 1:1 adduct, while reactions with alkyl halides can give either the 1:1 adduct or the 1:2 disilane radical adduct depending on the substrate (Scheme 1).^{12,13}

We herein report the synthesis of three new saturated N-heterocyclic silylenes, **5** (as a racemic mixture), **6**, and **7** (racemic), and the reactions of **5** toward a variety of substrates. The silylenes were characterized by 1H , ^{13}C , and ^{29}Si NMR, high-resolution mass spectrometry, and (for **5** and **7**) elemental analysis. The ^{29}Si resonance of **5** in C_6D_6 falls at $\delta +140.6$ ppm, slightly more deshielded than the resonances of **2** ($\delta +119$ ppm) and **4** ($\delta +123.4$ ppm). The UV–vis spectrum of **5** in *n*-heptane (ca. 2.6×10^{-4} M) shows a band maximum at 279 nm ($\epsilon = 1700$ M $^{-1}$ cm $^{-1}$) and shoulders at 300 and 333 nm. Silylene **2** has similar band maxima at 268 and 292 nm, while silylene **4** shows maxima at 270 and 295 nm.



Silylene **6**, substituted with two methyl groups on the same backbone carbon, is a pale yellow liquid that exists solely as the monomeric species. The ^{29}Si resonance for **6** in C_6D_6 falls

* To whom correspondence should be addressed. E-mail: west@chem.wisc.edu.

(1) Hill, N. J.; West, R. *J. Organomet. Chem.* **2004**, *689*, 4165–4183.
(2) Denk, M.; Lennon, R.; Hayashi, R.; West, R.; Belyakov, A. V.; Verne, H. P.; Haaland, A.; Wagner, M.; Metzler, N. *J. Am. Chem. Soc.* **1994**, *116*, 2691–2692.
(3) Gehrhuis, B.; Lappert, M. F.; Heinicke, J.; Boose, R.; Blaser, D. *J. Chem. Soc., Chem. Commun.* **1995**, 1931–1932.
(4) Haaf, M.; Schmedake, T. A.; Paradise, B. J.; West, R. *Can. J. Chem.* **2000**, *78*, 1526–1533.
(5) West, R.; Denk, M. *Pure Appl. Chem.* **1996**, *68*, 785–788.
(6) Heinicke, J.; Oprea, A.; Kindermann, M. K.; Karpati, T.; Nyulaszi, L.; Veszpremi, T. *Chem.–Eur. J.* **1998**, *4*, 541–545.
(7) Kira, M.; Ishida, S.; Iwamoto, T.; Kabuto, C. *J. Am. Chem. Soc.* **1999**, *121*, 9722–9723.

(8) Li, W.; Hill, N. J.; Tomasik, A. C.; Bikzhanova, G.; West, R. *Organometallics* **2006**, *25*, 3802–3805.

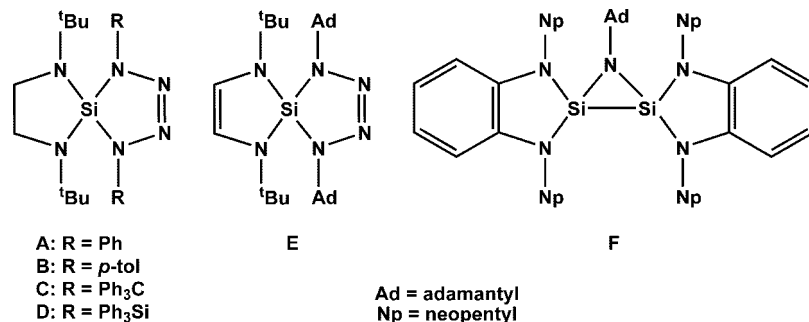
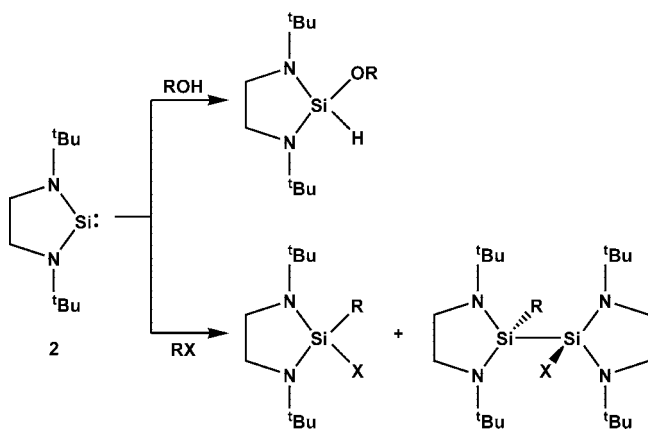


Figure 1. Products of silylenes **1**, **2**, and **3** with organic azides.

Scheme 1. Reactions of Silylene **2** with Alcohols and Alkyl Halides

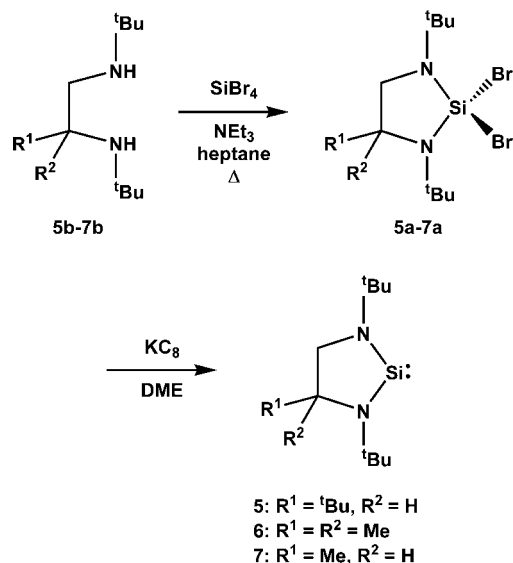


at $\delta +130.5$ ppm, in the same range as the resonances of **2**, **4**, and **5**. Silylene **7** has one methyl group in the backbone and can be viewed as the smallest structural perturbation of silylene **2**. It is a colorless liquid that exists exclusively as the monomeric species. The ²⁹Si NMR shift appears at 121.4 ppm, which is in between those of **2** and **4**. The observed trend in the ²⁹Si NMR shifts, **2** < **7** < **4** is what would be expected as the silylene structure becomes more deshielded upon the sequential addition of methyl groups.

The reason **4**, **5**, **6**, and **7** remain as monomers rather than tetramerizing like **2** is still under active investigation. The methyl or *tert*-butyl substituents on the ring carbon atoms contribute some steric effect, but inspection of models does not suggest that these groups should interfere with the oligomerization. Another possibility is that the alkyl substituent groups make the nitrogen atoms slightly better π -electron donors, stabilizing the monomeric silylenes. In either argument, it is clear that silylene **2** is a unique species.

Silylenes **5**, **6**, and **7** were prepared by the reduction of their corresponding dibromosilanes **5a**, **6a**, and **7a** with potassium graphite (KC₈) in dimethoxyethane (DME) at room temperature, as shown in Scheme 2.

Scheme 2. Synthesis of Silylenes **5**, **6**, and **7**



Diamines **5b**, **6b**, and **7b** were synthesized via methods derived from literature procedures.^{14–16} The diamines were converted to the dibromosilanes **5a**, **6a**, and **7a** by reaction with silicon tetrabromide in the presence of triethylamine.^{17,18} When

(15) Lai, J. T. *Tetrahedron Lett.* **1982**, 23, 595–598.

(16) D'Angeli, F.; Marchetti, P.; Cavicchioni, G.; Bertolasi, V.; Maran, F. *Tetrahedron: Asymmetry* **1991**, 2, 1111–1121.

(17) Synthesis of *rac*-2,2-dibromo-1,3,4-tri-*tert*-butyl-1,3,2-diazasilolidine (**5a**): A solution of the diamine (**5b**) (6.28 g, 27.5 mmol), triethylamine (12 mL), and heptane (125 mL) was stirred at 0 °C. SiBr₄ (11.0 g, 31.6 mmol) in 25 mL of heptane was added dropwise to the cooled solution. The reaction mixture was then fitted with a reflux condenser and refluxed for 2 d, after which it was cooled and filtered, and the solvent removed. The crude yellow oil was distilled in a Kugelrohr oven (110 °C, 1 Torr) to give a colorless oil. Yield: 8.60 g, 75.5%. ¹H NMR (C₆D₆): δ 1.00 (s, 9H); 1.28 (s, 9H); 1.33 (s, 9H); 2.77 (d, 1H, *J* = 5.8 Hz); 2.83 (d, 1H, *J* = 9.2); 2.89 (dd, 1H, *J* = 9.2, 5.8 Hz). ¹³C NMR (C₆D₆): δ 29.17; 30.07; 31.89; 36.48; 46.95; 53.33; 55.12; 62.64. ²⁹Si{¹H} NMR (C₆D₆): δ -50.06. High-resolution mass spectrometry: calcd for [C₁₄H₃₀N₂SiBr₂-CH₃]⁺ 397.0305, found 397.0310. Anal. Calcd for C₁₄H₃₀N₂SiBr₂: C, 40.59; H, 7.30; N, 6.76. Found: C, 40.38; H, 7.27; N, 6.67.

(18) 2,2-Dibromo-1,3-di-*tert*-butyl-4,4-dimethyl-1,3,2-diazasilolidine (**6a**): Yield: 8.29 g, 69%. ¹H NMR (C₆D₆): δ 1.17 (s, 6H); 1.28 (s, 9H); 1.44 (s, 9H); 2.56 (s, 2H). ¹³C NMR (C₆D₆): δ 29.42; 29.46; 33.62; 52.63; 54.85; 59.25; 60.14. ²⁹Si{¹H} NMR (C₆D₆): δ -60.96. High-resolution mass spectrometry: calcd for [C₁₂H₂₆N₂SiBr₂]⁺ 384.0227, found 384.0221. Anal. Calcd for C₁₂H₂₆N₂SiBr₂: C, 37.32; H, 6.78; N, 7.25. Found: C, 37.60; H, 6.55; N, 7.41. *rac*-2,2-Dibromo-1,3-di-*tert*-butyl-4-methyl-1,3,2-diazasilolidine (**7a**): Yield: 7.90 g, 76.5%. ¹H NMR (C₆D₆): δ 1.12 (d, 3H, *J* = 6.7 Hz); 1.26 (s, 9H); 1.27 (s, 9H); 2.29 (d, 1H, *J* = 8.6 Hz); 2.98 (dd, 1H, *J* = 8.3, 5.8 Hz); 3.03 (dq, 1H, *J* = 11.8, 6.0 Hz). ¹³C NMR (C₆D₆): δ 23.93; 29.57; 31.18; 50.19; 51.27; 52.58; 53.58. ²⁹Si{¹H} NMR (C₆D₆): δ -60.64. High-resolution mass spectrometry: calcd for [C₁₁H₂₄N₂SiBr₂]⁺ 370.0070, found 370.0065. Anal. Calcd for C₁₁H₂₄N₂SiBr₂: C, 35.49; H, 6.50; N, 7.53. Found: C, 35.34; H, 6.58; N, 7.70.

(9) Haaf, M.; Schmedake, T. A.; West, R. *Acc. Chem. Res.* **2000**, 33, 704–714.

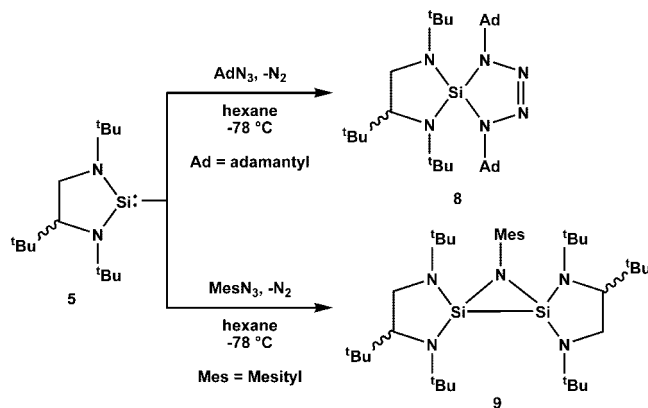
(10) Hill, N. J.; Moser, D. F.; Guzei, I. A.; West, R. *Organometallics* **2005**, 24, 3346–3349.

(11) Gehrhus, B.; Hitchcock, P. B.; Lappert, M. F. *Z. Anorg. Allg. Chem.* **2001**, 627, 1048.

(12) Moser, D. F.; Bosse, T.; Olson, J.; Moser, J. L.; Guzei, I. A.; West, R. *J. Am. Chem. Soc.* **2002**, 124, 4186–4187.

(13) Moser, D. F.; Naka, A.; Guzei, I. A.; Müller, T.; West, R. *J. Am. Chem. Soc.* **2005**, 127, 14730–14738.

(14) Gardiner, M. G.; Lawrence, S. M.; Raston, C. L. *Inorg. Chem.* **1996**, 35, 1349–1354.

Scheme 3. Reaction of **5** with AdN_3 and MesN_3 

the dibromosilanes were reduced with KC_8 in dimethoxyethane, the silylenes **5**, **6**, and **7** were obtained.^{19,20} The silylenes were purified by careful distillation at reduced pressure.

Silylene **5** shows reactivity similar to that of silylenes **1**–**4**. Treatment of 2 equiv of adamantyl azide with **5** in hexane at -78°C was accompanied by the evolution of N_2 and yielded the white solid **8**. A similar reaction between 2 equiv of **5** and 1 equiv of mesityl azide gives the azadisilacyclopropane derivative **9** quantitatively by NMR (Scheme 3). Formation of **8** and **9** is accompanied by a large upfield shift in the ^{29}Si NMR spectrum relative to the free silylene, from $\delta +140$ ppm for **5** to ca. $\delta -52$ ppm for **8** and $\delta -33$ ppm for **9**.

Single-crystal X-ray diffraction studies confirmed **8** to be a spirocyclic silatetrazoline, consisting of a central silicon atom coordinated to four separate nitrogen atoms (Figure 2). The SiN_4 core is comprised of two planar, orthogonal rings fused at the central silicon atom. The azadisilacyclopropane product **9** (Figure 3) provided the first crystallographic evidence for a compound of its type. The two silylene units in **9** are of the same enantiomer (the *R*-silylene), possibly indicating spontaneous resolution of the racemic mixture of **5**, although inspection of models does not indicate a strong steric reason for this preference. In addition, the ^1H NMR of the mother liquor does not show the detectable presence of the “*meso*” isomer.²¹

(19) Synthesis of *rac*-1,3,4-tri-*tert*-butyl-1,3-diaza-2-silacyclopentane-2-ylide (**5**): In a 250 mL Schlenk flask was placed potassium graphite (8.41 g, 62.3 mmol). To this flask was added 150 mL of DME. Then, *rac*-2,2-dibromo-1,3,4-tri-*tert*-butyl-1,3,2-diazasilolidine (**5a**) (8.60 g, 20.76 mmol) dissolved in 50 mL of DME was added dropwise. The reaction was monitored by ^1H NMR until all the starting material disappeared (~ 3 h). The reaction mixture was filtered and the solvent removed, resulting in a pale yellow oil. The yellow oil was vacuum distilled (95°C , 1 Torr) to give a very pale yellow liquid. Yield: 2.78 g, 52.7%. ^1H NMR (C_6D_6): δ 0.90 (s, 9H); 1.27 (s, 9H); 1.38 (s, 9H); 3.00 (d, 1H, $J = 10.5$ Hz); 3.14 (d, 1H, $J = 7.2$ Hz); 3.22 (dd, 1H, $J = 10.5, 7.2$ Hz). ^{13}C NMR (C_6D_6): δ 29.04; 32.01; 35.21; 35.48; 49.74; 53.54; 54.99; 67.12. $^{29}\text{Si}\{^1\text{H}\}$ NMR (C_6D_6): $\delta +140.59$. High-resolution mass spectrometry: calcd for $[\text{C}_{14}\text{H}_{30}\text{N}_2\text{Si}]^+$ 254.2173, found 254.2170. Anal. Calcd for $\text{C}_{14}\text{H}_{30}\text{N}_2\text{Si}$: C, 66.07; H, 11.88; N, 11.01. Found: C, 66.12; H, 12.09; N, 10.80.

(20) 1,3-Di-*tert*-butyl-4,4-dimethyl-1,3-diaza-2-silacyclopentane-2-ylide (**6**): Yield: 3.05 g, 62.8%. ^1H NMR (C_6D_6): δ 1.26 (s, 9H); 1.27 (s, 6H); 1.43 (s, 9H); 2.96 (s, 2H). ^{13}C NMR (C_6D_6): δ 30.77; 31.69; 36.35; 52.56; 55.09; 63.10; 65.09. $^{29}\text{Si}\{^1\text{H}\}$ NMR (C_6D_6): $\delta +130.47$. High-resolution mass spectrometry: calcd for $[\text{C}_{12}\text{H}_{26}\text{N}_2\text{Si}]^+$ 226.1860, found 226.1860. *rac*-1,3-Di-*tert*-butyl-4-methyl-1,3-diaza-2-silacyclopentane-2-ylide (**7**): Yield: 1.93 g, 52.0%. ^1H NMR (C_6D_6): δ 1.10 (d, 3H, $J = 6.8$ Hz); 1.26 (s, 9H); 1.31 (s, 9H); 2.63 (d, 1H, $J = 8.9$ Hz); 3.34–3.44 (m, 2H). ^{13}C NMR (C_6D_6): δ 26.16; 31.93; 34.14; 52.68; 53.55; 53.95; 55.43. $^{29}\text{Si}\{^1\text{H}\}$ NMR (C_6D_6): $\delta +121.43$. High-resolution mass spectrometry: calcd for $[\text{C}_{11}\text{H}_{24}\text{N}_2\text{Si}]^+$ 212.1704, found 212.1697. Anal. Calcd for $\text{C}_{11}\text{H}_{24}\text{N}_2\text{Si}$: C, 62.20; H, 11.39; N, 13.19. Found: C, 62.11; H, 11.54; N, 13.47.

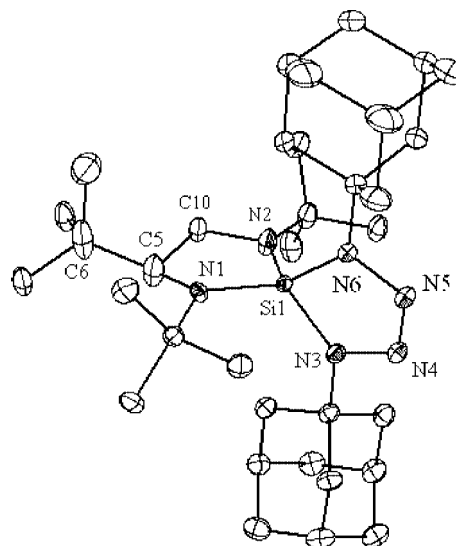


Figure 2. Thermal ellipsoid (40%) plot of **8** with H atoms omitted for clarity. Selected bond distances (\AA): Si–N(1) 1.7288(15), Si–N(2) 1.6934(17), Si–N(3) 1.7380(15), Si–N(6) 1.7384(16), N(3)–N(4) 1.383(2), N(4)–N(5) 1.267(2), N(5)–N(6) 1.383(2). Selected bond angles (deg): N(1)–Si–N(2) 96.59(8), N(3)–Si–N(6) 85.99(7). Selected torsion angles (deg): N(1)–C(5)–C(10)–N(2) 20.9(2). Planarity of C(5) (sum of angles) (deg): 343.34.

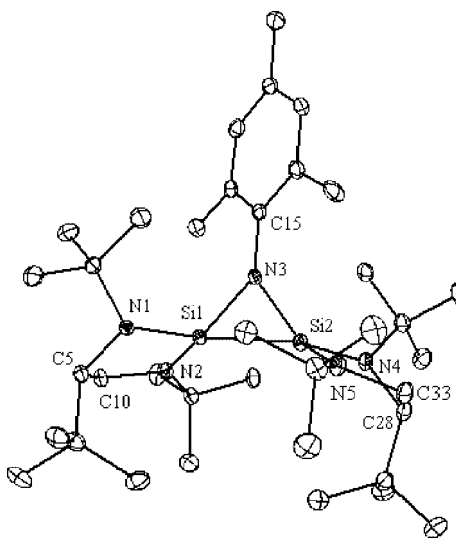


Figure 3. Thermal ellipsoid (40%) plot of **9** with H atoms omitted for clarity. Selected bond distances (\AA): Si(1)–Si(2) 2.2286(6), Si(1)–N(3) 1.7757(12), Si(2)–N(3) 1.7913(12). Selected bond angles (deg): N(3)–Si(1)–Si(2) 51.65(4), N(3)–Si(2)–Si(1) 51.02(4), Si(1)–N(3)–Si(2) 77.33(5). Selected dihedral angles (deg): N(1)–Si(1)–Si(2)–N(5) 24.79(9), N(2)–Si(1)–Si(2)–N(4) 19.86(9).

The Si–N_(silylene) bond distances in **8** are slightly longer than in the structural analogue **2** (Si–N 1.719(3) vs Si–N(1) 1.7288(15), Si–N(2) 1.6934(17) \AA , respectively),¹⁰ while the Si–N(azo) distances are very similar to each other (Si–N(3) 1.7380(15) and Si–N(6) 1.7384(16) \AA). The $\text{C}_2\text{N}_2\text{Si}$ ring

(21) Compound **9** has four stereogenic centers, which lead to 16 possible enantiomers (six are duplicates). Of the 10 stereographically unique possibilities, seven of them are sterically infeasible, as they contain *t*Bu groups, which conflict with the mesityl moiety. The three remaining enantiomers are *RSSR*, *SRRS*, and *RSRS* (the *meso* compound). The crystal of **9** represents the *RSSR* isomer. Presumably it is mixed with *SRRS*, as they are mirror images.

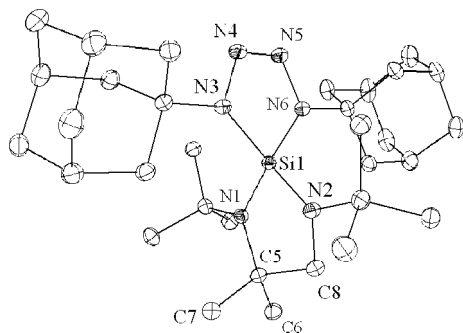


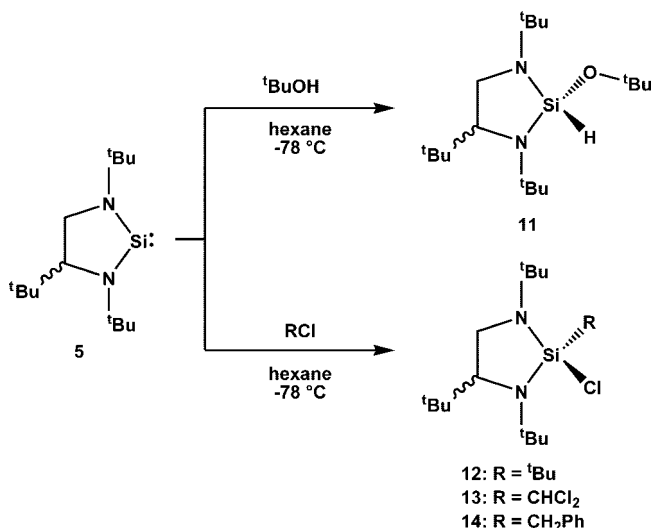
Figure 4. Thermal ellipsoid (40%) plot of **10** with H atoms omitted for clarity. Selected bond distances (Å): Si(1)–N(1) 1.7237(13), Si(1)–N(2) 1.7017(15), Si(1)–N(3) 1.7472(16), Si(1)–N(6) 1.7461(15), N(3)–N(4) 1.3869(16), N(4)–N(5) 1.2668(17), N(5)–N(6) 1.3813(17). Selected bond angles (deg): N(1)–Si(1)–N(2) 95.57(6), N(3)–Si(1)–N(6) 85.98(7), C(6)–C(5)–C(7) 108.52(11).

becomes somewhat planar due to the steric repulsion of the adamantyl groups, with the sum of angles around C(5) (343.34°) being a good indicator of this planarity. The N(3)–N(4) and N(5)–N(6) distances (1.383(2) Å) are typical of N–N single bonds, while the N(4)–N(5) distance is much shorter (1.267(2) Å), indicative of a N=N bond. The N–Si–N bond angles of the SiN₄ core are in the range 86.0–121.2° and thus significantly distorted from a regular tetrahedron.

Silylene **6** also reacts with adamantyl azide to yield the silatetrazoline **10** (Figure 4), which is analogous to compound **8** (Scheme 3). Crystals suitable for crystallographic studies were grown from a concentrated solution in tetrahydrofuran.

Silylene **5** reacts with *tert*-butanol in hexane at –78 °C via an expected insertion into the O–H bond to afford the corresponding *tert*-butoxyhydrosilane **11** in 78% isolated yield (Scheme 4). The ²⁹Si NMR shows the characteristic upfield shift from divalent silicon (δ +140 ppm) to tetravalent silicon (δ –43 ppm, $J_{\text{Si-H}} = 240$ Hz). Similar reactions with chlorocarbons are also observed. The reaction of **5** with ^tBuCl forms the 1:1 adduct **12** (²⁹Si $\delta = +2.24$ ppm), as expected with a probable preference for the “*trans*” isomer. The reactions of **1** and **2** with CHCl₃ and PhCH₂Cl give the 1:2 disilane adducts preferentially. However, the reactions of **5** with CHCl₃ and PhCH₂Cl give the 1:1 adducts **13** and **14** exclusively, which were obtained in 97% and 98% yield (by NMR), respectively (Scheme 4). This preference may be due to the increased steric bulk of **5**, which does not allow the insertion of a second silylene molecule to take place.

Scheme 4. Reaction of **5** with ^tBuOH, ^tBuCl, CHCl₃, and PhCH₂Cl



Although silylene **2** reacts with 2,3-dimethylbutadiene to afford a 1-silacyclopent-3-ene compound, the new silylene **5** catalyzes the polymerization of 2,3-dimethylbutadiene, as does the silylene **4**. This polymerization takes place even at very low concentrations of silylene.

Conclusion

Three new N-heterocyclic saturated silylenes, **5**, **6**, and **7**, which are monomeric in their pure state, have been synthesized. Reactions of **5** are similar to those for the unsubstituted analogue **2**, but unlike **2**, **5** does not undergo dimerizing additions to alkyl chlorides.

Further investigations regarding the reactivity of **5**, **6**, and **7** as well as theoretical calculations may shed light on the differences between **2** and its substituted analogues **5**, **6**, and **7**.

Acknowledgment. The authors thank Dr. Ilia Guzei for assistance with X-ray crystallographic studies and the National Science Foundation for support of this research.

Supporting Information Available: Text giving general experimental procedures, details of the preparation of **5**–**14** and their synthetic precursors, and spectroscopic information and CIF files giving X-ray structural information on **8**, **9**, and **10**. This material is available free of charge via the Internet at <http://pubs.acs.org>.

OM8006147

Synthesis and Structures of Titanium and Zirconium Trisiloxides

Clemens Krempner,^{*,†} Ulrike Jäger-Fiedler,[‡] Martin Köckerling,[‡] and Helmut Reinke[‡]

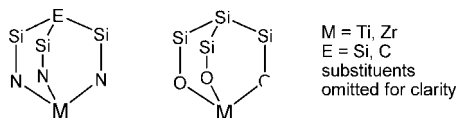
Department of Chemistry and Biochemistry, Texas Tech University, Lubbock, Texas 79409, and Institut für Chemie der Universität Rostock, A.-Einstein-Straussse 3a, D-18059 Rostock, Germany

Received September 24, 2008

Summary: The synthesis and structures of zirconium and titanium trisiloxides containing the tridentate ligand $[\text{MeSi}(\text{RMeSiO})_3]^{3-}$ (*rac-l,l-3*) ($\text{R} = \text{Si}(\text{SiMe}_3)_2\text{Me}$) are reported. Reactions of *rac-l,l-3* with $\text{M}(\text{OEt})_4$, where $\text{M} = \text{Ti}$ or Zr , gave tridentate complexes of formula $[\text{MeSi}(\text{RMeSiO})_3]\text{MOEt}$ (*l,l-4*, $\text{M} = \text{Ti}$; *l,l-5*, $\text{M} = \text{Zr}$). In striking contrast, treatment of *rac-l,l-3* with $\text{Zr}(\text{NEt})_4$ afforded the spirocyclic complex $\{[\text{MeSi}(\text{RMeSiO})_3]_2\text{Zr}\}\text{H}_2$ (*l,l-7*). These compounds feature bicyclooctane structures, which are hitherto unknown in the chemistry of metal siloxides.

Introduction

There has been considerable interest in recent years in the chemistry and structures of titanium and zirconium siloxides, as these well-defined compounds have found application in catalysis and as soluble precursors for silicate materials.¹ Synthetic and structural studies with respect to bidentate and tridentate siloxide complexes of titanium and zirconium have been reported by the groups of Feher,² Duchateau³ and Edelmann,⁴ employing incompletely condensed polyhedral oligosilsesquioxanes (POSS) as supporting ligands. Tridentate complexes, featuring a classical bicyclooctane structure, $\text{Si}(\text{SiO})_3\text{M}$, however, are hitherto unknown, although their nitrogen analogues, $\text{Si}(\text{SiN})_3\text{M}$ and $\text{C}(\text{SiN})_3\text{M}$, have been investigated in great detail by Gade and co-workers.⁵ We report here the synthesis and structures of the first titanium and zirconium trisiloxides derived from the trisilanol *rac-l,l-3*: $\text{MeSi}\{[\text{Me}(\text{Me}_3\text{Si})_2\text{Si}]\text{MeSiOH}\}_3$ (*rac-l,l-3*).



Results and Discussion

Recently, we reported the synthesis and isolation of the trisilanols *rac-l,l-3* and *rac-l,u-3*, obtained as mixtures (ratio *rac-l,l-3*/*rac-l,u-3* $\approx 1/3.5$) by hydrolysis of the chlorosilane *rac-l,u-2* in basic medium.⁶ We now have found that hydrolysis of *rac-l,l-2* in 1 M

* To whom correspondence should be addressed. E-mail: clemens.krempner@ttu.edu.

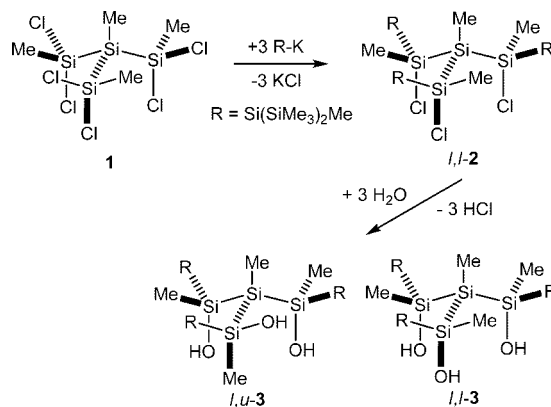
[†] Texas Tech University.

[‡] Institut für Chemie der Universität Rostock.

(1) Reviews: (a) Murugavel, R.; Voigt, A.; Walawalkar, M. G.; Roessky, H. W. *Chem. Rev.* **1996**, *96*, 2205. (b) King, L.; Sullivan, A. C. *Coord. Chem. Rev.* **1999**, *189*, 19. (c) Murugavel, R.; Bhattacharjee, M.; Roessky, H. W. *Appl. Organomet. Chem.* **1999**, *13*, 227–243. (d) Lorenz, V.; Fischer, A.; Gießmann, S.; Gilje, J. W.; Gun'ko, Y.; Jacob, K.; Edelmann, F. T. *Coord. Chem. Rev.* **2000**, *321*, 206–207. (e) Abbenhuis, H. C. L. *Chem.—Eur. J.* **2000**, *6*, 25–32. (f) Marciniak, B.; Maciejewski, H. *Coord. Chem. Rev.* **2001**, *223*, 301. (g) Fajdala, K. L.; Brutchey, R. L.; Tilley, T. D. *Topics Organomet. Chem.* **2005**, *16*, 69.

(2) (a) Feher, F. J. *J. Am. Chem. Soc.* **1986**, *108*, 3850. (b) Feher, F. J.; Walzer, F. J.; Blanski, R. L. *J. Am. Chem. Soc.* **1991**, *113*, 3618. (c) Feher, F. J.; Blanski, R. L. *J. Am. Chem. Soc.* **1992**, *114*, 5886. (d) Feher, F. J.; Tajima, T. L. *J. Am. Chem. Soc.* **1992**, *116*, 2145.

Scheme 1. Synthesis of 3



sulfuric acid furnished *rac-l,l-3* as the major product in yields of ca. 60%. Starting from $\text{MeSi}(\text{SiMe}_2\text{Cl})_3$ (**1**) and without purifying the chlorosilane *rac-l,l-2*, the trisilanol could be isolated in total yields of more than 50% based on **1** (Scheme 1). This allowed us to use *rac-l,l-3* as a precursor in the formation of transition metal trisiloxides that contain the tridentate ligand $[\text{MeSi}(\text{RMeSiO})_3]^{3-}$ (*rac-l,l-3*)-3H.

Suitable starting materials in the preparation of titanium and zirconium siloxides are the amides or alkoxides of these metals in Brønsted acid–base reactions with appropriate silanols. In fact, the stoichiometric reaction of *rac-l,l-3* with $\text{Ti}(\text{OEt})_4$ in hexanes at room temperature furnished $[\text{MeSi}(\text{RMeSiO})_3]\text{TiOEt}$ (*l,l-4*) as a yellow microcrystalline material in 74% yield. The analogous reaction with $\text{Zr}(\text{OEt})_4$ at elevated temperatures in heptanes gave the corresponding zirconium trisiloxide $[\text{MeSi}(\text{RMeSiO})_3]\text{ZrOEt}$ (*l,l-5*) as a colorless powder in 64% yields (Scheme 2). Both products could be identified by means of elemental analyses and multinuclear NMR spectroscopy. As in the free ligand *l,l-3*, the ¹H, ¹³C, and ²⁹Si NMR spectra (THF-*d*₈) of the C₃-symmetric products indicate that all three (RMeSiO)₃ groups are equivalent in solution with two sets of diastereotopic Me₃Si resonances and two singlets corresponding to the MeSiO and MeSi groups.

Interestingly, when a saturated hexane solution of the titanium compound **4** was exposed to air for several days, a yellow microcrystalline material was formed, which was identified by multinuclear NMR spectroscopy and X-ray crystallography as the

(3) (a) Duchateau, R. *Chem. Rev.* **2002**, *102*, 3525, and references cited therein. (b) Duchateau, R.; Dijkstra, T. W.; van Santen, R. A.; Yap, G. P. A. *Chem.—Eur. J.* **2004**, *10*, 3979.

(4) (a) Lorenz, V.; Edelmann, F. T. *Adv. Organomet. Chem.* **2005**, *53*, 101, and references cited therein. (b) Lorenz, V.; Giessmann, S.; Gun'ko, Y. K.; Fischer, A. K.; Gilje, J. W.; Edelmann, F. T. *Angew. Chem., Int. Ed.* **2004**, *43*, 4603.

(5) Gade, L. H. *Acc. Chem. Res.* **2002**, *35*, 575, and references cited therein.

(6) Krempner, C.; Jäger-Fiedler, U.; Köckerling, M.; Ludwig, R.; Wulf, A. *Angew. Chem., Int. Ed.* **2006**, *45*, 6755–6759.

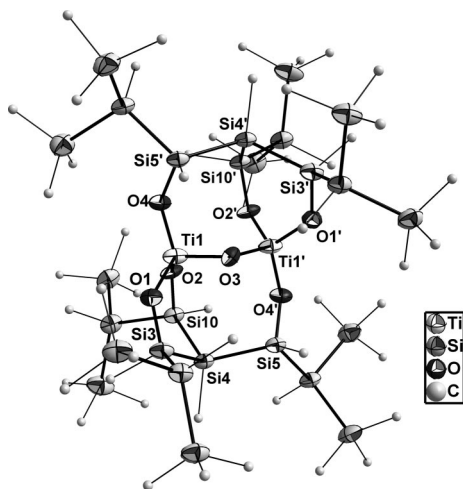
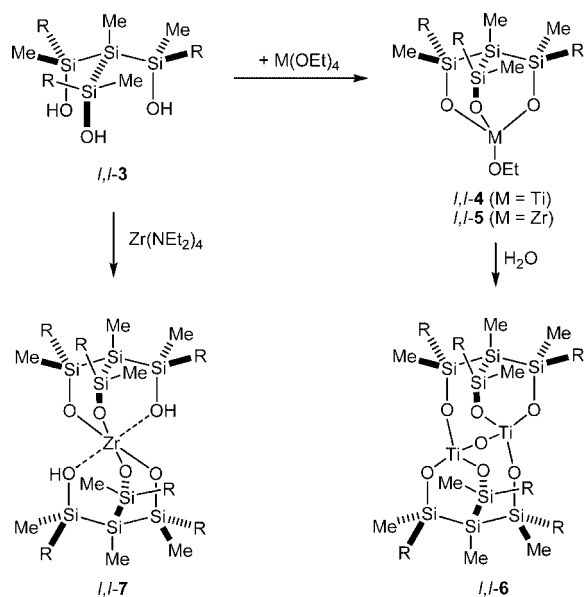


Figure 1. Molecular structure of **6** in the crystal. The thermal ellipsoids correspond to 30% probability. Hydrogen atoms are omitted for clarity. Selected bond lengths [Å] and angles [deg]: Ti1–O4 1.795(6), Ti1–O1 1.796(5), Ti1–O3 1.802(4), Ti1–O2 1.817(5), Si3–O1 1.683(6), Si5–O4 1.681(5), Si10–O2 1.680(6), Si4–Si10 2.400(3), Si4–Si5 2.401(5), Si3–Si4 2.396(5), O4–Ti1–O1 117.6(3), O4–Ti1–O3 103.1(2), O1–Ti1–O3 105.2(3), O4–Ti1–O2 115.0(2), O1–Ti1–O2 107.9(2), O3–Ti1–O2 107.0(3), Ti1–O3–Ti1 124.6(4).

Scheme 2. Synthesis of the Metal Trisiloxides 4–7



dinuclear titanium complex **6** (Scheme 2). In the ^1H , ^{13}C , and ^{29}Si NMR spectra of **6**, six signals for the SiMe_3 (1:1:1:1:1:1 ratio) and four signals for the SiMe groups (1:1:1:1 ratio) were observed, whereas the free ligand *rac*-**1,1,3** and the complexes **4** and **5** exhibit only two signals for the diastereotopic SiMe_3 groups (1:1 ratio) and two signals for the SiMe groups (1:3 ratio). Moreover, in the ^{29}Si NMR spectrum of **6**, the silicon atoms of the SiO moieties display three distinct signals appearing at 33.3, 27.9 and 26.0 ppm, respectively, indicating different chemical environments. By X-ray crystallography, the structure was determined unambiguously to be dinuclear, with the two tetracoordinated titanium atoms bridged by an oxygen atom (Figure 1). Each of the two siloxide ligands binds to the titanium atoms in a mono- and bidentate fashion as well. The inner Si–Si bonds [Si4–Si10 2.400(3), Si4–Si5 2.401(5), Si3–Si4 2.396(5) Å] are significantly elongated as compared to that of the free ligand *rac*-**1,1,3** (2.383(3) Å) and zirconium complex **7** (average value 2.36 Å), indicating consider-

able strain in the molecule. The Si–O and Ti–O distances are in the expected range for related tetravalent titanium siloxides.⁷ A similar structural motif has been observed in a dinuclear complex derived from the reaction of cyclo- $\text{Ph}_4(\text{SiO})_4(\text{OH})_4$ with $\text{Ti}(\text{O}-\text{SiMe}_3)_4$.⁸ In this case, however, a water molecule bridges both titanium atoms.

In addition, the structural interpretation has been confirmed by the independent synthesis of **6** from a wet sample of *l,l*-**3**⁹ and $\text{Ti}(\text{OEt})_4$ in *n*-heptane under a nitrogen atmosphere. The NMR spectroscopic data of the raw product are identical to those found for **6** derived from solutions of **4** being exposed to air. Besides **4**, small amounts of **6** could be detected in the ^1H NMR spectra, and with increased reaction time under reflux conditions the relative concentrations of both compounds continue to change; **6** becomes the major product, whereas the concentration of **4** decreases. From these results it is likely that the formation of dinuclear **6** arises from hydrolysis of the Ti–OEt bond sequence of **4**. This process may generate a reactive Ti–OH species, which then rapidly condenses or inserts into another molecule of **4** to form the oxo bridged titanium complex **6** after ligand scrambling.

Attempted reactions of *rac*-*l,l*-**3** with $\text{Ti}(\text{NET}_2)_4$ under various conditions resulted in mixtures of products that could not be identified. Also stoichiometric reactions of *rac*-*l,l*-**3** with $\text{Zr}(\text{NET}_2)_4$ did not give the expected product $[\text{MeSi}(\text{RMeSiO})_3]\text{ZrNEt}_2$; instead the formation of the spirocyclic zirconium trisiloxide *l,l*-**7** was observed as the main product (Scheme 2). Best yields (51%) were obtained when 2 equiv of *rac*-*l,l*-**3** and 1 equiv of $\text{Zr}(\text{NET}_2)_4$ in *n*-heptane were employed.

Complex **7**, whose structure was determined by X-ray crystallography, contains formally a Zr^{4+} ion, with two ligands coordinating (Figure 2). Because we could not find counter cations in the difference map, we propose compound **7** to be of formula $\{[\text{MeSi}(\text{RMeSiO})_3]_2\text{Zr}\}\text{H}_2$ ($\text{R} = \text{Si}(\text{SiMe}_3)_2\text{Me}$) in which two protons are weakly bonded to the oxygen atoms. However, four of the six coordinating OH-groups are deprotonated. Therefore, the coordination around the zirconium is not regular, but distorted octahedral, with four short Zr–O bonds (average length 2.008 Å, range 1.925–2.098 Å) and two longer ones (2.334 and 2.356 Å). The O atoms with the longer Zr–O bonds are carrying the protons. As expected, the average of the four Zr–O bond distances is slightly elongated as compared to tetracoordinated zirconium silsesquioxane complexes $[(c\text{-C}_6\text{H}_{11})_7\text{Si}_7\text{O}_{12}]\text{ZrCp}^*$ (1.96(3) Å),^{2a} and $[(c\text{-C}_5\text{H}_9)_7\text{Si}_7\text{O}_{11}(\text{OSiMePh}_2)]\text{ZrCp}_2$ (1.994(2), 1.995(2) Å),^{10a} the pentacoordinated species $\{[(c\text{-C}_5\text{H}_9)_7\text{Si}_7\text{O}_{12}]\text{ZrCH}_2\text{Ph}\}_2$ (1.958(5) Å)^{10b} and $[\text{Me}(\text{Me}_3\text{Si})_3\text{SiSiO}]_2\text{Zr} \cdot \text{NHEt}_2$ (2.020(2), 1.960(2) Å).¹¹ However, they compare well with compounds that have hexacoordinated zirconium, e.g. $[(c\text{-C}_5\text{H}_9)_7\text{Si}_7\text{O}_{11}$

(7) For comparison, see also: (a) Hoffmann, D.; Krempner, C.; Reinke, H. *J. Organomet. Chem.* **2002**, *662*, 1. (b) Krempner, C.; Koeckerling, M.; Reinke, H.; Weichert, K. *Inorg. Chem.* **2006**, *45*, 3203. (c) Krempner, C.; Reinke, H.; Weichert, K. *Polyhedron* **2007**, *26*, 3637. (d) Krempner, C.; Reinke, H.; Weichert, K. In *Organosilicon Chemistry*, Vol. VI; Auner, N., Weis, J., Eds.; VCH: Weinheim, 2005; p 344.

(8) Hirotsu, M.; Taruno, S.; Yoshimura, T.; Ueno, K.; Unno, M.; Matsumoto, H. *Chem. Lett.* **2005**, *34*, 1542.

(9) In the course of our studies we noticed that the yield and purity of titanium complex **4** is strongly influenced by the water content of the ligand precursor *l,l*-**2**. The latter, obtained as a finely divided powder from hydrolysis of *l,l*-**2**, contains significant amounts of water if not thoroughly dried under vacuum.

(10) (a) Skowronska-Ptasinska, M. D.; Duchateau, R.; van Santen, R. A.; Yap, G. P. A. *Organometallics* **2001**, *20*, 3519. (b) Duchateau, R.; Abbenhuis, H. C. L.; van Santen, R. A.; Meetsma, A.; Thiele, S.; K., H.; van, Tol; Maurits, F. H. *Organometallics* **1998**, *17*, 5663.

(11) Krempner, C.; Reinke, H.; Spannenberg, A.; Weichert, K. *Polyhedron* **2004**, *23*, 2475.

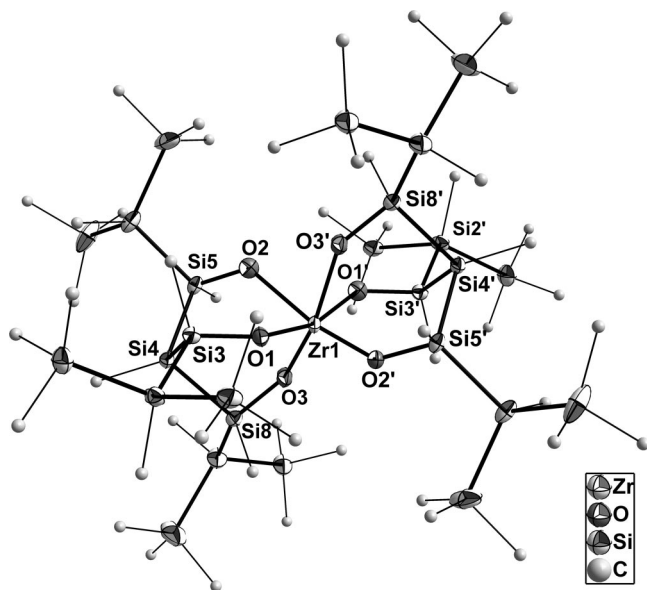


Figure 2. Molecular structure of **7** in the crystal. The thermal ellipsoids correspond to 30% probability. Hydrogen atoms are omitted for clarity. Only one of the two refined parts of the two disordered groups (and one Zr atom) is shown. Selected bond lengths [Å] and angles [deg]: Zr1–O1 2.075(2), Zr1–O2 2.334(2), Zr1–O3 1.932(2), O1–Si3 1.662(2), O2–Si5 1.676(2), O3–Si8 1.670(2), Si3–Si4 2.362(1), Si4–Si5 2.357(1), Si4–Si8 2.361(1), O1–Zr1–O1' 163.52(3), O1–Zr1–O2 83.74(8), O2–Zr1–O2' 168.18(5), O1–Zr1–O3 95.5(1), O2–Zr1–O3 88.0(1), O3–Zr1–O3' 168.63(6), Zr1–O2' 1.925(2), Zr1–O1' 2.098(2), Zr1–O3' 2.356(2) (symmetry operation for the primed atoms: $1-x, 2-y, -z$).

(OSiMe₃)₂Zr · 2THF (2.000(5) Å)^{10b} and the zirconate complex [O(SiPh₂O)₂]₃Zr[Li₂ · 3Pyr] (ca. 2.015–2.132 Å).¹²

The presence of OH groups in complex **7** is supported by IR spectroscopic measurements (nujol), which exhibit a sharp signal at 3605 cm⁻¹ indicative for a nonassociated Si–OH group. However, as in the free ligand *rac-l,l-3*, the MeRSiO moieties are equivalent in the ¹H, ¹³C and ²⁹Si NMR spectra, indicating a symmetric coordination environment of the central zirconium. Two sets of SiMe₃ groups (1:1 ratio), three SiMe groups (3:3:1 ratio), but none of the OH protons could be detected in the ¹H NMR (C₆D₆), which implies fluxional behavior of the OH protons.

It is somewhat surprising that diethylamine, which is released during the course of the reaction, does not abstract the OH protons to form the expected dianionic complex with H₂NET₂⁺ as the counteranion. We note that Ph₂(OH)Si–O–Si(OH)Ph₂ with pyridine readily forms its adduct [Ph₂(OH)SiOSi(O)Ph₂][PyrH]¹³ and reacts with Zr(NEt₂)₄ to give the hexa-coordinated zirconate [O(SiPh₂O)₂]₃Zr[H₂NET₂].¹⁴ The fact that *rac-l,l-3* can coordinate to the metal without being fully deprotonated^{15,16} is most likely due to its less pronounced acidity compared to siloxy substituted silanols such as Ph₂(OH)Si–O–Si(OH)Ph₂. This is plausible if

one considers that the acidity of silanols¹⁷ is progressively decreased as the substituents on the central SiOH moiety become more electropositive, consistent with the order (R₃SiO)₃SiOH > (Aryl)₃SiOH > R₃SiOH > (R₃Si)₃SiOH.¹⁸

In summary, tridentate titanium and zirconium trisiloxides derived from trisilanol *rac-l,l-3* were synthesized and structurally characterized. The titanium and zirconium derivatives **4**, **5**, and **7** represent the first examples of a metal siloxides featuring a bicycloctane structure, Si(SiO₃)₃M (M = Ti, Zr).

Experimental Section

General Remarks. The manipulation of air-sensitive compounds involved standard Schlenk line and dry box techniques. All solvents were distilled under argon from alkali metals prior to use. THF-*d*₈ and benzene-*d*₆ were dried over activated molecular sieves and stored in the glovebox. The compounds MeSi(SiMe₃)₃¹⁹ and MeSi(SiMeCl₂)₃²⁰ were prepared as previously described. Ti(OEt)₄ was purchased from Alfa Aesar and Zr(OEt)₄ from Aldrich. The ¹H, ¹³C, and ²⁹Si NMR spectra were obtained using Bruker AC 250 and ARX 300 spectrometers at 300 K if not otherwise stated. Microanalyses were carried out with a C/H/N/S-Analyzer Thermoquest Flash EA 1112 by addition of Pb₃O₄ for silicon containing compounds. MS: Intectra AMD 402.

Synthesis of *rac-l,l-3*. In a Schlenk flask with magnetic stirrer were placed rapidly Bu^tOK (12.93 g, 0.115 mmol) and MeSi(SiMe₃)₃ (30.32 g, 0.115 mol). After the flask was evacuated and refilled with argon three times, THF (300 mL) was added. The resulting yellow solution was stirred overnight to quantitatively form potassium silanide KSi(SiMe₃)₂Me. After the solvent had been replaced by *n*-pentane, the solution was transferred into a dropping funnel and slowly added to a vigorously stirred solution of MeSi(SiMeCl₂)₃ (**1**) (14.83 g, 0.0385 mol) in *n*-pentane (100 mL) at –78 °C. Stirring was continued for 30 min at –78 °C and the mixture was allowed to warm up to room temperature within 2 h. The reaction mixture was filtered, and the solution was concentrated and dried under high vacuum at 150 °C to afford raw *l,l-2* as a highly viscous oil, which upon standing slowly solidified. The raw material was dissolved in ether (150 mL) and 1 M H₂SO₄ (200 mL) was added. The mixture was vigorously stirred at room temperature for one day after which a white powder precipitated. The white powder was filtered, washed several times with water, acetone, and pentane, and carefully dried under high vacuum for 24 h at ca. 50 °C to afford 15.86 g (52%) of the title compound. The NMR spectroscopic data are identical to those previously reported.⁶

Caution! Compound **3** can contain significant amounts of water. Therefore, drying the sample under vacuum for 24 h at ca. 50 °C prior to use or storing dry samples in the Glove box is strongly recommended.

***l,l-4*:** A suspension of Ti(OEt)₄ (91 mg, 0.40 mmol), *rac-l,l-3* (300 mg, 0.38 mmol) and *n*-heptane (4 mL) was stirred for ca. 10 min at room temperature until the suspension became a clear solution. This solution was left overnight and subsequently stored in a freezer at –20 °C to give yellow crystals (250 mg, 74%) of the title compound. Mp 260–270 °C (dec.). ¹H NMR (THF-*d*₈, 300 MHz): δ 4.52 (br, OCH₂CH₃, 2 H), 1.29 (br, OCH₂CH₃, 3 H), 0.85 (s, OSiCH₃, 9 H), 0.38 (s, SiCH₃, 3 H), 0.32 (s, SiCH₃, 9 H), 0.23, 0.18 (2s, Si(CH₃)₃, 2 × 27 H). ¹³C NMR (THF-*d*₈, 125.8 MHz): δ 70.6 (OCH₂CH₃), 18.7 (OCH₂CH₃), 9.0 (OSiCH₃), 1.3, 1.0 (Si(CH₃)₃), –8.0, –9.7 (SiCH₃). ²⁹Si NMR (THF-*d*₈, 99.3 MHz): δ 27.8 (OSiCH₃), –8.9, –9.6

(12) Motevalli, M.; Shah, D.; Sullivan, A. C. *J. Chem. Soc., Dalton Trans.* **1993**, 2849.

(13) Gunko, Y. K.; Kessler, V. G.; Reilly, R. *Inorg. Chem. Commun.* **2004**, 7, 341.

(14) Hossain, M. A.; Hursthouse, M. B. *Inorg. Chim. Acta* **1980**, 44, L259.

(15) Similar observation were made for [(E)-(Me(Me₂Si)₃SiO)₂Al]H: Krempner, C.; Weichert, K.; Reinke, H. *Organometallics* **2007**, 26, 1386.

(16) Dimeric [Cl₂Zr(CpSiMe₂OH)]₂ is the only other known zirconium complex with two SiOH groups coordinated to the zirconium atoms: Ciruelos, S.; Cuence, T.; Gomez-Sal, R.; Manzanera, A.; Royo, P. *Polyhedron* **1998**, 17, 1055.

(17) Silanols are thought to be more acidic than their carbon counterparts, the alcohols; see also: West, R.; Baney, R. H. *J. Am. Chem. Soc.* **1959**, 81, 6145.

(18) Chandrasekhar, V.; Boomishankar, R.; Nagendran, S. *Chem. Rev.* **2004**, 104, 5847.

(19) Marsmann, H. C.; Raml, W.; Hengge, E. *Zeitschrift Naturf. B* **1980**, 35B, 1541.

(20) Herzog, U.; Richter, R.; Brendler, E.; Roewer, G. *J. Organomet. Chem.* **1996**, 507, 221.

(Si(CH₃)₃), -71.1, -78.4 (SiCH₃). Anal. calcd for C₂₇H₈₀O₄Si₁₃Ti (881.900): C, 36.77; H 9.14. Found: C, 36.51; H 9.07.

***l,l*-5**: A suspension of Zr(OEt)₄ (113 mg, 0.42 mmol), rac-*l,l*-3 (300 mg, 0.38 mmol), and *n*-heptane (10 mL) was stirred at room temperature overnight and at 100 °C for ca. 20 h. The resulting solution was cooled to room temperature and filtered. Colorless crystals of *l,l*-5 (225 mg, 64%) were obtained after cooling the solution in a freezer at ca. -20 °C. Mp 267 °C. ¹H NMR (THF-*d*₈, 300 MHz): δ 4.25 (br, OCH₂CH₃, 2 H), 1.30 (br, OCH₂CH₃, 3 H), 0.81 (s, OSiCH₃, 9 H), 0.31 (s, SiCH₃, 3 H), 0.29 (s, SiCH₃, 9 H), 0.22, 0.17 (2s, Si(CH₃)₃, 2 × 27 H). ¹³C NMR (THF-*d*₈, 125.8 MHz): δ 65.5 (OCH₂CH₃), 20.3 (OCH₂CH₃), 10.4 (OSiCH₃), 1.4, 1.1 (Si(CH₃)₃), -8.1, -9.5 (SiCH₃). ²⁹Si NMR (THF-*d*₈, 99.3 MHz): δ 16.4 (OSiCH₃), -9.0, -9.9 (Si(CH₃)₃), -70.7, 79.8 (SiCH₃). Anal. calcd for C₂₇H₈₀O₄Si₁₃Zr (925.257): C, 35.05; H 8.71. Found: C, 34.81; H 8.64.

***l,l*-6**: A stirred mixture of Ti(OEt)₄ (86 mg, 0.38 mmol), wet rac-*l,l*-3⁹ (300 mg, 0.38 mmol), and *n*-heptane (3 mL) was stirred at room temperature for 3 h at 100 °C and then cooled to room temperature. Yellow crystals of **6** (100 mg, 31%) were obtained after cooling the solution in a freezer at ca. 5 °C. Mp >230 °C. ¹H NMR (C₆D₆, 500 MHz): δ 1.25, 1.17, 0.90 (3s, OSiCH₃, 3 × 3 H), 0.68, 0.50, 0.49, 0.44 (4s, SiCH₃, 4 × 3 H), 0.42 (s, Si(CH₃)₃, 2 × 9 H), 0.39, 0.32, 0.28, 0.24, (4s, Si(CH₃)₃, 4 × 9 H). ¹³C NMR (C₆D₆, 125.8 MHz): δ 11.1, 9.7, 8.0 (OSiCH₃), 1.3, 1.3, 1.3, 1.2, 1.2 (Si(CH₃)₃), -7.9, -10.0, -10.2, -10.5 (SiCH₃). ²⁹Si NMR (C₆D₆, 99.4 MHz): δ 33.3, 27.9, 26.0 (OSiCH₃), -9.7, -9.9, -10.3, -12.3, -12.6, -13.8 (Si(CH₃)₃), -75.5, -76.3, -76.4, -76.5, (SiCH₃). Anal. calcd for C₅₀H₁₅₀O₇Si₂₆Ti₂ (1689.71): C, 35.54; H 8.95. Found: C, 35.70; H 9.10. - MS (70 eV): *m/z* (%): 1689 (60) [M⁺], 1500 (100) [M⁺ - Si(SiMe₃)₂Me].

***l,l*-7**: A stirred mixture of Zr(NEt₂)₄ (72 mg, 0.19 mmol), rac-*l,l*-3 (300 mg, 0.38 mmol), and *n*-heptane (3 mL) was heated to 100 °C for ca. 15 min until the suspension became a clear solution. Colorless crystals of *l,l*-7 (160 mg, 51%) were obtained after cooling slowly the hot solution to room temperature. Mp >230 °C. ¹H NMR (C₆D₆, 500 MHz): δ 1.07 (s, OSiCH₃, 9 H), 0.50 (s, SiCH₃, 3 H), 0.45 (s, SiCH₃, 9 H), 0.42, 0.28 (2s, Si(CH₃)₃, 2 × 27 H). ¹³C NMR (C₆D₆, 125.8 MHz): δ 9.9 (OSiCH₃), 1.8, 1.0 (Si(CH₃)₃), -9.7, -10.1 (SiCH₃). ²⁹Si NMR (C₆D₆, 99.4 MHz): δ -11.0, -12.2 (Si(CH₃)₃), -12.0 (OSiCH₃), -77.0, -80.8 (SiCH₃). IR (nujol): ν_{SiOH} = 3605 cm⁻¹. Anal. calcd for C₅₀H₁₅₂O₆Si₂₆Zr (1671.19): C, 35.93; H 9.17. Found: C, 35.72; H 9.29. MS (70 eV): *m/z* (%): 1656 (13) [M⁺ - CH₃], 1483 (57) [M⁺ - Si(SiMe₃)₂Me], 1467 (100) [M⁺ - Si(SiMe₃)₂Me - Me].

Crystal Structure Determination of 6 (CCDC 663365) and 7 (CCDC 663366). The relevant crystal data, data collection and refinement parameters are collected in Table 1. X-ray data were collected for **7** at low temperature (173(2) K) on a Bruker-Nonius Apex X8 diffractometer, equipped with a CCD detector and for **6** on a Siemens P4 diffractometer. Data were collected using graphite-monochromated Mo Kα radiation (λ = 0.71073 Å). Absorption correction for **7** was applied by using the SADABS routine. Both

Table 1. Crystal Data, Data Collection, and Structure Refinement Parameters for 6 and 7

	6	7
empirical formula	C ₅₀ H ₁₅₀ O ₇ Si ₂₆ Ti ₂	C ₅₀ H ₁₅₂ O ₆ Si ₂₆ Zr
fw, g/mol	1689.84	1671.20
crystal size, mm ³	0.38 × 0.34 × 0.32	0.43 × 0.19 × 0.18
<i>T</i> , K	293(2)	173(2)
cryst. sys.	monoclinic	monoclinic
space group, <i>Z</i>	<i>C</i> 2/ <i>c</i> , 4	<i>P</i> 2 ₁ / <i>c</i> , 2
<i>a</i> , Å	30.47(2)	14.6636(7)
<i>b</i> , Å	25.00(1)	26.479(2)
<i>c</i> , Å	16.228(9)	14.9466(7)
β, °	117.60(5)	115.082(2)
<i>V</i> , Å ³	10955(10)	5256.2(5)
<i>D</i> _{calcd} , g·cm ⁻³	1.025	1.056
μ, mm ⁻¹	0.463	0.434
no. of measured reflns.	5015 (up to 46°(2θ))	50770 (up to 52°(2θ))
no. of unique refln.	4276 (<i>R</i> _{int} = 0.0388)	10327 (<i>R</i> _{int} = 0.0421)
transm. factors, min, max	—	0.8666, 0.9260
no. parameters	384	387
<i>R</i> (<i>F</i>) ^a	0.0653	0.0683
<i>wR</i> 2(<i>F</i> ²) ^b	0.1761	0.1977
weighting, <i>A</i> , <i>B</i> ^c	0.0930, 0.0	0.0945, 4.53
GOF ^d	1.013	1.096

^a *R*1 = Σ|*F*_o - |*F*_c|| / Σ|*F*_c|; ^b *wR*2 = [Σ{*w*(*F*_o² - *F*_c²)²} / Σ{*w*(*F*_o²)²}]; ^c *w* = 1/[σ²(*F*_o²) + (*A*·*P*)² + *B*·*P*]; *P* = (*F*_o² + 2*F*_c²)/3; ^d GOF = [Σ{*w*(*F*_o² - *F*_c²)²} / (n - p)]^{1/2}, where *n* and *p* are the number of data and parameters.

structures were solved by direct methods (SHELXS-97),²¹ completed by subsequent difference Fourier techniques, and refined by full matrix least-squares refinements on *F*² (SHELXL-97)²¹ with initial isotropic thermal parameters. Anisotropic thermal parameters were used in the last cycles of refinement for all non-hydrogen atoms except those in disordered TMS groups. In **7** one TMS group is disordered and refined on two positions (as Si1A and Si1B), with an occupation of 63% for Me₃Si1A and 37% for Me₃Si1B as well as the Zr atom which is located slightly off the inversion center of Wyckoff site *1b*. It is refined with 50% occupation. The carbon atoms involved in this disordered TMS group are refined isotropically. The same procedure was applied to one of the methyl groups on Si7, which is refined as C11A (60% occupation) and C11B (40%). Hydrogen atoms were included in calculated positions in both structures and were refined with positional and thermal parameters riding on the attached atoms.

Supporting Information Available: Crystallographic data for **6** (CCDC 663365) and **7** (CCDC 663366) including CIF files. This material is available free of charge via the Internet at <http://pubs.acs.org>.

OM800930S

(21) Sheldrick, G. M. *SHELXSL-97 and SHELXL-97, Programs for Crystal Structure Solution and Refinement*; University of Göttingen: Göttingen, Germany, 1997.

Additions and Corrections

2008, Volume 27

Brian J. Anderson, David S. Glueck,* Antonio G. DiPasquale, and Arnold L. Rheingold: Substrate and Catalyst Screening in Platinum-Catalyzed Asymmetric Alkylation of Bis(secondary) Phosphines. Synthesis of an Enantiomerically Pure C_2 -Symmetric Diphosphine

Pages 4992–5001. The CIF files associated with this paper were not included in the original Supporting Information. The appropriate files are now available.

Supporting Information Available: CIF files giving crystallographic data for (*S,S*)-**6**, (*R,R*)-**6**, and *meso*-**7**. This material is available free of charge via the Internet at <http://pubs.acs.org>.

OM801124T

10.1021/om801124t

Published on Web 12/10/2008